Cobalt and Copper-Based Homogeneous Catalysis for C-C and C-N Bond Formation Reactions: Applications in Organic Synthesis and Sensing

A THESIS

Submitted by

ADWITIYA PAL

for the award of the degree

DOCTOR OF PHILOSOPHY (SCIENCE)

Department of Chemistry

Jadavpur University

Kolkata-700032, India

June, 2024

DECLARATION

I hereby declare that the research work embodied in the present thesis entitled **" Cobalt and Copper-Based Homogeneous Catalysis for C-C and C-N Bond Formation Reactions: Applications in Organic Synthesis and Sensing"** being submitted to Jadavpur University, Kolkata, has been carried out by me at Jadavpur University under the supervision of Dr. Arunabha Thakur, Assistant Professor, Jadavpur University. This work is original and has not been submitted in part or in full, for any degree whatsoever.

Adwitiya Pal 10/06/2024

(Adwitiya Pal)

Signature of Scholar with date

JADAVPUR UNIVERSITY
KOLKATA - 700 032

Dr. Arunabha Thakur
Assistant Professor
Department of Chemistry
Organic Chemistry Section

CERTIFICATE FROM THE SUPERVISOR

This is to certify that the thesis entitled "**Cobalt and Copper-Based Homogeneous Catalysis for C-C and C-N Bond Formation Reactions: Applications in Organic Synthesis and Sensing** " submitted by **Smt. Adwitiya Pal**, who got her name registered on 16/08/2019 for the award of Ph.D. (Science). Degree of Jadavpur University, is absolutely based upon her own work under the supervision of **Dr. Arunabha Thakur** and that neither this thesis nor any part of it has been submitted for either any degree/diploma or any other academic award anywhere before.

Thakur 10/06/2024

.....

(Dr. Arunabha Thakur)

Signature of Supervisor and date with seal

Dr. Arunabha Thakur
Assistant Professor
Department of Chemistry
Jadavpur University
Kolkata-700032, India

Phone : 033 2457 2779 (O), E-mail : arunabha.thakur@jadavpuruniversity.in / babuiitm07@gmail.com
Mobile : 9937760940, Webpage : https://sites.google.com/site/arunabhathakur3221/

Dedicated to my Family

Acknowledgement

Ph.D. degree course is a journey of training a tender mind with just an idea into a concrete base of research and it is not just the journey of the researcher but many other people who are directly or indirectly associated. Hence, as I approach towards the end of my doctoral research journey, there are so many wonderful people, who were behind the scenes, to whom I owe a debt of gratitude, for their contribution, support, and guidance towards my Ph.D. dissertation and I take this opportunity to thank them with all of my heart.

First and foremost, I would like to express my sincere gratitude to my Ph.D. supervisor, ***Dr. Arunabha Thakur***, Asst. Professor, Department of Chemistry, Jadavpur University, for providing me the opportunity to pursue Ph.D. in his research group. I am much obliged to him for leading me into the world of research with his constant guidance, valuable suggestions, and encouragement throughout the progression of my research. He always believed in my ideas and research proposals and provided ample liberty to conduct research work of my interest. He had always encouraged me to complete the projects within a limited timeline. It was his faith that enabled me to explore the fascinating field of transition metal-based catalysis and photocatalysis. His untiring determination, patience, research ethics, code of conduct, troubleshooting skills and perfectionist nature have shaped my character as a researcher. The training that I received from him in the last five years has prepared me well for the next challenges in my career and has developed me as an independent researcher. His zeal for excellence has always inspired me and set a good example for me in my career.

I am also thankful to the present and former Head of the Department, Section-in-Charge, Organic Chemistry Section and all the faculty members of the department of Chemistry, Jadavpur University.

I gratefully acknowledge my Research Advisory Committee member Dr. Indu Bhusan Deb, Principal Scientist, IICB for his valuable comments and yearly evaluation of my work. I convey my special acknowledgment to Jadavpur University, IACS and IICB for instrumental facilities and to Dr. Sumanta Jana (Microanalyst), Mr. Raju Biswas (NMR operator), Baby di (NMR operator), and other research scholars (acting as instrument operators) of the department of Chemistry, Jadavpur University, for their kind instrumental support in my research career.

I do not have words to express my thanks to the internet giants Google, Wikipedia, and Scifinder and Scihub which have made my work easier. It is because of these platforms that the knowledge in several disciplines related to my research is just a fingertip away from me.

I consider myself lucky enough to have experienced such a friendly lab environment with cooperative labmates during my Ph.D. tenure. It is because of them that I have never felt alone or depressed during my struggles in this once-in-a-lifetime journey to become a Ph.D. It is from the bottom of my heart that I acknowledge all the wonderful souls that I met in the lab since I joined. Senior labmates Dr. Sushil Ranjan Bhatta, Dr. Manisha Karmakar and all my juniors Mr. Krishna Mohan Das, Mr. Sayan Kumar Bag, Mr. Shubham Sau, and Mr. Suvendu Jana have helped me immensely in my lab work. I am also happy to have such labmates for keeping my social life alive during these 5 years and decorating my Ph.D. life with many beautiful memories. Without such huge support from past and present labmates, it would have been almost impossible for me to complete my work smoothly and joyfully.

I am also very much thankful to the former and present M.Sc. and project students of our lab, Mr. Sreejit Ghosh, Ms. Swagata Dasgupta, Ms. Balaka Ghosh, Ms. Rwitobrita Panda, Mr. Subhajit Bhuia, Mr. Abhradeep Dey and Ms. Soumita Dey for their kind cooperation and assistance in completing my work.

It is my pleasure to thank the neighbouring lab members from our department for their help in both academic and non-academic matters. Thanks to Dr. Biswajit Pabi, S. N. Bose National Centre for Basic Sciences for his cordial help in SEM measurements. I greatly appreciate and acknowledge the support received from other laboratories of Jadavpur University outside our lab for providing their facilities.

Collaborators played a big role in my doctoral research projects. Thus, my sincere gratitude goes to Dr. Bappaditya Goswami (IISER Kolkata), Dr. Atindra Nath Pal (S. N. Bose National Centre for Basic Sciences) and Dr. Bijan Mondal (Universitat Regensburg).

The motivation for pursuing higher studies in scientific research came right from the school days. Therefore, it will be a grave mistake if I do not acknowledge their efforts of teaching me. Thus, I take this platform to thank all of my teachers. The Chemistry Department of The University of Burdwan boosted my motivation to do Ph.D. So, the contribution from all of my teachers, especially, Prof. Pabitra Chattopadhyay, Prof. Bimalendu Ray, Prof. Bidyut Saha, Dr. Inul Ansari, and Dr. Sayani Ray is deeply acknowledged in this regard.

I also take this opportunity to convey my gratitude to my husband Mr. Tathagata Chatterjee for his unconditional love, support, and bearing with me during the entire phase of

my Ph.D. journey. He has witnessed all of my ups and downs, and has been my constant source of positivity and strength. The journey would have not been this smooth without the love, care, support and patience of my father-in-law Mr. Dipankar Chatterjee, and mother-in-law Mrs. Kalyani Chatterjee. They held me strong whenever I was low and had self-doubt.

Finally, it is time to mention the names of the two most important persons in my life, my mother Mrs. Mitali Pal and my father Mr. Asit Baran Pal. for their endless love and support throughout my life journey. They have always believed in me and provided me enough liberty to pursue the career of my choice and live life in my terms. It is the contribution of their selfless love, care, tenderness and countless sacrifices that I can write this thesis. They are the reason I am what I am today. Thank you for instilling in me a sense of discipline in life and building me up as an independent woman. A note of gratitude would never be enough for what you have contributed in my life. Last but not least, I would like to thank all my family members especially my big brother Dr. Pavel Pal, and my sister-in-law Dr. Rajlakshmi Mukherjee Pal for inspiring me toward higher studies.

Finally, I want to thank everyone who helped me finish my thesis and apologize for not naming everyone.

Adwitiya Pal

Date: 10/06/2024.

Adwitiya Pal
Department of Chemistry
Jadavpur University
Kolkata-700032, India.

Preface

The research embodied in the present thesis entitled "**Cobalt and Copper-Based Homogeneous Catalysis For C-C and C-N Bond Formation Reactions: Applications in Organic Synthesis and Sensing**" deals with the development of low-cost earth-abundant metal complex and salts of Co and Cu, in catalysis of C-C and C-N bond formations, which gives value-added synthetic intermediates as products.

Investigations described in this thesis have been carried out by the author at Jadavpur University, Jadavpur, Kolkata-700032, India during the time from January, 2019 to May, 2024 under the supervision of Dr. Arunabha Thakur. The entire work has been described and summarized within the six chapters of this thesis.

Chapter 1 is the general introduction which provides a comprehensive literature survey on the basic concept of catalysis that are relevant with my work. This chapter highlights the development of C-C and C-N bond formation reaction by Co and Cu-based catalytic systems by various research groups, followed by the applications of the developed molecules in total synthesis or as heavy ion detection probes.

Chapter 2 describes the development of a one-pot method for the synthesis of dimerized arene and heteroarene systems by employing 2 mol% of Co(II)-complex as catalyst along with Zn dust, at room temperature for 2-4 h. The Co(II)/Zn(0) system *in situ* generates Co(I) as the active catalyst. A range of substrates could be included in this methodology. The Co(II) catalyst is easy to synthesize, economically viable, thermally stable, and insensitive to air or moisture.

Chapter 3 describes the development of an unprecedented microwave-assisted $CoCl_2$-catalyzed acceptorless dehydrogenative coupling of benzyl alcohol and amine for the synthesis of *E*- aldimines, *N*-heterocycles and H_2 under mild condition, without any complicated exogenous ligand template, oxidant, or other additives. This environmentally benign methodology exhibits broad substrate scope (43 including 7 new products) with fair functional-group tolerance on the aniline ring. Controlled experiments, kinetic experiments, and Hammett analysis with variation in nature of substituents over the aniline ring were performed to reveal the insight of the reaction mechanism with different substituents.

Chapter 4 describes the development of the first Co(II) catalyzed one-component one-pot sustainable synthesis of acyl hydrazones only from acyl hydrazides under mild reaction conditions without using the traditional use of two components (usually acyl hydrazides and

aldehydes/ ketones/ alcohols/ styrene) as the coupling partners. This one-component procedure is found to be mild and has a high functional group tolerance, where a few of the resulting acyl hydrazones have been used as synthetic precursors and explored in various post-synthetic modifications to afford *N*-heterocyclic compounds. Furthermore, the *E/Z* isomerization around the C=N bond-bounded photoswitchable properties of a few products are also explored.

Chapter 5 presents an unprecedented visible light-mediated $CoCl_2$-catalyzed oxidative acylation of alkenes by aldehydes without any complicated ligand template in water solvent. This methodology includes aromatic as well as unactivated aliphatic substrates for both the alkene and aldehyde counterparts and also internal alkenes in aromatic system. The photocatalytic pathway has been studied by controlled and radical trapping experiments, intermediate detection by GCMS, and Hammett analysis.

Chapter 6 is divided into two parts 6.1 and 6.2, where the development of microwave-assisted Cu-catalyzed Glaser-Hay coupling has been described and the obtained products are explored for the detection of heavy metal ion Hg^{2+}. Comparison of the detection mode based on molecular structures have also been described comprehensively.

Each chapter (**Chapters 2** to **6**) begins with a short 'Introduction' followed by 'Results and discussion', 'Experimental Section', and 'Conclusion'. For convenience, 'References' are given at the end of each chapter. Overall summary and future scope, list of publications, list of poster presentations has been appended at the end of the thesis.

Abstract

Index No: 27/19/chem./26

Thesis title: "Cobalt and Copper-Based Homogeneous Catalysis For C-C and C-N Bond Formation Reactions: Applications in Organic Synthesis and Sensing."

The objective of the research work is to explore the use of low-cost earth-abundant metal complex and salts of Co and Cu, in catalysis of C-C and C-N bond formations, which gives value-added synthetic intermediates as products. To accomplish this aim, several new green and atom-economic methodologies with commercially available salts of Co and Cu have been developed. The products formed by these new methodologies have been explored in the applications of synthesis and metal sensing.

In the **first work**, a feasible one-pot synthesis of dimerized arene and heteroarene systems was achieved by employing 2 mol% of Co(II) catalyst along with Zn dust, at room temperature for 2-4 h. The Co(II)/Zn(0) system *in situ* generates Co(I) as the active catalyst. This catalyst can effectively substitute the expensive Pd catalysts and hygroscopic and air-sensitive $ZnCl_2$, generally employed to generate such dimerized heterocyclic cores. The Pd is replaced by the Co core and the anhydrous $ZnCl_2$ is replaced by the easy-to-handle and highly economic Zn dust, in its activated form. Where conventional methods use high temperature and/or longer reaction times, our synthetic strategy achieves the desired goal with a high % yield of products (70-89%) at room temperature with moderate reaction time (2-4 h) replacing expensive reagents at the same time. The Co(II) catalyst is easy to synthesize, economically viable, thermally stable, and insensitive to air or moisture. The catalyst has been well-characterized by EPR, IR, CV and UV-vis spectra and EDX studies. With a view to extend the Co-based catalysis with commercially available Co salt, an unprecedented microwave-assisted $CoCl_2$-catalyzed acceptorless dehydrogenative coupling of benzyl alcohol and amine for the synthesis of *E*- aldimines, *N*-heterocycles and H_2 under mild condition, without any complicated exogenous ligand template, oxidant, or other additives was developed in the **second work**. This environmentally benign methodology exhibits broad substrate scope (43 including 7 new products) with fair functional-group tolerance on the aniline ring. Detection of metal-associated intermediate by gas chromatography (GC) and HRMS, H_2 detection by GC and kinetic isotope effect reveal the mechanism of this $CoCl_2$ catalyzed reaction to be *via* acceptorless dehydrogenative coupling (ADC). Furthermore, kinetic experiments, and Hammett analysis with variation in nature of substituents over the aniline ring were performed

to reveal the insight of the reaction mechanism with different substituents. Stable imines were targeted next in the **third work**, by Co-catalysis, where, we have developed the first Co(II) catalyzed one-component one-pot sustainable synthesis of acyl hydrazones only from acyl hydrazides under mild reaction conditions. Traditional and contemporary methodologies use two components (usually acyl hydrazides and aldehydes/ ketones/ alcohols/ styrene) as the coupling partners. Our protocol, on the other hand, involves the *in situ* generation of aldehyde intermediate (detected by gas chromatography) from the acyl hydrazide, which then undergoes condensation with another molecule of the same acyl hydrazide in the same pot to yield acyl hydrazones in presence of mild base K_2CO_3 and low-cost $Co(OAc)_2 \cdot 4H_2O$ as catalyst. Some of the resulting acyl hydrazones have been used as synthetic precursors and explored in various post-synthetic modifications to afford *N*-heterocyclic compounds. Furthermore, photoswitchable properties of few synthesized acyl hydrazones are also explored using their *E/Z* isomerization around the C=N bond, as realized by high-pressure liquid chromatography (HPLC) and UV-vis spectroscopic studies. Unveiling the potential of $CoCl_2.6H_2O$ as catalyst, a one-step two-component visible light-mediated oxidative acylation of alkenes by aldehydes to synthesize *α,β*-epoxy ketone has been achieved in water at room temperature in the **fourth work**. The photocatalytic activity of Co(II) presented a remarkable achievement for synthesis of *α,β*-epoxy ketones from aldehydes and olefins, with a wide substrate compatibility including aromatic, hetero-aromatic and aliphatic aldehydes, styrenes with both electron-donating and withdrawing groups, *α*-substituted styrenes, stilbene, acrylates, and even the challenging unactivated aliphatic alkenes. Mechanistic studies including radical trapping experiments, intermediate detection by GCMS and Hammett analysis unveil the nature of the photocatalytic pathway.

After a series of reactions with Co-complex or salt as catalyst, we tried Cu-based C-C coupling in **fifth work**, where, a C_2-symmetric internally conjugated 1,3-di-alkyne system, containing phenolphthalein as a fluorophore and ferrocene as a redox moiety has been synthesized *via* microwave-assisted Cu(II) catalyzed Glaser-Hay coupling in neat condition for the first time. The compound was found to be highly selective towards Fe^{3+}, Cu^{2+} and Hg^{2+} ions *via* multi channels. Interestingly, Fe^{3+} and Cu^{2+} ions simply promote oxidation of ferrocene unit to ferrocenium ion without binding to the receptor whereas Hg^{2+} binds with the receptor, which was found to be the conjugated di-alkyne unit of the compound, as confirmed by ^{1}H, ^{13}C NMR and IR titrations and DFT calculations. The oxidation and binding phenomena were also investigated by optical and electrochemical analyses. Hg^{2+} ion interacts with the dialkyne

alkyne unit in more details, we have designed and synthesized two thermally stable probes, one acyclic another cyclic in the **sixth work**. The acyclic compound contains two terminal alkyne units, whereas the cyclic molecule has an internally conjugated C_2-symmetric 1,3-dialkyne unit. The acyclic probe with two terminal alkynes interacted with two Hg^{2+} ions whereas the cyclic probe with cage-like structure interacted with only one Hg^{2+} ion. Hg^{2+} ion can only interact with either alkyne unit at any instant in the probe to avoid steric repulsion between two Hg^{2+} ions. The differences in the selective responses of the cyclic and acyclic structures towards Hg^{2+} ion was thoroughly established by UV-vis, emission spectroscopy and electrochemical analysis along with theoretical (DFT) studies. The probable binding site of Hg^{2+} ion with the synthesized probes were determined by ^1H NMR and IR titrations, which indicated that terminal as well as conjugated di-alkyne unit interact with Hg^{2+} ion by a favorable soft-soft interaction. Furthermore, the sweeping motion of Hg^{2+} ion between the two alkyne units of the 1,3-dialkyne moiety, was also confirmed by DFT calculations. Unlike Hg^{2+} ion, Cu^{2+} and Fe^{3+} ions did not interact with the probes, rather they induced oxidation of ferrocene centre. Both the receptors and their corresponding metal complexes are stable in the physiological pH range (pH around 7) and thermally stable up to 60°C. This study focuses for the 1st time on the comparative responses of the acyclic and cyclic architectures of same molecular unit towards metal ion recognition and it supports the fact that the alkyne group in different environments behaves differently with the same soft metal.

10/06/2024

Dr. Arunabha Thakur
Assistant Professor
Department of Chemistry
Jadavpur University
Kolkata-700032, India

(Signature of the Supervisor date with official seal)

Adwitiya Pal 10/06/2024

(Signature of the Candidate with date)

Contents

Table of Contents

List of Figures

CHAPTER | 1

CHAPTER | 2

CHAPTER | 3

CHAPTER | 6

List of Schemes

CHAPTER | 1

CHAPTER | 2

CHAPTER | 3

CHAPTER | 4

CHAPTER | 5

CHAPTER | 6

List of Tables

CHAPTER | 2

CHAPTER | 3

CHAPTER | 4

CHAPTER | 5

CHAPTER | 6

Abbreviations

acac:	acetylacetone
ADC:	acceptorless dehydrogenative coupling
BHT:	butylated hydroxytoluene
BODIPY:	Fluorinated Boron-Dipyrromethene
DABCO:	1,4 Diazabicyclo[2.2.2]octane
DCM:	dichloromethane
DFT:	density functional theory
DTBP:	Di-*tert*-butyl peroxide
CB:	Conduction Band
COF:	Covalent-Organic Framework
COSY:	homonuclear correlation spectroscopy
CuAAC:	copper catalyzed azide-alkyne [3+2] cycloaddition
CV:	cyclic voltammetry
DL:	detection limit
DMSO:	dimethyl sulphoxide
DPV:	differential pulse voltammetry
EDTA:	ethylene diamine tetraacetate
EDX:	electron dispersive X-ray diffraction
EPR:	electron paramagnetic resonance
ESI-MS:	electrospray ionization mass spectrommetry
FT-IR:	Fourier-transform infra-red
GC:	gas chromatography
GCMS:	gas chromatography mass spectrommetry
HAT:	hydrogen atom transfer
HOMO:	highest occupied molecular orbital
HPLC:	high-pressure liquid chromatography
HRMS:	high-resolution mass spectrometry
HSQC:	heteronuclear single quantum coherence spectroscopy
HSAB:	hard-soft acid base
INT:	intermediate
IR:	infra-red
KIE:	kinetic isotope effect
LAS:	sodium-L-ascorbate
LED:	light emitting diode
LMCT:	ligand to metal charge transfer
LOD:	limit of detection
LUMO:	lowest unoccupied molecular orbital
m:	meta
MOF:	Metal-Organic Framework

NBO:	natural bond order
NMR:	nuclear magnetic resonance
NOESY:	nuclear overhauser effect spectroscopy
NP:	Nanoparticle
o:	ortho
p:	para
PMHS:	polymethylhydrosiloxane
py:	pyridine
RCM:	ring closing metathesis
RDS:	rate-determining step
SAC:	single atom catalysis
SEM:	scanning electron microscope
SET:	single electron transfer
TBAB:	tetrabutylammonium bromide
TBAP:	tetrabutyl ammonium perchlorate
TBHP:	*tert*-butyl hydroperoxide
TD-DFT:	time dependent density functional theory
TEMPO:	2,2,6,6-tetramethylpiperidine-*N*-oxide
TFA:	trifluoroacetic acid
TFE:	2,2,2-Trifluoroethanol
THF:	tetrahydrofuran
TLC:	thin layer chromatography
TS:	transition state
UV:	ultra-violet
VB:	Valence Band
Vis:	visible
WBI:	Wiberg Bond Index

Chapter 1

General Introduction

and

Literature survey

1.1. Catalysis:

The term "Catalysis" was first coined by *Jöns Jakob Berzelius* (1779-1848), the Swedish scientist in the year of 1836.[1] It comes from the combination of two Greek words "*kata*" *i.e.,* down and "*lyein*" *i.e.,* loosen. In the words of Berzelius catalysis is "the property of exerting on other bodies an action which is very different from chemical affinity. By means of this action, they produce decomposition in bodies, and form new compounds into the composition of which they do not enter".[2] In simple words, it is a process of amplifying the rate of a reaction by employing certain materials called "catalysts", which do not undergo any overall change during the course of the reaction.

This field of catalysis has gradually developed starting from 1540, when Valerius Cordus (1514-1544), a German physician, botanist, and pharmacist catalyzed the conversion of alcohol to ether with the aide of sulfuric acid to the present-day modern catalytic techniques.[3] In 1781, Antoine-Augustin Parmentier (1737-1813), a French agronomist and pharmacist, observed an enhanced sweet taste in presence of acetic acid in a mixture of potato starch, distilled water and potassium hydrogen tartrate.[4] The same reaction was revisited by the German chemist Johann Wolfgang Döbereiner (1780-1849).[5] He discovered that the starch when dissolved in water was fermented into sugar and then alcohol. Döbereiner also discovered the first catalytic action of an inorganic oxide, MnO_2, on the thermal decomposition reaction of $KClO_3$, which formed the basis of preparation of oxygen.[6] Later on, in the late 18th century, Johann Rudolph Deiman (1743-1808) (German-Dutch chemist and physician), Anthoni Lauwerenburg (1758-1820), Adrien Paets von Trootswijk (1752-1837) (Dutch businessman amateur chemist), Nicolas Bondt (1765- 1796), and Pieter Nieuwland (1764-1794) (a Dutch nautical scientist, mathematician, poet, and chemist), reported that preparation of ethylene was possible by treating 75 parts of concentrated sulfuric acid with 25 parts of alcohol, without heating, and alternatively by passing ether or alcohol vapors through a glass tube filled with alumina, or silica, or through an empty clay tube. The work had a considerable impact on the scientific community such that it was considered as the first systematic study of metal-catalyzed reaction. This was first reported on 1796, by Antoine Francois de Fourcroy (1755-1809).[7] The report held so much importance that it was recommended to publish in *Journal des Savants Etrangers* (one of the most primitive academic journals of Europe).[8] Following these preliminary experiments, came several other observations by various scientists worldwide like Humphry Davy,[9] Edmund Davy,[10] Louis-Jacques Thenard,[11] Johann Wolfgang Döbereiner[12] and others, and by the 1830s, the puzzle

was solved and the so-far unknown phenomenon took its present form and name. It is the contribution of all these Scientists, who shaped the field of catalysis as we see it today.

In contemporary times, catalysis is considered to be a unique chemical tool for sustainable development. It not only expedites a reaction to occur at a much lesser time, but also creates alternative pathways for wasteful and inefficient industrial processes, reducing the cost of valuable materials and enabling a sufficient amount of products with very low catalyst loadings, while remaining unchanged. Thus, the development of catalysis has made a tremendous impact on synthetic chemistry. Among the 12 principles of Green Chemistry, the 9th principle focuses on the use of catalysis over stoichiometric quantities of reagents. Catalysis plays a crucial role in sustaining our Nature by reducing the environmental footprint of chemical industries.

In the physical aspect, a catalyst minimizes the activation energy barrier for a chemical reaction (Figure 1.1), which would often otherwise be executed by high temperatures or a large excess of reagents. Such procedures are dangerous to handle in industrial scale and they are not atom economic. A catalyst, on the other hand, creates an atom economic pathway and since it remains principally unchanged in the whole process, can be reused and hence sub-stoichiometric amounts are sufficient to carry out a reaction effectively.

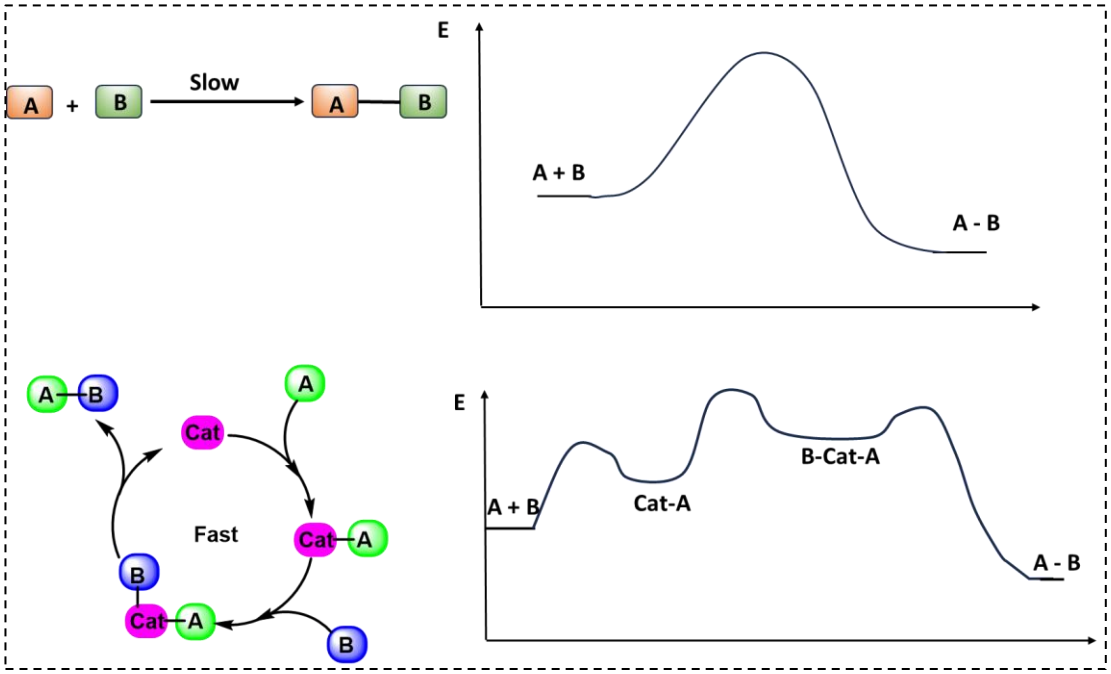

Figure 1.1: Change of activation energy barrier in catalyzed *vs.* non-catalyzed reactions.

The materials that can be called catalysts can vary from metal salts, metal complexes, metal-organic frameworks to pure covalent organic molecules, or even stimuli like light or electricity. Hence, catalysts can be classified according to their nature of miscibility (homogeneous or heterogeneous), composition (metallic, organometallic or organic molecule) and response to external stimuli (photocatalyst or electrocatalyst). They are elaborated in the following Scheme 1.1.

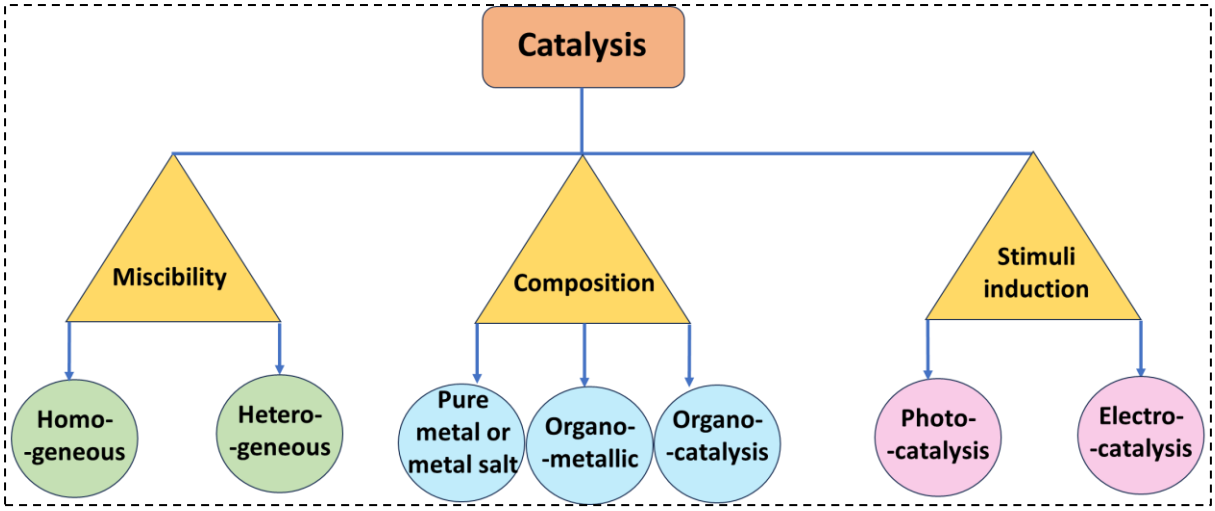

Scheme 1.1: Schematic presentation of the types of catalysis.

All these types of catalysis are discussed briefly in the following section:

1.1.1. Homogeneous catalysis: The process of catalysis where the catalyst is miscible in the reaction medium is called as homogeneous catalysis. A schematic representation of homogeneous catalysis is provided in Figure 1.2, where "C" represents the homogeneous catalyst, "R" the reactant and "P" the product, all in one phase of the solution. Homogeneous catalysis has established its foundation as an efficient way of chemical transformation using mild reaction conditions since all the reacting components including reagents, starting materials and catalyst are present in a single phase, mostly liquid phase. Homogeneous catalysis possesses some predominance over heterogeneous catalysis in terms of mild reaction conditions, higher activities, selectivities, and greater control of operating conditions. Examples of such catalysts are the general acid/base catalysis like ester hydrolysis, organometallic catalysts with soluble metal complexes, purely organic catalysts like thiazolium ions in Cannizzarro or enzymatic processes, Stetter reactions, etc.[13]

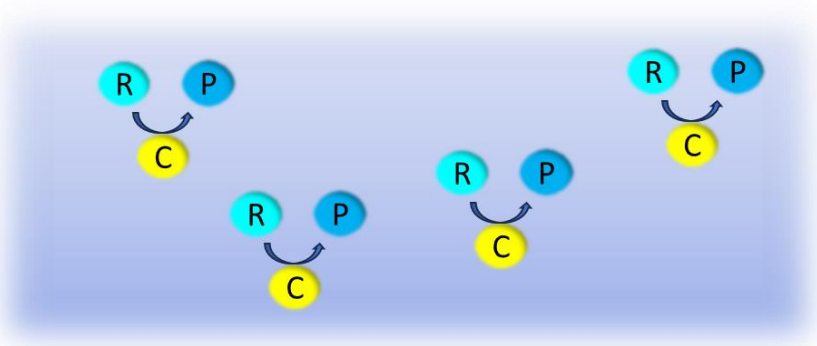

Figure 1.2: Diagrammatic representation of homogeneous catalysis.

1.1.2. Heterogeneous catalysis: On contrary to homogeneous catalysts, heterogeneous catalysts stay in a different phase (mostly in solid) than the substrates. Heterogeneous catalysts have the advantage of isolation and reusability of the catalyst in different catalytic cycles. This process is widely used in the chemical industries owing to its isolation from the reaction mixture. Examples are metal-organic framework (MOF) based catalysis where the MOF can be filtered off after each use. A schematic diagram of heterogeneous catalysis is shown in Figure 1.3, where the heterogeneous catalyst bed is represented as "C", reactant as "R" and product as "P".[14]

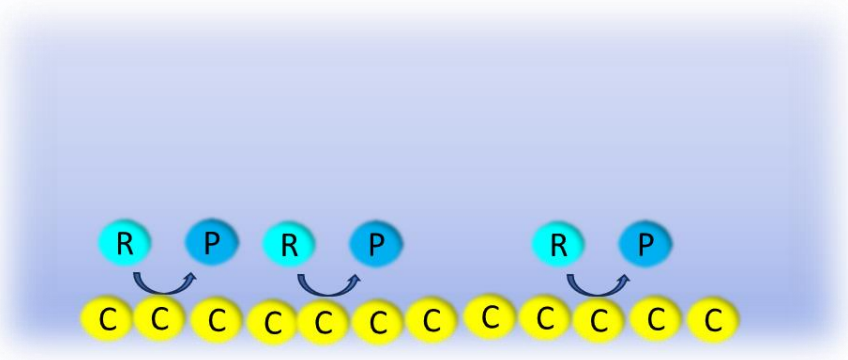

Figure 1.3: Diagrammatic representation of heterogeneous catalysis.

1.1.3. Pure metal or metal-salt based catalysis: This category of catalysis involves the use of metals as surface catalyst (principally heterogeneous) or commercially available metal-salts directly without any modification (homogeneous or heterogeneous depending on the medium) as catalyst for a reaction. Metal-based catalysis has developed over centuries and among metals, the transition metals (d-block elements) play a humongous and pivotal role in the catalysis of organic reactions crucial to the pharmaceutical industry. However, with time,

researchers are also exploring the catalytic activities of main group elements (s and p-block elements) like calcium (Ca), magnesium (Mg), aluminium (Al) or even non-metals like boron (B). One of the most trivial examples of metal-surface based catalysis is the reduction of olefinic bonds by H_2 over platinum (Pt) or palladium (Pd) surface.

1.1.4. Organometallic catalysis: This is a broad category of catalysis, which is directly linked with the previous one. Here, metal-ligand complexes (principally of transition metals) are prepared and administered within the reaction mixture to catalyze a reaction. Organometallic catalysis is very crucial to some reactions that can otherwise be not conducted by metal salts only. Often, the ligands act as the solubilizing or stabilizing factor or as electron source or sink or as labile temporary leaving groups in the catalytic cycle. For example, Lochbrunner, Opatz, and Heinze prepared a Cr(III)-polypyridine complex (**A**), where the suitable bite angle and electron-surplus nature of tripyridyl ligands (*N,N'*-dimethyl-*N,N'*-dipyridine-2-ylpyridine-2,6-diamine) created a homoleptic Cr(III) complex with a considerable energy difference between the $^4T_{2g}$ and ^2E_g states.[15] This led to a lengthening of the ^2E lifetime in the excited state (898μs), that promoted the visible-light-mediated cyanation in tertiary amines *via* singlet oxygen generation (Scheme 1.2).

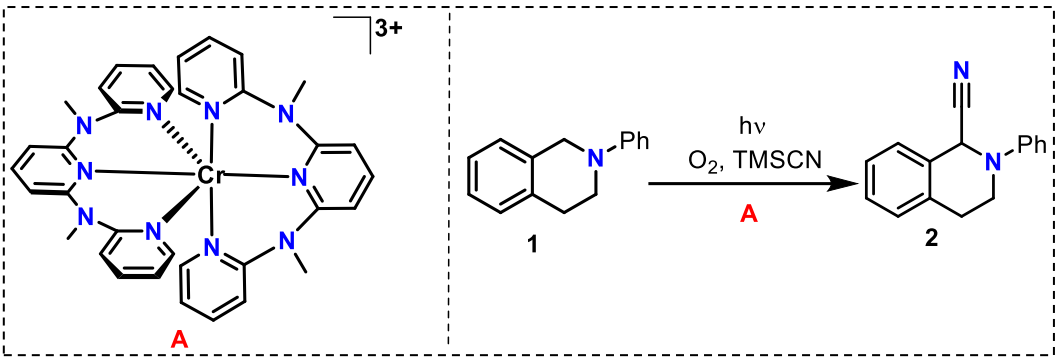

Scheme 1.2: Structure of the complex **A** ($[Cr(ddpd)_2]^{3+}$) and its catalyzed reaction.

1.1.5. Organocatalysis: Organocatalysis involves the use of organic molecules as catalysts for accelerating chemical reactions without the application of metals. This is considered as the "Hot Topic" in catalysis since it greatly promises to reduce the metal wastages caused by use of metal-based catalysts. These are primarily homogeneous in nature and are widely used in chemoselective reactions. Although this field is emerging nowadays, this kind of methodology has existed since a long time. One of the primitive organocatalyzed reactions was done by

Breding and Fiske in the year 1912, where the enantioselective addition of HCN to aldehydes was catalyzed by cinchona alkaloids (quinine or quinidine) (Scheme 1.3).[16]

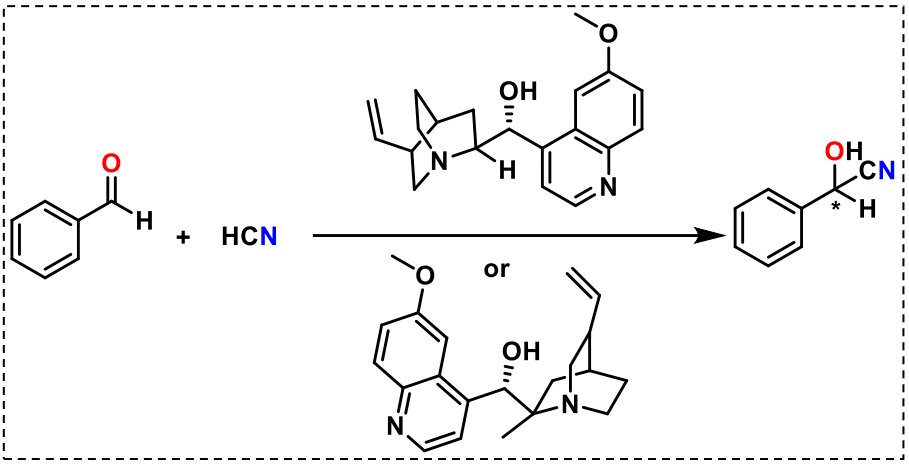

Scheme 1.3: Cinchona alkaloids (quinine and quinidine) in the catalysis of enantioselective HCN addition to aldehydes.

1.1.6. Photocatalysis: Photocatalysis involves the use of light to activate or excite the catalyst, called photocatalyst, which in the excited state catalyzes a reaction. The excited state of photocatalyst repeatedly interacts with the reactants, forming appropriate reaction intermediates, and regenerating itself after each cycle of interaction. This photonic excitation is known to create more impact on accelerating the reaction rather than the increase in temperature. The concept of photocatalysis is inspired by the biochemical reaction of conversion of CO_2 and H_2O into $C_6H_{12}O_6$ and O_2 by chlorophyll with the aid of light, known as photosynthesis occurring in nature. Contemporarily, the photocatalytic methods utilize either transition metals with labile d-electrons or organic molecules with conjugated π-cloud as the sensitizer or photocatalyst. In heterogeneous photocatalysis, the catalyst is a semiconductor whose electron traverses from valence band (VB) to conduction band (CB) when excited by light, and this transition induces the chemical reaction to proceed faster. For example, the photocatalyst formed from biosynthesized zinc oxide nanoparticles (ZnO NPs) can effectively break down organic waste materials under illumination (Figure 1.4).[17] On the other hand, in homogeneous transition metal-based photocatalytic system, the excitation of electron from lower to higher level (say, from t_{2g} to e_g) promotes the formation of intermediate, which leads to the product is more efficient and accelerated way, giving back the catalyst at the ground state. For example, the mononuclear Ir(III) complex $[Ir(tpy)(ppy)Cl]^+$, tpy is terpyridine and

ppy is 2-phenylpyridine selectively reduces CO_2 to CO upon irradiation of visible light (480 nm) without any additional photosensitizers (Figure 1.5).[18]

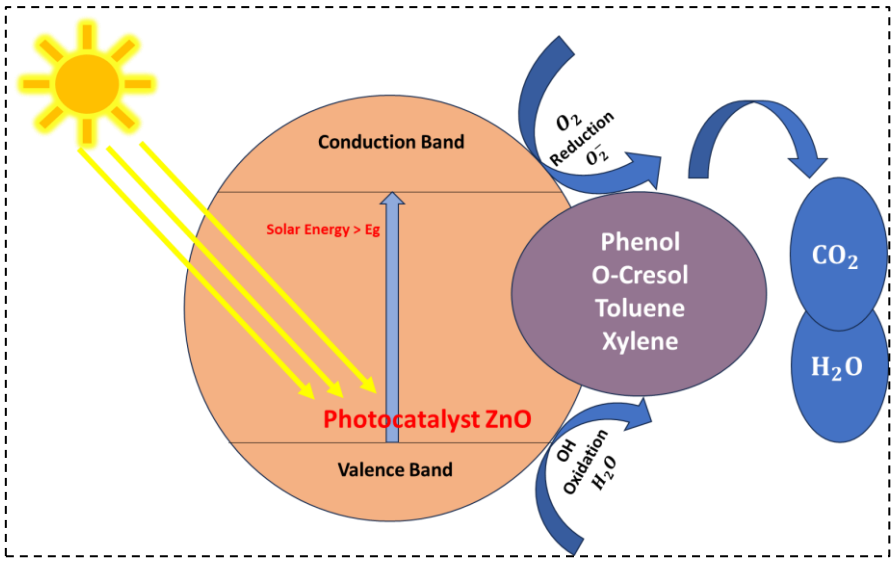

Figure 1.4: Scheme of photocatalytic mechanism occurring over a semiconductor like ZnO.

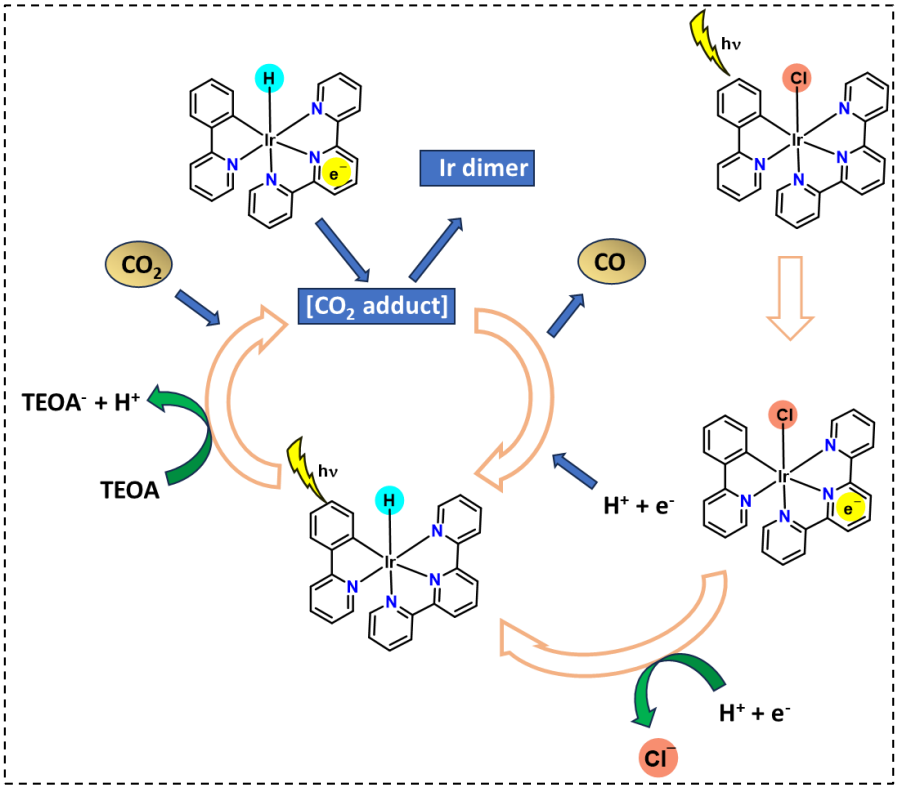

Figure 1.5: Mechanism for photocatalytic CO_2 reduction by $[Ir(tpy)(ppy)Cl]^+$ complex.

1.1.7. Electrocatalysis: Electrocatalysis involves the use of electrochemical reactions in catalyzing a reaction and the catalysts used for this purpose are called electrocatalysts. Often, the electrode, like platinized electrode, serve as electrocatalyst in a reaction set up of heterogeneous electrocatalysis,[19] whereas in homogeneous electrocatalysis, another electricity-cultivating agent soluble in the electrolyte is used as the electrocatalyst. They assist in transfer of electrons between the electrode surface and reactants, and may also facilitate intermediate chemical reactions included in the overall half-reaction.[20]

This major classification of catalysis is followed by other types also, like, single atom catalysis (SAC),[21] COF-based electrocatalysis,[22] catalysis by quantum dots[23] etc. Despite advancements in metal-free modern techniques, the contribution of transition metals in shaping the field of catalysis is highly significant. The importance of transition metals in catalysis is a vivacious topic, which needs a detailed discussion as follows:

1.2. Transition metal-based homogeneous catalysis:

The widespread use of transition metals in catalytic processes was originally inspired by the role of metalloenzymes in nature. At the advent of the 19th century, many metals, such as platinum, had been observed to show specific catalytic properties, thereby enabling the discovery of a trivial idea of homogeneous catalysis *via* an intermediate, which is supposed to be unstable. Intensive research carried out by Sabatier and his group enabled the discovery of nickel (Ni) and platinum (Pt) catalyzed hydrogenation reactions, which gave Sabatier the Nobel Prize in Chemistry in 1912.[24] This reaction ultimately became the foundation for the rapid growth of petrochemical industry. Other noble metals, like Ru, Rh, and Pd, were also explored to have superior catalytic activities in various reactions, so much so that the discovery of their complexes have been awarded the Nobel prize in 1973 (Wilkinson's catalyst-$[RhCl(PPh_3)_3]$)[25] for hydrofunctionalization across double bonds, in 2005 (Grubb's catalyst)[26] for olefin metathesis and in 2010 ($Pd(PPh_3)_4$)[27] for C-C cross coupling reactions (Figure 1.6). These reactions have formed the basis of many modern-day industrial processes for chemical synthesis.

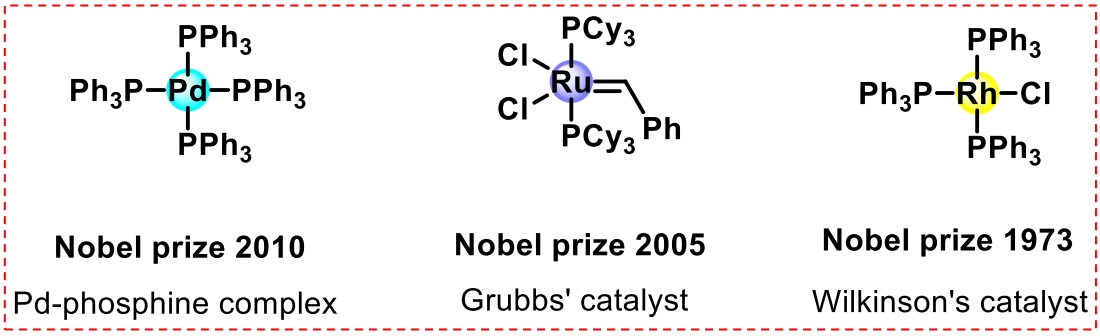

Figure 1.6: Nobel prizes awarded to discovery of metal complexes of Pd, Ru and Rh.

Transition metals in complexed form or metallic form or salt form have given many interesting results in synthetic organic chemistry, which have enabled discovery of several superior methodologies for chemical transformations and functionalizations. The most frequently used transition metal-based C-C cross-couplings are Negishi,[28] Stille,[29] Suzuki[30] and Sonogashira coupling[31] reactions using Pd and Ni/Cu catalysts, as indicated in Scheme 1.4.

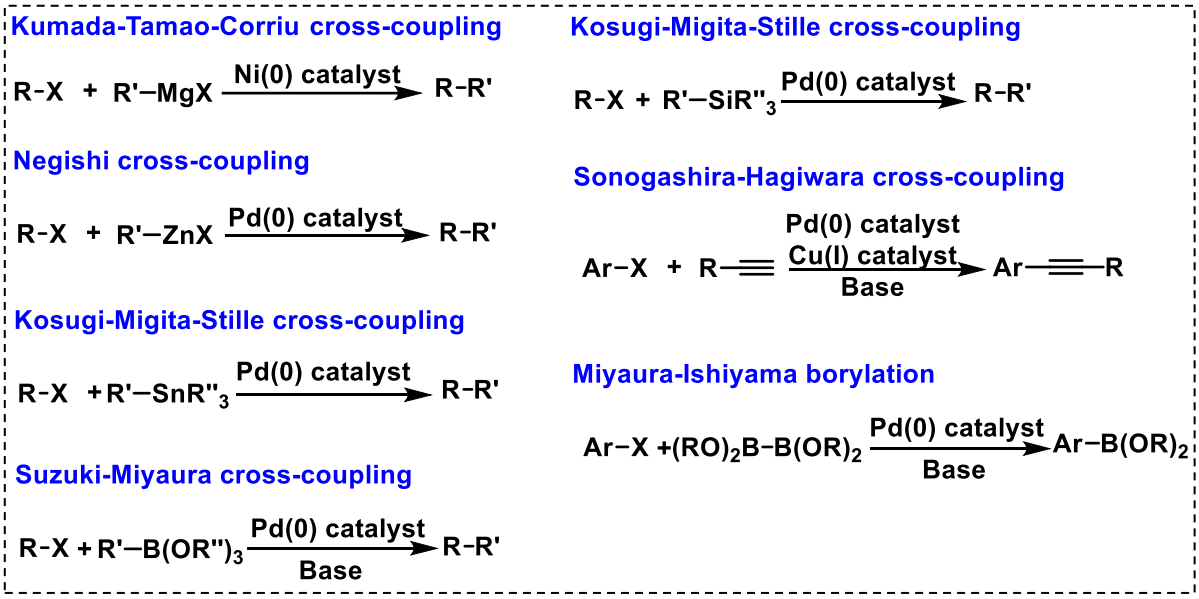

Scheme 1.4: The conventional C-C cross-coupling reactions by Pd and Ni catalyst.

Apart from single-transition-metal catalysis, dual-transition-metal catalysis is also emerging as good results in the productivity of desired compounds were observed, provided, the metals employed have synergistic effects.[32] As described in Scheme 1.5, each one of the two transition metal catalysts [M1] and [M2] activates reactants [S1] and [S2], with compatible and comparable rates of activation (say, k_1 and k_2). Incompatibility in rates would result in

superior reactivity and prolonged presence of one activated species only, which would encourage side reactions or even, decomposition diminishing the efficacy of reaction.

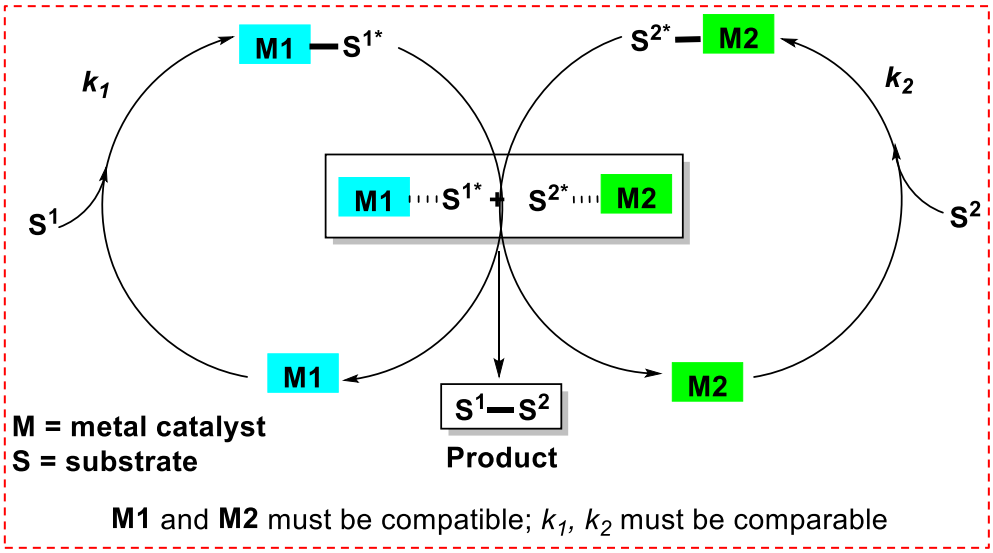

Scheme 1.5: Schematic presentation of dual metal catalysis.

Over time, modified versions of these reactions or new reactions have come into play. Although there are certain developments of organocatalysis, the indispensable role of transition metals in organic transformations cannot be replaced or denied till date. However, the expensive, sensitive and scarce metal-based catalysts of 4d and 5d transition series can be replaced by low-cost, air-stable, earth-abundant transition metal-based catalysts of 3d series on account of their similar reactivity. Cobalt (Co) and copper (Cu) are earth-abundant metals such that they constitute 0.003 % and 0.0068 % of earth's crust.[33] They can be utilized to substitute expensive catalysts like Ir, Ru, Rh, Pd etc. in important organic transformations. These metal ions are known to play irreplaceable roles in some organic transformations. A few examples are described as follows:

1.2.1. Cobalt-based C-C bond formations:

Cobalt is used in catalysis in three forms: either in the salt form, commonly in the +2 oxidation state, or can be reduced or oxidized to Co(I) and Co(III) species respectively (Scheme 1.6). Both the high-valent and low-valent Co species are less stable than the Co(II) species, unless otherwise stabilized by the external ligand system.

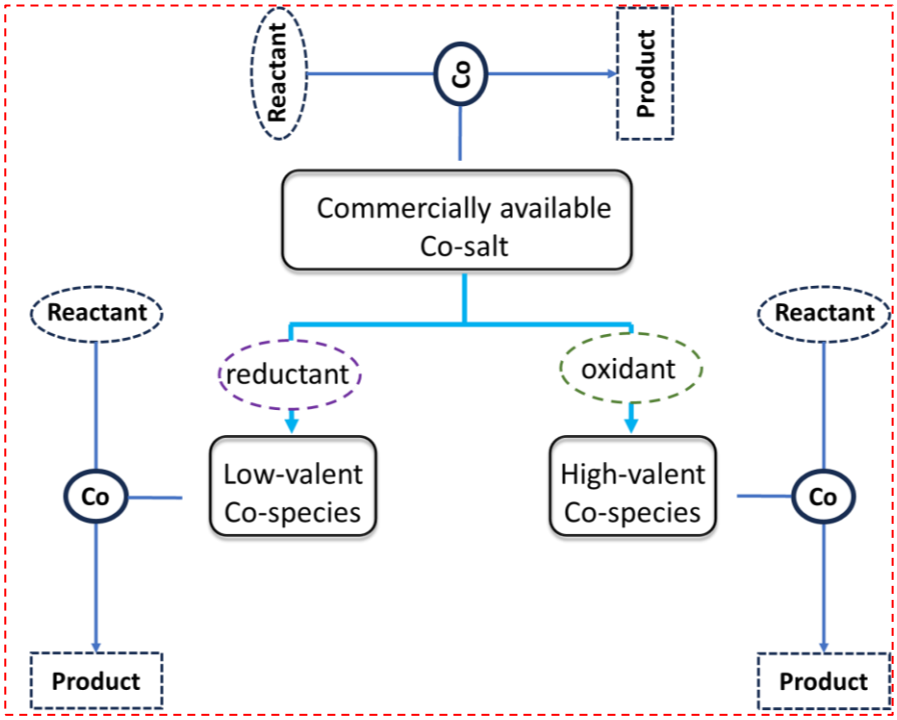

Scheme 1.6: Schematic presentation of Co-based catalysis.

Here, the cobalt-based C-C bond formations are categorically presented according to the kind of hybridization of the linked carbon atoms, as follows:

1.2.1.1. $C(sp^2)$-$C(sp^3)$ bond formation:

The $C(sp^2)$-$C(sp^3)$ bonds are generally obtained by the reaction between alkynes and alkenes. For example, Cheng and his group observed the formation of 3-alkenyl substituted cyclic ketones upon reacting internal alkynes with cyclic enones, like cycloheptenone, using CoI_2 as the catalyst in presence of Zn/ZnI_2 (Scheme 1.7a).[34] The enantioselectivity of the reaction is modulated by the application of chiral ligand (R)-BINAP in the reaction.

A variation of this methodology using (*R*,*R*,*S*,*S*)-Duanphos as chiral ligand in 1,4-dioxane gave the [3+2] addition product of internal alkynes with cyclic enones (cyclopentenone or cyclohexenone) (Scheme 1.7b) employing CoI_2/ ligand/Zn/ZnI_2 system.[35] One of the bicyclic products is presented here, where their enantioselectivities depend on the substitution pattern and also ring size of the cyclic enone reactant.

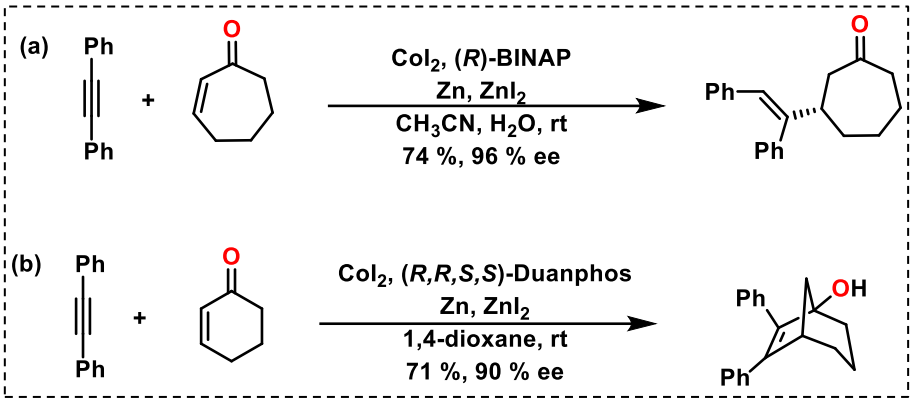

Scheme 1.7: Co/Zn catalyzed (a) allylic addition and (b) [3+2] cycloaddtion reaction by internal alkyne onto α,β-unsaturated cyclicketone.

Not only [3+2] cycloaddition, but also [2+2] cycloaddition, employing bicyclic alkenes with alkynes to form cyclobutene compounds, have been obtained by a similar cobalt-catalyzed methodology.[36] This reaction with $[CoI_2(PPh_3)_2]$, PPh_3, and Zn powder initiates with the reduction of Co(II) catalyst by Zn powder, to give Co(I) species, which gets complexed by the alkyne and the bicyclic alkene, followed by oxidative cyclometalation providing cobaltacyclopentene intermediate. This intermediate is responsible for producing the final product and regenerating the catalyst after reductive elimination (Scheme 1.8).

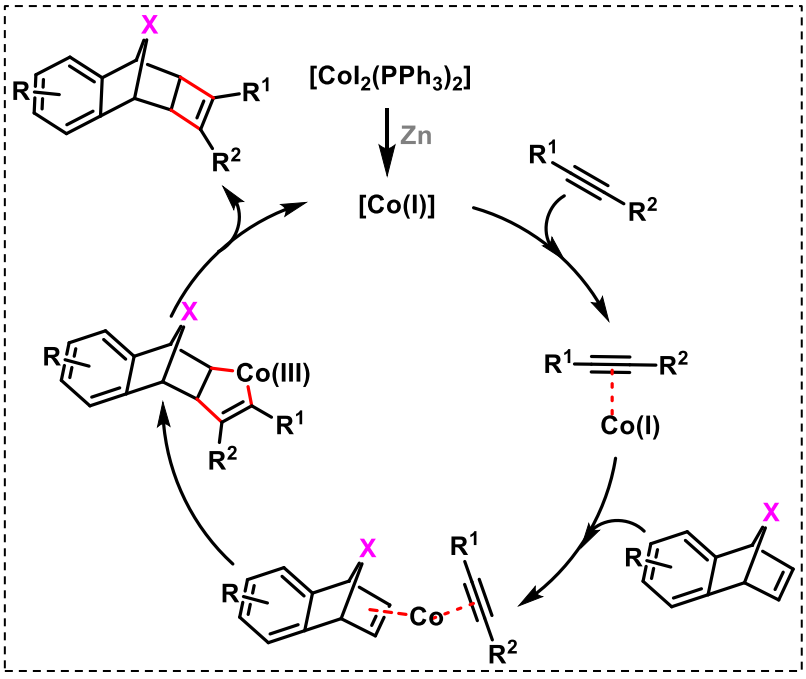

Scheme 1.8: Mechanistic cycle of Co(II)/Zn powder catalyzed [2+2] cycloaddition between 7-oxa and 7-aza benzonorbornadienes and alkynes.

1.2.1.2.C(sp^3)-C(sp^3) bond formation:

C(sp^3)-C(sp^3) bonds can be formed by the coupling of two C(sp^3) centres, which is very challenging, or by the common procedure of combining C(sp^2) with C(sp^3). The former coupling requires C(sp^3)-H bond activation, which is very much challenging till date. Such a C(sp^3)-C(sp^3) bond formation was accomplished by C(sp^3)-H bond activation by Kundu et al. in 2020, wherein, methyl-substituted *N*-heteroarenes were alkylated with alcohols using Co(II) catalyst (Scheme 1.9).[37] This reaction required 10 mol% of cobalt complex and 1.5 equiv. of KO^{t}Bu for 24 h in toluene at 150 °C. A variety of primary alcohols were reacted and the reaction of electron-donating benzyl alcohol with 2-methylquinoline gave high yields of products (78-88 %). However, the reactions of alcohols containing heteroatoms, like thiophen-2-ylmethanol and furan-2-ylmethanol, much lesser yields of products (~ 34 %) were obtained.

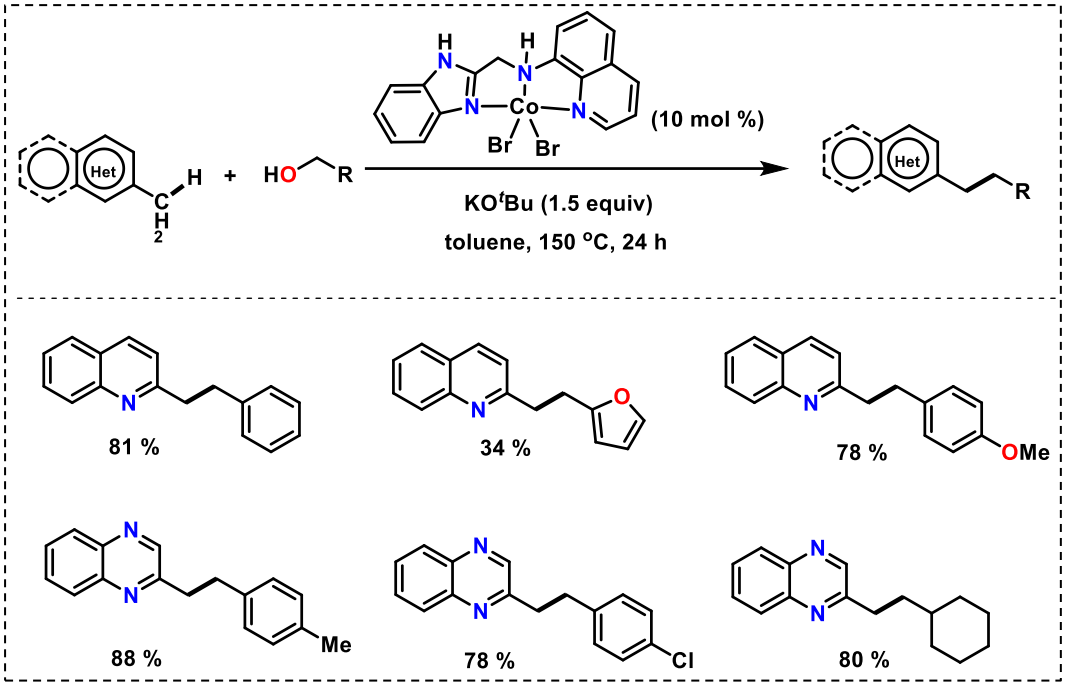

Scheme 1.9: Cobalt (Co)-catalyzed alkylation of 2-methylquinone.

For the coupling C(sp^2)-C(sp^3) leading to C(sp^3)-C(sp^3) bond, one of the most prevalent methods is the intermolecular oxidative alkylation/acylation of alkenes (styrenes) by alkanes (cyclo) or ethers. Such a transformation was developed by Liu and co-workers where C–C bonds were constructed between styrene and cyclic ethers *via* C(sp^3)-H activation using Co(II) complex in presence of an oxidant (here, TBHP) (Scheme 1.10).[38] The authors observed the substrates with ortho or meta-substitution on styrene had slightly lower reactivity than those with para- substitution. The mechanism proceeds through a free-radical pathway, where ^{t}BuO•

and ^{t}BuOO• were produced by Co(II)-catalyzed decomposition of TBHP (Scheme 1.11). A HAT (hydrogen atom transfer) from the ether by the generated radicals, followed by addition to styrene, coupling with ^{t}BuOO• and Kornblum–DeLaMare rearrangement in presence of DABCO gave the final product.

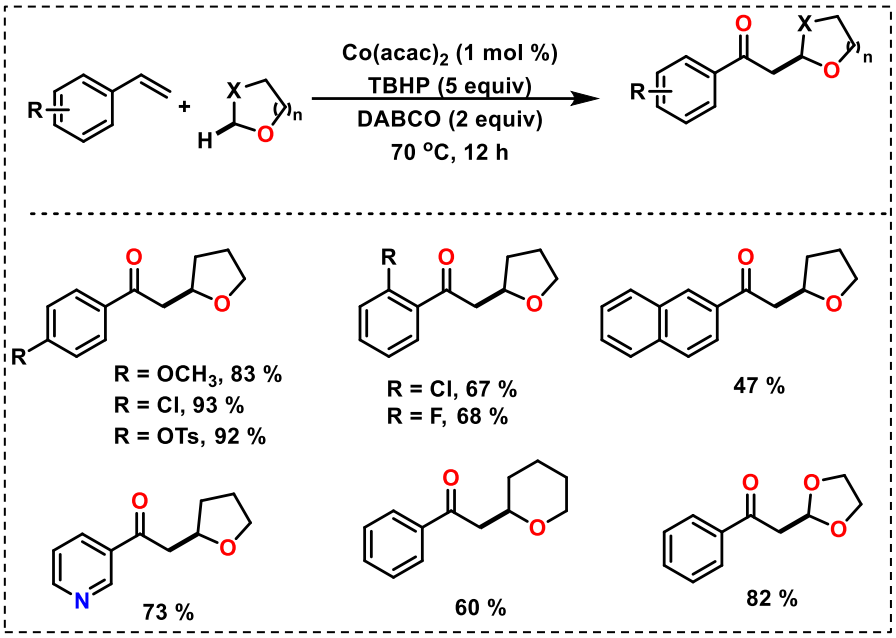

Scheme 1.10: Oxidative alkylation of styrene using Co(II)-catalyst.

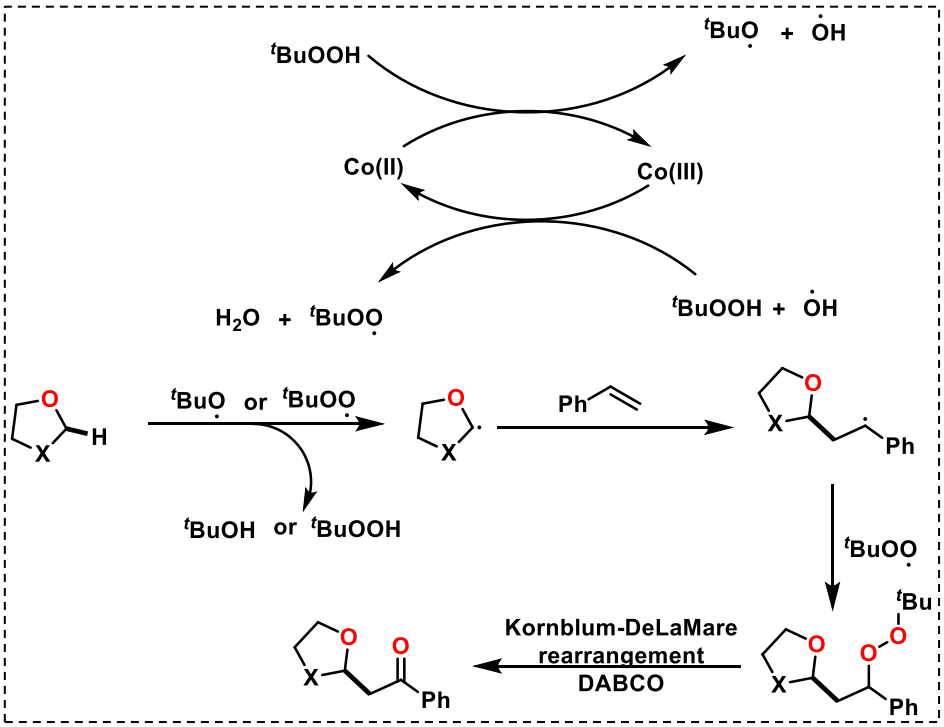

Scheme 1.11: Mechanism of the oxidative alkylation of styrene using Co(II)-catalyst.

After two years, in 2022, Wu et al. adopted a similar approach for C(sp^3)-C(sp^3) bond formation (Scheme 1.12) by a Co(II)-catalyzed multicomponent carbonylation for the preparing γ-aryl carboxylic acid esters.[39] Here the components of reaction *i.e.*, toluene (reactant and solvent), ethylene, carbon monoxide (CO), and ethanol are reacted in presence of $CoCl_2$ catalyst, PPh_3 as an additive, the pyridine derivative as ligand and di-*tert*-butylperoxide (DTBP) as the radical initiator at 120 °C for 24 h. Aliphatic primary alcohols like methanol, 3-phenylpropanol, *n*-butanol and 1-hexanol, or secondary alcohols could also produce corresponding products, however, tertiary alcohol like *tert*-butanol produced lower yield of product, and no product was obtained with phenols. Here also, the reaction proceeds through radical pathway (Scheme 1.13). The reaction is initiated with the generation of benzyl radical (by DTBP), which then adds to ethylene and the generated radical intermediate adds on to Co(II) to oxidize it to Co(III) in the complexed form. This Co(III) complex undergoes CO insertion and final reaction with alcohol furnishes the desired ester product regenerating the catalyst.

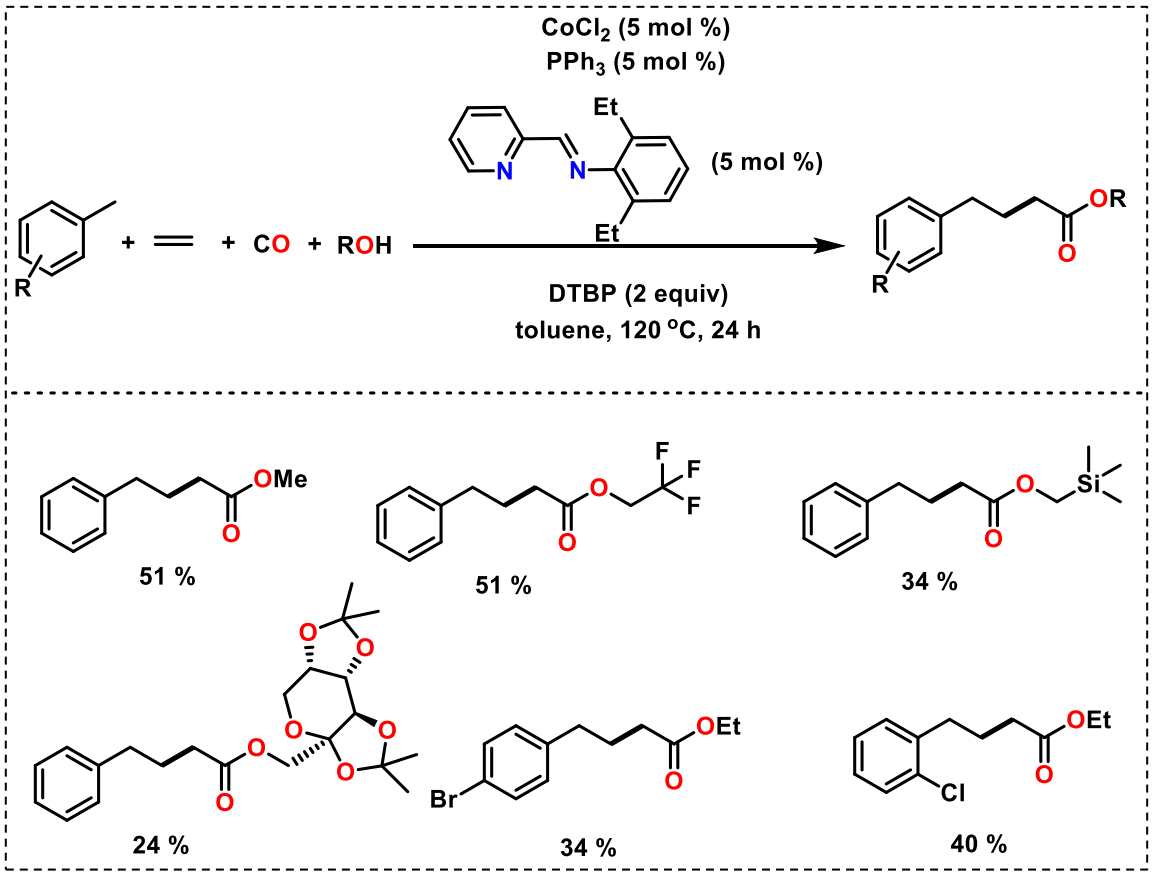

Scheme 1.12: Co(II)-catalysed multicomponent carbonylative acylation.

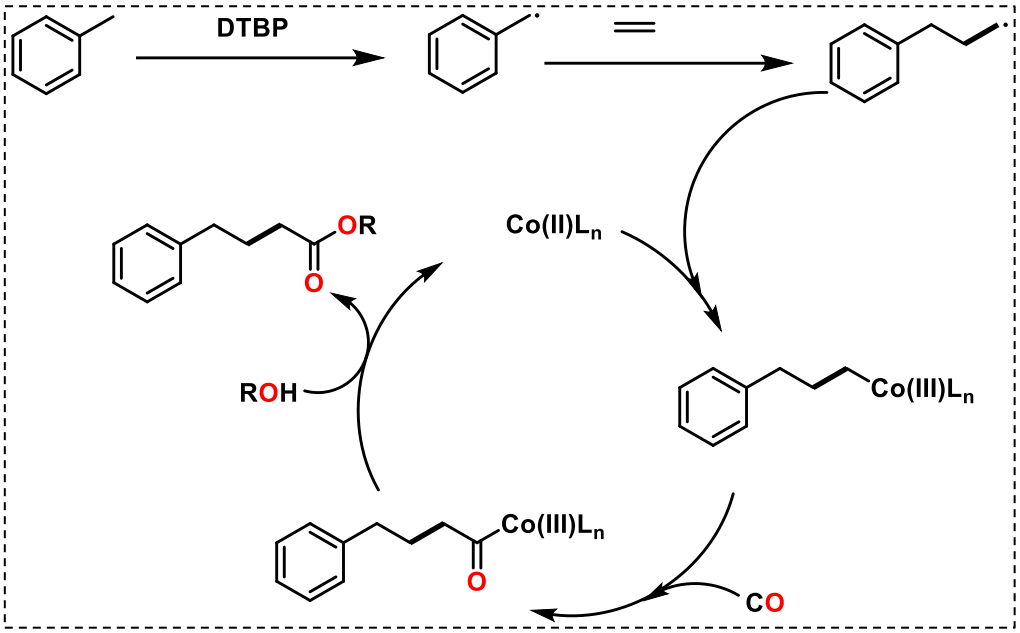

Scheme 1.13: Mechanism of Co(II)-catalysed multicomponent carbonylative acylation.

A recent development in this area is done by Wu and co-workers, where one-carbon-added alcohols have been obtained by Co-catalyzed hydroxymethylation of alkyl halides with CO as C-source and PMHS (polymethylhydrosiloxane) as H^- source (Scheme 1.14).[40] In this ligand-free synthesis, the $CoCl_2$ is the precatalyst, which gets reduced to the Co(I) complex, as indicated in Scheme 14. This Co(I) complex activates the alkyl halide giving alkyl radical and itself oxidizes to Co(II) species. CO is captured by the generated alkyl radical giving the acyl radical and subsequently the generated Co(II)-X_2 complex reacts with hydrosilane giving Co(II)X−H species, which captures the acyl radical to produce corresponding aldehyde by reductive elimination and regenerates the active catalyst Co(I) species. The Co-assisted reduction of aldehyde furnished the corresponding silyl-protected alcohol (Scheme 14, left cycle), from which the final product was obtained by NH_4F workup.

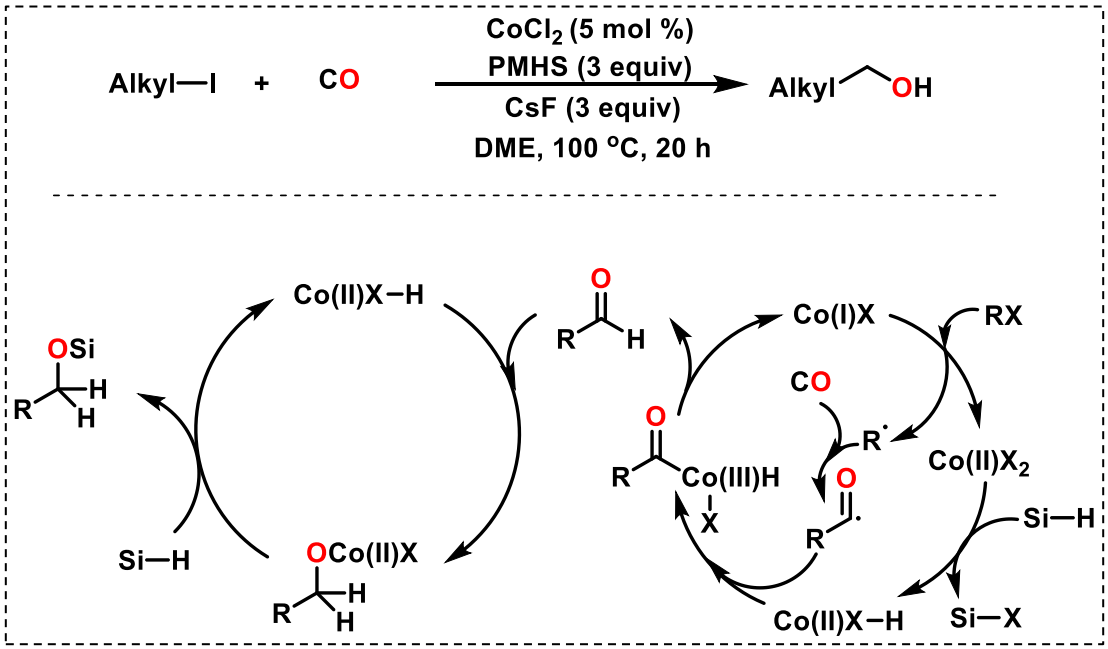

Scheme 1.14: Mechanism of Co(II)-catalyzed hydroxymethylation of alkyl halides.

1.2.1.3. C(sp^2)-C(sp^2) bond formation:

C(sp^2)-C(sp^2) bond formation is most commonly achieved by Pd-catalyzed reactions, however, some reports are there with Co-catalyst, coupling two C(sp^2) centres or C(sp^2) and C(sp) centres. In 2016, Wu and his group obtained the Co(II)-catalyzed homocoupling of benzamide derivatives (Scheme 1.15).[41] The authors also isolated two Co(III) complexes, with a difference in the orientation of the acac (acetylacetone) ligand, in 26% and 43% yields. The dimerized product was obtained from the biaryl-linked Co(III) complexes after demetallation.

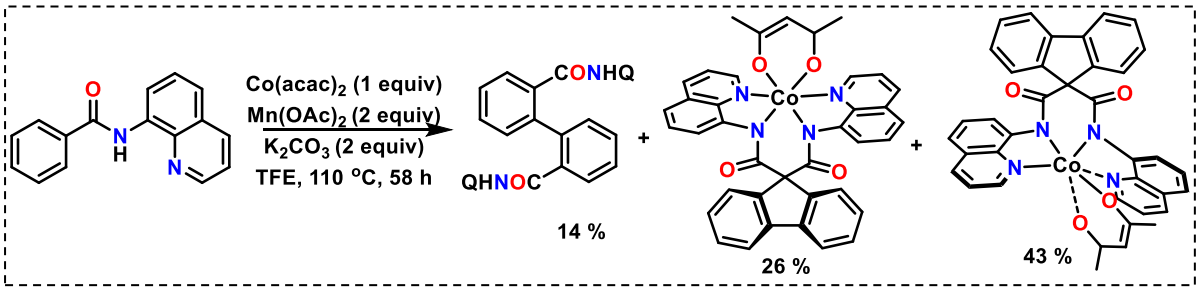

Scheme 1.15: Co-catalyzed benzamide dimerization.

Alkene alkyne coupling with *anti*-selectivity has been achieved by Petit and co-workers by using low-valent Co (0)-catalyzed C–H functionalization in aromatic imines with microwave irradiation (Scheme 1.16).[42] Here, non-diaryl acetylenes were found to be more active reactants.

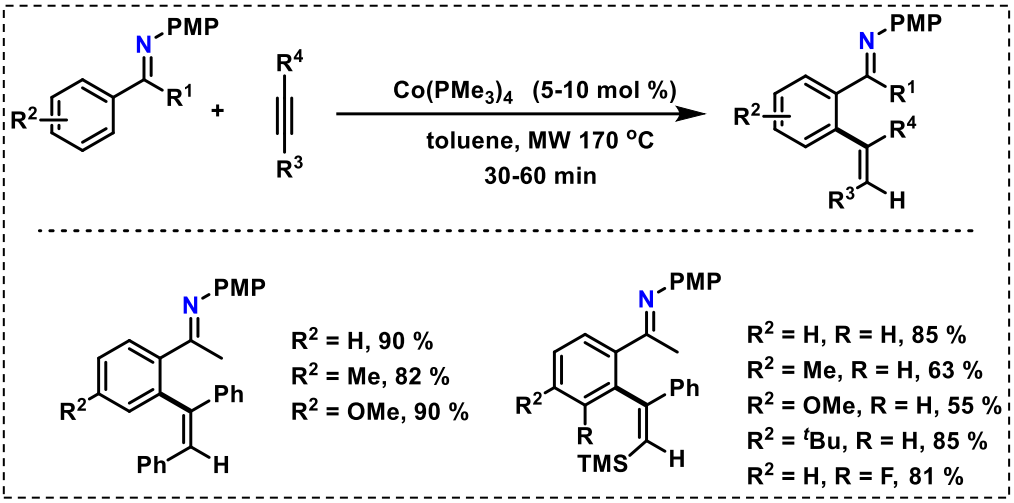

Scheme 1.16: Co-catalyzed hydroarylation of alkynes.

1.2.2. Cobalt-based C-N bond formations:

Cobalt-based catalytic systems are used not only for C-C bond formation reactions but also for C-X (X = heteroatom, like N, O, S, halogen) bond formations by several cross-coupling reactions. Interestingly, the C-N coupling has the potential to generate a variety of bioactive and synthetically important organic cores ranging from imine, amine, amide to several heterocycles like oxazoles, azines, oxazines, indoles, imidazoles, thiazoles, etc. Simple secondary or tertiary amines can be synthesized by cobalt(II)phthalocyanine-catalyzed reductive amination, *via* hydrosilylation of the intermediate imines generated *in situ*.[43] The cobalt(II)phthalocyanine catalyst activates the *in situ* generated imine by coordinating with the *N*-centre of imine for it to undergo hydrosilylation. As an example, the reductive amination of a benzaldehyde derivative (2,3,4-trimethoxybenzaldehyde) by an aniline derivative (4-methoxyaniline), is provided below (Scheme 1.17).

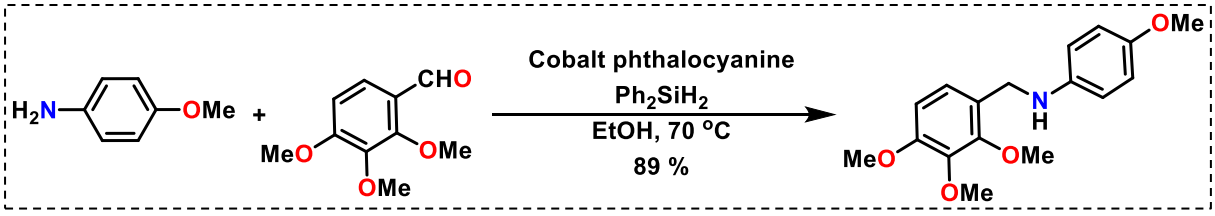

Scheme 1.17: Co-catalyzed reductive amination of aldehyde with amine.

Another way of formation of amines by C-N coupling *via* C(sp^3)–H activation was carried out by Loh's group in 2019, where, thioamides and anthranils were the starting

materials and Co(III) complex as the catalyst (Scheme 1.18).[44] Interestingly, the amination occured at the C(sp^3)–H bond of thioamide. It is reported that the anthranil derivatives with deactivating groups are more active than those with activating groups. Mechanistically, two alternative pathways are possible. One, where the reaction proceeds through a 5-membered cobaltacycle, through C(sp^3)–H bond activation, which upon coordination with anthranil undergoes migratory insertion and protonolysis with $AdCO_2H$ giving the product and the regenerated Co(III) active species. Alternatively, the formation of a Co(V)-nitrenoid species is possible *via* an intramolecular N–O cleavage, whereby insertion of the nitrenoid species into Co–C(sp^3) bond generates the common intermediate as in the first mechanistic route.

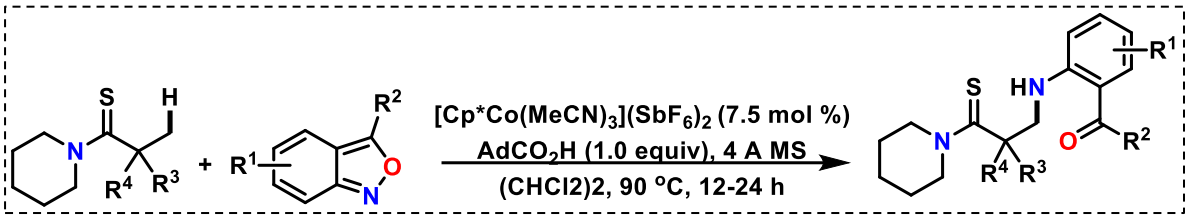

Scheme 1.18: Co-catalyzed C-N bond formation by C(sp^3)–H bond activation.

Not only amines, but imines and *N*-heterocycles can be prepared from amines (and alcohols) by acceptorless dehydrogenative coupling (ADC). It is a type of self or cross-coupling reaction, where hydrogen gas is eliminated even in the absence of any acceptor molecule within the reaction mixture. Often, the eliminated hydrogen can add up to the generated imine in presence of a metal catalyst to give amine as the final product. However, there are reports where the metal does not catalyze the hydrogenation reaction, giving imine, or even heterocycles by ADC. For example, Madsen and his group demonstrated the self and cross-coupling of aromatic and aliphatic amines to give imines by ADC (Scheme 1.19 a),[45] whereas, Balaraman and his group has explored the scope of pyrrole, pyridine and pyrazine derivatives by intramolecular ADC with a bridged bimetallic Co(II) complex (Scheme 1.19 b).[46]

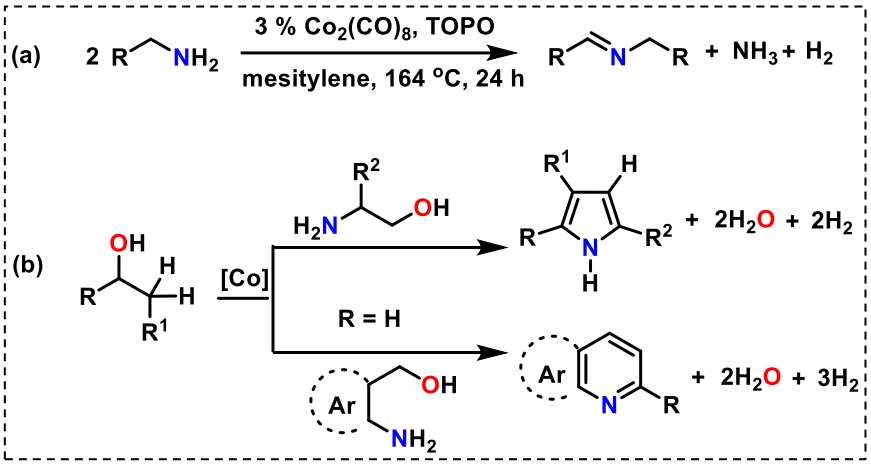

Scheme 1.19: Co-catalyzed C-N bond formation giving (a) imine, (b) heterocycles by ADC.

N-heterocycles like indoloisoquinolinones were synthesized after two years, in 2021, by Liu *et al.* using metallaphotoredox dearomatization reaction of indoles *via* [4 + 2] annulation with benzamides (Scheme 1.20)[47] $Co(OAc)_2$ served as the catalyst, $Ir(bt)_2(acac)$ as the photocatalyst, benzoylacetone as ligand, and sodium pivalate as additive, in TFE as solvent in presence of blue LED irradiation at room temperature. No additional oxidant was necessary owing to the photocatalytic autooxidation of the Co catalyst. The reaction proceeds through single electron transfer (SET) process. The detection of the shown intermediates established the mode of interaction and chelation of the Co(III) centre by nitrogenous ligands.

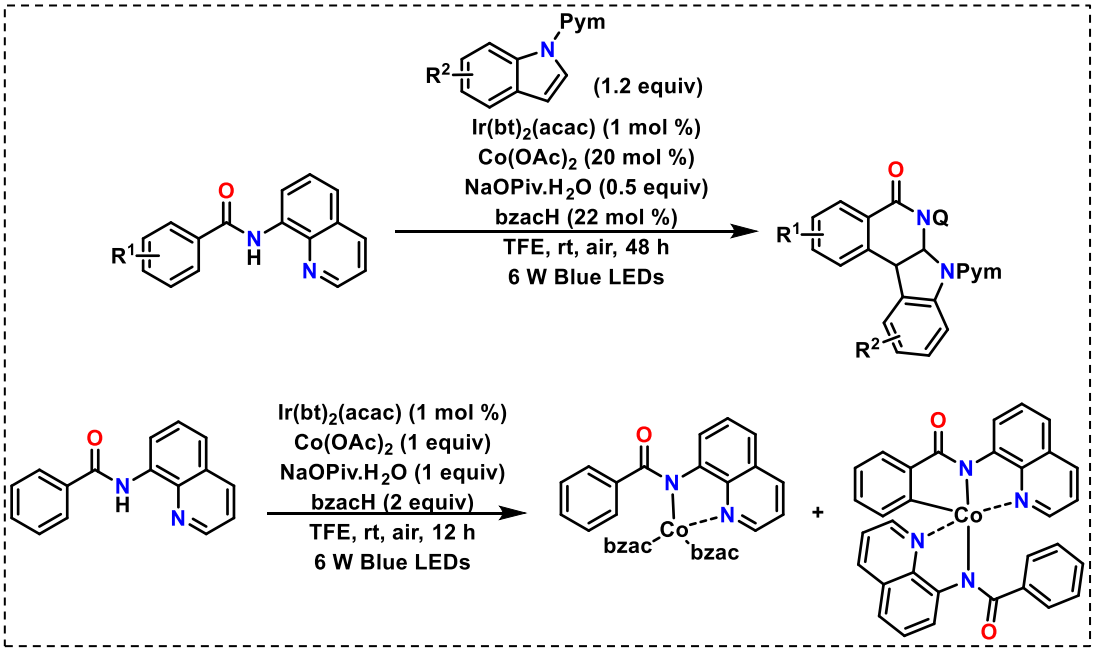

Scheme 1.20: Indoloisoquinolines developed *via* metallaphotoredox catalysis using Co(II) catalyst.

C-N bond formation is not necessarily a lone affair and can often be accompanied by C-C or C-O bond formations. For example, Co-catalyzed C-O and C-N bond formations by reaction between oxiranes and diaziridines in a stereospecific way (Scheme 1.21) can be achieved to develop tetrahydro-[1,3,4]-oxadiazines. The stereospecificity is delivered by engaging optically active oxiranes at room temperature. The mechanism is initiated by the coordination of oxirane O to $CoCl_2$, which when followed by the subsequent addition of azo methine imine, generated from diaziridine, leads to stereospecific ring opening giving the desired C-N and C-O coupled oxadiazine products.[48]

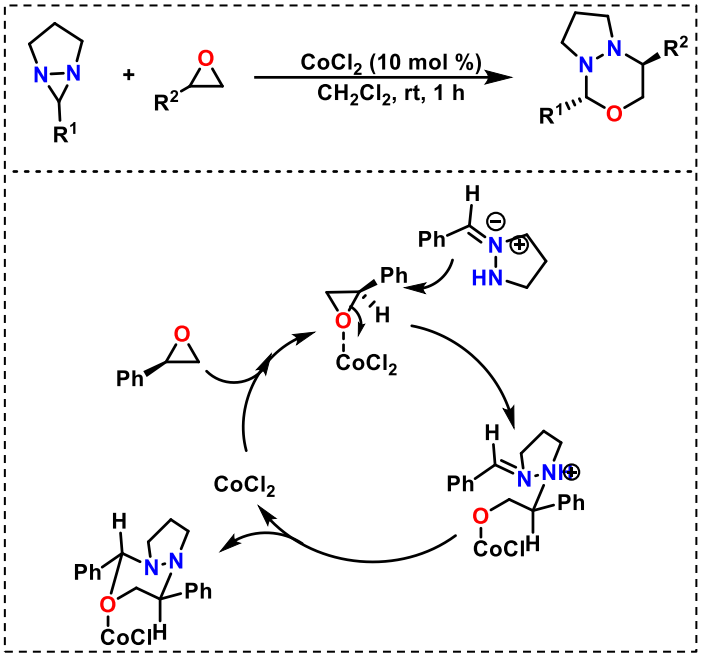

Scheme 1.21: $CoCl_2$-catalyzed stereospecific C-N and C-O bond formations.

1.2.3. Copper-based C-C bond formations:

The most prevalent copper-based C-C coupling reactions can principally be categorized into six broad divisions, as shown in Scheme 1.22. This includes Ullman coupling, giving homocoupling of two aryl groups, cross-dehydrogenative coupling, oxidative cross coupling, alkynylation (or alkenylation or allylation), cyanation and cross-coupling with organometallic reagents.

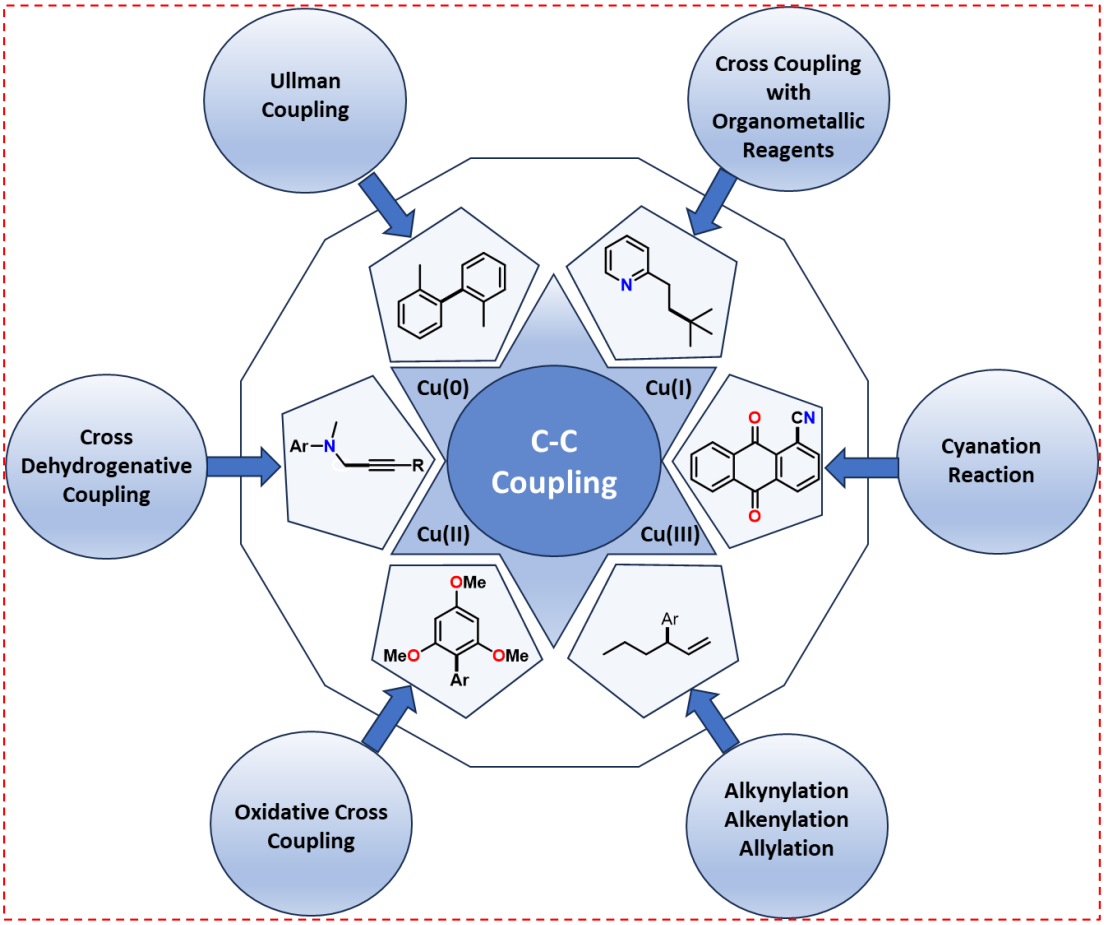

Scheme 1.22: Cu-catalyzed C-C bond formation reactions.

For example, Li, Zhang, and co-workers explored the cross-coupling between aryl halides and organo (aryl-, vinyl and alkynyl) tin reagent by Cu_2O nanoparticles (as catalyst) in tetrabutylammonium bromide (TBAB), in the presence of KF (Scheme 1.23).[49]

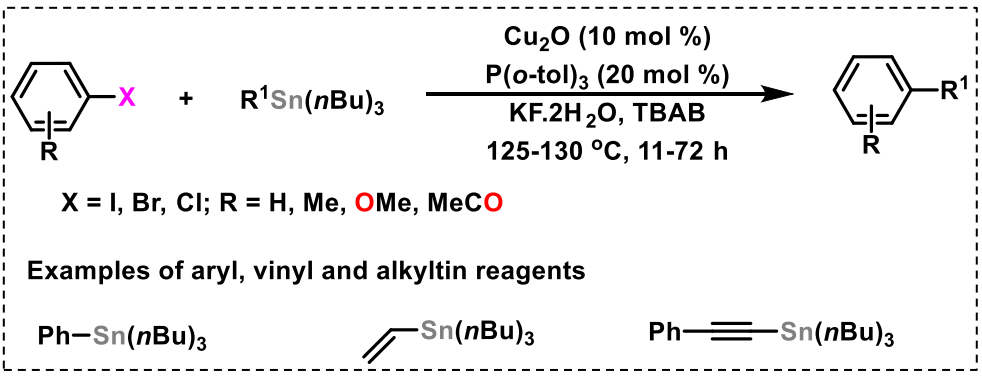

Scheme 1.23: Coupling of aryl/vinyl/alkyl tin reagents with aryl halides using Cu(II) catalyst.

Very recently, asymmetric C(sp^3)–C(sp^3) bond formation with fair stereocontrol over the two connecting C-centres, retaining all C/H substituents was also achieved by Cu(I)-catalyzed reductive coupling of two prochiral conjugate alkenes by using chiral ferrocene-catalyst in presence of diboron (Scheme 1.24). This transformation has included a wide range of coupling partners with terminal and internal enynes, and facilitates highly enantio- and diastereoselective synthesis of organoboron derivatives, with multiple stereocentres.[50]

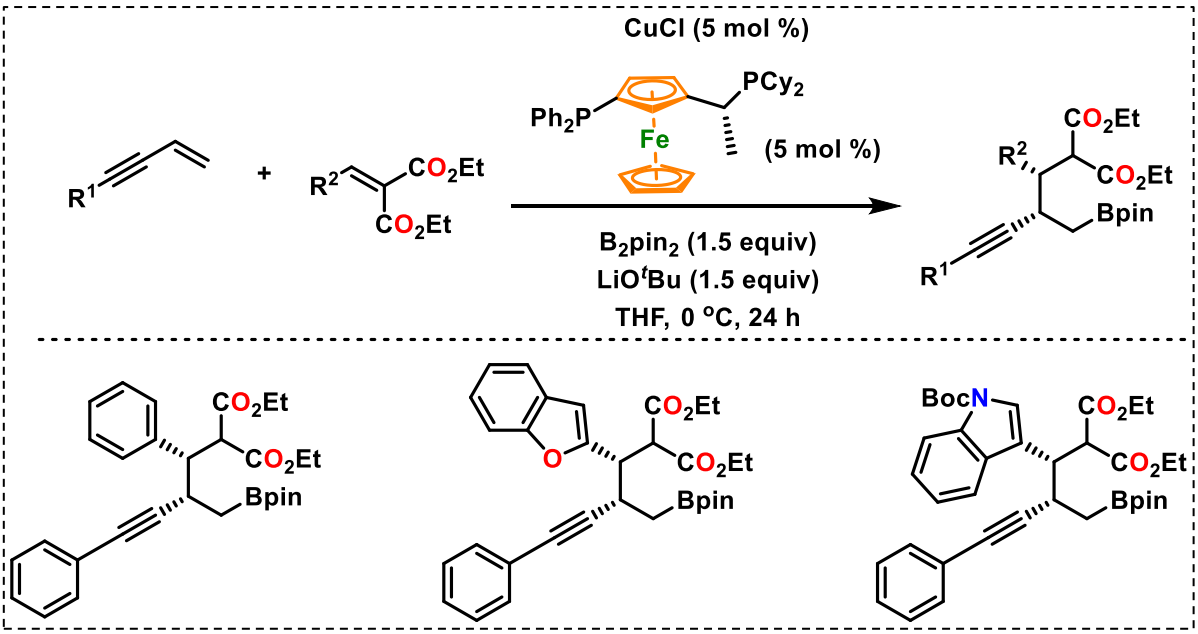

Scheme 1.24: Stereoselective coupling of alkenes by Cu(I) chloride as catalyst.

Cross-coupling reaction between aryl halides and organo (alkyl and aryl) boron compounds can also be catalyzed by commercially available Cu(I) iodide salt, apart from Pd (Scheme 1.25). The method includes a variety of heterocyclic and electron-deficient aryl bromides, which are challenging to be reacted.[51]

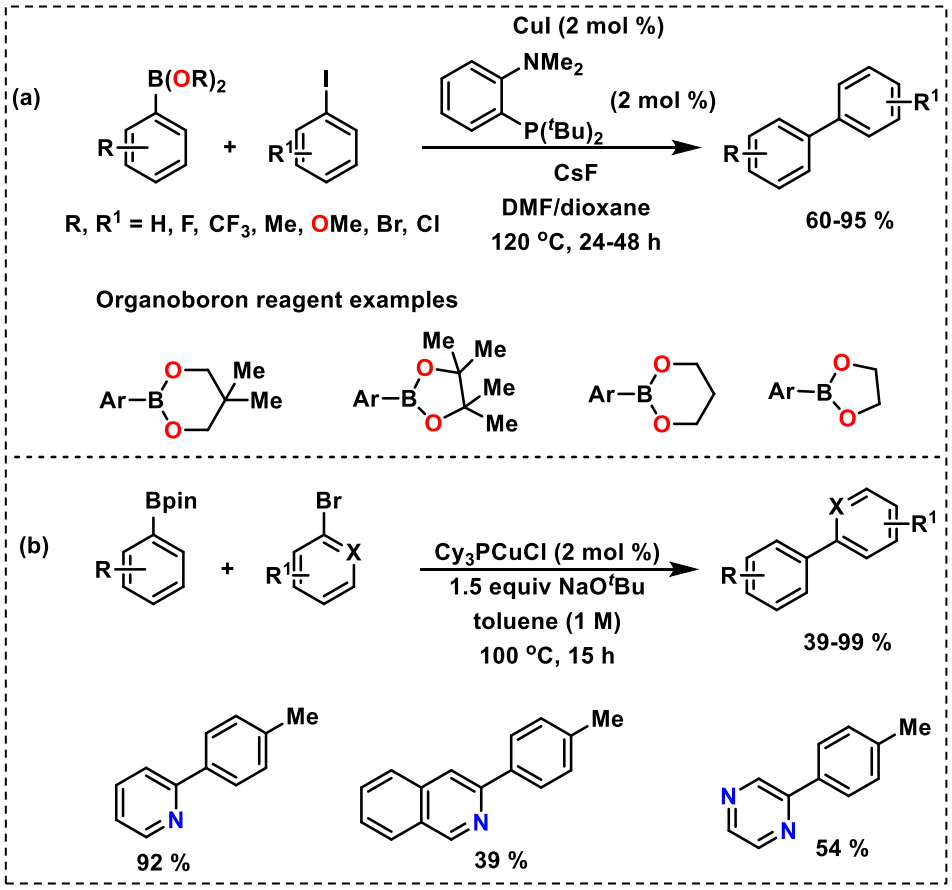

Scheme 1.25: Coupling between arylboron compounds and (a) aryl iodides (b) heterocyclic bromides using Cu(I) catalyst.

Another significant C-C coupling reaction by Cu^{2+} (Scheme 1.26) is the alkyne-alkyne coupling reaction where, terminal alkynes are coupled to synthesize internal 1,3-dialkyne system. These couplings are known by the name of Glaser coupling,[52] Hay coupling[53] or Eglinton coupling[54] depending upon the reaction conditions and oxidation state of Cu.

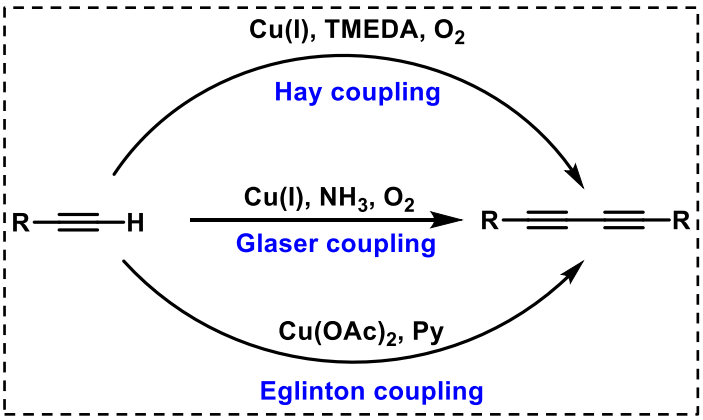

Scheme 1.26: Alkyne-alkyne homocoupling catalyzed by Cu.

1.3. Applications of molecules in synthesis and sensing:

The methodologies developed so far by several research groups can be utilized to synthesize several useful moieties. For example, one of the most promoted applications is in the field of synthesis, where the methodology, in one of the steps, can directly be utilized to prepare important molecular frameworks or natural product. Alternatively, the product obtained can be utilized for other applications like molecular labelling or bioimaging or metal ion sensing. For example, in the total synthesis of the bioactive alkaloid (+)-daphmanidin E having hexacyclic structure, with fused dihydro-pyrrole, as synthesized by Carreira *et al.*, the reaction of the iodide derivative (obtained after 19 steps from bicyclo[2.2.2]octadione) with cobaloxime under irradiation with sunlamp played a major step (Scheme 1.27).[55]

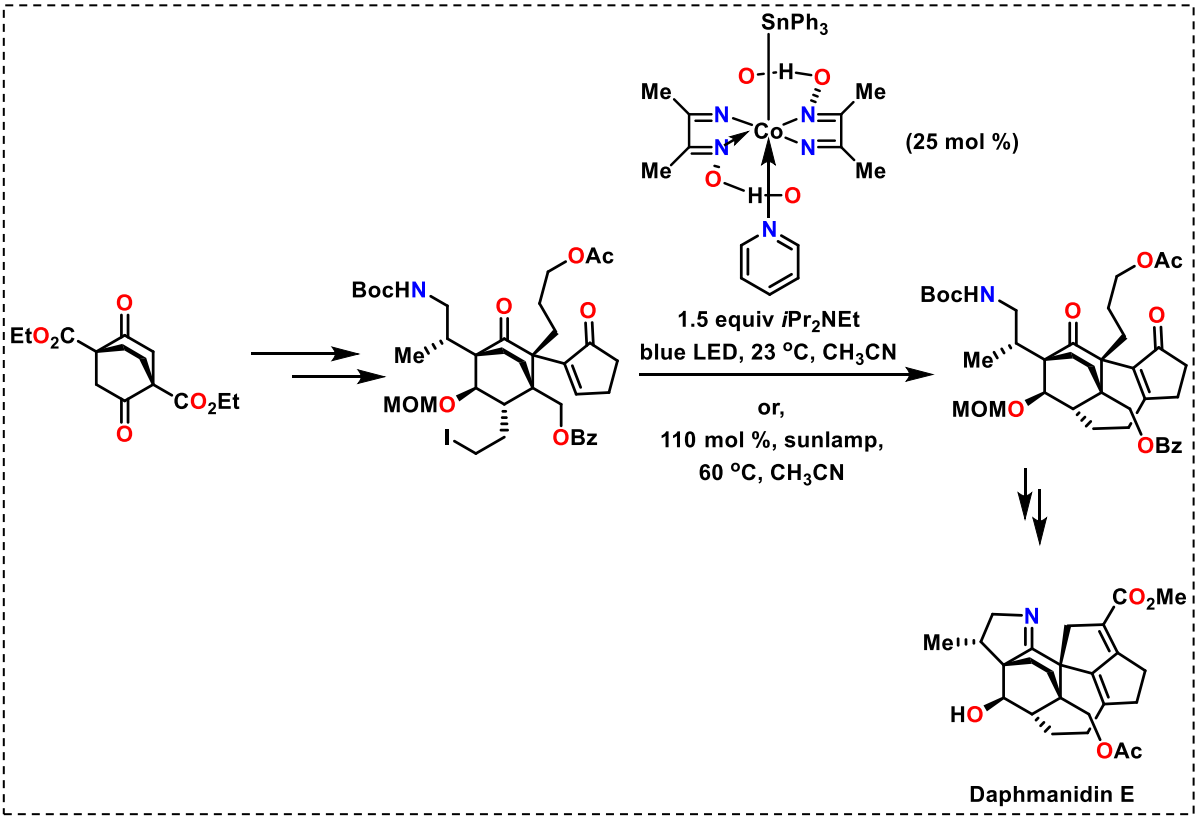

Scheme 1.27: Synthesis of daphmanidine E by Co-catalysis as one of the steps.

Another alkaloid, arboridinine, having a cage-shaped pentacyclic framework, was constructed *via* Co-catalyzed decarboxylative acetoxylation as one of the key steps, followed by saponification, which yielded (+)-arboridinine in good yields (20 % over two steps) (Scheme 1.28).[56]

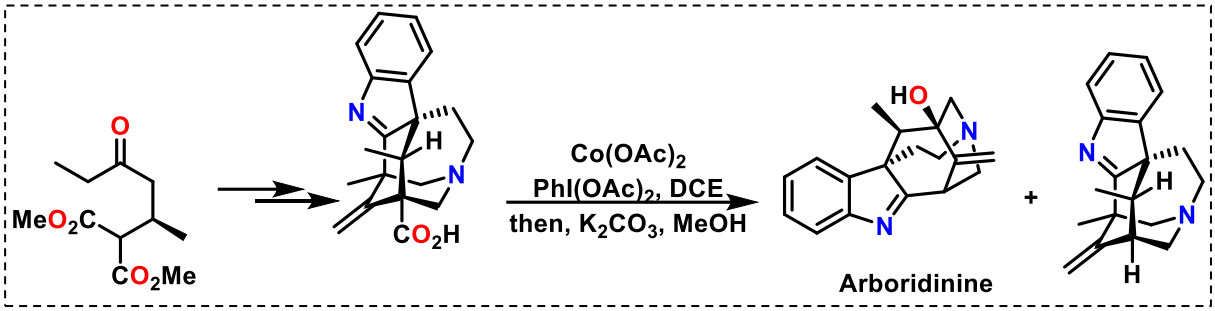

Scheme 1.28: Synthesis of arboridinine by Co-catalysis.

Not only Co-catalyzed reactions but also Cu-catalyzed reactions are utilized in the preparation of various useful derivatives. For example, in the total synthesis of martinellic acid, an unprecedented strategy, using Cu-catalyzed arylation reaction in *β*-amino ester by 1,4-diiodobenzene, was carried out by Ma and co-workers, for synthesizing the anilinic core of martinellic acid, (Scheme 1.29). Chemoselectivity of this C-N coupling reaction is impressive, since, the competitive reactions like arylation of unprotected alcohol or diamination of 1,4-diiodobenzene was not observed. The Cu-cross-coupled product was subjected to intramolecular Friedel-Crafts acylation, double C-/N-alkylation and Pd-catalyzed carbonylation as the major steps to obtain the final alkaloid martinellic acid.[57]

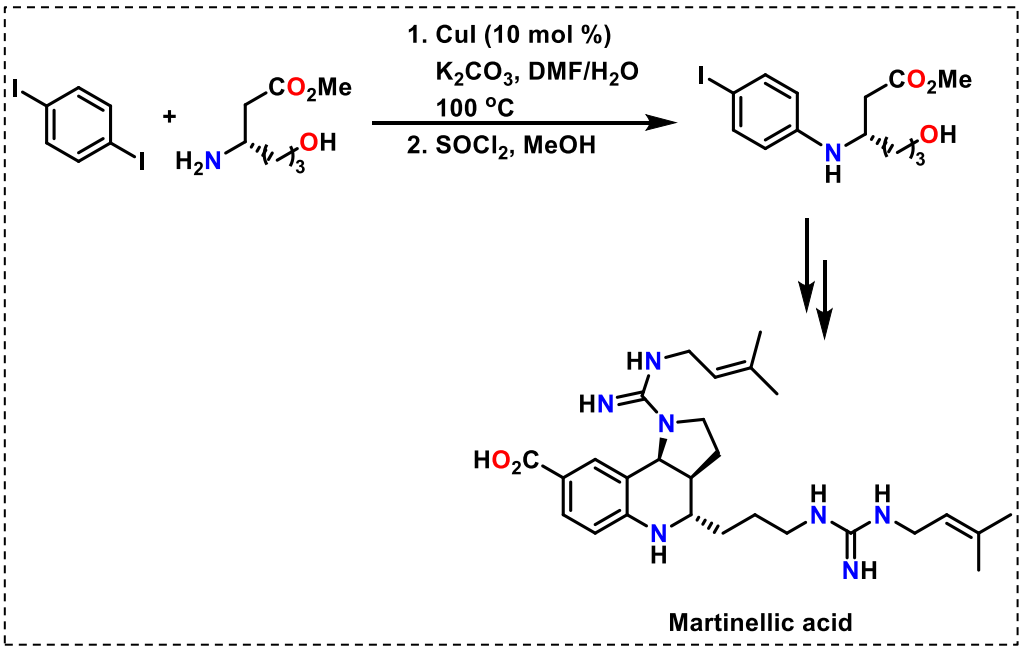

Scheme 1.29: Synthesis of martinellic acid by Cu-catalyzed C-N bond formation as one of the steps.

Macrocyclic cores like cytotrienins A–D were prepared by Cu(I)-catalyzed arylation of the corresponding amide derivative with the bromide derivative using the Buchwald protocol, to form anilide fragment, as one of the major steps (Scheme 1.30). 20 mol% CuI , 40 mol % *N,N'*-dimethylethylenediamine and K_2CO_3 were used under refluxing condition in toluene. This Cu-catalyzed amidation reaction, which could conveniently be performed (82% yield) on a large (multigram) scale, paved the way for the precursor macrocyclic core of cytotrienins (A-D), which were synthesized after ring-closing metathesis (RCM) from their corresponding acyclic dienes.[58]

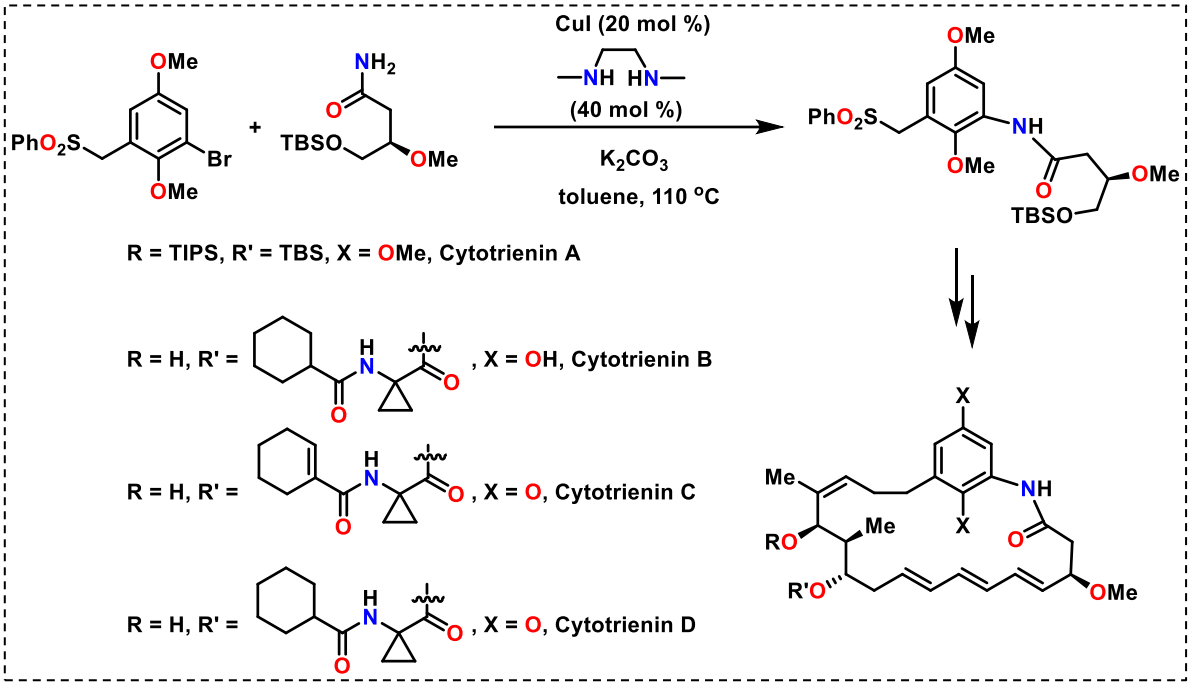

Scheme 1.30: Synthesis of cytotrienins A–D by Cu-catalyzed C-N bond formation as one of the key steps.

Other than synthetic applications, the C-C or C-N coupled compounds can be utilized in other applications as well, like applications in sensing of heavy metal ions, which is much in demand owing to the factors of increasing pollution and contamination. It is known to us that, metals, of any group and in any form, are an indispensable part of our surroundings.[59] They exist as elemental and ionic forms of various oxidation states. Metal ions are extensively utilized in the areas of industrial and analytical works.[60] They also take an imperative part in several biochemical processes.[61] Hence, recognizing them in a precise way is important and challenging at the same time.

Among the various detection techniques developed, the most reliable and explored ones are the photophysical studies like absorption spectroscopy, luminescence spectroscopy, colorimetric method, NMR spectroscopy and also electrochemical analysis. Among the various detection techniques, optical, spectroscopic and electrochemical strategies are most prevalent, enabling high sensitivity, rapid response, and cost-effective accuracy of analysis. Often, scientists have appended an electroactive group in the structural design of the detecting probes, to render them electrochemically active. Such an electroactive unit is ferrocene. It is by far, the most extensively used redox-active unit since its discovery in 1951[62] due to its exceptional electroanalytical property with d-π interactions between Fe-center and two cyclopentadienyl moieties in the sandwich form.[63] The lower oxidation potential of ferrocene makes the reversible oxidation of ferrocene (Fe^{2+}) to ferrocenium ion (Fe^{2+}) feasible, which makes its use as internal standard in electrochemical measurements possible.[64] Commercial availability, thermal, photochemical and aerobic stability[65] ease of functionalization and low biotoxicity,[66] altogether make ferrocene worth investigating. Notably, by incorporating ferrocene, the binding mode of the metal ion is not influenced as ferrocene does not directly bind to the metal ion, however, the binding phenomenon does change the oxidation and reduction potential of the ferrocene unit. This shift in potential in the complexed from the uncomplexed one accounts for the binding process in electrochemical studies. In the last decade, many research groups like Beer *et al.*, Martínez-Máñez *et al.*, Bryce *et al.*, among others, have produced many interesting results of metal ion detection, with their developed probes, containing ferrocene unit.[67] Some of the ferrocene-containing probes,[68] which can be synthesized by C-C and C-N coupling are shown below (Figure 1.7). The shown probes are all Hg^{2+} sensing probes and their development is important since Hg^{2+}, if consumed in an unregulated manner can give rise to several diseases and can even be fatal. The binding mode of one of the probes is shown in Figure 7 (below). The triazole-containing *C*2 symmetric probe contains two ferrocene units. Hg^{2+} coordination to N (triazole) and O (-OCH_2-) atoms induces a twisting intramolecularly giving enhancement of fluorescence, color change from yellow to bluish-green in acetonitrile-water solution, and a significant shift in the potential in the voltammetric studies (78 mV).[69]

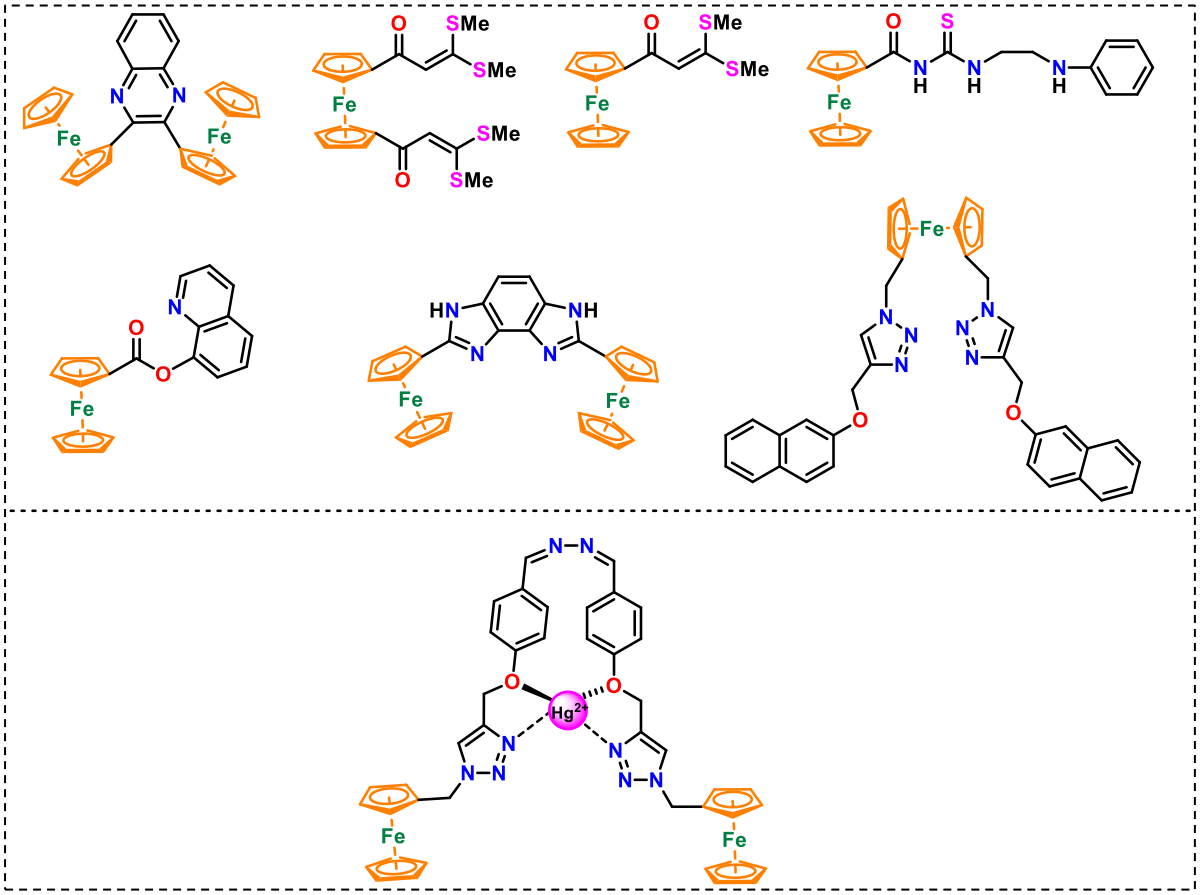

Figure 1.7: Some ferrocene-containing metal-ion detecting probes.

1.4. Objective of the thesis: The overall aim of this thesis is to:

- Explore the use of low-cost earth-abundant metal complex and salts of Co and Cu, in catalysis of C-C and C-N bond formations, which gives value-added synthetic intermediates as products.
- Develop new methodologies that are green and atom-economic.
- Explore the products formed by these new methodologies in applications of synthesis and metal sensing.

1.5. References

1. Wisniak, J. *Educación Química* **2010**, *21*, 60-69.
2. Berzelius, J.J., *Jahres-Bericht* **1835**, *14*, 237.
3. Cordus, V. *Le Guidon des Apotiquaires: C'est à dire, la Vraye Forme et Maniere de Composer les Médicamens, L. Cloquemin, E. Michel*, Lyons, **1575**.
4. Parmentier, A.A. *Expériences et Réflexions Relatives à l'Analyse du Blé et des Farines*, Paris, **1781**.
5. Döbereiner, J.W. *Versuche Über di Gährung, Schweiger J.* **1816**, *20*, 213-214.
6. Kauffman, G. *Enantiomer* **1999**, *4*, 609-619.
7. Fourcroy, A.F., *Ann. Chim.* **1797**, *21*, 48-71.
8. Passagez, A., *Bull. Soc. Chim.* **1935**, *2*, 1000-1002.
9. Davy, H., *Phil. Trans.* **1817**, *107*, 77-85.
10. Davy, E. *Phil. Trans.* **1820**, *110*, 108-125.
11. Thenard, P., Le Chimiste Thenard, Imprimerie Jobard, Dijon, **1950**.
12. Döbereiner, J.W., *Z. Chem. Physik.* **1828**, *54*, 412-426.
13. Kumar, A.; Daw**,** P.; Milstein, D. *Chem. Rev.* **2022**, *122*, 385−441.
14. Friend, C. M.; Xu, B. *Acc. Chem. Res.* **2017**, *50*, 517–521.
15. Otto, S.; Nauth, A. M.; Ermilov, E.; Scholz, N.; Friedrich, A.; Resch-Genger, U.; Lochbrunner, S.; Opatz, T.; Heinze, K. *ChemPhotoChem* **2017**, *1*, 344–349.
16. Bredig, G.; Fiske, W. S. *Biochemische Zeitschrift* **1912**, *46*, 7.
17. El Golli, A.; Contreras, S.; Dridi, C. *Sci. Reports* **2023**, *13*, 20809.
18. Sato, S.; Morikawa, T.; Kajino, T.; Ishitani, O. *Angew. Chem. Int. Ed.* **2013**, *52*, 988 –992.
19. Kotrel, S.; Bräuninger, S. "Industrial Electrocatalysis". *Handbook of Heterogeneous Catalysis*. **2008**.
20. Emil, R. *Cat. Today* **2017**, *309*, 263-268.
21. Guo, J.; Liu, H.; Lia, D.; Wang, J.; Djitcheu, X.; He, D.; Zhang, Q. *RSC Adv.* **2022**, *12*, 9373-9394.
22. J. Tang, C. Su, Z. Shao, *Small Methods* **2021**, *5*, 2100945.
23. Wang, X.; Sun, G.; Li, N.; Chen, P. *Chem. Soc. Rev.* **2016**, *45*, 2239-2262.
24. Che, M. *Cat. Today* **2013**, *218–219*, 162-171.
25. Knowles, W. S. *Angew. Chem. Int. Ed.* **2002**, *41*, 1998-2007.

26. Grubbs, R. H.; Trnka, T. M. "Ruthenium-Catalyzed Olefin Metathesis". In Murahashi, S. (ed.). *Ruthenium-Catalyzed Olefin Metathesis*. *Ruthenium in Organic Synthesis*. Weinheim: Wiley-VCH. **2004**, 153–177.
27. Miyaura, N.; Yamada, K.; Suzuki, A. *Chem. Rev.* **1979**, *95*, 2457–2483.
28. King A. O.; Okukado, N.; Negishi, E. *J. Chem. Soc., Chem.Commun.* **1977**, *19*, 683.
29. Stille, J. K. *Angew. Chem. Int. Ed. Engl.* **1986**, *25*, 508–524.
30. Miyaura, N.; Suzuki, A. *Chem. Comm.* **1979**, *19*, 866–867.
31. Sonogashira, K. *J. Organomet. Chem.* **2002**, *653***,** 46–49.
32. Kim, U. B.; Jung, D. J.; Jeon, H. J.; Rathwell, K.; Lee**,** S. -g. *Chem. Rev.* **2020,** *120***,** 13382−13433.
33. https://periodictable.com/Properties/A/CrustAbundance.an.html.
34. Wei, C. -H.; Mannathan, S.; Cheng, C. -H. *J. Am. Chem. Soc.* **2011**, *133*, 6942–6944.
35. Wei, C. -H.; Mannathan, S.; Cheng, C. -H. *Angew. Chem. Int. Ed.* **2012**, *51*, 10592–10595.
36. Chao, K. C.; Rayabarapu, D. K.; Wang, C. -C.; Cheng, C. -H. *J. Org. Chem.* **2001**, *66*, 8804−8810.
37. Mishra, A.; Dwivedi, A. D.; Shee S.; Kundu, S. *Chem. Commun.* **2020**, *56*, 249–252.
38. Chen, R.; Wang, K. -K.; Wang, Z. -Y.; Ma, X.; Wang, D.; Zhang, A. -a.; Liu, L. *Chem. Select* **2020**, *5*, 2078–2081.
39. Xu, J. -X.; Kuai C. -S.; Wu, X. -F. *J. Org. Chem.* **2022**, *87*, 6371–6377.
40. Yuan, Y.; Sun, N. -X.; Wang, C. -S.; Guo, K.; Wu, X. -F. *Org. Lett.* **2023**, *25*, 5084−5088.
41. Xie, Y.; Xu, D.; Sun, W. -W.; Zhang, S. -J.; Dong, X. -P.; Liu, B.; Zhou, Y.; Wu, B. *Asian J. Org. Chem.* **2016**, *5*, 961–965.
42. Fallon, B. J.; Derat, E.; Amatore, M.; Aubert, C.; Chemla, F.; Ferreira, F.; Perez-Luna, A.; Petit, M. *J. Am. Chem. Soc.* **2015**, *137*, 2448.
43. Kumar, V.; Sharma, U.; Verma, P. K.; Kumar, N.; Singh, B. *Adv. Synth. Catal.* **2012**, *354*, 870–878.
44. Liu, R. -H.; Shan, Q. -C.; Hu, X. -H.; Loh, T. -P. *Chem. Commun.* **2019**, *55*, 5519–5522.
45. Bottaro, F.; Takallou, A.; Chehaiber, A.; Madsen R. *Eur. J. Org. Chem.* **2019**, 7164–7168.
46. Midya, S. P.; Landge, V. G.; Sahoo, M. K.; Rana, J.; Balaraman, E. *Chem. Commun.* **2018**, *54*, 90.
47. Ban, Y. -L.; You, L.; Wang, T.; Wu, L. -Z.; Liu, Q. *ACS Catal.* **2021**, *11*, 5054–5060.
48. Maharana, P. K.; Sarkar, T.; Kar, S.; Purkayastha, S. K.; Guha, A. K.; Punniyamurthy, T. *J. Org. Chem.* **2023**, *88*, 9447−9458.

49. (a) Li, J. -H.; Tang, B. -X.; Tao, L. -M.; Xie, Y. -X.; Liang, Y.; Zhang, M. -B. *J. Org. Chem.* **2006**, *71*, 7488. (b) Thapa, S.; Shrestha, B.; Gurung S. K.; Giri, R. *Org. Biomol. Chem.* **2015**, *13*, 4816–4827.
50. Yoon, W. S.; Jang, W. J.; Yoon, W.; Yun, H.; Yun, J. *Nat. Commun.* **2022**, *13*, 2570.
51. Bergmann, A. M.; Oldham, A. M.; You, W.; Brown, M. K. *Chem. Commun.* **2018**, *54*, 5381-5384.
52. Glaser, C. *Annalen der Chemie und Pharmacie* **1870**, *154*, 137–171.
53. Hay, A. S. *J. Org. Chem.* 1962, **27**, 3320–3321.
54. Eglinton, G.; Galbraith, A. R. *J. Chem. Soc.* **1959**, 889.
55. Weiss, M. E.; Carreira, E. M. *Angew. Chem. Int. Ed.* **2011**, *50*, 11501-11505.
56. Zhang, Z.; Xie, S.; Cheng, B.; Zhai, H.; Li, Y. *J. Am. Chem. Soc.* **2019**, *141*, 7147–7154.
57. Ma D.; Qian, C. *Acc. Chem. Res.* **2008**, *41*, 1450.
58. Evano, G.; Schaus J. V.; Panek, J. S. *Org. Lett.* **2004**, *6*, 525.
59. (a) Kim, Y.; Nguyen, T. T. T.; Churchill, D.G.; Bioinorganic chemistry of the alkali metal ions. Springer International Publishing Switzerland 16 (**2016**). (b) Arevalo Jr, R.; Alkali and alkaline earth metals, Springer International Publishing Switzerland (outside the USA) (**2016**). (c) Williams, R. J. P. *Coord. Chem. Rev.* **1996**, *149*, 1-9.
60. (a) Liu, H.; Cheng, X. -B.; Jin, Z.; Zhang, R.; Wang, G.; Chen, L. -Q.; Liu, Q. -B.; Huang, J.-Q.; Zhang, Q. *Energy Chem.* **2019**, *1*, 100003-100025. (b) Hou, J.; Yang, M.; Ke, C.; Wei, G.; Priest, C.; Qiao, Z.; Wu, G.; Zhang, *J. Energy Chem.* **2020**, *2*, 100023-100062.
61. (a) Bhave, D. P.; Hong, J. A.; Keller, R. L.; Krebs, C.; Carroll, K. S. *ACS Chem. Biol.* **2012**, *7*, 306−315. (b) Kenney, G. E.; Rosenzweig, A. C. *ACS Chem. Biol.* **2012**, *7*, 260−268.
62. Kealy, T. J.; Pauson, P. L. *Nature* **1951**, *168*, 1039- 1040.
63. Beitollahi, H.; Khalilzadeh, M. A.; Tajik, S.; Safaei, M.; Zhang, K.; Jang, H. W.; Shokouhimehr, M. *ACS Omega* **2020**, *5*, 2049–2059.
64. (a) Fabre, B. *Acc. Chem. Res.* **2010**, *43*, 1509-1518. (b) Gagne, R. R.; Koval, C. A.; Lisensky, G. C. *Inorg. Chem.* 1980, *19*, 2854–2855.
65. Larik, F. A.; Saeed, A.; Fattah, T. A.; Muqadar, U.; Channar, P. A. *Appl. Organomet. Chem.* **2017**, *31*, 3664-3686.
66. Wu, J.; Wang, L.; Yu, H.; Abdin, Z.-ul-; Khan, R. U.; Haroon, M.; *J. Organomet. Chem.* **2017**, *828*, 38-51.
67. (a) Beer, P. D.; Chen, Z.; Drew, M. G. B.; Johnson, A. O. M.; Smith, D. K.; Spencer, P. *Inorg. Chim. Acta* **1996**, *246*, 143-150. (b) Beer, P. D.; Wild, K. Y. *Polyhedron* **1996**, *15*,

68. 775-780. (c) Chesney, A.; Bryce, M. R.; Batsanov, A. S.; Howard, J. A. K.; Goldenberg, L. M. *Chem. Commun.* **1998**, 677-678. (d) Lloris, J. M.; Martínez-Máñez, R.; Padilla-Tosta, M.; Pardo, T.; Soto, J.; Tendero, M. J. L. *J. Chem. Soc. Dalton Trans.* **1998**, 3657–3662. (e) Brindley, G. D.; Fox, O. D.; Beer, P. D. *J. Chem. Soc. Dalton Trans.* **2000**, 4354–4359.

69. (a) Zapata, F.; Caballero, A.; Molina, P.; Tárraga, A. *Sensors* **2010**, *10*, 11311-11321. (b) Ahamed, B. N.; Arunachalam, M.; Ghosh, P. *Inorg. Chem.* **2010**, *49*, 4447–4457.

70. Bhatta, S.R.; Mondal, B.; Lima, S.; Thakur, A. *Dalton Trans.* **2019**, *48*, 8209–8220.

Chapter 2

One-pot synthesis of dimerized arenes and heteroarenes under mild condition using Co(I) as active catalyst

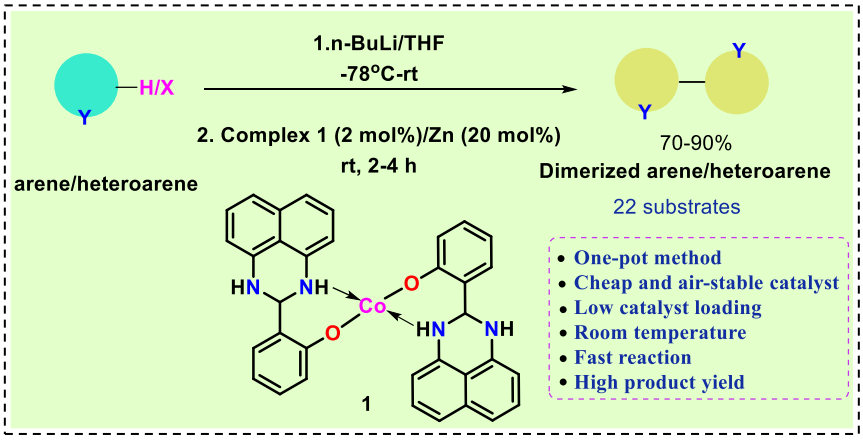

Representative Publication: *Org. Biomol. Chem.* **2022**, *20,* 8977–8987.

2.1. Introduction

Biaryl or biheteroaryl structural features are extensively found in metal-binding ligands, agrochemicals, pharmaceuticals, organic functional materials and natural products.[1] Natural products containing symmetrical bi(hetero)aryl cores (some of them are indicated in Figure 2.1) exhibit interesting biological activities.[2] The intriguing nature of dimerized organic molecules rendered the discovery of different methodologies for their atom economic synthesis. One of the most extensively utilized methods for the formation of biaryl moiety is the Cu-catalysed Ullmann reaction.[3] However, it is accompanied by harsh reaction conditions such as high Cu catalyst loading, addition of strong base, and high-temperature (> 200 ˚C), along with generation of large quantity of metal waste.[4] Other transition metals such as Ni, Pd, Co, and Fe have also been explored as catalysts, where bicomponent reactions between organic halides and organometallic reagents take place.[5,6] These methods have established themselves as standard for biaryl core synthesis, however, they require two independent reagents to be coupled and therefore, a one-pot single component *in situ* method for dimerization is much more advantageous. Lithium-halogen exchange is an example of such one-pot method,[7] where aryl lithium reagents are generated, followed by aryl-aryl dimerization catalysed by Pd, Mn, Fe, Cu, with or without additives (for aryl systems).[8]

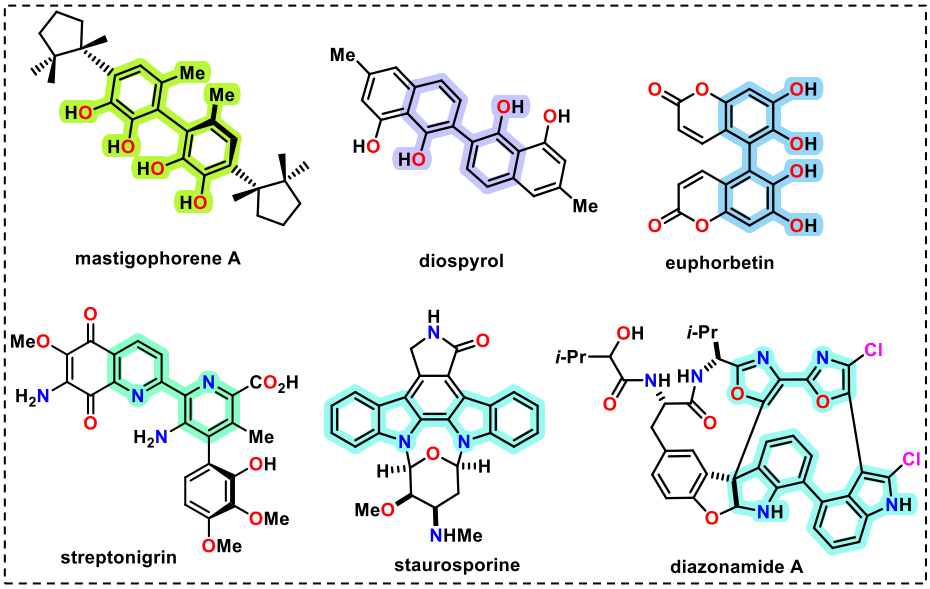

Figure 2.1: Some naturally occurring dimerized arene and heteroarene cores.

The synthetic methodology for biaryl compounds has been explored for more than a century.[9] Recently, Feringa and co-workers synthesized dimerized aromatic cores using *tert*-

butyl lithium and Pd catalyst (Scheme 2.1 entry 1).[10] This approach was also adopted by several other research groups later on with slight modifications (Scheme 2.1 entries 2 and 3).[8] However, the use of *tert*-butyl lithium is inconvenient as it demands several precautionary measures to handle. In the case of heteroarenes, dehydrogenative homocoupling is a well-explored dimerization method, that has been achieved by employing Pd(II)/Cu(II) catalysts.[11-15] However, as indicated in Scheme 1, the majority of reaction conditions for dimerized heteroarene formation require greater reaction times (Scheme 2.1 entries 4 and 5) using Pd catalyst.[16] In some cases, the reaction times have been decreased by increasing the temperature and catalyst loading.[15c]

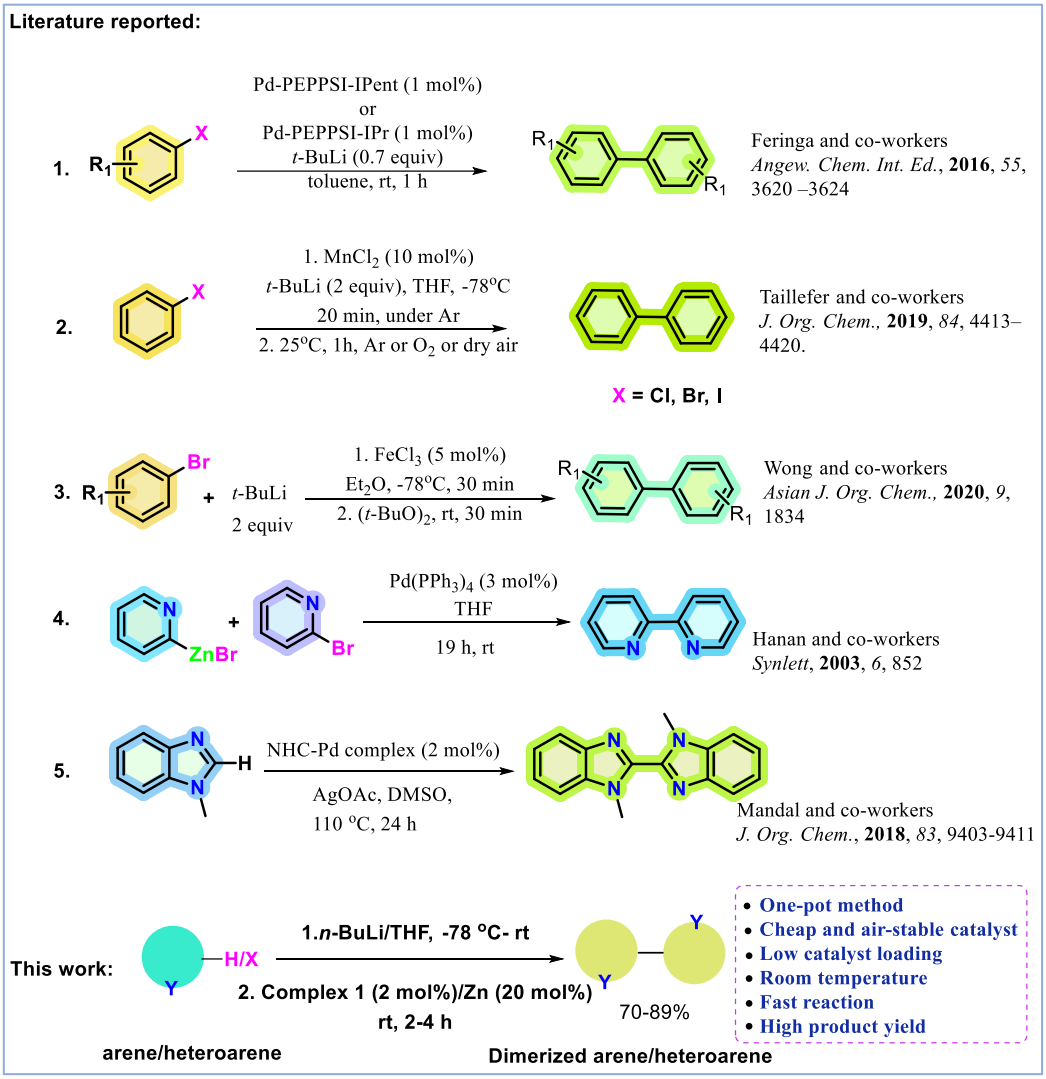

Scheme 2.1: Comparative representation of dimerization of heteroarenes.

With such background for dimerization reaction, there is still further scope for exploration of these reactions with milder conditions of temperature, time and easy-to-handle

cheap transition metal catalyst, such as cobalt, which is not explored yet for this purpose. With a view to replacing the existing expensive and widely used Pd catalyst with effective cheaper solutions for generating such dimerized cores, our quest to synthesize a Co-complex started.

Herein, we report a new methodology for the preparation of dimerized arenes and heteroarenes by lithium-halogen/acidic hydrogen exchange using *n*-BuLi, followed by action of Co(II)/Zn(0) catalyst system at 25 ˚C. The major advantages of this approach are the use of economically cheaper and air/moisture-stable Co catalyst, ease of product separation, faster reaction times than previously reported procedures[12-16] and hassle-free one-pot procedure at room temperature (Scheme 2.1).

2.2. Results and Discussions:

2.2.1. Synthesis of the Co(II) catalyst

The ligand **L1** is a condensation product, which can be synthesized in an atom economic way from 1,8-diaminonaphthalene and salicylaldehyde in a 1:1 molar ratio without any solvent and by only mechanical grinding at room temperature. The ligand has phenolic -OH and -NH as potential metal chelating sites. The white-colored crystalline ligand **L1** was subjected to react with $CoCl_2 \cdot 6H_2O$ in ethanol under reflux for 6 h, during which, green-colored precipitate of the complex **1** appeared. This complex **1** with ligand:metal ratio 2:1 is found to be formed under any stoichiometry of reactants taken, indicating that complex **1** is the most stable product out of all possibilities and the reaction is highly feasible.

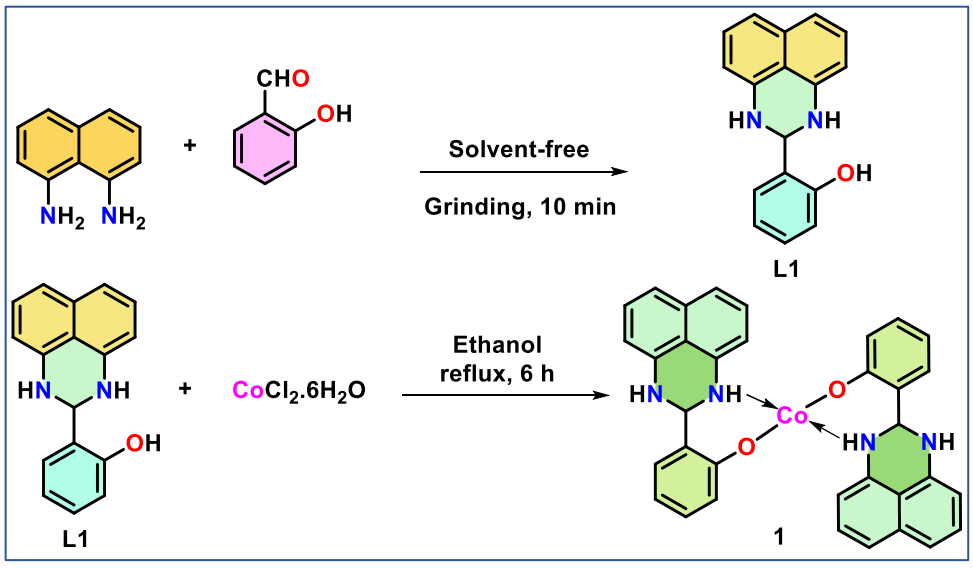

Scheme 2.2: Synthesis of the complex **1**.

Complex **1** is found to be stable under air, heat and moisture conditions. The ligand, as well as the complex, have been characterized by HRMS, IR, UV-vis spectra, CV, EPR and EDX studies.

2.2.2. Characterization of the Co(II) catalyst: HRMS, IR, UV-vis spectra, Cyclic voltammetry (CV), electron paramagnetic resonance (EPR) spectrum and electron dispersive X-ray (EDX) image of complex 1:

Complex **1** has been characterized by several methods such as UV-vis spectra, cyclic voltammetry (CV), electron paramagnetic resonance (EPR), IR spectra (Figure 2.2) and HRMS (Figure 2.6), and compared with the free ligand **L1**, wherever necessary. The ^{1}H NMR spectrum of complex **1** does not contain well-defined peaks as they get broadened due to the associated paramagnetism of the d^7 Co(II) centre. The HRMS data (Figure 2.6) indicates that the ligand to metal ratio in the complex is 2:1, with deprotonation of two phenolic-OH groups from the two ligands. The comparison of IR spectra of the free ligand **L1** and complex **1** shows that there is a broadening of the secondary amine stretching frequency at 3336 cm^{-1}, which indicates the involvement of the -NH group along with the oxygen atom (Figure 2.2a). The absence of Co-Cl stretching frequency in the 200-500 cm^{-1} wavenumber range[17] indicates the absence of Cl attached to the Co-centre.

The spectrophotometric method gives a unique characteristic spectral pattern for each compound. The UV-vis spectrum of the free ligand **L1** (CH_3CN, 3.12×10^{-5} M) at 22 ˚C gives four absorption peaks at 230 nm, 276 nm, 334 nm and 346 nm. The peaks may correspond to $\pi-\pi^*$ and $n-\pi^*$ transitions in the ligand (Figure 2.2b). In complex **1** (CH_3CN, 3.12×10^{-5} M), the absorption intensities of the peaks are decreased except 276 nm, along with blue-shift of around 12 nm of the peaks at 230 nm and 276 nm. An additional peak at 450 nm appears for complex **1**, which corresponds to the d-d transition of the associated metal ion.[18]

The anticipated structure of the complex, as obtained from IR and HRMS studies, indicates deprotonation of the two phenolic -OH groups, which is possible if the Co centre is in +2 oxidation state. However, to establish the anticipated oxidation state experimentally, cyclic voltammetry (CV) and electron paramagnetic resonance (EPR) studies have been conducted. In CV, a reversible one-electron reduction wave of the complex **1** (5×10^{-4} M) in 1:1 DMF:CH_3CN appears, with TBAP as supporting electrolyte at 0.05 Vs^{-1} scan rate at 22 ˚C. The E_{pa} is -1.059 V and E_{pc} is -0.693 V with ΔE = 0.366 V and $E_{1/2}$ = -0.876 V (Figure 2.2c),

corresponding to the Co(II)/Co(I) couple.[18,19] This supports the presence of Co(II) in the complex **1**. In addition, there is a quasireversible peak at 1.15 V.

The EPR spectrum of complex **1** shows a reversible wave with g = 2.007, which corresponds to the EPR signal of a one-electron system (ideally, g = 2.003)[20] (Figure 2.2d). This can only be possible if Co has an oxidation state of +2, giving a paramagnetic d^7 system in low spin square planar geometry. The superhyperfine splitting, which is supposed to be associated with such an arrangement with N and O donors in complex **1** is not visible as the EPR spectrum is recorded in $CHCl_3$ at 100 K temperature.

In addition to the aforementioned studies, the electron dispersive X-ray diffraction (EDX) pattern was taken for complex **1** as additional proof of the inclusion of Co-centre within the complex. The EDX image from scanning electron microscope (SEM) gives signals from Co K and L shells (Figure 2.2e), which proves that the element Co is present in the complex.

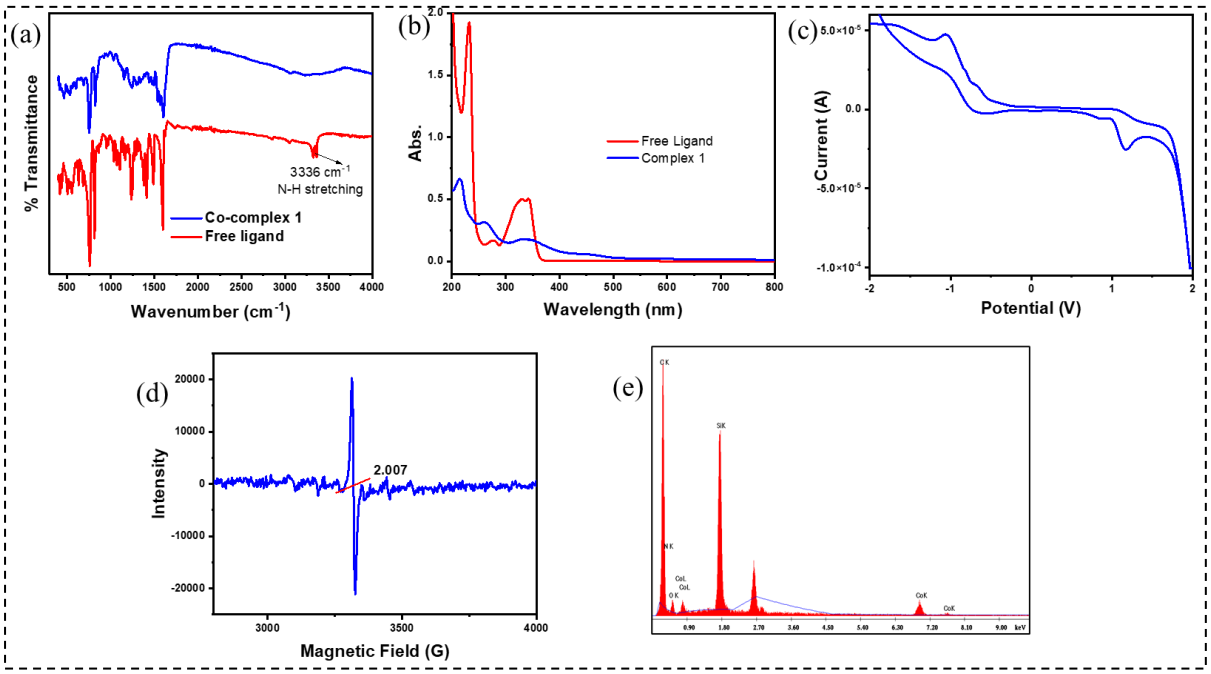

Figure 2.2 (a) IR spectra of free ligand **L1** and Co-complex **1** in solid state at 22 ˚C. (b) UV-vis spectra of free ligand (CH_3CN, 3.12×10^{-5} M) and Co-complex **1** (CH_3CN, 3.12×10^{-5} M) at 22 ˚C, (c) CV of complex **1** (DMF:CH_3CN 1:1, 5×10^{-4} M) with TBAP as supporting electrolyte at 0.05 Vs^{-1} scan rate at 22 ˚C, (d) EPR spectra of Co-complex **1** in $CHCl_3$ solvent at 100 K temperature, (e) EDX image of Co-complex **1** in solid state at 22 ˚C.

2.2.3. Catalytic activity

The dimerization of arene and heteroarene can generate a class of potential organic compounds having unique materialistic advantages or stable chelating agents with a convenient bite angle. With this approach, our synthesized complex **1**, coupled with air-stable Zn dust was subjected to catalyze dimerization reactions of arenes and heteroarenes. This Co(II)/Zn(0) couple forms a system of catalyst which selectively targets the C-C homocoupling at the activated (lithiated) site. The lithiation by *n*-BuLi is done prior to catalyst loading. The C-C coupling reaction occurs completely at room temperature within 2-4 h in the same pot as the lithiation.

2.2.4. Dimerization of arenes and heteroarenes

The optimization of the dimerization reaction of arenes was done taking iodobenzene as the model substrate. *n*-BuLi was added to the solution of iodobenzene in THF at room temperature to generate lithiated benzene within 1 h. The dimerization reaction was initially tested with 1 equiv anhydrous $ZnCl_2$ and 5 mol% $Pd(PPh_3)_4$, which gave the corresponding dimerized product within 8 h of reaction at room temperature (Table 2.1, Entry 1). The same reaction, when repeated with hydrated $ZnCl_2$, no product was formed (Table 2.1, Entry 2). Upon substituting the expensive and air-sensitive $Pd(PPh_3)_4$ with our synthesized Co(II) catalyst **1** (5 mol%), the reaction proceeded to completion within 8 h at room temperature (Table 2.1, Entry 3). Although, the expected Negishi type of coupling reaction with anhydrous $ZnCl_2$ went smoothly,[21] but use of anhydrous $ZnCl_2$ is disadvantageous as it is very expensive and hygroscopic in nature. Hence, we prompt to replace anhydrous $ZnCl_2$ with easy-to-handle activated Zn dust (1 equiv), as a cheaper alternative. The reaction went well with 5 mol% of the Co(II) catalyst **1** and 1 equiv activated Zn dust within 8 h at room temperature giving 78% yield of the product (Table 2.1, Entry 4). Increasing the catalyst loading or Zn dust loading, or both, did not alter the percentage of yield of product (Table 2.1, Entries 5-7). Since not more than 5 mol% of **1** and 1 equiv Zn was required for the reaction to take place at room temperature, we explored our observation upon decreasing the catalyst loading and the reaction time (Table 2.1, Entries 8-10). Upon decreasing the catalyst loading from 5 mol%, to 2 mol%, it was found that 78% of the product was formed after 2 h of reaction at room temperature (Table 2.1, Entry 11). Further decreasing the catalyst loading from 2 mol% afforded the desired product in low yield (Table 2.1, Entry 12). Hence keeping the catalyst loading at 2 mol%, the reaction time was decreased (Table 2.1, Entries 13-15), wherefrom it was observed that a minimum of 2 h is essential for the reaction to complete with 78 % yield of product (Table 2.1,

Entry 15). Same percentage of yield was also obtained by reducing the quantity of Zn dust to 20 mol% (Table 2.1, Entry 16). This is found to be the optimal condition for this reaction. Alternating the Co(II) source with $CoCl_2 \cdot 6H_2O$ produced the desired product in very low yield (Table 2.1, Entry 17). In absence of either of Zn or Co(II) complex, a feeble conversion to product takes place after 8 h of reaction at room temperature (Table 2.1, Entries 18, 19). The percentage yield of the product did not alter for an increased temperature of the reaction using catalyst **1** and Zn (Table 2.1, Entries 20, 21), which indicates that the reaction goes best at ambient conditions of room temperature for a period of 2 h within the same pot of lithiation using 20 mol% of activated Zn dust.

Table 2.1 Optimisation of the reaction conditions.[a]

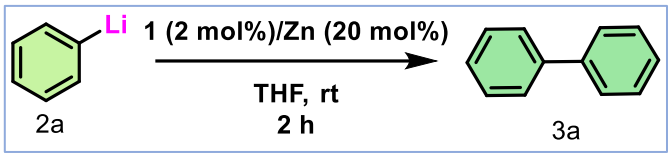

Entry	Catalyst (mol%)[a]	Zn source (equiv)	Temperature (°C)	Time (h)	% Yield[b]
1	$Pd(PPh_3)_4$ (5)	Anhy $ZnCl_2$ (1)	rt	8	80
2	$Pd(PPh_3)_4$ (5)	$ZnCl_2$ (1)	rt	8	NR
3	Catalyst **1** (5)	Anhy $ZnCl_2$ (1)	rt	8	78
4	Catalyst **1** (5)	Zn dust (1)	rt	8	78
5	Catalyst **1** (5)	Zn dust (2)	rt	8	78
6	Catalyst **1** (10)	Zn dust (1)	rt	8	78
7	Catalyst **1** (10)	Zn dust (2)	rt	8	78
8	Catalyst **1** (4)	Zn dust (1)	rt	8	78
9	Catalyst **1** (3)	Zn dust (1)	rt	8	78
10	Catalyst **1** (2.5)	Zn dust (1)	rt	8	78
11	Catalyst **1** (2)	Zn dust (1)	rt	8	78
12	Catalyst **1** (1.5)	Zn dust (1)	rt	8	65
13	Catalyst **1** (2)	Zn dust (1)	rt	6	78
14	Catalyst **1** (2)	Zn dust (1)	rt	4	78
15	Catalyst **1** (2)	Zn dust (1)	rt	2	78
16	Catalyst **1** (2)	Zn dust (20 mol%)	rt	2	78
17	$CoCl_2 \cdot 6H_2O$ (2)	Zn dust (20 mol%)	rt	2	24

18	-	Zn dust (20 mol%)	rt	8	18
19	Catalyst **1** (2)	-	rt	8	25
20	Catalyst **1** (2)	Zn dust (20 mol%)	45	4	77
21	Catalyst **1** (2)	Zn dust (20 mol%)	60	4	77

[a]Reaction conditions: **2a** (1 mmol), *n*-BuLi (1 mmol), 25 ˚C, solvent THF (5 ml). [b]Isolated yield after column chromatography. rt: room temperature, NR: No Reaction.

After completing the optimization for the aryl-aryl homo-coupling reaction, we have tried to apply this method for the coupling of hetero-arenes. After a set of optimizations (Table 2.2), we have observed that the maximum possible yield could be obtained by increasing the reaction time to 4 h (Table 2.2, Entry 10), keeping all other conditions same.

Table 2.2 Optimization of reaction conditions for the dimerization of heteroarenes.

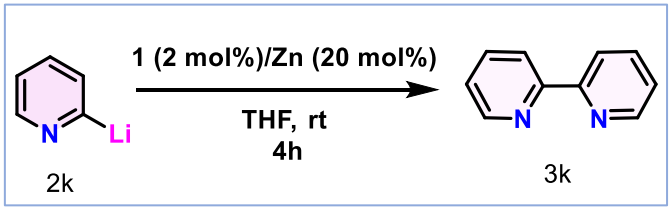

Entry	Catalyst (mol %)[a]	Zn source (equiv)	Temperature (˚C)	Time (h)	% Yield[b]
1	Catalyst **1** (2)	Zn dust (1)	rt	2	55
2	Catalyst **1** (2)	Zn dust (1)	rt	3	68
3	Catalyst **1** (2)	Zn dust (1)	rt	4	75
4	-	Zn dust (1)	rt	4	NR
5	Catalyst **1** (2)	-	rt	4	NR
6	Catalyst **1** (2)	Zn dust (1)	45	4	75
7	Catalyst **1** (2)	Zn dust (1)	60	4	75
8	Catalyst **1** (2)	Zn dust (20 mol%)	rt	2	55
9	Catalyst **1** (2)	Zn dust (20 mol%)	rt	3	68
10	Catalyst **1** (2)	Zn dust (20 mol%)	rt	4	75

[a]Reaction conditions: **2k** (1 mmol), Zn dust, cobalt catalyst, solvent THF (5 ml). [b]Isolated yield after column chromatography.

Since dimerized arene units are important with respect to their ligating behavior, optoelectronic properties or presence in natural products, our methodology can be explored as a step forward towards dimerization with lithium-halogen exchange mechanism for arenes.

With phenol derivative 2-bromophenol **2b**, the dimerization reaction occurred with 100% conversion to give biphenol system (**3b**), which can serve as a good ligating agent. Bromo derivatives of toluene (4-bromotoluene, **2c**) and anisole (3-bromoanisole, **2d**/ 4-bromoanisole, **2e**) successfully give corresponding dimerized products with high yields. Fluorinated phenol derivative such as 2-bromo-4-fluorophenol (**2f**) gives the corresponding dimer (**3f**) in moderate yield (74%), whereas dimerized product (**3g**) from 3,5-dimethoxybromobenzene (**2g**) is obtained in good yield (85%). The dimerized pyrene derivative (**3h**) finds its application in organic materials where a high conjugation is required (optoelectronic devices).[22] Naphthalene derivative such as 1-bromo-2-methyl naphthalene (**2i**) gave the corresponding binaphthyl system (**3i**) as the sole product, which, like the dimerized pyrene unit, is highly conjugated. Additionally, the coupling of *ortho*-disubstituted halobenzene to produce sterically hindered tetra-*ortho*-substituted biarenes is challenging and most of the literatures using the lithium-halogen exchange mechanism lack in exploring such reactions.[10] Our developed methodology has been utilized to produce such tetra-*ortho*-substituted sterically conjugated biaryl compound **3j**, although in a trace amount, using 1,3-dimethyl-2-bromobenzene (**2j**) as the starting material. Noteworthy to mention that, the optimized reaction condition for arenes does not work for non-halogenated phenyl derivatives, such as 1-methoxy naphthalene (lithiation at 2-position) or *N,N*-dimethyl aniline (lithiation at 4-position), which goes at par with the observations reported in the literature.[23,15b]

The optimised reaction condition has been applied for several heterocycles, containing C-X (X = Br, I) bond or activated C-H bond, such as 1-methyl benzimidazole (**2l**), benzothiazole (**2m**), 1-methyl indole (**2n**), 2-methylthiophene (**2o**) to give the corresponding dimerized products **3l-3o** in 75-80% yield (Table 2.3). This reaction condition can even be extended to the dimerization of metallocene, such as ferrocene (**2p**) to give biferrocene (**3p**) which is a potential source of intravalent charge transfer phenomenon.[24] For halogenated heteroarenes, containing highly acidic H atoms, such as 5-bromopiperidine (**2r**) and 3-bromopyridine (**2s**), a competition for lithiation exists between the C centre containing highly acidic H centre and the C centre attached to the halogen atom. As a result, a dimerized product devoid of the C_2 symmetry is obtained (**3r**) as the major product. Noteworthy to mention that the dimerization could not be obtained for *N*-BOC protected heterocycles, since the bond is highly susceptible to breakage, which results in the regeneration of the parent-NH containing heterocycle as soon as *n*-BuLi is charged to the reaction medium. Moreover, such coupling of substrates containing *N*-BOC group has not been reported by any other research group using

the lithium-halogen exchange mechanism.[23,15b] The cross-coupling of the heterocycles was attempted with the optimized reaction conditions by lithiation of both the heterocyclic components, however, in each case, the homocoupled product of the respective reactant was obtained as a major product along with some amount of cross-coupled product. The cross-coupling, with lithium-halogen/acidic H exchange strategy, has not been explored much,[9] which creates scope for further research in this field.

Table 2.3 Dimerization of arenes using the optimized reaction condition with Zn dust and catalyst **1**.[a]

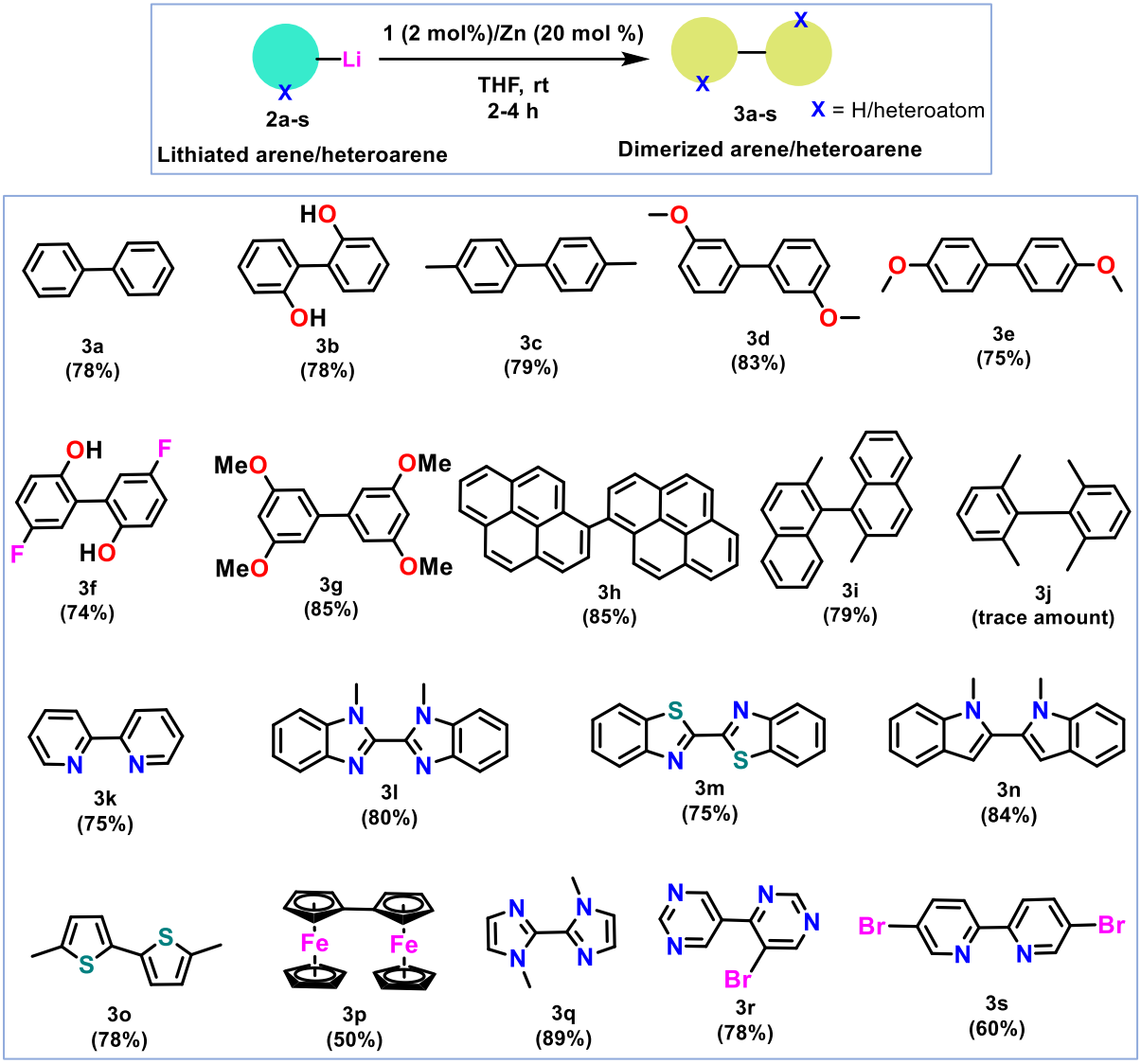

[a]Reaction conditions: **2a-s** (1 mmol), Zn dust (20 mol%), cobalt catalyst (2 mol%), solvent THF (5 ml), rt, 2 h (arenes). For heteroarenes, the reaction time for dimerization under this condition is 4 h. [b]Isolated yield after column chromatography.

For polyhaloarene substrates, the simple dimerization does not hold with our developed methodology, rather they undergo polymerization functionalizing all the available sites. With 1,3-dibromobenzene (**2t**), two products **3t** and **3u** were produced due to the unselective lithiation of the two *meta*-bromo groups (Scheme 2.3). The same holds good for 3-bromo-1-iodobenzene (**2v**).

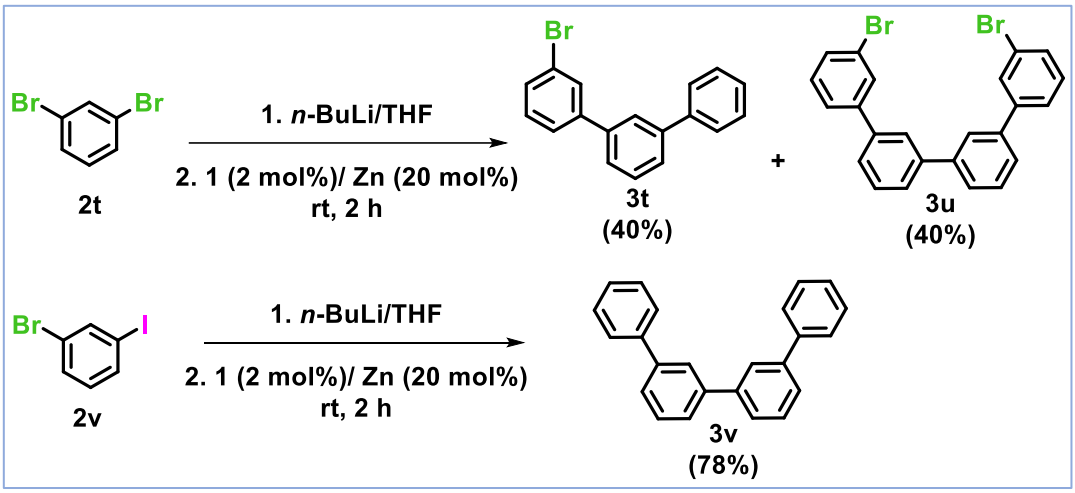

Scheme 2.3: Dimerization of polyhaloarenes using the optimized reaction condition with Zn dust and catalyst **1**.[a]

2.2.5. Gram-scale reaction

Gram-scale reaction has been explored with two substrates **2k** and **2o** to produce **3k** and **3o** respectively by our developed methodology (Scheme 2.4). The coupling reactions to construct **3k** and **3o** in gram-scale proceeded well with our optimized reaction conditions giving the dimerized products in 70 and 75% yield respectively.

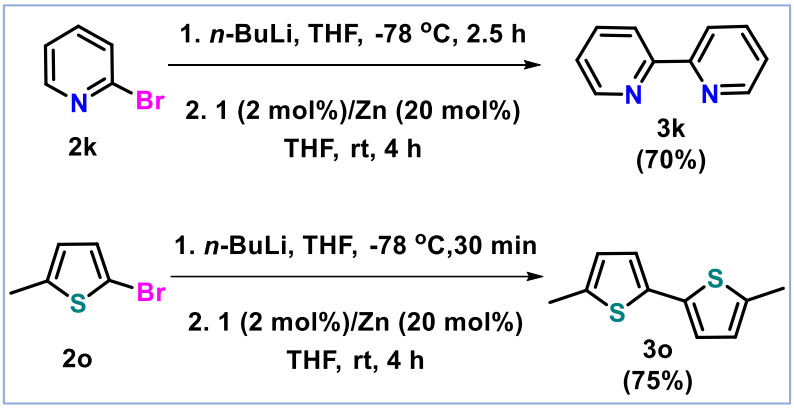

Scheme 2.4: Gram-scale reaction of **2k** and **2o** to produce **3k** and **3o** respectively using the optimized reaction conditions.

2.2.6. Plausible Mechanistic cycle

Literature reports about dimerized or cross-coupled products using bimetallic system of catalysts indicate that the two coupling components must attach together to the active catalyst from which the coupled product gets separated regenerating the catalyst.[15,25] Anticipating a free-radical mechanism, TEMPO (2,2,6,6-tetramethylpiperidine-*N*-oxide), a radical scavenger, was added to the reaction mixture after the addition of Zn(0) and Co(II) catalyst to the 2-lithiated pyridine. However, even after addition of radical scavenger, the desired product 2,2′-bipyridine was formed, indicating that the reaction mechanism does not undergo *via* a free-radical pathway. Co(II)/Zn(0) couple is well-known to catalyze hydrogenation/reduction reactions.[26] Further, Zn(0) is a well-known reducing agent, it is expected to reduce the Co(II) of the complex **1** to Co(I), as per several literature reports for such Co(II)/Zn(0) systems.[27] Since the reaction proceed smoothly with 20 mol% of the Zn dust, it is expected for Zn dust to act as a reducing agent in our case as well. The oxidized Zn^{2+} species probably act as a counterion to balance the charge of generated two monoanionic Co(I) complex. From the experimental observation and from the literature reports,[27,28] the most plausible mechanistic way for dimerization should be such that the reduced Co(I) attaches the two Ar groups from Ar-Li, (Ar is aryl or heteroaryl group) and the oxidation state of the Co centre simultaneously changes from +1 to +3 in one single step.[28] In the next step, the biaryl product is separated from the metallic core and the catalyst is regenerated (Scheme 2.5).

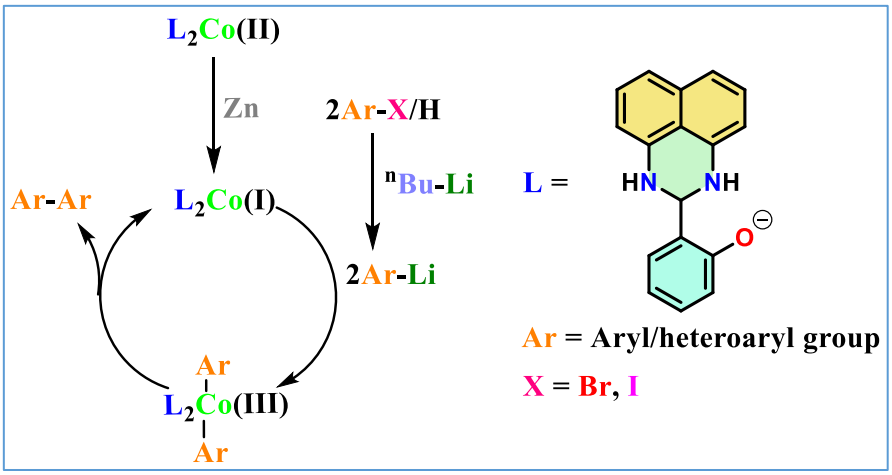

Scheme 2.5: Plausible mechanism for the catalytic cycle.

2.3. Conclusion

A new methodology for the synthesis of structurally beneficial dimerized arenes and heteroarenes, which are suitable candidates for natural product cores, organic devices, ligating agents etc., is devised by employing a sustainable catalyst system of a Co(II) catalyst, coupled with freshly activated Zn powder. The optimized reaction condition gives 70-89% of product yield by employing 2 mol% of the Co(II) catalyst at room temperature for 2-4 h. Where literature reported procedures use high temperature and long reaction times, our developed synthetic strategy is fast, occurs at room temperature, and requires very low catalyst loading. This methodology can be a step forward towards utilizing cheaper earth-abundant metals in replacing the expensive metals in the catalysis industry with high efficiency of output.

2.4. Experimental section:

2.4.1. Materials and reagents

THF or diethyl ether used for the reactions has been dried and distilled prior to use. Salicylaldehyde and 1,8-diaminonaphthalene were purchased from Sigma-Aldrich and were used without further purification. The ligand **L1** was prepared according to the literature reported procedure.[29] Lithiation of the substrates were carried out according to literature-reported procedures. Chromatography was carried out using 60-120 mesh silica gel in a column.

2.4.2. Instrumentation

^{1}H and ^{13}C NMR spectra were obtained with BRUKER 300 MHz FT-NMR spectrometers and the chemical shifts are reported in ppm, using tetramethylsilane as an internal standard and were referenced to the residual solvent as follows: $CDCl_3$ = 7.26 (^{1}H), 76.16 (^{13}C) ppm at room temperature. For ^{1}H NMR, coupling constants *J* are given in Hz and the resonance multiplicity is described as s (singlet), d (doublet), t (triplet), m (multiplet). UV-vis spectrum has been obtained in Shimadzu-UV-1900i spectrophotometer. X-band EPR spectrum was recorded using a Bruker Biospin EMX^{micro} spectrometer at 100 K. Perkin Elmer LX-1 FT-IR spectrophotometer has been used for obtaining the IR spectra of the ligand and the complex. EDX image has been obtained from field-emission scanning electron microscope (FE-SEM, QUANTA FEG 250) with an electron energy of 20 keV. Melting points have been recorded manually in melting point apparatus.

2.4.3. Synthesis

2.4.3.1. Synthesis of ligand L1: Salicylaldehyde (386 mg, 3.16 mmol) and 1,8-diaminonaphthalene (500 mg, 3.16 mmol) were taken in a mortar and were grounded well with a pestle for about 10 min until a brown powder was produced. The brown powder was dissolved in dichloromethane and purified by column chromatography in silica gel with EtOAc/hexane 1:19 as eluant. Pure ligand **L1** was obtained as white crystalline solid (743 mg, 2.84 mmol, yield 90%), which was recrystallized from dichloromethane/hexane solution to give transparent white crystals. ^{1}H NMR (300 MHz, $CDCl_3$): δ = 8.55 (s, 1H), 7.39-7.22 (m, 6H), 7.14-7.04 (m, 1H), 6.90 (t, 1H), 6.33 (t, 1H), 5.53 (s, 1H), 4.55 (s, 2H).

2.4.3.2. Synthesis of complex 1: In a 100 mL round-bottom flask, ligand **L1** (100 mg, 0.381 mmol) was dissolved in ethanol (10 mL). A solution of $CoCl_2 \cdot 6H_2O$ (45.35 mg, 0.190 mmol) in ethanol was added dropwise to the ligand solution with continuous stirring. The colorless ligand solution becomes green upon addition of $CoCl_2 \cdot 6H_2O$. The reaction mixture was refluxed for 8 h. A dark-green precipitate was formed, which was collected by filtration of the reaction mixture, washed with ethanol several times and allowed to dry in the air. Finally, the complex [Co(**L1**)$_2$] (**1**) was dried under vacuum for 2 h. Its yield and characterization data are as follows: yield: 80%. ESI-MS: calcd. for $C_{34}H_{26}CoN_4O_2$ $[M]^+$ = 581.1387, found 581.1381.

2.4.4. Lithiation of compounds

All reactions have been performed under N_2 atmosphere through Schlenk line using *n*-BuLi as the lithiating agent. Reactions, where -78 ˚C is required, have been done using acetone/liq N_2 mixture.

1. 1,1'-biphenyl (**3a**): Compound **3a** has been prepared from iodobenzene in THF, according to literature reported procedure.[30]
2. [1,1'-biphenyl]-2,2'-diol (**3b**): Compound **3b** has been prepared from 2-bromophenol in diethyl ether, according to literature reported procedure.[31]
3. 4,4'-dimethyl-1,1'-biphenyl (**3c**): Compound **3c** has been prepared from lithiation of 4-bromotoluene, according to literature reported procedure.[32]
4. 3,3'-dimethoxy-1,1'-biphenyl (**3d**): Compound **3d** have been prepared from 3-bromoanisole by slight modification of literature reported procedure.[33] One equivalent of *n*-BuLi (0.213 ml, 2.5 M in hexane) was added to THF solution 3-bromoanisole (100 mg, 0.534 mmol) at -78 ˚C and stirred at the same temperature for 30 min, during which time colourless precipitate could be observed.

5. 4,4'-dimethoxy-1,1'-biphenyl (**3e**): Compound **3e** have been prepared from 4-bromoanisole by slight modification of literature reported procedure.[34] One equivalent of *n*-BuLi (0.213 ml, 2.5 M in hexane) was added to THF solution 4-bromoanisole (100 mg, 0.534 mmol) at room temperature and stirred at the same temperature for 2 h, during which time colourless precipitate could be observed.
6. 6,6'-difluoro-[1,1'-biphenyl]-3,3'-diol (**3f**): The same procedure as for **3b** was followed.
7. 3,3',5,5'-tetramethoxy-1,1'-biphenyl (**3g**): Compound **3g** has been prepared from lithiation of 3,5-dimethoxy-1-bromobenzene, according to literature reported procedure.[35]
8. 1,1'-bipyrene (**3h**): Compound **3h** has been prepared from 2-bromopyrene in THF, according to literature reported procedure.[36]
9. 2,2'-dimethyl-1,1'-binaphthalene (**3i**): Compound **3i** has been prepared from lithiation of 1-bromo-2-methyl-naphthalene, according to literature reported procedure.[37]
10. 2,2',6,6'-tetramethyl-1,1'-biphenyl (**3j**): Compound **3j** has been prepared from lithiation of 1,3-dimethyl-2-bromobenzene, according to literature reported procedure.[38]
11. 2,2'-bipyridine (**3k**): Compound **3k** has been prepared from lithiation of 2-bromopyridine, according to literature reported procedure.[39]
12. 1,1'-dimethyl-1*H*,1'*H*-2,2'-bibenzo[d]imidazole (**3l**): Compound **3l** has been prepared from lithiation of 1-methylbenzimidazole, by slight modification of literature reported procedure.[40] n-BuLi (1 equivalent, 0.6 ml, 2.5 M in hexane) was added dropwise to a solution of 1-methylbenzimidazole in THF at -78 ˚C and the mixture was stirred for 2 h at -78 ˚C, after which, the temperature of the reaction mixture was allowed to rise to room temperature within another 1 h.
13. 2,2'-bibenzo[d]thiazole (**3m**): Compound **3m** has been prepared from lithiation of benzothiazole, according to literature reported procedure.[41]
14. 1,1'-dimethyl-1*H*,1'*H*-2,2'-biindole (**3n**): Compound **3n** has been prepared from lithiation of 1-methylindole, according to literature reported procedure.[42]
15. 5,5'-dimethyl-2,2'-bithiophene (**3o**): Compound **3o** has been prepared from lithiation of 2-methylthiophene, according to literature reported procedure.[43]
16. Biferrocene (**3p**): Compound **3p** has been prepared from lithiation of ferrocene, according to literature reported procedure.[44]
17. 1,1'-dimethyl-1*H*,1'*H*-2,2'-biimidazole (**3q**): Compound **3q** has been prepared from lithiation of 1-methylimidazole, according to literature reported procedure.[45]

18. 5-bromo-4,5'-bipyrimidine (**3r**): Compound **3r** has been prepared from 5-bromopyrimidine in THF, according to literature reported procedure.[46]
19. 5,5'-dibromo-2,2'-bipyridine (**3s**): Compound **3s** has been prepared from 3-bromopyridine in diethyl ether, according to procedure reported in patent.[47]
20. 3-bromo-1,1':3',1"-terphenyl (**3t**) and 3,3'"-dibromo-1,1':3',1":3",1'"-quaterphenyl (**3u**): Compounds **3t** and **3u** have been prepared by the lithiation of 1,3-dibromobenzene according to literature reported procedure.[48]
21. 1,1':3',1":3",1'"-quaterphenyl (**3v**): Compound **3v** has been prepared from lithiation of 1-iodo-3-bromobenzene, according to literature reported procedure.[49]

2.4.5. General procedure for the catalytic reaction

A Schlenk tube equipped with a stir bar was evacuated and back-filled with nitrogen successively for three times. The arene/heteroarene (1.0 mmol) was charged into it and dissolved in freshly dried THF solvent (5 ml). *n*-BuLi (1.0 mmol) was added dropwise to the solution after maintaining proper temperature condition (-78 ˚C/ 0 ˚C/ rt) for each substrate. After the lithiation is complete, Zn dust (0.2 mmol) and the catalyst **1** (0.02 mmol) were added successively at room temperature and the solution was stirred for 2-4 h at that temperature. After 2-4 h, the reaction mixture was extracted with EtOAc (3×20 ml) and water. The organic phase was dried by adding Na_2SO_4 and then under reduced pressure. The crude product was purified by column chromatography on silica gel (EtOAc/pet ether) to afford corresponding product.

2.4.6. Procedure for large-scale reactions

Large-scale (Gram-scale) reactions using the developed catalyst system have been optimized with 2-bromopyridine and 2-methylthiophene as the reactants. 1 g each of the reactants was taken in a Schlenk flask and 1 equivalent of *n*-BuLi was added at -78 ˚C and stirred for 2.5 h (for 2-bromopyridine) and 30 mins (for 2-methylthiophene) at that temperature. Zn dust (0.2 equiv) and catalyst **1** (0.02 equiv) were added to the reaction mixture and allowed to stir for 4 h. The reaction mixture was extracted with EtOAc (3×50 ml) and water. The organic phase was dried by adding Na_2SO_4 and then under reduced pressure. The crude product was purified by column chromatography on silica gel (EtOAc/pet ether) to afford corresponding products in 70 % (for 2-bromopyridine) and 75 % (for 2-methylthiophene) yield.

Table 2.4 Table for known and unknown compounds.

Known Compounds	Unknown compounds
3a-3t	**3u, 3v**

2.5. Analytical data of all synthesized compounds

n.b. Yields are reported after isolation by column chromatography

1,1'-biphenyl (**3a**): Colorless solid (yield 78%), m. p. 66 ˚C (lit[50a] 68-69 ˚C), ^{1}H NMR (300 MHz, $CDCl_3$): δ = 7.61 (dd, 2H, J_1 = 4.5 Hz, J_2 = 3 Hz), 7.45 (td, 2H, J_1 = 3 Hz, J_2 = 3 Hz), 7.35 (tt, 1H, J_1 = 3 Hz, J_2 = 6 Hz). ^{13}C NMR (75 MHz, $CDCl_3$): 140.9, 128.5, 127.0, 126.9.

[1,1'-biphenyl]-2,2'-diol (**3b**): Yellow liquid (yield 78%). ^{1}H NMR (300 MHz, $CDCl_3$): δ = 7.33-7.30 (m, 2H), 7.27-7.22 (m, 2H), 6.99 (t, 4H, *J* = 6Hz), 5.92 (s, 2H). ^{13}C NMR (75 MHz, $CDCl_3$): 154.1, 131.5, 129.5, 125.9, 120.9, 117.4.

4,4'-dimethyl-1,1'-biphenyl (**3c**): White solid (yield 79%), m. p. 116.8 ˚C (lit[50b] 119-120 ˚C), ^{1}H NMR (300 MHz, $CDCl_3$): δ = 7.47 (d, 2H, *J* = 9 Hz), 7.23 (d, 2H, *J* = 9 Hz), 2.39 (s, 3H). ^{13}C NMR (75 MHz, $CDCl_3$): 138.4, 136.8, 129.6, 126.9, 21.2.

3,3'-dimethoxy-1,1'-biphenyl (**3d**): Light Yellow solid (yield 83%), m. p. 40 ˚C (lit[50c] 41-42 ˚C), ^{1}H NMR (300 MHz, $CDCl_3$): δ = 7.36 (t, 1H, *J* = 6 Hz), 7.18 (dt, 1H, J_1 = 6 Hz, J_2 = 3 Hz), 7.14-7.12 (m, 1H), 6.91 (dd, 1H, J_1 = 6 Hz, J_2 = 3 Hz), 3.87 (s, 3H). ^{13}C NMR (75 MHz, $CDCl_3$): 160.0, 142.9, 129.9, 119.8, 113.1, 112.9, 55.4.

4,4'-dimethoxy-1,1'-biphenyl (**3e**): Colorless solid (yield 75%), m. p. 179.8 ˚C (lit[50b] 179-180 ˚C), ^{1}H NMR (300 MHz, $CDCl_3$): δ = 7.47 (d, 2H, *J* = 9 Hz), 6.95 (d, 2H, *J* = 9 Hz), 3.84 (s, 3H). ^{13}C NMR (75 MHz, $CDCl_3$): 158.8, 133.6, 127.8, 114.3, 55.5.

5,5'-difluoro-[1,1'-biphenyl]-2,2'-diol (**3f**): White solid (yield 74%), m. p. 148 ˚C (lit[50d] 147-149 ˚C), ^{1}H NMR (300 MHz, $CDCl_3$): δ = 7.02-6.79 (m, 3H). ^{19}F NMR (300 MHz, $CDCl_3$): δ = -121.3. ^{13}C NMR (75 MHz, $CDCl_3$): 120.5, 120.0, 119.5, 119.5, 116.5, 116.5.

3,3',5,5'-tetramethoxy-1,1'-biphenyl (**3g**): White solid (yield 85%), m. p. 109 ˚C (lit[50e]109-111 ˚C), ^{1}H NMR (300 MHz, $CDCl_3$): δ = 6.71 (d, 4H, *J* = 3 Hz), 6.47 (t, 2H, *J* = 3 Hz), 3.84 (s, 12H). ^{13}C NMR (75 MHz, $CDCl_3$): 161.1, 143.6, 105.6, 99.6, 55.6.

1,1'-bipyrene (**3h**): Light Yellowish-green solid (yield 85%), m. p. 320 ˚C (lit[50f] 327-328 ˚C), ^{1}H NMR (300 MHz, $CDCl_3$): δ = ^{1}H NMR (75 MHz, $CDCl_3$): 8.45 (s, 1H), 8.35 (t, 2H, *J* = 9 Hz), 8.27-8.14 (m, 12H), 8.09-8.02 (m, 3H). ^{13}C NMR (75 MHz, $CDCl_3$): 139.1, 138.1, 136.4, 131.4, 128.6, 128.1, 127.9, 127.6, 127.2, 126.2, 125.9, 125.5, 125.4, 125.0, 124.8, 123.9.

2,2'-dimethyl-1,1'-binaphthalene (**3i**): White solid (yield 79%), m. p. 79 ˚C (lit[50g] 77-79 ˚C), ^{1}H NMR (300 MHz, $CDCl_3$): δ = 7.89 (t, 4H, *J* = 6 Hz), 7.51 (d, 2H, *J* = 6 Hz), 7.43-7.38 (m, 2H), 7.21 (t, 2H, *J* = 6 Hz), 7.05 (d, 2H, *J* = 6 Hz), 2.04 (s, 6H). ^{13}C NMR (75 MHz, $CDCl_3$): 135.2, 134.4, 132.9, 132.3, 128.8, 128.0, 127.5, 126.2, 125.7, 125.0.

2,2',6,6'-tetramethyl-1,1'-biphenyl (**3j**): Yellow liquid (yield 20%), ^{1}H NMR (300 MHz, $CDCl_3$): δ = 7.07-6.97 (m, 6H), 2.44 (s, 12H).

2,2'-bipyridine (**3k**): Colorless solid (yield 75%), m. p. 70 ˚C (lit[50h] 71-72 ˚C), ^{1}H NMR (300 MHz, $CDCl_3$): δ = 8.69 (dt, 1H, J_1 = 3 Hz, J_2 = 3 Hz), 8.39 (dt, 1H, J_1 = 3 Hz, J_2 = 6 Hz), 7.82 (td, 1H, J_1 = 3 Hz, J_2 = 6 Hz), 7.31 (ddd, 1H, J_1 = 3 Hz, J_2 = 3 Hz). ^{13}C NMR (75 MHz, $CDCl_3$): 177.2, 149.3, 137.0, 123.8, 121.2.

1,1'-dimethyl-1*H*,1'*H*-2,2'-bibenzoimidazole (**3l**): Colorless solid (yield 80%), m. p. 208 ˚C (lit[50i] 208-209 ˚C), ^{1}H NMR (300 MHz, $CDCl_3$): δ = 7.88 (dd, 1H, J_1 = 3 Hz, J_2 = 6 Hz), 7.50 (dd, 1H, J_1 = 3 Hz, J_2 = 6 Hz), 7.44-7.34 (m, 2H), 4.34 (s, 3H). ^{13}C NMR (75 MHz, $CDCl_3$): 143.4, 142.7, 136.4, 124.1, 123.0, 120.5, 110.2, 32.6.

2,2'-dibenzothiazole (**3m**): White crystalline solid (yield 75%), m. p. 238 ˚C (lit[50j] 239-240 ˚C), ^{1}H NMR (300 MHz, $CDCl_3$): δ = 8.17 (dd, 1H, J_1 = 3 Hz, J_2 = 6 Hz), 7.99 (dd, 1H, J_1 = 3 Hz, J_2 = 6 Hz), 7.57 (td, 1H, J_1 = 3 Hz, J_2 = 6 Hz), 7.49 (td, 1H, J_1 = 6 Hz, J_2 = 9 Hz). ^{13}C NMR (75 MHz, $CDCl_3$): 161.7, 153.7, 135.9, 127.0, 126.8, 124.2, 122.2.

1,1'-dimethyl-1*H*,1'*H*-2,2'-biindole (**3n**): White solid (yield 84%), m. p. 164 ˚C (lit[50k] 172-174 ˚C), ^{1}H NMR (300 MHz, $CDCl_3$): δ = 7.69 (dt, 1H, J_1 = 3 Hz, J_2 = 6 Hz), 7.41 (dd, 1H, J_1 = 3 Hz, J_2 = 6 Hz), 7.31 (td, 1H, J_1 = 3 Hz, J_2 = 6 Hz), 7.19 (td, 1H, J_1 = 3 Hz, J_2 = 6 Hz), 3.72 (s, 1H). ^{13}C NMR (75 MHz, $CDCl_3$): 138.0, 131.7, 127.7, 122.4, 120.9, 120.2, 109.8, 104.5, 30.9.

5,5'-dimethyl-2,2'-bithiophene (**3o**): White solid (yield 78%), m. p. 58 ˚C (lit[50l] 59-61 ˚C), ^{1}H NMR (300 MHz, $CDCl_3$): δ = 6.87 (d, 1H, *J* = 3 Hz), 6.63 (d, 1H, *J* = 6 Hz), 2.46 (s, 3H). ^{13}C NMR (75 MHz, $CDCl_3$): 138.6, 135.6, 125.8, 123.0, 15.4.

Biferrocene (**3p**): Yellow solid (yield 50%), m. p. 236 ˚C (lit[50m] 239-240 ˚C), ^{1}H NMR (300 MHz, $CDCl_3$): δ = 4.35 (t, 2H, *J* = 3 Hz), 4.17 (t, 2H, *J* = 3 Hz), 3.99 (s, 5H). ^{13}C NMR (75 MHz, $CDCl_3$): 84.1, 69.3, 67.7, 66.5.

1,1'-dimethyl-1*H*,1'*H*-2,2'-biimidazole (**3q**): White solid (yield 89%), m. p. 104 ˚C (lit[50i] 105-106 ˚C), ^{1}H NMR (300 MHz, $CDCl_3$): δ = 7.11 (d, 1H), 6.96 (s, 1H), 4.03 (s, 3H). ^{13}C NMR (75 MHz, $CDCl_3$): 138.7, 127.9, 122.8, 35.5.

5-bromo-4,5'-bipyrimidine (**3r**): White solid (yield 78%), m. p. 112 ˚C (lit[50n] 119-120 ˚C), ^{1}H NMR (300 MHz, $CDCl_3$): δ = 9.35 (s, 1H), 9.26 (s, 2H), 9.24 (s, 1H), 9.00 (s, 1H). ^{13}C NMR

(75 MHz, $CDCl_3$): 160.7, 159.6, 159.0, 157.5, 157.24, 119.24. ESI-MS: calcd. for $C_8H_5N_4Br$ $[M+H]^+$ = 236.9775, found 236.976.

5,5'-dibromo-2,2'-bipyridine (**3s**): White solid (yield 60%), m. p. 204 ˚C (lit[50o] 205 ˚C), ^1H NMR (300 MHz, $CDCl_3$): δ = 8.88 (s, 2H), 8.64 (d, 2H, *J* = 3 Hz), 7.18 (d, 2H, *J* = 3 Hz). ^{13}C NMR (75 MHz, $CDCl_3$): 152.6, 148.5, 146.8, 135.4, 124.7.

3-bromo-1,1':3',1"-terphenyl (**3t**): Colorless oil (yield 40%). ^1H NMR (300 MHz, $CDCl_3$): δ = 7.70 (s, 2H), 7.58-7.40 (m, 7H), 7.36-7.29 (m, 4H). ^{13}C NMR (75 MHz, $CDCl_3$): 141.9, 133.3, 132.5, 132.2, 131.2, 130.9, 130.7, 130.5, 130.3, 130.1, 129.6, 129.4, 128.8, 128.3, 127.6, 125.9, 125.7, 123.1.

3,3'"-dibromo-1,1':3',1":3",1'"-quaterphenyl (**3u**): White liquid (yield 40%). ^1H NMR (300 MHz, $CDCl_3$): δ = 7.78 (t, 2H, *J* = 3 Hz), 7.71 (s, 1H), 7.57-7.49 (m, 10H), 7.33 (t, 3H, *J* = 6 Hz). ^{13}C NMR (75 MHz, $CDCl_3$): 143.2, 140.6, 132.0, 130.6, 130.5, 130.4, 130.3, 129.6, 126.8, 126.1, 126.0, 123.1. Anal. Calcd for $C_{24}H_{16}Br_2$, C, 62.10; H, 3.47. Found: C, 61.11; H, 4.27.

1,1':3',1":3",1'"-quaterphenyl (**3v**): Colorless oil (yield 78%). ^1H NMR (300 MHz, $CDCl_3$): δ = 7.98 (s, 1H), 7.78 (t, 2H, *J* = 3 Hz), 7.70 (d, 3H, *J* = 6 Hz), 7.57-7.49 (m, 9H), 7.33 (t, 3H, *J* = 6 Hz). ^{13}C NMR (75 MHz, $CDCl_3$): 140.6, 136.6, 136.4, 130.6, 130.5, 130.4, 129.6, 126.8, 126.0, 123.12. ESI-MS: calcd. for $C_{24}H_{18}$ $[M+Na]^+$ = 329.1306, found 329.1305. Anal. Calcd for $C_{24}H_{18}$, C, 94.08; H, 5.92. Found: C, 93.77; H, 5.43.

2.6. References

1. (a) Baudoin, O.; Gueritte, F. *Stud. Nat. Prod. Chem.* **2003**, *29*, 355-417. (b) Yang, Y.; Lan, J.; You, J. *Chem. Rev.* **2017**, *117*, 8787−8863.
2. Joule, J. A. Natural products containing nitrogen heterocycles-some highlights. 1990-2015, Chapter 4, Volume *119*, Advances in Heterocyclic Chemistry, **2016** Elsevier Inc.
3. (a) Ullmann, F.; Bielecki, J. *Ber. Dtsch. Chem. Ges.* **1901**, *34*, 2174-2185. (b) Hassan, J.; Sévignon, M.; Gozzi, C.; Schulz, E.; Lemaire, M. *Chem. Rev.* **2002**, *102,* 1359-1470.
4. (a) Yang, Q.; Zhao, Y.; Ma, D. *Org. Process Res. Dev.* **2022**, *26*, 1690−1750, (b) Ajitha, M. J.; Pary, F.; Nelson, T. L.; Musaev, D. G. *ACS Catal.* **2018**, *8*, 4829−4837, (c) Hassan, J.; Sévignon, M.; Gozzi, C.; Schulz, E.; Lemaire, M. *Chem. Rev.* **2002**, *102*, 1359-1469. (d) Sambiagio, C.; Marsden, S. P.; Blacker A. J.; McGowan, P. C. *Chem. Soc. Rev.* **2014**, *43*, 3525-3550.
5. (a) Metal-catalyzed cross-coupling reactions and more, Vol 1 (Eds.: de Meijere, A.; Bräse, S.; Oestreich, M.), Wiley-VCH, Weinheim, **2013**; (b) Transition metals for organic synthesis

(Eds.: Beller, M.; Bolm, C.), Wiley-VCH, Weinheim, **2004**. (c) Newkome, G. R.; Hager, D. C. *J. Org. Chem.* **1982**, *47*, 599–601.

6. (a) Savage, S. A.; Smith A. P.; Fraser, C. L. *J. Org. Chem.* **1998**, *63*, 10048–10051. (b) Luzung, M. R.; Patel J. S.; Yin, J. *J. Org. Chem.* **2010**, *75*, 8330−8332. (c) Lützen A.; Hapke, M. *Eur. J. Org. Chem.* **2002**, 2292–2297. (d) Zeng, J.; Liu, K. M.; Duan, X. F. *Org. Lett.* **2013**, *15*, 5342-5345. (e) Hammann, J. M.; Lutter, F. H.; Haas, D. Knochel, P. *Angew. Chem. Int. Ed.* **2017**, *56*, 1082-1086.
7. (a) Lithium Compounds in Organic Synthesis (Eds.: Luisi, R.; Capriati, V.), Wiley-VCH, Weinheim, **2014**. (b) Snieckus, V. *Chem. Rev.* **1990**, *90*, 879-933. (c) Board, J.; Cosman, J. L.; Rantanen, T.; Singh, S. P.; Snieckus, V. *Platinum Met. Rev.* **2013**, *57*, 234-258.
8. (a) Liu, Y.; Bergès, J.; Zaid, Y.; Chahdi, F. O.; Lee, A. V. D.; Harakat, D.; Clot, E.; Jaroschik, F.; Taillefer, M. *J. Org. Chem.* **2019**, *84*, 4413−4420. (b) Wang, Z. -Y.; Peng X. -S.; Wong, H. N. C. *Asian J. Org. Chem.* **2020**, *9*, 1834. (c) Scherpf, T.; Steinert, H.; Großjohann, A.; Dilchert, K.; Tappen, J.; Rodstein I.; Gessner, V. H. *Angew. Chem. Int. Ed.* **2020**, *59*, 20596–20603.
9. (a) Synthesis of Biaryls (Ed.: Cepanec, I.), Elsevier, Amsterdam, **2004**. (b) Bringmann, G.; Walter, R.; Weirch, R. *Angew. Chem. Int. Ed. Engl.* **1990**, *29*, 977-991. (c) Bringmann, G.; Price Mortimer, A. J.; Keller, P. A.; Gresser, M. J.; Garner, J.; Breuning, M. *Angew. Chem. Int. Ed.* **2005**, *44*, 5384-5427. (d) Wencel-Delord, J.; Panossian, A.; Leroux, F. R.; Colobert, F. *Chem. Soc. Rev.* **2015**, *44*, 3418-3430.
10. Buter, J.; Heijnen, D.; Vila, C.; Hornillos, V.; Otten, E.; Giannerini, M.; Minnaard, A. J.; Feringa, B. L. *Angew. Chem. Int. Ed.* **2016**, *55*, 3620–3624.
11. (a) Hull, K. L.; Lanni, E. L.; Sanford, M. S. *J. Am. Chem. Soc.* **2006**, *128*, 14047−14049. (b) Xia, J. -B.; Wang, X. -Q.; You, S. -L. *J. Org. Chem.* **2009**, *74*, 456−458. (c) Li, N. -N.; Zhang, Y. -L.; Mao, S.; Gao, Y. -R.; Guo D. -D.; Wang, Y. -Q. *Org. Lett.* **2014**, *16*, 2732−2735.
12. (a) Zhu, M.; Fujita, K.; Yamaguchi, R. *Chem. Commun.* **2011**, *47*, 12876−12878. (b) Li, Y.; Jin, J.; Qian W.; Bao, W. *Org. Biomol. Chem.* **2010**, *8*, 326−330. (b) Monguchi, D.; Yamamura, A.; Fujiwara, T.; Somete, T.; Mori, A. *Tetrahedron Lett.* **2010**, *51*, 850−852.
13. Truong, T.; Alvarado, J.; Tran, L. D.; Daugulis, O. *Org. Lett.* **2010**, *12*, 1200−1203.
14. Liang, Z.; Zhao, J.; Zhang, Y. *J. Org. Chem.* **2010**, *75*, 170−177.

15. (a) Masui, K.; Ikegami, H.; Mori, A. *J. Am. Chem. Soc.* **2004**, *126*, 5074−5075. (b) Kim, S. -H.; Rieke, R. D. *Tetrahedron* **2010**, *66*, 3135-3146. (c) Sreejyothi, P.; Sau, S. C.; Vardhanapu, P. K.; Mandal, S. K. *J. Org. Chem.* **2018**, *83*, 9403−9411.
16. Fang, Y. -Q.; Hanan, G. S. *Synlett* **2003**, 852–854.
17. Clark, R. J. H. *Spectrochim. Acta* **1965**, *21*, 955-963.
18. Stubbert, B. D.; Peters, J. C.; Gray, H. B. *J. Am. Chem. Soc*. **2011**, *133*, 18070–18073.
19. Shiekh, R. A.; Rahman, I. A.; Malik, M. A.; Masudi, S. M.; Luddin, N. *Int. J. Electrochem. Sci.* **2012**, *7*, 12829 –12845.
20. (a) Hagen, W. R. *Dalton Trans.* **2006**, 4415–4434. (b) Stoll, S.; Schweiger, A. *J. Magnetic Resonance* **2006**, *178*, 42-55.
21. (a) Liu, F.; Zhong, J.; Zhou, Y.; Gao, Z.; Walsh, P. J.; Wang, X.; Ma, S.; Hou, S.; Liu, S.; Wang, M.; Wang, M.; Bian, Q. *Chem. Eur. J.* **2018**, *24*, 2059-2064. (b) Haas, D.; Hammann, J. M.; Greiner, R.; Knochel, P. *ACS Catal.* **2016**, *6*, 1540−1552.
22. (a) Perepichka, D. F.; Rosei, F. *Science* **2009**, *323*, 216–217. (b) Colson, J. W.; Dichtel, W. R. *Nat. Chem.* **2013**, *5*, 453–465. (c) Gutzler, R.; Perepichka, D. F. *J. Am. Chem. Soc.* **2013**, *135*, 16585–16594.
23. Long, C. -Y.; Chen, H.; Ma, C.; Zhao, B. -W.; Li, S. -H.; Cui, Y.; Yang, X.; Ni, S. -F.; Wang, X. -Q. *Org. Lett.* **2022**, *24*, 4155–4159.
24. LeVanda, C.; Bechgaard, K.; Cowan, D. O.; Rausch, M. D. *J. Am. Chem. Soc.* **1977**, *99*, 2964–2968.
25. Zhang, S.; Kolluru, L.; Vedula, S. K.; Whippie, D.; Jin, J. *Tetrahedron Lett.* **2017**, *58*, 3594–3597.
26. Timelthaler, D.; Topf, C. *J. Org. Chem.* **2019**, *84*, 11604–11611.
27. (a) Hirano, M. *ACS Catal.* **2019**, *9*, 1408−1430. (b) Herbort, J. H.; Lalisse, R. F.; Hadad, C. M.; RajanBabu, T. V. *ACS Catal.* **2021**, *11*, 9605−9617. (c) Hilt, G.; Lüers, S.; Harms, K. *J. Org. Chem.* **2004**, *69*, 624-630. (d) Nogi, K.; Fujihara, T.; Terao, J.; Tsuji, Y. *J. Am. Chem. Soc.* **2016**, *138*, 5547−5550. (e) Aresta, M.; Rossi, M.; Sacco, A. *Inorg. Chim. Acta* **1969**, *3*, 227-231. (f) Ma, B.; Snyder, J. K. *Organometallics* **2002,** *21,* 4688-4695.
28. Biswas, S.; Parsutkar, M. M.; Jing, S. M.; Pagar, V. V.; Herbort, J. H.; RajanBabu, T. V. *Acc. Chem. Res.* **2021**, *54*, 4545−4564.
29. Harry, N. A.; Radhika, S.; Neetha, M.; Anilkumar, G. *J. Heterocyclic Chem.* **2020**, *57*, 2037–2043.

30. Roberts, A. J.; Kennedy, A. R.; McLellan, R.; Robertson, S. D.; Hevia, E. *Eur. J. Inorg. Chem.* **2016**, *2016*, 4752-4760.
31. Yu, X.; Zhang, L.; Hana, X.; Wang, J.; Tian, Y.; Liu, G. *J. Organometal. Chem.* **2017**, *833*, 50-53.
32. DeMott, J. C.; Bhuvanesh, N.; Ozerov, O. V. *Chem. Sci.* **2013**, *4*, 642-649.
33. Beak, P.; Selling, G. W. *J. Org. Chem.* **1989**, *54*, 5574-5580.
34. Harder, S.; Boersma, J.; Brandsma, L.; Kanters, J. A.; Duisenberg, A. J. M.; Van Lenthe, J. H. *Organometallics* **1990**, *9*, 511-516.
35. Punch, K. A.; Piggott, M. J. *Org. Biomol. Chem.* **2014**, *12*, 2801-2810.
36. Fang, Q.; Li, J.; Li, S.; Duan, R.; Wang, S.; Yi, Y.; Guo, X.; Qian, Y.; Huang, W.; Yang, G.; *Chem. Commun.* **2017**, *53*, 5702-5705.
37. Hoffend, C.; Diefenbach, M.; Januszewski, E.; Bolte, M.; Lerner, H. -W.; Holthausen, M. C.; Wagner, M. *Dalton Trans.* **2013**, *42*, 13826-13837.
38. Dupont, J.; Beydoun, N.; Pfeffer, M. *J. Chem. Soc., Dalton Trans.* **1989**, 1715-1720.
39. García-Romero, Á.; Plajer, A. J.; Miguel, D.; Wright, D. S.; Bond, A. D.; Álvarez, C. M.; García-Rodríguez, R. *Inorg. Chem.* **2020**, *59*, 7103-7116.
40. Kojima, H.; Yamamoto, K.; Kinoshita, Y.; Inoue, H. *J. Het. Chem.* **1992**, *29*, 1473-1476.
41. Hidenori, C.; Megumi, I.; Keiji, O.; Kazuyoshi, I. *Bull. Chem. Soc. Jpn.* **1988**, *61*, 3637-3648.
42. Gao, B.; Li, S.; Wu, P.; Moses, J. E.; Sharpless, K. B. *Angew. Chem. Int. Ed.* **2018**, *57*, 1939-1943.
43. Takeda, N.; Kobori, Y.; Okamura, K.; Yasui, M.; Ueda, M. *Org. Lett.* **2020**, *22*, 9740-9744.
44. Erb, W.; Mongin, F. *Synthesis* **2019**, *51*, 146–160.
45. Vagedes, D.; Kehr, G.; König, D.; Wedeking, K.; Fröhlich, R.; Erker, G.; Mück-Lichtenfeld, C.; Grimme, S. *Eur. J. Inorg. Chem.* **2002**, *2002*, 2015-2021.
46. Au Yeung, K. H.; Kühne, T.; Eisenhut, F.; Kleinwächter, M.; Gisbert, Y.; Robles, R.; Lorente, N.; Cuniberti, G.; Joachim, C.; Rapenne, G.; Kammerer, C.; Moresco, F. *J. Phys. Chem. Lett.* **2020**, *11*, 6892-6899.
47. Seiji, A.; Toshiaki, Y.; Tomohide, M.; Chieno, M. JP2009023914A.
48. Matera, C.; Quadri, M.; Sciaccaluga, M.; Pomè, D. Y.; Fasoli, F.; De Amici, M.; Fucile, S.; Gotti, C.; Dallanoce, C.; Grazioso, G. *Eur. J. Med. Chem.* **2016**, *108*, 392-405.
49. Fukumoto, H.; Ando, M.; Shiota, T.; Izumiya, H.; Kubota, T. *Macromolecules* **2017**, *50*, 865−871.

50. (a) Cheng, J.; Tang L.; Xu, J. *Adv. Synth. Catal.* **2010**, *352*, 3275-3286. (b) Stibingerova, I.; Voltrova, S.; Kocova, S.; Lindale, M.; Srogl, J. *Org. Lett.* **2016**, *18*, 312–315. (c) Zeng, M.; Du, Y.; Qi, C.; Zuo, S.; Li, X.; Shao, L.; Zhang, X. -M. *Green Chem.* **2011**, *13*, 350-356. (d) Long, C. -Y.; Chen, H.; Ma, C.; Zhao, B. -W.; Li, S. -H.; Cui, Y.; Yang, X.; Ni, S. -F.; Wang, X. -Q. *Org. Lett.* **2022**, *24*, 4155–4159. (e) Chaumont, C.; Mobian, P.; Kyritsakas, N.; Henry, M. *CrystEngComm* **2013**, *15*, 6845–6862. (f) Nefedov, V. A.; *Russian J. Org. Chem.* **2007**, *43*, 1163–1166. (g) Ikunaka, M.; Maruoka, K.; Okuda, Y.; Ooi, T. *Org. Proc. Res. Dev.* **2003**, *7*, 644–648. (h) Yuan, C.; Zheng, L.; Zhao, Y. *Molecules* **2019**, *24*, 3678. (i) Li, Y.; Jin, J.; Qian, W.; Bao, W. *Org. Biomol. Chem.* **2010**, *8*, 326-330. (j) Rahim, A.; Shaik, S. P.; Baig, M. F.; Alarific, A.; Kamal, A. *Org. Biomol. Chem.* **2018**, *16*, 635-644. (k) X.-H. Xu, G.-K. Liu, A. Azuma, E. Tokunaga, and N. Shibata, *Org. Lett.* **2011**, *13*, 4854–4857. (l) Li, Y.; Wang, J.; Huang, M.; Wang, Z.; Wu, Y.; Wu, Y. *J. Org. Chem.* **2014**, *79*, 2890–2897. (m) Macdonald, A. C.; Trotter, J. *Acta Cryst.* **1964**, *17*, 872. (n) Gronowitz, S.; Röe, J.; *Acta Chem. Scand.* **1965**, *19*, 1741-1748. (o) Schwab, P. F. H.; Fleischer, F.; Michl, J. *J. Org. Chem.* **2002**, *67*, 443–449.

Spectroscopic details

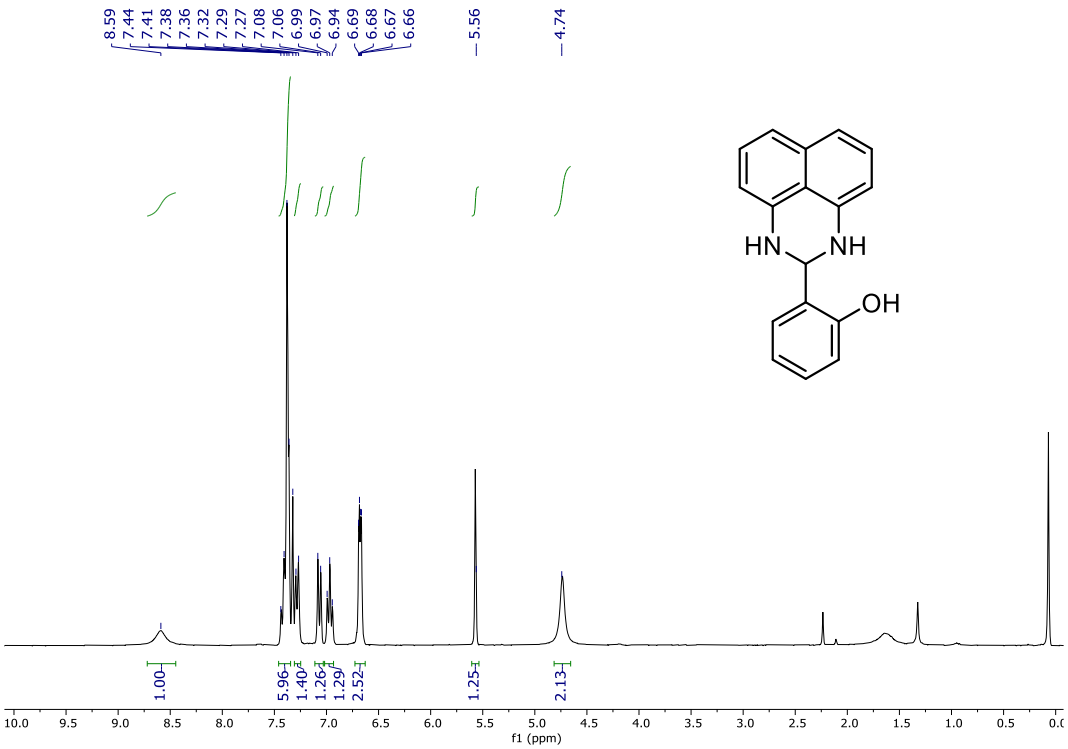

Figure 2.3. ^{1}H NMR spectra of ligand **L1** in $CDCl_3$.

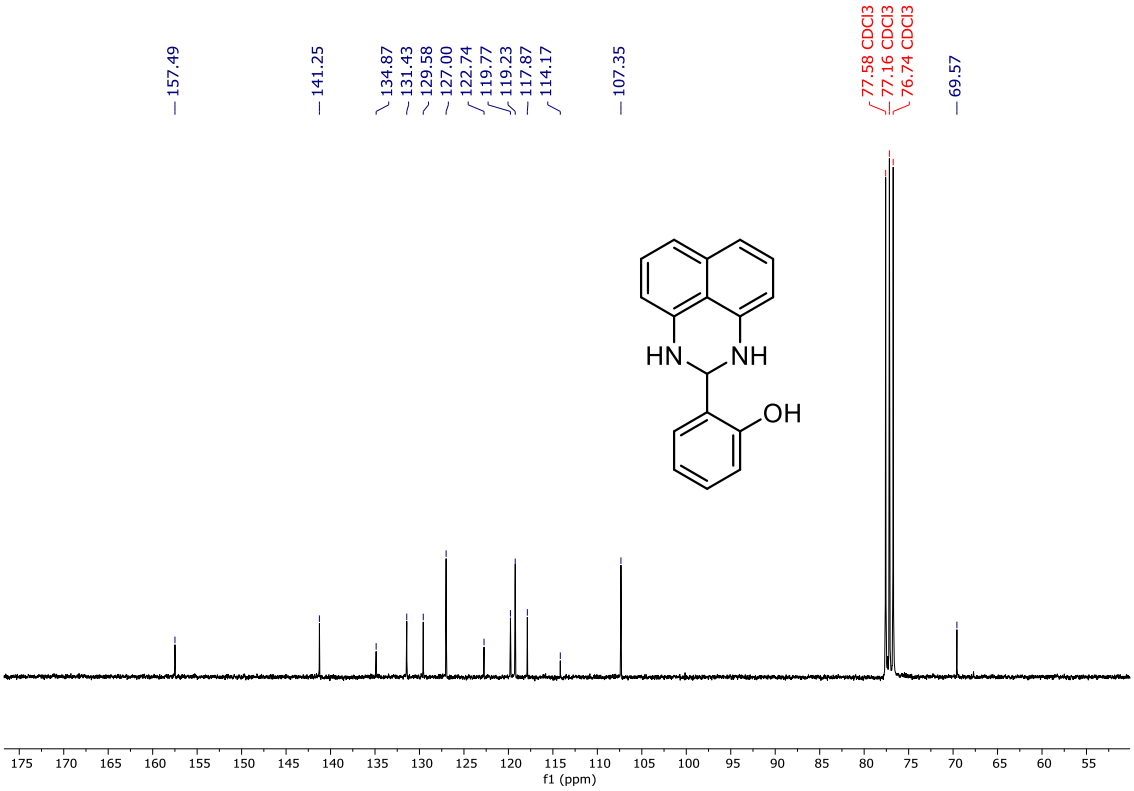

Figure 2.4. ^{13}C NMR spectra of ligand **L1** in $CDCl_3$.

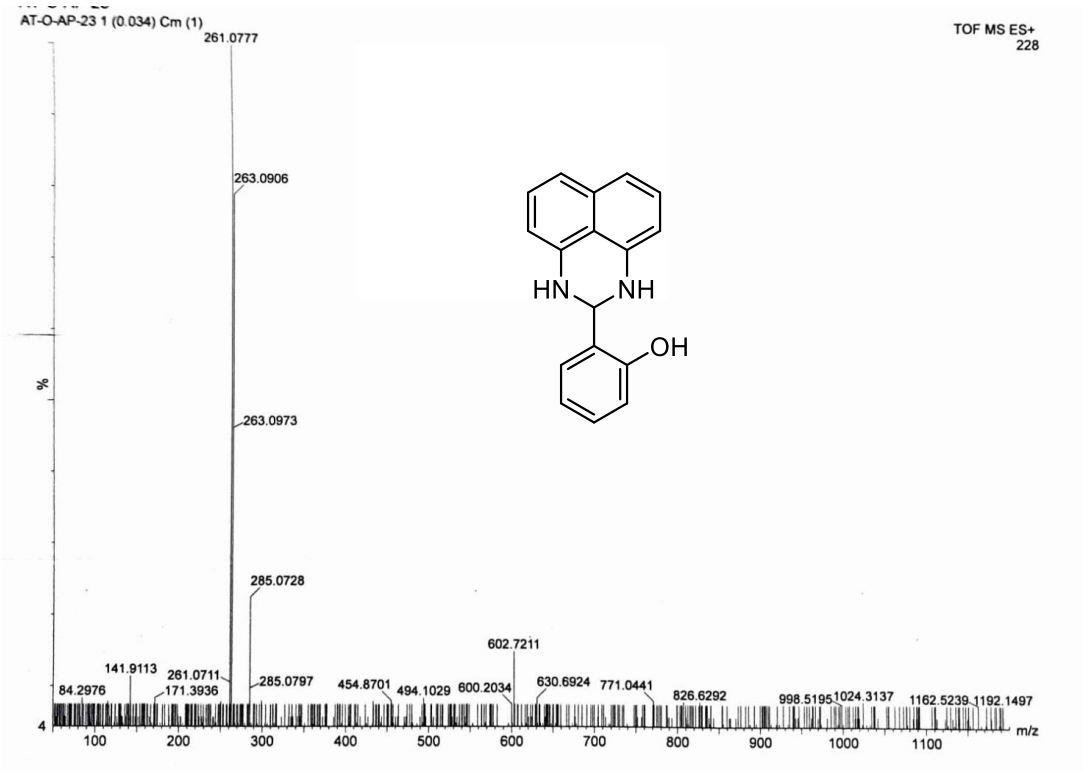

Figure 2.5. HRMS of ligand **L1**.

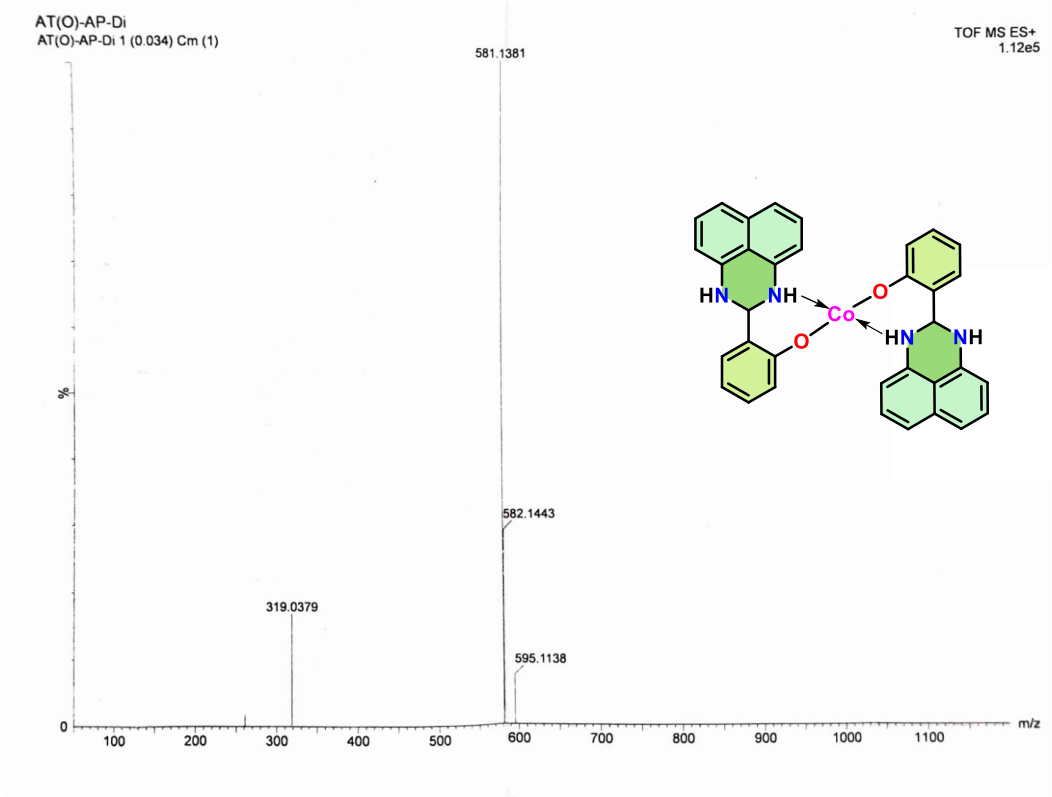

Figure 2.6. HRMS of complex **1**.

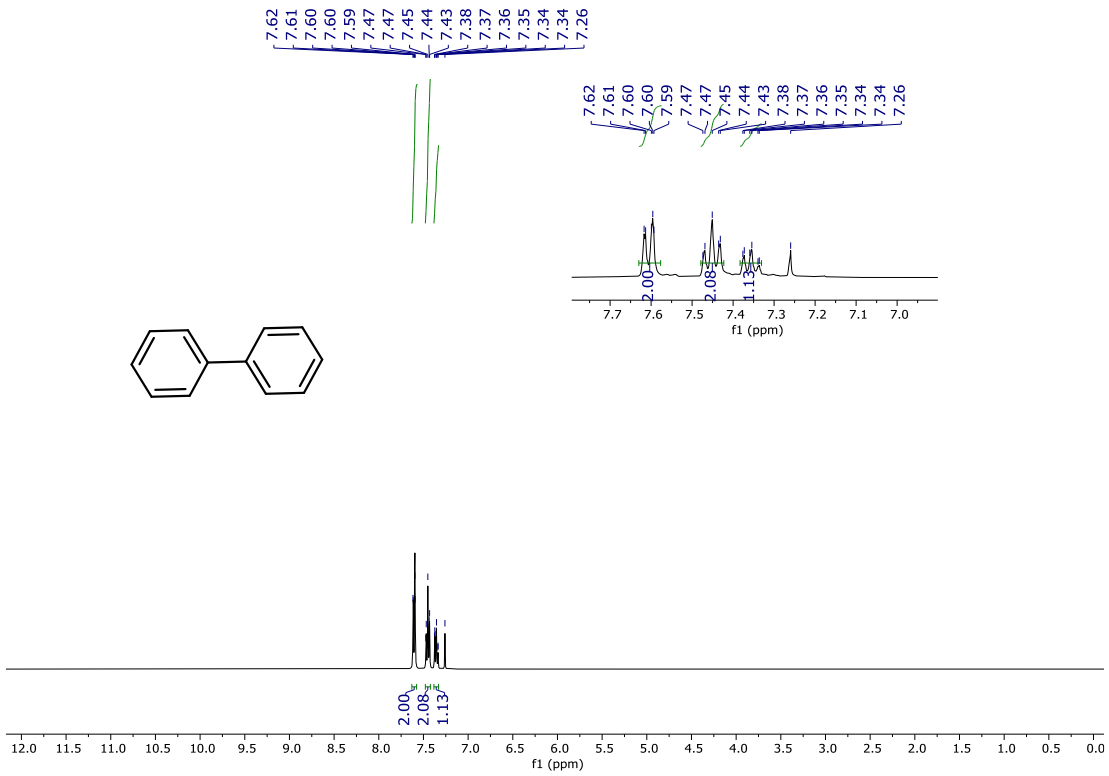

Figure 2.7. ^{1}H NMR spectra of compound **3a** in $CDCl_3$.

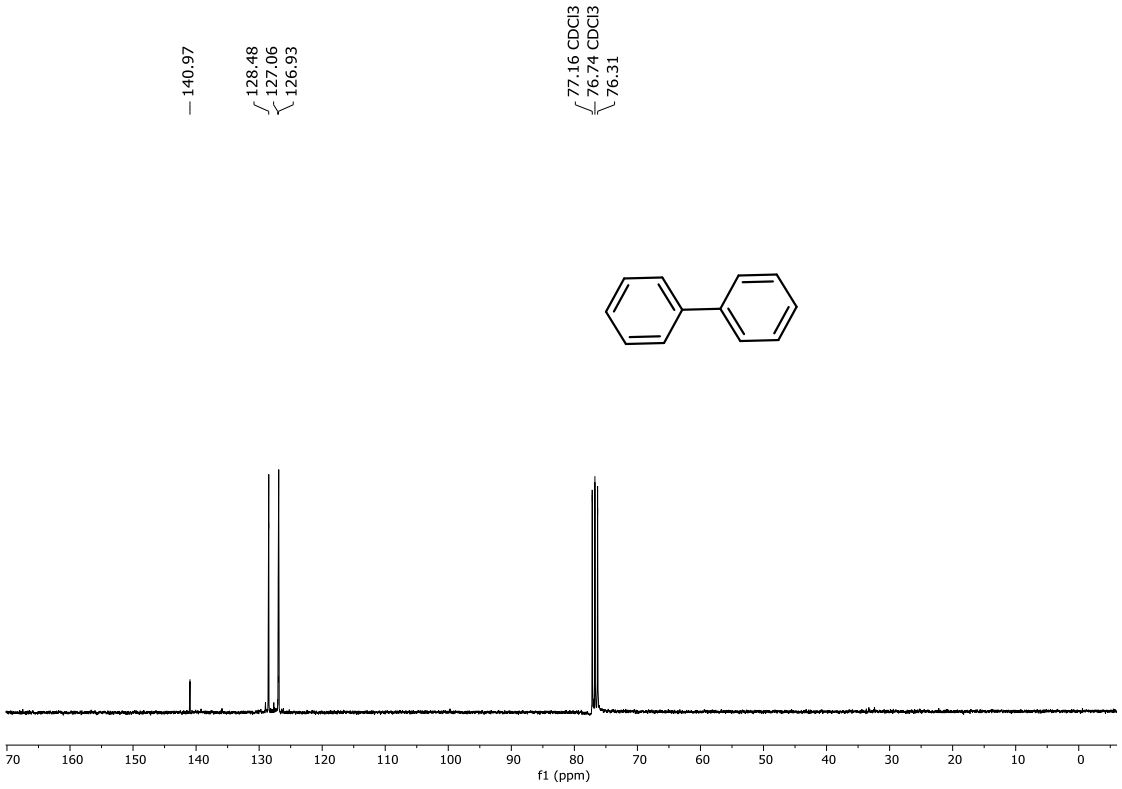

Figure 2.8. ^{13}C NMR spectra of compound **3a** in $CDCl_3$.

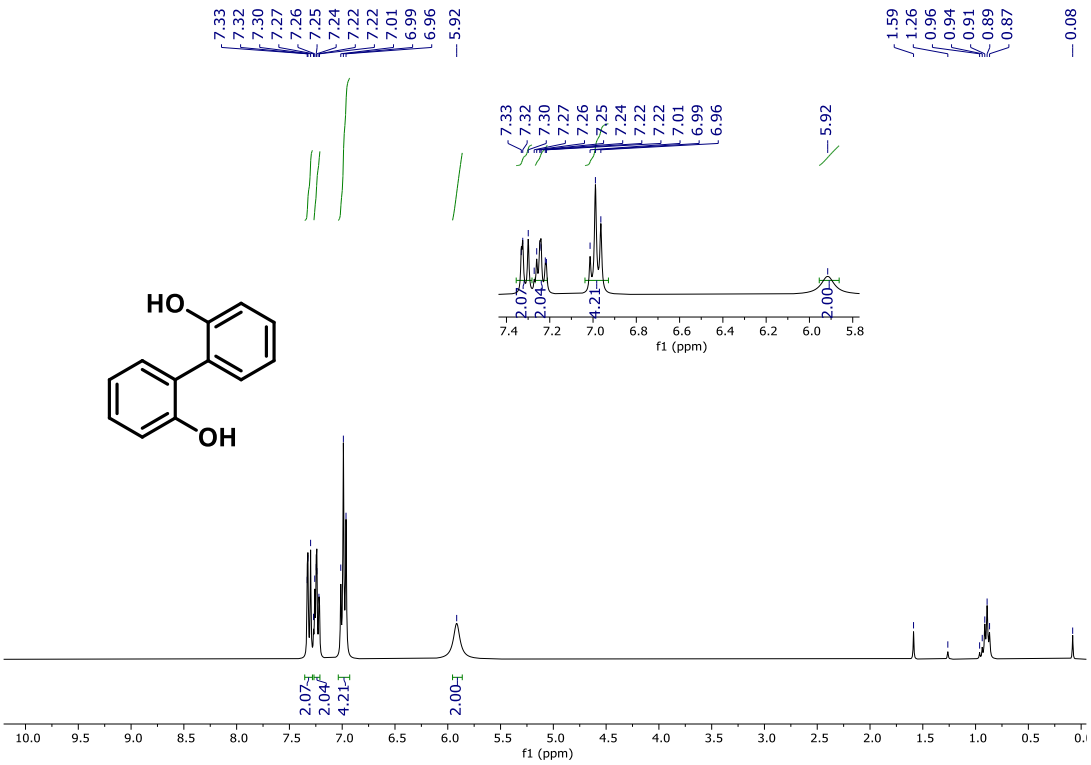

Figure 2.9. ^{1}H NMR spectra of compound **3b** in $CDCl_3$.

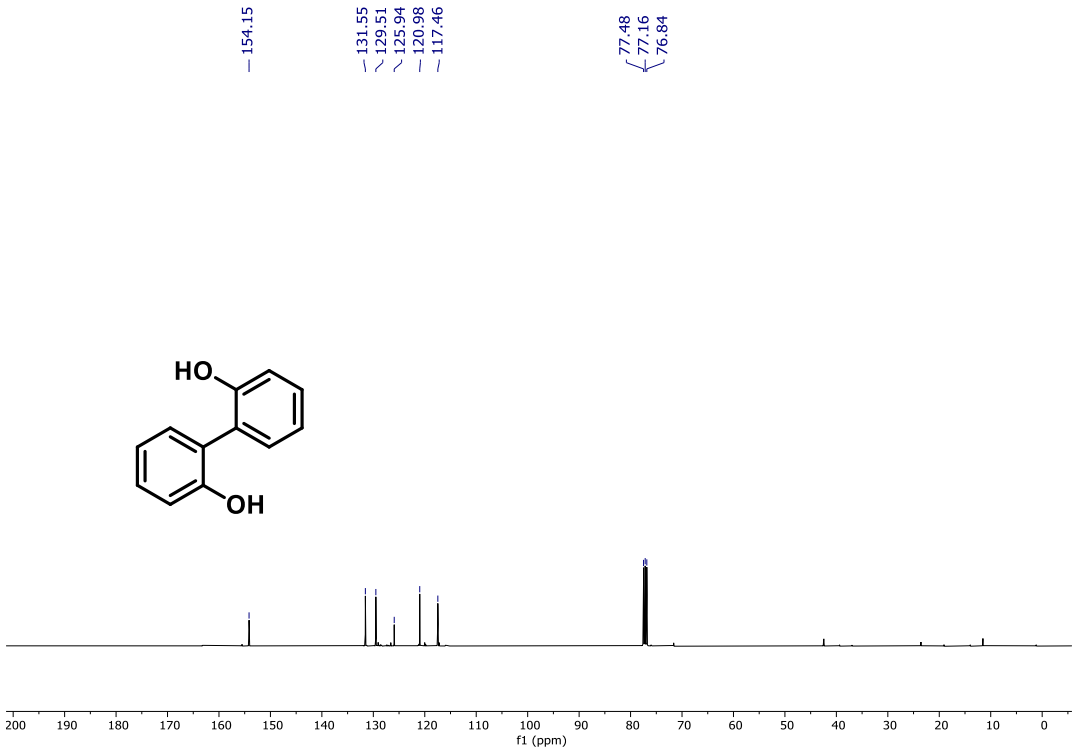

Figure 2.10. ^{13}C NMR spectra of compound **3b** in $CDCl_3$.

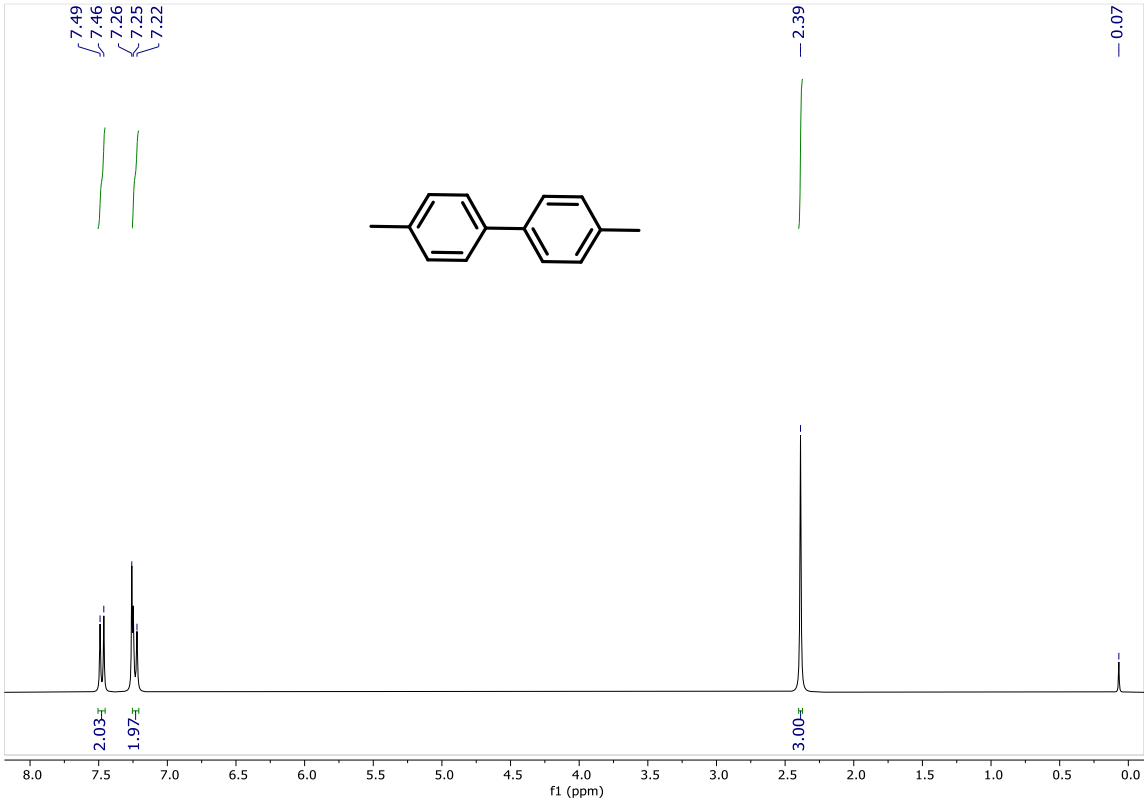

Figure 2.11. ^{1}H NMR spectra of compound **3c** in $CDCl_3$.

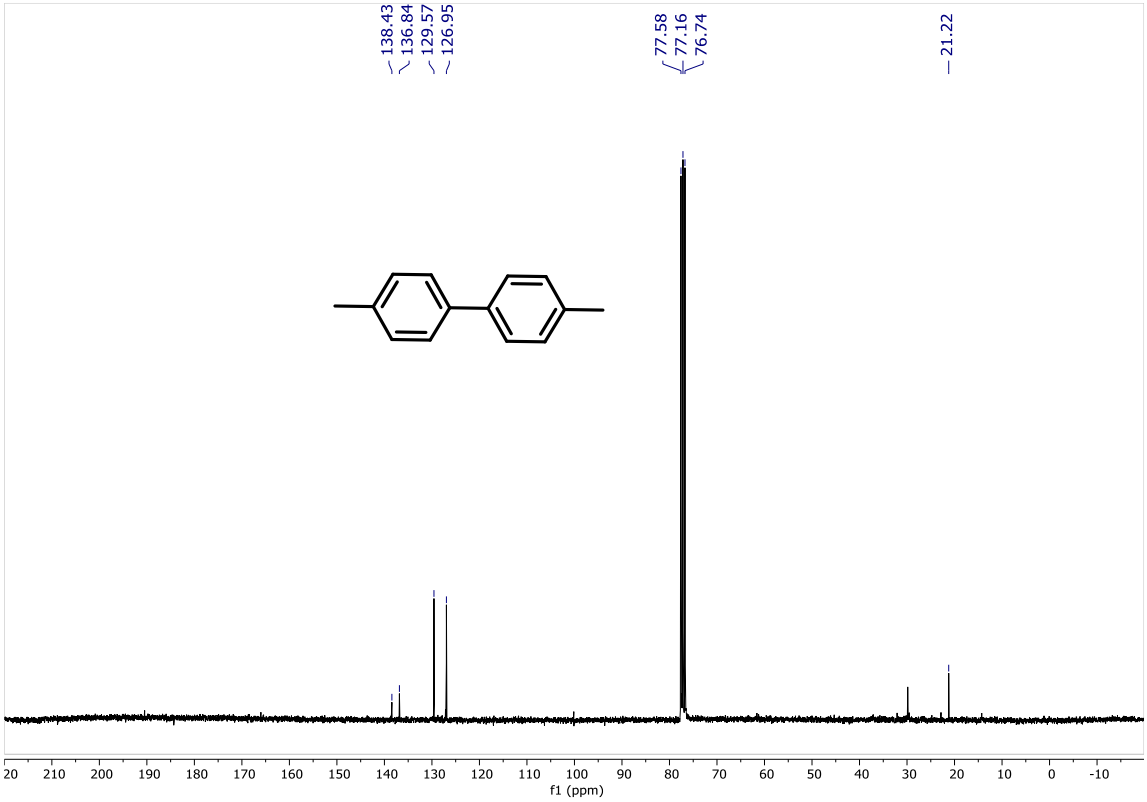

Figure 2.12. ^{13}C NMR spectra of compound **3c** in $CDCl_3$.

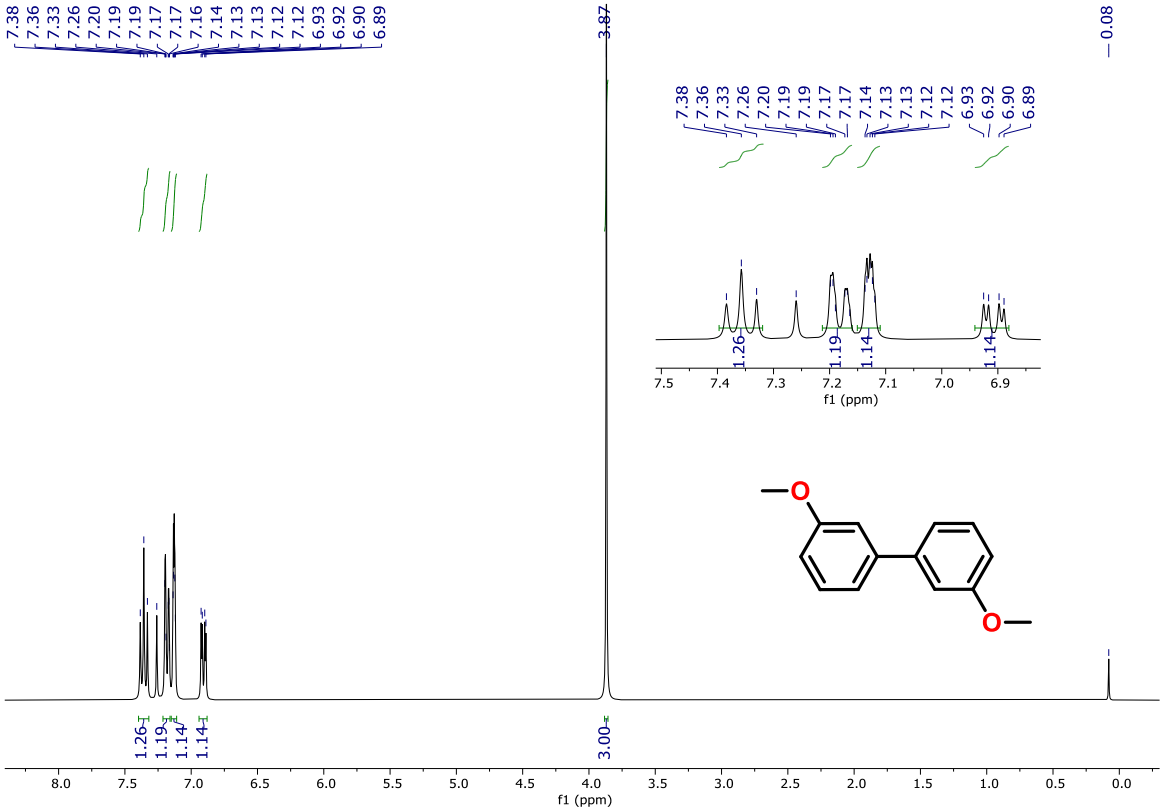

Figure 2.13. ^{1}H NMR spectra of compound **3d** in $CDCl_3$.

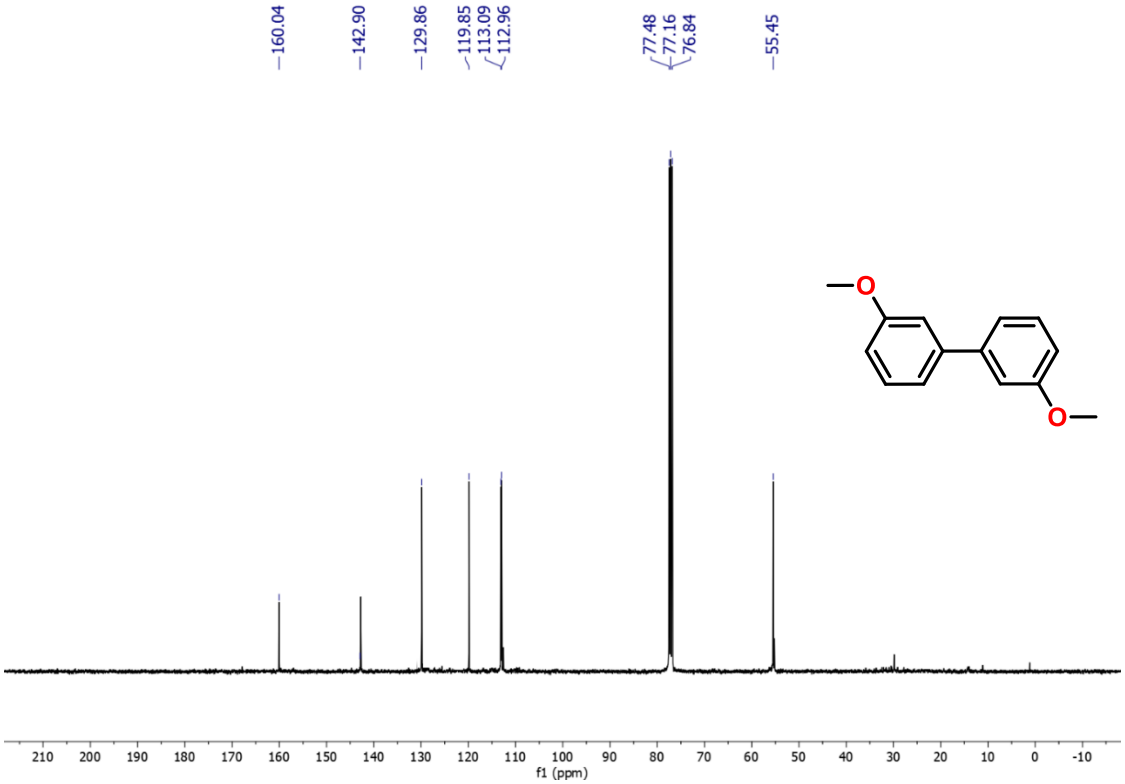

Figure 2.14. ^{13}C NMR spectra of compound **3d** in $CDCl_3$.

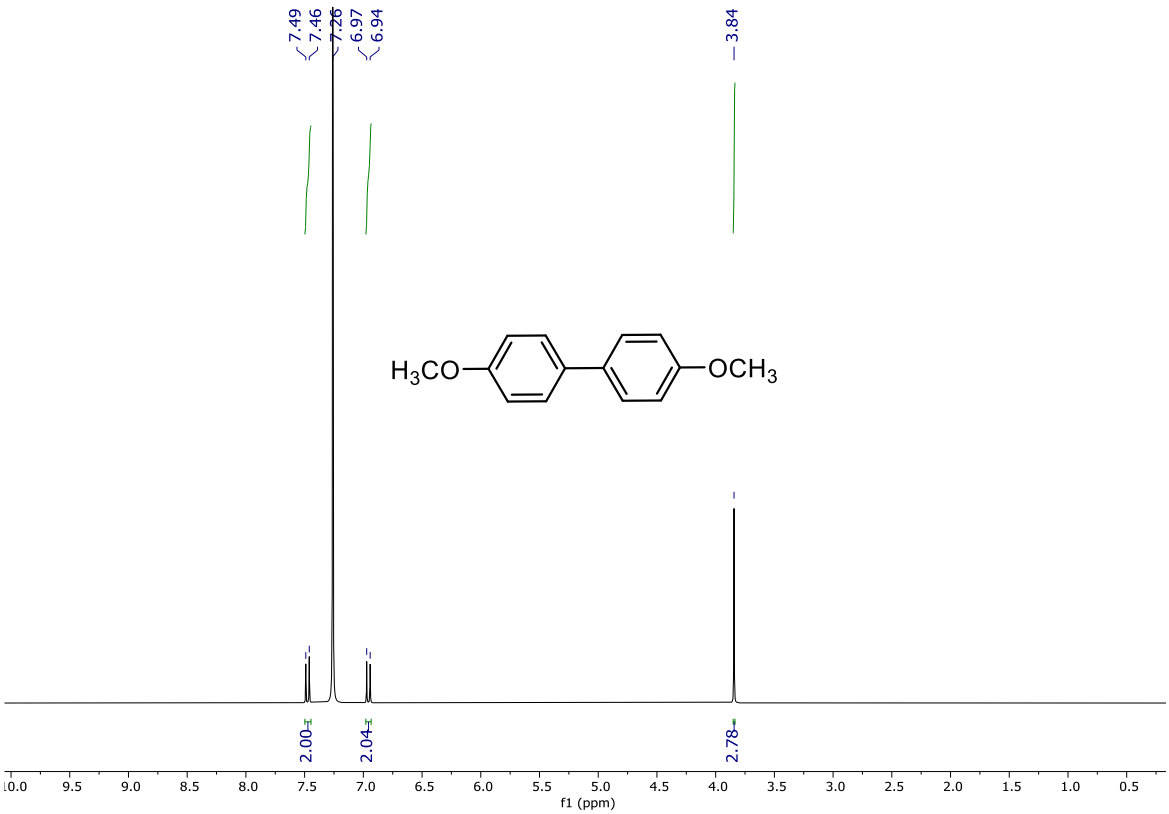

Figure 2.15. ^{1}H NMR spectra of compound **3e** in $CDCl_3$.

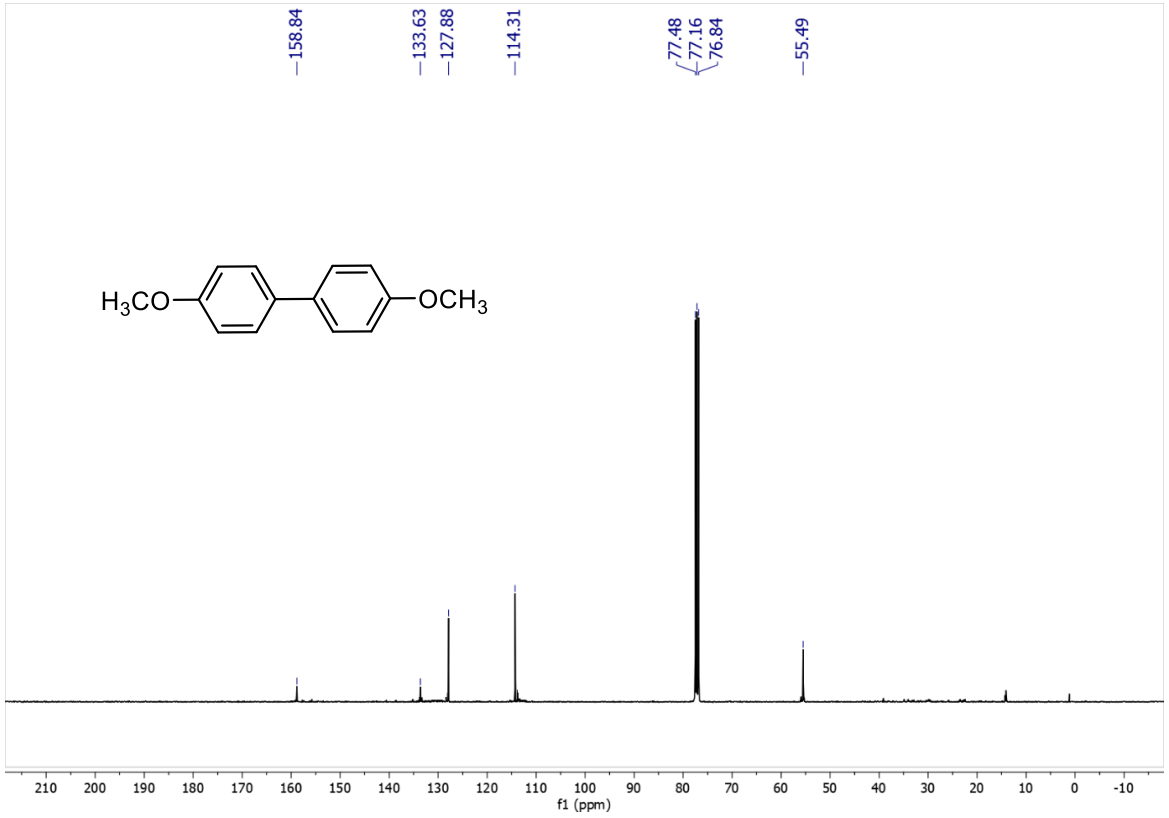

Figure 2.16. ^{13}C NMR spectra of compound **3e** in $CDCl_3$.

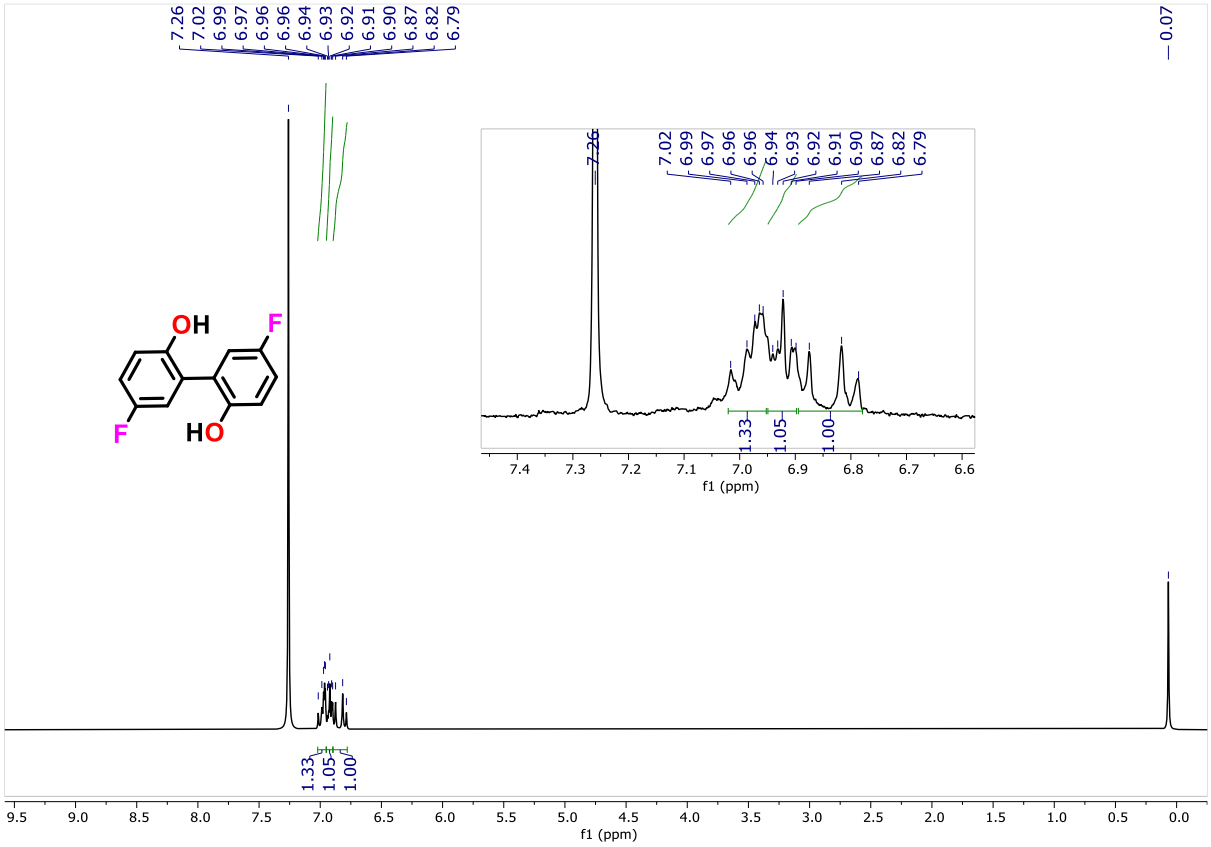

Figure 2.17. ^{1}H NMR spectra of compound **3f** in $CDCl_3$.

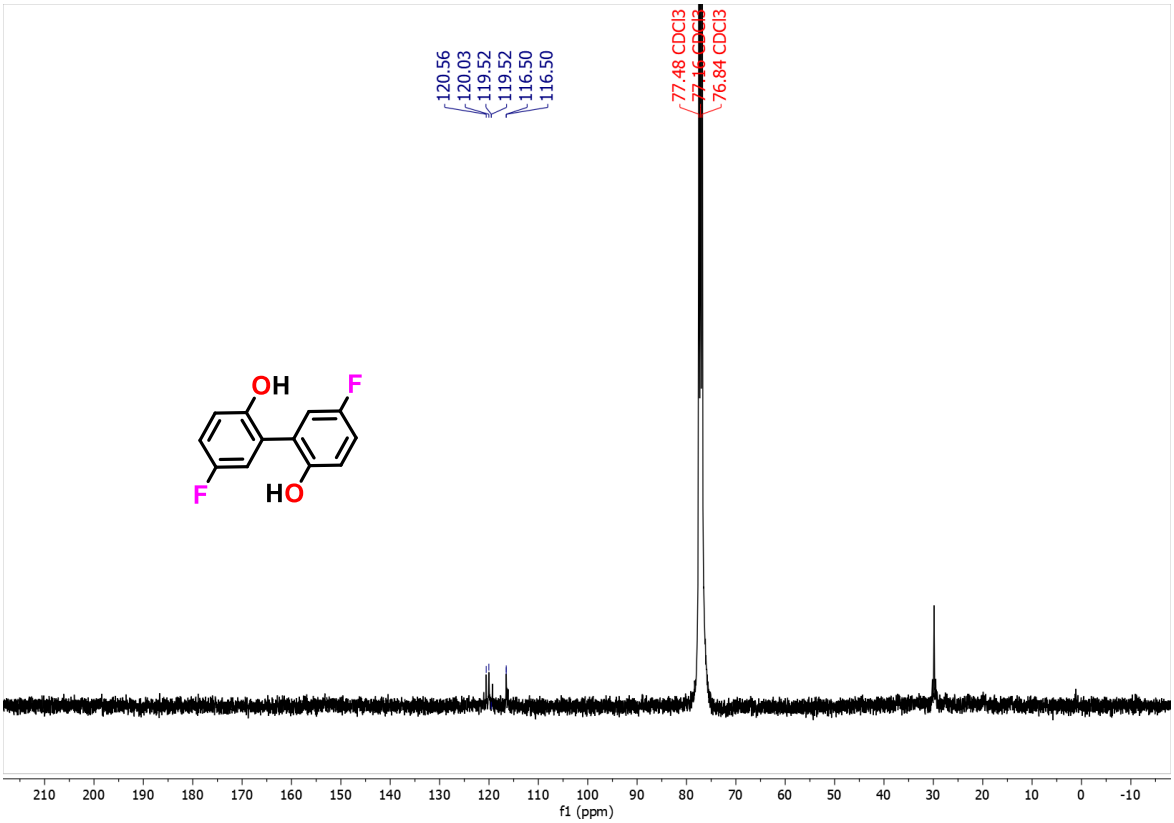

Figure 2.18. ^{13}C NMR spectra of compound **3f** in $CDCl_3$.

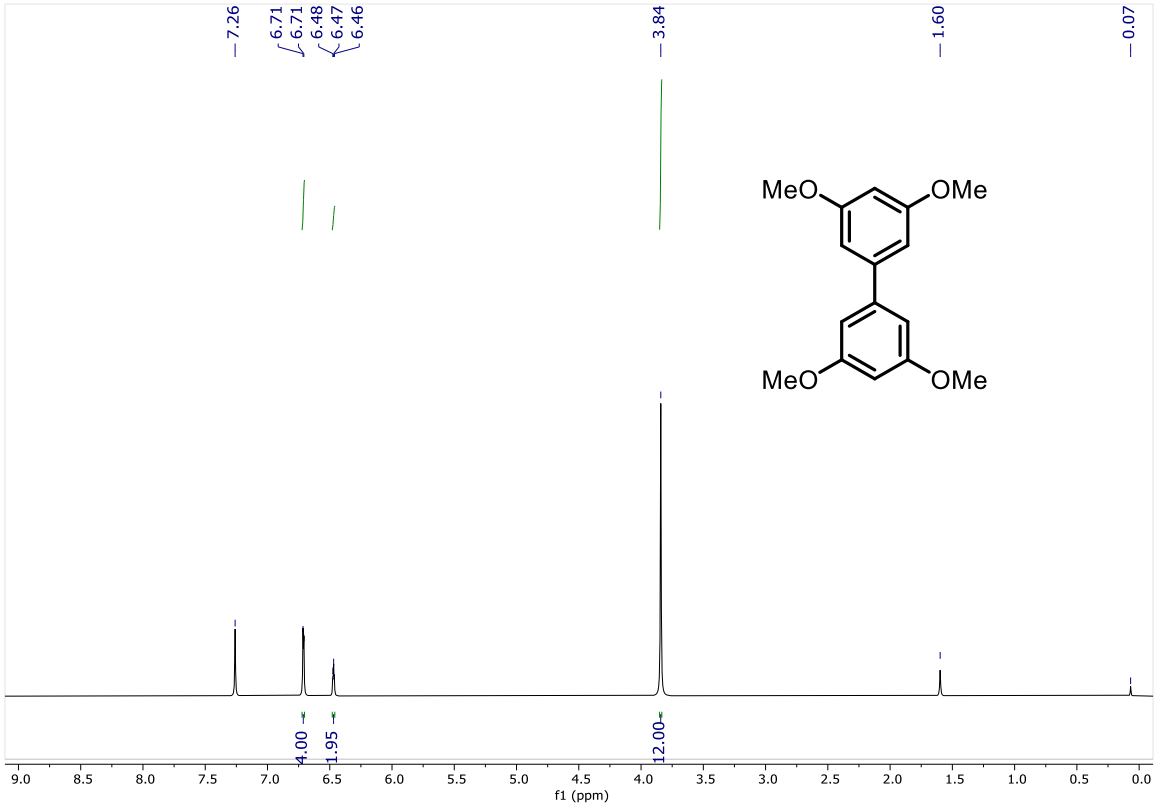

Figure 2.19. ^{1}H NMR spectra of compound **3g** in $CDCl_3$.

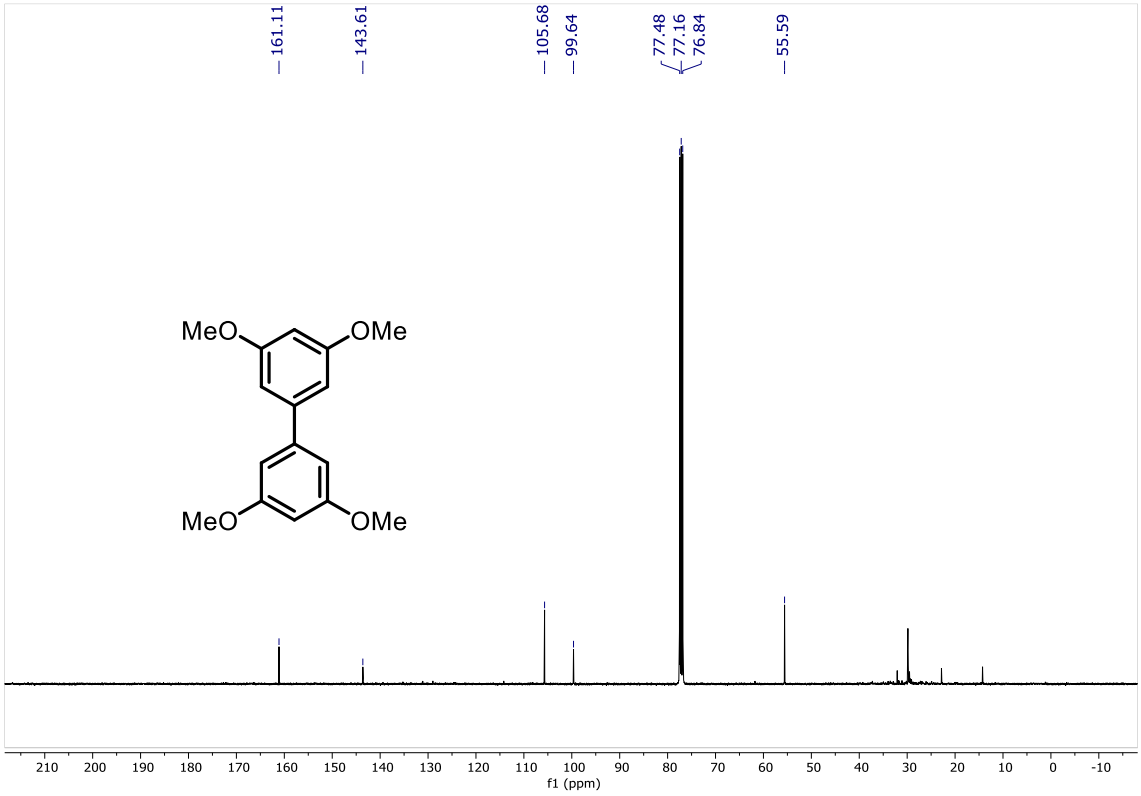

Figure 2.20. ^{13}C NMR spectra of compound **3g** in $CDCl_3$.

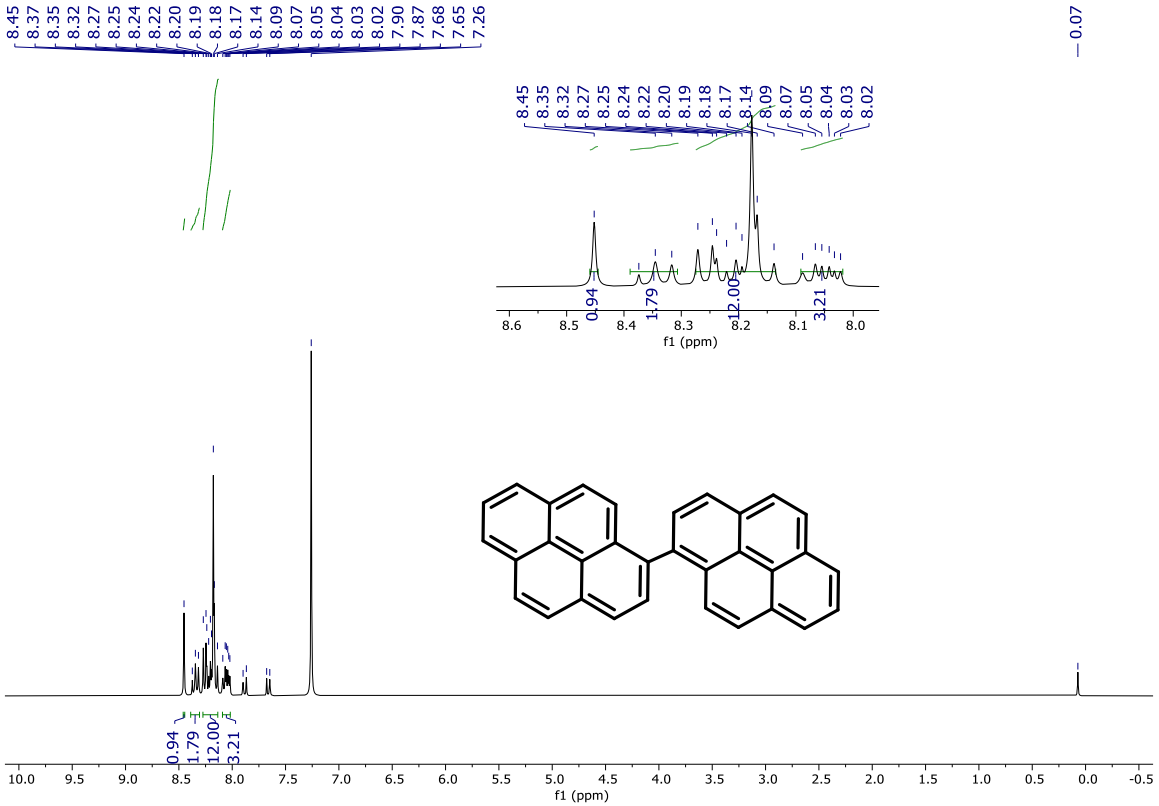

Figure 2.21. ^{1}H NMR spectra of compound **3h** in $CDCl_3$.

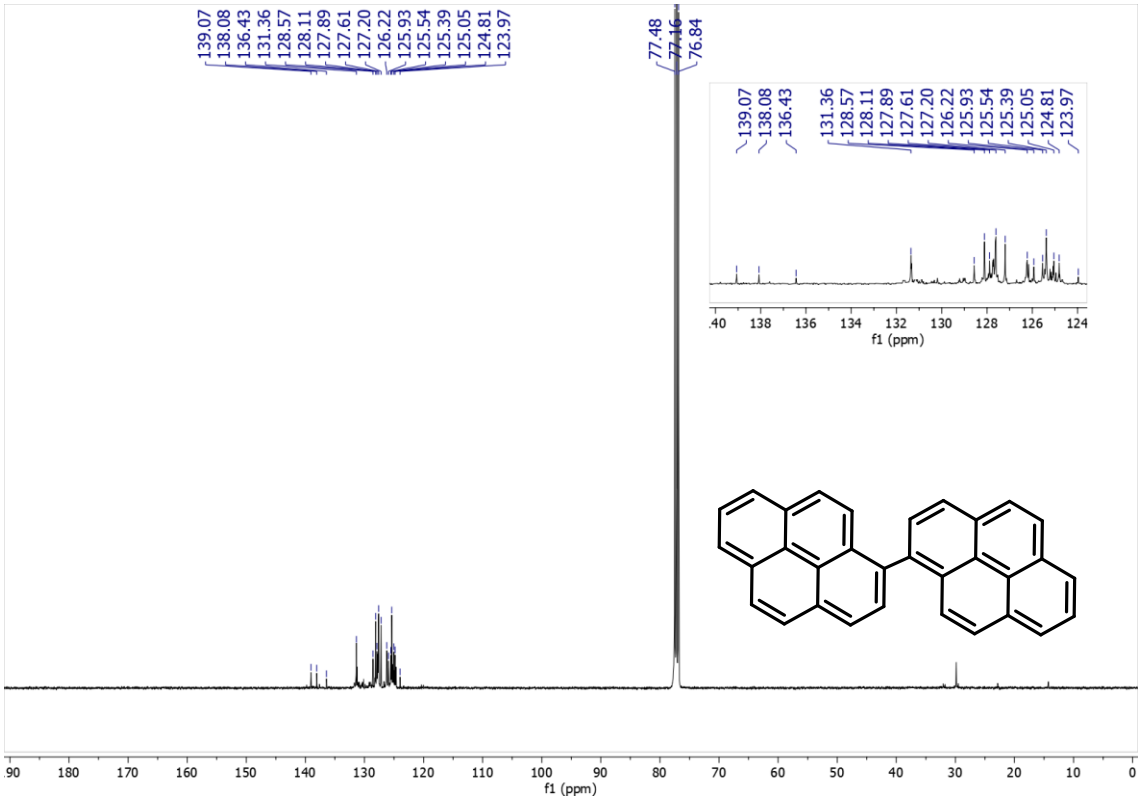

Figure 2.22. ^{13}C NMR spectra of compound **3h** in $CDCl_3$.

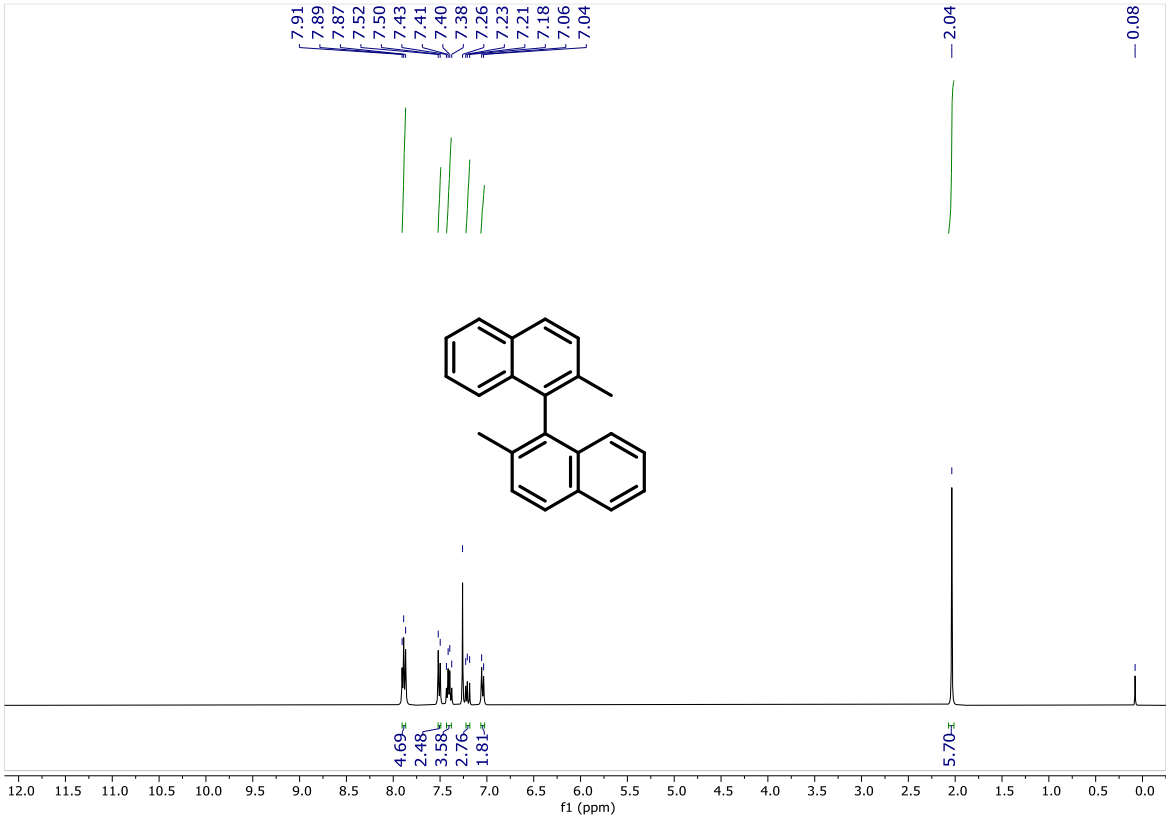

Figure 2.23. ^{1}H NMR spectra of compound **3i** in $CDCl_3$.

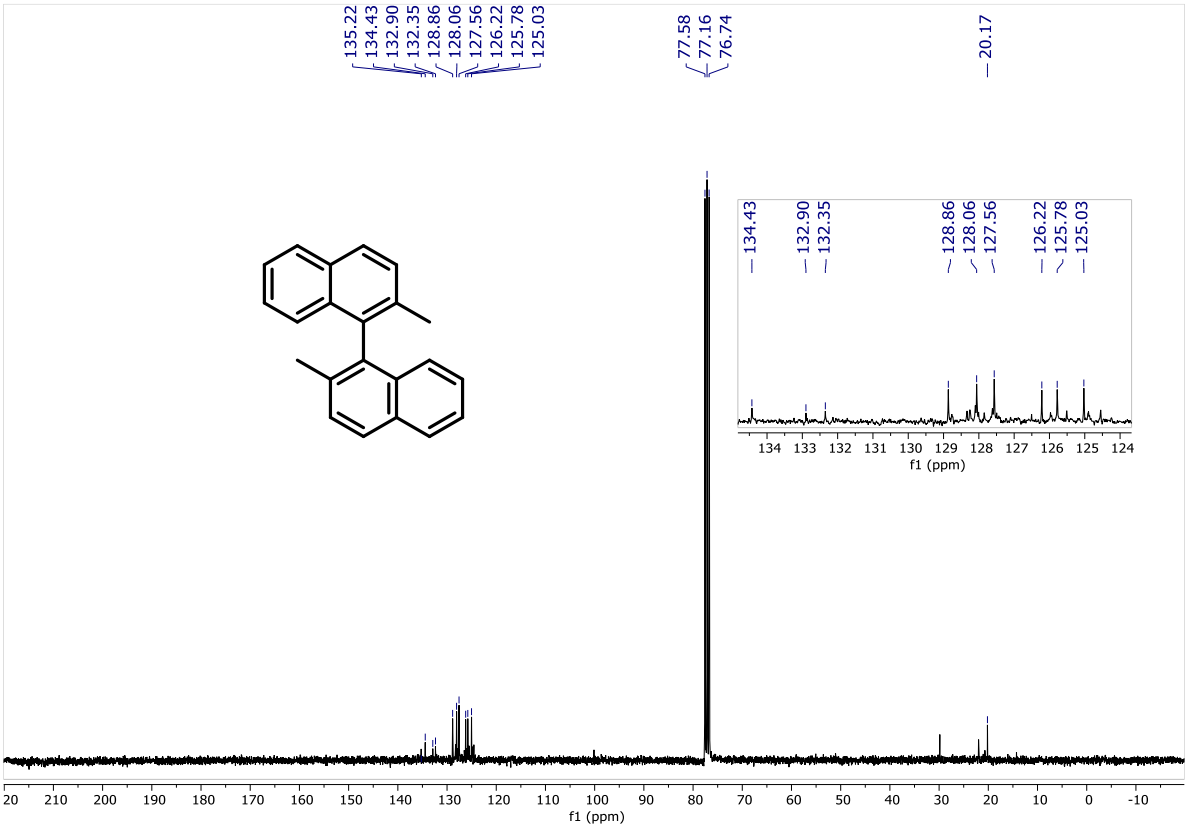

Figure 2.24. ^{13}C NMR spectra of compound **3i** in $CDCl_3$.

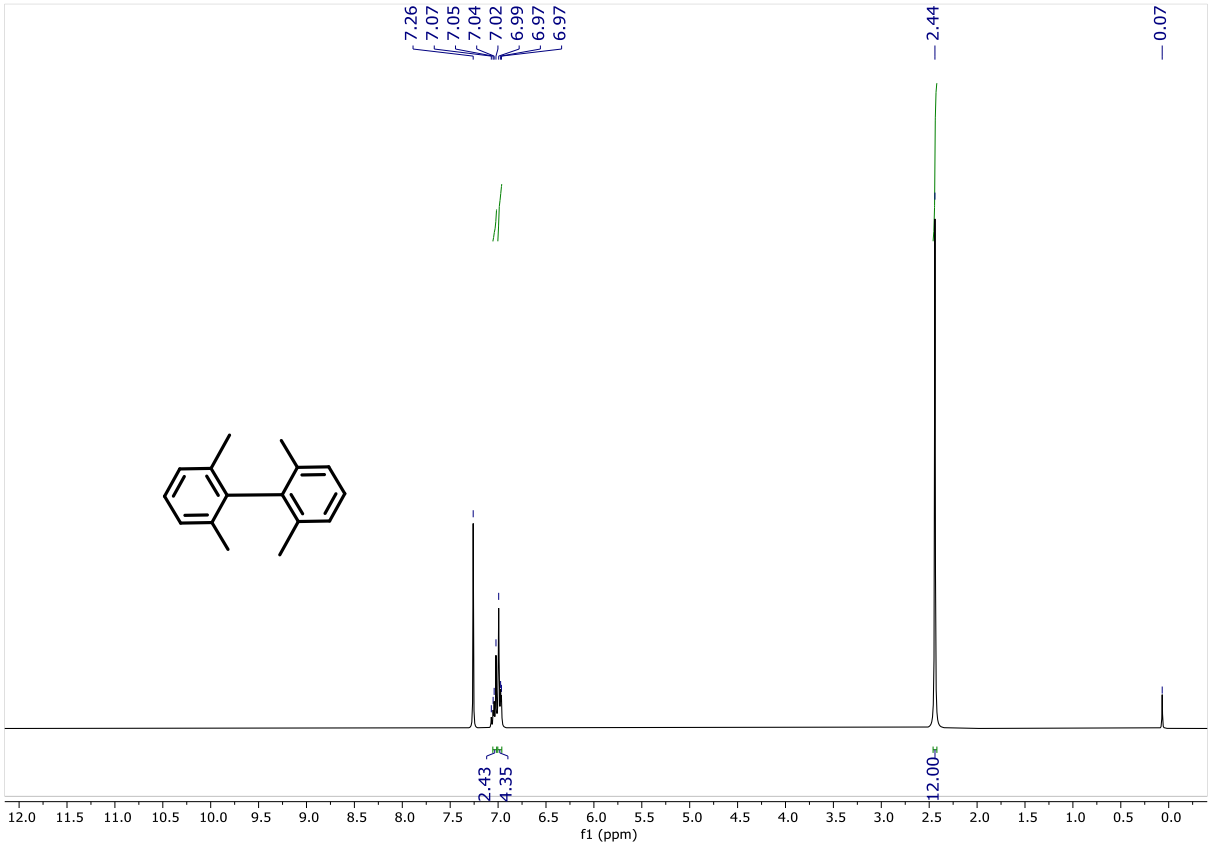

Figure 2.25. ^{1}H NMR spectra of compound **3j** in $CDCl_3$.

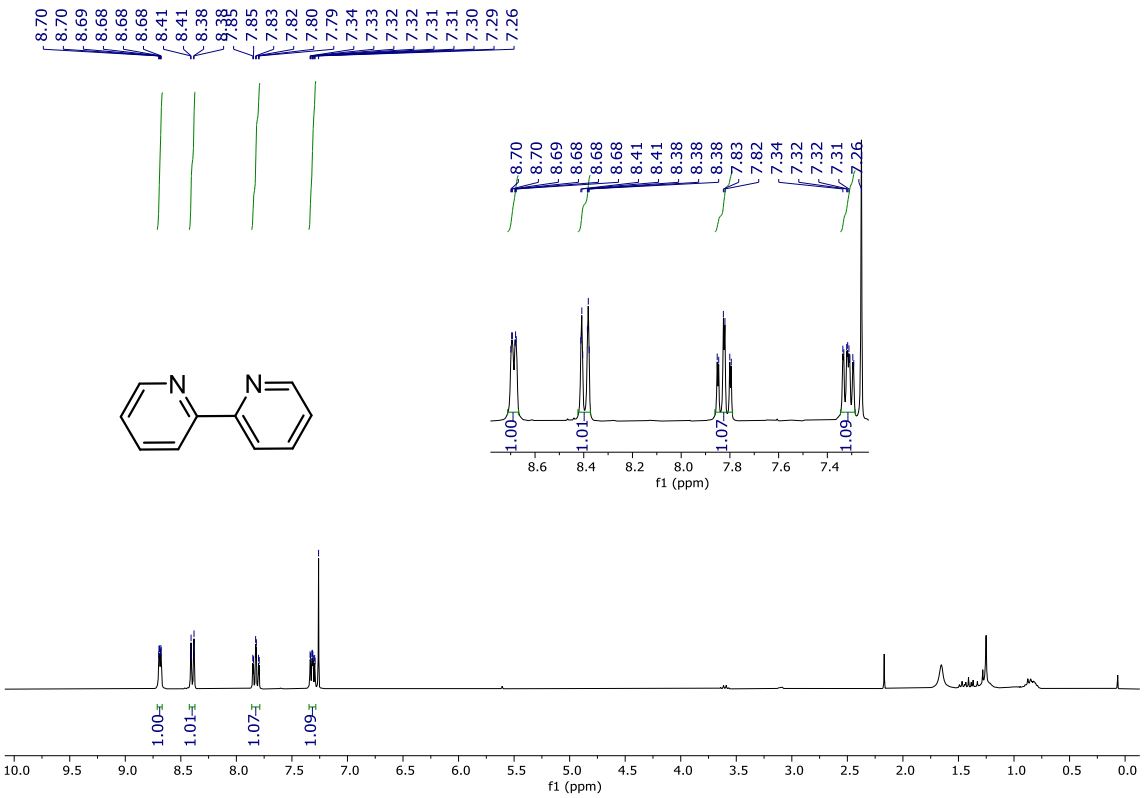

Figure 2.26. ^{1}H NMR spectra of compound **3k** in $CDCl_3$.

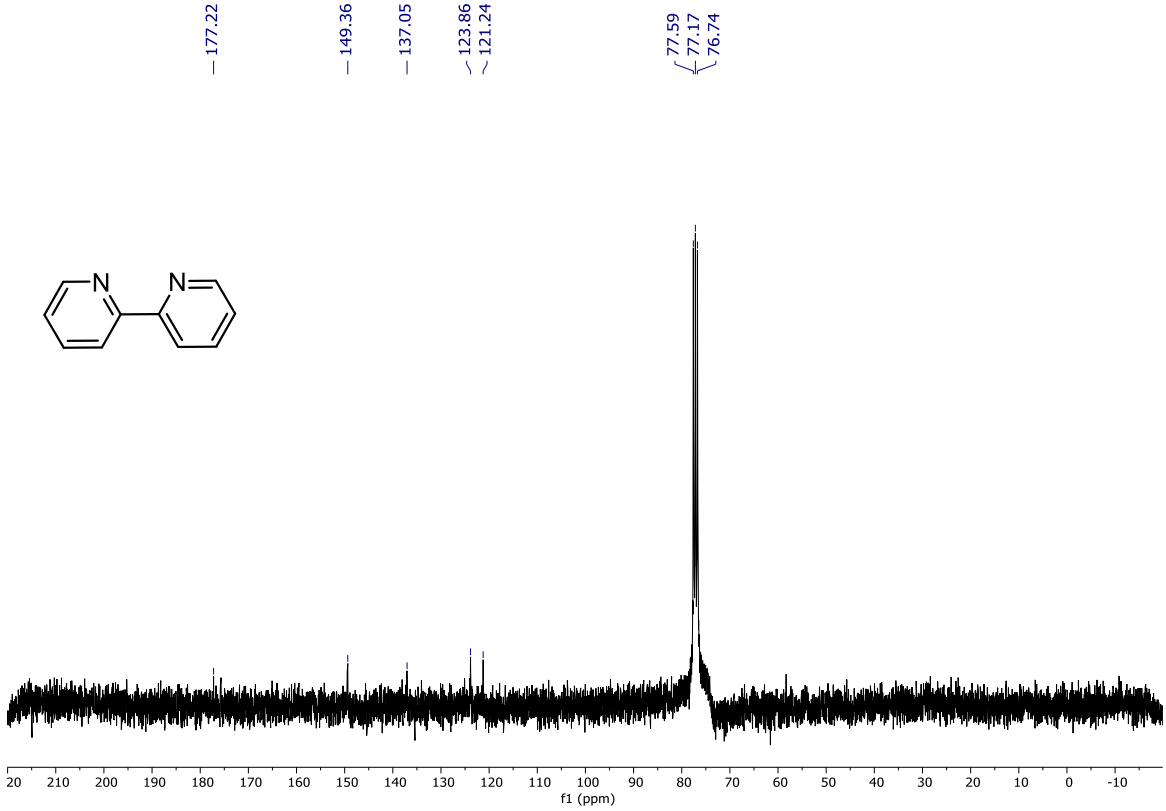

Figure 2.27. ^{13}C NMR spectra of compound **3k** in $CDCl_3$.

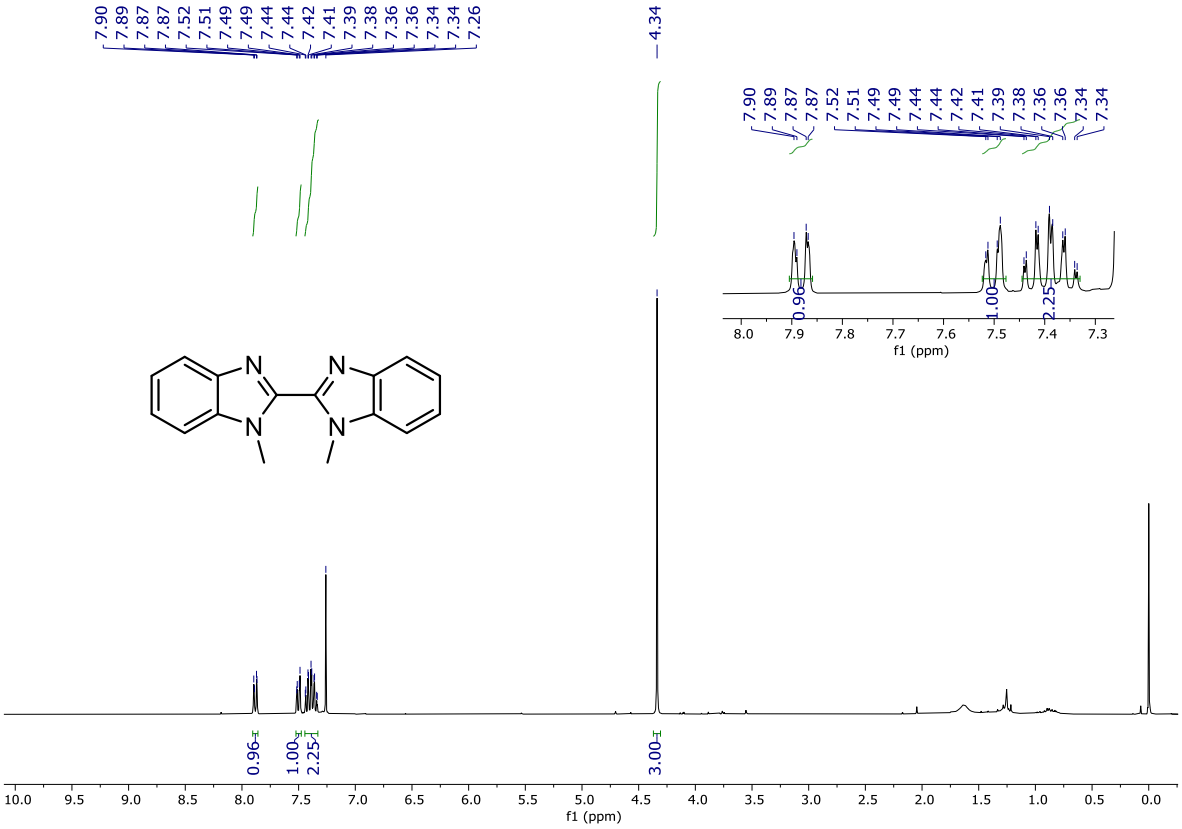

Figure 2.28. ^{1}H NMR spectra of compound **3l** in $CDCl_3$.

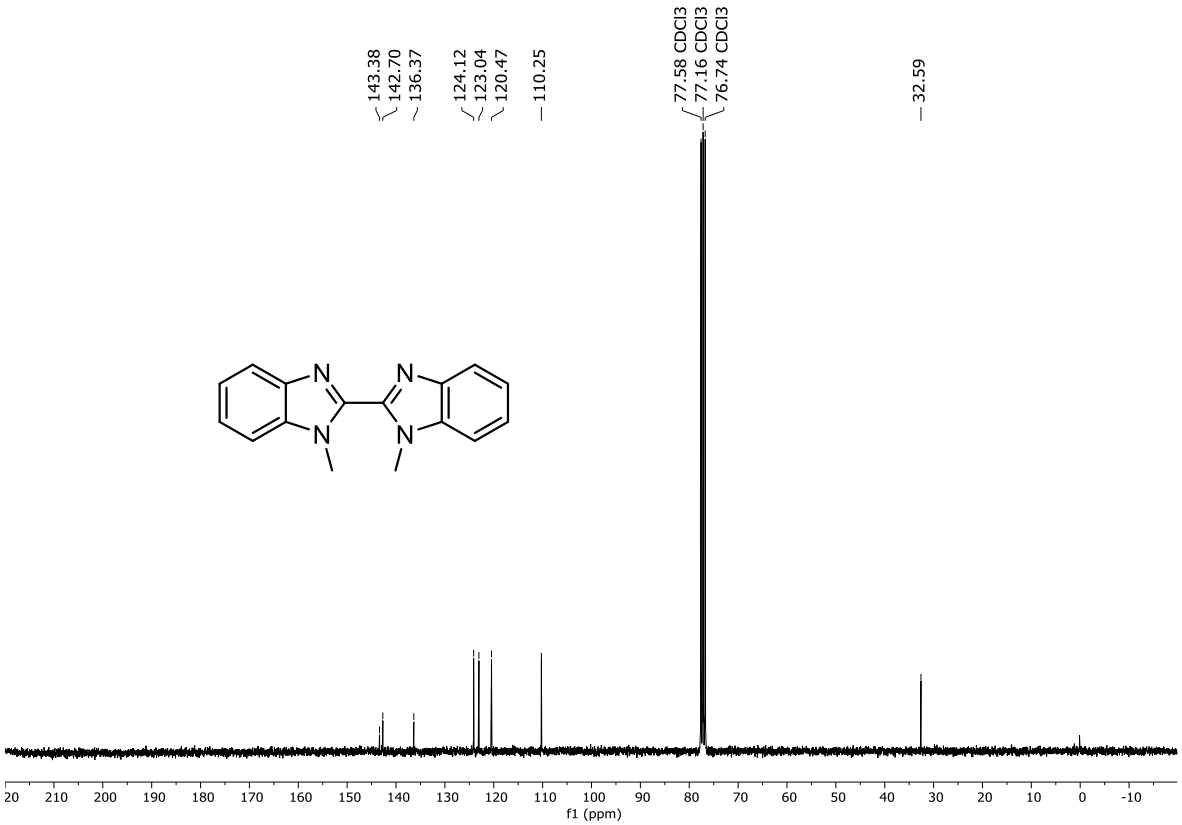

Figure 2.29. ^{13}C NMR spectra of compound **3l** in $CDCl_3$.

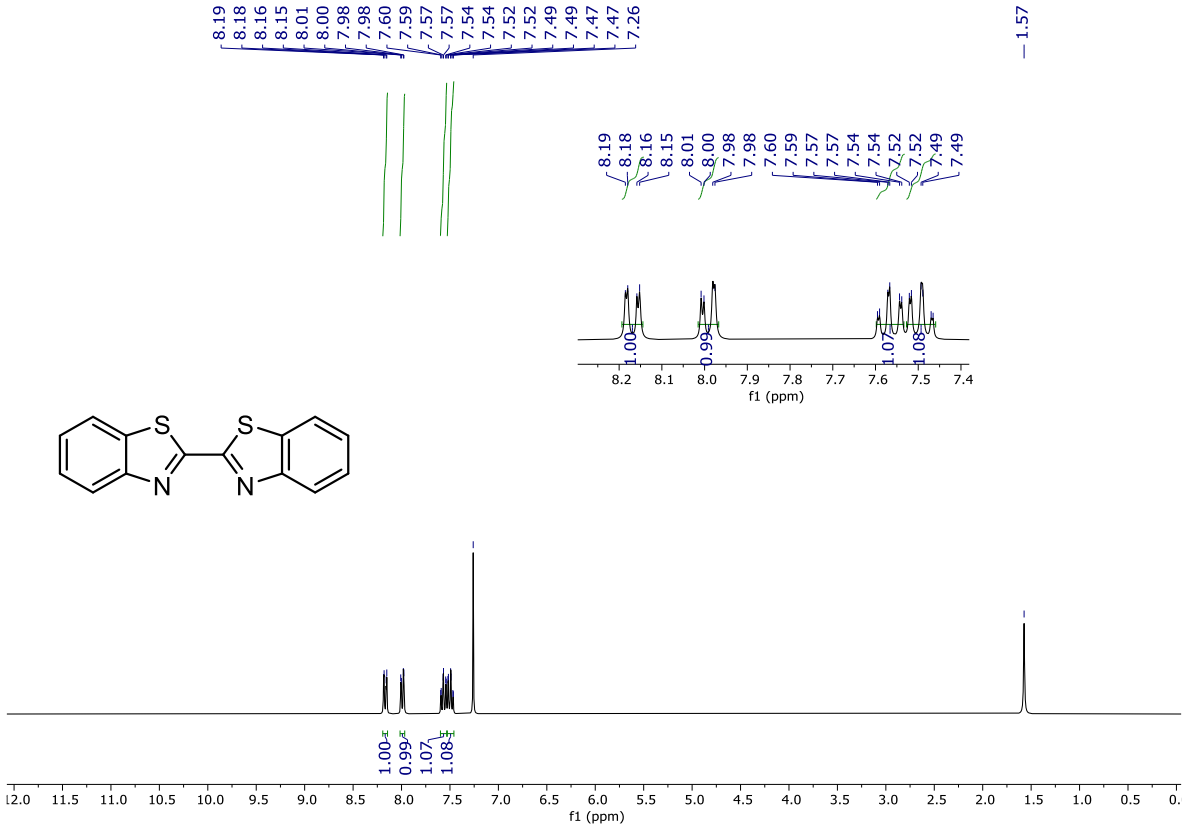

Figure 2.30. ^{1}H NMR spectra of compound **3m** in $CDCl_3$.

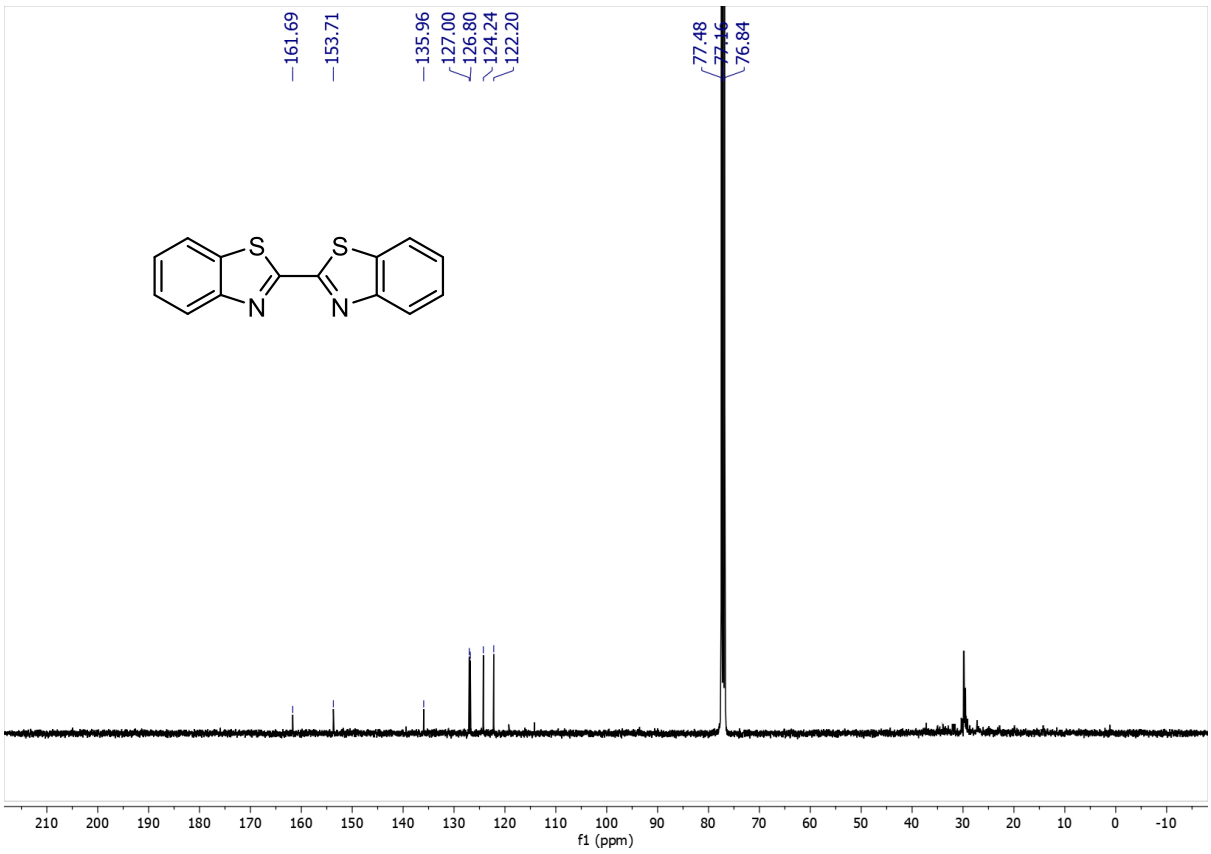

Figure 2.312. ^{13}C NMR spectra of compound **3m** in $CDCl_3$.

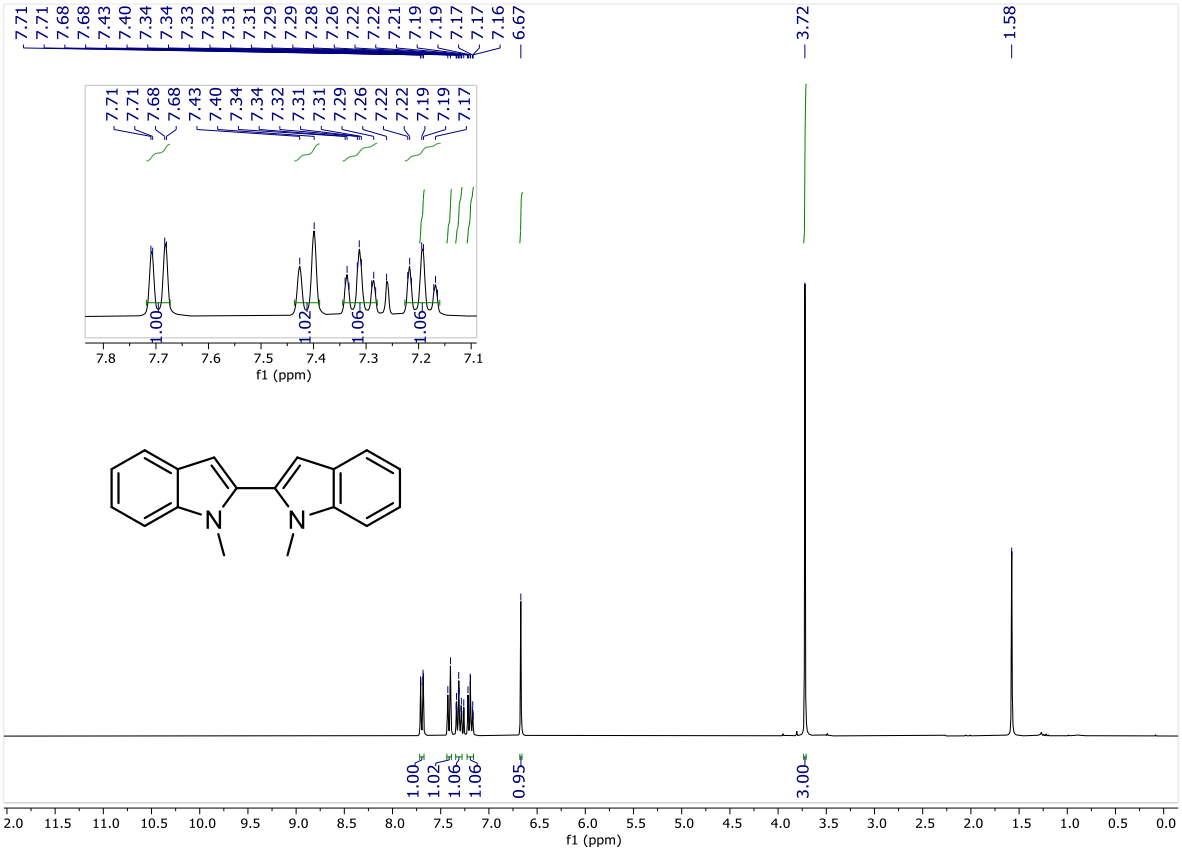

Figure 2.32. ^{1}H NMR spectra of compound **3n** in $CDCl_3$.

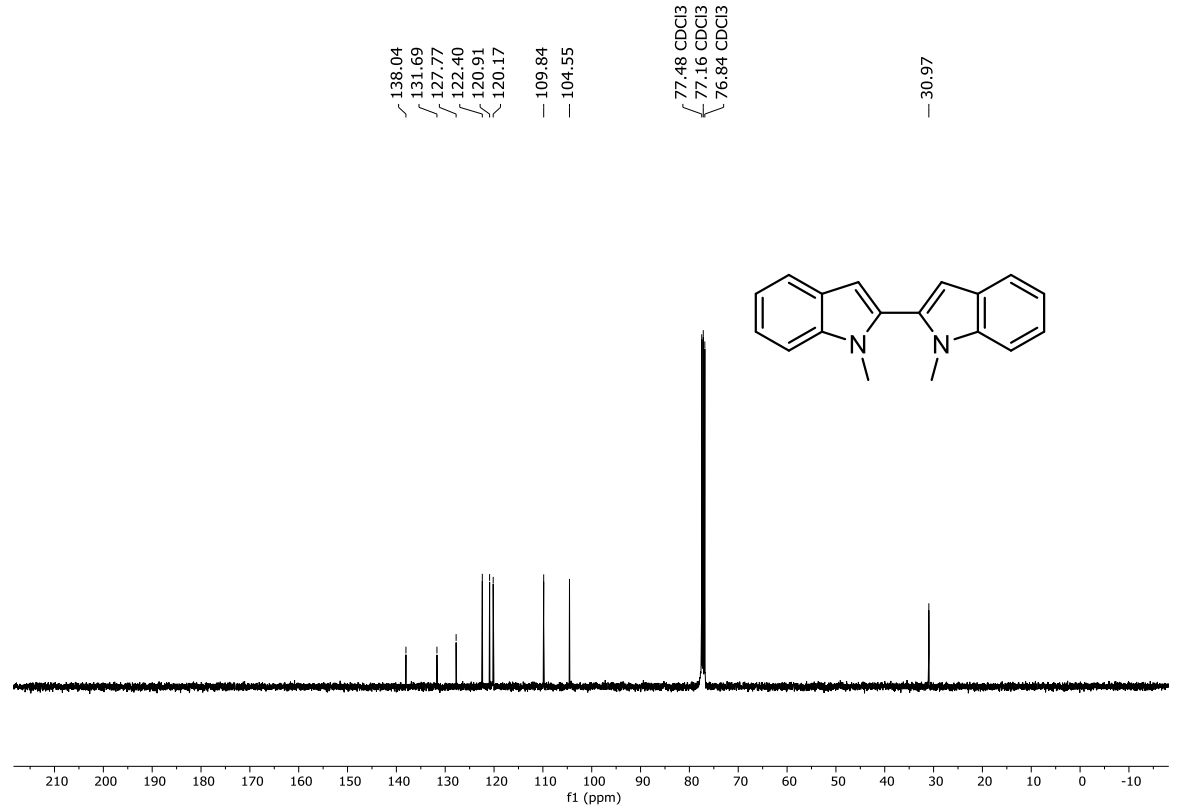

Figure 2.33. ^{13}C NMR spectra of compound **3n** in $CDCl_3$.

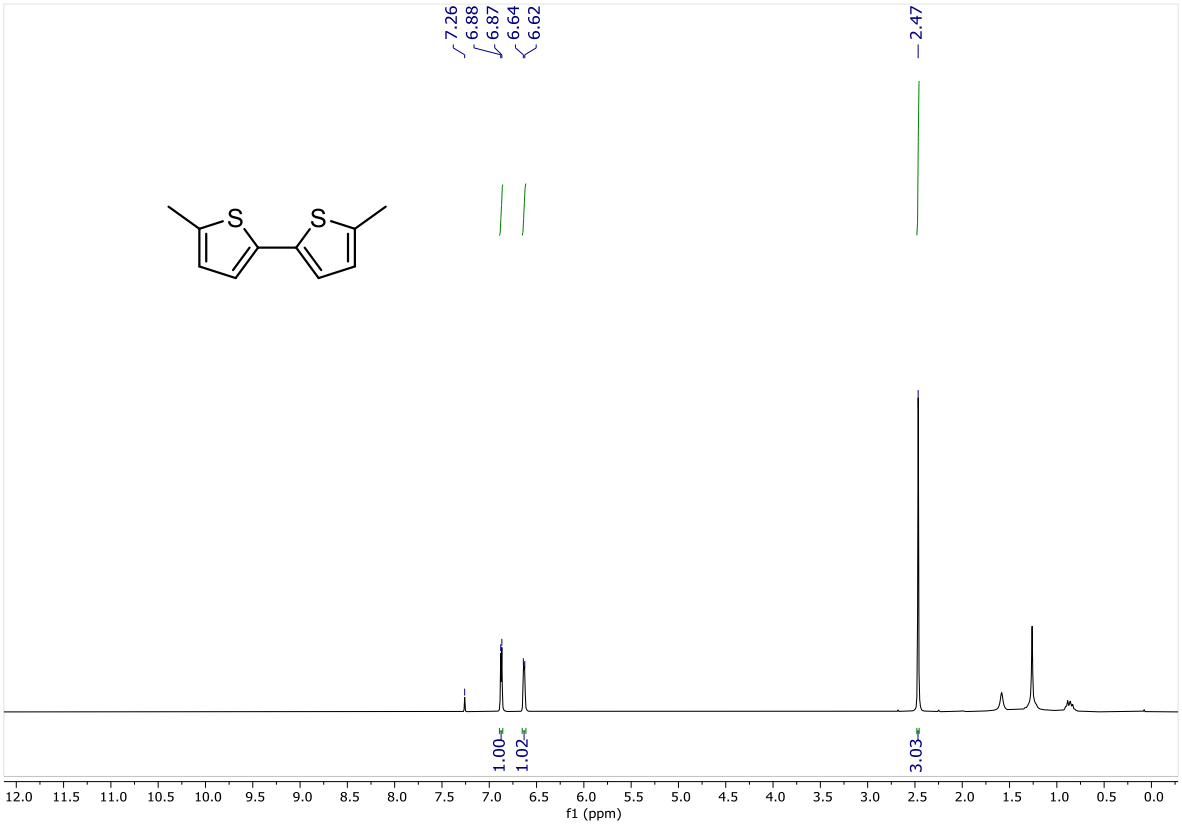

Figure 2.34. ^{1}H NMR spectra of compound **3o** in $CDCl_3$.

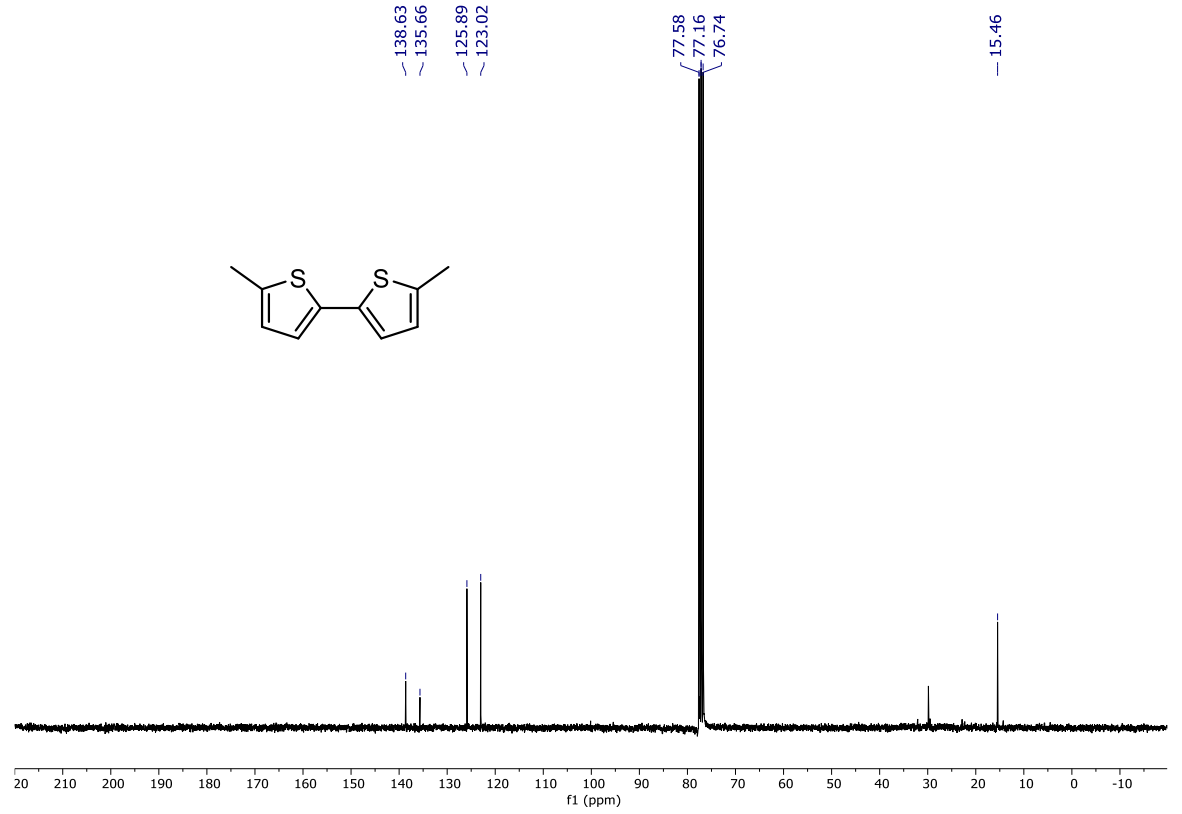

Figure 2.35. ^{13}C NMR spectra of compound **3o** in $CDCl_3$.

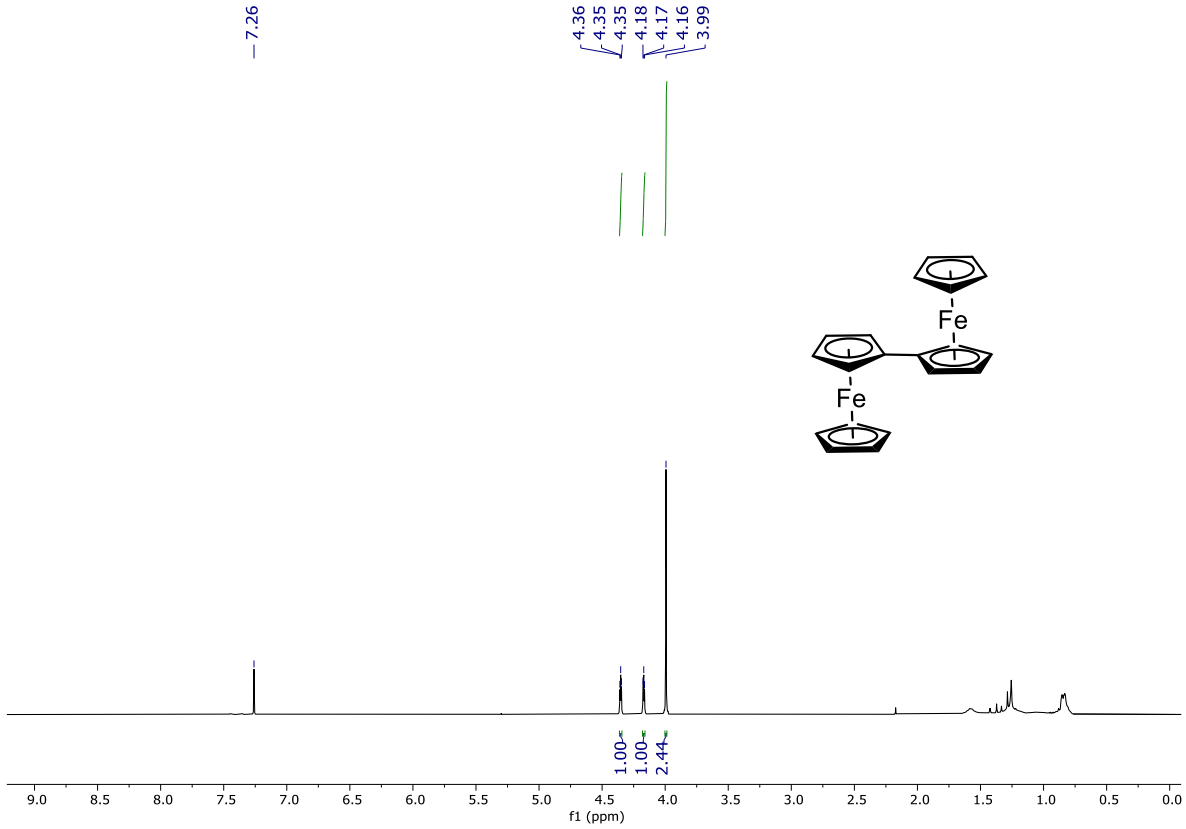

Figure 2.36. ^{1}H NMR spectra of compound **3p** in $CDCl_3$.

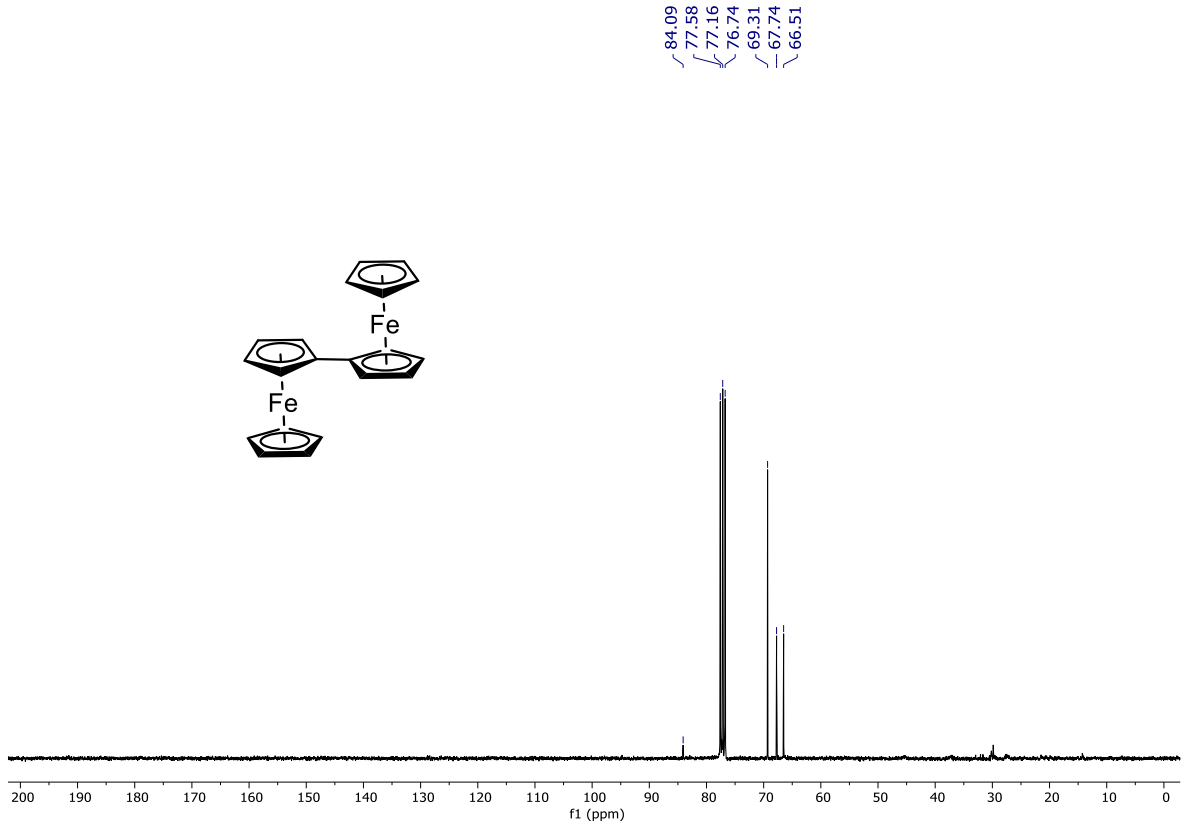

Figure 2.37. ^{13}C NMR spectra of compound **3p** in $CDCl_3$.

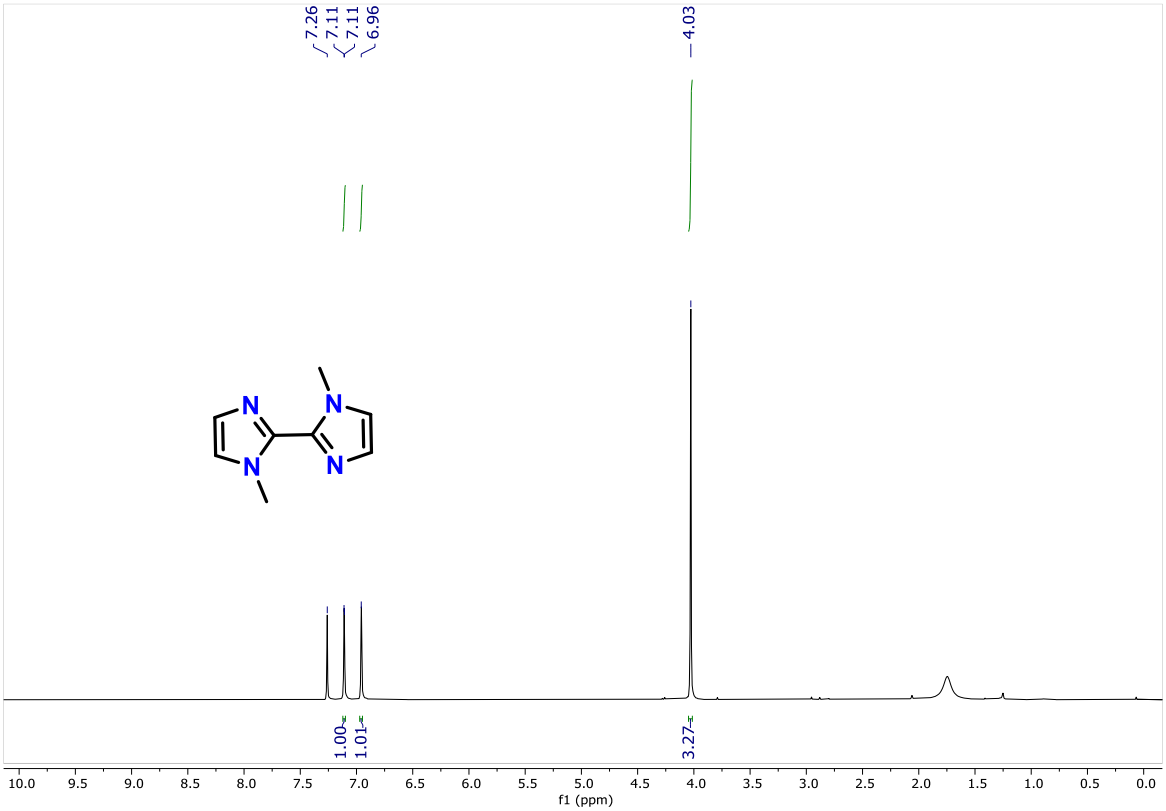

Figure 2.38. ^{1}H NMR spectra of compound **3q** in $CDCl_3$.

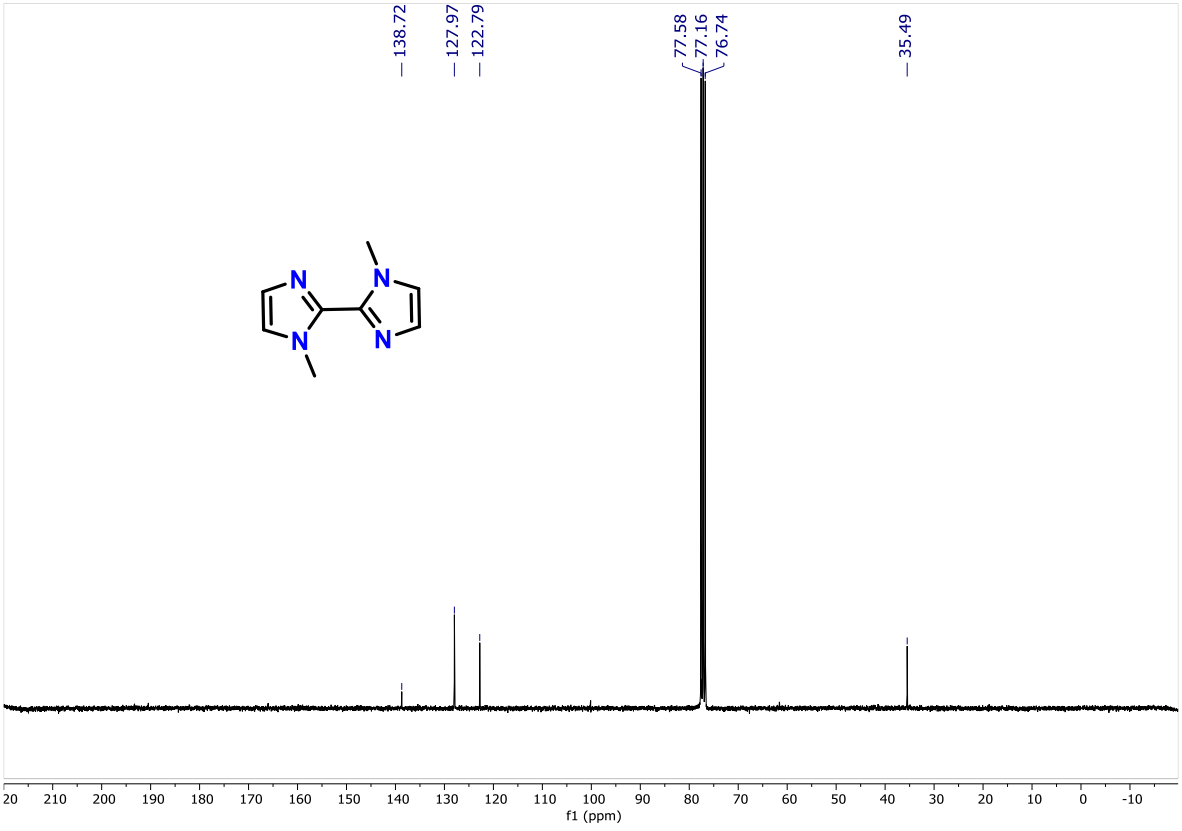

Figure 2.39. ^{13}C NMR spectra of compound **3q** in $CDCl_3$.

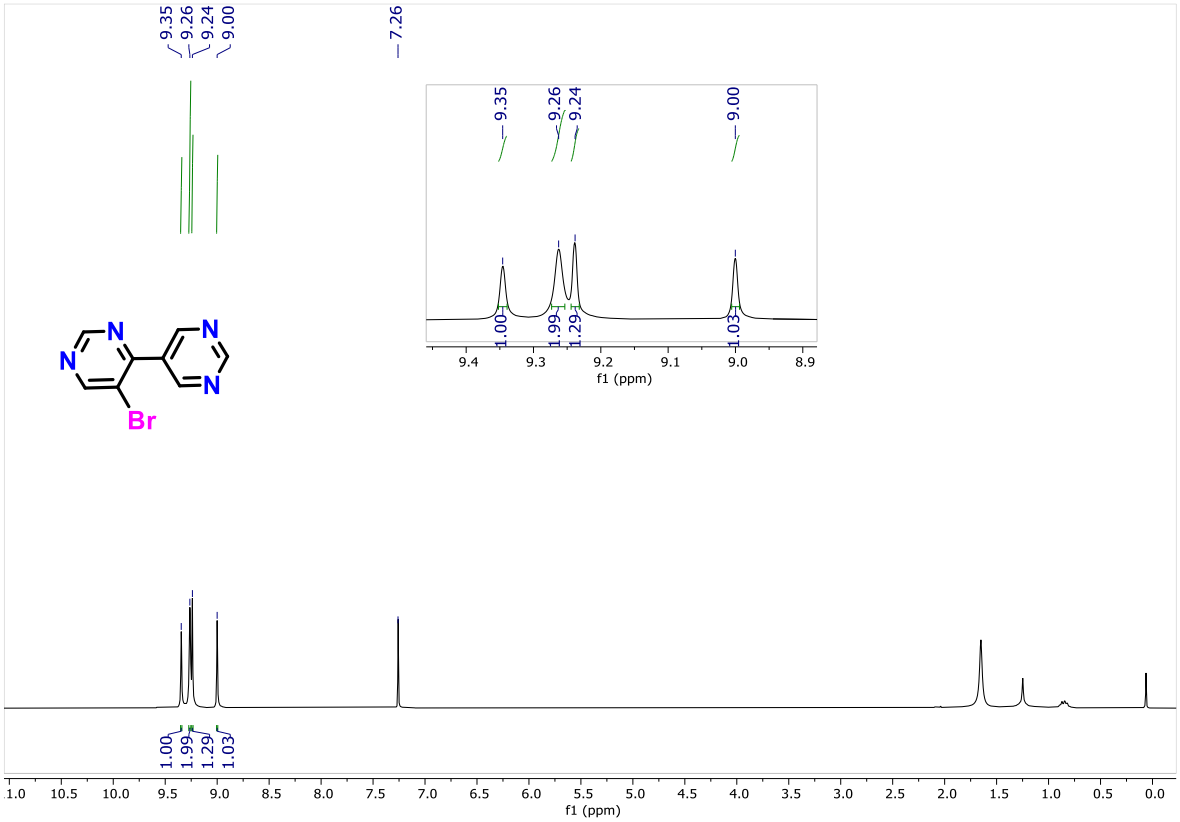

Figure 2.40. ^{1}H NMR spectra of compound **3r** in $CDCl_3$.

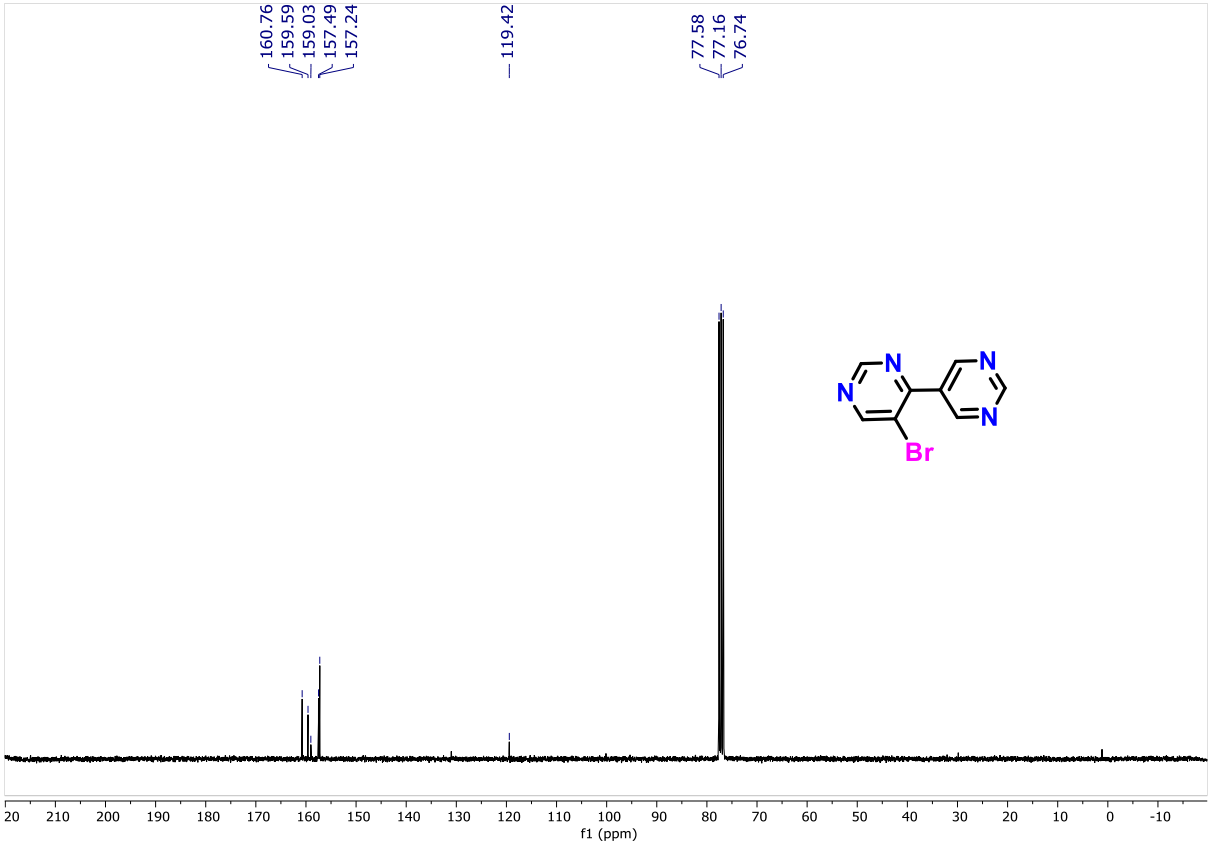

Figure 2.41. ^{13}C NMR spectra of compound **3r** in $CDCl_3$.

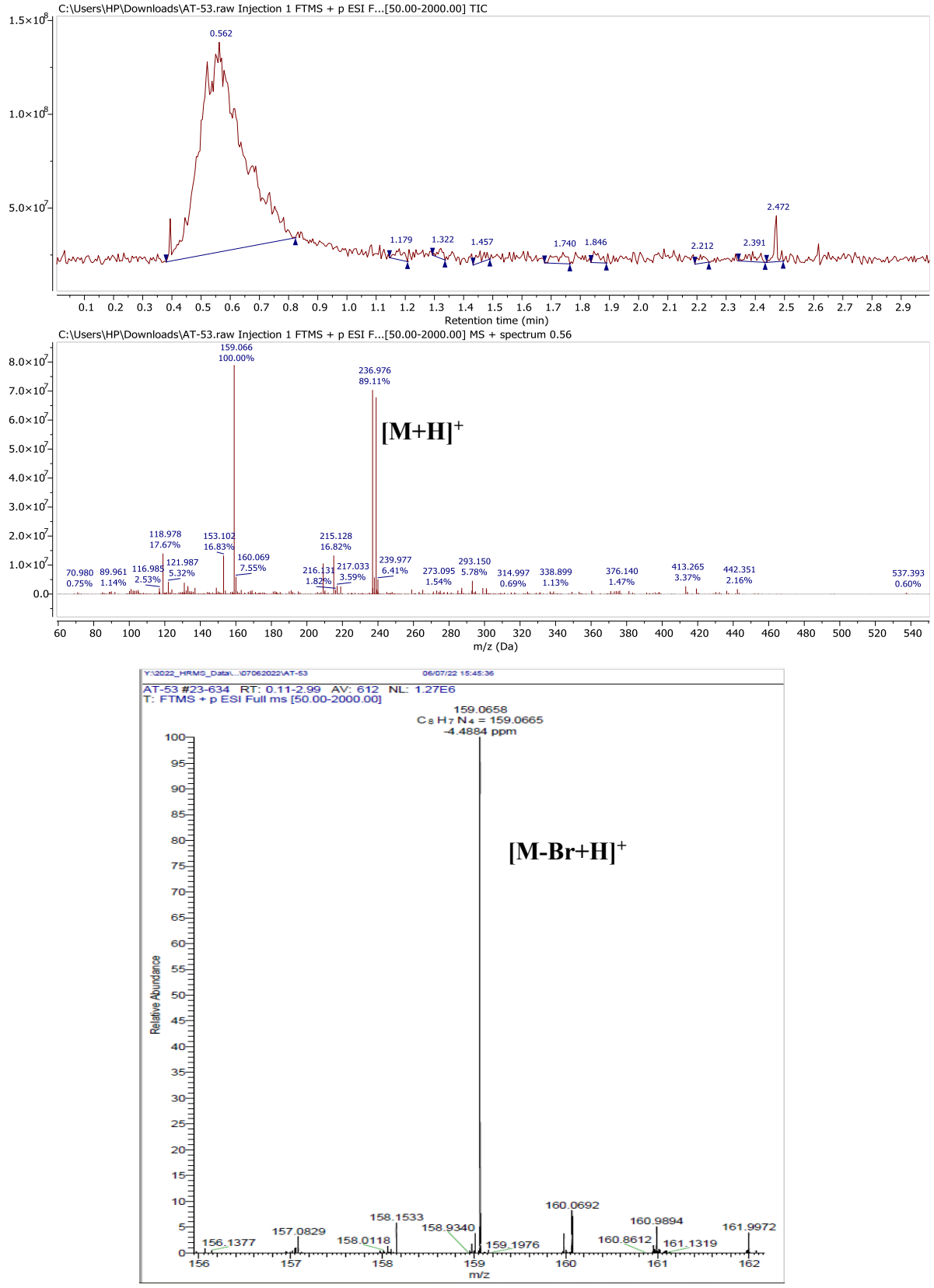

Figure 2.42. HRMS of compound **3r**.

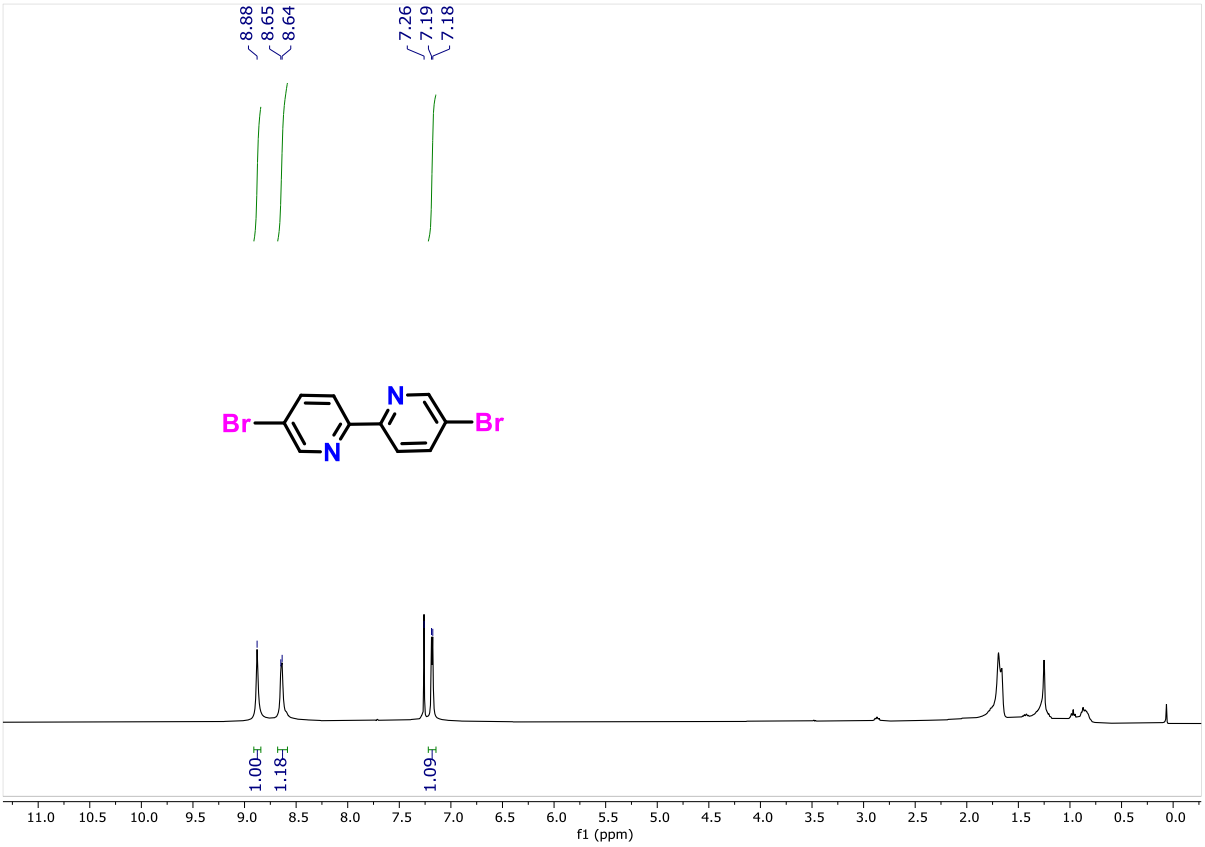

Figure 2.43. ^{1}H NMR spectra of compound **3s** in $CDCl_3$.

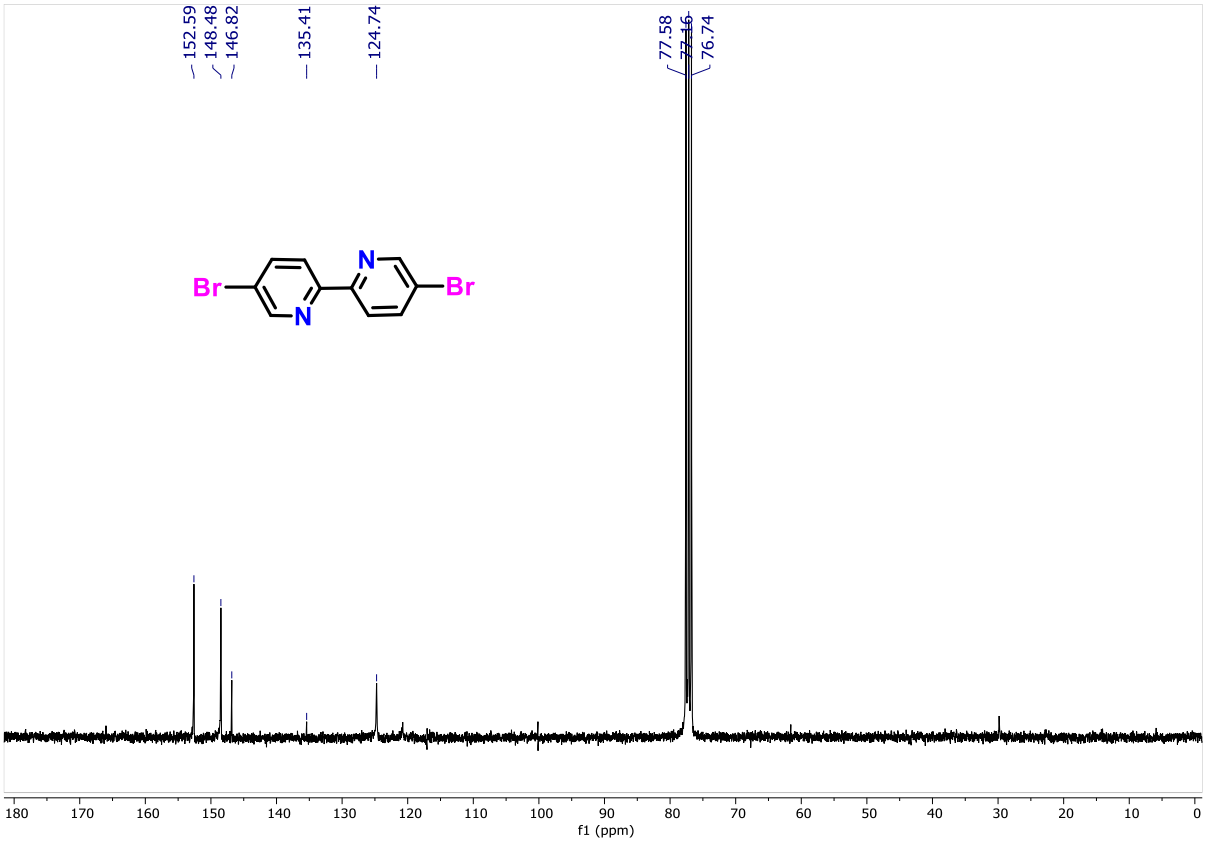

Figure 2.44. ^{13}C NMR spectra of compound **3s** in $CDCl_3$.

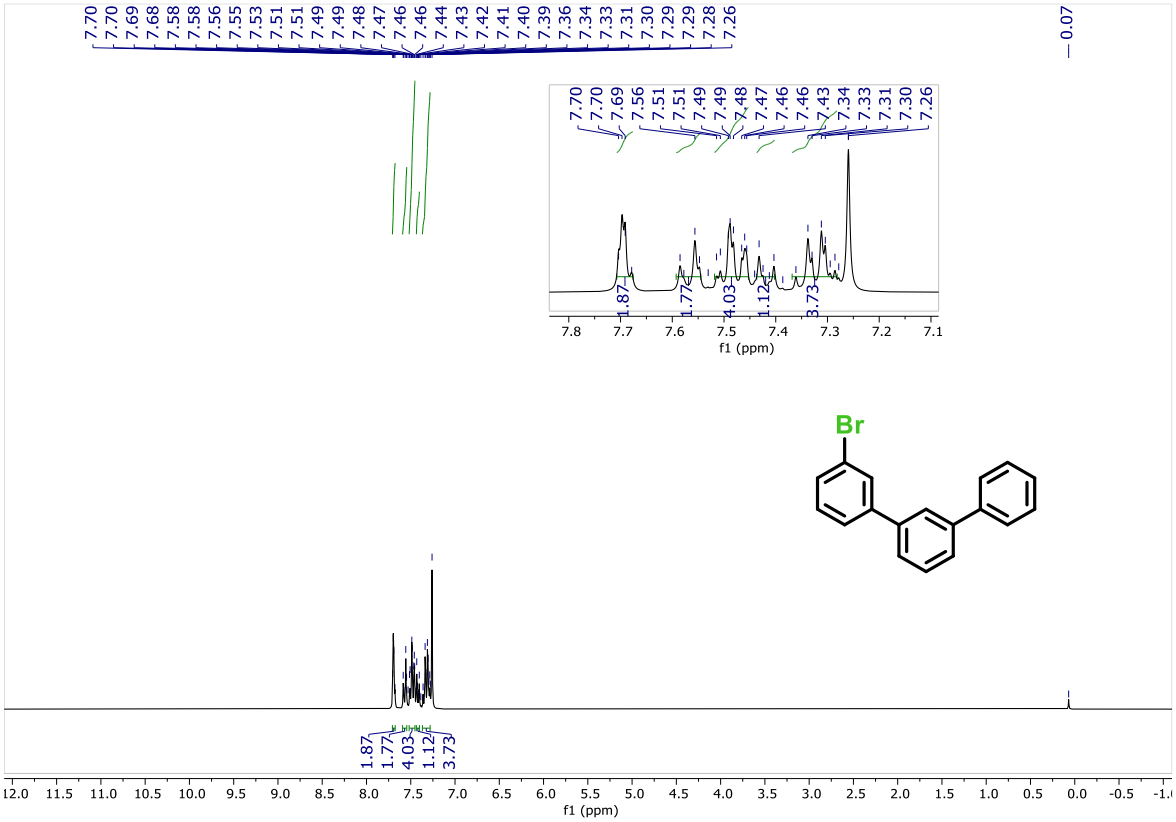

Figure 2.45. ^{1}H NMR spectra of compound **3t** in $CDCl_3$.

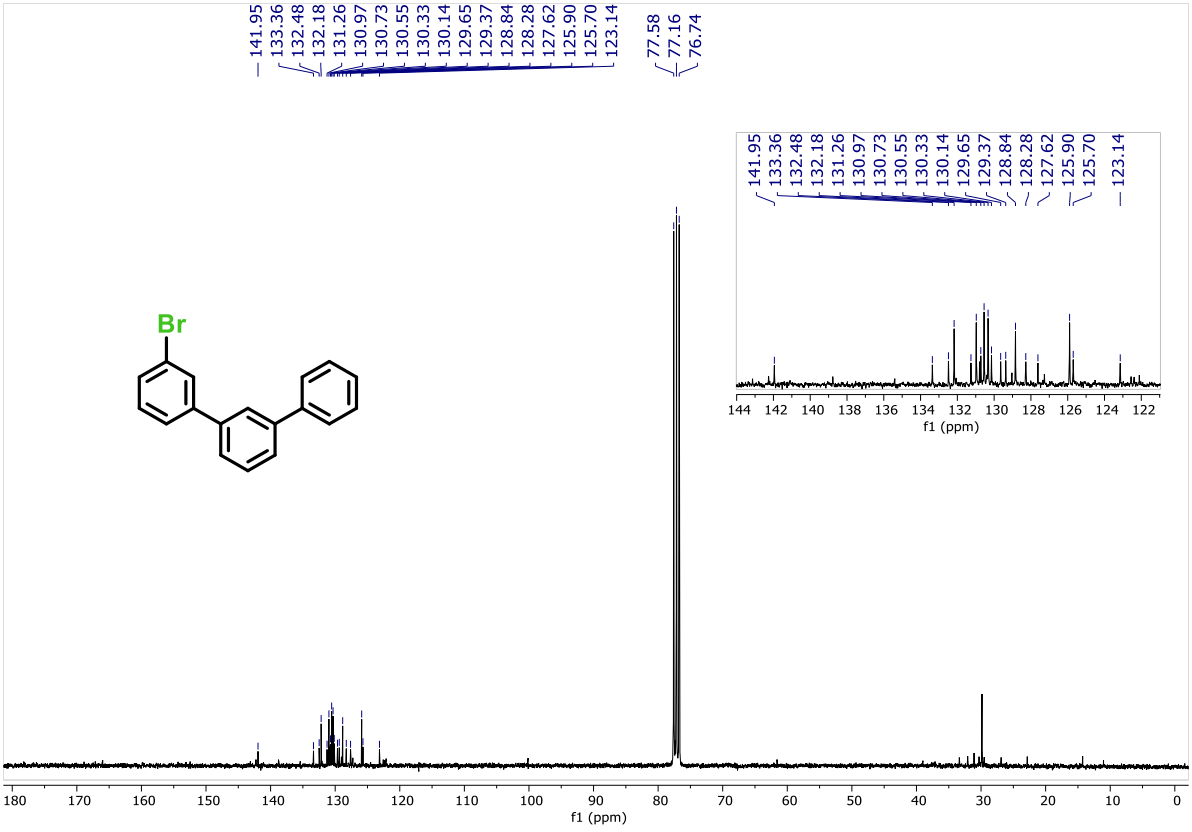

Figure 2.46. ^{13}C NMR spectra of compound **3t** in $CDCl_3$.

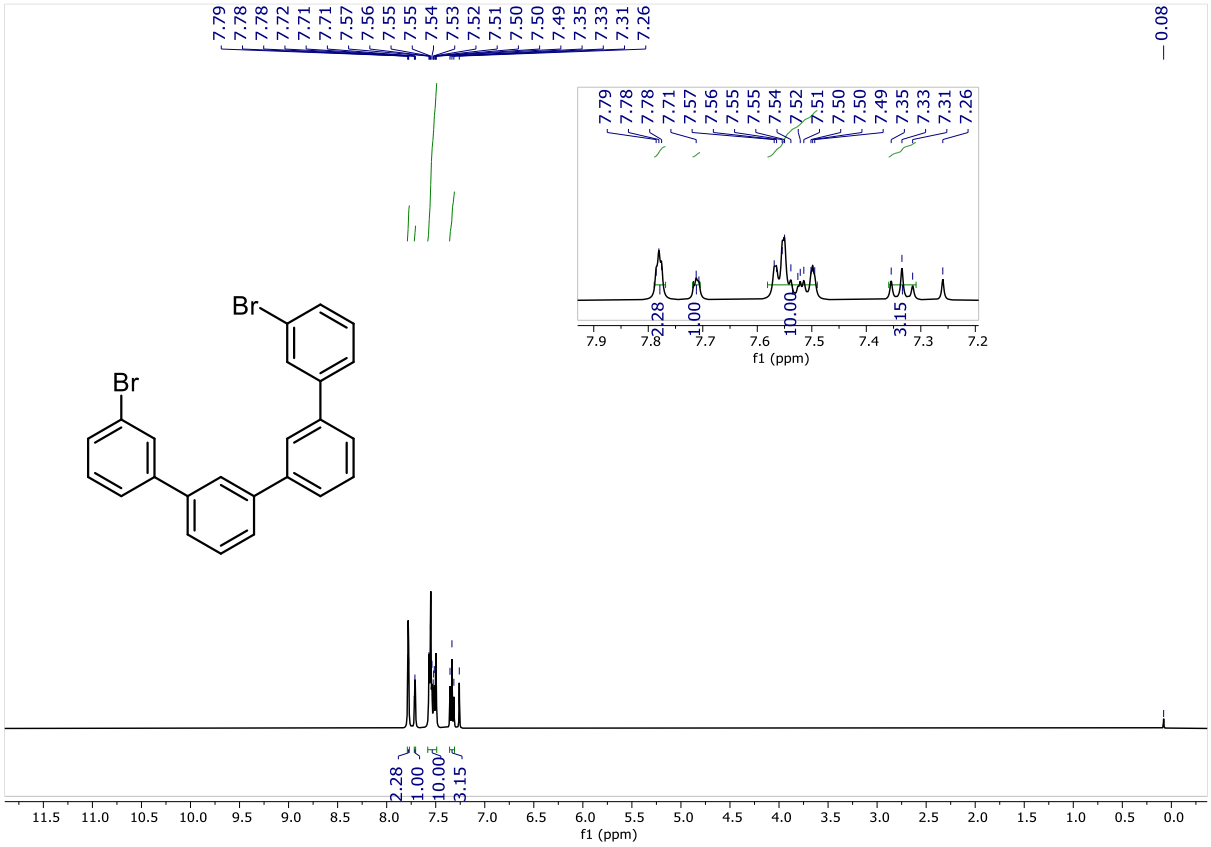

Figure 2.47. ^{1}H NMR spectra of compound **3u** in $CDCl_3$.

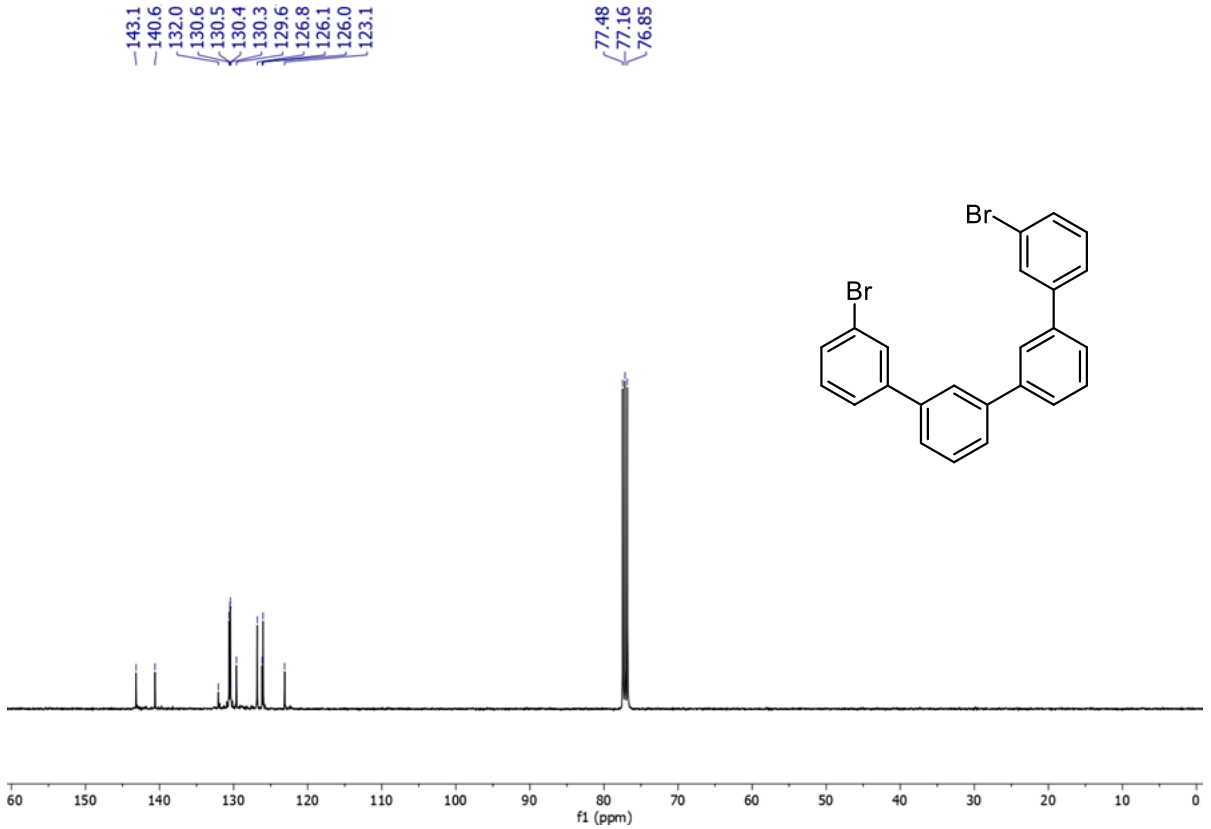

Figure 2.48. ^{13}C NMR spectra of compound **3u** in $CDCl_3$.

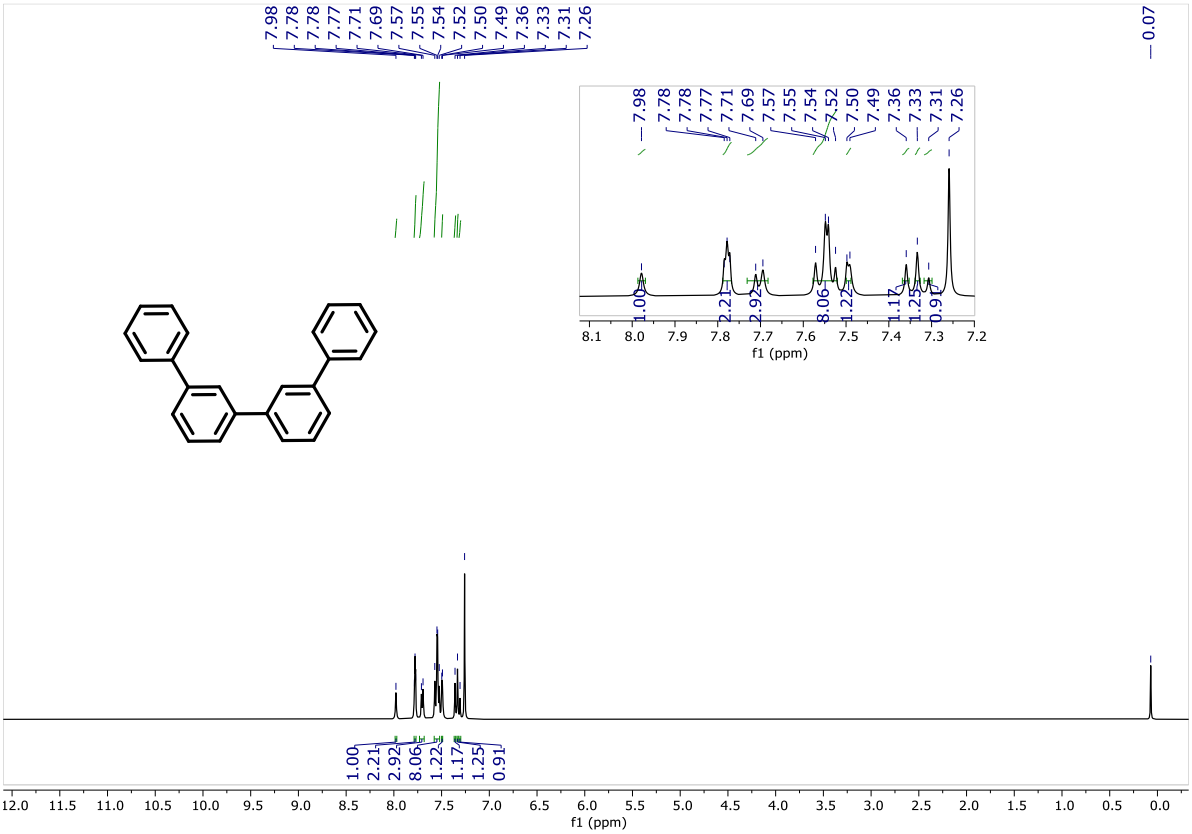

Figure 2.49. ^{1}H NMR spectra of compound **3v** in $CDCl_3$.

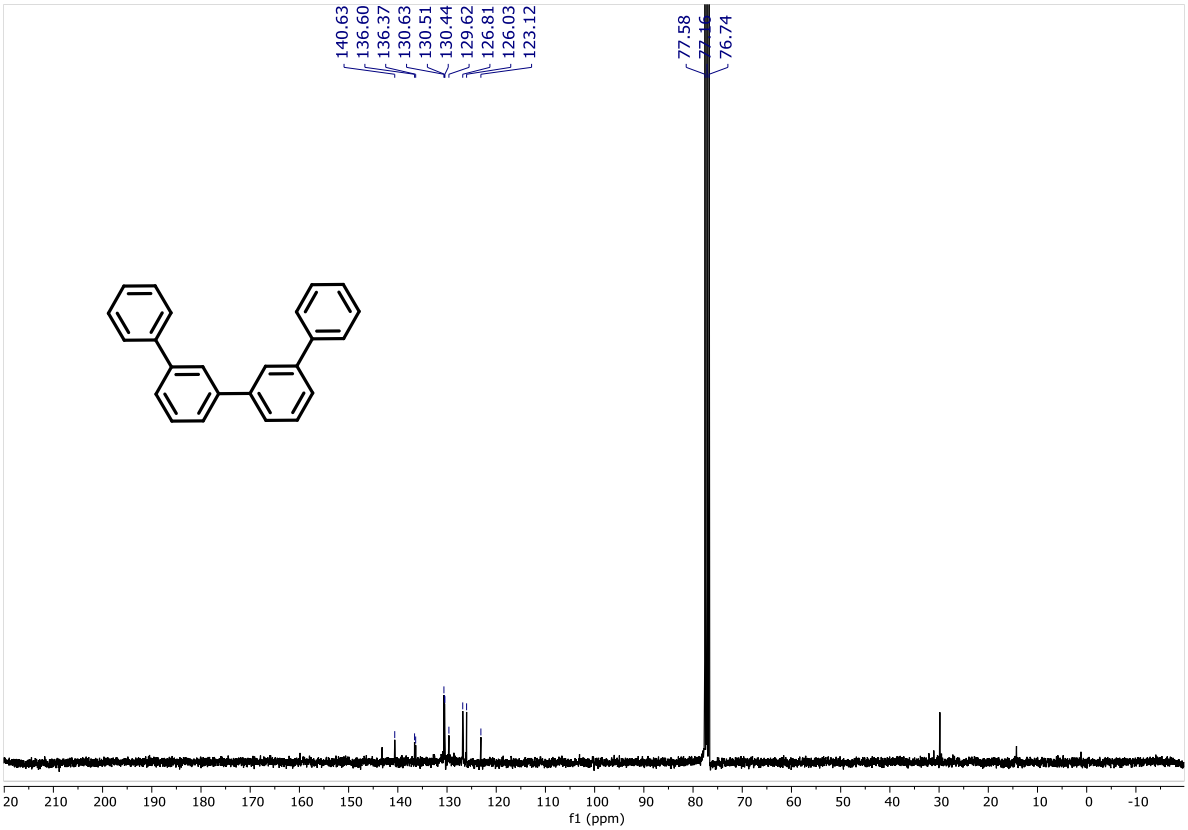

Figure 2.50. ^{13}C NMR spectra of compound **3v** in $CDCl_3$.

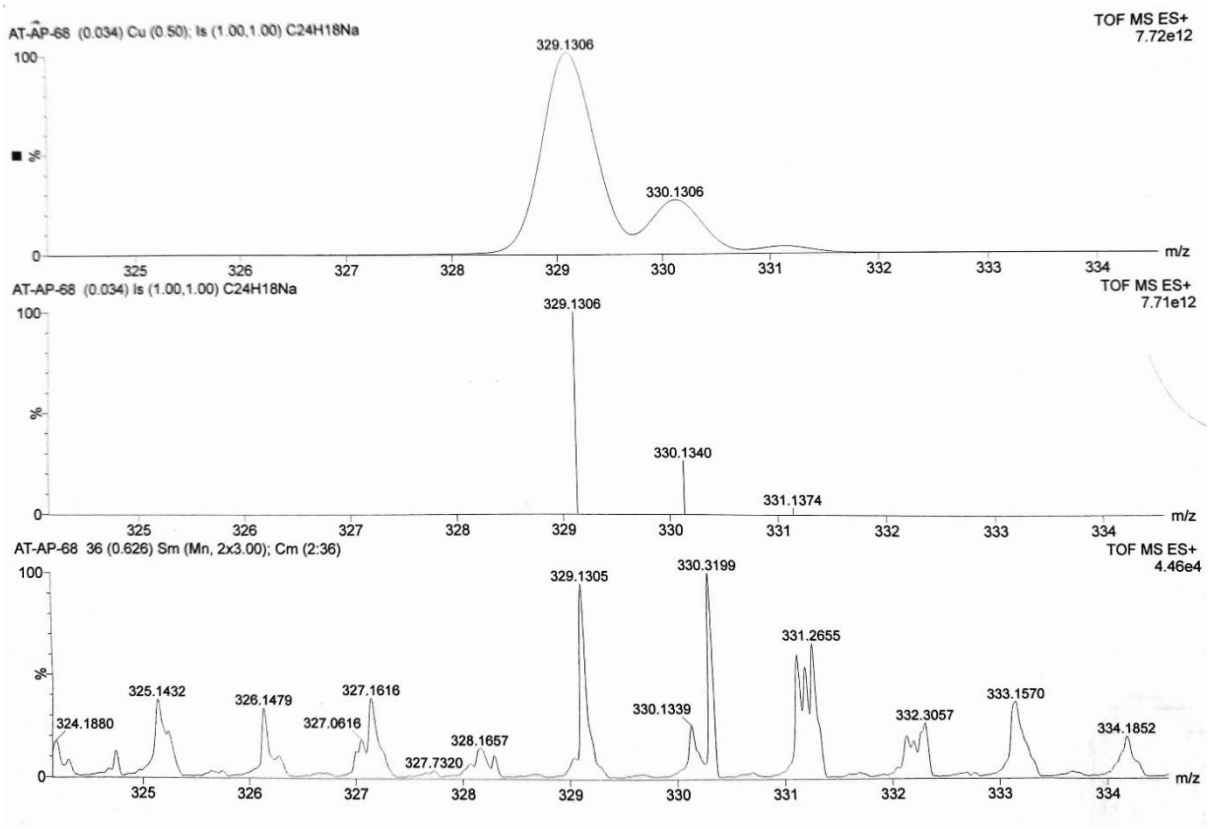

Figure 2.51. HRMS of compound **3v** $[M+Na]^+$.

Chapter 3

Microwave-assisted synthesis of *E*-aldimines, *N*-heterocycles and H_2 by dehydrogenative coupling of benzyl alcohol and aniline derivatives using $CoCl_2$ as catalyst

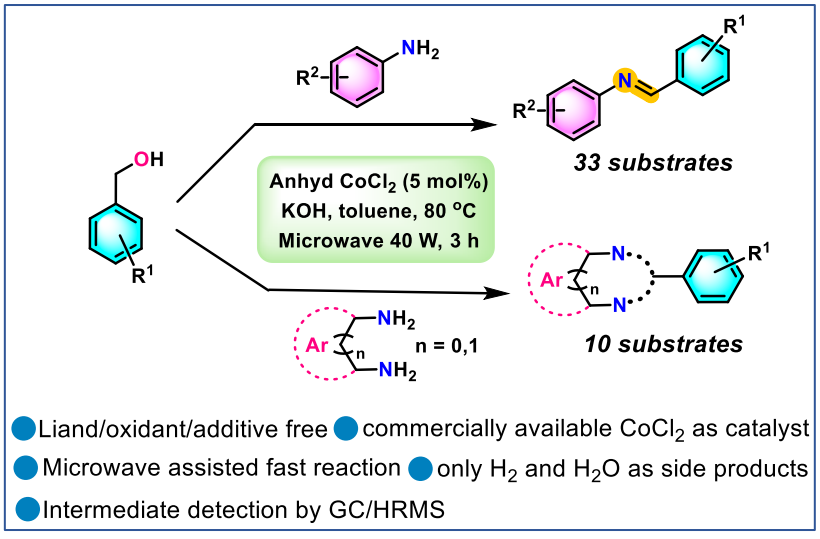

Representative Publication: *J. Org. Chem.* **2023**, *88,* 8955–8968.

3.1. Introduction

Imines constitute a major class of nitrogenous organic intermediates and are widely used in the broader areas of chemistry, biology, pharmacy and agriculture.[1] Owing to their unique structural features, they can also serve as ligands in coordination compounds. Among imines, aldimines are formed by the reaction between aldehydes and amines. A significant number of naturally occurring macrocycles like koranimine,[2] nostocyclopeptide A1[3] and lobatamide C[4] (Figure 3.1) contain such aldimine linkage. The most trivial way of producing aldimines is by the acid catalyzed condensation between aldehyde and amine. However, conventional acid/base-catalyzed condensation between aldehyde and amine is now replaced by versatile alternative methods, such as, condensation of primary amines *via* oxidation,[5] hydroamination of alkynes by amines,[6] oxidation of secondary amines,[7] etc. The greenest technique among the contemporary procedures is acceptorless dehydrogenative coupling (ADC), between amines and alcohols.[8] Dehydrogenative coupling between primary alcohols and derivatives of 1,2-phenylenediamine or 1,8 naphthalene diamines produce *N*-heterocycles specially benzimidazoles and hexahydropyrimidine derivatives respectively by an environmentally benign methodology. Benzimidazole, hexahydropyrimidine and their derivatives are important building blocks in the pharmaceutical industry, owing to their important biological activities such as antiulcer, anticancer, antifungal, antiarrhythmic, antihelmintic, antihistaminic, and antiviral activities.[9]

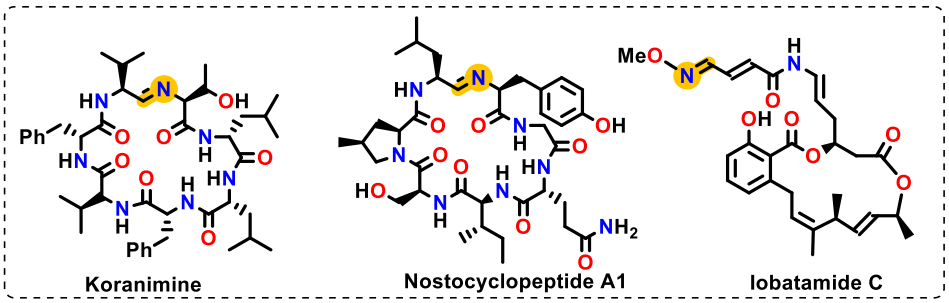

Figure 3.1 Some naturally occurring aldimines.

ADC mechanism provides superior advantages over conventional methods, firstly, since it is acceptorless, hence, no hydrogen acceptor is required, however, catalytic incorporation of the generated hydrogen into unsaturated organic molecules can give rise to tandem reactions in the same pot. Secondly, water and hydrogen are the only possible by-

products, hence less waste is generated. Thirdly, normally unreactive alcohols, or alcohols that are obtained from industrial wastes or biomass feedstock[10] can also be used consumed directly by this mechanism.

Significant recent advancements in the coupling of alcohol and amine[11-15] consist of homogeneous as well as heterogeneous catalysts[16] using precious transition metals like Ru,[11] Pd,[12a] Mo,[12b] Au,[12a,12c] and lanthanides like Ce.[12c,12f] Catalysts even based on cheap metals such as Cu,[13] Mn,[14] Fe,[15a] Ni[15b] or Co[8,17] have also been used however in the form of metal-ligand complex or oxide/mixed oxide forms or as nanoparticles (Scheme 3.1a). For example, a Mn-pincer complex was used to synthesize imine by the reaction between benzyl alcohol and benzyl amine at 135 ˚C for 60 h.[18] Subsequently, a Ru-complex was utilized for the reaction between benzyl alcohol and *n*-hexyl amine to obtain a mixture of imine and amide after 18 h under reflux.[11g] The same reaction when conducted with cyclohexyl amine, or aniline derivatives by ligand-assisted $Mo(CO)_6$ or Mn-complex gave imine selectively after 48-60 h of reaction at 164 ˚C. [12b,14a] All these methodologies have significantly advanced this field, however the major drawbacks are- use of expensive, sensitive, and capricious ligands, *e.g.*, phosphine ligands or phosphorus containing pincer molecules, not-easily-accessible precious metal complexes,[19] prior preparation of complexes or nanoparticles or mixed oxides, use of oxidant or other additives, harsh reaction conditions, such as high reaction temperatures, long time, inert atmosphere protection, and often, formation of by-products such as amide, ester or amine.[11a] Often a dimerized azo compound can be witnessed by the self-condensation of the amine derivatives in the basic medium.[20] Owing to increasing environmental and economic concerns, direct earth-abundant metal salts as catalysts have emerged as a desirable alternative to precious metal-ligand based catalysts or other sensitive procedures. Hence, the current interest revolves around building up environmentally benign and atom-economic methodology, avoiding all the undesired side products, with low-cost and earth-abundant readily available metal salts, without complicated ligand template under mild reaction condition.

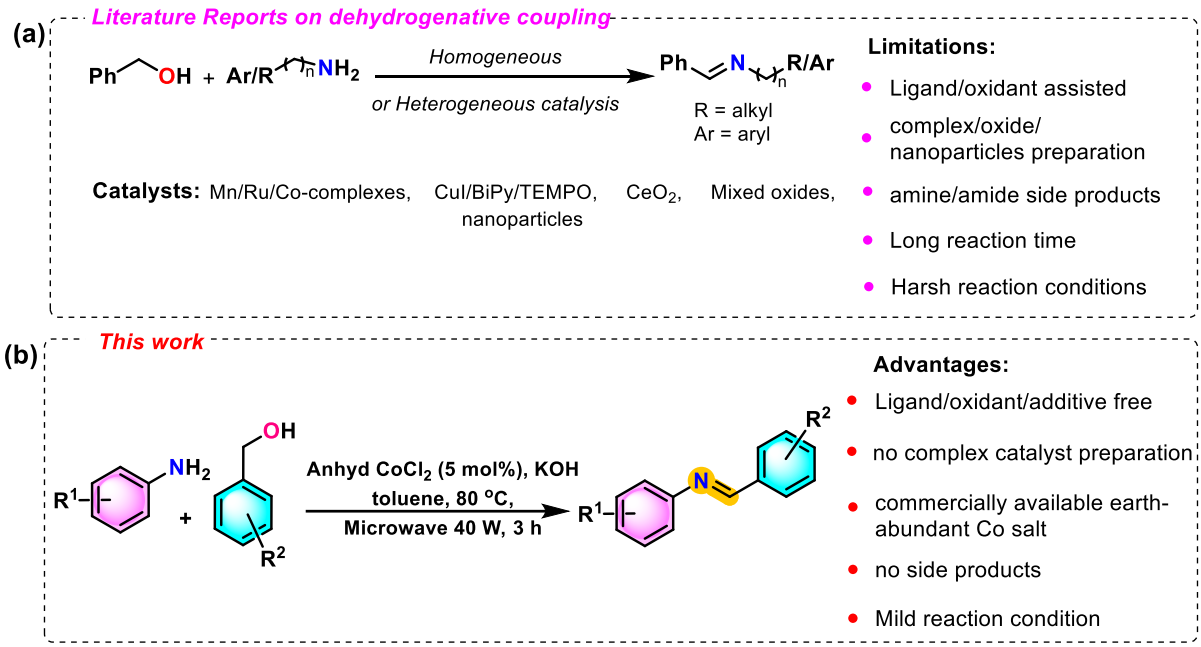

Scheme 3.1 (a) Literature reports on ADC-based alcohol-amine coupling, (b) Our synthetic scheme.

As a part of our continuous effort to develop Co-based catalyst in organic transformations,[21] since Co has limited toxicity and is found in various biological systems, we have developed an unprecedented green approach towards ADC of aniline with benzyl alcohol derivatives catalyzed by commercially available anhydrous $CoCl_2$, under microwave irradiation. To our knowledge, this is the first report of ADC-based homogeneous catalysis using commercially available earth-abundant simple Co metal salt under microwave irradiation, giving maximum product yield within very short time (3 h) and devoid of any ligand, oxidant or additives. This method yields *E*-aldimines selectively (Scheme 3.1b) along with H_2 and water, with no amine/amide/ester/azo as by-products, even in sealed tube. We have also extended this methodology to develop *N*-heterocycles with 1,8-diaminonaphthalene and 1,2-phenylenediamine units having the amino groups in close proximity.

3.2. Results and Discussions:

We started our initial optimization with aniline (**1a**) and benzyl alcohol (**2a**) as the model substrates. Since majority of the literature reported procedures require a longer reaction time, we started our optimization with 12 h of reaction time with 10 mol % of catalyst and 1 equiv of base at 90 ˚C in an oil bath (Table 3.1 entry 1), which gave 85 % product yield. Upon reducing the catalyst loading from 10 to 5 mol%, the product yield was found to remain same (Table 3.1 entry 2), however, further reduction (3 %) gave a fall in product yield (73 %) (Table

3.1 entry 3). The reaction time and temperature were then screened (Table 3.1 entries 4-8) and the maximum yield of product (85 %) was obtained for 5 mol % catalyst loading and 1 equiv base for 5 h under 80 ˚C heating (Table 3.1 entry 6). With a vision to reduce the reaction time further, we optimized the reaction using microwave reactor (Table 3.1 entries 9-17) and found the optimized condition to be with 5 mol% $CoCl_2$, 1 equiv KOH at 80 ˚C for 3 h under closed-vessel system of microwave reactor with 40 W power (Table 3.1, entry 9). The successful completion of the reaction even in presence of ligating agent PMe_3 (0.2 equiv) or catalyst poison Hg(0) suggests that the reaction follows a homogeneous catalytic pathway. Upon increasing the reaction time to 4 or 6 h under microwave reactor, no increase in product yield was obtained (Table 3.1, entries 10,11), whereas upon decreasing the reaction time to 2 h, a substantial decrease of yield (60 %) was observed (Table 3.1, entry 12). Increase in the quantity of base (1.5 equiv) did not produce any further effect in the overall yield of product, however decreasing the base loading to 0.8 equiv reduced the yield of product (60 %) (Table 3.1 entries 15,16). Since, similar yields were obtained for both KOH and KO^{t}Bu bases (Table 3.1 entry 17) in both inert and aerobic conditions, hence, all the further reactions were performed with KOH base under aerobic atmosphere, for convenience, under microwave reactor.

Table 3.1 Optimization of catalyst loading for reaction between aniline and benzyl alcohol.[a]

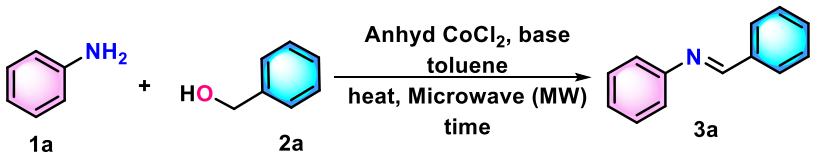

Entry	Mole % of anhyd $CoCl_2$	Base (equivalence)	Temperature (˚C)	Time (h)	% yield[b]
1	10	KOH (1)	90	12	85
2	5	KOH (1)	90	12	85
3	3	KOH (1)	90	12	73
5	5	KOH (1)	90	8	85
6	5	KOH (1)	80	5	85
7	5	KOH (1)	45	5	16
8	5	KOH (1)	60	5	29
9	**5**	**KOH (1)**	**80, MW**	**3**	**85, 84[c]**
10	5	KOH (1)	80, MW	4	85

11	5	KOH (1)	80, MW	6	85
12	5	KOH (1)	80, MW	2	60
13	5	KOH (1)	45, MW	3	18
14	5	KOH (1)	60, MW	3	30
15	5	KOH (0.8)	80, MW	3	60
16	5	KO^{t}Bu (1.5)	80, MW	3	84

[a]The reaction were performed taking **1a** (0.5 mmol) and **2a** (0.5 mmol). MW: Microwave reaction under closed vessel system. [b]GC yield with diphenyl as the standard. [‡]Equivalence taken with respect to the amine. All the reactions in normal heating have been performed under both nitrogenous and aerial conditions. Microwave reactions are performed under air in sealed tube closed vessel system. Other than microwave reactions, all the other heating reactions has been carried out in oil bath. [c]PMe_3 (0.2 equiv) was added in the reaction.

To explore the generalization of the methodology, a range of substrates containing electron-donating/withdrawing substituents were used (Table 3.2-3.4). A total of 43 substrates, including 7 new derivatives, were explored with this methodology. Aniline derivatives containing electron-donating groups, such as, *p*-toluidine (**1b**), 2,4-dimethylaniline (**1c**), 3,4-dimethylaniline (**1d**), *p*-anisidine (**1e**), 4-(4-tolyloxy)aniline (**1f**), 1-naphthylamine (**1g**) reacted with benzyl alcohol giving the corresponding imine derivatives (**3b**-**3g**) as the sole products in high yields (82-89 %). For sterically hindered aniline, such as 2,4-dimethoxyaniline (**1h**), the yield of product (**3h**) is moderate (79 %), despite containing two activating groups. Other sterically crowded anilines, such as 2,6-diisopropylaniline, 2,5-diethoxyaniline, prevented the formation of products even with elevated temperature and time, probably due to hindrance around the lone pair of N, inhibiting its reactivity. Deactivated haloanilines (**1i**-**1m**) reduced the yield of the products (**3i**-**3m**) to some extent (70-78 %) and it maintained the descending order of yield from bromo to fluoro derivatives. Thus, activating groups on aniline would facilitate the lone pair on N to attack the electrophile (*vide infra*), which in turn promotes the imine formation. On the other hand, deactivating groups pull the N lone pair towards the aniline ring decreasing its feasibility to attack the electrophile and extent of this deceleration becomes higher for more electronegative substituents on aniline ring.[22] Noteworthy to mention that, under heating conditions in an oil-bath, the time taken for the reaction of all the substrates vary from 5 h to 9 h, (Table 3.2).

Table 3.2 Substrate scope of aldimine formation from benzyl alcohol and substituted anilines.[a]

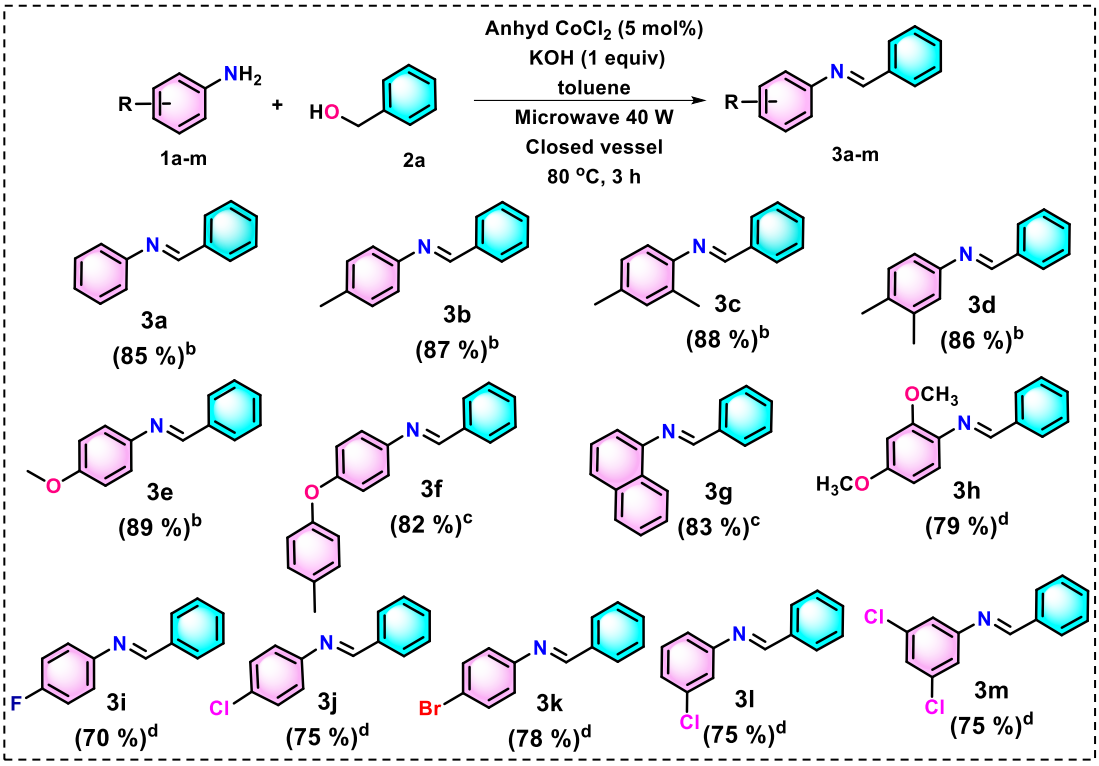

[a]Reaction condition Table 3.1 entry 9, 1 mmol scale. GC yields are obtained under microwave heating with biphenyl as internal standard. [b]5 h reaction time under heating in oil bath, [c]7 h reaction time under heating in oil bath, [d]9 h reaction time under heating in oil bath.

Successful application of our developed methodology to substituted aniline derivatives, rendered us to explore further with substitutions over the benzyl alcohol counterpart (Table 3.3). Unlike in anilines, in case of benzyl alcohol, deactivating substituents enhance the rate of reaction, however the stability of the corresponding aldimine derivatives gets deteriorated. The aldimine synthesis was explored with four derivatives of benzyl alcohol *viz.*, 4-chloro (**2b**), 3-nitro (**2c**) and 4-nitro (**2d**) and 4-fluoro (**2e**) which gave moderate to good yields (70-85 %) of products (**3n**-**3ae**). No product was obtained by employment of electron-donating group such as -OMe or -$N(Me)_2$ in the benzyl alcohol system, due to decrease in electrophilicity of the aldehyde intermediate involved (*vide infra*). The stability of the products containing electron-withdrawing groups in both the aniline and benzyl alcohol rings (**3t**-**3x**) is extremely poor. Although this methodology is excellent for aromatic systems, it does not work well for aliphatic amines and alcohols.

Table 3.3 Substrate scope of aldimine formation from benzyl alcohol derivatives and substituted anilines.[a]

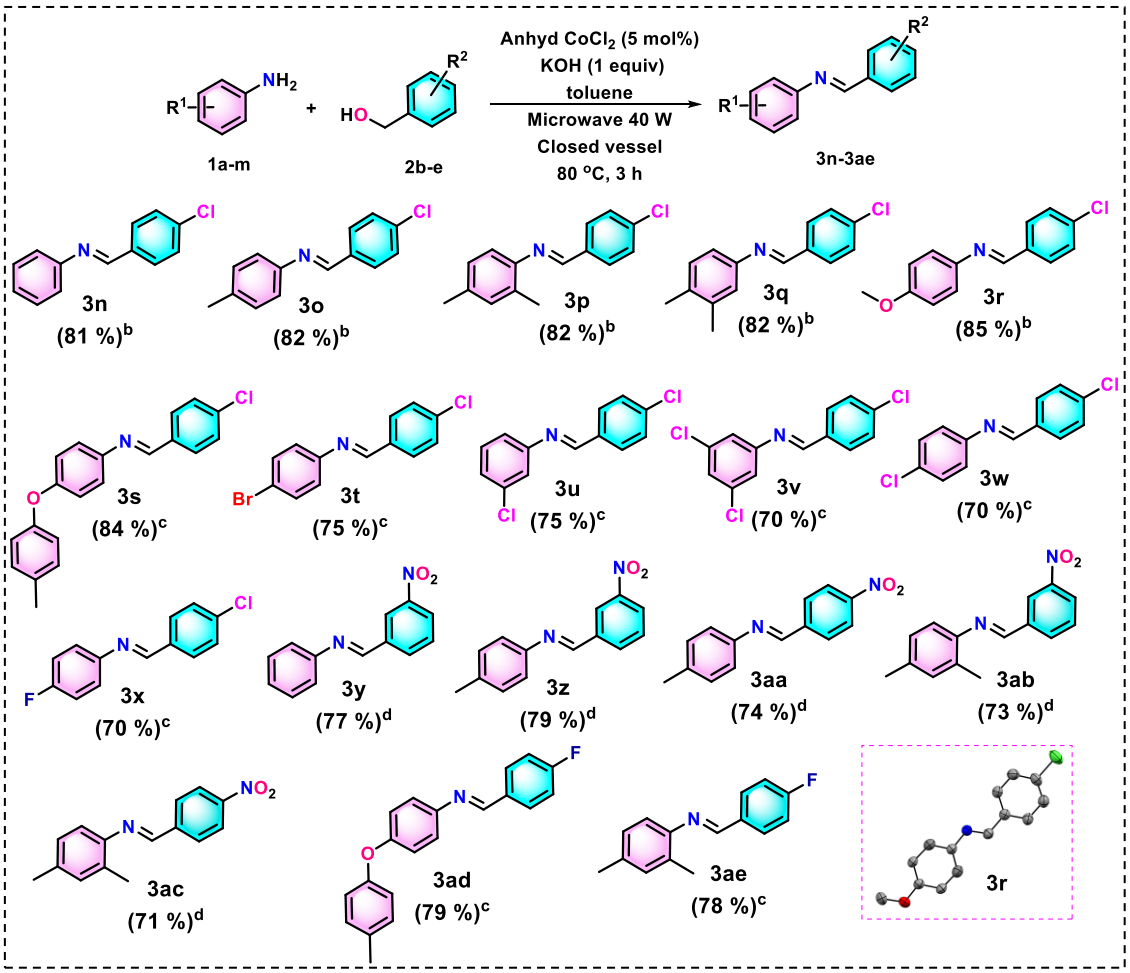

[a]Reaction condition Table 3.1 entry 9, 1 mmol scale. GC yields are obtained under microwave heating with biphenyl as internal standard. [b]5 h reaction time under heating in oil bath, [c]7 h reaction time under heating in oil bath, [d]9 h reaction time under heating in oil bath.

With a view to extend the methodology to diamine systems, reactions between three diamine systems (4,4'-(((perfluoropropane-2,2-diyl)bis(4,1-phenylene))bis(oxy))dianiline (**1n**), 1,8-diaminonaphthalene (**1o**) and *o*- phenylene diamine (**1p**)) with benzyl alcohol derivatives were observed (Table 3.4). For diamine systems, where the two amino groups are widely separated, like 4,4'-(((perfluoropropane-2,2-diyl)bis(4,1-phenylene))bis(oxy)) dianiline (**1n**), two aldimine linkages were formed (**3af** and **3ag**). However, diamines like, 1,8-diaminonaphthalene (**1o**) and *o*- phenylene diamine (**1p**), where the amino groups are in close proximity tend to form the most stable 5/6 membered cyclic products *i.e.*, hexahydropyrimidine derivatives (**3ah-3aj**) with the former one and two types of benzimidazole derivatives (**3ak-3ao** and **3ap/3aq**) with the latter one, regardless of the equivalence (1 or 2 equiv with respect to

aniline derivative) of the benzyl alcohol used. The formation of cyclic products was further confirmed by single crystal X-ray diffraction analysis of **3ap**.

Having obtained the optimized reaction conditions, we explored the applicability of the methodology in large scale. Gram-scale synthesis of compounds **3a**, **3b** and **3e** (Scheme 3.2) were accomplished under the optimized standard microwave conditions and the respective yields were found to be 80 %, 75 % and 85 %.

The geometrical configuration of all the resulting aldimine is confirmed to be *E*-selective from ^{1}H-^{1}H 2D NOESY (Figure 3.2a) and COSY spectrum of **3e** (Figure 3.92), and also from single crystal X-ray diffraction analysis of **3r** (Table 3.3). Monitoring the consumption of amine (*p*-anisidine), conversion of benzyl alcohol to benzaldehyde intermediate and production of the corresponding aldimine **3e** by GC (Figures 3.2b and 3.2c) suggests that the benzyl alcohol is almost completely consumed and benzaldehyde is formed in the reaction mixture. However, the *p*-anisidine is not completely consumed and it coexists with both the intermediate (benzaldehyde) and product in the reaction mixture, maintaining a particular ratio of concentrations after a certain time (5 h) under heating condition (Figure 3.2b). Further, as shown in Figure 3.2c, the percent yield of product (aldimine) is less than the percent conversion of benzyl alcohol to benzaldehyde. Both of these observations suggest the existence of an equilibrium of the product with its corresponding amine and aldehyde counterparts.[23]

In order to gain more insight on the generation of the benzaldehyde intermediate from benzyl alcohol and to identify the RDS, kinetic isotope effect was observed with deuterated alcohol. The optimized reaction was conducted with (benzyl alcohol)-*α*-*d* and aniline, wherefrom, a mixture of deuterated and non-deuterated imine products was obtained with Ph-CH=N-Ph/Ph-CD=N-Ph ratio around 1:3. This kinetic isotope effect (Figure 3.2c) suggests that H is abstracted around 3 times faster than deuterium and the benzaldehyde generation from benzyl alcohol is the rate-determining step. Similar results were also obtained for aldimines formed from benzyl alcohol and *p*-anisidine and 4-chloroaniline separately, where the Ph-CH=N-Ar/Ph-CD=N-Ar ratio is ~1:3 both for *p*-anisidine and 4-chloroaniline (Figures 3.118 and 3.119), suggesting that this rate-determining step is basically independent of the nature of substituent over the aniline ring.

Table 3.4 Substrate scope for reaction between from benzyl alcohol and diamines.[a]

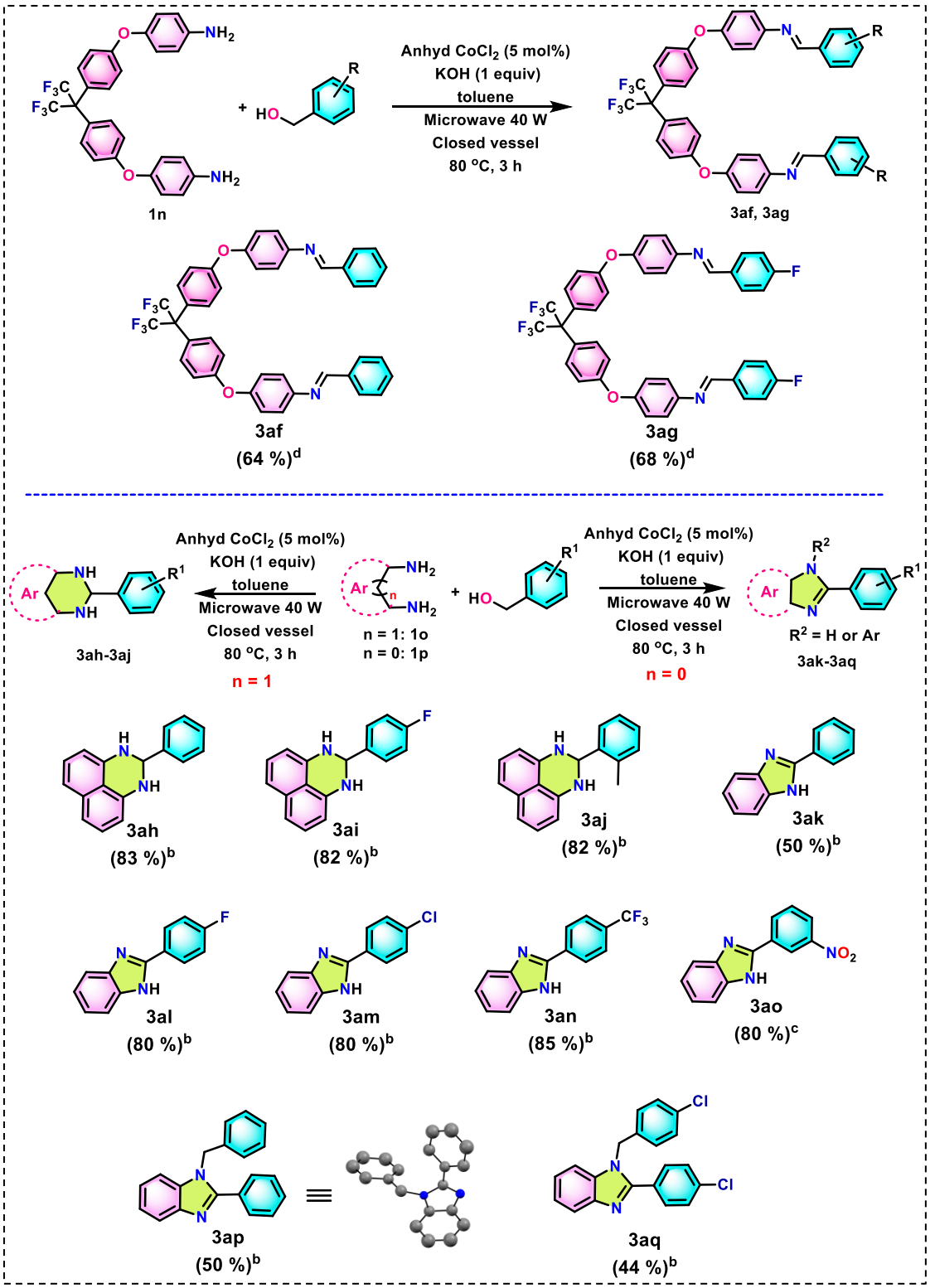

[a]Reaction condition Table 3.1 entry 9, 1 mmol scale. GC yields are obtained under microwave heating with biphenyl as internal standard. [b]5 h reaction time under heating in oil bath, [c]7 h reaction time under heating in oil bath, [d]9 h reaction time under heating in oil bath.

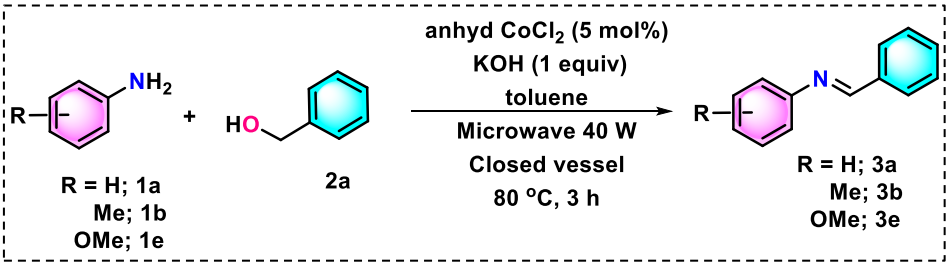

Scheme 3.2 Gram-scale reaction.

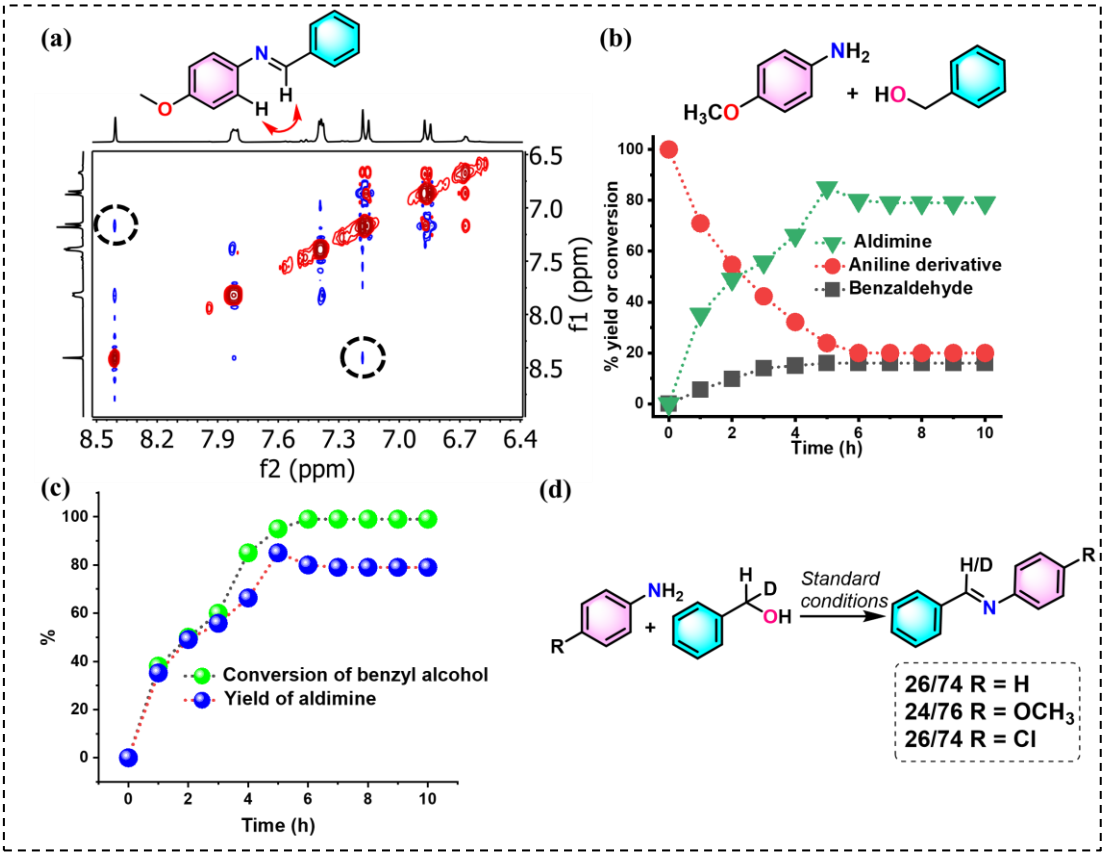

Figure 3.2 (a) ^{1}H-^{1}H 2D NOESY spectrum; (b) Variation of concentrations[a] of aldimine, benzaldehyde and *p*-anisidine with time; (c) Variation of percent conversion of benzyl alcohol and percent yield of aldimine with time; (d) Kinetic isotope effect in aldimine formation. [a]GC concentrations with diphenyl as the standard.

It is witnessed from the GC yields of aldimines that, the reaction is more feasible when aniline contains electron-donating substituents, rather than when it contains electron-withdrawing substituents (Figure 3.3a). Thus, the yield of imine increases gradually from unsubstituted aniline (**3a**) (85 %) to methyl substituted ones (**3b**-**3d**) (86-88 %) to methoxy substituted aniline (**3e**) (89 %) and from 4-fluoroaniline (**3h**) (70 %) to 4-bromoaniline (**3j**) (78 %) *via* 3/4-chloroaniline (**3i** and **3k**) (75 %). To gain insight on such variation of yields, the

role of substituents over the reaction mechanism was observed by Hammett plot, for which kinetic studies were essential. Kinetic studies were performed through monitoring the reaction between benzyl alcohol and *p*-anisidine with time by GC, taking four different ratios (Sets A-D) of benzyl alcohol (BA) and aniline derivative (A) (Figure 3.3b). Calculations suggested a first-order rate dependency of the reaction on both the benzyl alcohol and *p*-anisidine. Subsequently, Hammett plot with a range of diverse substituents on the aniline system (Figure 3.3c) was obtained from the percent consumption of the starting aniline derivatives, as observed from GC. This resulted in a V-shaped curve with a negative slope having $\rho = -3.53$ for electron-donating substituents whereas a positive slope with $\rho = 2.71$ for electron-withdrawing ones. The analysis of this curve suggests the formation of an intermediate with positive charge density (TS-A) (Figure 3.3c, inset) for electron-donating substrates and negative charge density for electron-withdrawing substrates (TS-B) (Figure 3.3c, inset).[24]

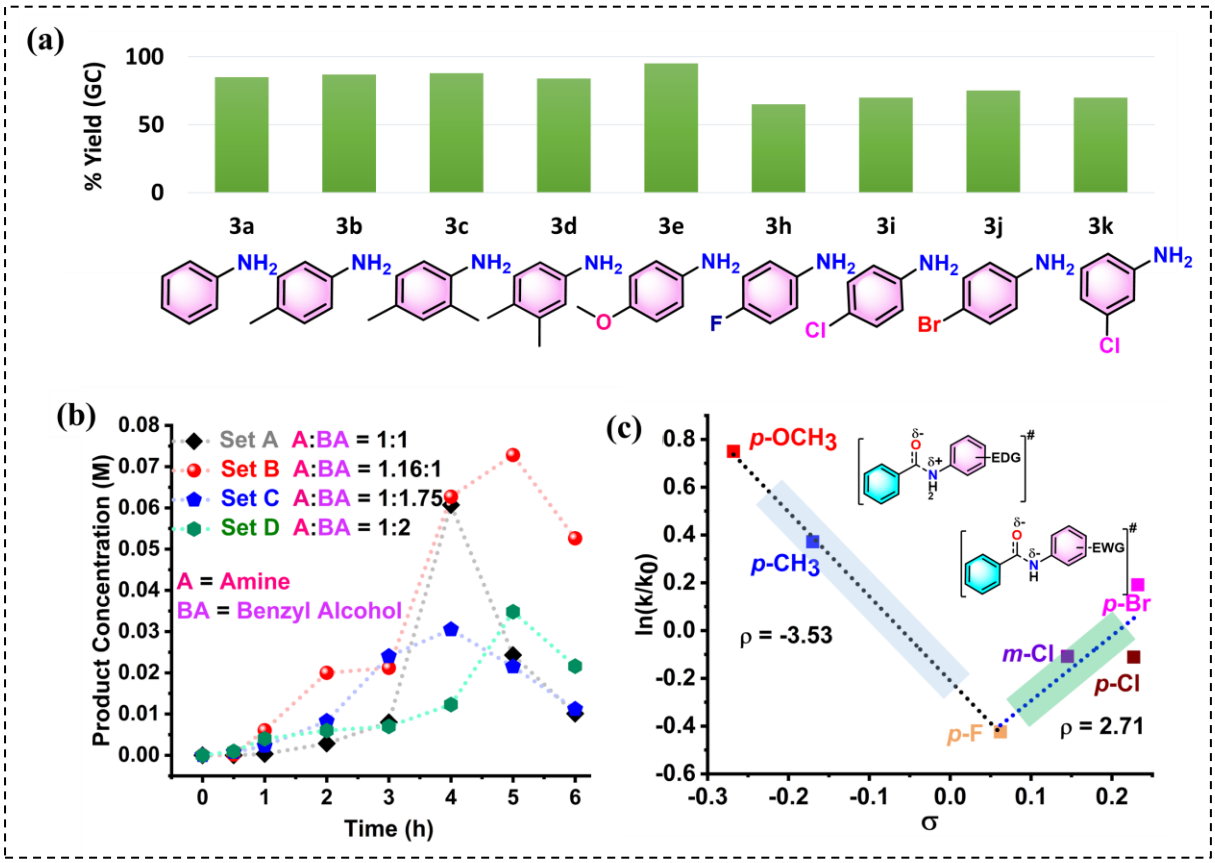

Figure 3.3 (a) Comparison of yields of aldimines with variation in the substituents of aniline for the reaction with benzyl alcohol; (b) Variation of GC yield of product with reaction time for the reaction between benzyl alcohol and *p*-anisidine to determine order of the reaction; (c) Hammett plot for different substituents in the aniline ring.

Such a Hammett plot indicates that, for electron-donating groups, the reaction may initiate from the lone pair of the N atom, whereas for electron-withdrawing groups, deprotonation from the N atom (more acidic H's) may lead to the negative charge density on the intermediate (TS-B). The latter mechanism may not be stable enough, as it involves two negative charge centres in near vicinity, which justifies the poor yield of the products with electron-withdrawing groups over aniline system (Scheme 3.3).[25]

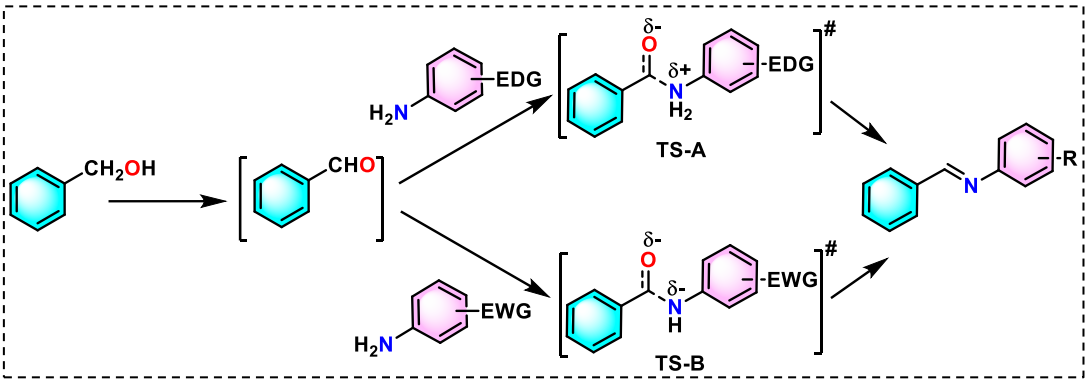

Scheme 3.3 Mechanism of product formation through variation in plausible transition states (TS-A and B).

To validate the results obtained from Hammett plot, three competition experiments with substituted aniline derivatives were conducted (Scheme 3.4). The first set of competition experiment was observed between aniline and *p*-anisidine for reaction with benzyl alcohol, the second one between aniline and 4-bromoaniline and the third one between *p*-anisidine and 4-bromoaniline. In all the sets, the aldimine products corresponding to the electron-withdrawing 4-bromoaniline was minimum whereas, that corresponding to the electron-donating *p*-anisidine was maximum. Competition experiment yet again proves the feasibility of imine formation with electron-donating substituents on aniline, even in the presence of electron-withdrawing aniline derivatives in the same pot.

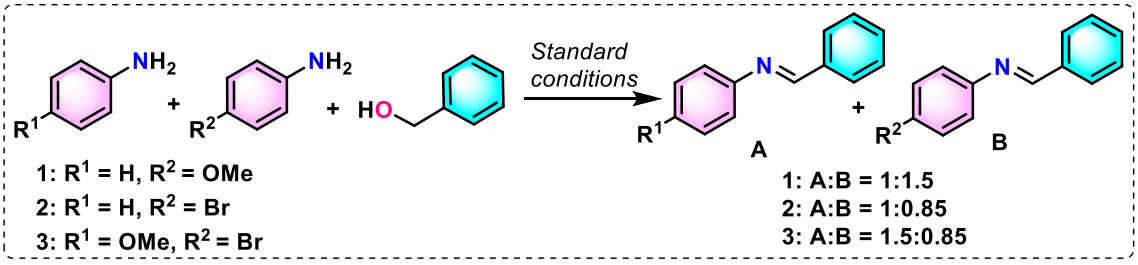

Scheme 3.4 Competition experiments with electron-donating and electron-withdrawing substituents on the aniline ring.

A series of controlled experiments were conducted to find out the exact mechanism of the reaction. H_2 gas was detected by GC from the reaction mixture of benzyl alcohol and aniline derivatives (Scheme 3.5(i)), suggesting the mechanism to be ADC *i.e.*, the alcohol first gets converted to aldehyde (by releasing H_2) and then amine reacts with aldehyde to produce corresponding aldimine. Hence, benzaldehyde is the reaction intermediate, and it was also detected in GCMS from the reaction mixture. Controlled experiments for the dehydrogenation of benzyl alcohol to benzaldehyde suggest the active role of both $CoCl_2$ and KOH (Scheme 3.5(ii)) without any requirement for aniline. However, its presence accelerated the dehydrogenation, indicating the existence of an equilibrium between benzyl alcohol and benzaldehyde, which moves forward upon consumption of aldehyde by amine.[11c,11e] Similar equilibration was also obtained for two other benzyl alcohol derivatives (4-chlorobenzylalcohol and 3-nitrobenzylalcohol) as well (Figures 3.109, 3.110). Absence of base produces a minute amount of benzaldehyde, whereas absence of $CoCl_2$ does not produce benzaldehyde from benzyl alcohol at all. Subsequently, the overall reaction was found to be most feasible in presence of both base and catalyst, the reaction was too sluggish to occur in absence of the catalyst and no product were obtained in absence of the base under the optimized reaction condition (Scheme 3.5(iii)). Condensation between amine and the generated aldehyde was found to be independent of the presence of catalyst (Scheme 3.5(iv), left). To investigate whether any radical pathway is involved in the reaction mechanism, benzyl alcohol was reacted with aniline under standard conditions in presence of radical scavenger 2,2,6,6-tetramethyl-1-piperidinyloxy (TEMPO) and butylated hydroxytoluene (BHT). It was observed that the desired imine product was obtained in normal yield even in presence of TEMPO/BHT, which proves that radical pathway is not involved in the whole reaction (Scheme 3.5(iv), right) mechanism.

Taking inference from all these controlled experiments, the plausible mechanism (Scheme 3.6) is suggested to be such that proton is abstracted from benzyl alcohol by the base and the deprotonated species chelates with the $CoCl_2$ to form intermediate **C**. The species **D**, formed from this intermediate **C** by elimination of Cl was detected by GC and HRMS from the reaction mixtures (Figures 3.104-3.106). The intermediate **C** gives the corresponding aldehyde by abstracting H from the chelated benzyl alcohol and eliminating it as H_2, which was again detected by GC. The generated benzaldehyde (detected by GC) then undergoes condensation with amine, already present in the reaction mixture, to give *E*-aldimine selectively. The $CoCl_2$

catalyst does not promote the parallel borrowing hydrogen, or β-hydrogen elimination mechanism, which is could produce amine or any other side product.

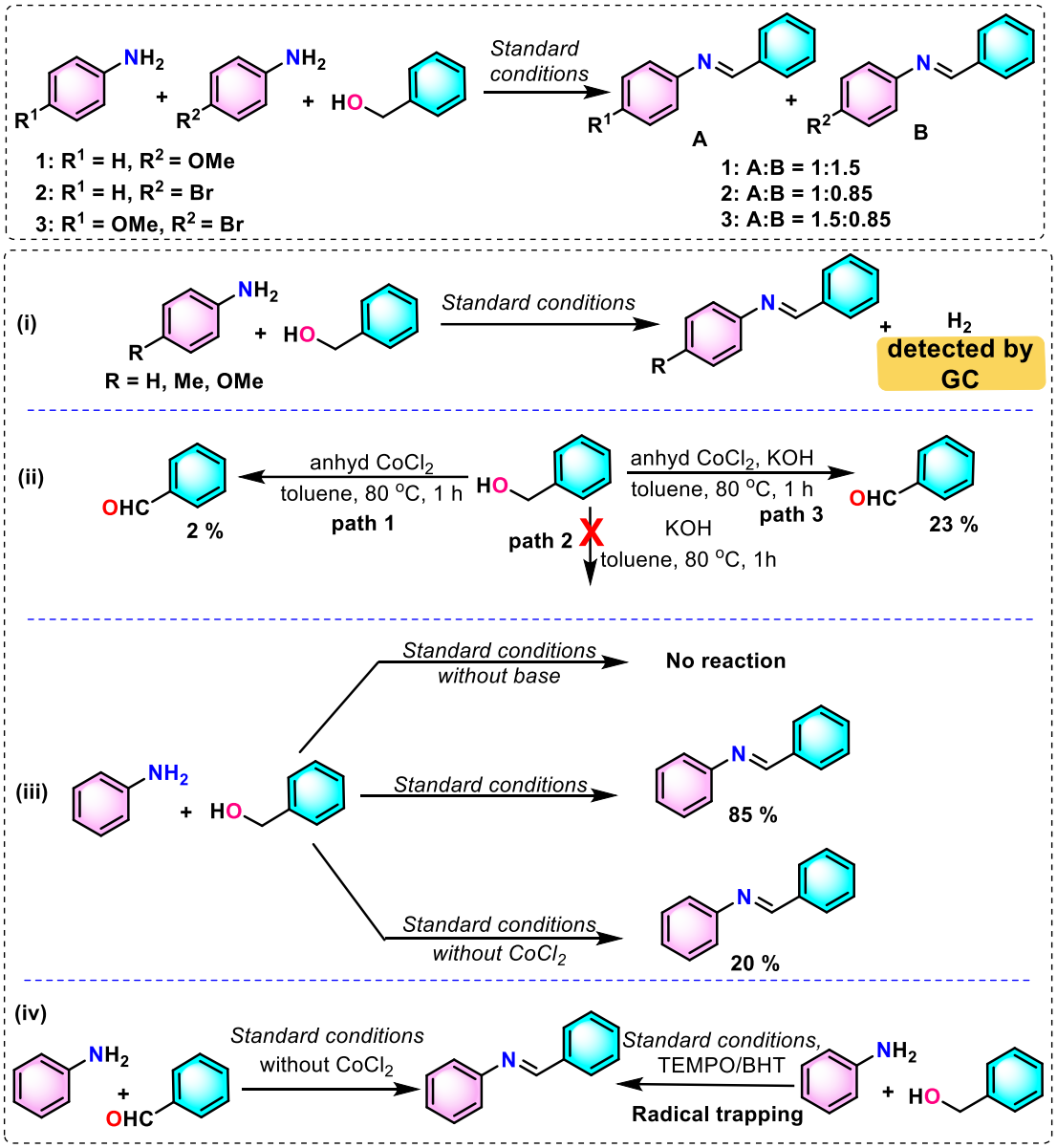

Scheme 3.5 Controlled experiments to determine the mechanism of reaction.

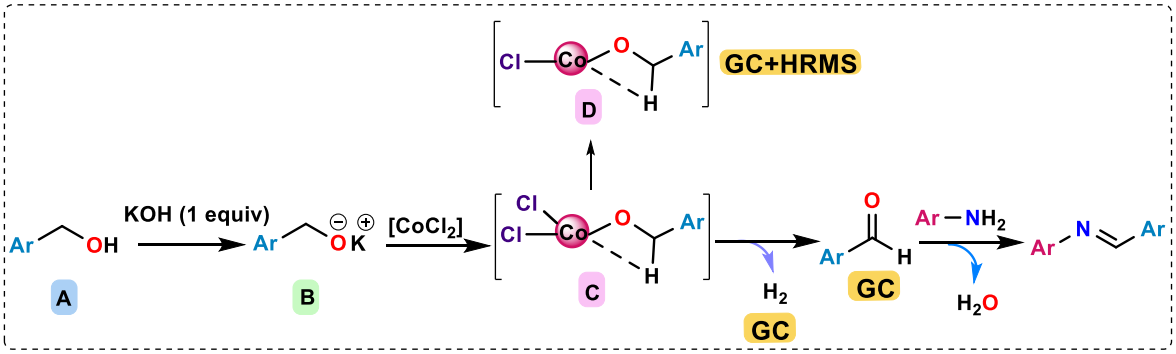

Scheme 3.6 Plausible mechanism of imine formation reaction.

3.3. Conclusion

Herein, we have explored an easy, fast, convenient, and atom-economic methodology of *E*-aldimine and *N*-heterocycles synthesis (43 substrates including 7 new) *via* acceptorless dehydrogenative coupling between aromatic primary amines and benzyl alcohols by using low-cost commercially available $CoCl_2$ catalyst under a microwave reactor for the first time. The catalytic reaction liberates H_2 under basic conditions and produces only H_2O as side-product. A variety of aniline and benzyl alcohol derivatives furnished the reaction with moderate to good yield without the need of inert atmosphere protection. Kinetic and mechanistic studies involving GC, intermediate identification by HRMS, kinetic isotope effect and Hammett analysis sheds light on the detailed nature of the ADC mechanism of catalytic cycle and imine formation.

3.4. Experimental section:

3.4.1. Materials and reagents

Commercially available toluene has been used for reaction without further distillation. Anhydrous $CoCl_2$ was purchased from Spectrochem and used directly for reaction. KOH and KO^tBu were purchased from SRL. All the commercially available amine and benzyl alcohol derivatives were used directly without further purification. $NaBD_4$ was purchased from Sigma-Aldrich. TEMPO, BHT and PMe_3 were purchased from Sigma Aldrich. Analytical thin layer chromatography (TLC) was performed on pre-coated silica gel 60 F_{254}. Visualization on TLC was achieved with UV light (254 nm). Column Chromatography was carried out using activated neutral alumina as the stationary phase.

3.4.2. Instrumentation

^1H and ^{13}C NMR spectra were obtained with BRUKER 300 MHz and 400 MHz FT-NMR spectrometers and the chemical shifts are reported in ppm, using tetramethylsilane as an internal standard and were referenced to the residual solvent as follows: $CDCl_3$ = 7.26 (^1H), 76.16 (^{13}C) ppm, DMSO = 2.51 (^1H), 39.50 (^{13}C) at room temperature. For ^1H NMR, coupling constants *J* are given in Hz and the resonance multiplicity is described as s (singlet), d (doublet), t (triplet), m (multiplet), dd (doublet of doublet), dt (doublet of triplet), td (triplet of doublet), tt (triplet of triplet), q (quartet) br s (broad singlet). ^{13}C NMR spectra were fully decoupled by

broadband proton decoupling. Structural assignments were made with additional information from gCOSY and gNOESY experiments. High-resolution mass spectra (HRMS) were obtained from Waters (Xevo G2 Q-TOF) mass spectrometer in electrospray ionization mode (ESI+), CHN analysis was performed on a CHNS analyser. GC studies of the reaction mixture were obtained from PerkinElmer Gas Chromatograph Clarus 590 and H_2 detection by GC was obtained using TCD detector from Agilent 8860 (G2790A). CEM microwave reactor (Discover System, Model no. 908010) was used for reactions in microwave. For reactions that require heating, oil bath and microwave reactor were used. Reactions in microwave reactor are all performed in sealed condition of closed vessel system.

3.4.3. General procedure for the reaction of benzyl alcohols with amines:

3.4.3.1. Under normal heating: In a round-bottomed flask, amine (1 mmol), benzyl alcohol (1 mmol), base (KOH, 1. mmol) and anhydrous $CoCl_2$ (0.05 mmol) were taken and dissolved in toluene at room temperature. The temperature of the reaction mixture was allowed to rise to 80 ˚C in an oil bath and the temperature was maintained for 5-9 h. After 5-9 h, water was added to the reaction mixture, stirred well and the organic layer was extracted with EtOAc (3×20 ml). The combined organic layers was washed with brine and dried under Na_2SO_4. The crude product was purified by column chromatography with activated neutral Al_2O_3 as the stationary phase and hexane as the mobile phase.

3.4.3.2. Microwave reaction: In a closed-system vessel of the microwave reactor, amine (1 mmol), benzyl alcohol (1 mmol), base (KOH, 1 mmol), and anhydrous $CoCl_2$ (0.05 mmol) were added and dissolved in toluene at room temperature. Then the vessel was placed into the microwave reactor with power 40 W and temperature 80 ˚C for 3 h, after which, the vessel was cooled down and water was added to the reaction mixture. The organic layer was extracted with EtOAc (3×20 ml). The combined organic layers was washed with brine and dried under Na_2SO_4. The crude product was purified by column chromatography with activated neutral Al_2O_3 as the stationary phase and hexane as the mobile phase.

3.4.4. Gram-Scale reaction: Aniline (1 g, 10.75 mmol, 1 equiv), benzyl alcohol (1 equiv, 10.75 mmol, 1.11 ml), KOH (1 equiv, 10.75 mmol, 603 mg) and anhydrous $CoCl_2$ (0.05 equiv, 0.537 mmol, 69 mg) were taken in the tube of the closed vessel system and dissolved in toluene (20 ml) at room temperature. Then the vessel was placed into the microwave reactor with power 40 W and temperature 80 ˚C for 3 h, after which, the vessel was cooled down and water was added to the reaction mixture. The organic layer was extracted with EtOAc (3×50 ml). The combined

organic layers was washed with brine and dried under Na_2SO_4. The crude product was purified by column chromatography with activated neutral Al_2O_3 as the stationary phase and hexane as the mobile phase to obtain the product in 80 % yield (1.5 g). Similar scale reactions were also repeated with *p*-anisidine and *p*-toluidine.

3.4.5. Procedure for detection of hydrogen gas evolution: In a round-bottomed flask, amine (1 mmol), benzyl alcohol (1 mmol), base (KOH, 1 mmol) and anhydrous $CoCl_2$ (0.05 mmol) were taken and dissolved in toluene at room temperature. The temperature of the reaction mixture was allowed to rise to 80 ˚C in an oil-bath and the temperature was maintained for 5 h. After 5 h, the gas from above the reaction mixture was taken and examined for H_2 evolution *via* gas chromatography.

3.4.6. Homogeneity test for imine formation reaction: In a closed-system vessel of the microwave reactor, aniline (0.5 mmol), benzyl alcohol (0.5 mmol), base (KOH, 0.5 mmol), anhydrous $CoCl_2$ (0.025 mmol) and biphenyl (0.5 mmol) as internal standard were added and dissolved in toluene at room temperature. The ligating agent PMe_3 (0.2 equiv, 0.1 mmol) was then added and the vessel was placed into the microwave reactor with power 40 W and temperature 80 ˚C for 3 h, after which, the vessel was cooled down. The reaction mixture was tested directly for GC yield.

3.4.7. Controlled reactions:

3.4.7.1. ***Benzyl alcohol to benzaldehyde:***

Path 1: Benzyl alcohol (63 µl, 0.609 mmol) and anhyd $CoCl_2$ (2.61 mg, 0.0203 mmol) were dissolved in toluene (5 ml) in a round-bottomed flask and was heated to 80 ˚C in an oil-bath for 1 h. Water was then added to the reaction mixture and the reaction mixture extracted with EtOAc (2×15 ml). The organic layer was dried under Na_2SO_4 and evaporated and the obtained crude was examined in TLC. A minute amount of aldehyde (around 2 %) was obtained.

Path 2: Benzyl alcohol (63 µl, 0.609 mmol) and KOH (34 mg, 0.609 mmol) were dissolved in toluene (5 ml) in a round-bottomed flask and was heated to 80 ˚C in an oil-bath for 1 h. Water was then added to the reaction mixture and the reaction mixture extracted with EtOAc (2×15 ml). The organic layer was dried under Na_2SO_4 and evaporated and the obtained crude was examined in TLC. Aldehyde was not obtained.

Path 3: Benzyl alcohol (63 µl, 0.609 mmol), anhyd $CoCl_2$ (2.61 mg, 0.0203 mmol) and KOH (34 mg, 0.609 mmol) were dissolved in toluene (5 ml) in a round-bottomed flask and was heated to 80 ˚C in an oil-bath for 1 h. Water was then added to the reaction mixture and the reaction mixture extracted with EtOAc (2×15 ml). The organic layer was dried under Na_2SO_4 and

evaporated and the obtained crude was examined in TLC. Aldehyde was obtained in a comparatively larger amount (around 23 %).

3.4.7.2. ***Benzyl alcohol and amine to aldimine:*** Aniline (43 μl, 0.47 mmol), benzyl alcohol (49 μl, 0.47 mmol), anhyd $CoCl_2$ (3 mg, 0.023 mmol), and KOH (26.37 mg, 0.47 mmol) were dissolved in toluene (5 ml) in MW closed vessel tube and was heated to 80 ˚C for 3 h. Water was then added to the reaction mixture and the reaction mixture extracted with EtOAc (2×15 ml). The organic layer was dried under Na_2SO_4 and evaporated and the obtained crude was examined in TLC. In first case, the reaction was conducted without the base, in second case with both base and catalyst and in third case without the catalyst.

3.4.7.3. ***Aldehyde and amine to imine:***

Path 1: Aniline (43 μl, 0.47 mmol), benzaldehyde (48 μl, 0.47 mmol) and KOH (26.37 mg, 0.47 mmol) were dissolved in toluene (5 ml) in a round-bottomed flask and was heated to 80 ˚C for 1 h. Water was then added to the reaction mixture and the reaction mixture extracted with EtOAc (2×15 ml). The organic layer was dried under Na_2SO_4 and evaporated and the obtained crude was examined in TLC. Product was formed with 85 % yield.

Path 2: Aniline (43 μl, 0.47 mmol), benzaldehyde (48 μl, 0.47 mmol), anhyd $CoCl_2$ (3 mg, 0.023 mmol) and KOH (26.37 mg, 0.47 mmol) were dissolved in toluene (5 ml) in a round-bottomed flask and was heated to 80 ˚C for 1 h. Water was then added to the reaction mixture and the reaction mixture extracted with EtOAc (2×15 ml). The organic layer was dried under Na_2SO_4 and evaporated and the obtained crude was examined in TLC. Product was formed in same quantity as above.

3.4.7.4. ***Radical trapping experiment:*** Aniline (43 μl, 0.47 mmol), benzyl alcohol (73 μl, 0.705 mmol), anhyd $CoCl_2$ (3 mg, 0.023 mmol), KOH (39.66 mg, 0.707 mmol) and TEMPO (220 mg, 1.41 mmol) or BHT (311 mg, 1.41 mmol) were dissolved in toluene (5 ml) in a round-bottomed flask and was heated to 80 ˚C in microwave for 3 h. Water was then added to the reaction mixture and the reaction mixture extracted with EtOAc (2×15 ml). The organic layer was dried under Na_2SO_4 and evaporated and the obtained crude was examined in TLC. Product was formed (85 %) without any hindrance.

3.4.8. Preparation of deuterated benzyl alcohol: A Schlenk flask was charged with benzaldehyde (0.199 mmol) and THF (2 ml) under nitrogen atmosphere and cooled to 0 ˚C. $NaBD_4$ (1.2 equiv) was added and the solution was stirred for 3 h at room temperature. Upon completion of the reaction, as monitored by TLC, water was added to the reaction mixture and product was extracted by washing with EtOAc (3×10 ml), dried over Na_2SO_4 and solvent was

evaporated. Product was purified by preparative TLC to obtain pure deuterated benzyl alcohol as transparent liquid.

3.4.9. Kinetic isotope effect experiment: Aniline (11 μl, 0.12 mmol), benzyl alcohol (12.5 μl, 0.12 mmol), anhyd $CoCl_2$ (0.77 mg, 0.006 mmol), and KOH (6.73 mg, 0.12 mmol) were dissolved in toluene (2 ml) in MW closed vessel tube and was heated to 80 ˚C for 3 h. The reaction vessel was cooled and toluene was evaporated. The reaction mixture was dissolved in $CDCl_3$, added mesitylene (5 μl, 0.37 mmol) as external standard and the ^1H NMR was recorded.

3.5. Analytical data of all synthesized compounds

n.b. Compounds **3h**, **3l**, **3v**, **3w**, and **3ab** are unstable, so NMR of reaction mixture has been recorded.

(*E*)-*N*,1-diphenylmethanimine (**3a**): White solid (GC yield 85%, isolated yield ~ 75%, 135 mg), ^1H NMR (300 MHz, $CDCl_3$): δ = 8.46 (s, 1H), 7.91 (q, J_1 = 3 Hz, J_2 = 9 Hz, 2H), 7.49-7.47 (m, 3H), 7.40 (t, J = 9 Hz, 2H), 7.23 (t, J = 9 Hz, 3H). $^{13}C\{^1H\}$ NMR (75 MHz, $CDCl_3$): δ = 160.6, 152.2, 136.3, 131.5, 129.9, 129.3, 128.9, 126.1, 121.0. ESI-MS: calcd. for $C_{13}H_{11}N$ $[M+H]^+$ = 182.0969, found 182.0983.

(*E*)-1-phenyl-*N*-(*p*-tolyl)methanimine (**3b**): White solid (GC yield 87%, isolated yield ~ 73%, 142 mg), ^1H NMR (300 MHz, $CDCl_3$): δ = 8.47 (s, 1H), 7.90 (q, J_1 = 6 Hz, J_2 = 3 Hz, 2H), 7.47 (t, J = 3 Hz, 3H), 7.17 (q, J_1 = J_2 = 9 Hz, 4H), 2.38 (s, 3H). $^{13}C\{^1H\}$ NMR (75 MHz, $CDCl_3$): δ = 159.8, 159.7, 149.6, 136.5, 135.9, 131.3, 129.9, 128.8, 120.9, 21.1.

(*E*)-*N*-(2,4-dimethylphenyl)-1-phenylmethanimine (**3c**): White solid (GC yield 88%, isolated yield ~ 80%, 167 mg), ^1H NMR (300 MHz, $CDCl_3$): δ = 8.39 (s, 1H), 7.93 (q, J_1 = 3 Hz, J_2 = 9 Hz, 2H), 7.49 (t, J = 3 Hz, 3H), 7.07-7.03 (m, 2H), 6.88 (d, J = 9 Hz, 1H), 2.38 (s, 3H), 2.36 (s, 3H). $^{13}C\{^1H\}$ NMR (75 MHz, $CDCl_3$): δ = 158.8, 148.6, 136.7, 135.5, 132.1, 131.2, 131.1, 128.8, 128.7, 127.3, 117.5, 21.1, 17.9.

(*E*)-*N*-(3,4-dimethylphenyl)-1-phenylmethanimine (**3d**): Yellow liquid (GC yield 86%, isolated yield ~ 78%, 163 mg), ^1H NMR (300 MHz, $CDCl_3$): δ = 8.47 (s, 1H), 7.89 (q, J_1 = 3 Hz, J_2 = 7.5 Hz, 2H), 7.47 (t, J = 3 Hz, 3H), 7.15 (d, J = 9 Hz, 1H), 7.05-6.98 (m, 2H), 2.30 (s, 3H), 2.28 (s, 3H). $^{13}C\{^1H\}$ NMR (75 MHz, $CDCl_3$): δ = 159.6, 149.9, 137.5, 136.5, 134.6, 131.3, 130.4, 129.9, 128.8, 122.4, 118.2, 20.0, 19.5.

(*E*)-*N*-(4-methoxyphenyl)-1-phenylmethanimine (**3e**): White solid (GC yield 89%, isolated yield ~ 83%, 175 mg), ^1H NMR (300 MHz, $CDCl_3$): δ = 8.53 (s, 1H), 7.93 (q, J = 3 Hz, 2H),

7.51 (t, J = 3 Hz, 3H), 7.28 (d, J = 9 Hz, 2H), 6.98 (d, J = 9 Hz, 2H), 3.88 (s, 3H). $^{13}C\{^1H\}$ NMR (75 MHz, $CDCl_3$): δ = 158.6, 145.1, 136.6, 131.2, 128.9, 128.7, 122.3, 114.5, 55.6.

(*E*)-1-phenyl-*N*-(4-(p-tolyloxy)phenyl)methanimine (**3f**): White solid (GC yield 82%, isolated yield ~ 72%, 206 mg), ^1H NMR (300 MHz, $CDCl_3$): δ = 8.52 (s, 1H), 7.94 (q, J_1 = 6 Hz, J_2 = 7.5 Hz, 2H), 7.52 (t, J_1 = 3 Hz, J_2 = 6 Hz, 3H), 7.26 (d, J = 9 Hz, 2H), 7.19 (d, J = 9 Hz, 2H), 7.05 (d, J = 9 Hz, 2H), 6.98 (d, J = 9 Hz, 2H), 2.39 (s, 3H). $^{13}C\{^1H\}$ NMR (75 MHz, $CDCl_3$): δ = 159.5, 156.3, 155.1, 147.1, 136.4, 133.0, 131.4, 130.4, 128.9, 128.8, 122.4, 119.2, 119.0, 20.8. ESI-MS: calcd. for $C_{20}H_{17}NO$ $[M+H]^+$ = 288.1388, found 288.1395.

(*E*)-*N*-(naphthalen-1-yl)-1-phenylmethanimine (**3g**): Brown solid (GC yield 83%, isolated yield ~ 70%, 161 mg), ^1H NMR (300 MHz, $CDCl_3$): δ = 8.67 (dd, J_1 = 3 Hz, J_2 = 7.5 Hz, 1H), 8.21 (dd, J_1 = 3 Hz, J_2 = 7.5 Hz, 1H,), 7.89 (dd, J = 9 Hz, 2H), 7.80 (td, J_1 = 3 Hz, J_2 = 6 Hz, 1H), 7.72 (td, J = 6 Hz, 2H), 7.55 (td, J = 6 Hz, 1H), 7.51-7.46 (m, 2H), 7.24 (d, J = 12 Hz, 1H), 6.78 (dd, J_1 = 3 Hz, J_2 = 7.5 Hz, 1H), 6.68 (d, J = 9 Hz, 1H). $^{13}C\{^1H\}$ NMR (75 MHz, $CDCl_3$): δ = 155.6, 146.4, 134.2, 133.3, 131.5, 130.7, 128.1, 127.2, 126.9, 126.3, 126.3, 125.8, 125.6, 124.2, 114.8.

(*E*)-*N*-(2,4-dimethoxyphenyl)-1-phenylmethanimine (**3h**): Brown liquid (GC yield 79%), NMR of reaction mixture has been provided. This compound has not been isolated.

(*E*)-*N*-(4-fluorophenyl)-1-phenylmethanimine (**3i**): Yellow liquid (GC yield 70%, isolated yield ~ 61%, 121 mg), ^1H NMR (300 MHz, $CDCl_3$): δ = 8.45 (s, 1H), 7.89 (q, J = 3 Hz, 2H), 7.49-7.47 (m, 3H), 7.22-7.19 (m, 2H), 7.08 (t, J_1 = 6 Hz, J_2 = 9 Hz, 2H). $^{13}C\{^1H\}$ NMR (75 MHz, $CDCl_3$): δ = 160.3, 141.4, 131.6, 128.9, 127.4, 127.3, 122.4, 116.1, 115.9.

(*E*)-*N*-(4-chlorophenyl)-1-phenylmethanimine (**3j**): White solid (GC yield 75%, isolated yield ~ 65%, 139 mg), ^1H NMR (300 MHz, $CDCl_3$): δ = 8.44 (s, 1H), 7.91-7.88 (m, 2H), 7.50-7.48 (m, 3H), 7.35 (dd, J = 3 Hz, 2H), 7.15 (dd, J = 3 Hz, 2H). $^{13}C\{^1H\}$ NMR (75 MHz, $CDCl_3$): δ = 160.8, 150.6, 136.1, 134.6, 131.8, 129.4, 128.9, 122.3, 116.4.

(*E*)-*N*-(4-bromophenyl)-1-phenylmethanimine (**3k**): White solid (GC yield 78%, isolated yield ~ 67%, 174 mg), ^1H NMR (300 MHz, $CDCl_3$): δ = 8.43 (s, 1H), 7.89 (q, J = 3 Hz, 2H), 7.52-7.47 (m, 5H), 7.09 (d, J = 9 Hz, 2H). $^{13}C\{^1H\}$ NMR (75 MHz, $CDCl_3$): δ = 160.9, 151.2, 136.1, 132.3, 131.8, 129.0, 128.9, 122.7, 119.5.

(*E*)-*N*-(3-chlorophenyl)-1-phenylmethanimine (**3l**): White solid (GC yield 75%), NMR of reaction mixture has been provided. This compound has not been isolated.

(*E*)-*N*-(3,5-dichlorophenyl)-1-phenylmethanimine (**3m**): Yellow solid (GC yield 75%, isolated yield ~ 63 %, 157 mg), ^1H NMR (300 MHz, $CDCl_3$): δ = 8.40 (s, 1H), 7.88 (q, J_1 = 3 Hz, J_2 =

7.5 Hz, 2H), 7.53-7.48 (m, 3H), 7.22 (t, J = 3 Hz, 1H), 7.08 (d, J = 3 Hz, 2H). $^{13}C\{^1H\}$ NMR (75 MHz, $CDCl_3$): δ = 162.4, 154.2, 135.6, 135.4, 132.3, 129.3, 129.0, 125.7, 119.7.

(*E*)-1-(4-chlorophenyl)-*N*-phenylmethanimine (**3n**): Yellow liquid (GC yield 81%, isolated yield ~ 73%, 157 mg), ^1H NMR (300 MHz, $CDCl_3$): δ = 8.31 (s, 1H), 7.73 (d, J_1 = 3 Hz, J_2 = 9 Hz, 2H), 7.36-7.27 (m, 4H), 7.17-7.09 (m, 3H). $^{13}C\{^1H\}$ NMR (75 MHz, $CDCl_3$): δ = 158.9, 151.8, 137.5, 134.8, 130.1, 129.3, 129.2, 126.3, 120.9.

(*E*)-1-(4-chlorophenyl)-*N*-(p-tolyl)methanimine (**3o**): Yellow solid (GC yield 82%, isolated yield ~ 72%, 164 mg), ^1H NMR (300 MHz, $CDCl_3$): δ = 8.43 (s, 1H), 7.83 (dt, J_1 = 3 Hz, J_2 = 9 Hz, 2H), 7.44 (d, J = 9 Hz, 2H), 7.17 (q, J_1 = 9 Hz, J_2 = 12 Hz, 4H), 2.38 (s, 3H). $^{13}C\{^1H\}$ NMR (75 MHz, $CDCl_3$): δ = 158.1, 149.2, 137.3, 136.3, 134.9, 130.0, 129.2, 120.9, 115.6, 21.2.

(*E*)-1-(4-chlorophenyl)-*N*-(2,4-dimethylphenyl)methanimine (**3p**): Yellow liquid (GC yield 82%, isolated yield ~ 72%, 175 mg), ^1H NMR (300 MHz, $CDCl_3$): δ = 8.36 (d, J = 12 Hz, 1H), 7.94-7.90 (m, 1H), 7.85 (d, J = 9 Hz, 1H), 7.49-7.43 (m, 2H), 7.05 (s, 1H), 7.02 (d, J = 6 Hz, 1H,), 6.85 (d, J = 9 Hz, 1H), 2.34 (s, 6H). $^{13}C\{^1H\}$ NMR (75 MHz, $CDCl_3$): δ = 157.3, 148.2, 137.1, 135.8, 132.3, 131.3, 129.9, 129.1, 128.8, 127.4, 117.3, 21.1, 17.9.

(*E*)-1-(4-chlorophenyl)-*N*-(3,4-dimethylphenyl)methanimine (**3q**): Yellow liquid (GC yield 82%, isolated yield ~ 70%, 170 mg), ^1H NMR (300 MHz, $CDCl_3$): δ = 8.43 (s, 1H), 7.83 (d, J = 9 Hz, 2H), 7.43 (d, J = 9 Hz, 2H), 7.15 (d, J = 9 Hz, 1H), 7.03-6.97 (m, 2H), 2.30 (s, 3H), 2.28 (s, 3H). $^{13}C\{^1H\}$ NMR (75 MHz, $CDCl_3$): δ = 157.9, 149.5, 137.6, 137.2, 135.0, 131.1, 129.9, 129.6, 129.2, 122.4, 118.2, 20.0, 19.5.

(*E*)-1-(4-chlorophenyl)-*N*-(4-methoxyphenyl)methanimine (**3r**): White solid (GC yield 85%, isolated yield ~ 76%, 186 mg), ^1H NMR (300 MHz, $CDCl_3$): δ = 8.43 (s, 1H), 7.81 (d, J = 9 Hz, 2H), 7.42 (d, J = 9 Hz, 2H), 7.23 (d, J = 9 Hz, 2H), 6.93 (d, J = 9 Hz, 2H), 3.83 (s, 3H). $^{13}C\{^1H\}$ NMR (75 MHz, $CDCl_3$): δ = 158.6, 156.8, 144.5, 137.0, 135.1, 129.8, 129.1, 122.3, 114.5, 55.6.

(*E*)-1-(4-chlorophenyl)-*N*-(4-(p-tolyloxy)phenyl)methanimine (**3s**): White solid (GC yield 84%, isolated yield ~ 73%, 234 mg), ^1H NMR (300 MHz, $CDCl_3$): δ = 8.44 (s, 1H), 7.83 (d, J = 6 Hz, 2H), 7.44 (d, J = 9 Hz, 2H), 7.21 (d, J = 9 Hz, 2H), 7.15 (d, J = 9 Hz, 2H), 7.01 (d, J = 9 Hz, 2H), 6.93 (d, J = 9 Hz, 2H). $^{13}C\{^1H\}$ NMR (75 MHz, $CDCl_3$): 158.9, 158.1, 131.1, 130.1, 129.9, 129.6, 129.2, 126.4, 124.5, 120.9, 119.9, 119.1, 118.1, 21.2. ESI-MS: calcd. for $C_{20}H_{16}ClNO$ $[M\text{-}Cl+K]^+$ = 325.0868, found 325.0867.

(*E*)-*N*-(4-bromophenyl)-1-(4-chlorophenyl)methanimine (**3t**): White solid (GC yield 75%, isolated yield ~ 67%, 197 mg), ^{1}H NMR (300 MHz, $CDCl_3$): δ = 8.40 (s, 1H), 7.85-7.82 (m, 2H), 7.54-7.50 (m, 2H), 7.45 (d, *J* = 9 Hz, 2H), 7.09 (d, *J* = 6 Hz, 2H). $^{13}C\{^{1}H\}$ NMR (75 MHz, $CDCl_3$): δ = 159.3, 132.4, 132.2, 131.1, 130.2, 129.6, 129.3, 122.7, 116.9.

(*E*)-*N*-(3-chlorophenyl)-1-(4-chlorophenyl)methanimine (**3u**): White liquid (GC yield 75%, isolated yield ~ 65%, 162 mg), ^{1}H NMR (300 MHz, $CDCl_3$): δ = 8.39 (s, 1H), 7.83 (d, *J* = 9 Hz, 2H), 7.52 (d, *J* = 9 Hz, 1H), 7.46 (d, *J* = 6 Hz, 2H), 7.32 (t, *J* = 9 Hz, 1H), 7.21 (d, *J* = 9 Hz, 2H). $^{13}C\{^{1}H\}$ NMR (75 MHz, $CDCl_3$): δ = 159.9, 153.1, 137.9, 134.4, 131.1, 130.3, 129.6, 129.3, 126.2, 121.0, 119.5.

(*E*)-1-(4-chlorophenyl)-*N*-(3,5-dichlorophenyl)methanimine (**3v**): White liquid (GC yield 70%). NMR of reaction mixture has been provided. Compound has not been isolated.

(*E*)-*N*,1-bis(4-chlorophenyl)methanimine (**3w**): White solid (GC yield 70%), NMR of reaction mixture has been provided. Compound has not been isolated.

(*E*)-1-(4-chlorophenyl)-*N*-(4-fluorophenyl)methanimine (**3x**): White solid (GC yield 70%, isolated yield ~ 60%, 139 mg), ^{1}H NMR (300 MHz, $CDCl_3$): δ = 8.41 (s, 1H), 7.83 (d, *J* = 9 Hz, 2H), 7.45 (d, *J* = 9 Hz, 2H), 7.20 (dd, J_1 = 6 Hz, J_2 = 3 Hz, 2H), 7.08 (t, *J* = 9 Hz, 2H). $^{13}C\{^{1}H\}$ NMR (75 MHz, $CDCl_3$): δ = 162.7, 158.7, 147.8, 137.6, 134.7, 130.1, 129.3, 122.4, 116.2.

(*E*)-1-(3-nitrophenyl)-*N*-phenylmethanimine (**3y**): Yellow liquid (GC yield 77%, isolated yield ~ 67%, 151 mg), ^{1}H NMR (300 MHz, $CDCl_3$): δ = 8.75 (t, *J* = 3 Hz, 1H), 8.55 (s, 1H), 8.33 (dq, J_1 = 3 Hz, J_2 = 6 Hz, 1H), 8.25 (tt, J_1 = 3 Hz, J_2 = 6 Hz, 1H), 7.67 (t, *J* = 9 Hz, 1H), 7.44 (tt, J_1 = 3 Hz, J_2 = 6 Hz, J_3 = 9 Hz, 2H), 7.32-7.24 (m, 3H). $^{13}C\{^{1}H\}$ NMR (75 MHz, $CDCl_3$): δ = 157.3, 151.0, 138.0, 134.7, 134.2, 129.9, 129.5, 127.0, 125.7, 123.7, 121.1.

(*E*)-1-(3-nitrophenyl)-*N*-(p-tolyl)methanimine (**3z**): Yellow liquid (GC yield 79%, isolated yield ~ 65 %, 156 mg), ^{1}H NMR (300 MHz, $CDCl_3$): δ = 8.74 (t, *J* = 3 Hz, 1H), 8.56 (s, 1H), 8.31 (dq, J_1 = 3 Hz, J_2 = 9 Hz, 1H), 8.25 (dt, J_1 = 3 Hz, J_2 = 6 Hz, 1H), 7.66 (t, J_1 = 9 Hz, J_2 = 6 Hz, 1H), 7.20 (t, J_1 = 9 Hz, J_2 = 6 Hz, 4H), 2.39 (s, 3 H). $^{13}C\{^{1}H\}$ NMR (75 MHz, $CDCl_3$): δ = 156.4, 148.4, 137.1, 134.1, 130.1, 129.9, 128.7, 125.5, 124.7, 123.6, 121.1, 21.2.

(*E*)-1-(4-nitrophenyl)-*N*-(p-tolyl)methanimine (**3aa**): Yellow liquid (GC yield 74%, isolated yield ~ 64%, 153 mg), ^{1}H NMR (300 MHz, $CDCl_3$): δ = 8.56 (d, *J* = 3 Hz, 1H), 8.34-8.31 (m, 2H), 8.10-8.06 (m, 2H), 7.27-7.19 (m, 4H), 2.39 (s, 3H). $^{13}C\{^{1}H\}$ NMR (75 MHz, $CDCl_3$): δ = 156.5, 149.3, 141.9, 137.4, 130.6, 130.1, 129.4, 127.2, 124.5, 124.1, 121.1, 21.2.

(*E*)-*N*-(2,4-dimethylphenyl)-1-(3-nitrophenyl)methanimine (**3ab**): Yellow liquid (GC yield 73%), NMR of reaction mixture has been provided. Compound has not been isolated.

(*E*)-*N*-(2,4-dimethylphenyl)-1-(4-nitrophenyl)methanimine (**3ac**): Yellow liquid (GC yield 71%, isolated yield ~ 60%, 152 mg), ^{1}H NMR (300 MHz, $CDCl_3$): δ = 8.48 (s, 1H), 8.32 (d, *J* = 9 Hz, 2H), 8.07 (d, *J* = 9 Hz, 2H), 7.08 (s, 1H), 7.04 (d, *J* = 6 Hz, 1H), 6.91(d, *J* = 6 Hz, 1H), 2.38 (s, 3H), 2.35 (s, 3H). ^{13}C{^{1}H} NMR (75 MHz, $CDCl_3$): δ = 155.6, 147.5, 142.2, 136.9, 133.1, 131.6, 130.6, 129.4, 127.5, 124.1, 117.0, 21.1, 17.9. ESI-MS: calcd. for $C_{15}H_{14}N_2O_2$ $[M+H]^+$ = 255.1133, found 255.1132. Anal. Calcd for $C_{15}H_{14}N_2O_2$, C, 70.85; H, 5.55; N, 11.02. Found: C, 69.68; H, 4.89; N, 10.42.

(*E*)-1-(4-fluorophenyl)-*N*-(4-(p-tolyloxy)phenyl)methanimine (**3ad**): Yellow liquid (GC yield 79%, isolated yield ~ 70%, 213 mg), ^{1}H NMR (300 MHz, $CDCl_3$): δ = 8.44 (s, 1H), 7.89 (q, J_1 = 6 Hz, J_2 = 3 Hz, 2H), 7.20 (d, *J* = 9 Hz, 2H), 7.14 (d, *J* = 9 Hz, 4H), 7.01 (d, *J* = 9 Hz, 2H), 6.93 (d, *J* = 9 Hz, 2H), 2.34 (s, 3H). ^{13}C{^{1}H} NMR (75 MHz, $CDCl_3$): δ = 157.9, 156.4, 132.3, 130.8, 130.4, 130.2, 122.3, 120.7, 119.2, 119.1, 117.7, 116.2, 115.9, 20.8. ESI-MS: calcd. for $C_{20}H_{16}FNO$ $[M+H]^+$ = 306.1294, found 306.1284.

(*E*)-*N*-(2,4-dimethylphenyl)-1-(4-fluorophenyl)methanimine (**3ae**): Yellow liquid (GC yield 78%, isolated yield ~ 68%, 154 mg), ^{1}H NMR (300 MHz, $CDCl_3$): δ = 8.34 (s, 1H), 7.94-7.89 (m, 2H), 7.16 (t, *J* = 7.5 Hz, 2H), 7.05-7.00 (m, 2H), 6.85 (d, *J* = 6 Hz, 1H), 2.34 (s, 6H). ^{13}C{^{1}H} NMR (75 MHz, $CDCl_3$): δ = 157.3, 148.4, 135.6, 132.4, 131.3, 130.7, 127.3, 117.4, 116.1, 115.9, 21.0, 17.9. ESI-MS: calcd. for $C_{15}H_{14}FN$ $[M+H]^+$ = 228.1188, found 228.1164.

(1*E*,1'*E*)-*N*,*N*'-((((perfluoropropane-2,2-diyl)bis(4,1phenylene))bis(oxy))bis(4,1-phenylene))bis(1-phenylmethanimine) (**3af**): White solid (GC yield 64%, isolated yield ~ 50%, 347 mg), ^{1}H NMR (300 MHz, $CDCl_3$): δ = 8.49 (s, 1H), 7.91 (t, *J* = 3 Hz, 2H), 7.48 (d, *J* = 3 Hz, 3H), 7.36 (d, *J* = 6 Hz, 3H), 7.12-7.00 (m, 2H), 6.98 (d, *J* = 6 Hz, 3H). ^{13}C{^{1}H} NMR (75 MHz, $CDCl_3$): δ = 160.1, 136.9, 131.9, 131.7, 131.6, 128.9, 122.6, 121.8, 120.8, 117.4, 117.3, 116.4, 116.3, 116.2, 64.0. Anal. Calcd for $C_{41}H_{28}F_6N_2O_2$, C, 70.89; H, 4.06; N, 4.03. Found: C, 70.81; H, 4.00; N, 3.92.

(1*E*,1'*E*)-*N*,*N*'-((((perfluoropropane-2,2-diyl)bis(4,1-phenylene))bis(oxy))bis(4,1-phenylene))bis(1-(4-fluorophenyl)methanimine) (**3ag**): White solid (GC yield 68%, isolated yield ~ 55%, 401 mg), ^{1}H NMR (300 MHz, $CDCl_3$): δ = 8.45 (s, 1H), 7.91 (q, J_1 = 6 Hz, J_1 = 9 Hz, 2H), 7.36 (d, *J* = 9 Hz, 2H), 7.24-7.09 (m, 6H), 6.98 (d, *J* = 9 Hz, 2H). ^{13}C{^{1}H} NMR (75 MHz, $CDCl_3$): δ = 158.5, 154.2, 148.2, 131.9, 130.9, 130.8, 122.5, 121.9, 120.8, 117.4,

116.4, 116.3, 115.9, 100.1, 61.6. ESI-MS: calcd. for $C_{41}H_{26}F_8N_2O_2$ $[M+H]^+$ = 731.1945, found 731.1944.

2-phenyl-2,3-dihydro-1*H*-perimidine (**3ah**): Yellow solid (GC yield 83%, isolated yield ~ 80%, 197 mg), ^{1}H NMR (300 MHz, $CDCl_3$): δ = 7.68 (q, *J* = 3 Hz, 2H), 7.49 (t, *J* = 3 Hz, 3H), 7.33-7.28 (m, 4H), 6.57 (dd, J_1 = 3 Hz, J_2 = 3 Hz, 2H), 5.52 (s, 1H), 4.58 (br s, 2H). ^{13}C{^{1}H} NMR (75 MHz, $CDCl_3$): δ = 142.2, 140.2, 135.0, 129.7, 128.9, 128.0, 127.0, 118.0, 113.6, 106.0, 68.5.

2-(4-fluorophenyl)-2,3-dihydro-1*H*-perimidine (**3ai**): White solid (GC yield 82%, isolated yield ~ 78%, 206 mg), ^{1}H NMR (300 MHz, $CDCl_3$): δ = 7.64 (q, *J* = 3 Hz, 2H), 7.30-7.27 (m, 2H), 7.26-7.24 (m, 2H), 7.15 (t, *J* = 6 Hz, 2H), 6.55 (d, *J* = 6 Hz, 2H), 5.48 (s, 1H), 4.50 (br s, 2H). ^{13}C{^{1}H} NMR (75 MHz, $CDCl_3$): δ = 164.8, 162.4, 142.1, 135.1, 129.9, 127.0, 118.2, 116.0, 115.8, 106.1, 67.8.

2-(*o*-tolyl)-2,3-dihydro-1*H*-perimidine (**3aj**): White solid (GC yield 82%, isolated yield ~ 75%, 195 mg), ^{1}H NMR (400 MHz, $CDCl_3$): δ = 7.80 (d, *J* = 8 Hz, 1H), 7.37-7.28 (m, 8H), 6.55 (d, *J* = 4 Hz, 2H), 5.75 (s, 1H), 4.48 (br s, 2H), 2.55 (s, 3H). ^{13}C{^{1}H} NMR (100 MHz, $CDCl_3$): δ = 142.5, 137.7, 136.7, 135.1, 131.0, 129.2, 128.2, 126.9, 126.7, 117.9, 113.7, 106.1, 65.3, 19.2.

2-phenyl-1*H*-benzo[*d*]imidazole (**3ak**): Yellow solid (GC yield 50%, isolated yield ~ 44%, 85 mg), ^{1}H NMR (300 MHz, $CDCl_3$): δ = 8.07 (q, *J* = 3 Hz, 2H), 7.65 (q, *J* = 3 Hz, 2H), 7.45 (t, *J* = 3 Hz, 3H), 7.37 (d, *J* = 6 Hz, 1H), 7.28 (t, *J* = 3 Hz, 1H), 4.71 (s, 1H). ^{13}C{^{1}H} NMR (75 MHz, $CDCl_3$): δ = 151.6, 130.4, 129.8, 129.2, 126.7, 123.2, 29.8.

2-(4-fluorophenyl)-1*H*-benzo[*d*]imidazole (**3al**): Yellow solid (GC yield 80%, isolated yield ~ 78%, 165 mg), ^{1}H NMR (300 MHz, $CDCl_3$): δ = 7.68 (d, *J* = 6 Hz, 2H), 7.18 (t, *J* = 6 Hz, 2H), 6.81-6.76 (m, 4H), 5.46 (br s, 1H). ^{13}C{^{1}H} NMR (75 MHz, $CDCl_3$): δ = 143.2, 137.9, 131.5, 124.4, 117.8, 117.2.

2-(4-chlorophenyl)-1*H*-benzo[*d*]imidazole (**3am**): Pale yellow solid (GC yield 80%, isolated yield ~ 79%, 180 mg), ^{1}H NMR (300 MHz, DMSO-d_6): δ = 13.04 (br s, 1H), 8.17 (d, *J* = 9 Hz, 2H), 7.63 (d, *J* = 9 Hz, 3H), 7.55 (d, *J* = 6 Hz, 1H), 7.22 (d, *J* = 3 Hz, 2H). ^{13}C{^{1}H} NMR (75 MHz, DMSO-d_6): δ = 150.3, 143.7, 135.1, 134.7, 129.2, 129.1, 128.3, 123.0, 122.1, 119.0, 111.6.

2-(4-(trifluoromethyl)phenyl)-1*H*-benzo[*d*]imidazole (**3an**): White solid (GC yield 85%, isolated yield ~ 80%, 209 mg), ^{1}H NMR (300 MHz, DMSO-d_6): δ = 13.19 (br s, 1H), 8.38 (d, *J* = 6 Hz, 2H), 7.93 (d, *J* = 9 Hz, 2H), 7.71 (d, *J* = 6 Hz, 1H), 7.58 (d, *J* = 6 Hz, 1H), 7.26 (t, *J*

= 6 Hz, 2H). $^{13}C\{^{1}H\}$ NMR (75 MHz, DMSO-d_6): δ = 149.7, 133.9, 129.9, 129.6, 127.2, 126.1, 126.1, 126.0, 125.9, 125.5, 123.3, 122.8, 122.2, 119.3, 111.7.

2-(3-nitrophenyl)-1*H*-benzo[*d*]imidazole (**3ao**): Yellow solid (GC yield 80%, isolated yield ~ 74%, 176 mg), ^{1}H NMR (400 MHz, $CDCl_3$): δ = 7.68 (d, *J* = 8 Hz, 2H), 7.18 (t, *J* = 8 Hz, 2H), 6.79 (t, *J* = 10 Hz, 4H), 5.48 (br s, 1H). $^{13}C\{^{1}H\}$ NMR (100 MHz, $CDCl_3$): δ = 143.3, 137.9, 131.5, 124.4, 117.8, 117.2.

1-benzyl-2-phenyl-1*H*-benzo[*d*]imidazole (**3ap**): Yellow solid (GC yield 50%, isolated yield ~ 44%, 125 mg), ^{1}H NMR (300 MHz, $CDCl_3$): δ = 7.87 (d, *J* = 6 Hz, 1H), 7.67 (d, *J* = 9 Hz, 2H), 7.44 (d, *J* = 6 Hz, 3H), 7.31 (d, *J* = 6 Hz, 4H), 7.25-7.21 (m, 2H), 7.08 (d, *J* = 3 Hz, 2H), 5.45 (s, 2H). $^{13}C\{^{1}H\}$ NMR (75 MHz, $CDCl_3$): δ = 154.2, 136.4, 136.1, 130.2, 129.4, 129.2, 128.9, 127.9, 126.1, 123.3, 122.9, 120.0, 110.7, 48.6.

1-(4-chlorobenzyl)-2-(4-chlorophenyl)-1*H*-benzo[*d*]imidazole (**3aq**): Yellow solid (GC yield 44%, isolated yield ~ 40%, 141 mg), ^{1}H NMR (400 MHz, $CDCl_3$): δ = 7.82 (d, *J* = 12 Hz, 1H), 7.55 (d, *J* = 8 Hz, 1H), 7.40 (d, *J* = 8 Hz, 1H), 7.30-7.29 (m, 3H), 7.23-7.21 (m, 1H), 7.16 (d, *J* = 8 Hz, 1H), 6.98 (d, *J* = 8 Hz, 2H), 5.02 (s, 2H). $^{13}C\{^{1}H\}$ NMR (100 MHz, $CDCl_3$): δ = 153.0, 143.3, 136.5, 134.8, 130.6, 129.7, 129.5, 129.3, 128.9, 127.4, 123.6, 123.2, 120.4, 110.4, 47.9.

3.6. References

1. (a) Hadjipavlou-Litina, D. J.; Geronikaki, A. A. *Drug Des. Discovery* **1998**, *15*, 199. (b) Rappoport, Z. J.; Liebman, F. The chemistry of hydroxylamines, oximes and hydroxamic acids; *Wiley*: New York, **2009**; 609. (c) Guillena, G.; Ramón, D. J.; Yus, M. *Chem. Rev.* **2010**, *110*, 1611–1641. (d) Pera-Titus, M.; Shi, F. *ChemSusChem* **2014**, *7*, 720–722. (e) Orr, S. A.; Andrews, P. C.; Blair, V. L. *Chem. Eur. J.* **2021***, 27,* 2569.
2. Malins, L. R.; deGruyter, J. N.; Robbins, K. J.; Scola, P. M.; Eastgate M. D.; Ghadiri, M. R.; Baran, P. S. *J. Am. Chem. Soc.* **2017**, *139*, 5233−5241.
3. Evans, B. S.; Ntai, I.; Chen, Y.; Robinson, S. J.; Kelleher, N. L. *J. Am. Chem. Soc.* **2011**, *133*, 7316−7319.
4. Poulsen, T. B. *Acc. Chem. Res.* **2021**, *54*, 1830−1842.
5. (a) Su, F.; Mathew, S. C.; Möhlmann, L.; Antonietti, M.; Wang, X.; Blechert, S. *Angew. Chem., Int. Ed.* **2011**, *50*, 657−660. (b) Chen, B.; Wang, L.; Dai, W.; Shang, S.; Lv, Y.; Gao,

S. *ACS Catal.* **2015**, *5*, 2788−2794. (c) Chen, B.; Wang, L.; Gao, S. *ACS Catal*. **2015**, *5*, 5851−5876.

6. (a) Pohlki, F.; Doye, S. *Angew. Chem., Int. Ed.* **2001**, *40*, 2305−2308. (b) Johnson, J. S.; Bergman, R. G. *J. Am. Chem. Soc.* **2001**, *123*, 2923−2924. (c) Li, Y.; Shi, Y.; Odom, A. L. *J. Am. Chem. Soc.* **2004**, *126*, 1794−1803. (d) Ryken, S. A.; Schafer, L. L. *Acc. Chem. Res*. **2015**, *48*, 2576−2586.
7. (a) Éll, A. H.; Samec, J. S. M.; Brasse, C.; Bäckvall, J. -E. *Chem. Commun*. **2002**, 1144−1145. (b) Largeron, M.; Chiaroni, A.; Fleury, M. -B. *Chem. Eur. J*. **2008**, *14*, 996−1003 (c) Jiang, G.; Chen, J.; Huang, J.-S.; Che, C. -M. *Org. Lett*. **2009**, *11*, 4568−4571. (d) Yamaguchi, K.; Mizuno, N. *Angew. Chem., Int. Ed*. **2003**, *42*, 1480−1483. (e) Sonobe, T.; Oisaki, K.; Kanai, M. *Chem. Sci*. **2012**, *3*, 3249−3255. (f) Yuan, H.; Yoo, W.-J.; Miyamura, H.; Kobayashi, S. *J. Am. Chem. Soc.* **2012**, *134*, 13970−13973.
8. Paudel, K.; Xu, S.; Hietsoi, O.; Pandey, B.; Onuh, C.; Ding, K. *Organometallics* **2021**, *40*, 418−426.
9. (a) Horton, D. A.; Bourne, G. T.; Smythe, M. L. *Chem. Rev.* **2003**, *103*, 893−930. (b) Undevia, S. D.; Innocenti, F.; Ramirez, J.; House, L.; Desai, A. A.; Skoog, L. A.; Singh, D. A.; Karrison, T.; Kindler, H. L.; Ratain, M. J. *Eur. J. Cancer* **2008**, *44*, 1684−1692. (c) Sarges, R.; Howard, H. R.; Browne, R. G.; Lebel, L. A.; Seymour, P. A.; Koe, B. K. *J. Med. Chem.* **1990**, *33*, 2240−2254.
10. Barta, K.; Ford, P. C. *Acc. Chem. Res.* **2014**, *47*, 1503−1512.
11. (a) Gnanaprakasam, B.; Zhang, J.; Milstein, D. *Angew. Chem. Int. Ed.* **2010**, *49*, 1468−1471, (b) Maggi, A.; Madsen, R. *Organometallics* **2012**, *31*, 451−455, (c) Zheng, Y.; Nie, X.; Long, Y.; Ji, L.; Fu, H.; Zheng, X.; Chen, H.; Li, R. *Chem. Commun.* **2019**, *55*, 12384−12387, (d) Saha, B.; Rahaman, S. M. W.; Daw, P.; Sengupta, G.; Bera, J. K. *Chem. Eur. J.* **2014**, *20*, 6542−6551, (e) Srimani, D.; Ben-David, Y.; Milstein, D. *Angew. Chem., Int. Ed.* **2013**, *52*, 4012−4015, (f) Zeng, G.; Li, S. *Inorg. Chem.* **2011**, *50*, 10572−10580, (g) Higuchi, T.; Tagawa, R.; Iimuro, A.; Akiyama, S.; Nagae, H.; Mashima, K. *Chem. Eur. J.* **2017**, *23*, 12795−12804,
12. (a) Soulé, J. -F.; Miyamura, H.; Kobayashi, S. *Chem. Commun.* **2013**, *49*, 355−357, (b) Azizi, K.; Madsen, R. *ChemCatChem* **2018**, *10*, 3703−3708, (c) Corma, A.; Navas, J.; Sabater, M. J. *Chem. Eur. J.* **2012**, *18*, 14150−14156, (d) Tamura, M.; Tomishige, K. *Angew. Chem. Int. Ed.* **2015**, *54*, 864−867, (e) Wu, S.; Wang, Y.; Cao, Q.; Zhao, Q.; Fang, W. *Chem.*

Eur. J. **2021**, *27*, 3019−3028, (f) Bain, J.; Cho, P.; Voutchkova-Kostal, A. *Green Chem.* **2015**, *17*, 2271−2280,

13. (a) Tian, H.; Yu, X.; Li, Q.; Wang, J.; Xu, Q. *Adv. Synth. Catal.* **2012**, *354*, 2671−2677, (b) Pérez, J. M.; Cano, R.; Yus, M.; Ramón, D. J. *Eur. J. Org. Chem.* **2012**, 4548−4554,
14. (a) Azizi, K.; Akrami, S.; Madsen, R. *Chem. Eur. J.* **2019**, *25*, 6439−6446, (b) Chen, B.; Li, J.; Dai, W.; Wanga, L.; Gao, S. *Green Chem.* **2014**, *16*, 3328−3334, (c) Chai, H.; Yu, K.; Liu, B.; Tan, W.; Zhang, G. *Organometallics* **2020**, *39*, 217−226,
15. (a) Jaiswal, G.; Landge, V. G.; Jagadeesan, D.; Balaraman, E. *Green Chem.* **2016**, *18*, 3232−3238, (b) Bera, A.; Sk, M.; Singh, K.; Banerjee, D. *Chem. Commun.* **2019**, *55*, 5958−5961, (c) Jin, Y.; Cao, Y.; Fang, G.; Ruan, F.; Ke, Q. *ChemCatChem* **2019**, *11*, 3178−3181, (d) Ruch, S.; Irrgang, T.; Kempe, R. *Chem. Eur. J.* **2014**, *20*, 13279−13285, (e) Trincado, M.; Banerjee, D.; Grützmacher, H. *Energy Environ. Sci.* **2014**, *7*, 2464−2503.
16. Wang, L.; Jv, X.; Wang, R.; Ma, L.; Liu, J.; Sun, J.; Shi, T.; Zhao, L.; Zhang, X.; Wang, B. *ACS Sustainable Chem. Eng.* **2022**, *10*, 8342−8349.
17. Daw, P.; Ben-David, Y.; Milstein, D. *ACS Catal.* **2017**, *7*, 7456−7460.
18. Mukherjee, A.; Nerush, A.; Leitus, G.; Shimon, L. J. W.; David, Y. B.; Jalapa, N. A. E.; Milstein, D. *J. Am. Chem. Soc.* **2016**, *138*, 4298−4301.
19. Zhang, E.; Tian, H.; Xu, S.; Yu, X.; Xu, Q. *Org. Lett.* **2013**, *15*, 2704−2707.
20. Zhao, R.; Tan, C.; Xie, Y.; Gao, C.; Liu, H.; Jiang, Y. *Tetrahedron Lett.* **2011**, *52*, 3805–3809.
21. Pal, A.; Thakur, A. *Org. Biomol. Chem.* **2022**, *20*, 8977−8987.
22. Hande, A. E.; Ramesh, V. B.; Prabhu, K. R. *Chem. Commun.* **2018**, *54*, 12113−12116.
23. (a) Hine, J.; Yeh, C. Y. *J. Am. Chem. Soc.* **1967**, *89*, 2669−2676, (b) Kovaříček, P.; Meister, A. C.; Flídrová, K.; Cabot, R.; Kovaříčková, K.; Lehn, J. -M. *Chem. Sci.* **2016**, *7*, 3215−3226.
24. Ballesteros-Soberanas, J.; Bilanin, C.; Leyva-Perez, A. *ACS Org. Inorg. Au* **2023**, *3*, 13−18.
25. Melanson, J. A.; Figliola, C.; Smithen, D. A.; Kajetanowicz, A. K.; Thompson, A. *Org. Biomol. Chem.* **2017**, *15*, 144−152.

Spectroscopic details

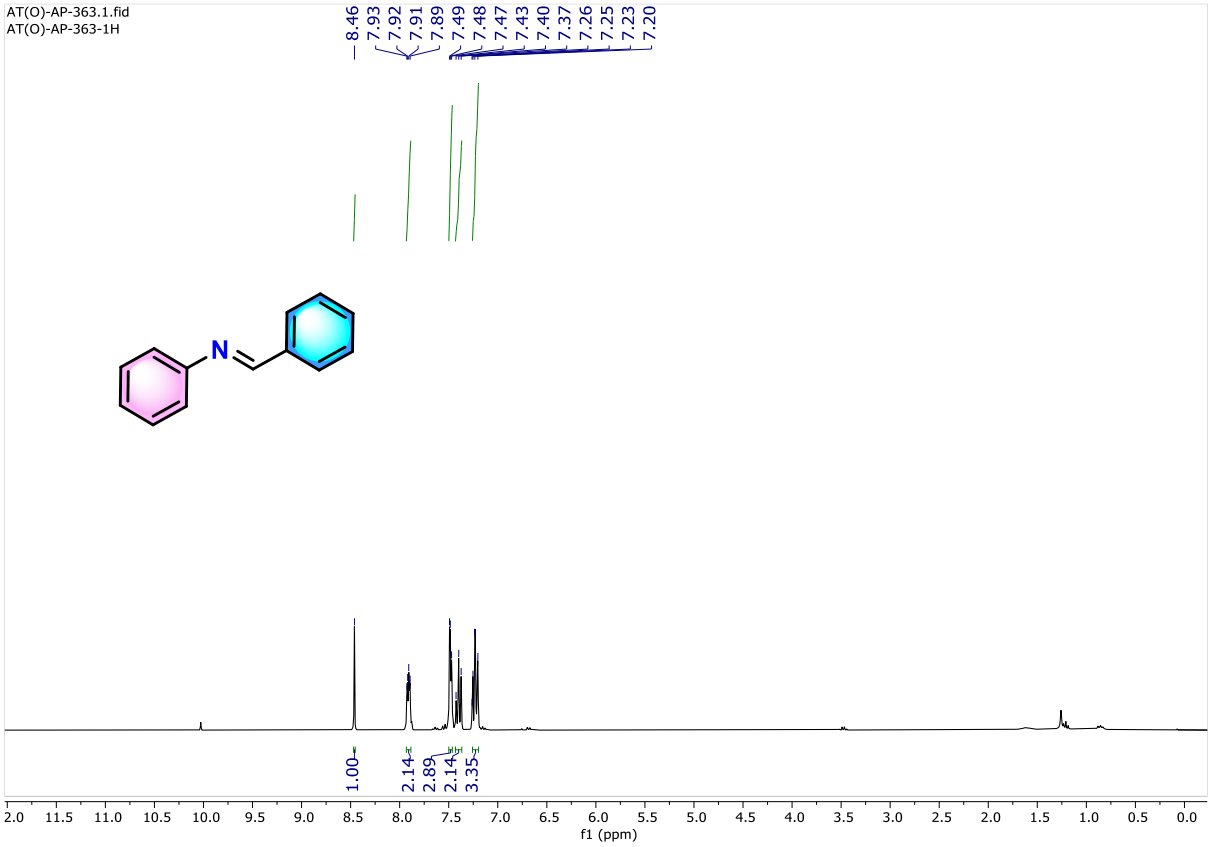

Figure 3.4. ^{1}H NMR (300 MHz) spectrum of **3a** in $CDCl_3$.

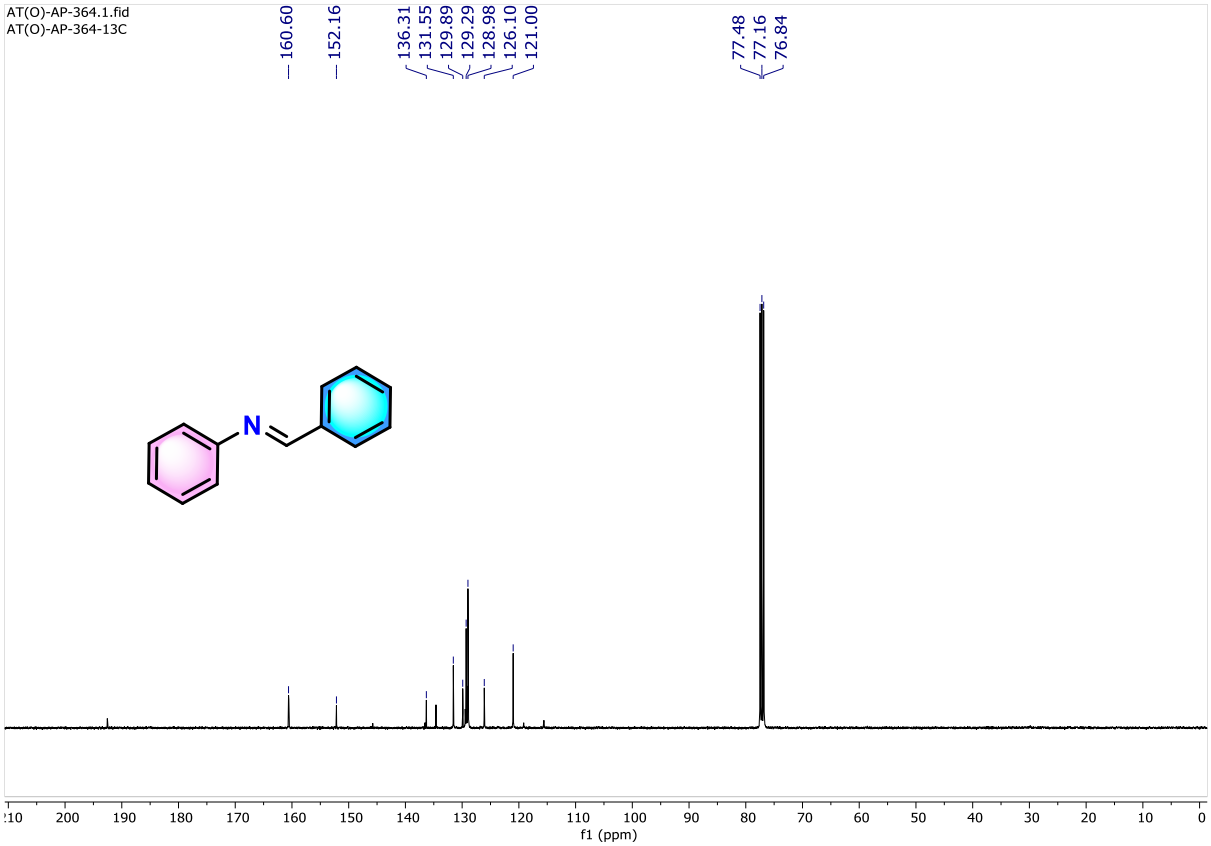

Figure 3.5. $^{13}C\{^{1}H\}$ NMR (75 MHz) spectrum of **3a** in $CDCl_3$.

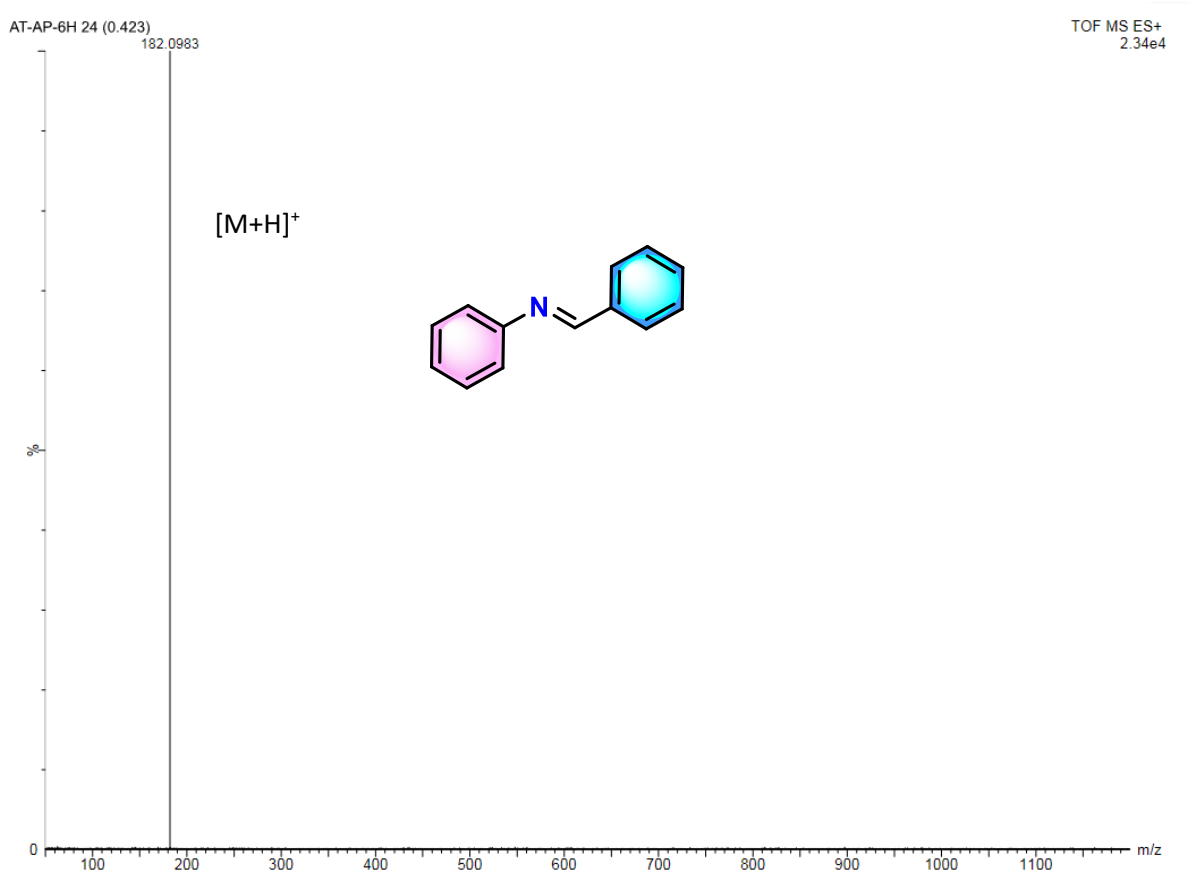

Figure 3.6. HRMS of **3a** compound.

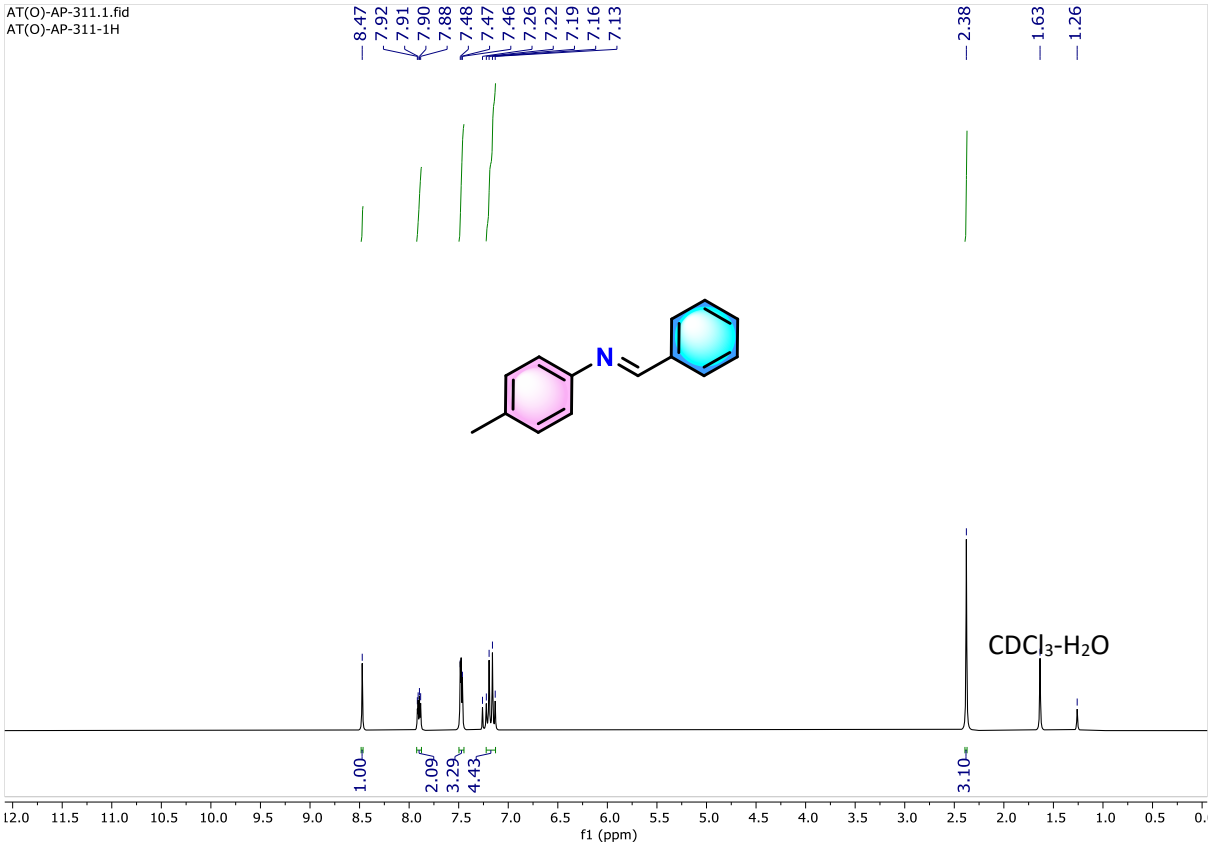

Figure 3.7. ^{1}H NMR (300 MHz) spectrum of **3b** in $CDCl_3$.

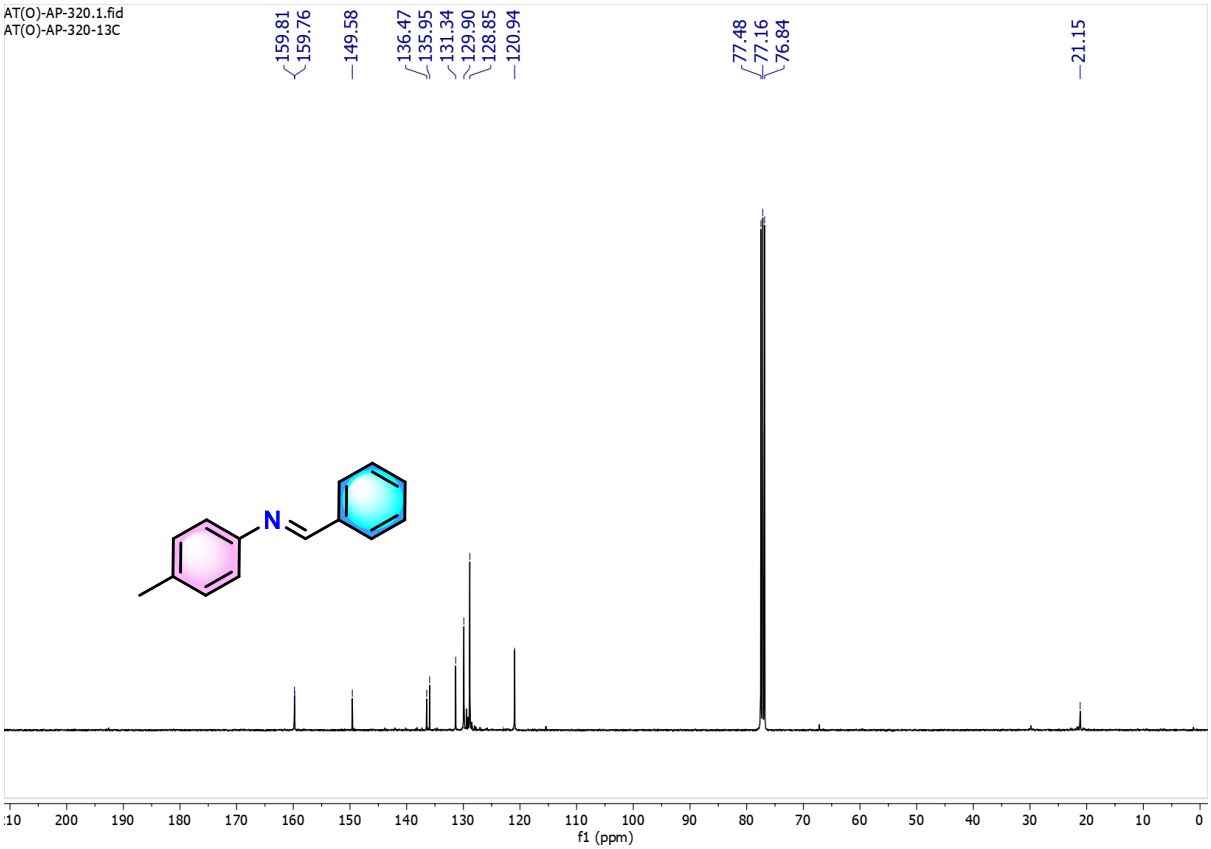

Figure 3.8. $^{13}C\{^{1}H\}$ NMR (75 MHz) spectrum of **3b** in $CDCl_3$.

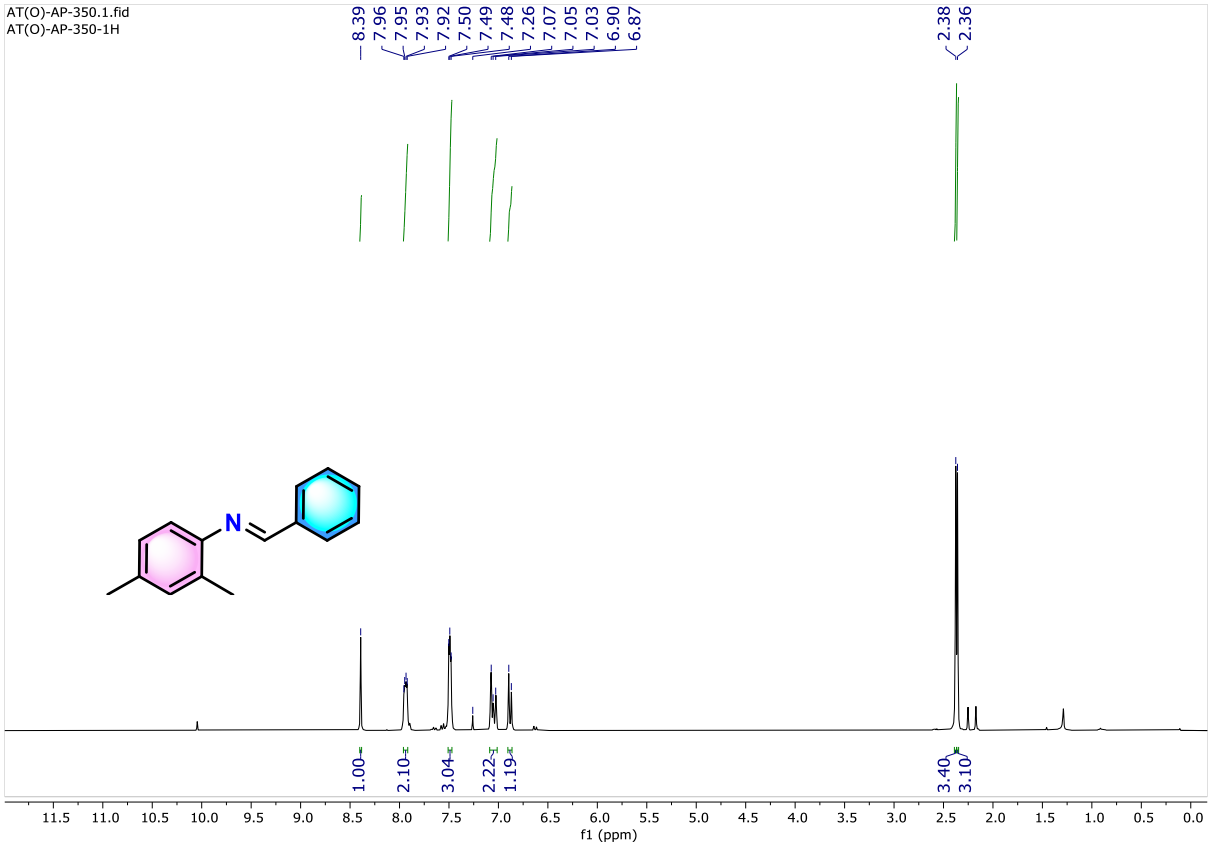

Figure 3.9. ^{1}H NMR (300 MHz) spectrum of **3c** in $CDCl_3$.

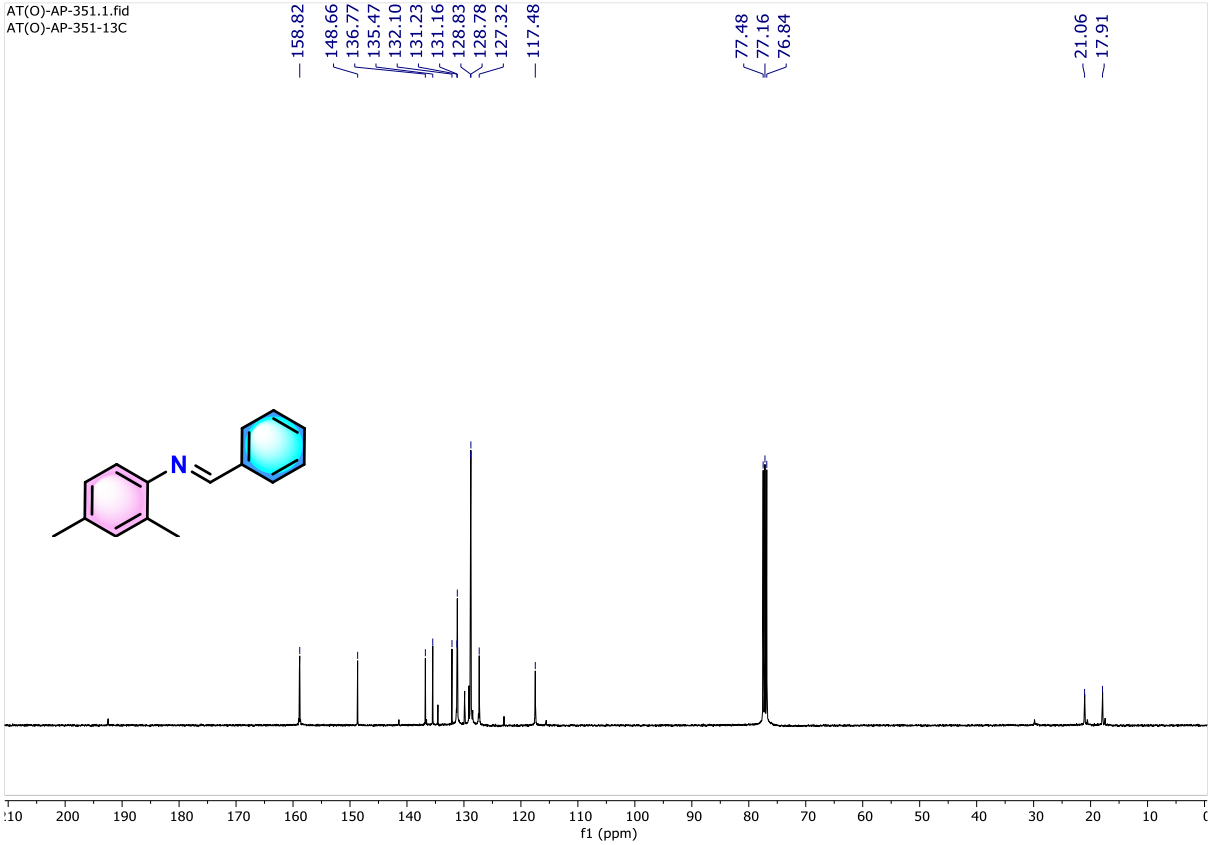

Figure 3.10. $^{13}C\{^{1}H\}$ NMR (75 MHz) spectrum of **3c** in $CDCl_3$.

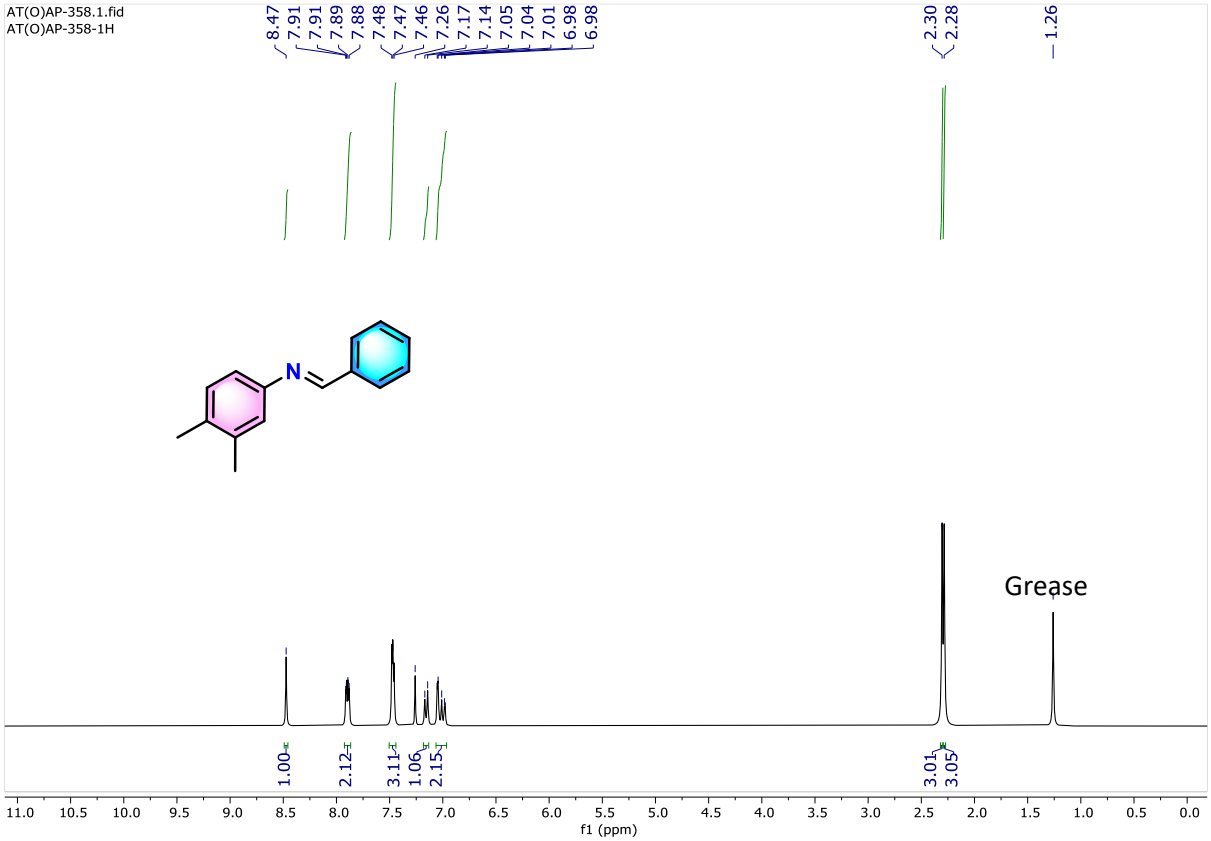

Figure 3.11. ^{1}H NMR (300 MHz) spectrum of **3d** in $CDCl_3$.

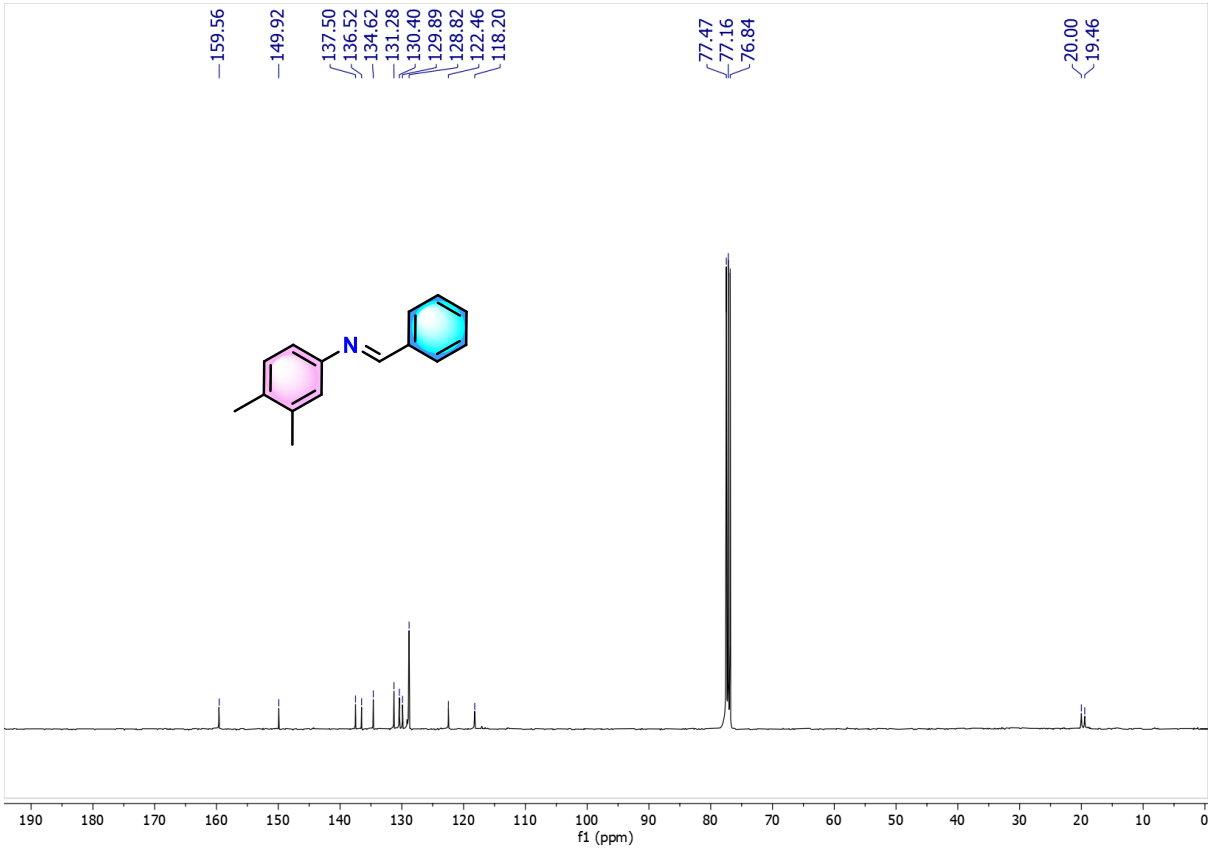

Figure 3.12. $^{13}C\{^{1}H\}$ NMR (75 MHz) spectrum of **3d** in $CDCl_3$**.**

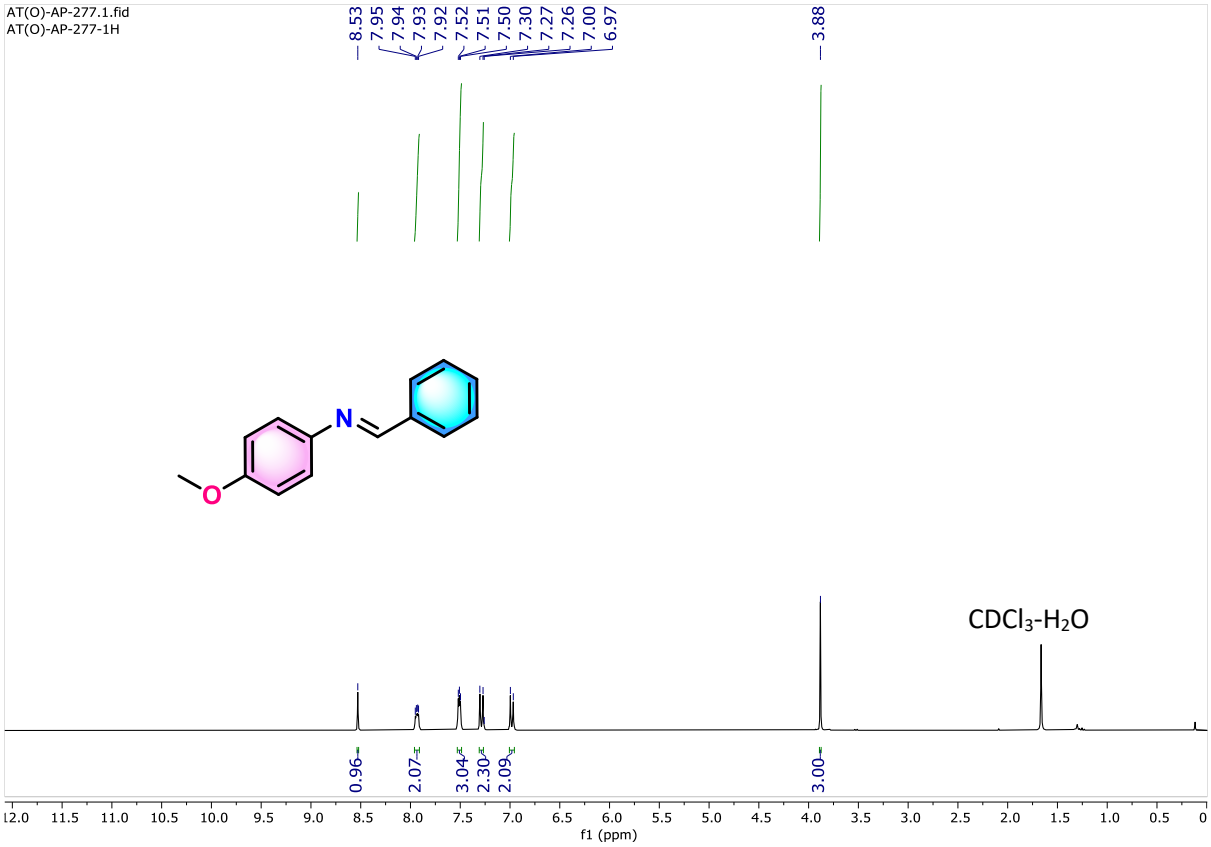

Figure 3.13. ^{1}H NMR (300 MHz) spectrum of **3e** in $CDCl_3$**.**

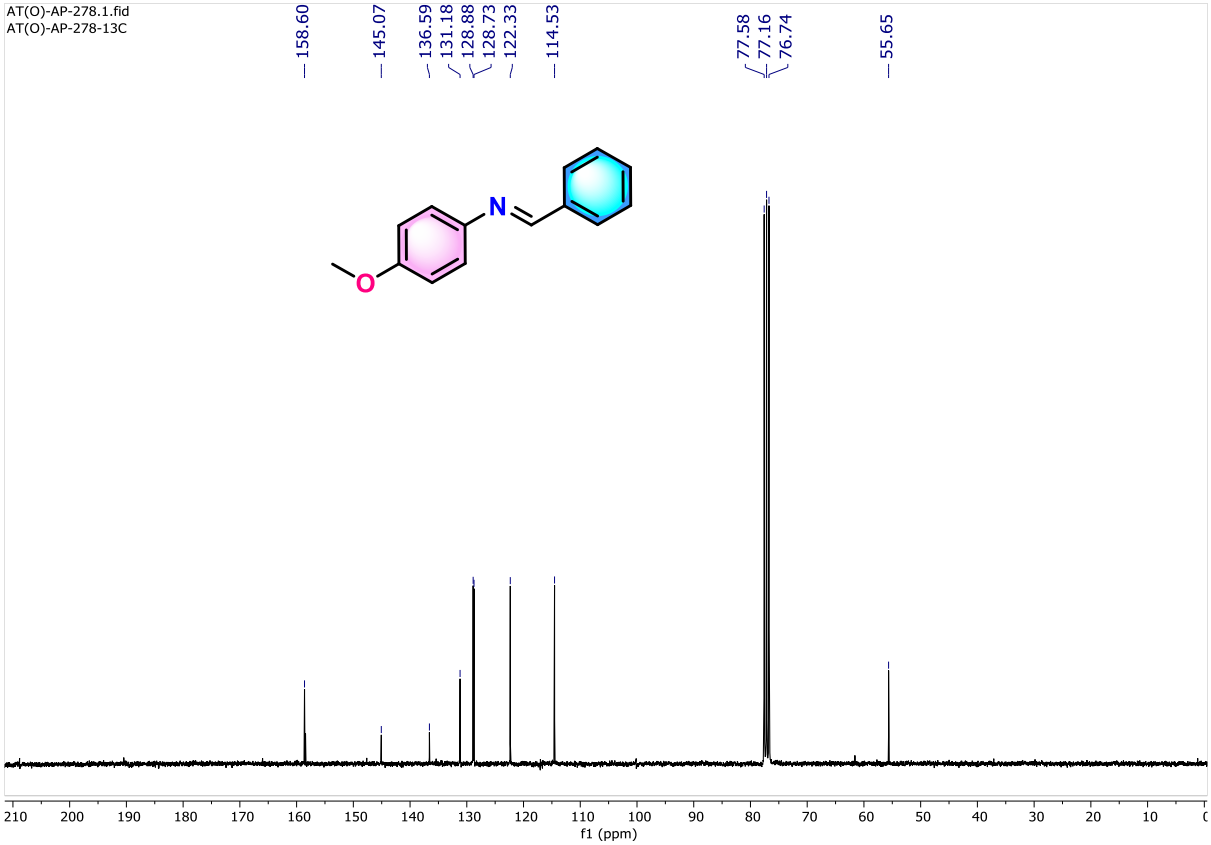

Figure 3.14. $^{13}C\{^{1}H\}$ NMR (75 MHz) spectrum of **3e** in $CDCl_3$**.**

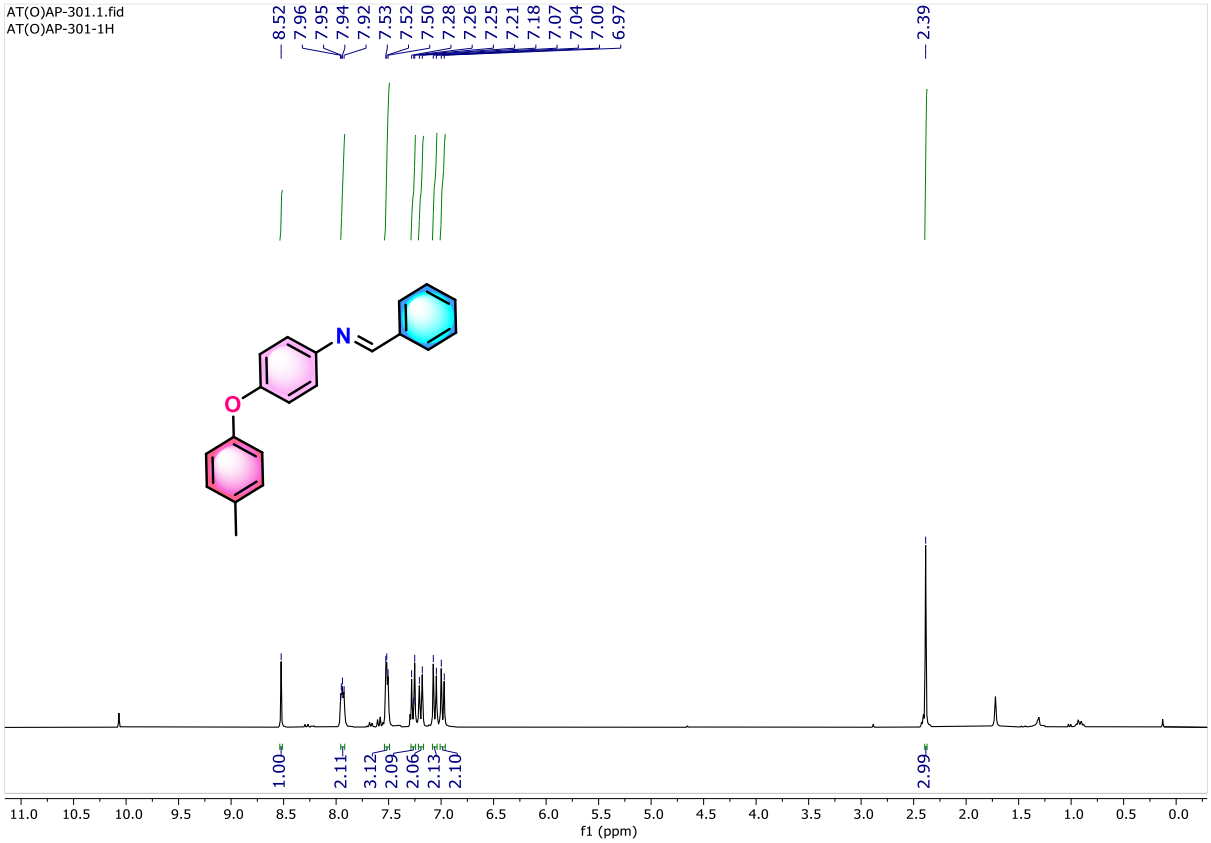

Figure 3.15. ^{1}H NMR (300 MHz) spectrum of **3f** in $CDCl_3$.

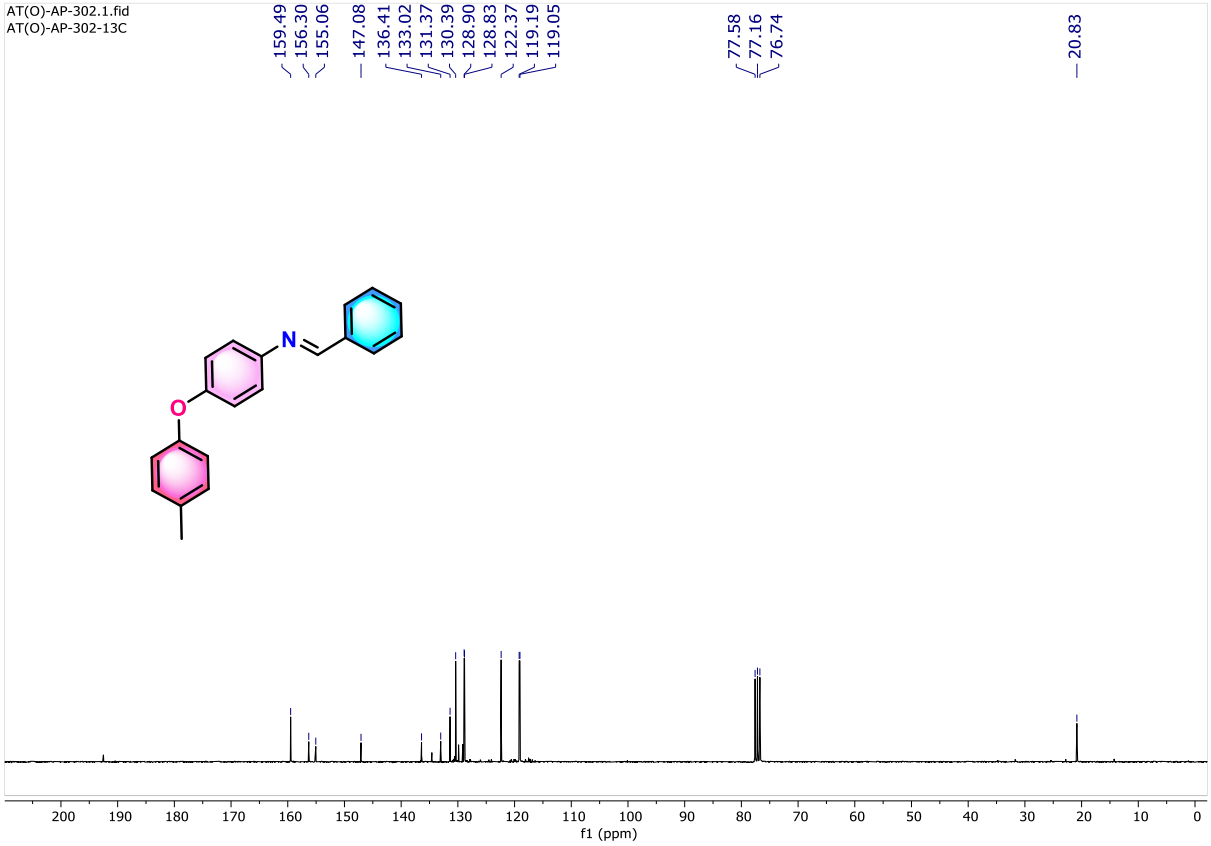

Figure 3.16. $^{13}C\{^{1}H\}$ NMR (75 MHz) spectrum of **3f** in $CDCl_3$.

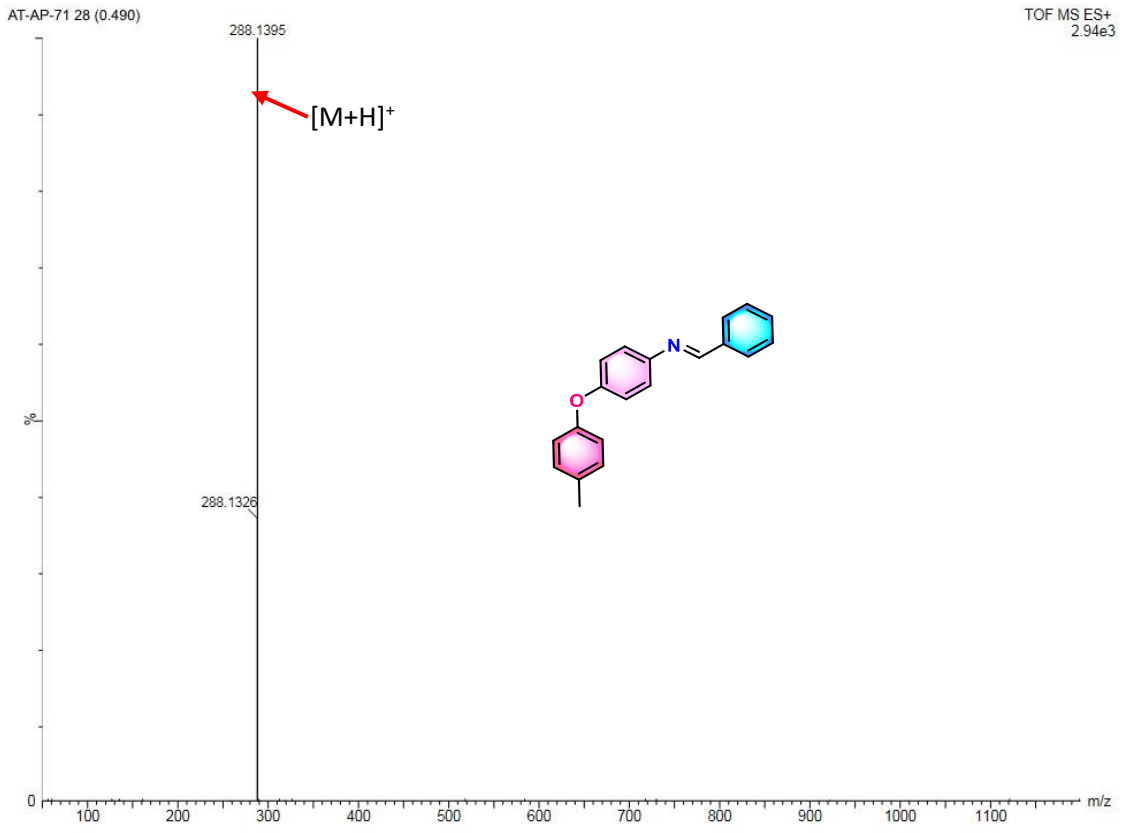

Figure 3.17. HRMS of **3f** compound.

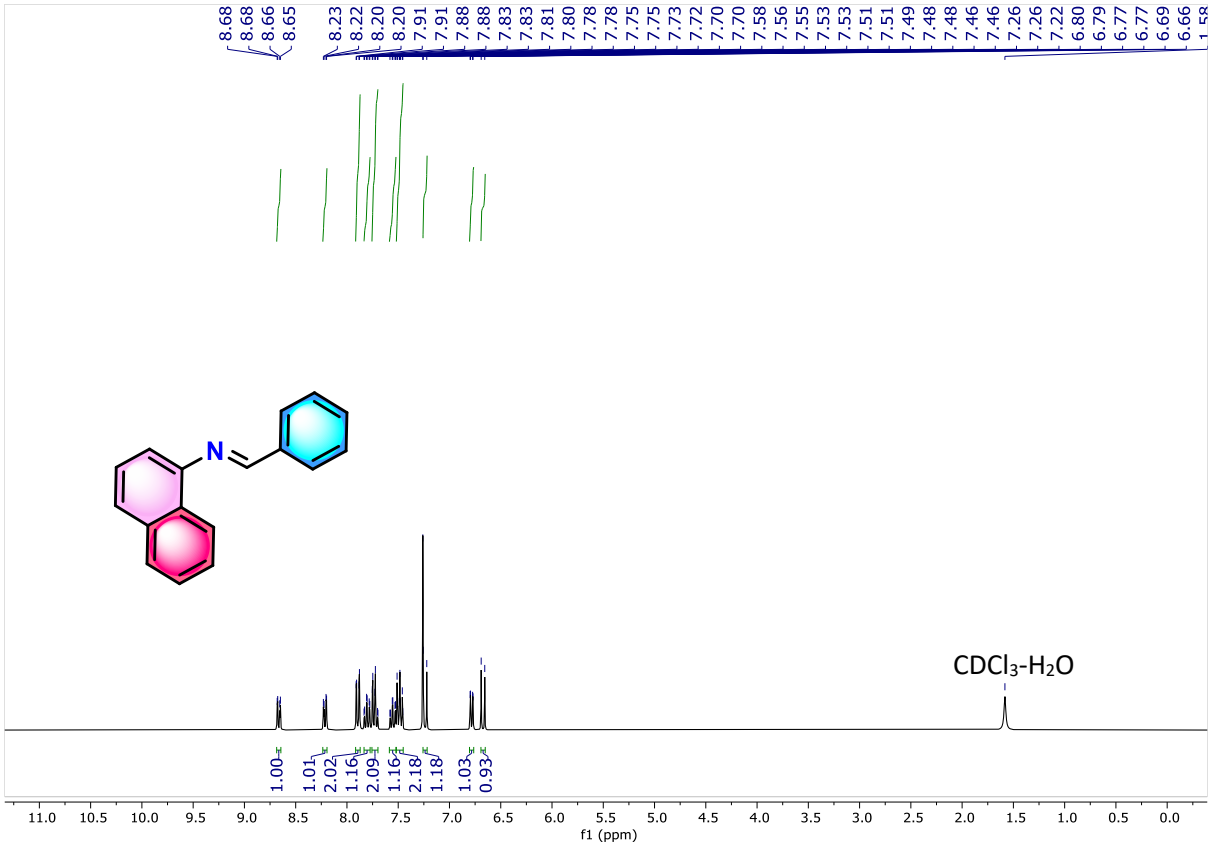

Figure 3.18. ^{1}H NMR (300 MHz) spectrum of **3g** in $CDCl_3$.

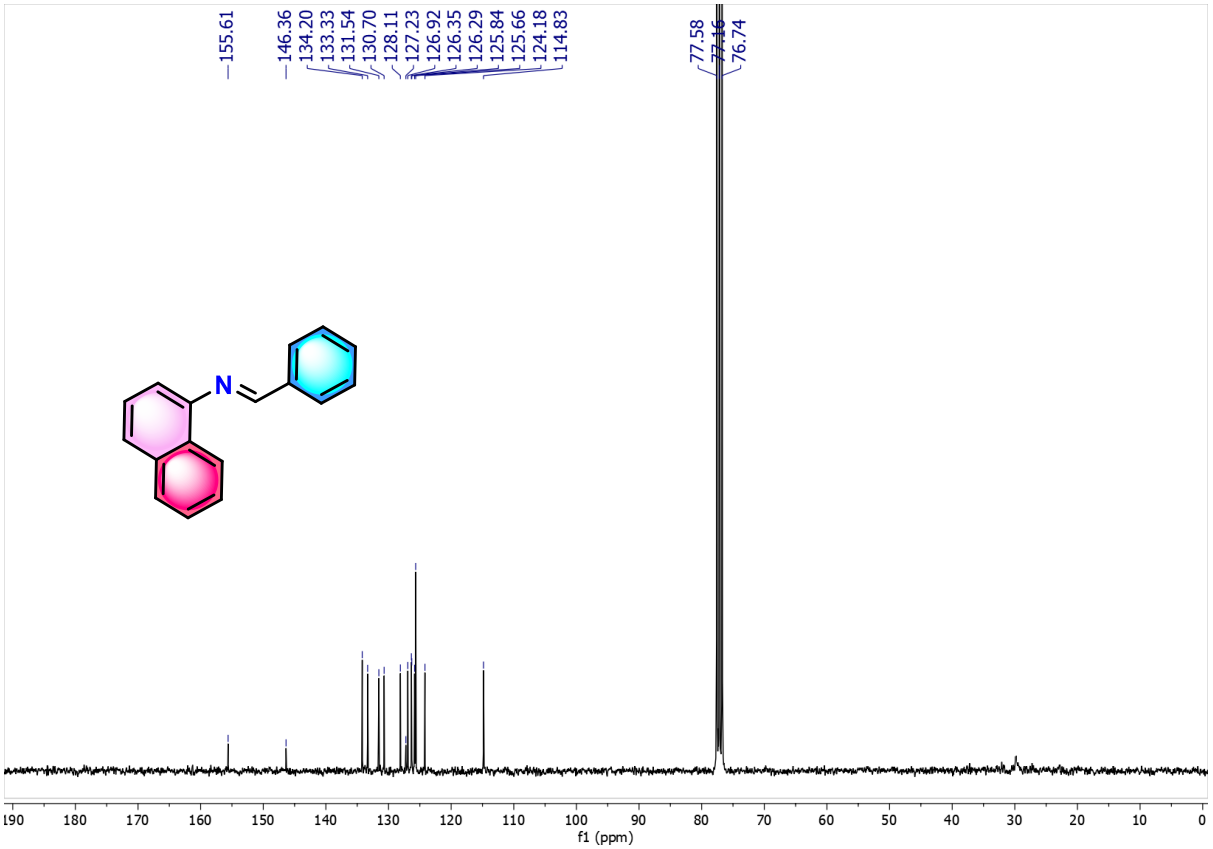

Figure 3.19. $^{13}C\{^{1}H\}$ NMR (75 MHz) spectrum of **3g** in $CDCl_3$**.**

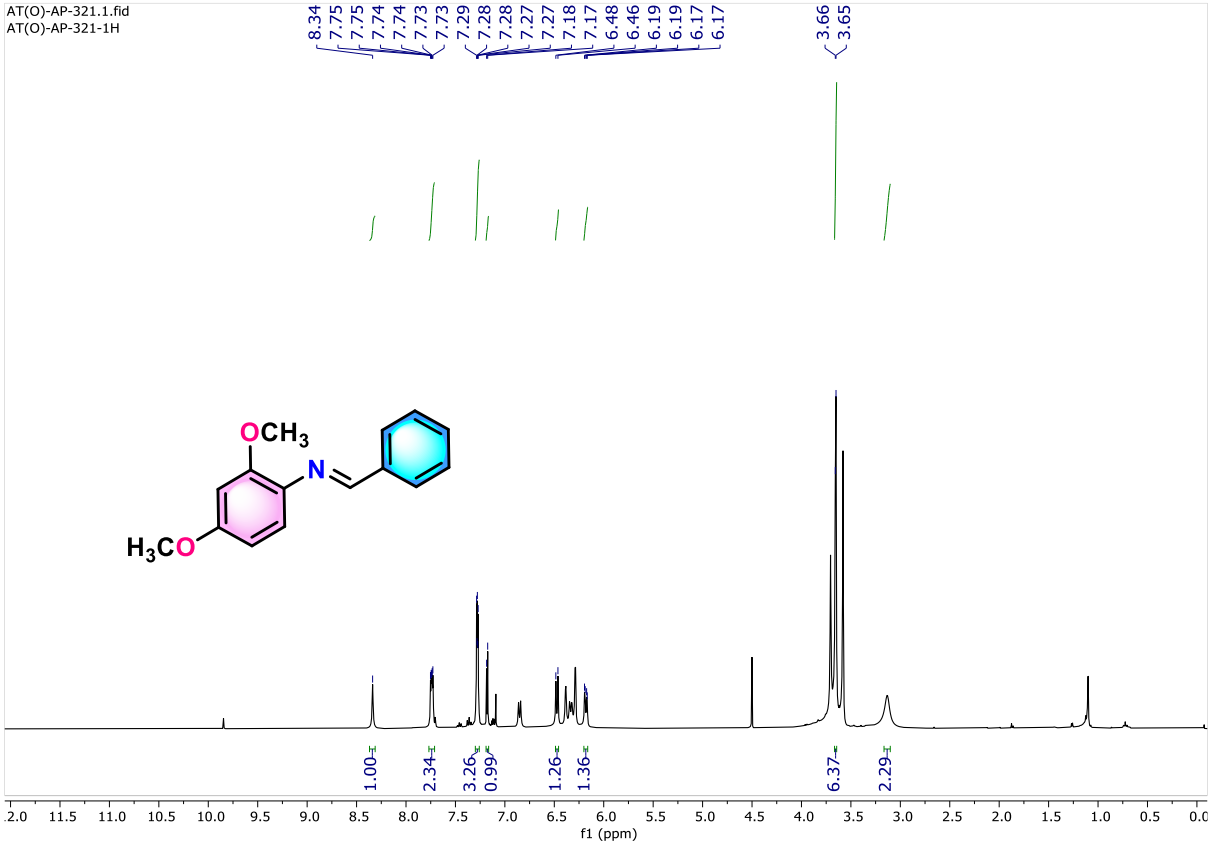

Figure 3.20. ^{1}H NMR (300 MHz) spectrum of **3h** (Reaction Mixture) in $CDCl_3$. The peak at 8.34 ppm shows the imine H.

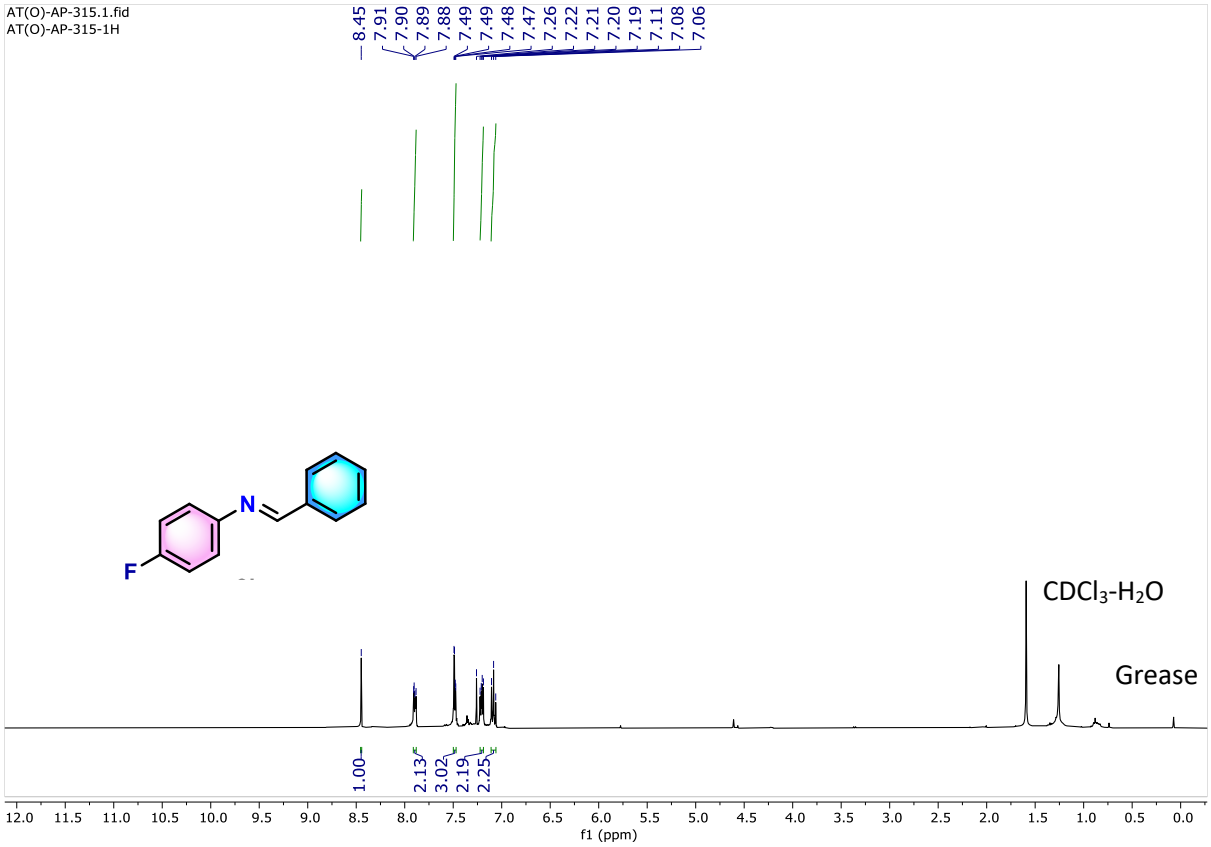

Figure 3.21. ^{1}H NMR (300 MHz) spectrum of **3i** in $CDCl_3$**.**

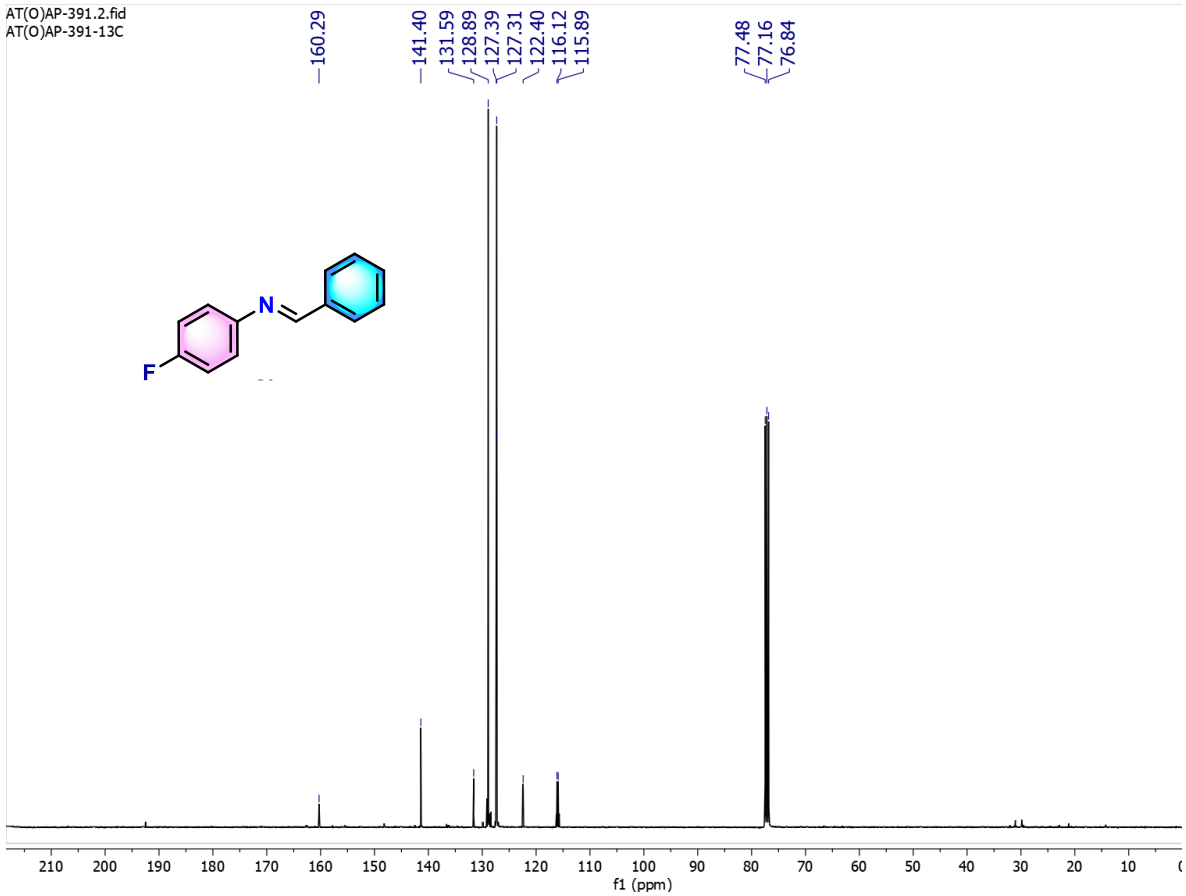

Figure 3.22. $^{13}C\{^{1}H\}$ NMR (75 MHz) spectrum of **3i** in $CDCl_3$**.**

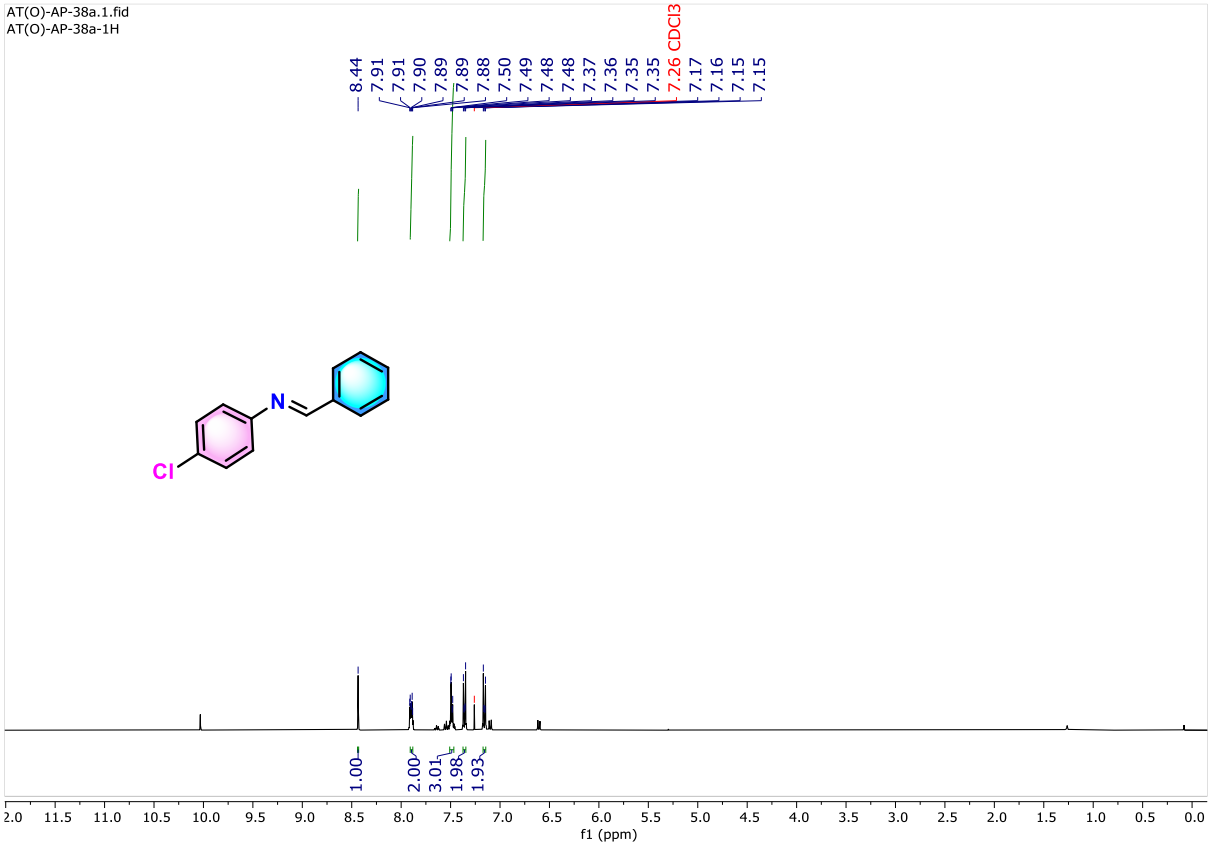

Figure 3.23. ^{1}H NMR (300 MHz) spectrum of **3j** in $CDCl_3$**.**

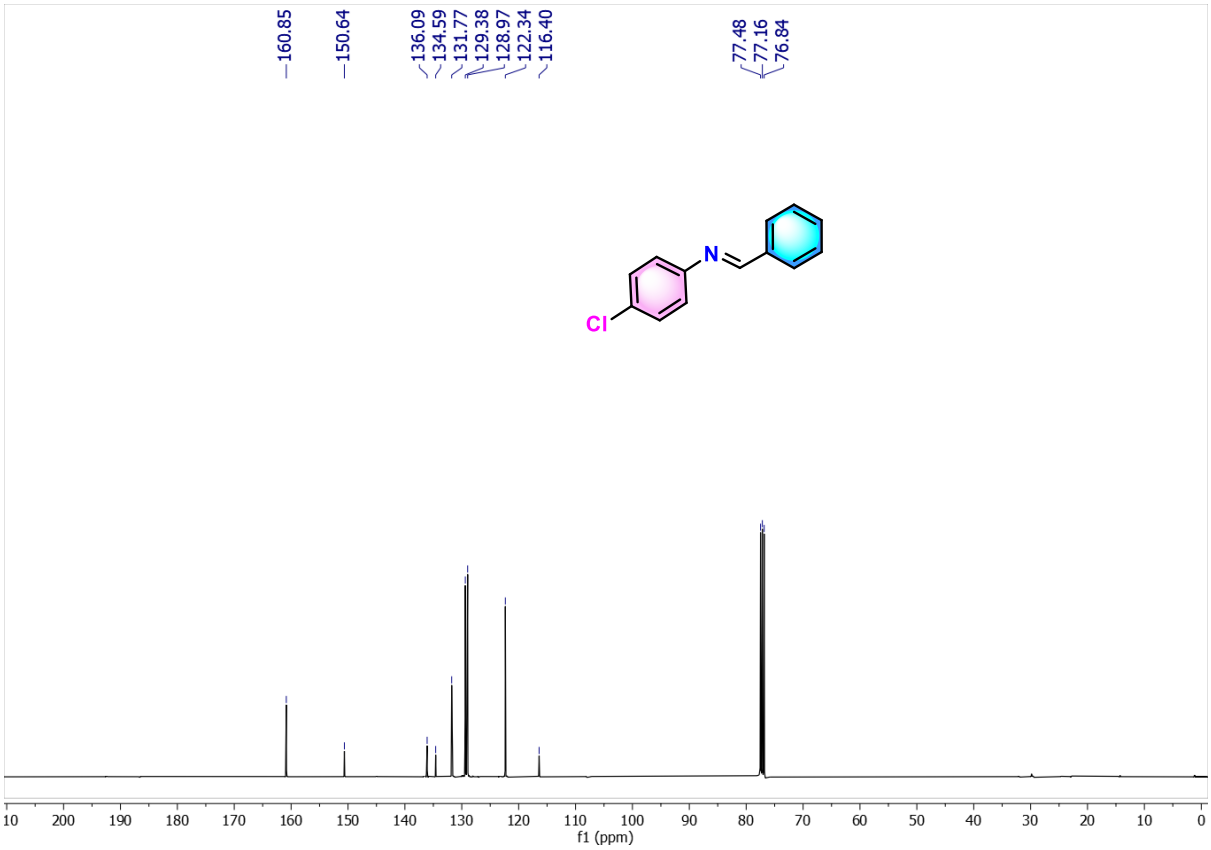

Figure 3.24. $^{13}C\{^{1}H\}$ NMR (75 MHz) spectrum of **3j** in $CDCl_3$.

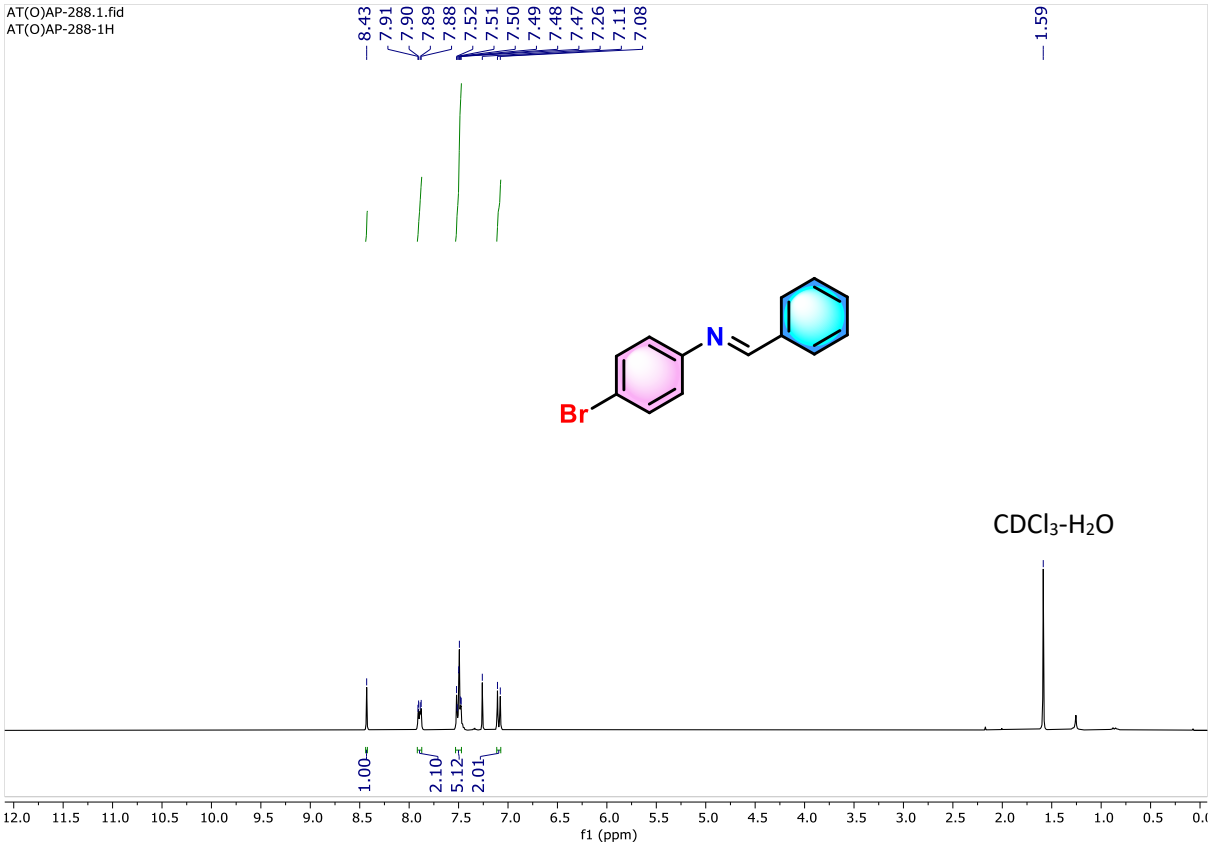

Figure 3.25. ^{1}H NMR (300 MHz) spectrum of **3k** in $CDCl_3$**.**

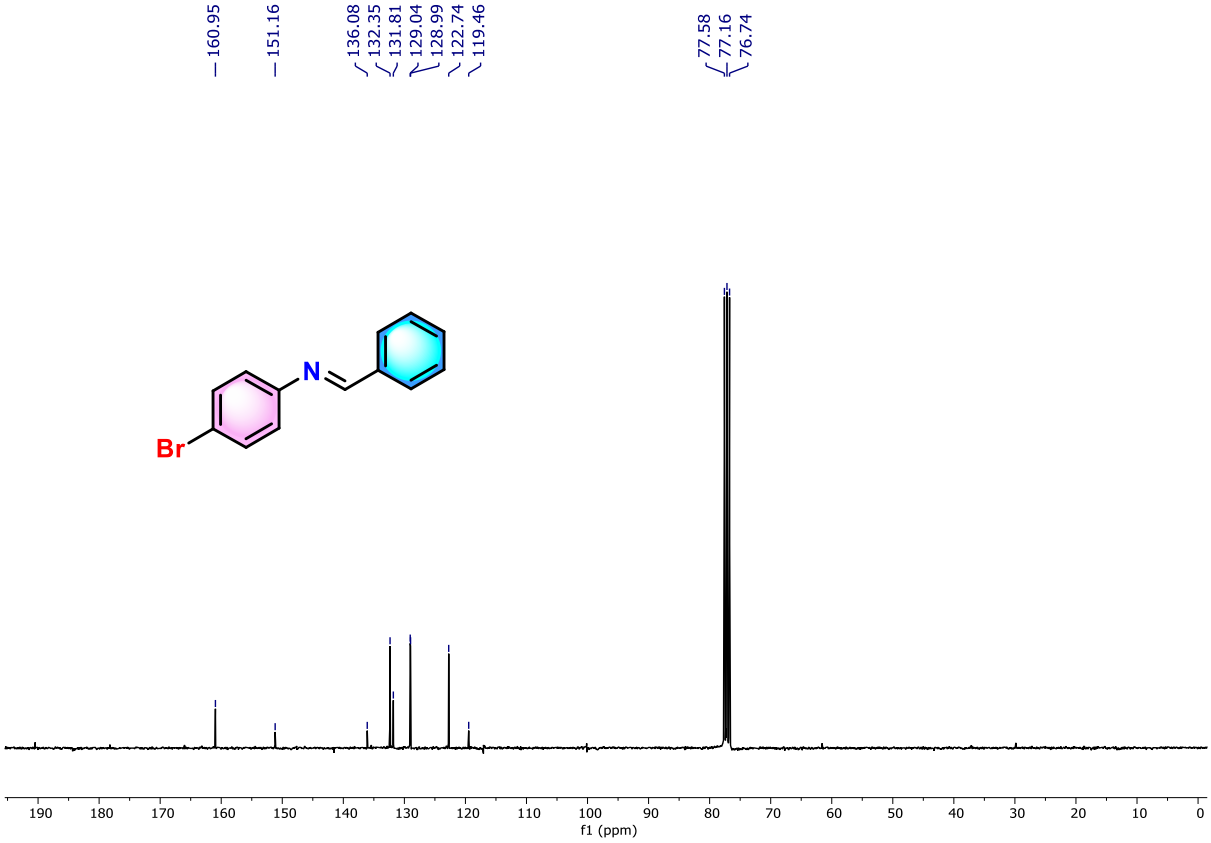

Figure 3.26. ^{13}C{^{1}H} NMR (75 MHz) spectrum of **3k** in $CDCl_3$**.**

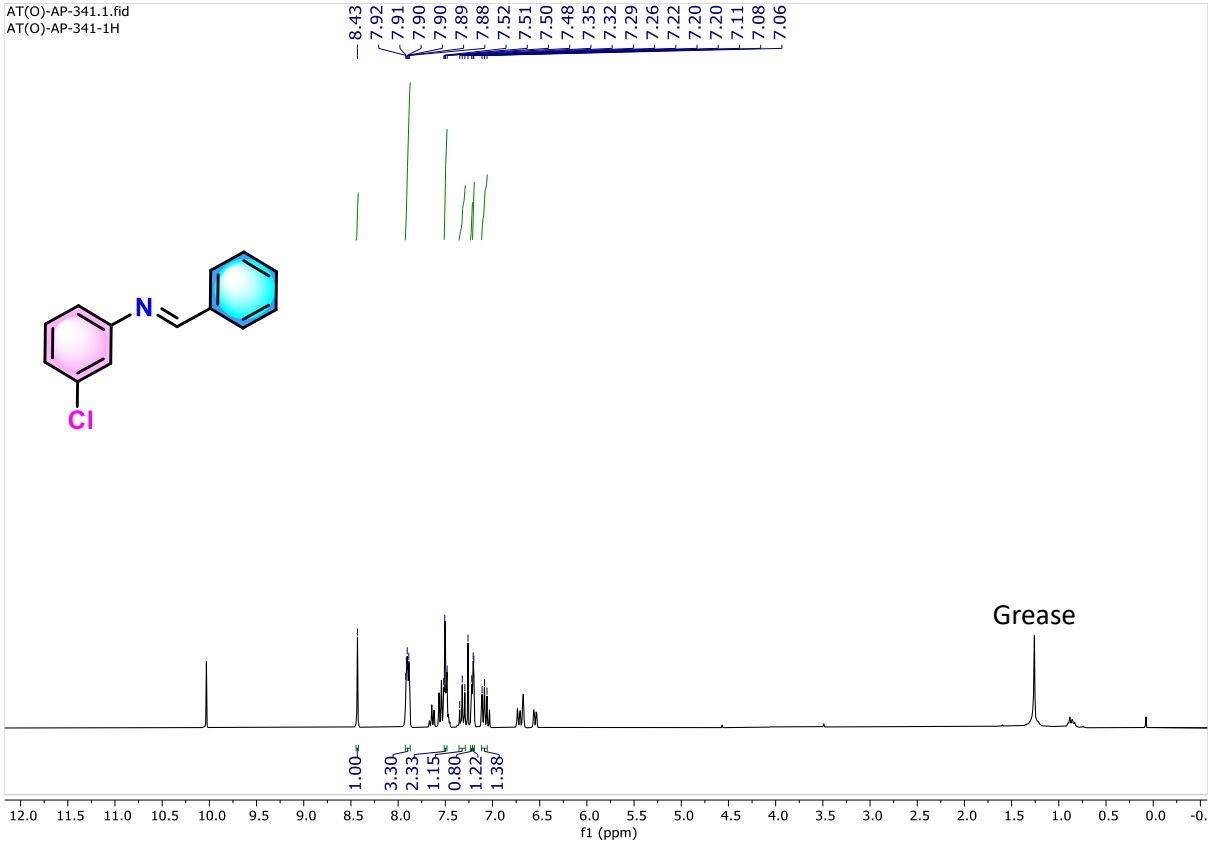

Figure 3.27. ^{1}H NMR (300 MHz) spectrum of **3l** (Reaction Mixture) in $CDCl_3$. The peak at 8.43 ppm shows the imine H.

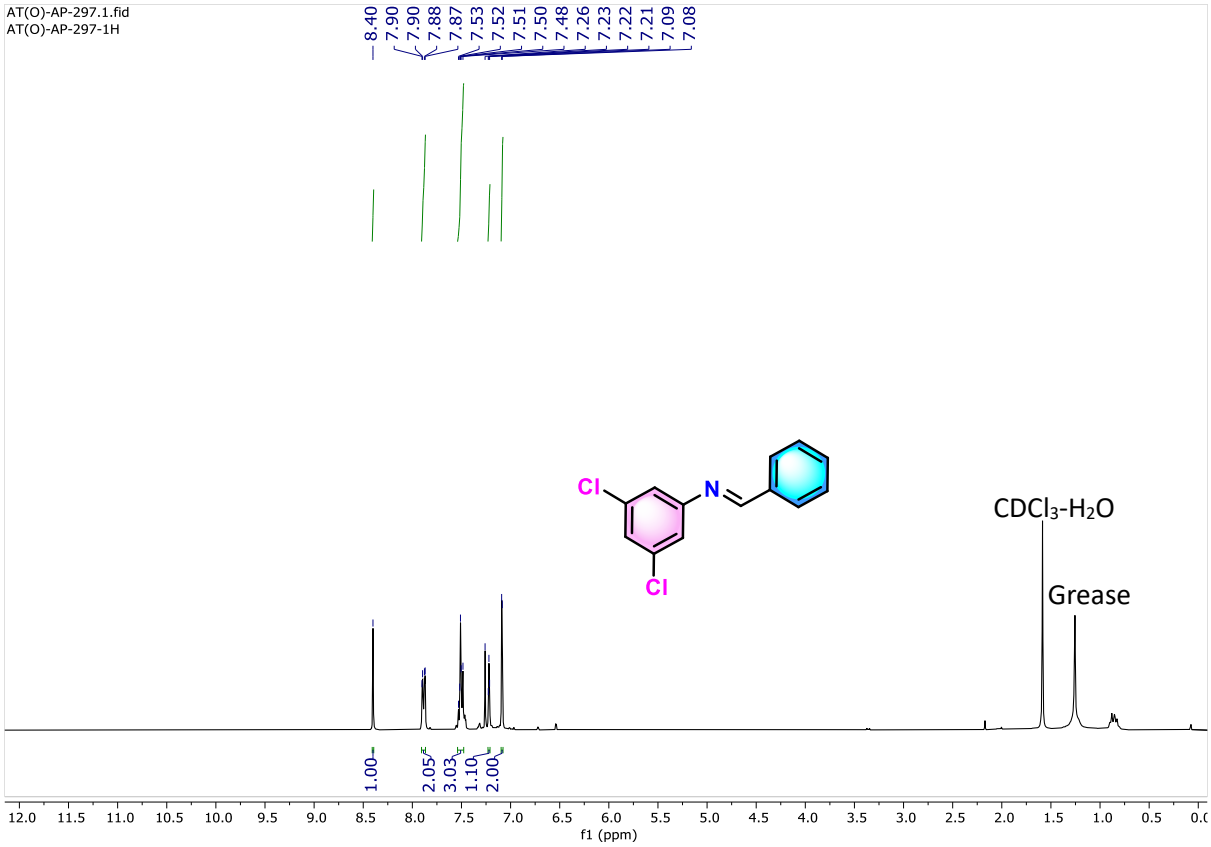

Figure 3.28. ^{1}H NMR (300 MHz) spectrum of **3m** in $CDCl_3$**.**

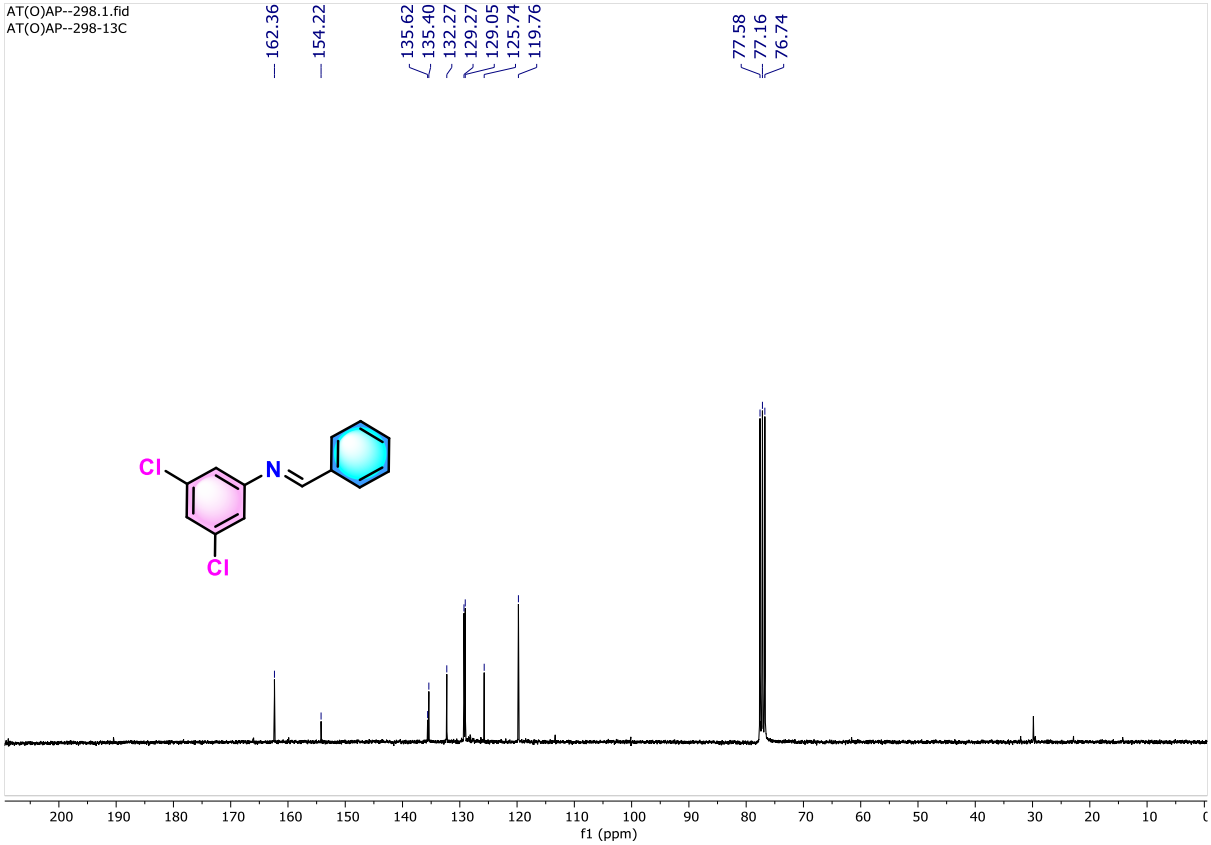

Figure 3.29. $^{13}C\{^{1}H\}$ NMR (75 MHz) spectrum of **3m** in $CDCl_3$

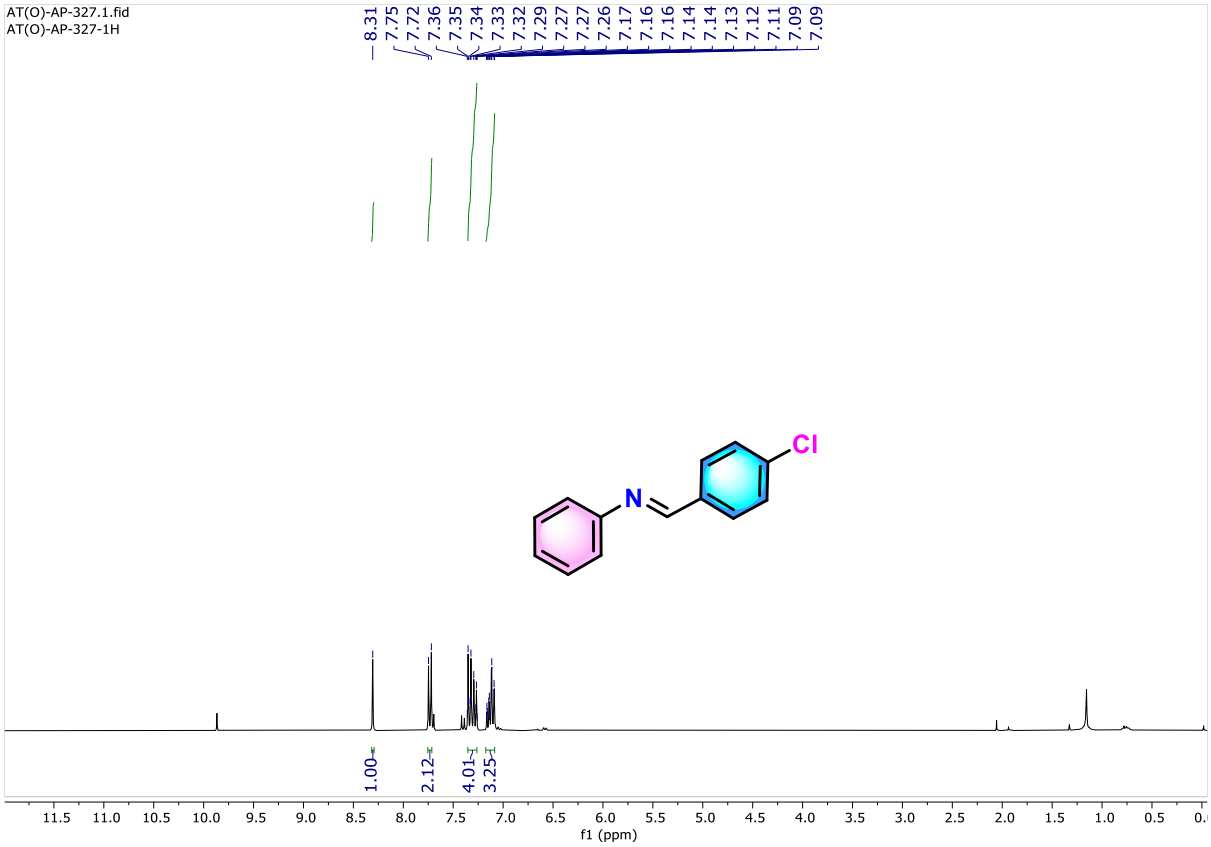

Figure 3.30. ^{1}H NMR (300 MHz) spectrum of **3n** in $CDCl_3$**.**

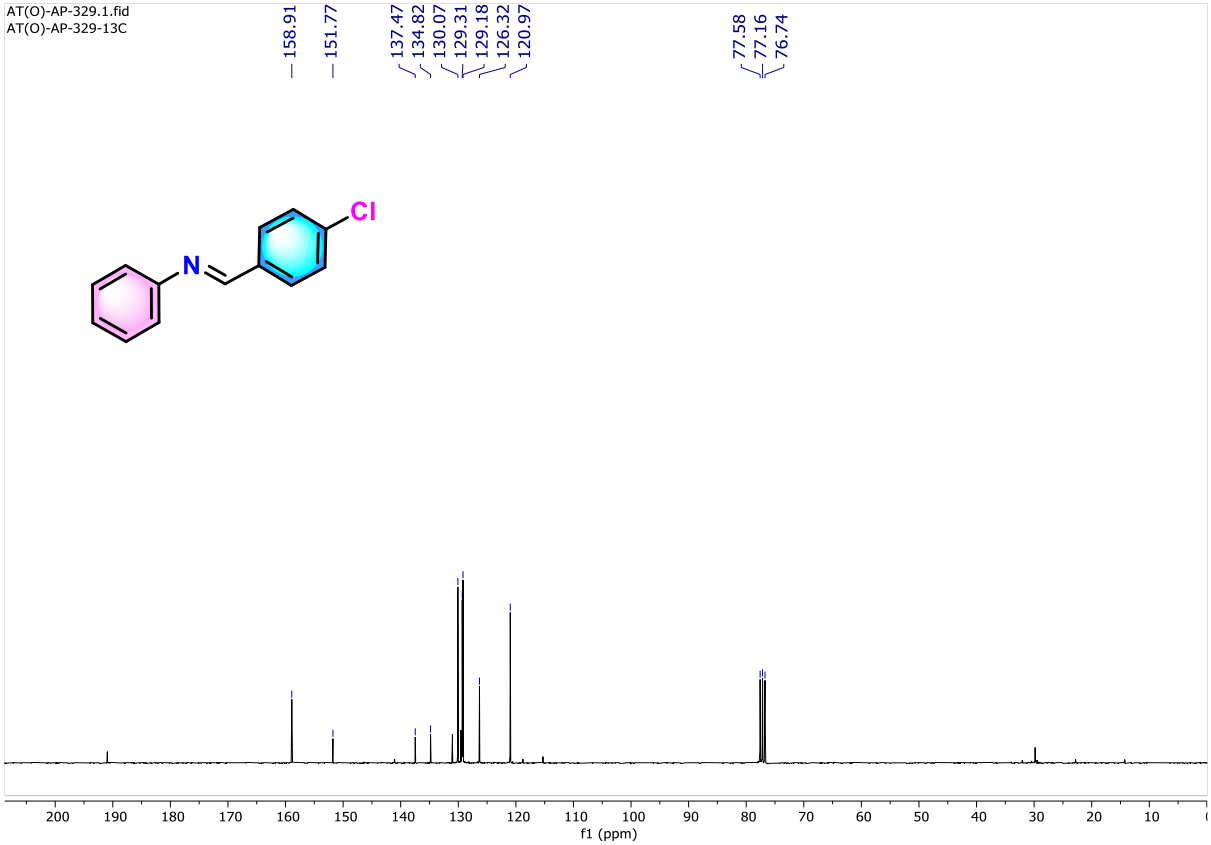

Figure 3.31. $^{13}C\{^{1}H\}$ NMR (75 MHz) spectrum of **3n** in $CDCl_3$**.**

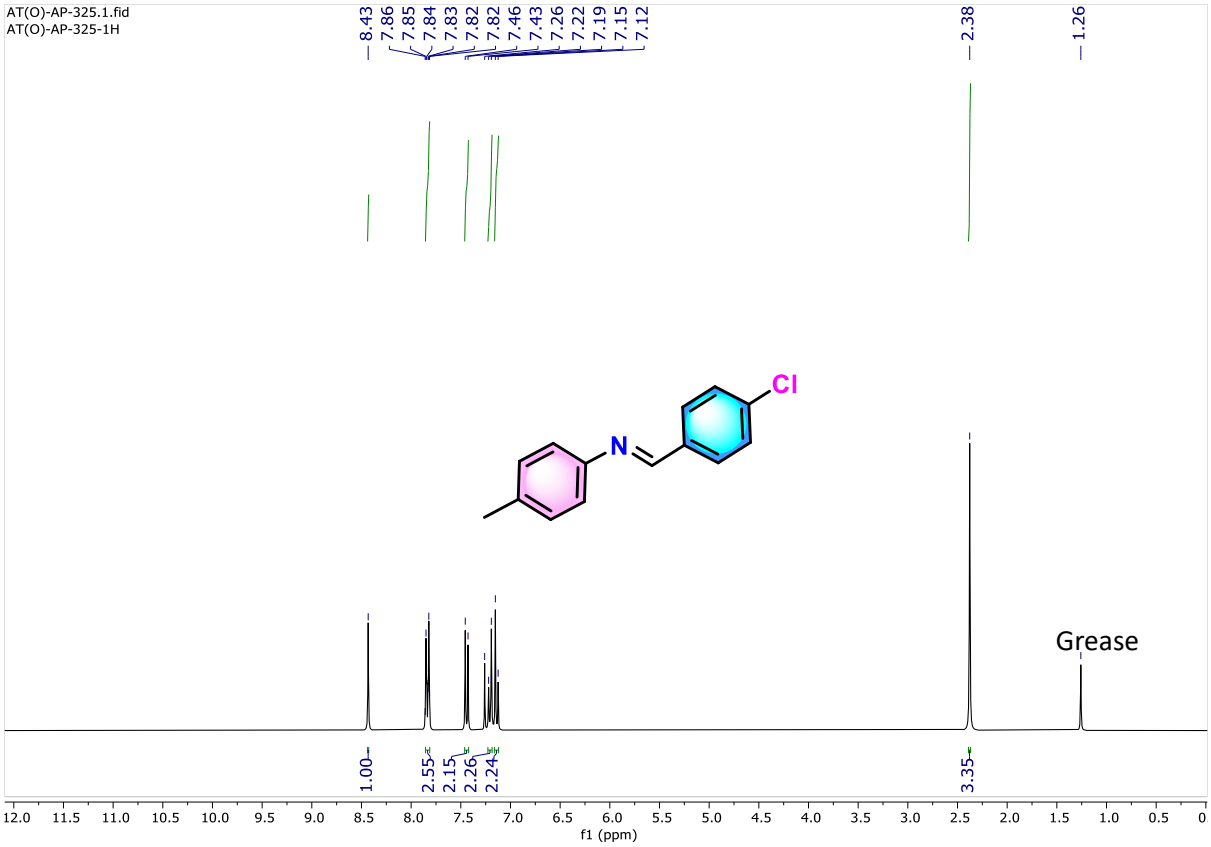

Figure 3.32. ^{1}H NMR (300 MHz) spectrum of **3o** in $CDCl_3$**.**

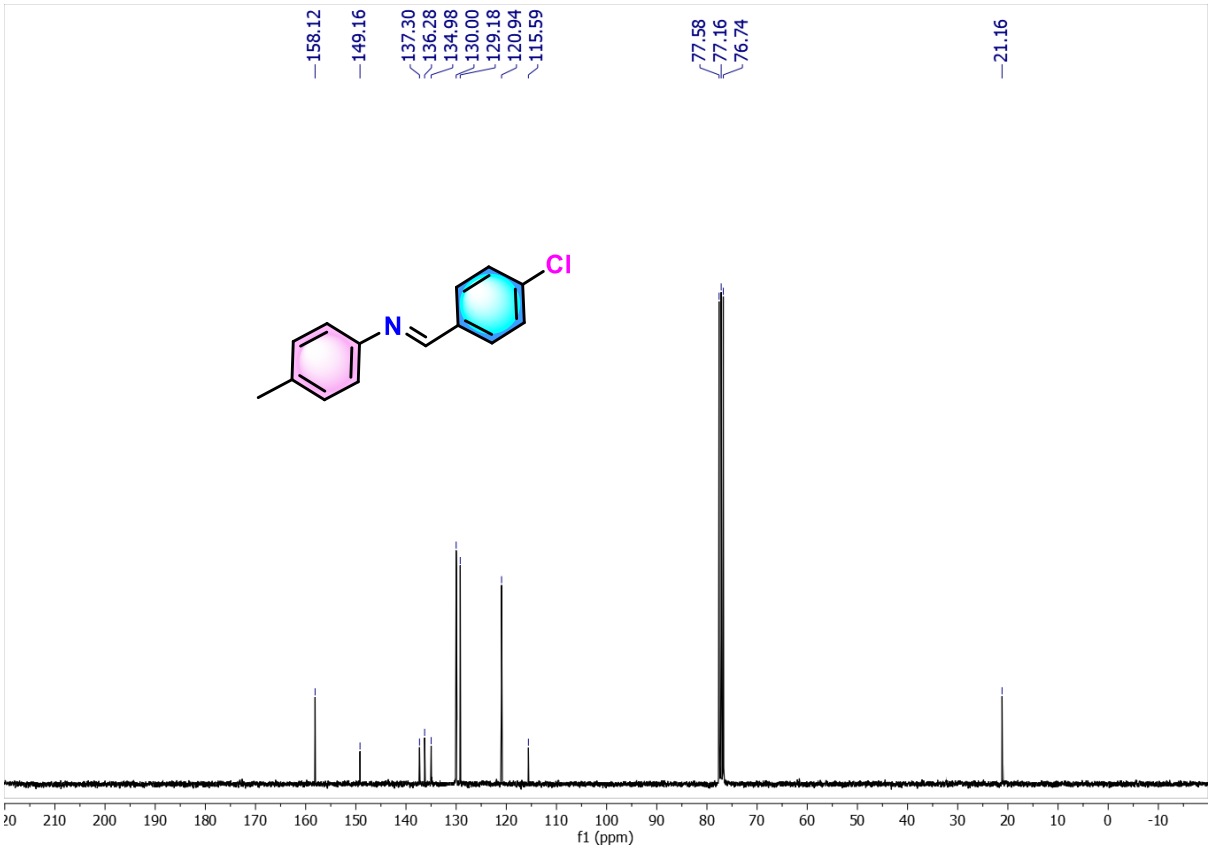

Figure 3.33. $^{13}C\{^{1}H\}$ NMR (75 MHz) spectrum of **3o** in $CDCl_3$**.**

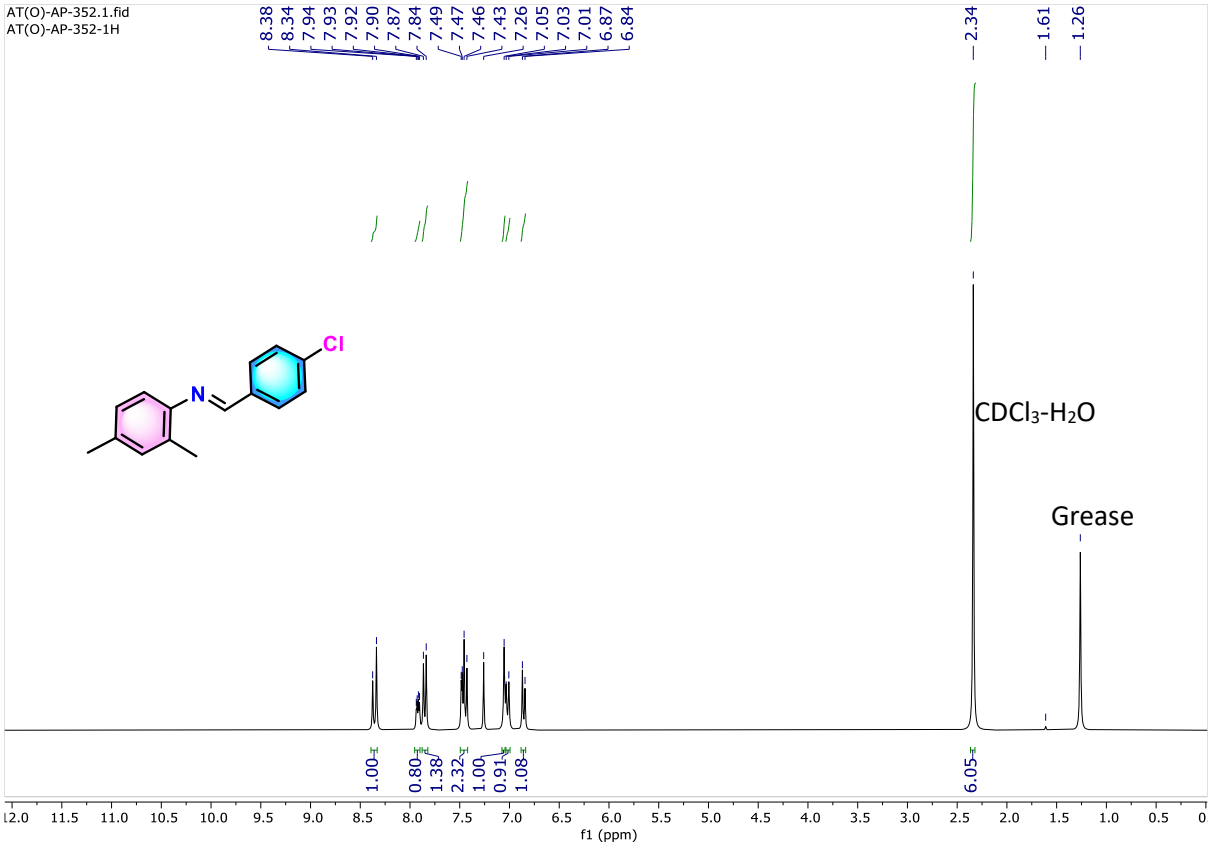

Figure 3.34. ^{1}H NMR (300 MHz) spectrum of **3p** in $CDCl_3$**.**

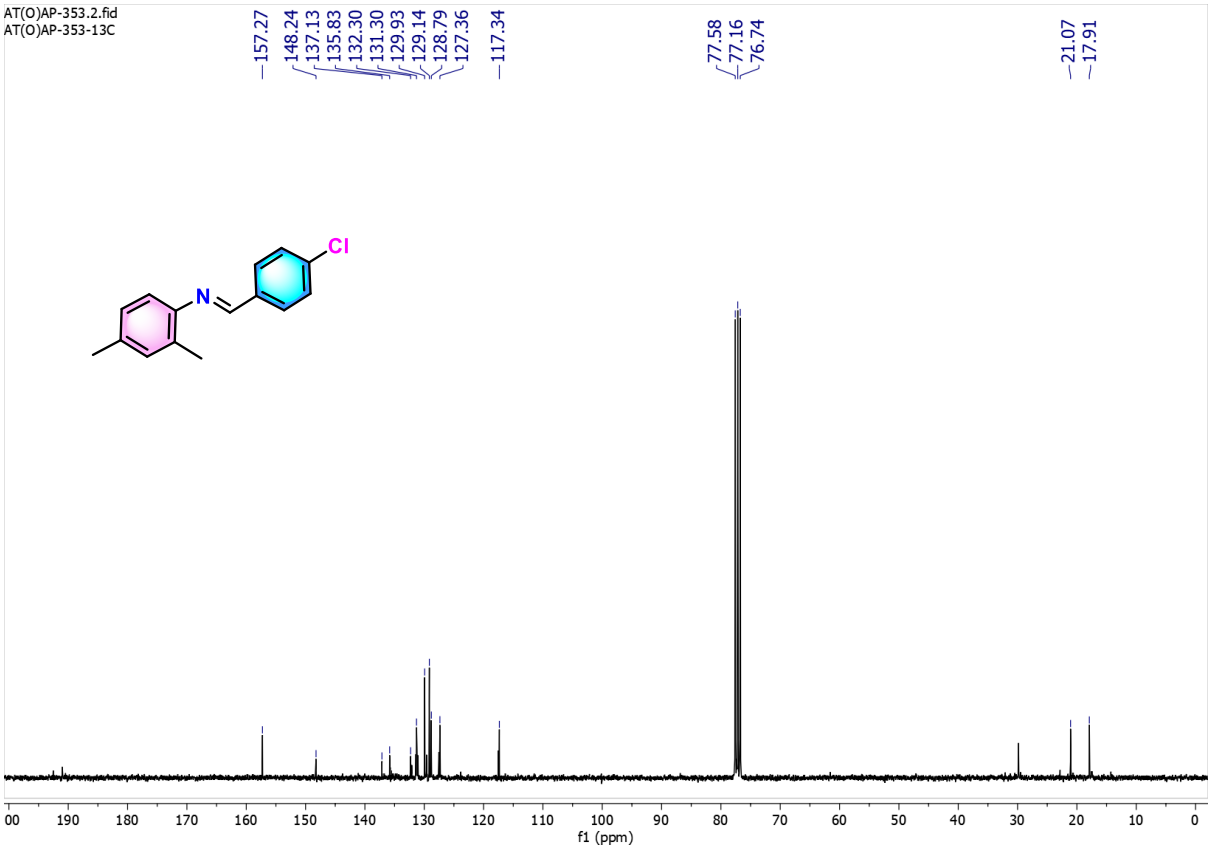

Figure 3.35. $^{13}C\{^{1}H\}$ NMR (75 MHz) spectrum of **3p** in $CDCl_3$.

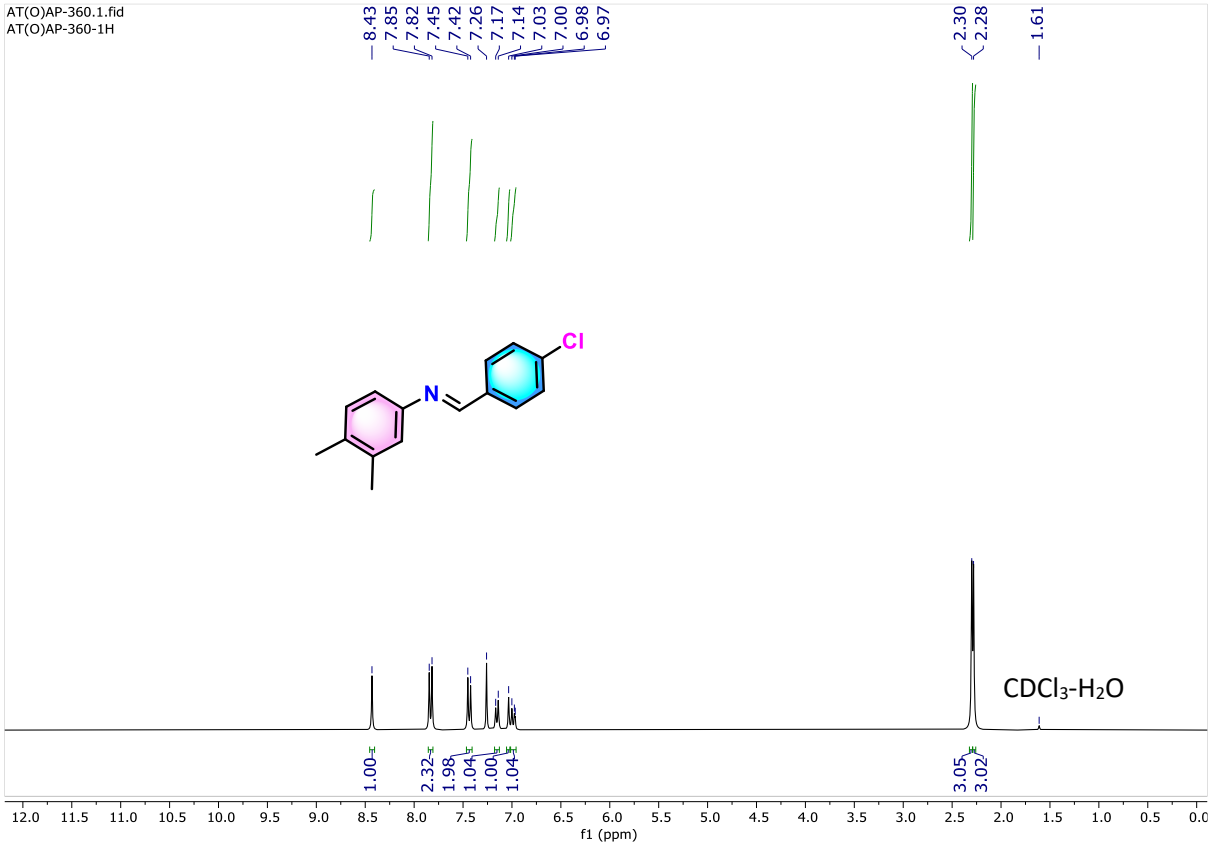

Figure 3.36. ^{1}H NMR (300 MHz) spectrum of **3q** in $CDCl_3$.

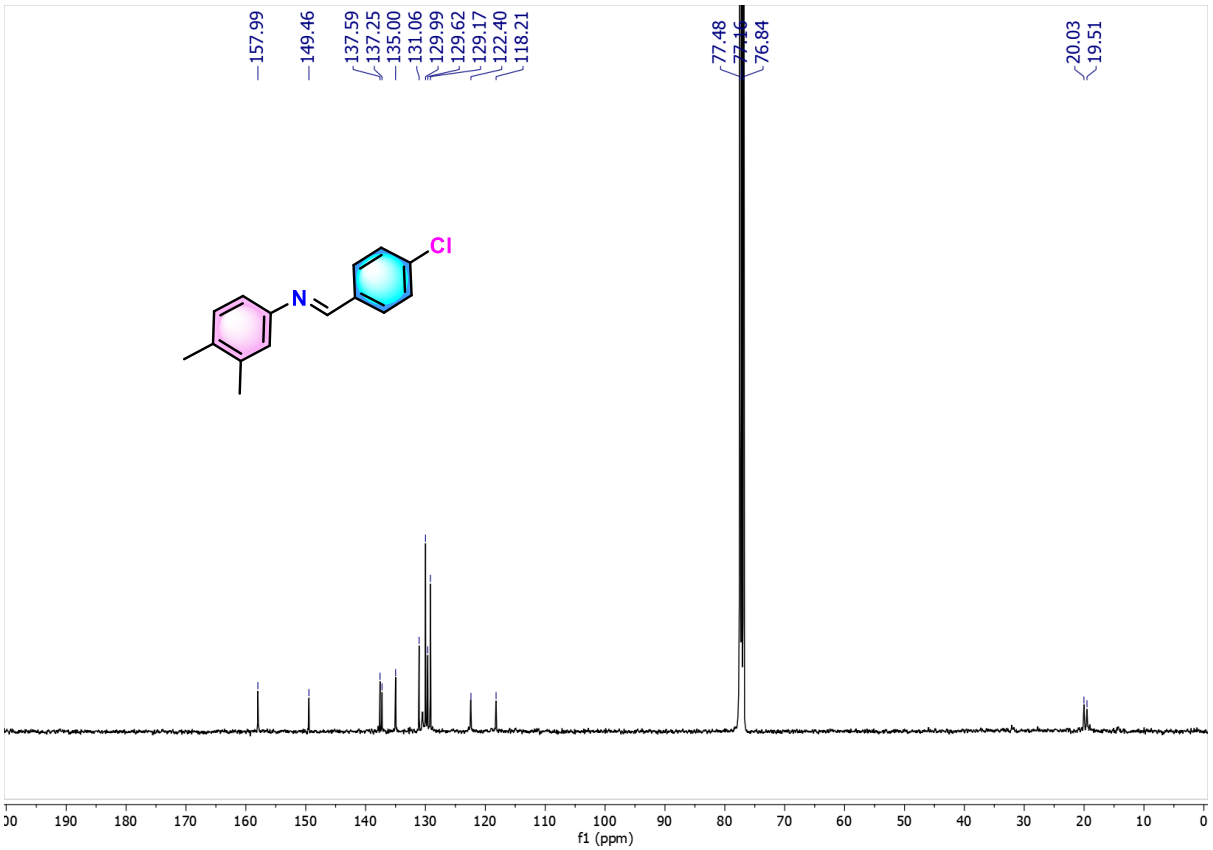

Figure 3.37. $^{13}C\{^{1}H\}$ NMR (75 MHz) spectrum of **3q** in $CDCl_3$**.**

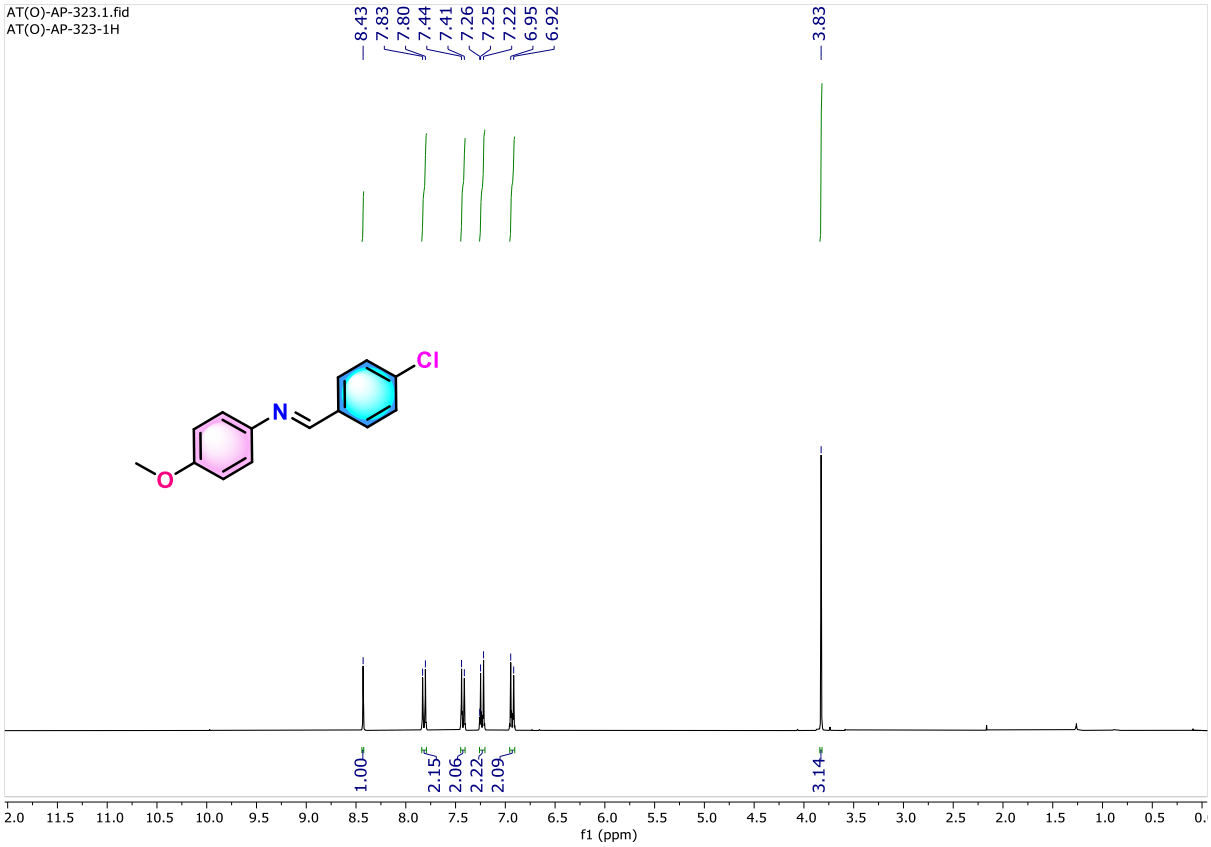

Figure 3.38. ^{1}H NMR (300 MHz) spectrum of **3r** in $CDCl_3$**.**

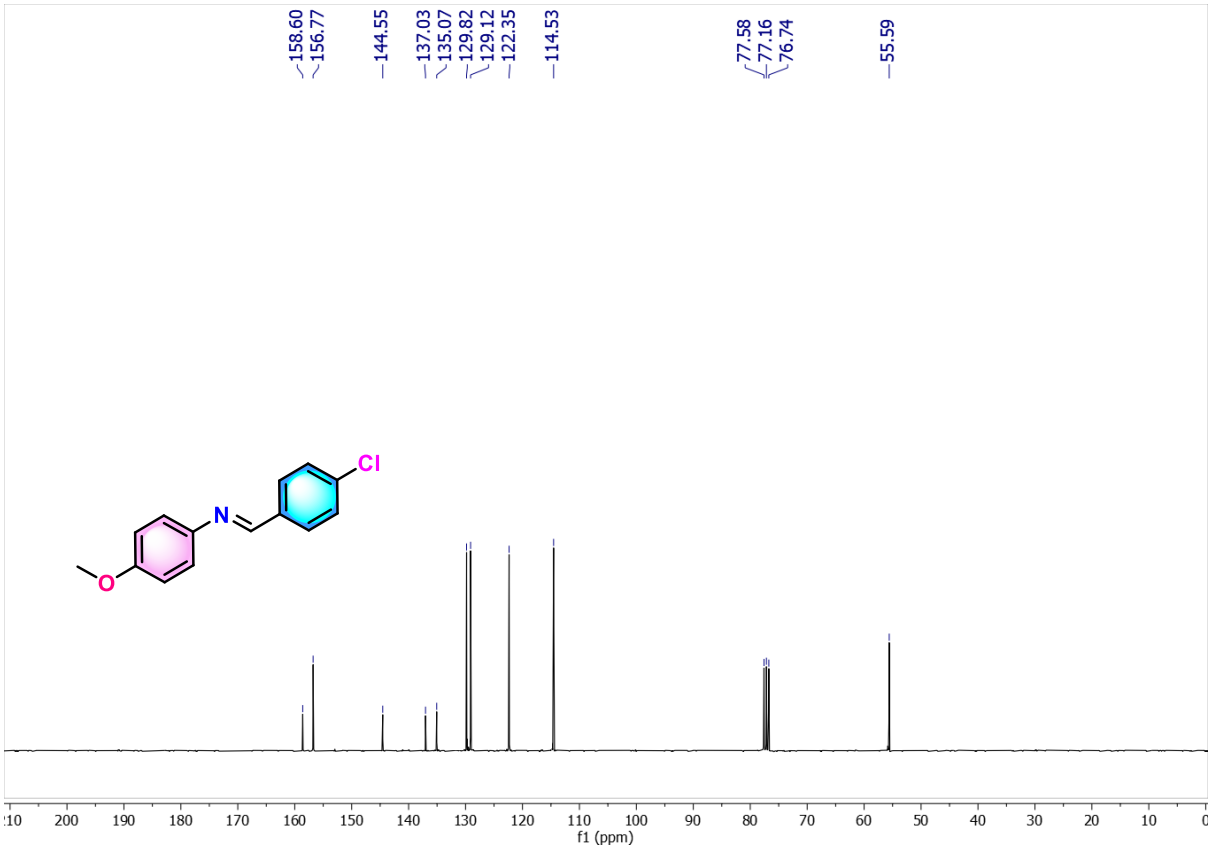

Figure 3.39. $^{13}C\{^{1}H\}$ NMR (75 MHz) spectrum of **3r** in $CDCl_3$**.**

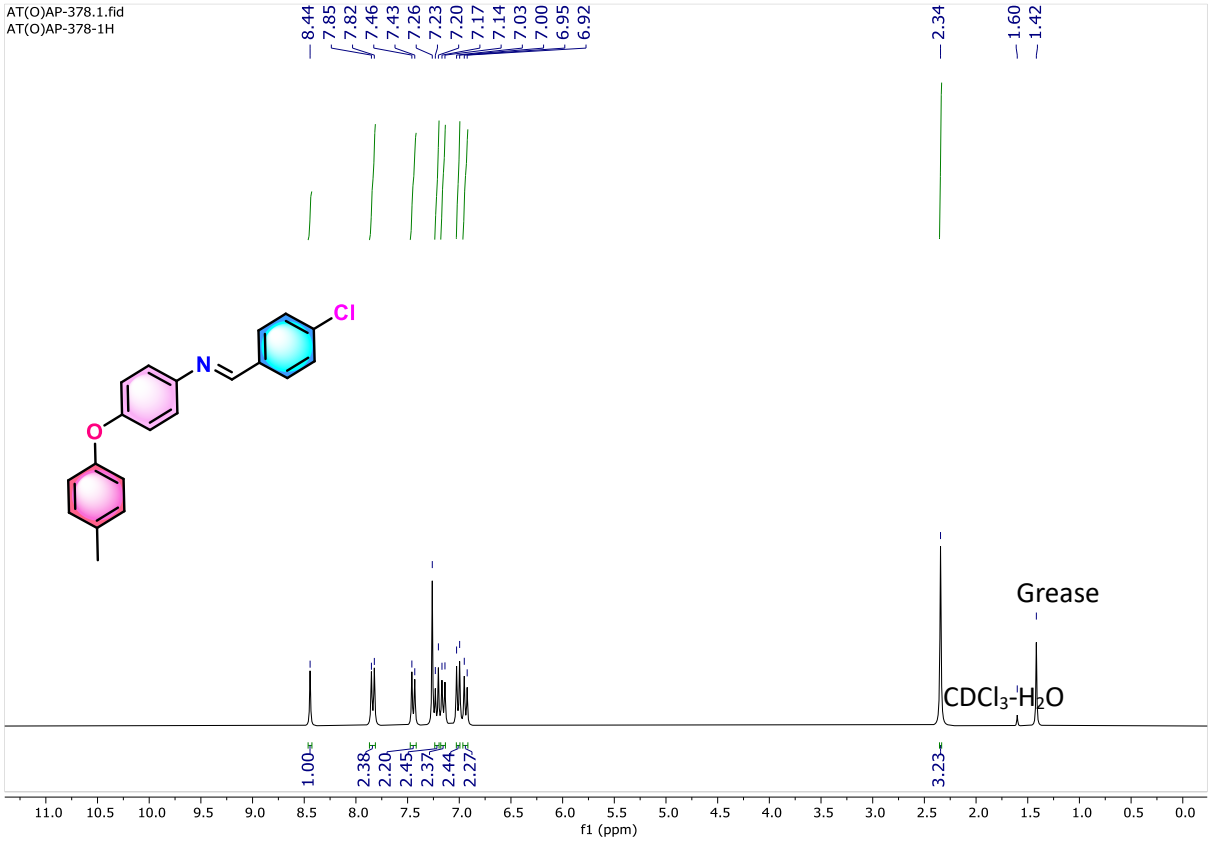

Figure 3.40. ^{1}H NMR (300 MHz) spectrum of **3s** in $CDCl_3$.

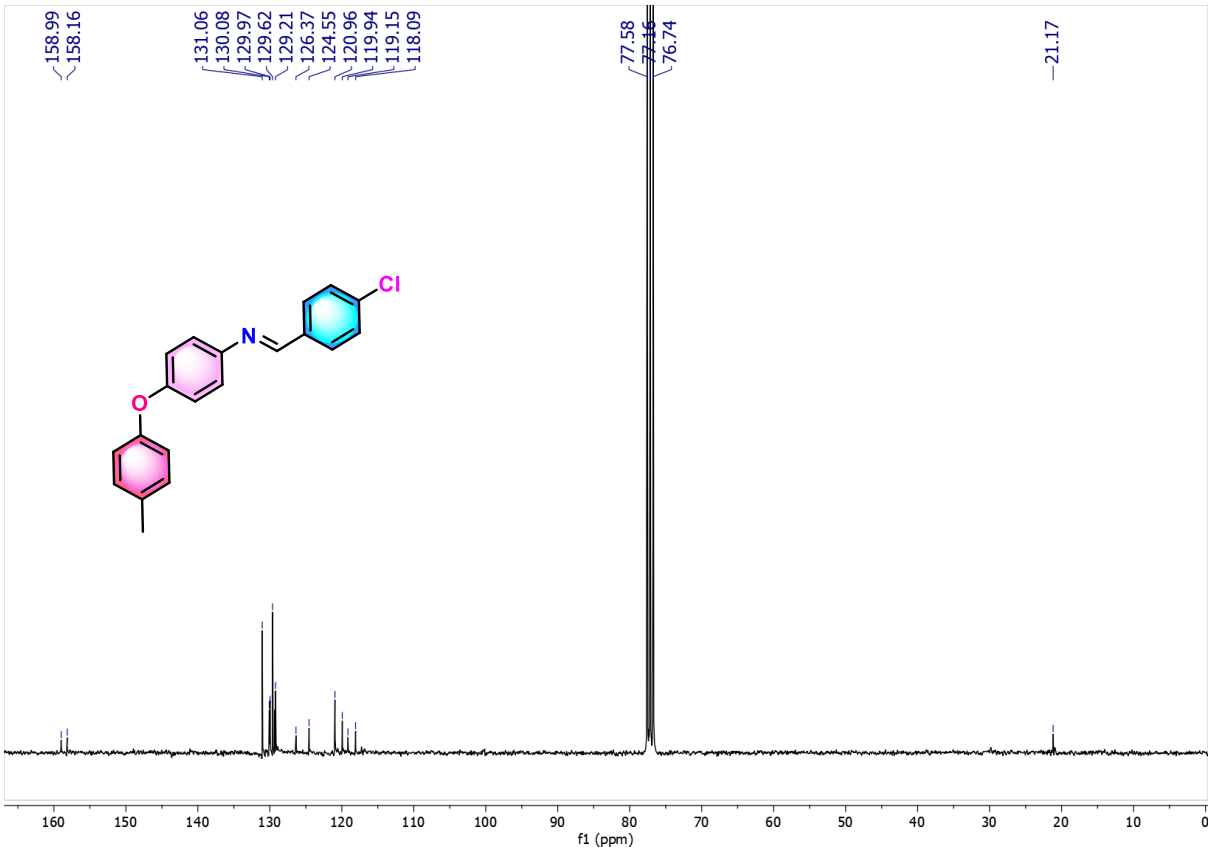

Figure 3.41. $^{13}C\{^{1}H\}$ NMR (75 MHz) spectrum of **3s** in $CDCl_3$.

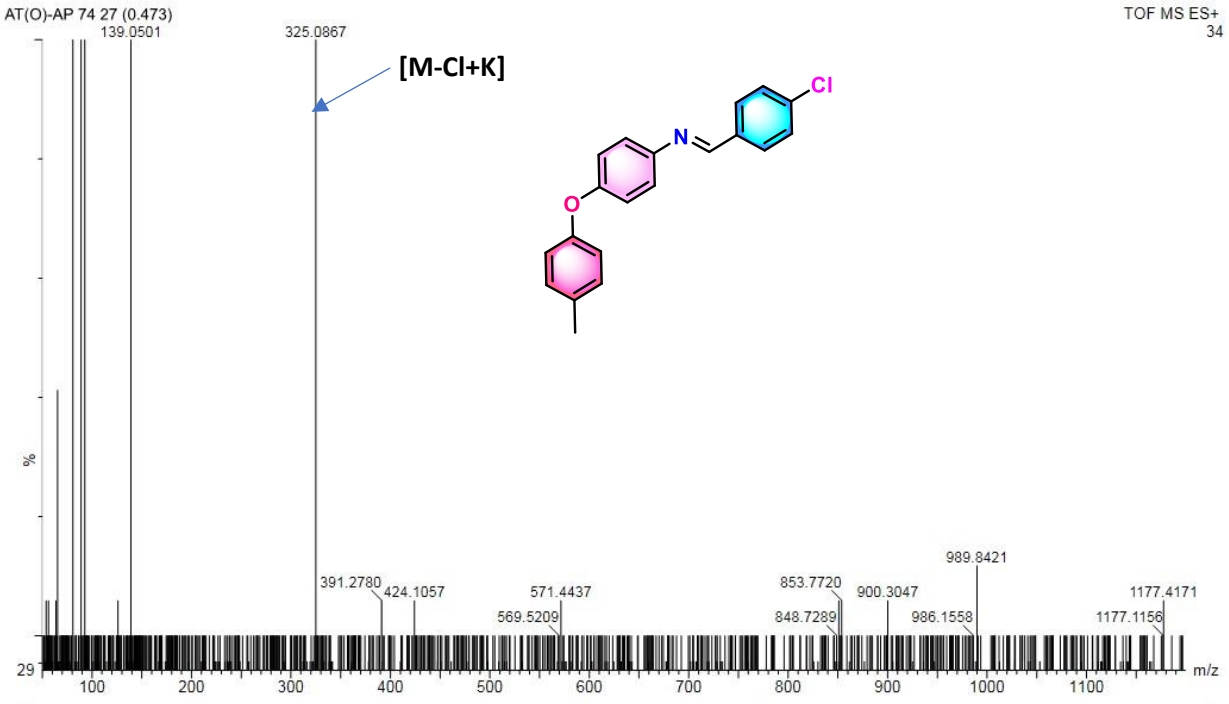

Figure 3.42. HRMS of **3s** compound.

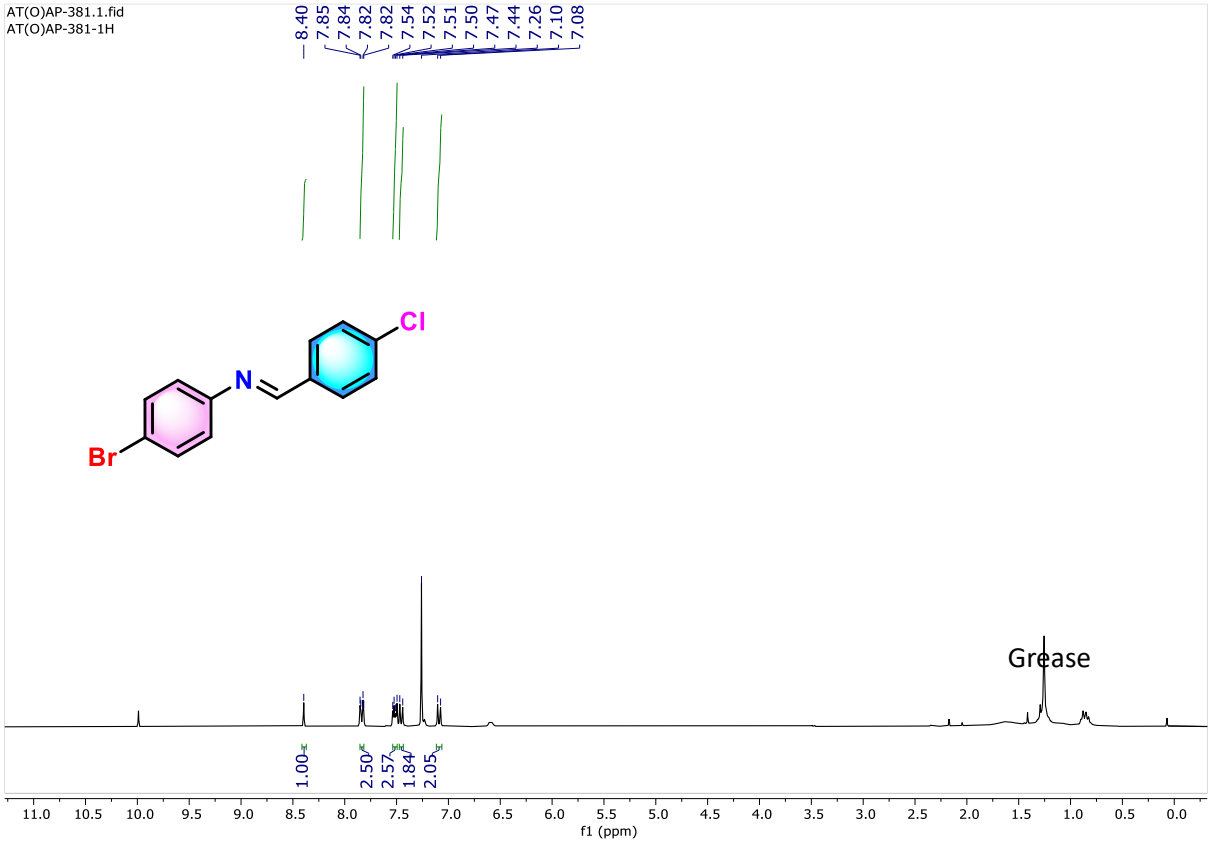

Figure 3.43. ^{1}H NMR (300 MHz) spectrum of **3t** in $CDCl_3$.

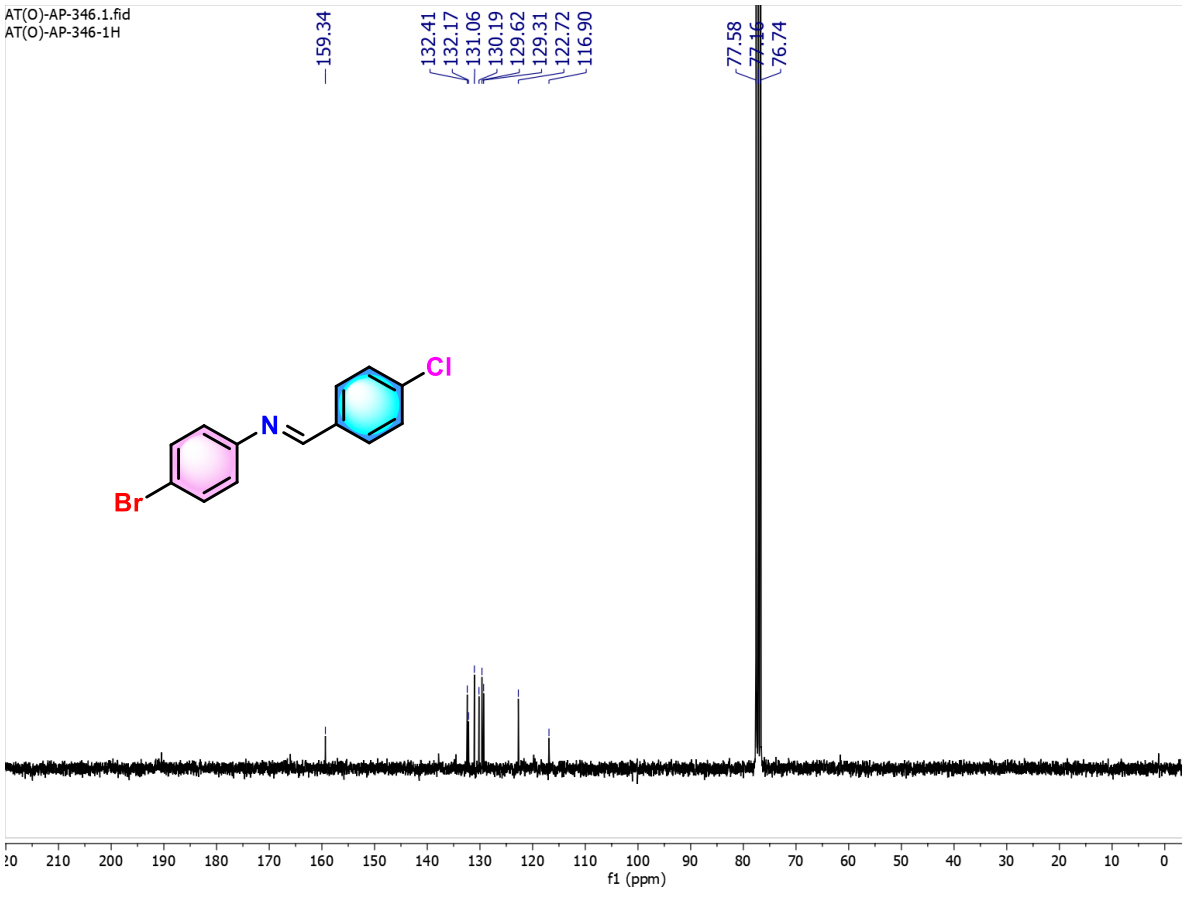

Figure 3.44. ^{13}C{^{1}H} NMR (75 MHz) spectrum of **3t** in $CDCl_3$.

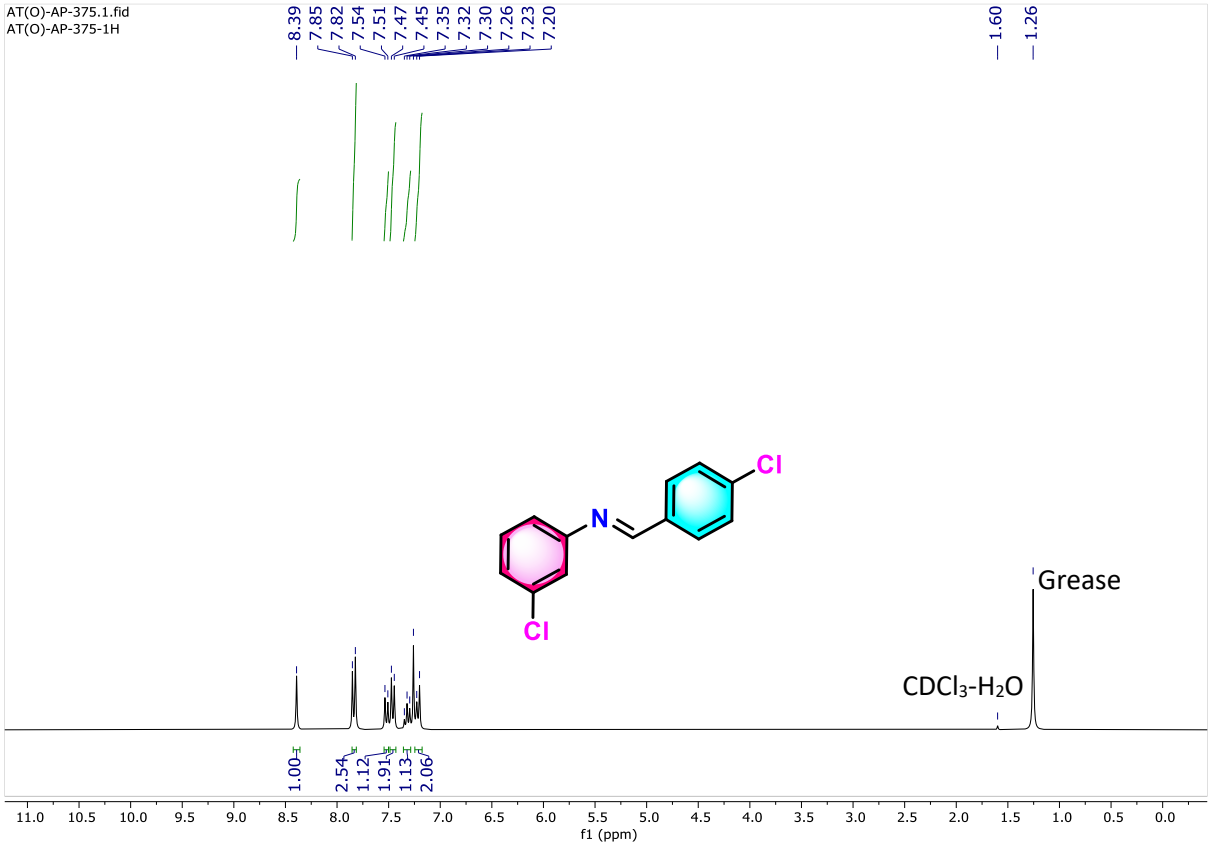

Figure 3.45. ^{1}H NMR (300 MHz) spectrum of **3u** in $CDCl_3$.

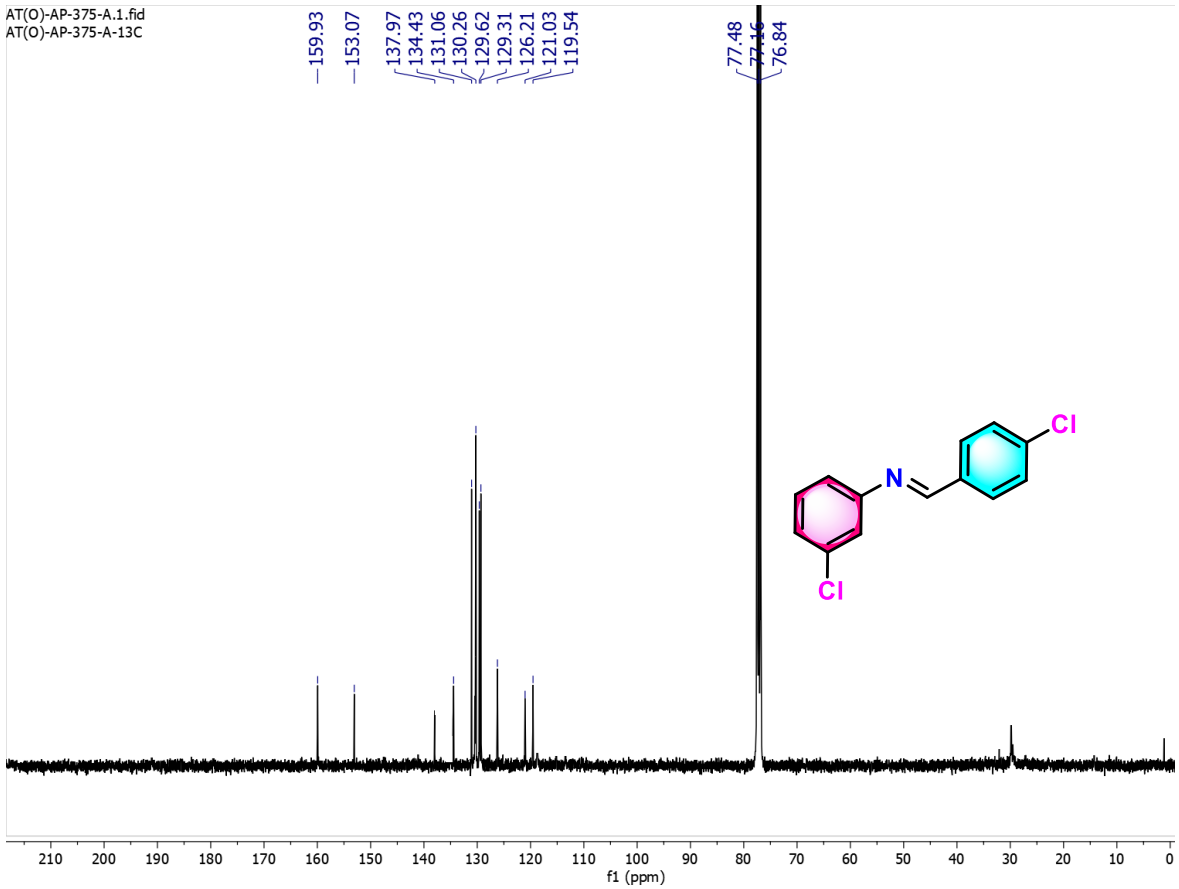

Figure 3.46. $^{13}C\{^{1}H\}$ NMR (75 MHz) spectrum of **3u** in $CDCl_3$.

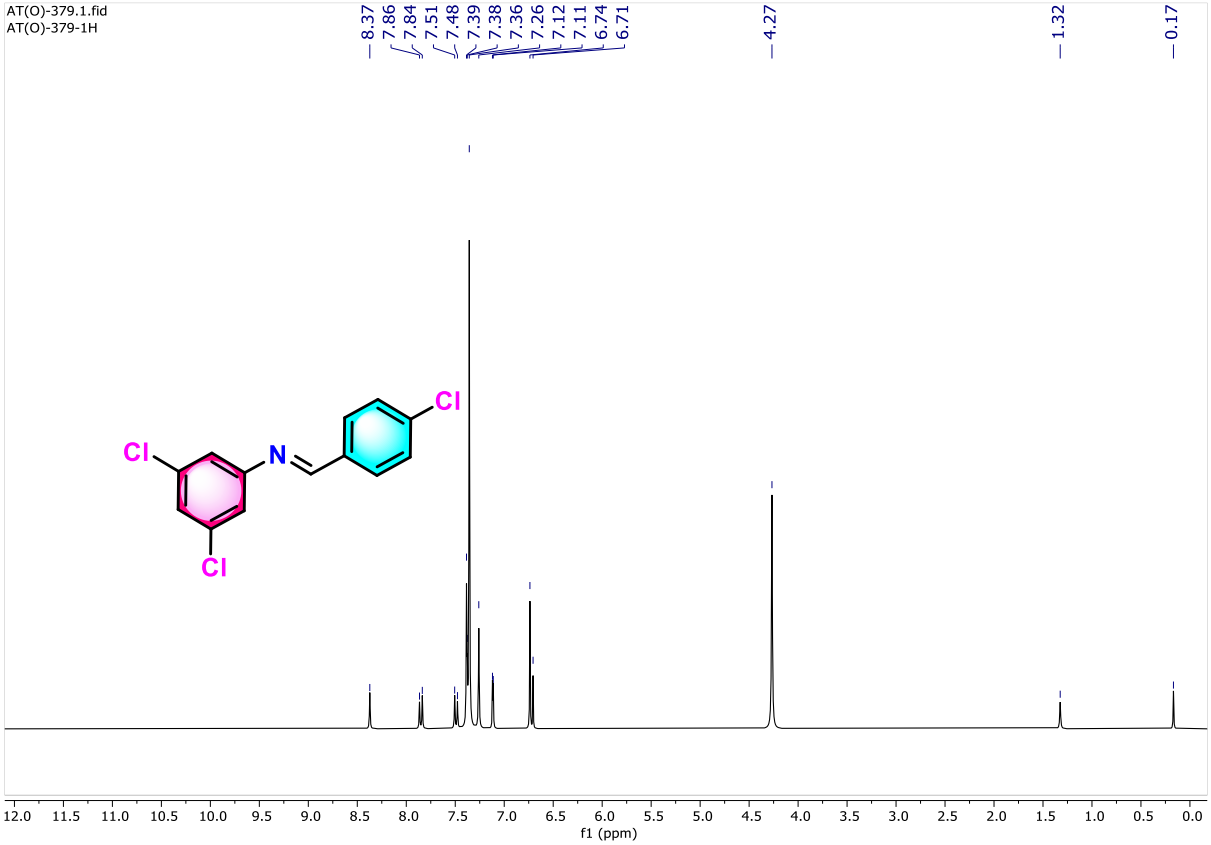

Figure 3.47. ^{1}H NMR (300 MHz) spectrum of **3v** in $CDCl_3$ (Reaction Mixture). The peak at 8.37 ppm shows the imine H.

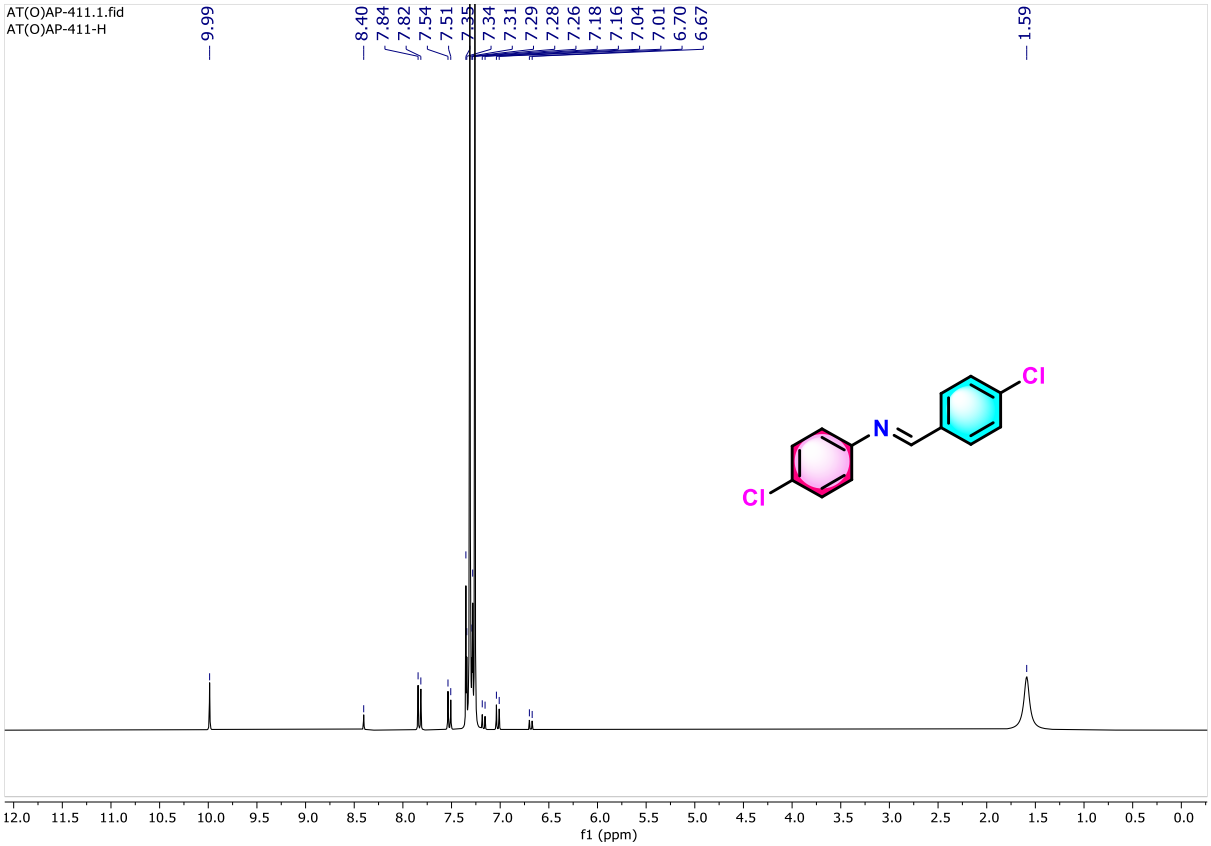

Figure 3.48. ^{1}H NMR (300 MHz) spectrum of **3w** in $CDCl_3$ (Reaction Mixture). The peak at 8.40 ppm shows the imine H.

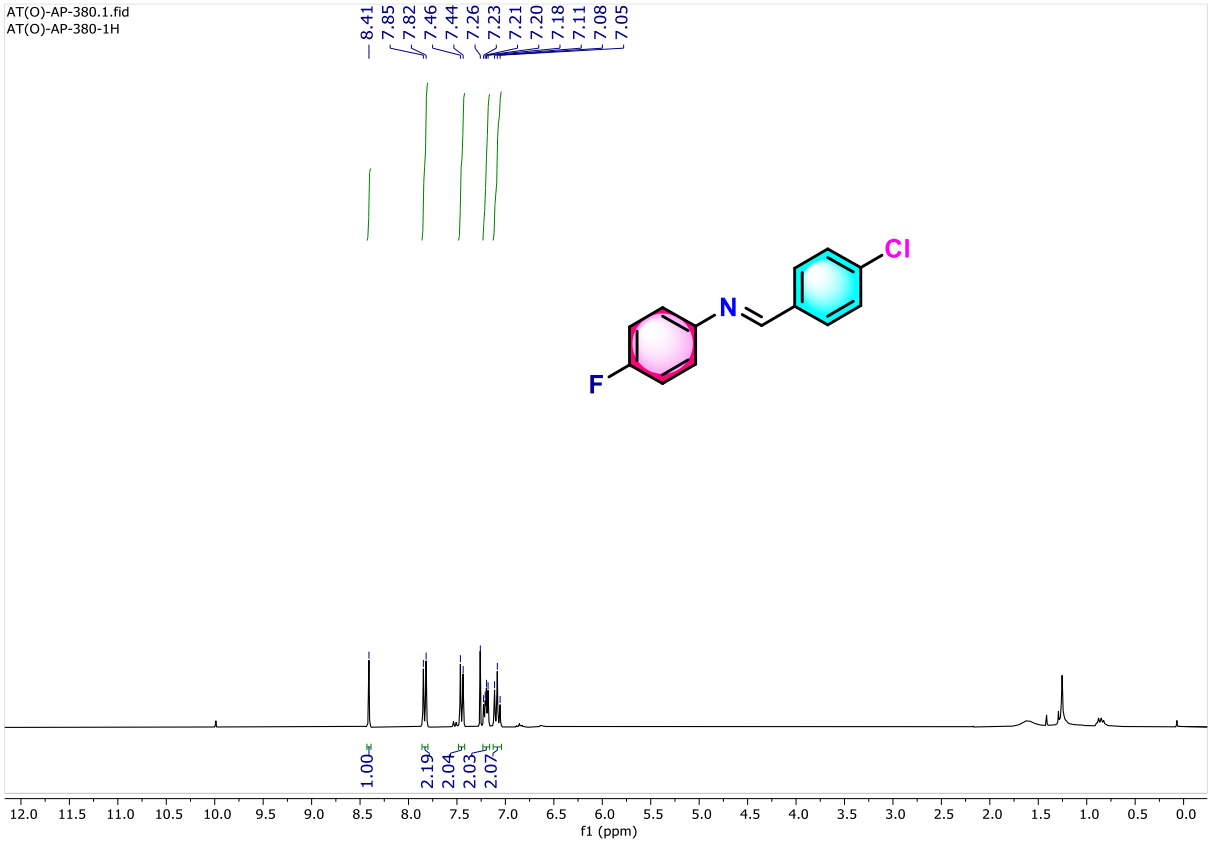

Figure 3.49. ^{1}H NMR (300 MHz) spectrum of **3x** in $CDCl_3$.

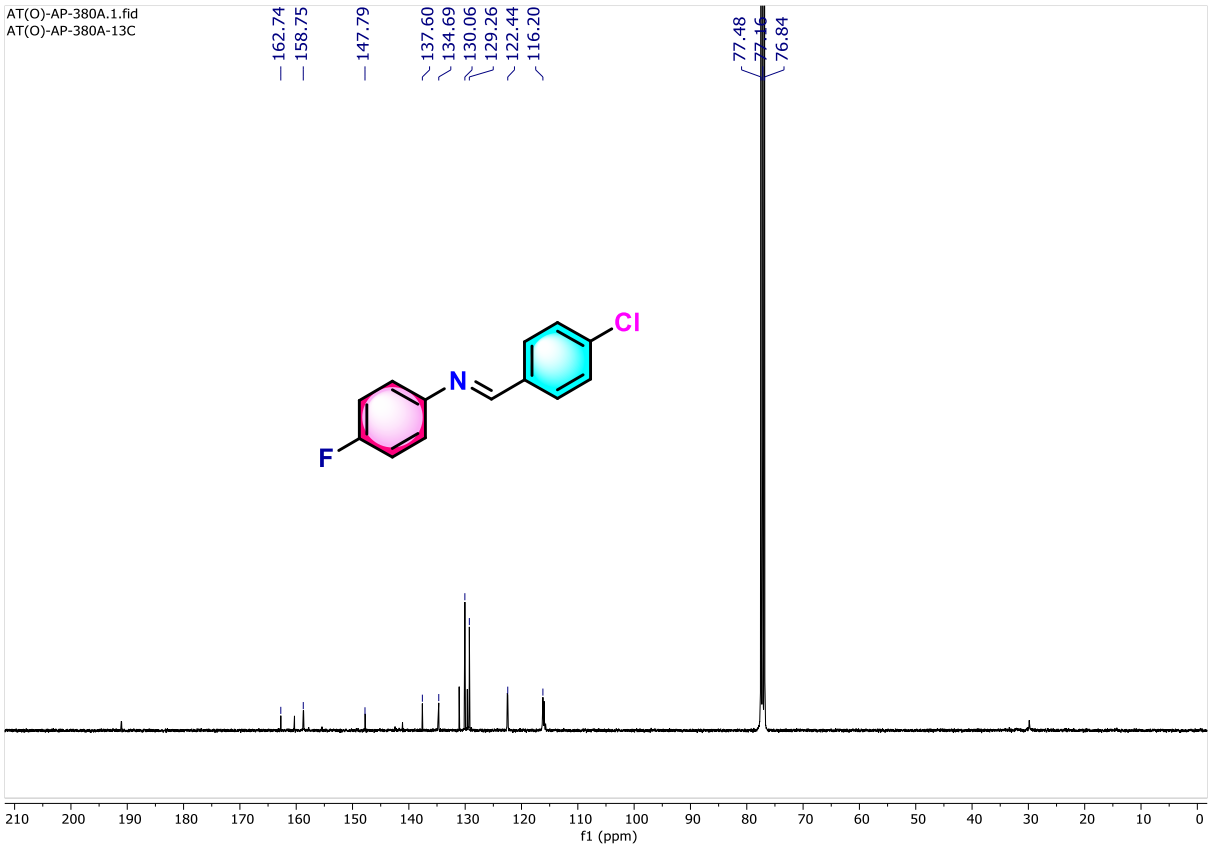

Figure 3.50. $^{13}C\{^{1}H\}$ NMR (75 MHz) spectrum of **3x** in $CDCl_3$.

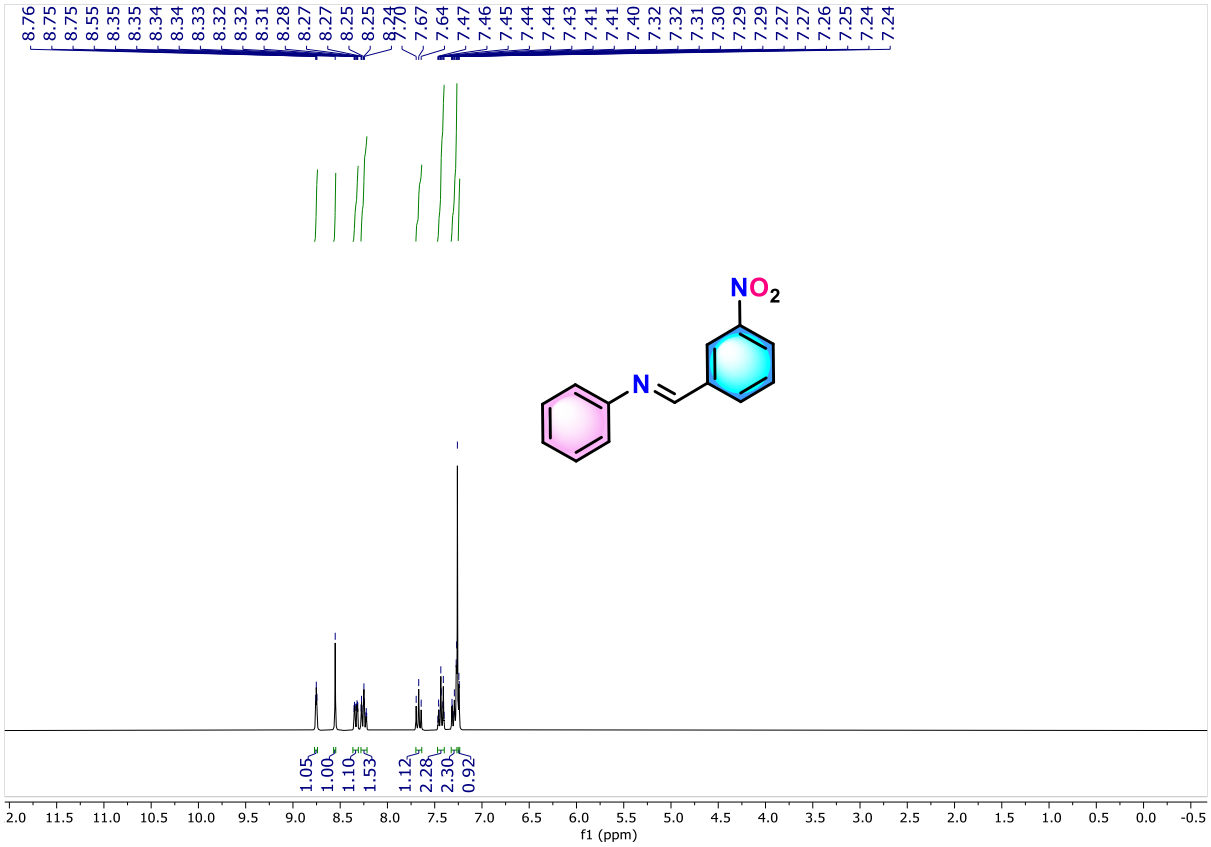

Figure 3.51. ^{1}H NMR (300 MHz) spectrum of **3y** in $CDCl_3$.

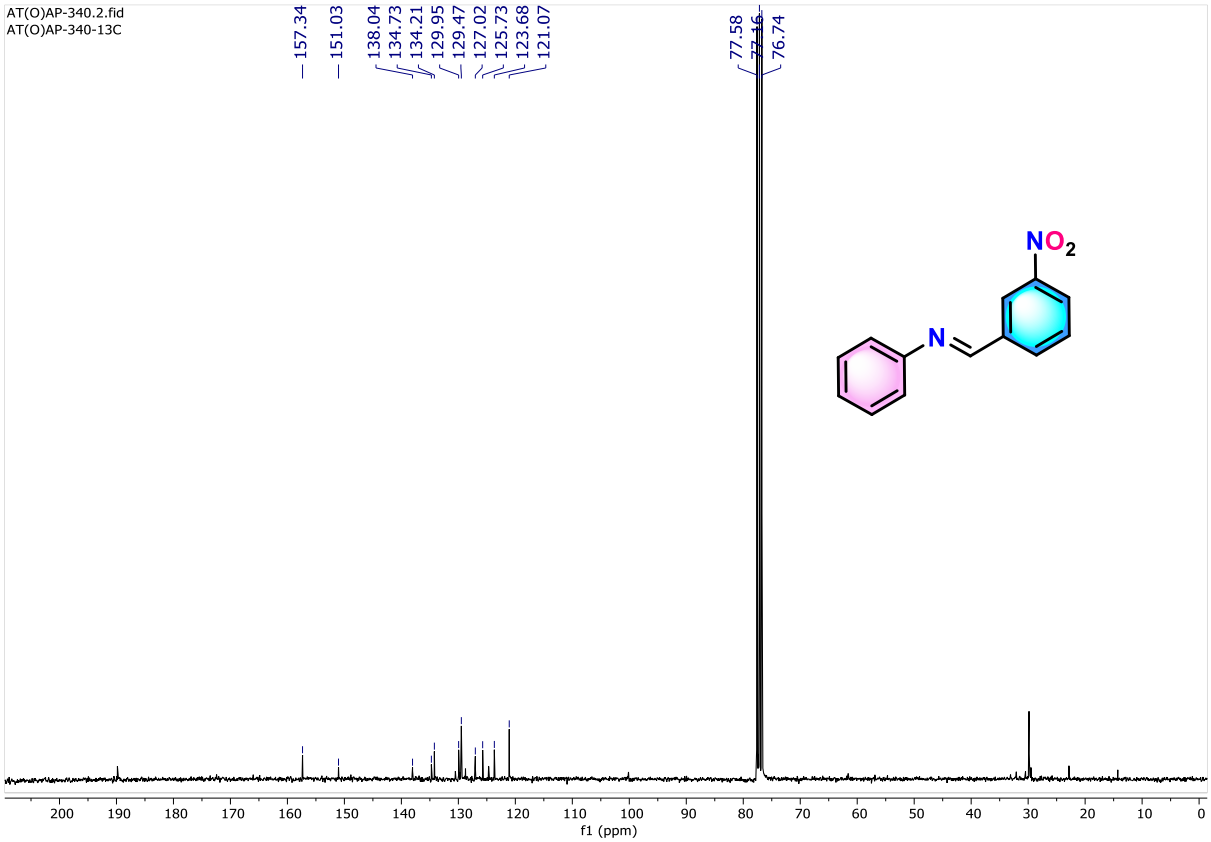

Figure 3.52. $^{13}C\{^{1}H\}$ NMR (75 MHz) spectrum of **3y** in $CDCl_3$.

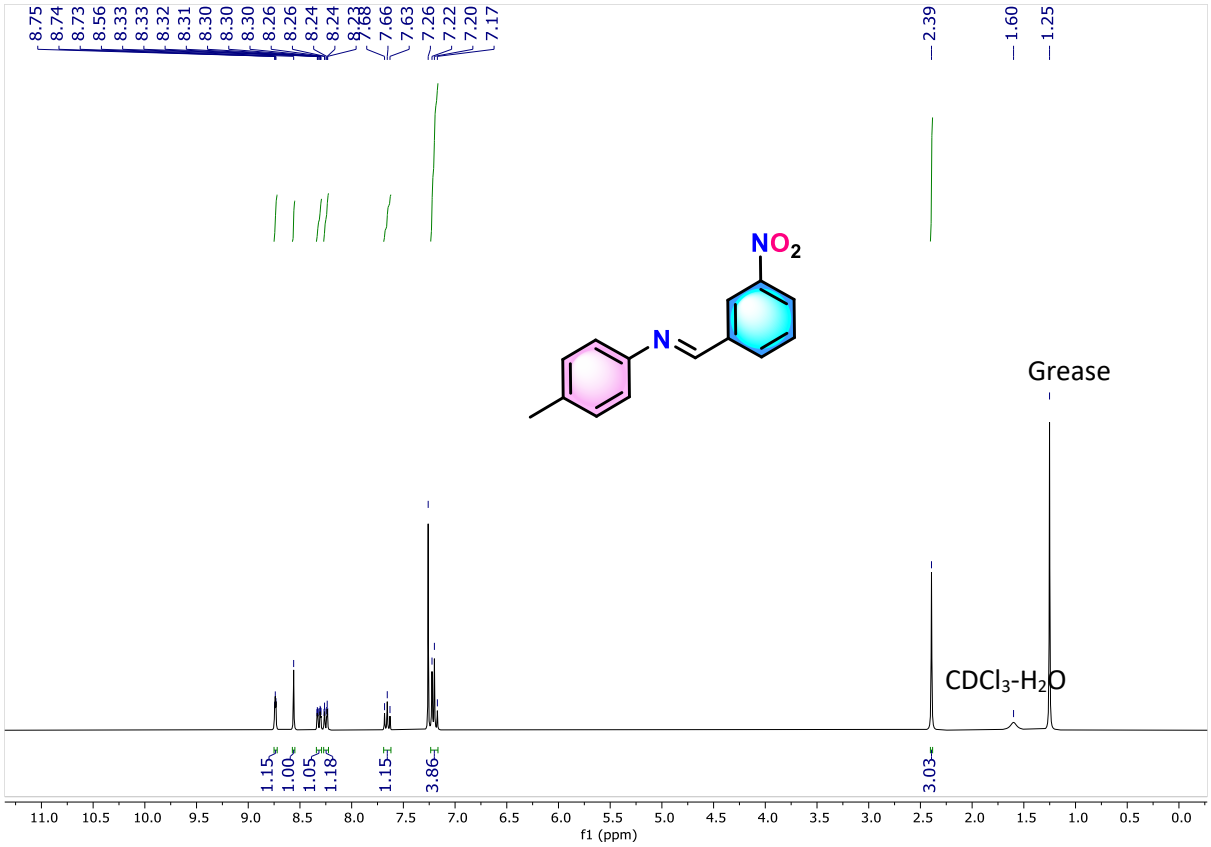

Figure 3.53. ^{1}H NMR (75 MHz) spectrum of **3z** in $CDCl_3$**.**

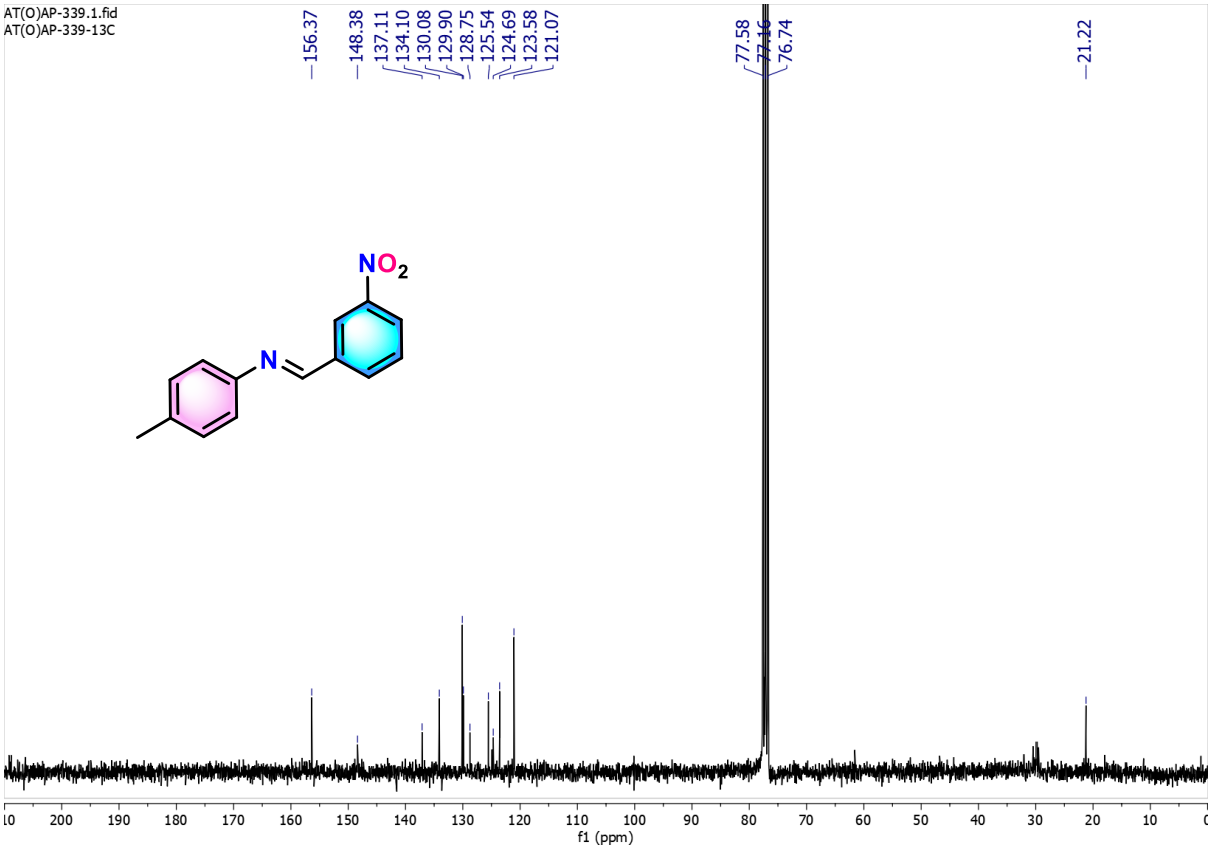

Figure 3.54. $^{13}C\{^{1}H\}$ NMR (75 MHz) spectrum of **3z** in $CDCl_3$**.**

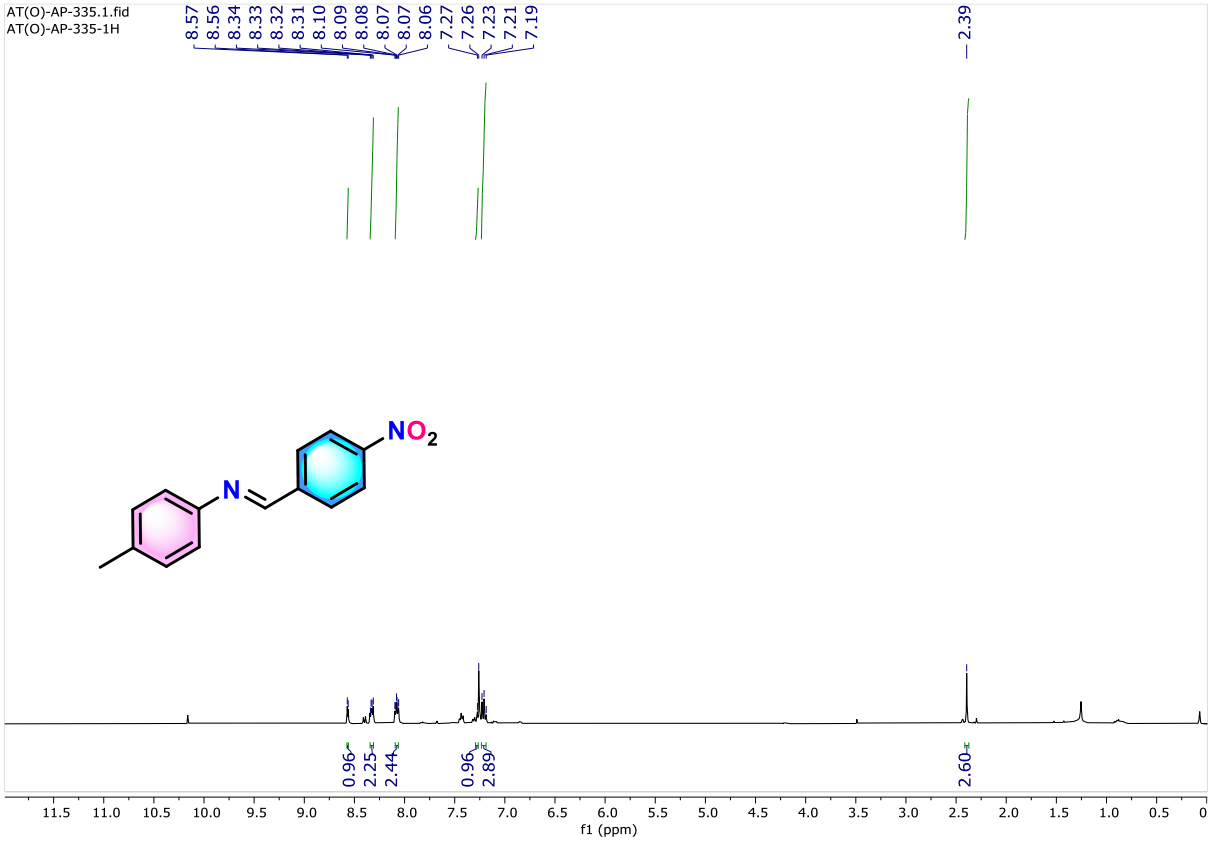

Figure 3.55. ^{1}H NMR (300 MHz) spectrum of **3aa** in $CDCl_3$**.**

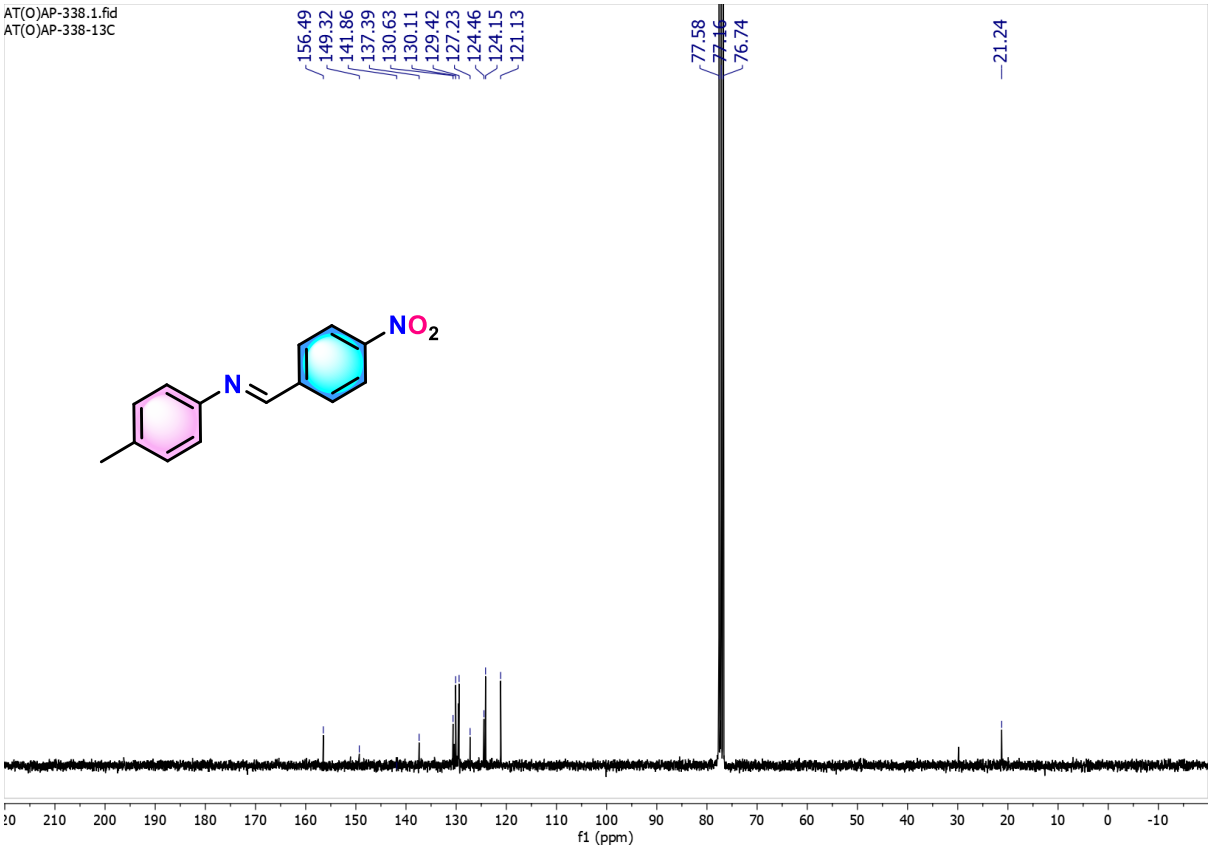

Figure 3.56. $^{13}C\{^{1}H\}$ NMR (75 MHz) spectrum of **3aa** in $CDCl_3$**.**

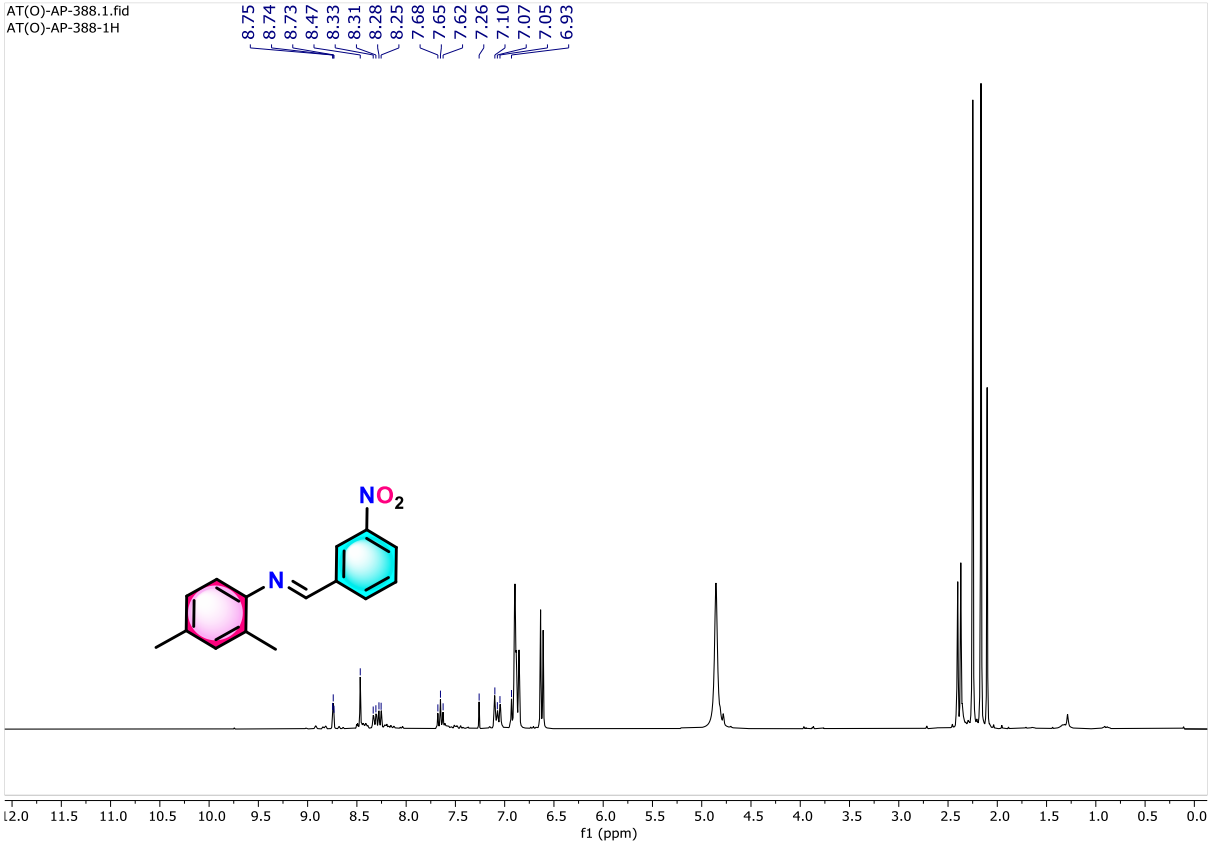

Figure 3.57. ^{1}H NMR (300 MHz) spectrum of **3ab** in $CDCl_3$ (Reaction mixture). The peak at 8.47 ppm shows the imine H.

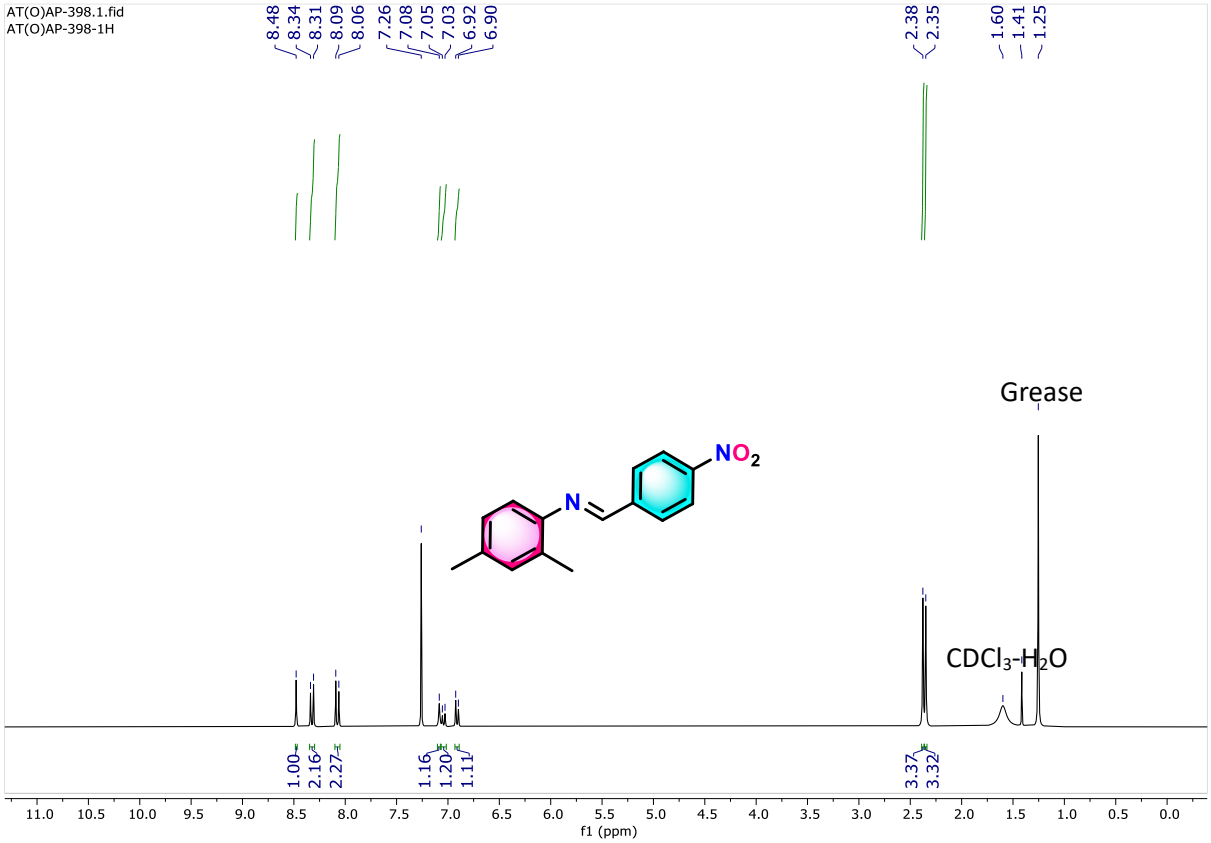

Figure 3.58. ^{1}H NMR (300 MHz) spectrum of **3ac** in $CDCl_3$.

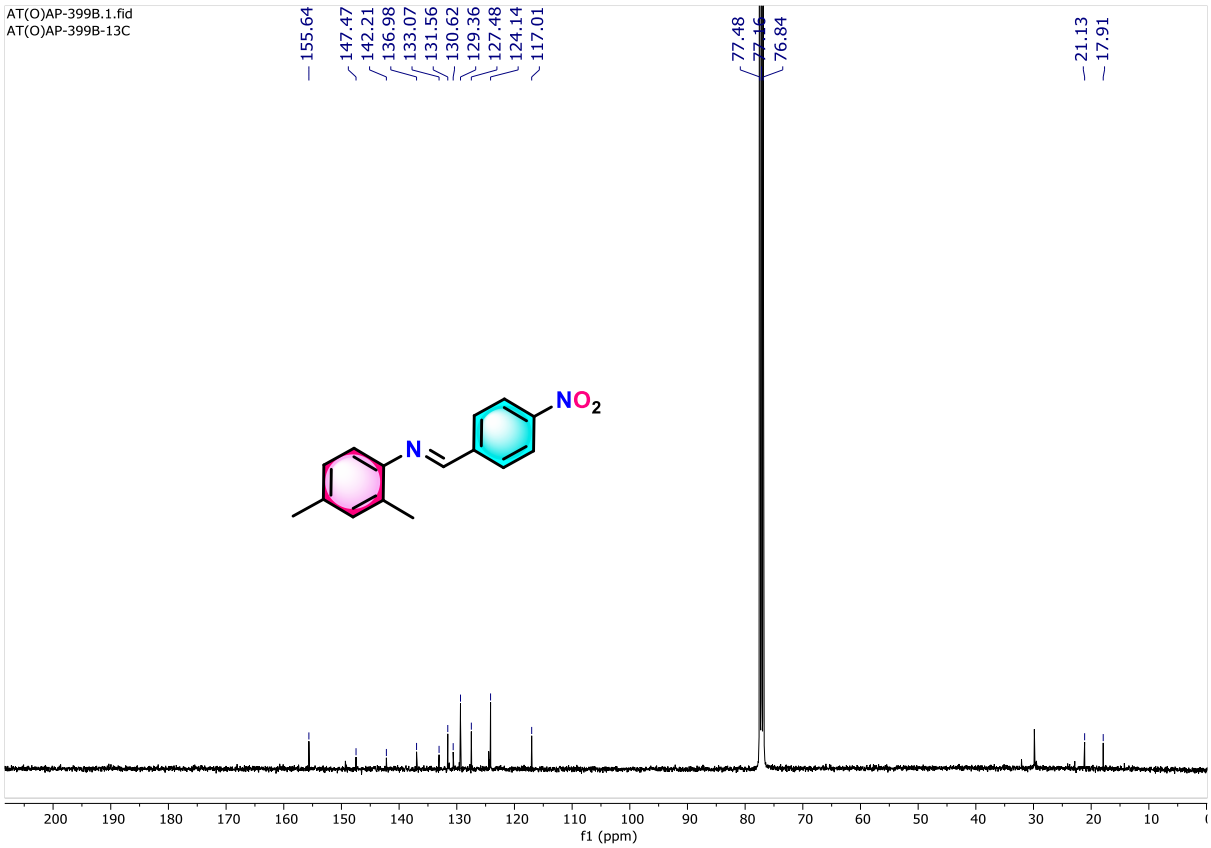

Figure 3.59. $^{13}C\{^{1}H\}$ NMR (75 MHz) spectrum of **3ac** in $CDCl_3$.

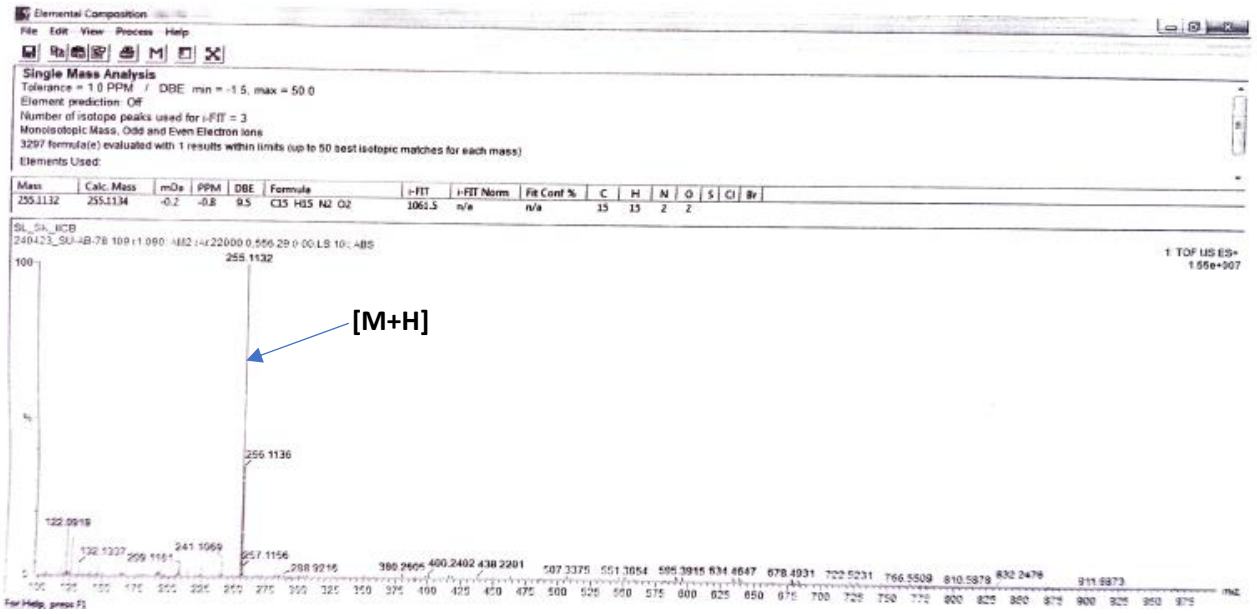

Figure 3.60. HRMS of **3ac**.

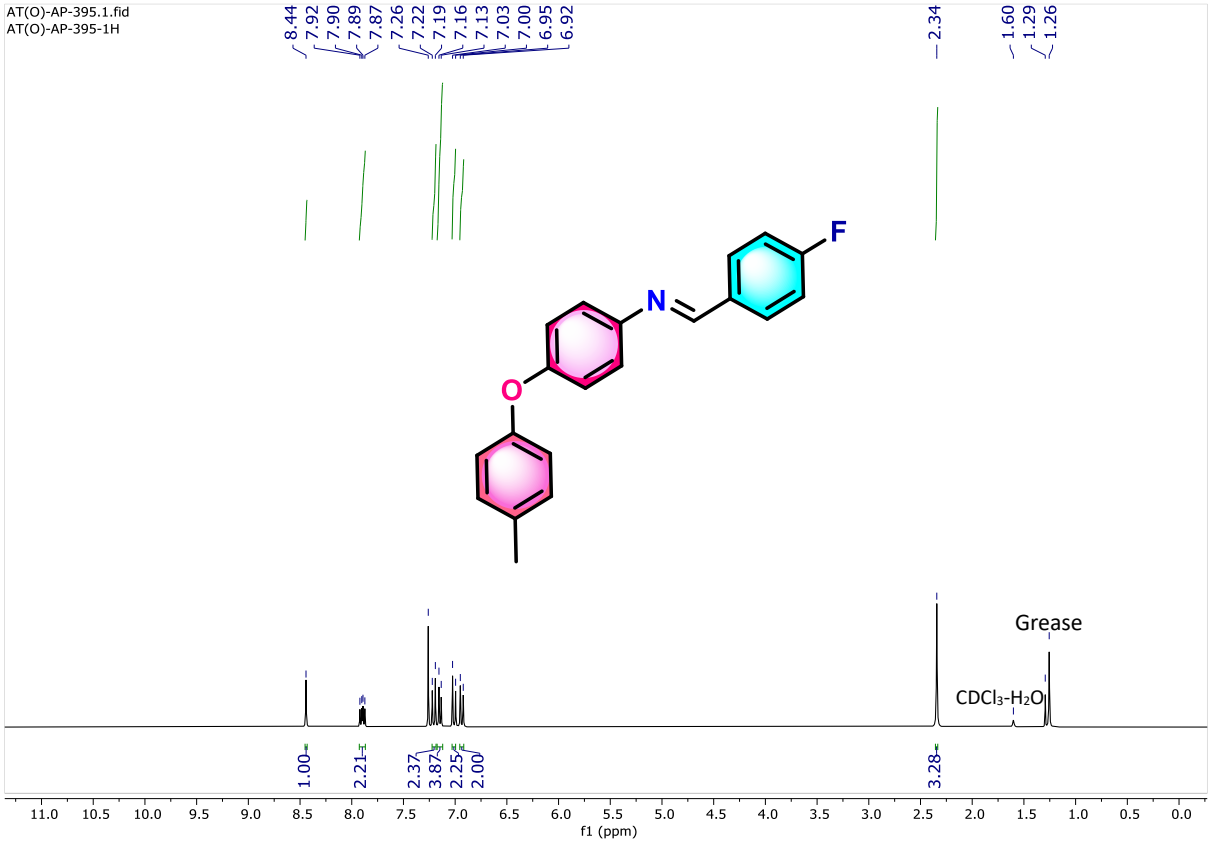

Figure 3.61. ^{1}H NMR (300 MHz) spectrum of **3ad** in $CDCl_3$.

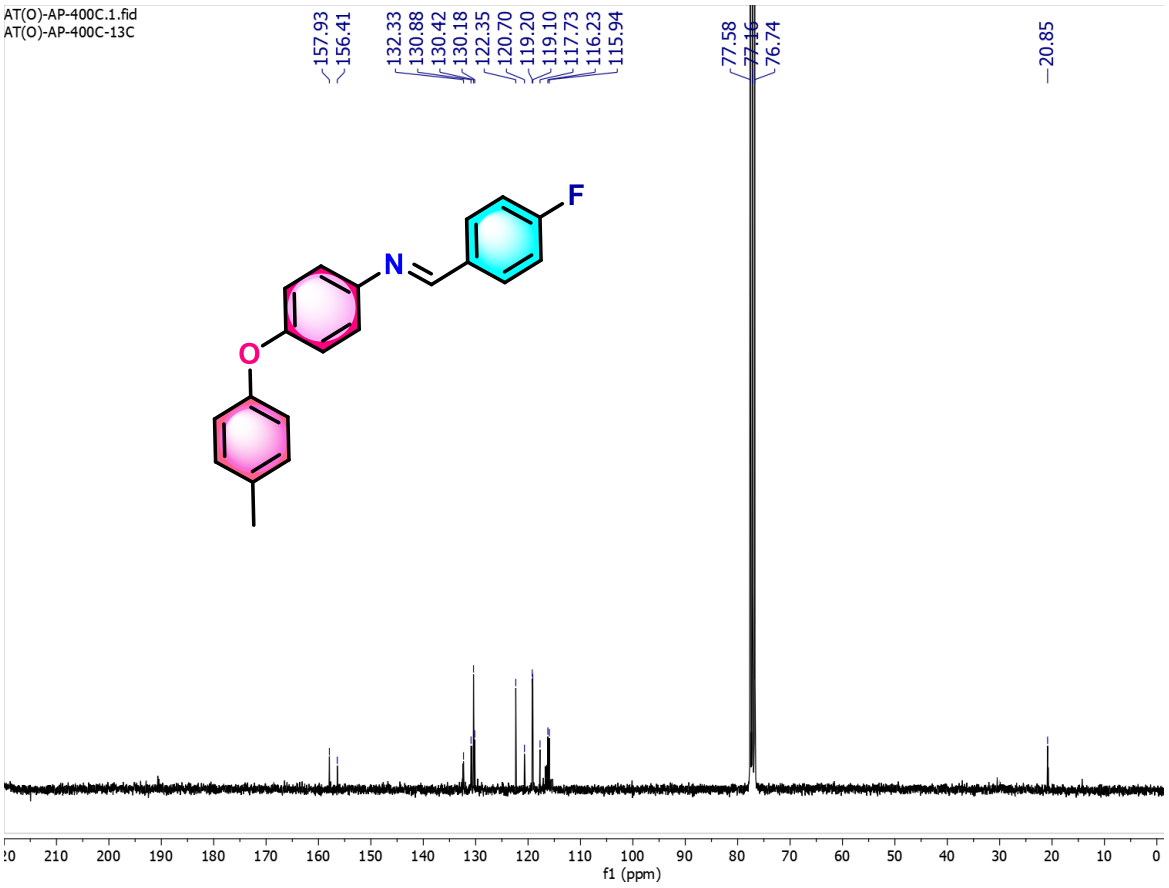

Figure 3.62. $^{13}C\{^{1}H\}$ NMR (75 MHz) spectrum of **3ad** in $CDCl_3$.

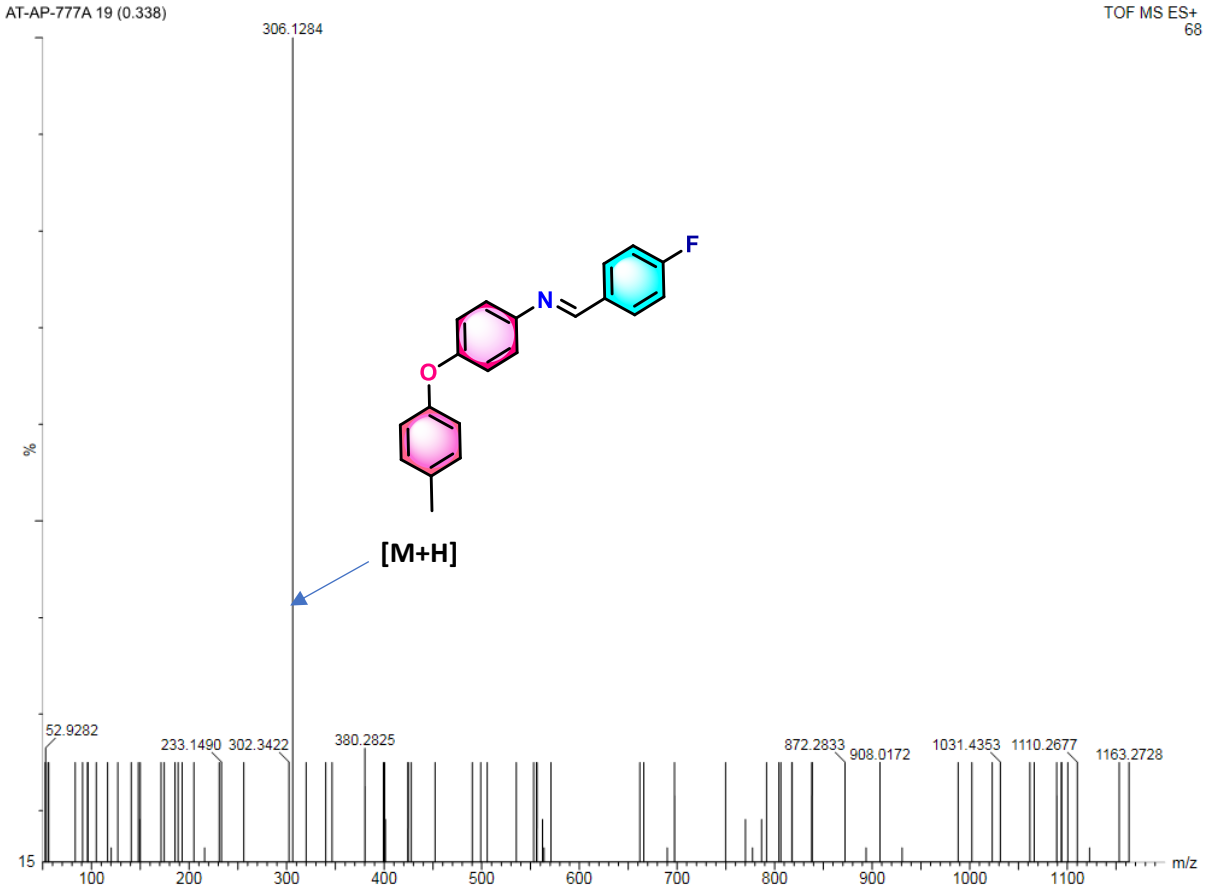

Figure 3.63. HRMS of **3ad** compound.

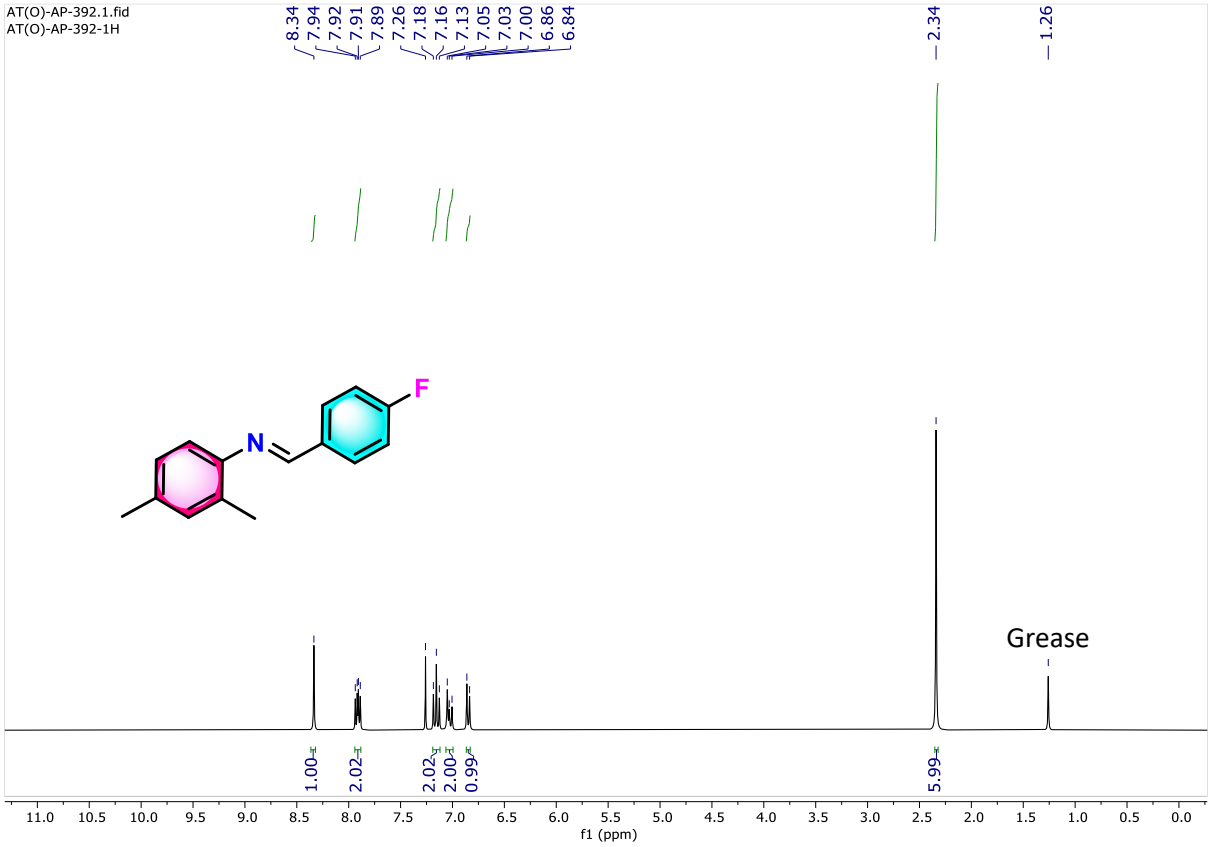

Figure 3.64. ^{1}H NMR (300 MHz) spectrum of **3ae** in $CDCl_3$.

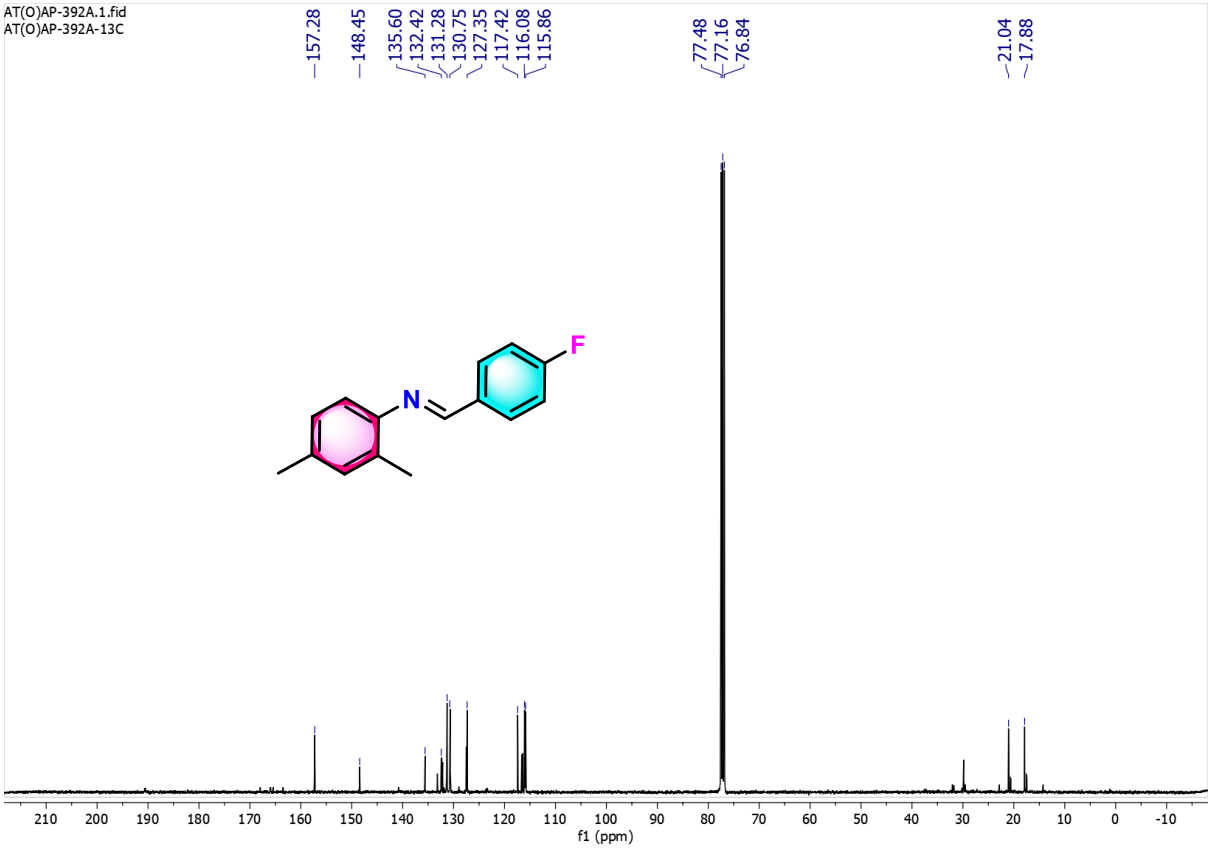

Figure 3.65. $^{13}C\{^{1}H\}$ NMR (75 MHz) spectrum of **3ae** in $CDCl_3$.

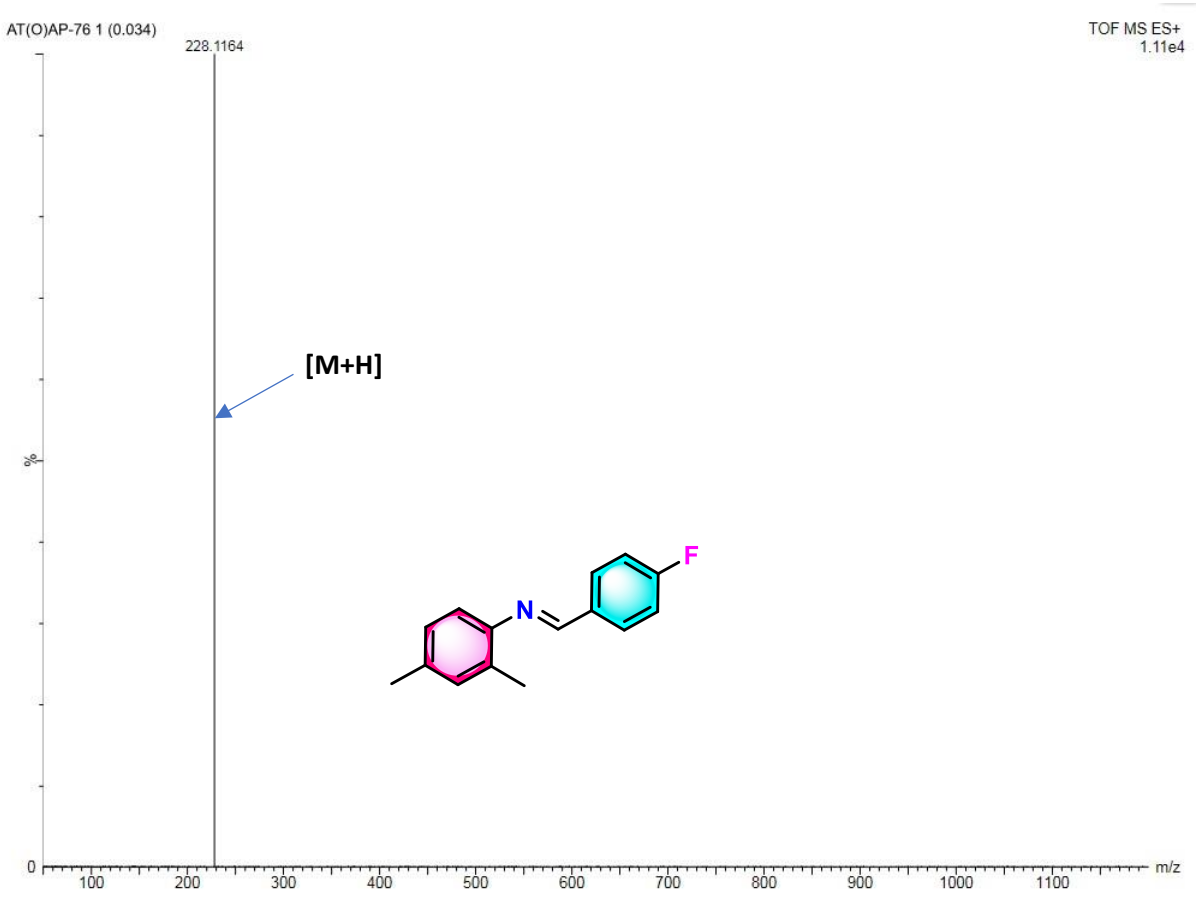

Figure 3.66. HRMS of **3ae.**

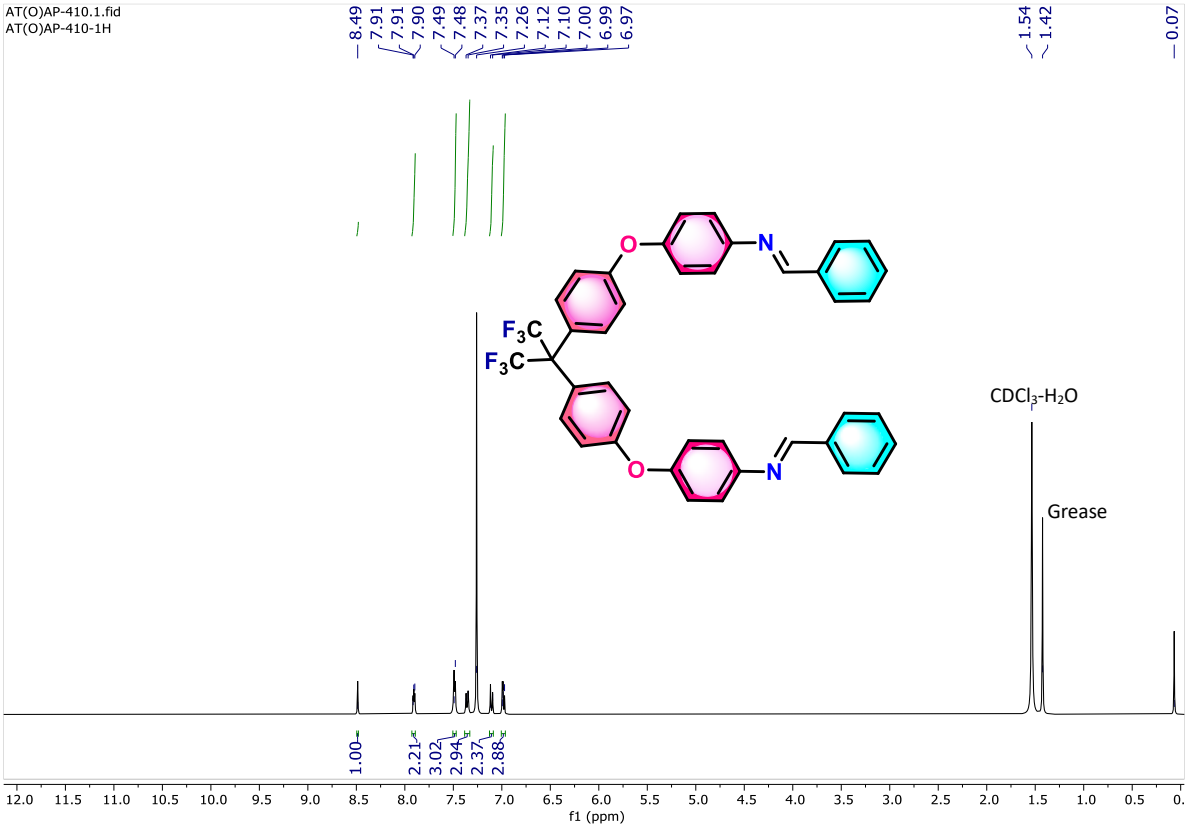

Figure 3.67. ^{1}H NMR (300 MHz) spectrum of **3af** in $CDCl_3$.

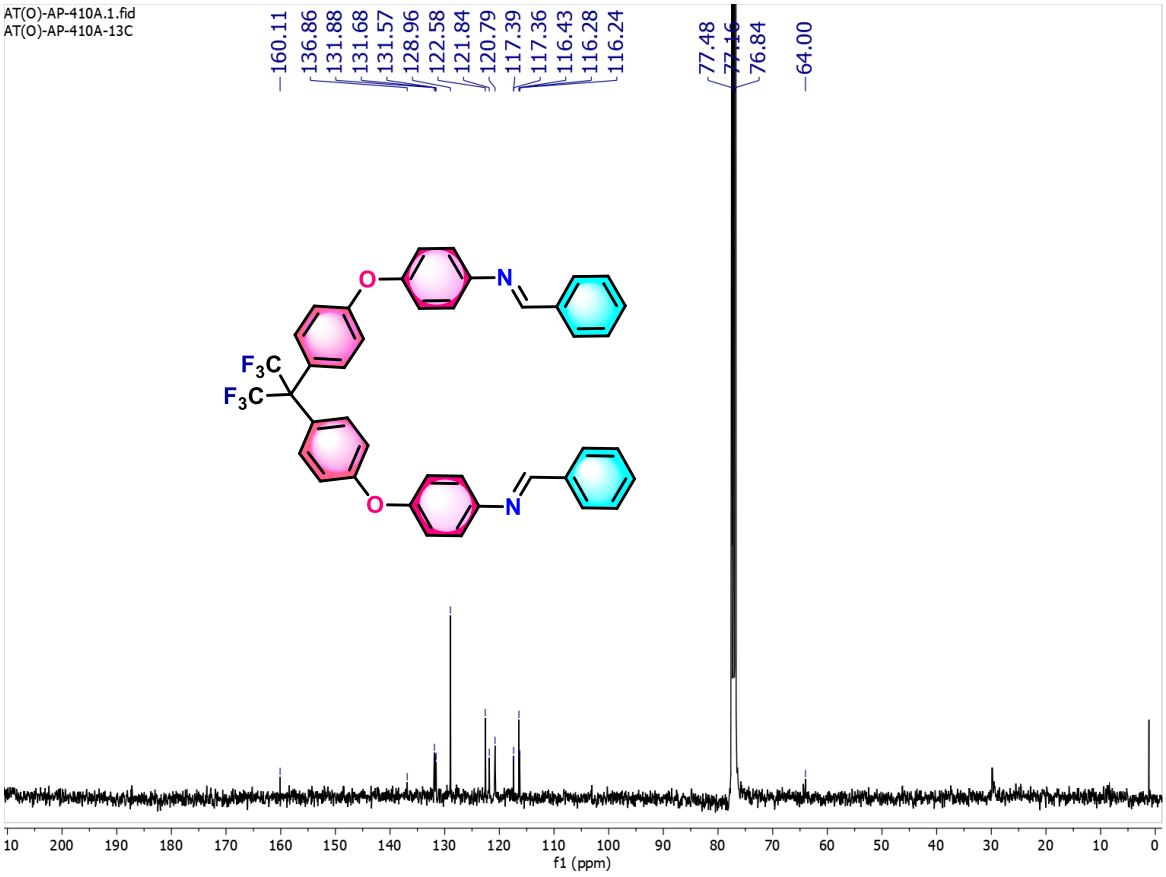

Figure 3.68. $^{13}C\{^{1}H\}$ NMR (75 MHz) spectrum of **3af** in $CDCl_3$.

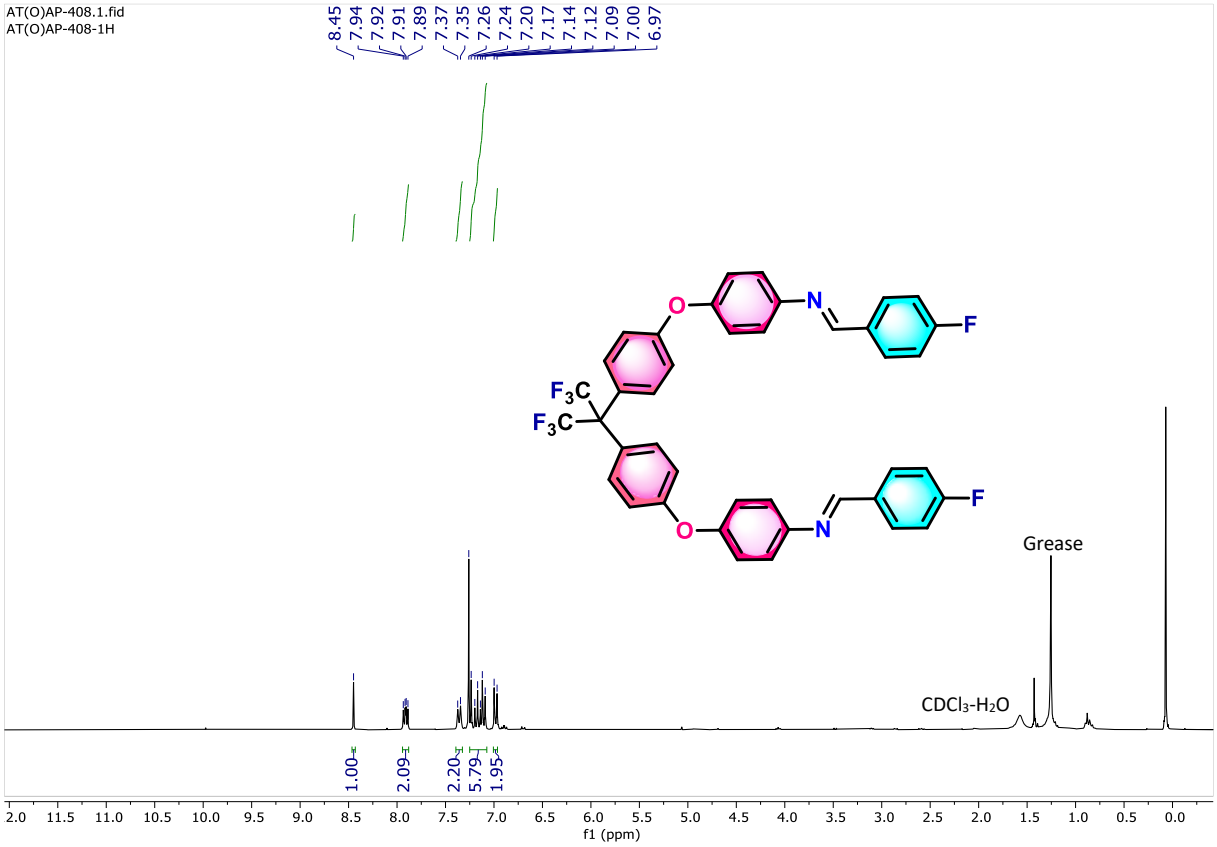

Figure 3.69. ^{1}H NMR (300 MHz) spectrum of **3ag** in $CDCl_3$.

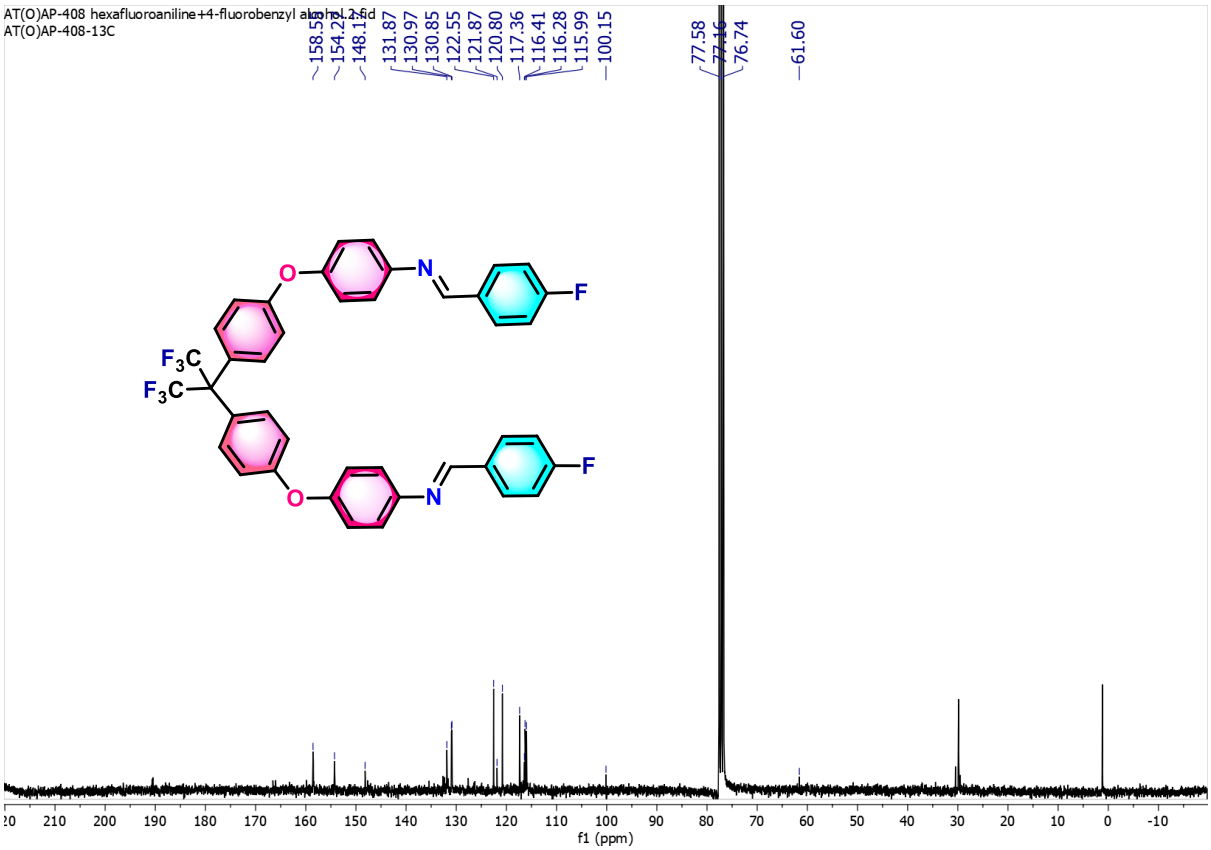

Figure 3.70. $^{13}C\{^{1}H\}$ NMR (75 MHz) spectrum of **3ag** in $CDCl_3$.

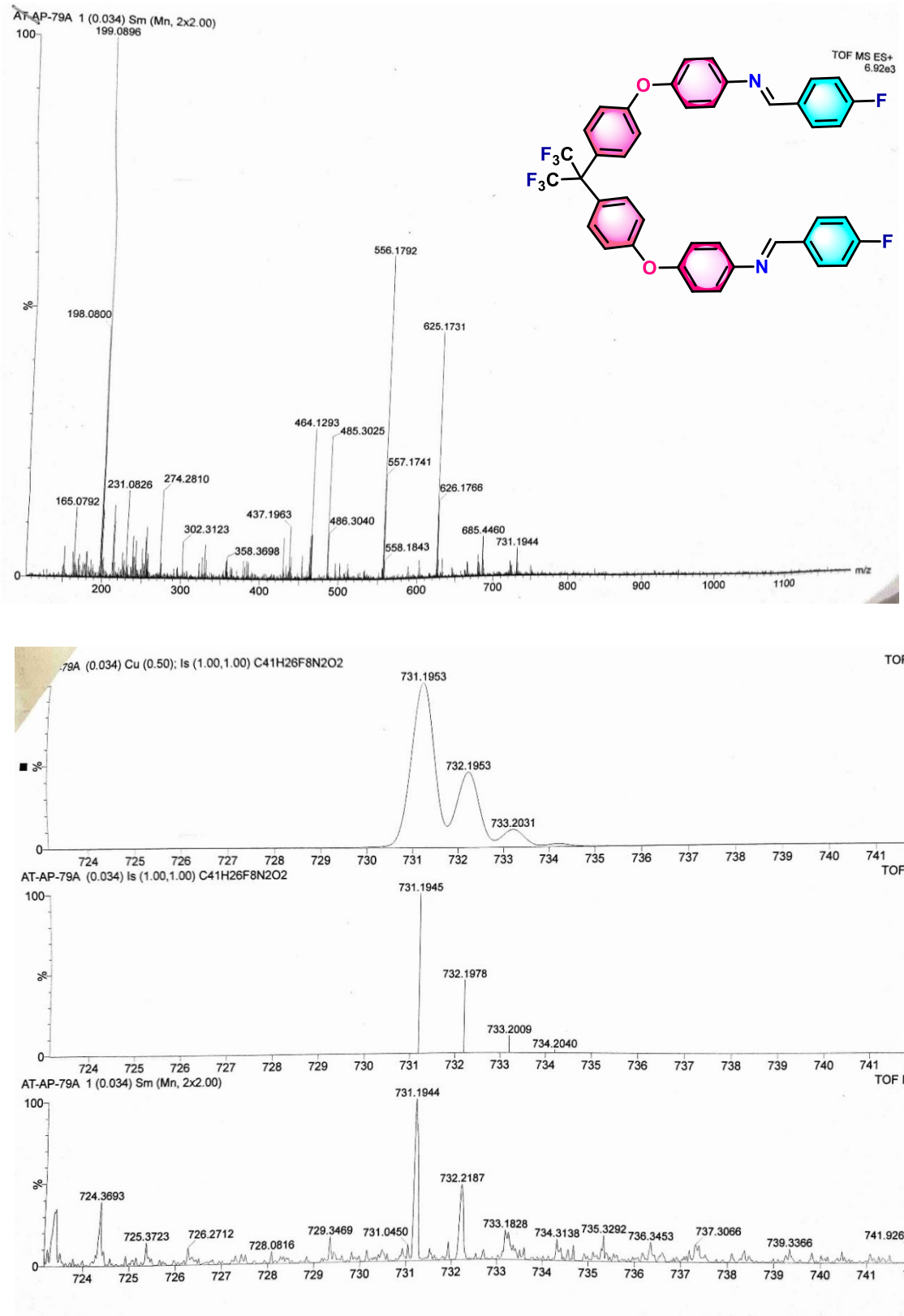

Figure 3.71. HRMS of **3ag** compound.

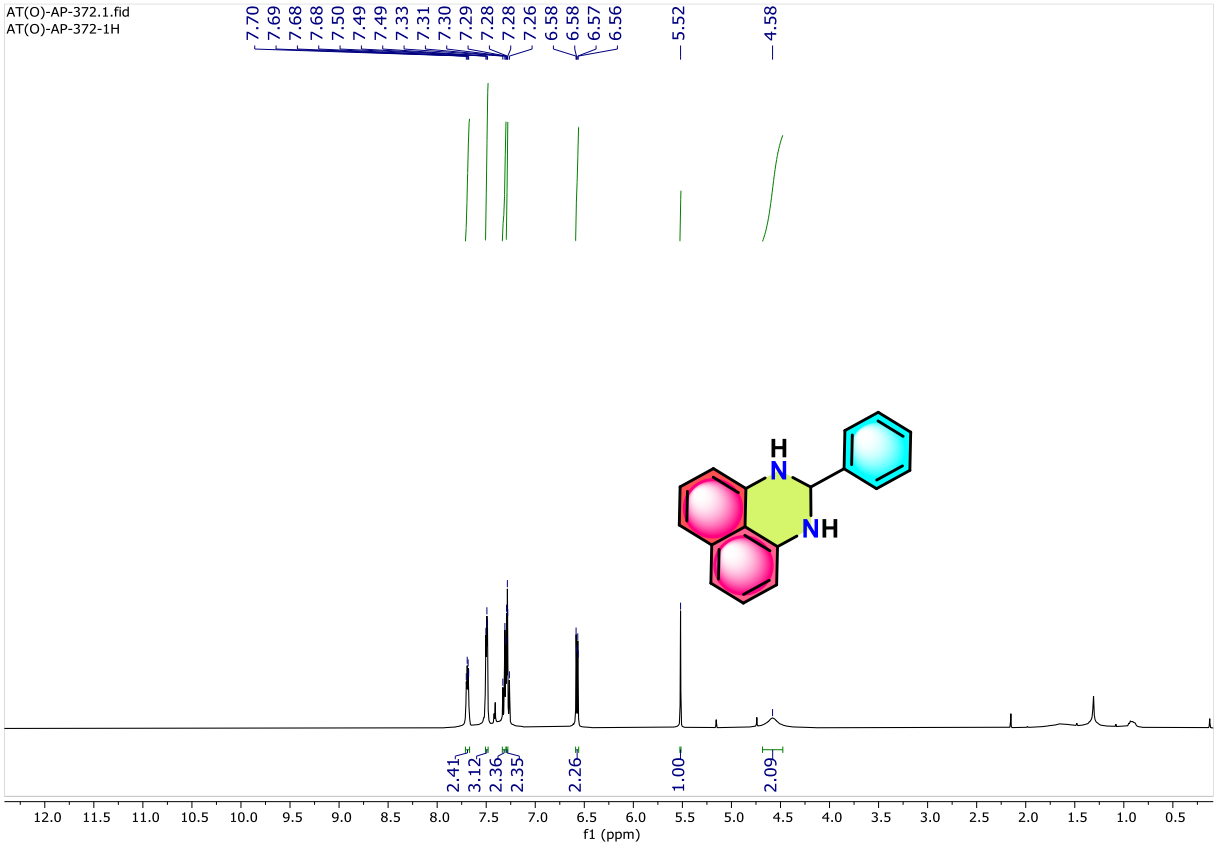

Figure 3.72. ^{1}H NMR (300 MHz) spectrum of **3ah** in $CDCl_3$**.**

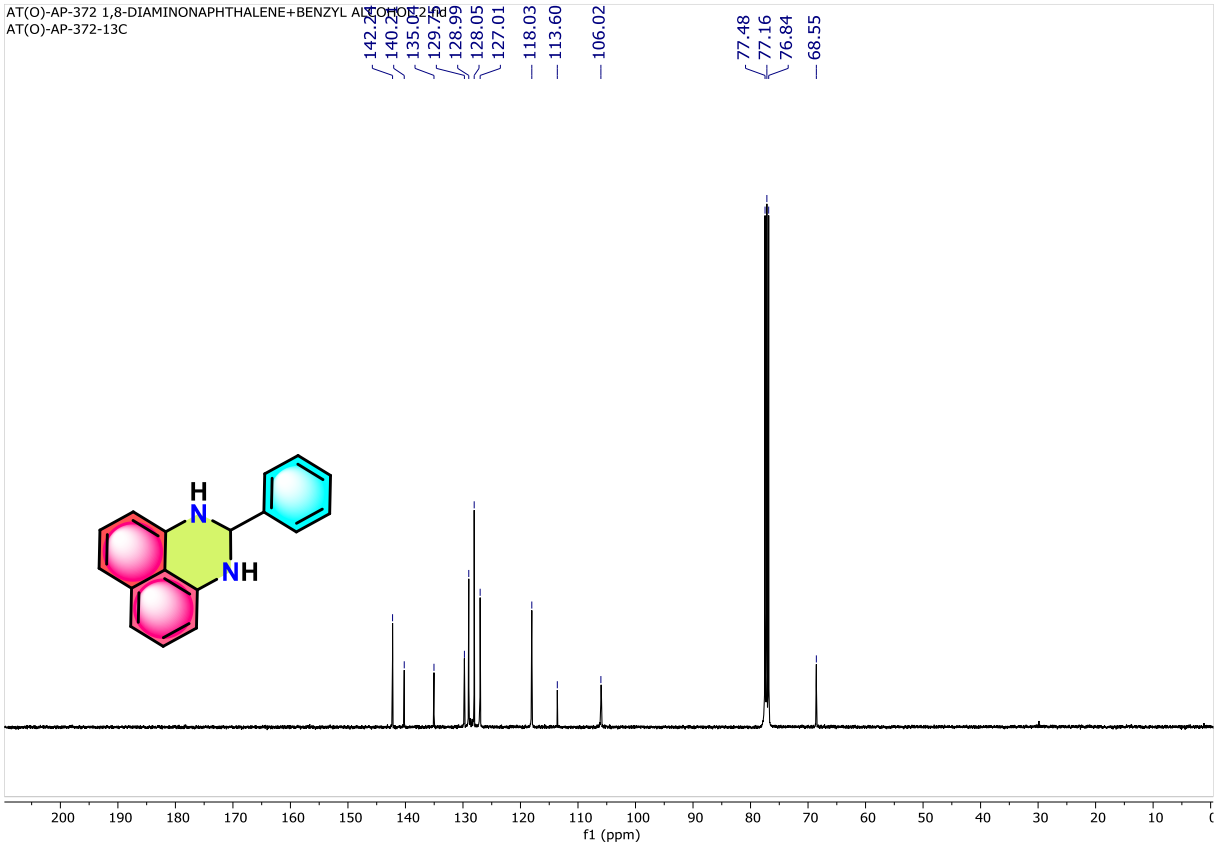

Figure 3.73. $^{13}C\{^{1}H\}$ NMR (75 MHz) spectrum of **3ah** in $CDCl_3$**.**

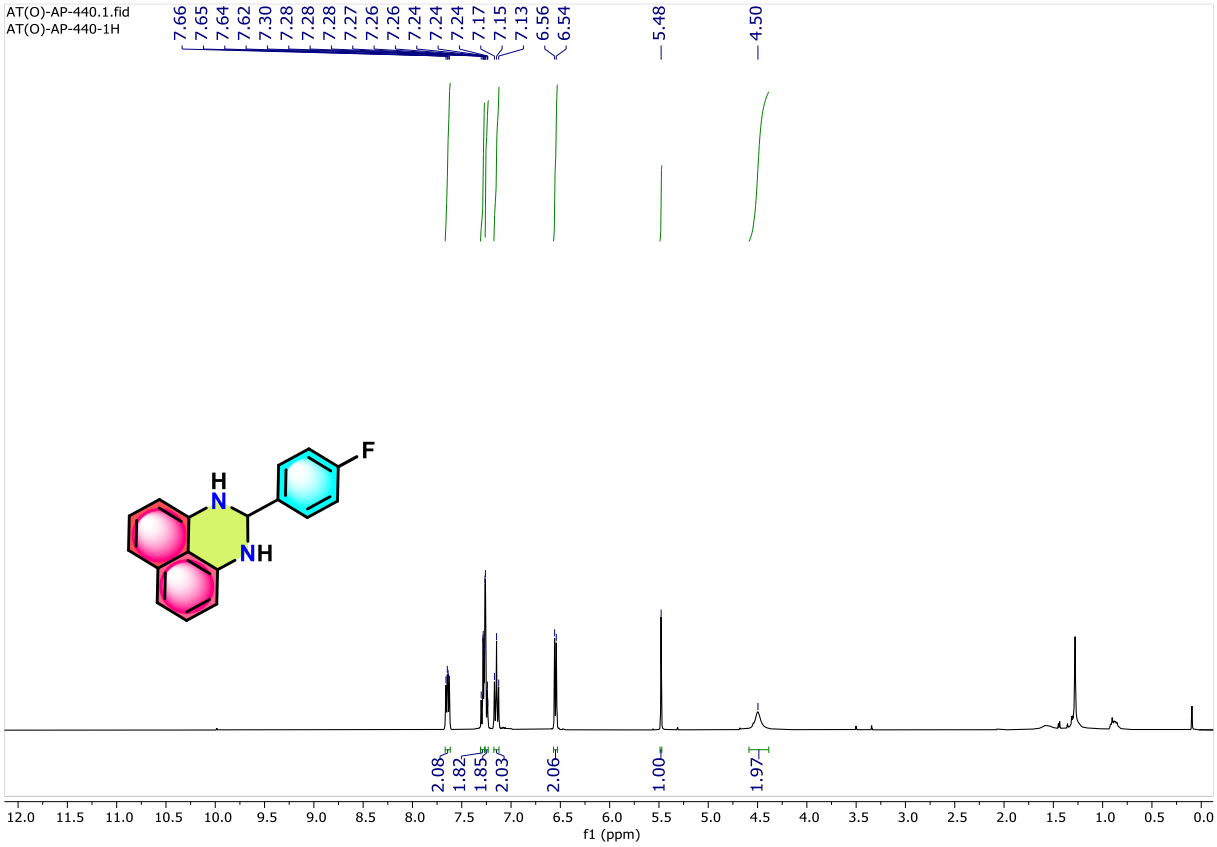

Figure 3.74. ^{1}H NMR (300 MHz) spectrum of **3ai** in $CDCl_3$**.**

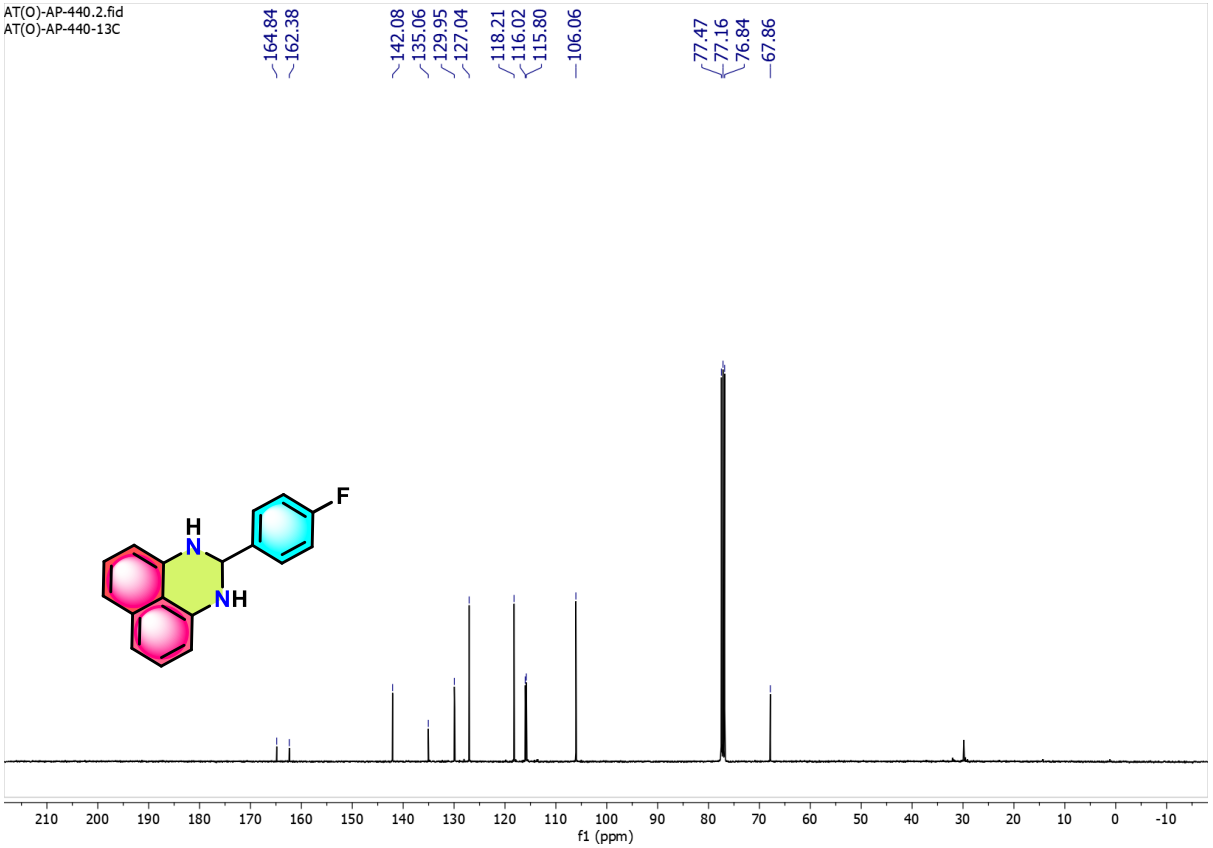

Figure 3.75. $^{13}C\{^{1}H\}$ NMR (75 MHz) spectrum of **3ai** in $CDCl_3$**.**

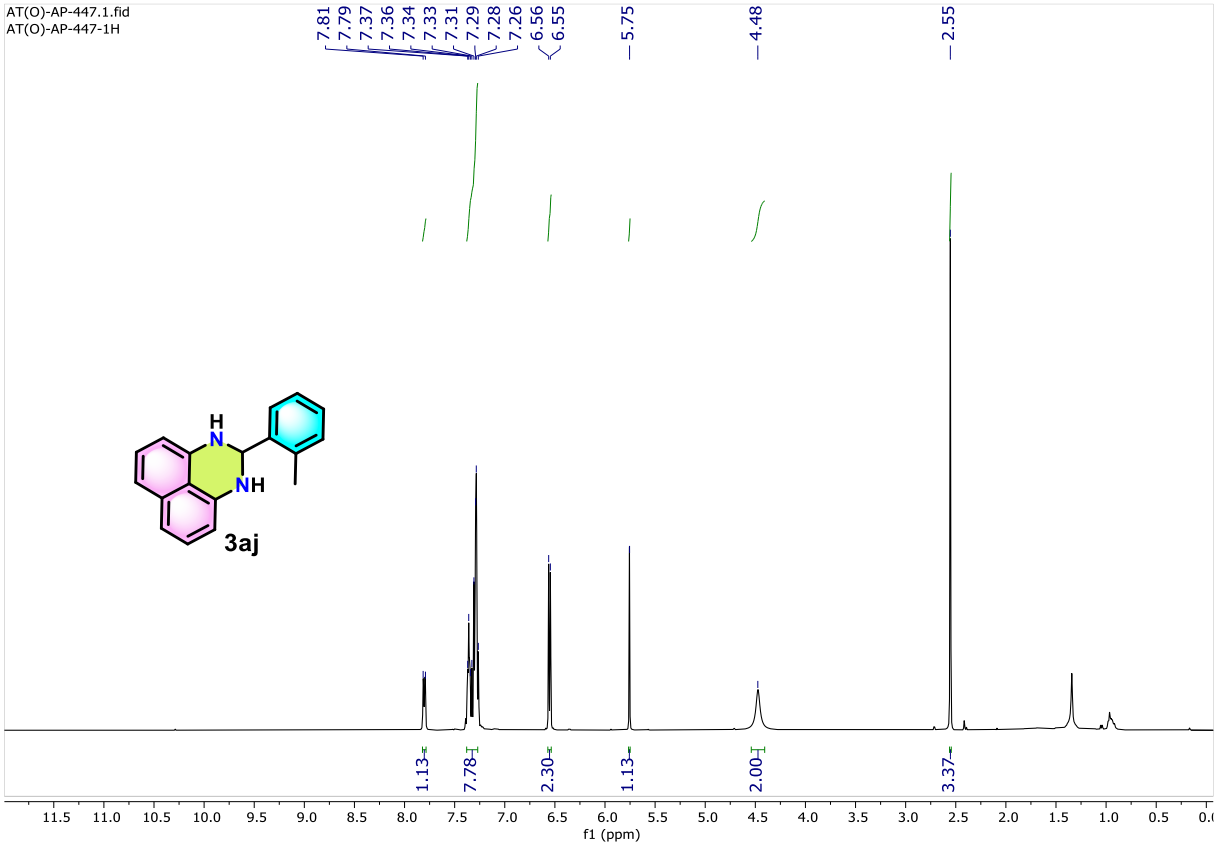

Figure 3.76. ^{1}H NMR (400 MHz) spectrum of **3aj** in $CDCl_3$**.**

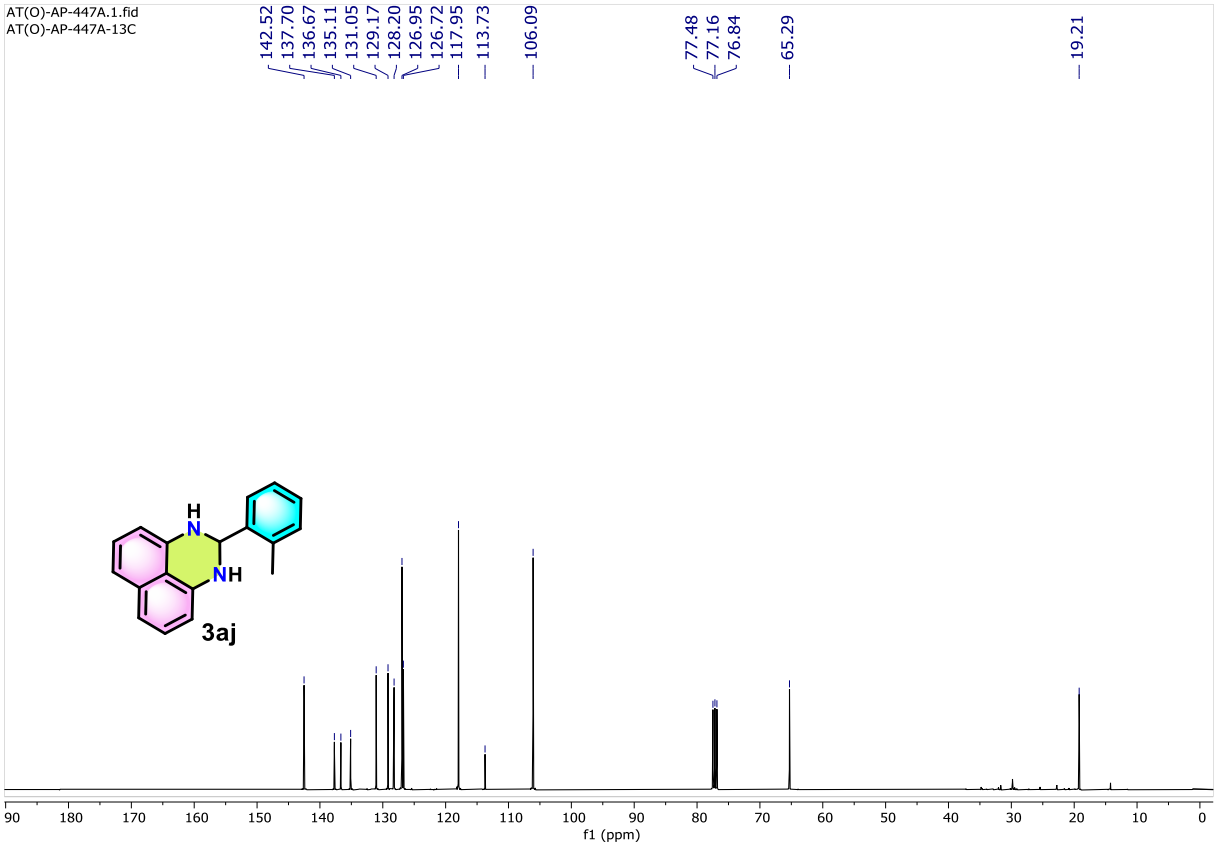

Figure 3.77. $^{13}C\{^{1}H\}$ NMR (100 MHz) spectrum of **3aj** in $CDCl_3$**.**

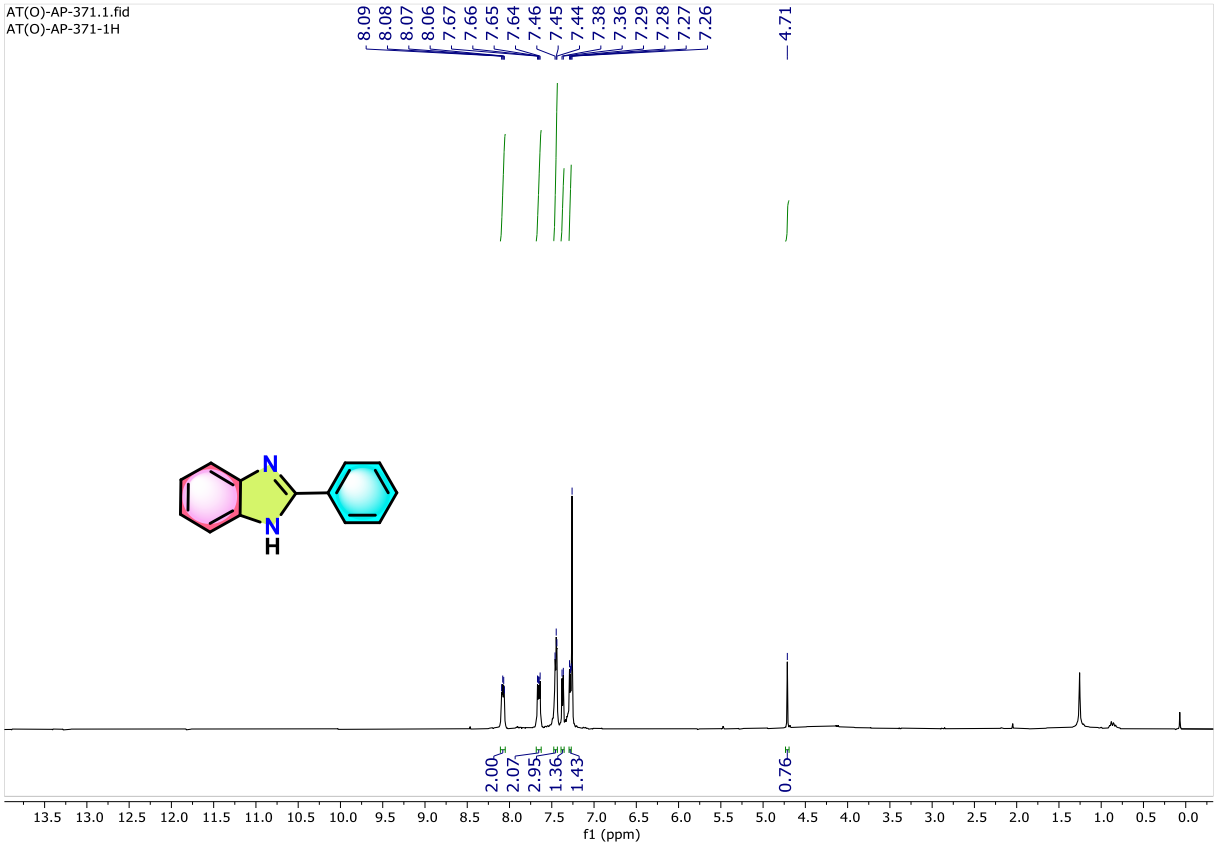

Figure 3.78. ^{1}H NMR (300 MHz) spectrum of **3ak** in $CDCl_3$.

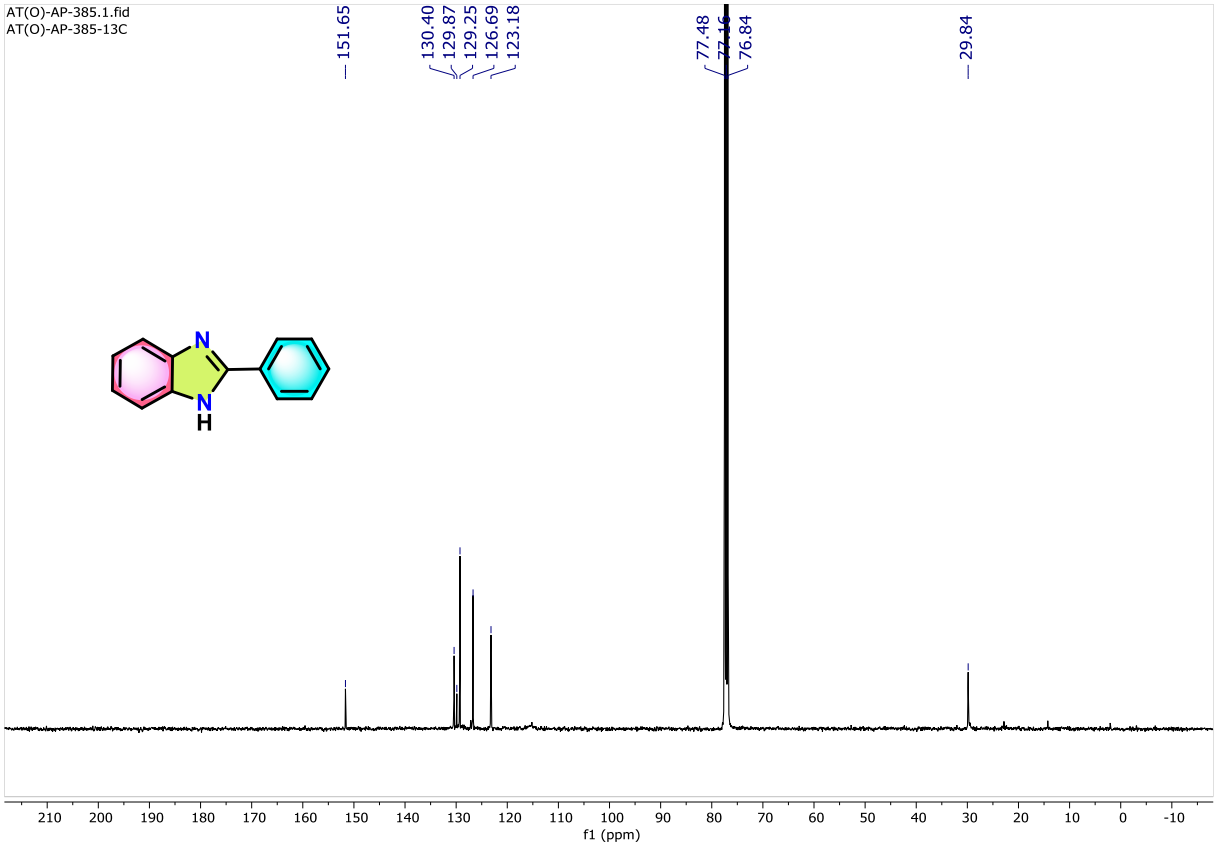

Figure 3.79. $^{13}C\{^{1}H\}$ NMR (75 MHz) spectrum of **3ak** in $CDCl_3$**.**

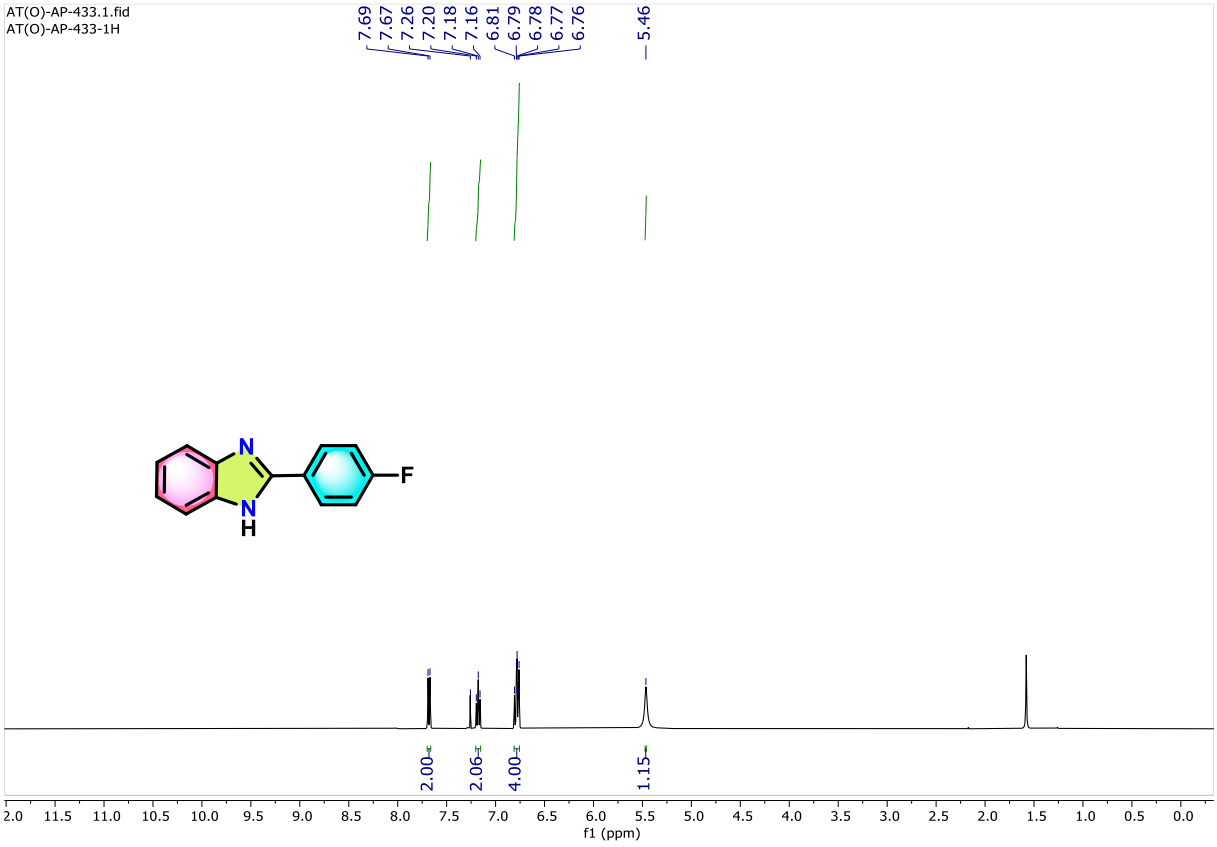

Figure 3.80. ^{1}H NMR (300 MHz) spectrum of **3al** in $CDCl_3$.

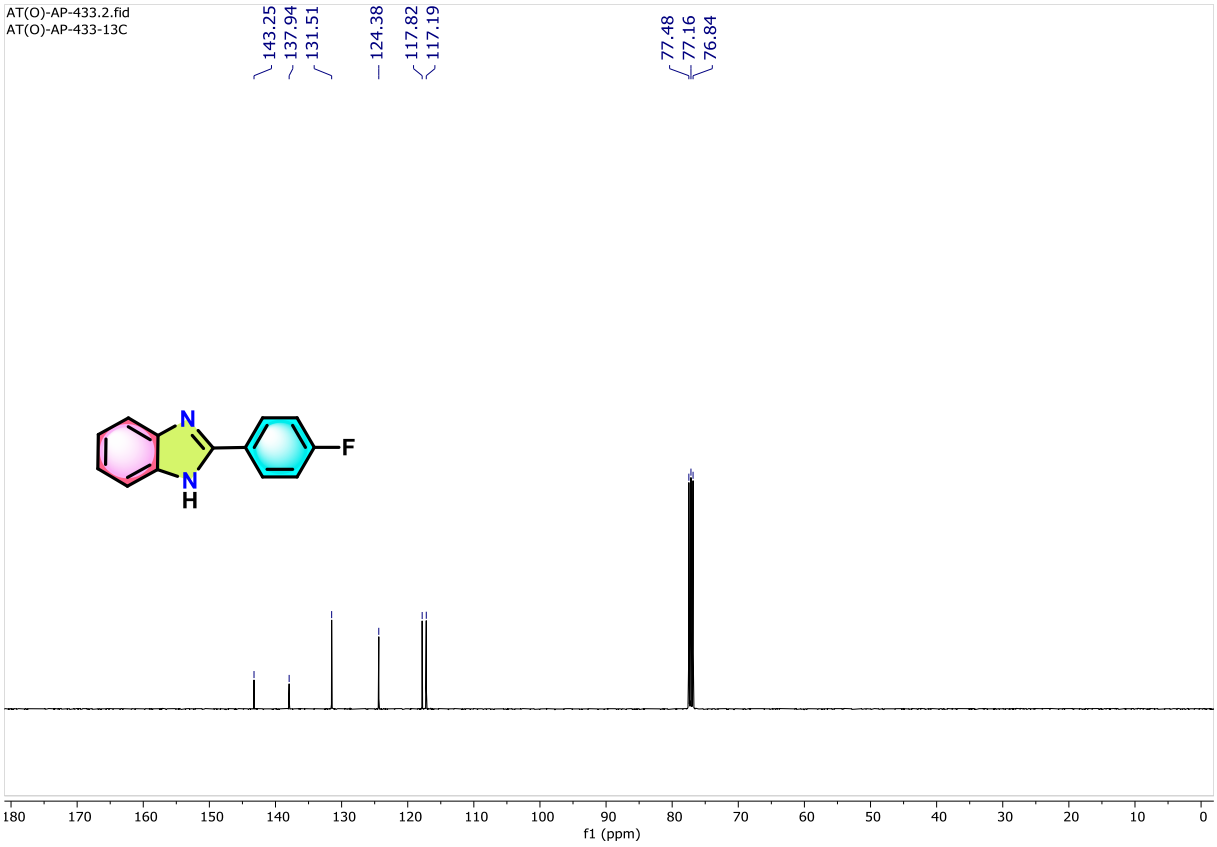

Figure 3.81. $^{13}C\{^{1}H\}$ NMR (75 MHz) spectrum of **3al** in $CDCl_3$**.**

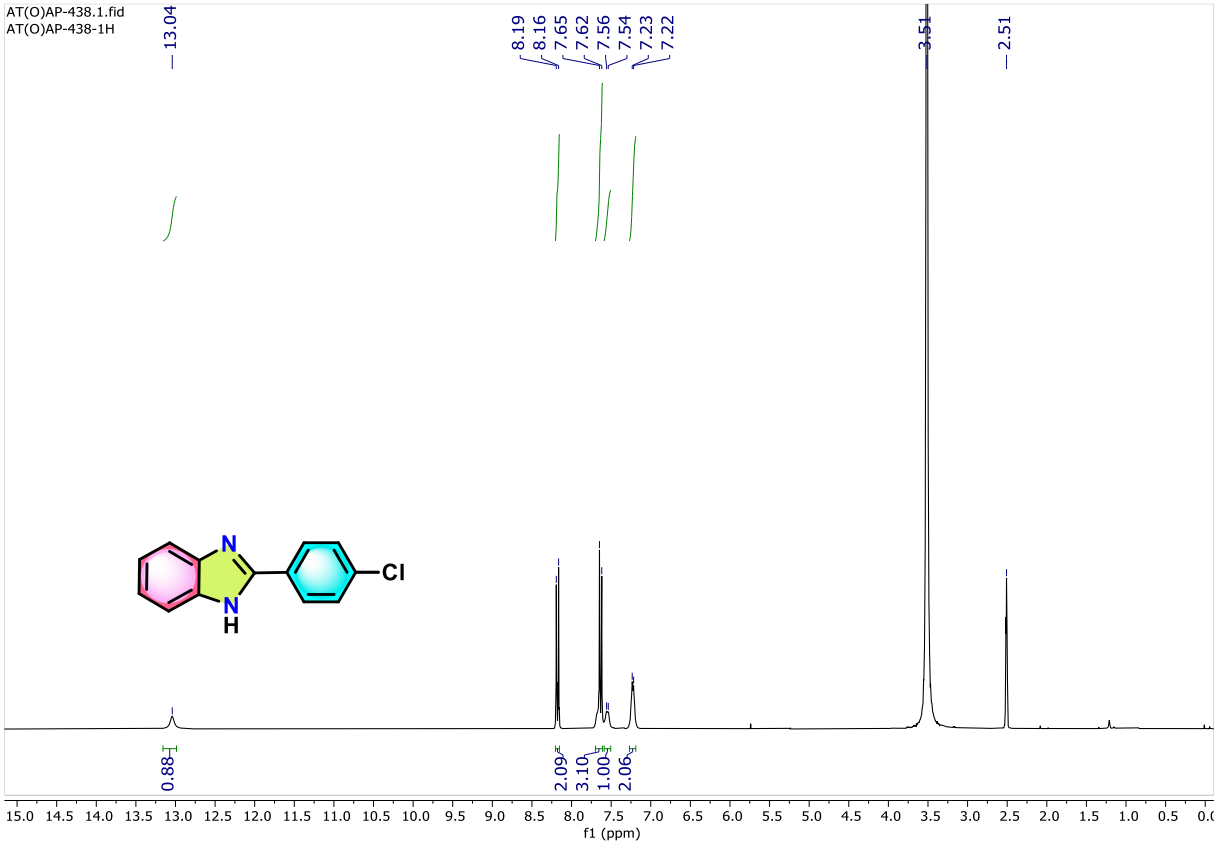

Figure 3.82. ^{1}H NMR (300 MHz) spectrum of **3am** in DMSO-d_6.

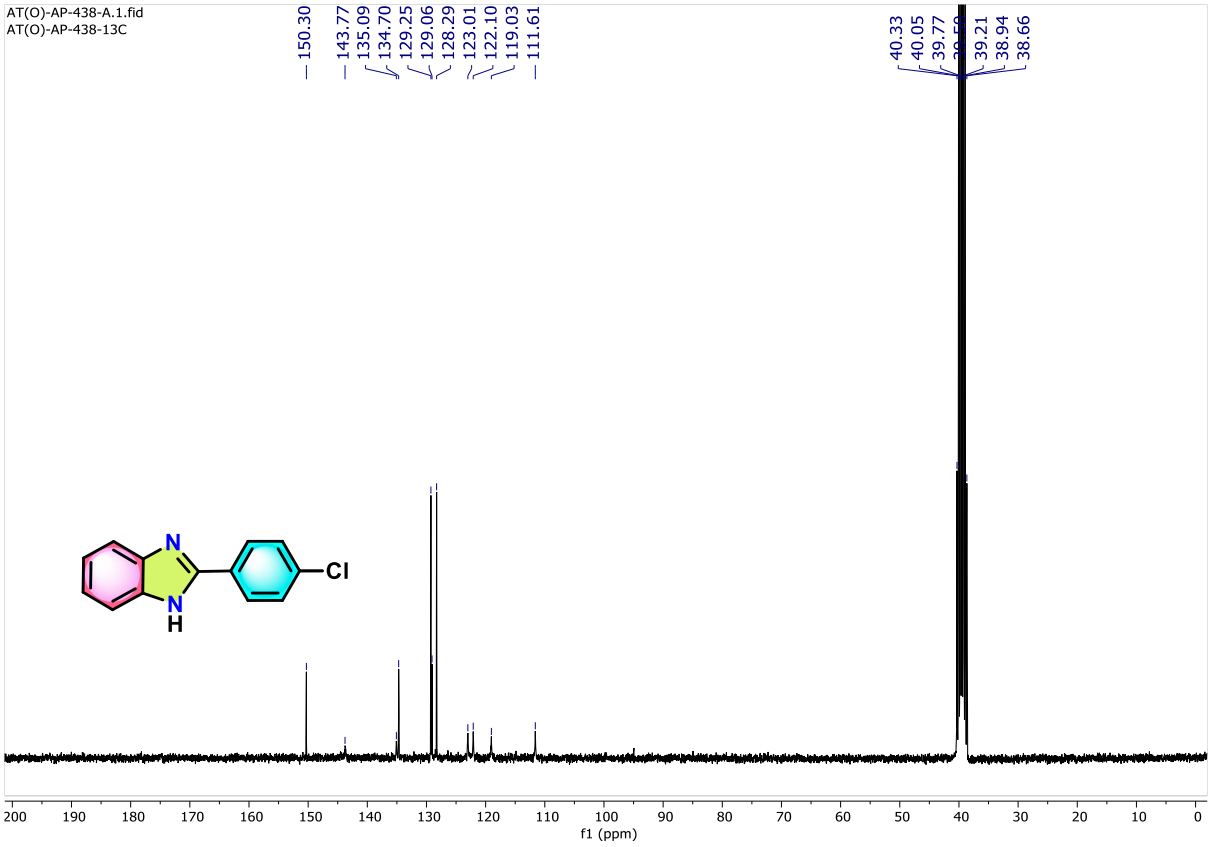

Figure 3.83. ^{13}C{^{1}H} NMR (75 MHz) spectrum of **3am** in DMSO-d_6.

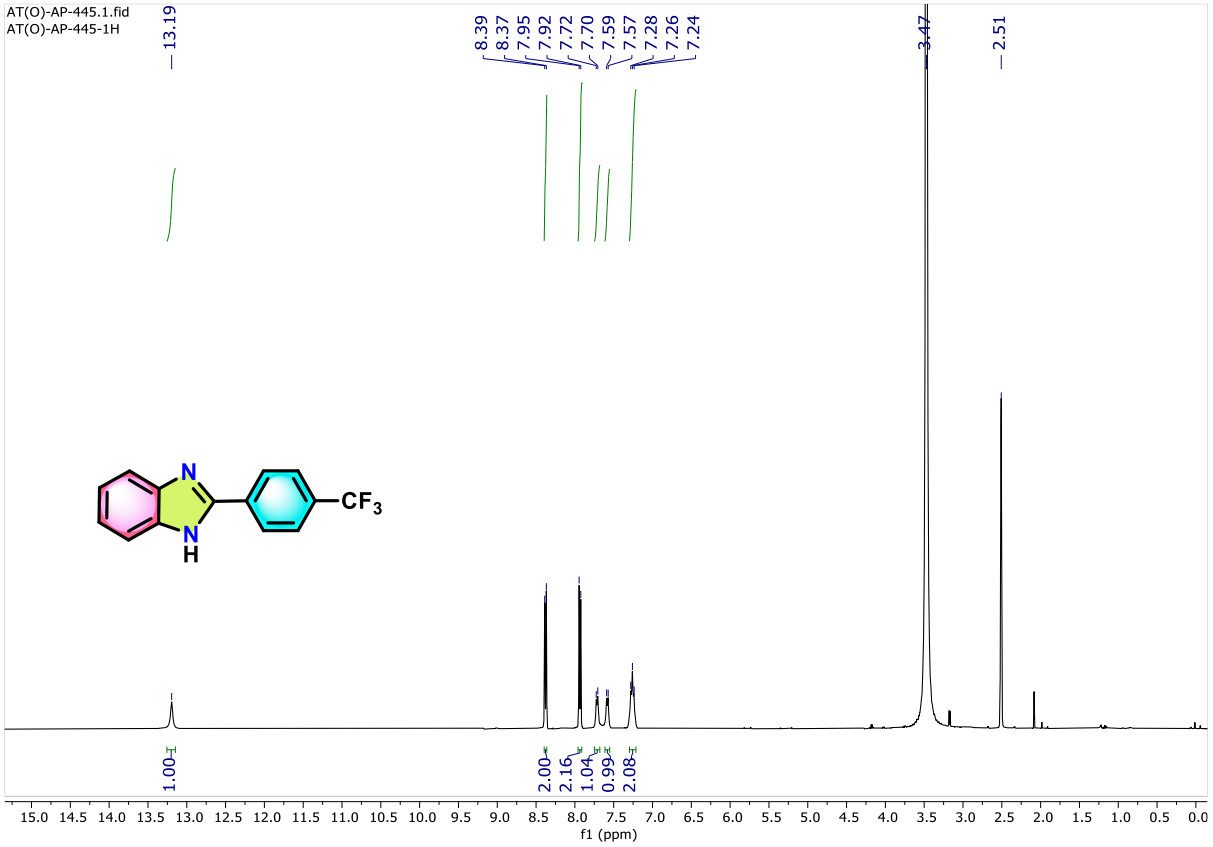

Figure 3.84. ^{1}H NMR (300 MHz) spectrum of **3an** in DMSO-d_6.

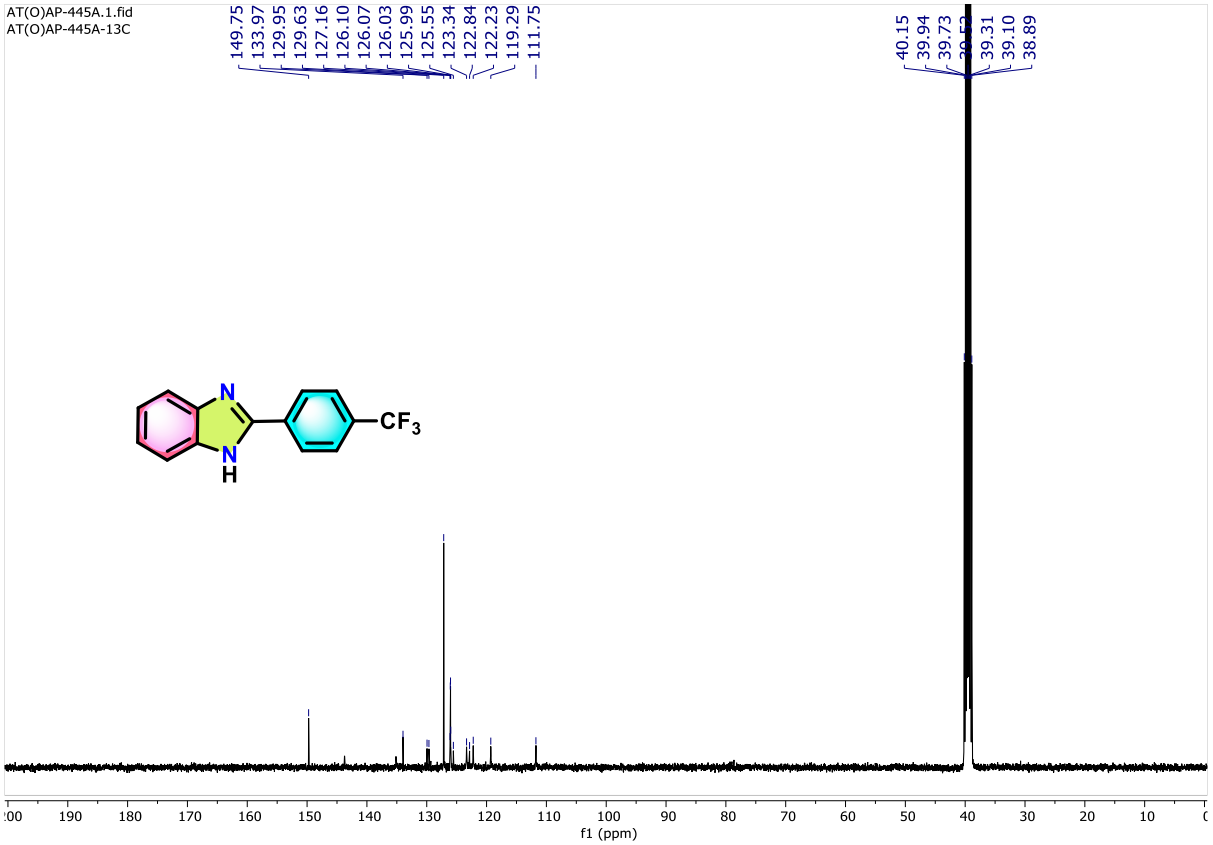

Figure 3.85. ^{13}C{^{1}H} NMR (75 MHz) spectrum of **3an** in DMSO-d_6.

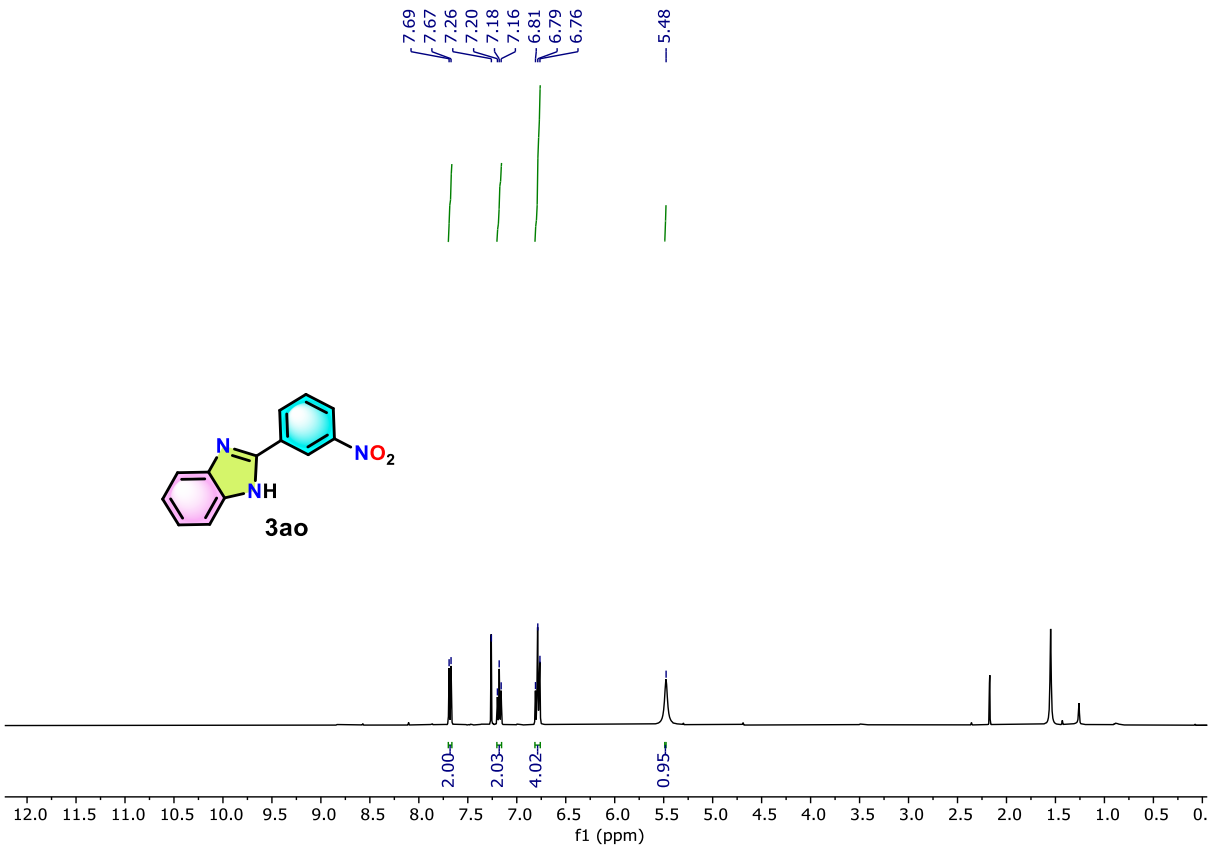

Figure 3.86. ^{1}H NMR (400 MHz) spectrum of **3ao** in $CDCl_3$.

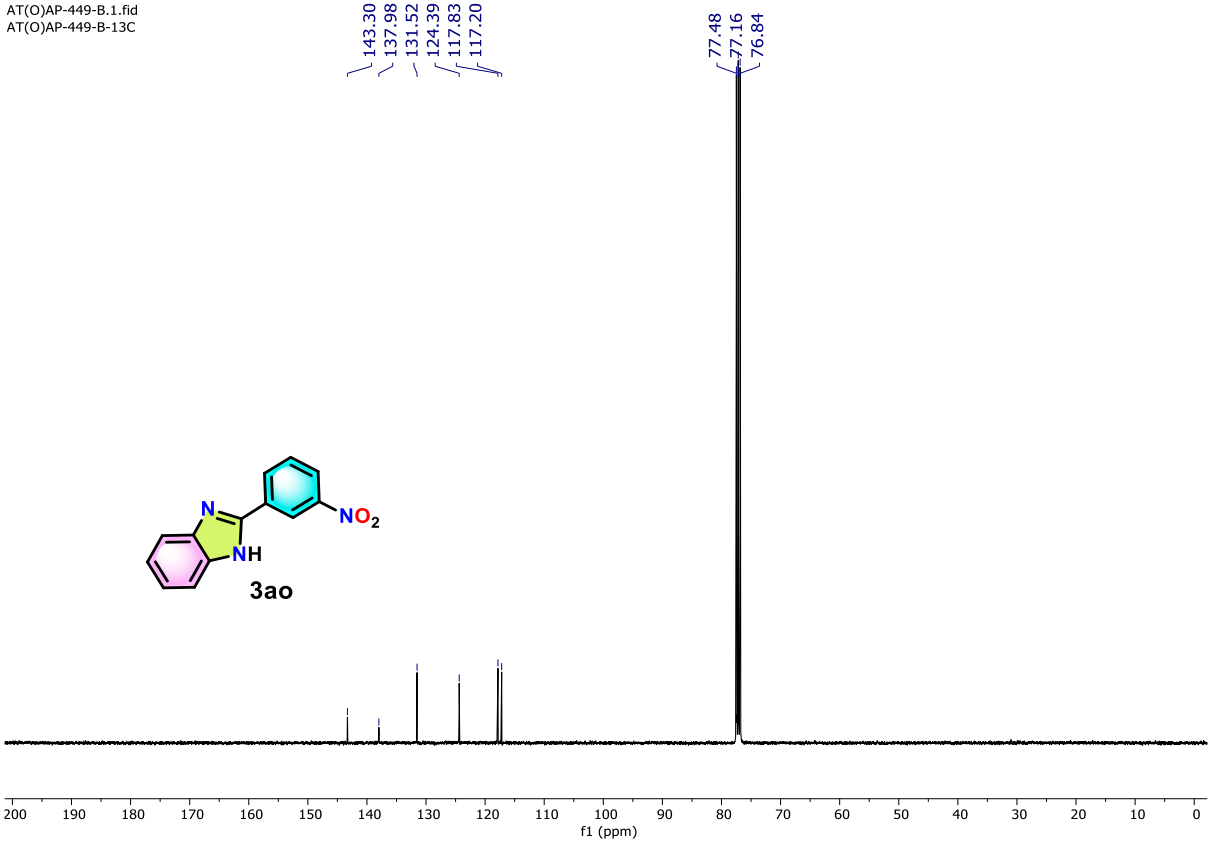

Figure 3.87. $^{13}C\{^{1}H\}$ NMR (100 MHz) spectrum of **3ao** in $CDCl_3$**.**

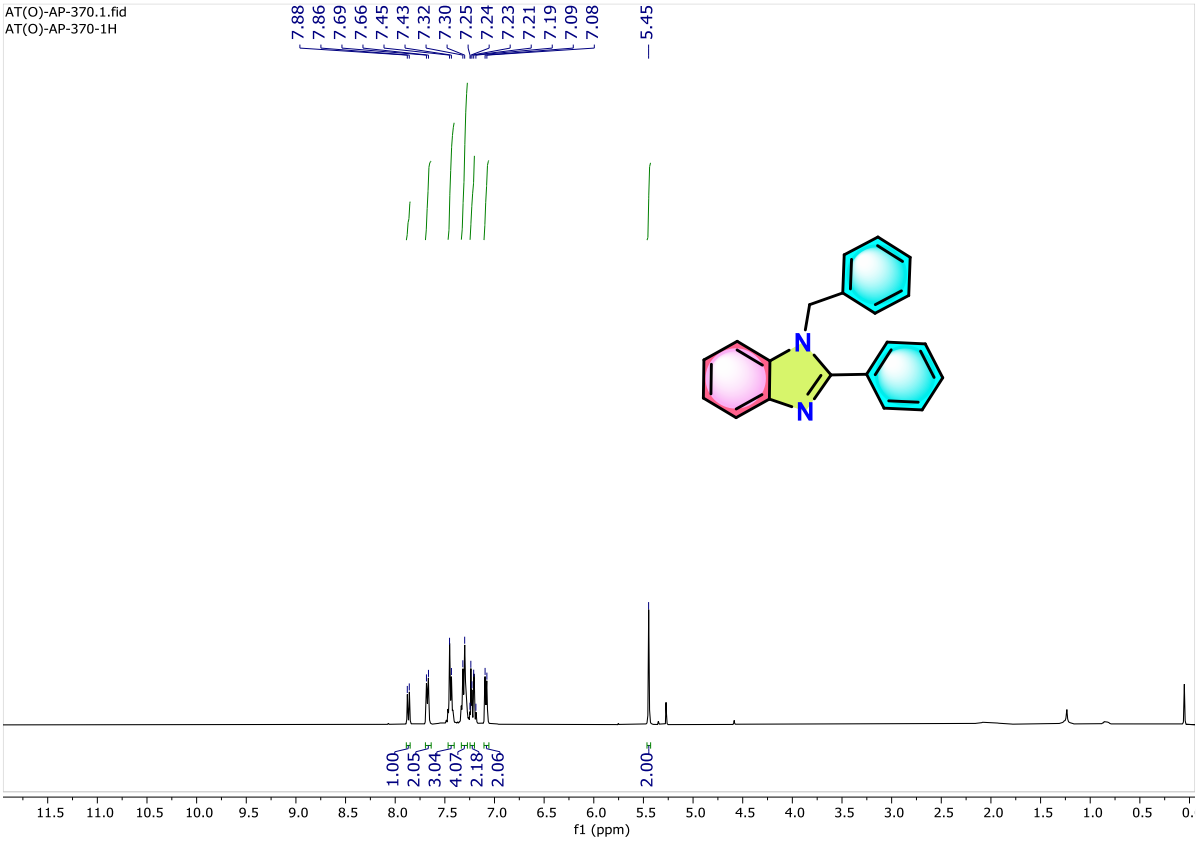

Figure 3.88. ^{1}H NMR (300 MHz) spectrum of **3ap** in $CDCl_3$.

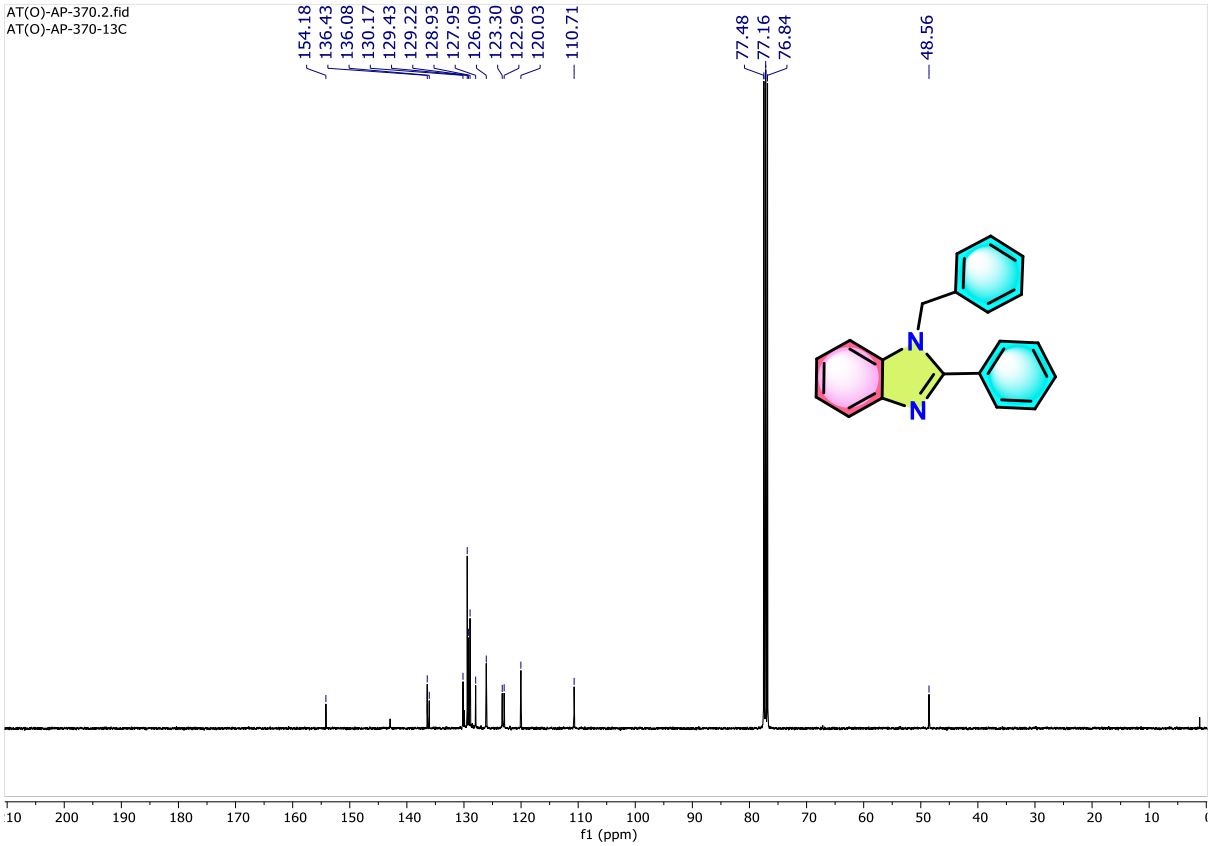

Figure 3.89. $^{13}C\{^{1}H\}$ NMR (75 MHz) spectrum of **3ap** in $CDCl_3$**.**

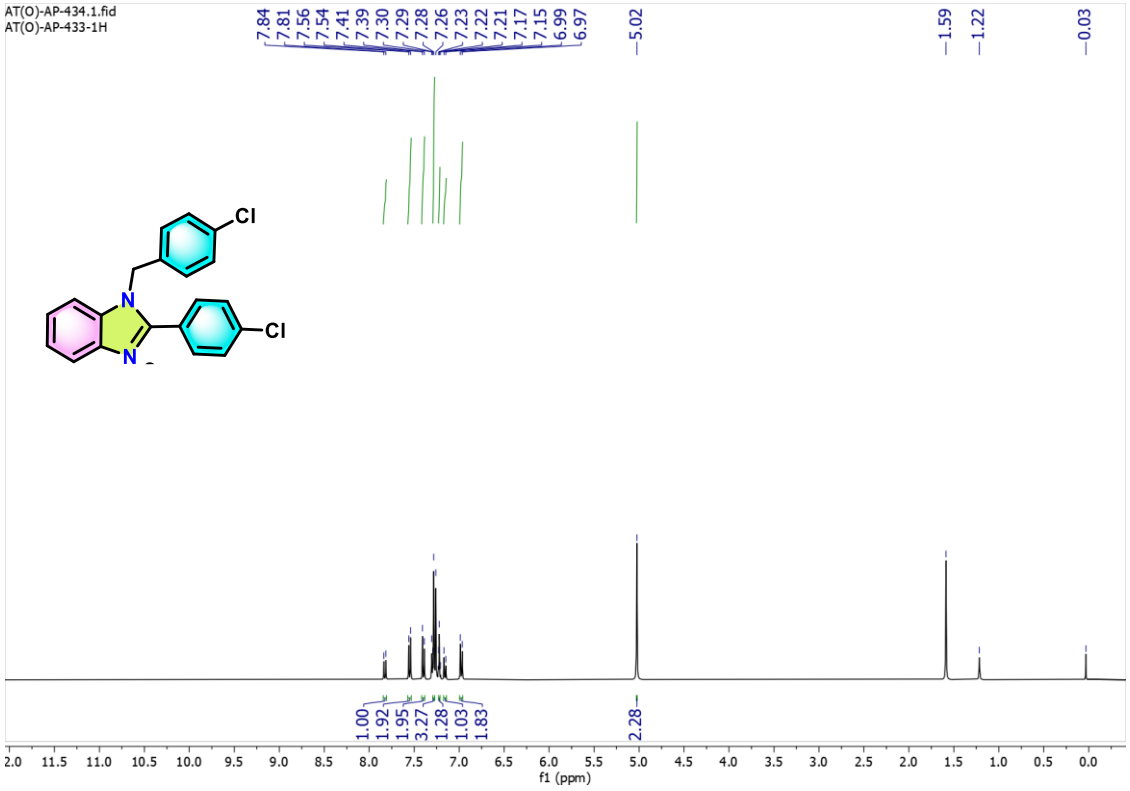

Figure 3.90. ^{1}H NMR (400 MHz) spectrum of **3aq** in $CDCl_3$**.**

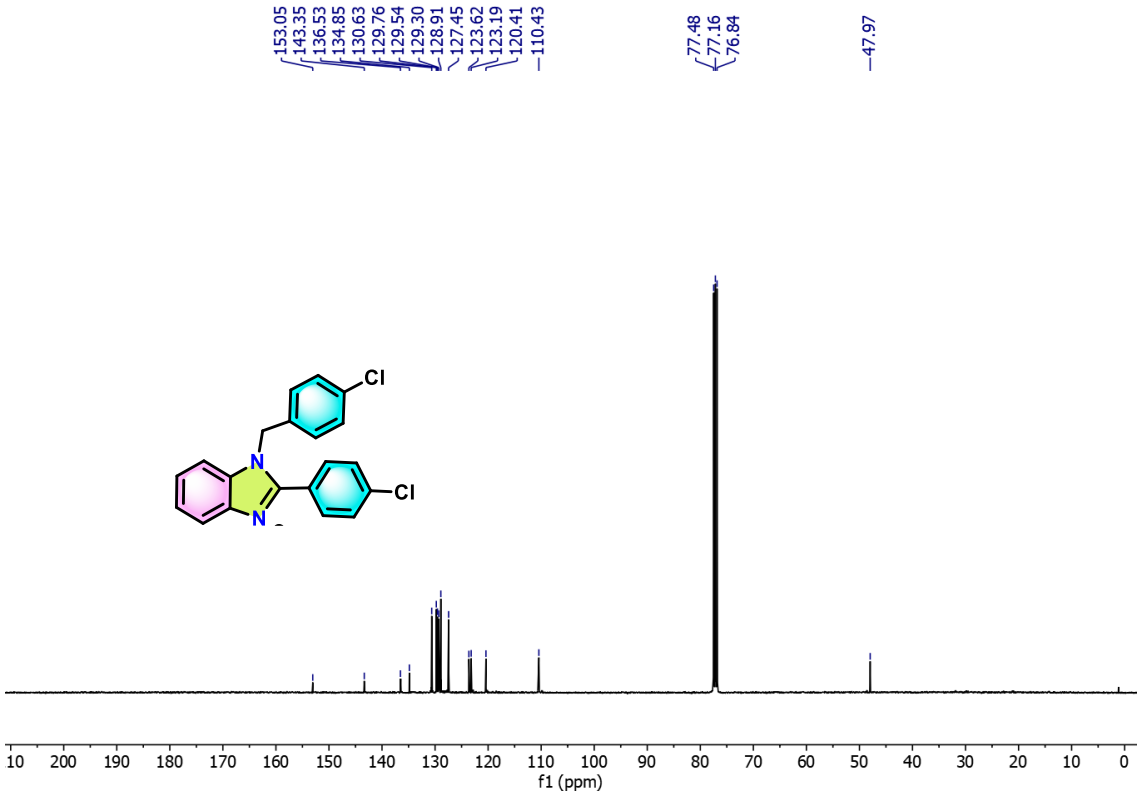

Figure 3.91. $^{13}C\{^{1}H\}$ NMR (100 MHz) spectrum of **3aq** in $CDCl_3$.

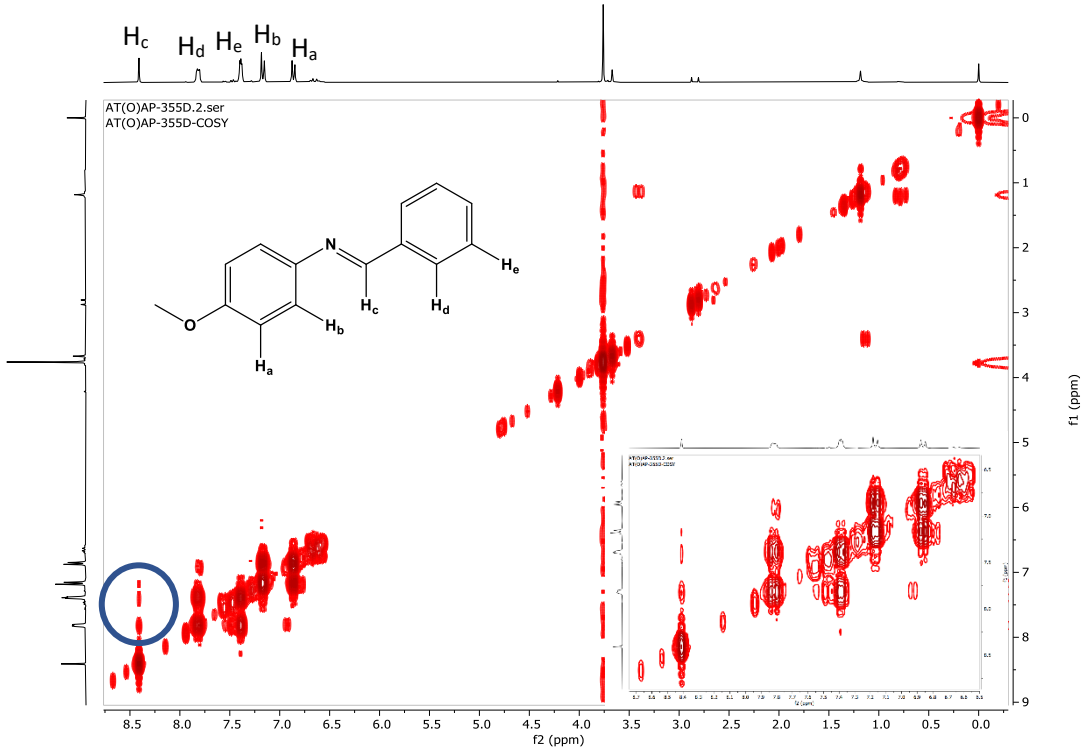

Figure 3.92a. ^{1}H-^{1}H 2D-COSY spectrum of **3e**. The encircled area shows the through-bond interaction of H_c-H_b, H_c-H_e and H_c-H_d (from top to bottom).

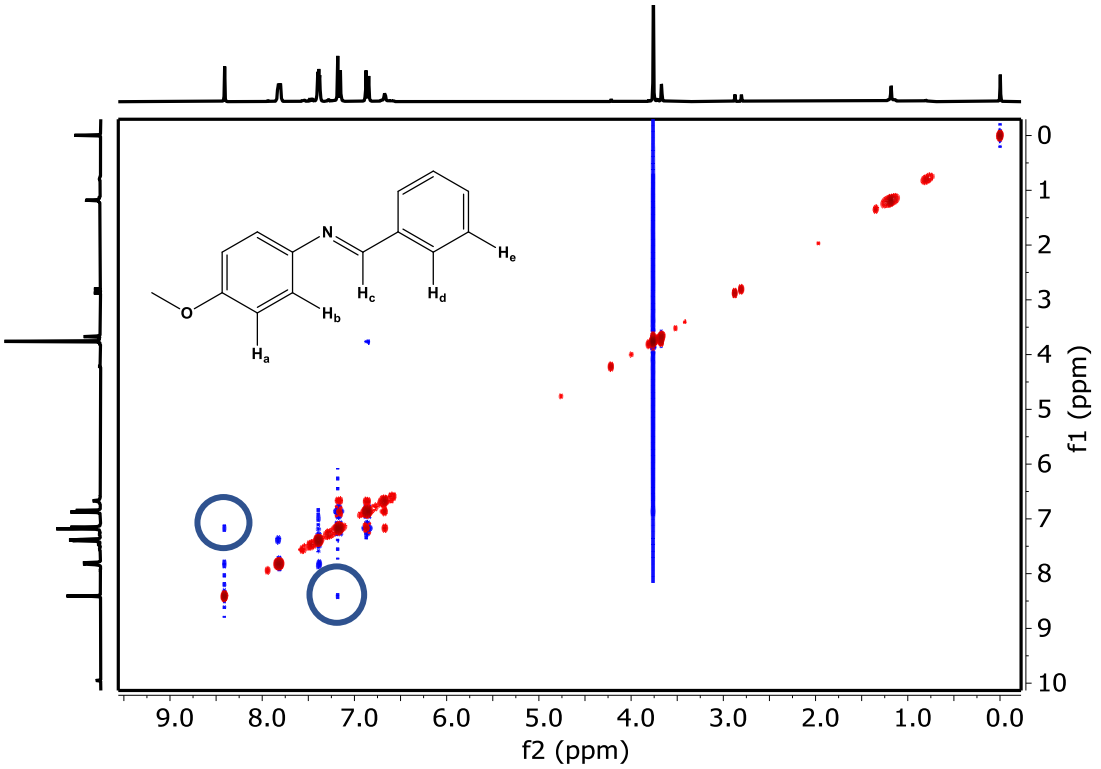

Figure 3.92b. ^{1}H-^{1}H 2D-NOESY spectrum of **3e**. The encircled area shows the through-space interaction of H_c-H_b.

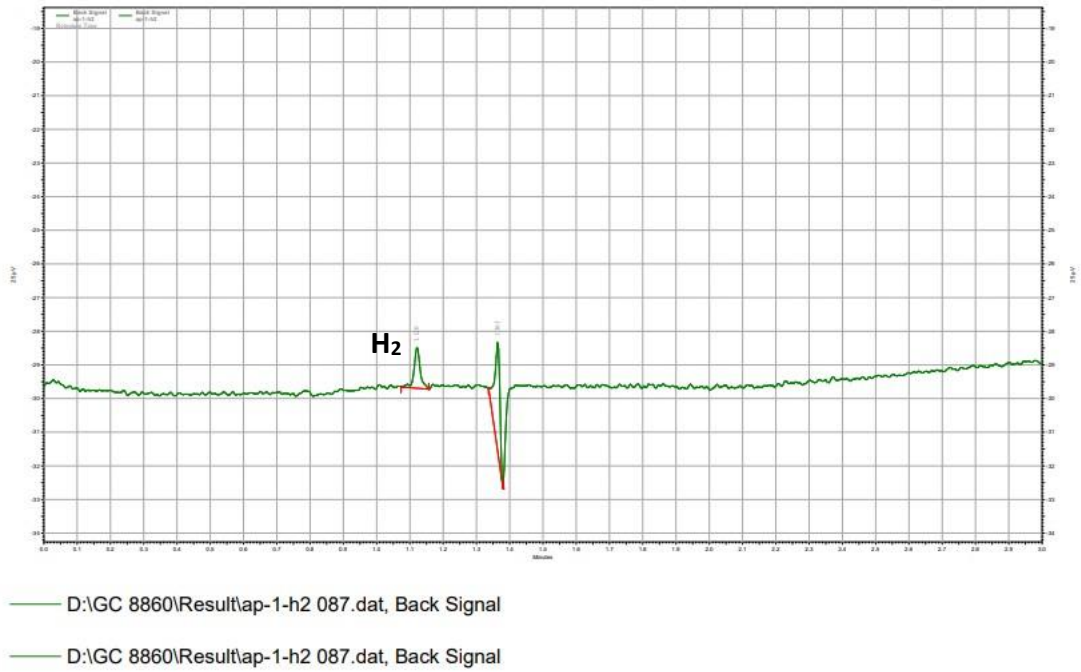

Figure 3.93. Gas Chromatogram of the reaction mixture of **3e** showing evolution of H_2 gas.

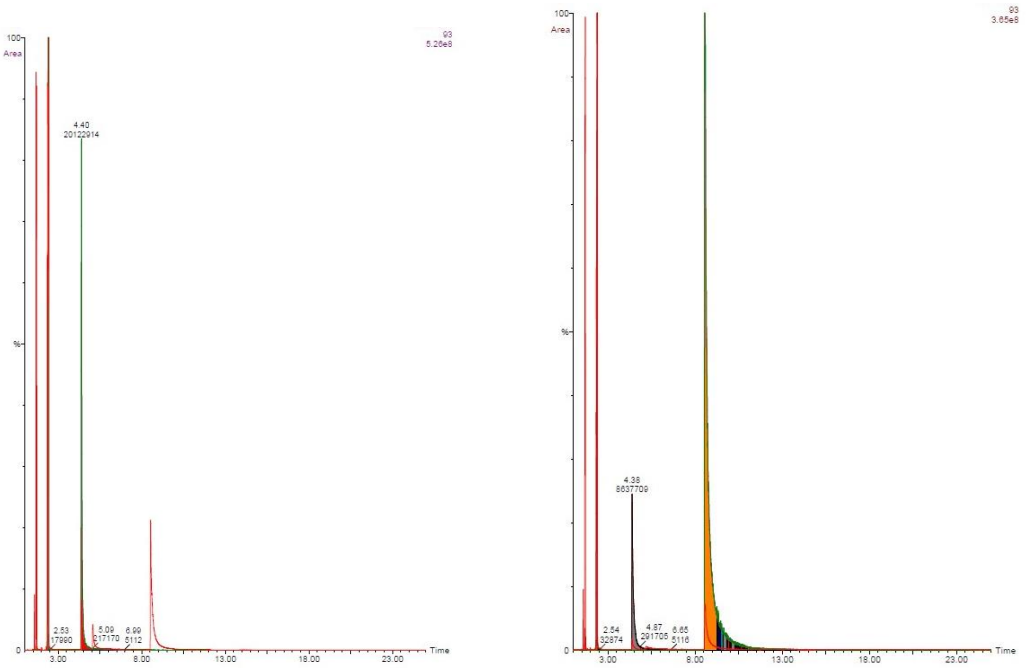

Figure 3.94. Gas Chromatogram of the reaction mixture of **3a** at zero time and after 5 h for Hammett analysis.

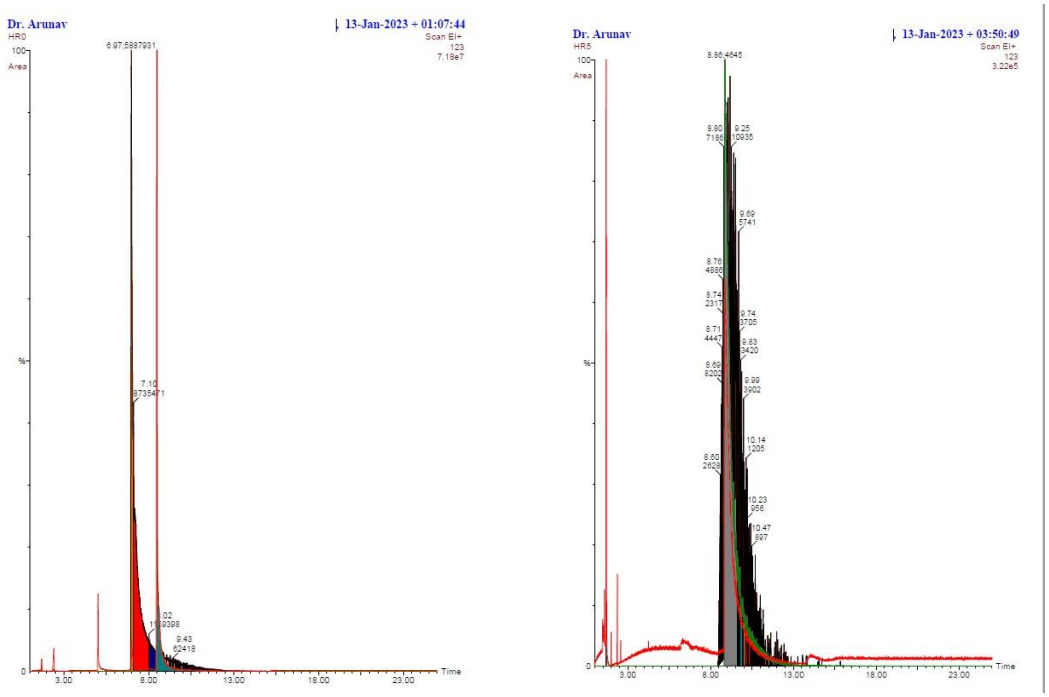

Figure 3.95. Gas Chromatogram of the reaction mixture of **3e** at zero time and after 5 h for Hammett analysis.

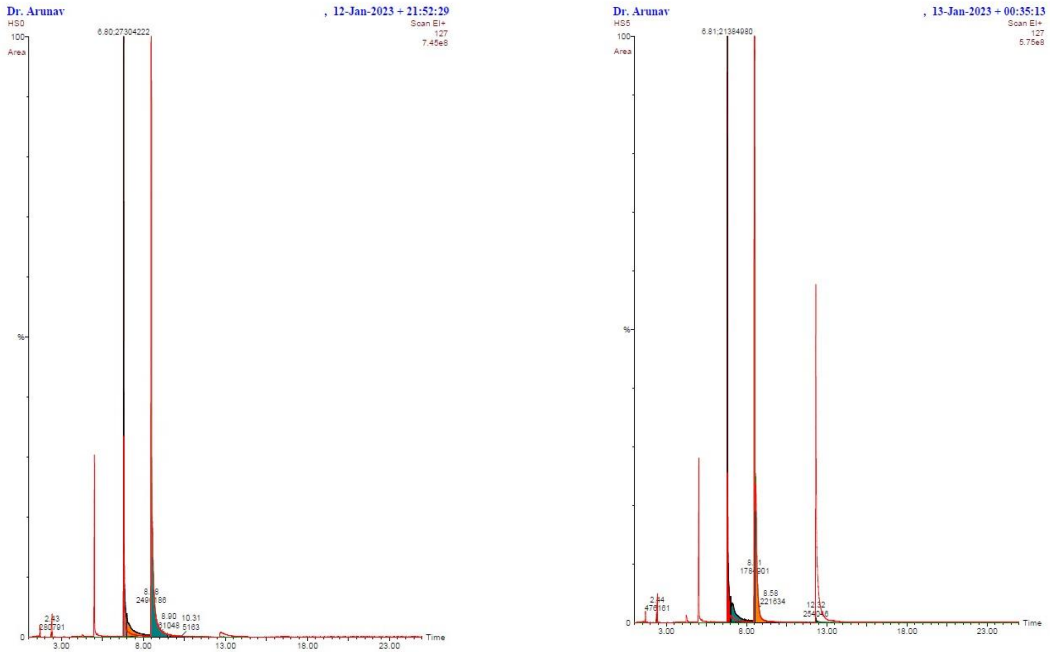

Figure 3.96. Gas Chromatogram of the reaction mixture of **3i** at zero time and after 5 h for Hammett analysis.

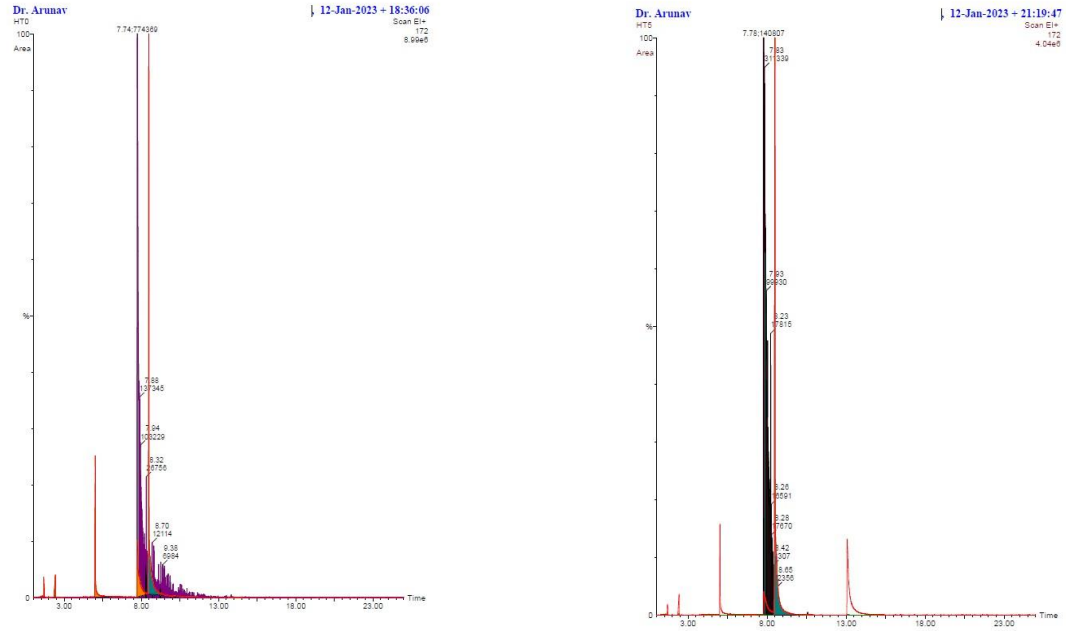

Figure 3.97. Gas Chromatogram of the reaction mixture of **3j** at zero time and after 5 h for Hammett analysis.

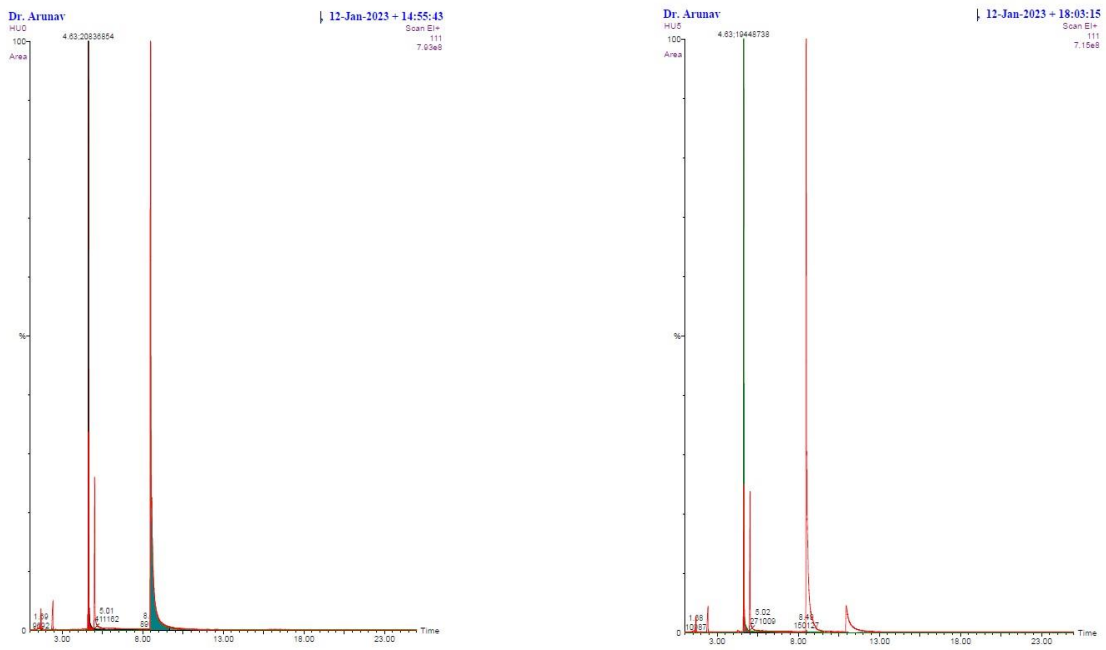

Figure 3.98. Gas Chromatogram of the reaction mixture of **3k** at zero time and after 5 h for Hammett analysis.

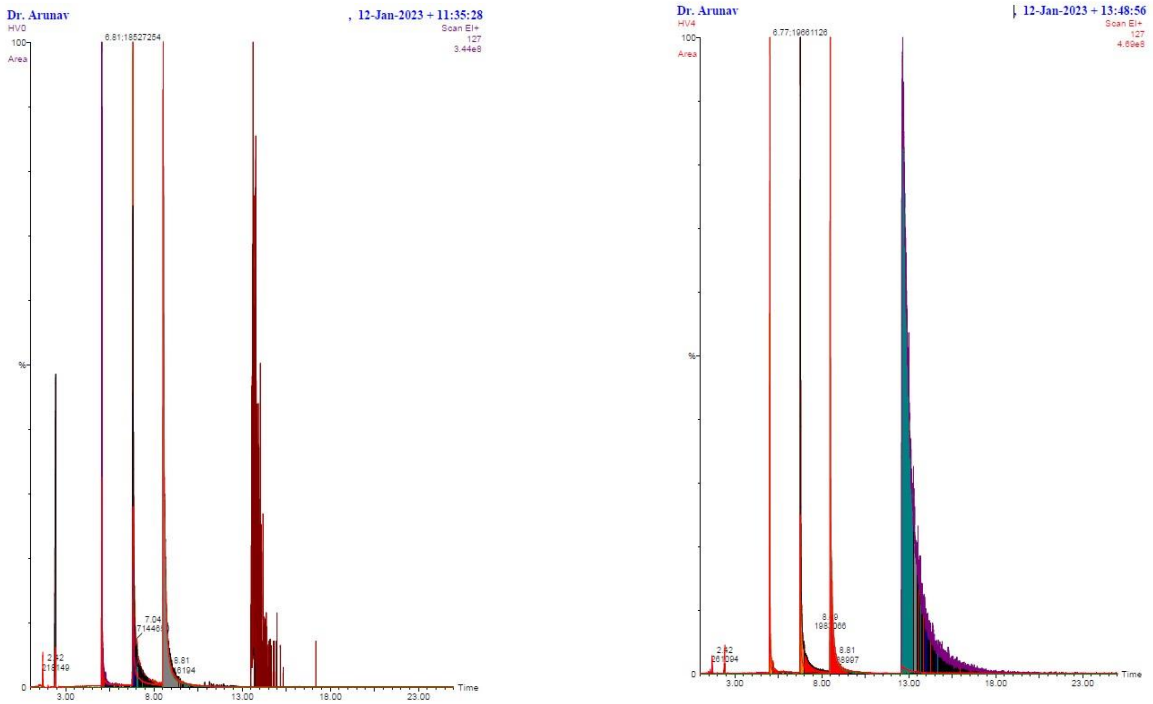

Figure 3.99. Gas Chromatogram of the reaction mixture of **3l** at zero time and after 5 h for Hammett analysis.

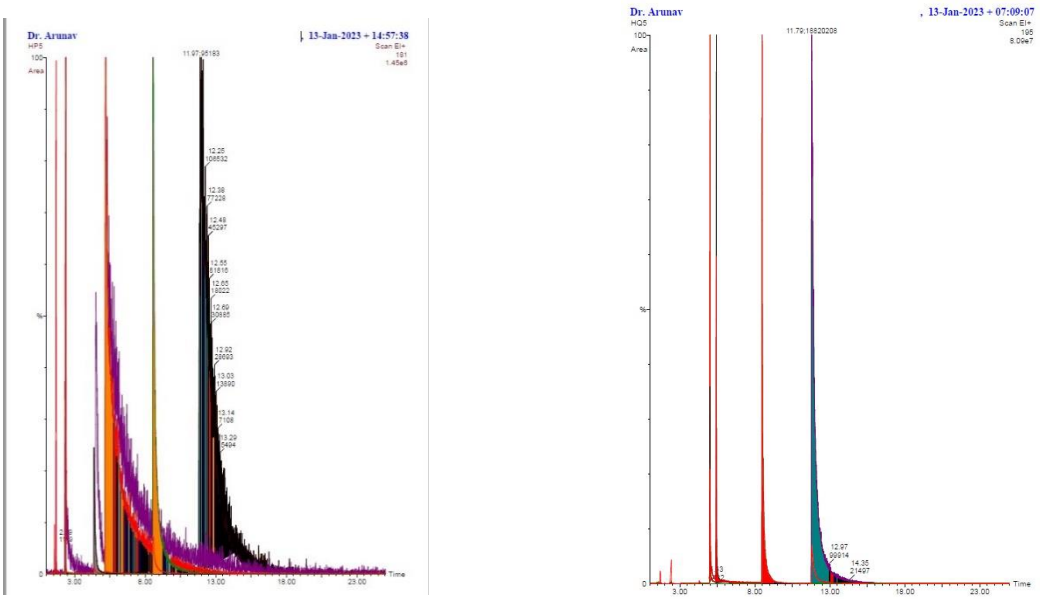

Figure 3.100. Gas Chromatogram of the product **3a** and **3b** in the reaction mixture.

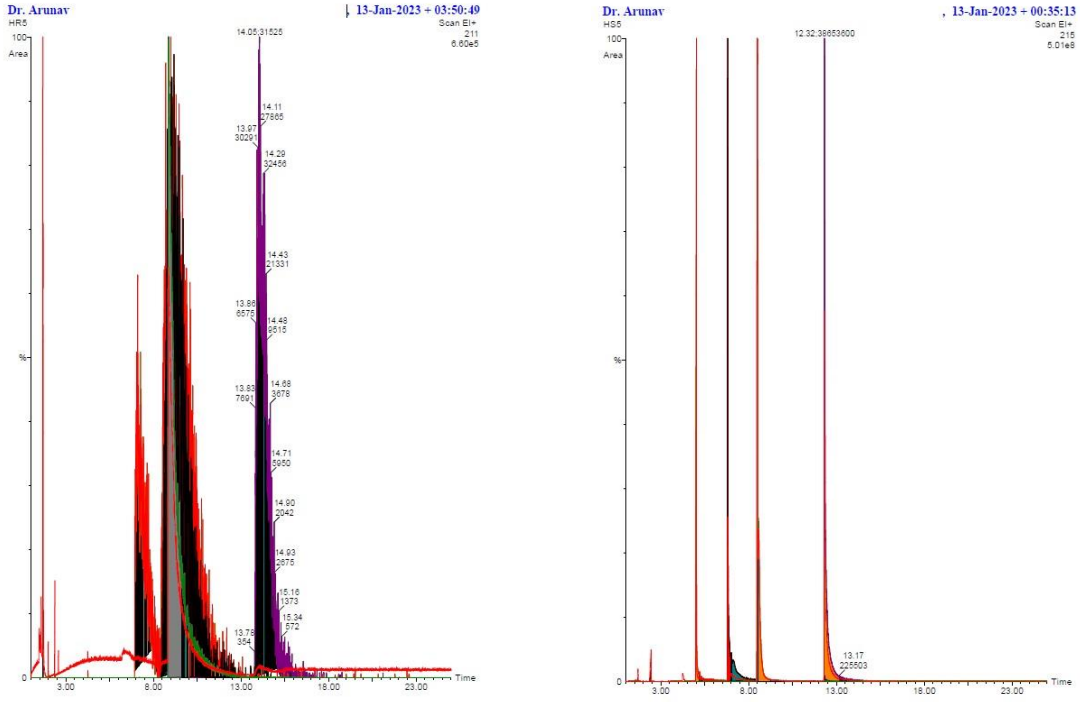

Figure 3.101. Gas Chromatogram of the product **3e** and **3i** in the reaction mixture.

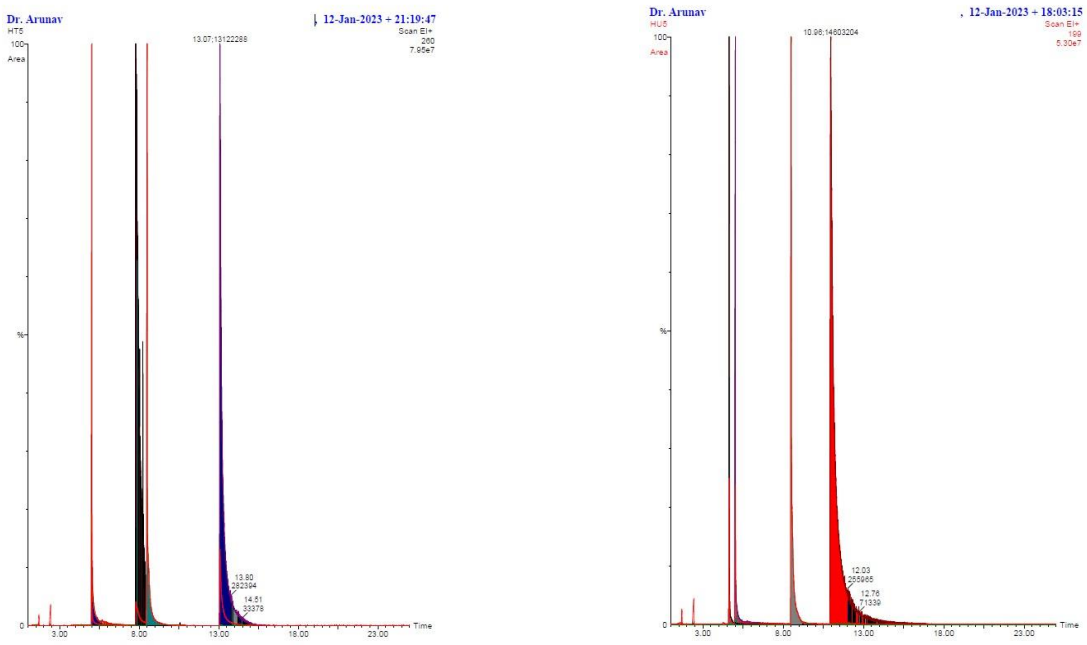

Figure 3.102. Gas Chromatogram of the product **3j** and **3k** in the reaction mixture.

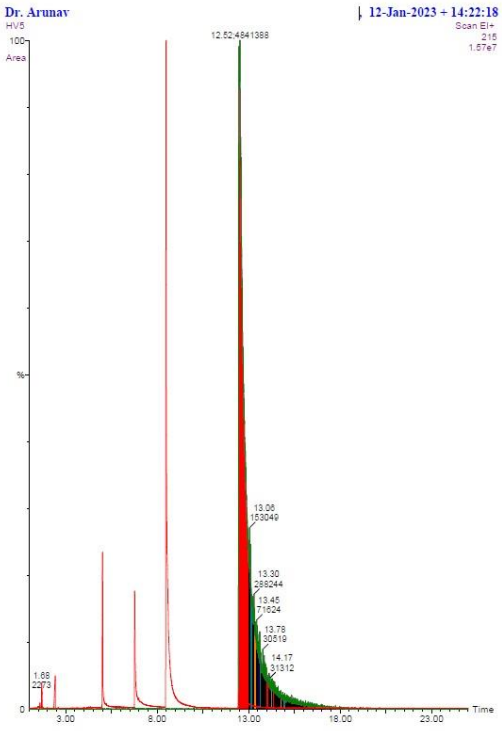

Figure 3.103. Gas Chromatogram of the product **3l** in the reaction mixture.

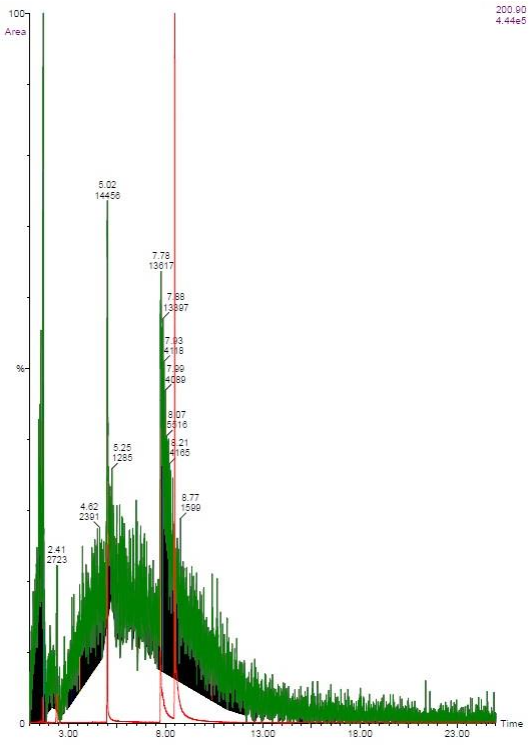

Figure 3.104. Gas Chromatogram of the intermediate **D** in the reaction mixture of **3i**.

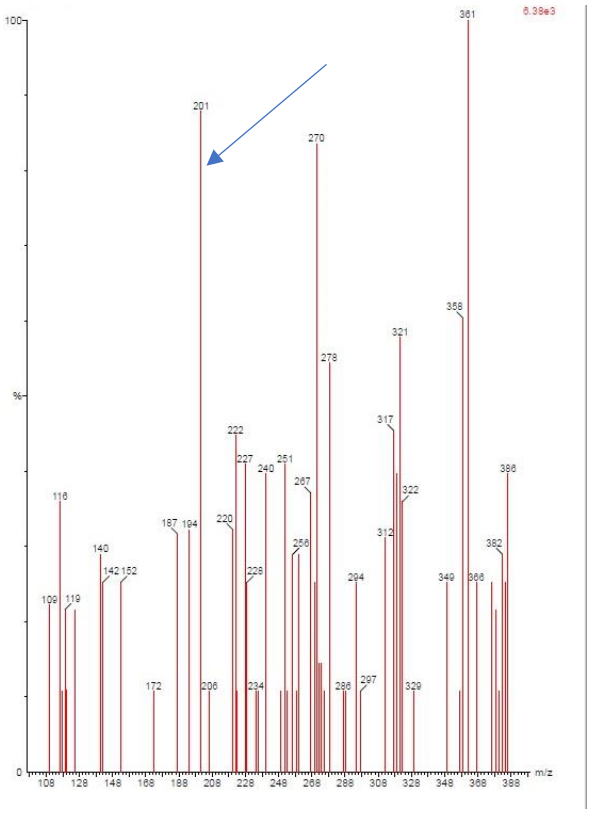

Figure 3.105. GC spectrum of the intermediate **D** in the reaction mixture of **3i**.

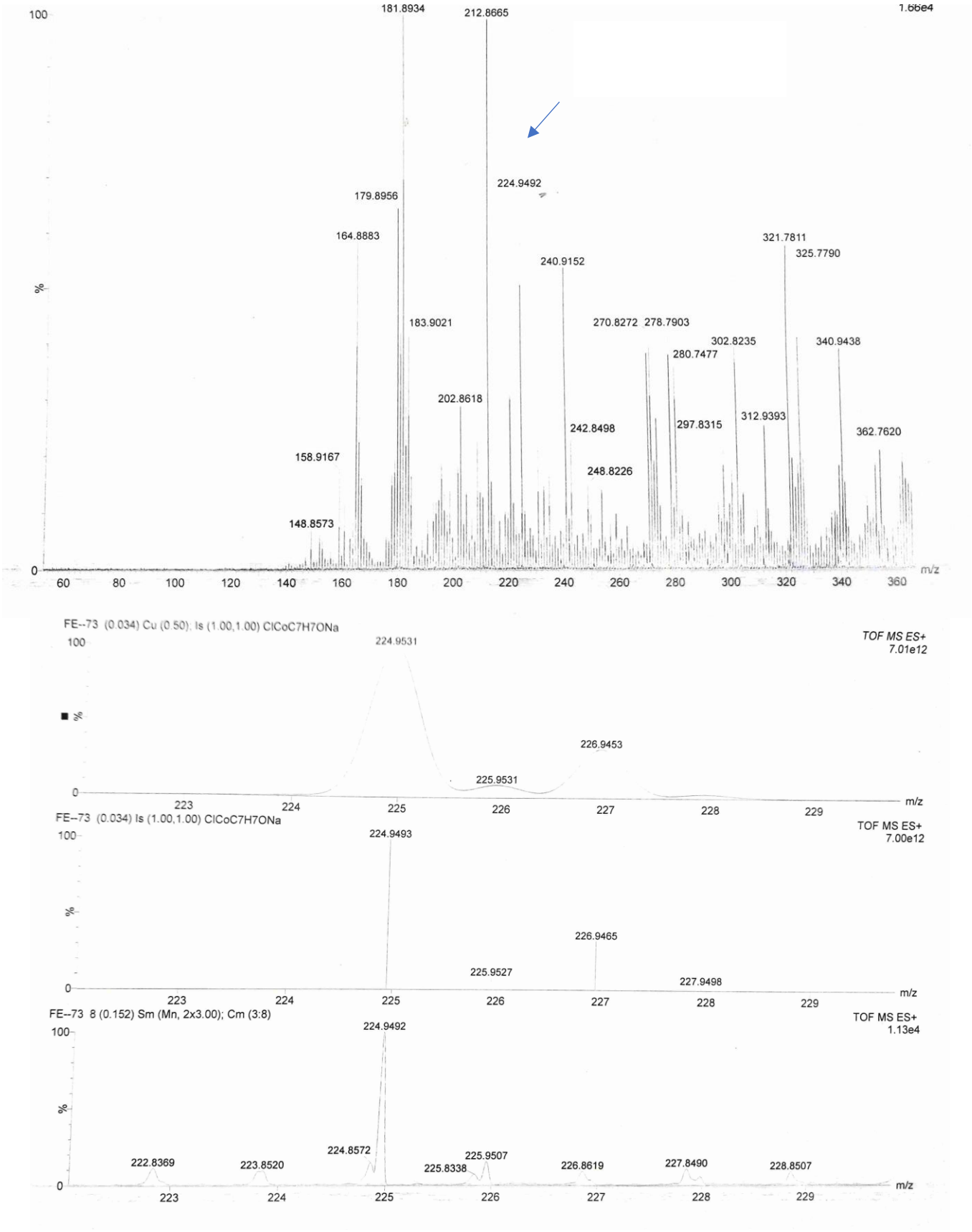

Figure 3.106. HRMS of the intermediate **D**.

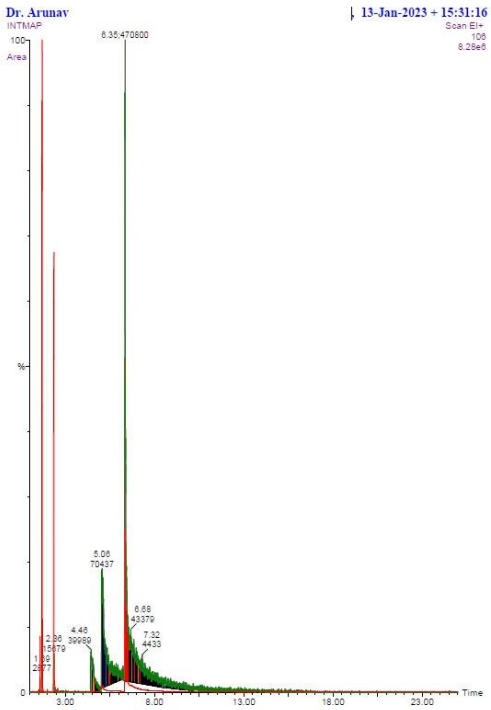

Figure 3.107. Gas Chromatogram of the benzaldehyde produced in the reaction between benzyl alcohol and $CoCl_2$ in presence of base KOH.

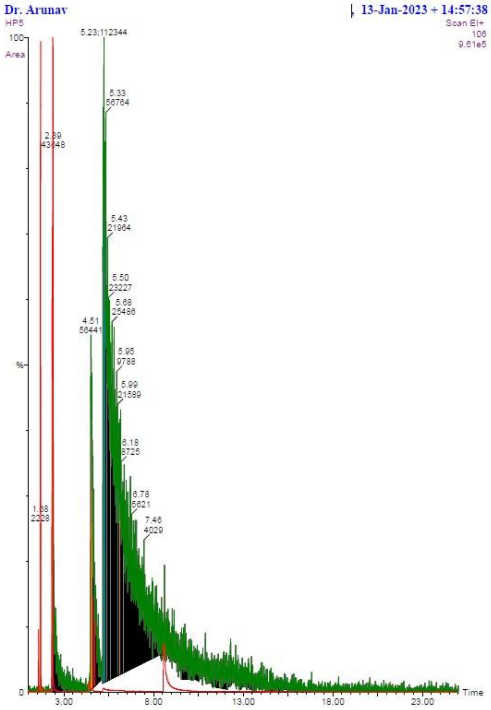

Figure 3.108. Gas Chromatogram of the benzaldehyde produced after the addition of aniline in the reaction mixture of **3a**.

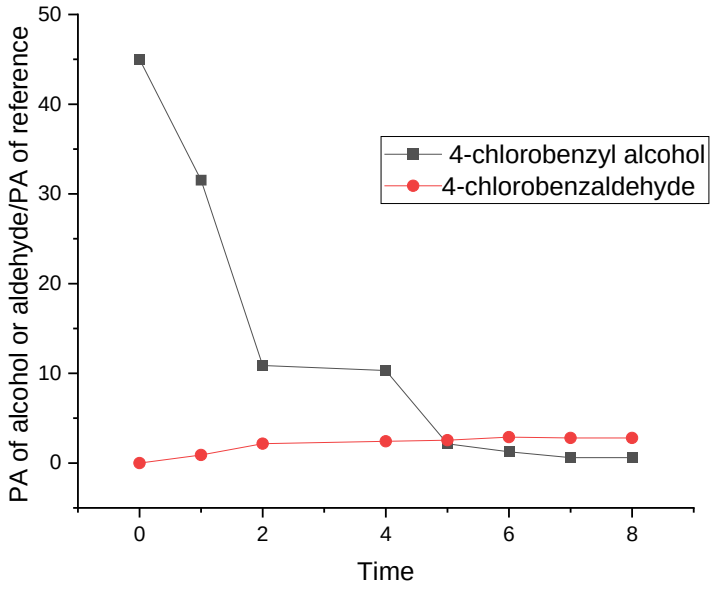

Figure 3.109. Equilibrium between 4-chlorobenzyl alcohol and its corresponding aldehyde obtained from GC. PA: Peak area.

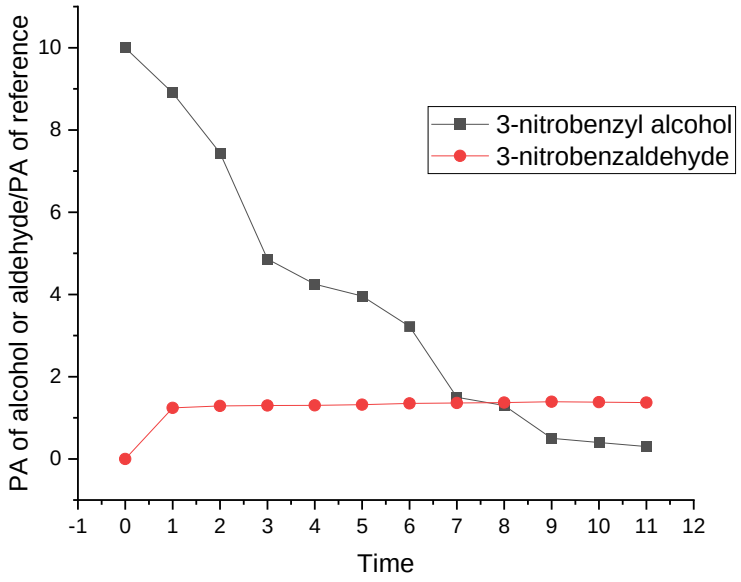

Figure 3.110. Equilibrium between 3-nitrobenzyl alcohol and its corresponding aldehyde obtained from GC. PA: Peak area.

Experimental Details for Kinetic Study:

Kinetic study was performed by taking the standard reaction of benzyl alcohol and *p*-anisidine. All the reactions were done by following the standard reaction protocol. Amount of product and reactant in each reaction was measured by gas chromatography using biphenyl as internal standard.

Now, both benzyl alcohol and *p*- anisidine were involved in the reaction. We can assume that rate of the reaction is only dependent on the concentration of benzyl alcohol and *p*- anisidine.

So, Rate = k.[benzyl alcohol]^x[*p*-anisidine]^y ……..(1)

[x = order with respect to benzyl alcohol; y = order with respect to *p*-anisidine; k = rate constant]

Determination of order with respect to *p*-anisidine:

Set	Amine	Alcohol	Base	$CoCl_2$	Toluene	Biphenyl
A	1.5 mmol	1.5 mmol	1.5 mmol	0.05 mmol	10 mL	1.5 mmol
B	1.75 mmol	1.5 mmol	1.5 mmol	0.05 mmol	10 mL	1.5 mmol

From the different sets of experiment (Set A and Set B) the following product formation plot was observed:

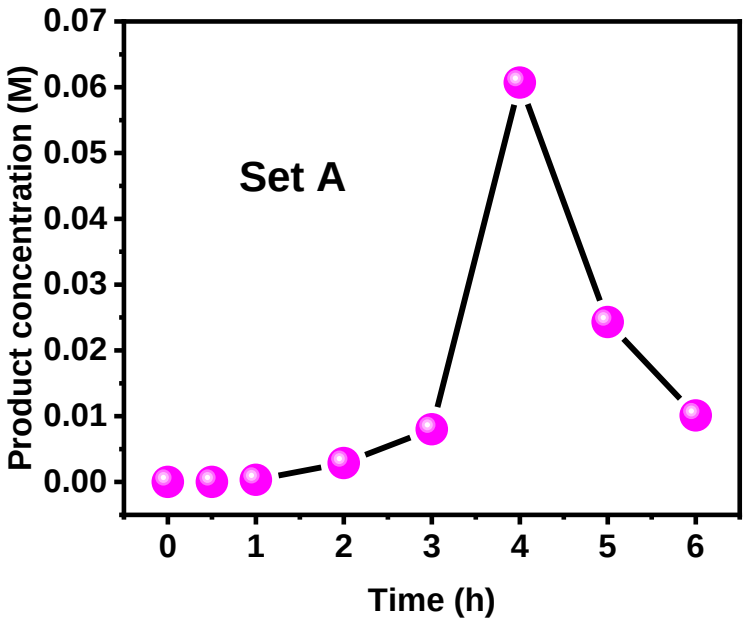

Figure 3.111. Product formation plot in Set A (amine = 1.5 mmol and benzyl alcohol 1.5 mmol).

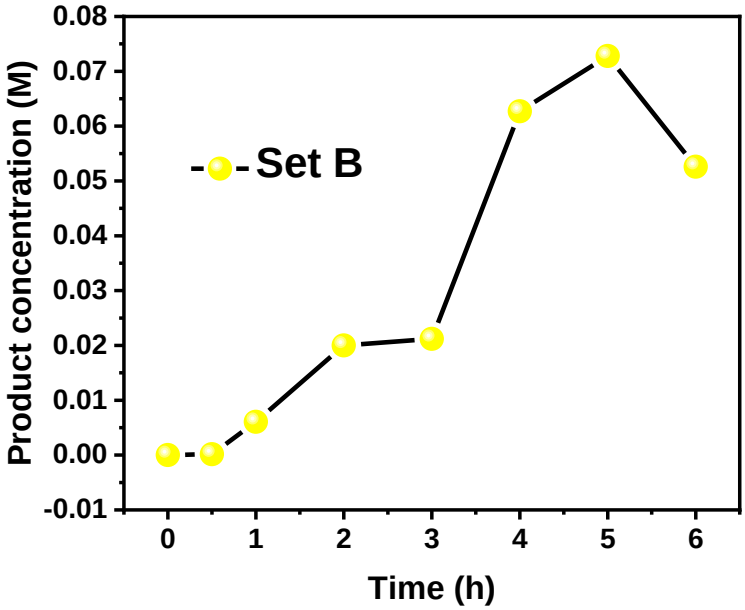

Figure 3.112. Product formation plot in Set B (amine = 1.75 mmol and benzyl alcohol 1.5 mmol).

From the equation (1) we got, Rate = k.[benzyl alcohol]^x[*p*-anisidine]^y

So, Rate 1 = k.[benzyl alcohol]^x[*p*-anisidine]^y

or, 1.33 = k.[1.5]^x[1.5]^y ……(2)

And, Rate 2= k.[benzyl alcohol]^x[*p*-anisidine]^y

or, 1.63 = k. [1. 5]^x[1.75]^y ……(3)

Hence, from equation (2) and (3) we get, [Rate 1/Rate 2] = [1.5 /1.75]^y

or, y = [log(Rate 1) - log(Rate 2)] / [log(1.5) - log(1.75)]

or, y = [log(1.33) – log(1.63)] / [log(1.5) – log(1.75)]

or, y = 1.00

So, order with respect to aniline derivatives is **~ 1.0**

Determination of order with respect to benzyl alcohol:

Set	Amine	Alcohol	Base	$CoCl_2$	Toluene	Biphenyl
C	1 mmol	1.75 mmol	1.5 mmol	0.05 mmol	10 mL	1 mmol
D	1 mmol	2 mmol	1.5 mmol	0.05 mmol	10 mL	1 mmol

From the different sets of experiment (Set A and Set B) the following product formation plot was observed:

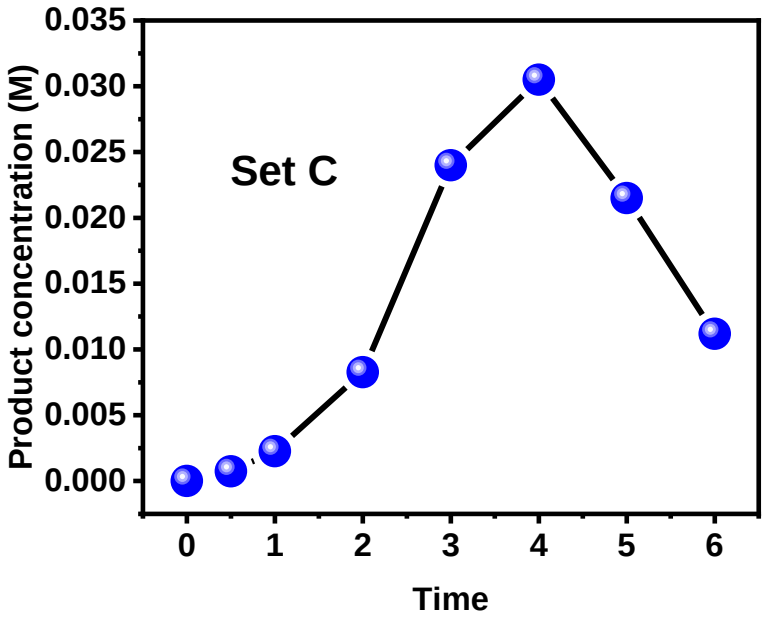

Figure 3.113. Product formation plot in Set C (amine = 1 mmol and benzyl alcohol 1.75 mmol).

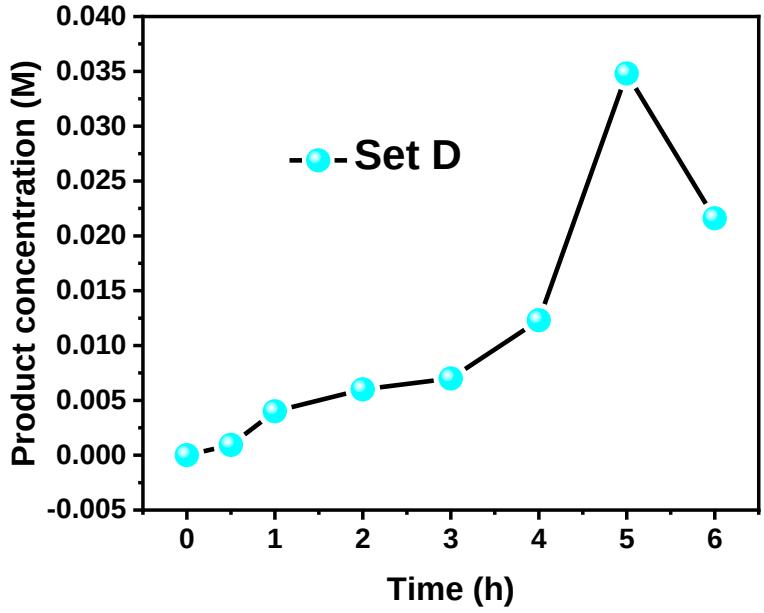

Figure 3.114. Product formation plot in Set D (amine = 1 mmol and benzyl alcohol 2 mmol).

From the equation (1) we got, Rate = k.[benzyl alcohol]^{x}[*p*-anisidine]^{y}

So, Rate 1 = k.[benzyl alcohol]^{x}[*p*-anisidine]^{y}

or, 1.48 = k.[1.75]^{x}[1]^{y} ……(2)

And, Rate 2= k.[benzyl alcohol]^{x}[*p*-anisidine]^{y}

or, 1.86 = k. [2]^{x}[1]^{y} …….(3)

Hence, from equation (2) and (3) we get, [Rate 1/Rate 2] = [1.75 /2]^{x}

or, y = [log(Rate 1) - log(Rate 2)] / [log(1.75) - log(2)]

or, y = [log(1.48) – log(1.86)] / [log(1.75) – log(2)]

or, y = 1.5~ 1.0

So, order with respect to benzyl alcohol derivatives is **~ 1.0**

Hammett Analysis of Aniline derivatives

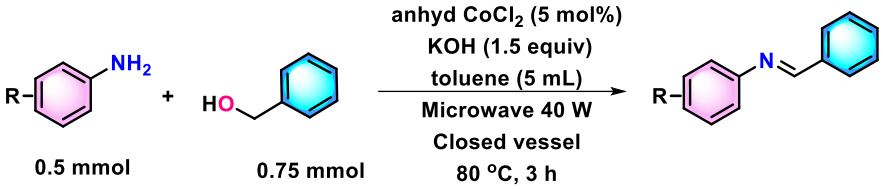

Procedure: All the reactions were done using the General Procedure in 0.5 mmol scale. The reactions were taken out after stipulated time and the consumption of aniline derivative was monitored using gas chromatography (GC) technique. The rate constants (k) were calculated using initial slope method with appropriate rate equation and order of the reactants.

Variable parameter: Substituents on aniline system.

R = H

Sr. No.	Time (h)	Conc. of aniline (M)
1	0	0.1
2	1	0.096
3	2	0.086
4	3	0.078
5	4	0.048
6	5	0.042

σ_{para} = 0

k_0 = 0.186

R = *p*-CH_3

Sr. No.	Time (h)	Conc. of aniline (M)
1	0	0.1
2	1	0.092
3	2	0.068
4	3	0.054
5	4	0.03
6	5	0.01

σ_{para} = -0.170

k = 0.438

log(k/k_0) = 0.372

R = *p*-OCH$_3$

Sr. No.	Time (h)	Conc. of aniline (M)
1	0	0.1
2	1	0.06
3	2	0.05
4	3	0.0166
5	4	0.00166
6	5	6.6E-4

σ_{para} = -0.268

k = 1.056

log(k/k$_0$) = 0.75

R = *p*-Cl

Sr. No.	Time (h)	Conc. of aniline (M)
1	0	0.1
2	1	0.098
3	2	0.078
4	3	0.058
5	4	0.056
6	5	0.054

σ_{para} = 0.227

k = 0.144

log(k/k$_0$) = -0.111

R = *p*-Br

Sr. No.	Time (h)	Conc. of aniline (M)
1	0	0.1
2	1	0.098
3	2	0.096
4	3	0.09
5	4	0.07
6	5	0.016

σ_{para} = 0.232

k = 0.29

log(k/k$_0$) = 0.192

R = *p*-F

Sr. No.	Time (h)	Conc. of aniline (M)
1	0	0.1
2	1	0.086
3	2	0.084
4	3	0.078
5	4	0.074
6	5	0.068

σ_{para} = 0.062

k = 0.07

log(k/k$_0$) = -0.424

R = *m*-Cl

Sr. No.	Time (h)	Conc. of aniline (M)
1	0	0.1
2	1	0.0998
3	2	0.097
4	3	0.094
5	4	0.0854
6	5	0.04

σ_{meta} = 0.373

k = 0.145

log(k/k$_0$) = -0.108

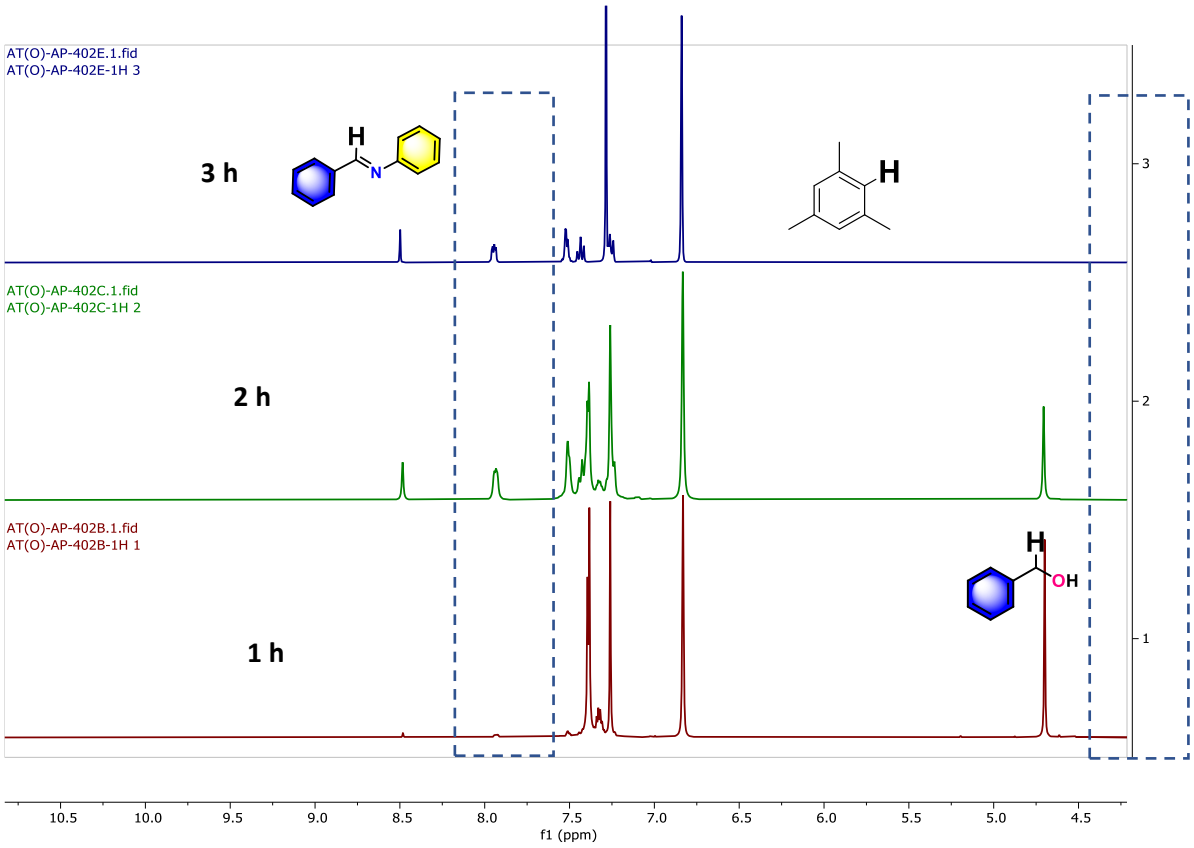

Figure 3.115. Monitoring the reaction between aniline (0.5 mmol scale) and benzyl alcohol under microwave reactor by ^{1}H NMR (300 MHz) spectra with mesitylene (2 equiv) as reference.

Preparation of deuterated benzyl alcohol:

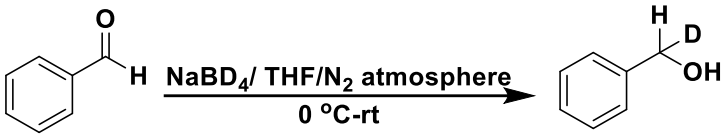

Deuterium incorporation experiment:

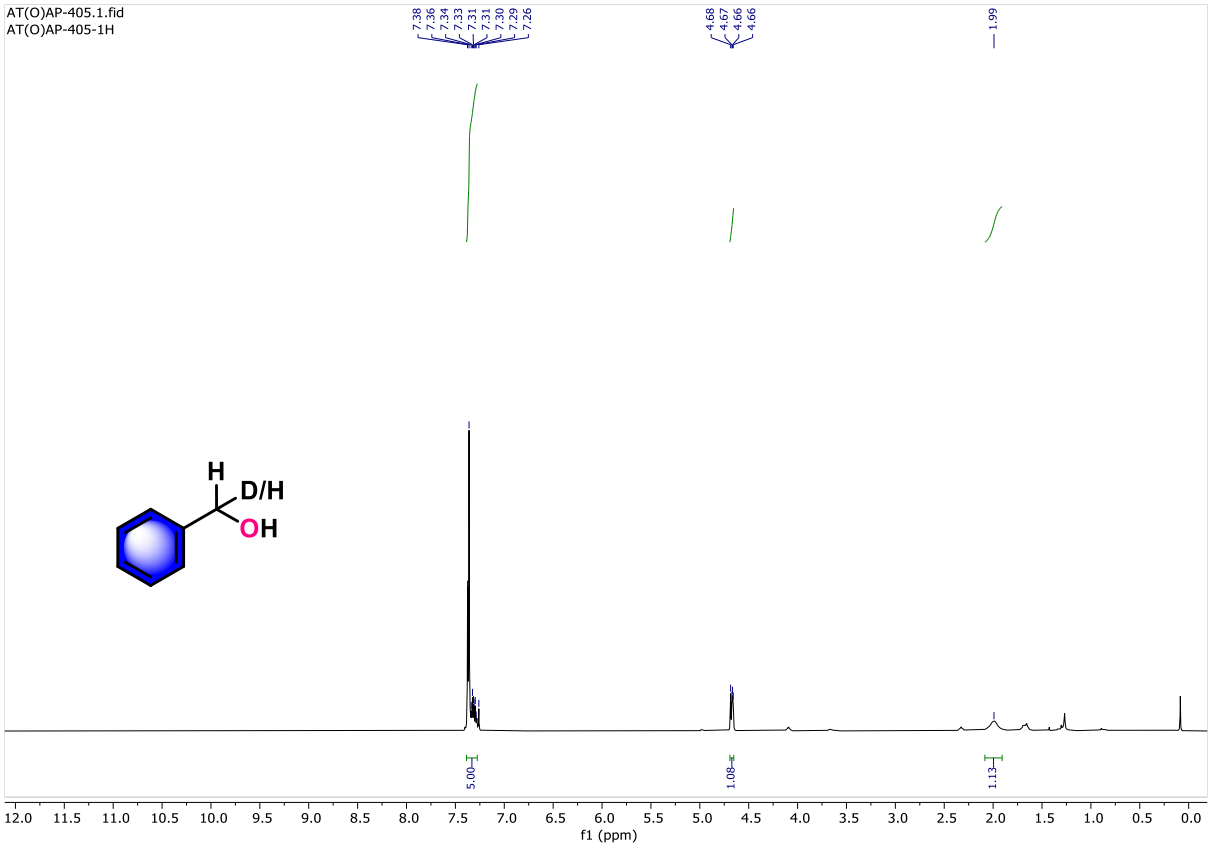

Figure 3.116. ^{1}H NMR (300 MHz) spectrum of deuterated benzyl alcohol.

For 100 % incorporation of D, 5 aromatic H corresponds to 1 alkyl H

Hence for 1.08 alkyl H, % incorporation of D is 92 %.

Kinetic isotope effect experiment:

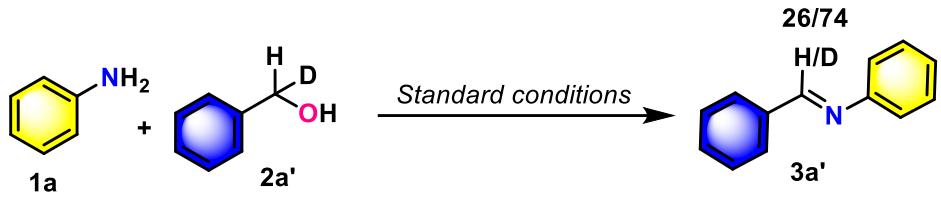

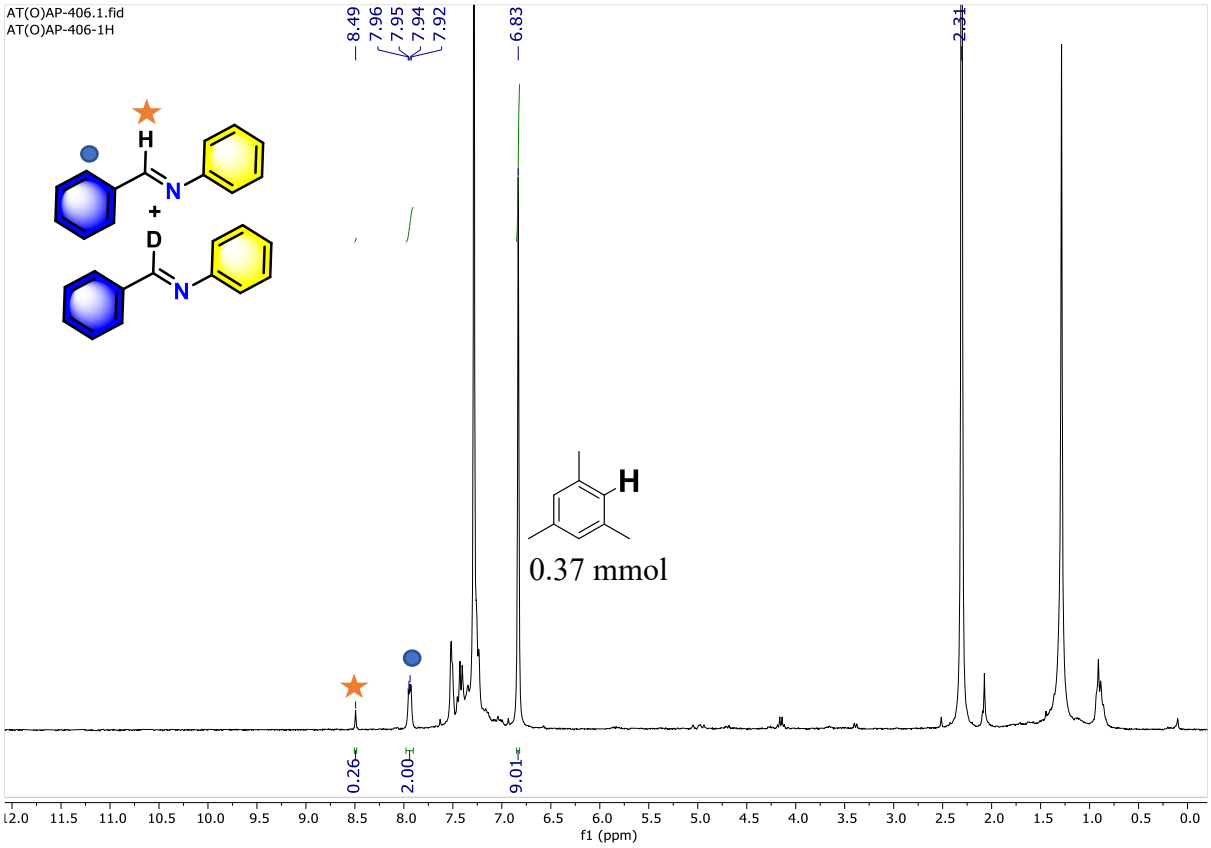

Figure 3.117. Kinetic isotope effect obtained from ^{1}H NMR (300 MHz) spectrum for the reaction between aniline and benzyl alcohol.

2 H in 7.94 ≡ 1 H in 8.49

Hydrogenated imine: Deuterated imine = 0.26: (1-0.26) = 0.26: 0.74 = 1 : 2.8

Kinetic isotope effect experiment:

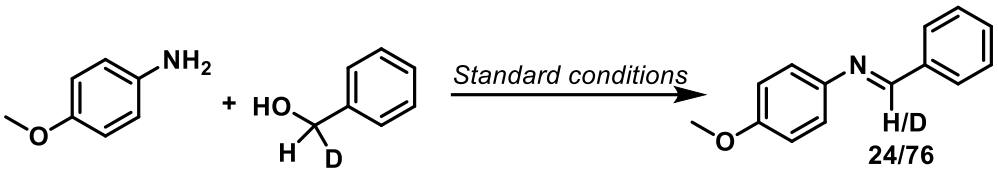

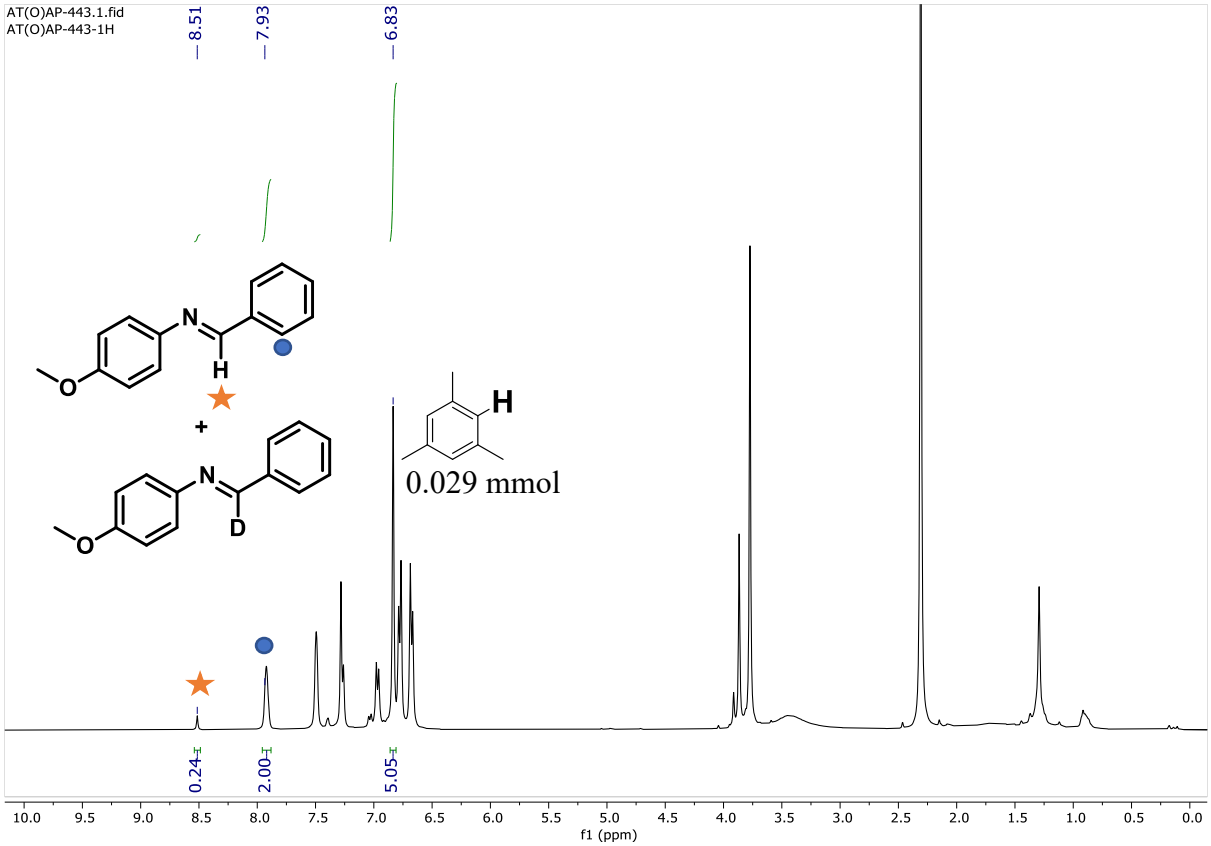

Figure 3.118. Kinetic isotope effect obtained from ^{1}H NMR (300 MHz) spectrum for the reaction between *p*-anisidine and benzyl alcohol.

2 H in 7.93 ≡ 1 H in 8.51

Hydrogenated imine: Deuterated imine = 0.24: (1-0.24) = 0.24: 0.76 = 1 : 3.16

Kinetic isotope effect experiment:

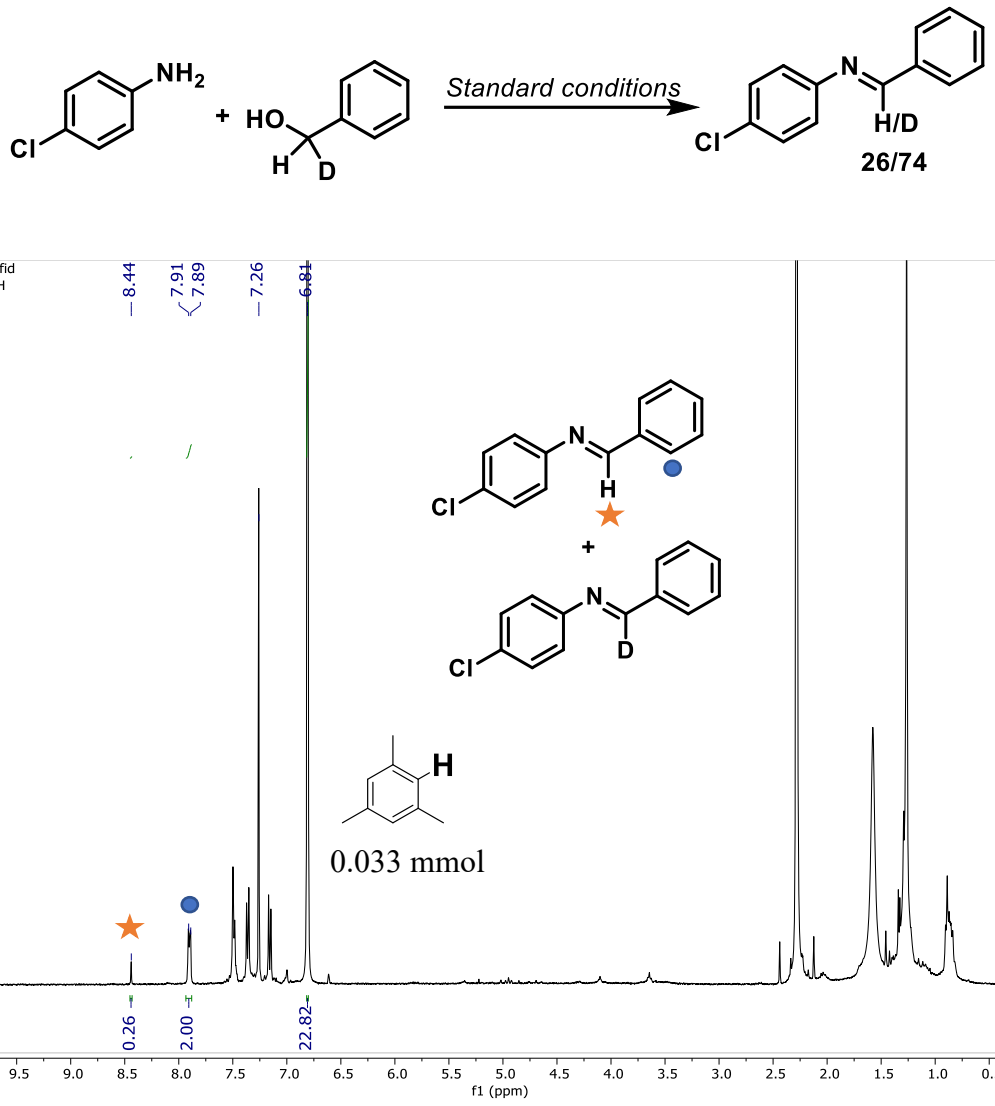

Figure 3.119. Kinetic isotope effect obtained from ^{1}H NMR (300 MHz) spectrum for the reaction between *p*-chloroaniline and benzyl alcohol.

2 H in 7.88 ≡ 1 H in 8.44

Hydrogenated imine: Deuterated imine = 0.26: (1-0.26) = 0.26: 0.74 = 1 : 2.8

Chapter 4

Co(II) acetate assisted direct synthesis of acyl hydrazones from acyl hydrazides under mild condition

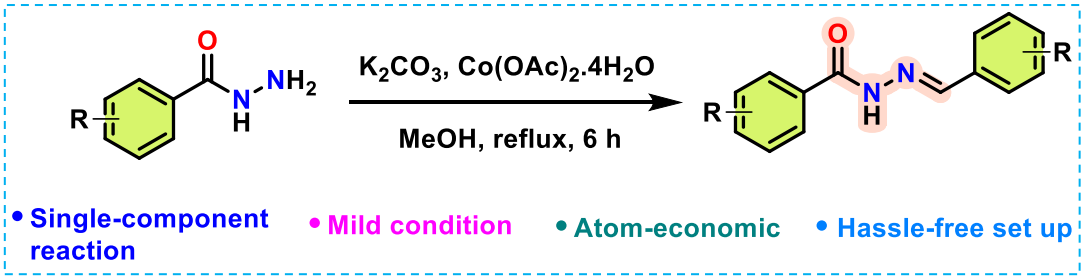

Representative Publication: *Chem. Asian J.* **2023**, *e202300755.*

4.1. Introduction

Hydrazones are an important class of nitrogenous organic substrates, which contain isomerizable C=N bond, just like imines, however, usually they are much more stable than imines.[1] The higher stability of hydrazones/acyl hydrazones has rendered them to be utilized in various fields of dynamic covalent chemistry.[2,3] For example, they are a common intermediate in the preparation of bioconjugates,[4,5] and they serve as excellent bi or tridentate (for acyl hydrazones) ligands in coordination chemistry.[6,7] This functionality also appears on several biologically active ingredients,[8,9] some of which are indicated in Figure 4.1.

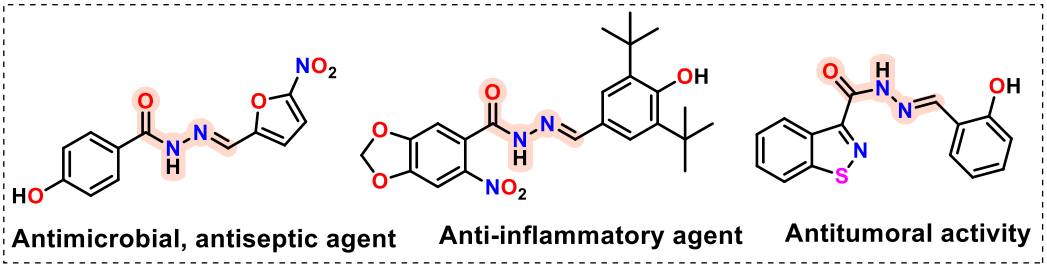

Figure 4.1 Some acyl hydrazones as potent bioactives.

In addition, the isomerization of acyl hydrazones along the C=N bond can give rise to functionally important molecular photoswitches and this can be modulated by the steric and electronic relation between the moieties on each side of the hydrazone core.[10] Acyl hydrazones are known to have several intriguing applications by virtue of their *E/Z* switching behavior,[11] like metalloselection and network switching process[11b] or information storage devices.[12] The *E/Z* switching behavior can best be realized by UV-vis spectra or ^{1}H NMR studies.

The synthesis of acyl hydrazones is known in the literature to occur *via* two-component reaction between an acyl hydrazide part and an aldehyde or ketone or styrene or alcohol under various reaction conditions (Scheme 4.1). In addition to two- components, the reactions also need external stimulus, like acid[13] (e.g. TFA), base[14] (e.g. pyrrolidine, aniline) or microwave irradiation[15] in order to make the reaction faster (Scheme 4.1a). Ding *et al.* reported a photocatalytic pathway using methylene blue and blue LED light to synthesize acyl hydrazones from acyl hydrazide and styrene (Scheme 4.1b).[16] Contemporary methodologies also use alcohols as a source of aldehydes, generated *in situ*, which then couple with acyl hydrazides when catalyzed by electrochemical means[17] or metal complexes like Fe/Ru complex[18] (Scheme 4.1c). All of these traditional and contemporary ways of acyl hydrazone synthesis rely on two reacting components, which often require special precautions, inert atmosphere, or prior

preparation of expensive catalysts or special reaction set-up (in case of photocatalysis). In contrast, a one-component methodology is atom-economic and much more convenient. It is known for a long time that acyl hydrazides can produce aldehydes in presence of base,[19] however, that methodology is not well-explored or utilized in modern-day synthesis of acyl hydrazones owing to the prolonged time of conversion (> 200 h). Hence, synthesis of acyl hydrazones, only from one-component, *i.e.*, acyl hydrazide may be achievable in presence of a base and an efficient catalyst.

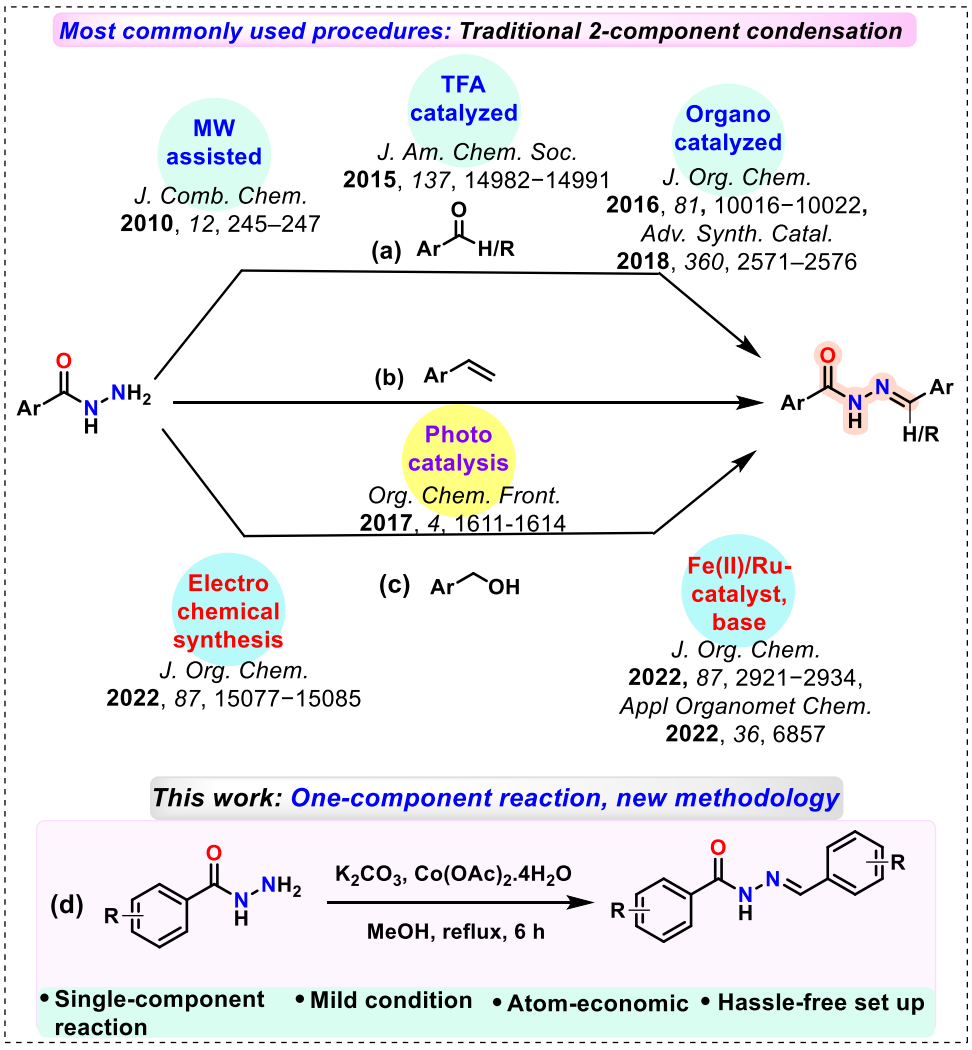

Scheme 4.1 Literature reported traditional two-component reaction *vs* our synthetic scheme on one-component reaction for the synthesis of acyl hydrazones.

Pertaining to our ongoing effort in developing low-cost Co-based catalysts in important organic transformations,[20] we have here explored an all-new chemistry of facile synthesis of

the acyl hydrazones using commercially available $Co(OAc)_2 \cdot 4H_2O$ as catalyst (Scheme 4.1d). To the best of our knowledge, this is the first report of one-component coupling of acyl hydrazides to transform into acyl hydrazones at a high conversion rate affording good to excellent yield of products under mild condition. This method involves a smaller number of reactants compared to the traditional two-component method, hence it is highly atom-economic and user-friendly to produce green by-products such as water and nitrogen gas. Furthermore, the reactions were carried out with earth-abundant metal salt as catalyst which is always desirable owing to increasing economic and environmental concerns. The reaction can also be successfully carried out to obtain good to excellent yield of product at a bulk scale and does not require any special sophisticated arrangements. We have also extended this methodology to heterocycles and aliphatic units to establish a broad generality of this method.

4.2. Results and Discussions:

With a view to explore *N*-methylation of acyl hydrazides by alcohol as methylating agent and commercially available low-cost and air-stable $Co(OAc)_2 \cdot 4H_2O$ as catalyst, we started our reaction taking the simplest acyl hydrazide (**3a**) as the model substrate and 5 mol % $Co(OAc)_2 \cdot 4H_2O$ and 1.5 equiv base K_2CO_3 in methanol and refluxed it for 12 h (Table 4.1 entry 1). The starting material was consumed in the reaction mixture; however, a mixture of products was formed, with no major one. Upon doubling the catalyst and base loading a single major product was formed with 100 % consumption of the starting material (Table 4.1 entry 3). The product was, however, not the *N*-methylated product, as expected, rather it was the acyl hydrazone derivative **4a** (as indicated in the schematic of Table 4.1, confirmed by NMR, HRMS and single crystal X-ray diffraction studies) occurred by coupling of two units of the same acyl hydrazide in a specific fashion. Variation in the solvent from methanol to ethanol to isopropanol to *tert*-butanol did vary the product yield, along with the formation of a number of side-products, however, the same acyl hydrazone product was found as the major product in each case (Table 4.1 entries 3-6). Variation of the base did not reproduce the same yields as earlier (Table 4.1 entries 7-9). With NaOEt base, a comparatively similar amount of product was obtained as with K_2CO_3 (Table 4.1, entry 10), however owing to the ease of availability and low-cost nature, K_2CO_3 was a more lucrative option. With organic bases like DBU or imidazole, the desired product was not detected at all (Table 4.1, entries 11, 12). Notably with $CoCl_2.6H_2O$ as catalyst, a minute amount of product was obtained (Table 4.1 entry 13) and with another

metal salt $CuCl_2.2H_2O$, the desired product was not formed (Table 4.1 entry 14). Upon reducing the time of reflux from 12 h to 6 h, the yield of product remained unaltered (90 %) (Table 4.1 entry 15), however upon further reducing it to 5 h the yield of product got reduced (80 %) (Table 4.1 entry 16). Reduction of reaction temperature also reduced the yields of product (Table 4.1 entries 17,18). Hence the optimized condition was found to be with catalyst $Co(OAc)_2 \cdot 4H_2O$ (10 mol %) and base K_2CO_3 (3 equiv) under reflux condition for 6 h (Table 4.1 entry 15). The successful completion of the reaction even in presence of ligating agent PMe_3 (0.2 equiv) or Hg(0) as catalyst poison (Table 4.1 entry 15) suggests that the reaction follows a homogeneous catalytic pathway. All the reactions were performed under aerobic atmosphere.

Table 4.1 Optimization of reaction conditions for transformation of acyl hydrazide to acyl hydrazone.[a]

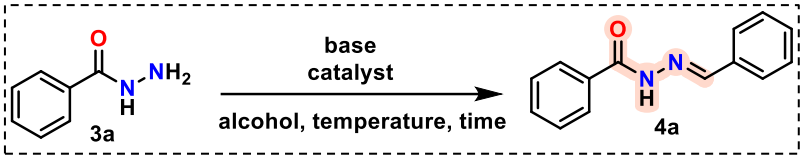

Entry	Catalyst (mole %)	Base (equiv) [b]	Solvent	Temp (°C)[c]	Time (h)	% yield[d]
1	$Co(OAc)_2.4H_2O$ (5)	K_2CO_3 (1.5)	MeOH	reflux	12	< 10
2	$Co(OAc)_2.4H_2O$ (10)	K_2CO_3 (1.5)	MeOH	reflux	12	50
3	$Co(OAc)_2.4H_2O$ (10)	K_2CO_3 (3)	MeOH	reflux	12	90
4	$Co(OAc)_2.4H_2O$ (10)	K_2CO_3 (3)	EtOH	reflux	12	50
5	$Co(OAc)_2.4H_2O$ (10)	K_2CO_3 (3)	Isopropanol	reflux	12	70
6	$Co(OAc)_2.4H_2O$ (10)	K_2CO_3 (3)	^{t}BuOH	reflux	12	65
7	$Co(OAc)_2.4H_2O$ (10)	KOH (1)	MeOH	reflux	12	65
8	$Co(OAc)_2.4H_2O$ (10)	NaOH (1)	MeOH	reflux	12	60
9	$Co(OAc)_2.4H_2O$ (10)	Na_2CO_3(3)	MeOH	reflux	12	50
10	$Co(OAc)_2.4H_2O$ (10)	NaOEt (3)	MeOH	reflux	12	70
11	$Co(OAc)_2.4H_2O$ (10)	DBU (3)	MeOH	reflux	12	ND
12	$Co(OAc)_2.4H_2O$ (10)	Imidazole (3)	MeOH	reflux	12	ND
13	$CoCl_2.6H_2O$ (10)	K_2CO_3 (3)	MeOH	reflux	12	10
14	$CuCl_2.2H_2O$ (10)	K_2CO_3 (3)	MeOH	reflux	12	ND

15	**$Co(OAc)_2.4H_2O$ (10)**	**K_2CO_3 (3)**	**MeOH**	**reflux**	**6**	**90, 88[e]**
16	$Co(OAc)_2.4H_2O$ (10)	K_2CO_3 (3)	MeOH	reflux	5	80
17	$Co(OAc)_2.4H_2O$ (10)	K_2CO_3 (3)	MeOH	50	6	75
18	$Co(OAc)_2.4H_2O$ (10)	K_2CO_3 (3)	MeOH	40	6	60

[a] The reactions were performed taking **3a** (0.5 mmol). [b] Equivalence taken with respect to substrate. [c] All the reactions, which require refluxing, have been performed under aerial conditions with reflux condenser and heating in oil bath. [d] Isolated yield by column chromatography. [e] PMe_3 (0.2 equiv) or Hg(0) was added in the reaction. ND: not detected.

The generalization of this methodology has been explored with a range of substrates containing activating/deactivating substituents (Table 4.2). A total of 22 substrates, were explored with this methodology. Acyl hydrazide derivatives containing activating groups, such as, 2/3/4-methyl (**3b-d**), 4-methoxy (**3e**), 3,4-dimethoxy (**3f**), and 3,5-dimethoxy (**3g**) produced good yields of products (**4b-4g**). Acyl hydrazides, where a strong electron- donating group is present as substituent, tend to produce the corresponding amide derivative. For example, for acyl hydrazides with 4-amino and 2-hydroxy derivatives, the desired acyl hydrazone derivatives were not obtained by this methodology, rather the corresponding amide derivatives were obtained as the major product. It can be the mixed effect of electron-donation and presence of acidic H (N*H* or O*H*) that hamper the mechanism containing base, giving the undesired product. To ascertain this, reactions with 3-amino, 4-hydroxy and 2-thiol substituents were also performed and they too did not produce the desired product(s) as well. This result imply that the presence of acidic hydrogen is discordant with this optimized reaction condition, regardless of their position with respect to the acyl group in the aromatic ring. With 4-dimethoxymethyl group (**3h**), product (**4h**) was obtained seamlessly with a high yield (92 %). Substrates with deactivating groups such as chloro, bromo, iodo, fluoro, nitro and trifluoromethyl groups (**3i-3q**) all gave good to excellent yield of desired products (**4i-4q**). Steric hindrance did not play much of a role in this type of reaction, as can be observed from the yields of 2-bromo (**4k**), 2-iodo (**4m**) derivatives. However, for diacyl hydrazides, the poor solubility of the compounds in methanol, or any other alcoholic solvent, poses a great problem in carrying out reactions with them. The geometrical configuration of the acyl hydrazone derivatives is confirmed to be *E*-selective from single crystal X-ray diffraction analysis of **4a** (Table 2). However, for *ortho*-substituted products (**4b**, **4i**, **4k**), there may be presence of both syn and anti-periplanar *E* isomers,[21] evolved as a result of rotation around the C(O)-NH bond, as can be observed from

the duplicity in signals (not necessarily in the ratio of 1:1) in the ^{1}H NMR spectra. This was not the co-existence of *E* and *Z* isomers, rather the two conformational stages of the molecule which is more evident for *ortho*-substituted products owing to the steric crowding around the C-N, leading to more bond rotation in order to gain stability. The rotational barrier for the two rotamers (*syn* and *anti*-periplanar) is easily surpassed at 27 ˚C for most of the derivatives.[22] The coexistence of *syn* and *anti*-periplanar configurations can only be detected by ^{1}H NMR by duplicity of signals, and not by UV-vis spectroscopy or HPLC. Interestingly, for bulky substituent like *ortho*-iodo (as in **4m**), the rotational barrier is too high to be surpassed at room temperature, such that, no duplicity in ^{1}H NMR signal was obtained, indicating the presence of only one rotamer in the solution at room temperature. This rendered us to investigate more into the configurational stability and the *E* to *Z* and *vice versa* switching behavior in presence of lights of different wavelengths by spectrophotometric methods (*vide infra*). The successful reactions of acyl hydrazides motivated us to explore more into other substrates like heterocycles and aliphatic chains. The thiophene hydrazides (**3r**, **3s**) reacted well under the optimized condition giving the desired products (**4r**, **4s**) (Table 4.2).

However, the aliphatic chains like the hydrazides obtained from capric acid (**3t**), myristic acid (**3u**) and palmitic acid (**3v**) reacted in a different way giving the corresponding homocoupled amide derivatives in all the cases (**4t**-**v**) (Table 4.3).[19] This is possibly because of more electrophilic character of the carbonyl carbon in aliphatic hydrazides rather than aromatic ones, such that the lone pair of N attacks the carbonyl carbon in aliphatic unit readily and gives the corresponding homo-coupled product after elimination of a hydrazine unit.[23]

A methodology is useful in practical sense when it can be reproduced in an industrial scale. Hence, we have explored the applicability of this methodology in large (gram) scale. Gram-scale synthesis of compounds **4a, 4d** and **4j** (Scheme 4.2) was accomplished under the optimized standard reaction conditions and the isolated yields were found to be 80, 75 and 82 % respectively. The applicability of the synthesized hydrazone core was explored synthetically by further reacting it under various conditions to achieve functionally important products or cores (Scheme 4.2). For example, *N*-propargylation of the amide N was done by using propargyl bromide in presence of base and the product (**5**) was further utilized for a [3+2] cycloaddition reaction between the terminal alkyne and azidomethylferrocene, catalyzed by $CuSO_4$ and sodium ascorbate to obtain a new product **6**. The *N*-propargylated product **5** has the potential to be utilized in several other reactions owing to the terminal alkyne unit. Another modification

was done by a ring-formation reaction where an oxadiazole ring was prepared directly from the acyl hydrazone product by microwave irradiation in presence of $KMnO_4$.

Table 4.2 Substrate scope of acylhydrazone formation from acyl hydrazides.[a]

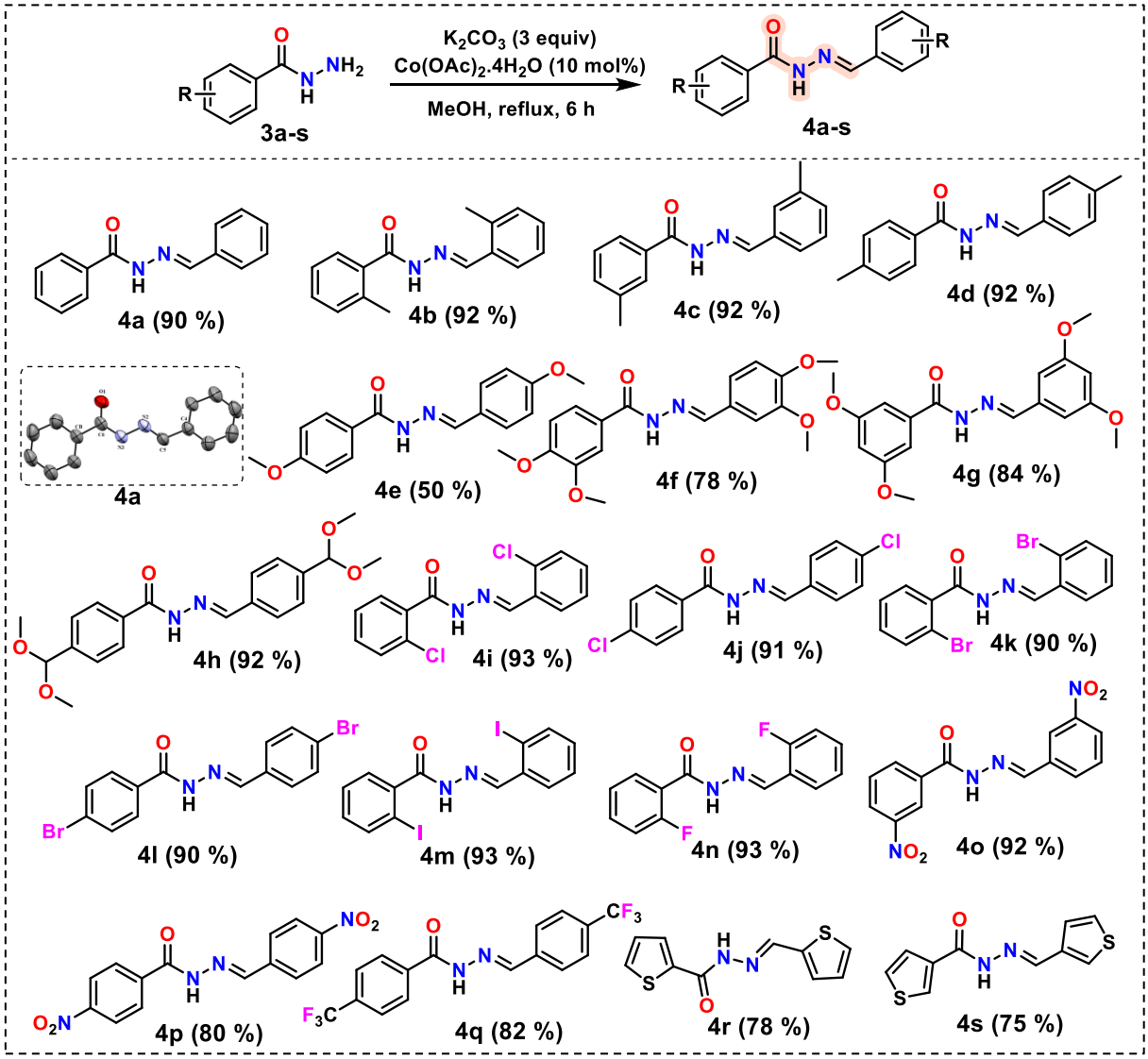

[a]Reaction condition: Table 1 entry 15, 1 mmol scale. Isolated yields are obtained after column chromatography.

Table 4.3 Substrate scope of reaction in aliphatic frameworks.[a]

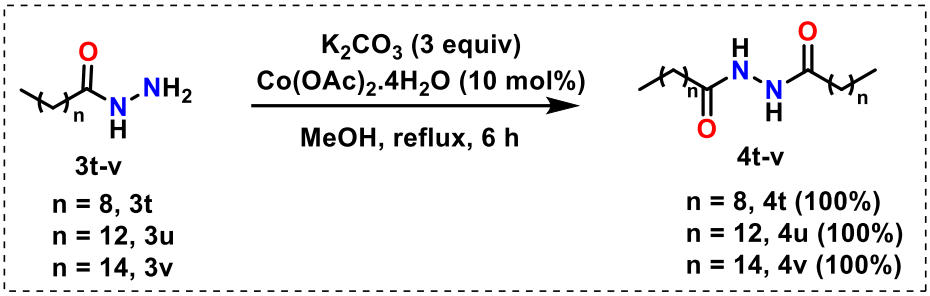

[a] Reaction condition: Table 1 entry 15, 1 mmol scale. Isolated yields are obtained after column chromatography.

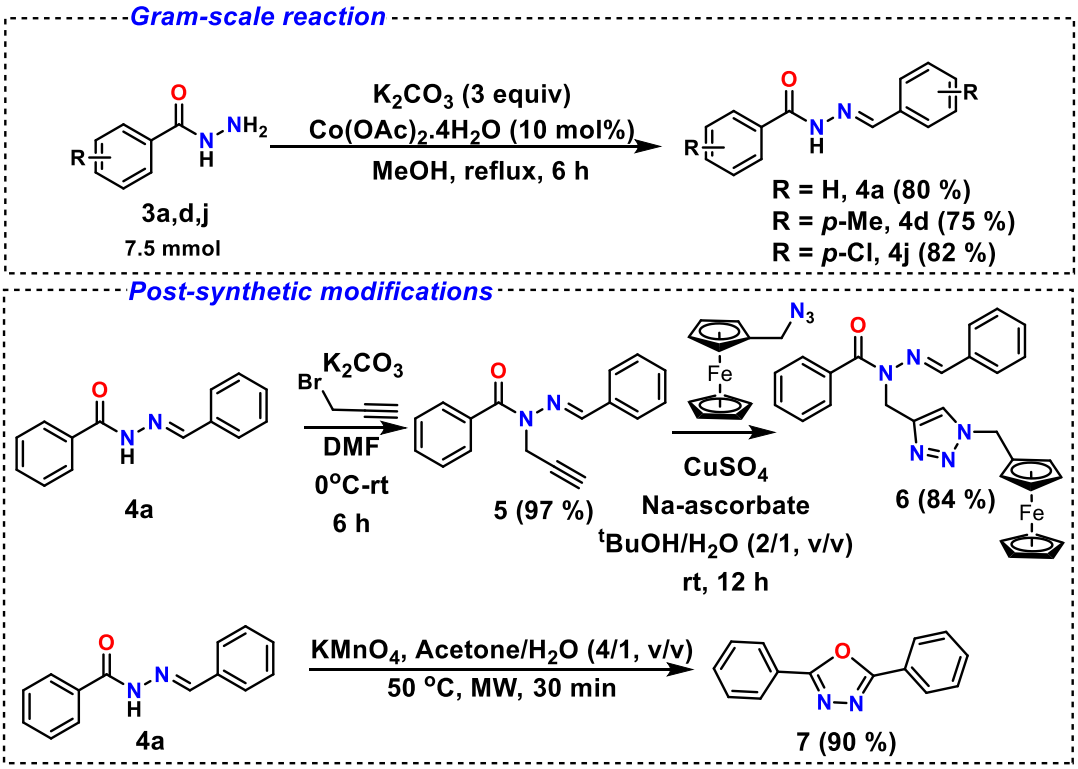

Scheme 4.2 Gram-scale reactions and post-synthetic modifications from acylhydrazone **4a**.

Apart from the synthetic utility as a core for bioactive compounds, these acyl hydrazone derivatives can also serve as tunable photoswitches owing to their reversible *E*/*Z* isomerization around the C=N bond upon alternatively shining UV lights of proper wavelength. Each compound has its unique optimum wavelength of light for *E*/*Z* switching. For example, when 2-methyl derivative **4b** in CH_3CN (1.5×10^{-5} M) was irradiated with 254 nm UV light gradually up to 25 minutes (Figure 4.2a), the absorption band of *E*-isomer at 290.5 nm ($\varepsilon = 5.11 \times 10^4$ lit mol^{-1} cm^{-1}) got slightly blue shifted to 283.3 nm ($\varepsilon = 3.61 \times 10^4$ lit mol^{-1} cm^{-1}) along with diminishing absorption intensity which corroborated with the formation of the *Z* isomer.

Appearance of clear isosbestic point at 261.7 nm signifies the equilibrated transition among the two isomers. Similar studies were conducted with compounds **4i** and **4h**. In **4i** (CH_3CN, 3.33 $\times 10^{-5}$ M), the absorption band of *E*-isomer at 290.5 nm ($\varepsilon = 3.65\times10^4$ lit mol^{-1} cm^{-1}) shifted to that of *Z* isomer at 283.9 nm ($\varepsilon = 2.39\times10^4$ lit mol^{-1} cm^{-1}) after irradiation of 254 nm light gradually for 35 minutes, along with the appearance of isosbestic point at 260.6 nm (Figure 4.2b). For 4h, there exists two absorption bands at 293.7 nm ($\varepsilon = 5.24\times10^4$ lit mol^{-1} cm^{-1}) and 225.3 nm ($\varepsilon = 4.82\times10^4$ lit mol^{-1} cm^{-1}) for the *E* isomer. Upon irradiating by 254 nm light gradually up to 20 minutes, the absorption intensity at 293.7 nm was diminished and slightly blue-shifted to 292.8 nm ($\varepsilon = 4.21\times10^4$ lit mol^{-1} cm^{-1}), with a slight red shift (1.02 nm) in the 225.02 nm peak (Figure 4.2c). The *E* isomer was regenerated from the *Z* isomer of **4h** by irradiating with 365 nm light for 10 minutes (Figure 2d). The *E* to *Z* isomerization was also realized by HPLC studies, where the retention times of *E* isomers of **4b**, **4h**, and **4i** at 5.61, 5.58, and 6.53 min shifted to 5.51, 5.61 and 6.45 min respectively after irradiation with 254 nm light (Figure 4.3). The change is very subtle for this *E*/*Z* isomerization, as realized by HPLC.

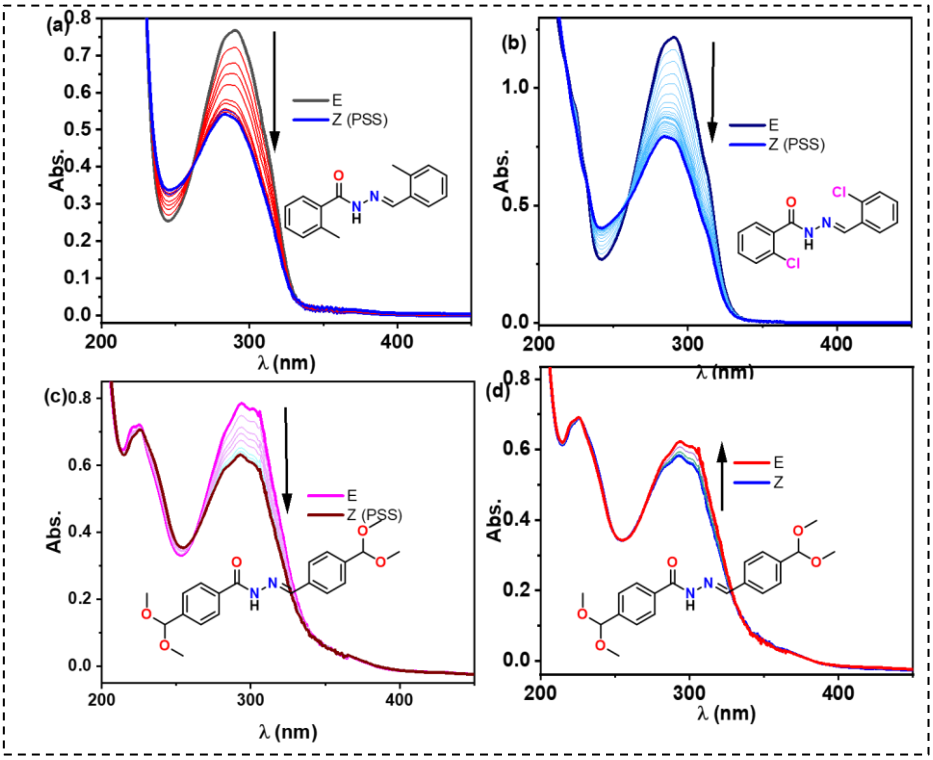

Figure 4.2 (a) *E* to *Z* isomerization of (E)-2-methyl-*N*'-(2-methylbenzylidene)benzohydrazide **4b** by UV light (254 nm), (b) *E* to *Z* isomerization of (*E*)-2-chloro-*N*'-(2-chlorobenzylidene) benzohydrazide **4i** by UV light (254 nm), (c) *E* to *Z* isomerization of (*E*)-4-(dimethoxymethyl)-*N*'-(4-(dimethoxymethyl)benzylidene) benzohydrazide **4h** by UV light (254 nm), (d) *Z* to *E*

isomerization of (*E*)-4-(dimethoxymethyl)-*N*'-(4-(dimethoxymethyl) benzylidene) benzohydrazide **4h** by UV light (365 nm), detected by UV-vis spectroscopy.

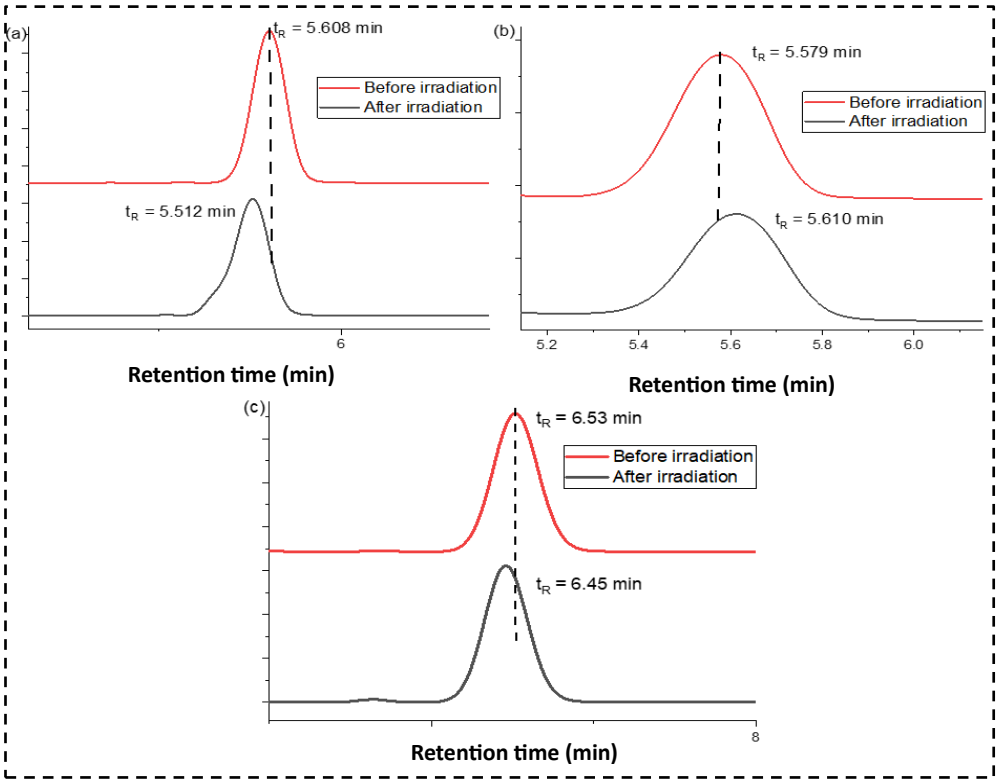

Figure 4.3 HPLC of compound (a) **4b**, (b) **4h** and (c) **4i** dissolved in MeOH and eluted in MeOH:H_2O (7:3, v/v).

To shed light on the reaction mechanism, a series of controlled experiments were conducted. The reaction of **3a** was repeated in identical conditions separately without base and without catalyst and it was found that in both cases, product **4a** was obtained in minute amount. This indicates the requirement of both the base and catalyst for the completion of the reaction at a quicker pace (Scheme 4.3(i)). The reaction mixture of **3a** under standard conditions with both base and catalyst was investigated at different time intervals by GC. The presence of benzaldehyde was detected after 1.5 h of reaction (Scheme 4.3(ii)), however, could not be detected after longer hours. This observation suggests that a part of the hydrazide molecules undergo dissociation to give benzaldehyde, which is expected to be the reaction intermediate. To investigate the involvement of metal catalyst in the condensation step as well, a reaction between **3a** and commercially available benzaldehyde was carried out in presence and absence of $Co(OAc)_2 \cdot 4H_2O$ (Scheme 4.3(iii)), wherefrom product formation was detected at the same rate in both the cases. This excludes the catalytic association of $Co(OAc)_2 \cdot 4H_2O$ in the condensation step. Speculating about an involved radical pathway, the reaction of **3a** was

performed under standard conditions in presence of radical scavenger 2,2,6,6-tetramethyl-1-piperidinyloxy (TEMPO) and butylated hydroxytoluene (BHT), from which the product 4a was obtained in undiminished yield (89 %). This indicates that no radical mechanism is involved in the whole reaction (Scheme 4.3(iv)) mechanism.

Taking inference from the controlled reactions and literature reports, the most probable mechanism (Scheme 4.4) is suggested to be such that K_2CO_3 induces the deprotonation of the NH_2 group, which then ligates the Co-centre by neutral O and anionic NH groups and hence the Co changes from Co(II) to Co(III) in ligated form. This Co-ligated acyl hydrazide species in presence of base, transforms into benzaldehyde (by the elimination of N_2), and regenerates the Co(II) catalyst. This *in situ* generated benzaldehyde (detected by GCMS) undergoes condensation with another molecule of acyl hydrazide to generate the corresponding acyl hydrazone derivative.

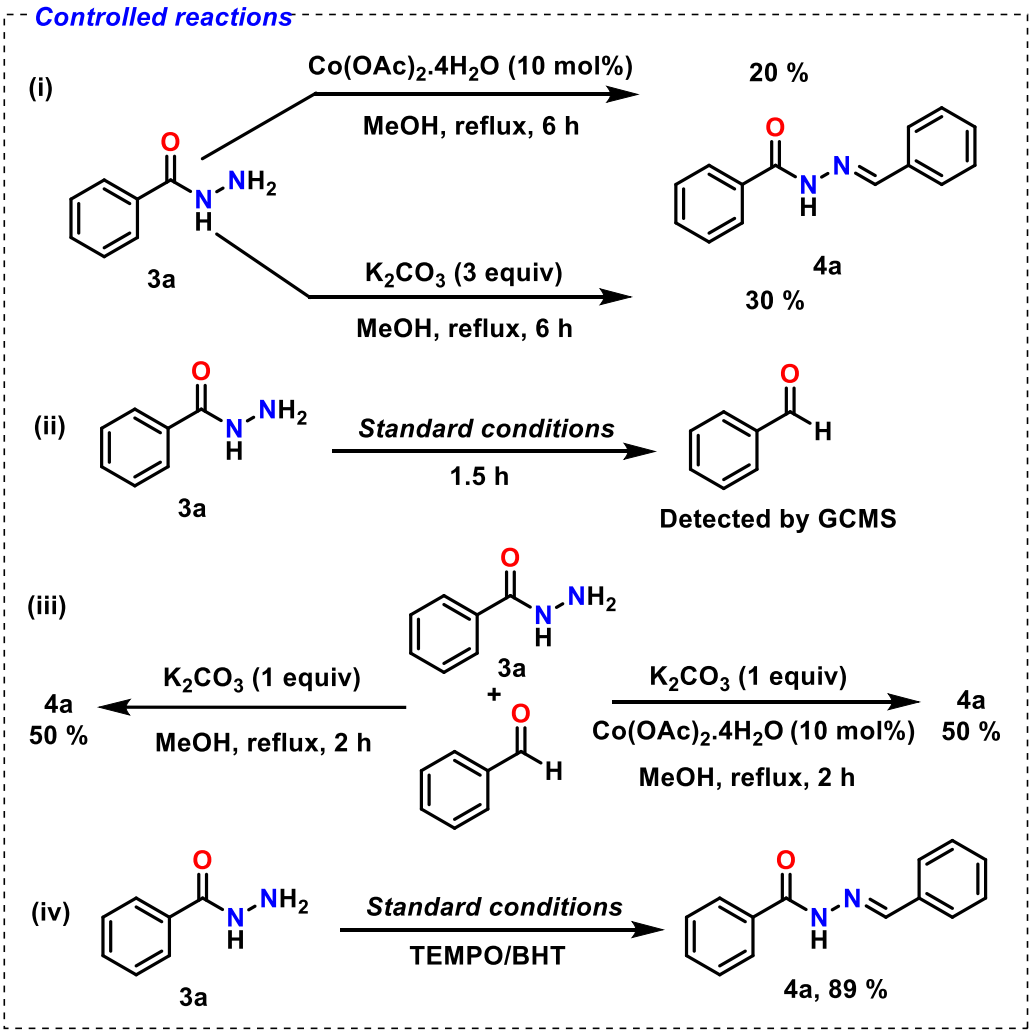

Scheme 4.3 Controlled experiments to determine the mechanism of reaction.

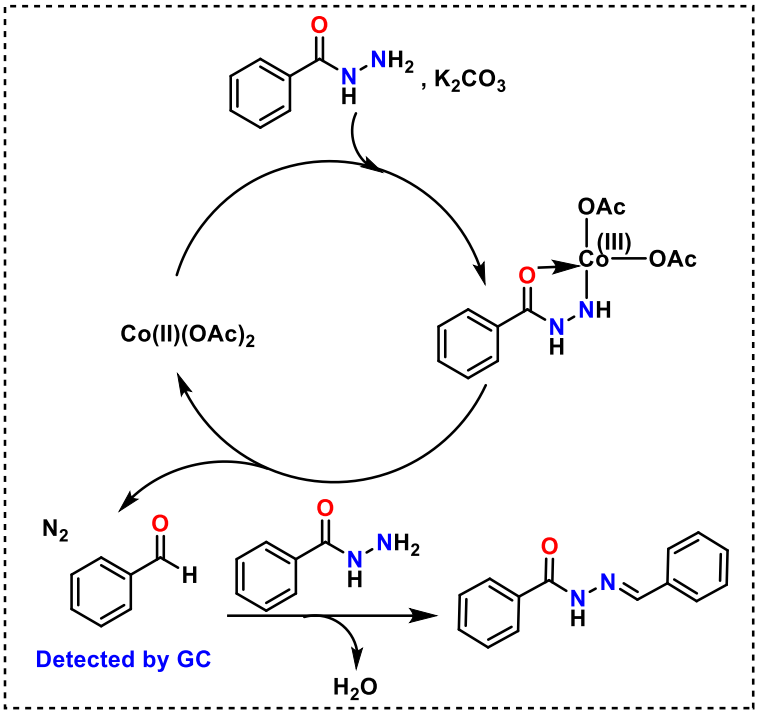

Scheme 4.4 Plausible mechanism of hydrazone formation reaction.

4.3. Conclusion

In conclusion, we have developed an easy-to-use and sustainable one-pot methodology catalyzed by commercially available $Co(OAc)_2 \cdot 4H_2O$ salt where acyl hydrazone derivatives can directly be synthesized in excellent yields from acyl hydrazides without the need for another component to be coupled. The reaction proceeds under mild conditions and exhibits a wide substrate scope. Further useful synthetic modification for the synthesis of *N*-heterocycles has also been demonstrated with the resulting acyl hydrazone derivatives. With respect to the wide utility of the resulting hydrazone products as synthetic intermediates and ligating species in coordination chemistry, this new environmentally benign methodology can serve as a practically hassle-free and atom-economic technique for acyl hydrazones. A pronounced application of the acyl hydrazone derivatives is the modulation of its *E/Z* switchability, which has been explored and may be useful to construct organic molecular photoswitches.

4.4. Experimental section:

4.4.1. Materials and reagents

Commercially available methanol has been used for reaction without further distillation. $Co(OAc)_2 \cdot 4H_2O$ and K_2CO_3 were purchased from Spectrochem and used directly for reaction. All the commercially available carboxylic acid derivatives were used directly without further

purification. TEMPO, BHT and PMe_3 were purchased from Sigma Aldrich. Analytical thin layer chromatography (TLC) was performed on pre-coated silica gel 60 F_{254}. Visualization on TLC was achieved with UV light (254 nm). Column Chromatography was carried out using silica gel as the stationary phase.

4.4.2. Instrumentation

^{1}H and ^{13}C NMR spectra were obtained with BRUKER 300 MHz and 400 MHz FT-NMR spectrometers and the chemical shifts are reported in ppm, using tetramethylsilane as an internal standard and were referenced to the residual solvent as follows: $CDCl_3$ = 7.26 (^{1}H), 76.16 (^{13}C) ppm, DMSO = 2.51 (^{1}H), 39.50 (^{13}C) at room temperature. For ^{1}H NMR, coupling constants *J* are given in Hz and the resonance multiplicity is described as s (singlet), d (doublet), t (triplet), m (multiplet), dd (doublet of doublet), dt (doublet of triplet), td (triplet of doublet), tt (triplet of triplet), q (quartet) br s (broad singlet). ^{13}C NMR spectra were fully decoupled by broadband proton decoupling. High-resolution mass spectra (HRMS) were obtained from Waters (Xevo G2 Q-TOF) mass spectrometer in electrospray ionization mode (ESI+), CHN analysis was performed on a CHNS analyser. GC studies of the reaction mixture were obtained from PerkinElmer Gas Chromatograph Clarus 590. CEM microwave reactor was used for microwave reaction. For reactions under heating, oil bath was used.

4.4.3. General procedure for the preparation of acyl hydrazones from carboxylic acid derivatives:

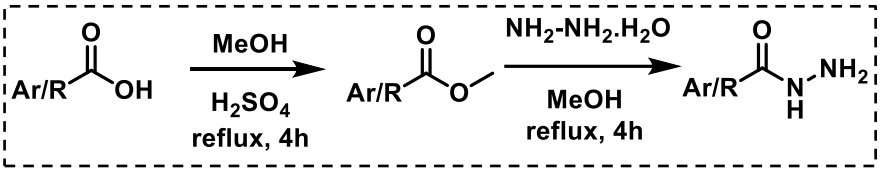

In a round-bottomed flask, carboxylic acid derivatives (1 mmol) were dissolved in MeOH (8 mL) and catalytic amount of H_2SO_4 was added. The reaction mixture was refluxed for 4 h and water was added to the reaction mixture after cooling it. The ester derivative was extracted by washing with EtOAc (3×20 mL) and the mixed organic layer was washed with brine, dried under Na_2SO_4 and solvent evaporated. To this ester derivative, hydrazine hydrate (6 mmol) and MeOH (8 mL) were added and the reaction mixture was refluxed for 4h. Then, water was added to the reaction mixture, stirred well and the organic layer was extracted with EtOAc (3×20 mL). The combined organic layers was washed with brine and dried under Na_2SO_4. The crude product was purified by column chromatography with silica gel as the stationary phase and EtOAc as the mobile phase.

4.4.4. General procedure for the preparation of acyl hydrazones from acyl hydrazides: In a round-bottomed flask, acyl hydrazide (1 mmol), K_2CO_3 (3 mmol), and $Co(OAc)_2 \cdot 4H_2O$ (0.10 mmol) were mixed in methanol (6 mL) at room temperature. The round-bottomed flask was attached with a reflux condenser and the temperature of the reaction mixture was allowed to rise in an oil bath and the refluxing condition was maintained for 6 h. After 6 h, water was added to the reaction mixture, stirred well and the organic layer was extracted with EtOAc (3×20 mL). The combined organic layers was washed with brine and dried under Na_2SO_4. The crude product was purified by column chromatography with silica gel as the stationary phase and 20-50 % EtOAc in hexane as the mobile phase.

4.4.5. Gram-Scale reaction: In a round-bottomed flask, acyl hydrazide **3a**/**3d**/**3j** (7.5 mmol), K_2CO_3 (22.5 mmol), and $Co(OAc)_2.4H_2O$ (0.75 mmol) were mixed in methanol (50 mL) at room temperature. The round-bottomed flask was attached with a reflux condenser and the temperature of the reaction mixture was allowed to rise in an oil bath and the refluxing condition was maintained for 6 h. After 6 h, water was added to the reaction mixture, stirred well and the organic layer was extracted with EtOAc (3×20 mL). The combined organic layers was washed with brine and dried under Na_2SO_4. The crude product was purified by column chromatography with silica gel as the stationary phase and 10-50 % EtOAc in hexane as the mobile phase, which produced products **4a**, **4d** and **4j** in 80, 75 and 82 % yields respectively.

4.4.6. Homogeneity test for the catalytic reaction: In a round-bottomed flask, acyl hydrazide (1 mmol), K_2CO_3 (3 mmol), and $Co(OAc)_2.4H_2O$ (0.10 mmol) were mixed in methanol (6 mL) at room temperature. The ligating agent PMe_3 (0.2 equiv, 0.2 mmol) was then added and the vessel was refluxed for 6 h. The reaction mixture was tested by TLC, where it was observed that the product was formed with 100% conversion of starting material.

4.4.7. Controlled reactions: (i) Without base: In a round-bottomed flask, acyl hydrazide **3a** (1 mmol), and $Co(OAc)_2 \cdot 4H_2O$ (0.10 mmol) were mixed in methanol (6 mL) at room temperature. The round-bottomed flask was attached with a reflux condenser and the temperature of the reaction mixture was allowed to rise in an oil bath and the refluxing condition was maintained for 6 h. After 6 h, water was added to the reaction mixture, stirred well and the organic layer was extracted with EtOAc (3×20 mL). The combined organic layers was washed with brine and dried under Na_2SO_4. The crude product was purified by column chromatography with silica gel as the stationary phase and 20% EtOAc in hexane as the mobile phase to obtain **4a** in 20 % yield.

(ii) Without catalyst: In a round-bottomed flask, acyl hydrazide **3a** (1 mmol), and K_2CO_3 (3 mmol) were mixed in methanol (6 mL) at room temperature. The round-bottomed flask was attached with a reflux condenser and the temperature of the reaction mixture was allowed to rise in an oil bath and the refluxing condition was maintained for 6 h. After 6 h, water was added to the reaction mixture, stirred well and the organic layer was extracted with EtOAc (3×20 mL). The combined organic layers was washed with brine and dried under Na_2SO_4. The crude product was purified by column chromatography with silica gel as the stationary phase and 20% EtOAc in hexane as the mobile phase to obtain **4a** in 30 % yield.

(iii) Benzaldehyde detection: In a round-bottomed flask, acyl hydrazide **3a** (1 mmol), K_2CO_3 (3 mmol), and $Co(OAc)_2{\cdot}4H_2O$ (0.10 mmol) were mixed in methanol (6 ml) at room temperature. The round-bottomed flask was attached with a reflux condenser and the temperature of the reaction mixture was allowed to rise in an oil bath and the refluxing condition was maintained for 1.5 h, after which an aliquot was taken directly from the reaction mixture, diluted with EtOAc and examined by GCMS for the presence of benzaldehyde intermediate.

(iv) Condensation step: In a round-bottomed flask, acyl hydrazide **3a** (1 mmol), benzaldehyde (1 mmol), K_2CO_3 (3 mmol), and $Co(OAc)_2{\cdot}4H_2O$ (0.10 mmol) and were mixed in methanol (6 mL) at room temperature. In another round-bottomed flask, acyl hydrazide **3a** (1 mmol), benzaldehyde (1 mmol) and K_2CO_3 (2 mmol) were mixed in methanol (6 mL) at room temperature. Both the flasks were attached with reflux condensers and heated under refluxing conditions. TLC was examined at each hour up to 6 h, during which it was observed that the rate of formation of product **4a** in both conditions is same.

(v) Radical pathway: Acyl hydrazide **3a** (136 mg, 1 mmol), K_2CO_3 (414 mg, 3 mmol), $Co(OAc)_2{\cdot}4H_2O$ (24.9 mg, 0.1 mmol), and TEMPO (468.75 mg, 3 mmol) or BHT (661 mg, 3 mmol) were dissolved in methanol (15 mL) in a round-bottomed flask and was refluxed for 6 h. Water was then added to the reaction mixture and the reaction mixture extracted with EtOAc (2×15 mL). The organic layer was dried under Na_2SO_4 and evaporated and the obtained crude was examined in TLC. Product was formed (85 %) without any hindrance.

4.4.8. Post-synthetic modifications: (a) *N*-propargylation: The procedure was adapted from literature report.[24] To a stirred solution of acyl hydrazone **4a** (224 mg, 1 mmol) in DMF, K_2CO_3 (3 mmol) was added at 0 ˚C and stirred for 30 minutes. Propargyl bromide was then added dropwise at 0 ˚C and the reaction mixture was stirred for 6 h allowing the temperature of reaction mixture to rise to room temperature. After completion of reaction, water (20 mL) was added to the reaction mixture and the product was extracted by ethyl acetate (3×20 mL). The

combined organic layers were washed with brine, dried over Na_2SO_4 and evaporated to dryness. The crude product was purified by column chromatography using silica gel (100-200 mesh) bed and 10 % EtOAc in hexane as the eluant to obtain the pure product **5** (0.97 mmol, 254 mg).

(b) Click Reaction: In a round-bottomed flask, compound **5** (200 mg, 0.76 mmol) and monoazidomethylferrocene (183 mg, 0.76 mmol) were taken and dissolved in 10 mL ^{t}BuOH. $CuSO_4.5H_2O$ (73 mg, 0.456 mmol) and sodium ascorbate (181 mg, 0.912 mmol) were dissolved in 2.5 mL water separately and added to the reaction vessel successively. The resulting reaction mixture was allowed to stir for 6 h, after which water (10 mL) was added to the reaction mixture. The product was extracted by ethyl acetate (3×20 mL). The combined organic layers were washed with brine, dried over Na_2SO_4 and evaporated to dryness. The crude product was purified by column chromatography using silica gel (100-200 mesh) bed and 50 % EtOAc in hexane as the eluant to obtain the pure product **6** (0.64 mmol, 321 mg) as pale-yellow solid.

(c) Oxadiazole: This reaction was done according to literature reported procedure.[25] Compound **4** (100 mg, 0.45 mmol) and $KMnO_4$ (211.4 mg, 1.34 mmol) were dissolved in 5 mL acetone /water (4/1, *v/v*) and transferred to a teflon vessel. The vessel was reacted in microwave reactor at 50 ˚C for 30 min under closed-vessel system. Then, water (10 mL) was added to the reaction mixture and the product was extracted by dichloromethane (3×10 mL). The combined organic layers were washed with brine, dried over Na_2SO_4 and evaporated to dryness. The crude product was purified by column chromatography using silica gel (100-200 mesh) bed and 5 % EtOAc in hexane as the eluant to obtain the pure product **7** (0.405 mmol, 90 mg) as white solid.

4.4.9. UV-vis studies: 1.5×10^{-5} M solutions of the products were prepared in CH_3CN for recording UV-Vis spectra at 22 ˚C.

4.4.10. HPLC studies: Compounds were dissolved in methanol to prepare a 10^{-3} M solution and the solution used for elution was methanol:water (7:3, *v/v*) at 22 ˚C. Irradiation for 30 mins was done taking solution in quartz cuvette.

4.5. Analytical data of all synthesized compounds

(*E*)-*N'*-benzylidenebenzohydrazide (**4a**)[26]: White solid (isolated yield ~ 90%, 101 mg), ^{1}H NMR (400 MHz, DMSO-d_6): δ = 11.85 (s, 1H), 8.46 (s, 1H), 7.92 (d, *J* = 6 Hz, 2H), 7.74 (d, *J* = 6 Hz, 2H), 7.60 (t, *J* = 6 Hz, 1H), 7.53 (t, *J* = 6 Hz, 2H), 7.46 (d, *J* = 6 Hz, 3H). $^{13}C\{^{1}H\}$ NMR (100 MHz, DMSO-d_6): δ = 163.3, 147.9, 134.4, 133.4, 131.9, 130.2, 128.9, 128.6, 127.7, 127.2. ESI-MS: calcd. for $C_{14}H_{12}N_2O$ $[M+Na]^+$ = 247.0847, found 247.0847.

(*E*)-2-methyl-*N*′-(2-methylbenzylidene)benzohydrazide (**4b**): White solid (isolated yield ~ 92%, 115 mg), ^{1}H NMR (400 MHz, DMSO-d_6): δ = 11.71 (s, 1H), 11.70 (s, 0.35H) 8.60 (s, 1H), 8.30 (s, 0.34H), 7.85 (dd, J_1 = 6 Hz, J_2 = 3Hz, 1H), 7.46-7.38 (m, 2H), 7.33-7.24 (m, 7H), 7.20-7.12 (m, 1H), 2.41 (s, 3H), 2.39 (s, 3H), 2.25 (s, 1H), 2.21 (s, 1H). ^{13}C{^{1}H} NMR (100 MHz, DMSO-d_6): δ = 165.1, 146.1, 143.1, 136.8, 135.9, 135.2, 132.2, 130.9, 130.6, 129.9, 129.7, 127.4, 126.2, 125.8, 125.6, 19.3, 18.9. ESI-MS: calcd. for $C_{16}H_{16}N_2O$ $[M+Na]^+$ = 275.1160, found 275.1161.

(*E*)-3-methyl-*N*′-(3-methylbenzylidene)benzohydrazide (**4c**): White solid (isolated yield ~ 92%, 116 mg), ^{1}H NMR (400 MHz, DMSO-d_6): δ = 11.78 (s, 1H), 8.41 (s, 1H), 7.74-7.71 (m, 2H), 7.56 (s, 1H), 7.50 (d, *J* = 12 Hz, 1H), 7.40 (d, *J* = 4 Hz, 2H), 7.35 (t, J_1 = 12 Hz, J_2 = 8 Hz, 1H), 7.25 (d, *J* = 12 Hz, 1H), 2.39 (s, 3H), 2.36 (s, 3H). ^{13}C{^{1}H} NMR (100 MHz, DMSO-d_6): δ = 165.9, 163.2, 147.7, 138.1, 137.8, 134.3, 132.3, 130.8, 128.7, 128.4, 128.1, 127.3, 124.8, 124.5, 21.0, 20.9.

(*E*)-4-methyl-*N*′-(4-methylbenzylidene)benzohydrazide (**4d**): White solid (isolated yield ~ 92%, 115.7 mg), ^{1}H NMR (400 MHz, DMSO-d_6): δ = 11.71 (s, 1H), 8.41 (s, 1H), 7.81 (d, *J* = 12 Hz, 2H), 7.61 (d, *J* = 12 Hz, 2H), 7.32 (d, *J* = 12 Hz, 2H), 7.27 (d, *J* = 8 Hz, 2H), 2.38 (s, 3H), 2.34 (s, 3H). ^{13}C{^{1}H} NMR (100 MHz, DMSO-d_6): δ = 163.0, 147.7, 141.8, 139.9, 131.7, 130.6, 129.5, 129.1, 127.7, 127.1, 114.9, 21.1.

(*E*)-4-methoxy-*N*′-(4-methoxybenzylidene)benzohydrazide (**4e**)[27]: White solid (isolated yield ~ 50%, 71 mg), ^{1}H NMR (400 MHz, DMSO-d_6): δ = 11.59 (s, 1H), 8.38 (s, 1H), 7.88 (d, *J* = 8 Hz, 2H), 7.66 (d, *J* = 12 Hz, 2H), 7.03 (q, J_1 = 8 Hz, J_2 = 4 Hz, 4H), 3.83 (s, 3H), 3.80 (s, 3H). ^{13}C{^{1}H} NMR (100 MHz, DMSO-d_6): δ = 162.4, 161.9, 160.7, 147.1, 129.4, 128.6, 127.0, 125.6, 114.3, 113.7, 55.4, 55.3.

(*E*)-*N*′-(3,4-dimethoxybenzylidene)-3,4-dimethoxybenzohydrazide (**4f**)[28]: White solid (isolated yield ~ 78%, 134.1 mg), ^{1}H NMR (400 MHz, DMSO-d_6): δ = 11.84 (s, 1H), 8.40 (s, 1H), 7.56 (d, *J* = 8 Hz, 1H), 7.50 (s, 1H), 7.45 (s, 1H), 7.18 (d, *J* = 4 Hz, 1H), 7.05 (d, *J* = 12 Hz, 1H), 7.01 (d, *J* = 8 Hz, 1H), 3.81 (s, 6H), 3.80 (s, 6H). ^{13}C{^{1}H} NMR (100 MHz, DMSO-d_6): δ = 163.4, 152.1, 151.1, 149.4, 148.7, 148.4, 127.5, 125.6, 122.4, 121.5, 111.8, 111.5, 111.2, 108.9, 56.1, 56.0, 56.0, 55.9.

(*E*)-*N*′-(3,5-dimethoxybenzylidene)-3,5-dimethoxybenzohydrazide (**4g**): White solid (isolated yield ~ 84%, 144.5 mg), ^{1}H NMR (400 MHz, $CDCl_3$): δ = 9.22 (s, 1H), 8.20 (s, 1H), 6.93 (d, *J* = 20 Hz, 4H), 6.62 (t, *J* = 4 Hz, 1H), 6.51 (t, *J* = 4 Hz, 1H), 3.84 (s, 6H), 3.82 (s, 6H). ^{13}C{^{1}H} NMR (100 MHz, DMSO-d_6): δ = 170.4, 160.8, 160.5, 148.1, 136.4, 135.4, 105.7, 105.0, 103.6,

102.4, 59.8, 55.6, 55.4. Anal. Calcd for $C_{18}H_{20}N_2O_5$, C, 62.78; H, 5.85; N, 8.13. Found: C, 62.55; H, 5.88; N, 8.01.

(*E*)-4-(dimethoxymethyl)-*N*′-(4-(dimethoxymethyl)benzylidene)benzohydrazide (**4h**): White solid (isolated yield ~ 92%, 171.3 mg), ^{1}H NMR (400 MHz, $CDCl_3$): δ = 9.46 (s, 1H), 8.35 (s, 1H), 7.86 (s, 2H), 7.75 (s, 2H), 7.55 (d, *J* = 4 Hz, 2H), 7.47 (d, *J* = 8 Hz, 2H), 5.44 (s, 1H), 5.40 (s, 1H). ^{13}C{^{1}H} NMR (100 MHz, $CDCl_3$): δ = 164.0, 148.5, 142.4, 140.7, 133.9, 127.8, 127.7, 127.3, 102.8, 102.5, 52.9, 52.8. ESI-MS: calcd. for $C_{20}H_{24}N_2O_5$ $[M+Na]^+$ = 395.1583, found 395.1585.

(*E*)-2-chloro-*N*′-(2-chlorobenzylidene)benzohydrazide (**4i**)[29]: White solid (isolated yield ~ 93%, 136 mg), ^{1}H NMR (400 MHz, DMSO-d_6): δ = 12.19 (s, 1H), 8.68 (s, 0.66 H), 8.44 (s, 0.34 H), 8.06-8.03 (m, 1H), 7.60-7.52 (m, 3H), 7.49-7.45 (m, 3H), 7.35 (d, *J* = 12 Hz, 1H). ^{13}C{^{1}H} NMR (100 MHz, DMSO-d_6): δ = 168.8, 162.6, 144.0, 140.3, 135.7, 135.0, 133.3, 133.0, 131.7, 131.6, 131.3, 131.2, 130.7, 130.4, 129.9, 129.9, 129.8, 129.8, 129.3, 129.0, 128.8, 127.7, 127.5, 127.3, 127.0, 126.9, 126.2.

(*E*)-4-chloro-*N*′-(4-chlorobenzylidene)benzohydrazide (**4j**)[30]: White solid (isolated yield ~ 91%, 133 mg), ^{1}H NMR (400 MHz, DMSO-d_6): δ = 12.0 (s, 1H), 8.44 (s, 1H), 7.94 (d, *J* = 12 Hz, 2H), 7.76 (d, *J* = 12 Hz, 2H), 7.61 (d, *J* = 12 Hz, 2H), 7.53 (d, *J* = 8 Hz, 2H). ^{13}C{^{1}H} NMR (100 MHz, DMSO-d_6): δ = 162.1, 146.8, 136.7, 134.6, 133.2, 132.0, 129.6, 129.0, 128.8, 128.6.

(*E*)-2-bromo-*N*′-(2-bromobenzylidene)benzohydrazide (**4k**)[31]: White solid (isolated yield ~ 90%, 172 mg), ^{1}H NMR (400 MHz, $CDCl_3$): δ = 9.21 (s, 1H), 9.12 (s, 1H), 8.56 (s, 1H), 8.24 (d, *J* = 8 Hz, 1H), 8.20 (s, 1H), 7.65 (s, 3H), 7.58-7.51 (m, 3H), 7.44-7.32 (m, 7H), 7.20-7.18 (m, 2H). ^{13}C{^{1}H} NMR (100 MHz, $CDCl_3$): δ = 162.4, 157.4, 146.6, 133.8, 133.1, 133.1, 132.9, 131.6, 128.7, 127.8, 124.3, 122.0, 120.3, 111.6. Anal. Calcd for $C_{14}H_{10}Br_2N_2O$, C, 44.01; H, 2.64; N, 7.33. Found: C, 43.97; H, 2.54; N, 7.27.

(*E*)-4-bromo-*N*′-(4-bromobenzylidene)benzohydrazide (**4l**)[32]: White solid (isolated yield ~ 90%, 172 mg), ^{1}H NMR (400 MHz, DMSO-d_6): δ = 11.99 (s, 1H), 8.42 (s, 1H), 7.87 (d, *J* = 8 Hz, 2H), 7.75 (d, *J* = 12 Hz, 2H), 7.71-7.66 (m, 4H). ^{13}C{^{1}H} NMR (100 MHz, DMSO-d_6): δ = 162.4, 147.1, 133.6, 132.4, 131.9, 131.6, 129.8, 129.1, 125.7, 123.5.

(*E*)-2-iodo-*N*′-(2-iodobenzylidene)benzohydrazide (**4m**): White solid (isolated yield ~ 93 %, 220 mg), ^{1}H NMR (400 MHz, DMSO-d_6): δ = 11.87 (s, 1H), 8.46 (s, 1H), 7.92 (d, *J* = 8 Hz, 2H), 7.74 (d, *J* = 4 Hz, 2H), 7.54 (t, *J* = 8 Hz, 2H), 7.47 (d, *J* = 8 Hz, 2H). ^{13}C{^{1}H} NMR (100 MHz, DMSO-d_6): δ = 163.3, 148.0, 134.4, 133.4, 131.9, 130.2, 128.9, 128.6, 127.7, 127.2. Anal. Calcd for $C_{14}H_{10}I_2N_2O$, C, 35.32; H, 2.12; N, 5.88. Found: C, 35.30; H, 2.22; N, 5.76.

(*E*)-2-fluoro-*N*′-(2-fluorobenzylidene)benzohydrazide (**4n**): White solid (isolated yield ~ 93%, 121 mg), ^{1}H NMR (400 MHz, $CDCl_3$): δ = 9.77 (d, *J* = 20 Hz, 1H), 8.48 (s, 1H), 8.25-8.16 (m, 2H), 7.59-7.51 (m, 1H), 7.44-7.38 (m, 1H), 7.37-7.31 (m, 1H), 7.23-7.15 (m, 2H), 7.13-7.06 (m, 1H). ^{13}C{^{1}H} NMR (100 MHz, $CDCl_3$): δ = 163.0, 161.7, 160.5, 160.2, 160.1, 159.3, 141.9, 134.3, 132.7, 132.3, 127.7, 125.4, 124.7, 121.5, 119.9, 116.4, 116.1, 115.9, 115.7.

(*E*)-3-nitro-*N*′-(3-nitrobenzylidene)benzohydrazide (**4o**)[33]: Yellow solid (isolated yield ~ 92%, 144 mg), ^{1}H NMR (400 MHz, DMSO-d_6): δ = 12.47 (s, 1H), 8.77 (s, 1H), 8.59 (d, *J* = 8 Hz, 2H), 8.46 (d, *J* = 8 Hz, 1H), 8.39 (d, *J* = 8 Hz, 1H), 8.29 (d, *J* = 16 Hz, 1H), 8.19 (d, *J* = 12 Hz, 1H), 7.86 (t, *J* = 12 Hz, 1H), 7.78 (t, *J* = 12 Hz, 1H). ^{13}C{^{1}H} NMR (100 MHz, DMSO-d_6): δ = 161.4, 148.3, 147.8, 146.5, 136.0, 134.5, 134.3, 133.6, 130.6, 130.5, 126.6, 124.6, 122.5, 121.2.

(*E*)-4-nitro-*N*′-(4-nitrobenzylidene)benzohydrazide (**4p**)[34]: Yellow solid (isolated yield ~ 80%, 125.5 mg), ^{1}H NMR (400 MHz, DMSO-d_6): δ = 10.67 (s, 1H), 10.14 (s, 1H), 8.35 (d, *J* = 12 Hz, 2H), 8.12 (d, *J* = 8 Hz, 2H), 7.63 (d, *J* = 12 Hz, 2H), 6.58 (d, *J* = 12 Hz, 2H,). ^{13}C{^{1}H} NMR (100 MHz, DMSO-d_6): δ = 164.7, 152.4, 149.5, 138.6, 130.1, 129.1, 125.0, 123.8, 118.9, 112.8.

(*E*)-4-(trifluoromethyl)-*N*′-(4-(trifluoromethyl)benzylidene)benzohydrazide (**4q**)[35]: White solid (isolated yield ~ 82%, 147 mg), ^{1}H NMR (400 MHz, DMSO-d_6): δ = 12.24 (s, 1H), 8.54 (s, 1H), 8.12 (d, *J* = 8 Hz, 3H), 7.97 (d, *J* = 8 Hz, 1H), 7.92 (d, *J* = 8 Hz, 3H), 7.83 (d, *J* = 8 Hz, 1H). ^{13}C{^{1}H} NMR (100 MHz, DMSO-d_6): δ = 164.8, 162.3, 146.9, 138.1, 137.0, 136.3, 128.7, 128.5, 127.9, 125.8, 125.8, 125.7.

(*E*)-*N*′-(thiophen-2-ylmethylene)thiophene-2-carbohydrazide (**4r**)[36]: White solid (isolated yield ~ 78%, 92 mg), ^{1}H NMR (300 MHz, DMSO-d_6): δ = 11.80 (d, *J* = 15 Hz, 1H), 8.63 and 8.29 (s, 1H), 8.03-7.86 (m, 2H), 7.66 (d, *J* = 3 Hz, 1H), 7.46 (d, *J* = 3 Hz, 1H), 7.21 (q, *J* = 3 Hz, 1H), 7.14 (q, *J* = 3 Hz, 1H). ^{13}C{^{1}H} NMR (75 MHz, DMSO-d_6): 161.2, 142.9, 138.9, 135.0, 134.7, 131.9, 131.0, 129.1, 128.1, 126.8.

(*E*)-*N*′-(thiophen-3-ylmethylene)thiophene-3-carbohydrazide (**4s**): White solid (isolated yield ~ 75%, 88 mg), ^{1}H NMR (400 MHz, DMSO-d_6): δ = 11.59 (s, 1H), 8.44 (s, 1H), 8.25 (d, *J* = 4 Hz, 1H), 7.91 (d, 1H), 7.63-7.61 (m, 1H), 7.57 (d, *J* = 8 Hz, 1H), 7.49 (d, *J* = 4 Hz, 1H). ^{13}C{^{1}H} NMR (100 MHz, DMSO-d_6): δ = 158.9, 143.3, 137.6, 136.2, 129.8, 128.3, 127.7, 127.2, 127.0, 124.9. Anal. Calcd for $C_{10}H_8N_2OS_2$, C, 50.83; H, 3.41; N, 11.85. Found: C, 50.53; H, 3.40; N, 11.78.

N′-decanoyldecanehydrazide (**4t**): White solid (isolated yield ~ 100%, 170 mg), ^{1}H NMR (300 MHz, $CDCl_3$): δ = 2.24-2.17 (m, 2H), 1.63 (br s, 2H), 1.34-1.25 (m, 12H), 0.87 (t, *J* = 6 Hz, 3H). $^{13}C\{^{1}H\}$ NMR (75 MHz, $CDCl_3$): δ = 173.9, 32.0, 29.8, 29.6, 29.5, 29.5, 29.4, 25.8, 22.8, 14.2.

N′-tetradecanoyltetradecanehydrazide (**4u**): White solid (isolated yield ~ 100%, 226 mg), ^{1}H NMR (300 MHz, $CDCl_3$): δ = 2.36 (t, *J* = 6 Hz, 2H), 1.63 (quin, *J* = 6 Hz, 2H), 1.35-1.25 (m, 20H), 0.88 (t, *J* = 6 Hz, 3H). $^{13}C\{^{1}H\}$ NMR (75 MHz, $CDCl_3$): δ = 179.5, 34.3, 32.1, 29.8, 29.8, 29.7, 29.6, 29.5, 29.4, 29.2, 24.9, 22.8, 14.2.

N′-palmitoylpalmitohydrazide (**4v**): White solid (isolated yield ~ 100%, 254 mg), ^{1}H NMR (300 MHz, $CDCl_3$): δ = 2.37 (t, *J* = 6 Hz, 2H), 1.63 (quin, *J* = 6 Hz, 2H), 1.25 (s, 24H), 0.88 (t, *J* = 6 Hz, 3H). $^{13}C\{^{1}H\}$ NMR (75 MHz, $CDCl_3$): δ = 179.3, 34.3, 32.1, 29.8, 29.8, 29.7, 29.6, 29.5, 29.4, 29.2, 25.1, 24.9, 22.8, 14.3.

(*E*)-*N′*-benzylidene-*N*-(prop-2-yn-1-yl)benzohydrazide (**5**)[37]: Colorless liquid (isolated yield ~ 97%, 177 mg), ^{1}H NMR (300 MHz, $CDCl_3$): δ = 7.99 (s, 1H), 7.78 (dt, *J* = 3 Hz, 2H), 7.56-7.52 (m, 2H), 7.51-7.44 (m, 3H), 7.35 (t, *J* = 3 Hz, 3H), 4.98 (d, *J* = 3 Hz, 2H), 2.33 (t, *J* = 3 Hz, 1H). $^{13}C\{^{1}H\}$ NMR (75 MHz, $CDCl_3$): δ = 170.3, 158.4, 140.7, 134.6, 130.7, 130.1, 129.9, 128.8, 127.5, 127.4, 76.8, 73.3, 54.7.

Compound **6**: Pale yellow solid (isolated yield ~ 84%, 205 mg), ^{1}H NMR (300 MHz, $CDCl_3$): δ = 8.35 (s, 1H), 7.74 (d, *J* = 6 Hz, 2H), 7.56 (s, 1H), 7.51-7.46 (m, 3H), 7.44-7.40 (m, 2H), 7.30 (t, *J* = 3 Hz, 3H), 5.43 (s, 2H), 5.25 (s, 2H), 4.25 (t, *J* = 3 Hz, 2H), 4.19 (t, *J* = 3 Hz, 2H), 4.14 (s, 5H). $^{13}C\{^{1}H\}$ NMR (75 MHz, $CDCl_3$): δ = 170.9, 142.7, 141.5, 134.8, 134.7, 130.7, 130.2, 129.8, 128.7, 127.5, 122.8, 80.7, 69.3, 69.1, 69.0, 50.3, 37.9.

2,5-diphenyl-1,3,4-oxadiazole (**7**)[38]: White solid (isolated yield ~ 90%, 100 mg), ^{1}H NMR (300 MHz, $CDCl_3$): δ = 8.17-8.14 (m, 2H), 7.57-7.52 (m, 3H). $^{13}C\{^{1}H\}$ NMR (75 MHz, $CDCl_3$): δ = 164.7, 131.9, 129.2, 127.1, 124.1.

4.6. References

1. (a) Kalia, J.; Raines, R. T. *Angew. Chem. Int. Ed.* **2008**, *47*, 7523-7526. (b) Canal-Martín, A.; Navo, C. D.; Sáez, E.; Molero, D.; Jiménez-Osés, G.; Pérez-Fernández, R. *Org. Biomol. Chem.* **2021**, *19*, 7202-7210. (c) Nguyen, R.; Huc, I. *Chem. Commun.* **2003**, 942-943. (d)

Demir, Y.; Tokali, F. S.; Kalay, E.; Türkes, C.; Tokali, P.; Aslan, O. N.; Sendil, K.; Beydemir, S. *Mol. Divers*. **2023**, *27*, 1713-1733.

2. (a) Corbett, P. T.; Leclaire, J.; Vial, L.; West, K. R.; Wietor, J. L.; Sanders, J. K. M.; Otto, S. *Chem. Rev.* **2006**, *106*, 3652-3711. (b) Lehn, J. M. *Chem. Soc. Rev.* **2007**, *36*, 151-160. (c) Belowich, M. E.; Stoddart, J. F. *Chem. Soc. Rev.* **2012**, *41*, 2003-2024. (d) Dirksen, A.; Dirksen, S.; Hackeng, T. M.; Dawson, P. E. *J. Am. Chem. Soc*. **2006**, *49*, 15602-15603. (e) Ladame, S. *Org. Biomol. Chem*. **2008**, *6*, 219-226. (f) Simpson, M. G.; Pittelkow, M.; Watson, S. P.; Sanders, J. K. M. *Org. Biomol. Chem.* **2010**, *8*, 1173-1180.
3. (a) Hu, J.; Gupta, S. K.; Ozdemir, J.; Beyzavi, H. *ACS Appl. Nano Mater.* **2020**, *3*, 6239-6269. (b) Marro, N.; Suo, R.; Naden, A. B.; Kay, E. R. *J. Am. Chem. Soc.* **2022**, *144*, 14310-14321. (c) Wilson, A.; Gasparini, G.; Matile, S. *Chem. Soc. Rev.* **2014**, *43*, 1948-1962.
4. (a) Ulrich, S.; Boturyn, D.; Marra, A.; Renaudet, O.; Dumy, P. *Chem. Eur. J.* **2014**, *20*, 34-41. (b) Agten, S. M.; Dawson, P. E.; Hackeng, T. M. J. *Pept. Sci*. **2016**, *22*, 271-279. (c) Socea, L. -I.; Barbuceanu, S.-F.; Pahontu, E. M.; Dumitru, A. -C.; Nitulescu, G. M.; Sfetea, R. C.; Apostol, T. -V. *Molecules* **2022**, *27*, 8719. (d) Bo, S.; Zhang, D.; Ma, M.; Mo, X.; Stabinska, J.; McMahon, M. T.; Shi, C.; Luo, L. *Pharmaceuticals* **2023**, *16*, 639.
5. (a) Shaw, T. A.; Powdrill, M. H.; Sherratt, A. R.; Garland, K.; Li, B. -J.; Beauchemin, A. M.; Pezacki, J. P. *RSC Med. Chem.* **2021**, *12*, 797-803. (b) Kolmel, D. K.; Kool, E. T. *Chem. Rev.* **2017**, *117*, 10358-10376. (c) Mailig, M.; Hymel, D.; Liu, F. *Org. Lett.* **2020**, *22*, 6677-6681.
6. (a) Wang, Y.; Zhang, F. L.; Liu, Z. J.; Yao, Z. J. *Inorg. Chem.* **2022**, *61*, 10310-10320. (b) Choudhary, S.; Morrow, J. R. *Angew. Chem.* **2002**, *114*, 4270-4272. (c) Chen, X.; Cai, Y.; Jiang, W.; Peng, G.; Fang, J.; Liu, J.; Tong, M.; Bao, X. *Inorg. Chem.* **2019**, *58*, 999-1002.
7. (a) Dasgupta, S.; Karim, S.; Banerjee, S.; Saha, M.; Das Saha, K.; Das, D. *Dalton Trans.* **2020**, *49*, 1232-1240. (b) Biliz, Y.; Hasdemir, B.; Kucuk, H. B.; Zaim, M.; Senturk, A. M.; Kirmizibekmez, A. M.; Kara, I. *ACS Omega.* **2023**, *8*, 20073-20084.
8. (a) Vicini, P.; Incerti, M.; La Colla, P.; Loddo, R. *Eur. J. Med. Chem*. **2009**, *44*, 1801-1807. (b) Kandile, N. G.; Mohamed, M. I.; Zaky, H.; Mohamed, H. M. *Eur. J. Med. Chem*. **2009**, *44*, 1989-1996. (c) Ajani, O. O.; Obafemi, C. A.; Nwinyi, O. C.; Akinpelu, D. A. *Bioorg. Med. Chem*. **2010**, *18*, 214-221. (d) Dascalu, A. -E.; Ghinet, A.; Lipka, E.; Furman, C.; Rigo, B.; Fayeulle, A.; Billamboz, M. *Bioorg. Med. Chem.* **2020**, *30*, 127220. (e) Rai, U. S.; Isloor, A. M.; Shetty, P.; Isloor, N.; Malladi, S.; Fun, H. -K. *Eur. J. Med. Chem*. **2010**, *45*, 6090-6094. (f) Kumar, P.; Narasimhan, B. *Mini-Rev. Med. Chem*. **2013**, *13*, 971-987.

9. (a) Park, K. D.; Liu, R.; Kohn, H. *Chem. Biol.* **2009**, *16*, 763-772. (b) Cui, P.; Cai, M.; Meng, Y.; Yang, Y.; Song, H.; Liu, Y.; Wang, Q. *Sci. Rep.* **2022**, *12*, 2935. (c) Wang, X. -L.; Zhang, Y. -B.; Tang, J. -F.; Yang, Y. -S.; Chen, R. -Q.; Zhang, F.; Zhu, H. -L.; *Eur. J. Med. Chem.* **2012**, *57,* 373-382. (d) Goff, G. L.; Ouazzani, J. *Bioorg. Med. Chem.* **2014**, *22,* 6529-6544. (e) Zhou, Y.; Luo, Y.; Yang, Y. -S.; Lu, L.; Zhu, H. -L. *Med. Chem. Commun.* **2016**, *7*, 1980-1987.
10. Chaur, M. N.; Collado, D.; Lehn, J. M. *Chem. Eur. J.* **2011**, *17*, 248-258.
11. (a) Ratjen, L.; Lehn, J. -M. *RSC Adv*. **2014**, *4*, 50554-50557. (b) Vantomme, G.; Jiang, S.; Lehn, J. M. *J. Am. Chem. Soc*. **2014**, *136*, 9509-9518. (c) Vantomme, G.; Lehn, J. -M. *Chem. Eur. J*. **2014**, *20*, 16188-16193. (d) Wezenberg, S. J. *Chem. Commun*. **2022**, *58*, 11045-11058.
12. Chaur, M. N.; Collado, D.; Lehn, J. M. *Chem. Eur. J.* **2011**, *17*, 248-258.
13. van Dijken, D. J.; Kovaříček, P.; Ihrig, S. P.; Hecht, S. *J. Am. Chem. Soc*. **2015**, *137*, 14982-14991.
14. (a) Morales, S.; Aceña, J. L.; García Ruano, J. L.; Cid, M. B. *J. Org. Chem*. **2016**, *81*, 10016-10022. (b) Trausel, F.; Fan, B.; van Rossum, S. A. P.; van Esch, J. H.; Eelkema, R. *Adv. Synth. Catal*. **2018**, *360*, 2571-2576.
15. Andrade, M. M.; Barros, M. T. *J. Comb. Chem.* **2010**, *12*, 245-247.
16. Ding, Y.; Li, H.; Meng, Y.; Zhang, T.; Li, J.; Chen, Q. Y.; Zhu, C. *Org. Chem. Front.* **2017**, *4*, 1611-1614.
17. Yavari, I.; Shaabanzadeh, S. *J. Org. Chem*. **2022**, *87*, 15077-15085.
18. (a) Mondal, R.; Guin, A. K.; Chakraborty, S.; Paul, N. D. *J. Org. Chem*. **2022**, *87*, 2921-2934. (b) Sundar, S.; Rengan, R.; Pennamuthiriyan, A.; Sémeril, D. *Appl. Organomet. Chem*. **2022**, *36*, e6857.
19. Niemann, C.; Hays, J. T. *J. Am. Chem. Soc.* **1943**, *65*, 482-484.
20. (a) Pal, A.; Das, K. M.; Thakur, A. *J. Org. Chem*. **2023**, *88*, 8955-8968. (b) Pal, A.; Das, K. M.; Thakur, A. *Org. Biomol. Chem.* **2022**, *20*, 8977-8987.
21. Munir, R.; Javid, N.; Zia-ur-Rehman, M.; Zaheer, M.; Huma, R.; Roohi, A.; Athar, M. M.; *Molecules* **2021**, *16*, 4908.
22. Hincapié-Otero, M. M.; Joaqui-Joaqui, A.; Polo-Cerón, D. *Univ. Sci.* **2021**, *26*, 193–215.
23. Sailu, B.; Komaraiah, A.; Reddy, P. S. N. *Syn. Commun.* **2006**, *36*, 1907-1910.
24. Yadav, A.; Kaushik, C. P.; Kumar, M. *J. Mol. Struc.* **2023**, *1283*, 135163.
25. Rostamizadeh, S.; Ghasem Housaini, S. A. *Tetrahedron Lett.* **2004**, *45*, 8753-8756.

26. Nun, P.; Martin, C.; Martinez, J.; Lamaty, F. *Tetrahedron* **2011**, *67*, 8187-8194.
27. Taha, M.; Naz, H.; Rasheed, S.; Ismail, N. H.; Abd Rahman, A.; Yousuf, S.; Choudhary, M. I. *Molecules* **2014**, *19*, 1286-1301.
28. Kümmerle, A. E.; Schmitt, M.; Cardozo, S. V. S.; Lugnier, C.; Villa, P.; Lopes, A. B.; Romeiro, N. C.; Justiniano, H.; Martins, M. A.; Fraga, C. A. M.; Bourguignon, J. -J.; Barreiro, E. J. *J. Med. Chem.* **2012**, *55*, 7525-7545.
29. Zou, D. -H.; Guan, H.; Zhang, X. -H. *Acta Cryst.* **2009**, *E65*, o2871.
30. Veeramanikandan, S.; Sherine, B. H. *Pharma Chemica* **2015**, *7*, 70-84.
31. Tsefrikas, V. M.; Arns, S.; Merner, P. M.; Warford, C. C.; Merner, B. L.; Scott, L. T.; Bodwell, G. J. *Org. Lett.* **2006**, *8*, 5195-5198.
32. Kumar, P.; Narasimhan, B.; Ramasamy, K.; Mani, V.; Mishra, R. K.; Majeed, A. B. A. *Current Topics in Med. Chem.* **2015**, *15*, 1050-1064.
33. Kumar, P.; Narasimhan, B.; Sharma, D.; Judge, V.; Narang, R. *Eur. J. Med. Chem.* **2009**, *44*, 1853-1863.
34. Han, X.; Zhu, X.; Hong, Z.; Wei, L.; Ren, Y.; Wan, F.; Zhu, S.; Peng, H.; Guo, L.; Rao, L.; Feng, L.; Wan, J. *J. Chem. Inf. Model.* **2017**, *57*, 1426–1438.
35. Krátký, M.; Bősze, S.; Baranyai, Z.; Stolaříková, J.; Vinšová, J. *Bioorg. Med. Chem. Lett.* **2017**, *27*, 5185-5189.
36. van Dijken, D. J.; Kovaříček, P.; Ihrig, S. P.; Hecht, S. *J. Am. Chem. Soc.* **2015**, *137*, 14982–14991.
37. Yadav, A.; Kaushik, C. P.; Kumar, M. *J. Mol. Struc.* **2023**, *1283*, 135163.
38. Bhujabal, Y. B.; Vadagaonkar, K. S.; Kapdi, A. R. *Asian J. Org. Chem.* **2019**, *8*, 289.

Spectroscopic details

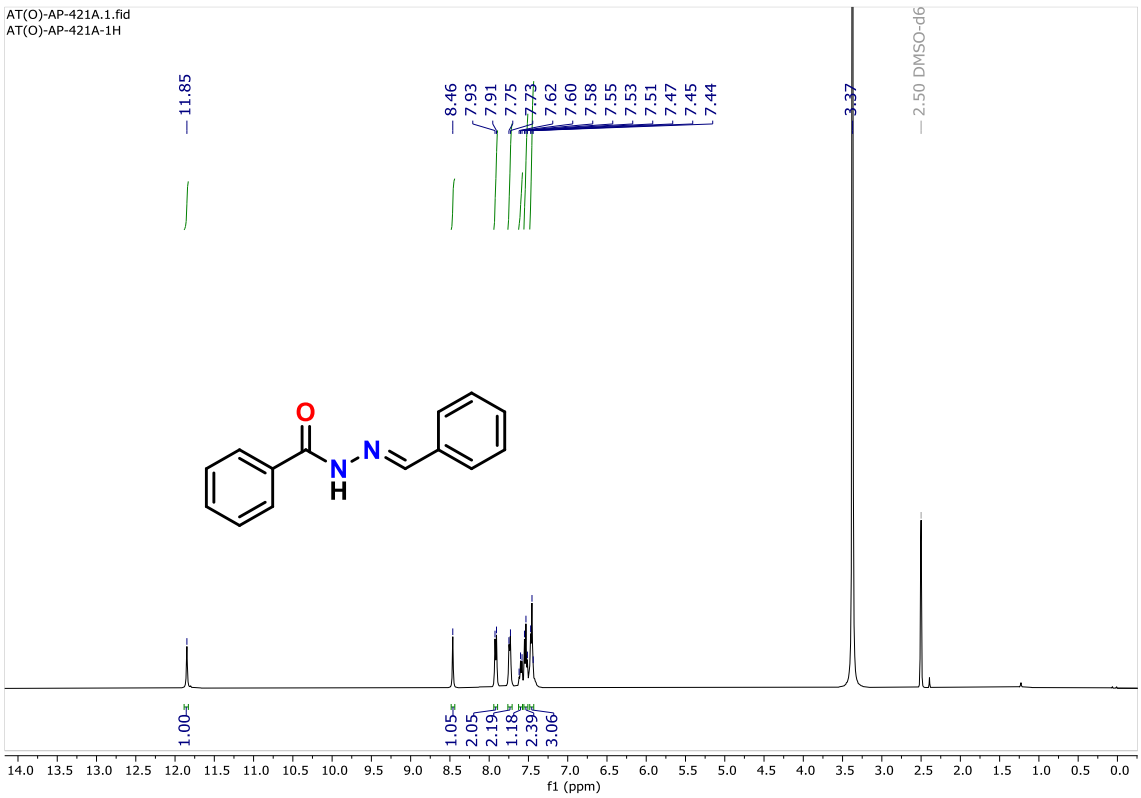

Figure 4.4. ^{1}H NMR (400 MHz) spectrum of **4a** in DMSO-d_6.

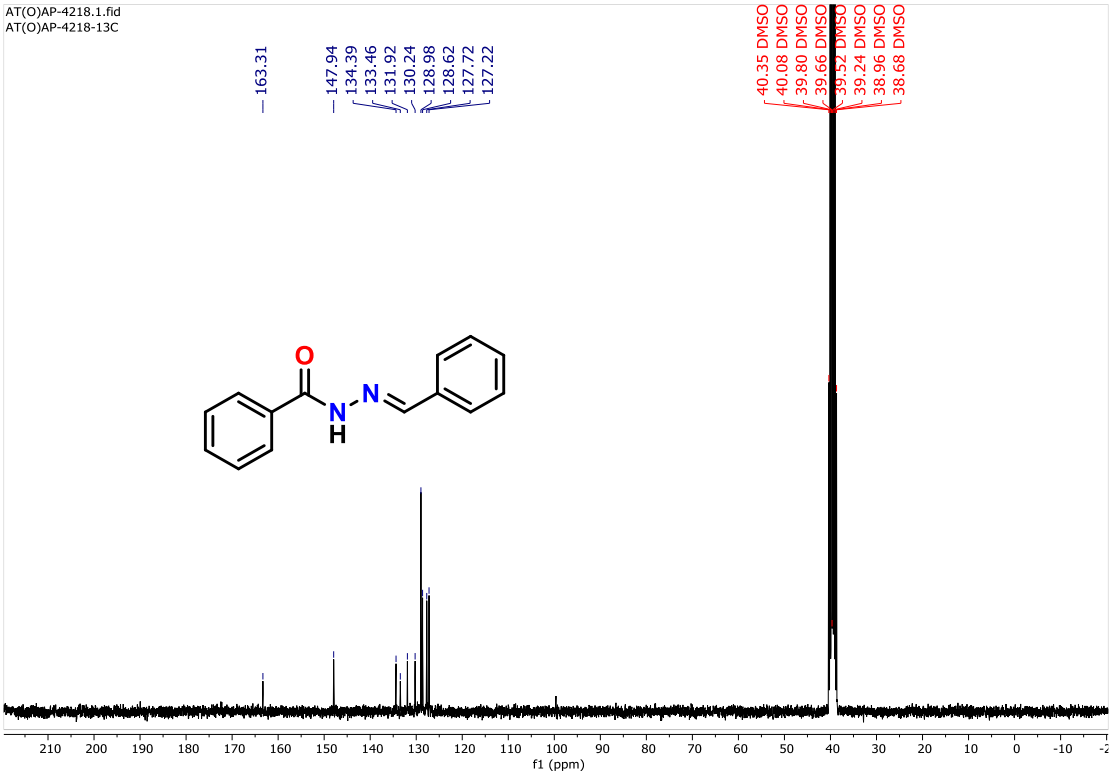

Figure 4.5. $^{13}C\{^{1}H\}$ NMR (100 MHz) spectrum of **4a** in DMSO-d_6.

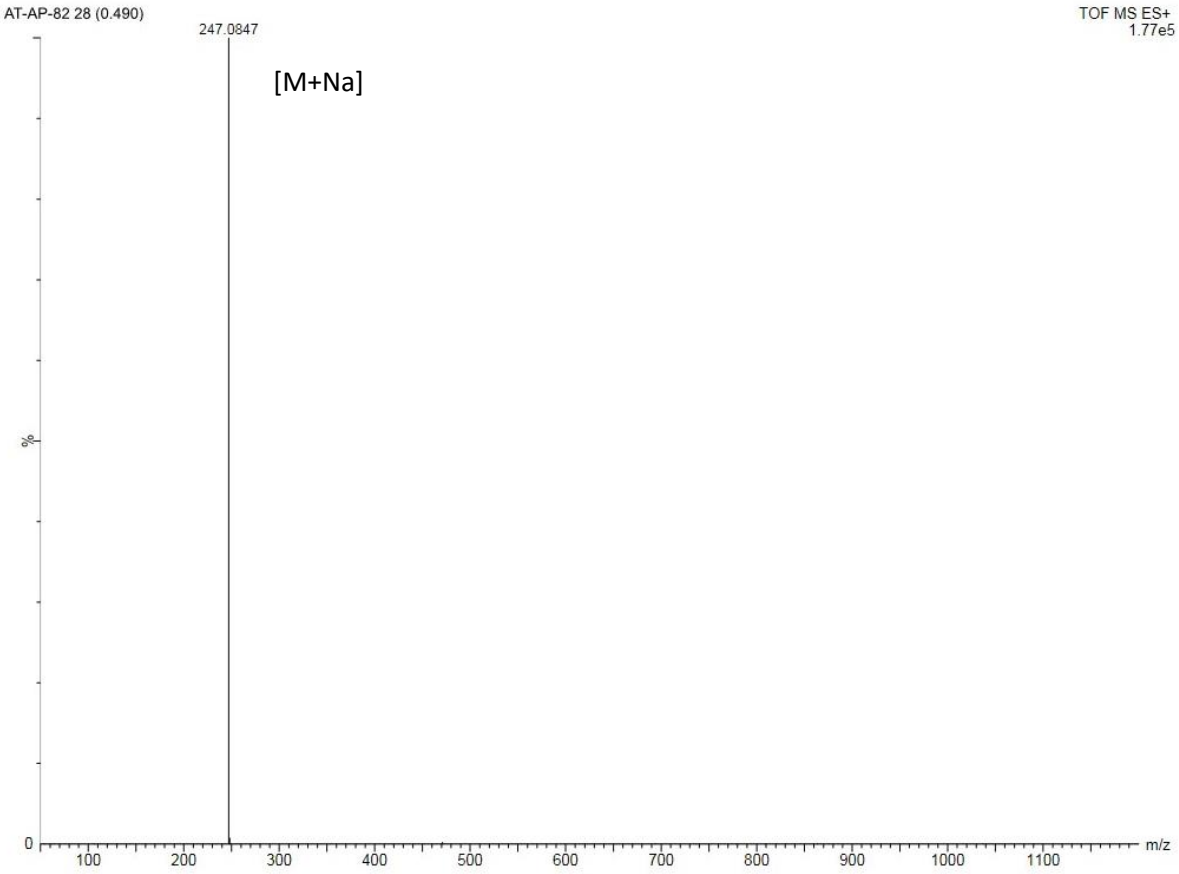

Figure 4.6. HRMS of **4a**.

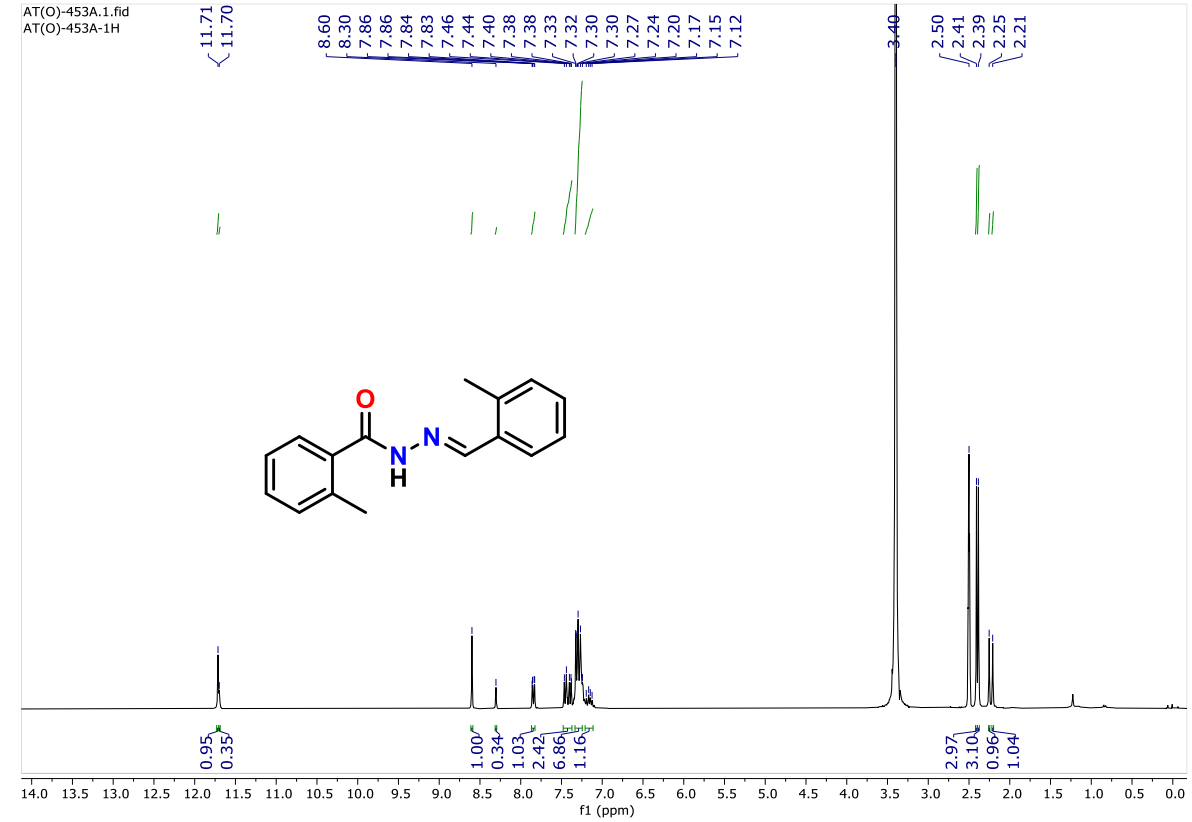

Figure 4.7. ^{1}H NMR (400 MHz) spectrum of **4b** in DMSO-d_6.

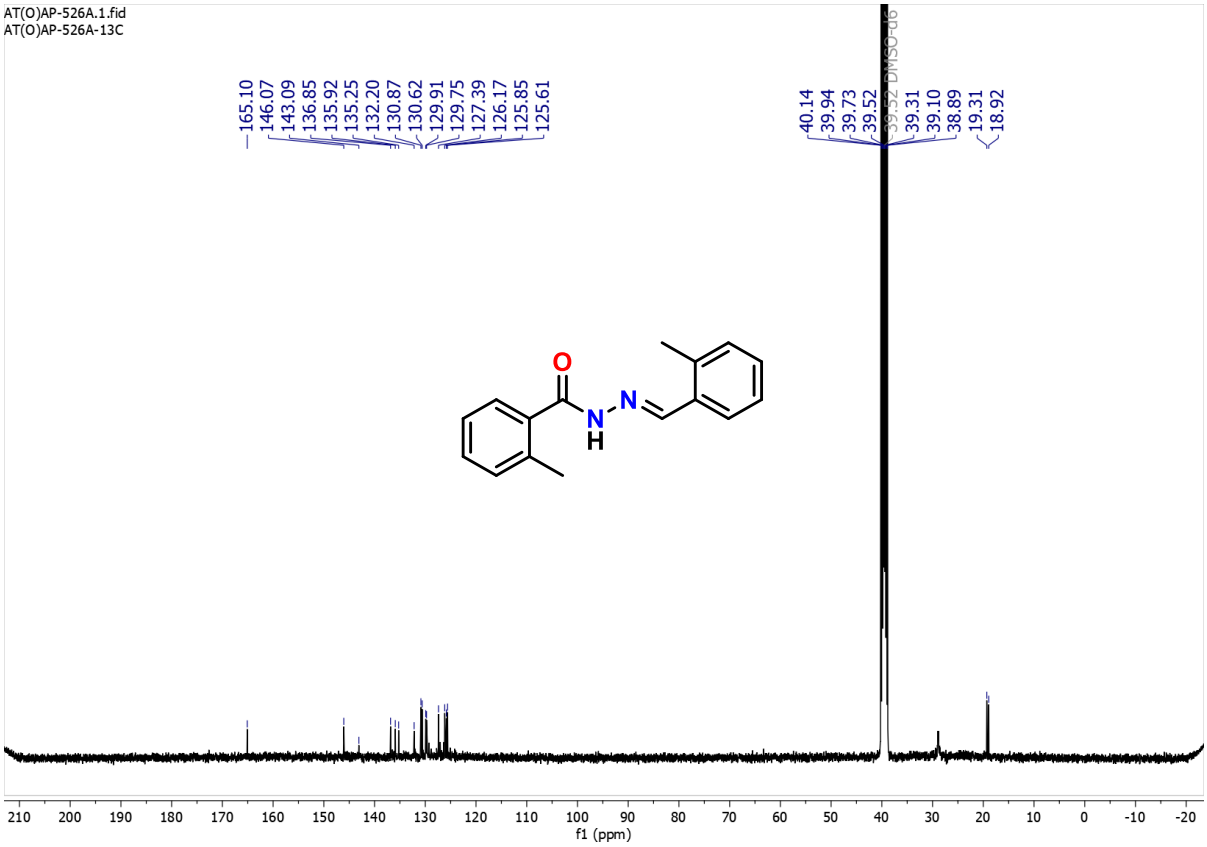

Figure 4.8. $^{13}C\{^{1}H\}$ NMR (100 MHz) spectrum of **4b** in DMSO-d_6.

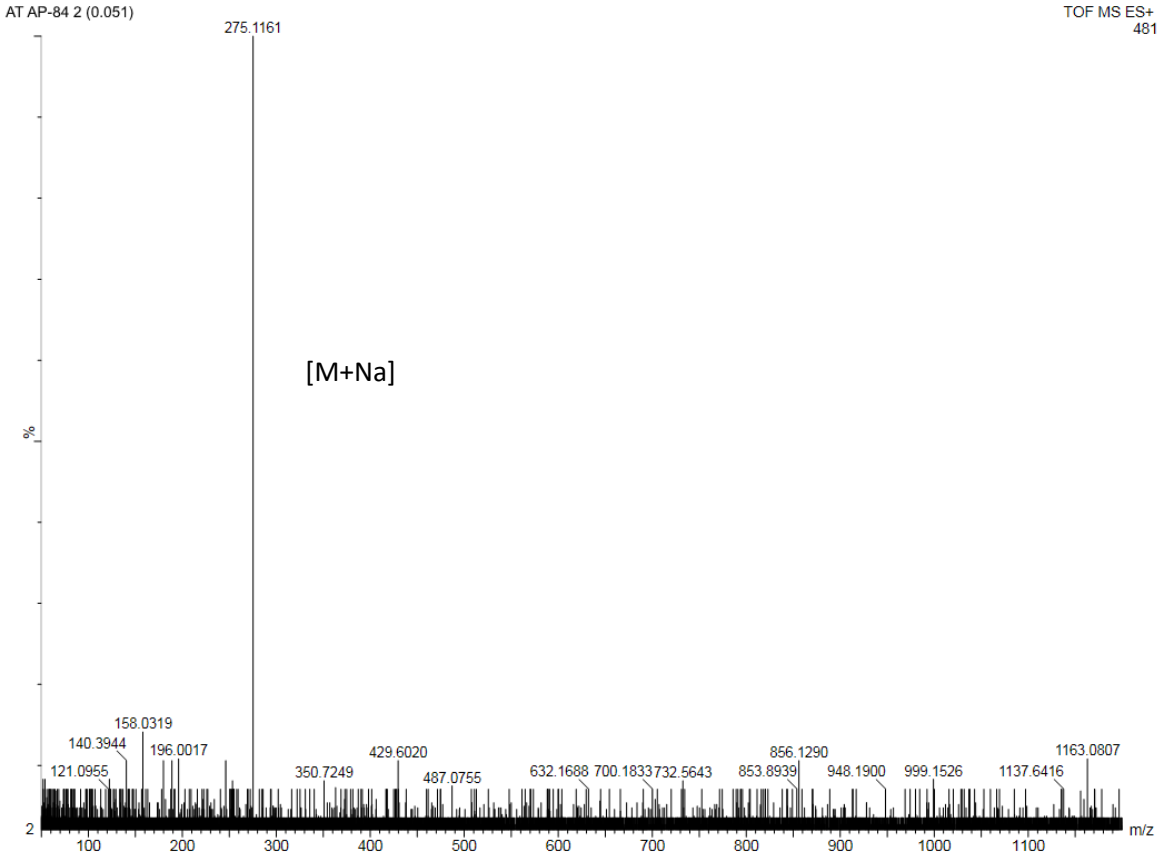

Figure 4.9. HRMS of **4b**.

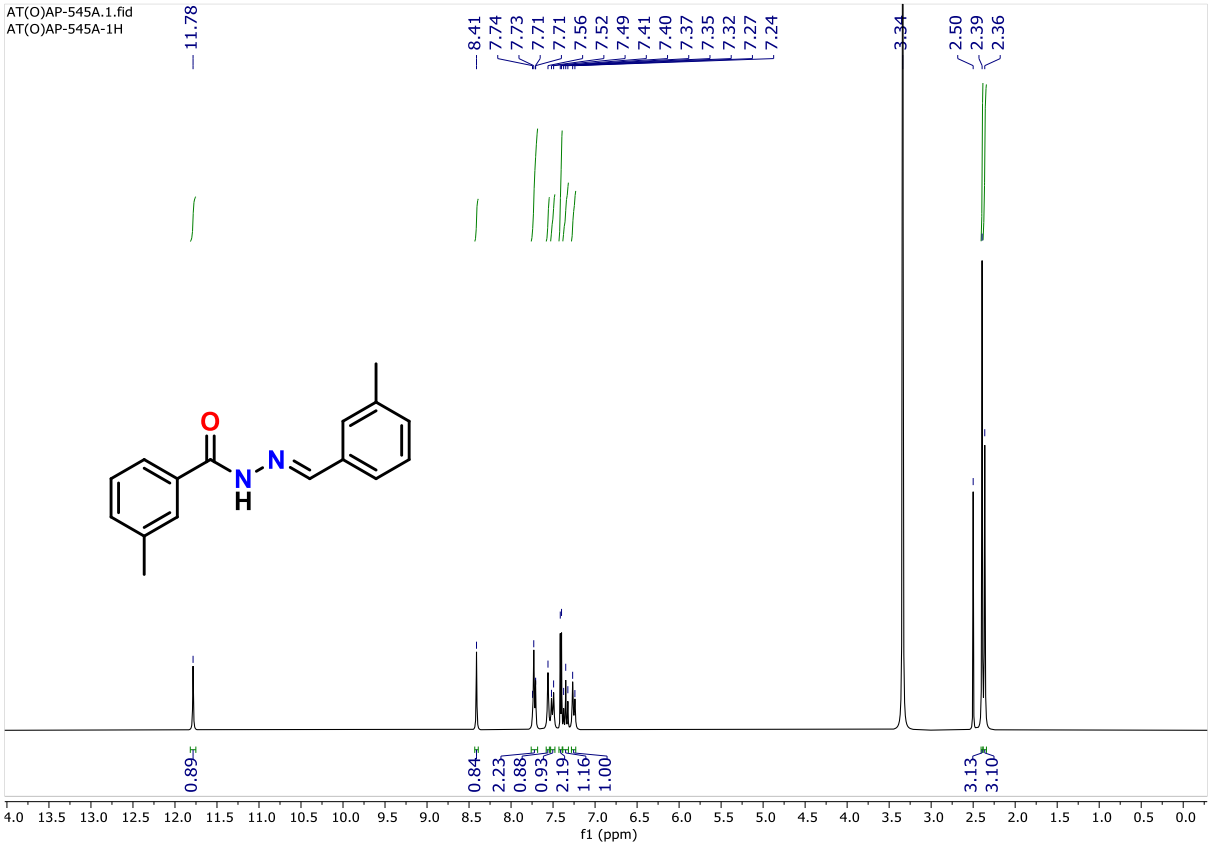

Figure 4.10. ^{1}H NMR (400 MHz) spectrum of **4c** in DMSO-d_6.

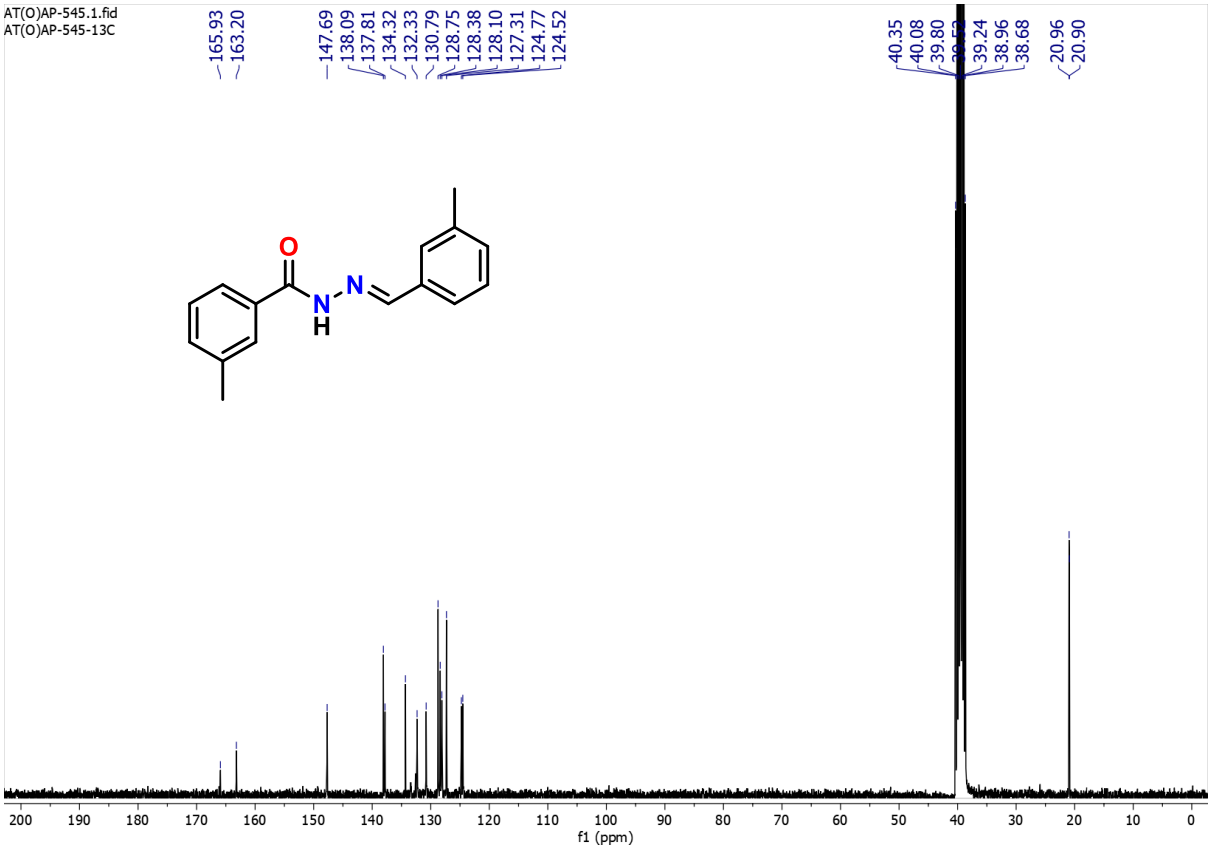

Figure 4.11. $^{13}C\{^{1}H\}$ NMR (100 MHz) spectrum of **4c** in DMSO-d_6.

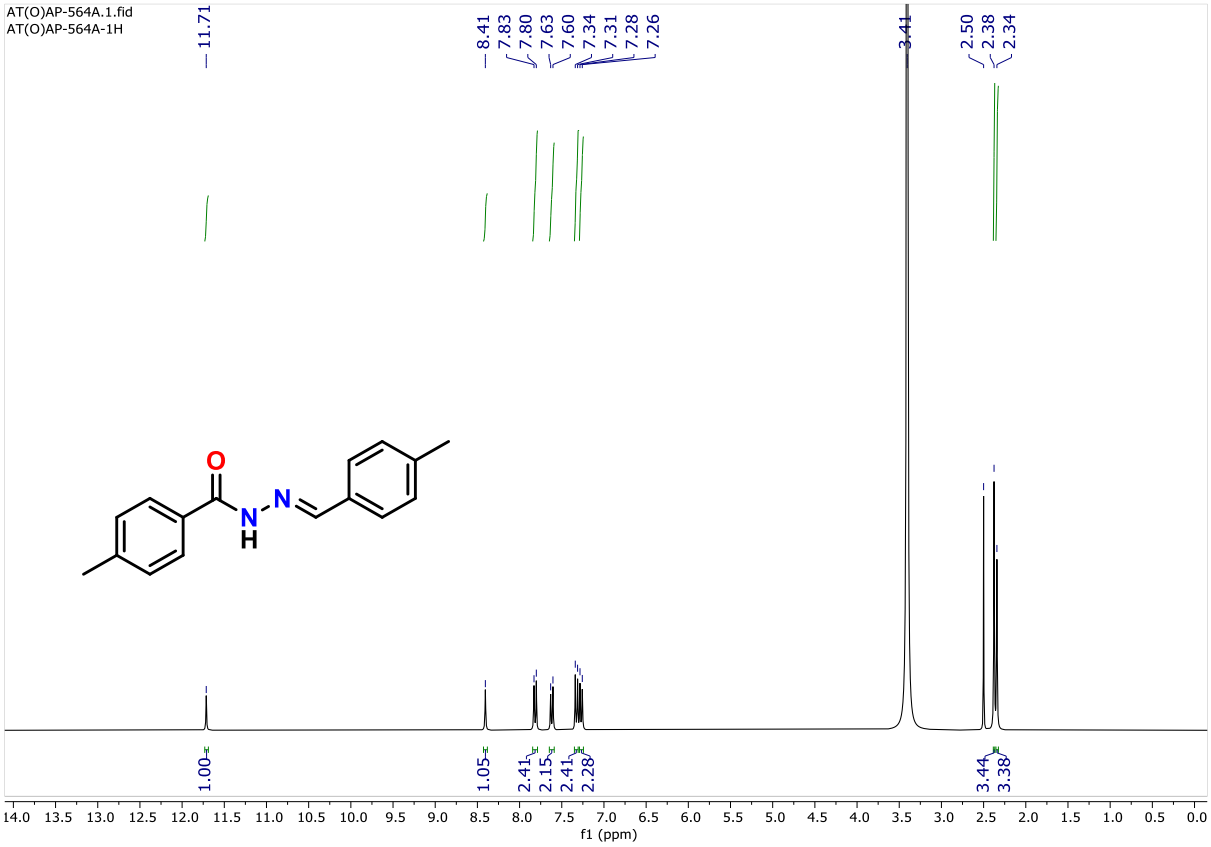

Figure 4.12. ^{1}H NMR (400 MHz) spectrum of **4d** in DMSO-d_6.

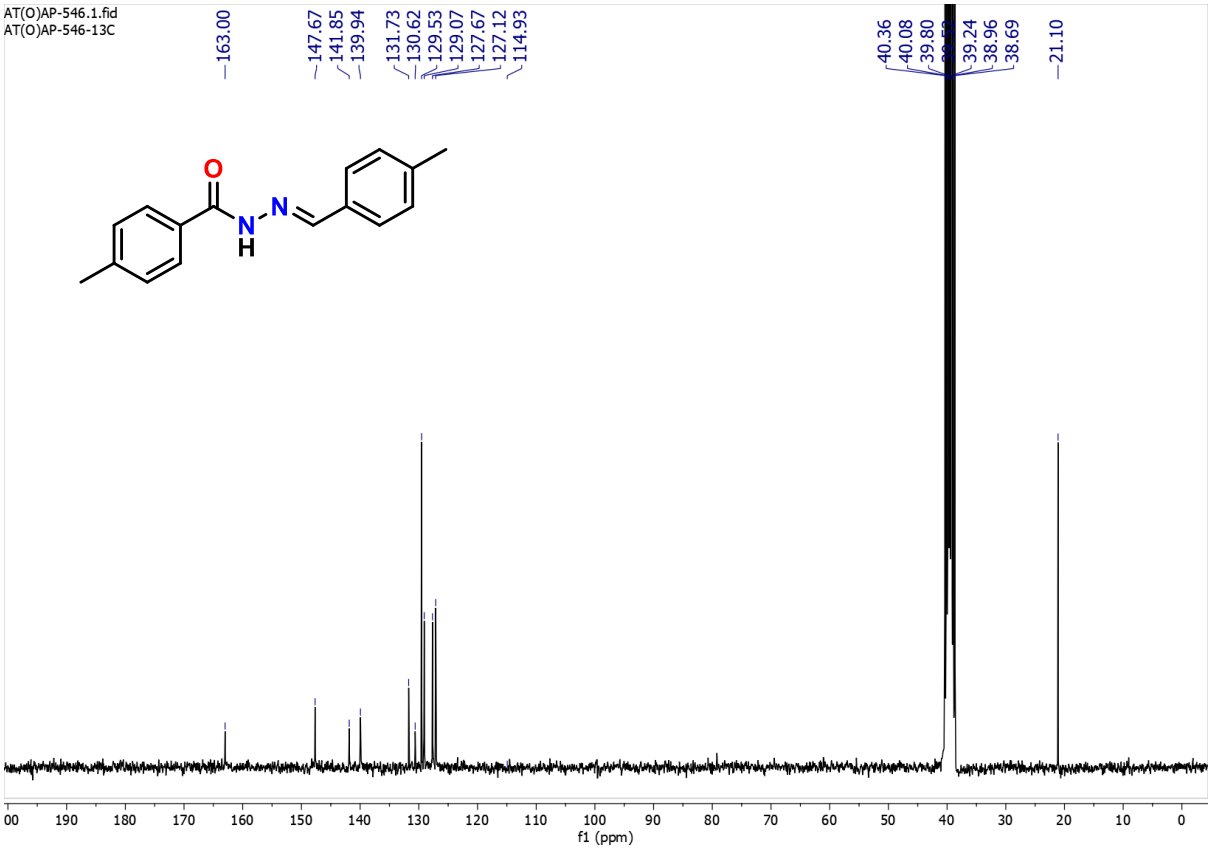

Figure 4.13. $^{13}C\{^{1}H\}$ NMR (100 MHz) spectrum of **4d** in DMSO-d_6.

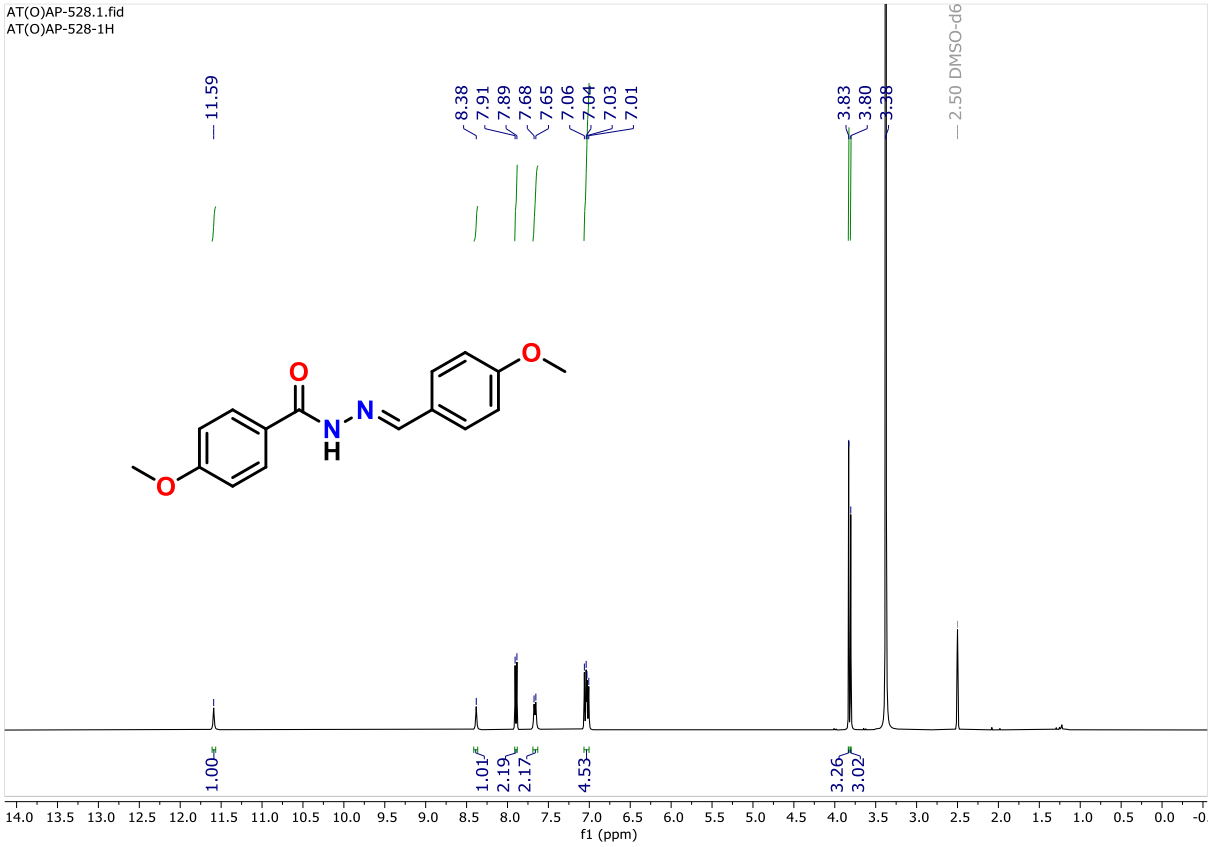

Figure 4.14. ^{1}H NMR (400 MHz) spectrum of **4e** in DMSO-d_6.

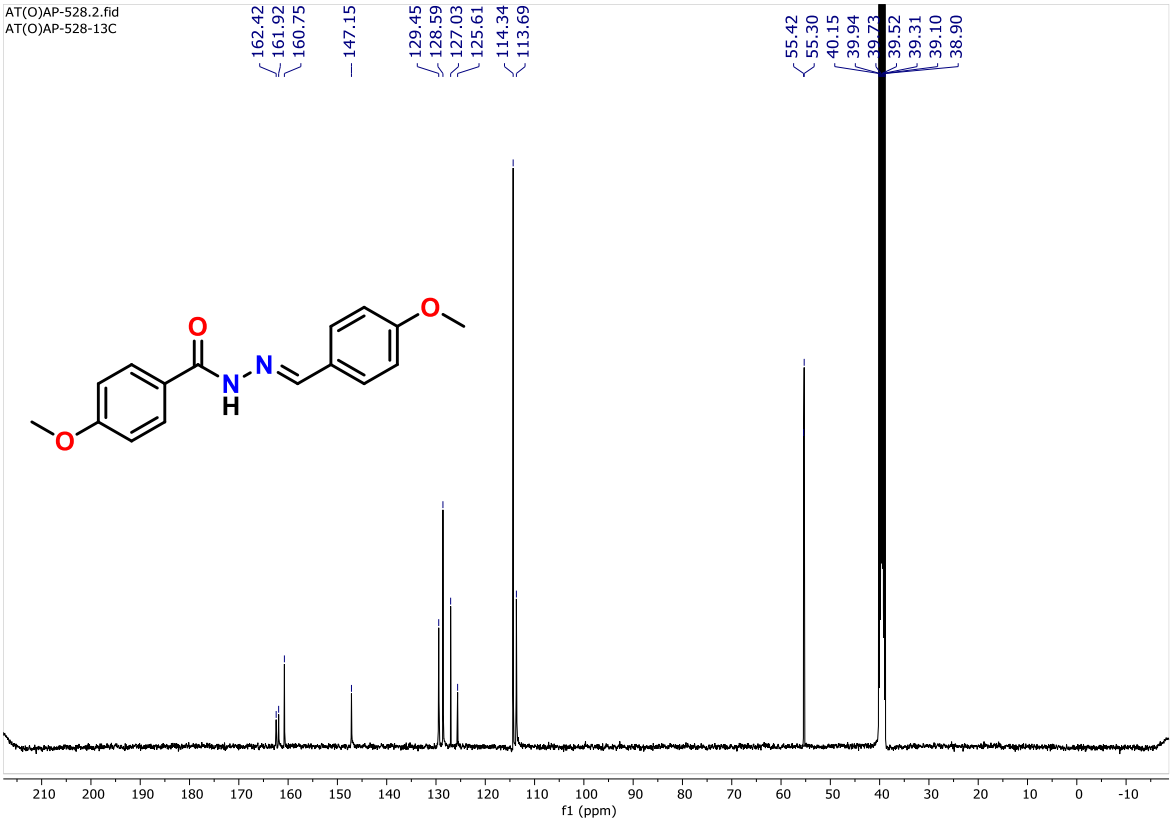

Figure 4.15. $^{13}C\{^{1}H\}$ NMR (100 MHz) spectrum of **4e** in DMSO-d_6.

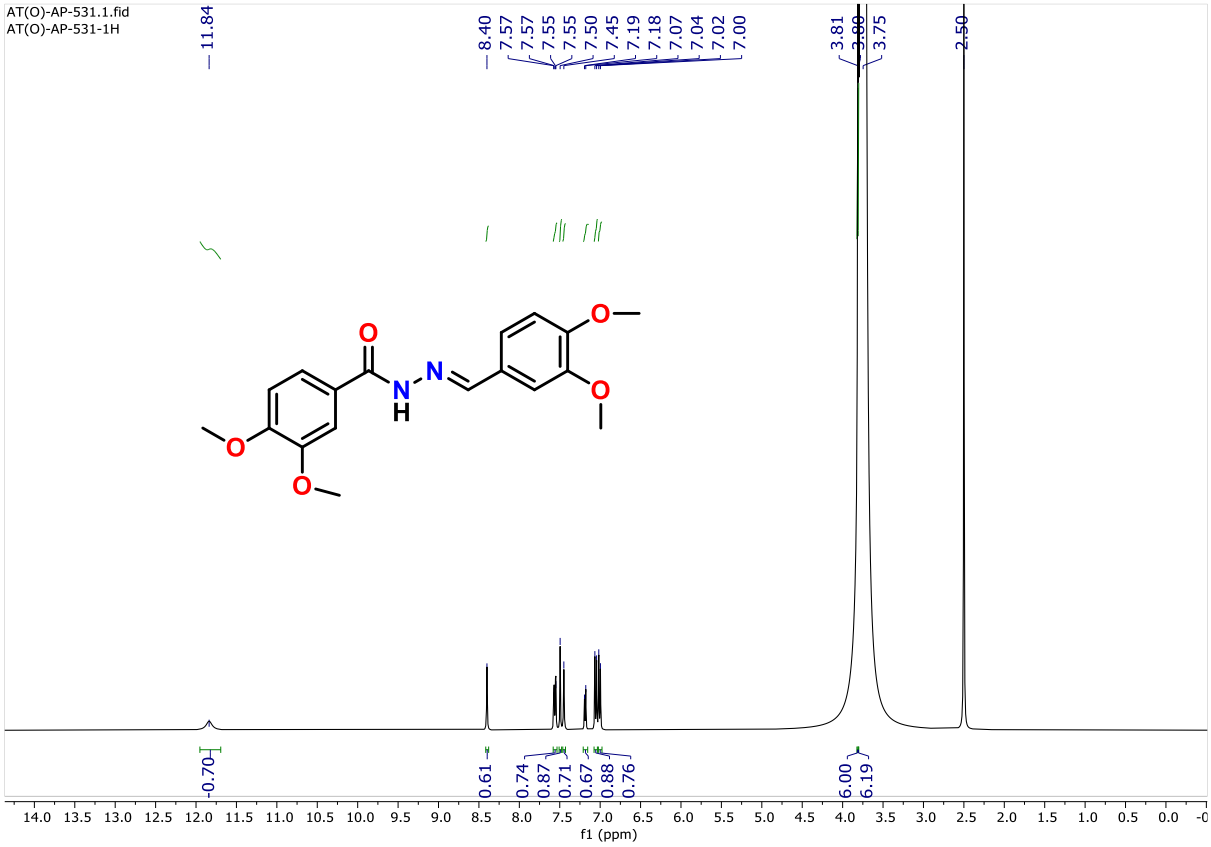

Figure 4.16. ^{1}H NMR (400 MHz) spectrum of **4f** in DMSO-d_6.

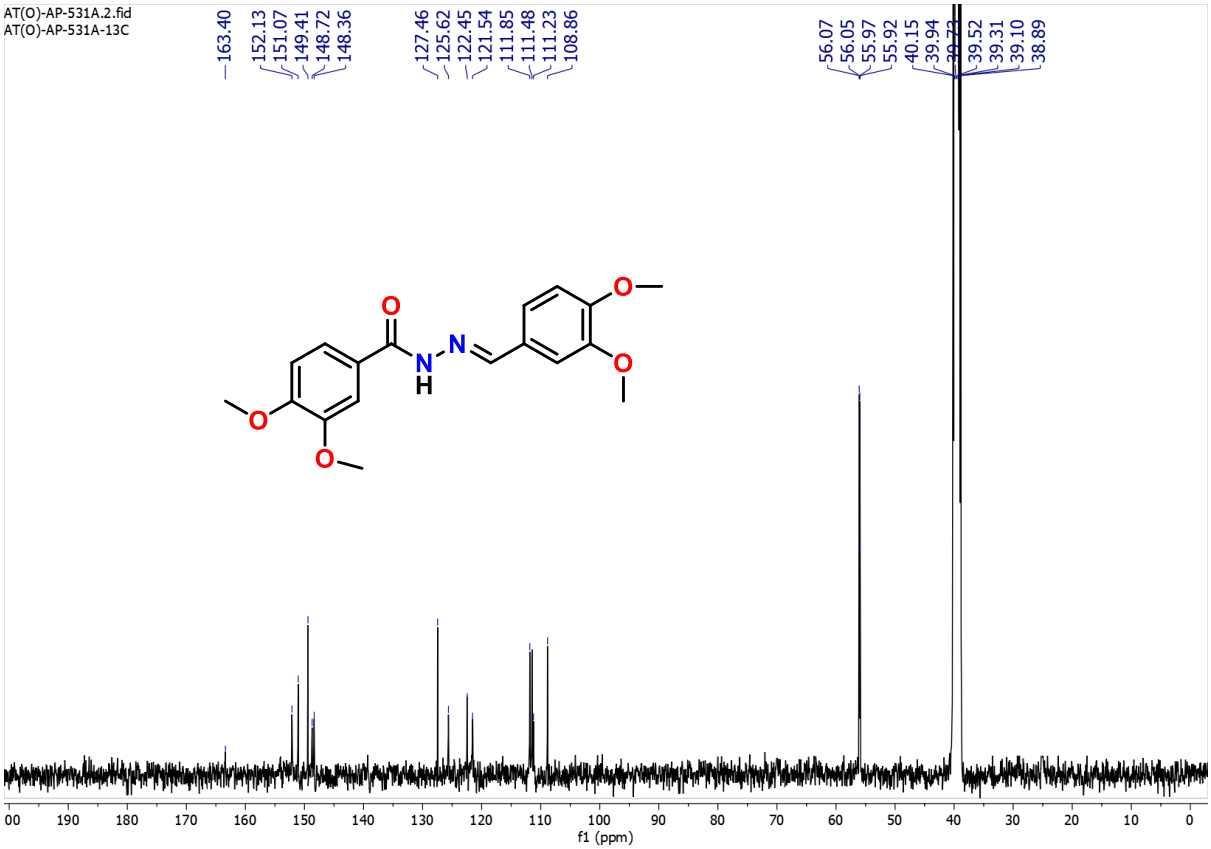

Figure 4.17. $^{13}C\{^{1}H\}$ NMR (100 MHz) spectrum of **4f** in DMSO-d_6.

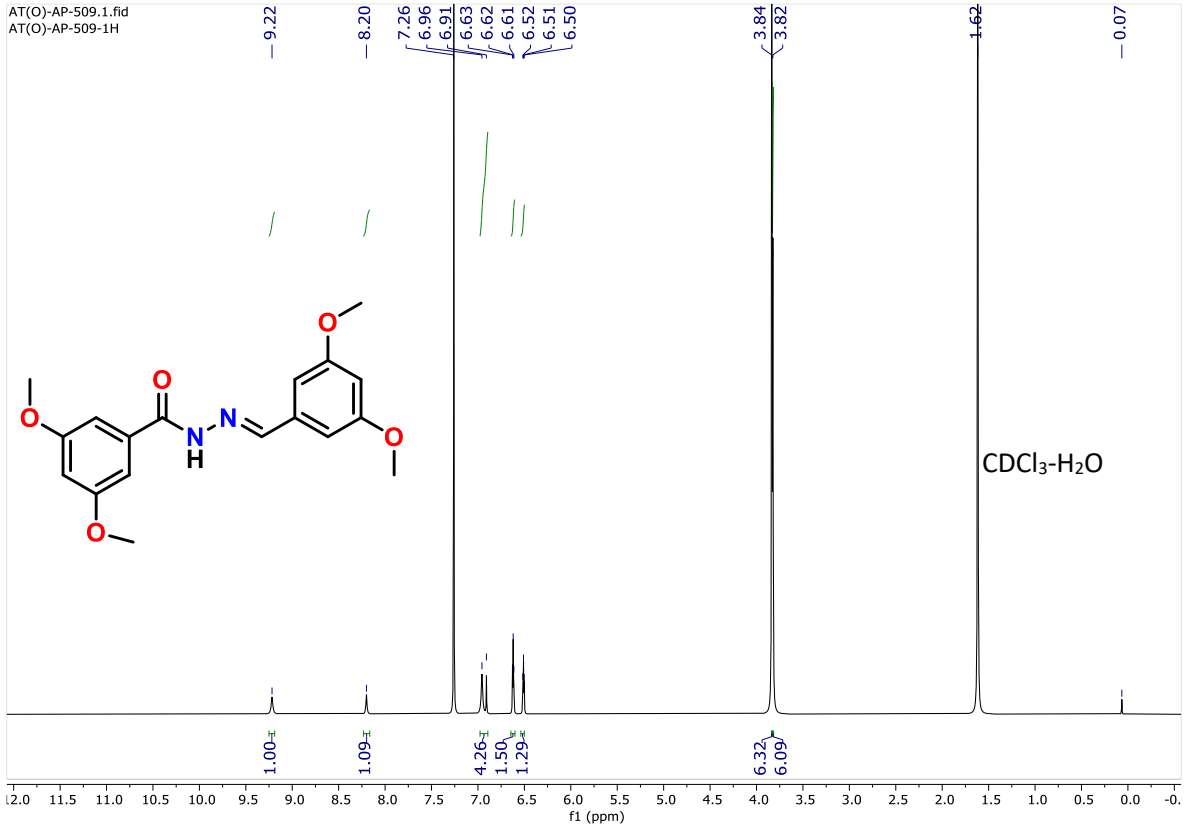

Figure 4.18. ^{1}H NMR (400 MHz) spectrum of **4g** in $CDCl_3$.

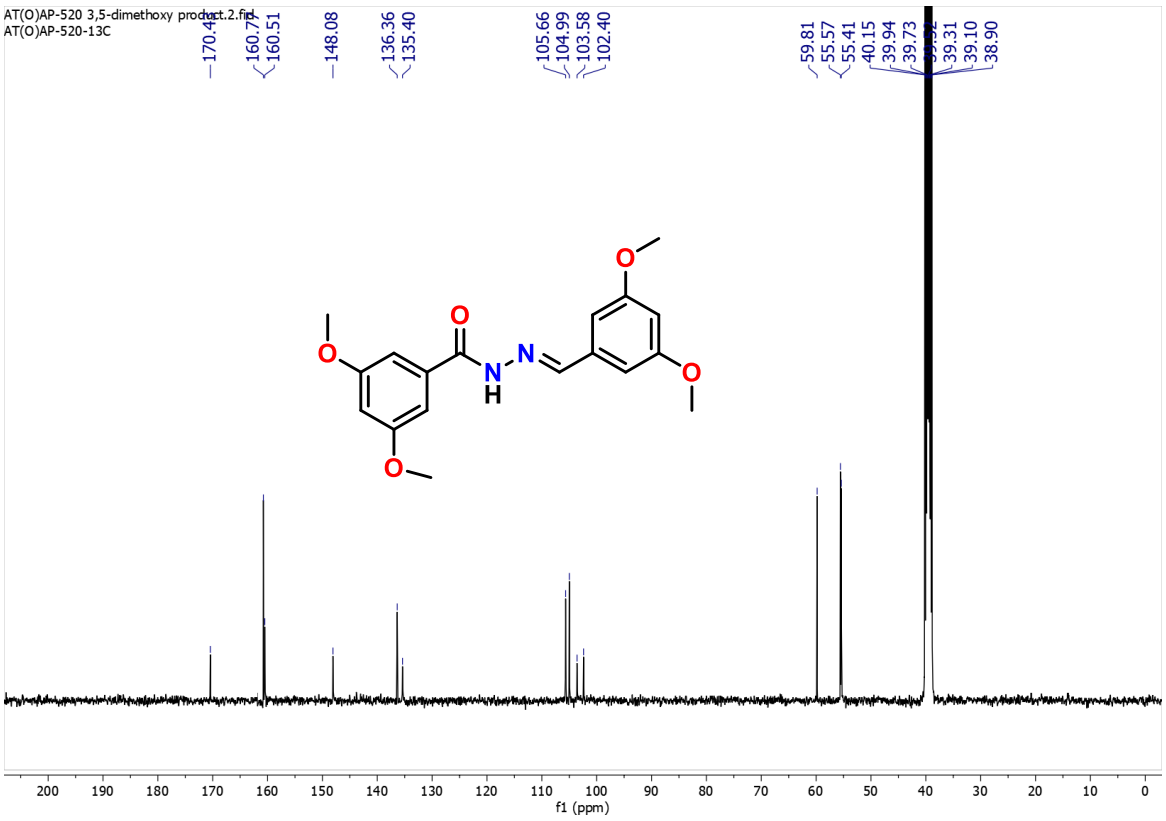

Figure 4.19. $^{13}C\{^{1}H\}$ NMR (100 MHz) spectrum of **4g** in DMSO-d_6.

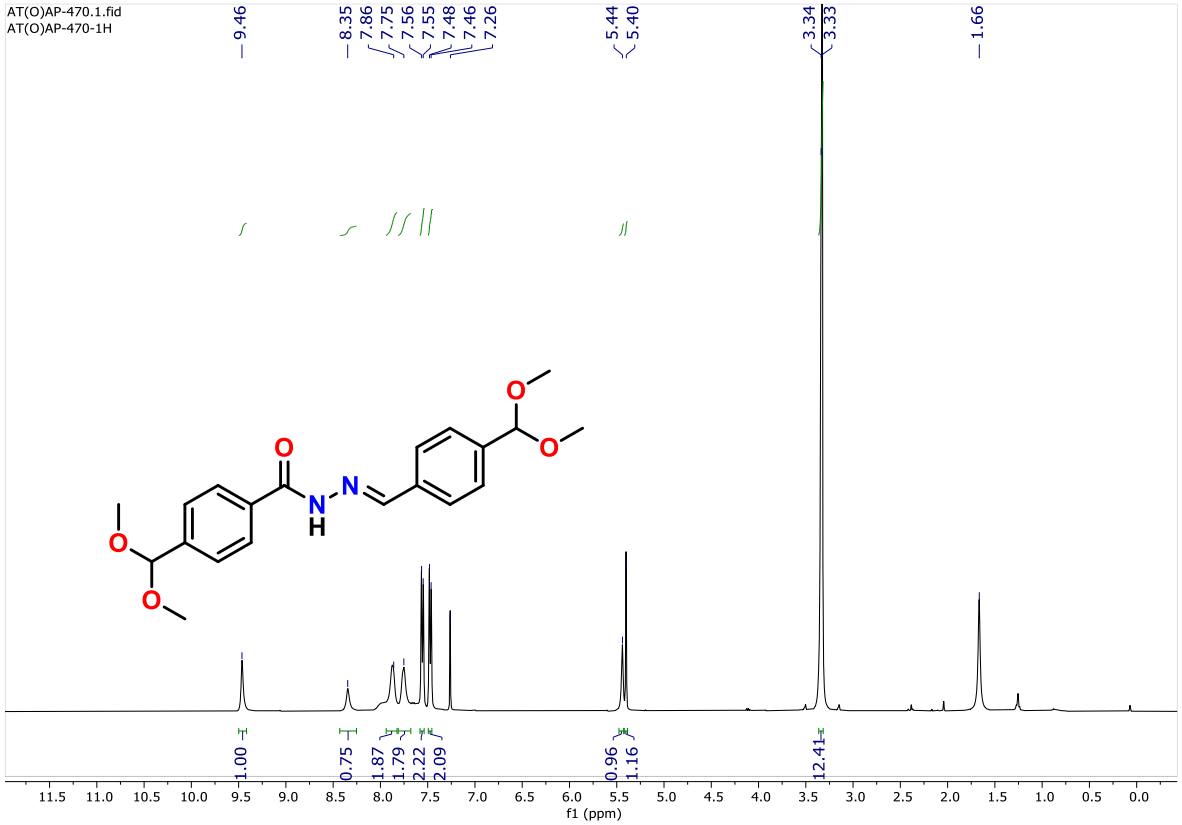

Figure 4.20. ^{1}H NMR (400 MHz) spectrum of **4h** in $CDCl_3$.

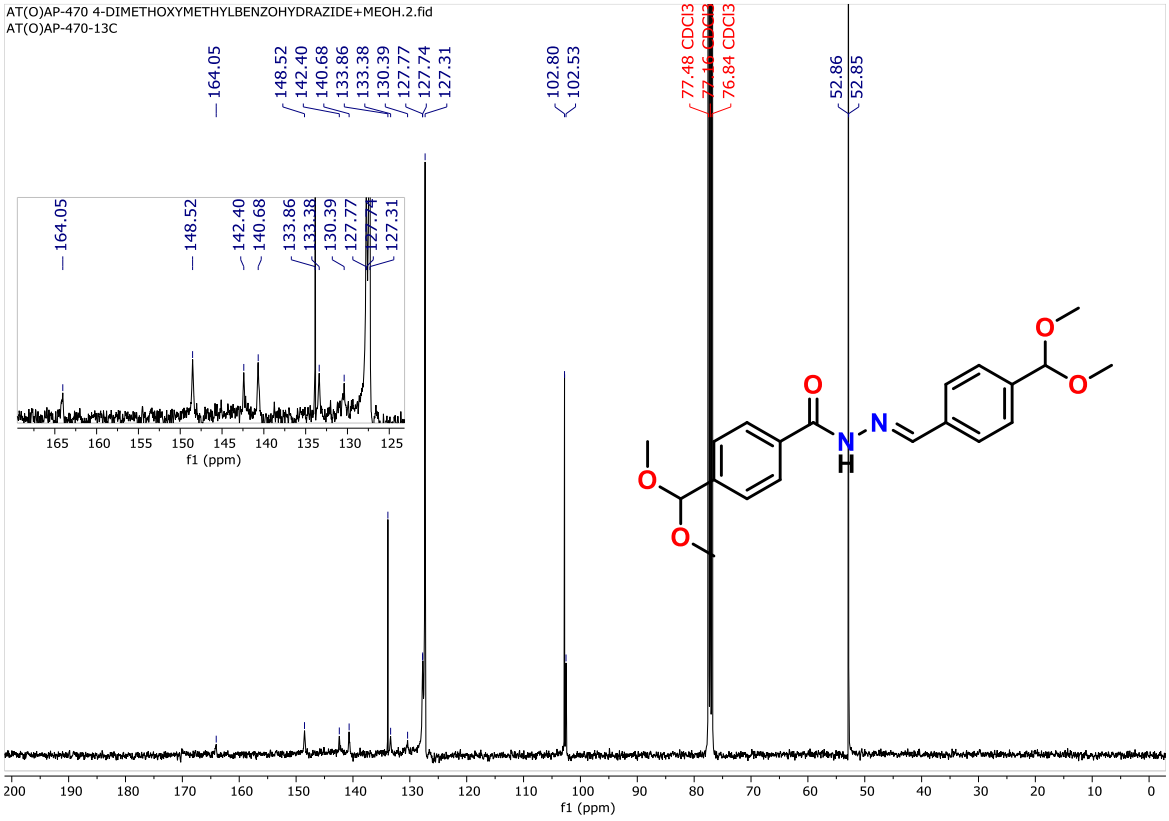

Figure 4.21. $^{13}C\{^{1}H\}$ NMR (100 MHz) spectrum of **4h** in $CDCl_3$.

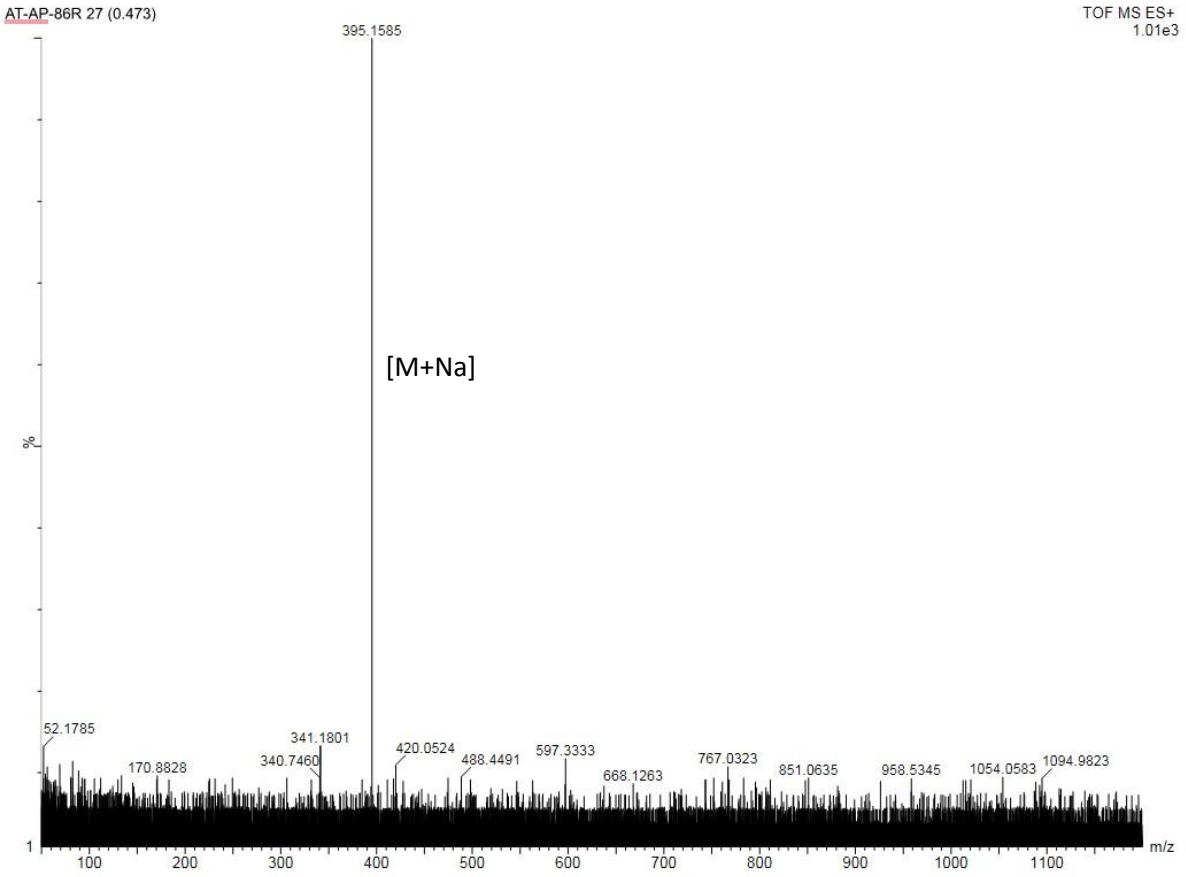

Figure 4.22. HRMS of **4h**.

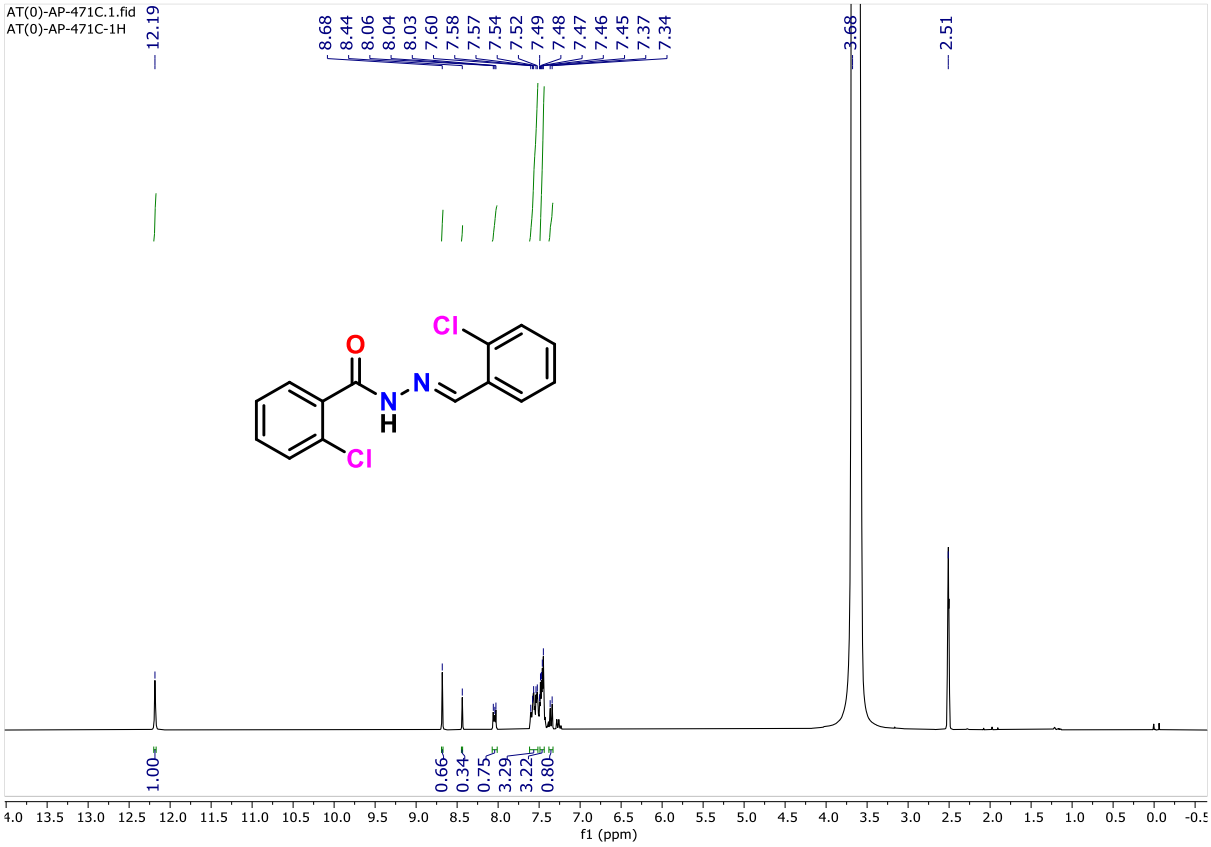

Figure 4.23. ^{1}H NMR (400 MHz) spectrum of **4i** in DMSO-d$_6$.

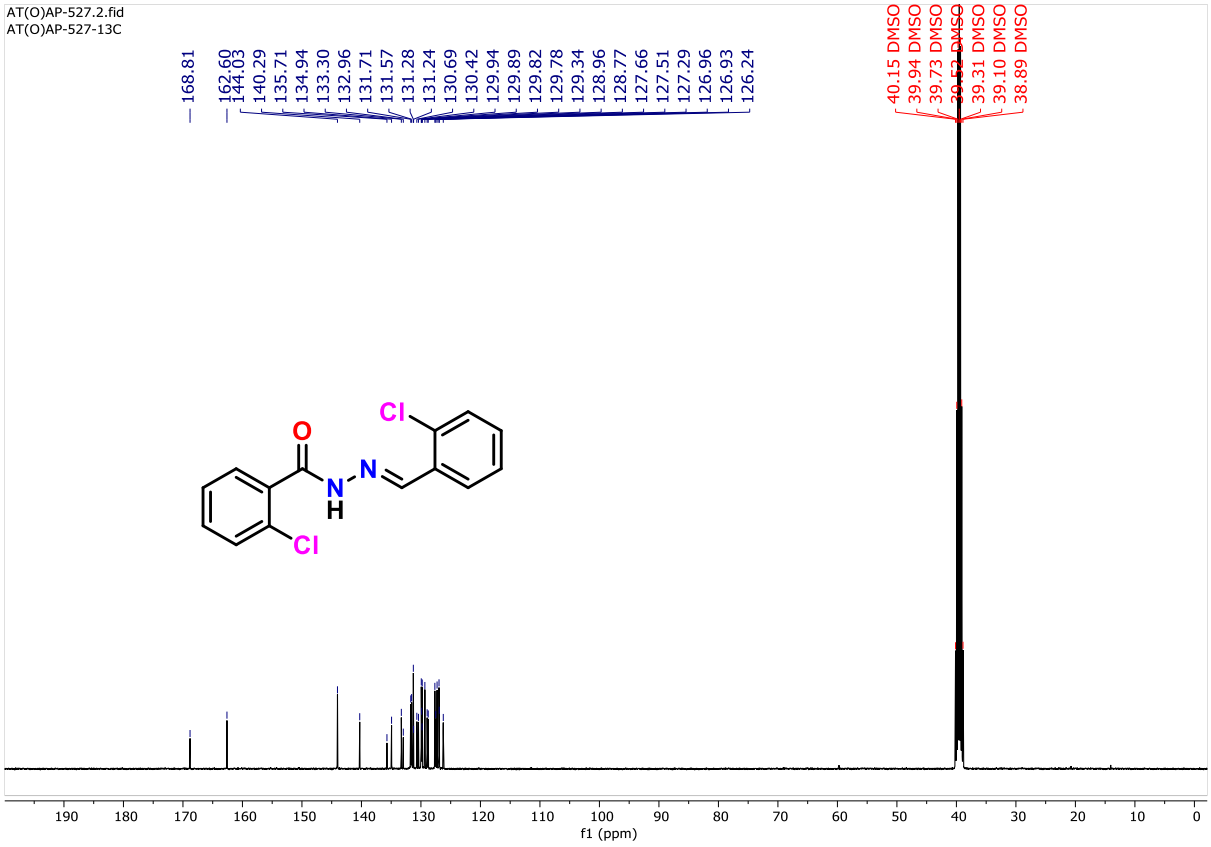

Figure 4.24. ^{13}C{^{1}H} NMR (100 MHz) spectrum of **4i** in DMSO-d$_6$.

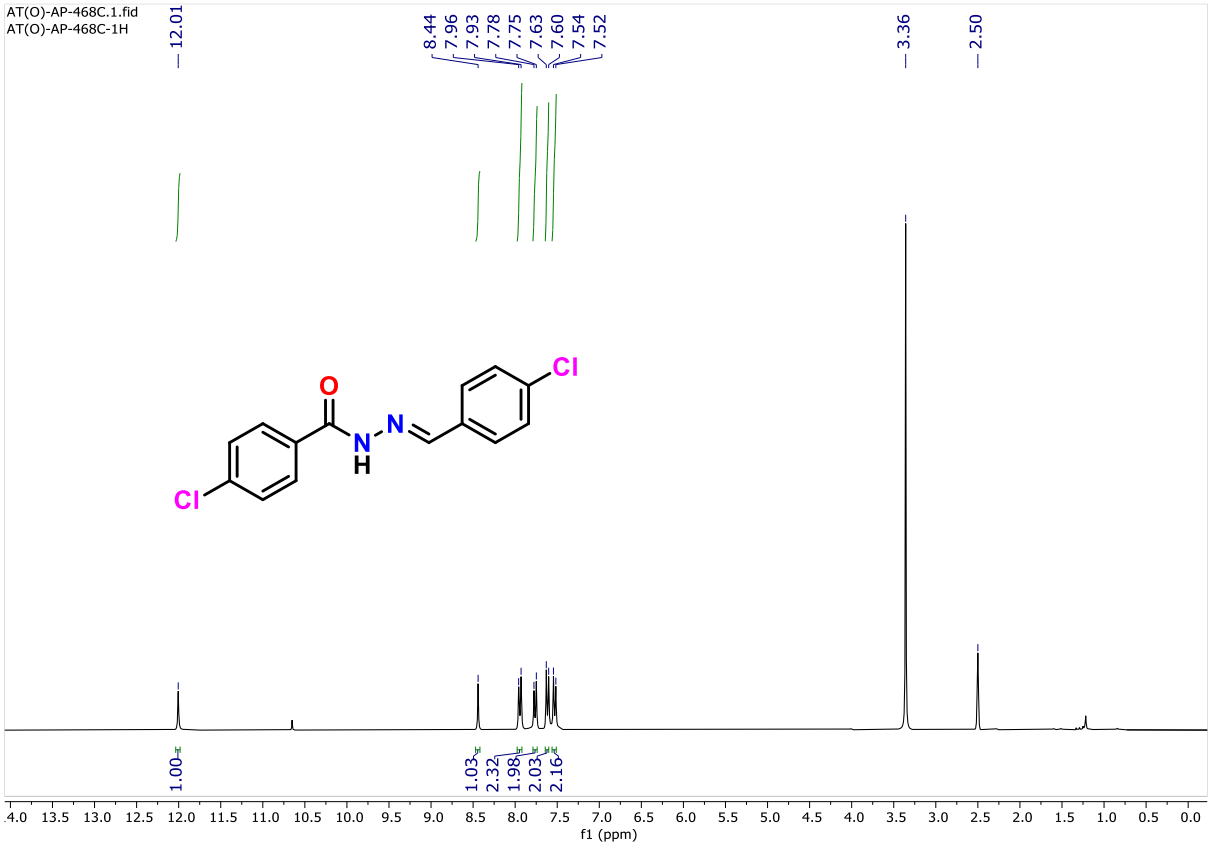

Figure 4.25. ^{1}H NMR (400 MHz) spectrum of **4j** in DMSO-d_6.

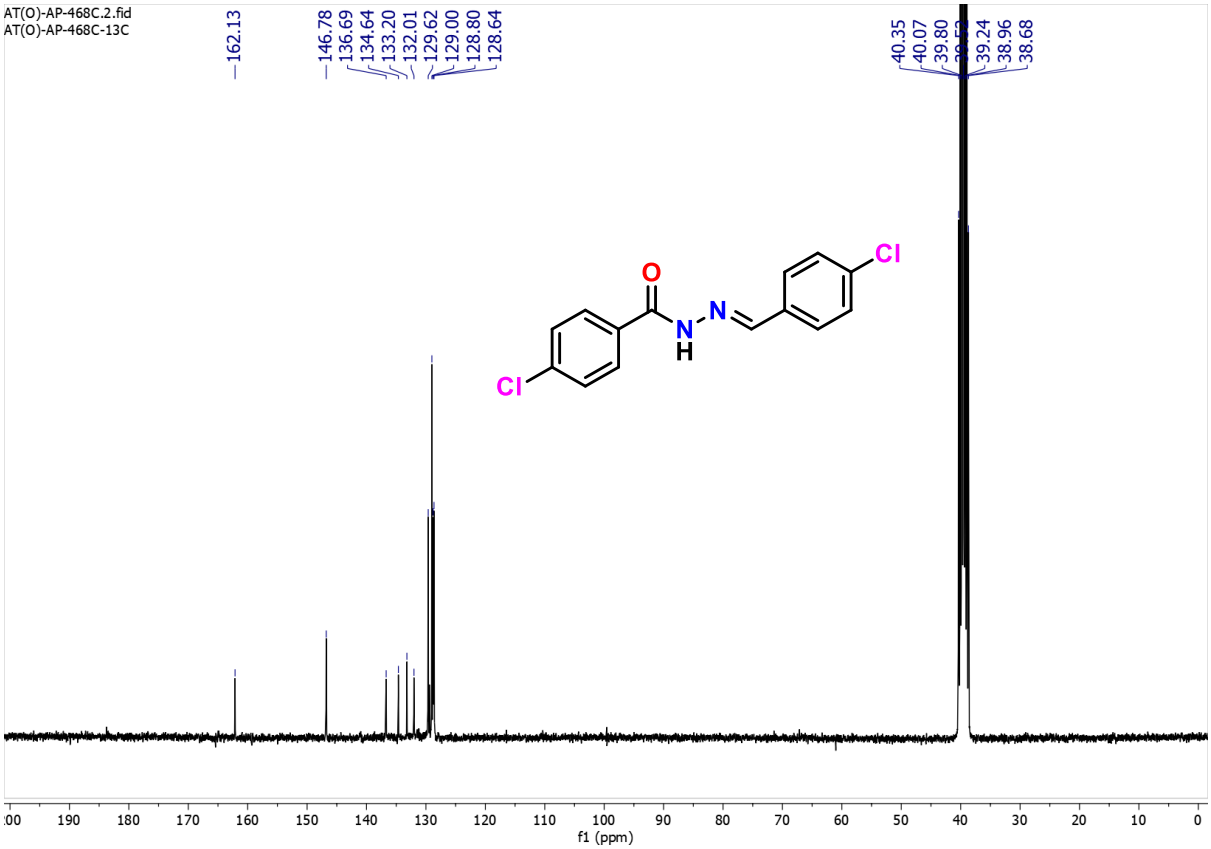

Figure 4.26. $^{13}C\{^{1}H\}$ NMR (100 MHz) spectrum of **4j** in DMSO-d_6.

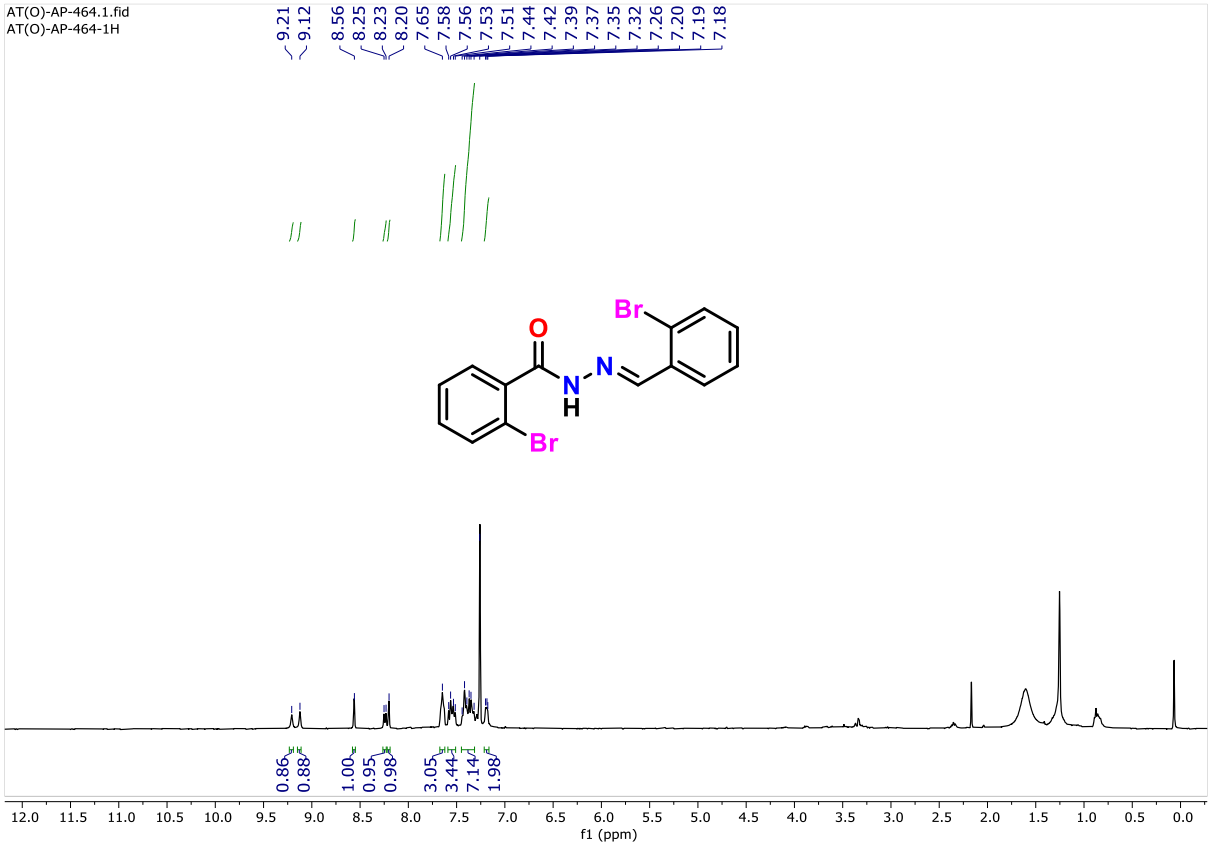

Figure 4.27. ^{1}H NMR (400 MHz) spectrum of **4k** in $CDCl_3$.

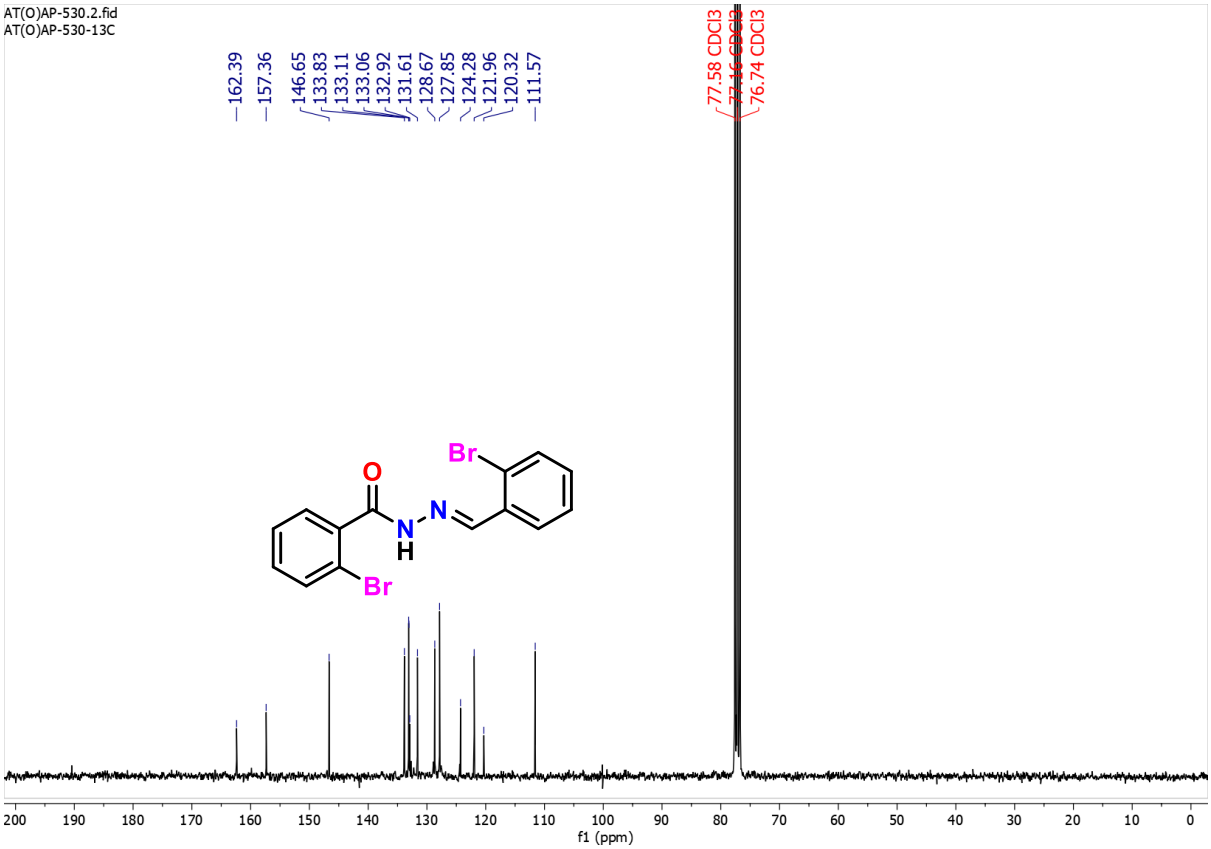

Figure 4.28. $^{13}C\{^{1}H\}$ NMR (100 MHz) spectrum of **4k** $CDCl_3$.

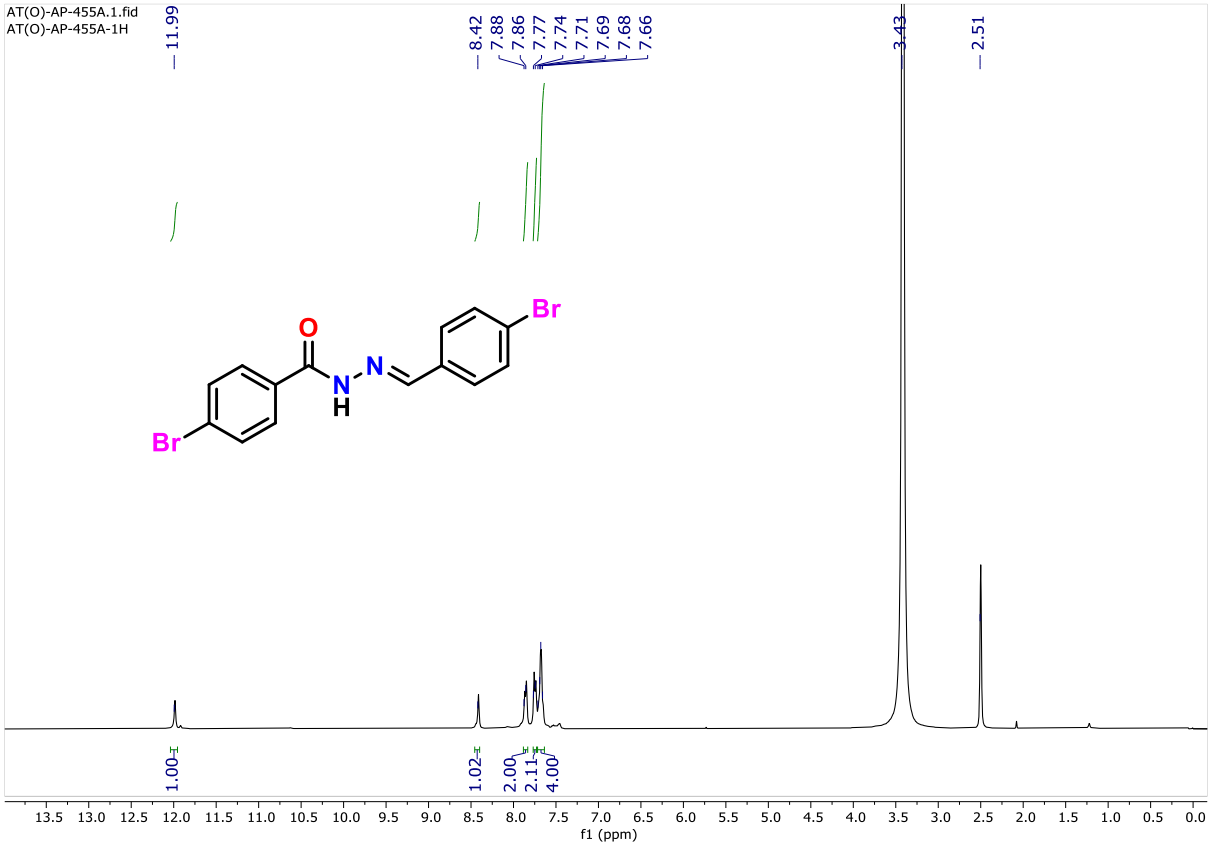

Figure 4.29. ^{1}H NMR (400 MHz) spectrum of **4l** in DMSO-d_6.

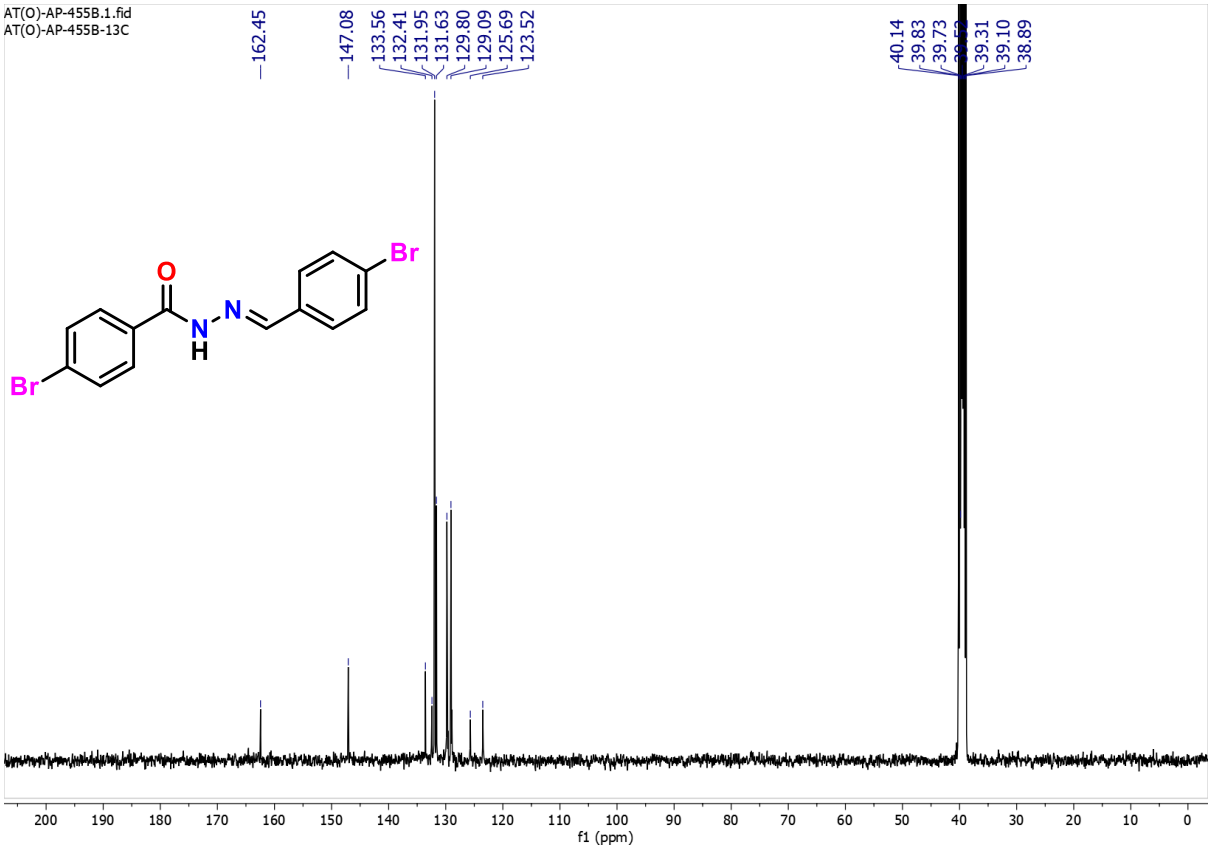

Figure 4.30. $^{13}C\{^{1}H\}$ NMR (100 MHz) spectrum of **4l** in DMSO-d_6.

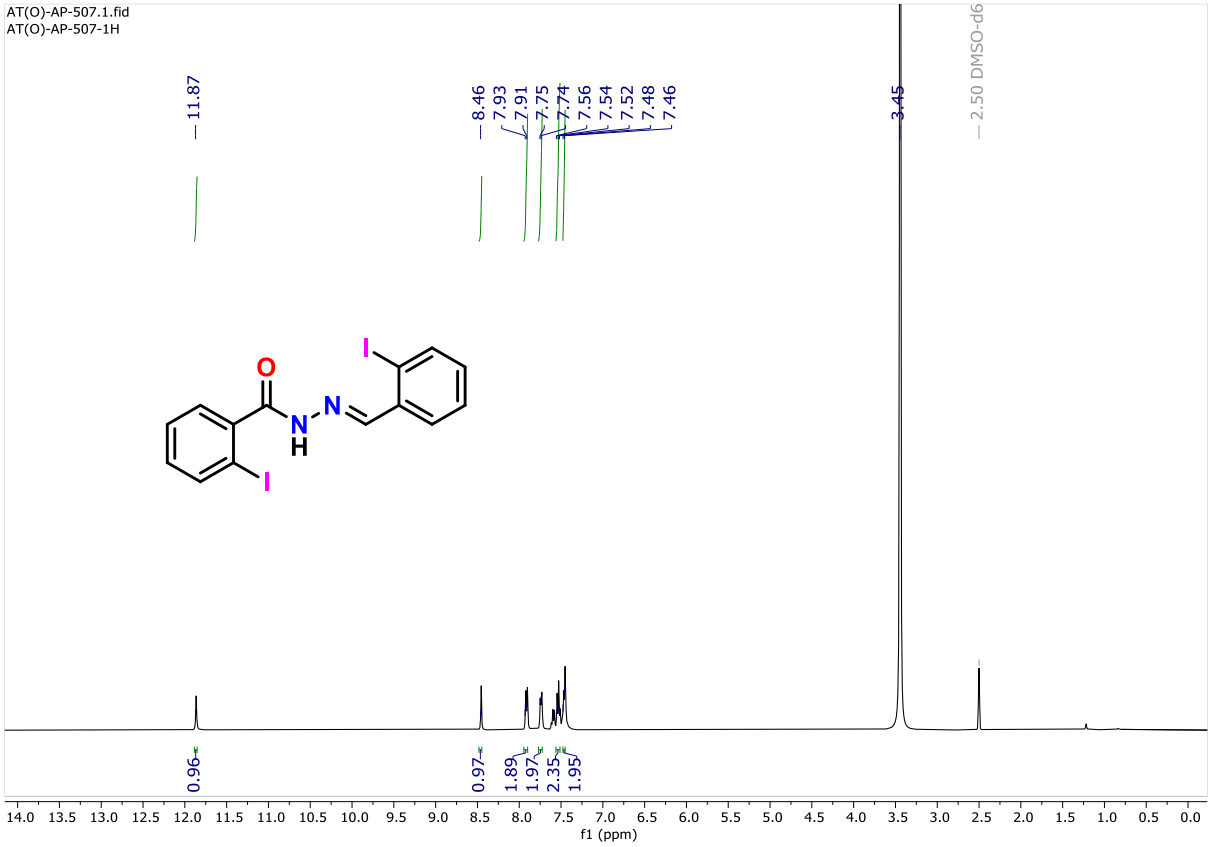

Figure 4.31. ^{1}H NMR (400 MHz) spectrum of **4m** in DMSO-d_6.

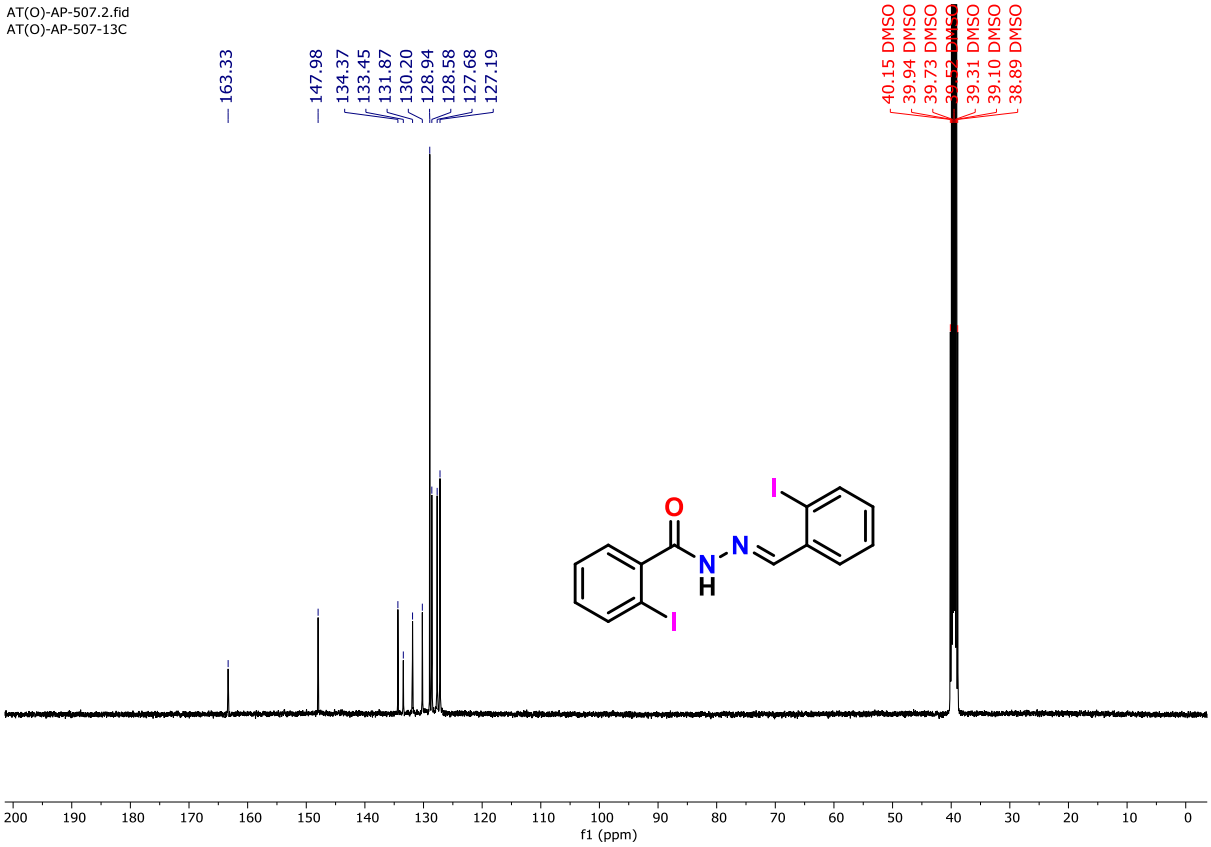

Figure 4.32. $^{13}C\{^{1}H\}$ NMR (100 MHz) spectrum of **4m** in DMSO-d_6.

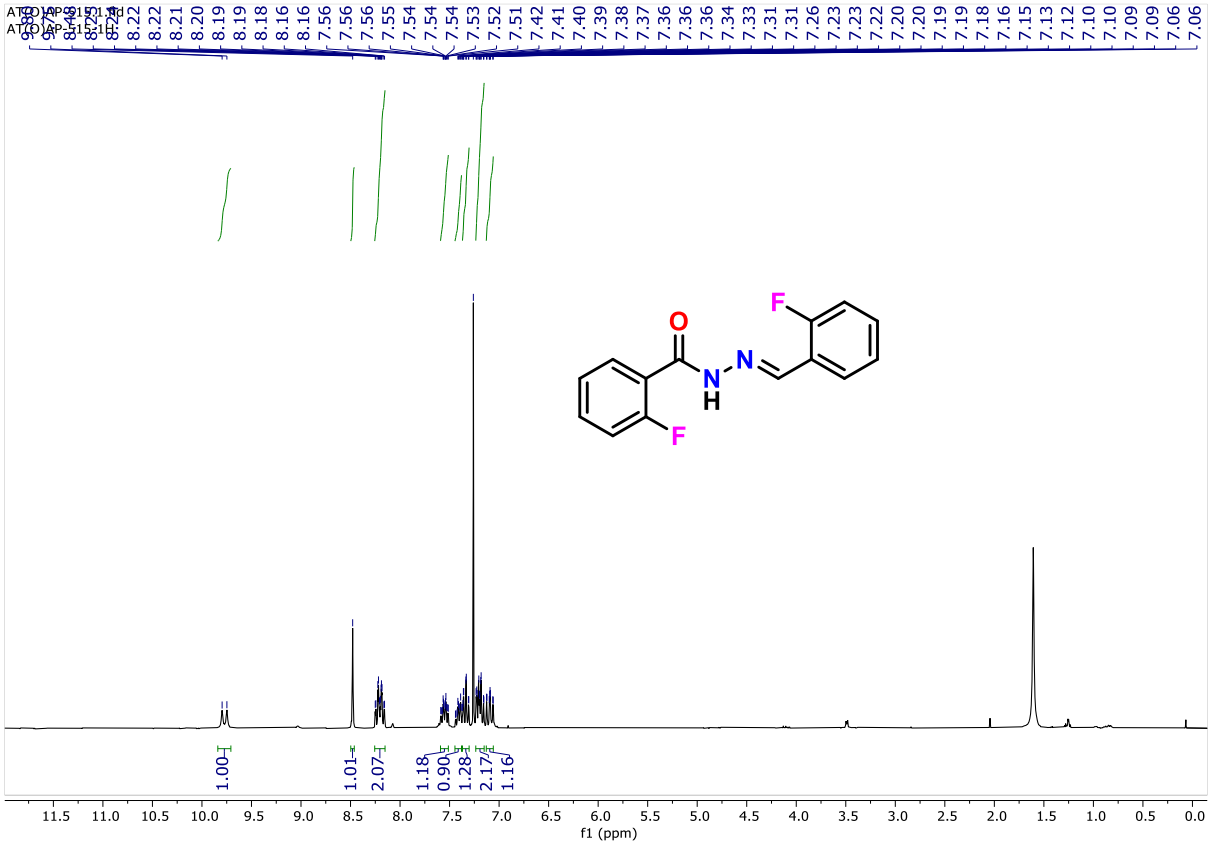

Figure 4.33. ^{1}H NMR (400 MHz) spectrum of **4n** in $CDCl_3$.

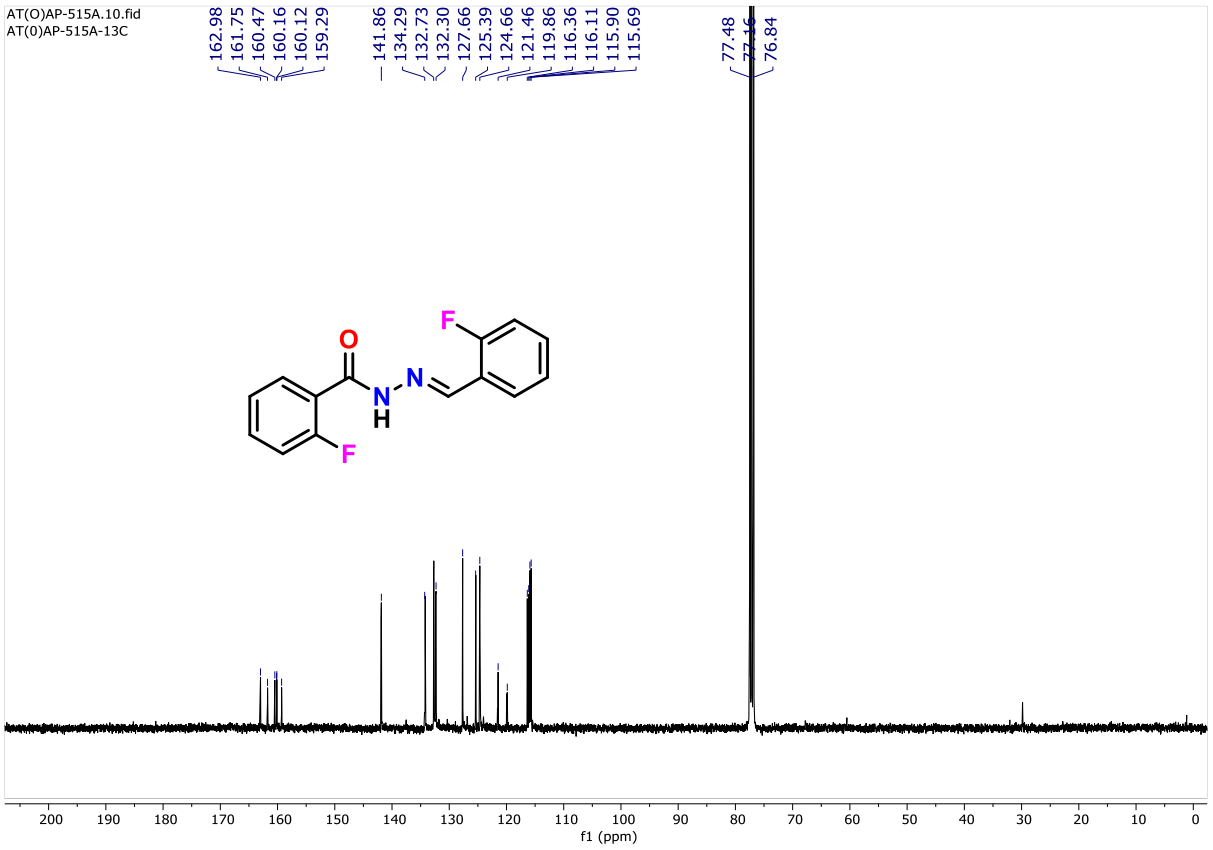

Figure 4.34. $^{13}C\{^{1}H\}$ NMR (100 MHz) spectrum of **4n** in $CDCl_3$.

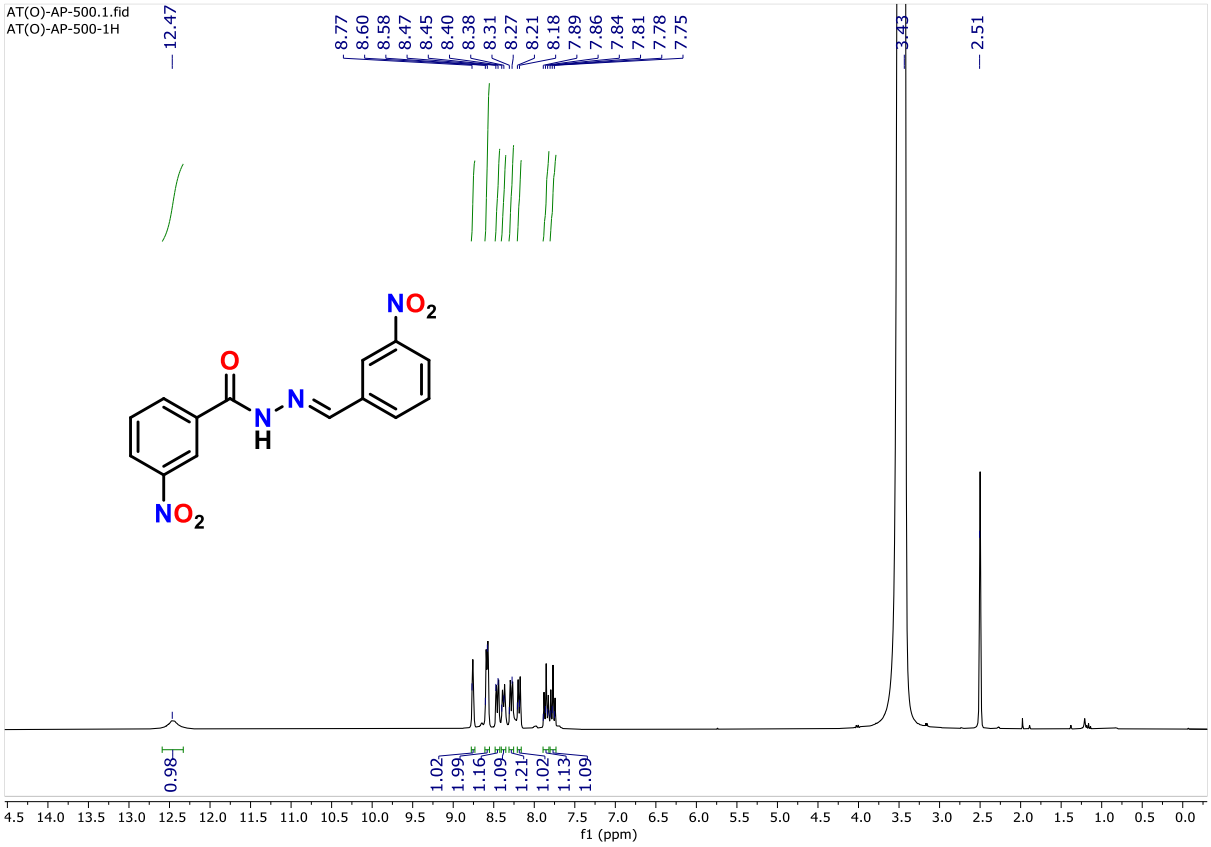

Figure 4.35. ^{1}H NMR (400 MHz) spectrum of **4o** in DMSO-d$_6$.

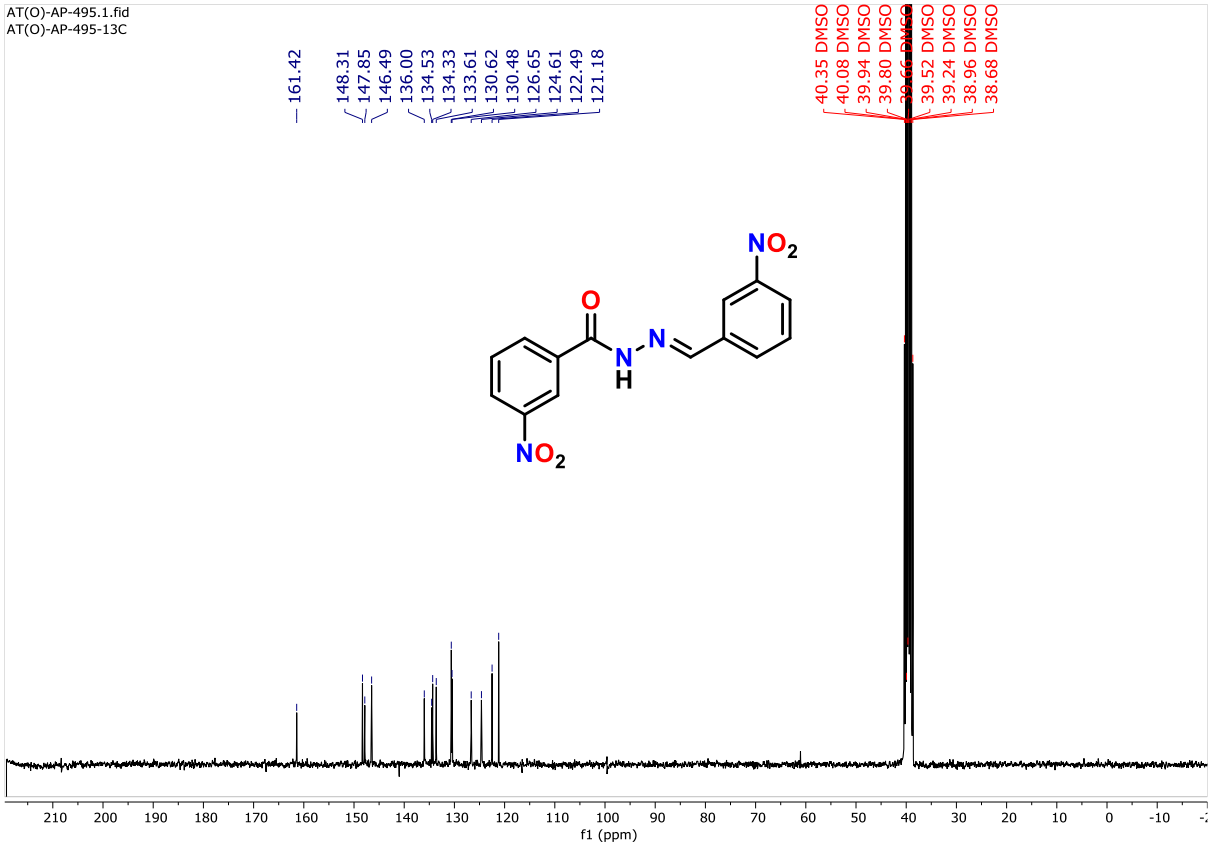

Figure 4.36. ^{13}C{^{1}H} NMR (100 MHz) spectrum of **4o** in DMSO-d$_6$.

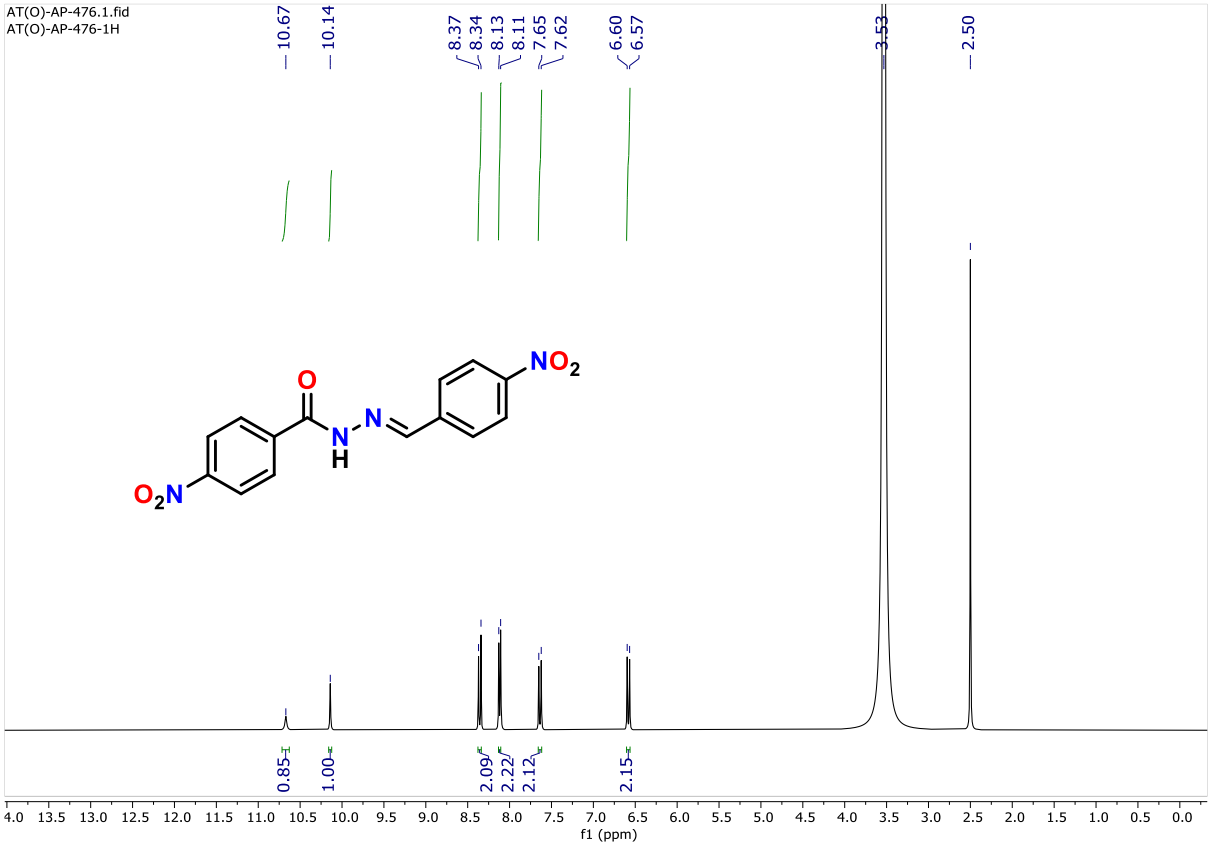

Figure 4.37. ^{1}H NMR (400 MHz) spectrum of **4p** in DMSO-d_6.

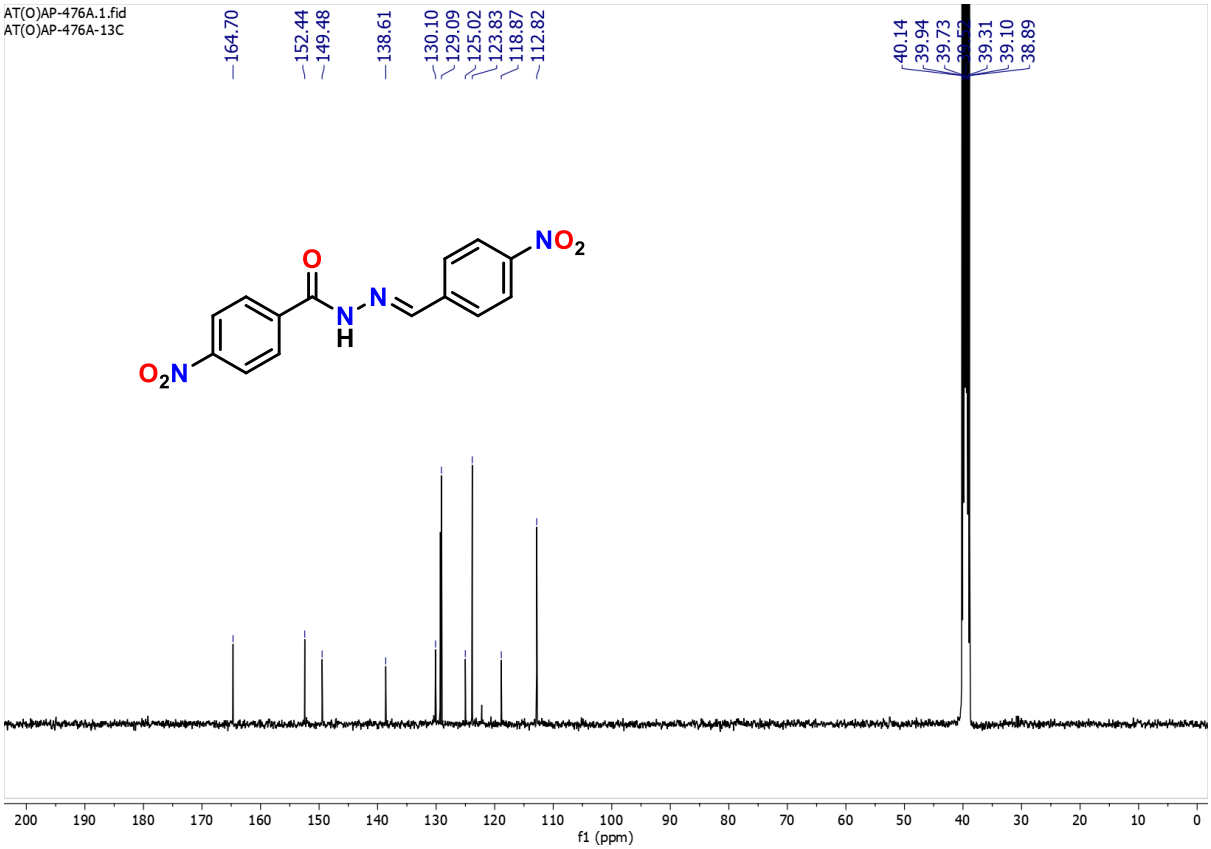

Figure 4.38. $^{13}C\{^{1}H\}$ NMR (100 MHz) spectrum of **4p** in DMSO-d_6.

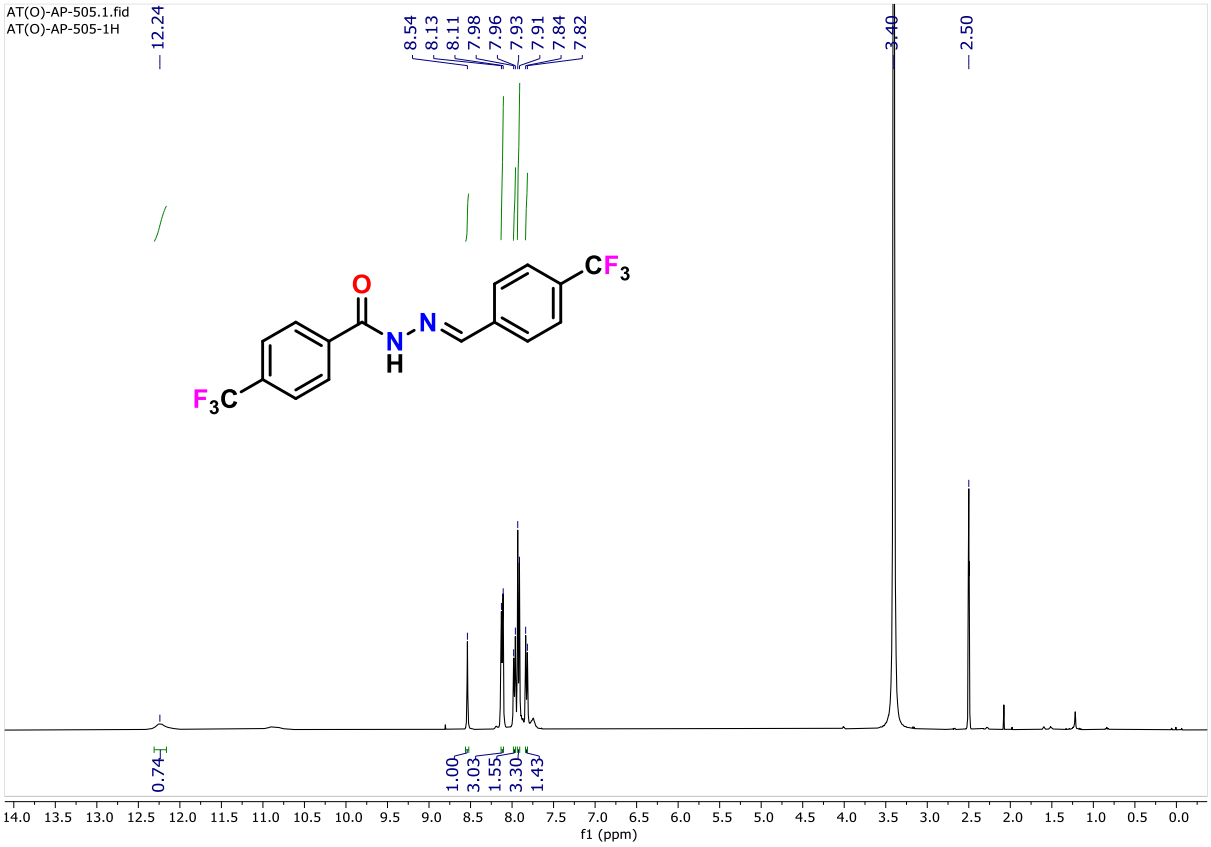

Figure 4.39. ^{1}H NMR (400 MHz) spectrum of **4q** in DMSO-d_6.

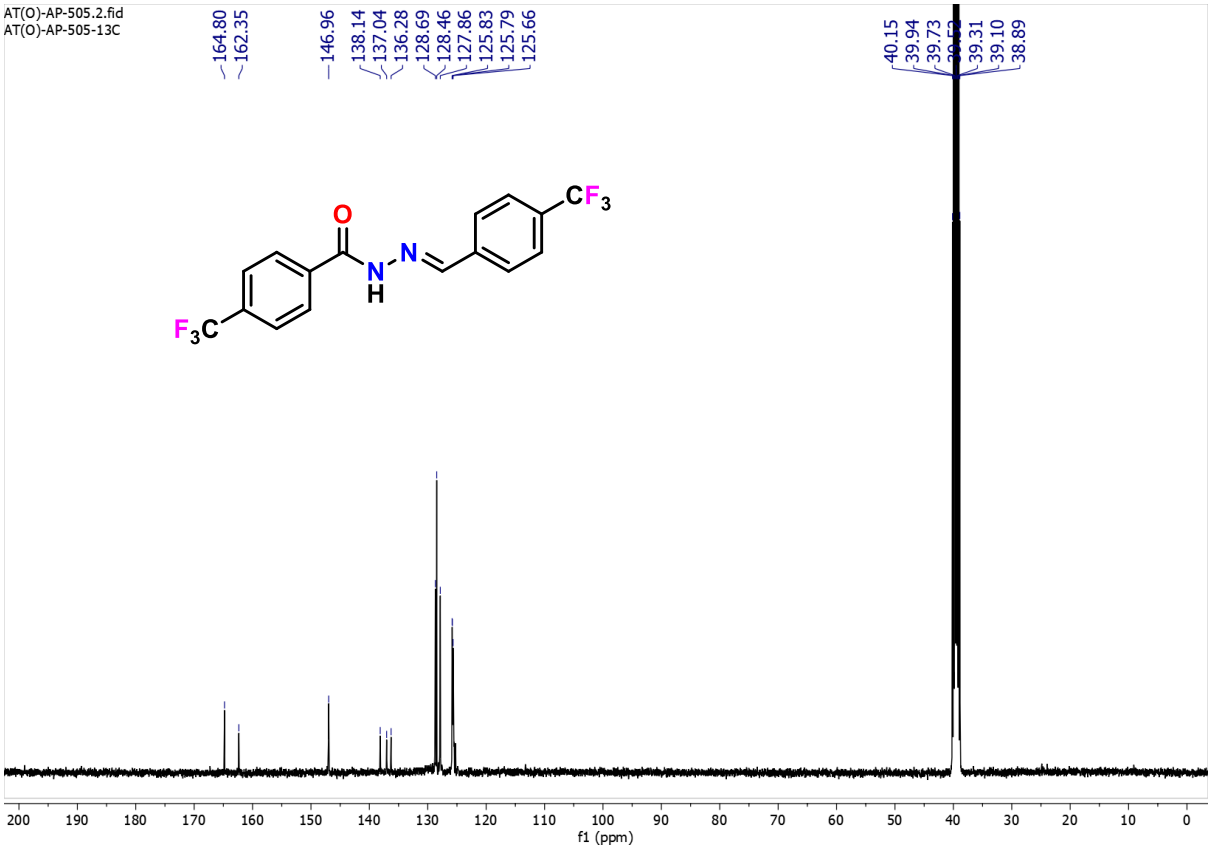

Figure 4.40. $^{13}C\{^{1}H\}$ NMR (100 MHz) spectrum of **4q** in DMSO-d_6.

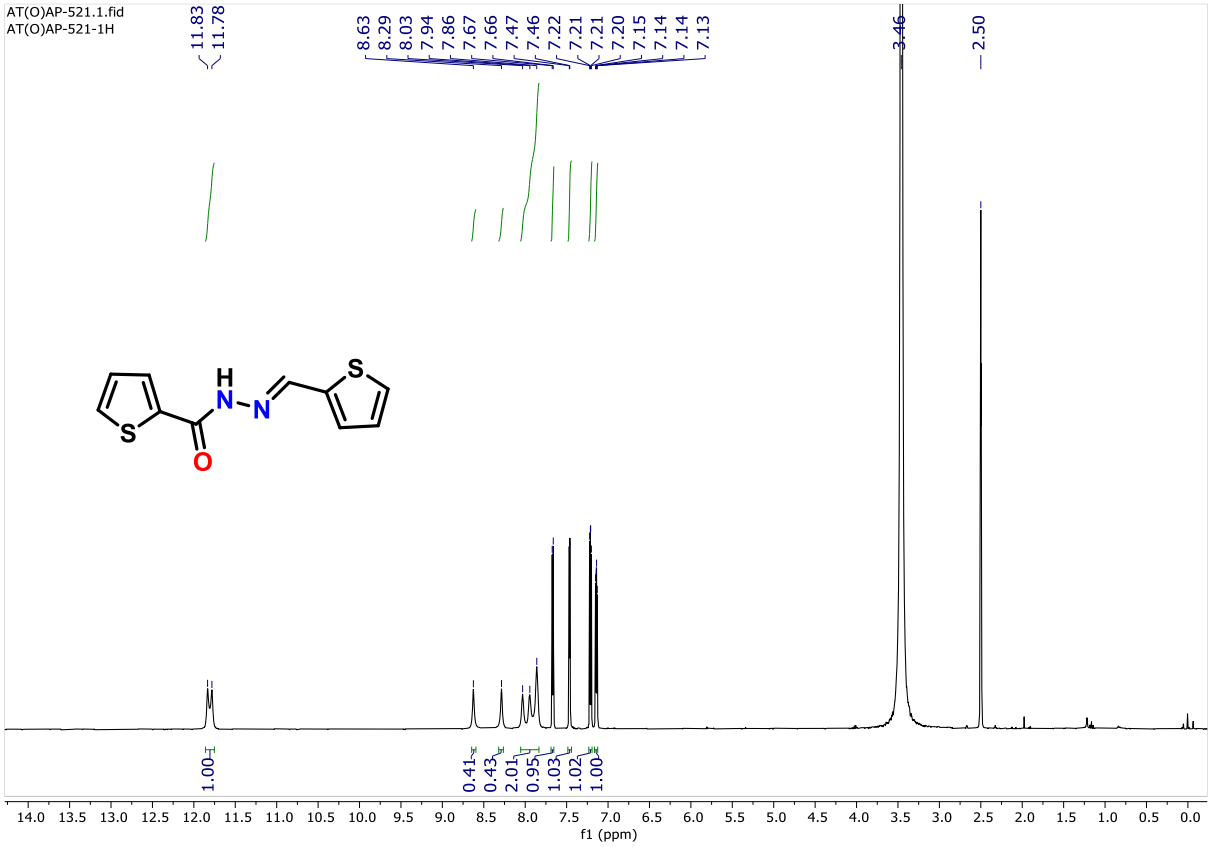

Figure 4.41. ^{1}H NMR (300 MHz) spectrum of **4r** in DMSO-d_6.

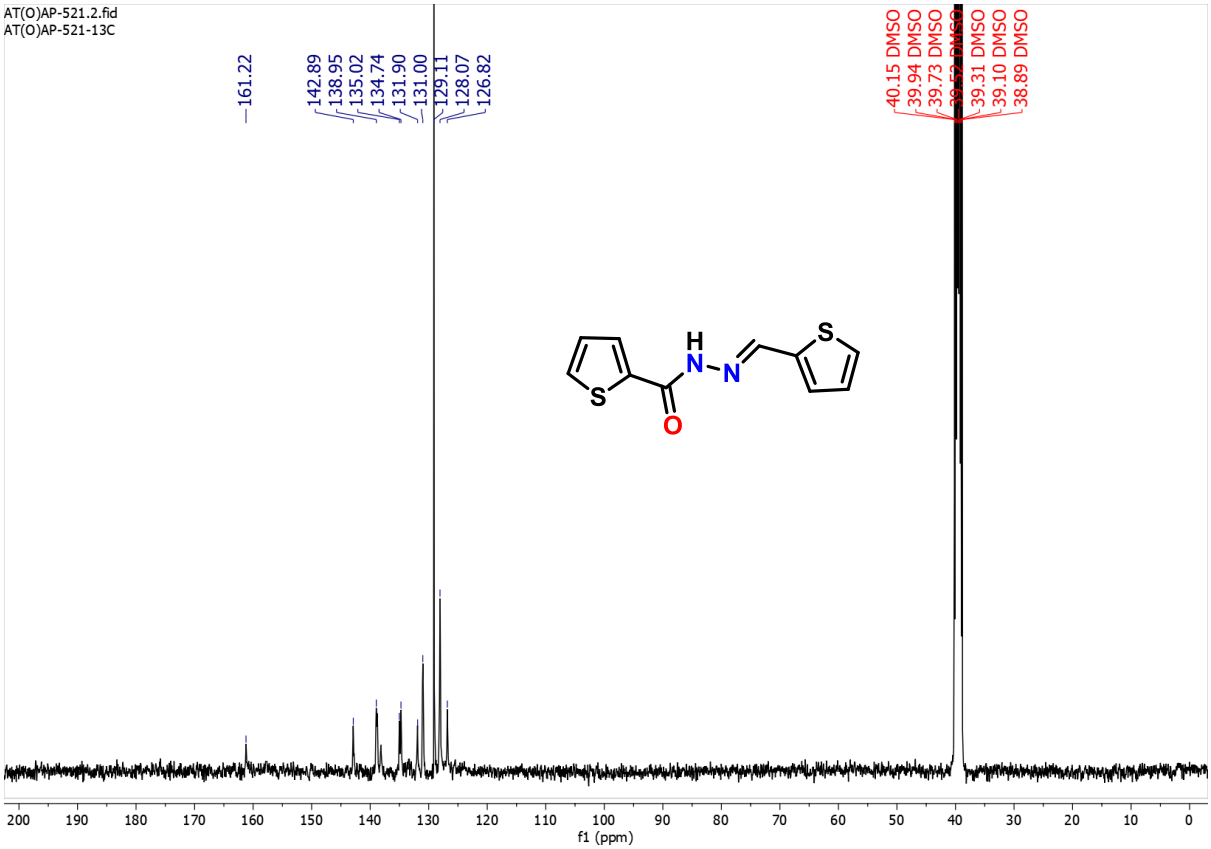

Figure 4.42. $^{13}C\{^{1}H\}$ NMR (75 MHz) spectrum of **4r** in DMSO-d_6.

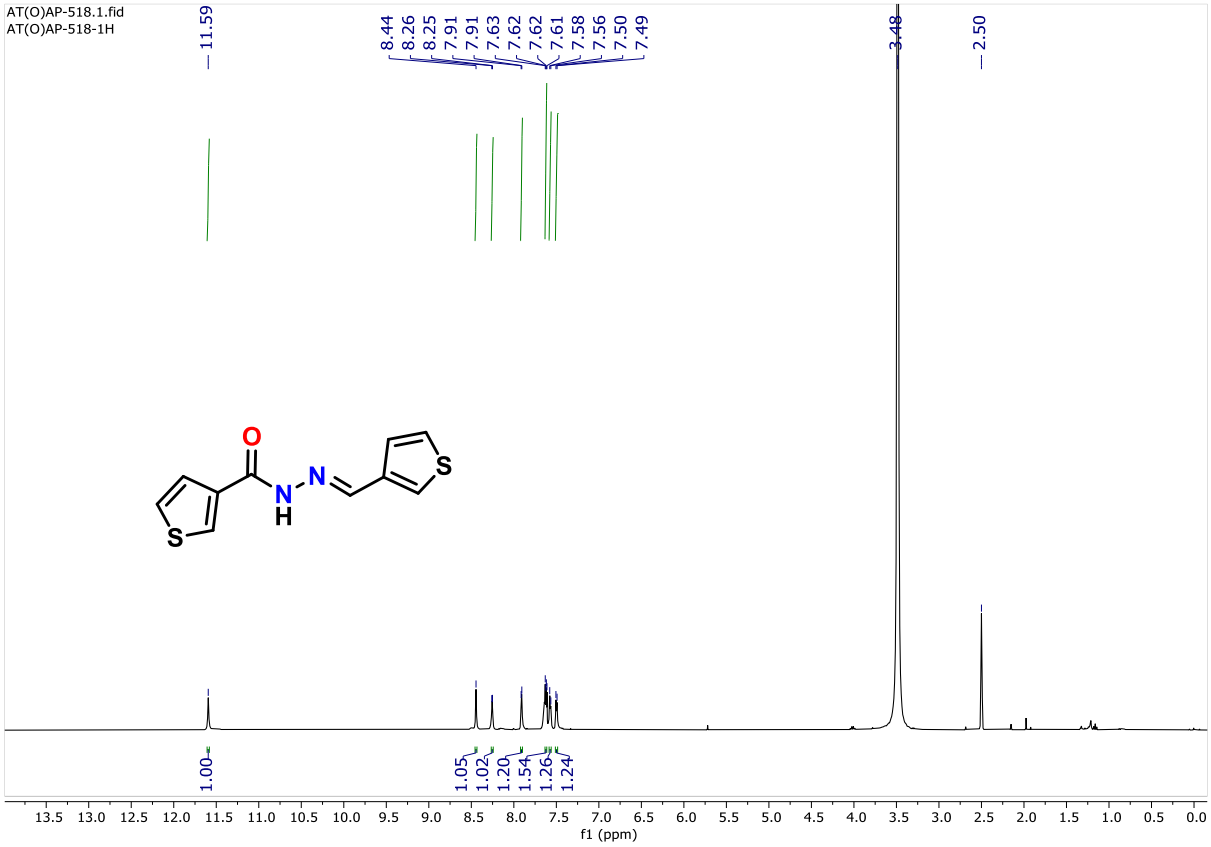

Figure 4.43. ^{1}H NMR (400 MHz) spectrum of **4s** in DMSO-d_6.

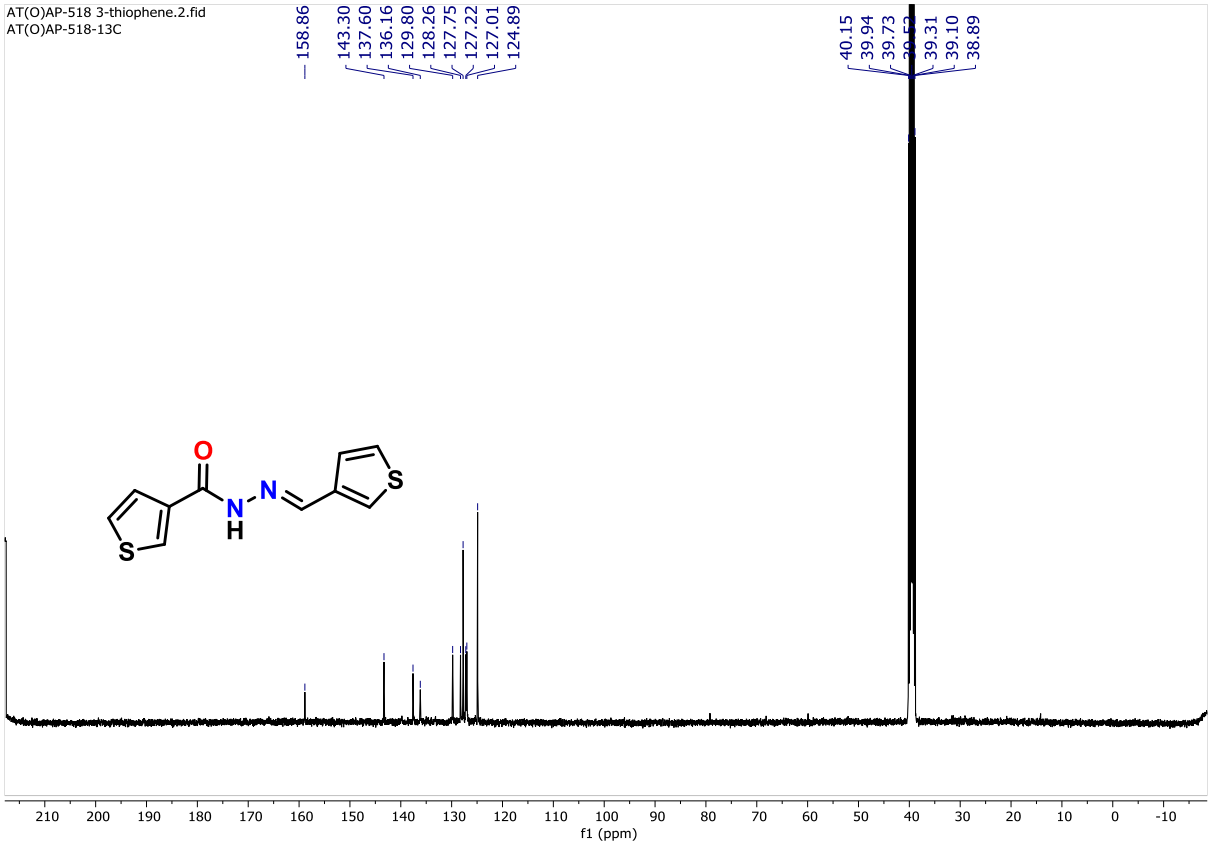

Figure 4.44. $^{13}C\{^{1}H\}$ NMR (100 MHz) spectrum of **4s** in DMSO-d_6.

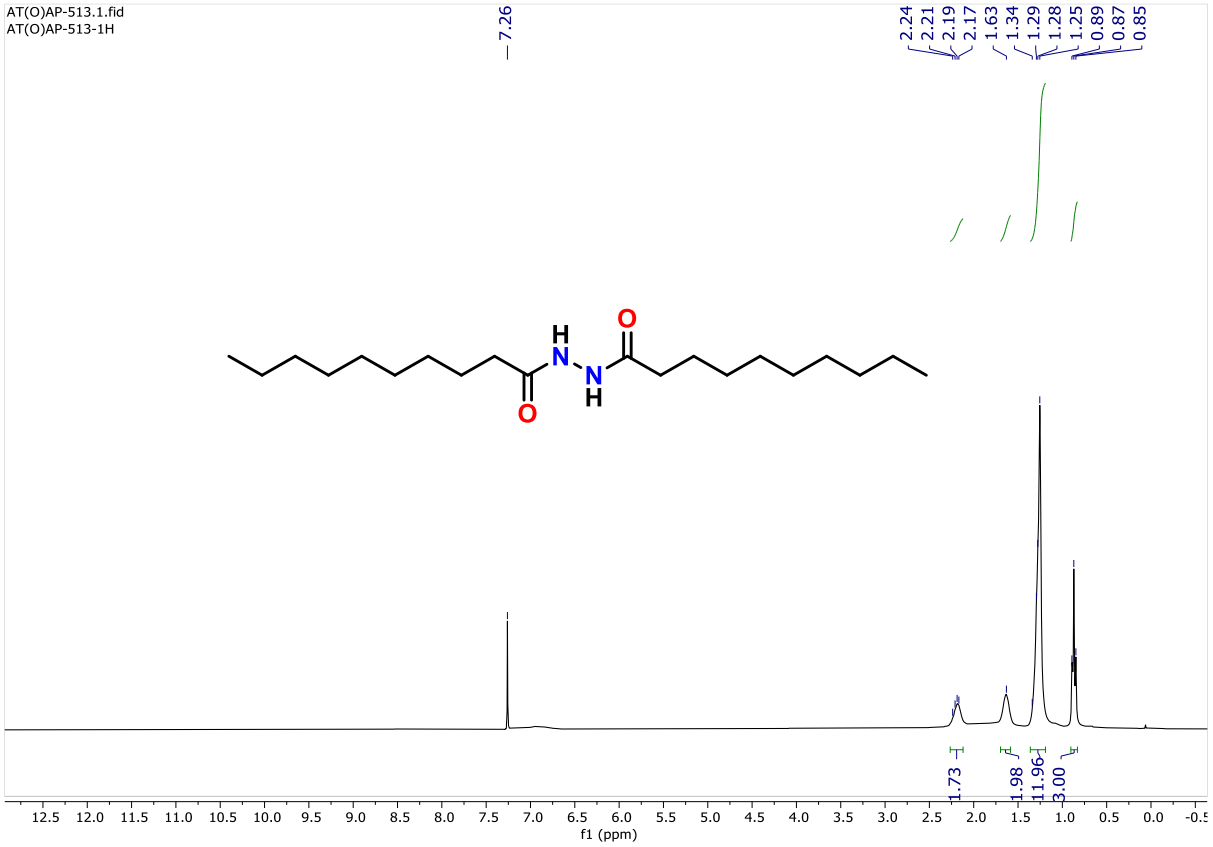

Figure 4.45. ^{1}H NMR (300 MHz) spectrum of **4t** in $CDCl_3$.

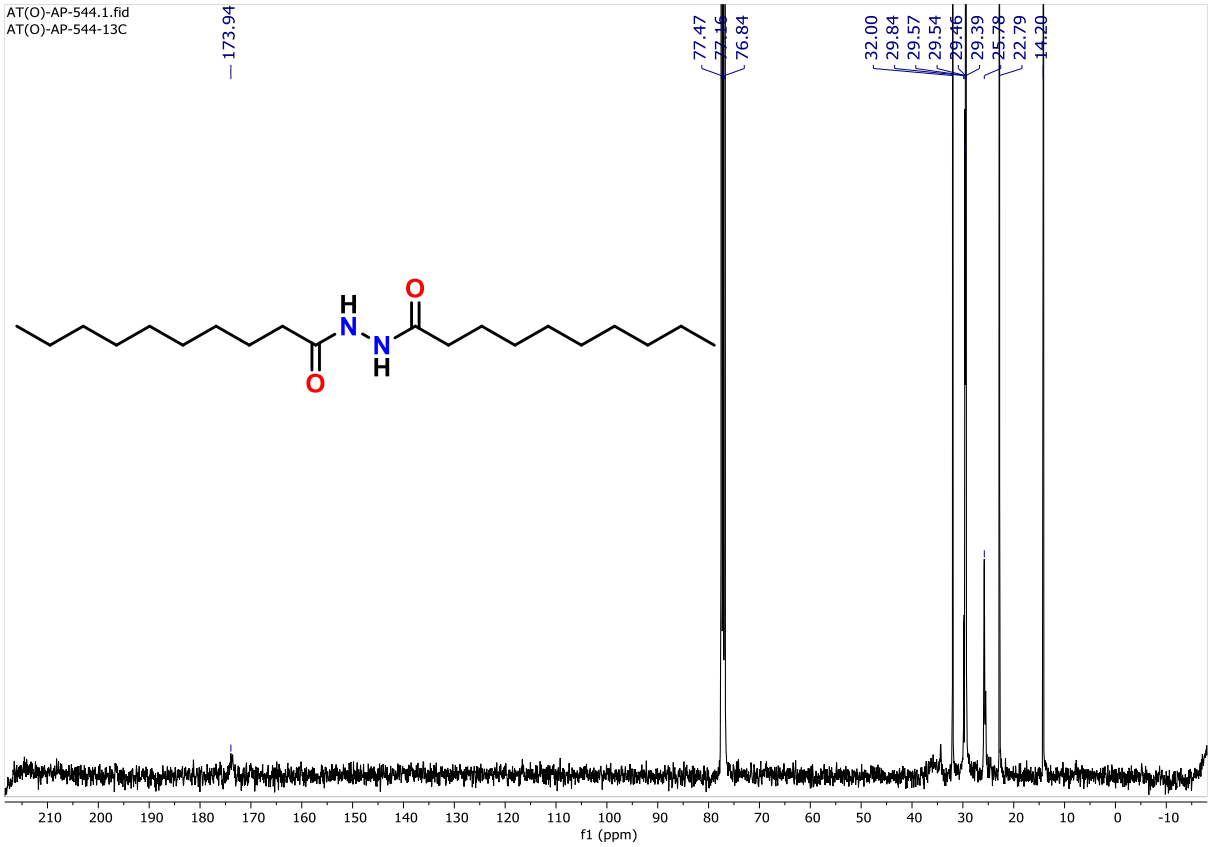

Figure 4.46. $^{13}C\{^{1}H\}$ NMR (75 MHz) spectrum of **4t** in $CDCl_3$.

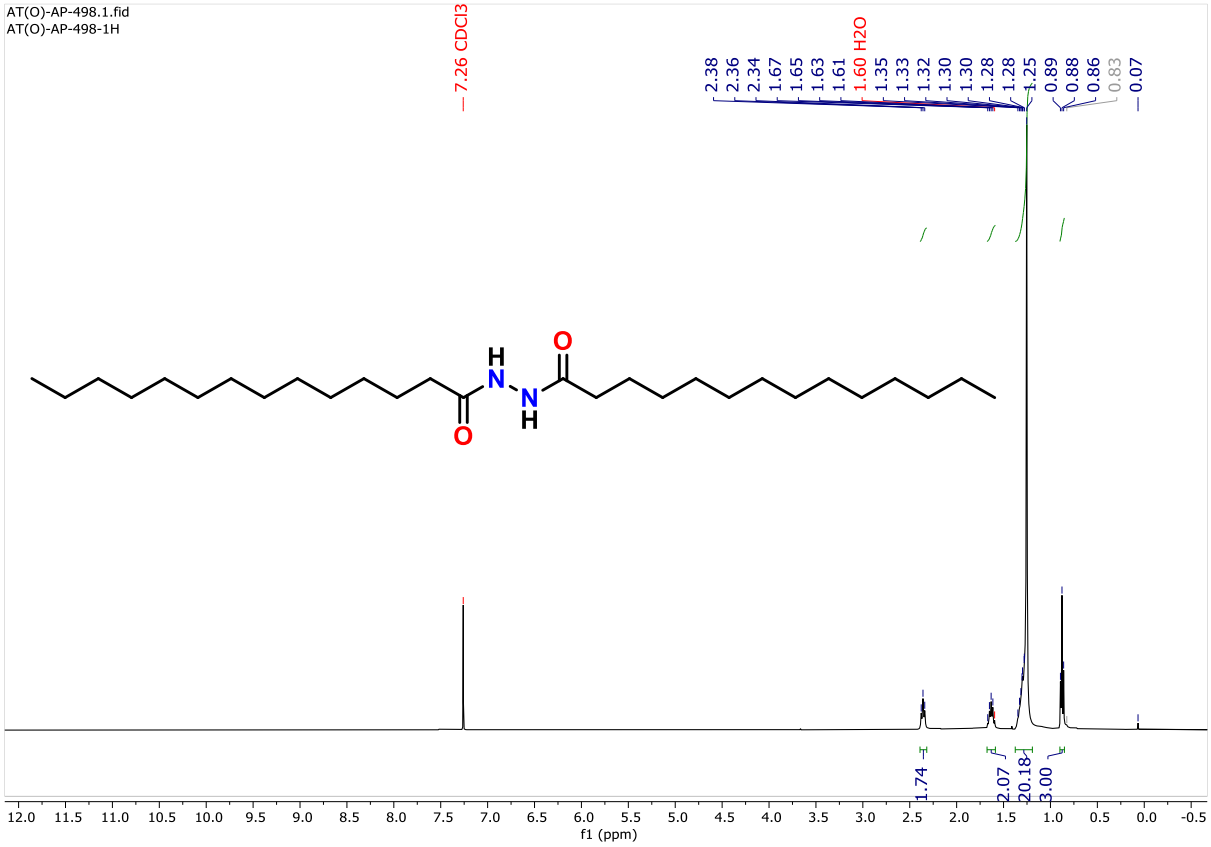

Figure 4.47. ^{1}H NMR (300 MHz) spectrum of **4u** in $CDCl_3$.

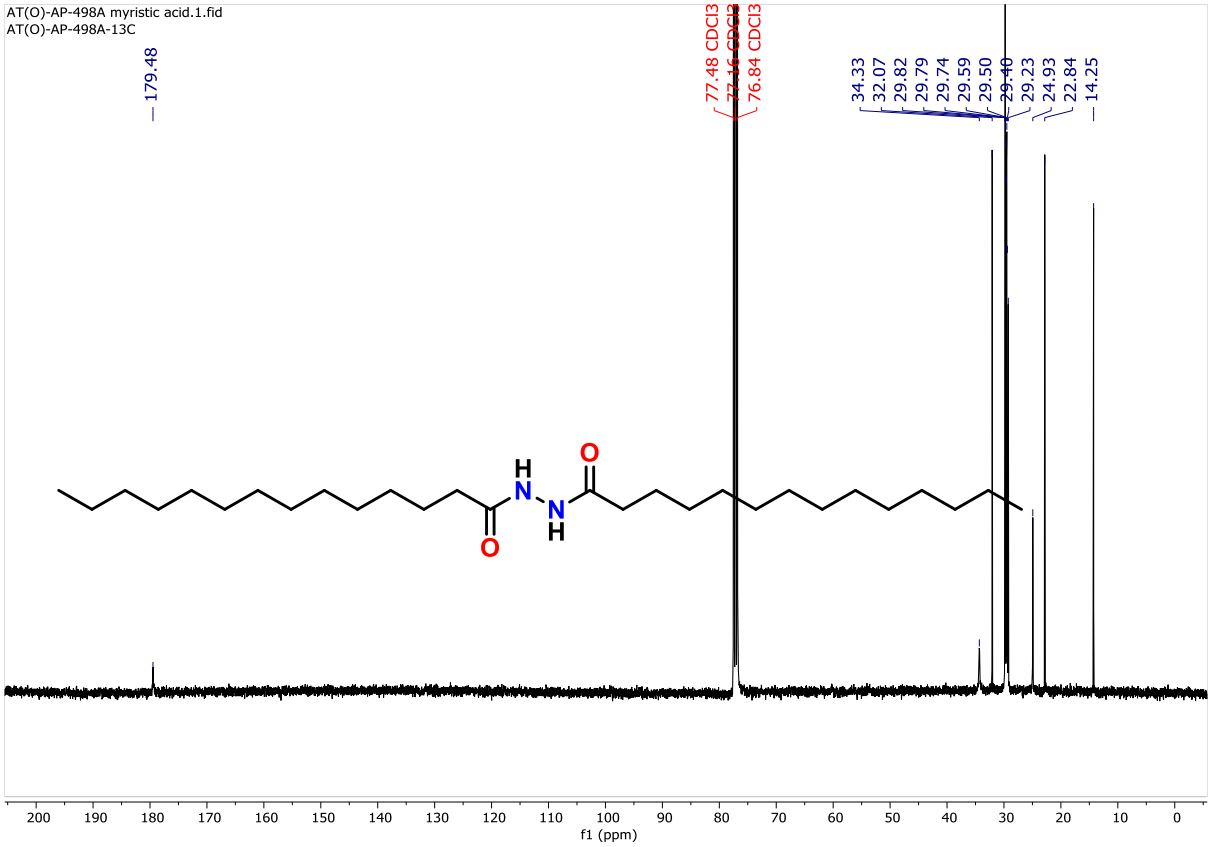

Figure 4.48. $^{13}C\{^{1}H\}$ NMR (75 MHz) spectrum of **4u** in $CDCl_3$.

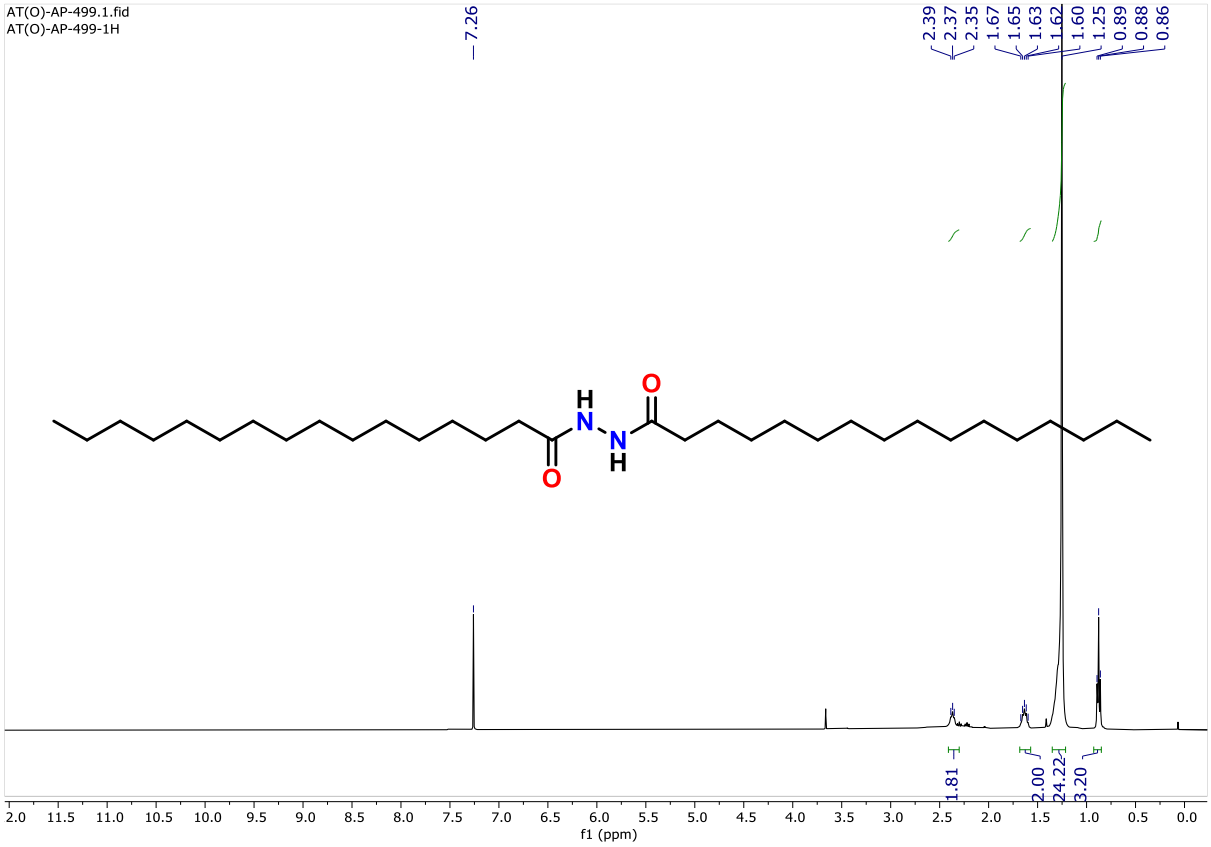

Figure 4.49. ^{1}H NMR (300 MHz) spectrum of **4v** in $CDCl_3$.

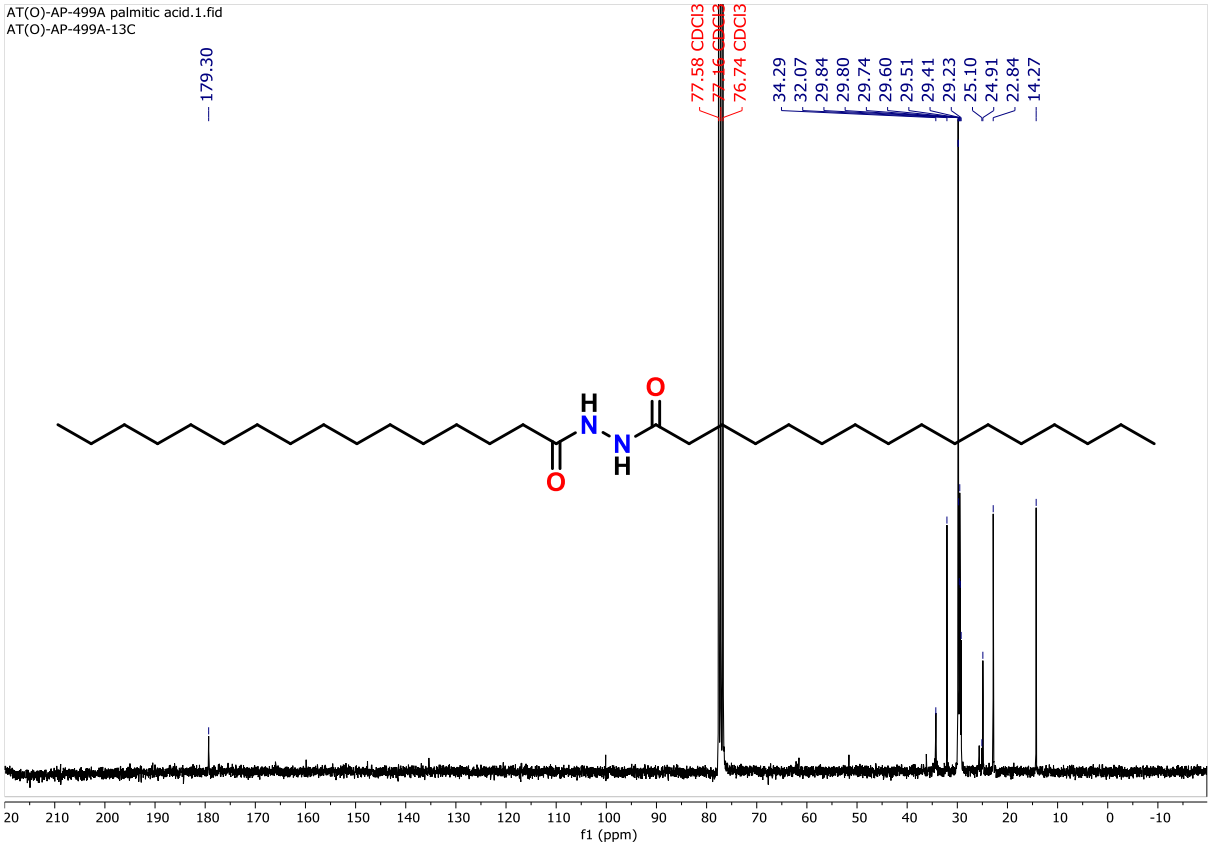

Figure 4.50. $^{13}C\{^{1}H\}$ NMR (100 MHz) spectrum of **4v** in $CDCl_3$.

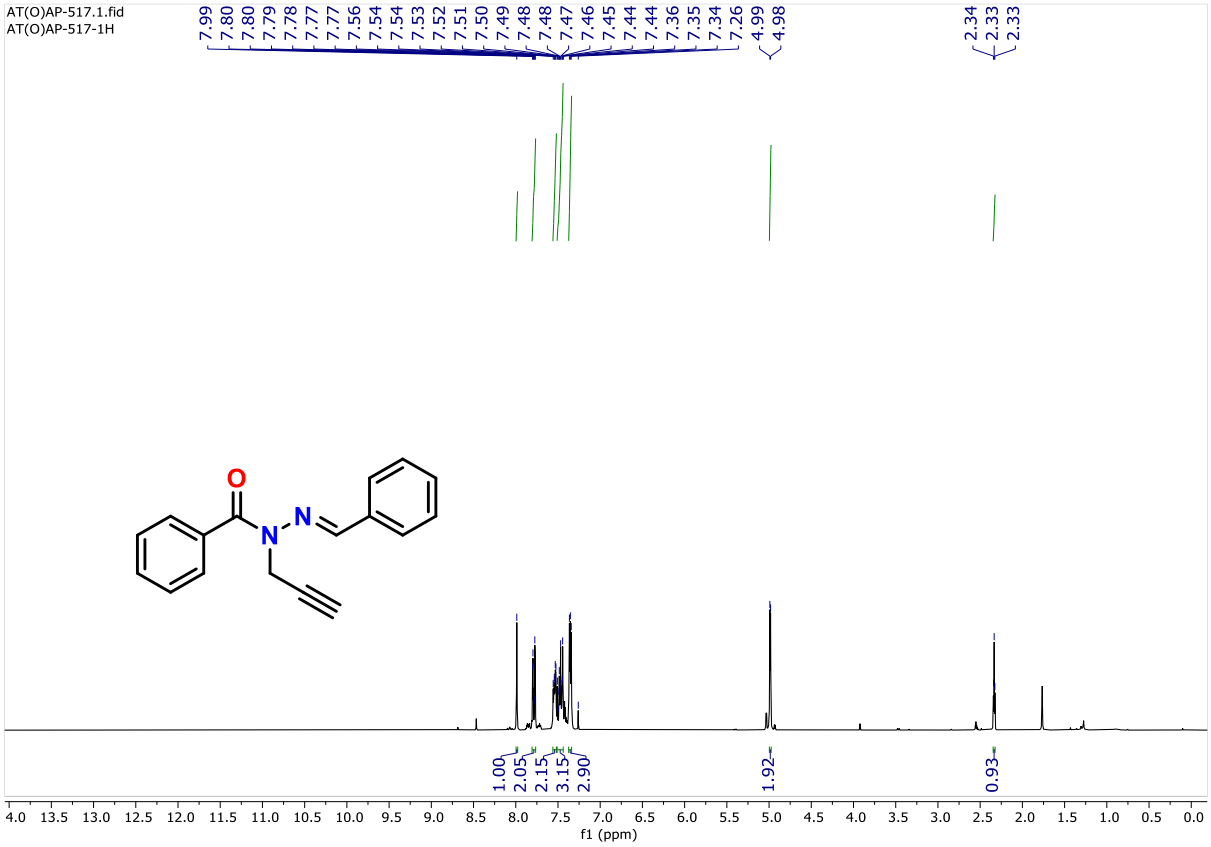

Figure 4.51. ^{1}H NMR (300 MHz) spectrum of **5** in $CDCl_3$.

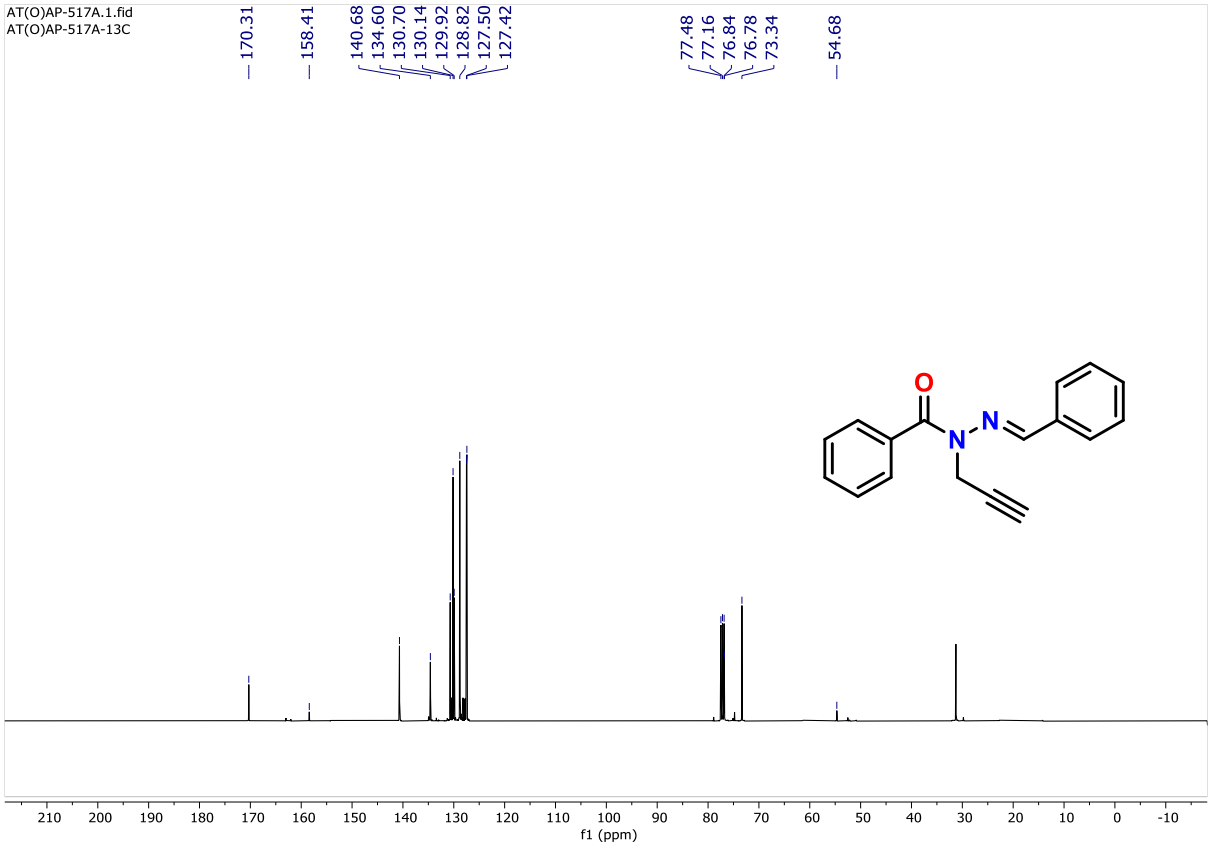

Figure 4.52. $^{13}C\{^{1}H\}$ NMR (75 MHz) spectrum of **5** in $CDCl_3$.

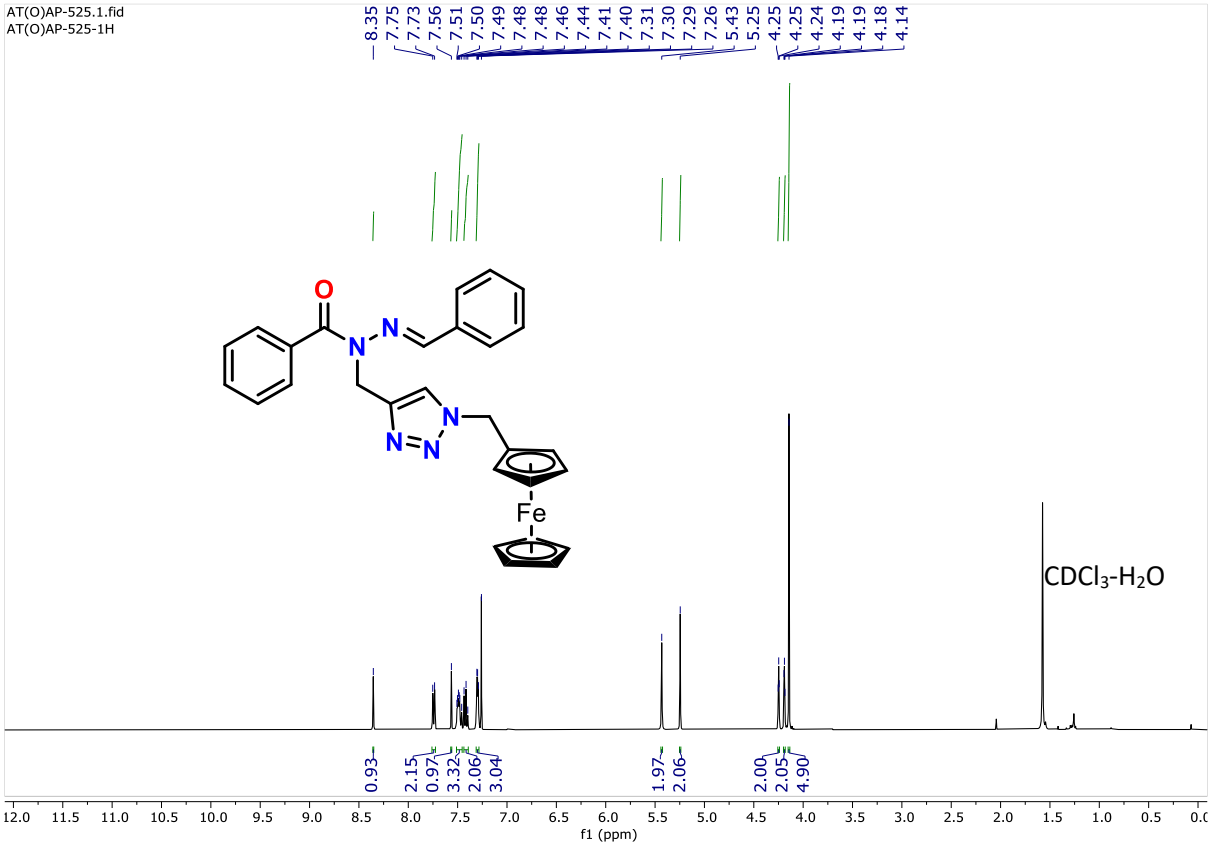

Figure 4.53. ^{1}H NMR (300 MHz) spectrum of **6** in $CDCl_3$.

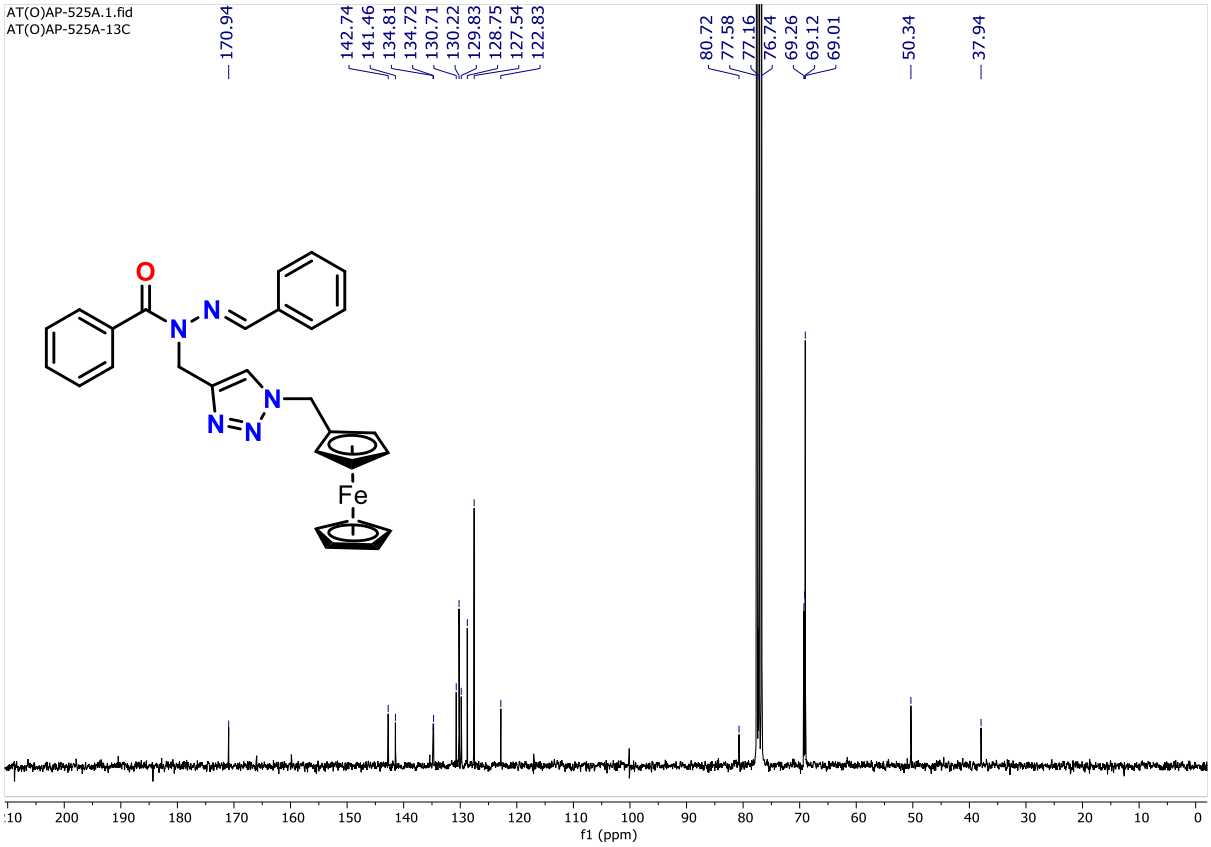

Figure 4.54. $^{13}C\{^{1}H\}$ NMR (75 MHz) spectrum of **6** in $CDCl_3$.

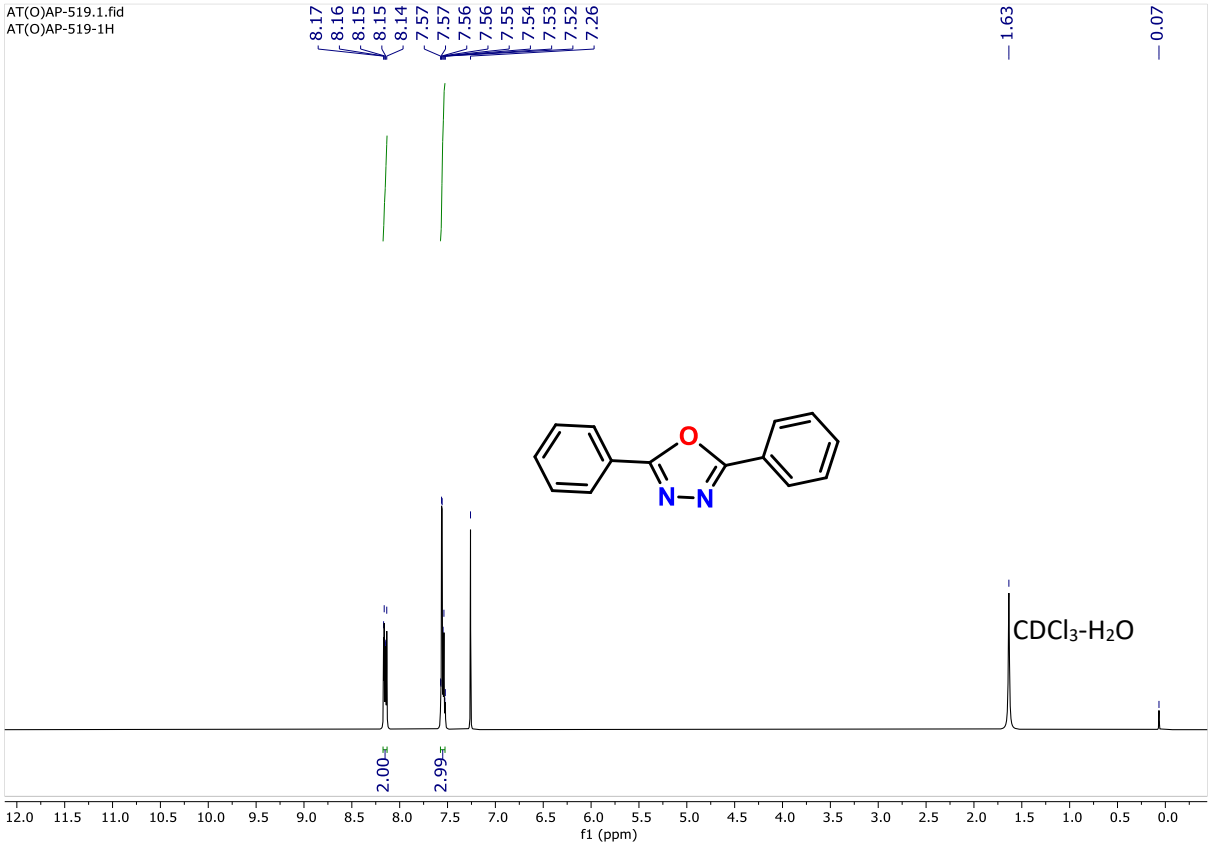

Figure 4.55. ^{1}H NMR (300 MHz) spectrum of **7** in $CDCl_3$.

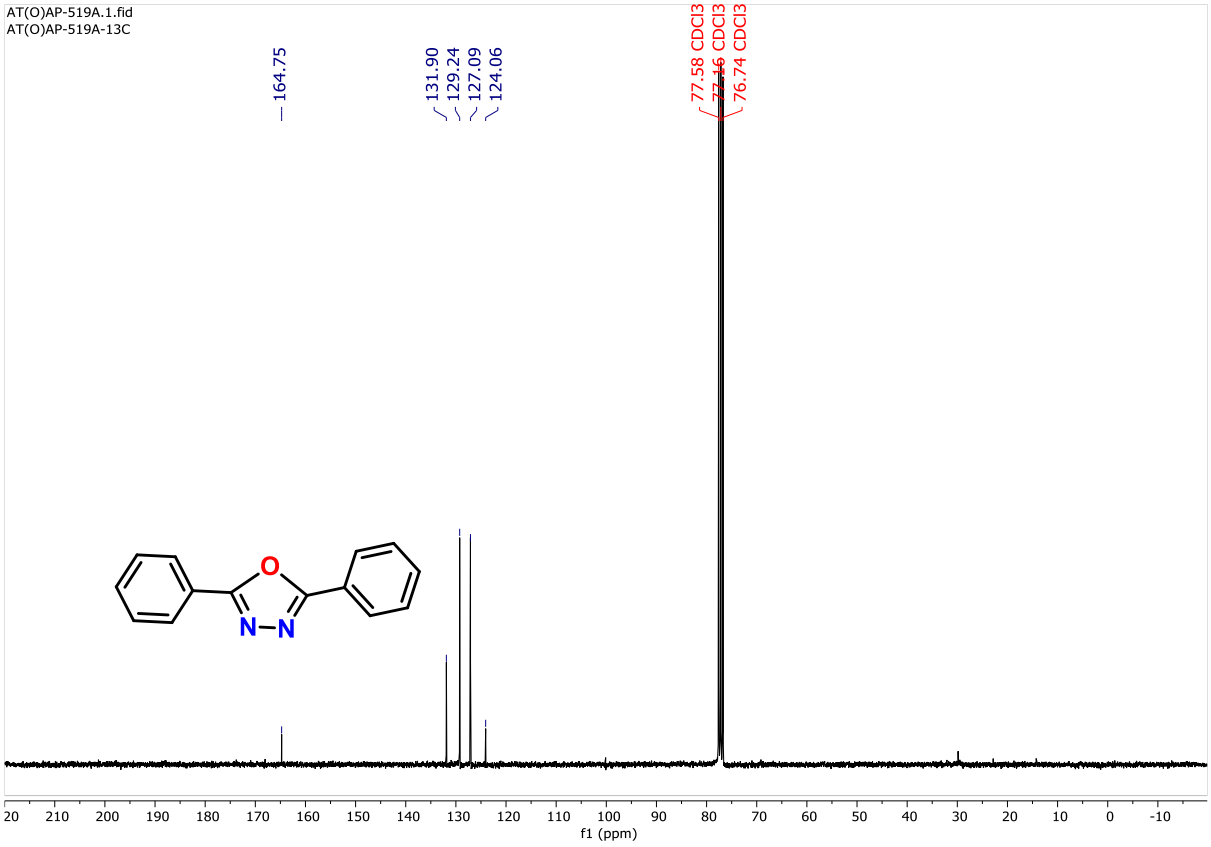

Figure 4.56. $^{13}C\{^{1}H\}$ NMR (75 MHz) spectrum of **7** in $CDCl_3$.

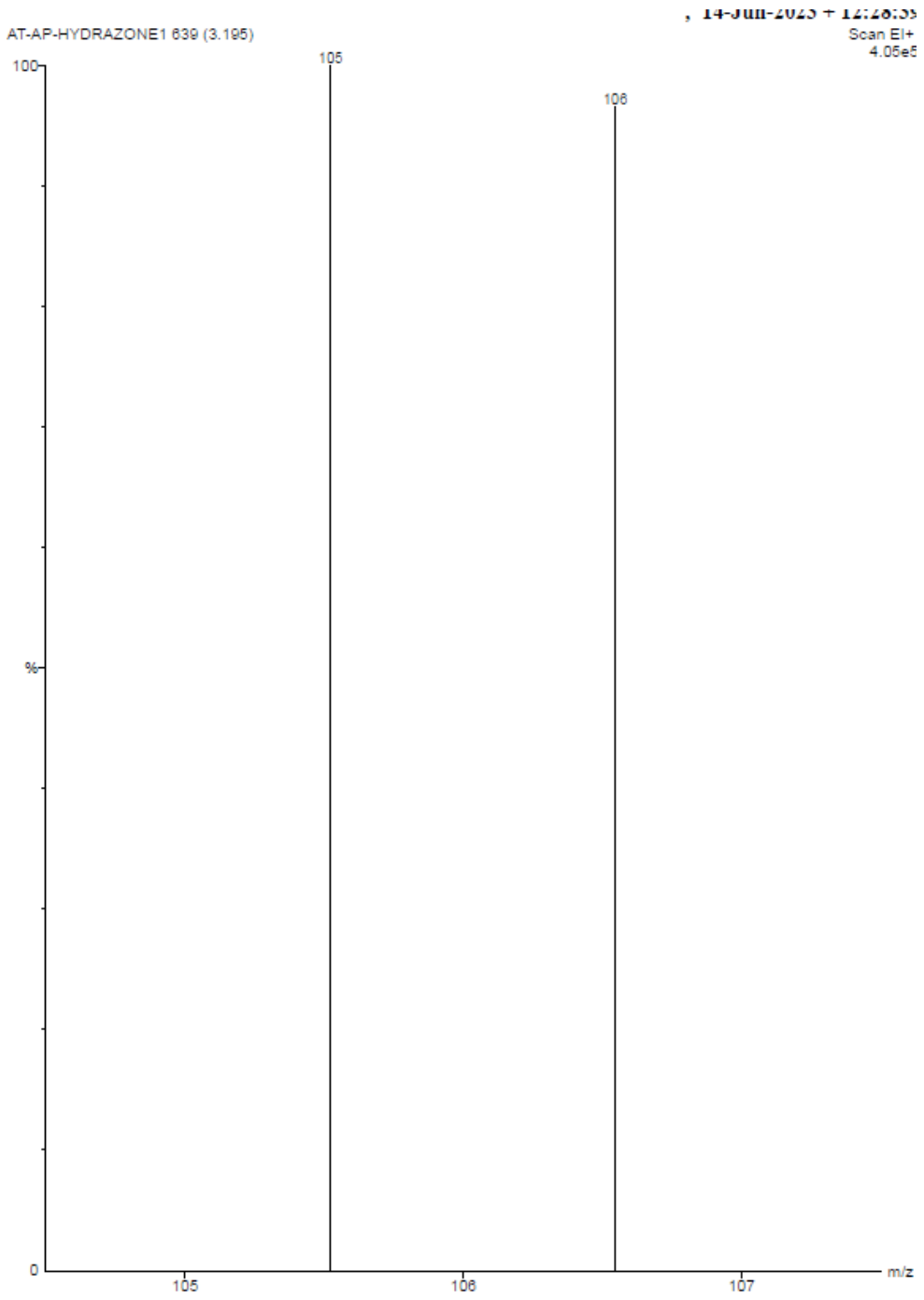

Figure 4.57: GCMS of benzaldehyde intermediate obtained from reaction mixture of **4a** after 1.5 h of reaction.

Chapter 5

Visible light-mediated Co(II) catalyzed synthesis of α,β-epoxy ketones by oxidative coupling of alkenes and aldehydes in water

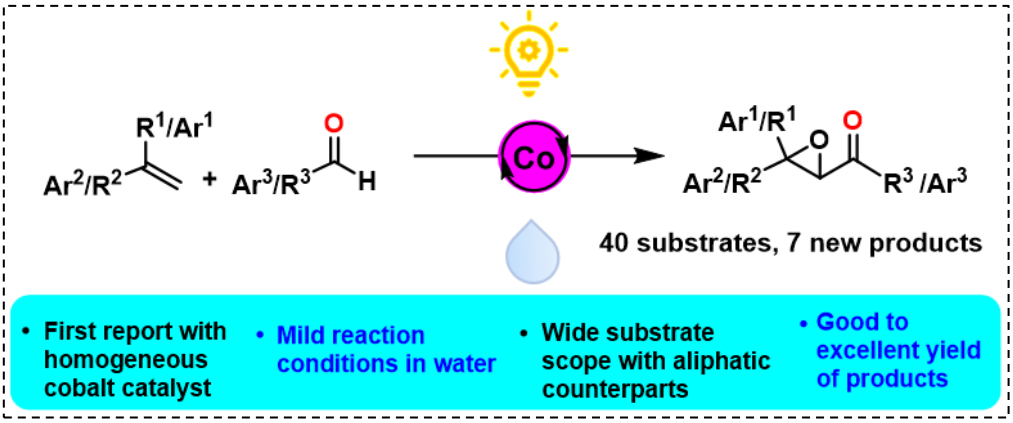

Communicated

5.1. Introduction

α,β-epoxy ketones form a class of synthetic intermediates that are often used as crucial precursors for important organic reactions leading to natural products and drug candidates.[1] A variety of synthetic procedures have been explored for the synthesis of *α,β*-epoxy ketones, the most common among which is the epoxidation of *α,β*-unsaturated ketones[2] with hydroperoxides in alkaline medium[3] or by electrogenerated peroxodicarbonate reagent (Scheme 5.1, 1).[4] Alternative synthetic strategies include γ-elimination reaction from *β*-peroxy ketones (Scheme 5.1, 2),[5] which gives enantiomerically pure starting material along with *α,β*-epoxy ketone, as a side product. Compared to these methods, a one-step, two-component reaction[6] between aldehydes and alkenes directly to produce *α,β*-epoxy ketones can stand out as aldehydes and alkenes are both abundant chemical feedstocks, and their functionalizations represent a unique avenue to access versatile complex molecules.[7-12] Great progress have been made by several research groups like Souza *et al.*,[8] Liu *et al.*,[10] and others, in exploring the scope and pathway of the reaction between styrenes and aromatic aldehydes, and to some extent aliphatic aldehydes. However, the substrate scope could not be extended to alkenes in general, including, internal alkenes, acrylates, and more importantly, aliphatic alkenes. Souza *et al.*[8] has shown the formation of ketone products upon using aliphatic alkene chains with methylene blue as the catalytic photosensitizer. Hence, a simple but versatile methodology that can include all kinds of alkenes and aldehydes to give *α,β*-epoxy ketones selectively in good yields has remained virtually unexplored.

In this context, herein, we report a visible-light-mediated Co(II) chloride catalyzed reaction as a comprehensive methodology for oxidative coupling between aldehydes and alkenes (aliphatic and aromatic substrates in both partners) in water at room temperature for the first time to obtain *α,β*-epoxy ketones. Compared to the expensive transition metals that are used in this transformation,[7] cobalt (Co) is inexpensive, earth-abundant, exhibits lower toxicity,[13] and is unexplored in this reaction. This Co-based photocatalytic oxidative acylation of alkenes by aldehydes is easily reproducible, even in a multigram scale, requires mild reaction conditions, and can address the challenges of limited substrate scope that prevail in the existing reports, owing to the absence of effective complexation or activation of the alkene unit by the catalytic method.

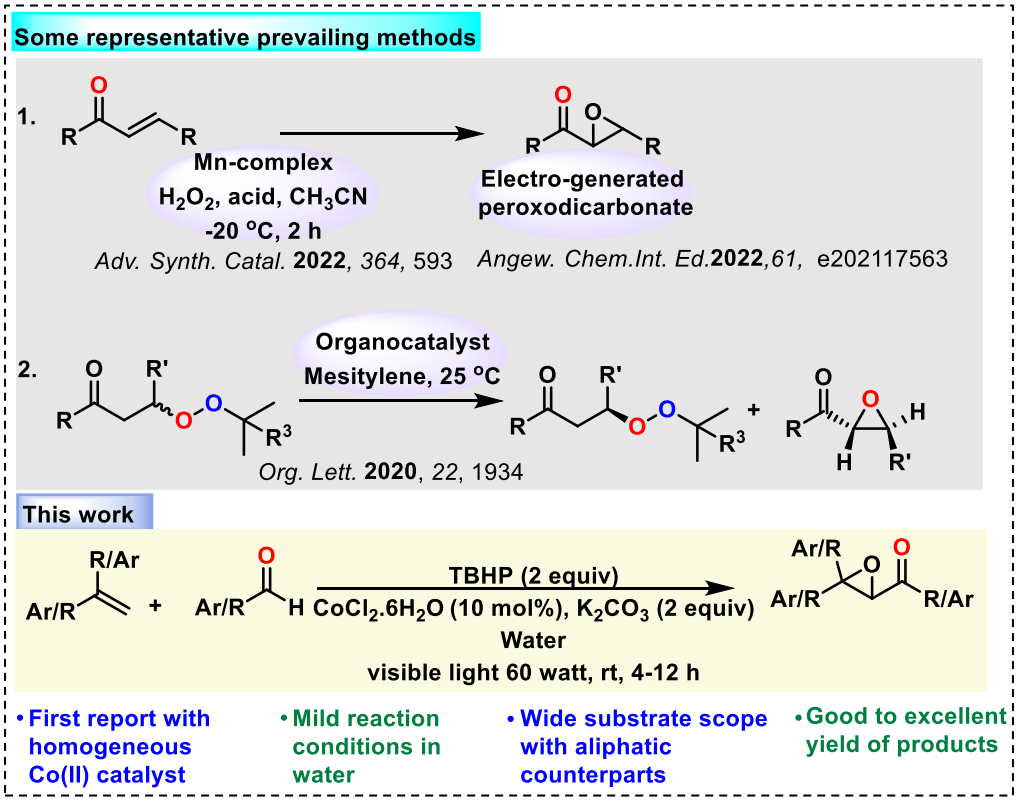

Scheme 5.1 Representative literature reports *vs* our developed methodology for synthesis of *α,β*-epoxy ketones.

5.2. Results and Discussions:

We initialized our reaction with styrene (**1a**) and benzaldehyde (**2a**) as the model substrates. A string of different reaction conditions was employed (Table 5.1) and screening was done concerning oxidant, base, time, temperature, and irradiation of visible light (60 watt). TBHP (3 equivalent), as the oxidant, K_2CO_3 (2 equivalent) as base and anhydrous $CoCl_2$ (10 mol %) as the catalyst were employed for a reaction of 12 h in acetonitrile solvent at room temperature, wherefrom compound **3a** was obtained in 80 % yield (Table 5.1 entry 1). Upon replacing $CoCl_2$ with $Co(OAc)_2{\cdot}4H_2O$, product was not obtained (Table 5.1 entry 11). After a rigorous screening, the most suitable condition was found to be with 10 mol % $CoCl_2.6H_2O$, K_2CO_3 2 equiv, TBHP 2 equiv in acetonitrile or water for 6 h at room temperature (Table 5.1 entries 12,15,16). Notably, this reaction is specific to the acetonitrile or water or acetonitrile-water mixture (1/1, *v/v*) solvent and product was not obtained at all in other solvents like toluene, or methanol. Next, we observed if light would have a role in catalyzing the reaction, by employing 60 watt visible light source during the reaction, and as per our speculation, the product yield increased considerably (80 to 87 %) within a minimal time (4 h) of reaction, keeping all other conditions same. Hence the optimized condition was found to be with TBHP (2 equivalent),

K_2CO_3 (2 equivalent), $CoCl_2.6H_2O$ (10 mol %) in water for 4 h at room temperature under 60 watt visible light irradiation (Table 5.1, entry 19).

Table 5.1 Optimisation of the reaction conditions.[a]

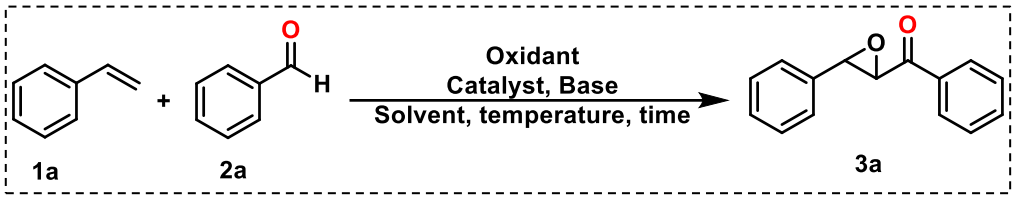

Entry	*Catalyst (Mole %)*	*Base (equivalence)*	*Oxidant (equivalence)*	*Vis Light (60 watt)*	*Solvent (5 mL)*	*Temperature (°C)*	*Time (h)*	*% yield[b]*
1	$CoCl_2$ (10)	K_2CO_3 (2)	TBHP (3)	Off	CH_3CN	rt	12	80
2	$CoCl_2$ (10)	K_2CO_3 (2)	TBHP (3)	Off	CH_3CN	rt	8	80
3	$CoCl_2$ (10)	K_2CO_3 (2)	TBHP (3)	Off	CH_3CN	rt	4	80
4	$CoCl_2$ (10)	K_2CO_3 (2)	TBHP (3)	Off	CH_3CN	50	4	80
5	$CoCl_2$ (10)	K_2CO_3 (2)	TBHP (3)	Off	CH_3CN	70	4	80
6	$CoCl_2$ (10)	K_2CO_3 (2)	TBHP (3)	Off	CH_3CN	100	4	80
7	$CoCl_2$ (10)	K_2CO_3 (2)	TBHP (2)	Off	CH_3CN	rt	4	80
8	$CoCl_2$ (10)	K_2CO_3 (1)	TBHP (2)	Off	CH_3CN	rt	4	70
9	$CoCl_2$ (5)	K_2CO_3 (2)	TBHP (2)	Off	CH_3CN	rt	4	70
10	$CoCl_2$ (10)	KOH (2)	TBHP (2)	Off	CH_3CN	rt	4	80
11	$Co(OAc)_2.4H_2O$ (10)	K_2CO_3 (2)	TBHP (2)	Off	CH_3CN	rt	4	ND
12	$CoCl_2.6H_2O$ (10)	K_2CO_3 (2)	TBHP (2)	Off	CH_3CN	rt	4	80
13	$CoCl_2$ (10)	K_2CO_3 (2)	TBHP (2)	Off	CH_3OH	rt	4	ND
14	$CoCl_2$ (10)	K_2CO_3 (2)	TBHP (2)	Off	Toluene	rt	4	ND
15	$CoCl_2.6H_2O$ (10)	K_2CO_3 (2)	TBHP (2)	Off	Water	rt	4	80
16	$CoCl_2.6H_2O$ (10)	K_2CO_3 (2)	TBHP (2)	Off	CH_3CN:Water (4:1)	rt	4	80
17	$CoCl_2.6H_2O$ **(10)**	**K_2CO_3 (2)**	**TBHP (2)**	**On**	**CH_3CN**	**rt**	**4**	**87**

18	$CoCl_2.6H_2O$ (10)	K_2CO_3 (2)	TBHP (2)	On	CH_3CN:Water (4:1)	rt	4	87
19	$CoCl_2.6H_2O$ **(10)**	**K_2CO_3 (2)**	**TBHP (2)**	**On**	**Water**	**rt**	**4**	**87**

[a]The reaction were performed taking **1a** (0.5 mmol) and **2a** (0.5 mmol). [‡]Equivalence taken with respect to styrene. All the reactions have been performed aerial conditions. [b]isolated yield after column chromatography. ND = Not Detected.

.

With the optimized reaction condition in hand, the acclimatization of aldehydes in the reaction with styrene was started (Table 5.2). An array of benzaldehyde derivatives with electron-donating/withdrawing substituents were investigated. Electron-donating groups, such as, 2/3-methyl (**2b**,**c**), 4-*tert*-butyl (**2d**), 2/4-methoxy (**2e**,**f**), 4-*N,N*-dimethyl (**2g**), 1-naphthyl (**2h**) and 4-phenyl (**2i**) were all smoothly accommodated to give the corresponding epoxy ketone derivatives (**3b**-**3i**) as the single products in high yields (72-87 %). Reactions with electron-withdrawing groups like 4-fluoro (**2j**), 3-chloro (**2k**) and 3-nitro (**2l**) also gave good yield (70-72 %) of products (**3j**-**l**). Extending the methodology to aliphatic aldehydes like pentanal, hexanal, and octanal (**2m**-**2o**) gave good yields (~ 80 %) of the corresponding products (**3m**-**3o**). Notably, aldehydes with heteroaryl cores (**2p**, **2q**) can also be included into this reaction giving their corresponding epoxy ketones (**3p**, **3q**) in high yield (77-80 %). Hence this methodology goes well with any kind of aldehydes, aromatic, heteroaromatic, or aliphatic with a fair functional group tolerance.

Next, we explored the substrate scope of the styrene derivatives (Table 5.3) with benzaldehyde fixed as the aldehyde counterpart. Both electron-donating and electron-withdrawing substituents like 4-phenyl (**1b**), 4-chloro (**1c**), 4-*tert*-butyl (**1d**) and 1-naphthyl styrenes (**1e**) all reacted well with benzaldehyde within 4 h to give 70-80 % product (**4a**-**4d**) yield. The reaction displayed good efficacy with α-substituted styrenes, like α- methyl (**1f**) and α-phenyl (**1g**) styrene substrates, as well. Their reaction with benzaldehyde derivatives giving the desired epoxy ketones (**4e**-**4l**) in good yield (70-80 %), account for the versatility of the reaction. Satisfyingly, the reaction of benzaldehyde with aromatic internal alkene (stilbene, **1h**) remained unimpeded under standard reaction conditions, giving 60 % yield of corresponding product (**4m**) after 12 h of reaction.

Table 5.2 Substrate scope of benzaldehydes in reaction with styrene for *α,β*-epoxy ketones formation.[a]

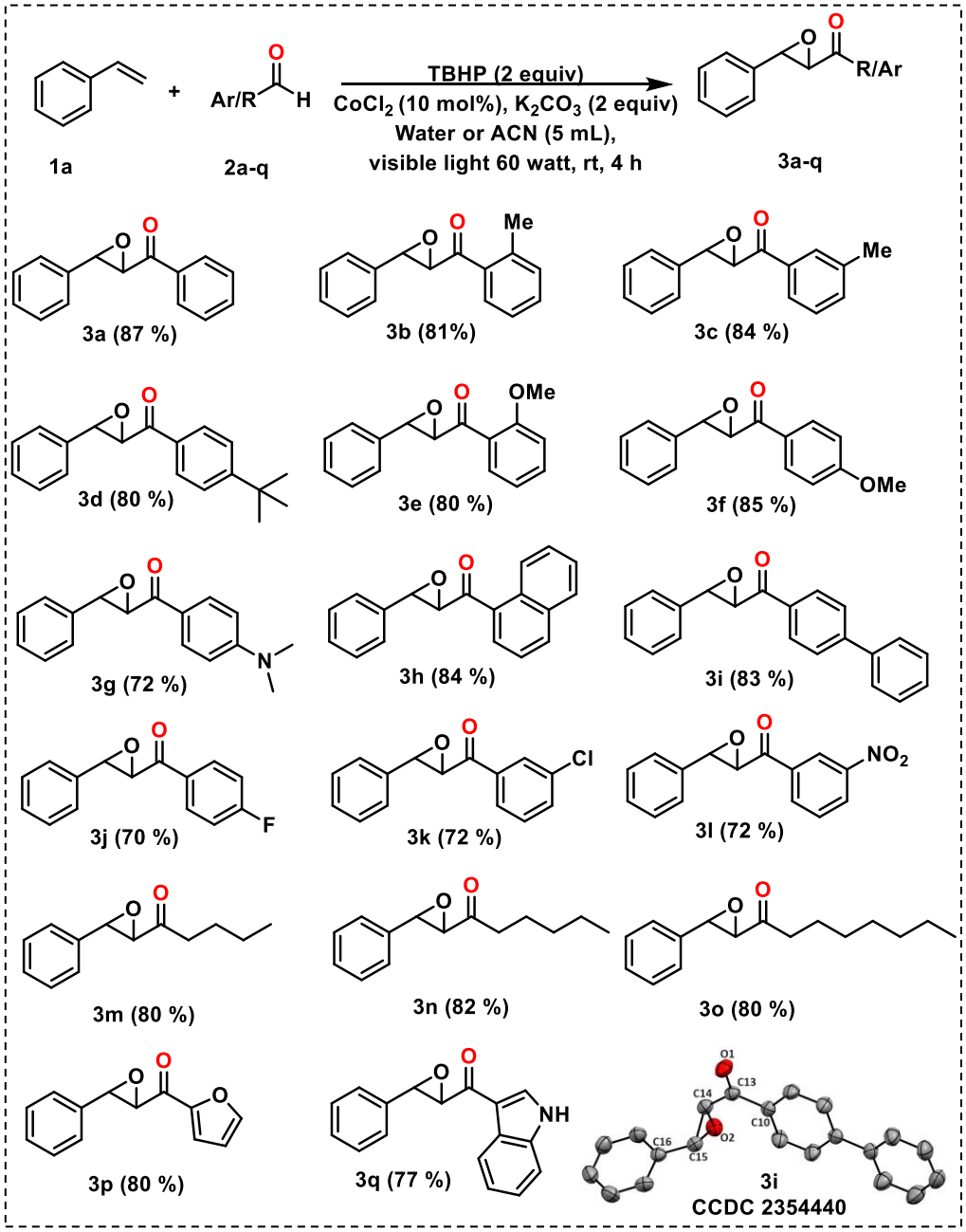

[a]Reaction condition Table 5.1 entry 19, 1 mmol scale. Isolated yields are obtained after column chromatography. ORTEP representation of compound **3i** is given with thermal ellipsoids drawn at the 50% probability level; hydrogen atoms are omitted for clarity.

Then, we were interested in investigating the generality of this reaction methodology by using aliphatic alkenes. Envisioning the challenges revolving around fuctionalization of unactivated aliphatic alkenes, the scope of aliphatic alkenes were explored by taking unactivated long chains (1-hexene **1i** and 1-octene **1j**), bromo derivatives (allyl bromide **1k**, 5-

bromopent-1-ene **1l**) and ester derivatives (ethyl acrylate **1m** and butyl acrylate **1n**) (Table 5.4, top). In all the cases, the reaction did very well such that the corresponding epoxy ketone products could be obtained in moderate yields (50-60 %) for unactivated alkenes (**5a-5d**) and in high yields (~ 79 %) for the activated ones (esters) (**5e**, **5f**). The inclusion of aliphatic alkenes to the direct two-component coupling is challenging and has not been achieved in considerable yield to date.[12] Extending this methodology, we have also explored four intramolecular cyclizations, which gave good yields (70-82 %) of products (**6a-6d**), in acetonitrile (Table 5.4, bottom).

Table 5.3 Substrate scope of styrene in reaction with benzaldehydes for *α,β*-epoxy ketones formation.[a]

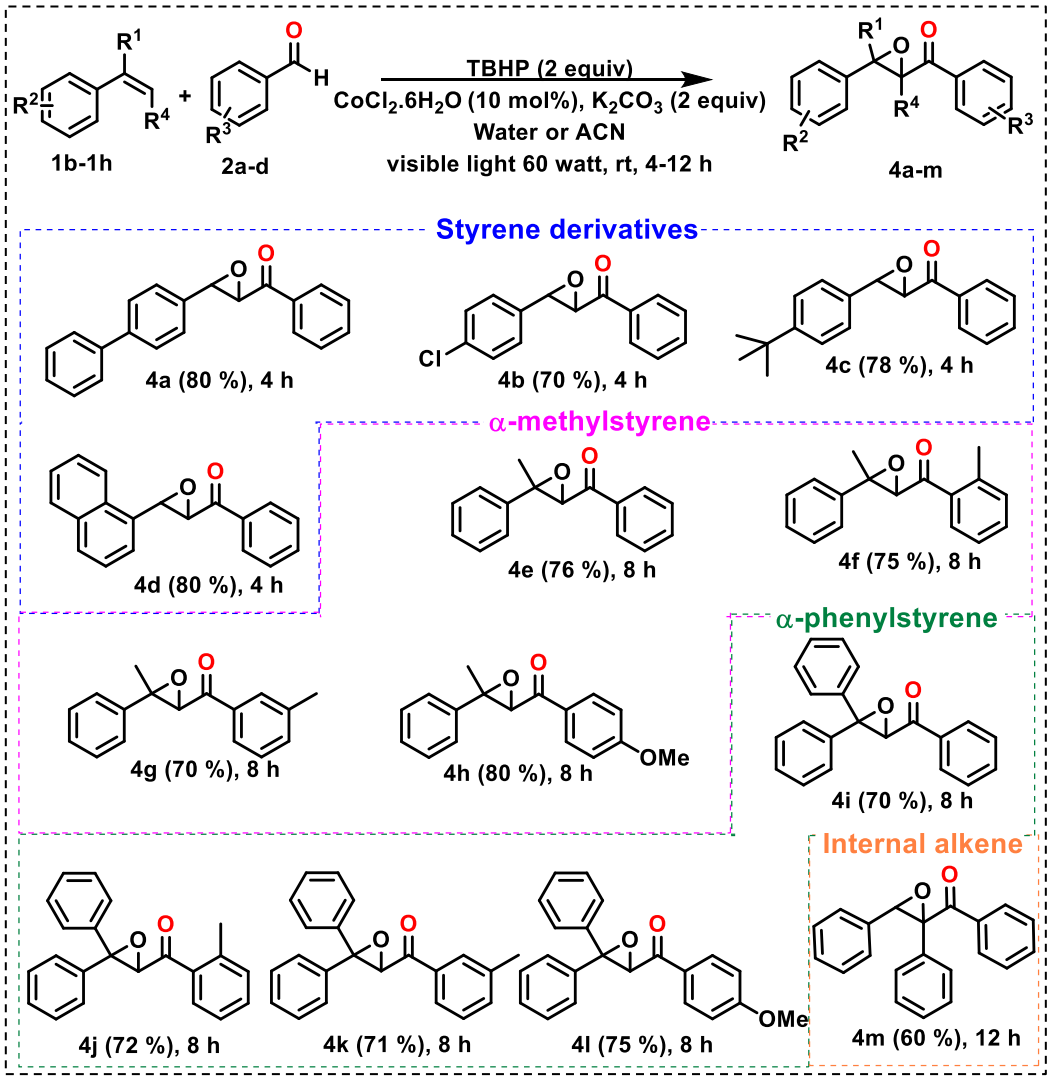

[a]Reaction condition Table 5.1 entry 19, 1 mmol scale. Isolated yields are obtained after column chromatography.

Table 5.4 Substrate scope of aliphatic alkenes in reaction with benzaldehydes and in intramolecular way for *α,β*-epoxy ketones formation.[a]

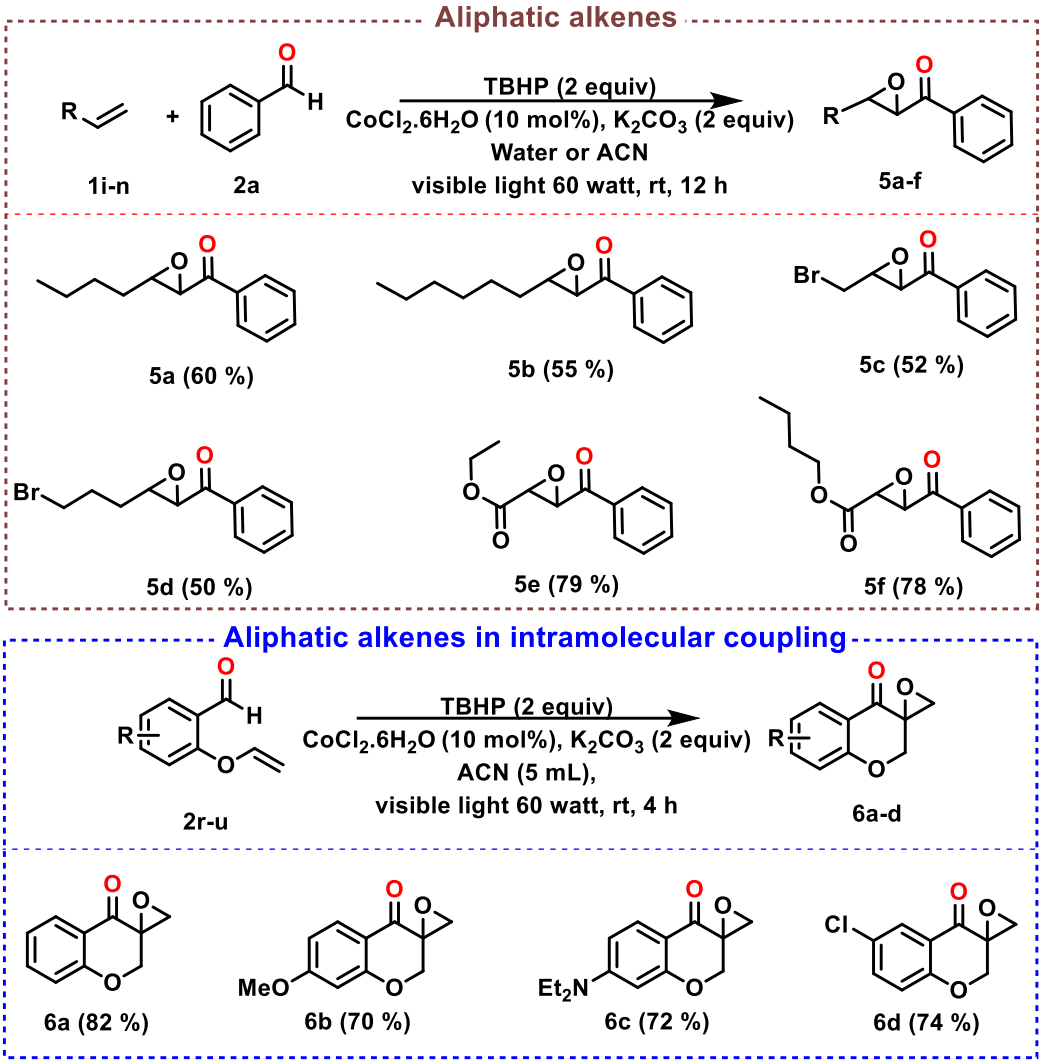

[a]Reaction condition Table 5.1 entry 19, 1 mmol scale. Isolated yields are obtained after column chromatography.

To probe the scalability of the optimized methodology, we accomplished the synthesis of **3a**, **3b** and **3c** in gram-scale (1 g) (Scheme 5.2), wherefrom, respective yields of 78 %, 75 % and 75 % were found. The synthetic application of this methodology was also explored by subjecting compound **3a** to several post-synthetic modifications, which would give structurally important organic derivatives. Upon reaction of **3a** with $SnCl_2$ in CH_2Cl_2, an alcohol derivative (**7**) was obtained in 90 % yield. Pyrazine derivative (**8**) could be obtained in 80 % yield by reaction of **3a** with *o*-phenylenediamine. Reaction with hydroxylamine hydrochloride in presence of pyridine was expected to give the corresponding isooxazoline derivative, however, the obtained compound is **9**. Upon reaction with hydrazine hydrate in ethanol under reflux for

6 h, pyrazoline derivative **10** was obtained, whereas upon reaction under same conditions in presence of catalytic amount of H_2SO_4, compound **13** was obtained. Upon reaction with Zn/NH_4Cl, three compounds **11**, **12** and **9** were obtained in 40, 30 and 30 % yields respectively.

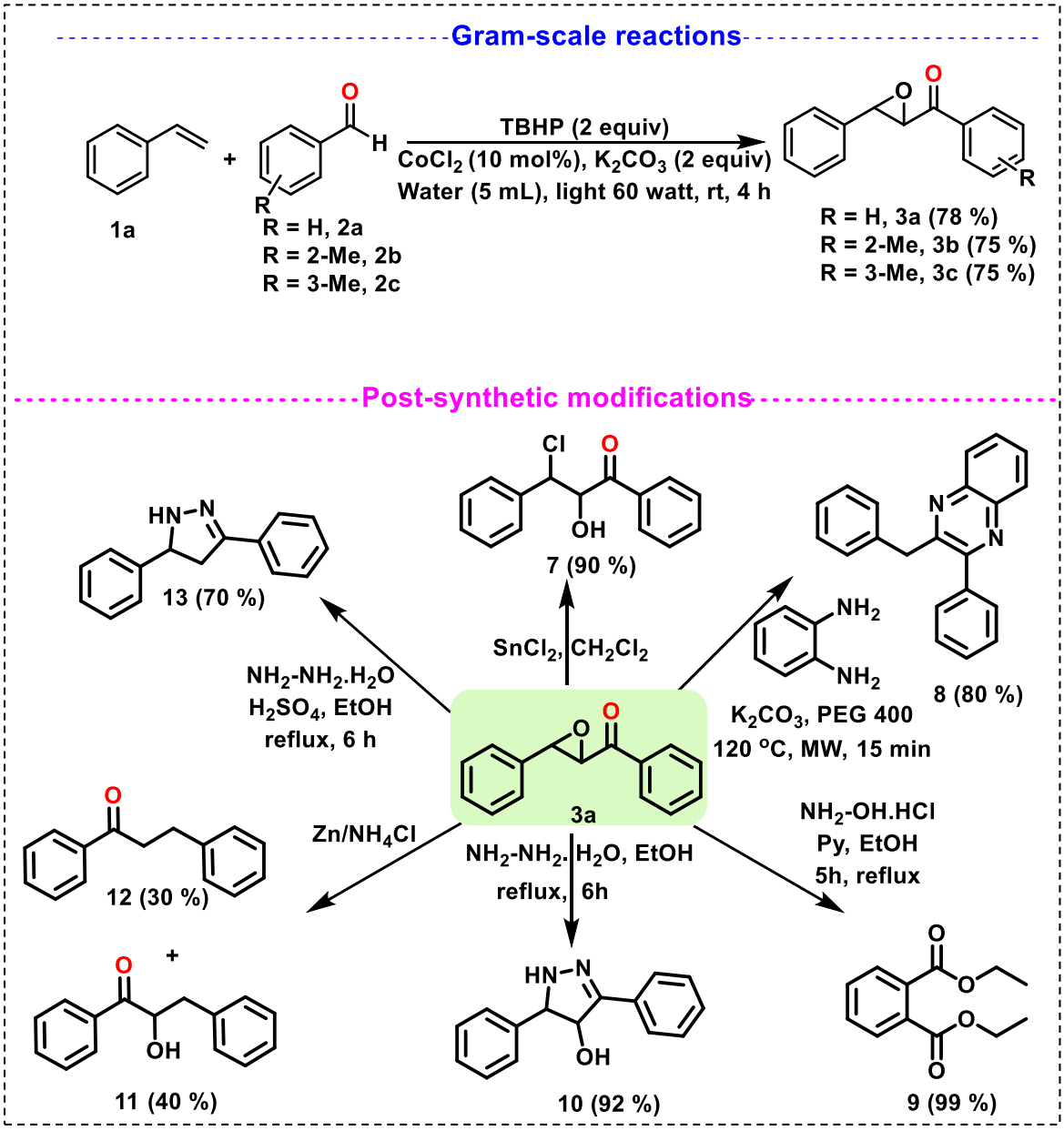

Scheme 5.2. Gram-scale reactions and post-synthetic modifications.

To ascertain the reaction mechanism, a series of controlled experiments and Hammett plot by competitive ^1H NMR analysis with electron-donating/withdrawing groups on benzaldehyde were conducted. The Hammett plot (Figure 5.1a) shows a negative slope (ρ = -0.40285), indicating that the reaction proceeds through an electron-deficient transition state

(TS). Controlled reactions with benzaldehyde and styrene under standard conditions, revealed that a slight quantity of product (10 %) was obtained without the catalyst, however, the reaction did not proceed at all without oxidant. However, without base, a new 1,2-dicarbonyl compound (**14**) was formed in acetonitrile medium. The formation of the 1,2-dicarbonyl compound was reaffirmed from the product (**15**) obtained with *p*-methoxybenzaldehyde. With an anticipation of radical pathway, reactions under standard conditions were conducted in presence of radical scavengers 2,2,6,6-tetramethyl-1-piperidinyloxy (TEMPO) and butylated hydroxytoluene (BHT) (Figure 5.1b). The desired epoxy ketone was obtained in very low yield (< 10 %) in BHT and not at all in presence of TEMPO, which proves that the reaction proceeds through radical pathway. Additionally, TEMPO/BHT-trapped intermediates were identified by HRMS.

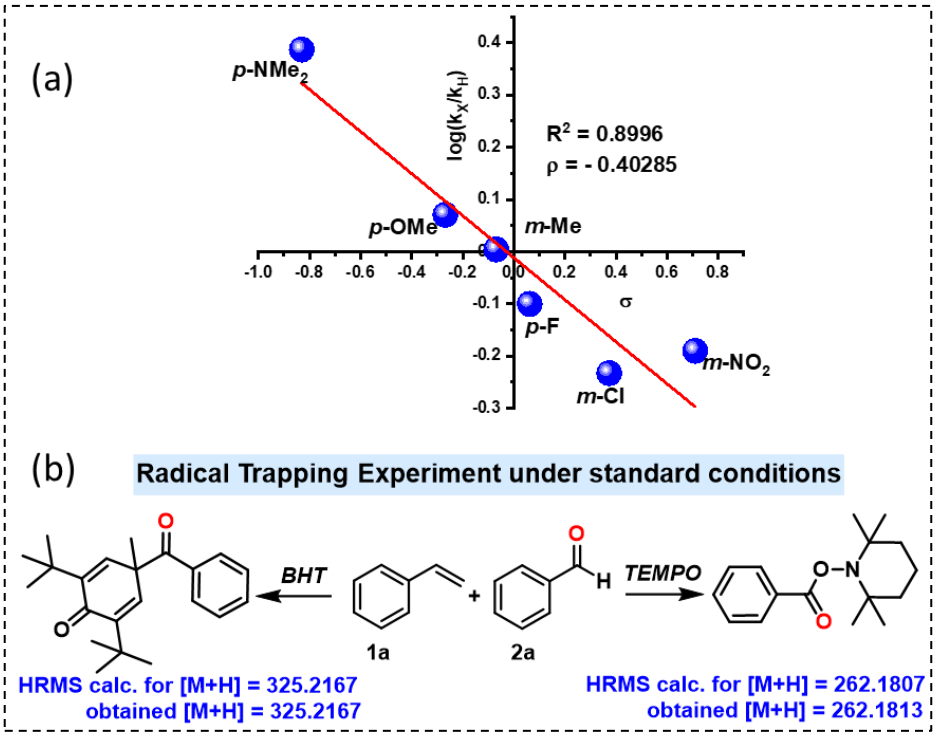

Figure 5.1. (a) Hammett plot for different substituents in the benzaldehyde ring. (b) TEMPO and BHT adducts of the generated radicals.

Based on the concurrence of experimental studies, the plausible mechanism of this reaction (Scheme 5.3) was proposed such that the acyl radical adds up to the Co(II) centre (**A**) to render (**B**), where the alkene too gets attached by a π-interaction. The light activates this chelated complex (**C**) to break the C-Co bond (**D**) and attach to the alkene end, which gives species **E,** as detected by GCMS (Figure 5.116). Finally, the ^{t}BuOȮ radical, formed from TBHP

adds to the **E** at the expense of C-Co bond breaking and the free catalyst is released along with **F**, which in presence of base (K_2CO_3) gives the product **G**.

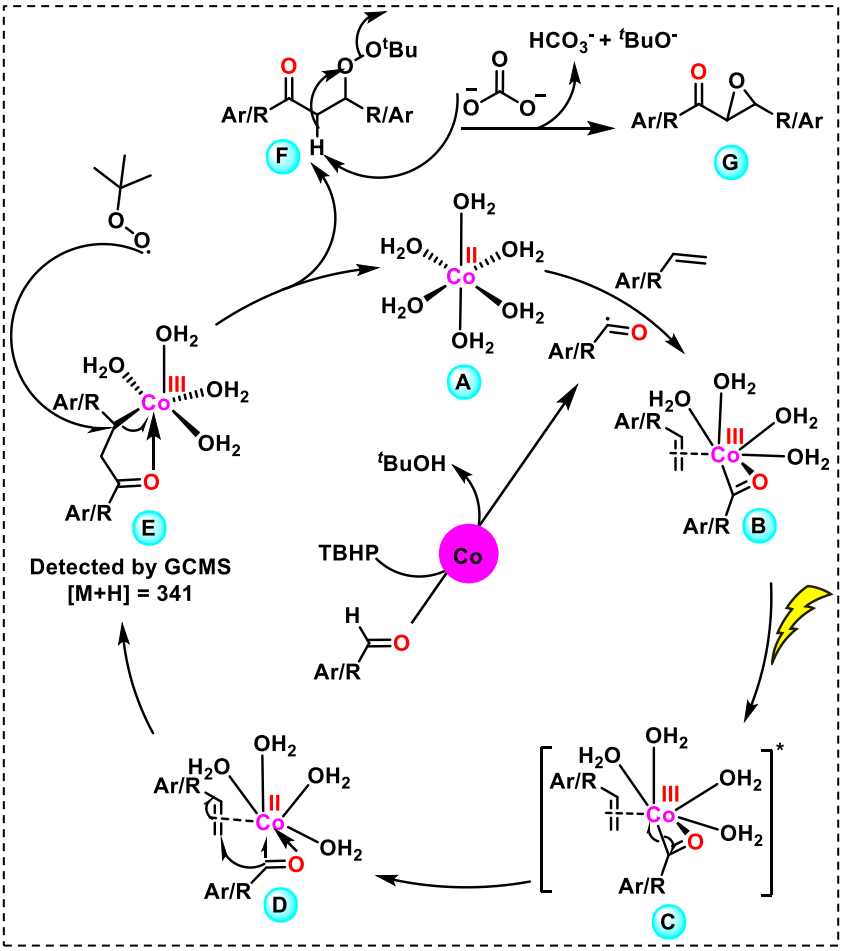

Scheme 5.3. Plausible mechanism of *α,β*-epoxy ketone formation reaction.

5.3. Conclusion

In conclusion, we have developed a first Co-based homogeneous photocatalytic route, which provides a straightforward and convenient yet powerful method for the synthesis of a wide range of *α,β*-epoxy ketones in water. This method is facile, low-cost, and is devoid of any harsh reaction conditions. The present photocatalyzed strategy features a good substrate scope including aliphatic analogues and diverse functional groups, providing innovative approaches to construct synthetically significant *α,β*-epoxy ketones and their various post-modified heterocycles. Mechanistic studies, and Hammett analysis have revealed that photoexcitation of Co is necessary for the inclusion of a wide substrate scope in good yields.

5.4. Experimental section:

5.4.1. Materials and reagents

Commercially available AR-grade acetonitrile has been used for reaction without further distillation. Anhydrous $CoCl_2$, $CoCl_2 \cdot 6H_2O$ and K_2CO_3 were purchased from Spectrochem chemicals, *tert*-butyl hydroperoxide was purchased from TCI and used directly for the reaction. All the commercially available aldehyde derivatives were purchased from Sigma-Aldrich and used without further purification. All the styrene derivatives were synthesized by literature-reported procedures. *n*-Buli (1.6 M, in hexane) was purchased from Spectrochem chemicals and THF was distilled by using Na and benzophenone under N_2 atmosphere. Analytical thin layer chromatography (TLC) was performed on pre-coated silica gel 60 F_{254}. Visualization on TLC was achieved with UV light (254 nm). Column Chromatography was carried out using silica gel as the stationary phase and EtOAc/hexane.

5.4.2. Instrumentation

^1H and ^{13}C NMR spectra were obtained with BRUKER 300 MHz FT-NMR spectrometers and the chemical shifts are reported in ppm, using tetramethylsilane as an internal standard and were referenced to the residual solvent as follows: $CDCl_3$ = 7.26 (^1H), 76.16 (^{13}C) ppm, DMSO = 2.51 (^1H), 39.50 (^{13}C) at room temperature. For ^1H NMR, coupling constants *J* are given in Hz and the resonance multiplicity is described as s (singlet), d (doublet), t (triplet), m (multiplet), dd (doublet of doublet), dt (doublet of triplet), td (triplet of doublet), tt (triplet of triplet), q (quartet). ^{13}C NMR spectra were fully decoupled by broadband proton decoupling. High-resolution mass spectra (HRMS) were obtained from Waters (Xevo G2 Q-TOF) mass spectrometer in electrospray ionization mode (ESI+).

5.4.3. General procedure for the reaction of alkene with aldehyde: An oven-dried round bottom flask equipped with a stir bar was charged with alkene (1 mmol, 1 equiv.) and aldehyde (2 mmol, 2 equiv.) in acetonitrile or water (3-4 ml) solvent. After that, TBHP (2 equiv., 70% in water), $CoCl_2 \cdot 6H_2O$ (10 mol%, 0.1 mmol, 0.1 equiv.) and K_2CO_3 (2 mmol, 2 equiv.) were added sequentially to the mixture of aldehyde and styrene. Then the reaction mixture was stirred at room temperature under an aerobic atmosphere for 4 h under 60 watt visible light irradiation. Thereafter, water was added to the reaction mixture (in case of reaction in acetonitrile solvent), stirred well and the organic layer was extracted with EtOAc (3×20 ml). The combined organic layer was washed with brine and dried under Na_2SO_4. The crude product was purified by column chromatography on silica gel (5% EtOAc/pet ether).

5.4.4. Gram-Scale reaction: An oven-dried round bottom flask equipped with a stir bar was charged with styrene derivatives **1a** (1 equiv.) and aldehydes **2a-2c** (2 equiv.) were dissolved in acetonitrile (3-4 ml) solvent. After that, TBHP (2 equiv., 70% in water), $CoCl_2 \cdot 6H_2O$ (10 mol%), and K_2CO_3 (2 equiv.) were added sequentially to the mixture of aldehyde and styrene. Then the reaction mixture was stirred at room temperature under an aerobic atmosphere with 60 watt visible light irradiation for 4 h. Thereafter, water was added to the reaction mixture, stirred well and the organic layer was extracted with EtOAc (3×20 ml). The combined organic layer was washed with brine and dried under Na_2SO_4. The crude products were purified by column chromatography on silica gel (5% EtOAc/pet ether).

5.4.5. Controlled reactions:

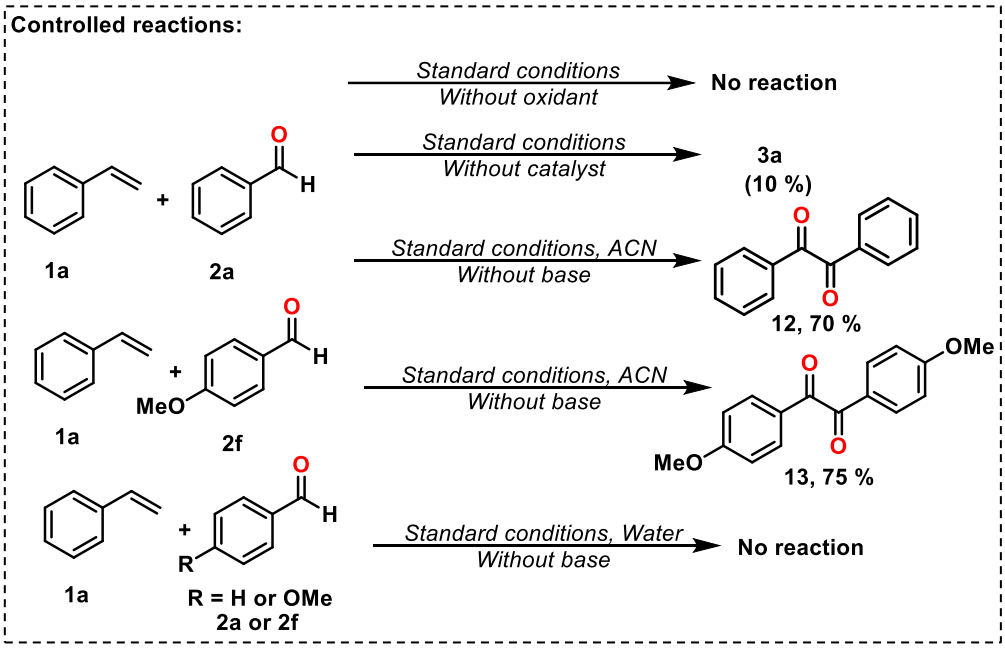

Figure 5.2. Controlled reactions for determining reaction mechanism.

5.4.5.1. Reaction 1: An oven-dried round bottom flask equipped with a stir bar was charged with styrene **1a** (1 mmol, 1 equiv.) and benzaldehyde **2a** (2 mmol, 2 equiv.) in acetonitrile/water (3-4 ml) solvent. After that, $CoCl_2 \cdot 6H_2O$ (10 mol%, 0.1 mmol, 0.1 equiv.) and K_2CO_3 (2 mmol, 2 equiv.) were added sequentially to the mixture of aldehyde and styrene. Then the reaction mixture was stirred at room temperature under an aerobic atmosphere for 4 h under 60-watt visible light irradiation. Thereafter, water was added to the reaction mixture (in case of reaction in acetonitrile solvent), stirred well and the organic layer was extracted with EtOAc (3×20 ml).

The combined organic layer was washed with brine and dried under Na_2SO_4. The product formed was observed by thin-layer chromatography.

5.4.5.2. Reaction 2: An oven-dried round bottom flask equipped with a stir bar was charged with styrene **1a** (1 mmol, 1 equiv.) and benzaldehyde **2a** (2 mmol, 2 equiv.) in acetonitrile or water (3-4 ml) solvent. After that, TBHP (2 equiv., 70% in water) and K_2CO_3 (2 mmol, 2 equiv.) were added sequentially to the mixture of aldehyde and styrene. Then the reaction mixture was stirred at room temperature under an aerobic atmosphere for 4 h under 60-watt visible light irradiation. Thereafter, water was added to the reaction mixture (in case of reaction in acetonitrile solvent), stirred well and the organic layer was extracted with EtOAc (3×20 ml). The combined organic layer was washed with brine and dried under Na_2SO_4. The product formed was observed by thin-layer chromatography.

5.4.5.3. Reaction 3: An oven-dried round bottom flask equipped with a stir bar was charged with styrene **1a** (1 mmol, 1 equiv.) and benzaldehyde **2a** (2 mmol, 2 equiv.) in acetonitrile (3-4 ml) solvent. After that, TBHP (2 equiv., 70% in water) and $CoCl_2 \cdot 6H_2O$ (10 mol%, 0.1 mmol, 0.1 equiv.) were added sequentially to the mixture of benzaldehyde and styrene. Then the reaction mixture was stirred at room temperature under an aerobic atmosphere for 4 h under 60-watt visible light irradiation. Thereafter, water was added to the reaction mixture, stirred well and the organic layer was extracted with EtOAc (3×20 ml). The combined organic layer was washed with brine and dried under Na_2SO_4. The crude product was purified by column chromatography on silica gel (5% EtOAc/pet ether).

5.4.5.4. Reaction 4: An oven-dried round bottom flask equipped with a stir bar was charged with styrene **1a** (1 mmol, 1 equiv.) and benzaldehyde **2f** (2 mmol, 2 equiv.) in acetonitrile (3-4 ml) solvent. After that, TBHP (2 equiv., 70% in water) and $CoCl_2 \cdot 6H_2O$ (10 mol%, 0.1 mmol, 0.1 equiv.) were added sequentially to the mixture of aldehyde and styrene. Then the reaction mixture was stirred at room temperature under an aerobic atmosphere for 4 h under 60-watt visible light irradiation. Thereafter, water was added to the reaction mixture, stirred well and the organic layer was extracted with EtOAc (3×20 ml). The combined organic layer was washed with brine and dried under Na_2SO_4. The crude product was purified by column chromatography on silica gel (5% EtOAc/pet ether).

5.4.5.5. Reaction 5: An oven-dried round bottom flask equipped with a stir bar was charged with styrene **1a** (1 mmol, 1 equiv.) and benzaldehyde **2a** (2 mmol, 2 equiv.) in water (3-4 ml) solvent. After that, TBHP (2 equiv., 70% in water) and $CoCl_2 \cdot 6H_2O$ (10 mol%, 0.1 mmol, 0.1 equiv.) were added sequentially to the mixture of benzaldehyde and styrene. Then the reaction mixture was stirred at room temperature under an aerobic atmosphere for 4 h under 60-watt visible light irradiation. Thereafter, the organic layer was extracted with EtOAc (3×20 ml). The combined organic layer was washed with brine and dried under Na_2SO_4 and the formation of any product was observed by thin-layer chromatography.

5.4.6. Radical trapping experiment: An oven-dried round bottom flask equipped with a stir bar was charged with styrene **1a** (1 mmol, 1 equiv.) and benzaldehyde **2a** (2 mmol, 2 equiv.) and TEMPO/BHT (4 mmol, 4 equiv) in acetonitrile (3-4 ml) solvent. After that, TBHP (2 equiv., 70% in water), $CoCl_2 \cdot 6H_2O$ \ (10 mol%), K_2CO_3 (2 equiv.), and were added sequentially to the mixture of benzaldehyde and styrene. Then the reaction mixture was analyzed directly by GCMS and HRMS.

5.4.7. Post-Synthetic Modifications:

5.4.7.1. Synthesis of compound 7: Compound **7** was synthesized by slight modification of literature reported procedure.[14] An oven-dried round bottom flask equipped with a stir bar was charged with compound **3a** (50 mg, 0.223 mmol, 1 equiv.) and $SnCl_2$ (60.37 mg, 0.2676 mmol, 1.2 equiv.) were dissolved in dichloromethane (5 ml) solvent. Then the reaction mixture was stirred at room temperature under an aerobic atmosphere for one hour. Thereafter, water was added to the reaction mixture, stirred well and the organic layer was extracted with EtOAc (3×10 ml). The combined organic layer was washed with brine and dried under Na_2SO_4. The crude product was purified by column chromatography on silica gel (5% EtOAc/pet ether).

5.4.7.2. Synthesis of compound 8: Compound **8** was synthesized by slight modification of literature reported procedure.[15] An oven-dried round bottom flask equipped with a stir bar was charged with compound **3a** (50 mg, 0.233 mmol, 1 equiv.) and *o*-phenylene diamine (24.084 mg, 0.233 mmol, 1 equiv.) were dissolved in polyethylene glycol (PEG) (5 ml) solvent. After that Cs_2CO_3 (72.65 mg, 0.233 mmol, 1 equiv.) was added to the mixture of **3a** and *o*-phenylene diamine. Then the reaction mixture was stirred at 160 ˚C temperature under an aerobic

atmosphere for 2 h. Thereafter, water was added to the reaction mixture, stirred well and the organic layer was extracted with EtOAc (3×10 ml). The combined organic layer was washed with brine and dried under Na_2SO_4. The crude product was purified by column chromatography on silica gel (20 % EtOAc/pet ether).

5.4.7.3. Synthesis of compound 9: An oven-dried round bottom flask equipped with a stir bar was charged with compound **3a** (50 mg, 0.233 mmol, 1 equiv.) and hydroxylamine hydrochloride (15.50 mg, 0.233 mmol, 1 equiv.), dissolved in ethanol (10 mL). Then pyridine (10 μL, 0.6 equiv.) was added to the reaction mixture and was refluxed for 5 hours. Thereafter, water was added to the reaction mixture, stirred well and the organic layer was extracted with EtOAc (3×20 ml). The combined organic layer was washed with brine and dried under Na_2SO_4. The crude product was purified by column chromatography on silica gel (5% EtOAc/pet ether).

5.4.7.4. Synthesis of compound 10: Compound **10** was synthesized according to literature reported procedure.[16] An oven-dried round bottom flask equipped with a stir bar was charged with compound **3a** (50 mg, 0.223 mmol, 1equiv.) and hydrazine hydrate (0.350 mmol, 1.5 equiv.), dissolved in ethanol (15 ml) solvent. Then the reaction mixture was refluxed for 6 hours. Thereafter, water was added to the reaction mixture, stirred well and the organic layer was extracted with EtOAc (3×20 ml). The combined organic layer was washed with brine and dried under Na_2SO_4. The crude product was purified by column chromatography on neutral alumina (15 % EtOAc/pet ether).

5.4.7.5. Synthesis of compounds 11 and 12: Compounds **11** and **12** were synthesized according to literature reported procedure.[17] An oven-dried round bottom flask equipped with a stir bar was charged with compound **3a** (50 mg, 0.223 mmol, 1 equiv.), dissolved in ethanol (20 ml) solvent. Then Zn dust (29 mg, 0.446 mmol, 2 equiv.) and NH_4Cl (24 mg, 0.446 mmol, 2 equiv.) were added to the reaction mixture. The reaction mixture was refluxed for 30 minutes. Thereafter, Zn was filtered out and ethanol was removed under vacuum. Then water was added to the reaction mixture, stirred well and the organic layer was extracted with dichloromethane (3×20 ml). The combined organic layer was washed with brine and dried under Na_2SO_4. The products (**9**, **11** and **12)** formed were purified by column chromatography on silica gel (2-5% EtOAc/pet ether).

5.4.7.6. Synthesis of compound 13: An oven-dried round bottom flask equipped with a stir bar was charged with compound **3a** (50 mg, 0.223 mmol, 1 equiv.) and hydrazine hydrate (0.350 mmol, 1.5 equiv.), dissolved in ethanol (15 mL) solvent. Then catalytic amount of conc. H_2SO_4 was added to the reaction mixture and then was stirred for 24 hours under reflux. Thereafter, water was added to the reaction mixture, stirred well and the organic layer was extracted with EtOAc (3×20 ml). The combined organic layer was washed with brine and dried under Na_2SO_4 and the solvent was evaporated to dryness. The crude product was redissolved in ethanol and pure compound **13** was recrystallized.

Table 5.5 Classification of synthesized compounds as known and unknown.

Known	**Unknown**
3a, 3b, 3c, 3d, 3e, 3f, 3g, 3h, 3i, 3j, 3k, 3l, 3m, 3n, 3o, 3p, 3q, 4a, 4b, 4c, 4d, 4e, 4f, 4g, 4h, 4i, 4m, 5a, 5b, 5c, 5e, 6a, 6d, 7, 8, 9, 10, 11, 12, 13, 14, 15,	**4j, 4k, 4l, 5d, 5f, 6b, 6c**

Table 5.6: Crystallographic details of compound **3i**.

Empirical formula	$C_{21}H_{16}O_2$
Formula weight	300.34
Crystal size (mm)	0.36 X 0.3 X 0.25
Crystal system	orthorhombic
Space group	*Pca2(1)*
a [Å]	a=6.149(3)
b [Å]	b=7.582(3)
c [Å]	c=32.785(13)
α [°]	90
β [°]	90
γ [°]	90
volume [Å^3]	1528.5(11)
Z	4
F(000)	632.0
μ MoK$_\alpha$ [mm^{-1}]	0.083
Temperature [K]	298
R_{int}	0.0235
Range of h, k, l	–7/7, –9/9, –42/42
$\theta_{min/max}$ (°)	2.759/27.466
GOF on F^2	1.155
Final R indices [I > 2σ(I)]	*R*1 = 0.0431 *wR*2 = 0.1164
R indices [all data]	*R*1 = 0.0442 *wR*2 = 0.1171

5.5. Analytical data of all synthesized compounds

Phenyl(3-phenyloxiran-2-yl)methanone (**3a**)[18]: White solid (Isolated yield ~ 87%, 195 mg), ^{1}H NMR (300 MHz, $CDCl_3$): δ = 8.04-8.0 (m, 2H), 7.63 (tt, J_1 = 1.35 Hz, J_2 = 2.1 Hz, J_3 = 7.5 Hz 1H), 7.52-7.46 (m, 2H), 7.41-7.37 (m, 5H), 4.30 (d, J = 3 Hz, 1H), 4.08 (d, J = 3 Hz, 1H). ^{13}C{^{1}H} NMR (75 MHz, $CDCl_3$): δ = 193.2, 135.6, 134.1, 129.2, 129.0, 128.9, 128.5, 125.9, 61.2, 59.5.

(3-phenyloxiran-2-yl)(*o*-tolyl)methanone (**3b**): Yellow oil (Isolated yield ~ 81%, 193 mg), ^{1}H NMR (300 MHz, $CDCl_3$): δ = 7.68 (dd, J_1 = 1.5 Hz, J_2 = 7.8 Hz, 1H), 7.45-7.36 (m, 7H), 7.3-7.27 (m, 2H), 4.10 (d, J = 2.1 Hz, 1H), 4.03 (d, J = 2.1 Hz, 1H), 2.55 (s, 3H). ^{13}C{^{1}H} NMR (75 MHz, $CDCl_3$): δ = 196.7, 139.0, 135.6, 135.5, 132.4, 132.2, 129.2, 129.1, 128.9, 125.9, 62.5, 59.6, 21.1.

(3-phenyloxiran-2-yl)(*m*-tolyl)methanone (**3c**): Yellow oil (Isolated yield ~ 84%, 200 mg), ^{1}H NMR (300 MHz, $CDCl_3$): δ = 7.83-7.78 (m, 2H), 7.45-7.34 (m, 8H), 4.29 (d, J = 1.8 Hz, 1H), 4.07 (d, J = 1.8 Hz, 1H), 2.41 (s, 3H). ^{13}C{^{1}H} NMR (75 MHz, $CDCl_3$): δ =193.4, 139.0, 135.7, 135.7, 134.9, 129.2, 128.9, 128.8, 125.9, 125.8, 61.1, 59.6, 21.5.

(4-(*tert*-butyl)phenyl)(3-phenyloxiran-2-yl)methanone (**3d**): White liquid (Isolated yield ~ 80%, 224 mg), ^{1}H NMR (300 MHz, $CDCl_3$): δ = 7.96 (d, J = 9Hz, 2H), 7.50 (d, J = 9 Hz, 2H), 7.40-7.35 (m, 5H), 4.28 (d, J = 1.8 Hz, 1H), 4.06 (d, J = 1.8 Hz, 1H), 1.34 (s, 9H). ^{13}C{^{1}H} NMR (75 MHz, $CDCl_3$): δ =192.7, 158.1, 150.7, 135.8, 133.1, 129.1, 128.9, 128.5, 126.0, 61.2, 59.4, 35.4, 31.1.

(2-methoxyphenyl)(3-phenyloxiran-2-yl)methanone (**3e**)[19]: White solid (Isolated yield ~ 80%, 203 mg), ^{1}H NMR (300 MHz, $CDCl_3$): δ = 7.83 (dd, J_1 = 1.8 Hz, J_2 = 7.8 Hz, 1H), 7.55-7.49 (m, 1H), 7.41-7.38 (m, 5H), 7.08-7.03 (m, 1H), 6.93 (d, J = 12 Hz, 1H), 4.31 (d, J = 1.8 Hz, 1H), 4.01 (d, J = 1.8 Hz, 1H), 3.60 (s, 3H). ^{13}C{^{1}H} NMR (75 MHz, $CDCl_3$): δ = 195.0, 159.7, 136.7, 135.0, 130.9, 128.8, 128.7, 126.2, 125.9, 121.2, 111.7, 64.6, 59.9, 55.7.

(4-methoxyphenyl)(3-phenyloxiran-2-yl)methanone (**3f**)[20]: White solid (Isolated yield ~ 85%, 216 mg), ^{1}H NMR (300 MHz, $CDCl_3$): δ = 8.01 (d, J = 9 Hz, 2H), 7.40-7.35 (m, 5H), 6.95 (d, J = 9 Hz, 2H), 4.25 (d, J = 1.8 Hz, 1H), 4.07 (d, J = 1.8 Hz, 1H), 3.88 (s, 3H). ^{13}C{^{1}H} NMR (75 MHz, $CDCl_3$): δ = 191.5, 164.4, 135.9, 130.9, 129.1, 128.9, 128.8, 125.9, 114.3, 61.0, 59.3, 55.7.

(4-(dimethylamino)phenyl)(3-phenyloxiran-2-yl)methanone (**3g**): Brown liquid (Isolated yield ~ 72%, 192 mg), ^{1}H NMR (300 MHz, $CDCl_3$): δ = 7.94 (d, J = 9 Hz, 2H), 7.39-7.35 (m, 5H,), 6.65 (d, J = 9 Hz, 2H), 4.24 (d, J = 3 Hz, 1H), 4.07 (d, J = 3 Hz, 1H), 3.07 (s, 6H). ^{13}C{^{1}H}

NMR (75 MHz, $CDCl_3$): δ = 190.4, 154.1, 136.3, 130.8, 128.9, 128.8, 125.9, 123.7, 111.1, 110.9, 60.8, 59.1, 40.1.

naphthalen-1-yl(3-phenyloxiran-2-yl)methanone (**3h**): Colorless liquid (Isolated yield ~ 84%, 230 mg), ^{1}H NMR (300 MHz, $CDCl_3$): δ = 8.67 (d, *J* = 6 Hz, 1H), 8.05 (d, *J* = 9 Hz, 1H), 7.98 (dd, J_1 = 1.2 Hz, J_2 = 7.2 Hz, 1H), 7.91 (dd, J_1 = 2.1 Hz, J_2 = 8.1 Hz, 1H), 7.67-7.61 (m, 1H), 7.60-7.55 (m, 1H), 7.54-7.49 (m, 1H), 7.41-7.39 (m, 5H), 4.26 (d, *J* = 1.8 Hz, 1H), 4.15 (d, *J* = 1.8 Hz, 1H). ^{13}C{^{1}H} NMR (75 MHz, $CDCl_3$): δ = 196.4, 135.6, 134.1, 133.9, 133.1, 130.4, 129.2, 129.0, 128.9, 128.7, 128.6, 127.0, 126.0, 125.6, 124.5, 62.8, 59.8.

[1,1'-biphenyl]-4-yl(3-phenyloxiran-2-yl)methanone (**3i**)[21]: White solid (Isolated yield ~ 83%, 249 mg), ^{1}H NMR (300 MHz, $CDCl_3$): δ = 8.09 (d, *J* = 9 Hz, 2H), 7.71 (d, *J* = 9 Hz, 2H), 7.64-7.61 (m, 2H), 7.51-7.43 (m, 3H), 7.42-7.39 (m, 5H), 4.33 (d, *J* = 3 Hz, 1H), 4.11 (d, *J* = 3 Hz, 1H). ^{13}C{^{1}H} NMR (75 MHz, $CDCl_3$): δ = 192.8, 146.9, 139.7, 135.7, 134.3, 129.2, 129.1, 128.9, 128.6, 127.6, 127.4, 126.3, 125.9, 61.2, 59.6.

(4-fluorophenyl)(3-phenyloxiran-2-yl)methanone (**3j**): Brown liquid (Isolated yield ~ 70%, 160 mg), ^{1}H NMR (300 MHz, $CDCl_3$): δ = 8.10 - 8.03 (m, 2H), 7.42 -7.34 (m, 5H), 7.20-7.12 (m, 2H), 4.24 (d, *J* = 3 Hz, 1H), 4.07 (d, *J* = 3 Hz, 1H). ^{13}C{^{1}H} NMR (75 MHz, $CDCl_3$): δ = 191.7, 168.1, 164.7, 135.4, 131.4, 131.2, 129.3, 128.9, 125.9, 116.4, 116.1, 61.2, 59.4.

(3-chlorophenyl)(3-phenyloxiran-2-yl)methanone (**3k**)[22]: White solid (Isolated yield ~ 72%, 186 mg), ^{1}H NMR (300 MHz, $CDCl_3$): δ = 7.99 (t, *J* = 1.8Hz, 1H), 7.89 (dt, J_1 = 1.3 Hz, J_2 = 9 Hz, 1H), 7.61-7.58 (m, 1H), 7.46-7.42 (m, 1H), 7.42-7.35 (m, 5H), 4.23 (d, *J* = 1.8 Hz, 1H), 4.08 (d, *J* = 1.8 Hz, 1H). ^{13}C{^{1}H} NMR (75 MHz, $CDCl_3$): δ = 192.3, 137.0, 135.4, 135.3, 134.1, 130.4, 129.3, 128.9, 128.5, 126.6, 125.9, 61.2, 59.6.

(3-nitrophenyl)(3-phenyloxiran-2-yl)methanone (**3l**)[18]: Yellow solid (Isolated yield ~ 72%, 193 mg), ^{1}H NMR (300 MHz, $CDCl_3$): δ = 8.88 (t, *J* = 1.95Hz, 1H), 8.50 – 8.46 (m, 1H), 8.36 (dt, J_1 = 1.5 Hz, J_2 = 9 Hz, 1H), 7.72 (t, *J* = 7.5 Hz, 1H), 7.44-7.35 (m, 5H), 4.27 (d, *J* = 1.8 Hz, 1H), 4.12 (d, *J* = 1.8 Hz, 1H). ^{13}C{^{1}H} NMR (75 MHz, $CDCl_3$): δ = 191.8, 136.6, 134.9, 134.1, 130.3, 129.5, 129.1, 128.3, 125.9, 123.6, 61.4, 59.7.

1-(3-phenyloxiran-2-yl)pentan-1-one (**3m**)[23]: White solid (Isolated yield ~ 80 %, 163 mg), ^{1}H NMR (300 MHz, $CDCl_3$): δ = 7.38 – 7.35 (m, 3H), 7.30 – 7.27 (m, 2H), 3.96 (d, *J* = 2.1 Hz, 1H), 3.52 (d, *J* = 2.1 Hz, 1H), 2.61-2.40 (m, 2H), 1.62-1.59 (m, 2H), 1.42-1.34 (m, 2H), 0.95-0.90 (m, 3H). ^{13}C{^{1}H} NMR (75 MHz, $CDCl_3$): δ = 206.3, 135.4, 129.1, 128.8, 125.8, 63.3, 58.2, 37.7, 25.3, 22.4, 13.9.

1-(3-phenyloxiran-2-yl)hexan-1-one (**3n**)[24]: White solid (Isolated yield ~ 82 %, 179 mg), ^{1}H NMR (300 MHz, $CDCl_3$): δ = 7.25 – 7.21 (m, 3H), 7.17 – 7.13 (m, 2H), 3.83 (d, *J* = 3 Hz, 1H), 3.38 (d, *J* = 3 Hz, 1H), 2.48-2.24 (m, 2H), 1.53-1.46 (m, 2H), 1.24-1.17 (m, 4H), 0.80-0.75 (m, 3H). $^{13}C\{^1H\}$ NMR (75 MHz, $CDCl_3$): δ = 206.3, 135.4, 129.1, 128.8, 125.8, 63.3, 58.2, 37.9, 31.4, 22.9, 22.5, 14.0.

1-(3-phenyloxiran-2-yl)octan-1-one (**3o**): White solid (Isolated yield ~ 80 %, 197 mg), ^{1}H NMR (300 MHz, $CDCl_3$): δ = 7.36 – 7.35 (m, 3H), 7.28 – 7.27 (m, 2H), 3.96 (s, 1H), 3.51 (s, 1H), 2.58-2.38 (m, 2H), 1.70-1.60 (m, 2H), 1.30-1.27 (m, 8H), 0.89-0.86 (m, 3H). $^{13}C\{^1H\}$ NMR (75 MHz, $CDCl_3$): δ = 206.3, 135.4, 129.1, 128.8, 125.8, 63.3, 58.2, 37.9, 31.8, 29.1, 26.3, 23.3, 22.7, 14.2.

furan-2-yl(3-phenyloxiran-2-yl)methanone (**3p**)[20]: Yellow oil (Isolated yield ~ 80 %, 171 mg), ^{1}H NMR (300 MHz, $CDCl_3$): δ = 7.67 (dd, J_1 = 0.9 Hz, J_2 = 1.8 Hz, 1H), 7.45 (d, *J* = 3.6 Hz 1H), 7.40-7.32 (m, 5H), 6.59 (dd, J_1 = 1.8 Hz, J_2 = 3.6 Hz, 1H), 4.14 (t, J_1 = 2.1 Hz, 3H). $^{13}C\{^1H\}$ NMR (75 MHz, $CDCl_3$): δ = 182.2, 151.3, 147.8, 135.5, 129.2, 128.8, 125.9, 119.7, 112.8, 60.8, 59.7.

(1*H*-indol-3-yl)(3-phenyloxiran-2-yl)methanone (**3q**): Brown solid (Isolated yield ~ 77 %, 202 mg), ^{1}H NMR (300 MHz, DMSO-d_6): δ = 12.20 (s, 1H), 8.66 (d, *J* = 3 Hz, 1H), 8.24-8.21 (m, 1H), 7.85 (t, *J* = 9 Hz, 1H), 7.53-7.50 (m, 1H), 7.47-7.40 (m, 4H), 7.27-7.23 (m, 2H). $^{13}C\{^1H\}$ NMR (75 MHz, $CDCl_3$): δ = 188.0, 140.0, 136.9, 136.7, 135.7, 129.3, 128.9, 126.8, 123.8, 122.7, 121.8, 115.8, 112.8, 60.4, 58.5.

(3-([1,1'-biphenyl]-4-yl)oxiran-2-yl)(phenyl)methanone (**4a**): Yellow liquid (Isolated yield ~ 80%, 240 mg), ^{1}H NMR (300 MHz, $CDCl_3$): δ = 7.61-7.57 (m, 6H), 7.47-7.43 (m, 4H), 7.38-7.34 (m, 4H), 3.93-3.91 (m, 1H), 3.18 (dd, J_1 = 3Hz, J_2 = 6Hz, 1H), 2.85 (dd, J_1 = 1.95 Hz, J_2 = 4 Hz, 1H). $^{13}C\{^1H\}$ NMR (75 MHz, $CDCl_3$): δ = 192.0, 141.3, 140.8, 136.7, 133.5, 130.4, 129.2, 128.9, 128.7, 127.8, 127.5, 127.4, 126.1, 63.2, 58.5.

(3-(4-chlorophenyl)oxiran-2-yl)(phenyl)methanone (**4b**)[25]: Yellow solid (Isolated yield ~ 70%, 181 mg), ^{1}H NMR (300 MHz, $CDCl_3$): δ = 8.0 (dd, J_1 = 1.05 Hz, J_2 = 6 Hz, 2H), 7.63 (tt, J_1 = 1.05 Hz, J_2 = 6 Hz, 1H), 7.50 (t, *J* = 6 Hz 2H), 7.39-7.37 (m, 2H), 7.33-7.30 (m, 2H), 4.24 (d, *J* = 3 Hz, 1H), 4.06 (d, *J* = 3 Hz, 1H,). $^{13}C\{^1H\}$ NMR (75 MHz, $CDCl_3$): δ = 191.9, 135.5, 135.1, 134.2, 134.1, 129.2, 129.1, 128.5, 127.3, 61.1, 58.8.

(3-(4-(*tert*-butyl)phenyl)oxiran-2-yl)(phenyl)methanone (**4c**): Yellow oil (Isolated yield ~ 78%, 218 mg), ^{1}H NMR (300 MHz, $CDCl_3$): δ = 8.03-8.00 (m, 2H), 7.64-7.59 (m, 1H), 7.50 (d, *J* = 6 Hz, 2H), 7.45-7.42 (m, 2H), 7.33-7.30 (m, 2H), 4.31 (d, *J* = 3 Hz, 1H), 4.05 (d, *J* = 3

Hz, 1H), 1.34 (s, 9H). $^{13}C\{^{1}H\}$ NMR (75 MHz, $CDCl_3$): δ = 193.4, 152.5, 135.7, 134.1, 132.6, 129.0, 128.5, 125.9, 125.8, 61.1, 59.6, 34.9, 31.4.

(3-(naphthalen-2-yl)oxiran-2-yl)(phenyl)methanone (**4d**)[26]: Yellow liquid (Isolated yield ~ 80%, 219 mg), ^{1}H NMR (300 MHz, $CDCl_3$): δ = 8.10-8.07 (m, 2H), 8.02-7.99 (m, 1H), 7.94-7.91 (m, 1H), 7.89-7.87 (m, 1H), 7.64-7.62 (m, 2H), 7.54-7.50 (m, 5H), 4.73 (d, *J* = 3 Hz, 1H), 4.31 (d, *J* = 3 Hz, 1H).$^{13}C\{^{1}H\}$ NMR (75 MHz, $CDCl_3$): δ = 193.5, 135.6, 134.3, 133.5, 131.9, 133.3, 129.1, 129.1, 129.0, 128.6, 126.9, 126.3, 125.7, 122.7, 122.6, 60.4, 58.0.

(3-methyl-3-phenyloxiran-2-yl)(phenyl)methanone (**4e**): White solid (Isolated yield ~ 76%, 180 mg), ^{1}H NMR (300 MHz, $CDCl_3$): δ = 7.98-7.95 (m, 2H), 7.65-7.60 (m, 1H), 7.52-7.48 (m, 4H), 7.44-7.37 (m, 3H), 4.16 (s, 1H), 1.64 (s, 3H). $^{13}C\{^{1}H\}$ NMR (75 MHz, $CDCl_3$): δ = 193.1, 140.5, 135.7, 134.1, 129.1, 128.9, 128.4, 125.3, 67.0, 63.0, 17.1.

(3-methyl-3-phenyloxiran-2-yl)(*o*-tolyl)methanone (**4f**): White solid (Isolated yield ~ 75%, 189 mg), ^{1}H NMR (300 MHz, $CDCl_3$): δ = 7.57 (dd, J_1 = 1.65 Hz, J_2 = 7.5 Hz 1H), 7.34-7.27 (m, 3H), 7.23-7.18 (m, 4H), 7.12-7.10 (m, 1H), 4.16 (s, 1H), 2.09 (s, 1H), 1.87 (s,1H). $^{13}C\{^{1}H\}$ NMR (75 MHz, $CDCl_3$): 196.6, 138.9, 136.8, 135.7, 131.9, 131.8, 129.1, 128.1, 128.0, 126.5, 125.5, 67.0, 64.9, 24.6, 20.3.

(3-methyl-3-phenyloxiran-2-yl)(*m*-tolyl)methanone (**4g**): White solid (Isolated yield ~ 70%, 176 mg), ^{1}H NMR (300 MHz, $CDCl_3$): δ = 7.49-7.46 (m, 4H), 7.39-7.37 (m, 2H), 7.35-7.32 (m, 3H), 4.1 (s, 1H), 2.42 (s, 3H), 1.63 (s, 3H). $^{13}C\{^{1}H\}$ NMR (75 MHz, $CDCl_3$): δ = 193.3, 145.1, 139.0, 134.9, 128.9, 128.8, 128.3, 128.2, 127.1, 125.7, 125.3, 75.3, 67.0, 29.8, 26.4.

(4-methoxyphenyl)(3-methyl-3-phenyloxiran-2-yl)methanone (**4h**): White solid (Isolated yield ~ 80%, 214 mg), ^{1}H NMR (300 MHz, $CDCl_3$): δ = 7.95 (2, *J* = 9 Hz, 2H), 7.50-7.36 (m, 5H), 6.95 (d, *J* = 9 Hz, 2H), 4.11 (s, 1H), 3.88 (s, 3H), 1.62 (s, 3H). $^{13}C\{^{1}H\}$ NMR (75 MHz, $CDCl_3$): δ = 191.5, 164.3, 140.7, 130.8, 128.8, 128.3, 125.2, 116.2, 114.3, 66.9, 62.6, 55.7, 17.2.

(3,3-diphenyloxiran-2-yl)(phenyl)methanone (**4i**): White solid (Isolated yield ~ 70%, 210 mg), ^{1}H NMR (300 MHz, $CDCl_3$): δ = 7.94-7.91 (m, 2H), 7.60-7.55 (m, 2H), 7.47-7.42 (m, 5H), 7.39-7.37 (m, 3H), 7.33-7.29 (m, 3H), 7.22-7.20 (m, 2H), 4.67 (s, 1H). $^{13}C\{^{1}H\}$ NMR (75 MHz, $CDCl_3$): δ = 192.1, 139.3, 135.9, 135.0, 133.8, 132.6, 130.2, 128.9, 128.8, 128.4, 128.2, 128.2, 127.1, 67.8, 67.0.

(3,3-diphenyloxiran-2-yl)(*o*-tolyl)methanone (**4j**): White solid (Isolated yield ~ 72%, 226 mg), ^{1}H NMR (300 MHz, $CDCl_3$): δ = 7.70 (dd, J_1 = 1.5 Hz, J_2 = 7.8 Hz, 1H), 7.43-7.40 (m, 2H), 7.37-7.28 (m, 6H), 7.23-7.19 (m, 4H), 7.16-7.11 (m, 1H), 4.53 (s, 1H), 2.18 (s, 3H). $^{13}C\{^{1}H\}$ NMR (75 MHz, $CDCl_3$): δ = 195.6, 139.4, 139.3, 135.5, 135.1, 132.1, 132.0, 129.3, 128.7,

128.6, 128.2, 128.1, 128.0, 127.2, 125.6, 67.9, 67.4, 20.6. HRMS (ESI, m/z) [M+Na] calcd. for $C_{22}H_{18}O_2$ 337.1204, found 337.1204.

(3,3-diphenyloxiran-2-yl)(*m*-tolyl)methanone (**4k**): White solid (Isolated yield ~ 71%, 222 mg), ^{1}H NMR (300 MHz, $CDCl_3$): δ = 7.83-7.68 (m, 3H), 7.45-7.27 (m, 10H), 7.25-7.22 (m, 1H), 4.15 (s, 1H), 2.41 (s, 3H). $^{13}C\{^1H\}$ NMR (75 MHz, $CDCl_3$): δ = 197.4, 143.9, 138.7, 137.9, 134.3, 133.4, 129.8, 129.1, 128.6, 128.2, 127.7, 127.2, 126.8, 126.3, 125.8, 26.4. HRMS (ESI, m/z) [M+Na] calcd. for $C_{22}H_{18}O_2$ 337.1204, found 337.1204.

(3,3-diphenyloxiran-2-yl)(4-methoxyphenyl)methanone (**4l**): White solid (Isolated yield ~ 75%, 252 mg), ^{1}H NMR (300 MHz, $CDCl_3$): δ = 7.94 (d, J = 9 Hz, 2H), 7.46-7.42 (m, 3H), 7.39-7.36 (m, 2H), 7.33-7.29 (m, 2H), 7.22-7.20 (m, 3H), 6.91 (d, J = 9 Hz, 2H), 4.62 (s, 1H), 3.86 (s, 3H). $^{13}C\{^1H\}$ NMR (75 MHz, $CDCl_3$): δ = 190.3, 164.0, 139.4, 135.2, 130.7, 128.7, 128.6, 128.3, 128.2, 128.1, 127.0, 126.5, 114.1, 67.5, 67.0, 55.6. HRMS (ESI, m/z) [M+H] calcd. for $C_{22}H_{18}O_3$ 337.1334, found 331.1328.

(2,3-diphenyloxiran-2-yl)(phenyl)methanone (**4m**): White solid (Isolated yield ~ 60%, 180 mg), ^{1}H NMR (300 MHz, $CDCl_3$): δ = 8.16-8.14 (m, 2H), 7.48-7.43 (m, 5H), 7.22-7.18 (m, 8H), 4.53 (s, 1H). $^{13}C\{^1H\}$ NMR (75 MHz, $CDCl_3$): δ = 195.4, 134.3, 133.9, 133.5, 132.6, 132.1, 130.0, 128.7, 128.3, 128.1, 128.0, 127.7, 126.9, 71.3, 63.2.

(3-butyloxiran-2-yl)(phenyl)methanone (**5a**): Colorless oil (Isolated yield ~ 60%, 122 mg), ^{1}H NMR (300 MHz, $CDCl_3$): δ = 8.01 (dd, J_1 = 3 Hz, J_2 = 6 Hz, 2H), 7.62 (tt, J_1 = 1.5 Hz, J_2 = 6 Hz, 1H), 7.52-7.48 (m, 2H), 4.01 (d, J = 1.5 Hz, 1H), 3.16-3.13 (m, 1H), 1.83-1.67 (m, 2H), 1.55-1.47 (m, 2H), 1.45-1.37 (m, 2H), 0.93 (t, J = 4.5 Hz, 3H). $^{13}C\{^1H\}$ NMR (75 MHz, $CDCl_3$): δ = 194.9, 135.8, 133.9, 128.9, 128.4, 60.2, 57.6, 31.8, 28.1, 22.6, 14.0.

(3-hexyloxiran-2-yl)(phenyl)methanone (**5b**): Colorless oil (Isolated yield ~ 55%, 127 mg), ^{1}H NMR (300 MHz, $CDCl_3$): δ = 8.03 - 8.0 (m, 2H), 7.61 (d, J = 6 Hz, 1H), 7.53-7.48 (m, 2H), 4.01 (d, J = 3 Hz, 1H), 3.17-3.13 (m, 1H), 1.80-1.72 (m, 2H), 1.42-1.41 (m, 2H), 1.33-1.28 (m, 8H), 0.86-0.83 (m, 3H). $^{13}C\{^1H\}$ NMR (75 MHz, $CDCl_3$): δ = 194.9, 133.9, 130.0, 128.9, 128.4, 68.6, 60.2, 32.1, 31.8, 29.2, 26.0, 22.7, 14.2.

(3-(bromomethyl)oxiran-2-yl)(phenyl)methanone (**5c**): Colorless oil (Isolated yield ~ 55%, 132 mg), ^{1}H NMR (300 MHz, $CDCl_3$): δ = 8.09 (dt, J_1 = 1.2 Hz, J_2 = 3.9 Hz, J_3 = 8.4 Hz, 2H), 7.61-7.58 (m, 1H), 7.49-7.47 (m, 2H), 5.11 (d, J = 3 Hz, 1H), 4.66 (dd, J_1 = 3 Hz, J_2 = 15 Hz, 1H), 4.18 (dd, J_1 = 6 Hz, J_2 = 12 Hz, 1H), 3.38-3.32 (m, 1H). $^{13}C\{^1H\}$ NMR (75 MHz, $CDCl_3$): δ = 190.2, 133.5, 133.2, 129.9, 128.7, 65.6, 63.7, 29.8.

(3-(3-bromopropyl)oxiran-2-yl)(phenyl)methanone (**5d**): Colorless oil (Isolated yield ~ 67%, 134 mg), ^{1}H NMR (300 MHz, $CDCl_3$): δ = 8.05-8.03 (m, 2H), 7.58-7.53 (m, 1H), 7.46-7.42 (m, 2H), 4.49 (d, *J* = 6 Hz, 1H), 4.34 (t, *J* = 6 Hz, 2H), 3.41 (t, *J* = 7.5 Hz, 1H), 1.88-1.81 (m, 4H). ^{13}C{^{1}H} NMR (75 MHz, $CDCl_3$): δ = 200.3, 133.1, 129.7, 128.5, 128.2, 65.0, 64.6, 38.5, 29.8, 26.5. HRMS (ESI, m/z) [M+H] calcd. for $C_{12}H_{13}BrO_2$ 269.0177, found 269.0178.

Ethyl 3-benzoyloxirane-2-carboxylate (**5e**): White solid (Isolated yield ~ 79%, 173 mg), ^{1}H NMR (300 MHz, $CDCl_3$): δ = 8.05 (dd, J_1 = 1.5 Hz, J_2 = 7.5 Hz, 2H), 7.71-7.65 (m, 1H), 7.57-7.52 (m, 2H), 4.47 (d, *J* = 3 Hz, 1H), 4.38-4.30 (m, 2H), 3.72 (d, *J* = 1.8 Hz, 1H), 1.37 (t, *J* = 7.5 Hz, 3H). ^{13}C{^{1}H} NMR (75 MHz, $CDCl_3$): δ = 192.0, 167.3, 134.6, 130.3, 129.1, 128.7, 62.5, 55.4, 53.2, 14.2.

Butyl 3-benzoyloxirane-2-carboxylate (**5f**): White solid (Isolated yield ~ 78%, 193 mg), ^{1}H NMR (300 MHz, $CDCl_3$): δ = 8.02 (dd, J_1 = 1.8 Hz, J_2 = 6 Hz, 2H), 7.69-7.63 (tt, J_1 = 1.6 Hz, J_2 = 7.5 Hz, 1H), 7.55-7.50 (m, 2H), 4.44 (d, *J* = 3 Hz, 1H), 4.30-4.21 (m, 2H), 3.69 (d, *J* = 3 Hz, 1H), 1.73-1.64 (m, 2H), 1.45-1.38 (m, 2H), 0.96 (t, *J* = 7.5 Hz, 3H). ^{13}C{^{1}H} NMR (75 MHz, $CDCl_3$): δ = 192.0, 167.4, 135.2, 134.6, 129.1, 128.7, 66.3, 55.4, 53.2, 30.6, 19.1, 13.8. HRMS (ESI, m/z) [M+Na] calcd. for $C_{14}H_{16}O_4$ 271.0946, found 271.0942.

Spiro[chromane-3,2'-oxiran]-4-one (**6a**): White solid (Isolated yield ~ 82%, 144 mg), ^{1}H NMR (300 MHz, $CDCl_3$): δ = 7.94 (dd, J_1 = 1.85 Hz, J_2 = 7.5 Hz, 1H), 7.57-7.51 (m, 1H), 7.11-7.03 (m, 2H), 4.62 (dd, J_1 = 1.2 Hz, J_2 = 12 Hz, 1H), 4.38 (d, *J* = 12 Hz, 1H), 3.37 (dd, J_1 = 1.2 Hz, J_2 = 6 Hz, 1H), 3.02 (d, *J* = 6 Hz, 1H). ^{13}C{^{1}H} NMR (75 MHz, $CDCl_3$): δ = 188.3, 161.9, 136.9, 127.5, 122.3, 121.9, 118.5, 70.9, 54.8, 53.1.

7-methoxyspiro[chromane-3,2'-oxiran]-4-one (**6b**): White solid (GC yield 75%, isolated yield ~ 70%, 144 mg), ^{1}H NMR (300 MHz, $CDCl_3$): δ = 7.87 (d, J = 9 Hz, 1H), 6.64 (dd, J_1 = 3 Hz, J_2 = 9 Hz, 1H), 6.46 (d, J = 3 Hz, 1H), 4.59 (d, J = 12 Hz, 1H), 4.38 (d, J = 12 Hz, 1H), 3.86 (s, 3H), 3.38 (d, J = 6 Hz, 1H), 2.98 (d, J = 6 Hz, 1H). ^{13}C{^{1}H} NMR (75 MHz, $CDCl_3$): δ = 186.6, 166.8, 164.0, 129.2, 115.9, 110.9, 101.3, 71.2, 55.9, 54.5, 52.7. HRMS (ESI, m/z) [M+H] calcd. for $C_{11}H_{10}O_4$ 207.0657, found 207.0666.

7-(diethylamino)spiro[chromane-3,2'-oxiran]-4-one (**6c**): White solid (Isolated yield ~ 70%, 172 mg), ^{1}H NMR (300 MHz, $CDCl_3$): δ = 7.74 (d, *J* = 6 Hz, 1H), 6.36 (dd, J_1 = 2.1 Hz, J_2 = 6.9 Hz, 1H), 6.06 (d, J = 1.8 Hz, 1H), 4.49-4.45 (m, 1H), 4.30 (t, *J* = 9 Hz, 1H), 3.90-3.87 (m, 1H), 3.39 (q, *J* = 6 Hz, 4H), 2.95-2.88 (m, 1H), 1.20 (t, *J* = 4.5 Hz, 6H) . ^{13}C{^{1}H} NMR (75 MHz, $CDCl_3$): δ = 192.3, 163.9, 154.0, 129.1, 106.7, 96.8, 68.7, 60.3, 47.0, 45.0, 12.7. HRMS (ESI, m/z) [M+H] calcd. for $C_{14}H_{17}NO_3$ 248.1287, found 248.1290.

6-chlorospiro[chromane-3,2'-oxiran]-4-one (**6d**): White solid (Isolated yield ~ 74%, 155 mg), ^{1}H NMR (300 MHz, $CDCl_3$): δ = 7.89 (d, J = 3 Hz, 1H), 7.49 (dd, J_1 = 3 Hz, J_2 = 9 Hz, 1H), 7.02 (d, J = 9Hz, 1H), 4.62 (d, J = 12 Hz, 1H), 4.40 (d, J = 12 Hz, 1H), 3.39 (d, J = 6 Hz, 1H), 3.03 (d, J = 6 Hz, 1H). ^{13}C{^{1}H} NMR (75 MHz, $CDCl_3$): δ = 187.3, 160.4, 139.4, 136.8, 126.7, 122.7, 120.3, 71.0, 54.6, 53.1.

3-chloro-2-hydroxy-1,3-diphenylpropan-1-one (**7**): White solid (Isolated yield ~ 90%, 234 mg), ^{1}H NMR (300 MHz, $CDCl_3$): δ = 7.95-7.92 (m, 2H), 7.71-765 (m, 1H), 7.58-7.53 (m, 4H), 7.42-7.34 (m, 3H), 5.41 (dd, J_1 = 2.1 Hz, J_2 = 7.5 Hz 2H), 5.25 (d, J = 3 Hz, 1H), 4.12 (d, J = 6 Hz, 1H). ^{13}C{^{1}H} NMR (75 MHz, $CDCl_3$): δ = 197.9, 138.3, 133.4, 133.8, 129.3, 128.9, 128.7, 128.1, 76.2, 63.9.

2-benzyl-3-phenylquinoxaline (**8**): White solid (Isolated yield ~ 80%, 237 mg), ^{1}H NMR (300 MHz, $CDCl_3$): δ = 8.16-8.10 (m, 2H), 7.78-7.74 (m, 2H), 7.49-7.44 (m, 5H), 7.17-7.13 (m, 3H), 6.99-6.97 (m, 2H), 4.41 (s, 2H). ^{13}C{^{1}H} NMR (75 MHz, $CDCl_3$): δ = 155.6, 154.5, 141.6, 141.1, 139.1, 138.3, 130.7, 129.9, 129.7, 129.4, 129.0, 128.6, 128.4, 126.5, 125.9, 42.4.

diethyl phthalate (**9**): White solid (Isolated yield ~ 99%, 220 mg), ^{1}H NMR (300 MHz, $CDCl_3$): δ = 7.71-7.69 (m, 2H), 7.51-7.49 (m, 2H), 4.35 (q, J = 6 Hz, 4H), 1.34 (t, J = 4.5 Hz, 6H). ^{13}C{^{1}H} NMR (75 MHz, $CDCl_3$): δ = 167.6, 132.3, 131.0, 128.9, 61.6, 14.1.

3,5-diphenyl-4,5-dihydro-1H-pyrazol-4-ol (**10**): White solid (Isolated yield ~ 92%, 219 mg), ^{1}H NMR (300 MHz, DMSO-d_6): δ = 7.70 (d, J = 6 Hz, 2H), 7.38-7.32 (m, 5H), 7.30-7.2 (m, 3H), 4.97 (d, J = 6 Hz, 1H), 4.55 (d, J = 6 Hz, 1H). ^{13}C{^{1}H} NMR (75 MHz, DMSO-d_6): δ = 149.8, 141.7, 132.8, 129.1, 129.0, 128.5, 127.9, 126.9, 126.2, 82.3, 72.3.

2-hydroxy-1,3-diphenylpropan-1-one (**11**): White solid (Isolated yield ~ 40%, 90 mg), ^{1}H NMR (300 MHz, $CDCl_3$): δ = 7.96 (dd, J_1 = 1 Hz, J_2 = 6 Hz, 2H), 7.59 (m, J_1 = 1.1 Hz, J_2 = 6 Hz 1H), 7.49-7.44 (m, 4H), 7.40-7.36 (m, 2H), 7.33-7.28 (m, 1H), 5.36 (t, J = 4.5 Hz, 1H), 3.57 (s, 1H), 3.38 (d, J = 3 Hz, 2H). ^{13}C{^{1}H} NMR (75 MHz, $CDCl_3$): δ = 200.4, 143.1, 136.7, 133.8, 128.9, 128.7, 128.3, 127.8, 125.9, 70.9, 47.5.

1,3-diphenylpropan-1-one (**12**): White solid (Isolated yield ~ 30%, 63 mg), ^{1}H NMR (300 MHz, $CDCl_3$): δ = 7.97-7.94 (m, 2H), 7.55 (tt, J_1 = 1.2 Hz, J_2 = 6 Hz, 1H), 7.45 (t, J = 6 Hz, 2H), 7.32-7.26 (m, 3H), 7.25-7.24 (m, 1H), 7.22-7.18 (m, 1H), 3.30 (t, J = 6 Hz, 2H), 3.07 (t, J = 6 Hz, 2H) . ^{13}C{^{1}H} NMR (75 MHz, $CDCl_3$): δ = 199.4, 141.4, 137.0, 133.2, 128.7, 128.6, 128.5, 128.2, 126.3, 40.6, 30.3.

3,5-diphenyl-4,5-dihydro-1H-pyrazole (**13**): White solid (Isolated yield ~ 70%, 155 mg), ^{1}H NMR (300 MHz, $CDCl_3$): δ = 7.74-7.71 (m, 3H), 7.39-7.30 (m, 6H), 7.30-7.27 (m, 1H), 6.05

(d, J = 9 Hz, 1H), 4.98 (t, J = 7.5 Hz, 1H), 4.54 (dd, J_1 = 3 Hz, J_2 = 6 Hz, 1H). $^{13}C\{^1H\}$ NMR (75 MHz, $CDCl_3$): δ = 149.2, 141.6. 132.8, 128.7, 128.6, 128.0, 127.5, 126.6, 125.8, 82.1, 72.2. benzil (**14**): White solid (Isolated yield ~ 70%, 147 mg), ^1H NMR (300 MHz, $CDCl_3$): δ = 8.13 (dt, J_1 = 3 Hz, J_2 = 6 Hz, 2H), 7.65-7.59 (m, 1H), 7.52-7.46 (m, 2H), 7.43-7.37 (m, 1H). $^{13}C\{^1H\}$ NMR (75 MHz, $CDCl_3$): δ = 172.1, 133.9, 130.3, 129.5, 128.6.

1,2-bis(4-methoxyphenyl)ethane-1,2-dione (**15**): White solid (Isolated yield ~ 75%, 202.5 mg), ^1H NMR (300 MHz, $CDCl_3$): δ = 8.07 (d, J = 9 Hz, 2H), 6.96 (d, J = 12 Hz, 2H), 3.88 (s, 3H). $^{13}C\{^1H\}$ NMR (75 MHz, $CDCl_3$): δ = 171.7, 164.2, 132.5, 121.8, 113.9, 55.6.

5.6. References

1. (a) Adam, W.; Saha-Möller, C. R.; Ganeshpure, P. A. *Chem. Rev.* **2001**, *101*, 3499-3548. (b) Xia, Q. -H.; Ge, H. -Q.; Ye, C. -P.; Liu, Z. -M.; Su, K. -X. *Chem. Rev.* **2005**, *105*, 1603-1662. (c) Climent, M. J.; Corma, A.; Iborra, S. *Chem. Rev.* **2011**, *111*, 1072-1133. (d) Kolb, H. C.; VanNieuwenhze, M. S.; Sharpless, K. B. *Chem. Rev*. **1994**, *94*, 2483-2547.
2. (a) Ottenbacher, R. V.; Bryliakov, K. P.; Talsi, E.P. *Adv. Synth. Catal.* **2011**, *353*, 885-889, (b) Sherstyuk, V. A.; Ottenbacher, R. V.; Talsi, E. P.; Bryliakov, K. P. *ACS Catal.* **2024**, *14*, 498-507. (c) Kadiri, M. Y. E.; Framery, E.; Andrioletti, B. *Tetrahedron Lett.* **2012**, *53*, 6335-6338.
3. (a) Choudary, B. M.; Kantam, M. L.; Ranganath, V. S.; Mahendar, K.; Sreedhar, B. *J. Am. Chem. Soc*. **2004**, *126*, 3396–3397. (b) Wang, Y.; Ye, J.; Liang, X. *Adv. Synth. Catal*. **2007**, *349*, 1033–1036. (c) Marigo, M.; Franzén, J.; Poulsen, T. B.; Zhuang, W.; Jørgensen, K. A. *J. Am. Chem. Soc*. **2005**, *127*, 6964–6965.
4. Seitz, A.-K.; Kohlpaintner, P. J.; Lingen, T. V.; Dyga, M.; Zirbes, F. S. M.; Waldvogel, S. R.; Gooßen, L. J. *Angew. Chem. Int. Ed.* **2022**, *61*, e202117563.
5. Hu, F.; Chen, Z.; Tan, Y.; Xu, D.; Huang, S.; Jia, S.; Gong, X.; Qin, W.; Yan, H. *Org. Lett.* **2020**, *22*, 1934-1940.
6. (a) Luo, W.; Yu, Z.; Qiu, W.; Yang, F.; Liu, X.; Tang, J. *Tetrahedron* **2011**, *67*, 5289-5292 (b) Crivoi, D.-G.; Segarra, A. M.; Medina, F. *J. Catal*. **2016**, *334*, 120-128.
7. Li, J.; Wang, Z. *Org. Lett*. **2015**, *17*, 5260−5263.
8. de Souza, G. F. P.; Bonacin, J. A.; Salles Jr., A. G. *J. Org. Chem.* **2018**, *83*, 8331−8340.
9. Zhang, C.-P.; Zhu, Y.-J.; Wang, D.; Qian, J.; Zhao, Y.-P.; Lian, C.; Zhang, Z.-H.; He, M.-Y.; Chen, S.-C.; Chen, Q. *Inorg. Chem.* **2023**, *62*, 17678−17690.
10. Liu, W.; Li, Y.; Li, Z. *J. Am. Chem. Soc*. **2011**, *133*, 10756–10759.

11. (a) Hu, Z.; Xia, F.; Yang, F.; Weng, J.; Yao, P.; Zheng, C.; Zhu, C., Tang, T.; Fu, W. *RSC Adv*. **2017**, *7*, 41204–41209. (b) Larionov, V. A.; Markelova, E. P.; Smol'yakov, A. F.; Savel'yeva, T. F.; Maleev, V. I.; Belokon, Y. N. *RSC Adv.* **2015**, *5*, 72764-72771. (c) Xiang, M.; Ni, X.; Yi, X.; Zheng, A.; Wang, W.; He, M.; Xiong, J.; Liu, T.; Ma, Y.; Zhu, P.; Zheng, X.; Tang, T. *ChemCatChem.* **2015**, *7*, 521-525. (d) Ke, Q.; Zhang, B.; Hu, B.; Jin, Y.; Lu, G. *Chem. Commun*. **2015**, *51*, 1012-1015. (e) Ashokkumar, V.; Siva, A. *Org. Biomol. Chem*. **2017**, *15*, 2551–2561.
12. Reddi, R. N.; Prasad, P. K.; Sudalai, A. *Angew. Chem. Int. Ed.* **2015**, *54*, 14150-14153.
13. Pal, A.; Das, K. M.; Thakur, A. *J. Org. Chem*. **2023**, *88*, 8955-8968.
14. Einhorn, C.; Luche, J.-L. *J. Chem. Soc., Chem. Commun.* **1986**, 1368-1369.
15. Tu, M.-S.; Xu, H.-W.; Fan, W.; Jiang, B.; Tu, S.-J. *J. Het. Chem*. **2015**, *52*, 719–725.
16. Bhat, B. A.; Puri, S. C.; Qurishi, M. A.; Dhar, K. L.; Qazi, G. N. *Synthetic Commun.* **2005**, *35*, 1135–1142.
17. Yao, Z.; Ye, D.; Liu, H.; Chen, K.; Jiang, H. *Synthetic Commun*. **2007**, *37*, 149–156.
18. Mahato, S.; Santra, S.; De, A.; Chatterjee, R.; Zyryanov, G. V.; Majee, A. *Chem. Select* **2018**, *3*, 7596-7601.
19. Jiang, B.; Li, H. -Z. Li, R. -J.; Zhang, J.; Zhang, Y. -X. *ACS Omega* **2022**, *7*, 21608-21614.
20. Shan, H.; Lu, C.; Zhao, B.; Yao, Y. *New J. Chem.* **2021**, *45*, 1043-1053.
21. Rapi, Z.; Bakó, P.; Keglevich, G.; Szöllősy, Á.; Drahos, L.; Botyánszki, A.; Holczbauer, T. *Tet. Asymm.* **2012**, *23*, 489-496.
22. Karaman, H. S.; Kılıç, H.; Şahin, E. *Tetrahedron Asymm.* **2017**, *28*, 1626-1632.
23. Xiang, M.; Ni, X.; Yi, X.; Zheng, A.; Wang, W.; He, M.; Xiong, J.; Liu, T.; Ma, Y.; Zhu, P.; Zheng, X.; Tang, T. *ChemCatChem* **2015**, *7*, 521-525.
24. Ashokkumar, V.; Siva, A. *Org. Biomol. Chem.* **2017**, *15*, 2551-2561.
25. Sivamani, J.; Ashokkumar, V.; Sadhasivam, V.; Duraimurugan, K.; Siva, A. *RSC Adv.* **2014**, *4*, 60293-60299.
26. Makó, A.; Rapi, Z.; Keglevich, G.; Szöllősy, Á.; Drahos, L.; Hegedűs, L.; Bakó, P. *Tetrahedron Asymm.* **2010**, *21*, 919-925.

Spectroscopic details

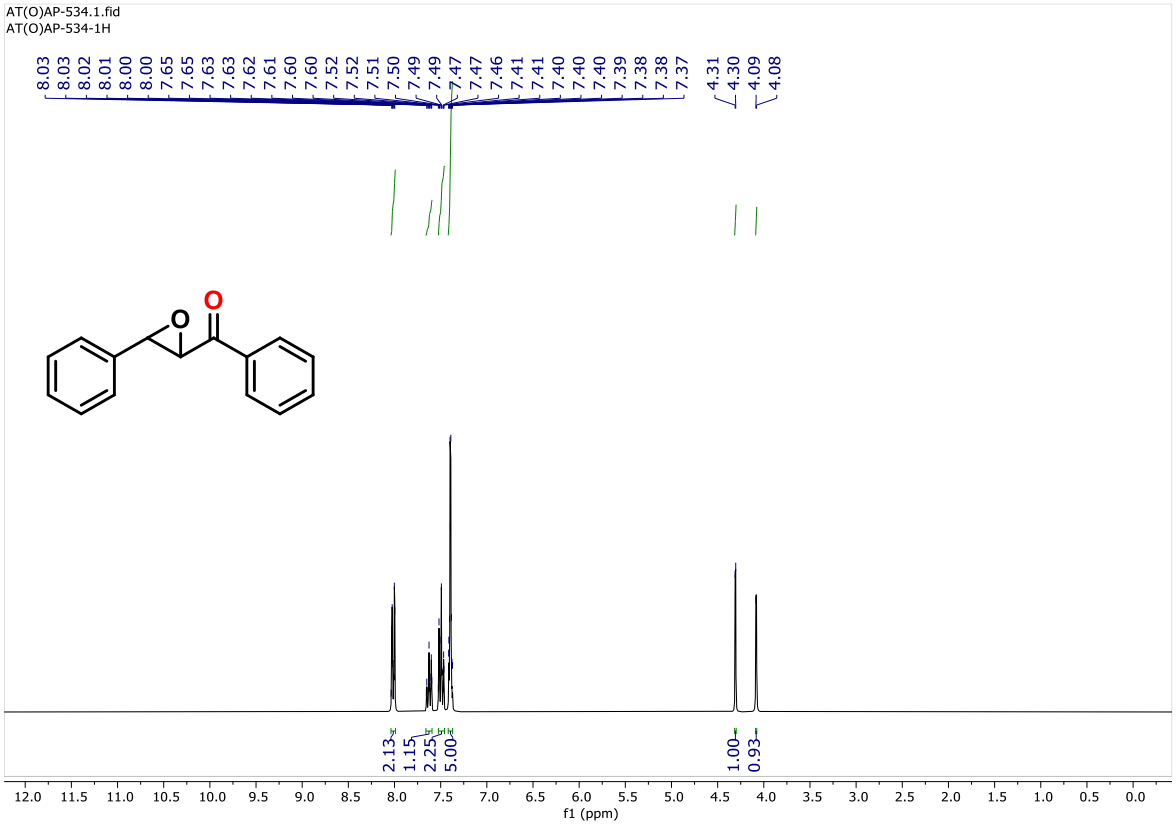

Figure 5.3. ^{1}H NMR (300 MHz) spectrum of **3a** in $CDCl_3$.

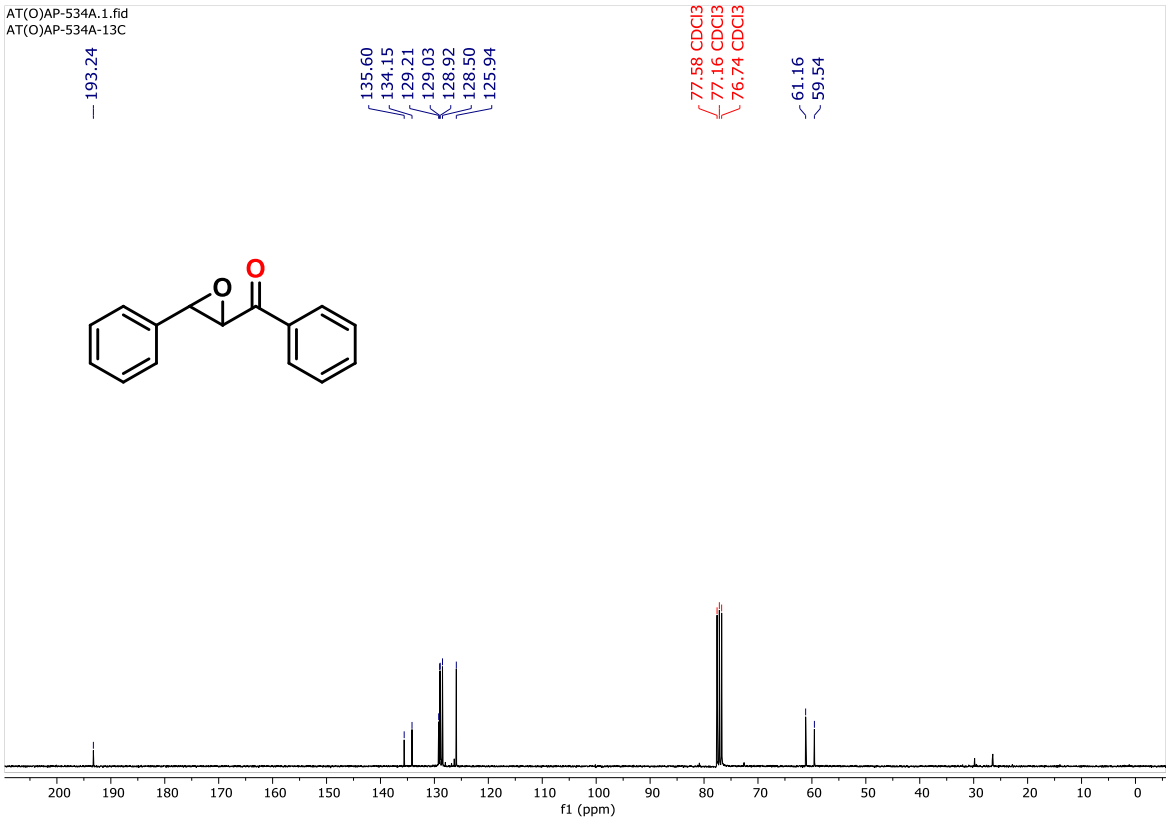

Figure 5.4. $^{13}C\{^{1}H\}$ NMR (75 MHz) spectrum of **3a** in $CDCl_3$.

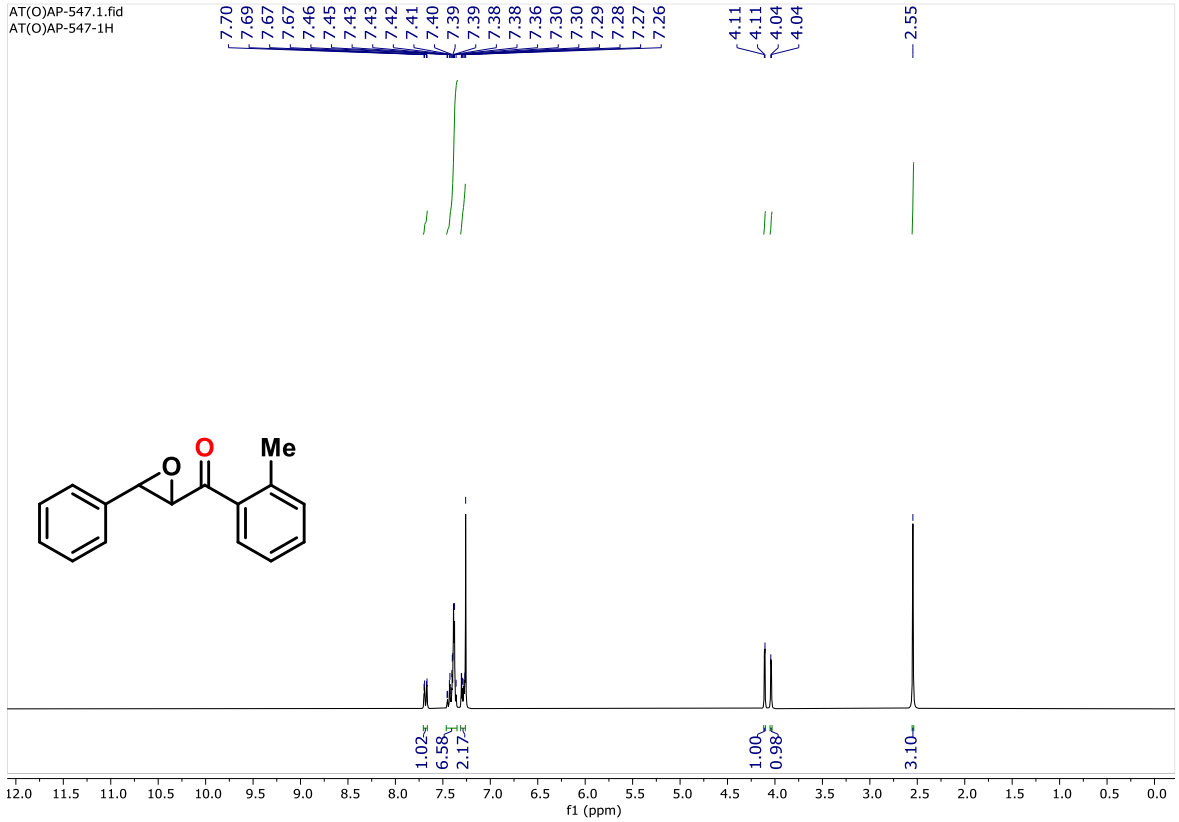

Figure 5.5. ^{1}H NMR (300 MHz) spectrum of **3b** in $CDCl_3$.

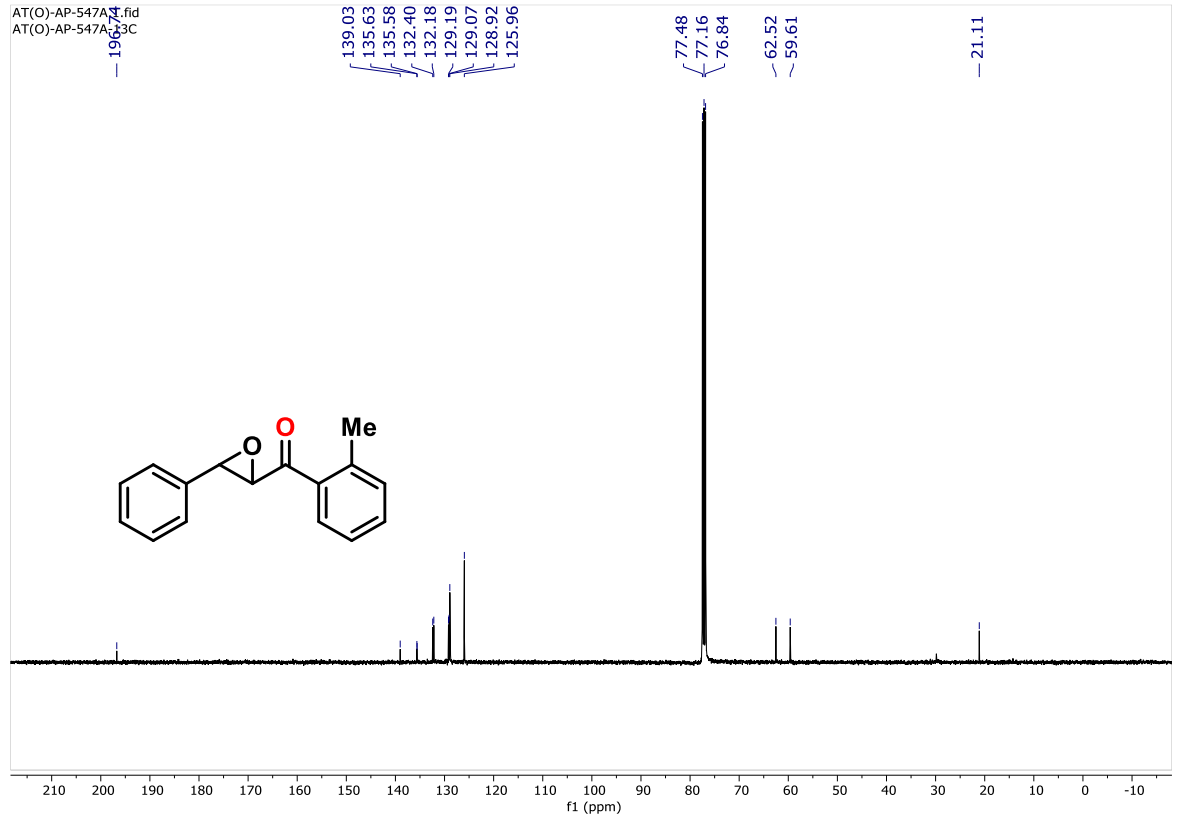

Figure 5.6. $^{13}C\{^{1}H\}$ NMR (75 MHz) spectrum of **3b** in $CDCl_3$.

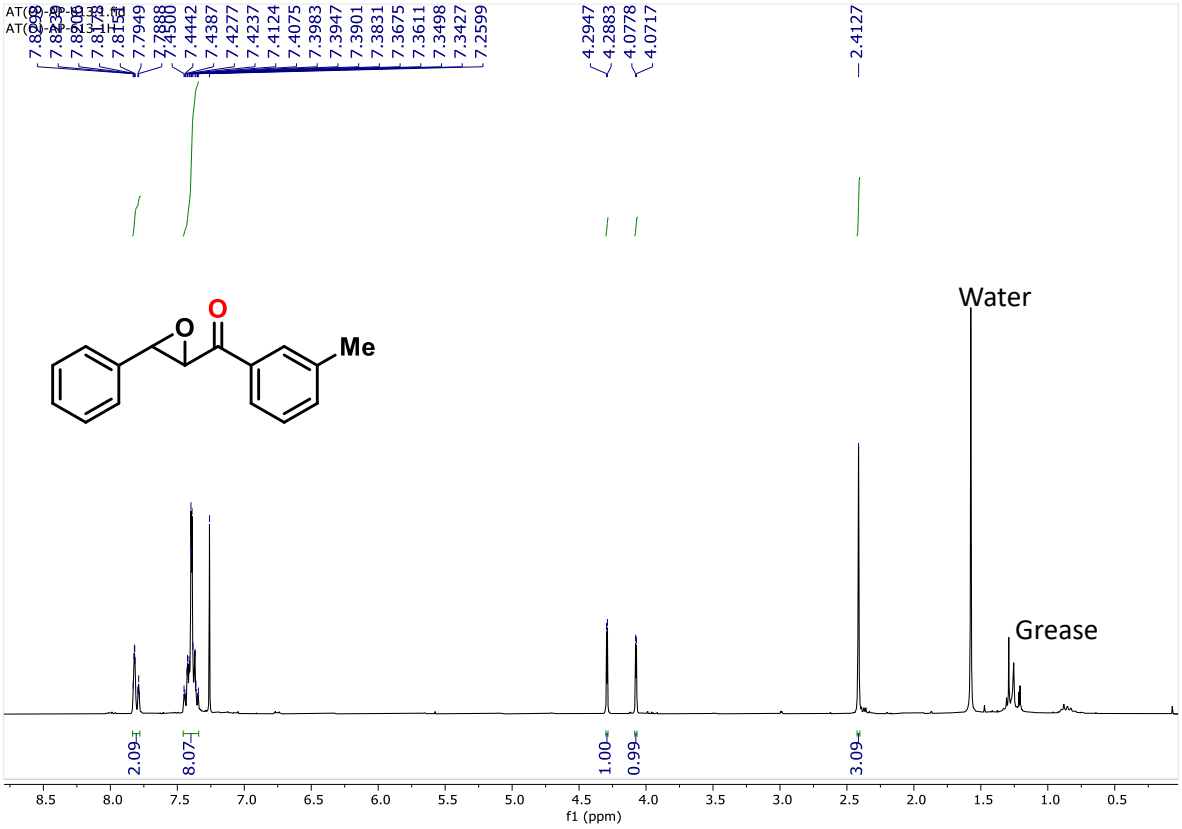

Figure 5.7. ^{1}H NMR (300 MHz) spectrum of **3c** in $CDCl_3$.

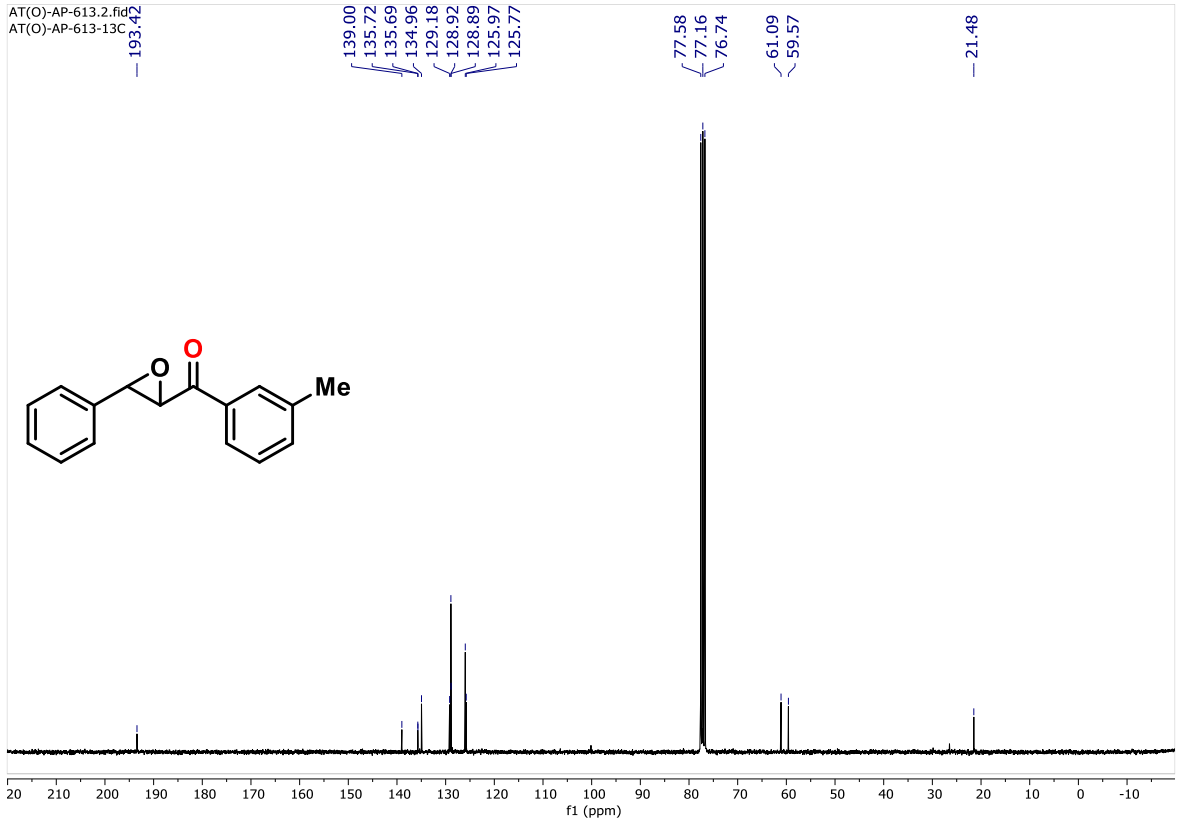

Figure 5.8. $^{13}C\{^{1}H\}$ NMR (75 MHz) spectrum of **3c** in $CDCl_3$.

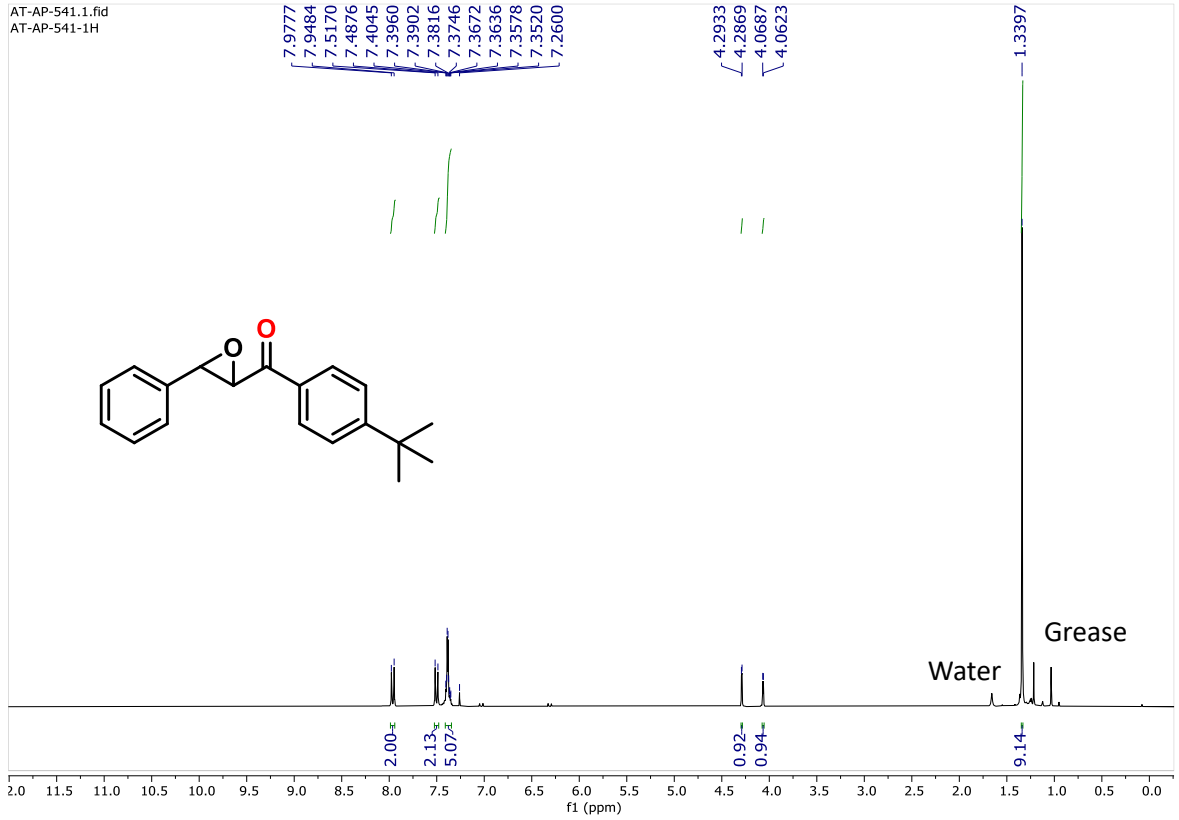

Figure 5.9. ^{1}H NMR (300 MHz) spectrum of **3d** in $CDCl_3$.

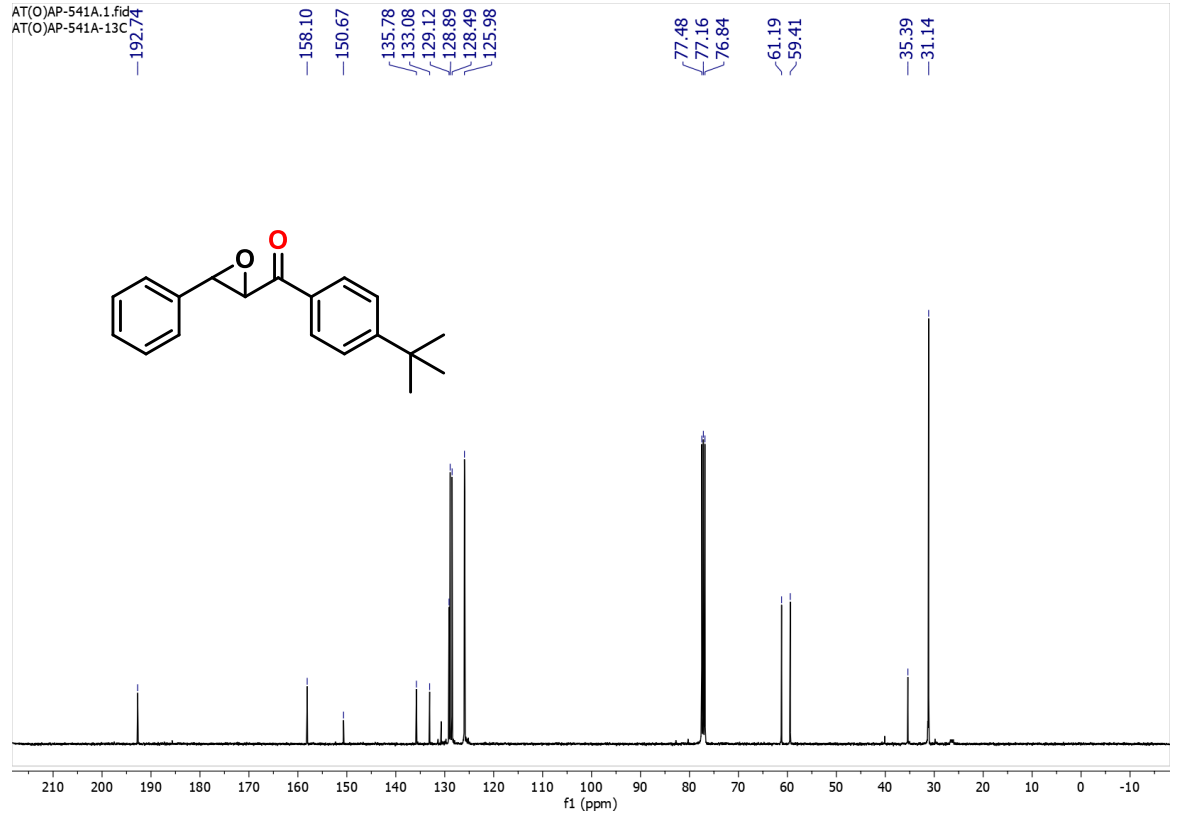

Figure 5.10. $^{13}C\{^{1}H\}$ NMR (75 MHz) spectrum of **3d** in $CDCl_3$.

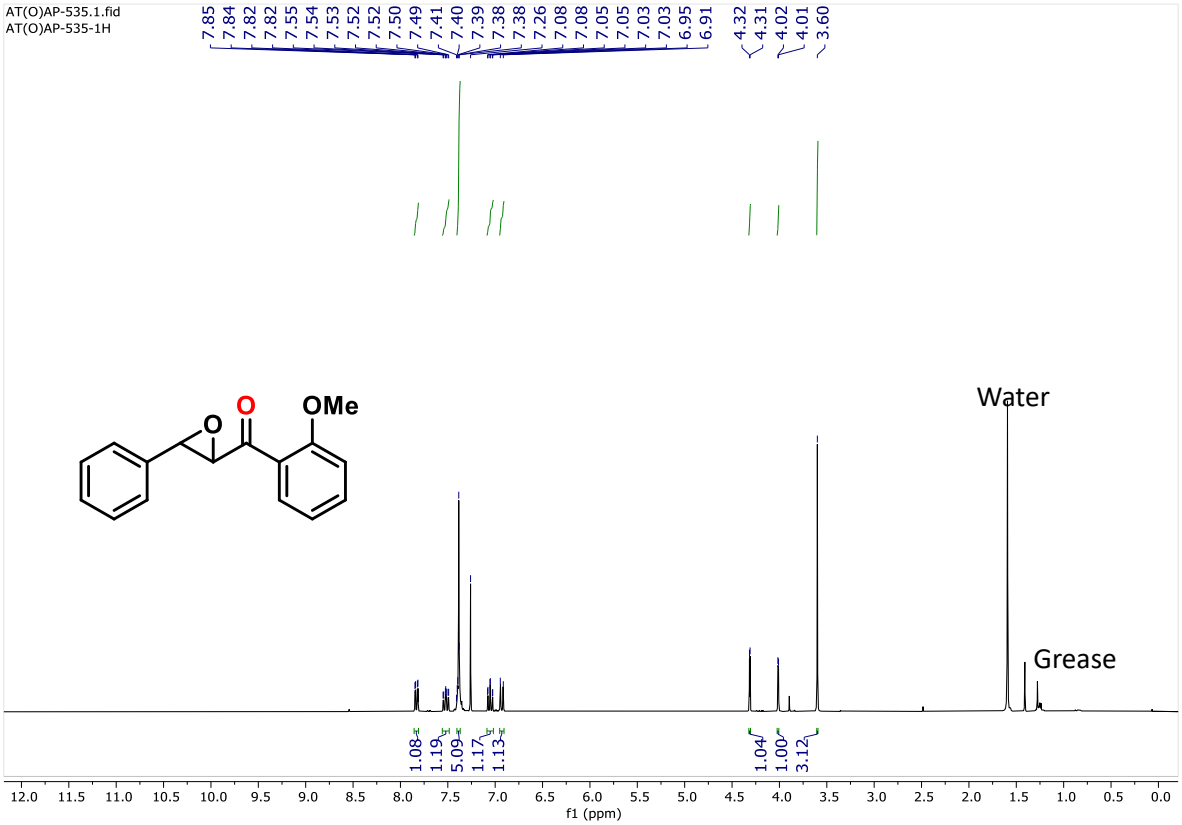

Figure 5.11. ^{1}H NMR (300 MHz) spectrum of **3e** in $CDCl_3$.

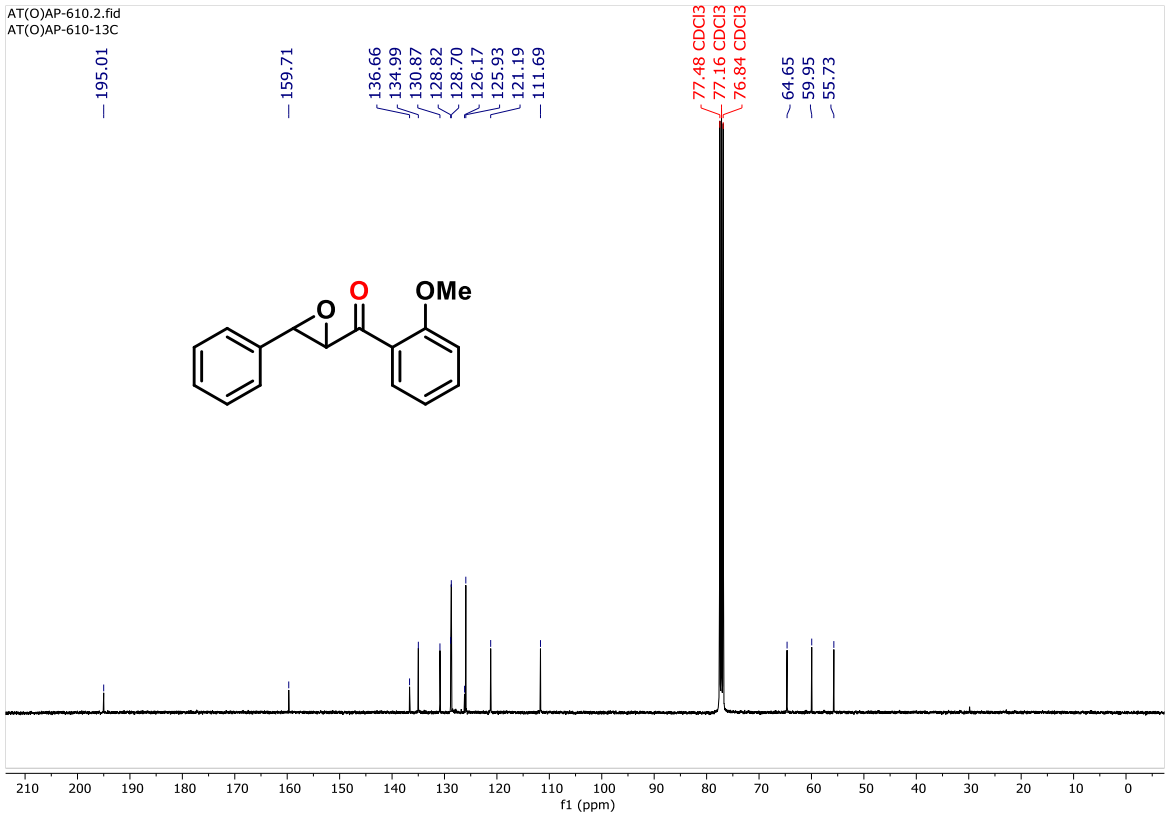

Figure 5.12. $^{13}C\{^{1}H\}$ NMR (75 MHz) spectrum of **3e** in $CDCl_3$.

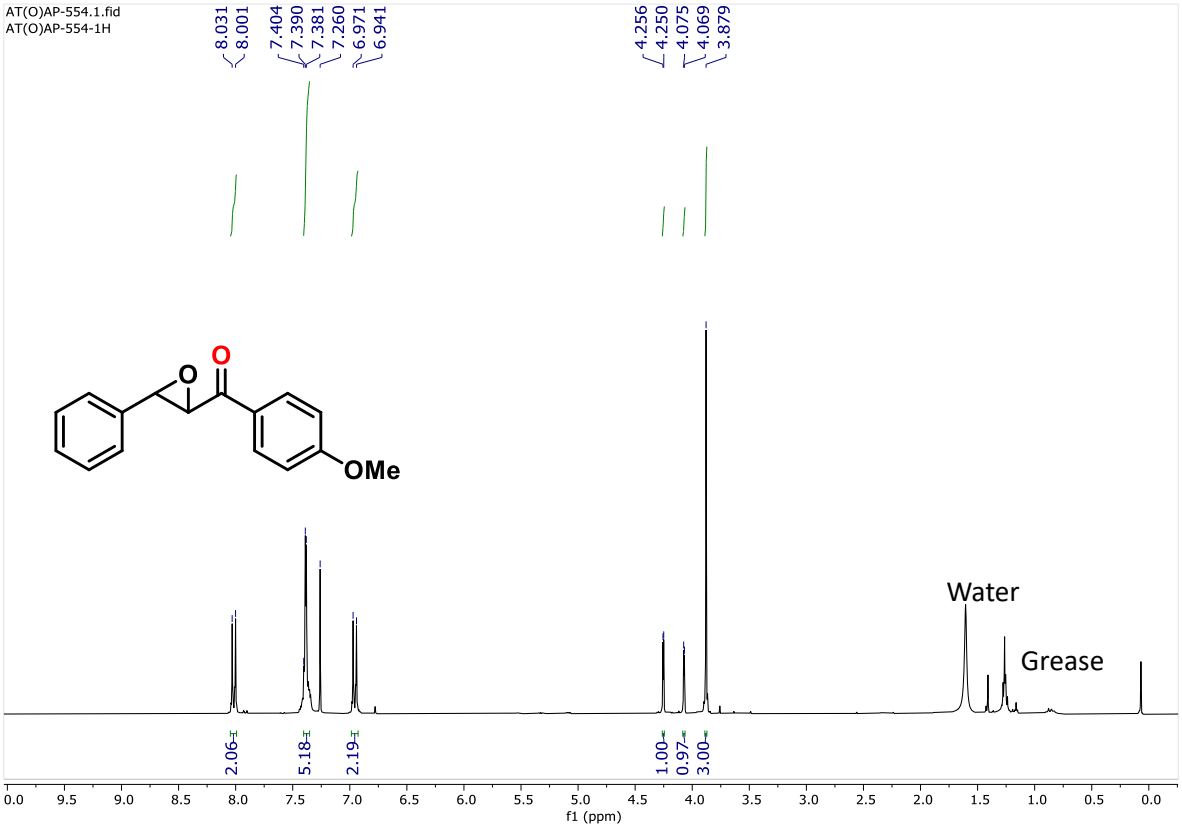

Figure 5.13. ^{1}H NMR (300 MHz) spectrum of **3f** in $CDCl_3$.

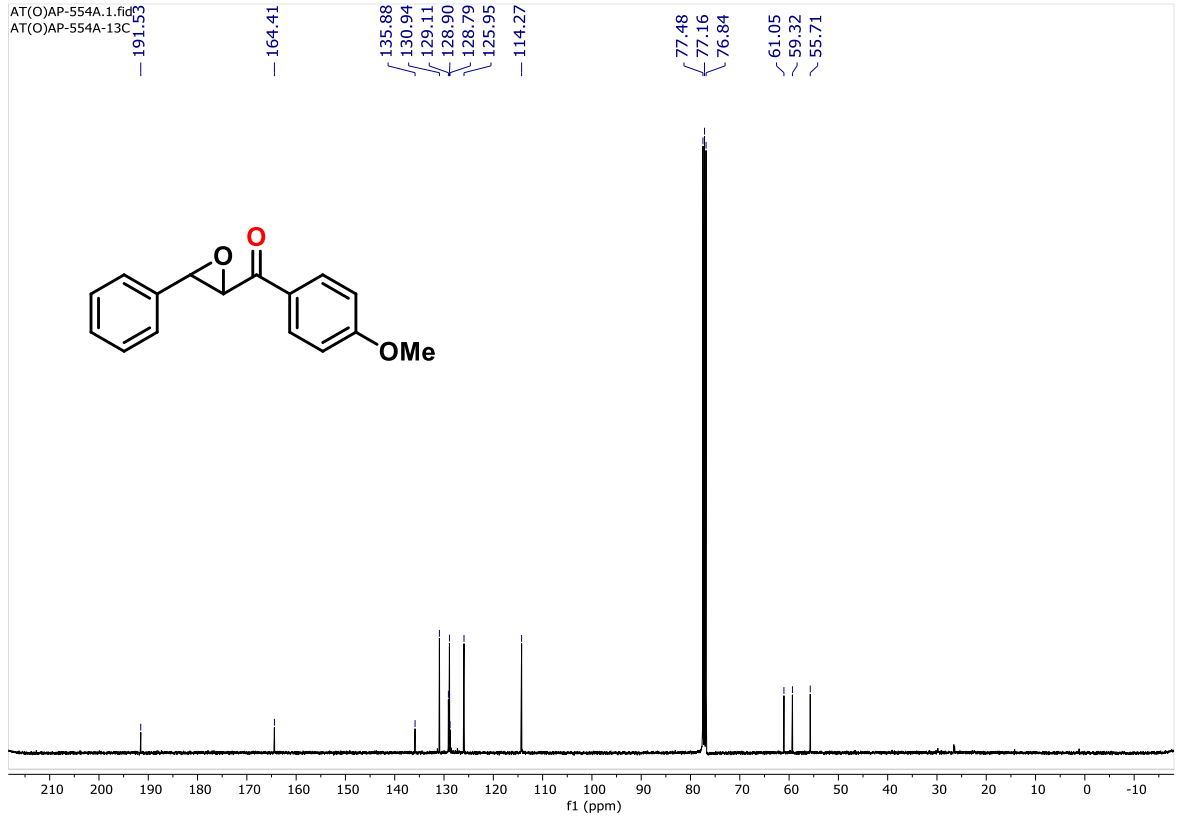

Figure 5.14. $^{13}C\{^{1}H\}$ NMR (75 MHz) spectrum of **3f** in $CDCl_3$.

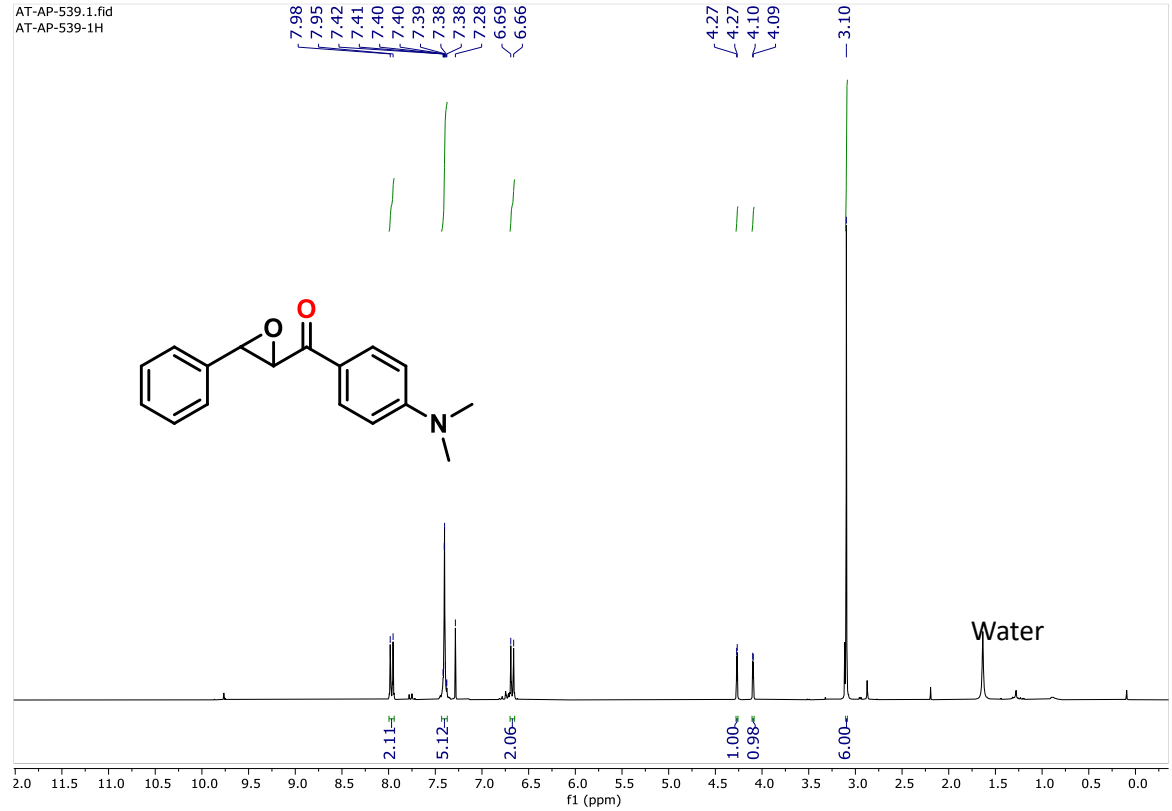

Figure 5.15. ^{1}H NMR (300 MHz) spectrum of **3g** in $CDCl_3$.

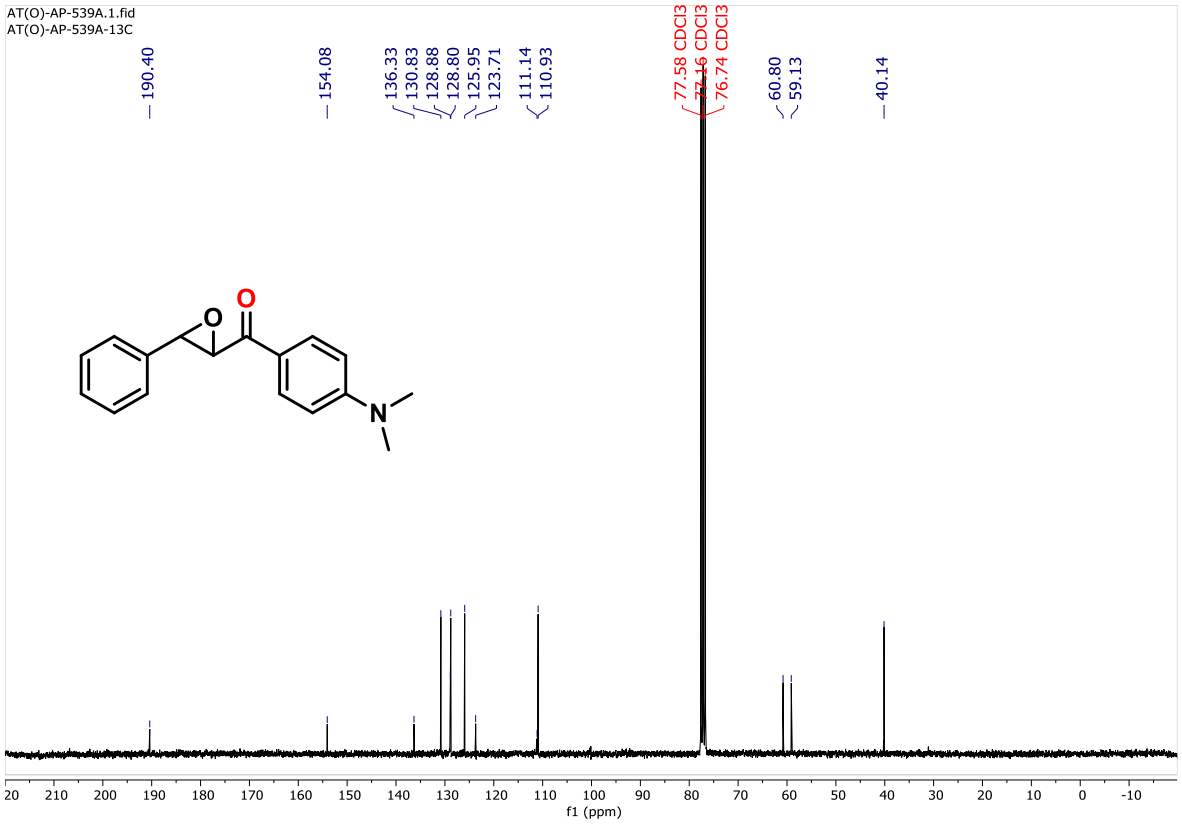

Figure 5.16. $^{13}C\{^{1}H\}$ NMR (75 MHz) spectrum of **3g** in $CDCl_3$.

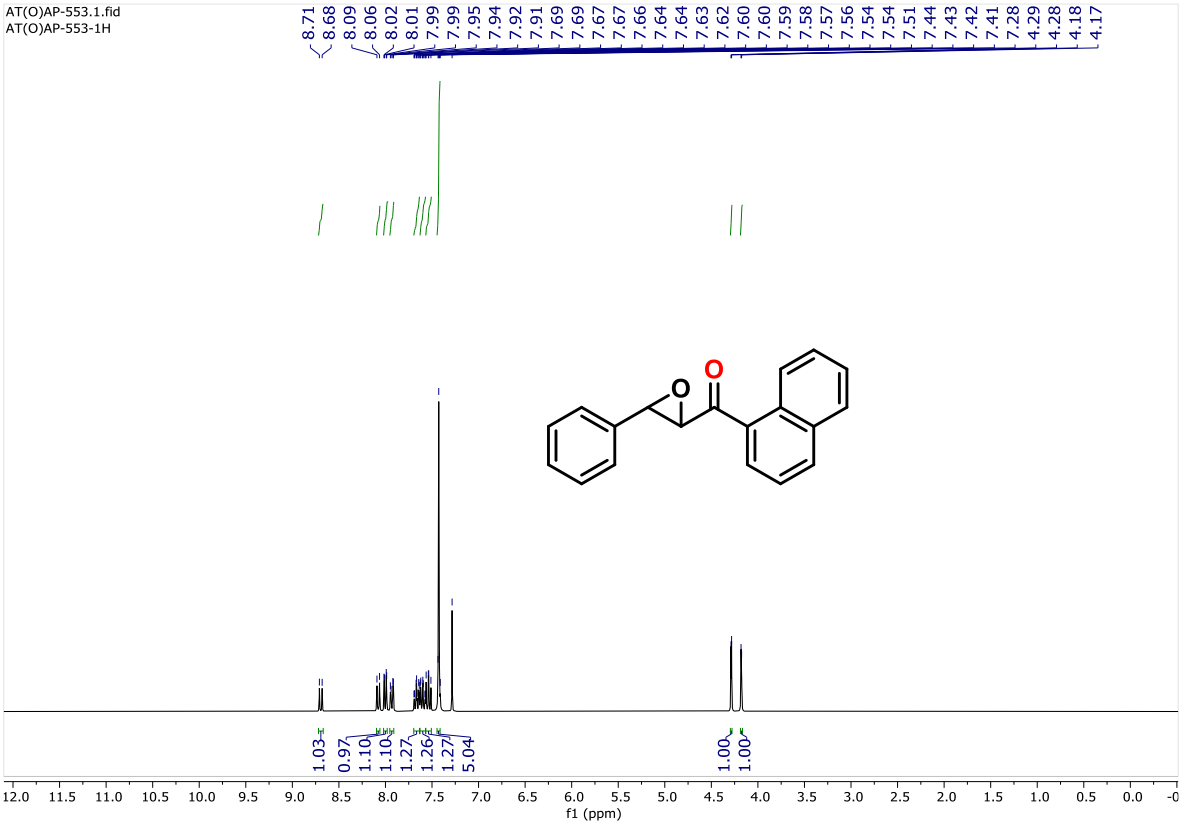

Figure 5.17. ^{1}H NMR (300 MHz) spectrum of **3h** in $CDCl_3$.

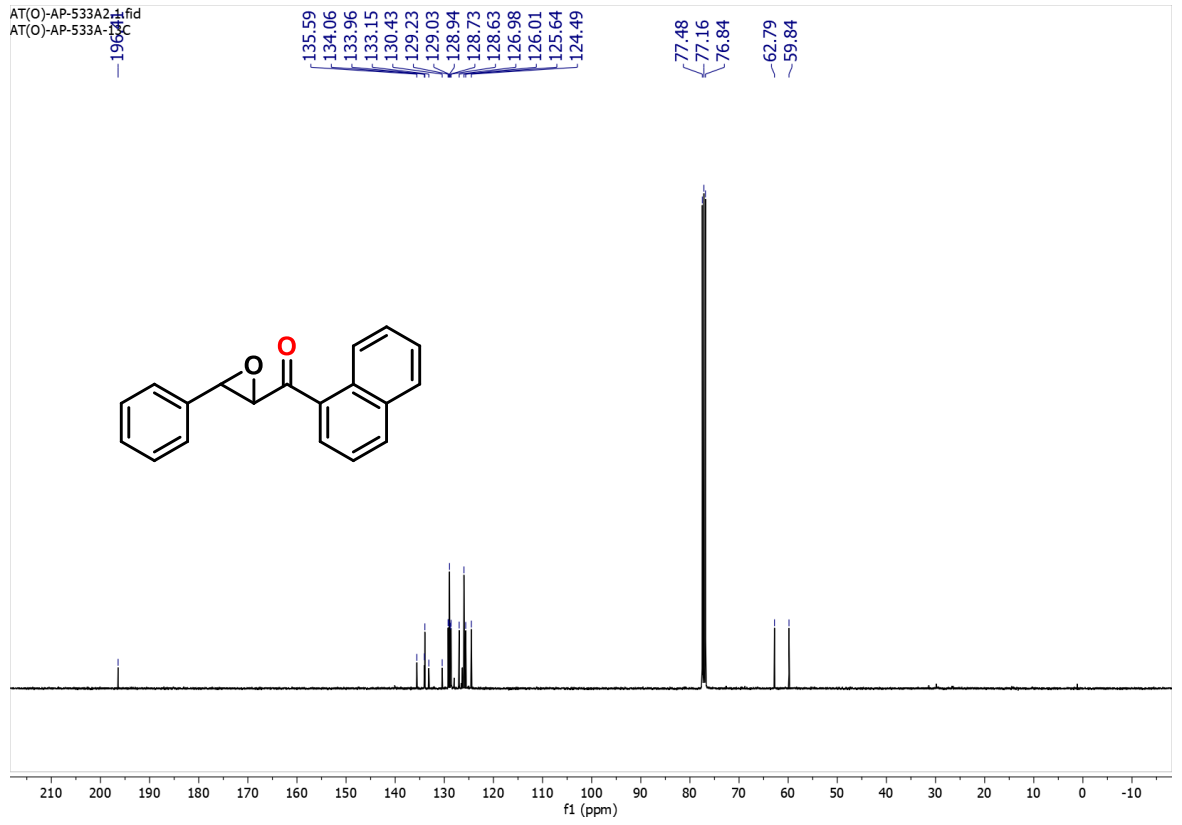

Figure 5.18. ^{13}C{^{1}H} NMR (75 MHz) spectrum of **3h** in $CDCl_3$.

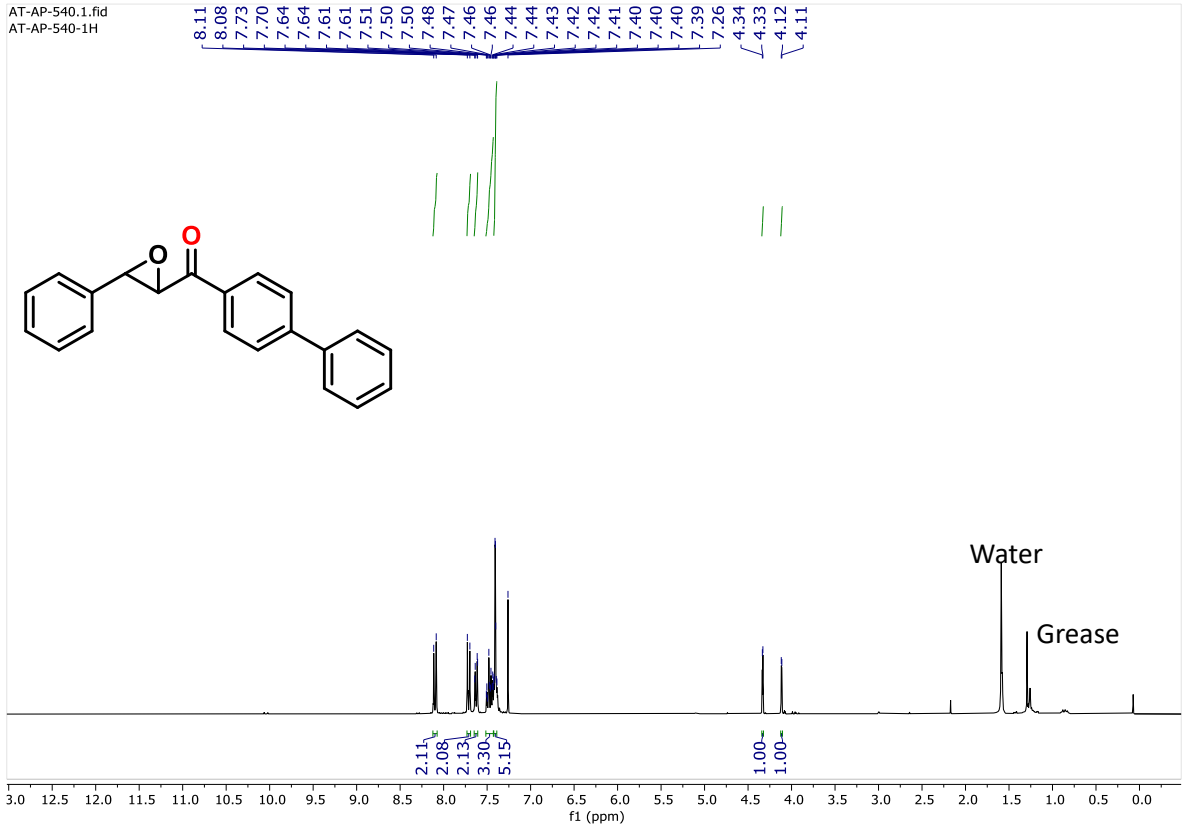

Figure 5.19. ^{1}H NMR (300 MHz) spectrum of **3i** in $CDCl_3$.

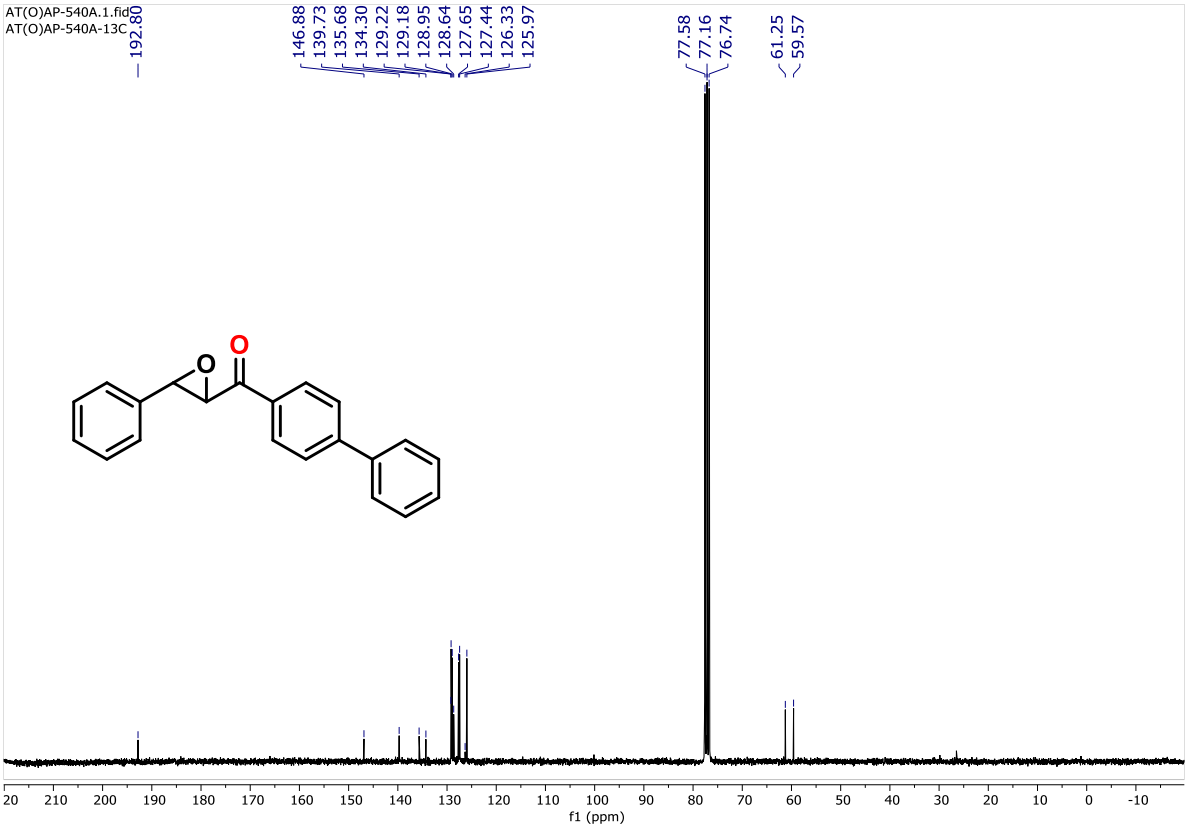

Figure 5.20. $^{13}C\{^{1}H\}$ NMR (75 MHz) spectrum of **3i** in $CDCl_3$.

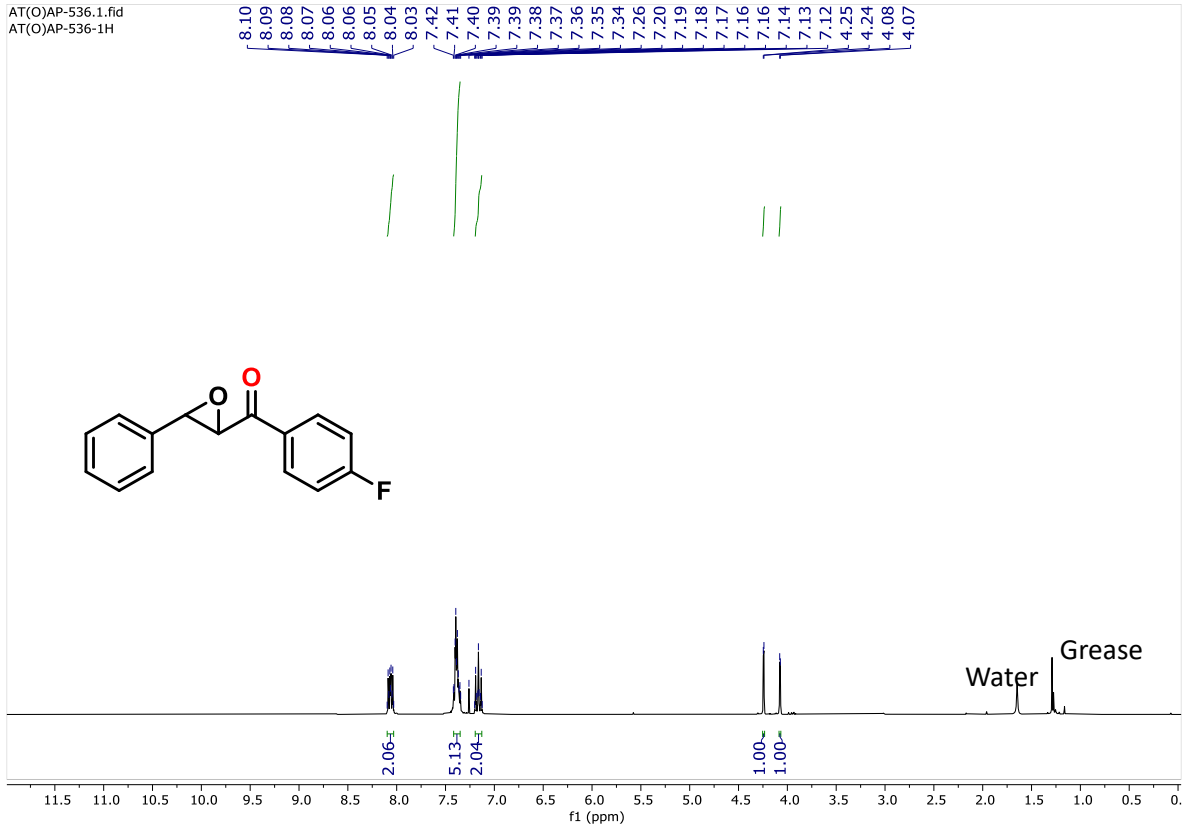

Figure 5.21. ^{1}H NMR (300 MHz) spectrum of **3j** in $CDCl_3$.

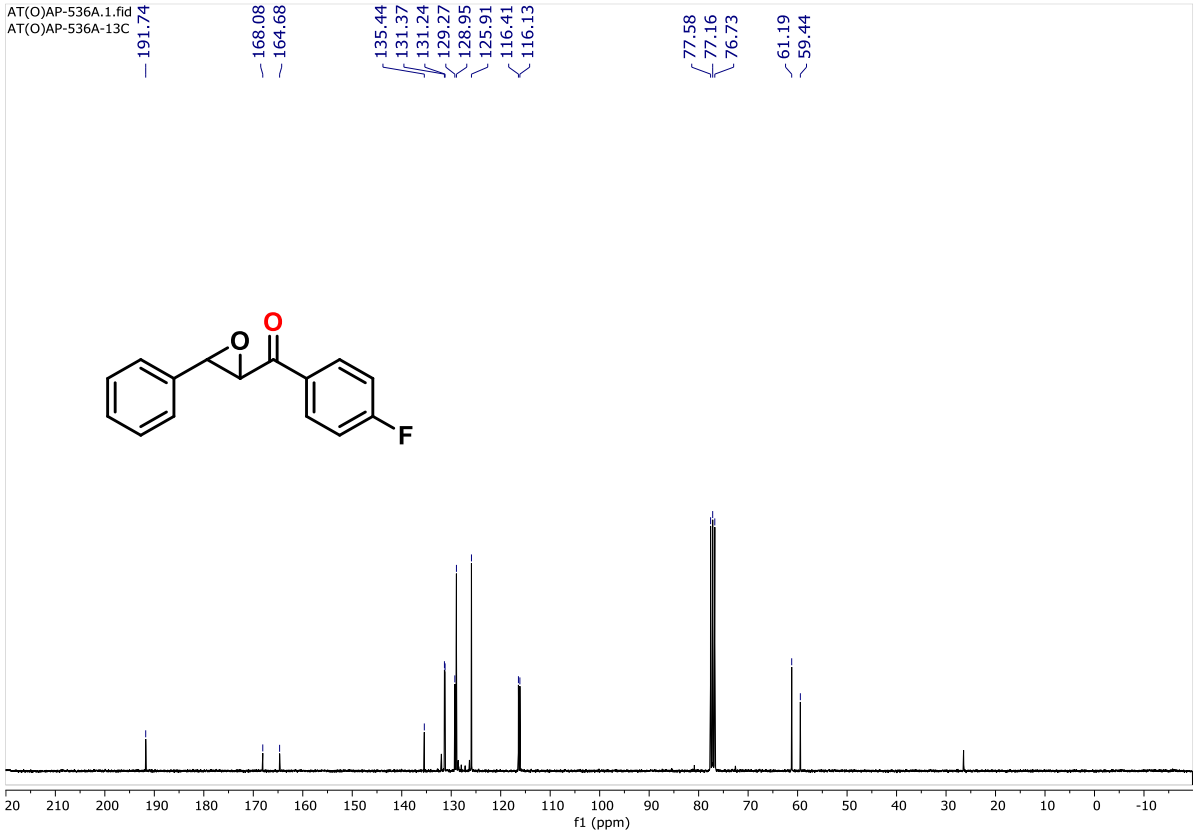

Figure 5.22. $^{13}C\{^{1}H\}$ NMR (75 MHz) spectrum of **3j** in $CDCl_3$.

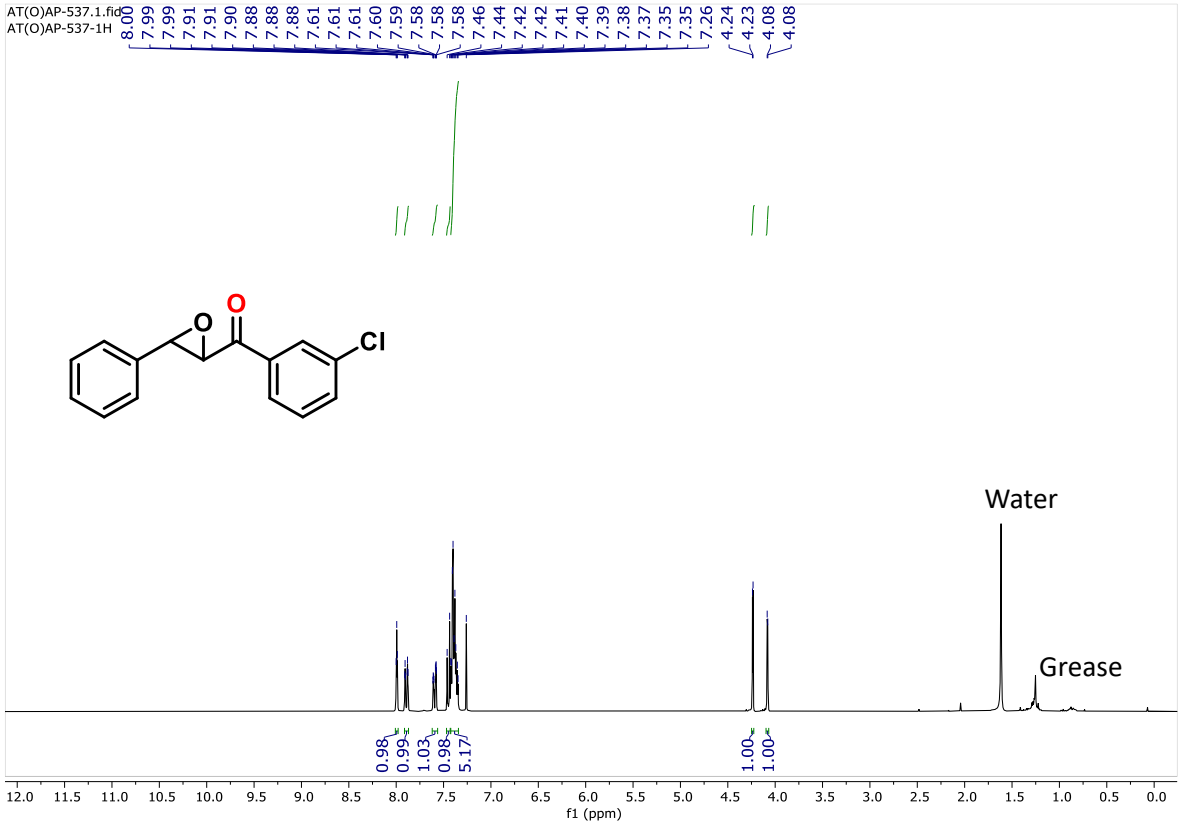

Figure 5.23. ^{1}H NMR (300 MHz) spectrum of **3k** in $CDCl_3$.

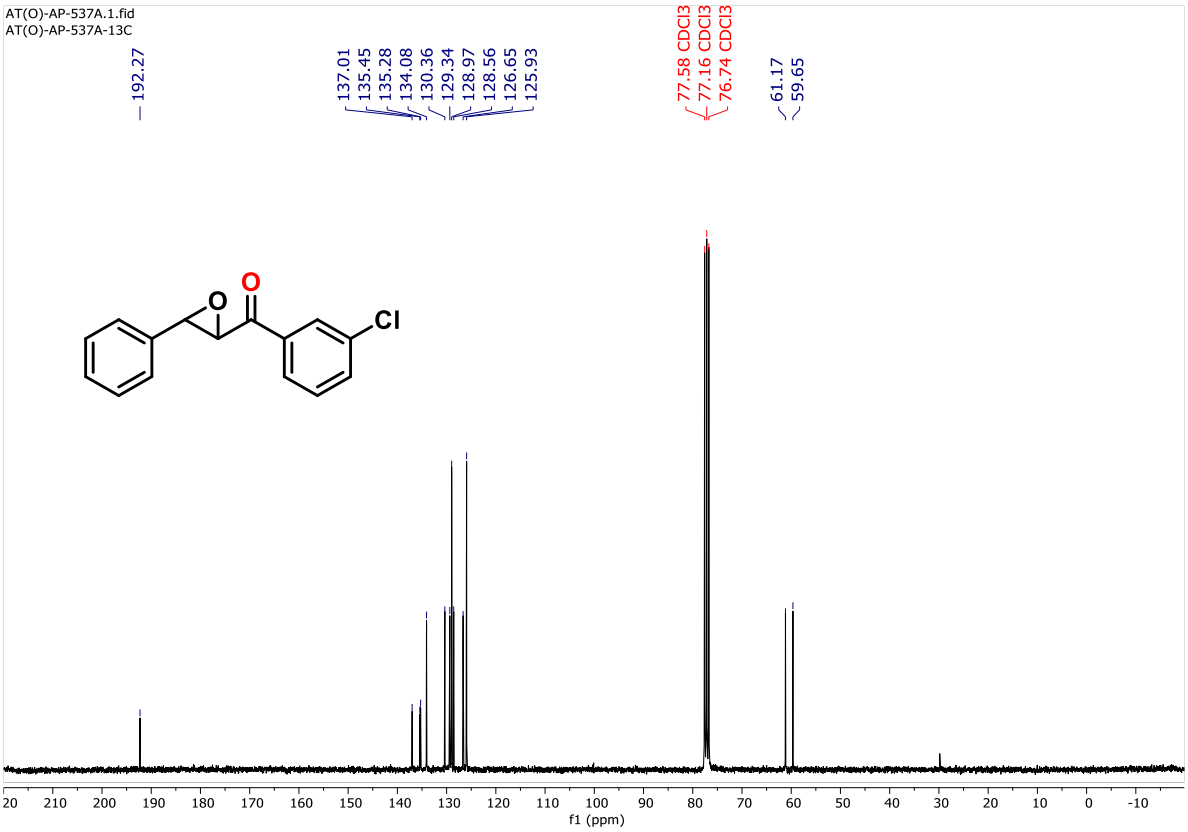

Figure 5.24. $^{13}C\{^{1}H\}$ NMR (75 MHz) spectrum of **3k** in $CDCl_3$.

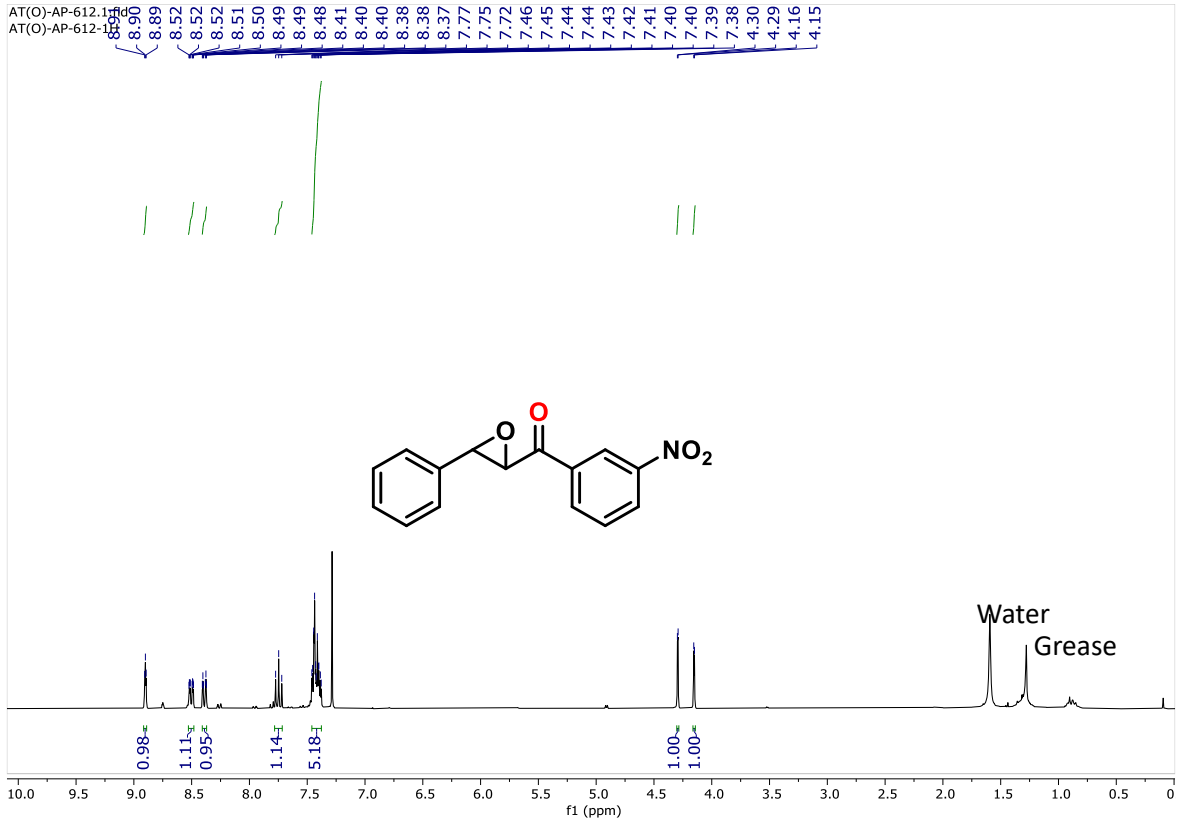

Figure 5.25. ^{1}H NMR (300 MHz) spectrum of **3l** in $CDCl_3$.

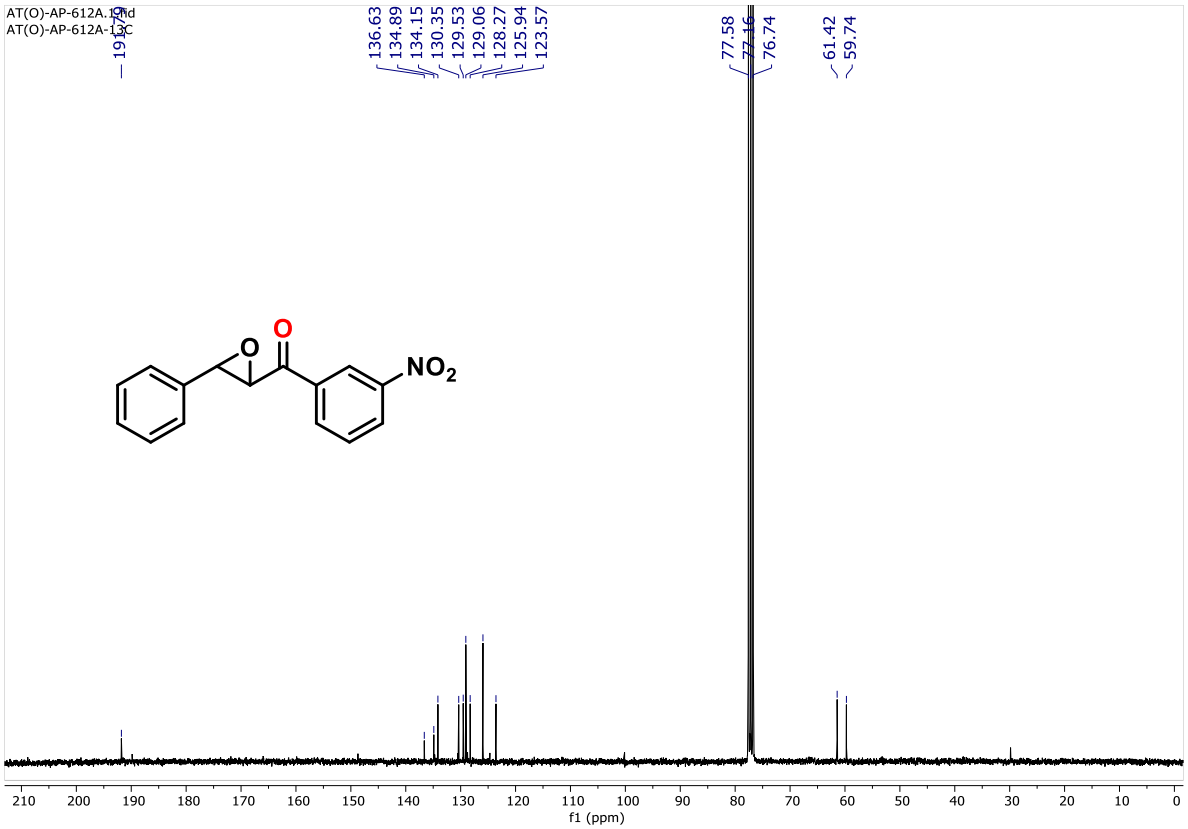

Figure 5.26. $^{13}C\{^{1}H\}$ NMR (75 MHz) spectrum of **3l** in $CDCl_3$.

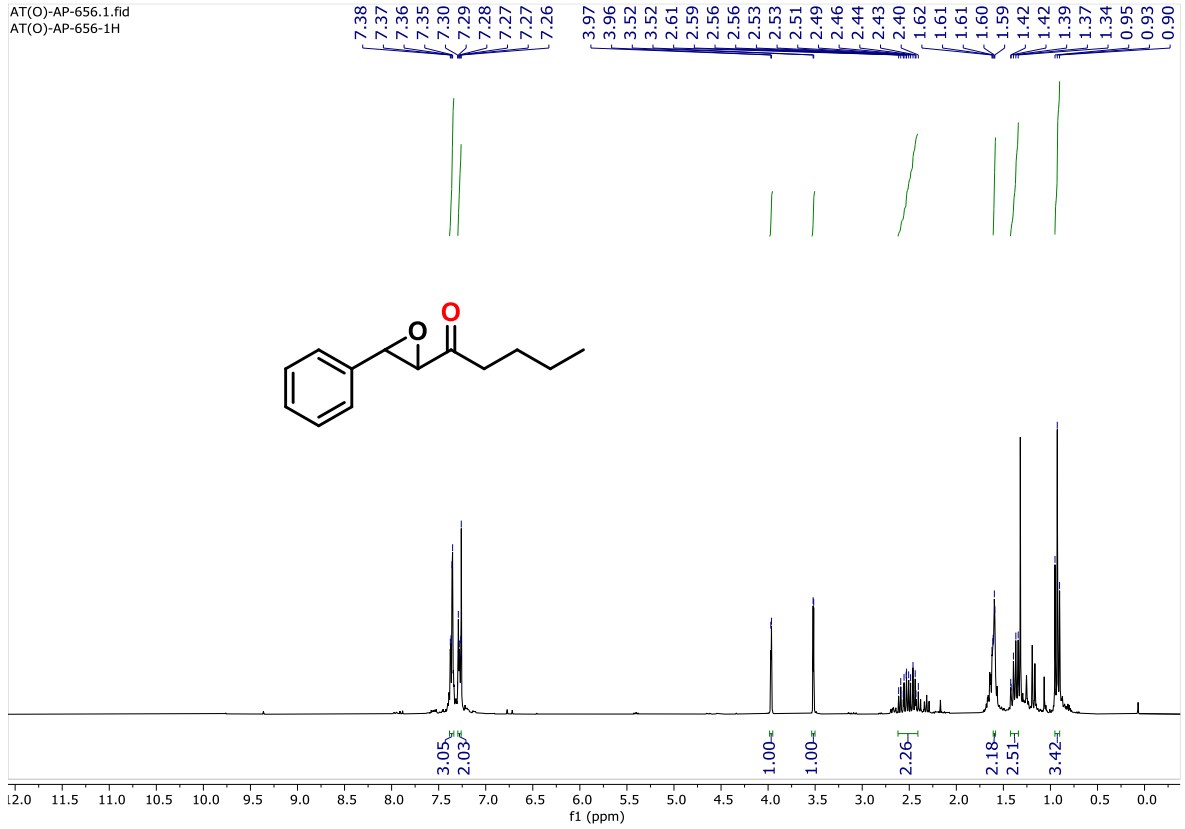

Figure 5.27. ^{1}H NMR (300 MHz) spectrum of **3m** in $CDCl_3$.

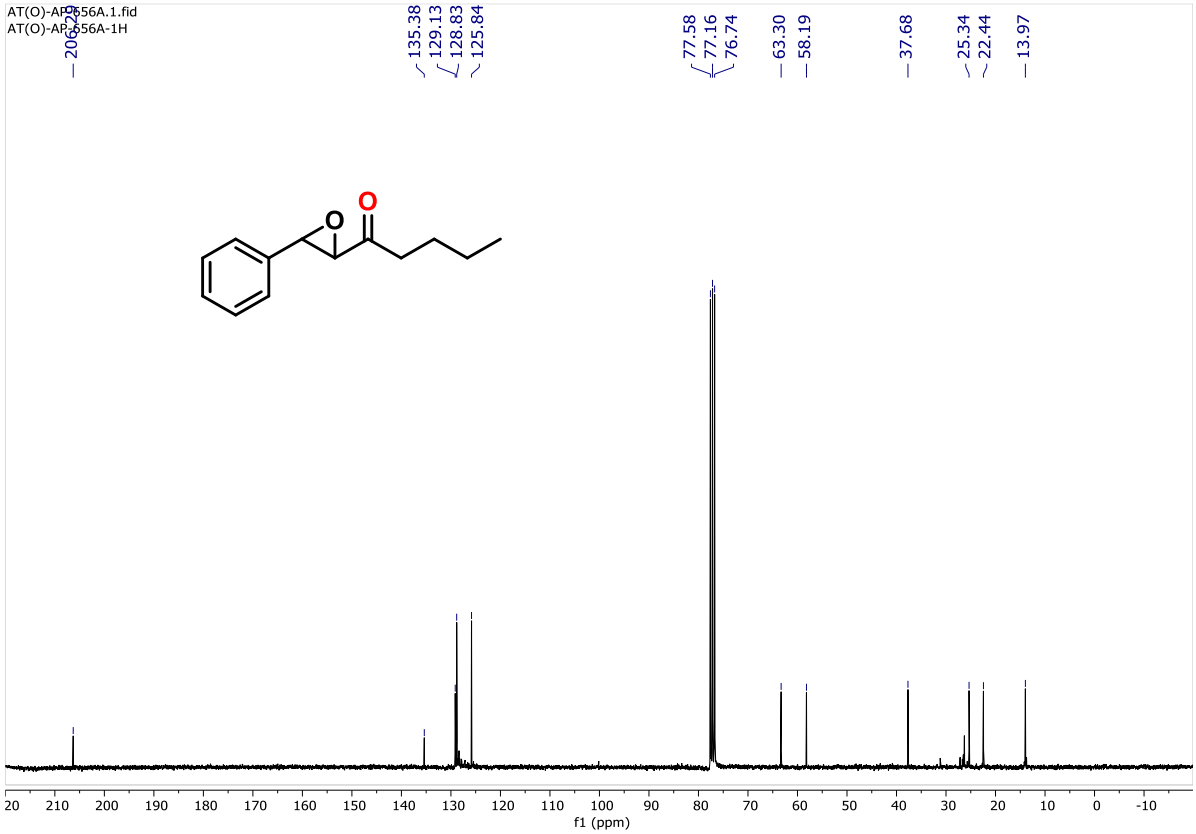

Figure 5.28. $^{13}C\{^{1}H\}$ NMR (75 MHz) spectrum of **3m** in $CDCl_3$.

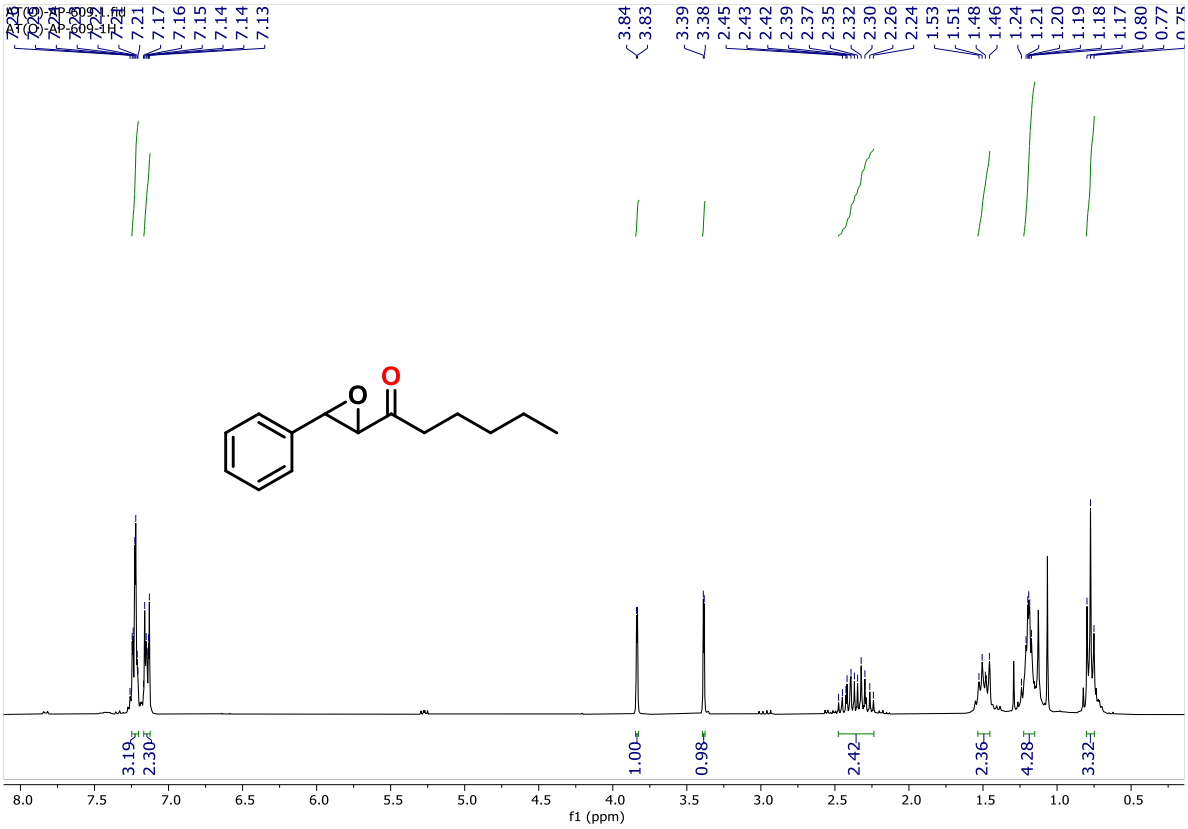

Figure 5.29. ^{1}H NMR (300 MHz) spectrum of **3n** in $CDCl_3$.

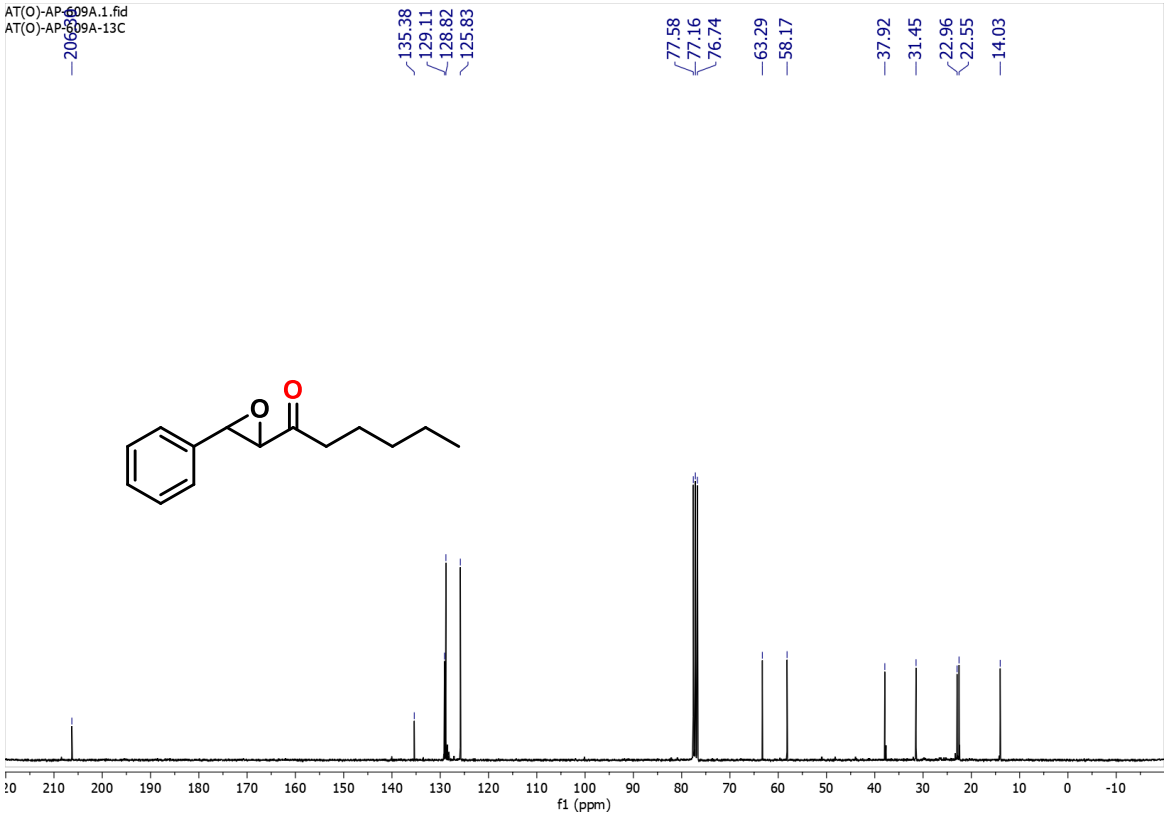

Figure 5.30. $^{13}C\{^{1}H\}$ NMR (75 MHz) spectrum of **3n** in $CDCl_3$.

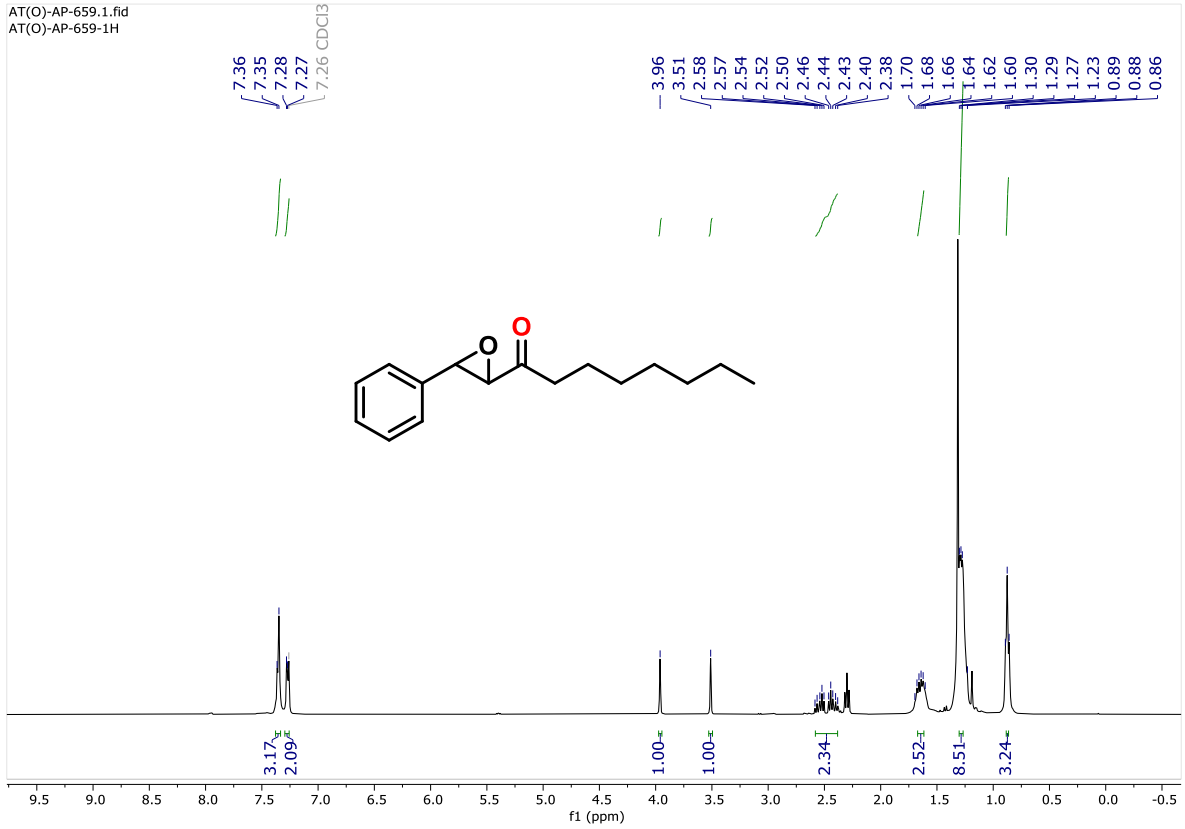

Figure 5.31. ^{1}H NMR (300 MHz) spectrum of **3o** in $CDCl_3$.

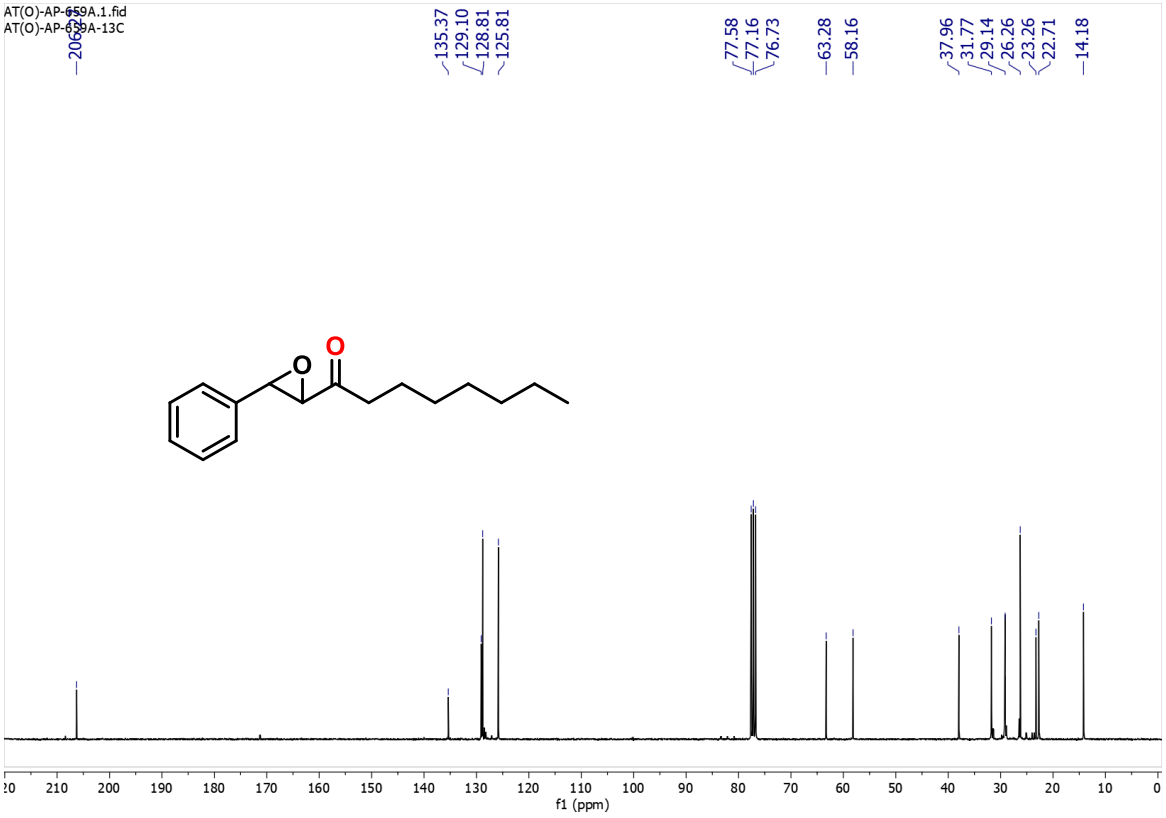

Figure 5.32. $^{13}C\{^{1}H\}$ NMR (75 MHz) spectrum of **3o** in $CDCl_3$.

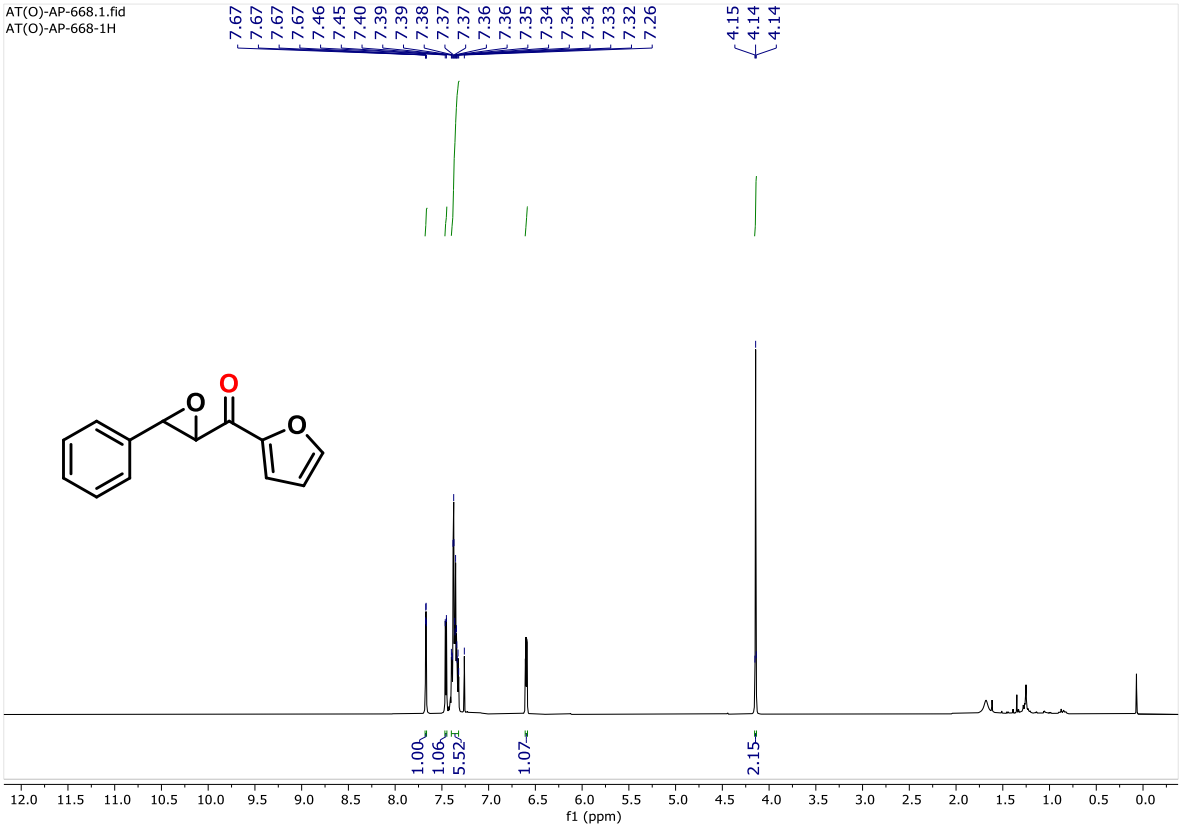

Figure 5.33. ^{1}H NMR (300 MHz) spectrum of **3p** in $CDCl_3$.

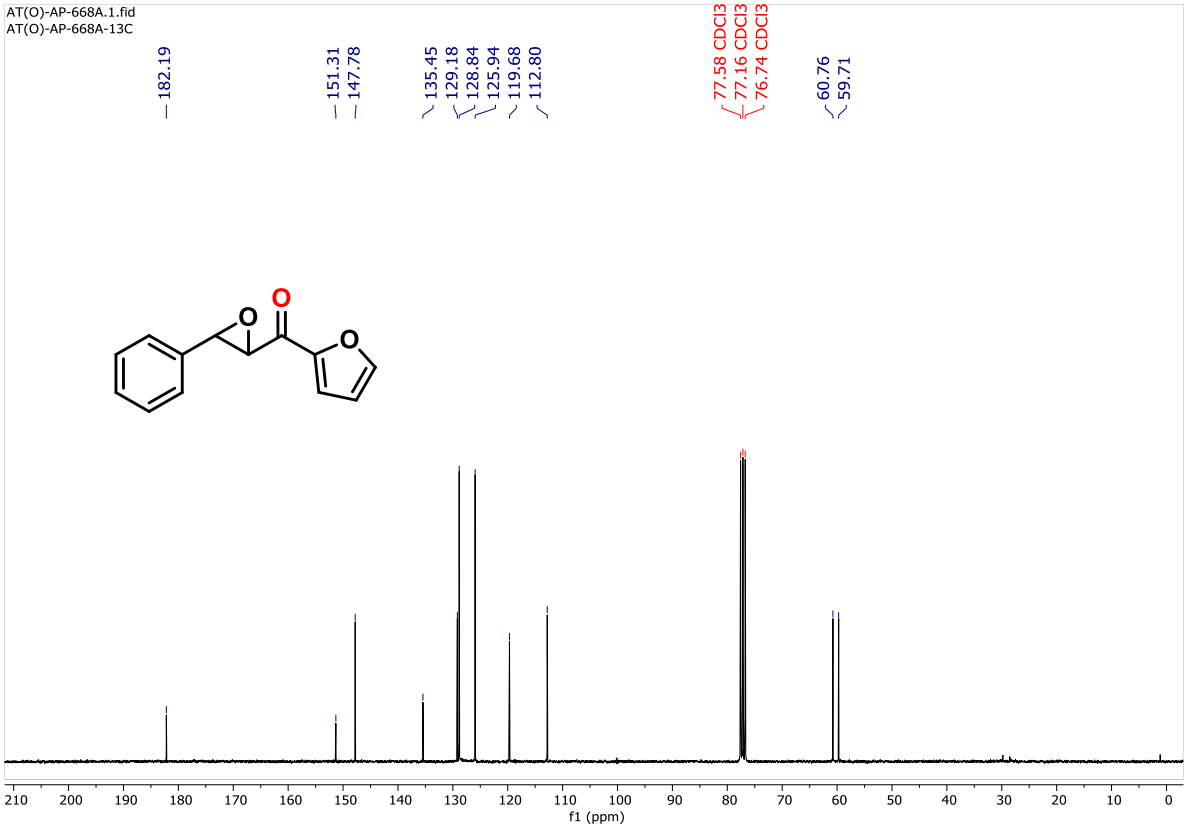

Figure 5.34. $^{13}C\{^{1}H\}$ NMR (75 MHz) spectrum of **3p** in $CDCl_3$.

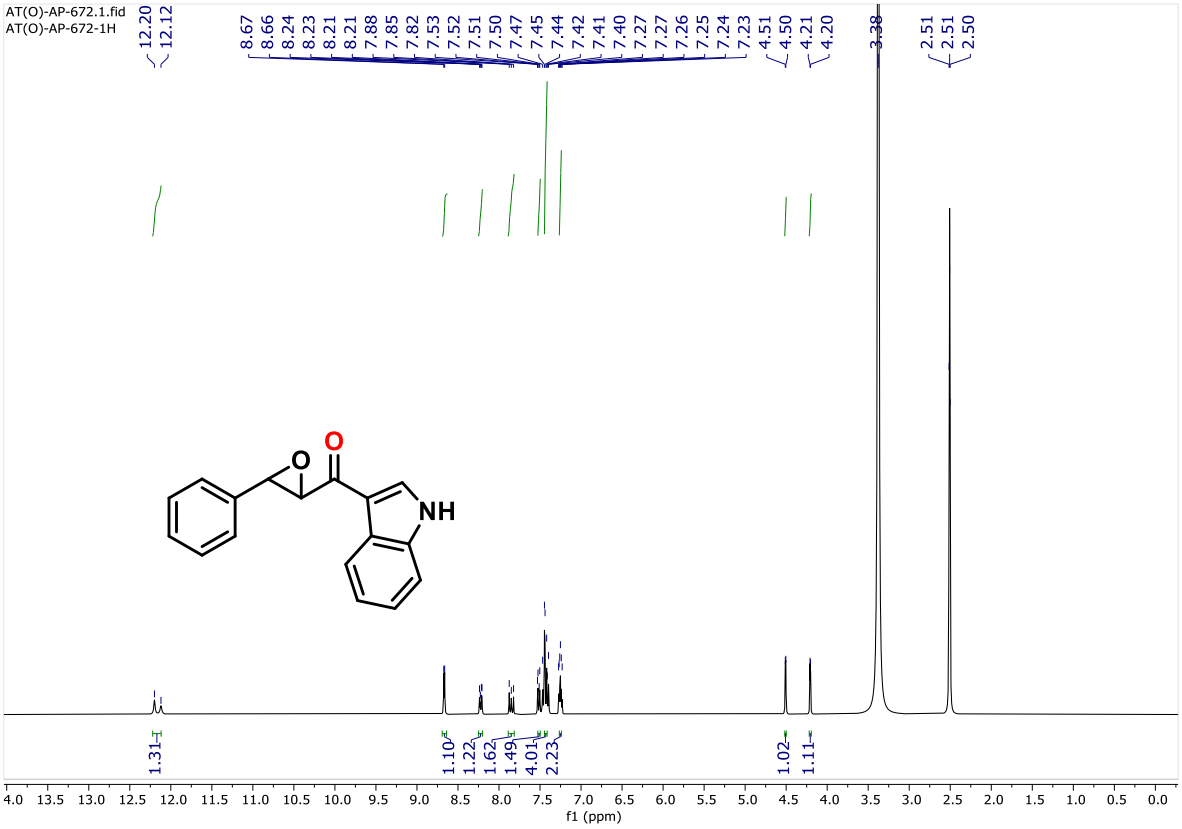

Figure 5.35. ^{1}H NMR (300 MHz) spectrum of **3q** in DMSO-d_6.

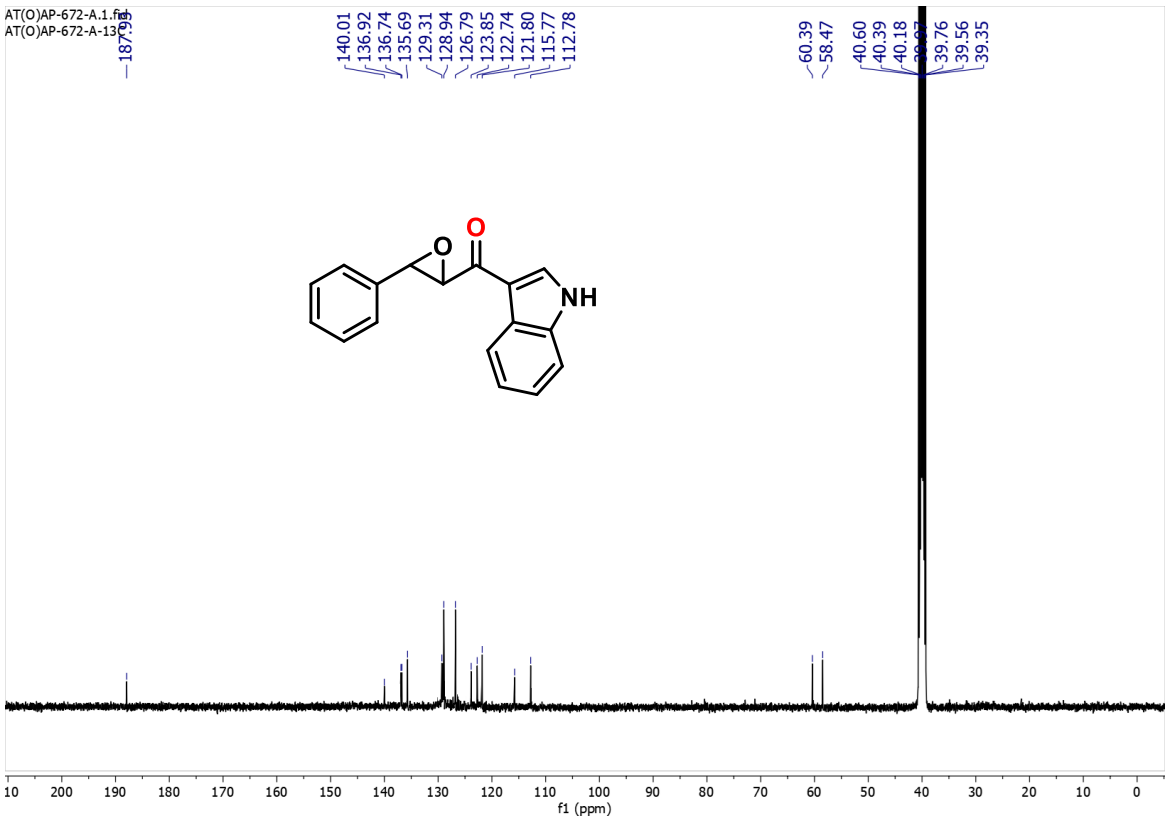

Figure 5.36. $^{13}C\{^{1}H\}$ NMR (75 MHz) spectrum of **3q** in DMSO-d_6.

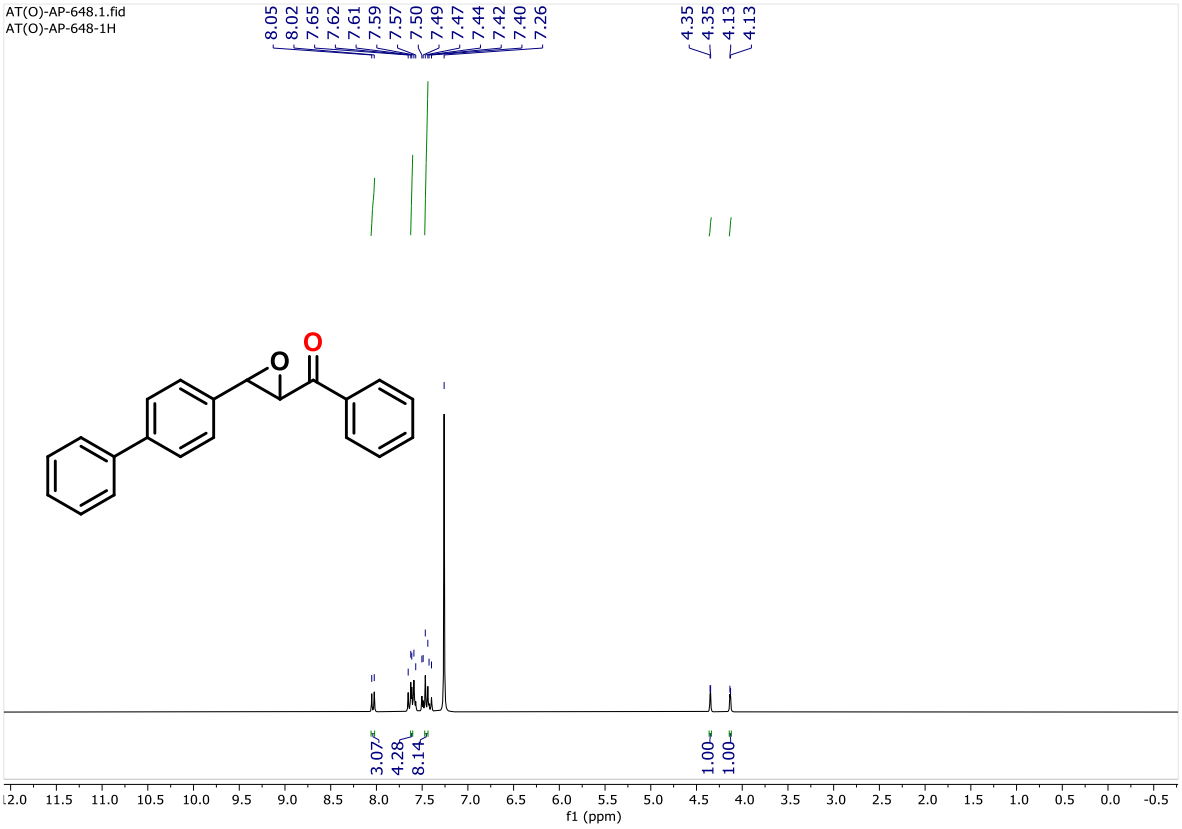

Figure 5.37. ^{1}H NMR (300 MHz) spectrum of **4a** in $CDCl_3$.

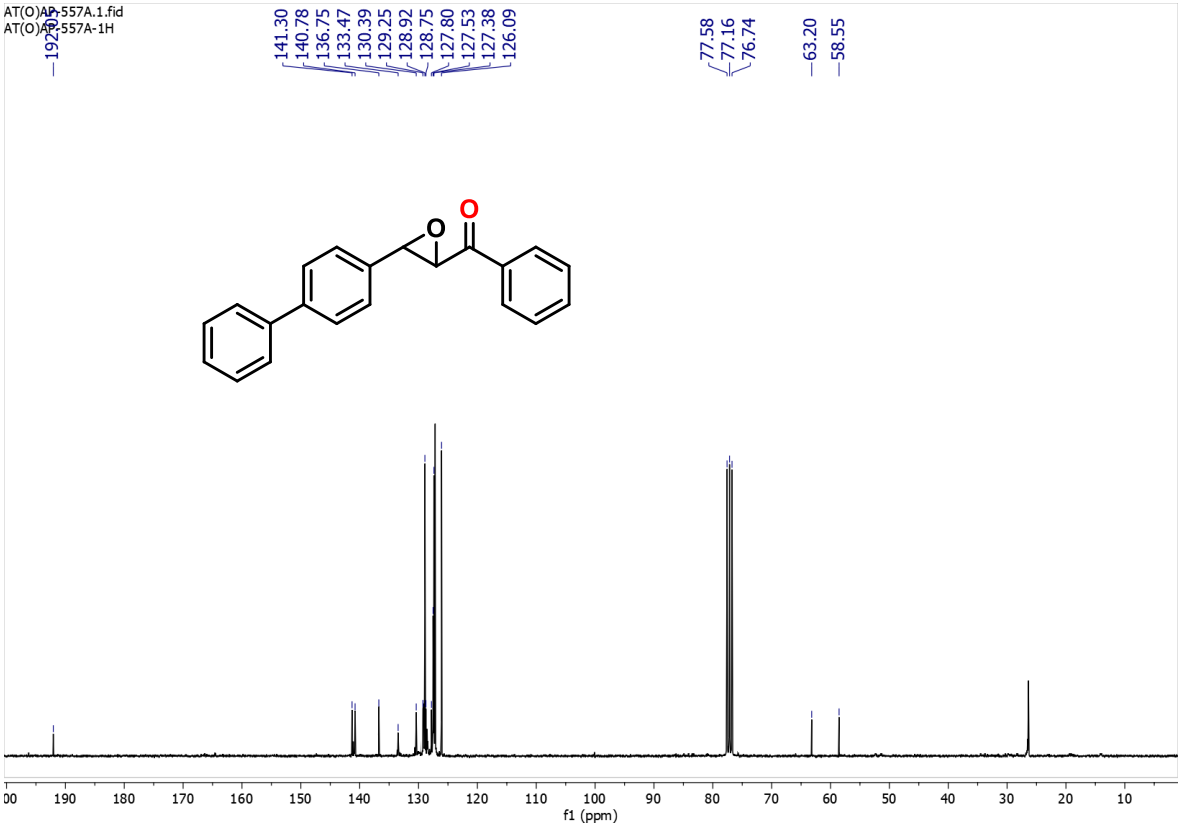

Figure 5.38. ^{13}C{^{1}H} NMR (75 MHz) spectrum of **4a** in $CDCl_3$.

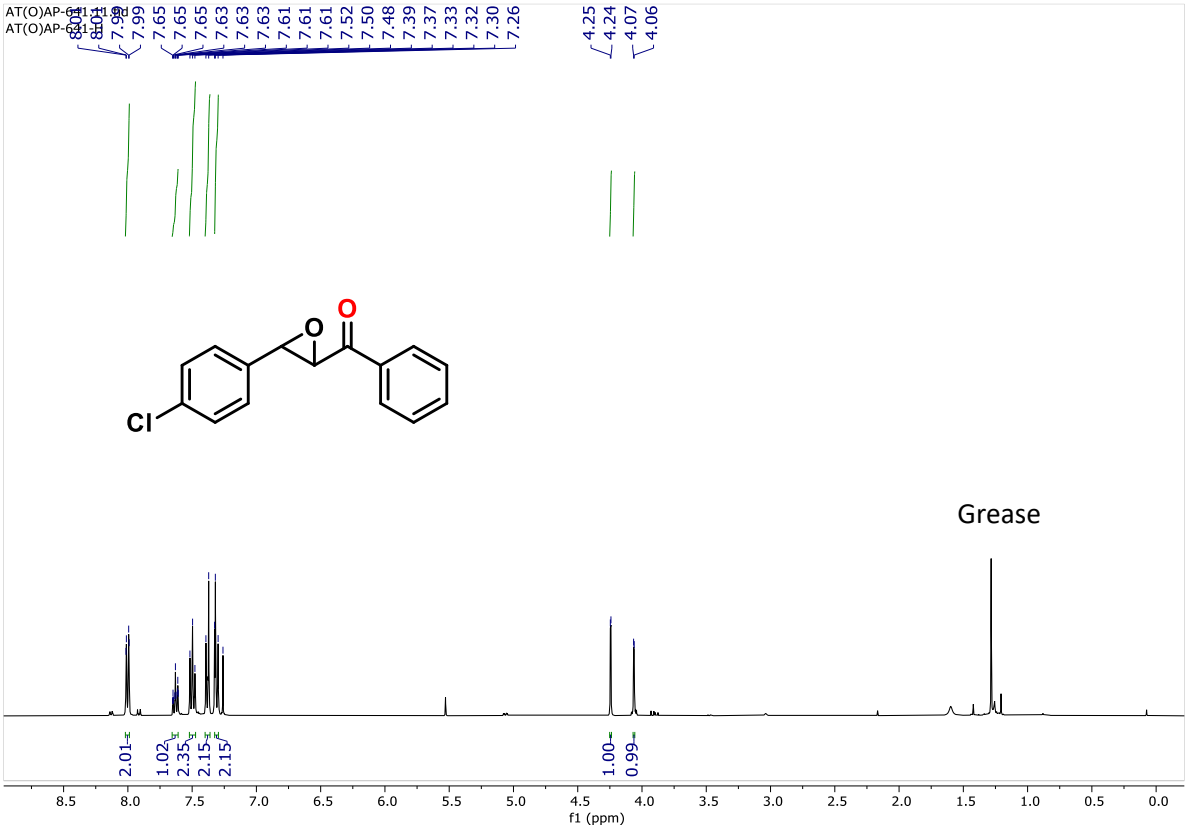

Figure 5.39. ^{1}H NMR (300 MHz) spectrum of **4b** in $CDCl_3$.

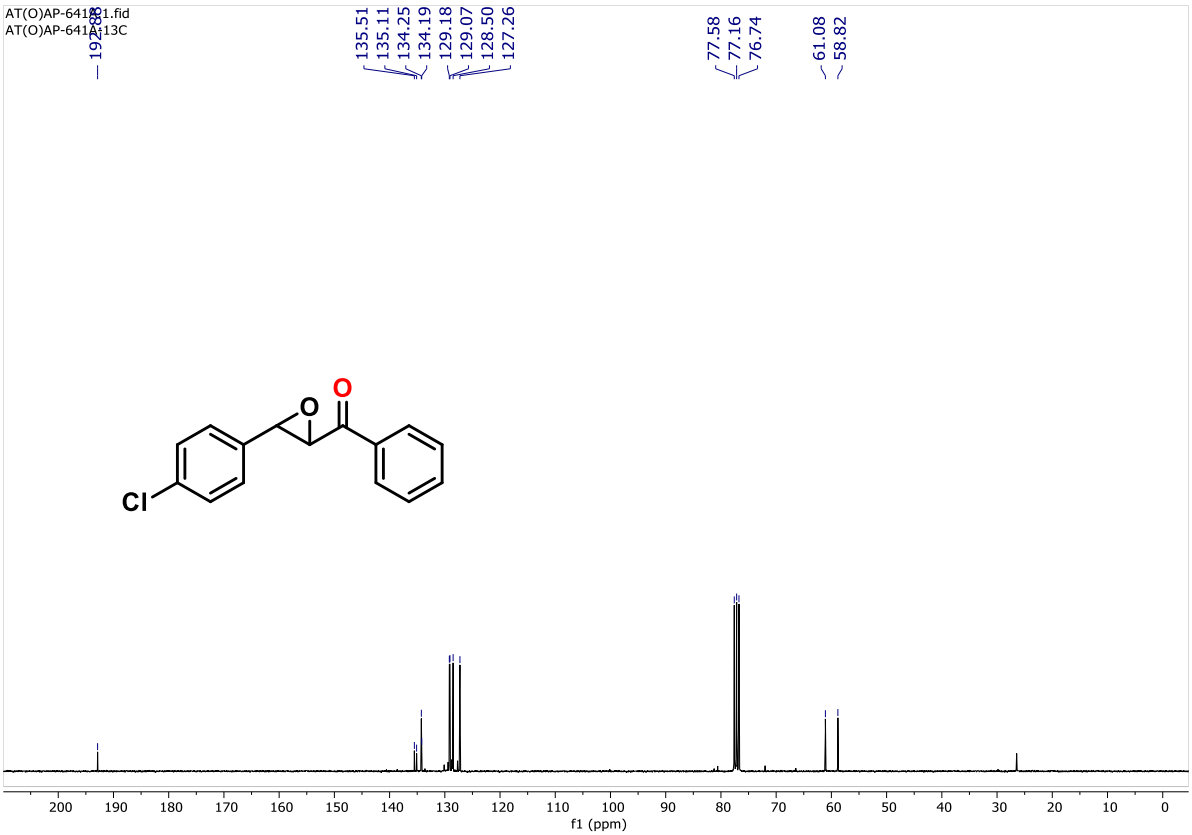

Figure 5.40. $^{13}C\{^{1}H\}$ NMR (75 MHz) spectrum of **4b** in $CDCl_3$.

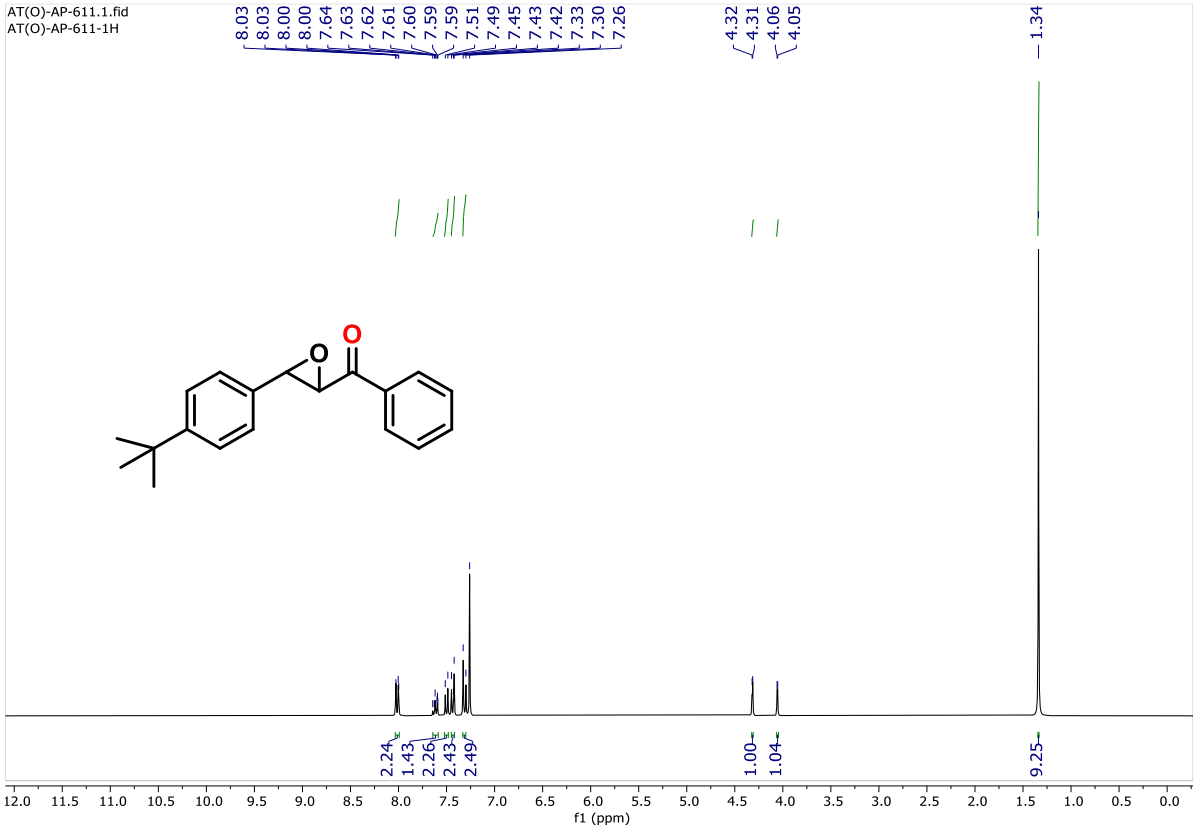

Figure 5.41. ^{1}H NMR (300 MHz) spectrum of **4c** in $CDCl_3$.

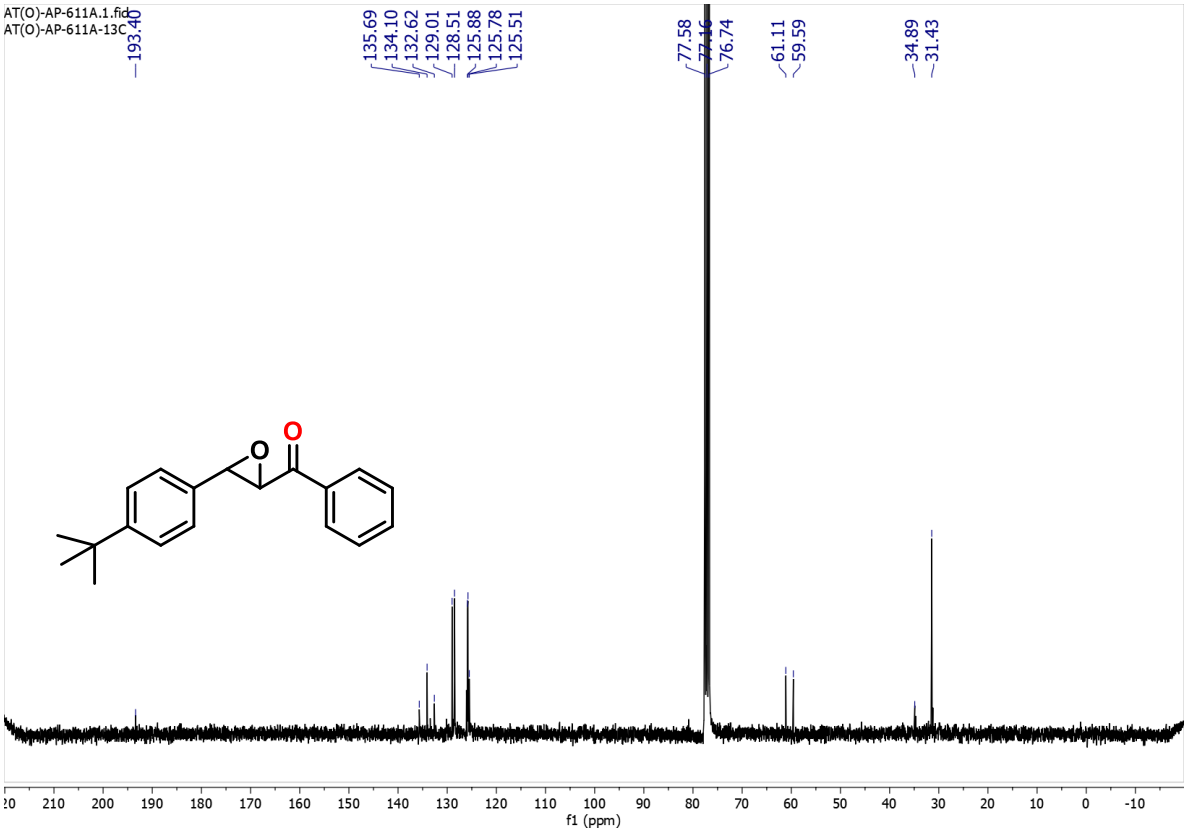

Figure 5.42. $^{13}C\{^{1}H\}$ NMR (75 MHz) spectrum of **4c** in $CDCl_3$.

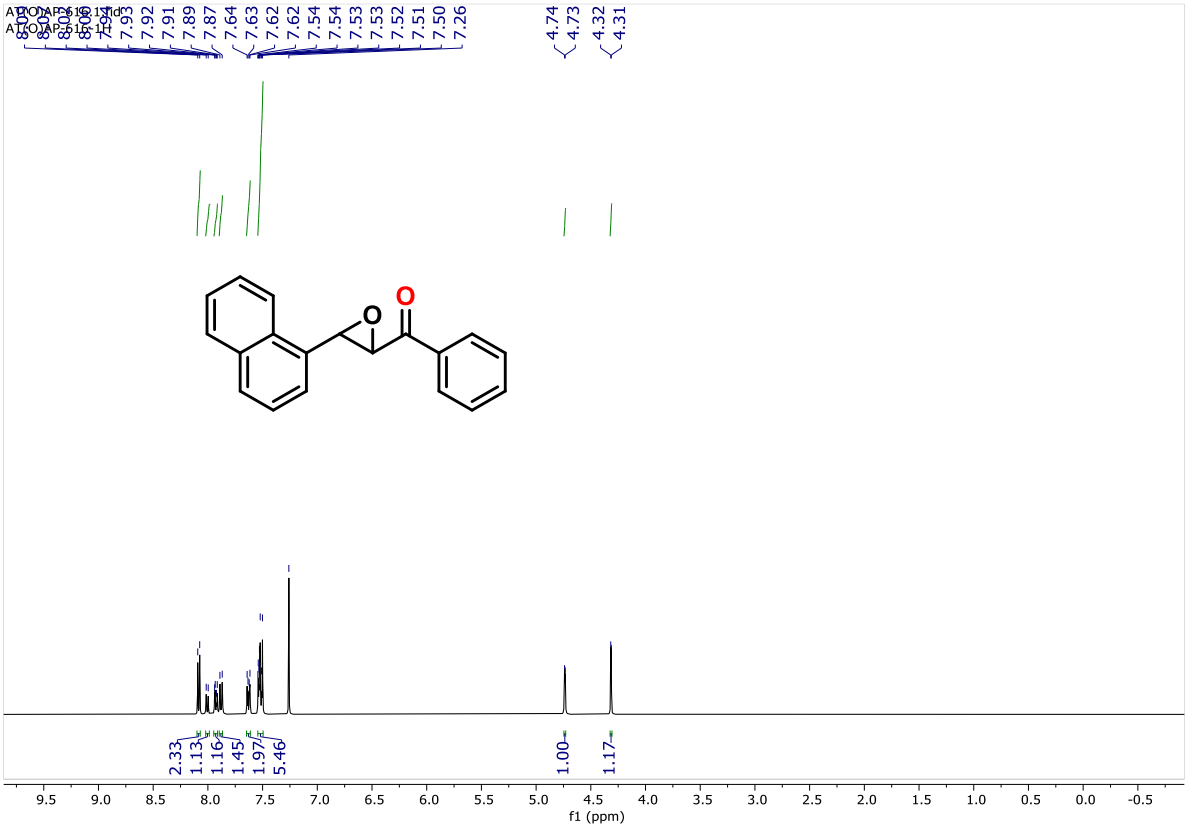

Figure 5.43. ^{1}H NMR (300 MHz) spectrum of **4d** in $CDCl_3$.

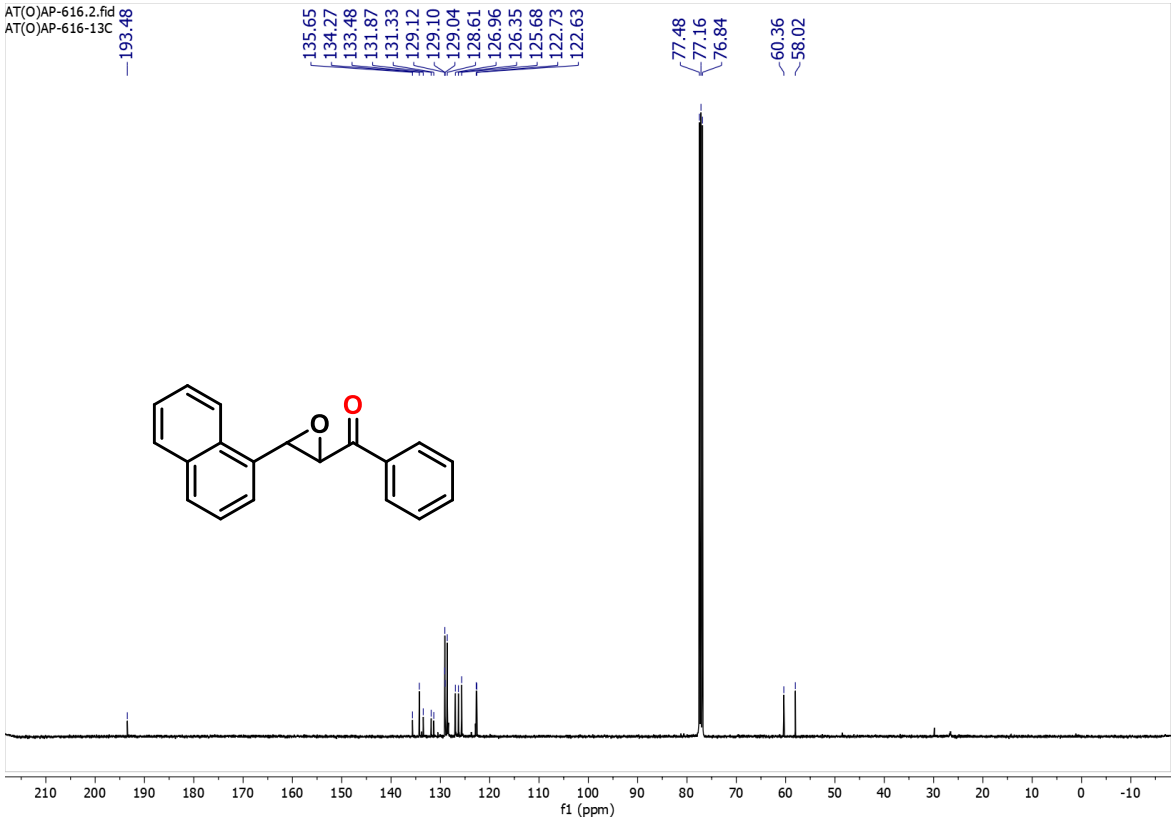

Figure 5.44. $^{13}C\{^{1}H\}$ NMR (75 MHz) spectrum of **4d** in $CDCl_3$.

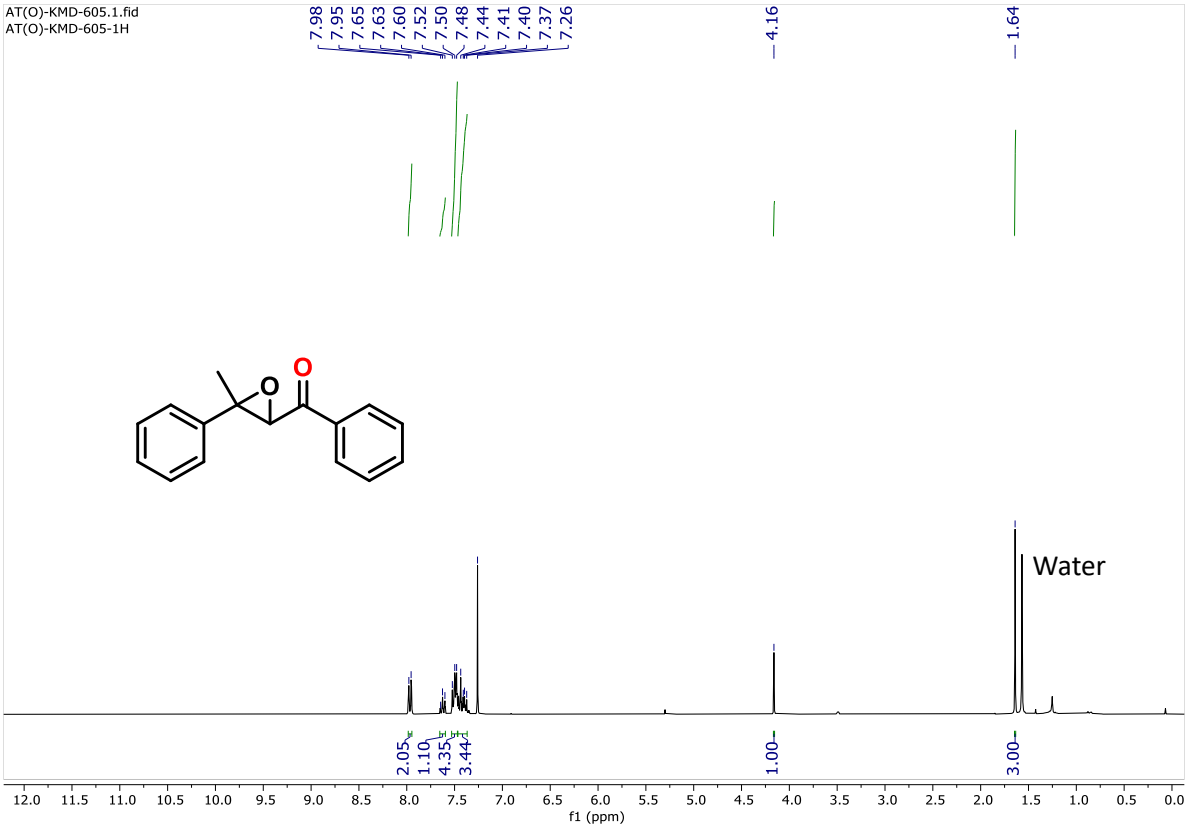

Figure 5.45. ^{1}H NMR (300 MHz) spectrum of **4e** in $CDCl_3$.

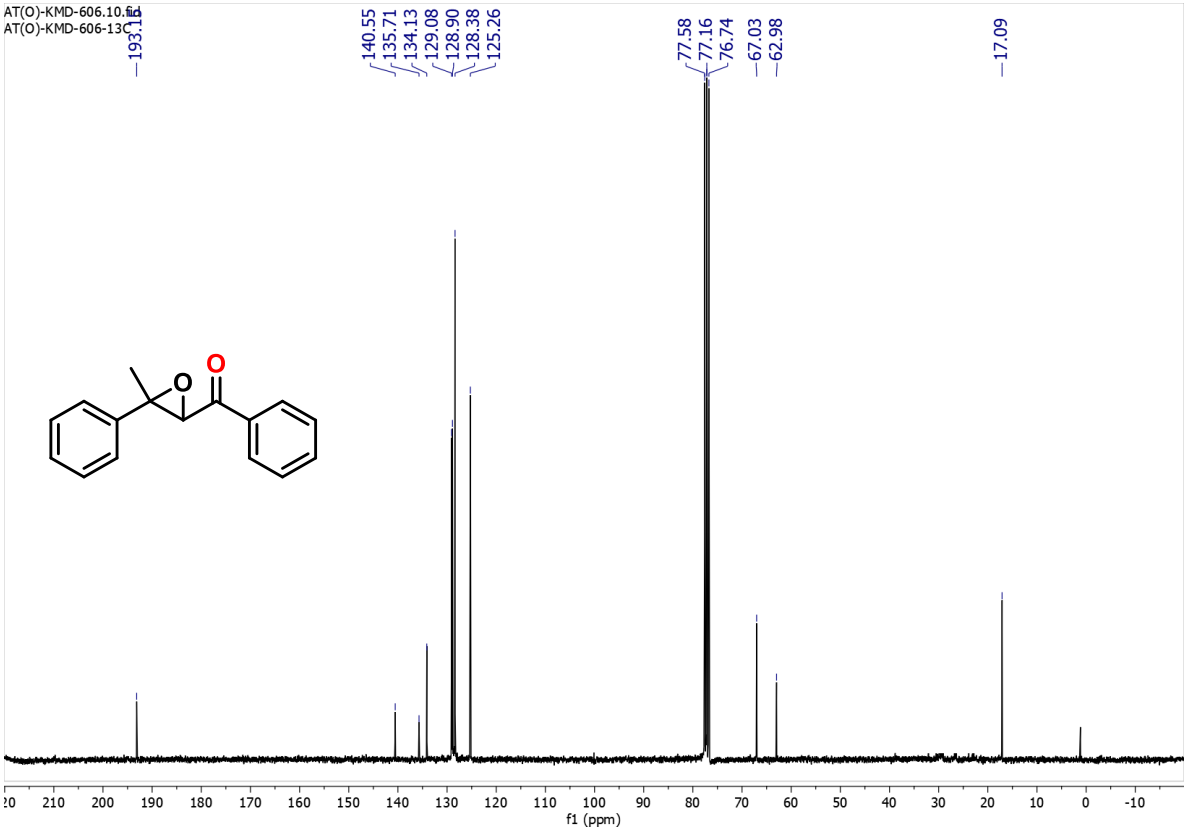

Figure 5.46. $^{13}C\{^{1}H\}$ NMR (75 MHz) spectrum of **4e** in $CDCl_3$.

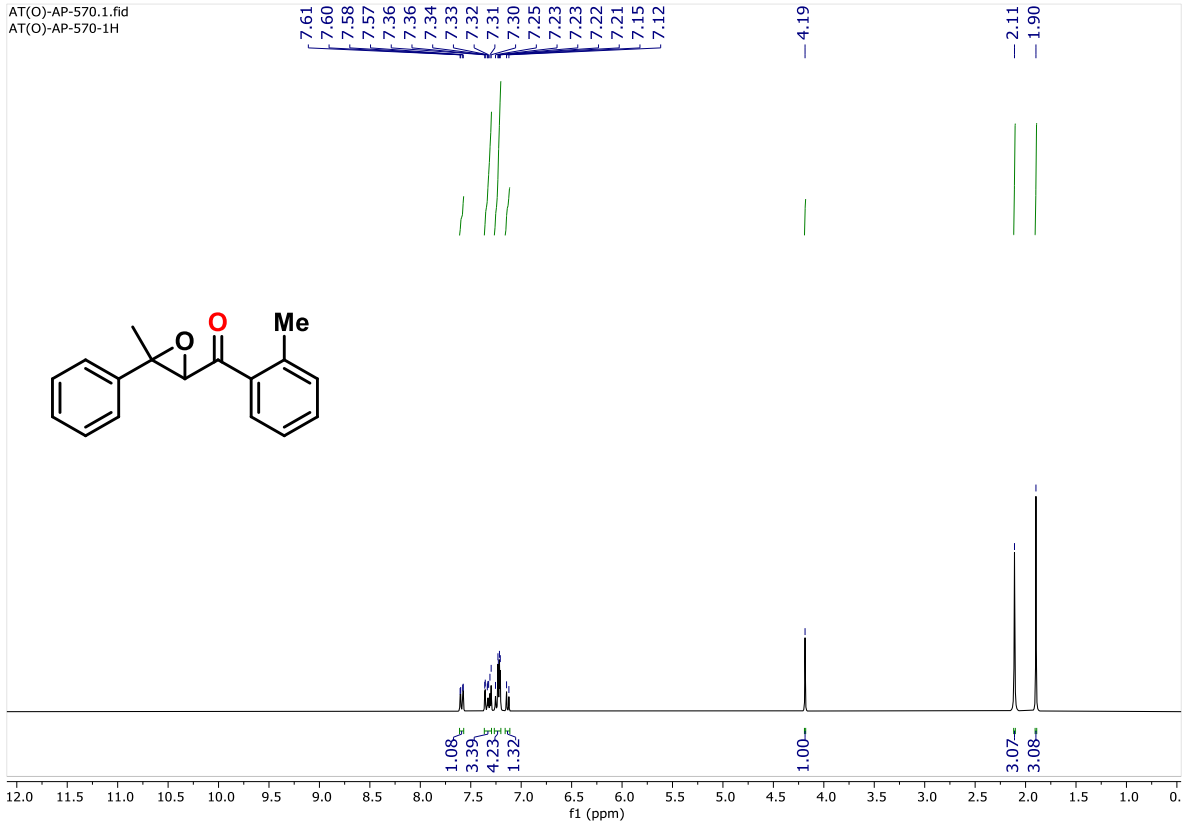

Figure 5.47. ^{1}H NMR (300 MHz) spectrum of **4f** in $CDCl_3$.

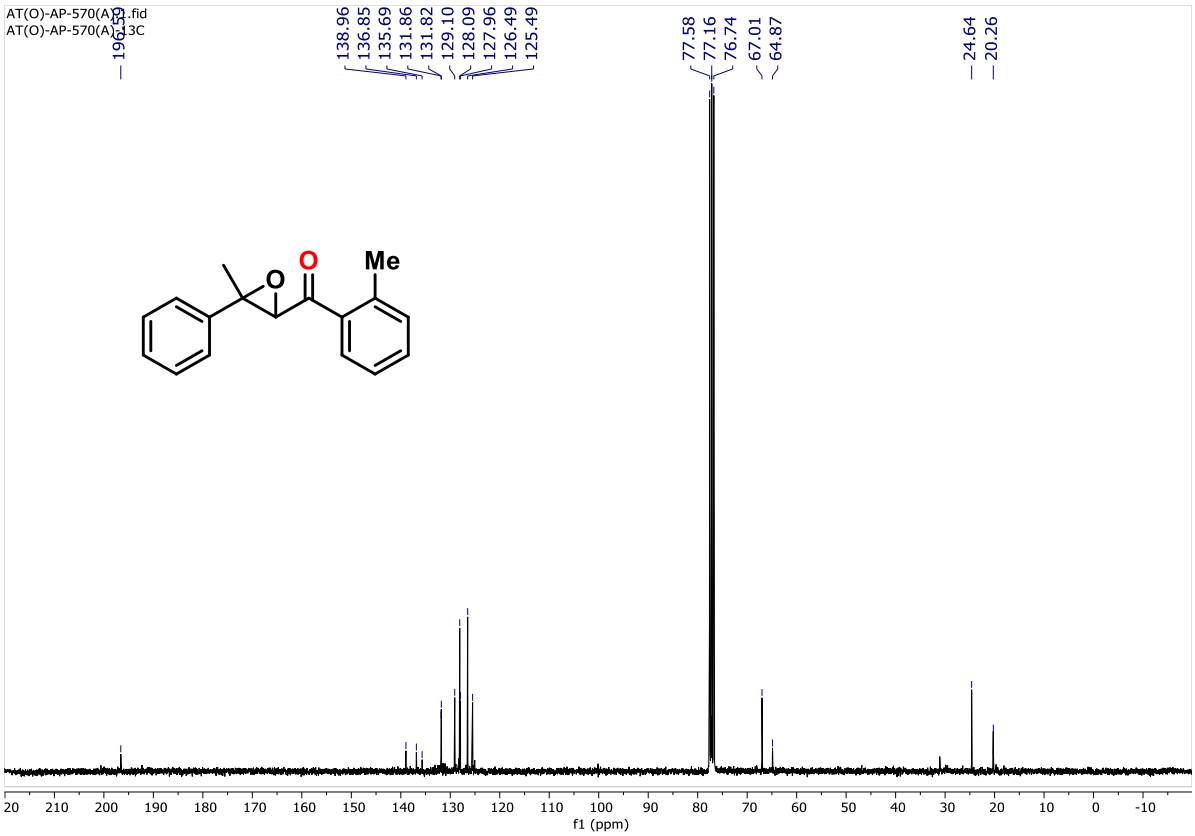

Figure 5.48. $^{13}C\{^{1}H\}$ NMR (75 MHz) spectrum of **4f** in $CDCl_3$.

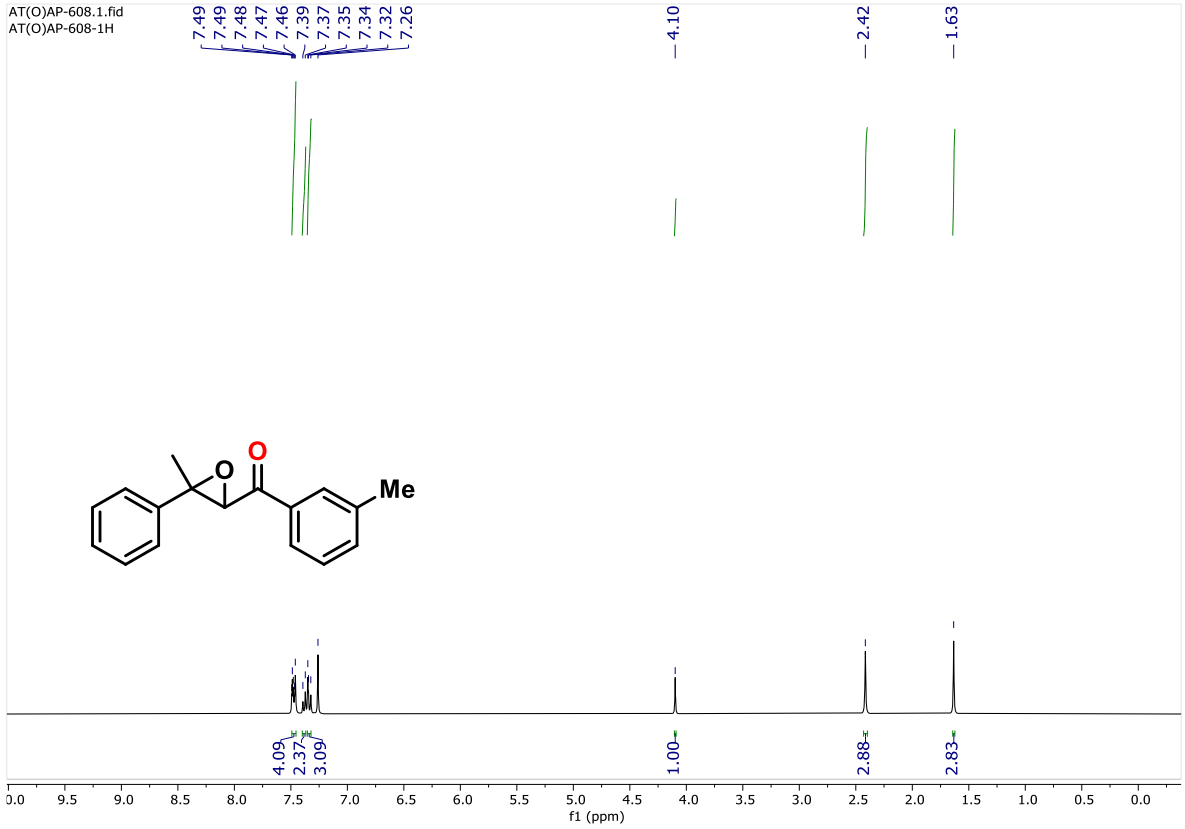

Figure 5.49. ^{1}H NMR (300 MHz) spectrum of **4g** in $CDCl_3$.

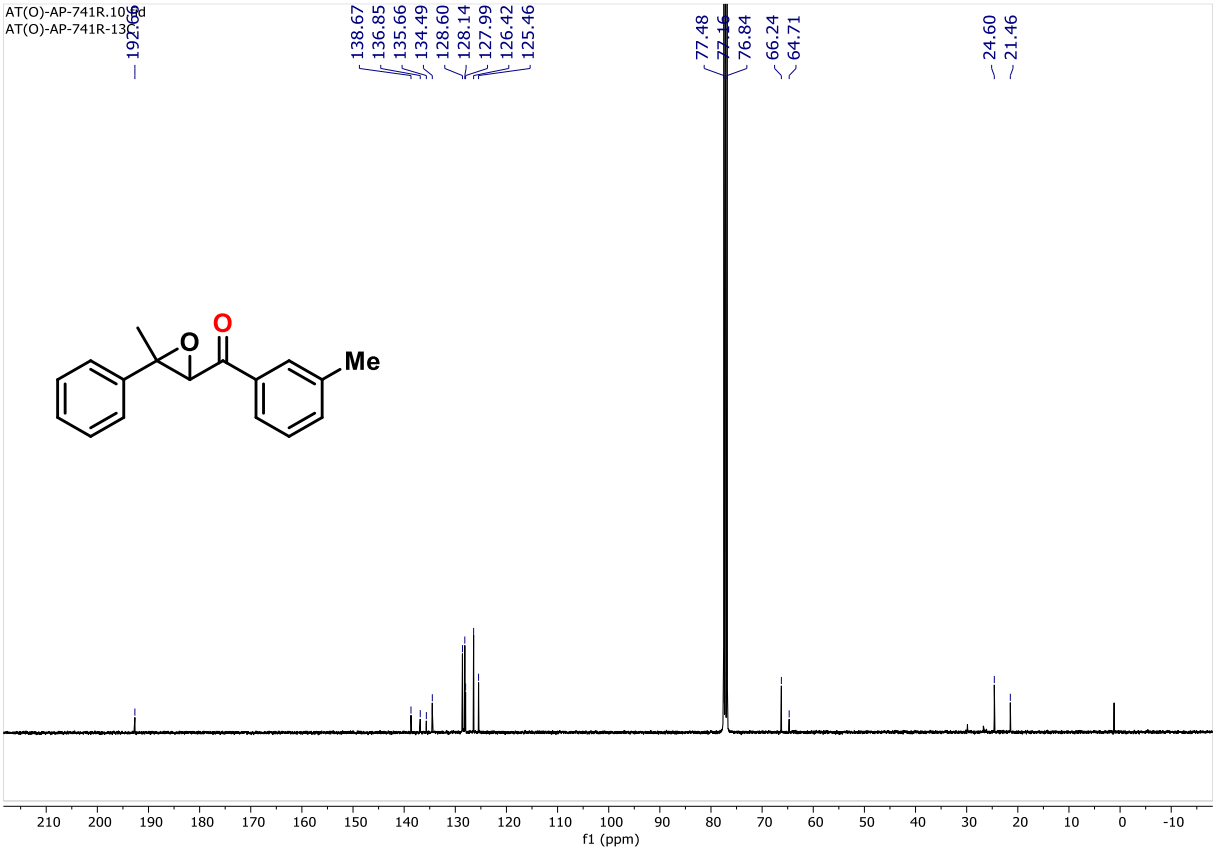

Figure 5.50. $^{13}C\{^{1}H\}$ NMR (75 MHz) spectrum of **4g** in $CDCl_3$.

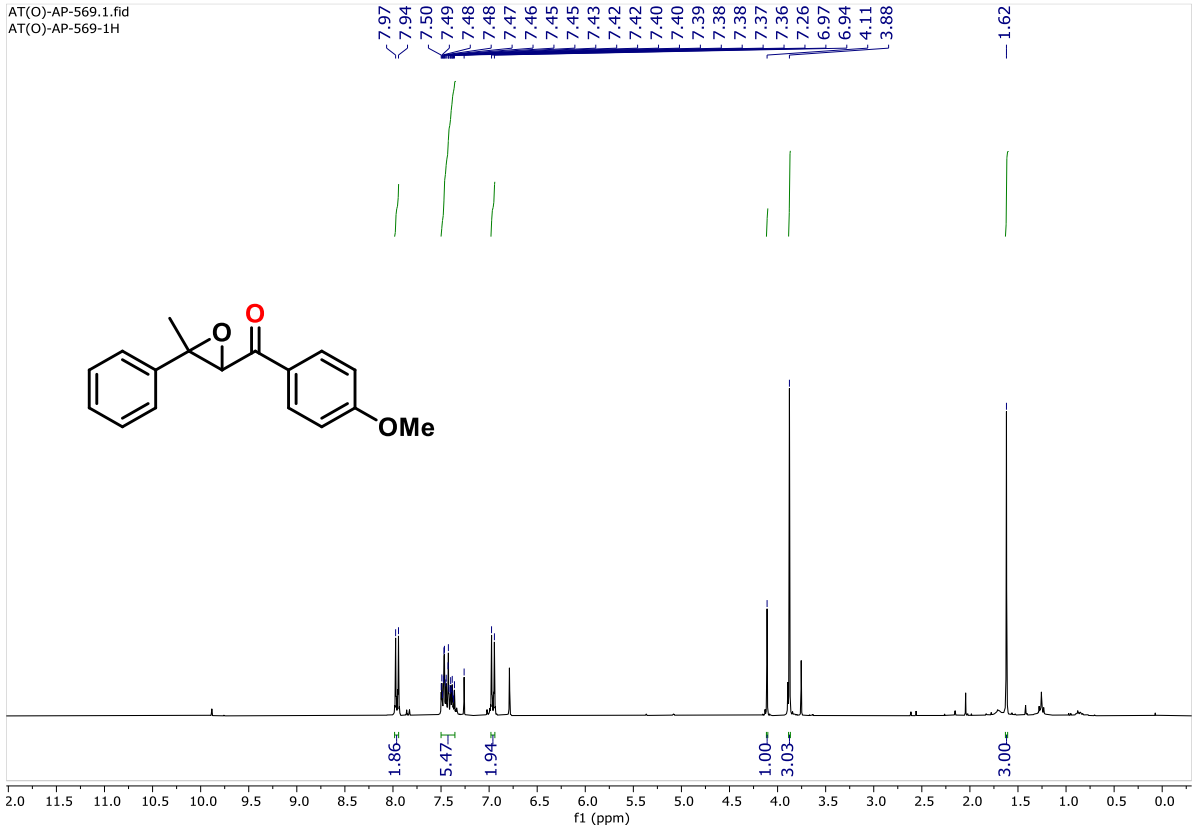

Figure 5.51. ^{1}H NMR (300 MHz) spectrum of **4h** in $CDCl_3$.

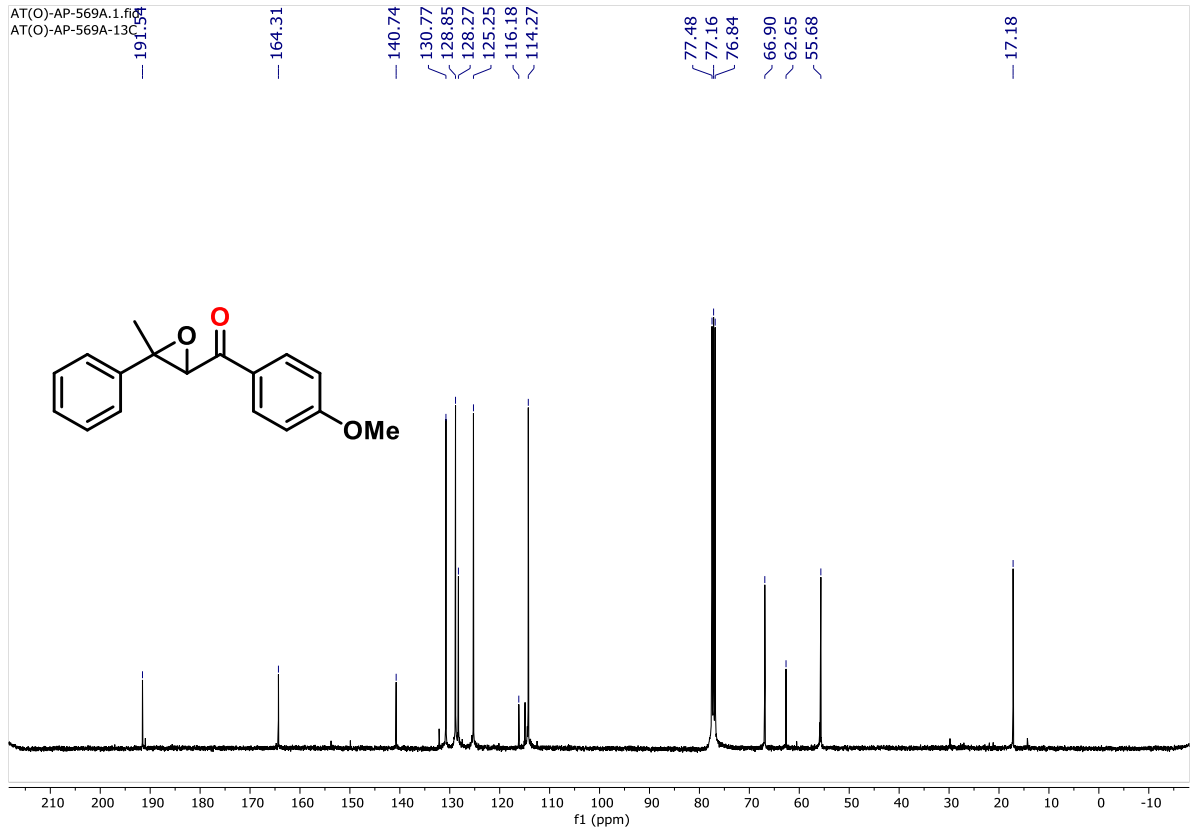

Figure 5.52. $^{13}C\{^{1}H\}$ NMR (75 MHz) spectrum of **4h** in $CDCl_3$.

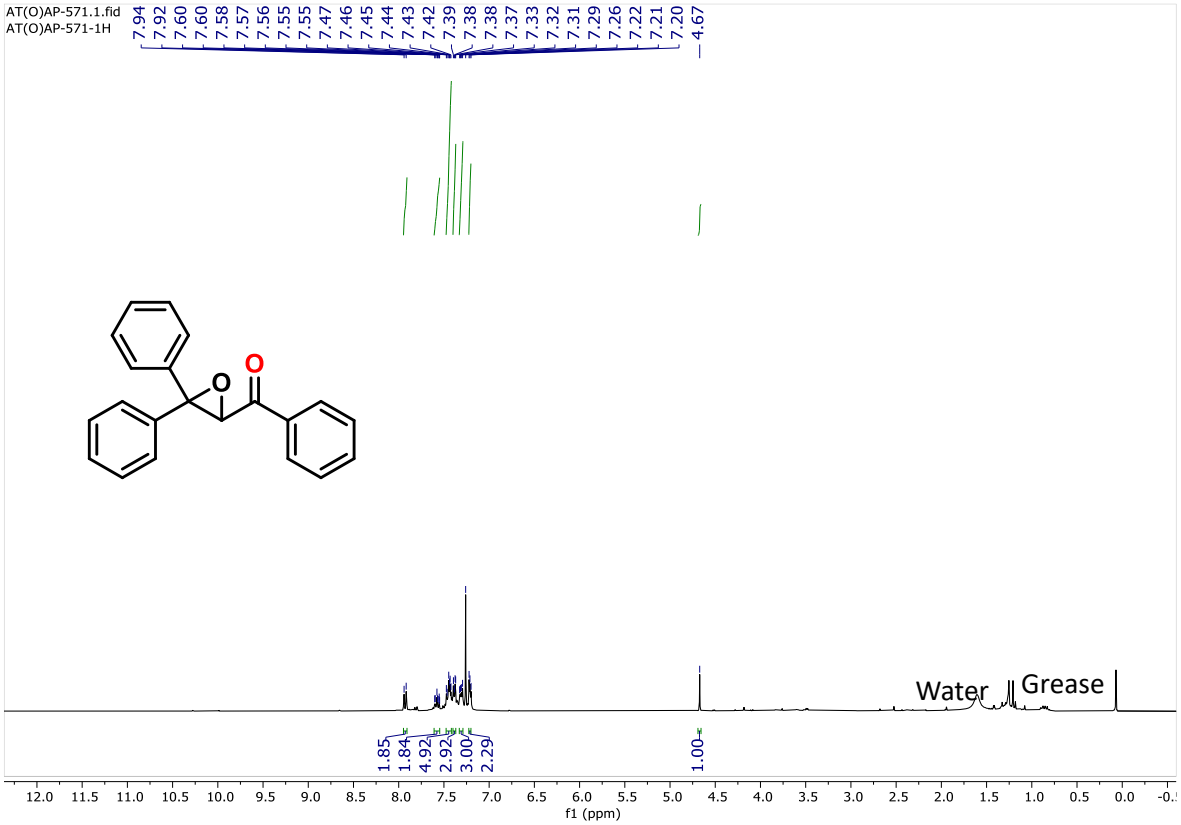

Figure 5.53. ^{1}H NMR (300 MHz) spectrum of **4i** in $CDCl_3$.

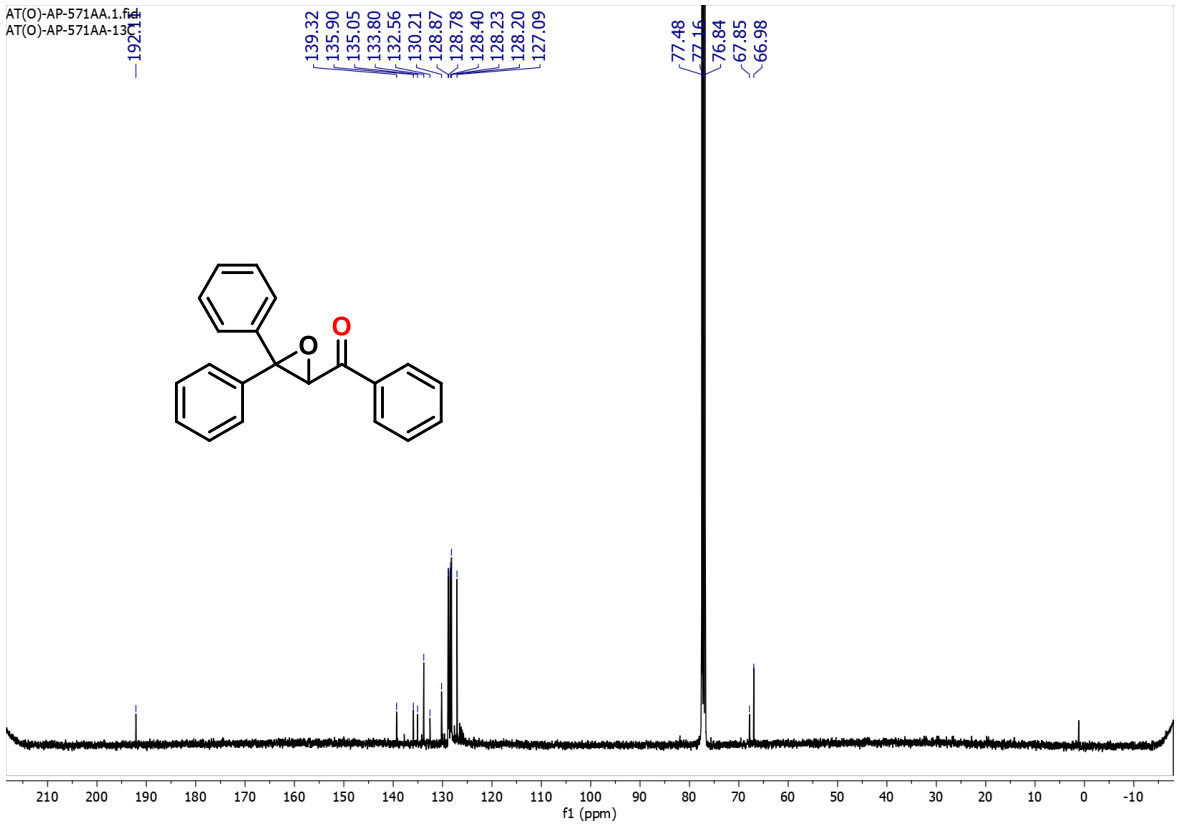

Figure 5.54. $^{13}C\{^{1}H\}$ NMR (75 MHz) spectrum of **4i** in $CDCl_3$.

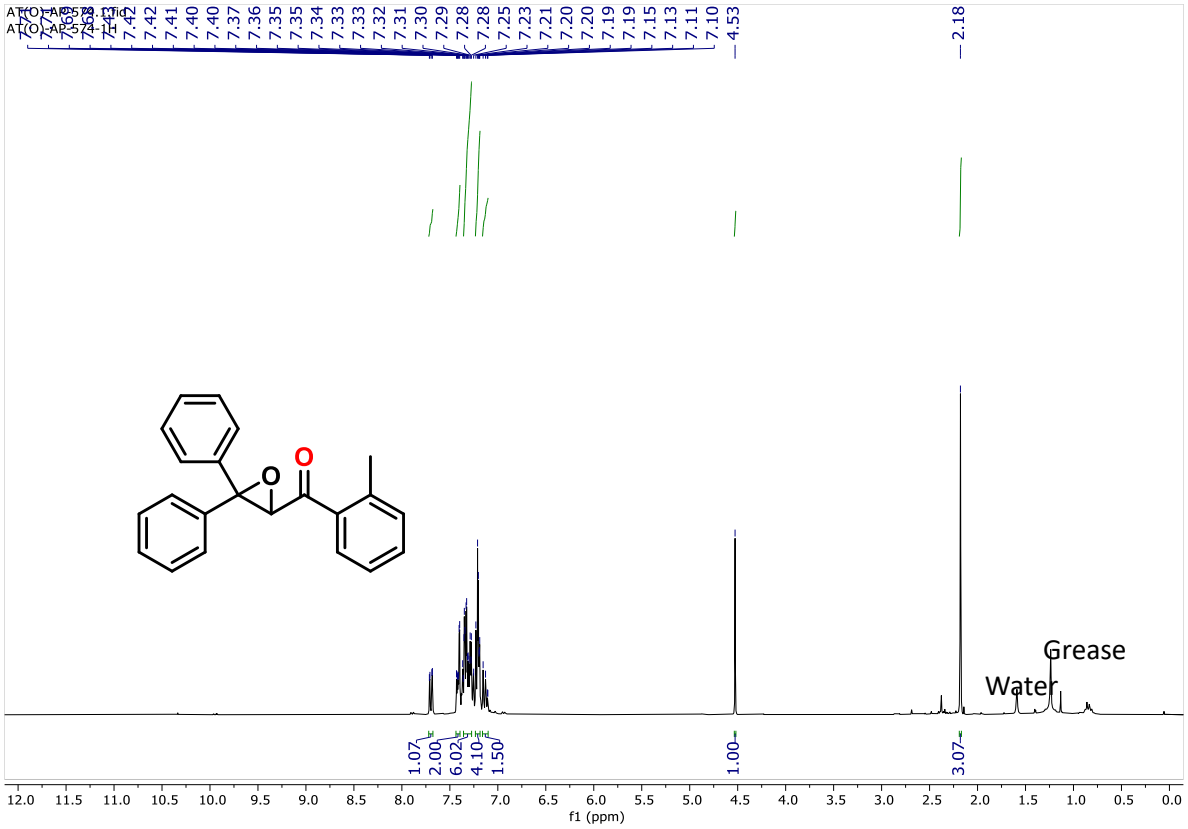

Figure 5.55. ^{1}H NMR (300 MHz) spectrum of **4j** in $CDCl_3$.

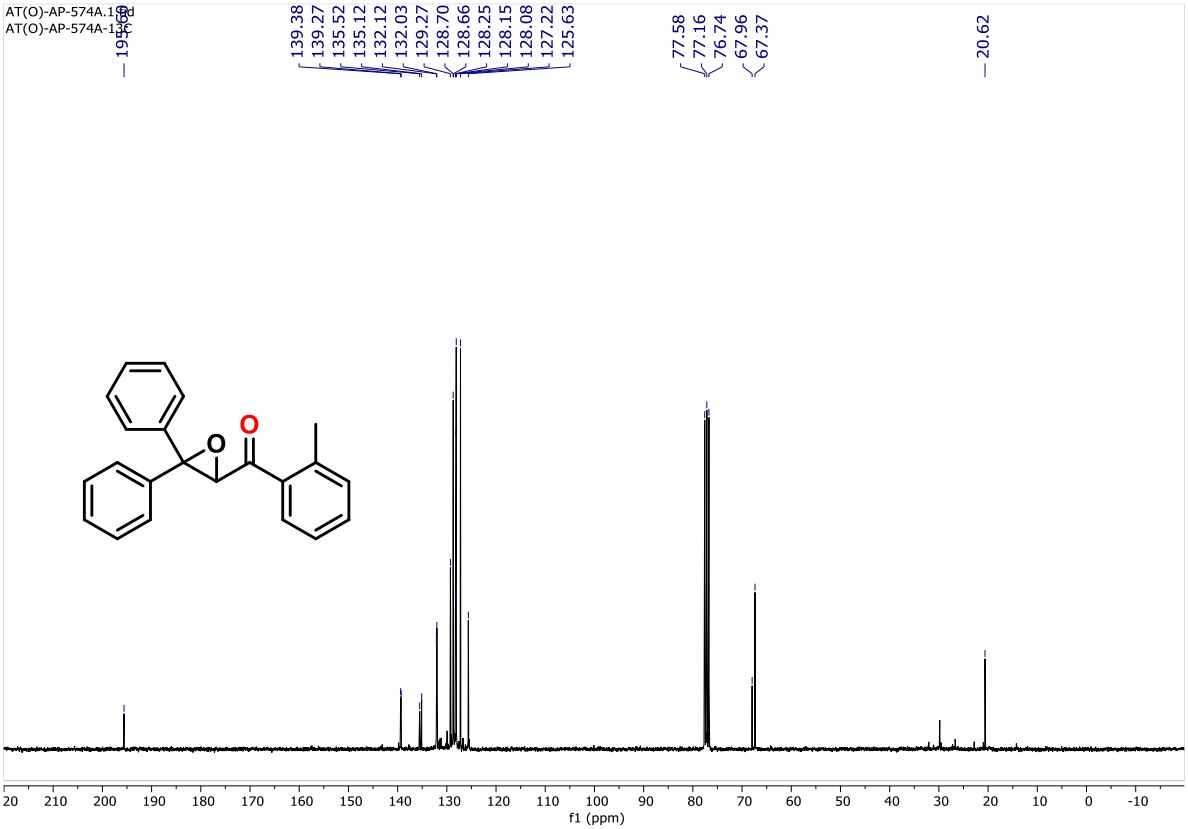

Figure 5.56. $^{13}C\{^{1}H\}$ NMR (75 MHz) spectrum of **4j** in $CDCl_3$.

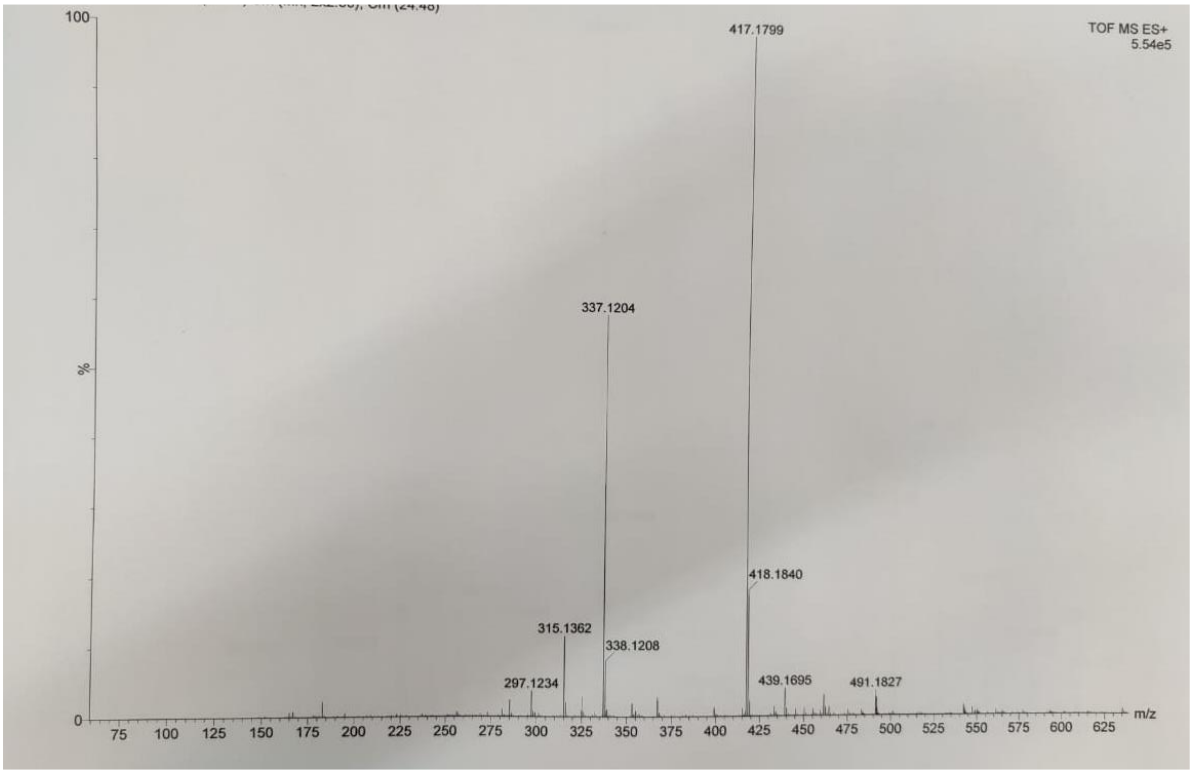

Figure 5.57. HRMS of **4j** compound.

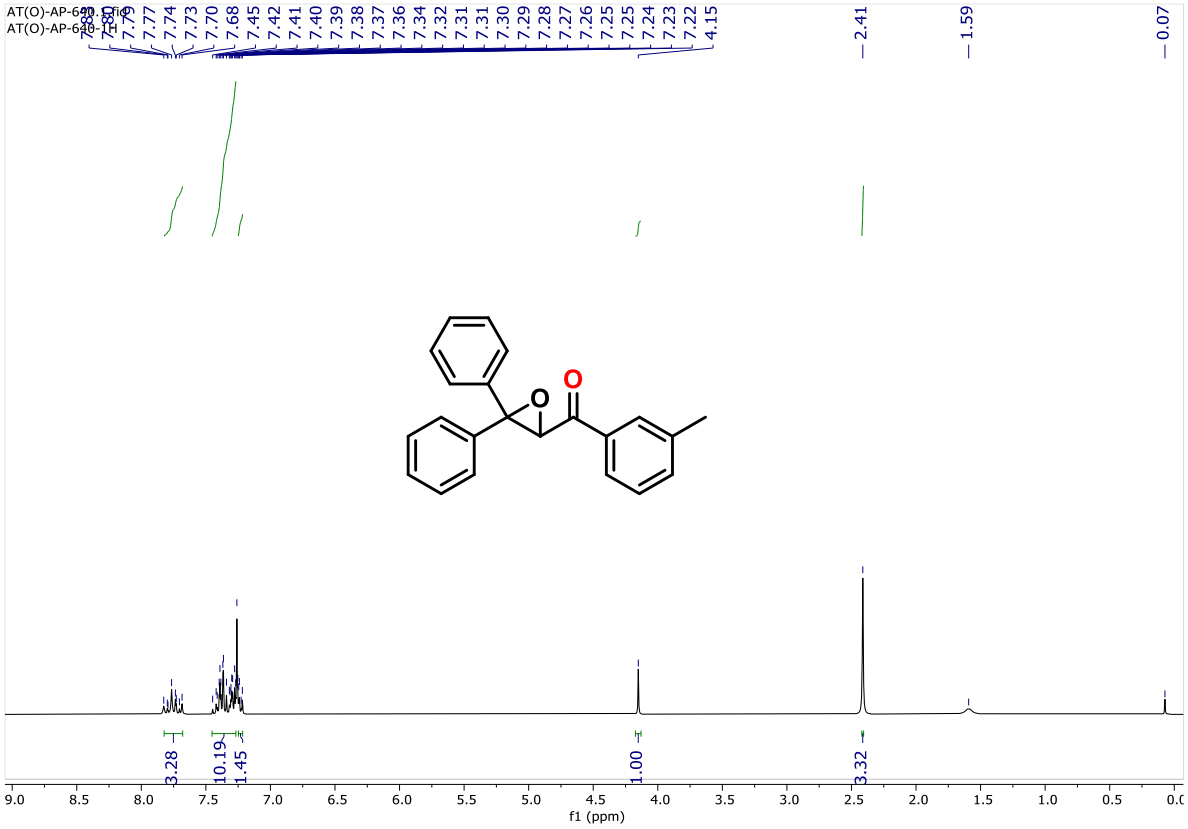

Figure 5.58. ^{1}H NMR (300 MHz) spectrum of **4k** in $CDCl_3$.

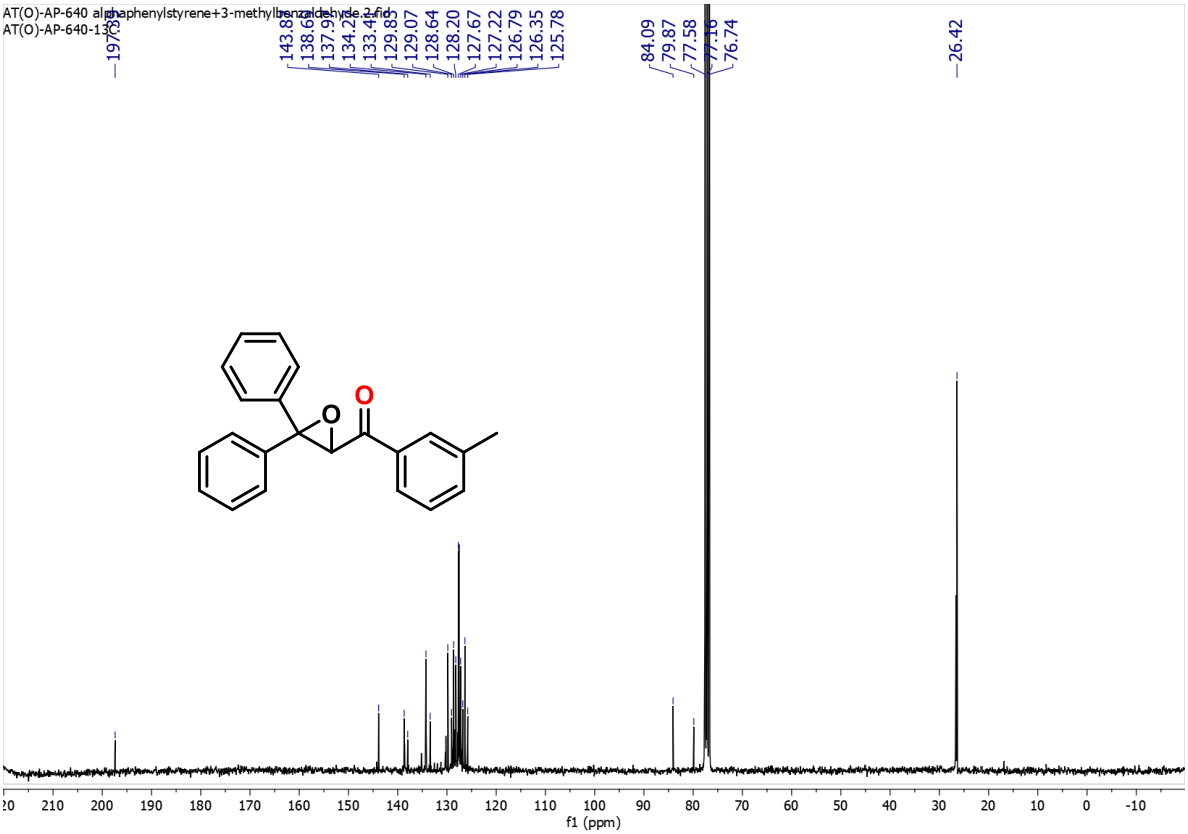

Figure 5.59. $^{13}C\{^{1}H\}$ NMR (75 MHz) spectrum of **4k** in $CDCl_3$.

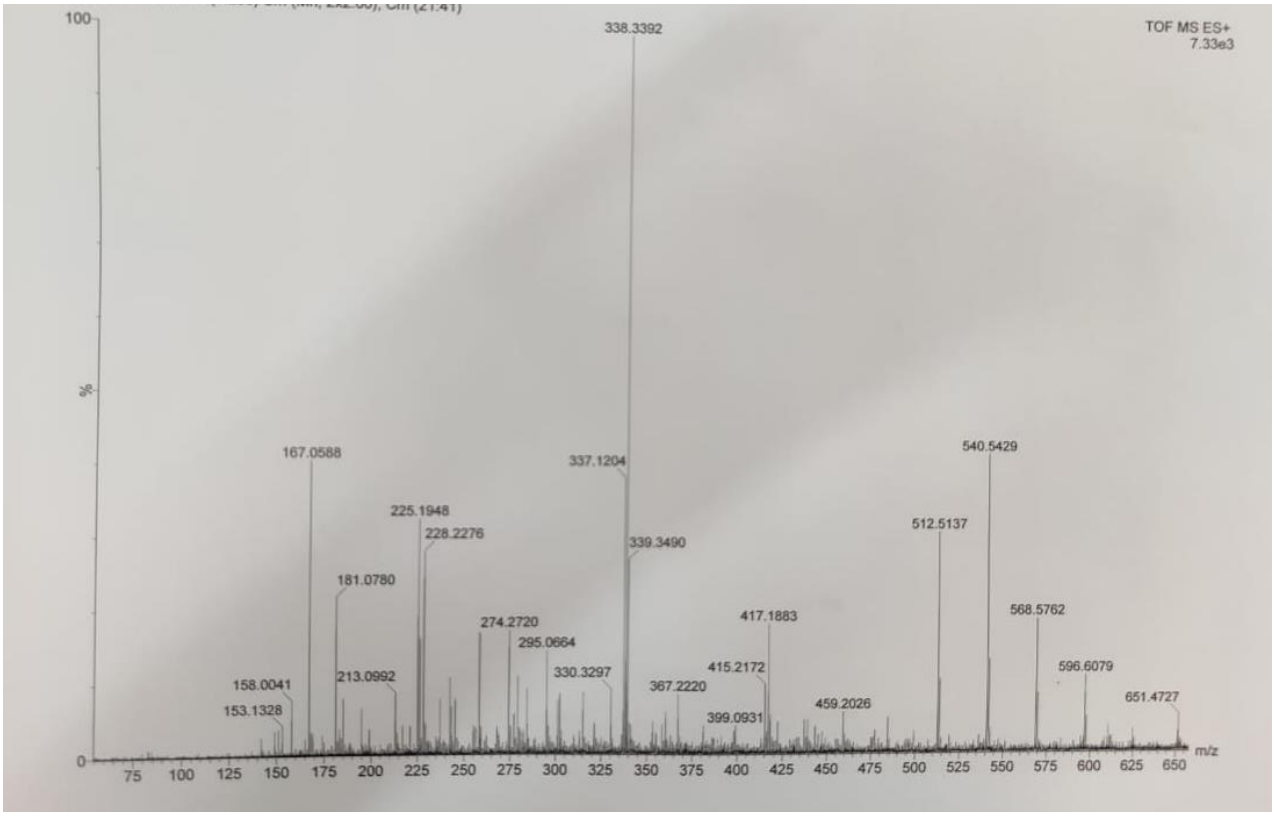

Figure 5.60. HRMS of **4k** compound

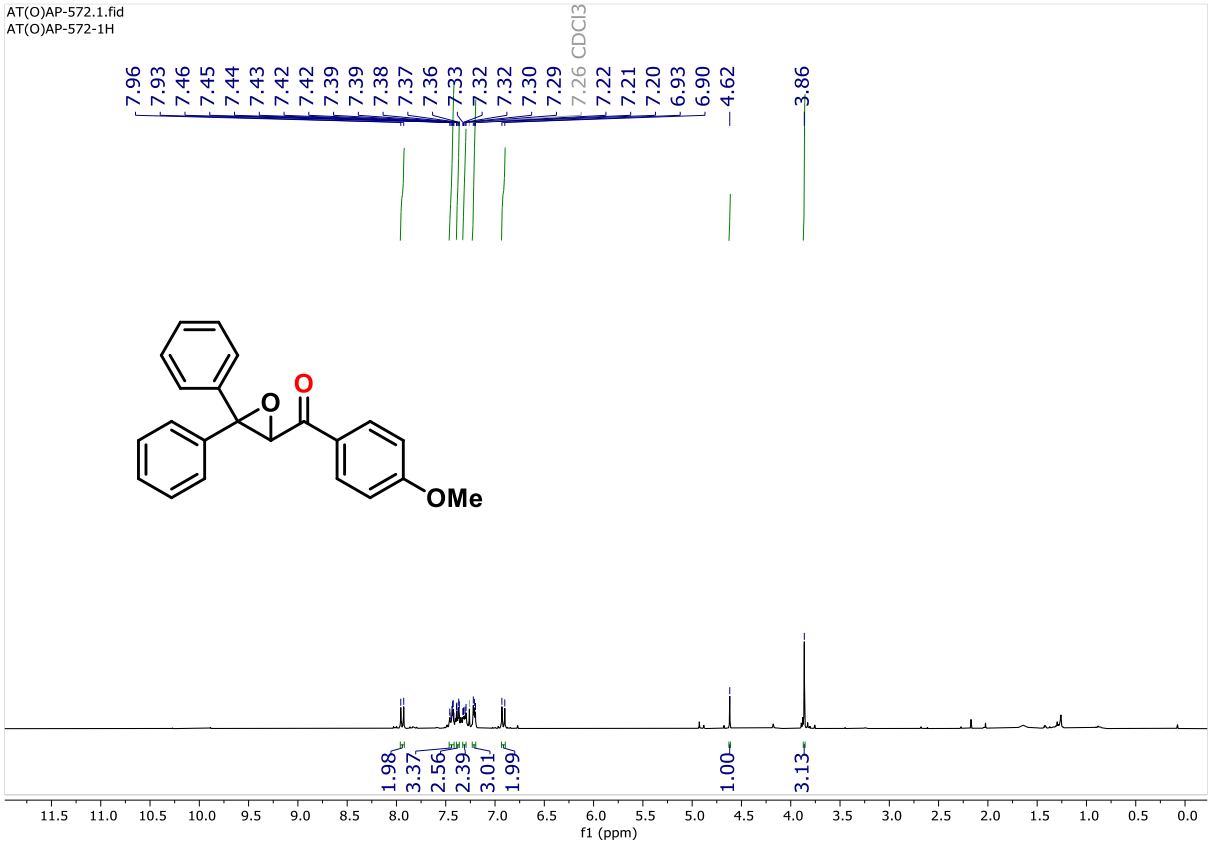

Figure 5.61. ^{1}H NMR (300 MHz) spectrum of **4l** in $CDCl_3$.

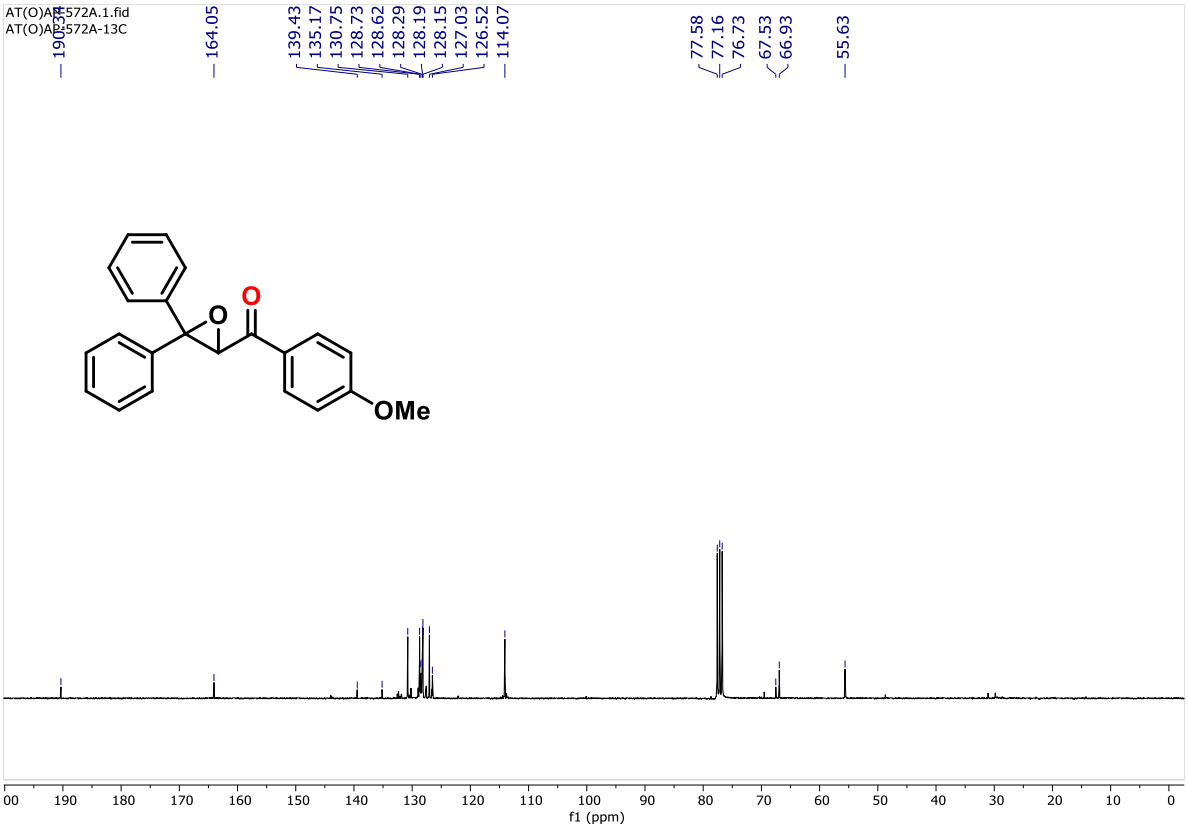

Figure 5.62. $^{13}C\{^{1}H\}$ NMR (75 MHz) spectrum of **4l** in $CDCl_3$.

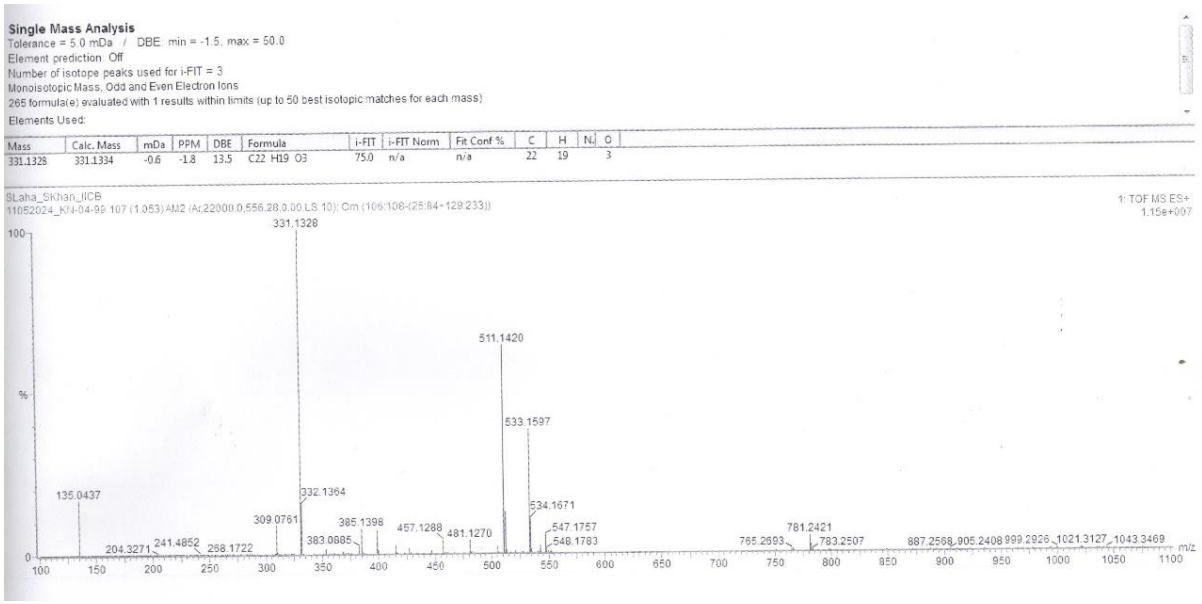

Figure 5.63. HRMS of **4l**.

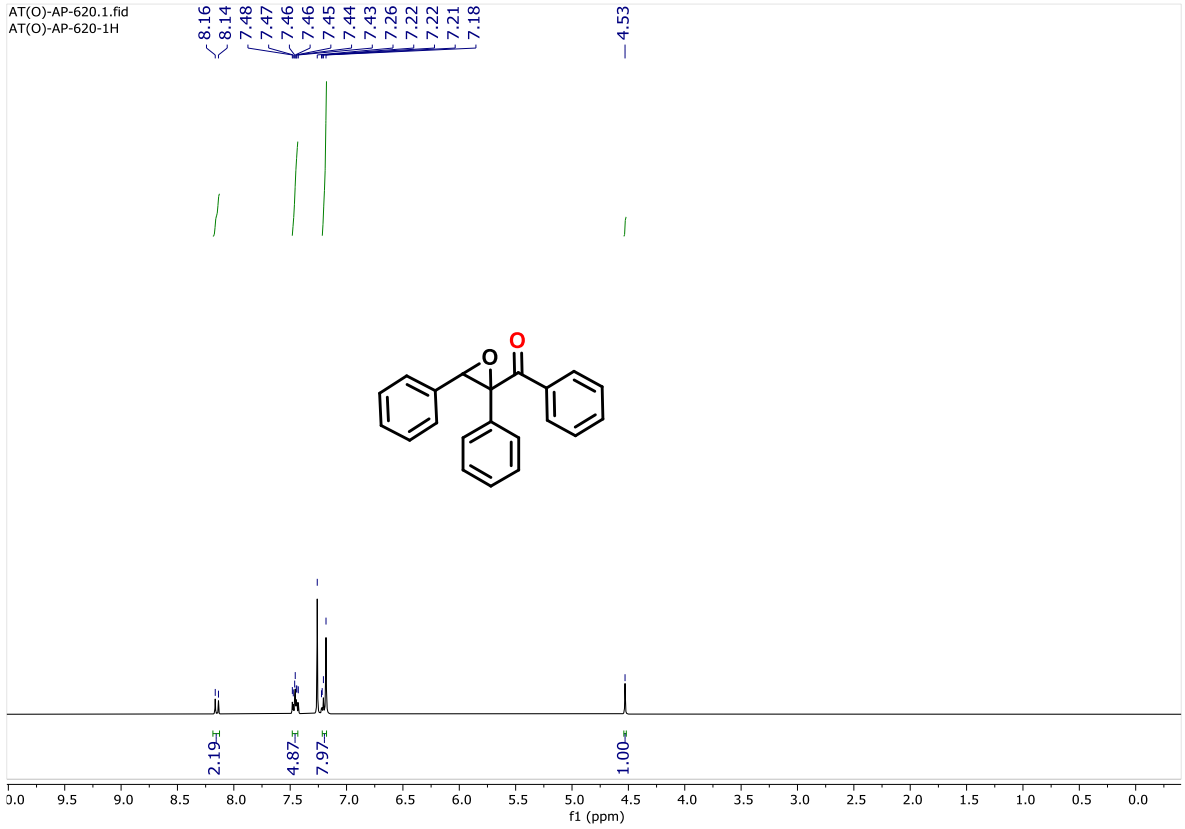

Figure 5.64. ^{1}H NMR (300 MHz) spectrum of **4m** in $CDCl_3$.

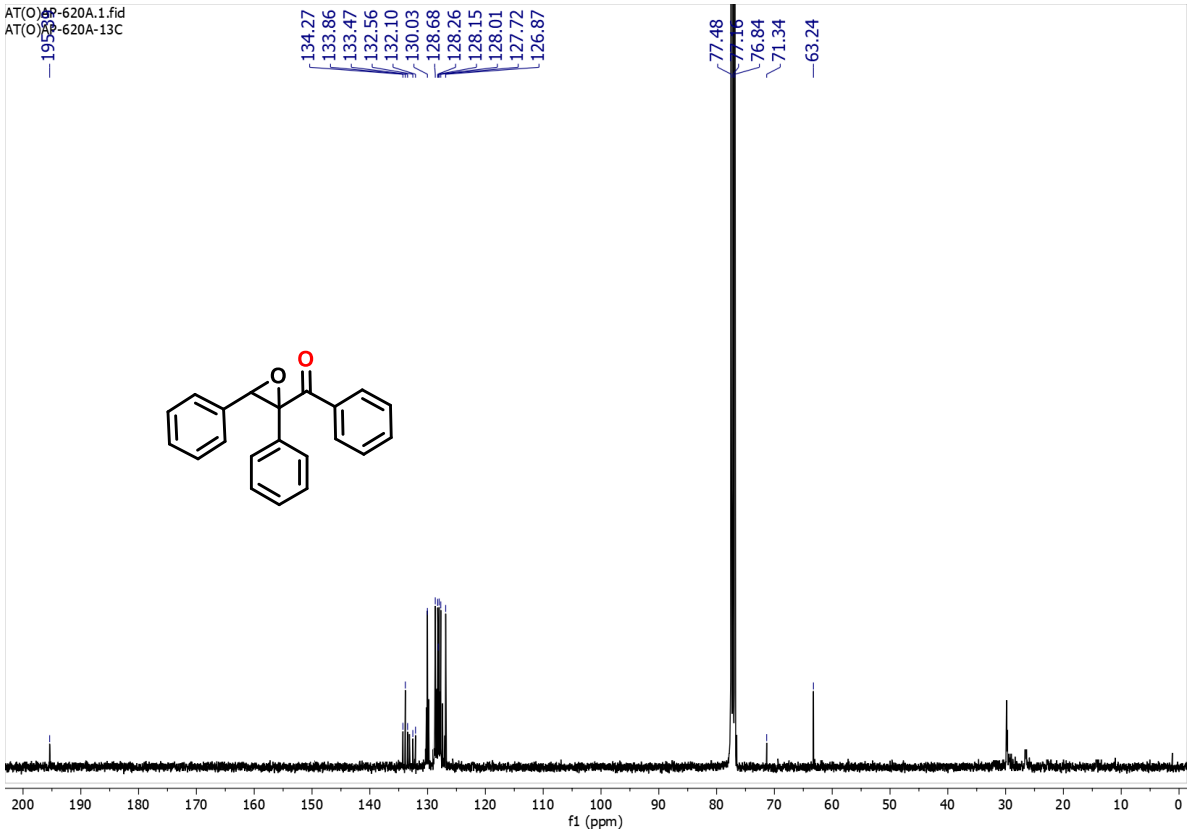

Figure 5.65. $^{13}C\{^{1}H\}$ NMR (75 MHz) spectrum of **4m** in $CDCl_3$.

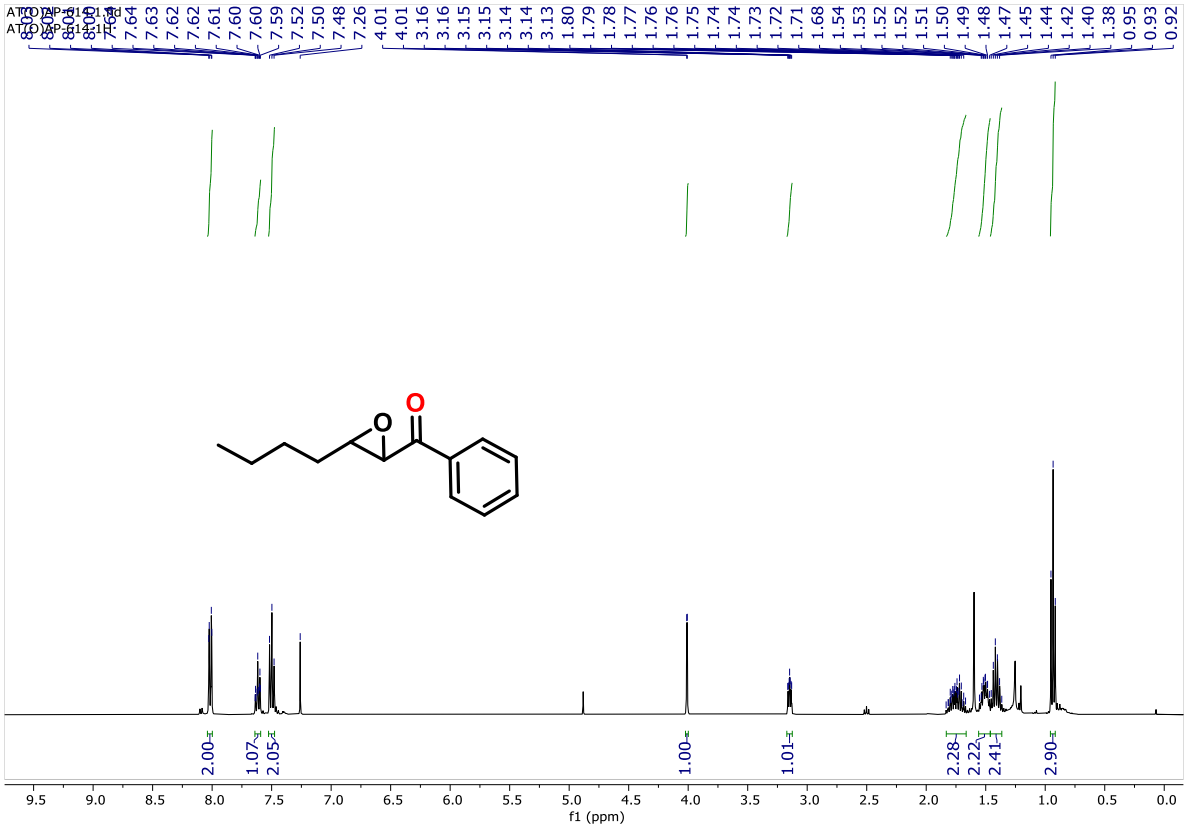

Figure 5.66. ^{1}H NMR (300 MHz) spectrum of **5a** in $CDCl_3$.

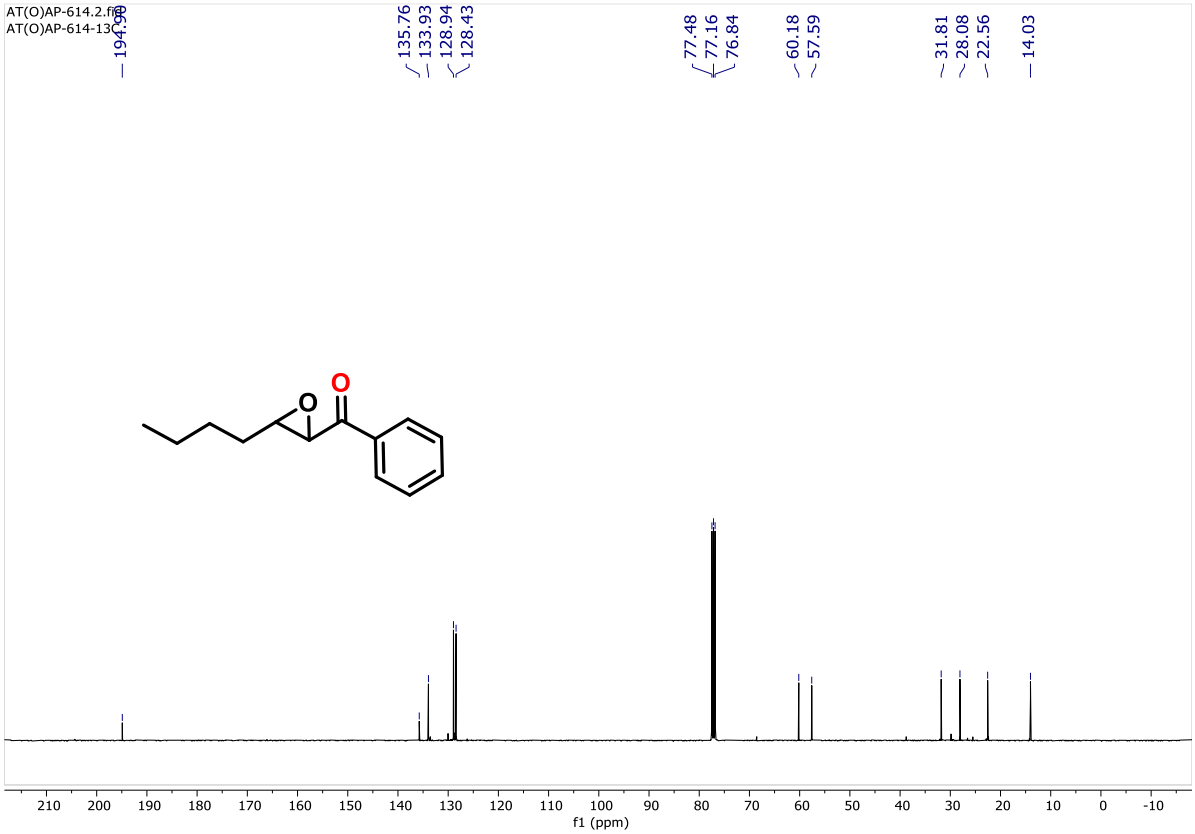

Figure 5.67. $^{13}C\{^{1}H\}$ NMR (75 MHz) spectrum of **5a** in $CDCl_3$.

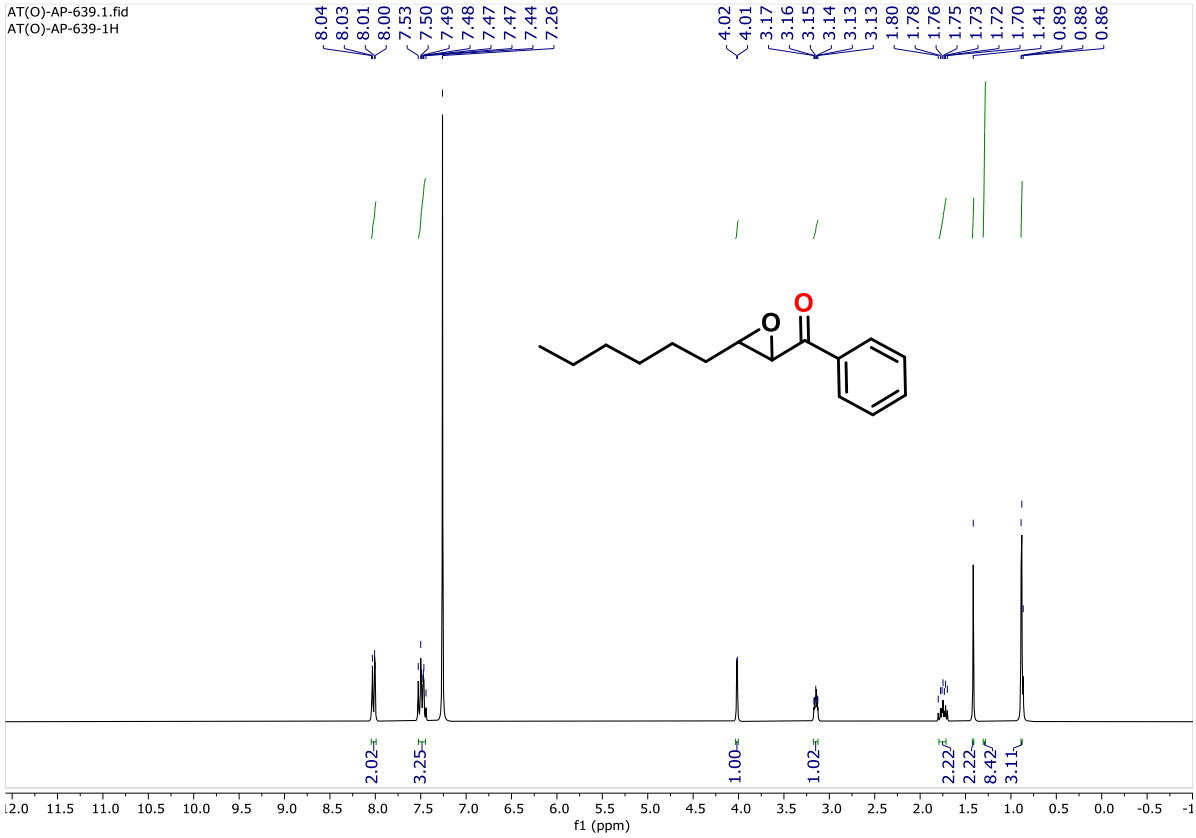

Figure 5.68. ^{1}H NMR (300 MHz) spectrum of **5b** in $CDCl_3$.

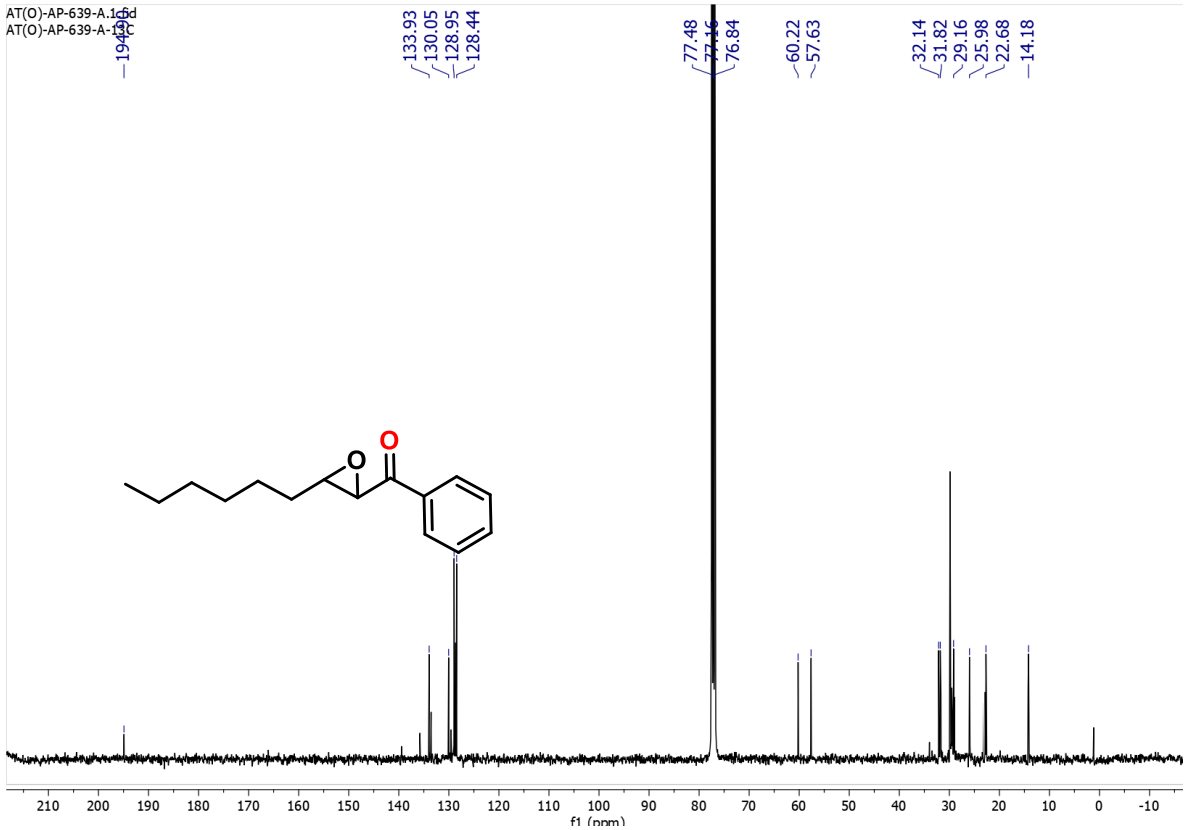

Figure 5.69. $^{13}C\{^{1}H\}$ NMR (75 MHz) spectrum of **5b** in $CDCl_3$.

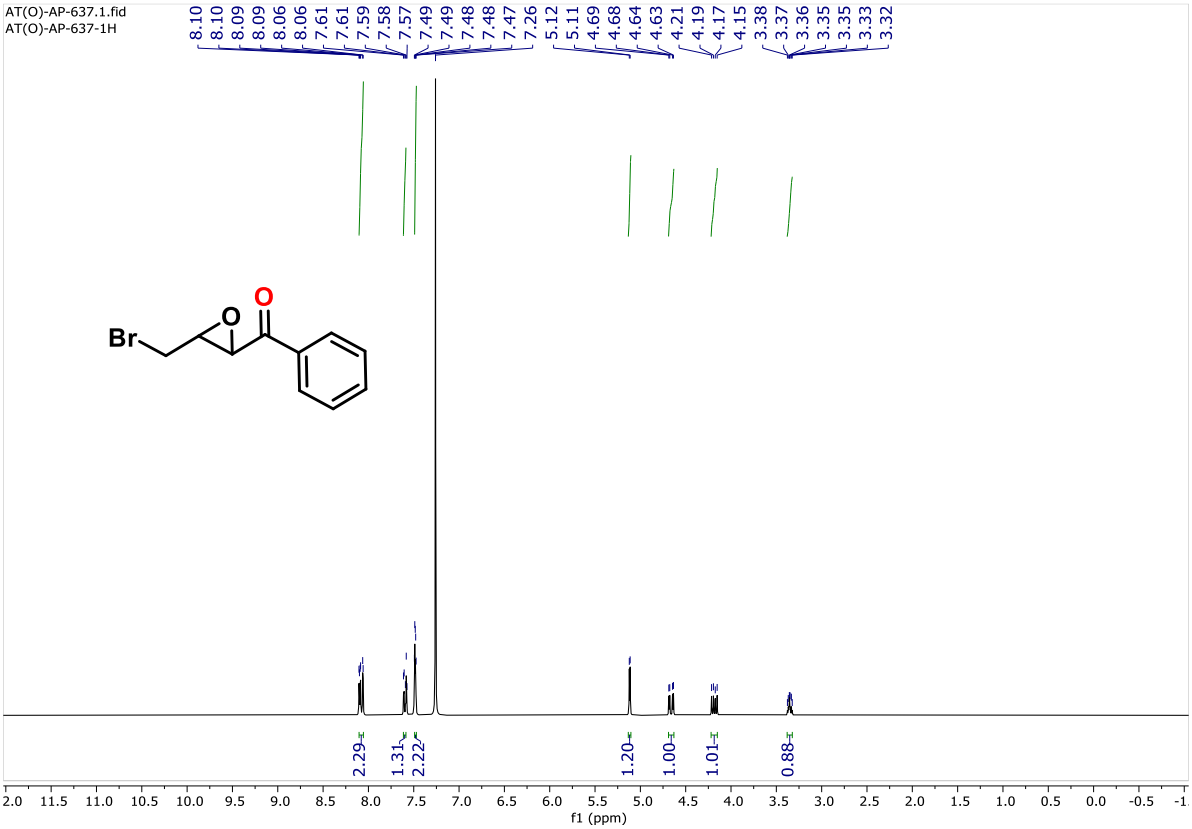

Figure 5.70. ^{1}H NMR (300 MHz) spectrum of **5c** in $CDCl_3$.

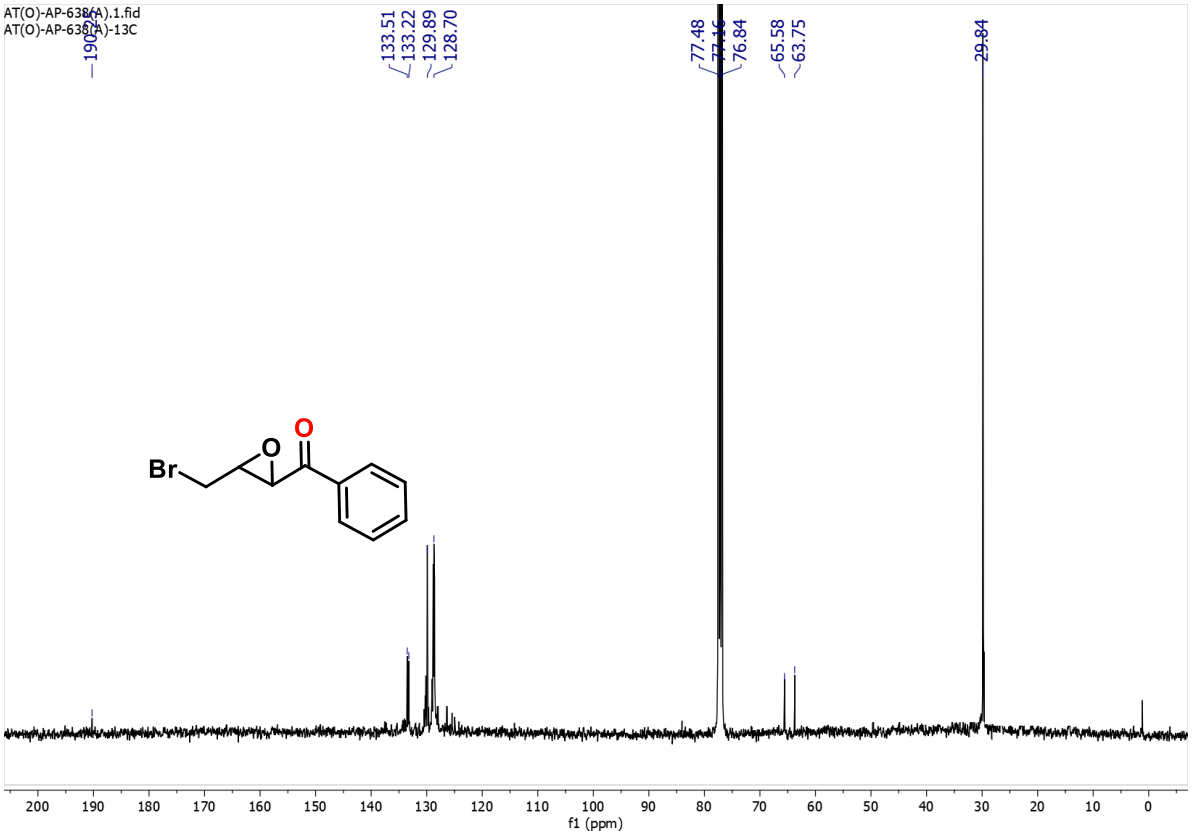

Figure 5.71. $^{13}C\{^{1}H\}$ NMR (75 MHz) spectrum of **5c** in $CDCl_3$.

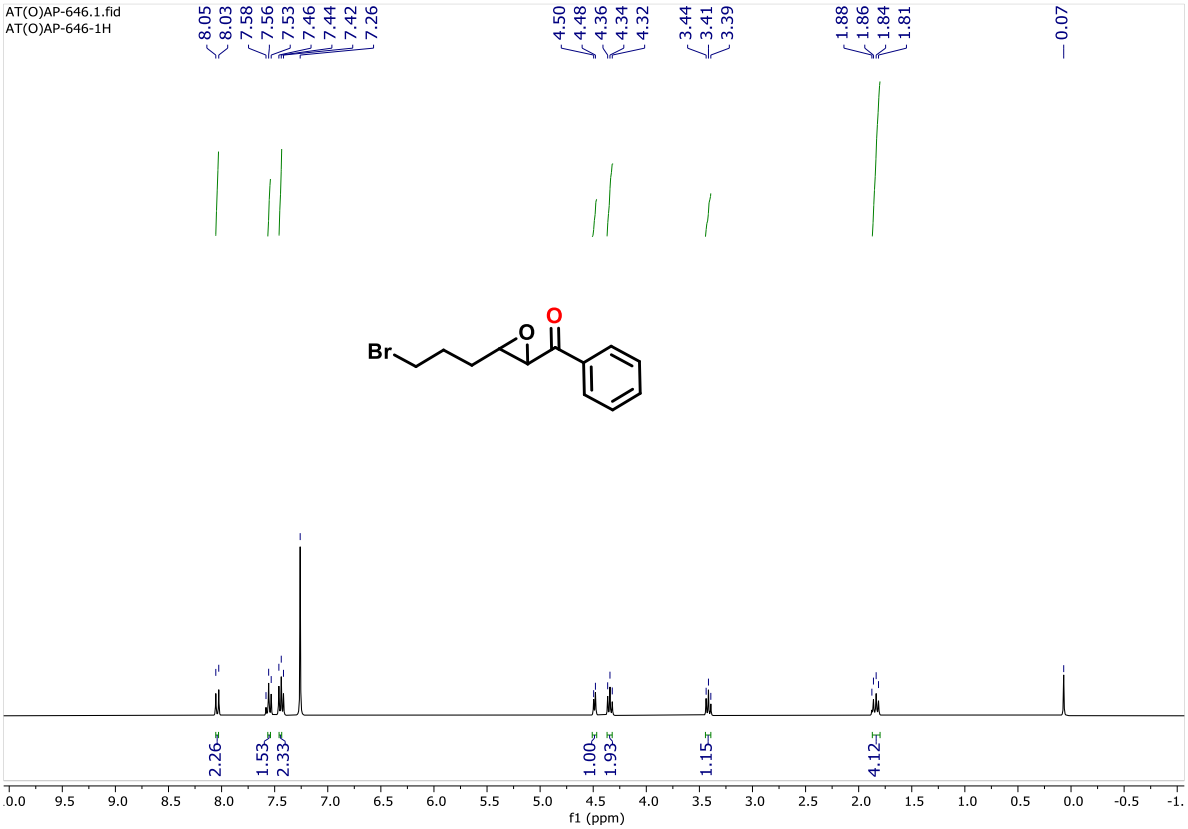

Figure 5.72. ^{1}H NMR (300 MHz) spectrum of **5d** in $CDCl_3$.

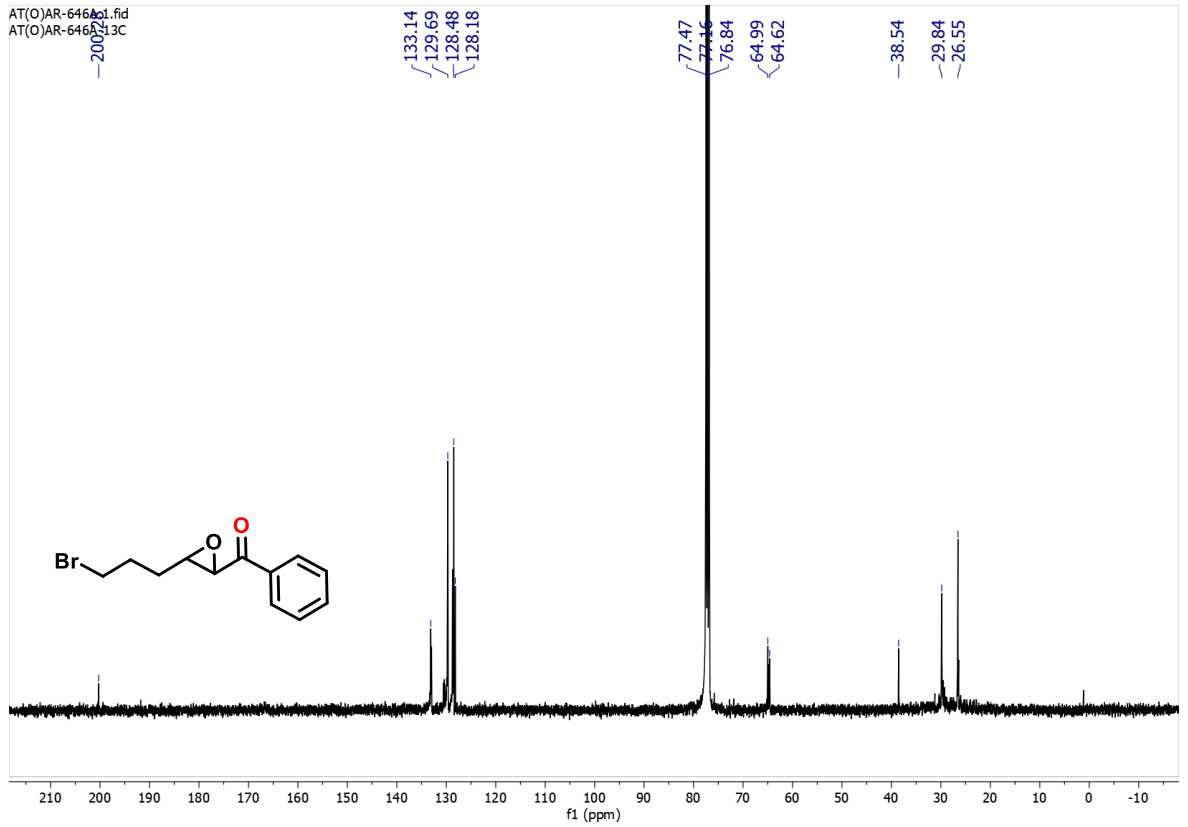

Figure 5.73. $^{13}C\{^{1}H\}$ NMR (75 MHz) spectrum of **5d** in $CDCl_3$.

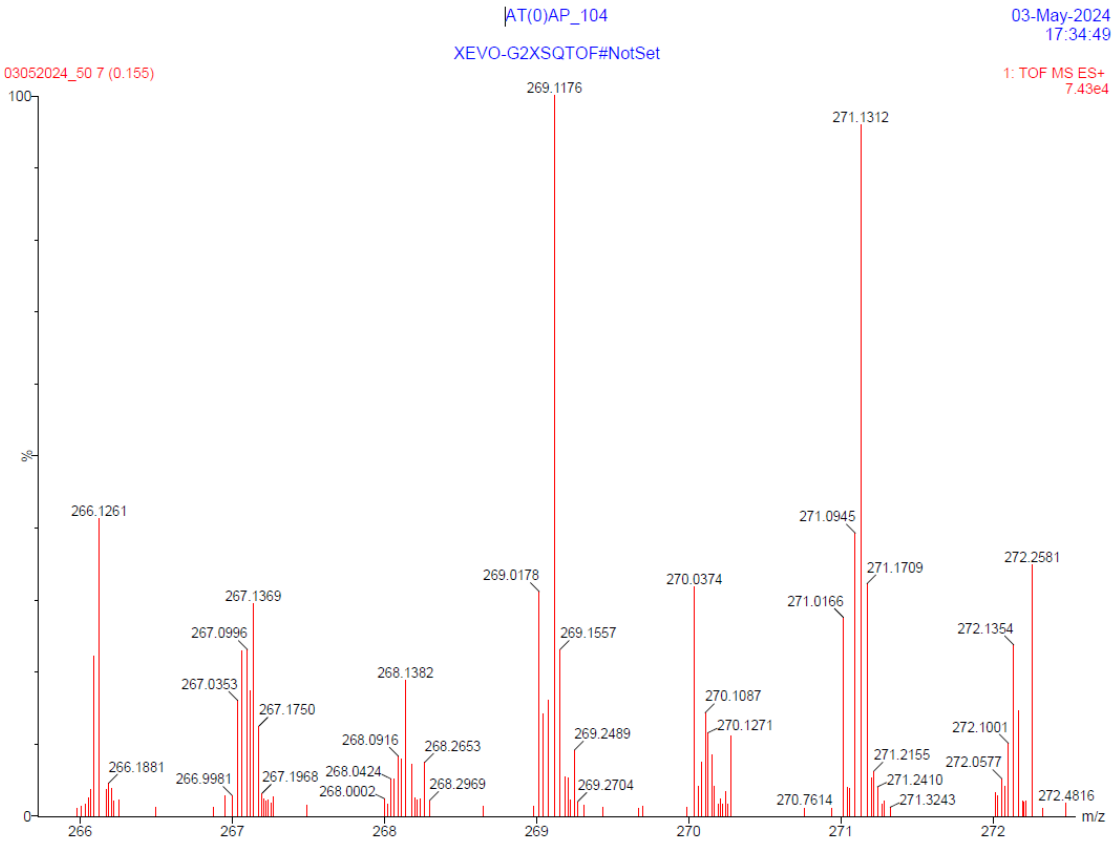

Figure 5.74. HRMS of **5d**.

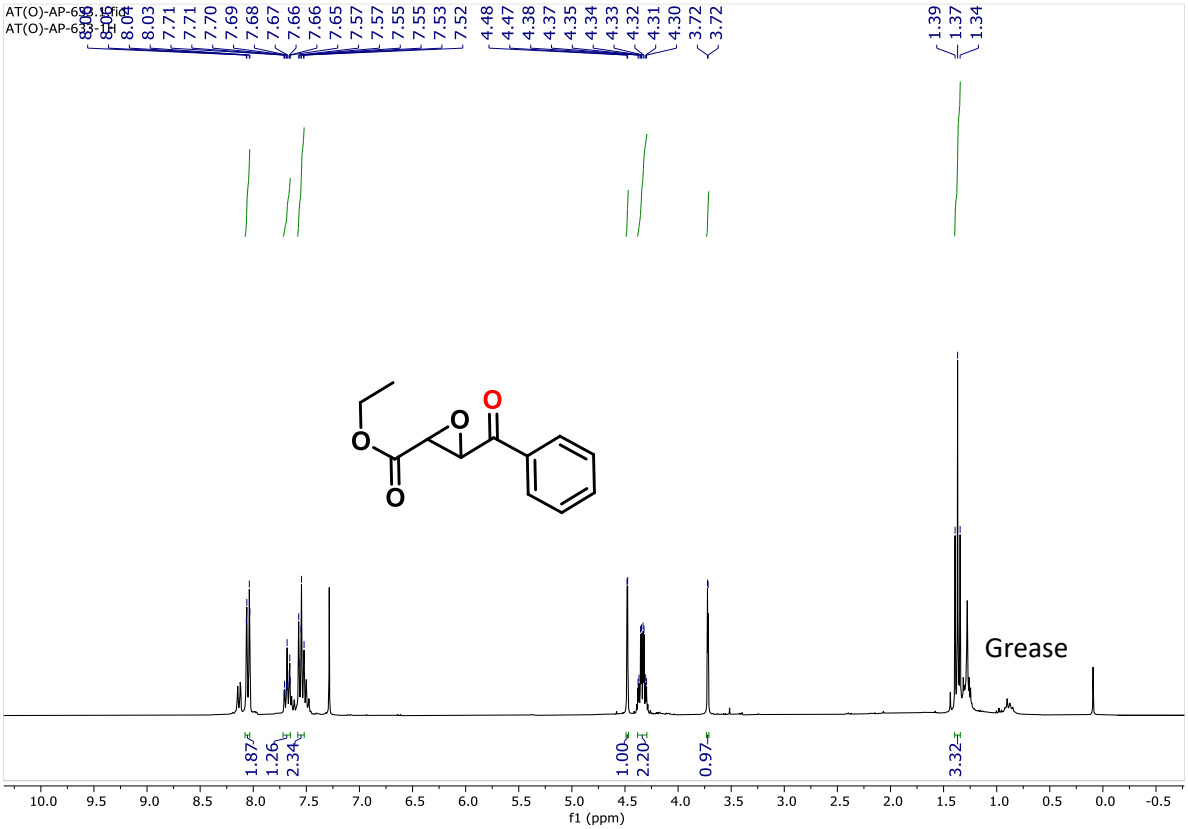

Figure 5.75. ^{1}H NMR (300 MHz) spectrum of **5e** in $CDCl_3$.

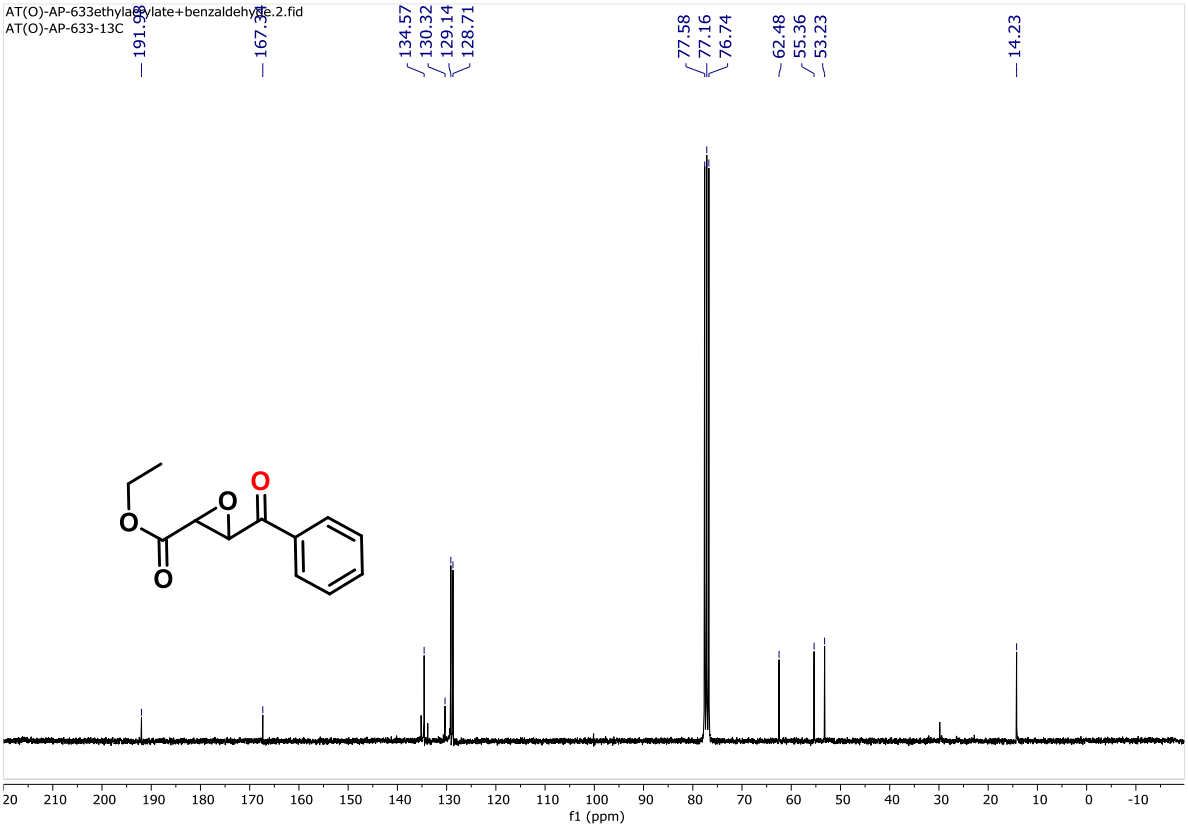

Figure 5.76. $^{13}C\{^{1}H\}$ NMR (75 MHz) spectrum of **5e** in $CDCl_3$.

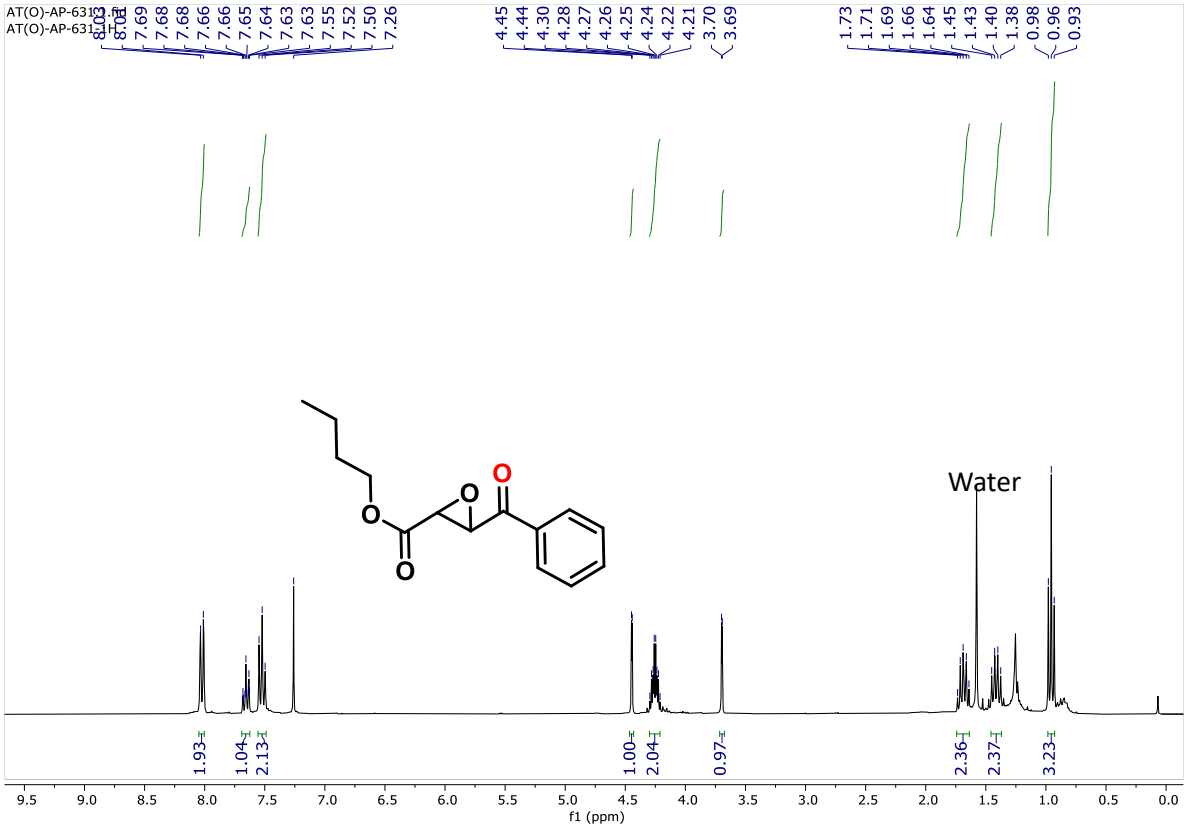

Figure 5.77. ^{1}H NMR (300 MHz) spectrum of **5f** in $CDCl_3$.

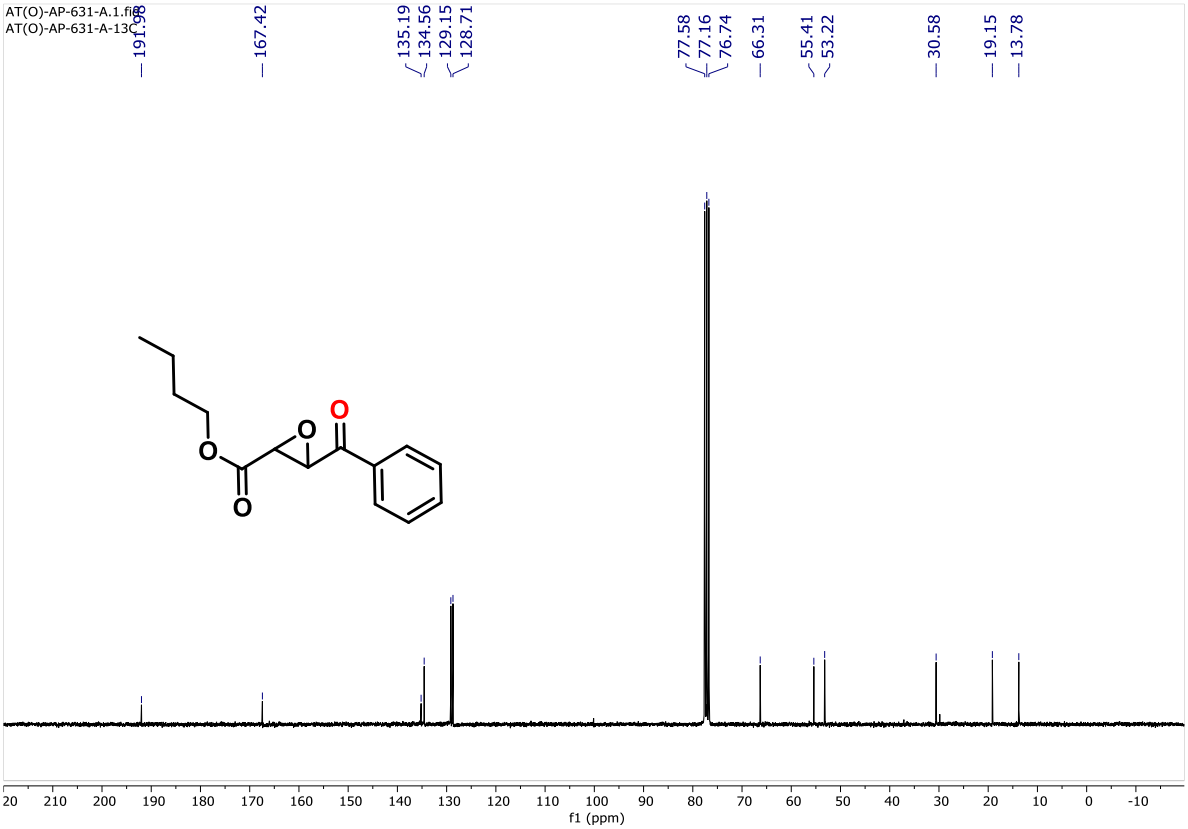

Figure 5.78. $^{13}C\{^{1}H\}$ NMR (75 MHz) spectrum of **5f** in $CDCl_3$.

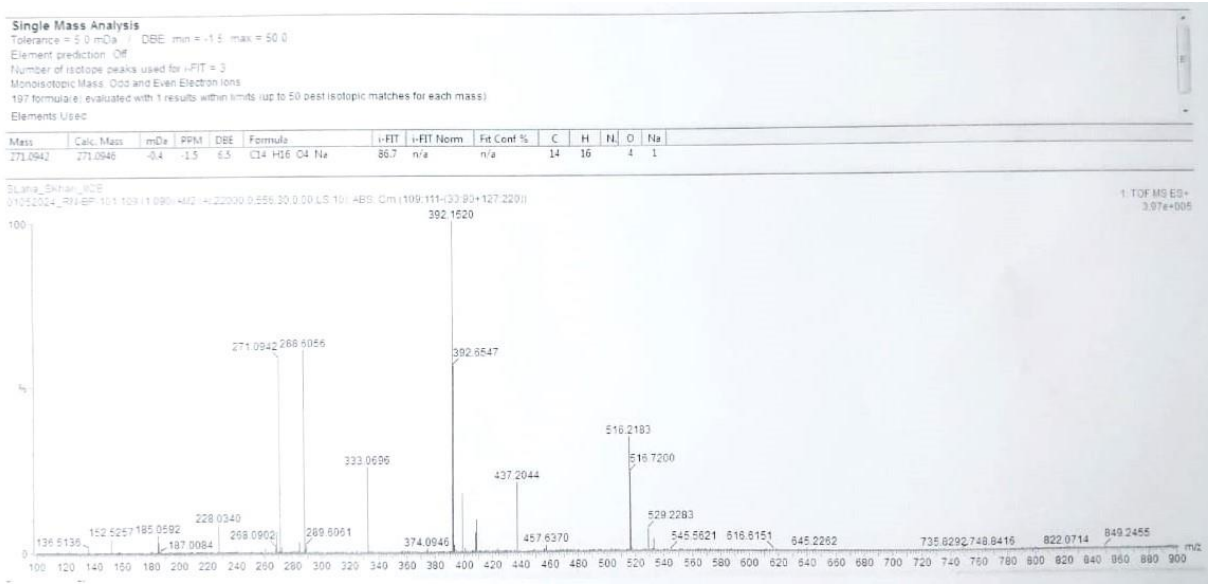

Figure 5.79. HRMS of **5f**.

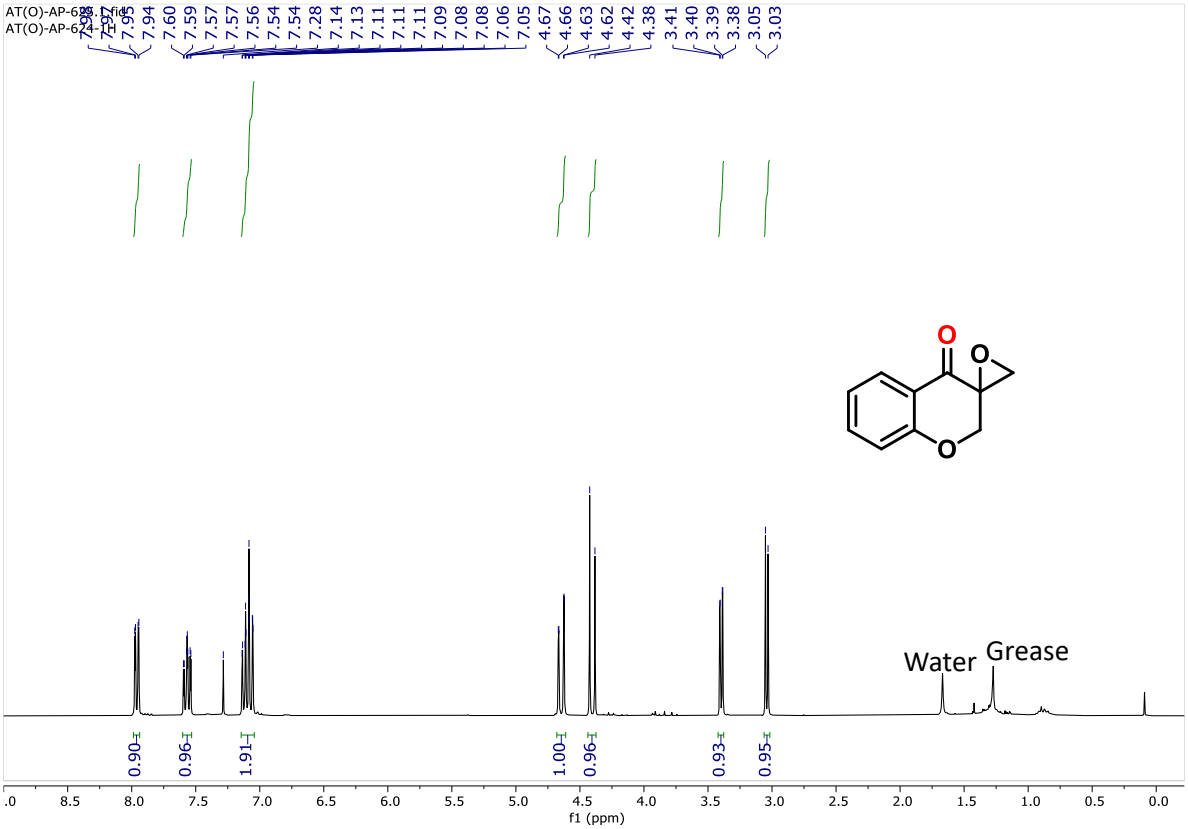

Figure 5.80. ^{1}H NMR (300 MHz) spectrum of **6a** in $CDCl_3$.

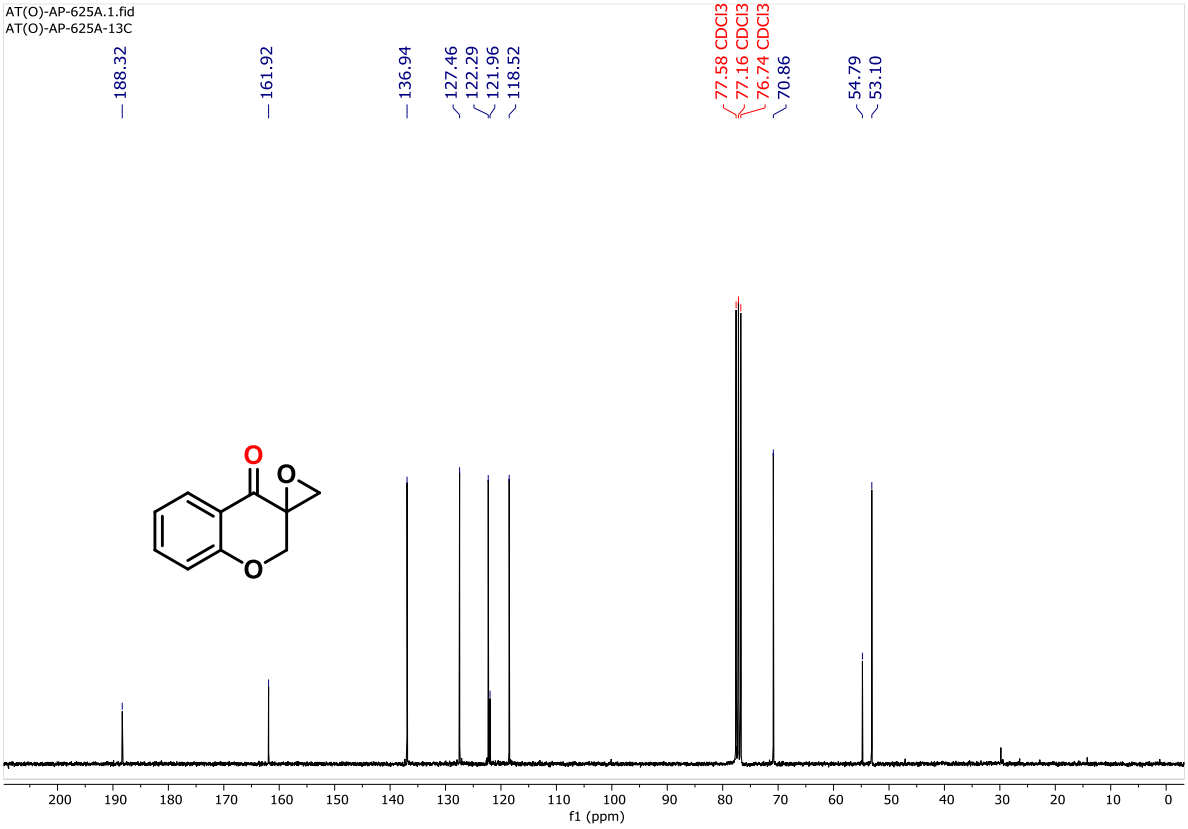

Figure 5.81. $^{13}C\{^{1}H\}$ NMR (75 MHz) spectrum of **6a** in $CDCl_3$.

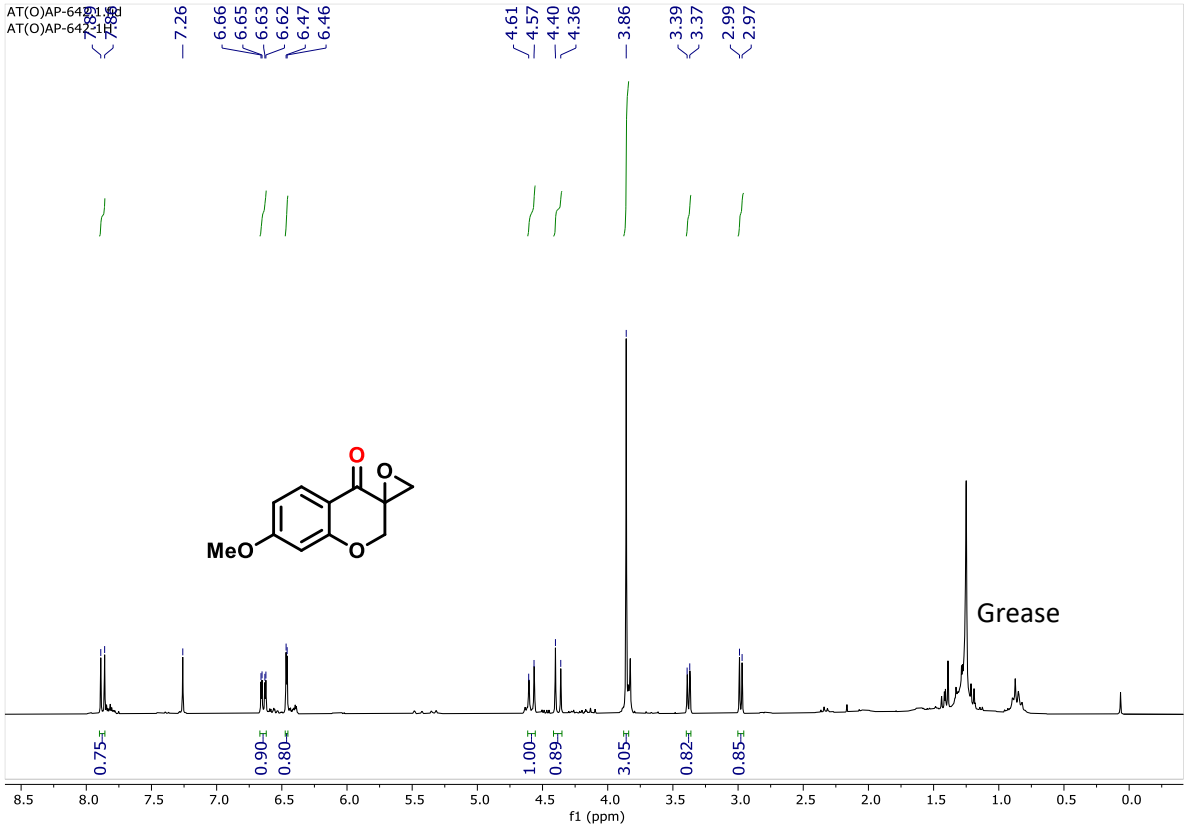

Figure 5.82. ^{1}H NMR (300 MHz) spectrum of **6b** in $CDCl_3$.

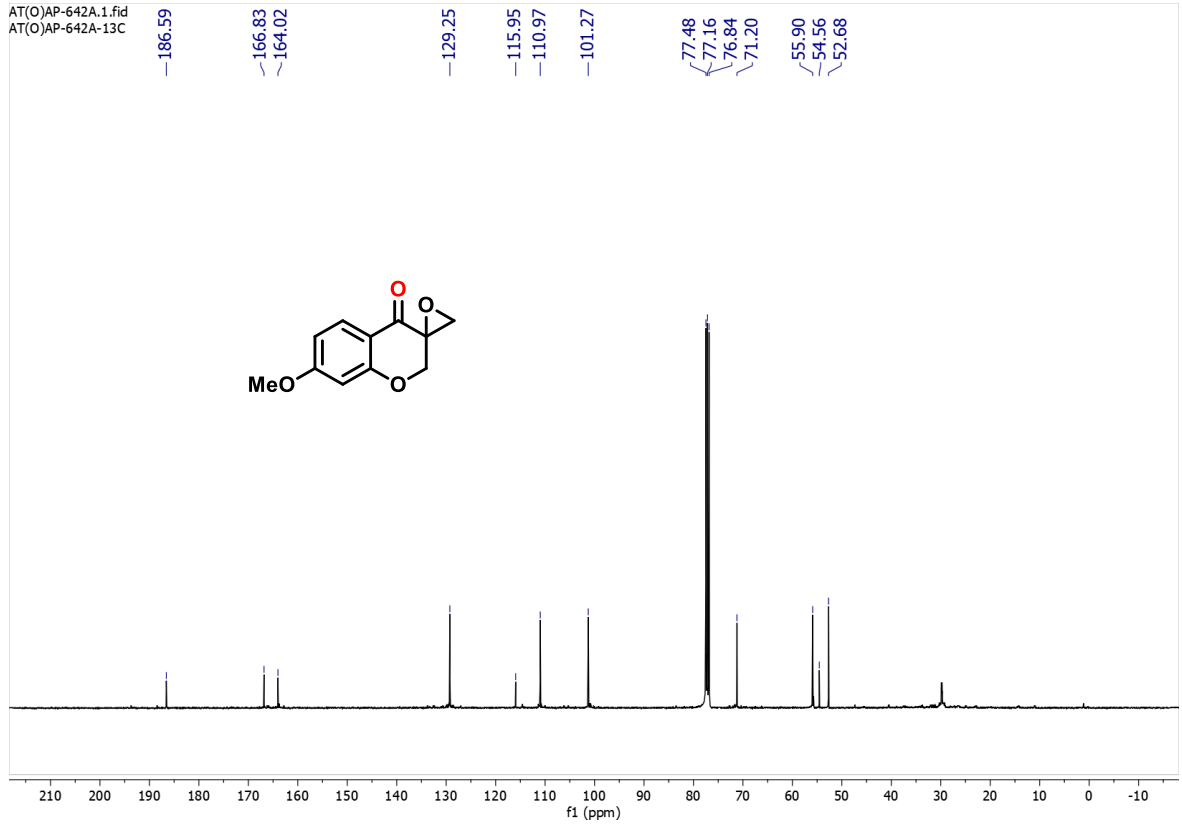

Figure 5.83. $^{13}C\{^{1}H\}$ NMR (75 MHz) spectrum of **6b** in $CDCl_3$.

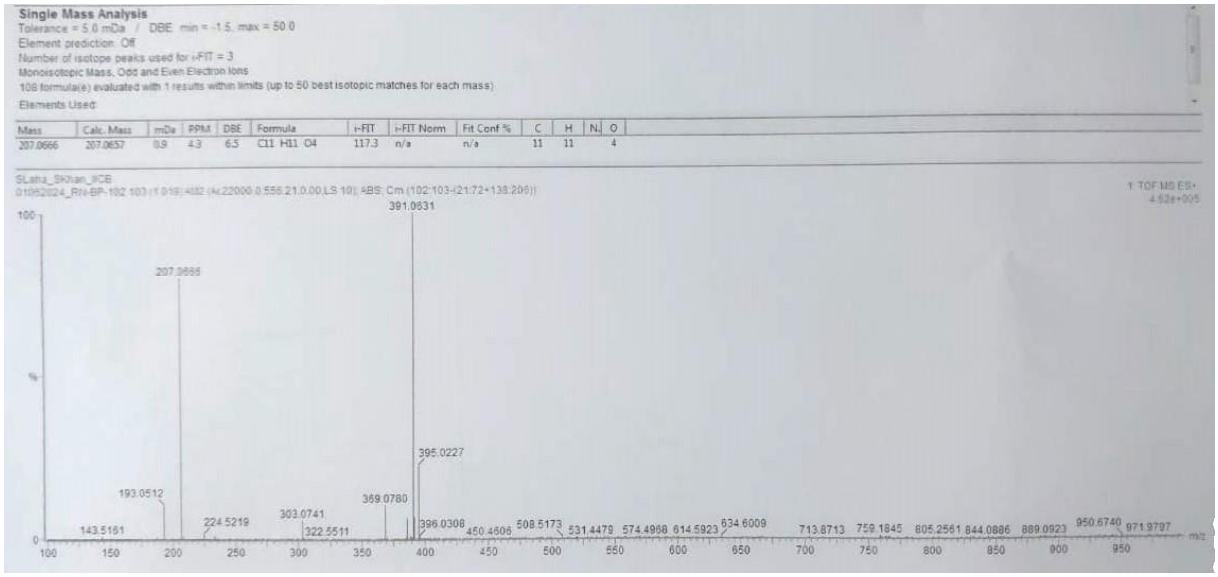

Figure 5.84. HRMS of **6b**.

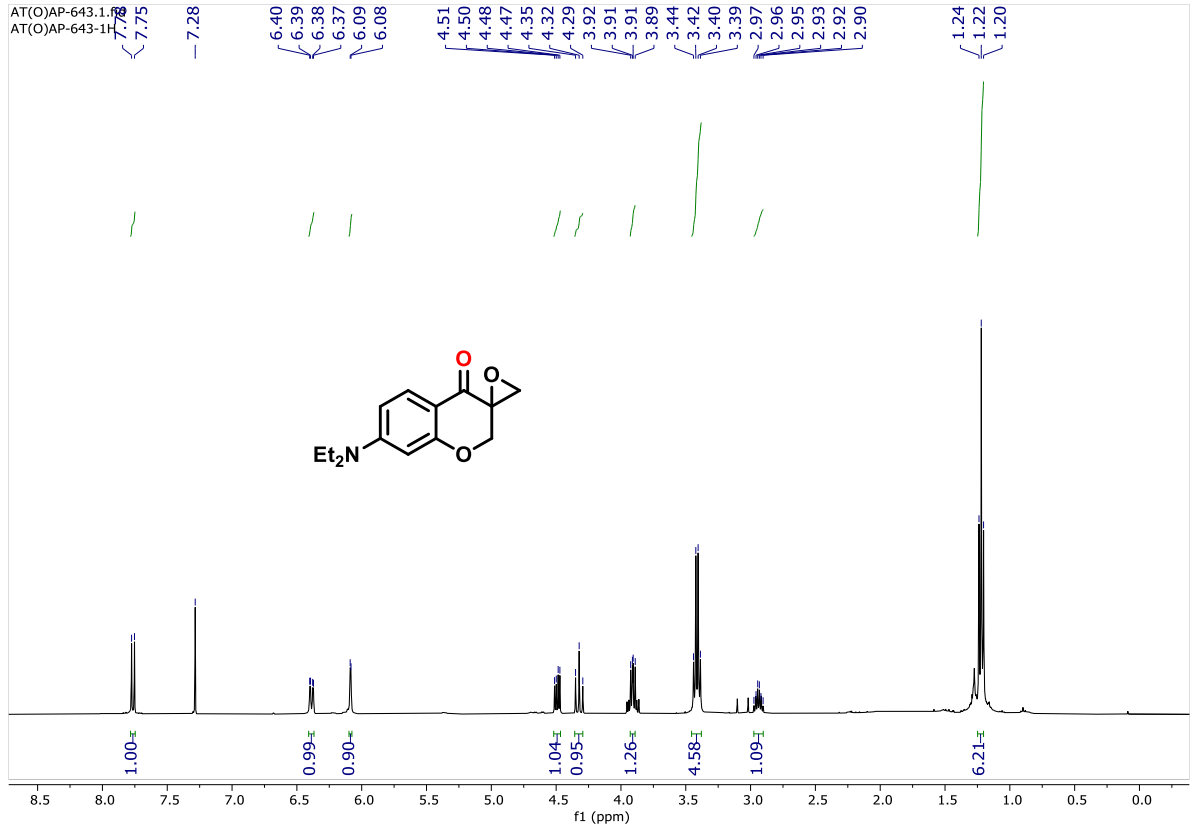

Figure 5.85. ^{1}H NMR (300 MHz) spectrum of **6c** in $CDCl_3$.

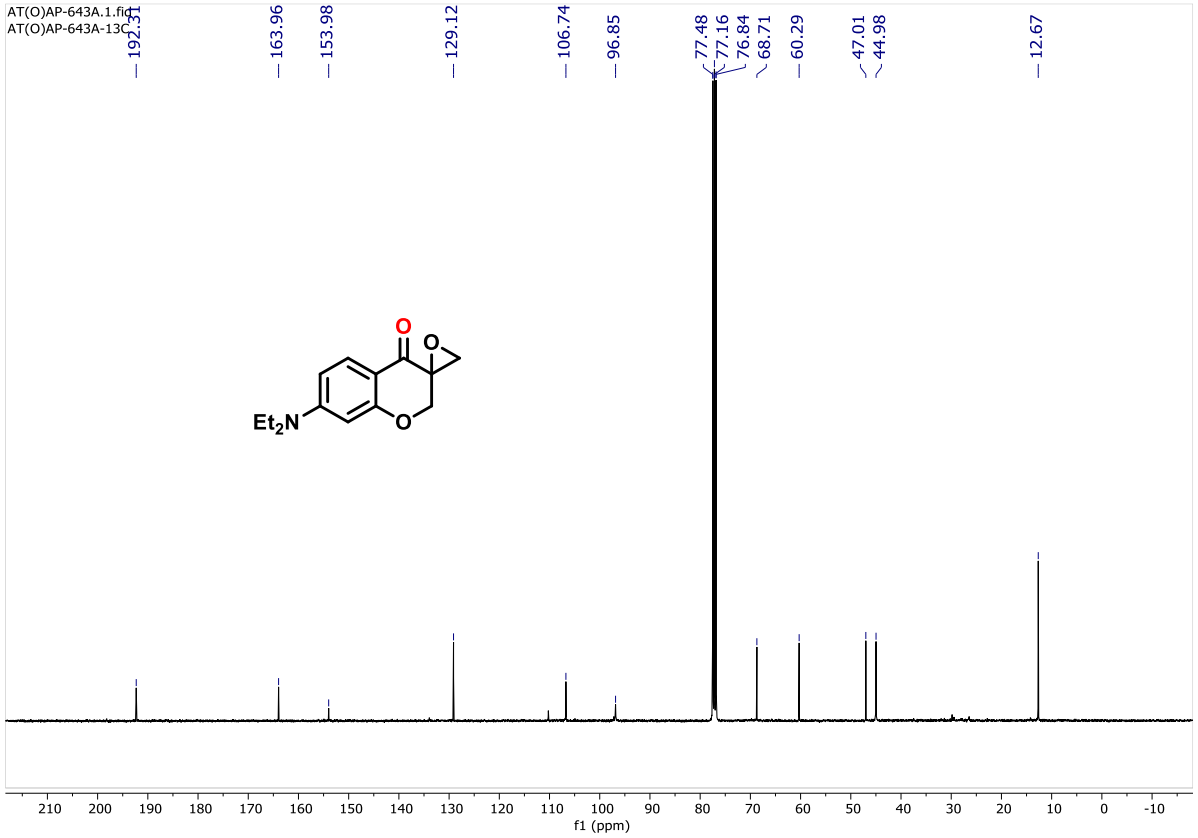

Figure 5.86. $^{13}C\{^{1}H\}$ NMR (75 MHz) spectrum of **6c** in $CDCl_3$.

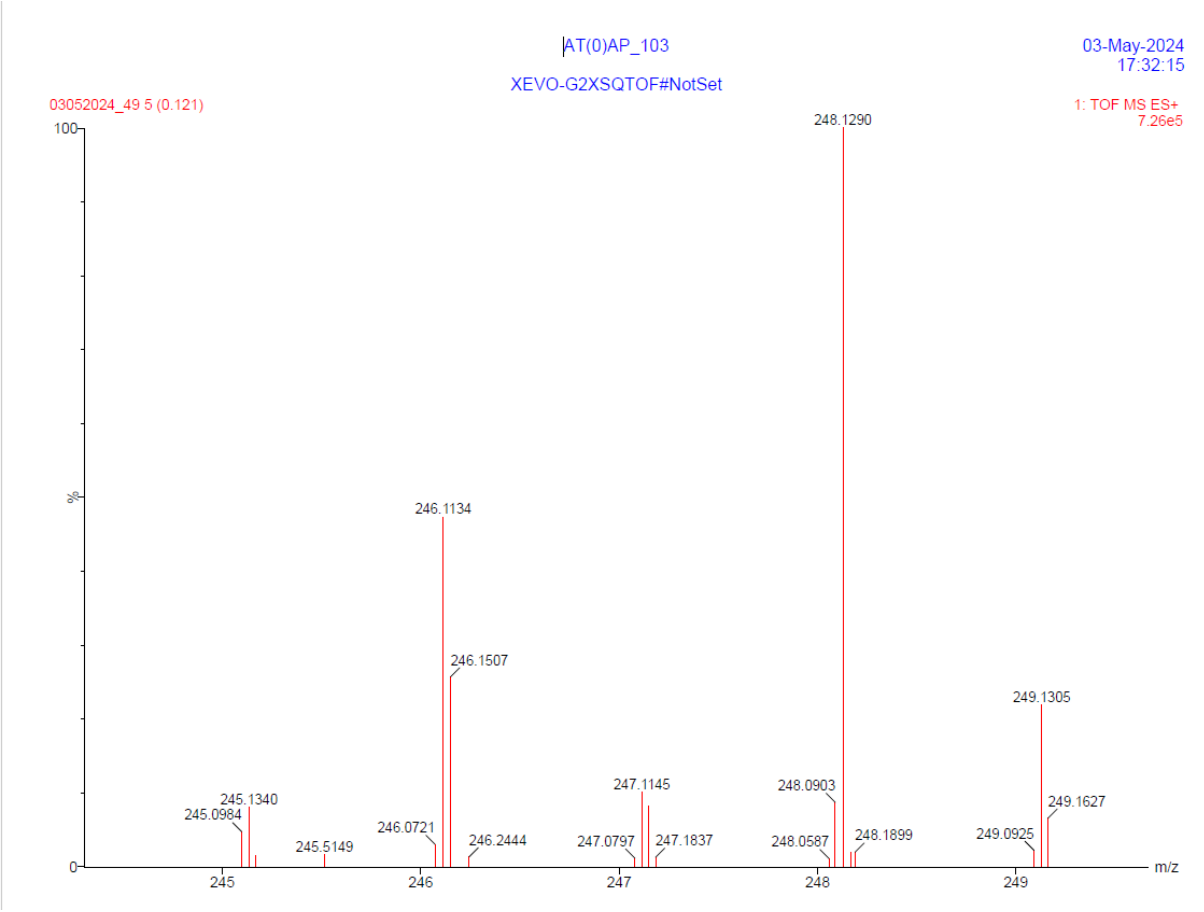

Figure 5.87. HRMS of **6c**.

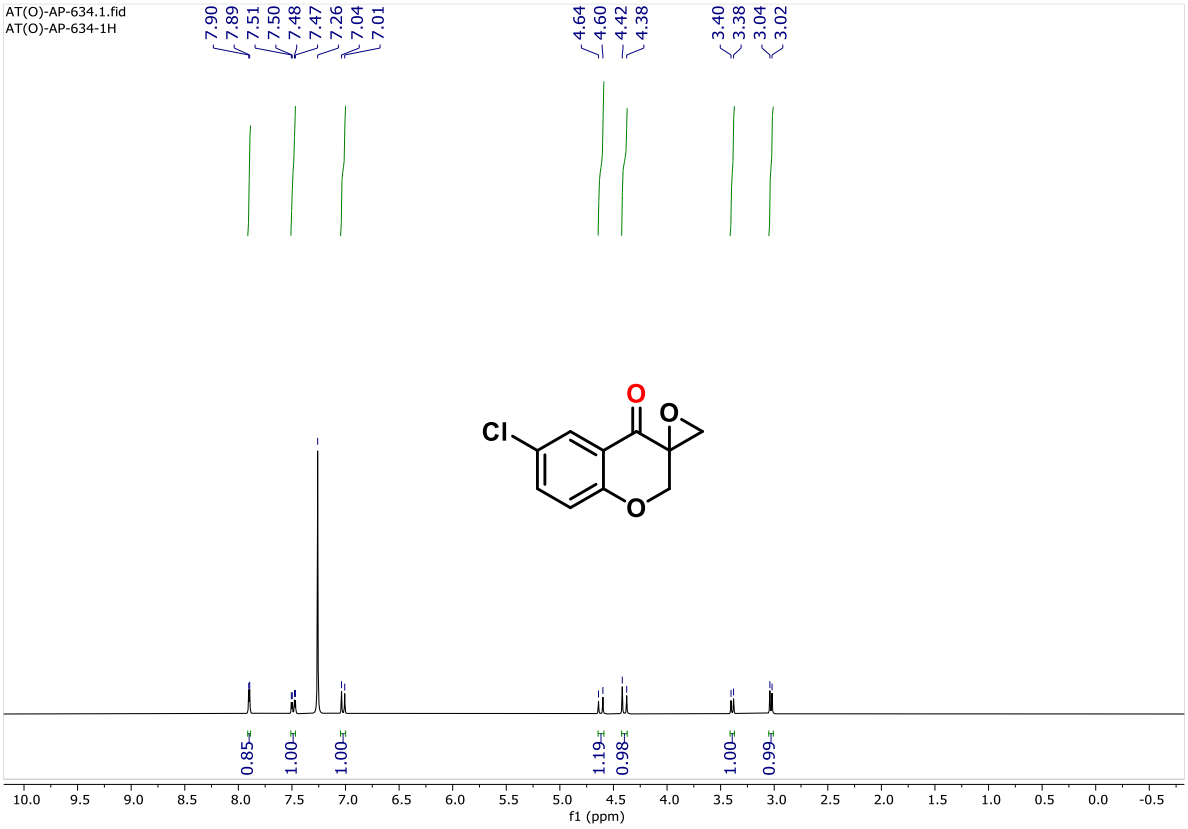

Figure 5.88. ^{1}H NMR (300 MHz) spectrum of **6d** in $CDCl_3$.

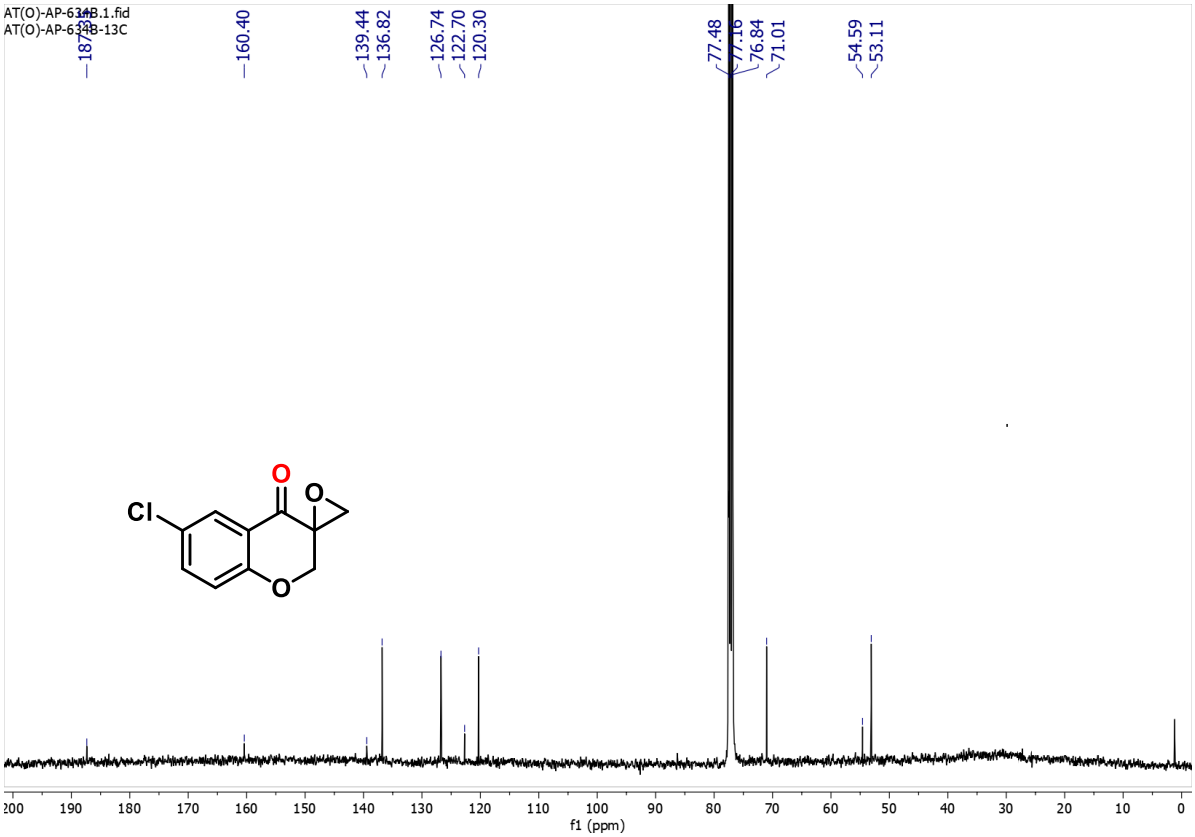

Figure 5.89. $^{13}C\{^{1}H\}$ NMR (75 MHz) spectrum of **6d** in $CDCl_3$.

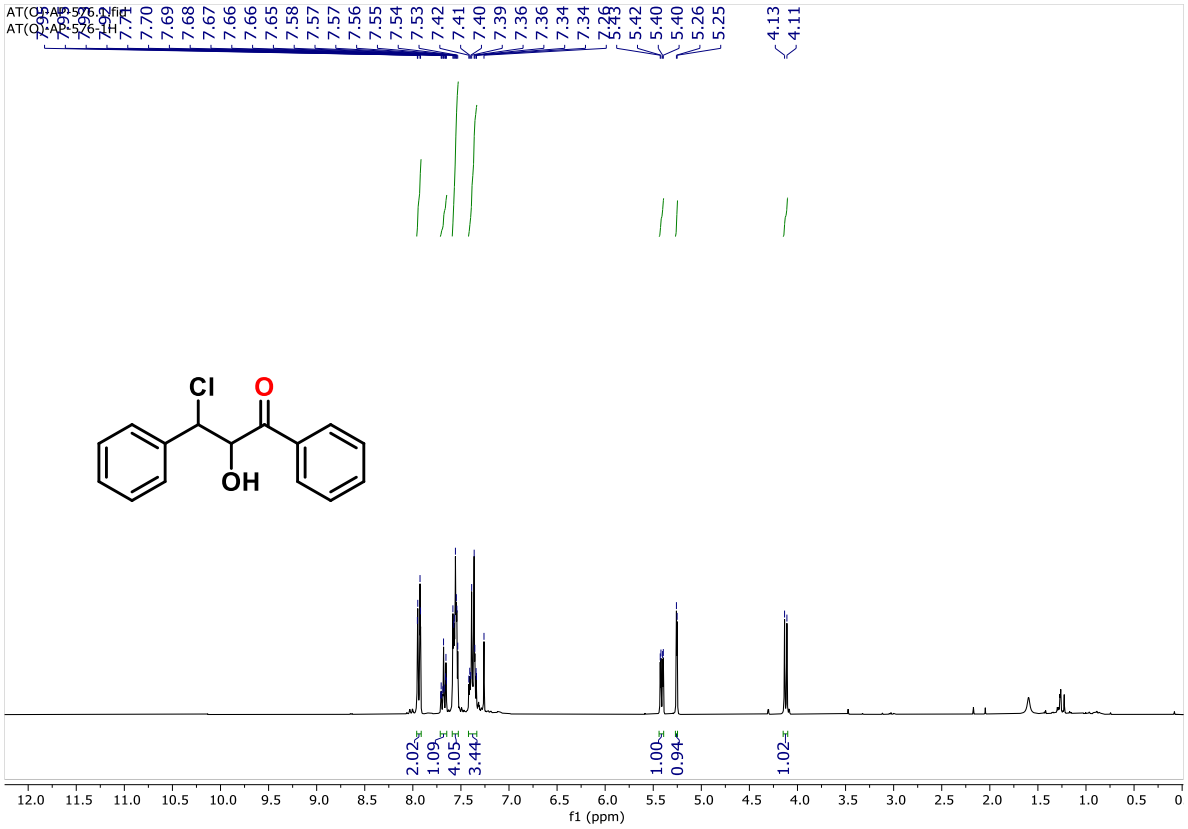

Figure 5.90. ^{1}H NMR (300 MHz) spectrum of **7** in $CDCl_3$.

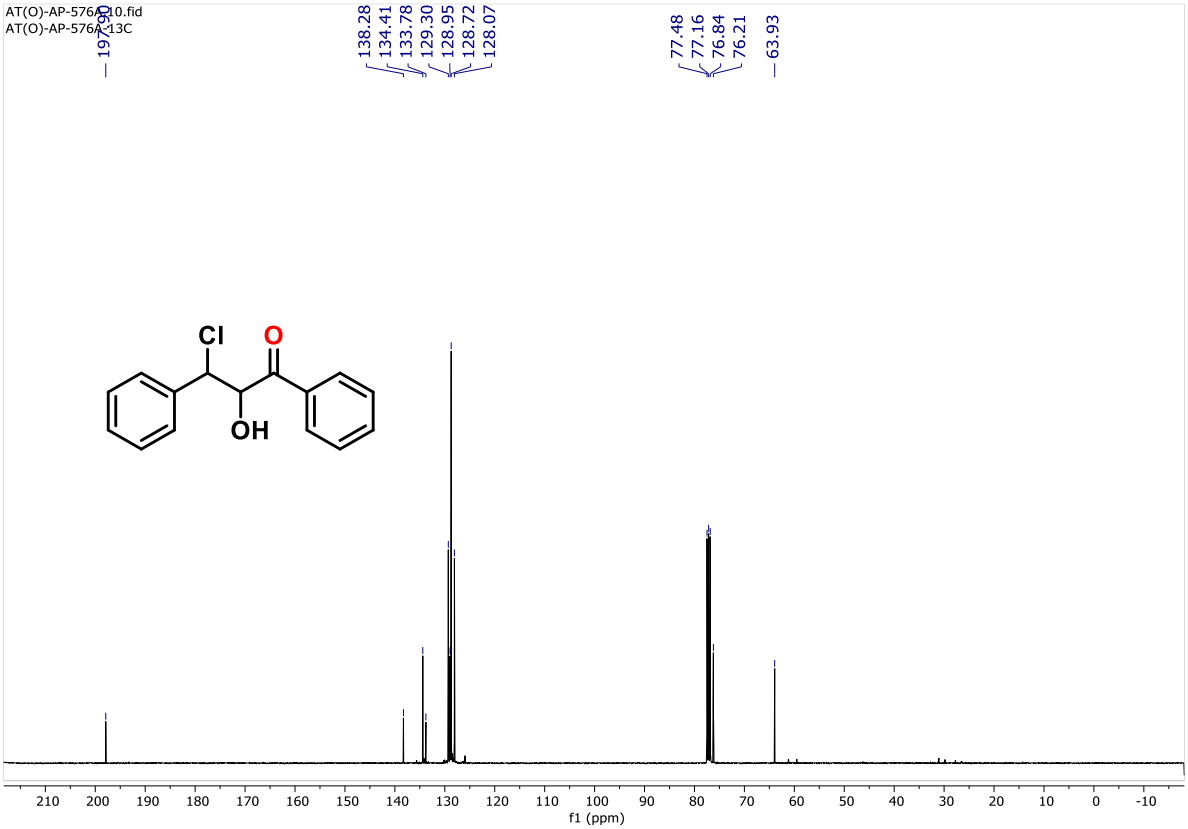

Figure 5.91. $^{13}C\{^{1}H\}$ NMR (75 MHz) spectrum of **7** in $CDCl_3$.

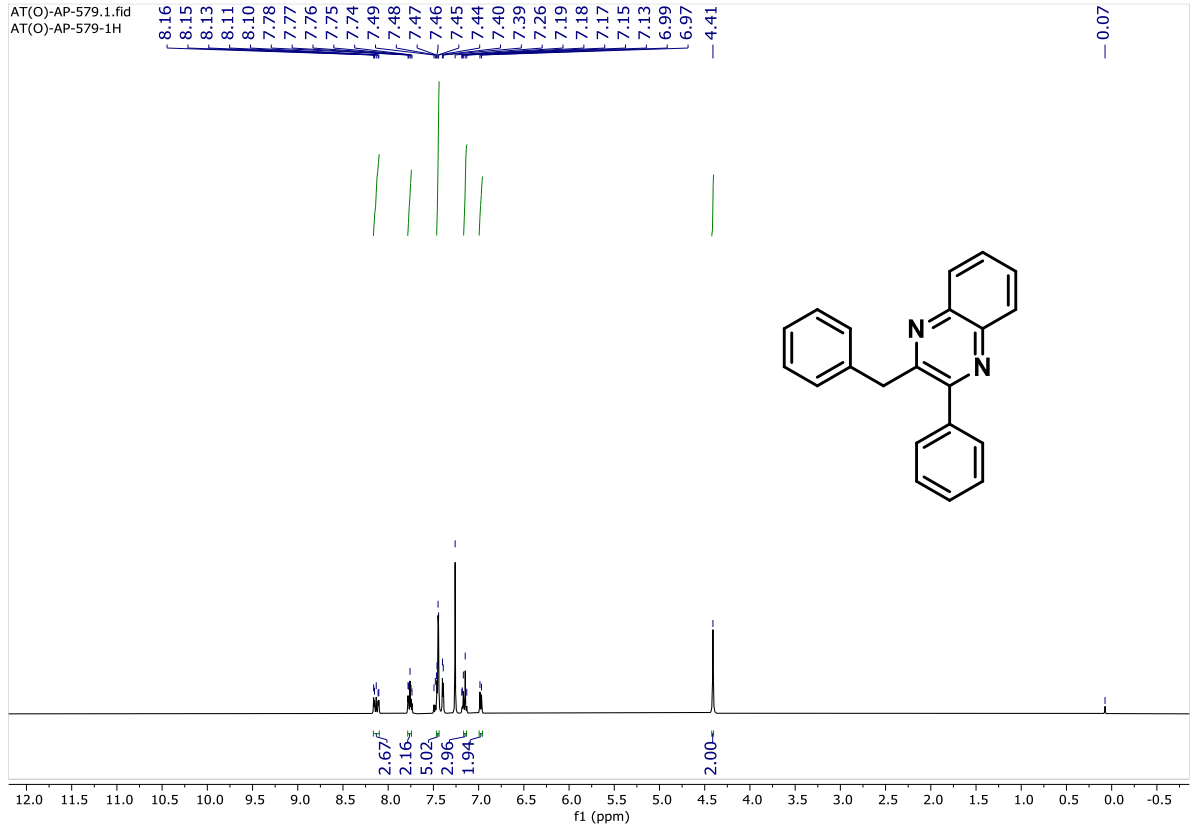

Figure 5.92. ^{1}H NMR (300 MHz) spectrum of **8** in $CDCl_3$.

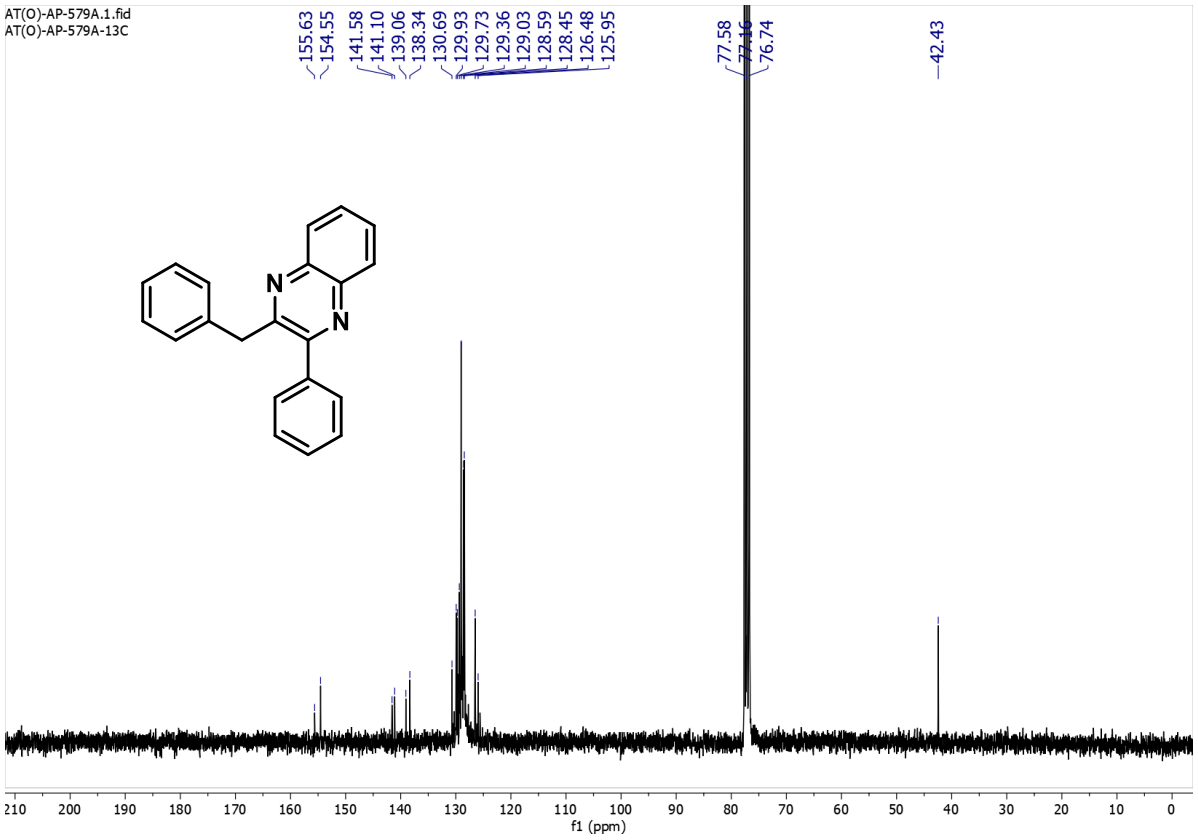

Figure 5.93. $^{13}C\{^{1}H\}$ NMR (75 MHz) spectrum of **8** in $CDCl_3$.

Figure 5.94. ^{1}H NMR (300 MHz) spectrum of **9** in $CDCl_3$.

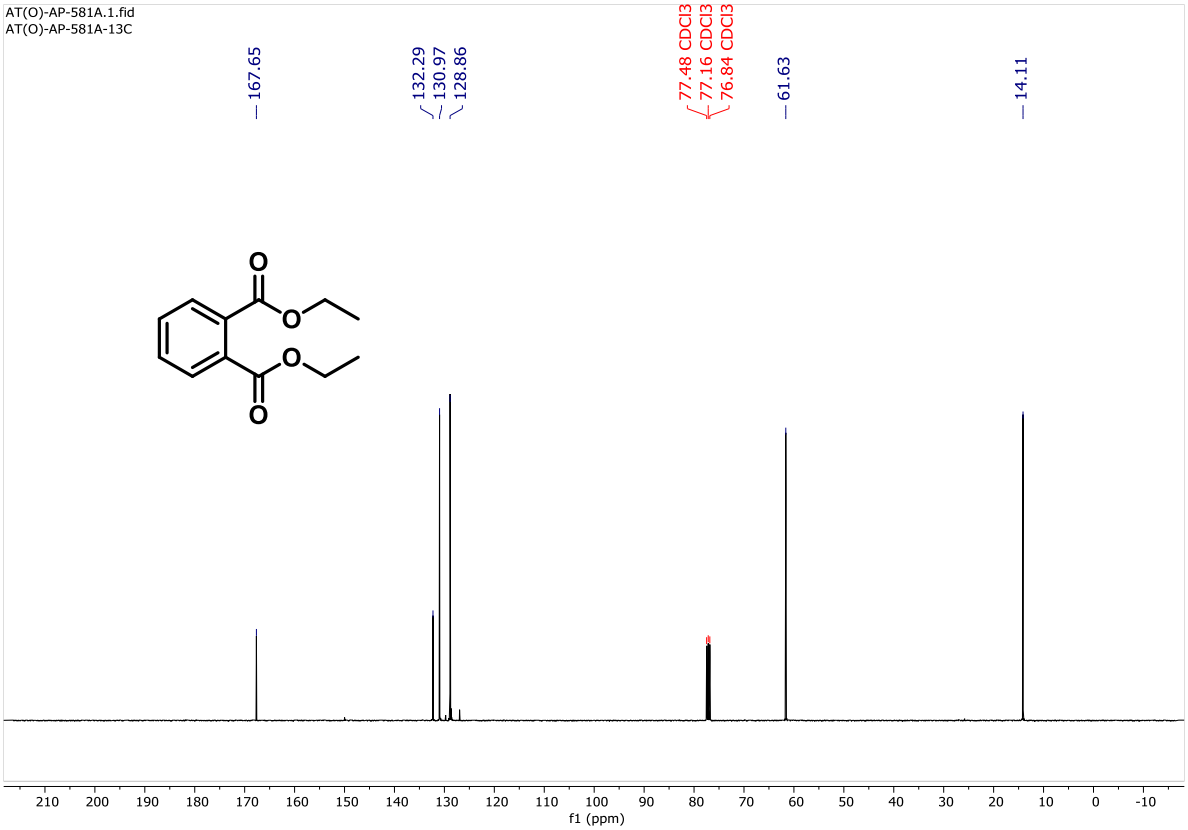

Figure 5.95. $^{13}C\{^{1}H\}$ NMR (75 MHz) spectrum of **9** in $CDCl_3$.

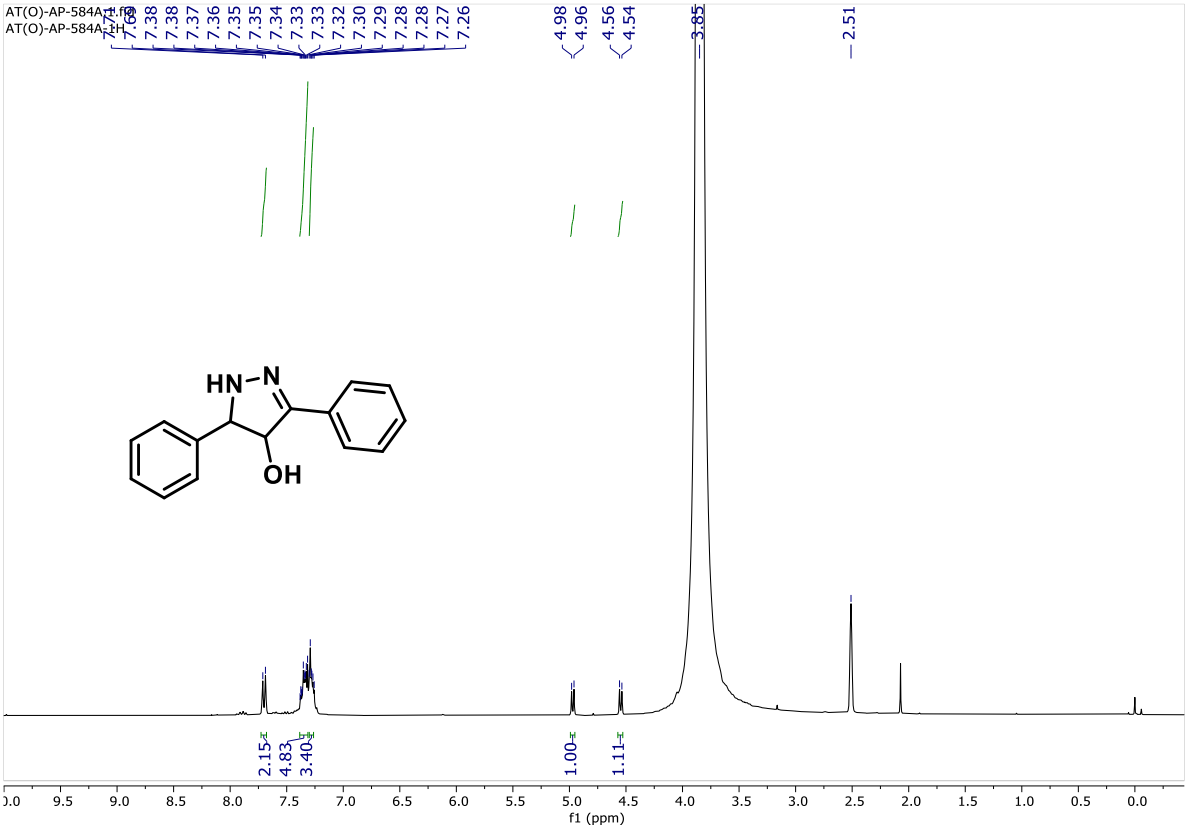

Figure 5.96. ^{1}H NMR (300 MHz) spectrum of **10** in DMSO-d_6.

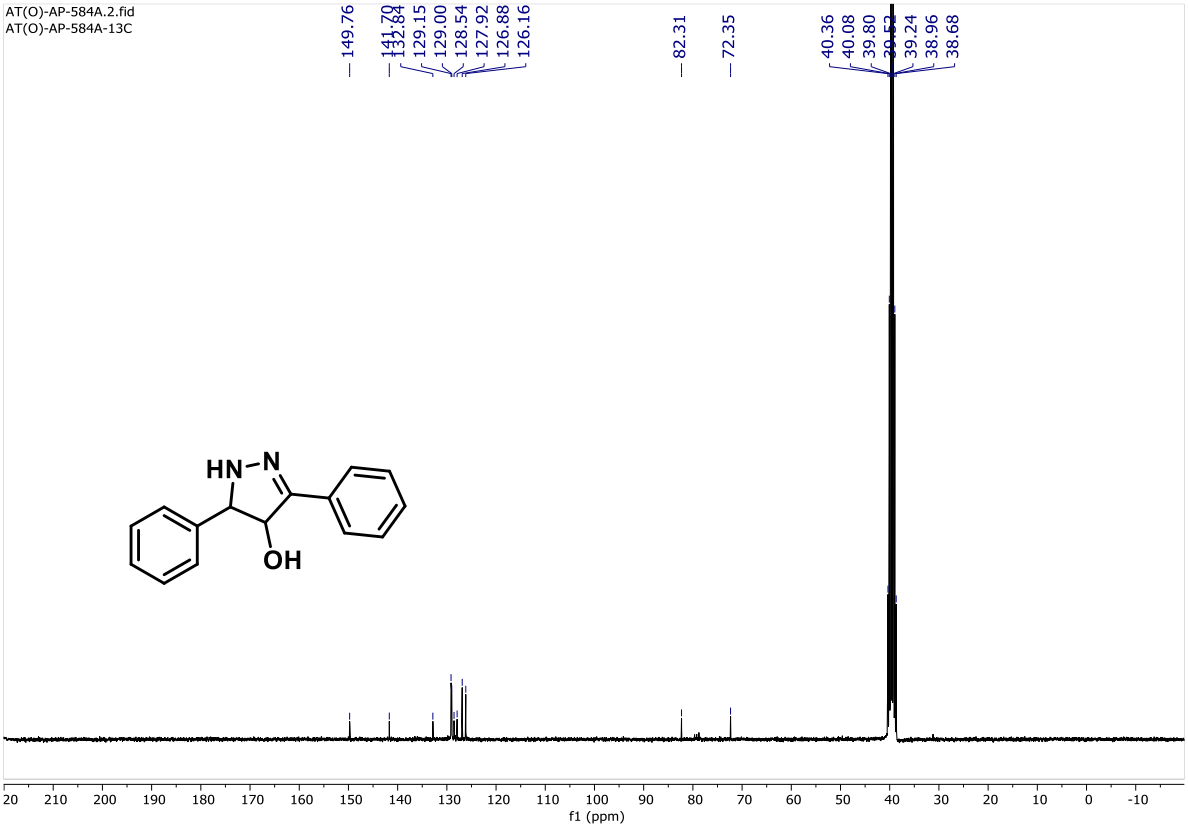

Figure 5.97. ^{13}C{^{1}H} NMR (75 MHz) spectrum of **10** in DMSO-d_6.

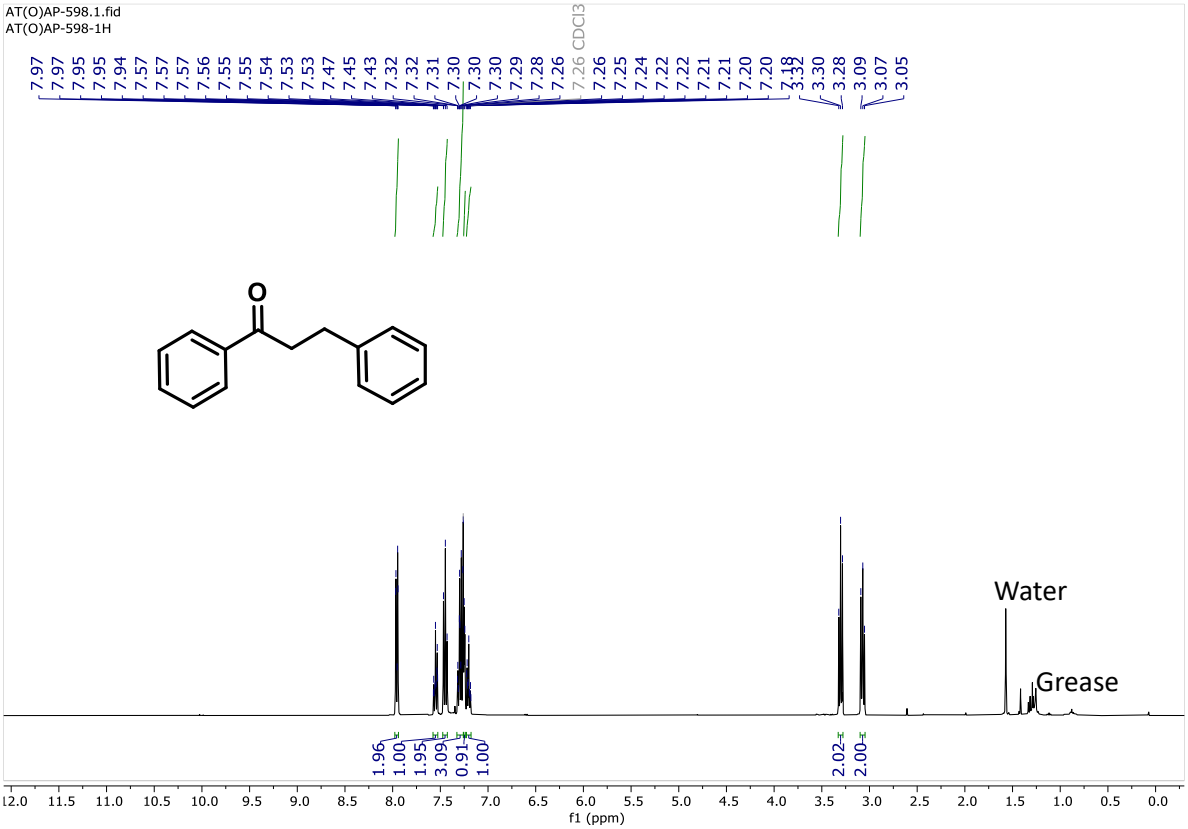

Figure 5.98. ^{1}H NMR (300 MHz) spectrum of **12** in $CDCl_3$.

Figure 5.99. $^{13}C\{^{1}H\}$ NMR (75 MHz) spectrum of **12** in $CDCl_3$.

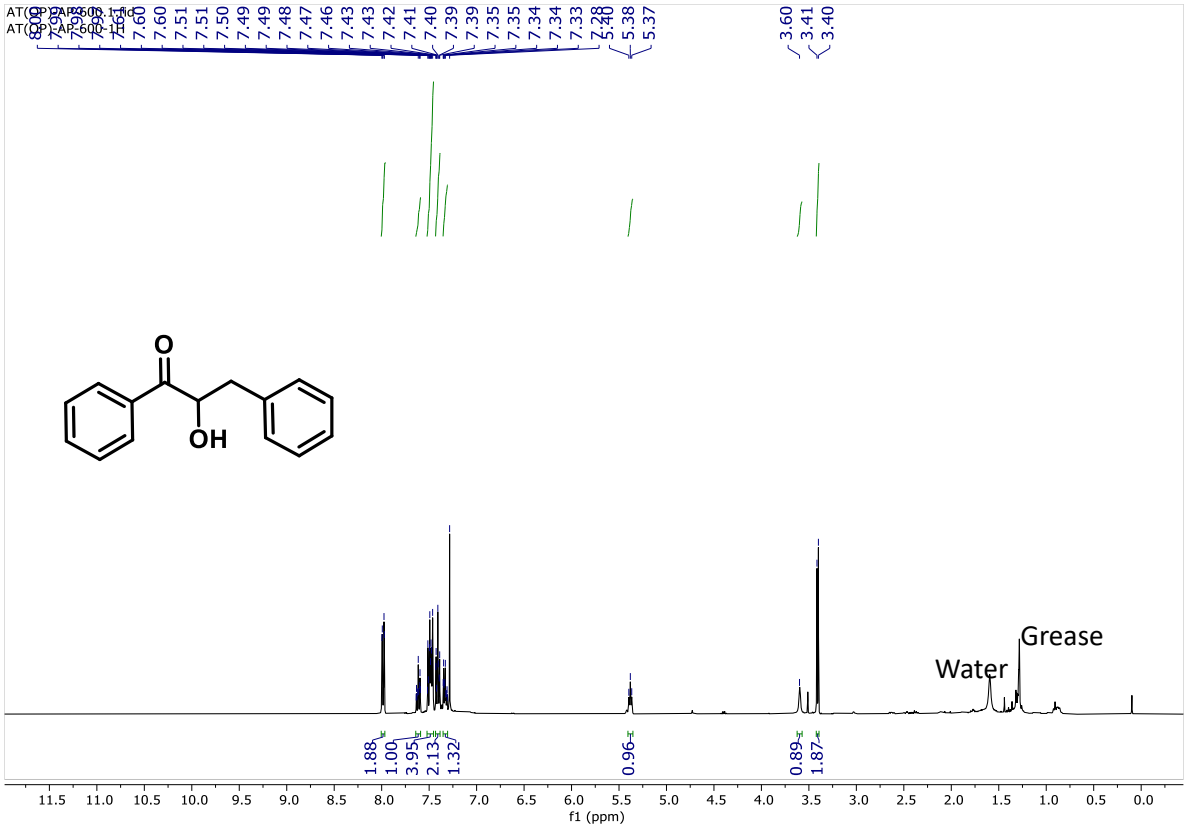

Figure 5.100. ^{1}H NMR (300 MHz) spectrum of **11** in $CDCl_3$.

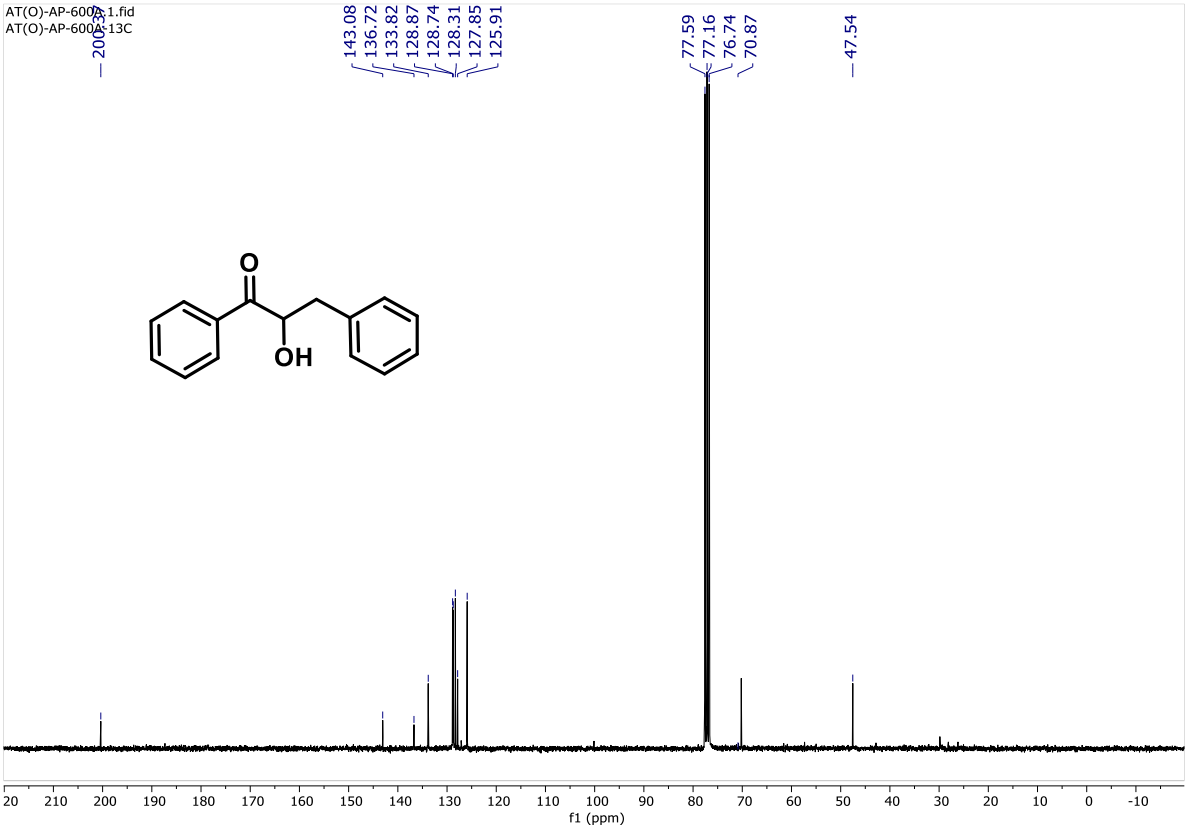

Figure 5.101. $^{13}C\{^{1}H\}$ NMR (75 MHz) spectrum of **11** in $CDCl_3$.

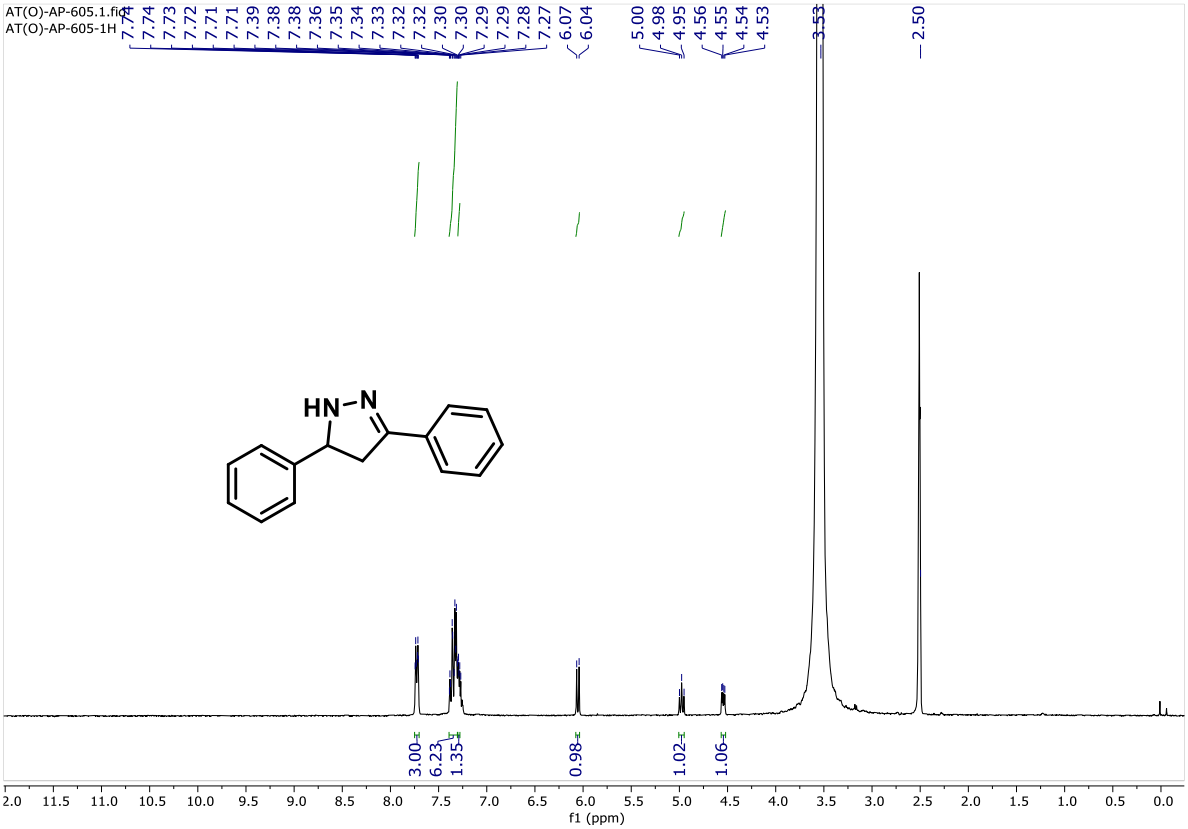

Figure 5.102. ^{1}H NMR (300 MHz) spectrum of **13** in DMSO-d_6.

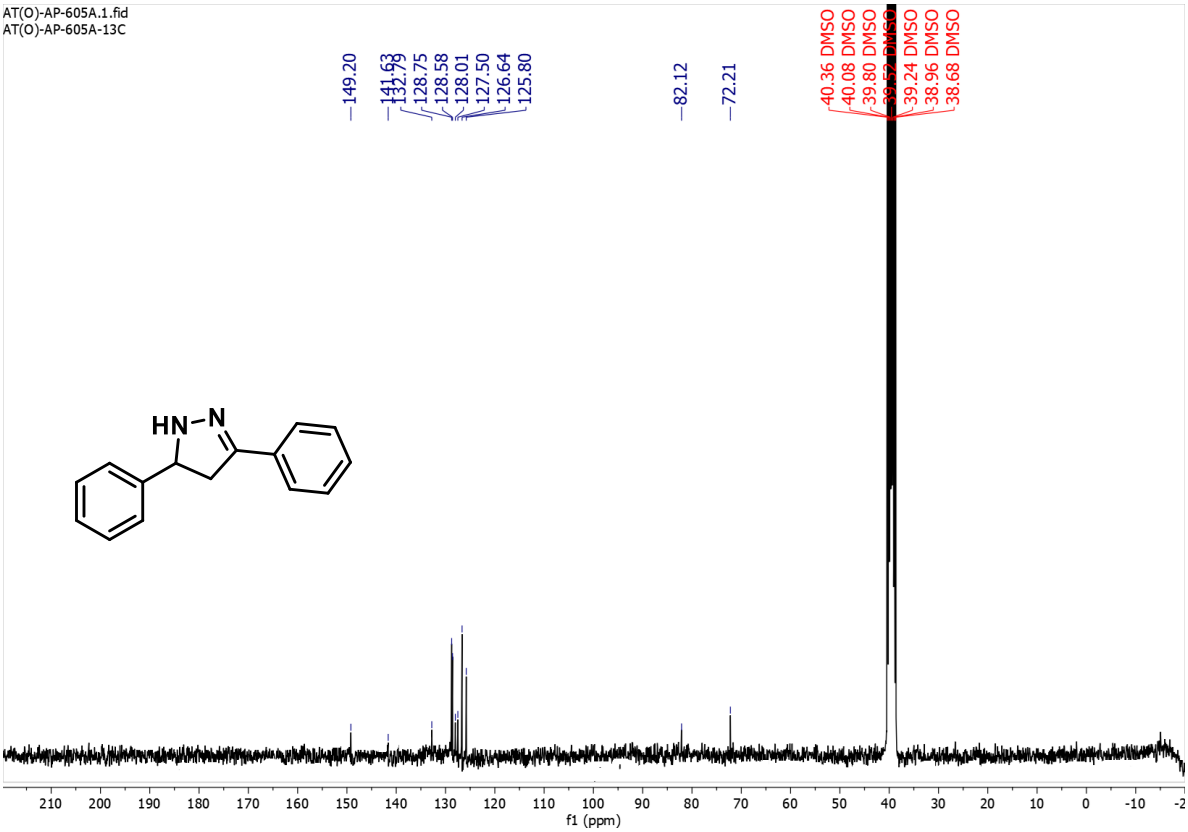

Figure 5.103. ^{13}C{^{1}H} NMR (75 MHz) spectrum of **13** in DMSO-d_6.

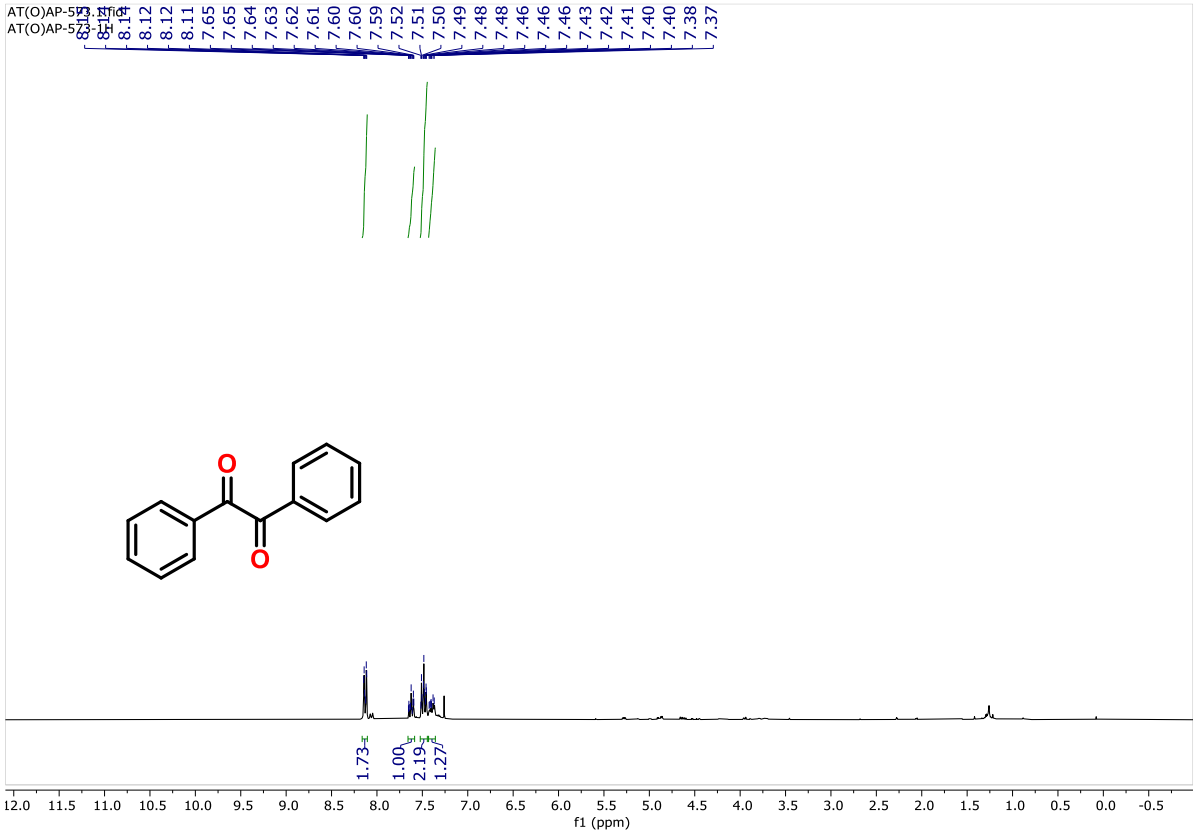

Figure 5.104. ^{1}H NMR (300 MHz) spectrum of **14** in $CDCl_3$.

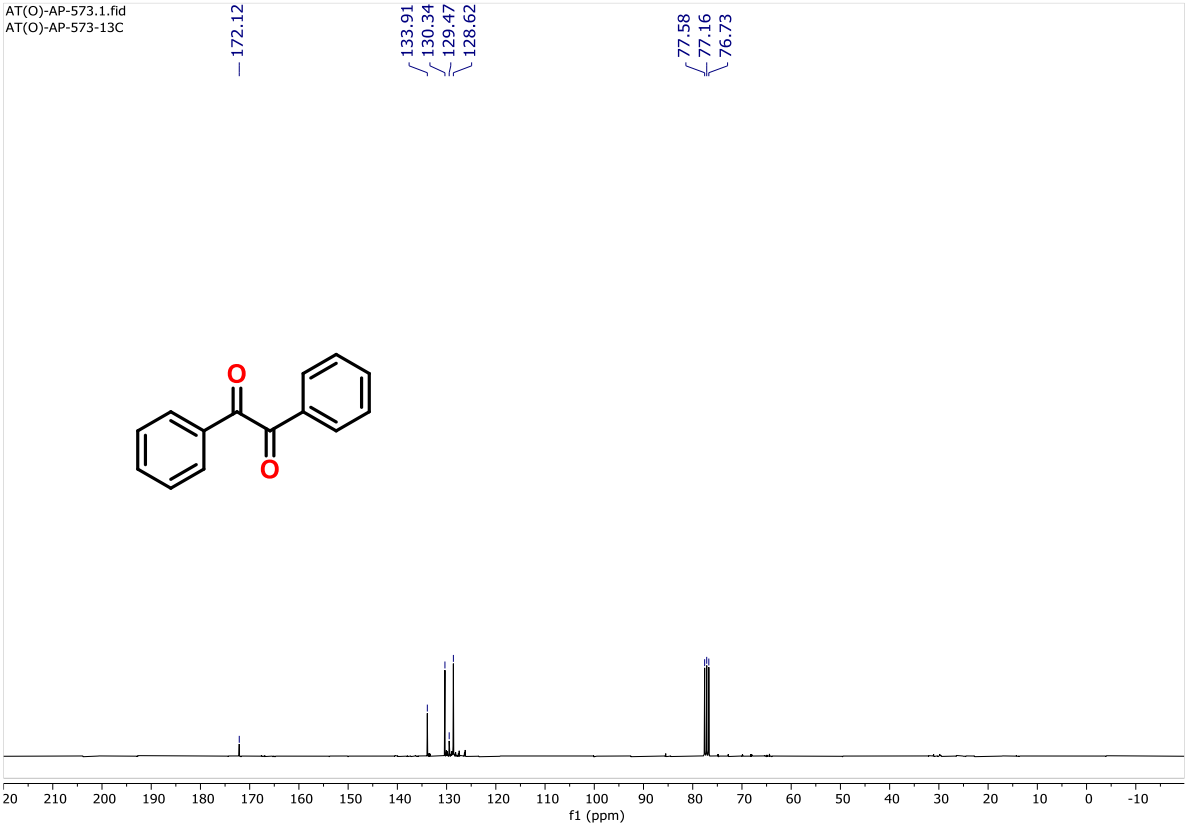

Figure 5.105. $^{13}C\{^{1}H\}$ NMR (75 MHz) spectrum of **14** in $CDCl_3$.

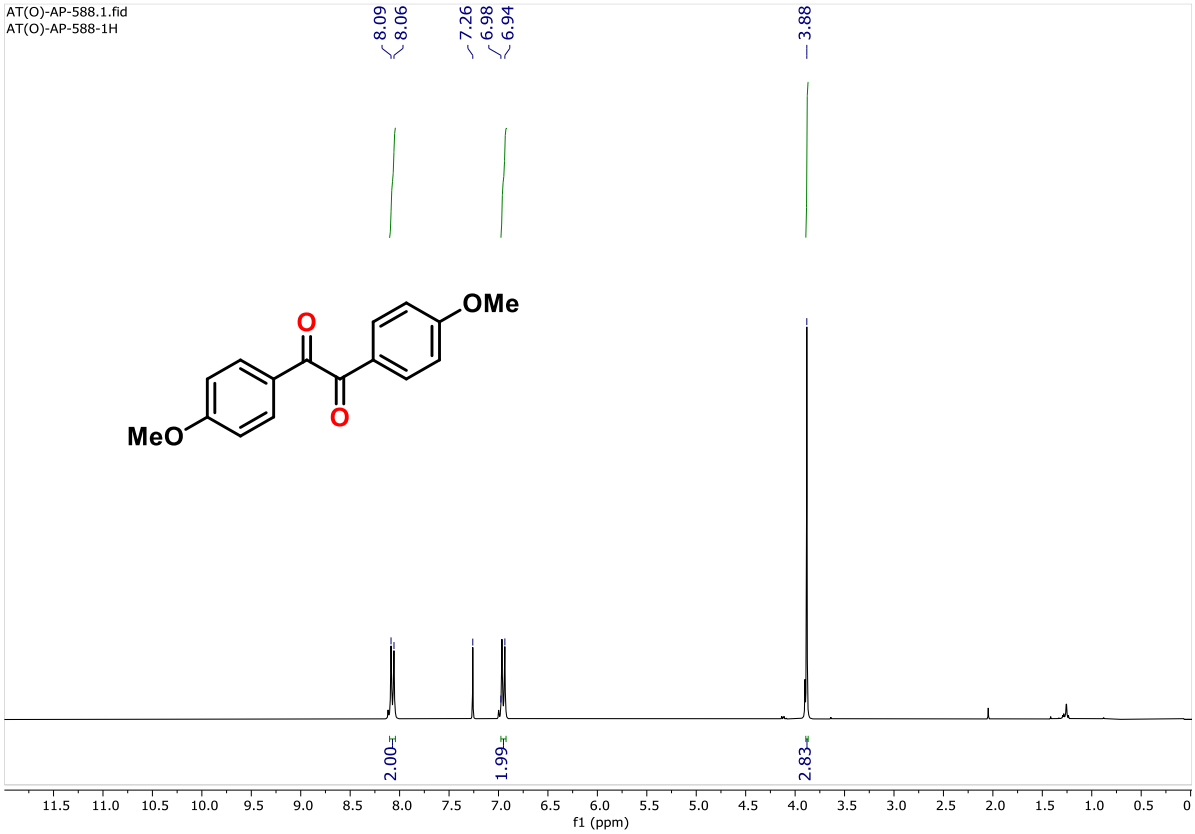

Figure 5.106. ^{1}H NMR (300 MHz) spectrum of **15** in $CDCl_3$.

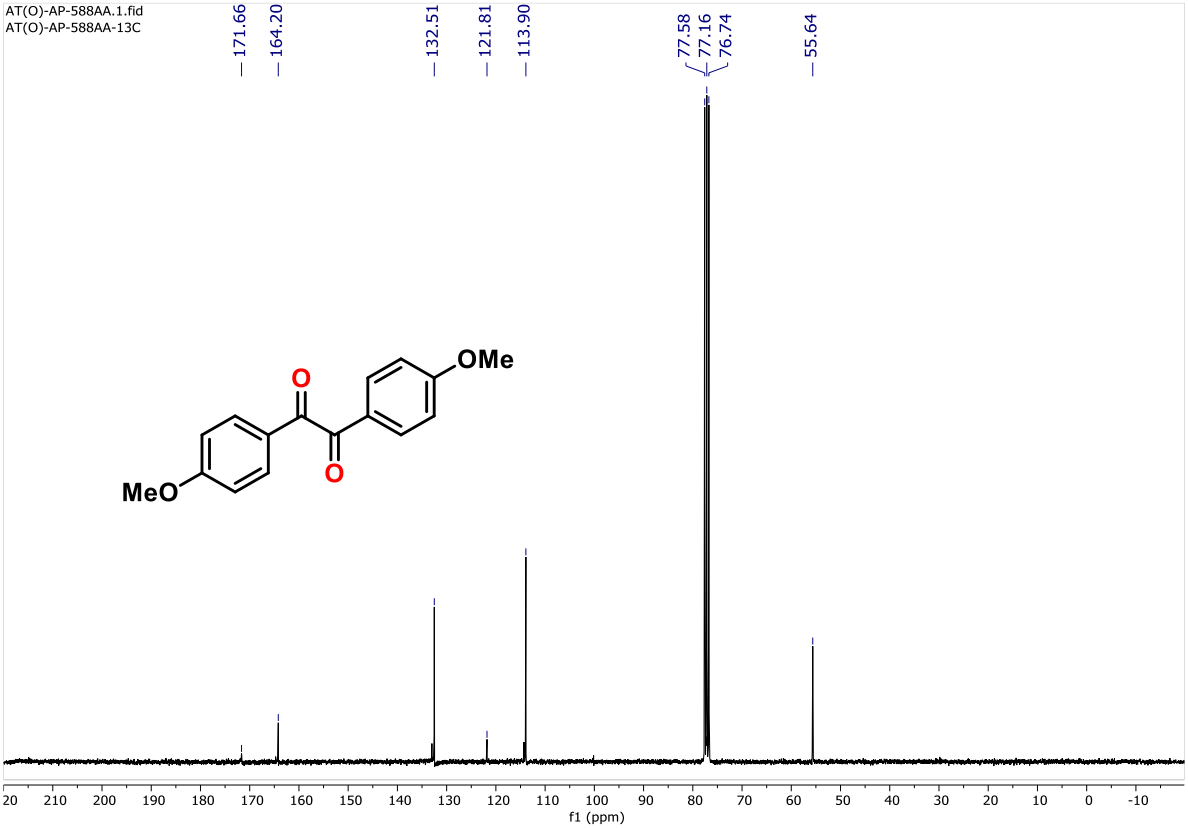

Figure 5.107. $^{13}C\{^{1}H\}$ NMR (75 MHz) spectrum of **15** in $CDCl_3$.

^{1}H NMR for Hammett analysis:

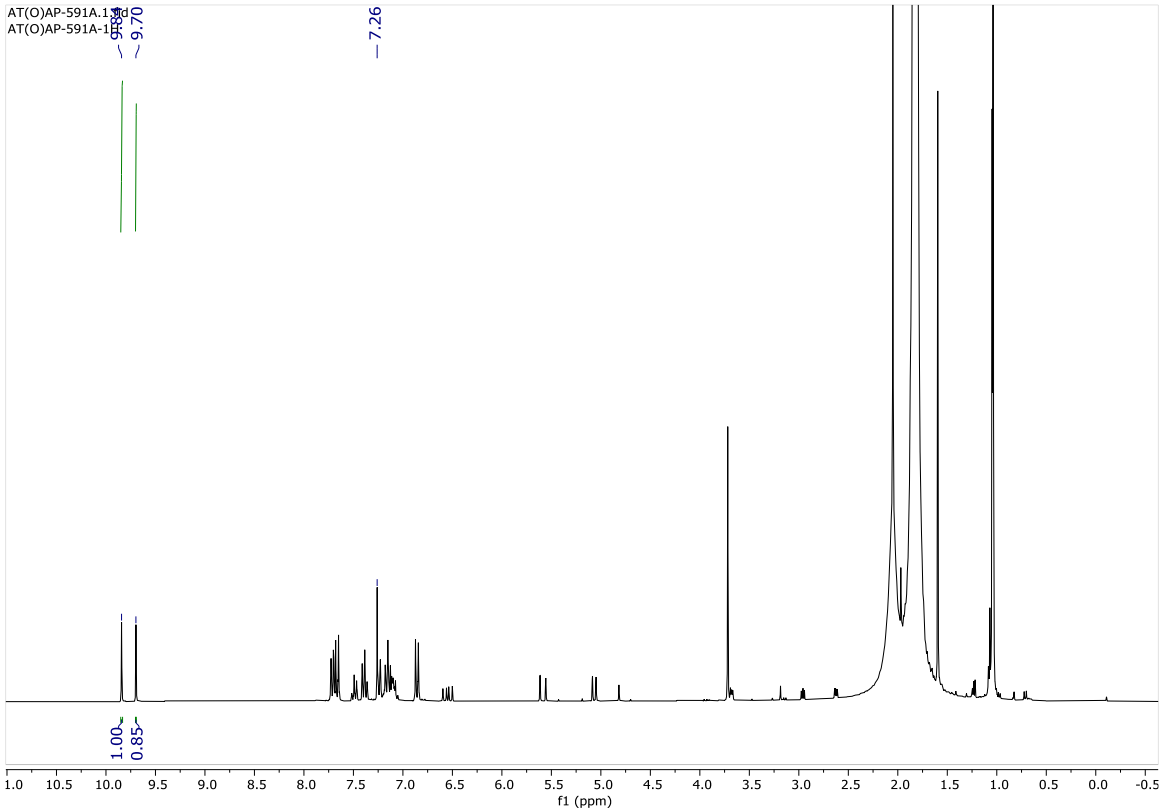

Figure 5.108. ^{1}H NMR for Hammett analysis between **3a** and **3f**.

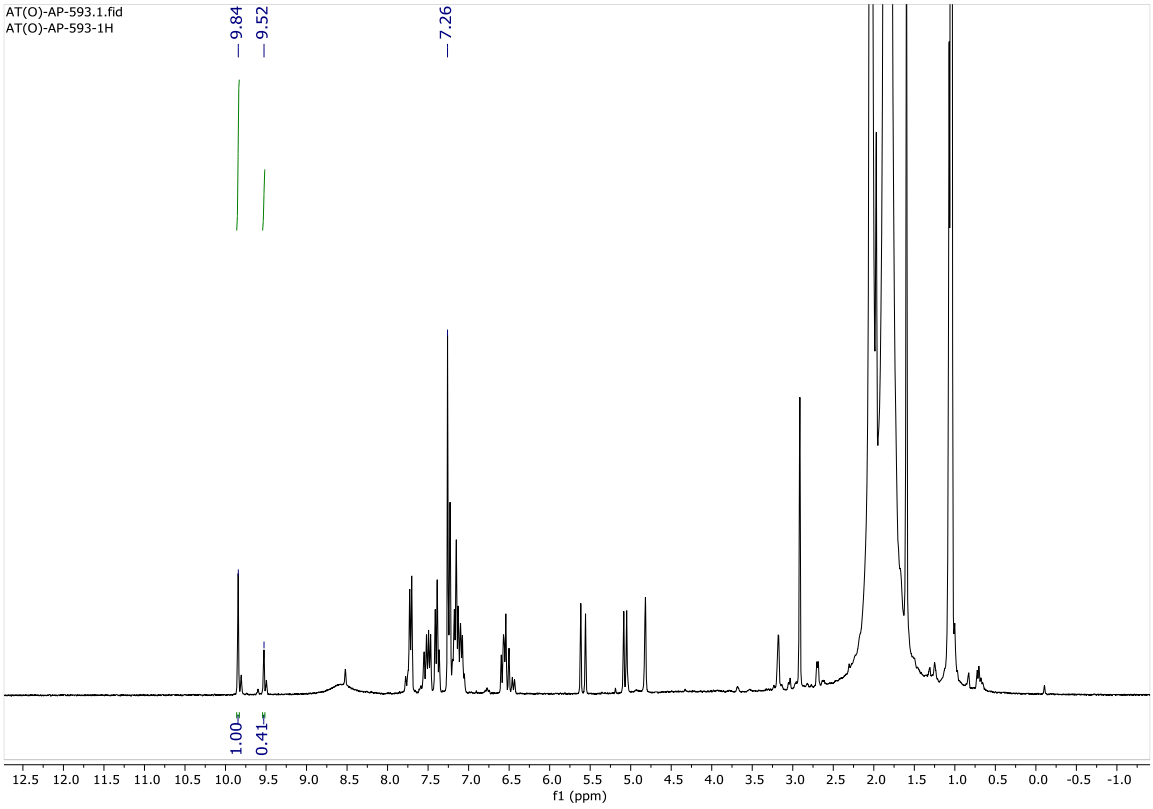

Figure 5.109. ^{1}H NMR for Hammett analysis between **3a** and **3g**.

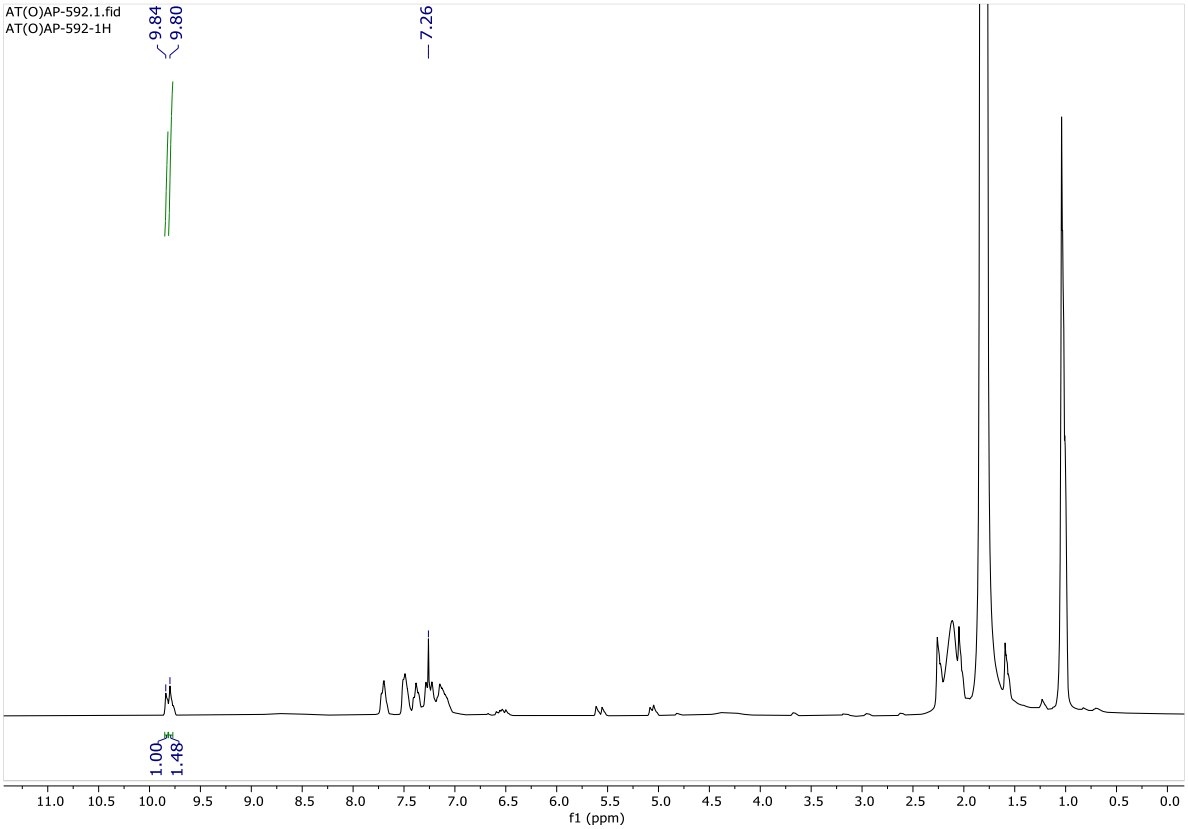

Figure 5.110. ^{1}H NMR for Hammett analysis between **3a** and **3c**.

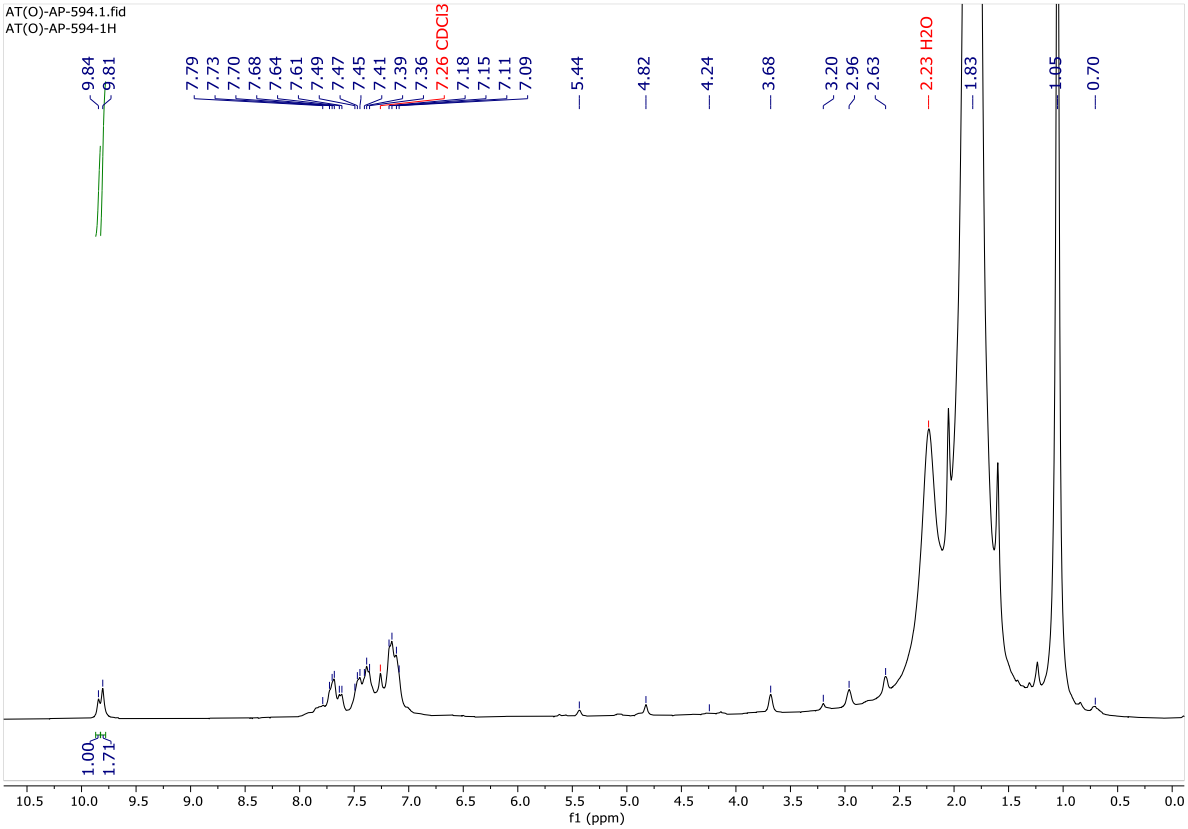

Figure 5.111. ^{1}H NMR for Hammett analysis between **3a** and **3k**.

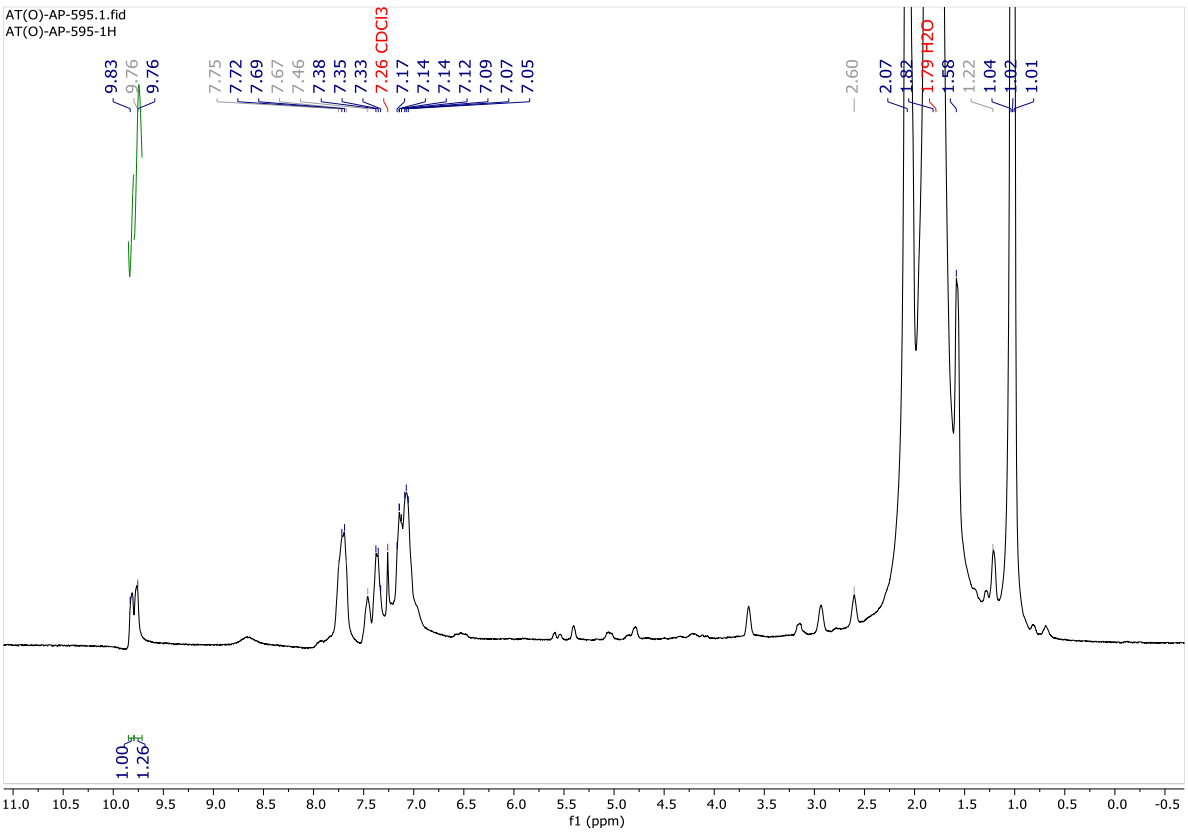

Figure 5.112. ^{1}H NMR for Hammett analysis between **3a** and **3j**.

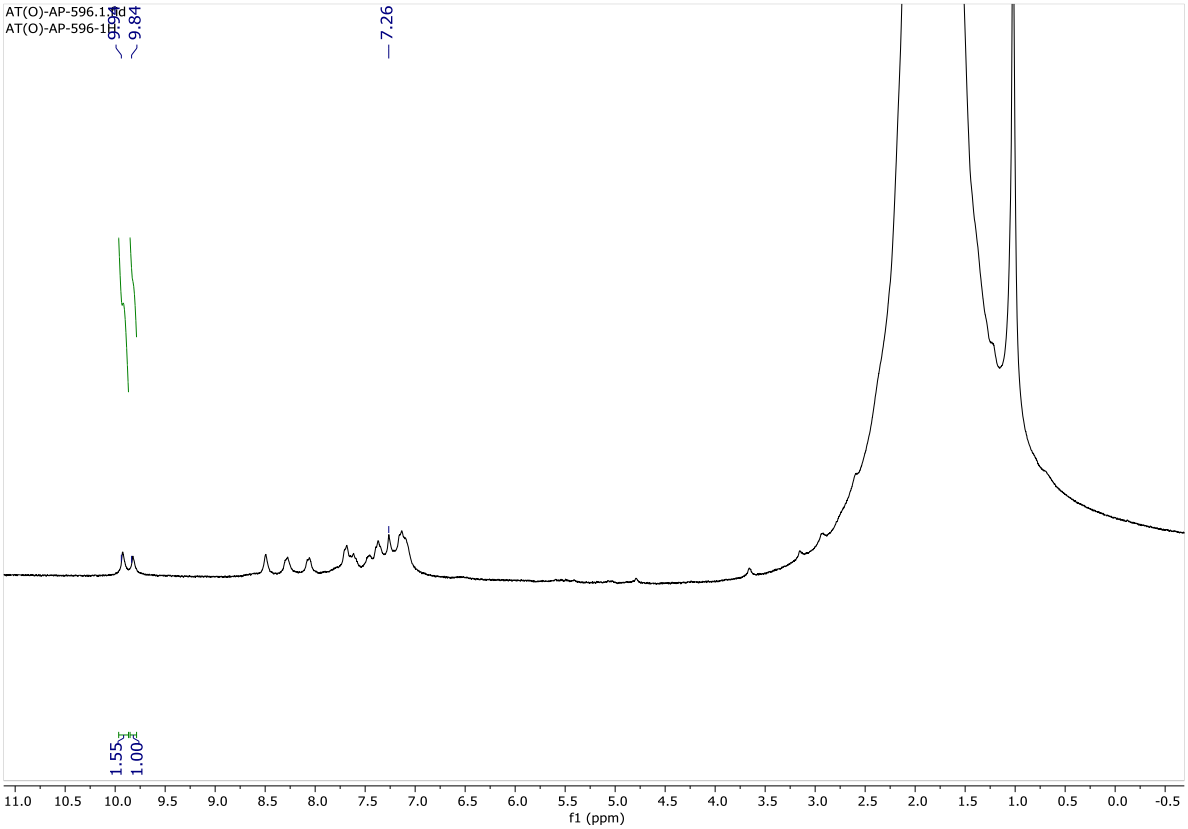

Figure 5.113. ^{1}H NMR for Hammett analysis between **3a** and **3l**.

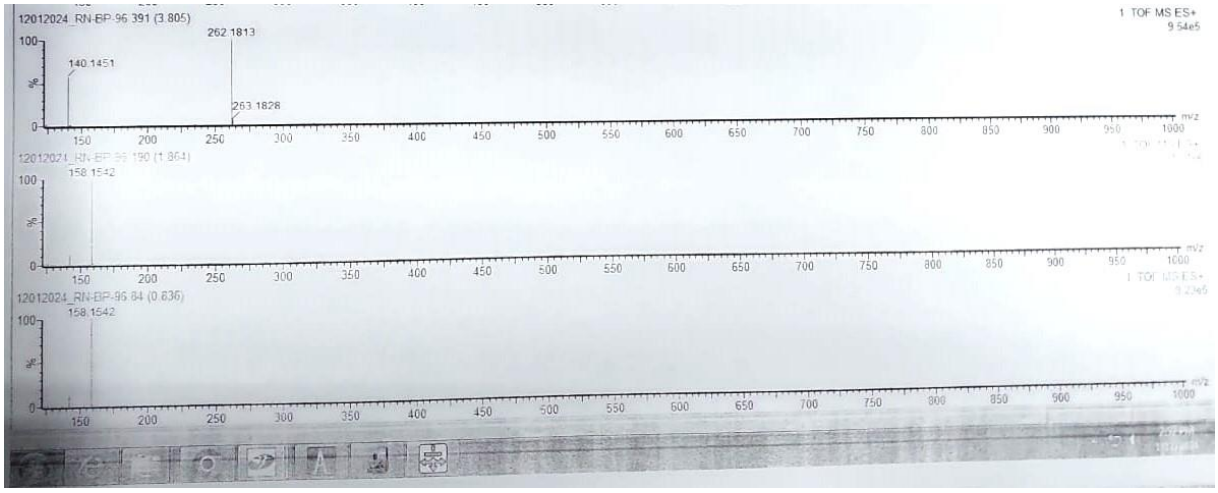

Figure 5.114. TEMPO adduct of generated acyl radical.

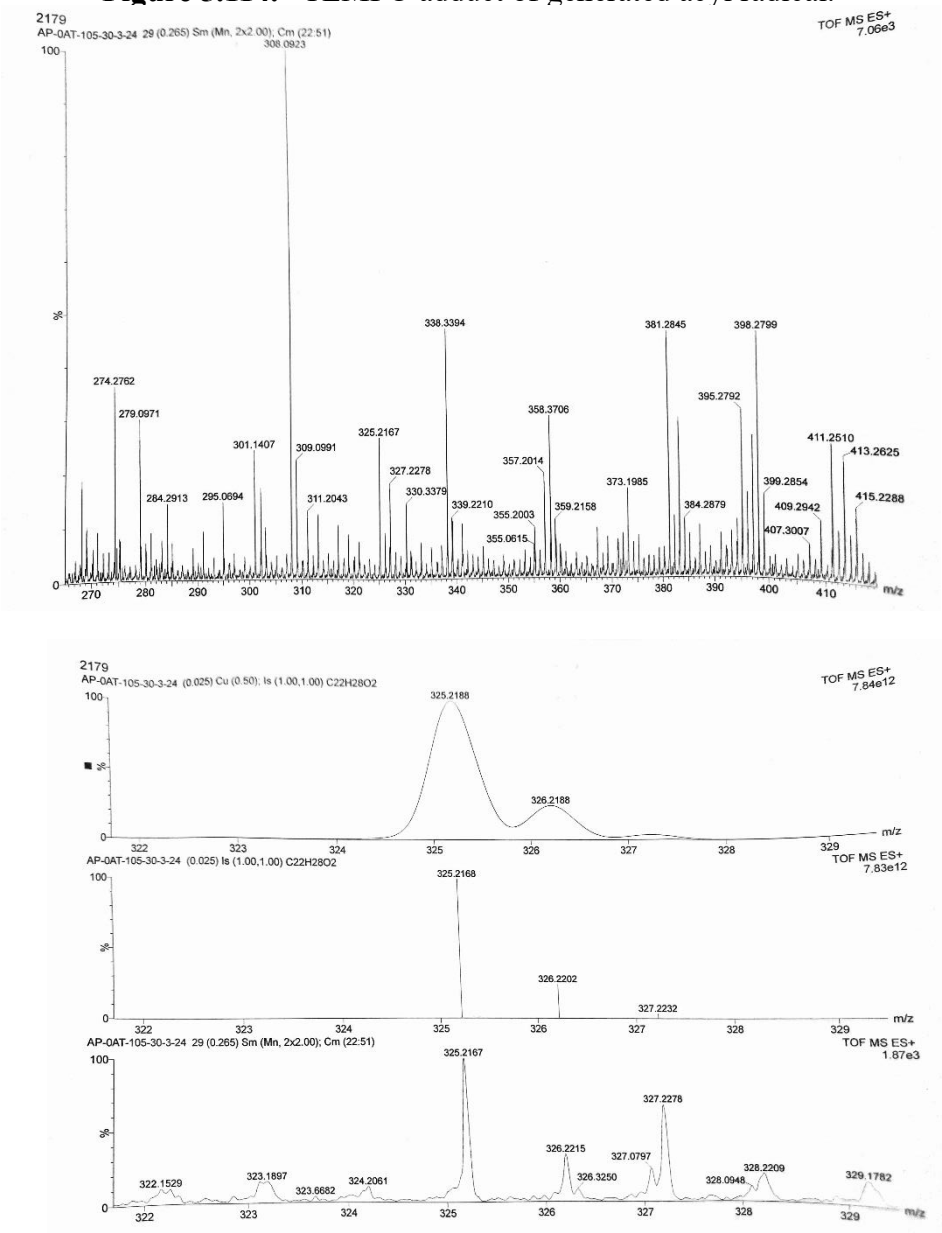

Figure 5.115. BHT adduct of generated acyl radical.

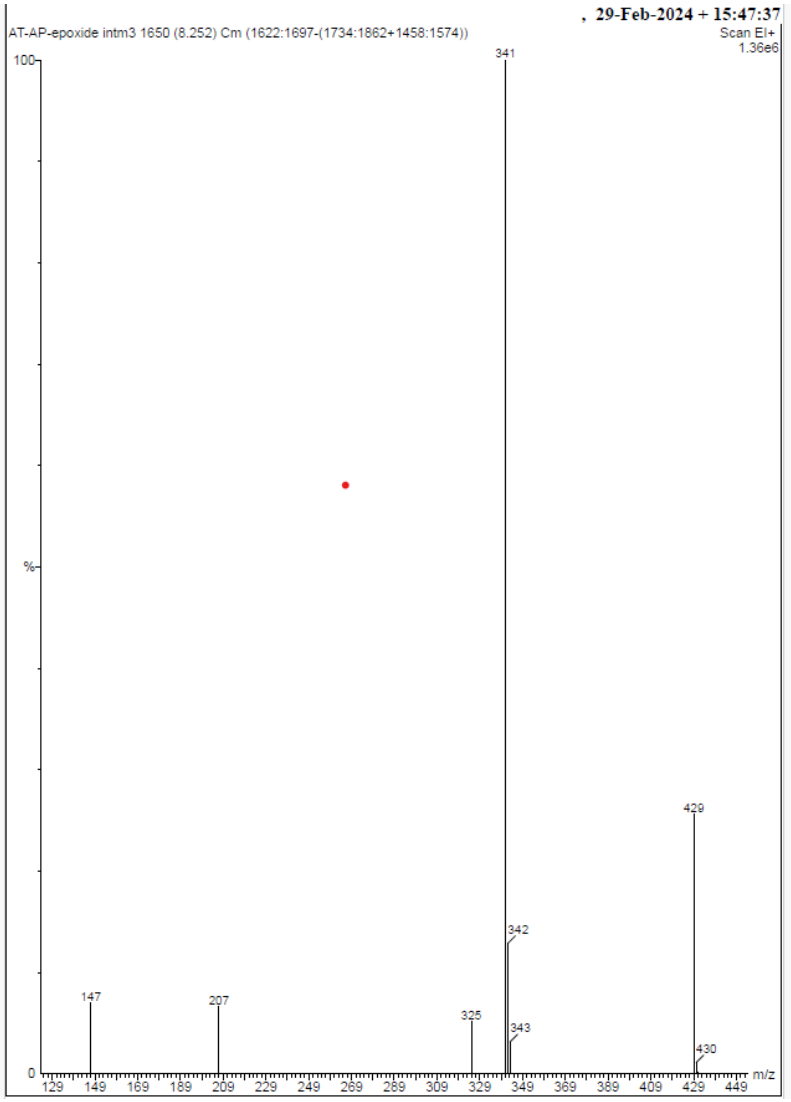

Figure 5.116. GCMS of intermediate **E**.

Chapter 6

Copper-catalyzed C-C bond formations and their application in sensing

Representative Publications:

Inorg. Chem. **2020**, *59,* 10099−10112.

New J. Chem. **2022**, *46*, 2989–3005.

This chapter is a little bit different from the previous ones. So far, we have discussed the use of Co as a catalyst in several organic reactions. This chapter is more application oriented where the potential of copper (Cu) catalyzed reaction in alkyne-alkyne homocoupling reaction is explored and discussed, and the synthesized molecules are utilized in selective heavy metal ion (Hg^{2+}) detection. This chapter is categorized into two divisions 6.1 and 6.2., which contain two different works with similar chemistry.

In 6.1, Cu-catalyzed alkyne-alkyne coupling has been developed by microwave-assisted technique and the synthesized internal 1,3-dialkyne unit containing molecule was subjected to metal ion detection, wherefrom, it was observed to have selective response towards Hg^{2+} ion. Detailed study on binding mode by spectrophotometric studies, emission spectral studies, voltammetric and NMR studies revealed an unusual binding pattern of Hg^{2+} by the conjugated 1,3-dialkyne unit converging with the HSAB principle. Extending this work, to find out whether this binding mode is universal, a cyclic 1,3-dialkyne unit containing molecule has been synthesized in 6.2, by the previously optimized microwave-assisted, Cu-catalyzed alkyne-alkyne coupling. As a part of comparison in the binding modes between internally conjugated 1,3-dialkyne unit and terminal alkyne unit, tests with metals ions have been conducted with both the cyclic 1,3-dialkyne molecule as well as its precursor containing two terminal alkyne units. The comparison has been comprehensively carried out by spectrophotometric studies, emission spectral studies, voltammetric and NMR studies, which shows in both the cases the alkyne units are involved, however, in the terminal alkynes the adjacent heteroatoms assist in binding two Hg^{2+} ion at a time, whereas in the cyclic 1,3-dialkyne molecule no heteroatom is involved in binding of one Hg^{2+} ion at a time. Additionally, theoretical studies have confirmed the stable mode of binding and the spectral changes associated with the interactions.

To function as a metal ion detection probe, a molecule needs to meet certain criteria like a binding centre with possibility of chelation, or a binding cavity with compatible cavity size or a possible hard-hard or soft-soft interaction between host and guest, or even an irreversible chemical change of the probe in presence of the metal (to function as chemodosimeter). Based on these criteria, selectivity of a probe towards a particular metal ion is developed, such that the detection can be performed even in presence of a variety of metal ions. For example, metal ions like Na^{+} and K^{+} are trapped in cavity of appropriate size and for that mostly crown ethers have been used. On the other hand, for heavy metal ions like Hg^{2+} ion, since it is a soft metal ion, soft centres like S play effective role in binding. This process consequently changes the properties of the probe in terms of energy transfer, electronic

distribution or excitation and emission properties, which can be realized by UV-vis, fluorescence spectra, voltammetric studies etc., as shown in Scheme 6.1. This chapter explores the changes in photophysical and electrochemical properties of the developed probes upon interaction with Hg^{2+} and its unusual binding pattern.

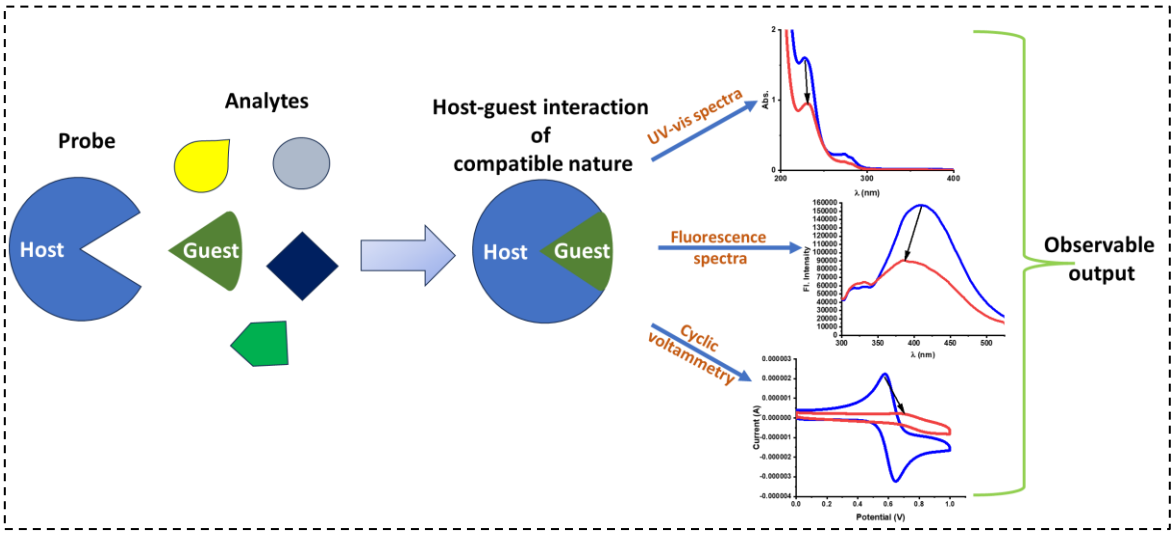

Scheme 6.1. Schematic diagram of selective sensing of an analyte by the probe.

6.1. Microwave Assisted Neat Synthesis of a Ferrocene Appended Phenolphthalein Di-yne: A Designed Synthetic Scaffold for Hg^{2+} Ion

This part of the chapter is taken from the work published in *Inorg. Chem.* **2020**, *59*, 10099−10112.

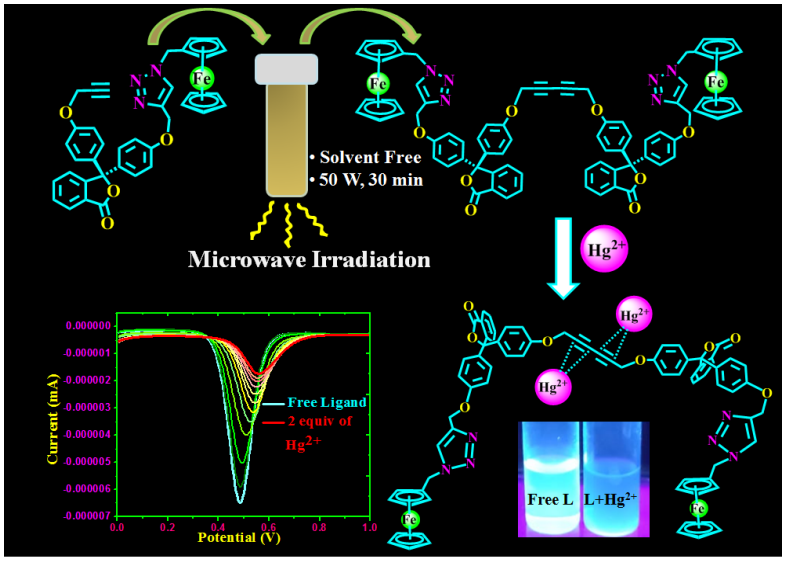

6.1.1. Introduction

1,3-di-ynes represent a unique class of intermediates in organic synthesis and one of the most vital blocks in many natural products and functional materials.[1,2] Conjugated alkynes are always advantageous because of their cylindrical electronic symmetry. The morphological beauty, as well as beneficial properties of conjugated di-ynes have fascinated scientists to explore its scope of synthesis and utilization. The di-yne moiety has been extensively utilized in many fields starting from nanoscience,[3] liquid crystals,[4−7] to antiviral activities,[8] providing a strong motivation for modern research. Furthermore, they are used in optoelectronics,[9] rotaxanes,[10,11] catenanes,[12] pharmaceuticals[13] and polymer science.[14] Mostly the di-yne molecular systems have been developed so far by alkyne homocoupling and a few by heterocoupling[15] using transition metal (*e.g.* Cu, Pd, Ni and Au) catalysts. Such compounds can be prepared by the conventional Glaser coupling, Eglinton coupling, Hay coupling,[16,17] as also by their modified versions.[10-12] As an advancement of the synthetic methodology, microwave assisted reaction in solvent phase[18] and in solvent-free medium under thermal condition[19] have

also been explored for alkyne-alkyne coupling reactions. However, a microwave assisted homogenous synthesis of 1,3-di-yne system in neat condition has not been explored earlier.

In spite of knowing the fact for last few decades that mercury has a strong propensity towards alkyne, a very few examples are known where alkyne systems have been explored as structural building blocks for metal ions especially for mercury ion sensing.[20,21] In this regard, a side-on coordination to Hg^{2+} ions by sterically accessible π-conjugation has been documented in case of mercury-ethynyl interaction.[22-24] A soft binding centre (base) prefers to bind to a soft metal ion (acid) according to HSAB principle.[25] Keeping this idea in mind, we have deliberately designed a structural motif, consisting of 1,3-di-yne system, which can interact and detect a soft Lewis acid, mercury. Mercury is one of the most investigated metal ions in the field of sensing owing to its extreme toxicity to the living species.[26-28] Mercury, in any form, for example, in elemental form, inorganic form as well as in organic form, shows different kinds of toxicity. Hence, the design and development of any potential probe, capable of detecting the released mercury, would be a step forward towards making the environment safer for the living species.

The design of metal ion sensors based on conjugated alkyne molecules may be the subject of growing interest due to its configurational as well as conformational rigidity.[29] Therefore, we have performed homocoupling of triazole based ferrocene appended phenolphthalein alkyne in a dry medium to generate a di-alkyne system that can be used as a potential metal ion sensor having multi-channels. Fluorescence spectroscopy is a widely used and reliable technique for the detection of various metal ions in a precise and non-destructive manner.[30-32] Phenolphthalein is taken as the fluorophore moiety so that fluorescence detection of the metal ion is possible and ferrocene is appended to make the molecule redox active. Phenolphthalein is a much popular pH indicator, but its scope of being used as the fluorophore in chemosensor molecules is not well-explored inspite of having a well-defined extended conjugation. In fact, it is not considered as an efficient fluorophore since it lacks structural rigidity due to the C-C single bond rotation.[33,34] Hence, the easiest way to turn it into an effective fluorophore is by restricting its feasible C-C bond rotation. Interestingly, we have circumvented this issue, which is the root cause for being non-fluorescent, by functionalizing the hydroxyl groups by bulky substituents and this modification has enabled us to convert it to a fluorescent derivative. On the other hand, the robustness in aerobic conditions, easy availability, economical affordability, ease of handling and storage and most importantly its precise redox property make ferrocene unit a topic of intensive research that has been well-

explored.[35]

Here in this present work, we have developed a ferrocene appended phenolphthalein di-yne system by microwave synthesis in a neat condition. The present system, an easy-to-make optical and electrochemical sensor, displayed a high selectivity towards Hg^{2+} ion. To the best of our knowledge, this is the first report of a conjugated di-alkyne system for the detection of Hg^{2+} ion. A series of experiments and DFT calculations unravel the binding mode of the present probe with Hg^{2+} ion.

6.1.2. Results and Discussions:

6.1.2.1. Synthesis of Compound 5

In this work, we have developed a conjugated di-yne bridged chromophore system by the homocoupling of two terminal alkynes with the pre-established protocol of the Eglinton coupling[36] with some advanced modifications. Microwave assisted synthesis of di-yne system by the homocoupling of two terminal alkynes are reported in solvent phase,[18] however, use of solvents, specially chlorinated solvents, make this strategy disadvantageous towards green synthesis. In this report, we have tried the microwave assisted homocoupling of two terminal alkynes in neat condition at slightly elevated temperature with low catalyst loading to obtain the desired product. After successfully synthesizing the conjugated di-yne bridged chromophore system *via* a modified method, we have investigated the metal ion sensing properties of the synthesized compound.

As shown in Scheme 6.1.1, phenolphthalein, **1** is converted into its dialkynyl derivative, **2** using K_2CO_3 as a base and propargyl bromide in DMSO at room temperature. Further, copper catalyzed azide-alkyne [3+2] cycloaddition (CuAAC) reaction of **2** with mono(azidomethyl)ferrocene afforded compounds **3** and **4** in 35% and 20% yield respectively. Conventional Eglinton coupling of compound **3** using $Cu(OAc)_2 \cdot H_2O$ and pyridine as a base as well as a solvent afforded compound **5** in low yield (30%). As an advancement of conventional Glaser coupling, Eglinton coupling, Hay coupling, microwave assisted heterogeneous as well as homogenous homocoupling of terminal alkynes is reported either in alumina surface[37] or in solvent phase.[18] Here, we wish to report a fast, solvent free microwave assisted homogeneous Eglinton coupling of terminal alkynes.

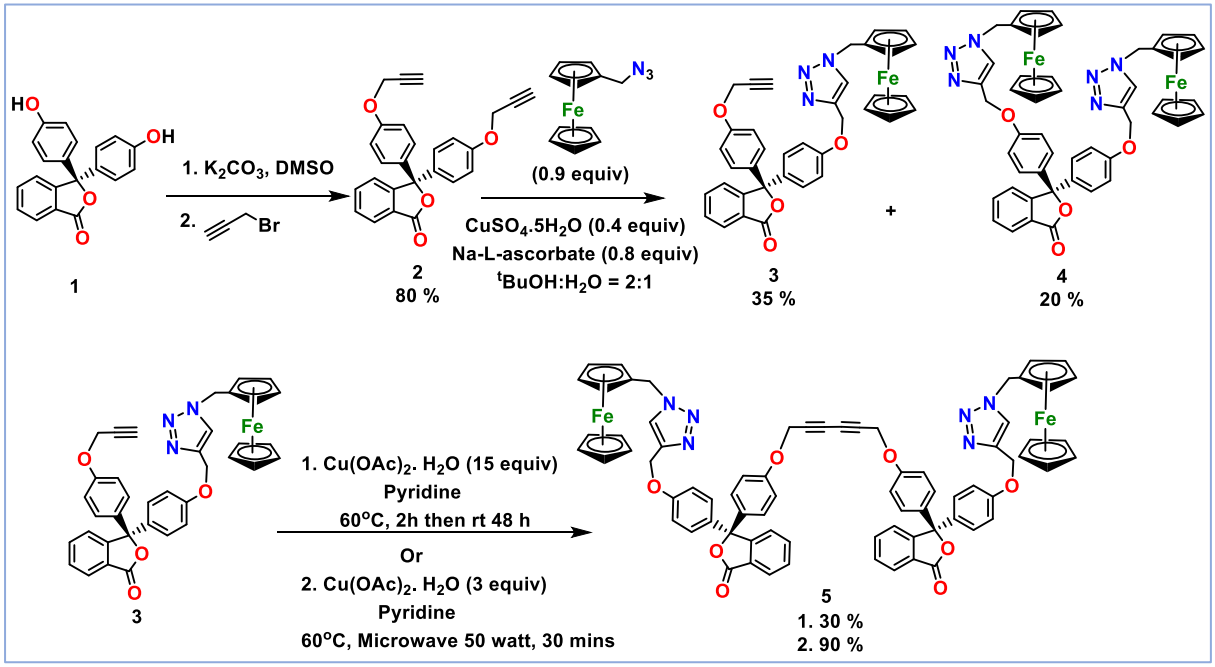

Scheme 6.1.1: Synthesis of compounds **3**, **4** and **5**.

As shown in Scheme 6.1.1 and Table 6.1.1, compound **5** can be achieved in 90% yield in just 30 min by employing microwave excitation to 50 watt at 60°C with low catalyst loading (3 equiv) compared to the conventional reaction method (15 equiv) mentioned earlier. For the further advancement of the reaction protocol, the reaction was performed in neat condition with only 3 equiv of pyridine (19µL) merely as a base and 3.7 equiv of $Cu(OAc)_2 \cdot H_2O$, giving 80% conversion, under microwave irradiation. This is the first report of homogenous Eglinton coupling in solvent free condition done under microwave irradiation and without any external solid support. All the synthesized compounds have been characterised by ^1H and ^{13}C NMR spectroscopy, HRMS, and elemental analysis.

Table 6.1.1 Optimization of microwave-assisted Eglinton coupling reaction in our specified substrate.

Sl. No.	Equiv of **3**	Equiv of Catalyst[#]	Equiv of Base / solvent	Temperature (°C)	Time (minutes)	% Conversion	% Yield
1	1	15	118 (5 mL)	60	10	20	6
2	1	15	118 (5 mL)	60	20	60	50
3	1	15	118 (5 mL)	60	30	100	90
4	1	1	118 (5 mL)	60	30	20	8

5	1	2	118 (5 mL)	60	30	65	49
6	**1**	**3**	**118 (5 mL)**	**60**	**30**	**100**	**90**
7	1	3	118 (5 mL)	25	30	10	5
8	1	3	118 (5 mL)	40	30	40	25
9	**1**	**3.7**	**3 (19µL)**	**60**	**30**	**80**	**40**

[#]catalyst is $Cu(OAc)_2 \cdot H_2O$.

6.1.2.2. UV-visible Absorption Studies

The UV-vis spectra of compound **5** (7.8×10^{-6} M) with stepwise addition of solutions of Na^+, K^+, Fe^{2+}, Fe^{3+}, Cu^{2+}, Cu^+, Hg^{2+}, Ag^+, Ca^{2+}, Mg^{2+}, Mn^{2+}, Zn^{2+}, Pb^{2+}, Co^{2+}, Cr^{3+}, Al^{3+} ions (7.8×10^{-6} M) are recorded separately in CH_3CN solvent. From this experiment, we have observed that the receptor **5** selectively responded towards Hg^{2+}, Cu^{2+} and Fe^{3+} ions (Figure 6.1.1) among all the aforementioned cations. The UV-vis spectra of compound **5** shows two absorption bands at $\lambda_{max}\sim$ 228 nm (ε = 81907 M^{-1} cm^{-1}) and 273 nm (ε = 13832 M^{-1} cm^{-1}), corresponding to the excitation of the phenolphthalein moiety.[38] After the addition of each aliquot of the metal ions, the absorbance decreases and it continues to fall gradually upto 2 equiv of each of Hg^{2+}, Cu^{2+} and Fe^{3+} ions (Figure 6.1.1(b)-(d)). On careful observation of the interaction of **5** with Cu^{2+} and Fe^{3+} ions (Figures 6.1.1(c),(d) inset), it is found that there occurs a small peak around 630 nm (ε = 7024 M^{-1} cm^{-1}) corresponding to the oxidation of Fe(II) of ferrocene unit to Fe(III) of ferrocenium ion.[39] This peak diminishes gradually on addition of L-sodium ascorbate (LAS) as a reducing agent (Figure 6.1.1(e),(f)). This phenomenon clearly indicates that the oxidation-reduction of the ferrocene unit in **5** is reversible. Interestingly, no such peak at high wavelength was observed upon addition of Hg^{2+} ion. It may be concluded that the kind of interaction of receptor **5** towards Hg^{2+} ion is different from that towards Cu^{2+} and Fe^{3+} ions. Anticipating that the interaction can be of binding type, we have calculated the binding ratio of Hg^{2+} with probe **5** by binding assays using the method of continuous variation (Job's plot) (Figure 6.1.1(b) inset) and it was found to be 2:1. Although our several attempts to obtain the mass spectra of the [**5**$\cdot$2Hg^{2+}] complex were unsuccessful, the binding ratio and composition were confirmed by elemental analysis of the isolated complex.

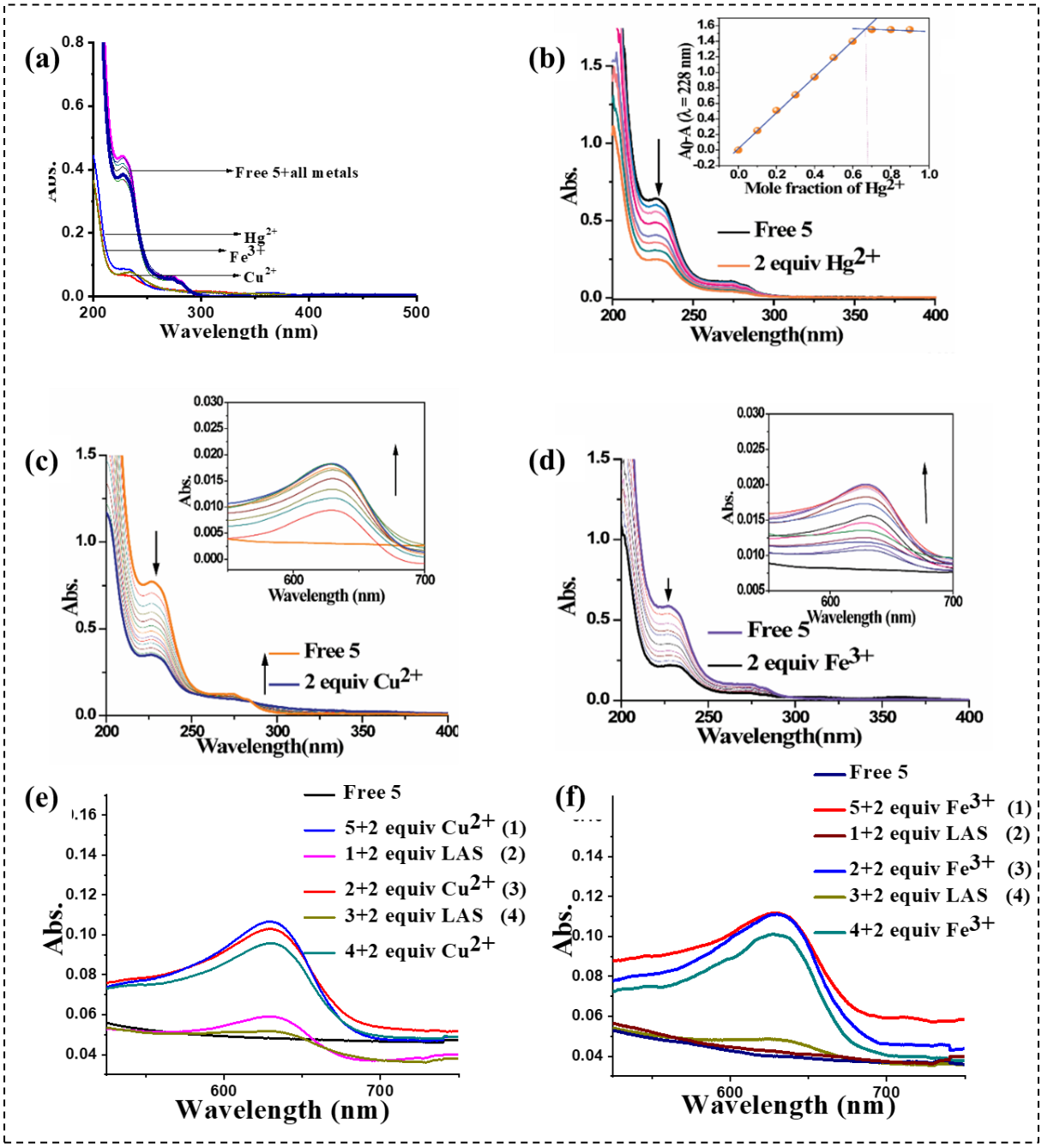

Figure 6.1.1 (a) Absorption spectra of compound **5** (7.8×10^{-6} M) (a) with all metals (7.8×10^{-6} M), and upon addition of up to (b) 2 equiv Hg^{2+} (The inset picture shows the Job's plot); (c) 2 equiv Cu^{2+} and (d) 2 equiv Fe^{3+} in CH_3CN solvent at room temperature (The inset pictures show the peak appearing due to oxidation of the ferrocene unit). Reversibility test of **5** (7.8×10^{-6} M) with (e) Cu^{2+} and (f) Fe^{3+} ions (7.8×10^{-6} M) in presence of Sodium-L-ascorbate (LAS) in CH_3CN solvent at room temperature.

6.1.2.3. Fluorescence Studies

To understand the properties of the synthesized molecule more clearly, fluorescence studies are indispensable as fluorescence spectroscopy acts as a supreme and precise analytical tool. We have modified the structure of phenolphthalein in order to make it a good fluorophore moiety and to obtain a considerable fluorescence emission intensity. Fluorescence spectra of **5** in presence of Na^+, K^+, Fe^{2+}, Fe^{3+}, Cu^{2+}, Hg^{2+}, Ag^+, Ca^{2+}, Mg^{2+}, Mn^{2+}, Zn^{2+}, Pb^{2+}, Co^{2+}, Cr^{3+}, Al^{3+} ions (as their perchlorate salts) and Cu^+ (as $[(CH_3CN)_4Cu]PF_6$) are recorded separately in CH_3CN solution (6.62×10^{-6} M) with excitation wavelength 273 nm. Excitation at 228 nm did not produce any considerable fluorescence intensity for **5**. No significant change was observed in the emission spectra of **5** after addition of the metal ions except for Hg^{2+}, Cu^{2+} and Fe^{3+} ions (Figure 6.1.2(a)). As shown in Figure 6.1.2(b), the addition of Hg^{2+} ion upto 2 equiv exhibited a gradual diminishing fluorescence emission intensity with a small blue shift ($\Delta\lambda$ = 10 nm) on excitation at 273 nm and no further change was observed on addition of Hg^{2+} ion beyond 2 equiv. It is known that alkyne units have two perpendicular π-electron clouds[40] and if two alkyne units are joined by a C-C single bond, that connecting single bond has slightly reduced bond length.[41, 42] Coordination of metal ion in this "triple-single-triple" bond unit can lead to a perturbation to the conjugation to a slight extent and eventually may lead to a blue shift in fluorescence spectra.[43] It is evident from ^1H, ^{13}C NMR and IR spectral data that, the alternate triple bonds are stable and prominent in our synthesized probe **5**. However, the change of the emission spectra ($\Delta\lambda$ = 10 nm) on addition of Hg^{2+} ion led us to conclude that, receptor **5** may bind Hg^{2+} ion through π-cloud *via* soft-soft interaction according to HSAB principle. The reversibility of this interaction of the probe **5** towards Hg^{2+} ion has also been investigated through the fluorescence spectroscopy by using aqueous solution of disodium EDTA (6.62×10^{-6} M) as the chelating agent (Figure 6.1.3(a),(b)). However, repeating the same experiment up to 2 equiv of Cu^{2+} and Fe^{3+} ions in a CH_3CN solution of compound **5**, fluorescence quenching, with no net shift of the intensity maxima were observed (Figure 6.1.3(c),(d)). Fe^{3+} and Cu^{2+} ions are known as efficient fluorescence quenchers[44,45] may be due to their paramagnetic nature and Hg^{2+} ion led to the fluorescence quenching may be *via* ligand-to-metal charge transfer (LMCT), which was verified by TD-DFT calculations (*vide-supra*). To get further insight into the quenching mechanism for Hg^{2+}, fluorescence lifetime measurement was performed. As shown in Figure 6.1.2(c), lifetime of the undisturbed molecule (1.9 ns) remains almost constant even after addition of 2 equiv Hg^{2+} ion (2.1 ns). Thus, the unchanged lifetime predicts the

formation of a non-fluorescent complex in the ground-state,[46] indicating a static quenching phenomenon.

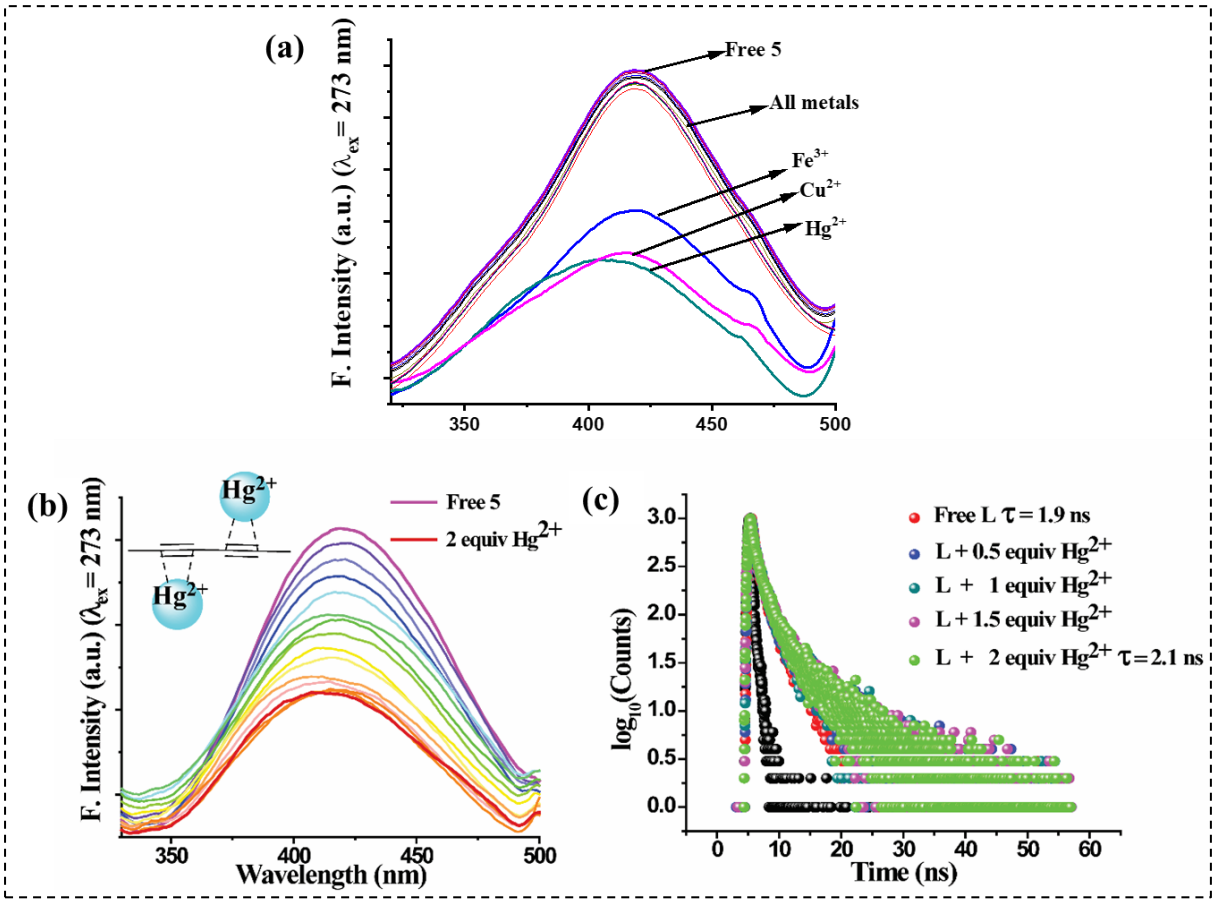

Figure 6.1.2 Fluorescence emission spectra of compound **5** (6.62×10^{-6} M) (a) with all metals, (b) upon addition of Hg^{2+} upto 2 equiv in CH_3CN solvent at room temperature; inset picture showing the probable interaction responsible for the quenching. (c) Mechanism of fluorescence quenching by fluorescence life-time study of **5** with Hg^{2+} at room temperature: Static Quenching.

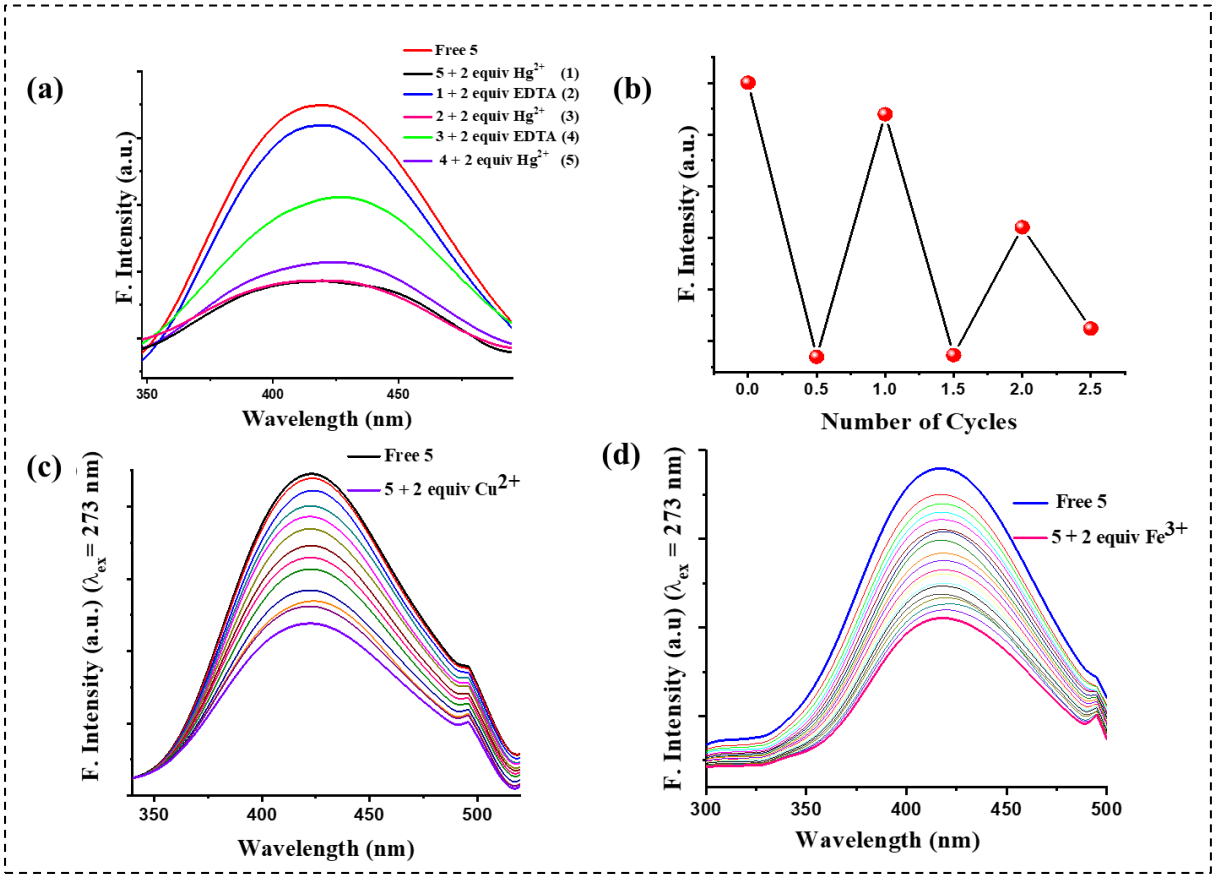

Figure 6.1.3 (a) Reversibility test of **5** (6.62×10^{-6} M) with Hg^{2+} (6.62×10^{-6} M) in CH_3CN by aqueous solution of disodium EDTA (6.62×10^{-6} M) at room temperature. (b) Results of the reversibility test represented in terms of number of cycles. Fluorescence emission titration spectra of compound **5** (6.62×10^{-6} M) upon addition of (c) Cu^{2+} ion (6.62×10^{-6} M), (d) Fe^{3+} metal ion (6.62×10^{-6} M) upto 2 equiv in CH_3CN solvent at room temperature.

In order to understand the sensitivity of the probe **5** (6.62×10^{-6} M), we have performed the fluorescence titration using Hg^{2+} ion (6.62×10^{-6} M) in CH_3CN solution. A detectable change in fluorescence spectra was observed only in presence of 0.015 equiv of Hg^{2+} ion, hence, the detection limit (DL) of Hg^{2+} with probe **5** is 9.9×10^{-8} M. Further, DL can also be precisely obtained *via* 3σ/S method,[47] where 'σ' is the standard deviation of the blank and 'S' is the slope of the calibration curve. A good linear relationship between the fluorescence intensity (data extracted from Figure 6.1.2(b)) and the concentration of Hg^{2+} was obtained (Figure 6.1.4(a)). Interestingly, the limit of detection was obtained in the same order as obtained from above method. Further, binding constant value with Hg^{2+} ion have been calculated according to Stern-Volmer equation,[48] $I/I_o = 1 + K[Q]$ (data plot Figure 6.1.4(b)), where K is called the quenching

constant, I is the intensity of fluorescence at the quencher concentration [Q], and I_o is its value without quencher. Binding constant value was found to be 6.8×10^3 M^{-1}, which indicate a weak interaction of Hg^{2+} with probe **5**.

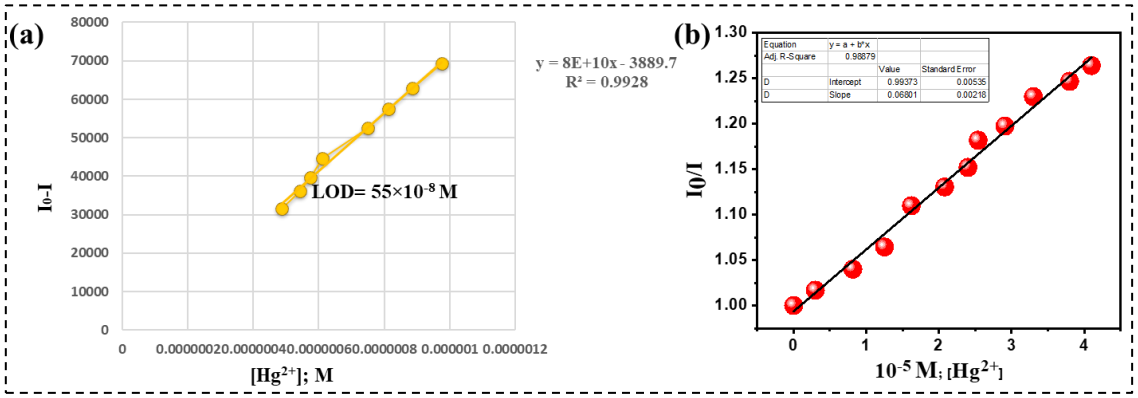

Figure 6.1.4 (a) LOD of **5** in presence of Hg^{2+} ion from fluorescence spectra by 3σ/S method. (b) Quantitive binding data for **5** with Hg^{2+} ion from the fluorescence titration.

6.1.2.4. Electrochemical Studies

The sole purpose of including ferrocene into the model of the probe is to carry out the various electrochemical studies of metal binding phenomenon due to its inherent reversible electrochemical nature.[49,50] Among the various electrochemical studies known, cyclic voltammetry (CV) and differential pulse voltammetry (DPV) experiments are explored for the cation recognition mechanism study for the receptor **5**. A reversible one electron oxidation process is observed for the receptor **5** (2.5×10^{-4} M) with a redox wave at $E_{1/2} = 0.503$ V due to oxidation of the Fe(II) of ferrocene to Fe(III) of ferrocenium ion and *vice versa*. The electrochemical behaviour of compound **5** was investigated in the presence of Fe^{3+}, Cu^{2+} and Hg^{2+} ions along with other metal ions (as their perchlorate salts) and Cu^+ as $[(CH_3CN)_4Cu]PF_6$ in CH_3CN (2.5×10^{-4} M) solvent containing 0.1 M $[(n\text{-}Bu)_4N]ClO_4$ as supporting electrolyte (Figure 6.1.5). No perturbation of the cyclic voltammogram (CV) was observed except in the case of Fe^{3+}, Cu^{2+} and Hg^{2+} ions. As shown in the Figure 6.1.6(a), stepwise addition of Hg^{2+} upto 2 equiv induced a significant shift of $\Delta E_{1/2}$ = 60 mV of compound **5**, indicating the formation of a new complex species, [**5**·$2Hg^{2+}$]. The DPV experiment also corroborated the same results as obtained from CV experiment (Figure 6.1.6(b)). A significant shift in potential of the complexed species was observed upon addition of Hg^{2+} ion.

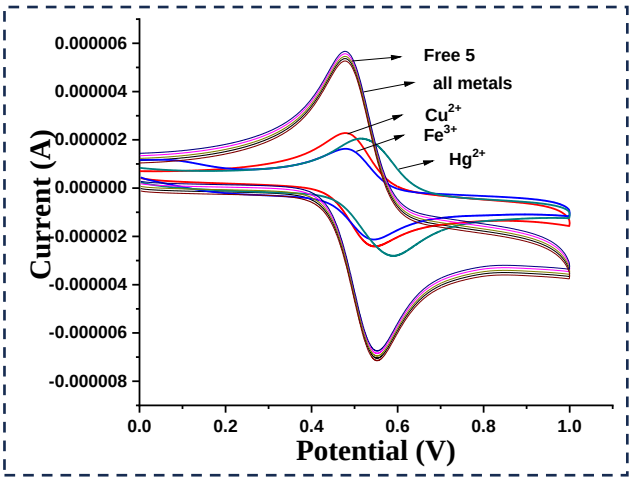

Figure 6.1.5 CV plot of compound **5** (2.5×10^{-4} M) in CH_3CN solvent with all metals (2.5×10^{-4} M) using $[(n\text{-}Bu)_4N]ClO_4$ as supporting electrolyte at room temperature at a scan rate of 0.05 Vs^{-1}.

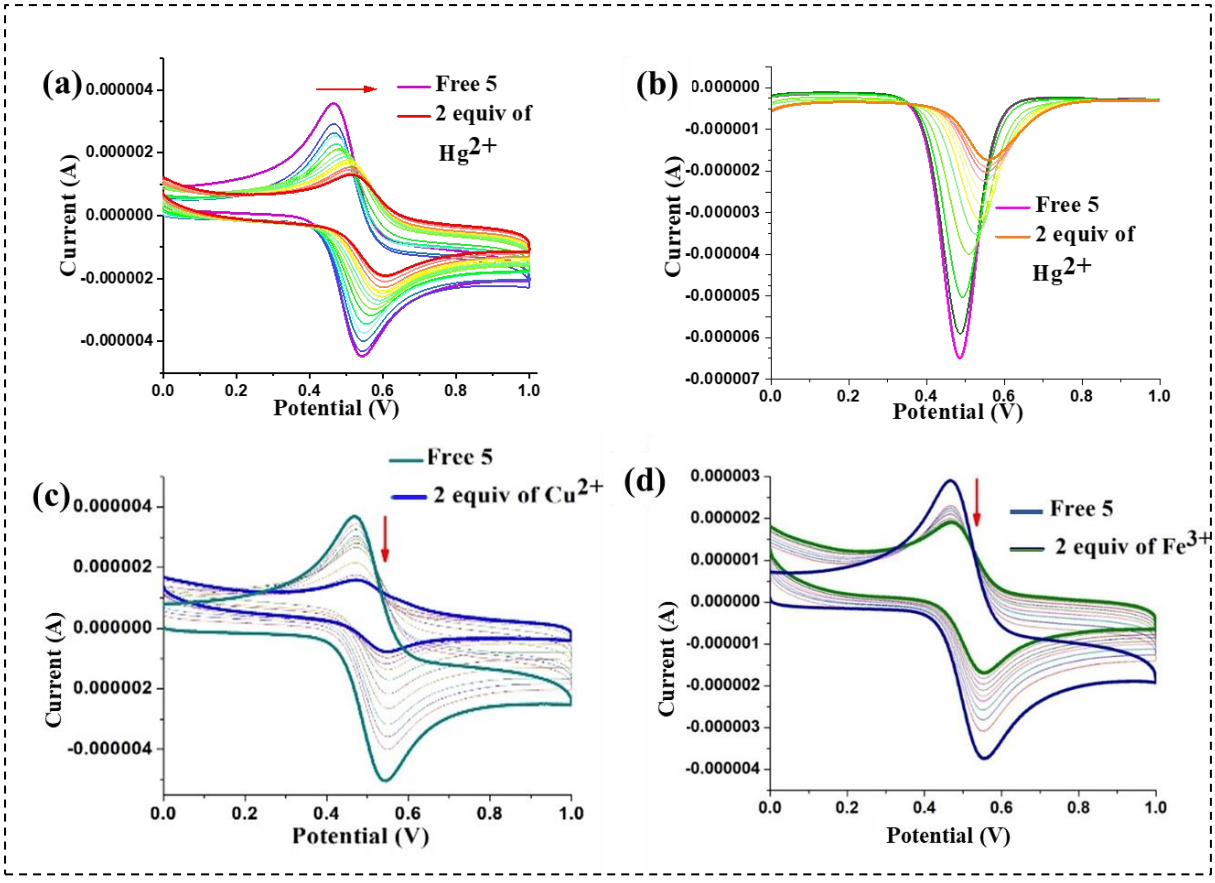

Figure 6.1.6 Evolution of (a) CV and (b) DPV of compound **5** (2.5×10^{-4} M) in CH_3CN solvent when $Hg(ClO_4)_2$ is added upto 2 equiv. CV of compound **5** (2.5×10^{-4} M) in CH_3CN solvent when (c) $Cu(ClO_4)_2$ (2.5×10^{-4} M), (d) $Fe(ClO_4)_3$ (2.5×10^{-4} M) is added upto 0-2 equiv at room temperature at a scan rate of 0.05 Vs^{-1} using $[(n\text{-}Bu)_4N]ClO_4$ as supporting electrolyte.

On the other hand, compound **5** did not exhibit any significant shift of $\Delta E_{1/2}$ upon addition of upto 2 equiv of Cu^{2+} and Fe^{3+} ions (Figures 6.1.6(c),(d)), only the current got diminished with each aliquot of metal addition, indicating oxidation of ferrocene to ferrocenium ion.[51] The responses of probe **5** towards the three metal ions remain unaffected by the presence of other metal ions.

6.1.2.5. ^{1}H and ^{13}C NMR and IR Titrations:

From all the above experiments, it may be concluded that the present probe, **5** binds with Hg^{2+} ion but the binding site cannot be assigned unambiguously as **5** has multiple probable binding sites. Therefore, in order to find out the actual binding site, ^{1}H NMR titration was conducted in d_6-DMSO at room temperature. Initially ^{1}H NMR of compound **5** in d_6-DMSO was recorded and then 2 equiv of Hg^{2+} ion in d_6-DMSO is added in two instalments consecutively (1 equiv + 1 equiv) and the corresponding ^{1}H NMR spectra were recorded. Surprisingly, as shown in Figure 6.1.7(a), no net shift of any of the peaks (not even the peak at 8.18 ppm, corresponding to –C*H* proton of triazole unit)[52] in the ^{1}H NMR spectra was observed after the addition of 2 equiv of Hg^{2+} ion. It imparts the idea that the heteroatoms (O, N) present in the probe are probably not contributing to the binding of metal ion, had it been so, the corresponding adjacent H atoms in the ^{1}H spectra of the complexed moiety would have been shifted.[50] Nevertheless, our original quest for determining the actual binding site unambiguously still remained unanswered.

In order to understand the binding site in detail, ^{13}C NMR titration was performed expecting some light on the binding mode for Hg^{2+} ion. As shown in Figure 6.1.7(b), addition of 2 equiv of Hg^{2+} into d_6-DMSO solution of compound **5**, led to the disappearance of the signals at 70.35 ppm and 76.19 ppm. Those signals at 70.35 ppm and 76.19 ppm are attributed to the alkyne carbons, which were confirmed from ^{1}H-^{13}C HSQC spectral data (Figure 6.1.7(c)) of **5** in d_6-DMSO. All other signals corresponding to aromatic carbons and triazole carbons show no obvious changes. This result clearly demonstrates that the conjugated alkyne part plays a vital role in interacting with the Hg^{2+} ion. The binding mode and this proposed mechanism has been further supported by IR titration and DFT studies (*vide supra*).

To further verify the proposed binding mode the IR titration was performed taking all the compounds in the solid state. Upon gradual addition of $Hg(ClO_4)_2$ upto 2 equiv, the peak at $\bar{\upsilon}$ = 2086 cm^{-1}, corresponding to C≡C stretching frequency, got disappeared (Figure 6.1.7(d)). This observation suggested the presence of some interaction between the di-alkyne unit and

metal ion and this result corroborated with our previous observation in ^{13}C NMR titration. Interestingly, no shifts were observed for the peak at $\bar{\upsilon}$ = 1752 cm^{-1}, corresponding to carbonyl moiety of the lactone ring, indicating no interaction with the Hg^{2+} ion. There is also a strong peak at $\bar{\upsilon}$ = 1085 cm^{-1}, corresponding to the Cl-O stretching frequency[53] of the ClO_4^- unit, which results due to the inclusion of $Hg(ClO_4)_2$ unit in **5**. Therefore, combining all the results from NMR and IR titration, it can be concluded that the plausible binding mode of Hg^{2+} ions is the conjugated di-alkyne unit in probe **5**.

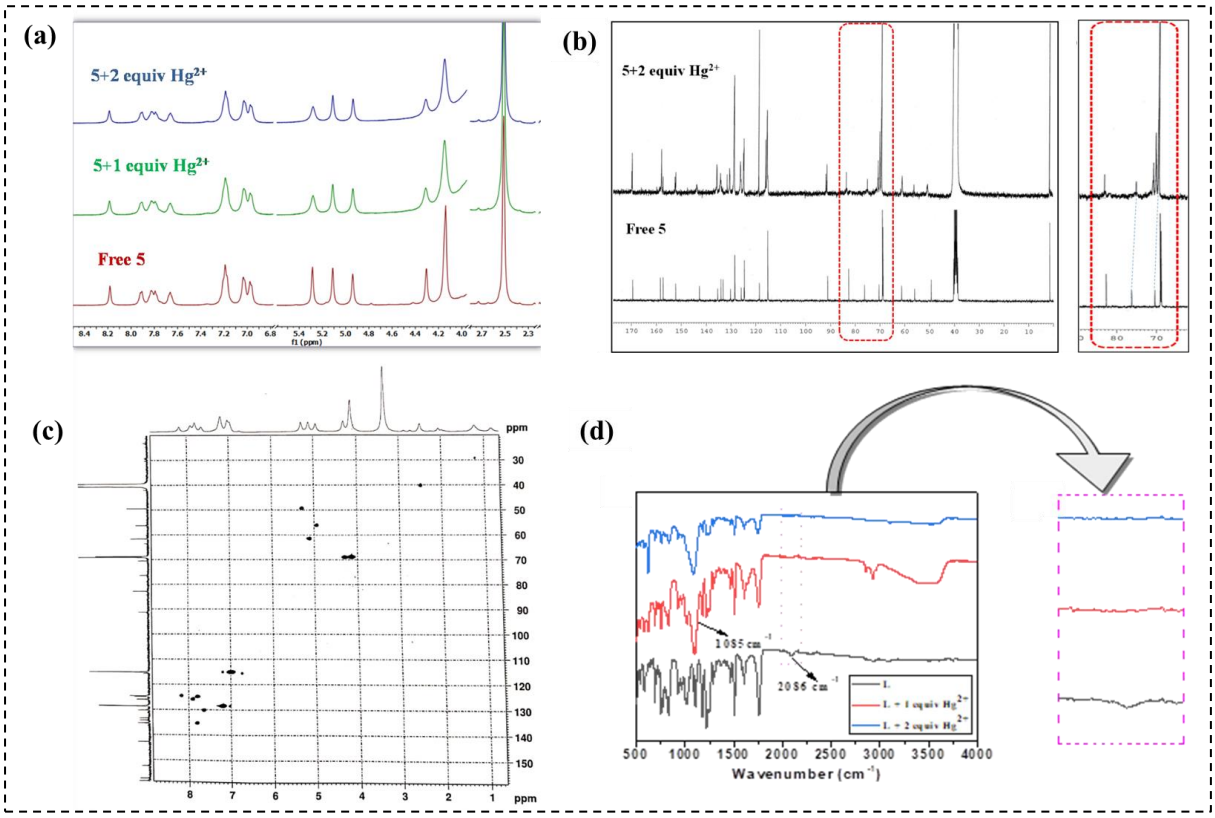

Figure 6.1.7 (a) ^{1}H NMR titration of compound **5** with $Hg(ClO_4)_2$ in d_6-DMSO solvent at room temperature. (b) ^{13}C NMR titration of compound **5** with 2 equiv Hg^{2+} ion in d_6-DMSO solvent at room temperature. Selected part from 65 ppm to 86 ppm is shown. (c) ^{1}H-^{13}C HSQC NMR spectra of compound **5** in DMSO-d_6 as solvent. (d) IR titration of **5** with 1 and 2 equiv $Hg(ClO_4)_2$ in solid state at room temperature. An enlarged image of the alkyne peak vanishing with addition of $Hg(ClO_4)_2$ is shown.

6.1.2.6. Naked-Eye Detection

A sensor, having prominent colour changing property in the visual range upon interaction with analytes, is a potential candidate for the practical application and this particular property of a sensor makes the preliminary qualitative analysis easier. To render the synthesized dialkyne moiety as a sensing probe, using its ground state complexation property, its visual detectability was qualitatively tested by naked eye. For that, each aforementioned metal ion (10^{-4} M) was added to a 10^{-4} M ligand solution and it showed colour changes from yellow to pale bluish green for Hg^{2+} and to light blue for Cu^{2+} and Fe^{3+} ions respectively (Figure 6.1.8(a)), supporting the results obtained from the previous experiments. Thus, naked eye detection makes the chemosensor molecule more susceptible to be applied practically. In fact, the quenching of fluorescence is also perceptible in the naked eye when the respective solutions of **5**, [**5**+Hg^{2+}], [**5**+Cu^{2+}] and [**5**+Fe^{3+}] are irradiated under 365nm UV lamp in dark. The irradiated pictures of **5** and [**5**+Hg^{2+}] are given in Figure 6.1.8(b) to understand the quenching of fluorescence easily.

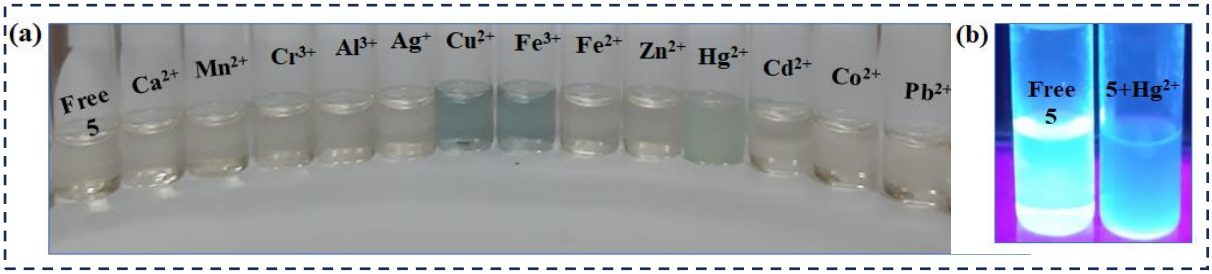

Figure 6.1.8 (a) Visual color changes observed for receptor **5** (10^{-4} M) in CH_3CN after addition of 1 equiv of several metal cations (10^{-4} M). (b) Irradiation of **5** and [**5**+Hg^{2+}] at 365 nm UV light under darkness in CH_3CN solvent to observe naked eye fluorescence quenching.

6.1.2.7. pH, Time and Temperature Effects

Phenolphthalein is well-known to be pH sensitive,[54] and therefore, it has widely been used as an indicator in acid-base titration. Thus, our designed probe, containing phenolphthalein, is expected to show pH sensitivity. Although structural modification in the phenolphthalein unit was carried out by functionalizing the phenolic –OH groups, but still there is the lactone moiety that has pH sensitivity.[55,56] Hence, the effects of pH on the fluorescence response of compound **5** and [**5**·2Hg^{2+}] complex are very important to be investigated to assess the overall applicability of the probe. A wide range of pH solutions from 2-12 in acetonitrile

were prepared taking **5** (6.62×10^{-6} M) and [**5**·$2Hg^{2+}$] (6.62×10^{-6} M) and their corresponding fluorescence spectra were recorded immediately. The spectra show that fluorescence intensities and characteristics of the free ligand as well as the complexed moiety remain intact in the pH range of 6-7, but change erratically on moving left or right in the pH scale. This experiment evidently demonstrated that, both compound **5** and [**5**·$2Hg^{2+}$] complex are stable in the biological pH range 6-7 (Figure 6.1.9(a)).

A fast response time is a promoting factor for a sensor to be used in real time. Therefore, the response time of compound **5** towards Hg^{2+} ion (2 equiv) (6.62×10^{-6} M) in CH_3CN solution was investigated by recording the changes of the fluorescence intensity of the complexed species with time at room temperature. As depicted in Figure 6.1.9(b), Hg^{2+} ion interacted with compound **5** within 1 min of its addition to the ligand solution. This can be observed from the sudden minimization of fluorescence intensity of the complexed species within the first 1 min. However, the fluorescence intensity remains almost unaltered upon rerecording the spectra after certain time intervals upto 10 min. From this study, we can conclude that the present probe has the response time of <1 min and this information will certainly allow this molecule to be used as a potential sensor probe.

Thermal stability is another primary condition to be fulfilled for a molecule to be employed as a potential sensing probe. Our developed probe has a high degree of stability at room temperature and it remains in the unperturbed form over the months. To explore the stability over a range of temperatures, we have recorded fluorescence spectra of both receptor **5** and its Hg^{2+} complex, [**5**·$2Hg^{2+}$] in different temperatures (within 25 °C-78 °C range) in acetonitrile solvent (Figure 6.1.9(c),(d)). The investigated result showed that the fluorescence intensity did not differ significantly with increasing temperature for both the free **5** (6.62×10^{-6} M) and [**5**·$2Hg^{2+}$] (6.62×10^{-6} M) system in acetonitrile. The unfluctuation in fluorescence intensities clearly indicated that the probe as well as the complexed entity are stable to temperature variation within the mentioned range. Since acetonitrile is used as the analytical solvent, fluorescence responses at temperatures above 78 °C could not be recorded.

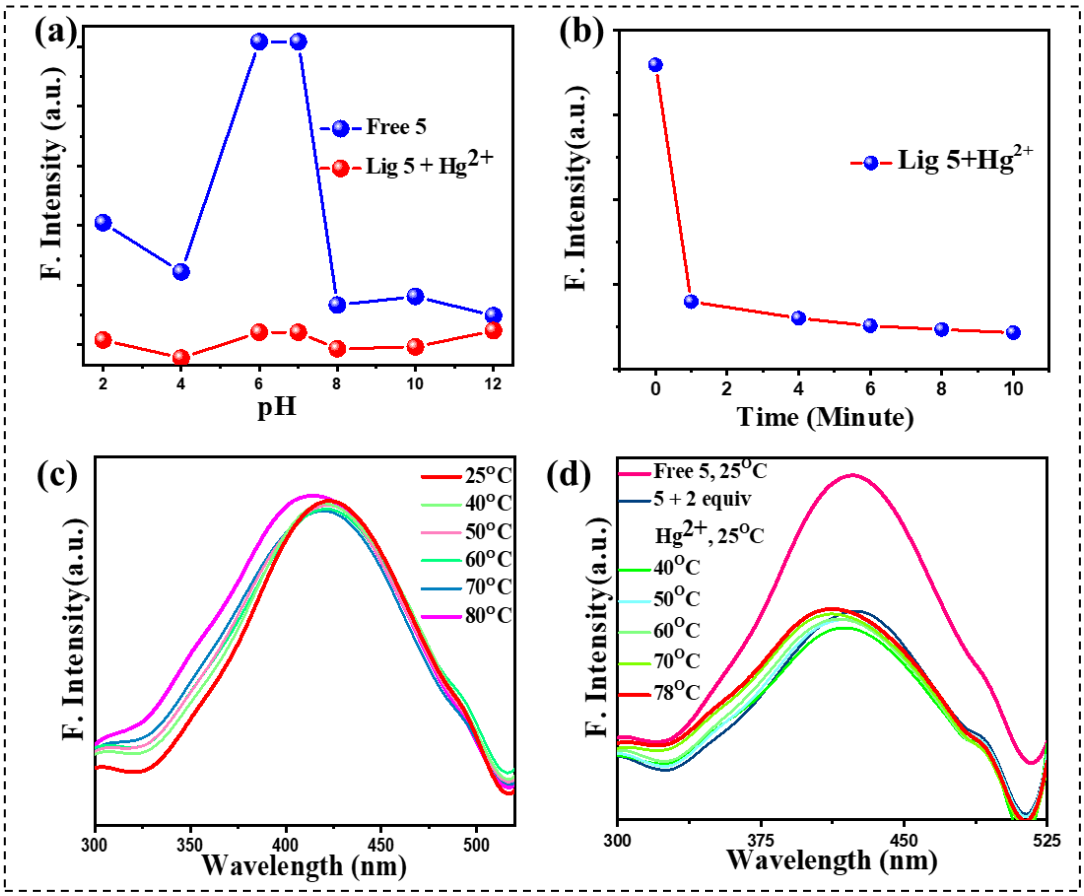

Figure 6.1.9 (a) Fluorescence response of compound **5** (6.62×10^{-6} M) as a function of pH (pH 2-12) in the absence and presence of Hg^{2+} (2 equiv) (6.62×10^{-6} M) metal ion in CH_3CN at room temperature. (b) Time-dependent fluorescence intensity changes of compound **5** (6.62×10^{-6} M) upon addition of 2 equiv Hg^{2+} (6.62×10^{-6} M) in CH_3CN solvent at room temperature. Examination of thermal stability of (c) **5** and (d) **5**+Hg^{2+} by fluorescence spectroscopy

6.1.2.8. Competitive Studies

After careful assessment about the nature of interaction of **5** with the three selected metal ions and the characteristics of the complex species, we are curious to know about the extent of restoration of those individual interactions in presence of each other metal ions (Hg^{2+}, Cu^{2+} and Fe^{3+}). Therefore, a competitive experiment was carried out by electrochemical analysis. At first, 2 equiv of Cu^{2+}/ Fe^{3+} ion was added into the CH_3CN solution of **5** and it promoted the oxidation of ferrocene to ferrocenium ion in probe **5**, with no shift in potential in CV. Further, addition of 2 equiv of Hg^{2+} to this solution led a shift in voltammetric wave towards anodic potential. This experiment indicated that Hg^{2+} ion is able to bind with the probe even after the oxidation of Fe(II) to Fe(III) of ferrocene unit of the probe (Figures 6.1.10(a),(b)).Interestingly, the same result was observed even in presence of excess Cu^{2+}/ Fe^{3+}

ions. This experimental result demonstrated that the binding interaction of Hg^{2+} ion remained unchanged in the presence of other responding cations even in excess. Moreover, we have also performed the experiment in the reverse way, *i.e.,* addition of 2 equiv of Hg^{2+} followed by the addition of 2 equiv of Cu^{2+}/ Fe^{3+} (Figure 6.1.10(c),(d)). The results showed that even after binding to Hg^{2+}, oxidation of the Fe(II) of ferrocene unit occurs in presence of Cu^{2+}/ Fe^{3+} ion. Therefore, from this competitive experiment we can conclude that the course of oxidation and binding are mutually exclusive *i.e.,* they are independent of each other and do not interfere in each other's mechanism (Figure 6.1.11).

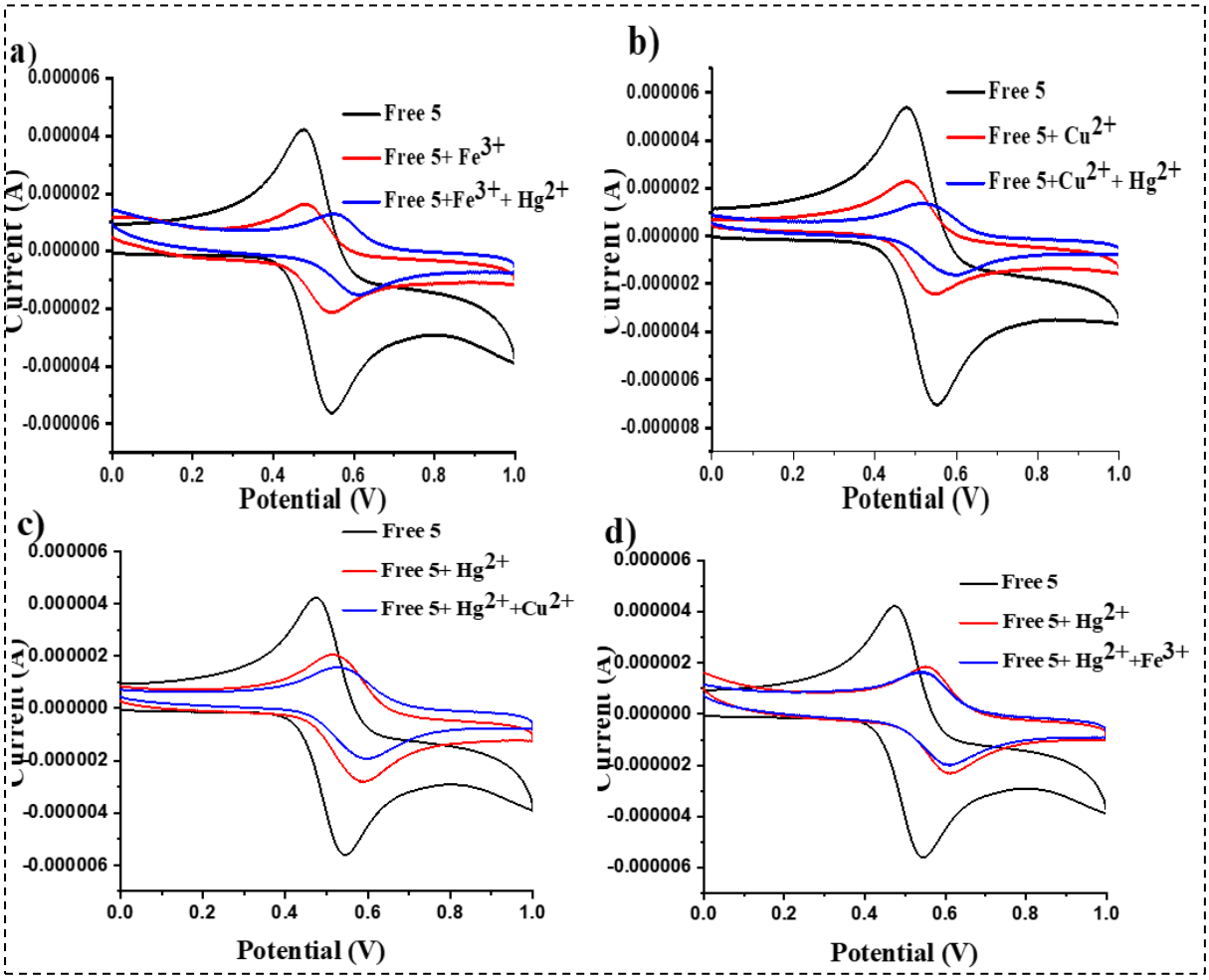

Figure 6.1.10 Competitive experiments with (a) and (d) Fe^{3+} and Hg^{2+}; (b) and (c) Cu^{2+} and Hg^{2+} in CH_3CN solvent at room temperature.

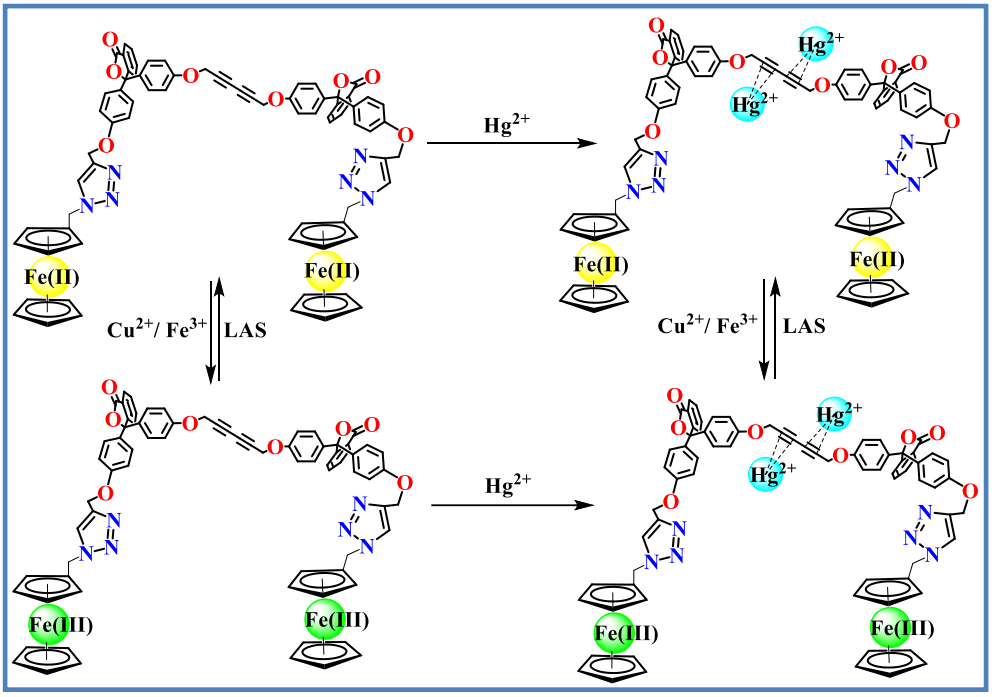

Figure 6.1.11. Schematic representation of binding mode with Hg^{2+} ion and competitive nature of interaction with all three metal ions.

6.1.2.9. Real Sample Analysis

To utilize the new sensor **5** practically, it's electrochemical sensing ability towards Hg^{2+} were quantitatively evaluated in two tap water samples, collected from Jadavpur University campus. They were filtered on a Whatman 41 filter paper and their pH were maintained around 6.5–7. Known concentrations of Hg^{2+} ion were added to the water samples separately and cyclic voltammetry (CV) spectra were recorded after addition of each aliquot of aqueous solution of Hg^{2+} ion to the ligand solution in CH_3CN (6.25×10^{-5} M). With each addition, shifts in potential were obtained for both water samples. The corresponding recovered Hg^{2+} ion concentrations were calculated from the equations y = (-4051x + 0.538) and y = (-2908x + 0.530), with correlation coefficients R^2 = 0.949 and R^2 = 0.992 for water sample-1 and water sample-2 respectively (Figure 6.1.12). The experimental concentration and percentage recovery values are shown in Table 6.1.2.

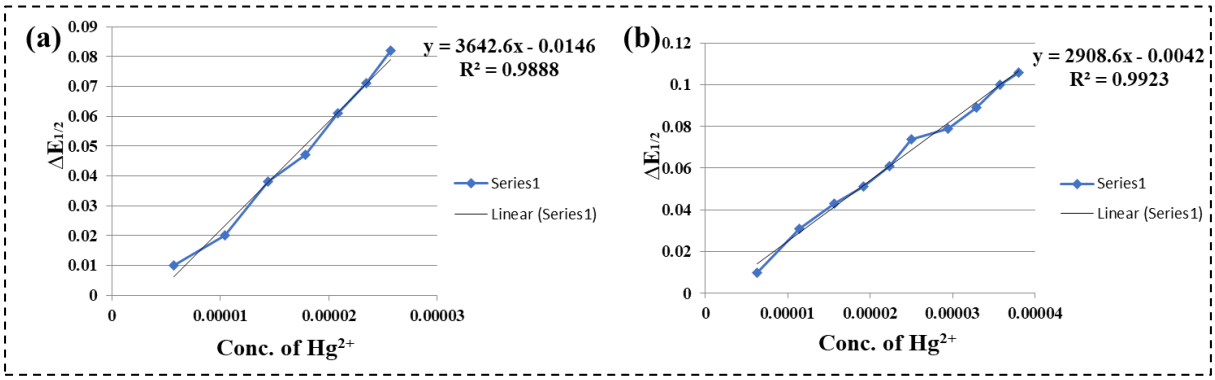

Figure 6.1.12 Linear regression plot for Hg^{2+} for (a) Pond Water and (b) Tap Water.

Table 6.1.2. Determination of recovered concentrations of Hg^{2+} ion in pond water and tap water samples.

Samples	Added metal conc. (M)	Recovered metal conc. (M)	% of Recovery	% Error
Water Sample-1	1.83×10^{-5}	1.73×10^{-5}	94.53	5.46
Water Sample-2	2.35×10^{-5}	2.31×10^{-5}	98.29	1.7

6.1.2.10. DFT Studies

In order to get the detailed information about the electronic structure and to understand the bonding scenario of the receptor towards Hg^{2+}, we have performed theoretical studies at the DFT level of theory. At first, few possible starting geometries are taken to optimize the geometry to obtain the global minima and geometry optimization of **5** and [**5**·$2Hg^{2+}$] was done by DFT calculations at B3LYP-D3/def2-SVP level of theory.[57] Their corresponding molecular orbital pictures are shown in Figures 6.1.13 and 6.1.14. The optimized structure of the receptor, **5** showed a linear structure of middle 1,3- di-alkyne unit and the two phenolphthalein-ferrocene moieties are oriented in *trans* fashion with respect to each other (Figure 6.1.15). Bond lengths are given respectively as C1-C2: 1.496Å; C2-C3: 1.250 Å; C3-C4: 1.407 Å; C4-C5: 1.25 Å; C5-C6: 1.496 Å. Analysis of bond lengths indicated a relatively shorter C3-C4 single bond which connects the two alkyne units and this observation is in agreement with literature report.[41,42] Further, it is confirmed by natural bond orbital (NBO) analysis at the same level of theory. Wiberg bond indices of the C1-C2, C2-C3, C3-C4, C4-C5 and C5-C6 bonds are 1.071, 2.610, 1.214, 2.610 and 1.070 respectively. The detailed bond lengths and Wiberg bond indices are depicted in the Table 6.1.3.

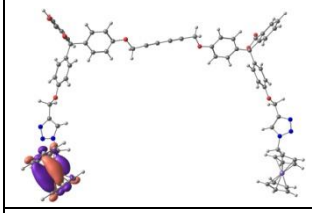	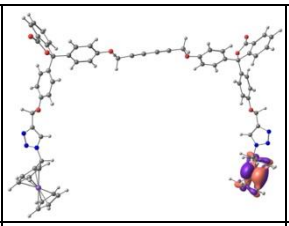	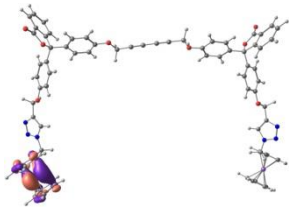	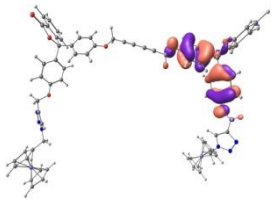
HOMO (-5.635eV)	HOMO-1 (-5.642eV)	HOMO-2 (-5.656eV)	HOMO-5 (-6.325eV)
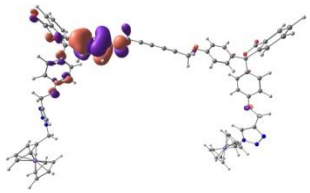	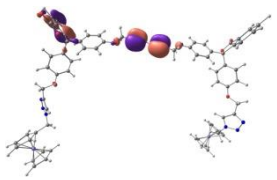	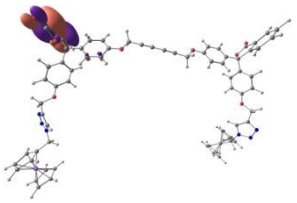	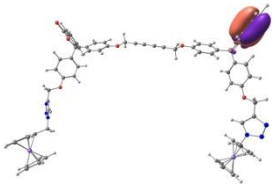
HOMO-9 (-6.514eV)	HOMO-21 (-7.447eV)	HOMO-28 (-7.58eV)	HOMO-29 (-7.585eV)
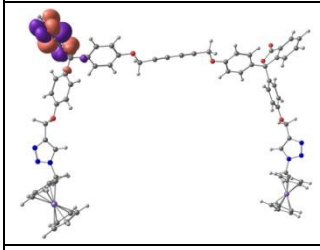	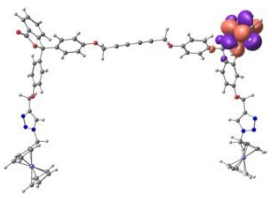	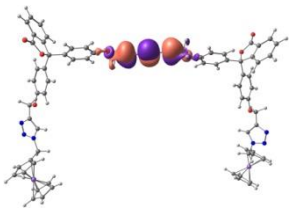	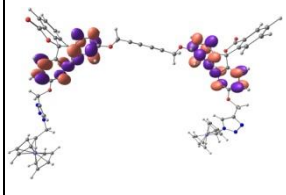
LUMO (-1.675eV)	LUMO+1 (-1.671eV)	LUMO+2 (-1.418eV)	LUMO+6 (-0.773eV)
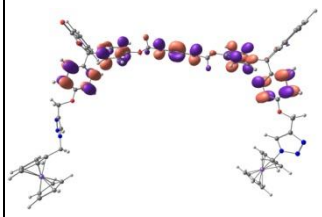	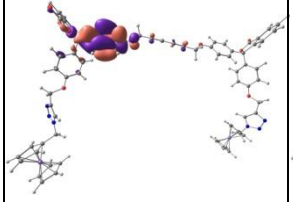	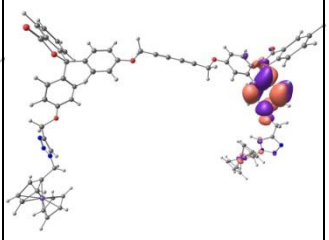	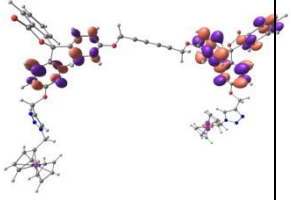
LUMO+7 (-0.72eV)	LUMO+10 (-0.465eV)	LUMO+11 (-0.426eV)	LUMO+12 (-0.359eV)
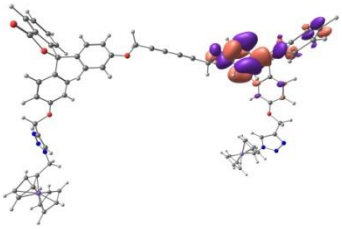			
LUMO+18 (-0.196eV)			

Figure 6.1.13. Frontiers MOs of the free ligand **5** with energy at B3LYPD3/def2SVP/CPCM (acetonitrile) level (Isosurface value=0.04).

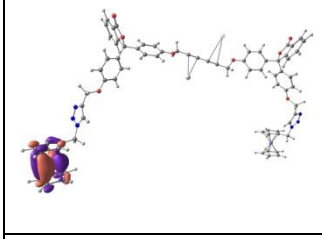	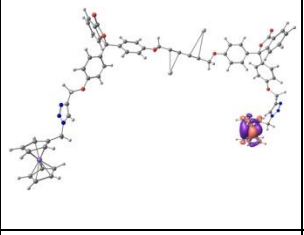	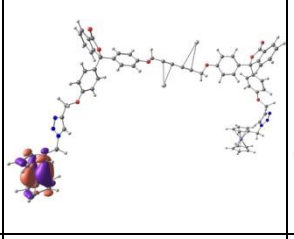	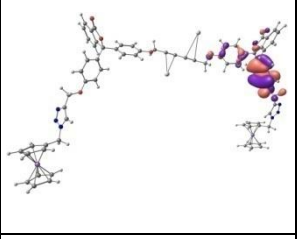
HOMO (-5.719eV)	HOMO-1 (-5.724eV)	HOMO-2 (-5.739eV)	HOMO-5 (-6.487eV)
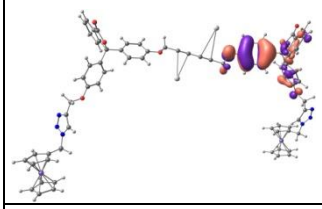	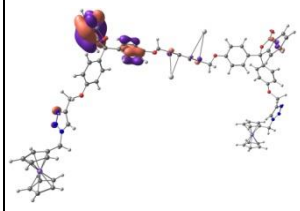	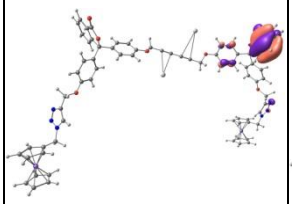	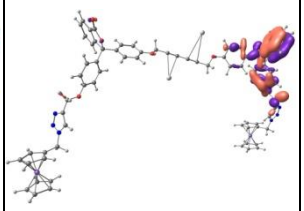
HOMO-8 (-6.73eV)	HOMO-29 (-7.73eV)	HOMO-30 (-7.74eV)	HOMO-65 (-10.564eV)
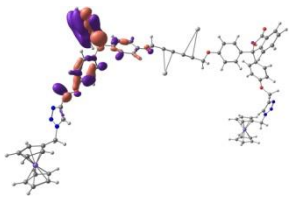	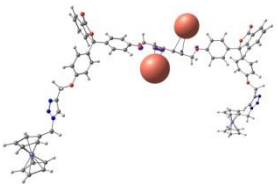	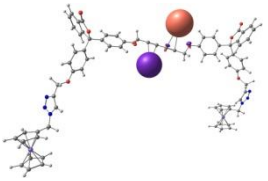	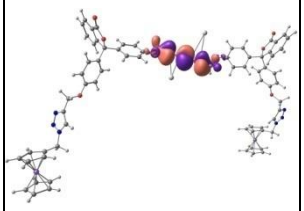
HOMO-66 (-10.565eV)	LUMO (-4.77ev)	LUMO+1 (-4.75ev)	LUMO+2 (-1.90ev)
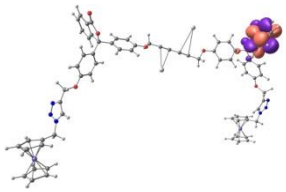	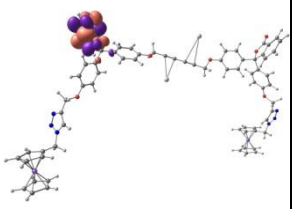	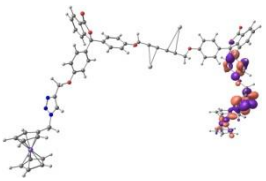	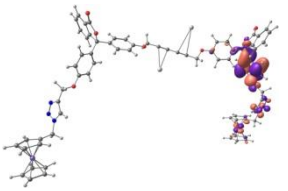
LUMO+3 (-1.82ev)	LUMO+4 (-1.81eV)	LUMO+11 (-0.63ev)	LUMO+14 (-0.52ev)

Figure 6.1.14. Frontiers MOs of [**5**·2Hg^{2+}] (involving only conjugated alkynes as binding unit) with energy at B3LYP-D3/def2SVP/CPCM (acetonitrile) level (Isosurface value=0.04).

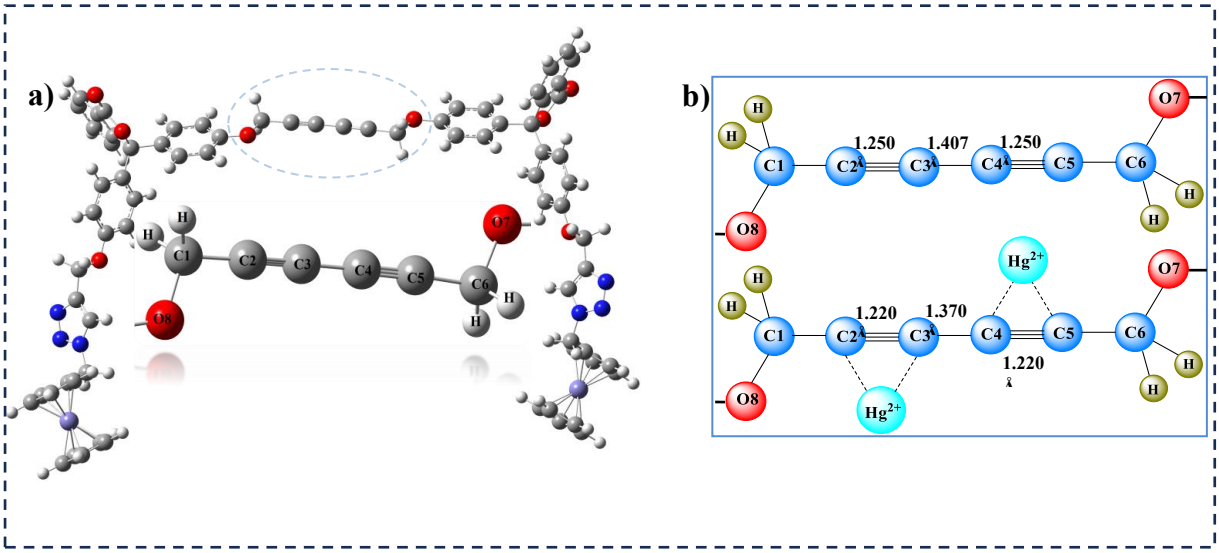

Figure 6.1.15. (a) Optimized structure of the receptor **5**. Zoomed structure of middle unit of receptor **5** to understand the bonding (inset). (b) Chemdraw structure of the conjugated binding unit before and after binding with Hg^{2+} alongwith the C-C bond lengths.

Table 6.1.3 The selected distances (Å) and Wiberg Bond Index (WBI) of **5** and [**5**·2Hg^{2+}] complex (involving only conjugated alkynes as binding unit) calculated at B3LYP-D3/def2-SVP/CPCM (acetonitrile) level (The zoomed portions of the main binding core of **5** and metal complex [**5**·2Hg^{2+}] with atom labelling are shown below the table).

	contact	Distance (Å)	WBI
Receptor[**5**]	**C1-C2/C5-C6**	1.496	1.071/1.070
	C2-C3/ C4-C5	1.250	2.610
	C3-C4	1.407	1.214
	C1-O8/ C6-O7	1.459	0.876
Complex	**C1-C2/C5-C6**	1.457	1.071/1.072
[5· 2Hg^{2+}]	**C2-C3/ C4-C5**	1.220	2.589
	C3-C4	1.370	1.215
	C1-O8/ C6-O7	1.422	0.872
Hg-Alkyne	**C2-Hg1**	3.551	0.0169
	C3-Hg1	3.601	0.0140
	C4-Hg1	3.569	0.0148
	C5-Hg2	3.549	0.0161

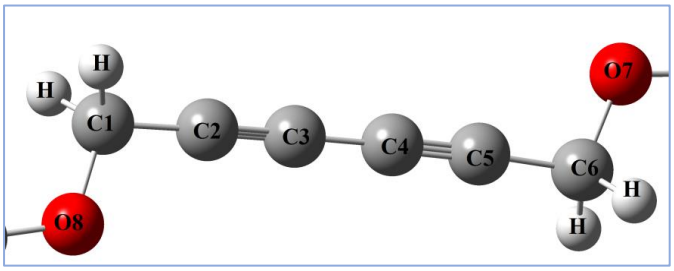

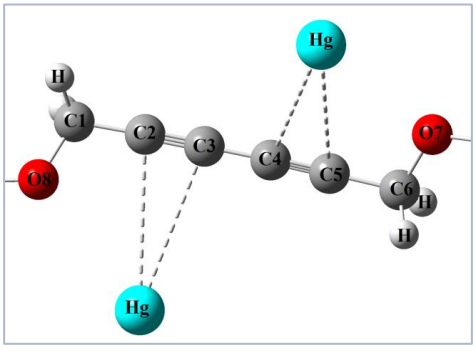

Now in order to understand the exact binding site of Hg^{2+} with receptor **5**, we have performed theoretical calculation with different model systems. We have tried to optimize all the possible structures of metal complexes with different binding sites and calculated their corresponding binding energies. Among all the possible geometries, the structure in which two Hg^{2+} ions bind with conjugated 1,3-di-yne unit is the energy-minimized structure with most stable conformation (Figure 6.1.16(a)). This result supports our experimental findings where the ligand to metal binding ratio was found to be 1:2. The binding energy of this optimized geometry is significantly high (13.64 Kcal/mol) as compared to the other optimized structures. Another geometry optimized structure involving O atom of $–OCH_2-$ unit adjacent to alkyne (Figure 6.1.16(b)) also exhibits the similar kind of binding energy (14.43 Kcal/mol). However, from the experimental results obtained from ^1H NMR and ^{13}C NMR titrations, the possibility of this optimized model can be eliminated as no shift of $–OCH_2-$ is observed in ^1H NMR as well as ^{13}C NMR titration of receptor **5** after addition of Hg^{2+} ion. Furthermore, natural bond analysis (NBO) at B3LYP-D3/def2-SVP level is performed to get insight of the bonding pattern of the [**5**·$2Hg^{2+}$]. Bond lengths (and WBI) are given as C1-C2: 1.457Å (1.071); C2-C3: 1.220 Å (2.589); C3-C4: 1.370 Å (1.215); C4-C5: 1.220 Å (2.589); C5-C6: 1.457 Å (1.072). From the energy minimized structure of the **5** and [**5**·$2Hg^{2+}$], we have observed that there is a change in alkyne bond lengths (1.25 Å to 1.22 Å) and middle C3-C4 bond length (1.40 Å to 1.37 Å) upon coordination of mercury to the receptor, indicating a weak interaction of the receptor with Hg^{2+} ion. To confirm it further we have done NBO calculation, which depicts a small change in Weiberg Bond Index from 2.610 to 2.589. This small change in WBI indicates the weak interaction of π-orbital of alkyne with the mercury ion. In the optimized structure, the bond distance between Hg and carbon atoms are in the range of 3.2-3.6 Å which corroborates with the value reported in the literature.[58] Therefore, from ^1H, ^{13}C NMR titrations and the combined DFT analysis it is confirmed that 2 Hg^{2+} ions bind with the 1,3-di-alkyne unit of the receptor and provided the more stable

conformation.

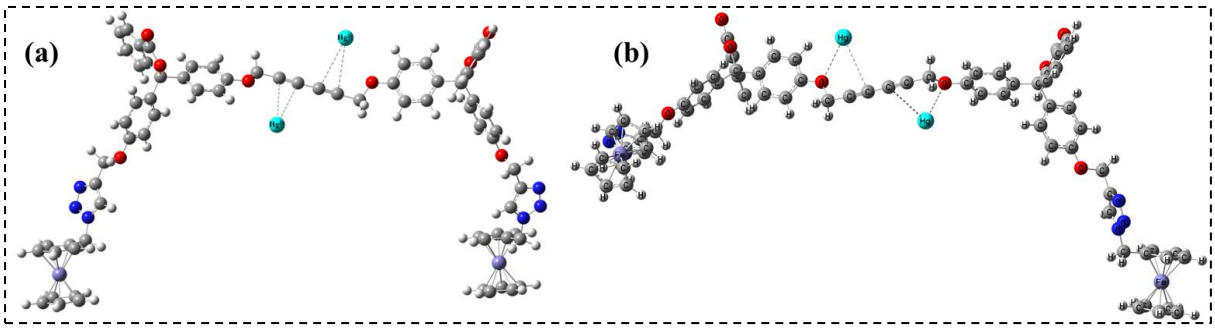

Figure 6.1.16 (a) Optimized structure of the complex [**5**·2Hg^{2+}]. (b) Alternate optimized structure of the complex [**5**·2Hg^{2+}], involving oxygen atoms along with conjugated alkynes as binding unit.

Further, to rationalize the detailed information about the UV−vis spectra, time-dependent DFT (TD-DFT) calculations at the B3LYP-D3/def2-SVP/CPCM (acetonitrile) level were performed. TD-DFT vertical excited state calculations of the receptor **5** predicts a HOMO-28 (phenolphthalein π type) to LUMO+1 (phenolphthalein π* type) transition with the band centered at 224 nm (oscillator strength $f = 0.18$) (Table 6.1.4), which is in close agreement with the experimental results. Similarly, TD-DFT calculations at the B3LYP-D3/def2-SVP/CPCM (acetonitrile) level on [**5**·2Hg^{2+}] predict a strong HOMO-29 (phenolphthalein π type) to LUMO+4 (phenolphthalein π* type) (Table 6.1.5) transition with the band centered at 225 nm (oscillator strength $f = 0.14$), and this is also in close agreement with the experimental UV−vis results. The calculated gaps between the orbitals involved in major transitions for both **5** and [**5**·2Hg^{2+}] complex are in the same range (5.91eV and 5.92eV respectively), which demonstrates no significant shifts in UV−vis absorption bands and this is clearly concurrent with the experimental findings.

Table 6.1.4 Major excited state transitions of Ligand **5** with Osc. Strength and λ_{ex}.

Molecule	λ_{ex}(nm)	Osc. Strength (*f*)	Major transition
Free Ligand [**5**]	224	0.18	H-28->L+1 (50%), H-9->L+12 (17%)
	223	0.13	H-9->L+6 (42%), H-9->L+7 (44%)

Table 6.1.5 Major excited state transitions of [**5**·2Hg^{2+}] (involving only conjugated alkynes as binding unit) with Osc. Strength and λ_{ex}.

Molecule	λ_{ex}(nm)	Osc. Strength (*f*)	Major transition
Hg^{2+} bound Ligand	221	0.10	H-66->L+1 (38%), H-65->L+1 (24%)
	222	0.10	H-66->LUMO (31%), H-65->L+1 (36%)
	224	0.13	H-30->L+3 (37%), H-5->L+14 (28%)
	225	0.14	H-29->L+4 (45%)
[**5**·2Hg^{2+}]	230	0.13	H-5->L+11 (64%)

Furthermore, to shed more light on fluorescence quenching mechanism, TD-DFT calculations were done at the same level of theory. TD-DFT calculations revealed that the mercury-centred empty orbital (LUMO) lies in between the fluorophore (phenolphthalein) transition orbitals (Figure 6.1.17). As a result, the electron in the excited state of the phenolphthalein-centred orbital (LUMO+4) got transferred to energetically favourable mercury-centred empty orbital (LUMO) instead of highly buried HOMO-29 state. Therefore, this type of orientation of orbitals might be providing an additional pathway for fluorescence quenching of receptor in presence of Hg^{2+} ion.

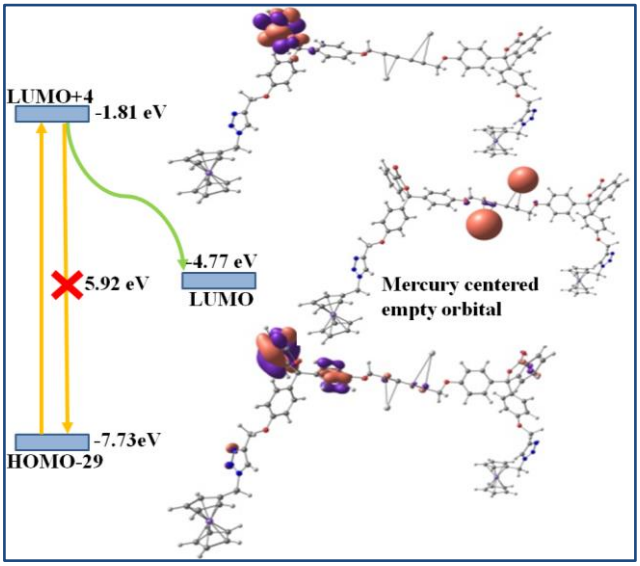

Figure 6.1.17 Schematic representation of fluorescence quenching due to Hg^{2+} ion binding to the receptor.

6.1.3. Conclusion

Herein, we have designed and synthesized a C_2-symmetric internally conjugated 1,3-di-alkyne system *via* microwave-assisted synthetic procedure in neat condition for the first time. The microwave-assisted synthesis of the probe in solution phase as well as in neat condition has paved the way for further modulation of greener ways in synthetic methodology. To the best of our knowledge, this is the first report of a conjugated 1,3-di-yne system, which has been exploited as a Hg^{2+} ion sensor. The synthesized molecule, containing ferrocene as redox unit and phenolphthalein as a fluorophore, was found to be highly selective towards the detection of Hg^{2+} ion whereas Fe^{3+} and Cu^{2+} merely promote the oxidation of ferrocene unit. Two Hg^{2+} ions bind with two-alkyne motifs by "soft-soft" interaction and this mode of binding was supported by NMR titration and DFT calculations along with optical and electrochemical experiments. We believe that we have demonstrated a new strategy using conjugated 1,3-di-yne unit for direct detection of Hg^{2+} using the concept of HSAB principle.

6.1.4. Experimental Section

6.1.4.1. Materials and reagents

Among the metal ions used, Na^+, K^+, Fe^{2+}, Fe^{3+}, Cu^{2+} and Hg^{2+} were purchased from Sigma Aldrich and Ag^+, Ca^{2+}, Mg^{2+}, Mn^{2+}, Zn^{2+}, Pb^{2+}, Co^{2+}, Cr^{3+}, Al^{3+} were purchased from Alfa Aesar, as their respective perchlorate salts and used directly without further purification. Cu^+ was purchased from Sigma Aldrich as $[(CH_3CN)_4Cu]PF_6$. NaH was purchased from Sigma Aldrich, Glacial AcOH from Merck. DMF and acetonitrile (HPLC) were purchased from Thermo Fisher Scientific and freshly distilled prior to use. Rest of the chemicals were purchased from local brand. Mono(azidomethyl)ferrocene was prepared according to literature reported procedure.[59] Chromatography was carried out using 60-120 mesh silica gel in a column of 2.5 cm diameter. All the necessary solvents were dried by conventional methods and distilled under N_2 atmosphere. The cyclic voltammetry (CV) was performed with a conventional three electrode configuration consisting of glassy carbon as working electrode, platinum as an auxiliary electrode and Ag/Ag^+ as a reference electrode. The experiment was carried out with 10^{-4} M solution of sample in CH_3CN containing 0.1 M (TBAP) [(*n*-$C_4H_9)_4NClO_4$] as supporting electrolyte. The working electrode was cleaned after each run. The cyclic voltammograms were recorded at a scan rate 0.05 Vs^{-1} and readings were taken considering ferrocene/ferrocenium couple as the standard. The UV-vis spectra were carried out

in CH_3CN solutions at c = 10^{-6} M and the fluorescence spectra were carried out at c = 10^{-6} M, as it is stated in the corresponding Figure captions.

6.1.4.2. Procedure of reversibility test of the interaction of Hg^{2+} with compound 5 by disodium EDTA

For the reversibility experiment, $Hg(ClO_4)_2 \cdot xH_2O$ was added to the CH_3CN solution of probe **5**. A decrease in the emission intensity can be observed, which reverses back nearly to its original form on introducing disodium EDTA as the chelating agent for Hg^{2+} ion. Repeated changes of fluorescence intensity can be observed on further addition of Hg^{2+} and Na_2EDTA alternatively. This proves the reversible nature of the interaction of receptor **5** with the Hg^{2+}. This experiment can be repeated at least 2 times without much loss in sensitivity.

6.1.4.3. Preparation of IR samples

The compound **5**, 1 equiv and 2 equiv of $Hg(ClO_4)_2$ were weighed separately and dissolved in acetonitrile then mixed together correspondingly to form **5**+1 equiv Hg^{2+} and **5**+2 equiv Hg^{2+}. The acetonitrile was the dried up in a rotary evaporator and then stored under vacuum for some time. Thus, we resulted in two sets of complexed species in the solid form. The IR spectra of the free ligand with these two sets of samples were recorded in solid form.

6.1.4.4. Preparation of samples for elemental analysis of the complex species:

For the elemental analysis of the [**5**·$2Hg^{2+}$] complex, pure **5** was taken in minimum amount of dichloromethane and 2 molar equiv $Hg(ClO_4)_2$ was dissolved in CH_3CN and the two solutions were mixed up gradually. The solvent mixture was evaporated in a rotary evaporator and then stored under vacuum for some time. The resulting green solid compound was washed several times with water, to remove excess perchlorate, if in case some amount of the added $Hg(ClO_4)_2$ remained unbounded to the probe. Following this, it was washed with dichloromethane, dried over Na_2SO_4 and kept under high vacuum for 5 hours. This sample was used for analysis. Anal. Calcd for $C_{74}H_{56}Fe_2N_6O_8Hg_2$, C, 53.10; H, 3.34; N, 5.02. Found: C, 54.04; H, 4.11; N, 5.84.

6.1.4.5. Instrumentation

^1H and ^{13}C NMR spectra were obtained with BRUKER 400 MHz and 300 MHz FT-NMR spectrometers respectively. For compound **2**, both ^1H and ^{13}C NMR spectra has been

taken in BRUKER 300 MHz FT-NMR spectrometer. The chemical shifts are reported in ppm, using tetramethylsilane as an internal standard and were referenced to the residual solvent as follows: $CDCl_3$ = 7.26 (^1H), 76.16 (^{13}C) ppm, DMSO = 2.51 (^1H), 39.50 (^{13}C) at room temperature. For ^1H NMR, coupling constants *J* are given in Hz and the resonance multiplicity is described as s (singlet), d (doublet), t (triplet), m (multiplet). IR spectral studies were done on Perkin Elmer LX-1 FTIR spectrophotometer. The absorption spectra were recorded with a SHIMADZU-2450 UV-vis spectrophotometer at room temperature. Fluorescence was recorded with SHIMADZU RF-5301pc spectrophotometer. CH Instruments Electrochemical Analyzer was used to perform the cyclic voltammetry (CV) and differential pulse voltammetry (DPV) studies. HRMS were taken using Quadruple-TOF (Q-TOF) micro MS system using electrospray ionization (ESI) technique. CHN analysis was performed on a CHNS analyser. Microwave optimization has been done in CEM microwave.

Caution! Metal perchlorate salts are potentially explosive in certain conditions. All due precautions should be taken while handling perchlorate salts!

6.1.4.6. Synthesis of Compounds 2, 3 and 5

6.1.4.6.1. Synthesis of compound 2

Phenolphthalein (500 mg, 1.57 mmol) was taken in a clean round-bottomed flask and dissolved in 10 mL of DMSO solvent. K_2CO_3 (867 mg, 6.28 mmol) was added to the solution and kept to stir for 30 mins after which propargyl bromide (0.5 mL, 6.28 mmol) was added and stirring was continued overnight. The reaction mixture was extracted with EtOAc, dried over Na_2SO_4 and solvent dried under vacuum. Column chromatography in 20% EtOAc in hexane gave pure compound **2** (3,3-bis(4-(prop-2-yn-1-yloxy)phenyl)isobenzofuran-1(3*H*)-one) (499 mg, 80% yield). ^1H NMR ($CDCl_3$, 300 MHz) δ = 7.91 (d, 1H, $H_{aromatic}$, J = 6 Hz), 7.70-7.67 (m, 1H, $H_{aromatic}$), 7.58-7.52 (m, 2H, $H_{aromatic}$), 7.30-7.25 (m, 4H, $H_{aromatic}$), 6.96-6.91 (m, 4H, $H_{aromatic}$), 4.68 (d, 4H, J = 2.4 Hz, OCH_2), 2.53 (t, 2H, J = 2.4 Hz, H_{alkyne}); ^{13}C NMR ($CDCl_3$,75 MHz) δ = 169. 8, 157.6, 152.4, 134.2, 133.9, 129.3, 128.6, 126.0, 125.5, 124.1, 114.7, 91.4, 78.3, 75.9, 55.8; HRMS *m/z* calcd for $C_{26}H_{18}O_4$ $[M+Na]^+$ 417.1102; found 417.0885.

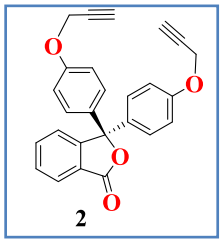

2

6.1.4.6.2. Synthesis of Compound 3

3,3-bis(4-(prop-2-yn-1-yloxy)phenyl)isobenzofuran-1(3*H*)-one (**2**) (1g, 2.53 mmol) and 0.9 equiv of mono(azidomethyl)ferrocene (554.48 mg, 2.3 mmol) were taken in a 100mL round bottom flask and dissolved in ^{t}BuOH (26mL) solvent. $CuSO_4 \cdot 5H_2O$ and Sodium-L-

ascorbate were dissolved in a total of 13mL of H_2O and added to the reaction mixture one by one at room temperature. After 1 h, a greenish suspension was formed which was allowed to stir overnight at room temperature. Reaction mixture was diluted with ethyl acetate and washed with distilled water. The organic phase was separated, dried over sodium sulphate and the solvent was removed under reduced pressure. Then the crude product was purified by silica gel column chromatography. Elution with 40% EtOAc/Hexane gave yellow coloured solid compound **3** (550mg, 0.86 mmol, yield 35 %) along with some amount of compound **4** (0.5 mmol, yield 20%) as side product. **3**: ^{1}H NMR ($CDCl_3$,400 MHz) δ = 7.93 (d, 1H, J = 8 Hz, $H_{aromatic}$), 7.69 (t, 1H, J = 8 Hz, $H_{aromatic}$), 7.57 (s, 1H, $H_{aromatic}$), 7.55 (s, 1H, $H_{triazole}$), 7.51 (d, 1H, J = 8 Hz, $H_{aromatic}$), 7.22-7.28 (m, 4H, $H_{aromatic}$), 6.92 (d, 4H, J = 8 Hz, $H_{aromatic}$), 5.30 (s, 2H, OCH_2), 5.15 (s, 2H, NCH_2), 4.68 (s, 2H, OCH_2), 4.28 (s, 2H, H_{Fc}), 4.22 (s, 2H, H_{Fc}), 4.17 (s, 5H, H_{Fc}), 2.53 (s, 1H, H_{alkyne}); ^{13}C NMR ($CDCl_3$,75 MHz) δ = 169.77, 158.32, 157.61, 152.42, 143.67, 134.12, 133.97, 133.52, 129.25, 128.65, 128.49, 125.96, 125.55, 124.02, 122.15, 114.70, 114.64, 91.45, 80.72, 78.27, 75.80, 69.09, 68.92, 62.061, 55.83, 50.16, 30.91; HRMS *m/z*calcd for $C_{37}H_{29}FeN_3O_4$ $[M]^+$ 635.1507; found 635.1900; Anal. Calcd for $C_{37}H_{29}FeN_3O_4$, C, 69.93; H, 4.60; N, 6.61. Found: C, 69.63; H, 4.48; N, 6.42.

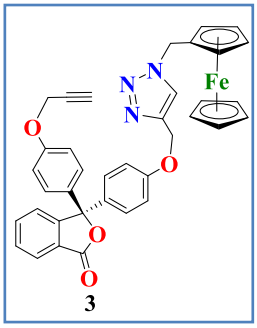

3

6.1.4.6.3. Synthesis of compound 5

The coupling reaction of compound **3** had been performed by two ways: one by slight modification of the already established procedure,[36] and another by taking the assistance of single focus microwave in closed reaction system.

By conventional way: Compound **3** (206 mg, 0.324 mmol) and 15 equiv of $Cu(OAc)_2 \cdot H_2O$ (971.25 mg, 4.86 mmol) were added in a 100 ml round bottom flask and dissolved in pyridine solvent (15mL) .The reaction mixture was stirred at room temperature for 2 h and then at 60°C for 2 h. The blue reaction mixture was cooled to room temperature and the stirring was continued for further 48 h. Cold water was added after which brown precipitate appeared and the reaction mixture was stirred for another 10 mins. Filtration of the brown precipitate under suction and successive washings with water and finally with ethanol gave us dry pyridine free product, which on further purification by silica gel column chromatography (60% EtOAC/Hex) gave a pale yellow coloured solid compound **5** (61 mg, yield 29.67%).

Microwave assisted reaction: This was done in closed reaction system whereby compound **3** (100 mg, 0.16 mmol) was taken into the closed system vessel containing a rice magnet, dissolved in pyridine solvent (5 mL) and then the catalyst $Cu(OAc)_2 \cdot H_2O$ (3 equiv, 100 mg, 0.5 mmol) was added. When the catalyst gets dissolved totally, the vessel was put to microwave radiation in the reactor under 50 watt power maintaining a constant 60°C for 30 mins. After cooling the reaction vessel it was taken out and the colour of the reaction mixture was seen to change from green (before the reaction) to yellowish green (after the reaction). The reaction mixture was poured into a vessel containing cold water (7 mL) and was left for sometime after which brown precipitate can be observed. It was filtered and washed successively with water (5×10 mL) and finally with ethanol (2 mL). The precipitate was re-dissolved in DCM and further purification was done by silica gel column chromatography after which pure **5** was obtained (91 mg, 0.072 mmol, yield 90 %).

For the neat reaction, **3** (50 mg, 0.078 mmol) was grinded well with 3.7 equiv $Cu(OAc)_2 \cdot H_2O$ (58 mg, 0.29 mmol) until a homogeneous powder was formed. Then it was poured into the glass tube for closed vessel reaction system along with 3 equiv of pyridine as base (19 µL, 0.234 mmol) and mixed properly then subjected to microwave irradiation at 50 watt power and 60°C for 30 minutes. Then it was cooled down and washed successively with water to remove any traces of pyridine. Finally, work up in EtOAc and removing the solvent under vacuum after drying on sodium sulphate gave compound **5** with 80% conversion of compound **3**.

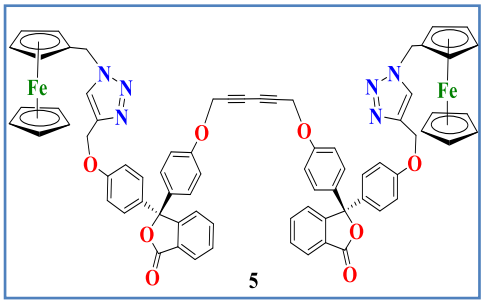

5

^{1}H NMR ($CDCl_3$,400 MHz)δ = 7.91 (d, 1H, J = 8 Hz, $H_{aromatic}$), 7.67 (t, 1H, J = 8 Hz, $H_{aromatic}$), 7.53(t, 1H, J = 8 Hz, $H_{aromatic}$), 7.49 (s, 1H, $H_{triazole}$), 7.48 (s, 1H, $H_{aromatic}$), 7.21 (t, 4H, J = 8 Hz, $H_{aromatic}$), 6.91-6.85 (m, 4H, $H_{aromatic}$), 5.26 (s, 2H, OCH_2), 5.13(s, 2H, OCH_2), 1.63(s, 2H, NCH_2), 4.26(s, 2H, H_{Fc}), 4.21(s, 2H, H_{Fc}), 4.16(s, 5H, H_{Fc}); ^{13}C NMR (d_6-DMSO,75 MHz) δ = 169.41, 158.26, 157.22, 152.19, 142.77, 135.38, 134.07, 133.22, 130.20, 128.45, 128.42, 125.87, 124.70, 124.55, 118.49, 115.08, 91.16, 82.63, 76.19, 70.35, 68.95, 68.91, 68.71, 61.26, 56.01, 49.31; HRMS (ESI) *m/z* calcd for $C_{74}H_{56}Fe_2N_6O_8$ $[M+H]^+$ 1269.2937; found 1269.2935; Anal. Calcd for $C_{74}H_{56}Fe_2N_6O_8$, C, 70.03; H, 4.45; N, 6.63. Found: C, 69.43; H, 4.38; N, 6.39.

6.1.4.7. Computational Studies

All computational calculations presented in this paper were performed by density functional theory (DFT) method using the Gaussian 16[60] program package. Full geometry optimizations were carried out using B3LYP (Becke, three parameter, Lee-Yang-Parr)-D3 level of theory.[61] The def2-SVP[57] basis set was employed for all the atoms with the conductor-like polarizable continuum model[62] (CPCM) using acetonitrile as a solvent. The vibrational frequency calculations were performed to ensure that the optimized geometries represent the local minima and that there are only positive eigen values. Natural bond orbital (NBO) analysis[63] and Wiberg bond indices (WBI)[64] were performed at the same level[57,61] using the NBO Version 3.1 program implemented in the Gaussian package. Orbital diagrams are rendered in the Chemcraft visualization software with an isosurface value 0.04.[65]

Table 6.1.6 Cartesian coordinates (Å) of the ligand **5**.

B3LYP-D3/def2-SVP-CPCM (acetonitrile)

Energy (a.u.) = -6308.37769

C	2.326882000000	3.229450000000	-0.031156000000
C	1.138897000000	3.490753000000	-0.113084000000
C	3.732552000000	2.857284000000	0.084664000000
C	-0.203121000000	3.764802000000	-0.192860000000
C	-1.398028000000	3.991815000000	-0.274508000000
C	-2.831963000000	4.249264000000	-0.352449000000
O	4.535487000000	3.825207000000	-0.580841000000
O	-3.518192000000	3.200956000000	0.322454000000
C	5.881134000000	3.626038000000	-0.633159000000
C	-4.877202000000	3.202185000000	0.330647000000
C	6.620504000000	4.593229000000	-1.335484000000
C	8.002872000000	4.475195000000	-1.450865000000
C	8.680420000000	3.386239000000	-0.879581000000
C	7.936273000000	2.428679000000	-0.181878000000
C	6.548518000000	2.539034000000	-0.048089000000
C	-5.483155000000	2.116610000000	0.991564000000
C	-6.866378000000	2.016765000000	1.042861000000
C	-7.688320000000	2.991104000000	0.444237000000
C	-7.076340000000	4.071833000000	-0.194483000000
C	-5.680667000000	4.185522000000	-0.261371000000
C	-11.015386000000	5.234757000000	-1.867030000000
C	-11.669696000000	6.024598000000	-0.903993000000
C	-11.504463000000	5.761130000000	0.457510000000
C	-10.668509000000	4.700635000000	0.814230000000
C	-10.012311000000	3.921406000000	-0.134683000000
C	-10.182230000000	4.171857000000	-1.495710000000
C	-10.334800000000	4.182472000000	2.157346000000
O	-9.518087000000	3.104702000000	1.993338000000
C	-9.202696000000	2.851871000000	0.584296000000
O	-10.679606000000	4.567603000000	3.246981000000
C	-9.704469000000	1.457889000000	0.205576000000
C	-9.222053000000	0.832557000000	-0.957773000000
C	-9.710721000000	-0.405823000000	-1.358147000000
C	-10.697986000000	-1.060743000000	-0.598422000000
C	-11.186970000000	-0.445220000000	0.563884000000
C	-10.689481000000	0.805204000000	0.951155000000
O	-11.101245000000	-2.269614000000	-1.062323000000
C	-12.087453000000	-3.005724000000	-0.334243000000
C	-12.329632000000	-4.297029000000	-1.037359000000
N	-13.267923000000	-4.433224000000	-2.016413000000
N	-13.231429000000	-5.648134000000	-2.479797000000
N	-12.268968000000	-6.310325000000	-1.820972000000
C	-11.677913000000	-5.511510000000	-0.903189000000
C	-12.047756000000	-7.738097000000	-2.069713000000
C	11.407249000000	4.583447000000	2.493916000000
C	12.243571000000	5.607897000000	2.014737000000
C	12.375717000000	5.829357000000	0.642084000000
C	11.660888000000	4.994471000000	-0.219500000000
C	10.843348000000	3.969570000000	0.249387000000
C	10.693105000000	3.755300000000	1.618897000000
C	11.573318000000	5.025370000000	-1.694308000000
O	10.696298000000	4.054924000000	-2.076043000000
C	10.204565000000	3.270344000000	-0.941199000000
O	12.122347000000	5.744837000000	-2.491140000000
C	10.659683000000	1.830176000000	-1.168930000000
C	10.207197000000	1.173579000000	-2.329949000000
C	10.571237000000	-0.137611000000	-2.599067000000
C	11.399564000000	-0.839954000000	-1.702243000000
C	11.871769000000	-0.194599000000	-0.552123000000
C	11.500899000000	1.134186000000	-0.299467000000

O	11.680619000000	-2.123211000000	-2.038609000000
C	12.388058000000	-2.950242000000	-1.126517000000
C	12.381304000000	-4.339847000000	-1.676037000000
N	13.328968000000	-5.261647000000	-1.354919000000
N	13.045877000000	-6.389251000000	-1.946878000000
N	11.920266000000	-6.210563000000	-2.648032000000
C	11.462406000000	-4.940863000000	-2.517611000000
C	11.396936000000	-7.279502000000	-3.503393000000
H	4.009210000000	2.785831000000	1.155368000000
H	3.878971000000	1.852866000000	-0.359739000000
H	-3.063317000000	5.229150000000	0.106724000000
H	-3.142757000000	4.302207000000	-1.413436000000
H	6.086869000000	5.431128000000	-1.788944000000
H	8.560365000000	5.232675000000	-2.003612000000
H	8.438749000000	1.567291000000	0.263463000000
H	6.011669000000	1.768119000000	0.503959000000
H	-4.842236000000	1.361928000000	1.451908000000
H	-7.323520000000	1.165917000000	1.552690000000
H	-7.681451000000	4.851619000000	-0.658957000000
H	-5.247218000000	5.042919000000	-0.775603000000
H	-11.162111000000	5.453784000000	-2.927457000000
H	-12.314107000000	6.845106000000	-1.227520000000
H	-12.007949000000	6.354123000000	1.224137000000
H	-9.684525000000	3.562504000000	-2.252538000000
H	-8.443760000000	1.315216000000	-1.552979000000
H	-9.334617000000	-0.896153000000	-2.257954000000
H	-11.949274000000	-0.922390000000	1.178848000000
H	-11.076398000000	1.267805000000	1.859813000000
H	-11.737194000000	-3.190532000000	0.695528000000
H	-13.029334000000	-2.432901000000	-0.285005000000
H	-10.876097000000	-5.850968000000	-0.254102000000
H	11.308975000000	4.433477000000	3.571775000000
H	12.784206000000	6.238052000000	2.724444000000
H	13.006962000000	6.627547000000	0.245858000000
H	10.037117000000	2.971647000000	2.002878000000
H	9.553271000000	1.703892000000	-3.025529000000
H	10.218325000000	-0.652233000000	-3.495012000000
H	12.527006000000	-0.703906000000	0.153775000000
H	11.882961000000	1.614893000000	0.601708000000
H	13.429232000000	-2.606428000000	-0.991055000000
H	11.899709000000	-2.924431000000	-0.134058000000
H	10.566432000000	-4.577575000000	-3.011930000000
H	-13.388066000000	-11.375543000000	-3.996695000000
C	-12.891406000000	-11.673801000000	-3.074404000000
H	-14.780135000000	-8.802974000000	-2.497581000000
H	-14.431454000000	-12.969011000000	-2.068651000000
C	-13.442148000000	-12.513854000000	-2.056507000000
H	-10.916065000000	-10.603576000000	-3.197524000000
C	-11.587062000000	-11.266005000000	-2.652216000000
H	-15.713555000000	-10.349424000000	-0.471547000000
C	-14.259010000000	-9.036175000000	-1.570040000000
C	-14.748509000000	-9.845787000000	-0.501329000000
Fe	-13.004963000000	-10.646300000000	-1.285877000000
C	-12.477850000000	-12.625760000000	-1.005922000000
C	-11.331080000000	-11.854935000000	-1.374324000000
C	-12.933221000000	-8.608300000000	-1.229924000000
C	-13.736477000000	-9.909894000000	0.507664000000
H	-12.604406000000	-13.180883000000	-0.077488000000
H	-10.431405000000	-11.718399000000	-0.775776000000
C	-12.618838000000	-9.139717000000	0.064818000000
H	-11.677232000000	-9.002832000000	0.595413000000
H	9.656325000000	-9.789630000000	-4.705739000000
C	10.089459000000	-9.821106000000	-5.704745000000
H	11.890890000000	-11.140700000000	-5.429928000000
C	11.268754000000	-10.534674000000	-6.086764000000
H	8.724105000000	-8.480644000000	-6.888126000000
C	9.597300000000	-9.130860000000	-6.856488000000
H	13.785633000000	-8.546350000000	-4.719405000000
C	11.968876000000	-7.233153000000	-4.888017000000
C	13.160106000000	-7.897045000000	-5.330327000000
Fe	11.517372000000	-8.509996000000	-6.414021000000
C	11.505757000000	-10.284019000000	-7.474775000000
C	10.472595000000	-9.416693000000	-7.950439000000
C	11.440058000000	-6.494652000000	-5.998165000000
C	13.350134000000	-7.588334000000	-6.710966000000
H	12.339736000000	-10.667352000000	-8.060992000000
H	10.382048000000	-9.023223000000	-8.961938000000
C	12.288964000000	-6.722137000000	-7.123068000000
H	14.148681000000	-7.967739000000	-7.346618000000
H	12.139166000000	-6.327589000000	-8.126964000000
H	10.531044000000	-5.894411000000	-5.985804000000
H	11.643861000000	-8.228402000000	-3.010030000000
H	10.304085000000	-7.177739000000	-3.528937000000
H	-12.236064000000	-7.904960000000	-3.137921000000
H	-10.989379000000	-7.948189000000	-1.868691000000
H	-13.797186000000	-10.470804000000	1.439280000000

Table 6.1.7 Cartesian coordinates (Å) of the mercury bound ligand [**5**·2Hg^{2+}] (involving only conjugated alkynes as binding unit).

B3LYP-D3/def2-SVP-CPCM (acetonitrile):

Energy (a.u.) = -6614.823612

C	-2.483568000000	-2.811463000000	-0.566355000000
C	-1.362624000000	-3.162869000000	-0.895855000000
C	-3.819264000000	-2.395800000000	-0.159902000000
C	-0.092408000000	-3.533649000000	-1.252452000000

C	1.040151000000	-3.871620000000	-1.556590000000
C	2.404058000000	-4.247950000000	-1.902587000000
O	-4.742747000000	-3.416318000000	-0.516484000000
O	3.259606000000	-3.911462000000	-0.815130000000
C	-6.008987000000	-3.372623000000	-0.011440000000
C	4.605927000000	-4.066155000000	-0.964992000000
C	-6.788212000000	-4.523211000000	-0.210737000000
C	-8.098992000000	-4.567978000000	0.256399000000
C	-8.659115000000	-3.469837000000	0.929375000000
C	-7.870518000000	-2.331925000000	1.125212000000
C	-6.551677000000	-2.271276000000	0.662081000000
C	5.402240000000	-3.534922000000	0.065837000000
C	6.784461000000	-3.655068000000	0.005716000000
C	7.410802000000	-4.304125000000	-1.075863000000
C	6.607720000000	-4.827148000000	-2.090798000000
C	5.211787000000	-4.708878000000	-2.050161000000
C	10.233836000000	-5.755143000000	-4.454189000000
C	10.743934000000	-6.984734000000	-3.999168000000
C	10.651478000000	-7.333480000000	-2.649927000000
C	10.031955000000	-6.425559000000	-1.788239000000
C	9.515554000000	-5.212606000000	-2.235724000000
C	9.617613000000	-4.852105000000	-3.578721000000
C	9.829100000000	-6.510504000000	-0.327008000000
O	9.232062000000	-5.352773000000	0.075017000000
C	8.930216000000	-4.461526000000	-1.048120000000
O	10.113944000000	-7.388395000000	0.448772000000
C	9.665629000000	-3.136913000000	-0.846518000000
C	9.245433000000	-1.986309000000	-1.536437000000
C	9.964213000000	-0.798810000000	-1.447650000000
C	11.126405000000	-0.727686000000	-0.657439000000
C	11.546630000000	-1.867790000000	0.045965000000
C	10.817532000000	-3.057715000000	-0.059080000000
O	11.760332000000	0.470534000000	-0.635512000000
C	12.992657000000	0.594612000000	0.079466000000
C	13.534349000000	1.965494000000	-0.138158000000
N	14.254350000000	2.294603000000	-1.248727000000
N	14.573643000000	3.553574000000	-1.195006000000
N	14.062548000000	4.059848000000	-0.062234000000
C	13.406642000000	3.105171000000	0.637913000000
C	14.350363000000	5.445095000000	0.322559000000
C	-9.498871000000	-4.571324000000	5.203983000000
C	-10.275159000000	-5.744394000000	5.186248000000
C	-10.927709000000	-6.144052000000	4.017866000000
C	-10.785558000000	-5.334822000000	2.888511000000
C	-10.029244000000	-4.166234000000	2.905157000000
C	-9.361792000000	-3.770352000000	4.063335000000
C	-11.319046000000	-5.527736000000	1.523819000000
O	-10.856265000000	-4.504949000000	0.750991000000
C	-10.068717000000	-3.537626000000	1.520391000000
O	-12.022562000000	-6.400433000000	1.079689000000
C	-10.801596000000	-2.201064000000	1.439068000000
C	-10.947691000000	-1.598342000000	0.174235000000
C	-11.605727000000	-0.385426000000	0.029597000000
C	-12.138676000000	0.272174000000	1.156864000000
C	-12.016139000000	-0.325559000000	2.419240000000
C	-11.353822000000	-1.554665000000	2.546307000000
O	-12.738694000000	1.462944000000	0.919378000000
C	-13.269198000000	2.210628000000	2.017947000000
C	-13.804434000000	3.501603000000	1.501028000000
N	-15.090510000000	3.644319000000	1.070661000000
N	-15.270841000000	4.863525000000	0.655161000000
N	-14.114254000000	5.526075000000	0.810927000000
C	-13.162591000000	4.717087000000	1.330666000000
C	-13.985636000000	6.915418000000	0.360207000000
H	-3.826198000000	-2.221792000000	0.932969000000
H	-4.082944000000	-1.439146000000	-0.649335000000
H	2.444232000000	-5.333033000000	-2.115461000000
H	2.715871000000	-3.718486000000	-2.822931000000
H	-6.342085000000	-5.372502000000	-0.734394000000
H	-8.694800000000	-5.466734000000	0.092683000000
H	-8.286607000000	-1.464308000000	1.640053000000
H	-5.975683000000	-1.360435000000	0.822325000000
H	4.911196000000	-3.030086000000	0.901099000000
H	7.395592000000	-3.237214000000	0.808619000000
H	7.057810000000	-5.342428000000	-2.939851000000
H	4.623961000000	-5.131668000000	-2.864343000000
H	10.323831000000	-5.497381000000	-5.512291000000
H	11.221199000000	-7.665109000000	-4.707835000000
H	11.050331000000	-8.276671000000	-2.270421000000
H	9.233467000000	-3.896785000000	-3.941631000000
H	8.343102000000	-2.017789000000	-2.150857000000
H	9.643401000000	0.096211000000	-1.984454000000
H	12.434635000000	-1.847826000000	0.676848000000
H	11.158967000000	-3.935039000000	0.491874000000
H	12.829405000000	0.413658000000	1.155423000000
H	13.718345000000	-0.149042000000	-0.292712000000
H	12.923472000000	3.298380000000	1.591674000000
H	-8.989408000000	-4.281126000000	6.125975000000
H	-10.359585000000	-6.347793000000	6.092651000000
H	-11.525603000000	-7.056994000000	3.975918000000
H	-8.749190000000	-2.866854000000	4.084530000000
H	-10.530651000000	-2.090945000000	-0.706796000000
H	-11.716416000000	0.086143000000	-0.948842000000
H	-12.426041000000	0.145747000000	3.311709000000
H	-11.273777000000	-1.997098000000	3.539817000000
H	-14.080531000000	1.643131000000	2.505160000000
H	-12.477704000000	2.397730000000	2.763205000000
H	-12.149790000000	5.052833000000	1.536394000000
H	16.871838000000	8.908021000000	-0.491733000000
C	16.617385000000	8.937600000000	0.566757000000
H	17.217820000000	5.642907000000	-0.390488000000
H	18.627275000000	9.106214000000	1.563950000000
C	17.543653000000	9.041372000000	1.651607000000
H	14.376889000000	8.732792000000	0.551604000000
C	15.300785000000	8.844737000000	1.117775000000
H	18.897533000000	5.806458000000	1.735570000000
C	16.933218000000	5.625882000000	0.660305000000
C	17.814052000000	5.706974000000	1.780548000000

Fe	16.468795000000	7.282565000000	1.792872000000
C	16.799322000000	9.013623000000	2.872648000000
C	15.413385000000	8.892222000000	2.542641000000
C	15.589891000000	5.554278000000	1.157939000000
C	17.023219000000	5.672400000000	2.972056000000
H	17.217155000000	9.053547000000	3.877740000000
H	14.589775000000	8.822002000000	3.252044000000
C	15.651320000000	5.568109000000	2.590916000000
H	14.793956000000	5.537917000000	3.262344000000
H	-14.112411000000	10.202145000000	0.142250000000
C	-13.738812000000	10.306641000000	-0.875527000000
H	-15.618997000000	10.252395000000	-2.109644000000
C	-14.534030000000	10.333746000000	-2.064001000000
H	-11.509370000000	10.395259000000	-0.586430000000
C	-12.364973000000	10.408950000000	-1.260120000000
H	-15.431904000000	6.964349000000	-2.228325000000
C	-13.512176000000	7.012889000000	-1.058537000000
C	-14.343734000000	7.008763000000	-2.226658000000
Fe	-13.225036000000	8.736203000000	-2.112867000000
C	-13.651607000000	10.451940000000	-3.183240000000
C	-12.311140000000	10.498267000000	-2.686418000000
C	-12.147155000000	7.095753000000	-1.491758000000
C	-13.496741000000	7.112245000000	-3.370875000000
H	-13.947230000000	10.477693000000	-4.231016000000
H	-11.407029000000	10.565437000000	-3.289853000000
C	-12.141104000000	7.165518000000	-2.917688000000
H	-13.826630000000	7.168767000000	-4.407155000000
H	-11.259868000000	7.270018000000	-3.548746000000
H	-11.276049000000	7.132944000000	-0.838901000000
H	-14.975824000000	7.374073000000	0.475154000000
H	-13.288292000000	7.422002000000	1.040259000000
H	14.455980000000	6.010733000000	-0.611882000000
H	13.477252000000	5.831682000000	0.864346000000
H	17.400162000000	5.740633000000	3.991428000000
Hg	1.833701000000	-1.255322000000	0.707072000000
Hg	-3.117732000000	-6.302332000000	-0.713424000000

Table 6.1.8 Cartesian coordinates (Å) of alternative optimized structure of the mercury bound ligand [**5**·2Hg^{2+}] (involving oxygen atoms along with the conjugated alkyne as binding unit).

B3LYP-D3/def2-SVP-CPCM (acetonitrile):

Energy (a.u.) = -6614.8248675

C	2.424737000000	1.342035000000	0.356330000000
C	1.404902000000	1.806673000000	-0.127406000000
C	3.649130000000	0.848471000000	0.971028000000
C	0.250866000000	2.312635000000	-0.665151000000
C	-0.766504000000	2.783894000000	-1.147272000000
C	-2.000000000000	3.329327000000	-1.697854000000
O	4.161214000000	1.874022000000	1.815426000000
O	-3.039129000000	3.140336000000	-0.743096000000
C	5.399277000000	1.744569000000	2.372341000000
C	-4.333166000000	3.385643000000	-1.090810000000
C	5.933179000000	2.905731000000	2.952813000000
C	7.180945000000	2.868133000000	3.568230000000
C	7.926379000000	1.678654000000	3.605647000000
C	7.386454000000	0.530724000000	3.015747000000
C	6.129378000000	0.550106000000	2.401358000000
C	-5.307001000000	2.905292000000	-0.197741000000
C	-6.653662000000	3.130481000000	-0.454646000000
C	-7.065122000000	3.833179000000	-1.603083000000
C	-6.085350000000	4.299928000000	-2.482512000000
C	-4.723142000000	4.078043000000	-2.241732000000
C	-9.258519000000	5.283930000000	-5.413996000000
C	-9.705450000000	6.583067000000	-5.110819000000
C	-9.758697000000	7.021989000000	-3.786070000000
C	-9.348356000000	6.130384000000	-2.792308000000
C	-8.897885000000	4.846974000000	-3.088402000000
C	-8.853187000000	4.398387000000	-4.407620000000
C	-9.324862000000	6.308021000000	-1.325500000000
O	-8.894717000000	5.137613000000	-0.774139000000
C	-8.551095000000	4.136407000000	-1.787407000000
O	-9.620374000000	7.263505000000	-0.652260000000
C	-9.450375000000	2.913833000000	-1.606639000000
C	-9.095559000000	1.685721000000	-2.191906000000
C	-9.955847000000	0.593938000000	-2.138227000000
C	-11.201260000000	0.700542000000	-1.491335000000
C	-11.556724000000	1.917320000000	-0.888156000000
C	-10.683501000000	3.009069000000	-0.955762000000
O	-11.976351000000	-0.412115000000	-1.500077000000
C	-13.303264000000	-0.339783000000	-0.971320000000
C	-13.994804000000	-1.633812000000	-1.231378000000
N	-14.531148000000	-1.939239000000	-2.447835000000
N	-15.049899000000	-3.130182000000	-2.399831000000
N	-14.854739000000	-3.615580000000	-1.164384000000
C	-14.202050000000	-2.715552000000	-0.392410000000
C	-15.427804000000	-4.908686000000	-0.778764000000
C	8.343167000000	0.202554000000	7.830445000000
C	8.855978000000	1.264885000000	8.595908000000
C	9.455014000000	2.361578000000	7.972481000000
C	9.530895000000	2.351036000000	6.578390000000
C	9.038211000000	1.294891000000	5.817158000000
C	8.422439000000	0.206158000000	6.432317000000
C	10.061626000000	3.381252000000	5.661901000000
O	9.853822000000	2.945672000000	4.387275000000
C	9.264162000000	1.605821000000	4.345298000000
O	10.579880000000	4.442711000000	5.900855000000
C	10.268810000000	0.699913000000	3.637785000000
C	10.627440000000	1.019844000000	2.313428000000

C	11.533437000000	0.240922000000	1.608936000000
C	12.109055000000	-0.897442000000	2.209443000000
C	11.769010000000	-1.220989000000	3.530507000000
C	10.858313000000	-0.417572000000	4.231387000000
O	12.967509000000	-1.603345000000	1.435835000000
C	13.536133000000	-2.814352000000	1.942878000000
C	14.392825000000	-3.410078000000	0.879211000000
N	15.748552000000	-3.270978000000	0.867387000000
N	16.230107000000	-3.856089000000	-0.190074000000
N	15.201385000000	-4.380527000000	-0.874180000000
C	14.028647000000	-4.124887000000	-0.250597000000
C	15.425866000000	-5.022535000000	-2.173494000000
H	3.433441000000	-0.068268000000	1.551604000000
H	4.383479000000	0.580675000000	0.188130000000
H	-1.864632000000	4.403742000000	-1.924334000000
H	-2.243321000000	2.817978000000	-2.648542000000
H	5.351598000000	3.830583000000	2.911189000000
H	7.585842000000	3.777886000000	4.012583000000
H	7.952155000000	-0.402868000000	3.024847000000
H	5.739792000000	-0.365686000000	1.956741000000
H	-4.978813000000	2.356799000000	0.689385000000
H	-7.403772000000	2.753242000000	0.243242000000
H	-6.368747000000	4.853763000000	-3.377911000000
H	-3.989917000000	4.462098000000	-2.950245000000
H	-9.230255000000	4.957829000000	-6.456468000000
H	-10.017241000000	7.247770000000	-5.919482000000
H	-10.110610000000	8.022363000000	-3.524962000000
H	-8.515082000000	3.389905000000	-4.653889000000
H	-8.133254000000	1.580932000000	-2.697917000000
H	-9.686268000000	-0.359626000000	-2.596395000000
H	-12.505477000000	2.033503000000	-0.365261000000
H	-10.977607000000	3.948719000000	-0.486477000000
H	-13.273439000000	-0.134240000000	0.112013000000
H	-13.857186000000	0.477535000000	-1.464563000000
H	-13.949115000000	-2.902127000000	0.647661000000
H	7.869264000000	-0.641405000000	8.336853000000
H	8.776015000000	1.232113000000	9.684346000000
H	9.847732000000	3.204856000000	8.544109000000
H	8.010119000000	-0.618202000000	5.847661000000
H	10.181443000000	1.893507000000	1.832665000000
H	11.812380000000	0.484586000000	0.581613000000
H	12.200892000000	-2.087049000000	4.031010000000
H	10.615010000000	-0.689495000000	5.259106000000
H	14.155363000000	-2.606893000000	2.832347000000
H	12.730628000000	-3.511348000000	2.232033000000
H	13.069156000000	-4.457126000000	-0.637937000000
H	-18.202732000000	-8.169118000000	-1.798355000000
C	-18.164518000000	-8.083646000000	-0.713372000000
H	-18.066896000000	-4.898639000000	-2.128678000000
H	-20.334107000000	-7.908380000000	-0.144668000000
C	-19.288995000000	-7.945339000000	0.159357000000
H	-15.956154000000	-8.116882000000	-0.283450000000
C	-16.978934000000	-8.055800000000	0.086211000000
H	-20.183727000000	-4.605742000000	-0.455262000000
C	-18.022961000000	-4.772443000000	-1.047862000000
C	-19.133942000000	-4.613895000000	-0.165871000000
Fe	-18.043628000000	-6.304758000000	0.329339000000
C	-18.798448000000	-7.832929000000	1.498265000000
C	-17.370700000000	-7.901409000000	1.453026000000
C	-16.826880000000	-4.775755000000	-0.257080000000
C	-18.630476000000	-4.504328000000	1.168560000000
H	-19.404571000000	-7.695037000000	2.392388000000
H	-16.698523000000	-7.823228000000	2.306227000000
C	-17.206721000000	-4.594628000000	1.114165000000
H	-16.524285000000	-4.566205000000	1.962542000000
H	16.196713000000	-7.133409000000	-4.591871000000
C	16.168278000000	-6.434615000000	-5.426767000000
H	18.250295000000	-5.581238000000	-5.439635000000
C	17.252275000000	-5.615661000000	-5.874383000000
H	14.042697000000	-6.595616000000	-6.146175000000
C	15.031604000000	-6.150885000000	-6.247381000000
H	17.361578000000	-3.154245000000	-3.410912000000
C	15.302224000000	-4.051092000000	-3.308718000000
C	16.340677000000	-3.186708000000	-3.788941000000
Fe	15.663827000000	-4.438339000000	-5.279313000000
C	16.785037000000	-4.825261000000	-6.971108000000
C	15.412922000000	-5.156329000000	-7.201768000000
C	14.120972000000	-3.788637000000	-4.079391000000
C	15.808447000000	-2.413425000000	-4.864374000000
H	17.365472000000	-4.084401000000	-7.519100000000
H	14.765122000000	-4.711691000000	-7.955984000000
C	14.438766000000	-2.785255000000	-5.044423000000
H	16.357400000000	-1.687322000000	-5.462358000000
H	13.764048000000	-2.391302000000	-5.803092000000
H	13.163176000000	-4.294785000000	-3.964014000000
H	16.433183000000	-5.456027000000	-2.135606000000
H	14.699706000000	-5.839877000000	-2.275376000000
H	-15.402320000000	-5.542486000000	-1.674243000000
H	-14.768517000000	-5.352931000000	-0.021772000000
H	-19.230349000000	-4.398218000000	2.071110000000
Hg	-2.385016000000	0.682880000000	1.235502000000
Hg	3.402731000000	4.747761000000	0.710907000000

6.2. Divergent Behaviour of Cyclic and Acyclic Alkyne towards Hg^{2+} ion: A Combined Experimental and Theoretical Studies

This part of the chapter is taken from the work published in *New J. Chem.* **2022**, *46,* 2989–3005.

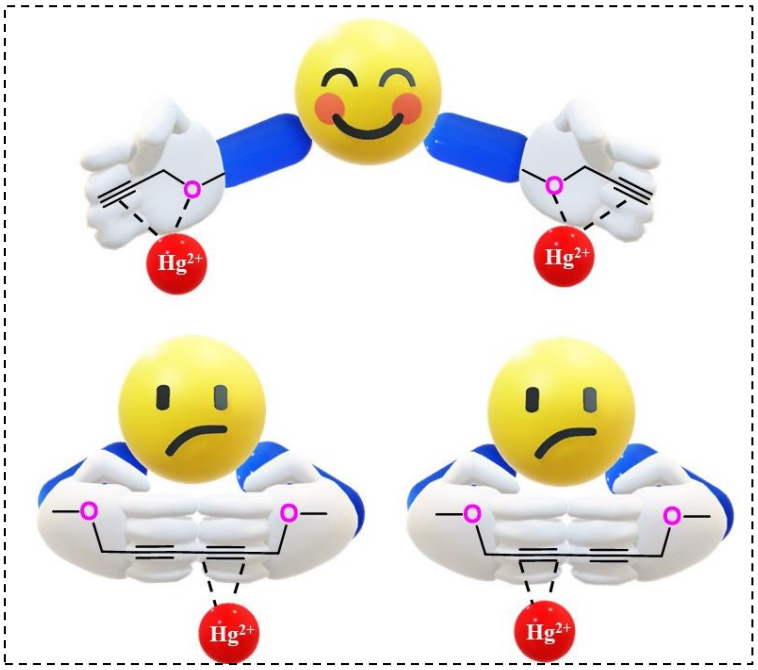

6.2.1. Introduction:

Alkyne is a versatile functional group in organic chemistry, and is able to undergo a wide variety of reactions and interactions.[66,67] In some cases, the alkyne group reacts with a specific analyte transforming itself into a new functional group[68,69] whereas, in some other cases, alkynes could be found to only interact through the π-cloud, producing π-complex with the restoration of its unique structural integrity.[70-72] Hence, the position of alkyne moiety in a molecule is a key factor in understanding its interacting capability. There ought to be some differences in the reactivity of the terminal alkyne unit with that of internally conjugated 1,3-dialkyne system, since the 1,3-dialkyne moiety has a more diffused and extended π-cloud than the terminal one. On the other hand, the terminal alkynes possess easy accessibility owing to their reduced steric bulk and presence of acidic hydrogen along with a feeble dipole moment.[66] Interestingly, among the 1,3-dialkyne systems, there may be cyclic and acyclic 1,3-dialkynes, which also have the probability to interact differently with an analyte.

The difference in cyclic and acyclic compounds in terms of their reactivity has been known for centuries.[73-79] There have been numerous studies on isolated terminal alkynes,

internally conjugated 1,3-dialkyne systems as well as oligoynes, both in cyclic and acyclic systems, which account for their stability and respective areas of applications.[2,9,40,80,81] For example, the conjugated alkyne systems in long-chain form or in cyclic form has been used up in a range of prospects from natural products to optoelectronics and this is solely dependent on the unique molecular information they carry.[40,80,82] However, a clear comparative picture of the cyclic and acyclic structures having alkyne functionality as the point of interest is rather rare. To conduct such a comparative study, the concerned probes should possess similar structural framework, then only the comparison of cyclic and acyclic perspectives can come into play. With this conscience, we have set out to investigate, for the first time, a comparative metal recognition property of a cyclic and an acyclic alkyne system bearing same molecular background. For this purpose, we have deliberately designed two similar structural motifs, consisting of terminal and internally conjugated 1,3-di-yne systems, which are known to have a strong affinity towards mercury, which behaves as a soft Lewis acid. Among several metal ions, those behaving as soft (acidic) ions are known to be preferred by the soft (basic) functionality (alkyne), according to HSAB principle.[25] In some cases, the alkyne transforms into carbonyl functionality upon interaction with Hg^{2+} ion[21,23,83] and in some cases the π-cloud of alkyne unit assists in mercury binding.[22] Mercury serves as a species of extreme toxicity to the environment and living species, regardless of its form as elemental, organic or inorganic, which justifies its widely explored arena of investigation.[27,28] Hence, any probe capable of detecting mercury selectively with promising and reproducible analytical results, would be a step forward in the research field of molecular recognition.

Keeping this idea and knowledge in mind, we have designed and synthesized two molecules **7** and **8** with identical structural backbone, by an "easy-to-make" synthetic method. The design of probes **7** and **8** consisted of ferrocene, phenolphthalein and 1,2,3-triazole units, all tied up together with a 1,3-dialkyne linkage for **8**. Phenolphthalein derivatives are known to provide good to moderate fluorescence when the phenolic -OH groups are derivatized with bulky substituents,[33,34] whereas ferrocene is a potential redox active unit capable of undergoing oxidation easily to generate the Fe^{2+}/Fe^{3+} redox couple.[35] The principle aim of inclusion of an electroactive moiety into the probes is to monitor the interaction by electroanalytical techniques. One step addition of two different units, alkyne and azide, *via* cycloaddition reaction afforded a triazole moiety which can act as an additional metal binding site.[50,84] Since our aim was to compare the nature of interaction of alkyne with analyte in the cyclic and acyclic forms, the alkynes were chosen to be terminal in the acyclic compound **7** and internally

conjugated 1,3-dialkyne in the cyclic form **8**. Remarkably, in the cyclic analogue **8**, the binding character is quite dissimilar to the acyclic one, **7**, the difference being attributed preliminarily to their different structural flexibility. The cyclic molecule **8** has a cage with 1,3-dialkyne as potential binding unit, as was found for the acyclic molecule, as well as heteroatoms from the phenolphthalein and 1,2,3-triazole units. In the structural design, the cage was supposed to conveniently and selectively bind to metal ions of compatible size.

Herein we report that, the cyclic molecule **8** with a cage-like structure gave dissimilar responses from that of its terminal alkyne-containing analogue **7**. The detailed interactions of both **7** and **8** with metal ions have been systematically investigated by the spectrophotometric (UV-Vis and fluorescence), electrochemical as well as NMR spectroscopic analysis along with quantum chemical calculations (DFT studies).

6.2.2. Results and Discussions:

6.2.2.1. Synthesis of compounds 7 and 8

Internally conjugated alkynes and isolated internal or terminal alkynes are known to be inherently different due to the presence of an acidic H atom in terminal alkynes. This structural contrast is expected to create reactivity difference in terminal and internal alkynes. There are some reactions where both the terminal and internal alkynes participate indifferently,[85-88] but there are others which are specific only for terminal alkynes such as reaction with base or alkyne-alkyne coupling reactions.[89-91] However, in order to unambiguously compare the differences in reactivity between terminal and internally conjugated alkynes, the basic molecular platform must be same only keeping the alkyne positions variable so that any factor other than the alkyne positions do not have any role to play in their difference in responses, if any. With such a vision to develop a comparative study, we have come up with the design of two molecules having similar structural background, with the only variations in their nature being acyclic (**7**), having two terminal alkynes and cyclic (**8**), having an embedded 1,3-dialkyne unit. As shown in Scheme 6.2.1, compound **2**, having two alkyne moieties was reacted with compound **6**, to yield compound **7** (35%) by the facile azide-alkyne [3+2] cycloaddition reaction using $CuSO_4 \cdot 5H_2O$ and sodium ascorbate in ^tBuOH:H_2O (2:1) solvent at room temperature for 24 h. Here, it is noteworthy to mention that there was a possibility for the formation of a 1:1 azide-alkyne coupling product, **9**. However, compound **9**

was not formed may be due to the possibility of formation of an unstable puckered and strained cyclic cage structure.

Compound **8** was synthesized by modified Glaser–Hay coupling under neat condition.[92] Treatment of compound **7** with $Cu(OAc)_2 \cdot H_2O$ as the catalyst and pyridine as the base in microwave condition afforded the cyclic compound **8**. The reaction was set up in closed reaction vessel in microwave reactor with a power of 50 watt under temperature of 60˚C for 30 mins to give compound **8** in 30% yield. Both the compounds **7** and **8** were characterized by ^1H, ^{13}C NMR, IR, HRMS and elemental analysis. Both the compounds are extremely stable to moisture, air or time, such that they retain their reactivity even after a year, being kept at room temperature.

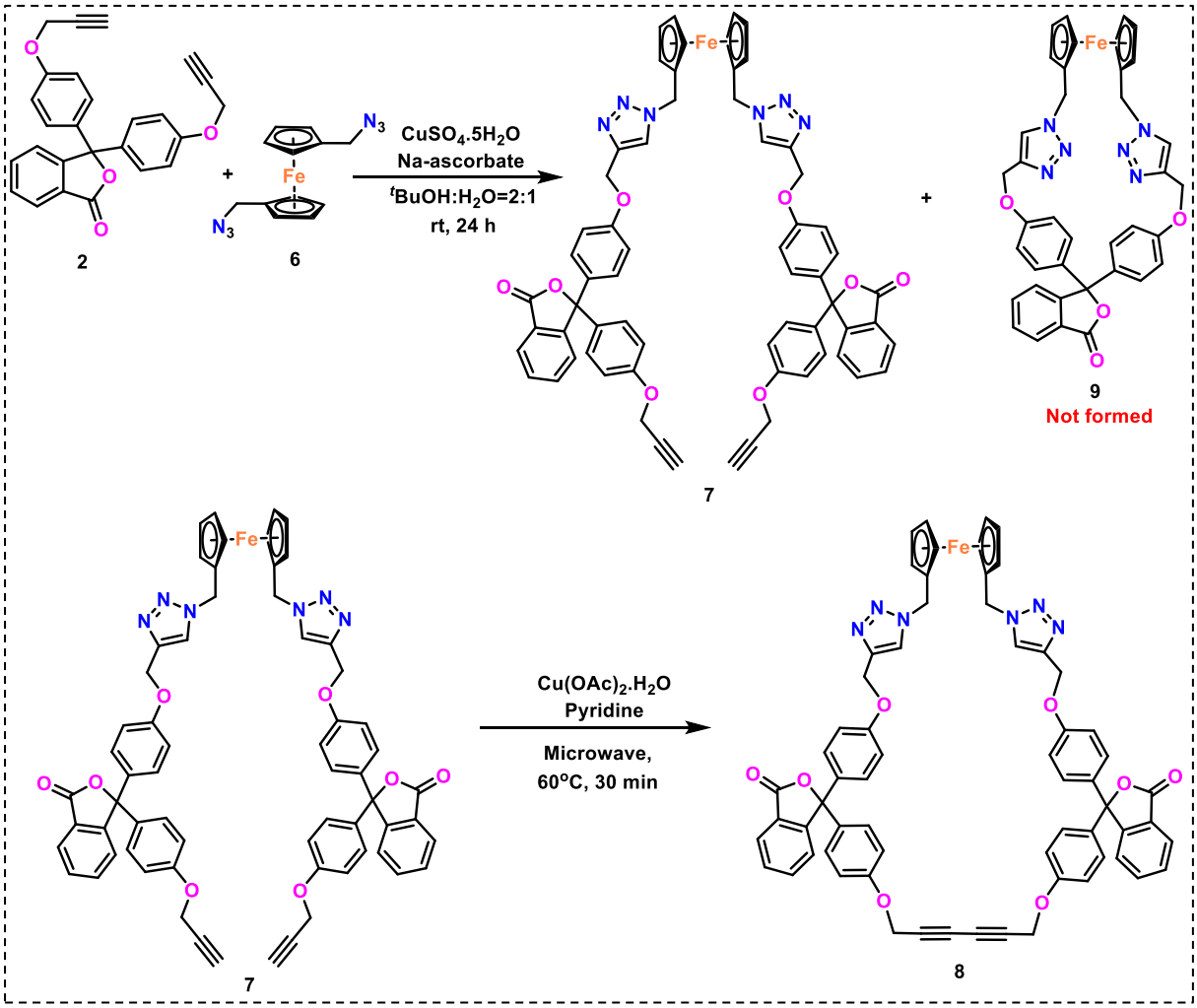

Scheme 6.2.1: Synthetic route for compounds **7** and **8**.

6.2.2.2. UV-visible absorption studies

Spectrophotometry is one of the preliminary and fundamental studies which gives some fingerprint information about the compounds of interest and assists in carrying out several other studies with that compound. Since the cyclic (**8**) and acyclic (**7**) alkyne containing compounds have the same fluorophoric unit, *i.e.*, phenolphthalein with similar conjugation around, they show similar pattern in their UV-vis absorption spectra. Each of compounds **7** and **8** (3.1×10^{-5} M, CH_3CN) possesses three absorption bands at around 227 nm, 273 nm and 281 nm which are closely associated with the phenolphthalein unit.[30] Since our synthesized compound **8**, containing a cavity, and **7**, having terminal alkynes are aimed to be compared in terms of molecular recognition of metal ions, hence they were spectrophotometrically tested with several metal ions (Figure 6.2.1(a), (b)), among which, Cu^{2+}, Fe^{3+} and Hg^{2+} are the only ones giving responses different from the free compounds. Titrations of the cyclic and acyclic compounds with Hg^{2+} ion provided a glimpse of their respective interaction patterns. As depicted in Figure 6.2.1(c), it can be seen that with gradual addition of Hg^{2+} ion (3.1×10^{-5} M, CH_3CN) into the free ligand **7**, the intensity of the three peaks decreased gradually with a distinct isosbestic point at around 249 nm along with a red shift of the 227 nm band through 4 nm for up to 2 equiv Hg^{2+} addition. However, in compound **8**, for the same experiment, similar results with an isosbestic point around 250 nm and with a slight red shift (3 nm) of the 227 nm peak for up to 1 equiv Hg^{2+} could be observed (Figure 6.2.1(d)) which was validated by quantum chemical calculations (*vide infra*). Interestingly, no significant changes could be found beyond the addition of 1 equiv of Hg^{2+} ions for probe **8**. Thus, from the titration profile with Hg^{2+} ion, it can be inferred that Hg^{2+} ion interacted with both **7** and **8**, but with different stoichiometry. Looking into the structures of **7** and **8**, it may be anticipated that molecule **8** is much more rigid as compared to **7**, since the terminal alkynes in **7** can adjust to a sterically more favourable conformation as compared to **8**. These structural features may contribute to the differences in the interaction rates as well as stoichiometries of interaction with the Hg^{2+} ion. Compound **7** was found to have a 1:2 ratio of interaction with Hg^{2+} ion, whereas, **8** was found to have a 1:1 ratio, as obtained from the Job's plot (inset: Figures 6.2.1(c) and (d)), where, "A" is absorbance of probe with each aliquot of Hg^{2+} ion addition, "A_0" denotes absorbance of free probe and "M_0" is the absorbance of free metal ion solution. Additionally, the formation of [**7**·$2Hg^{2+}$] and [**8**·Hg^{2+}] complexes were confirmed by elemental analysis (*vide infra*) and [**8**·Hg^{2+}] by HRMS.

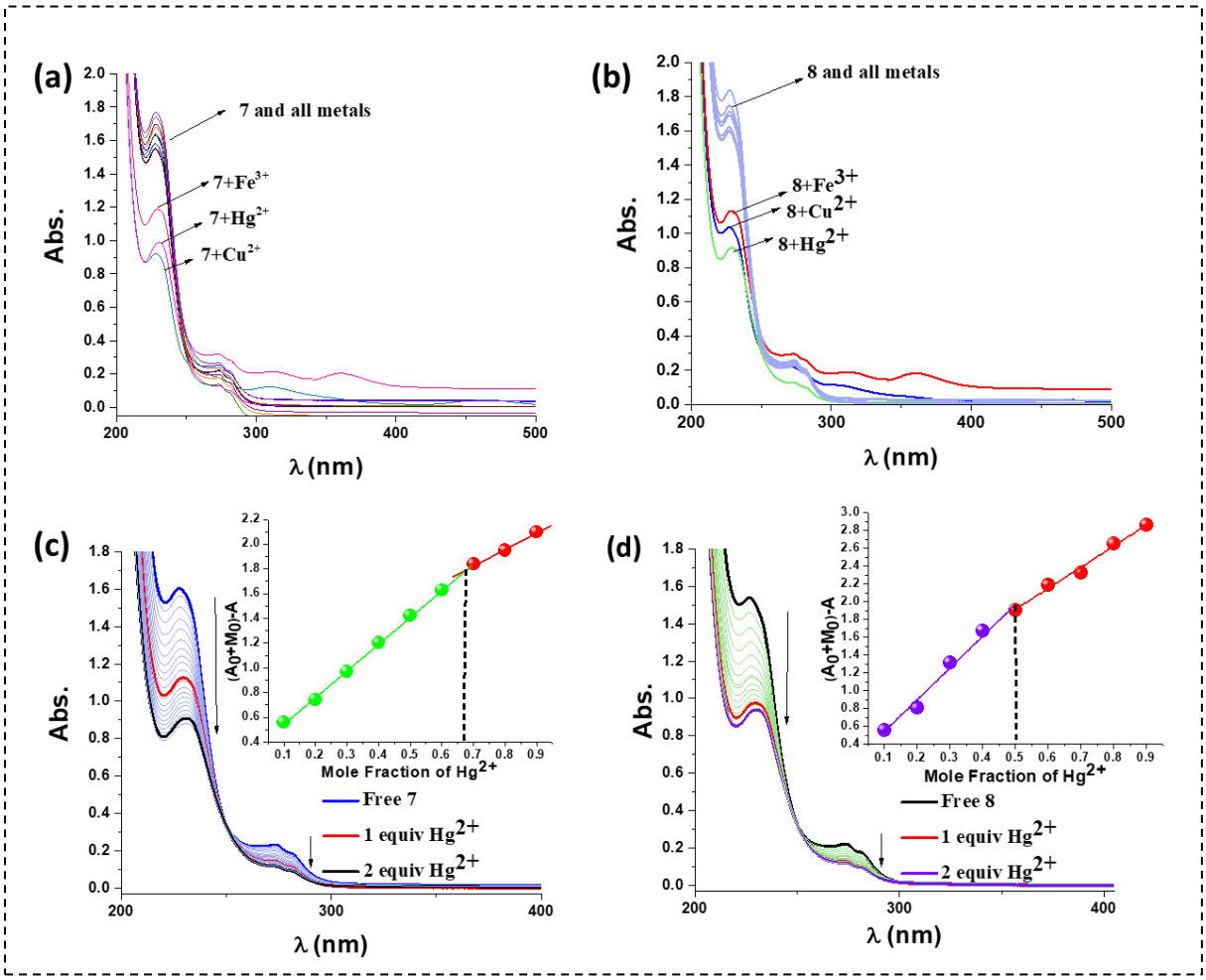

Figure 6.2.1. UV-vis titrations of compounds (a) **7** and (b) **8** in presence of several metal ions (CH_3CN, 3.12×10^{-5} M). UV-vis spectral changes of (c) **7** (inset: binding ratio of **7** with Hg^{2+} ion by Job's plot) and (d) **8** in presence of Hg^{2+} ion (3.1×10^{-5} M, CH_3CN) (inset: binding ratio of **8** with Hg^{2+} ion by Job's plot).

Compounds **7** and **8** (3.1×10^{-5} M, CH_3CN) are also found to interact with Cu^{2+} and Fe^{3+} ions (3.1×10^{-5} M, CH_3CN) (Figure 6.2.2) but in a different way. With Cu^{2+} ion, the titration curve of **7** gradually decreased in its original intensity but with the emergence of three new peaks at around 305, 358 and 461 nm and an isosbestic point at 257 nm could be observed (Figure 6.2.2(a)). Whereas, with Fe^{3+}, the original intensity of the peaks of free **7** decreased along with appearance of two new peaks at around 313 nm and 360 nm and a clear isosbestic point at 289 nm (Figure 6.2.2(b)). For compound **8**, similar observations were recorded with both the metal ions (Figures 6.2.2(c) and (d)) but with the isosbestic point with Cu^{2+} being located at 287 nm. Along with all those different peaks, low energy peaks in the range of 630-640 nm, characteristic for the formation of ferrocenium ion were observed for both **7** and **8**.[39]

Interestingly, addition of sodium-L-ascorbate as a reducing agent reversed back the oxidation peak to that of the original free receptor (Figure 6.2.3) indicating that Cu^{2+} and Fe^{3+} promote the oxidation of ferrocene unit to the ferrocenium ion. Beyond the addition of 1 equiv of analyte (Cu^{2+} and Fe^{3+} ions) to the solution of compounds **7** and **8**, no significant changes were observed in the UV-vis spectra indicating that no ferrocene unit was left to be oxidised. Since such a peak corresponding to the oxidation of ferrocene to ferrocenium does not occur in case of Hg^{2+} ion, hence it can be concluded that Cu^{2+} and Fe^{3+} ions are indulged in the redox type of interaction, and the only metal ion showing the binding phenomenon is the Hg^{2+} ion.

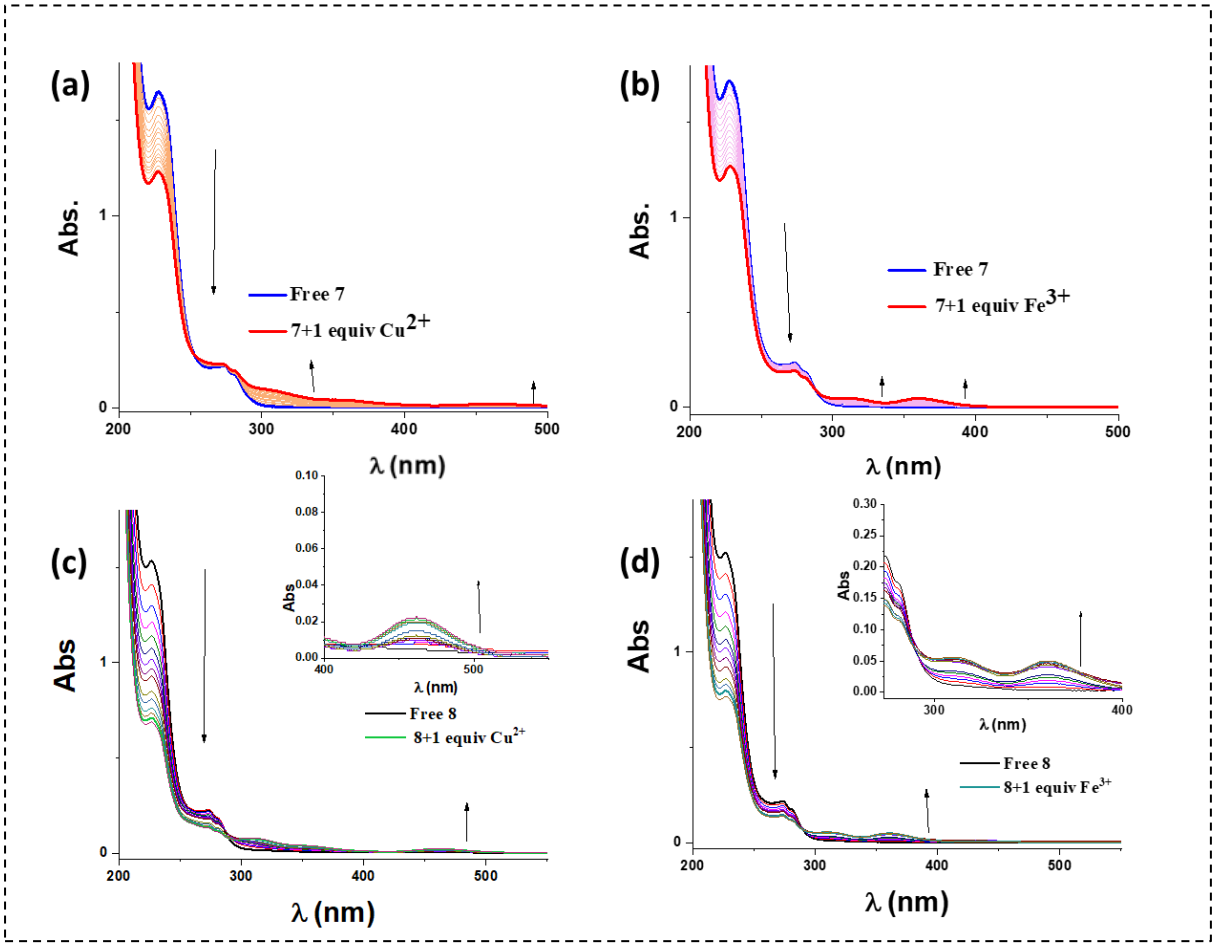

Figure 6.2.2: UV-vis titrations of compounds **7** and **8** in presence of up to 1 equiv Cu^{2+} and Fe^{3+} ions (CH_3CN, 3.12×10^{-5} M).

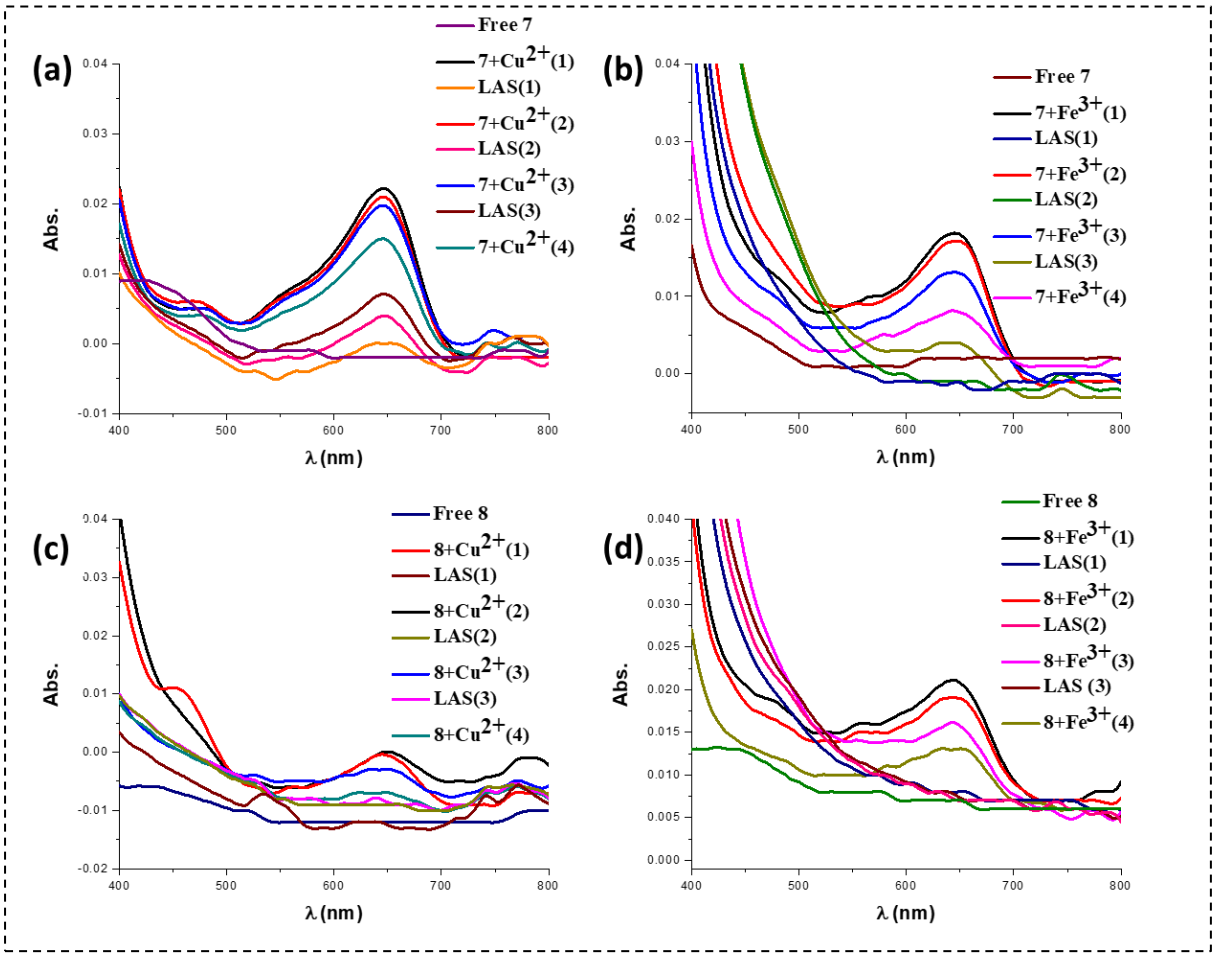

Figure 6.2.3: Reversible redox interactions of compounds **7** and **8** in presence of up to 1 equiv Cu^{2+} and Fe^{3+} ions (CH_3CN, 1×10^{-3} M) and LAS alternatively, obtained by UV-vis titrations.

6.2.2.3. Fluorescence studies

Fluorescence spectroscopy have been widely utilized to obtain some basic molecular information about any interaction of any probe with an external analyte. Its widespread precedence arises from its non-destructive nature giving instant highly sensitive results with high accuracy.[30-32] To obtain the detailed information about the photophysical properties of our synthesized probes fluorescence titration was carried out. As shown in Figure 2, compound **7** (9.7×10^{-7} M, CH_3CN), is found to emit at 409 nm, 330 nm and 296 nm and compound **8** (9.7×10^{-7} M, CH_3CN), at 411 nm, 382 nm and 286 nm, when both of them are excited by 273 nm light. Fluorescence titrations of **7** and **8** with several metal ions (Na^+, K^+, Fe^{2+}, Fe^{3+}, Cu^{2+}, Hg^{2+}, Ag^+, Ca^{2+}, Mg^{2+}, Mn^{2+}, Zn^{2+}, Pb^{2+}, Co^{2+}, Cr^{3+}, Al^{3+} ions (as their perchlorate salts) fetched some interesting results selectively for Hg^{2+}, Cu^{2+} and Fe^{3+} ions (9.7×10^{-7} M, CH_3CN) (Figure 6.2.4). Upon gradual addition of Hg^{2+} ion up to 2 equiv to a CH_3CN solution of **7**, quenching of the spectra at 409 nm and a blue shift of the peak (8 nm) was observed along with slight

enhancement of the peaks at 330 and 296 nm. An isoemmisive point at 352 nm was concomitantly produced, as evident from Figure 6.2.5(a). On the other hand, for compound **8**, with gradual addition of Hg^{2+} ion, the fluorescence intensity of the peak at 411 nm decreased with a blue shift of 19 nm, whereas that at 286 nm and 382 nm increased for up to 1 equiv Hg^{2+} addition, creating an isoemissive point at 352 nm (Figure 6.2.5(b)). In contrast to compound **7**, very insignificant change in spectral pattern or intensity of compound **8** after 1 equiv Hg^{2+} ion was observed, indicating the spectra became saturated after 1 equiv analyte addition. From these changes in emission spectra, it is evident that the binding phenomenon persists in both of the synthesized molecules, however with different ratio of interaction and these results corroborated with results obtained from UV-vis spectral analysis. This may provide a slight glimpse into mechanism of interaction as the initial interaction of the Hg^{2+} up to 1 equiv is feasible but beyond that, the interaction becomes sluggish as to provide no additional changes in the emission spectra for **8**. In order to get more insight about the fluorescence quenching phenomenon, fluorescence lifetime experiments were performed. Lifetime experiments of probes **7** and **8** with Hg^{2+} ion up to 2 equiv inferred a variation in results (Figures 6.2.5(c) and (d)). The lifetime of free **7** is calculated to be 4.56 ns, which got reduced to 1.9 ns after the addition of Hg^{2+} ion for the formation of the complexed species [**7**·2Hg^{2+}], whereas, the lifetime of probe **8**, changed insignificantly from 2.35 nm to 2.53 nm after 1 equiv Hg^{2+} ion addition and did not change for any further addition of Hg^{2+} ion. From the calculated average lifetimes and the exponential decay plots, it can be inferred that no or insignificant changes in the lifetimes of the complexed species occurs from that of the free ligands, suggesting a static quenching mechanism for both the interactions of **7** and **8** with 2 and 1 equiv Hg^{2+} ion respectively. Hence complexation with Hg^{2+} ion happens in the ground state only for both the probes, creating non-fluorescent complexes.[46] The limit of detection (LOD) found in case of **7** and **8** are 1.39×10^{-7} M and 2.78×10^{-7} M in acetonitrile, as obtained from the $3\sigma/S$ method, calculated with fluorescence titration data (Figures 6.2.6(a) and (b)). For the static quenching mechanism, the binding constants for the probes **7** and **8** were found to be 1.17×10^{5} M^{-1} and 1.88×10^{5} M^{-1} respectively, by using Stern-Volmer equation:[48] $Io/I = 1 + K[Q]$ (Figures 6.2.6(c) and (d)). The moderate binding constant values along with blue-shifts suggest weak binding associated with diminution of conjugation in the probes. This may point towards the involvement of the alkyne units in both the cyclic and acyclic forms since the interaction between the alkyne and Hg^{2+} ion by spreading the π-cloud of the alkyne is a prevalent weak interaction according to the HSAB principle.

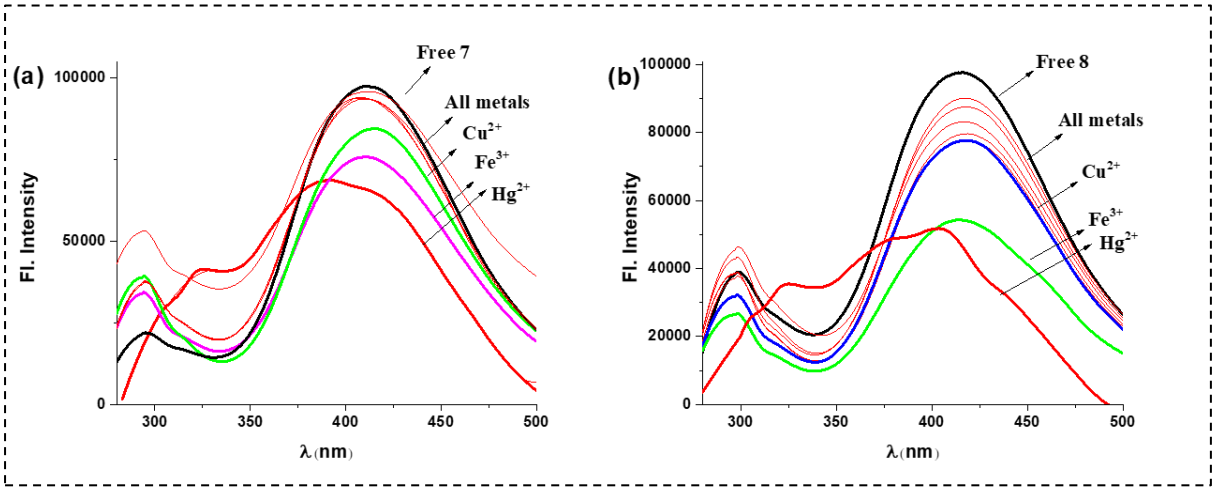

Figure 6.2.4: Fluorescence spectra of compounds (a) **7** and (b) **8** in presence of several metal ions (CH_3CN, 9.7×10^{-7} M).

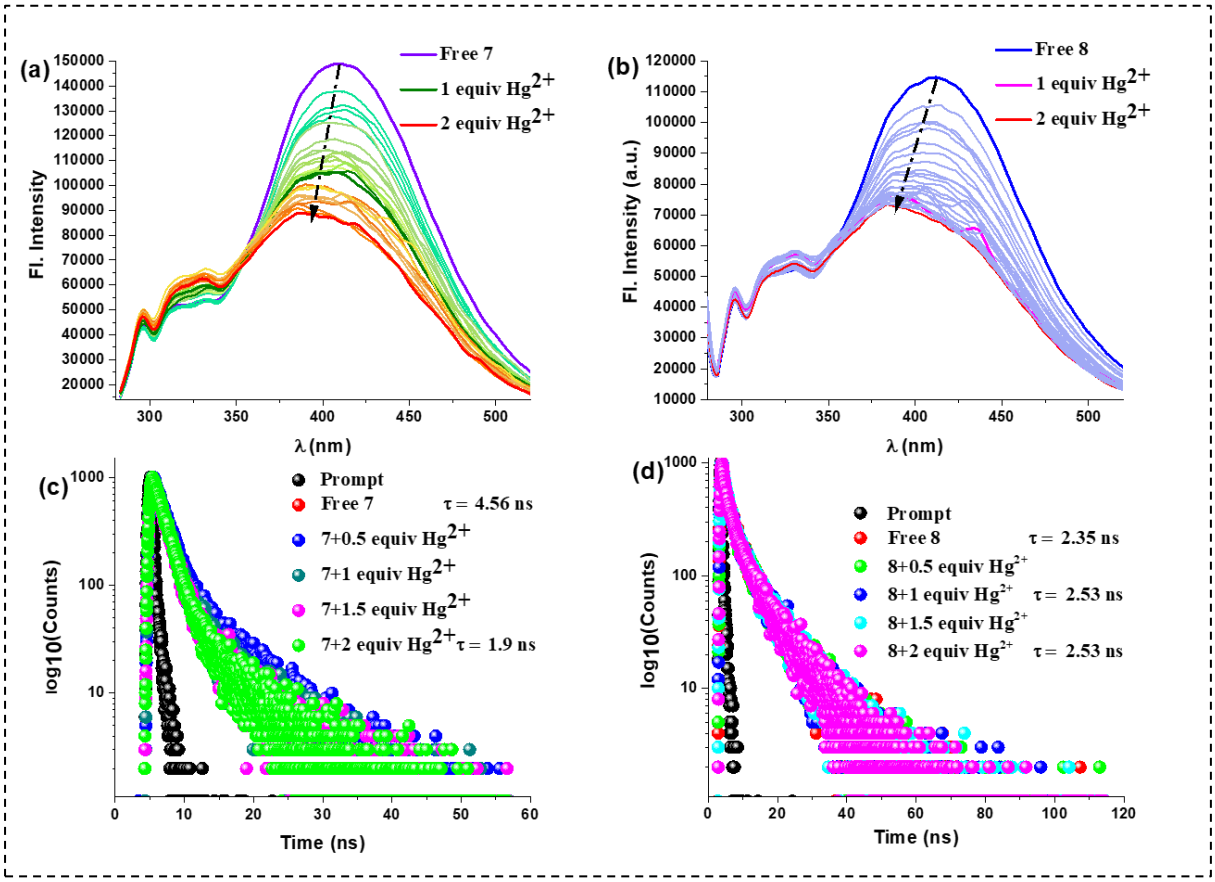

Figure 6.2.5. Fluorescence titrations of (a) **7** and (b) **8** with Hg^{2+} ions (9.7×10^{-7} M, CH_3CN); fluorescence lifetime titrations of (c) **7** and (d) **8** with Hg^{2+} ions (9.7×10^{-7} M, CH_3CN).

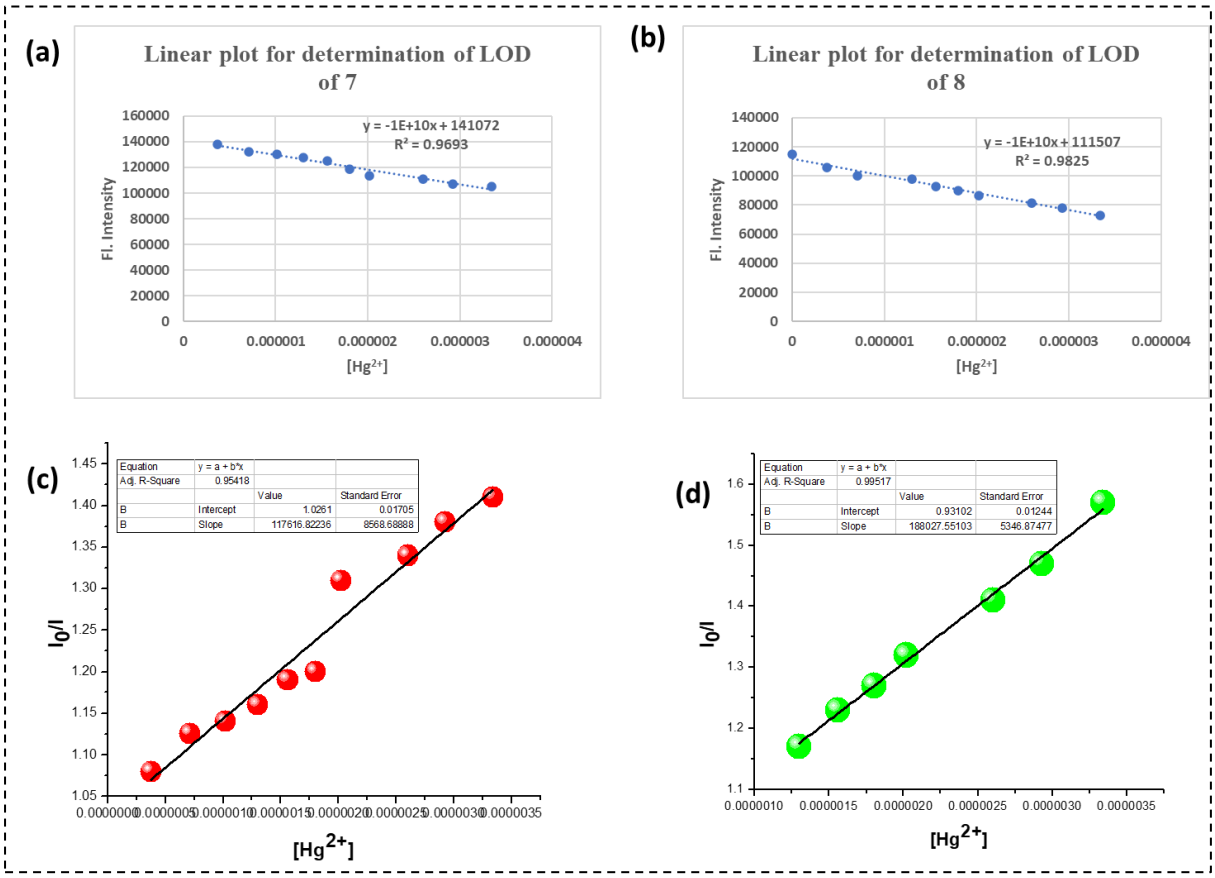

Figure 6.2.6: Linear plots for the determination of LOD for (a) **7** and (b) **8** from fluorescence experiments. Binding constant of compounds (c) **7** and (d) **8** by fluorescence titrations in presence of Hg^{2+}.

With gradual addition of Fe^{3+} and Cu^{2+} ions up to 1 equiv, prominent diminution of the emission spectra of both **7** and **8**, with no additional changes or generation of isoemissive point was observed (Figure 6.2.7). Interestingly, the spectral patterns of **7** and **8** got completely destroyed beyond 1 equiv of the analytes may be due to excess metal accumulation in the ligand system. A 1:1 interaction mode with these two metal ions with both the probes can be concluded and it also corroborated with the results obtained from the UV-vis spectral studies. So, in both Cu^{2+} and Fe^{3+} ions, a significant interaction happens in the ratio 1:1 with the probe **8**. Diminution of the emission spectra after addition of metal ions may be attributed to the paramagnetic nature of Fe^{3+} and Cu^{2+} ion.[45]

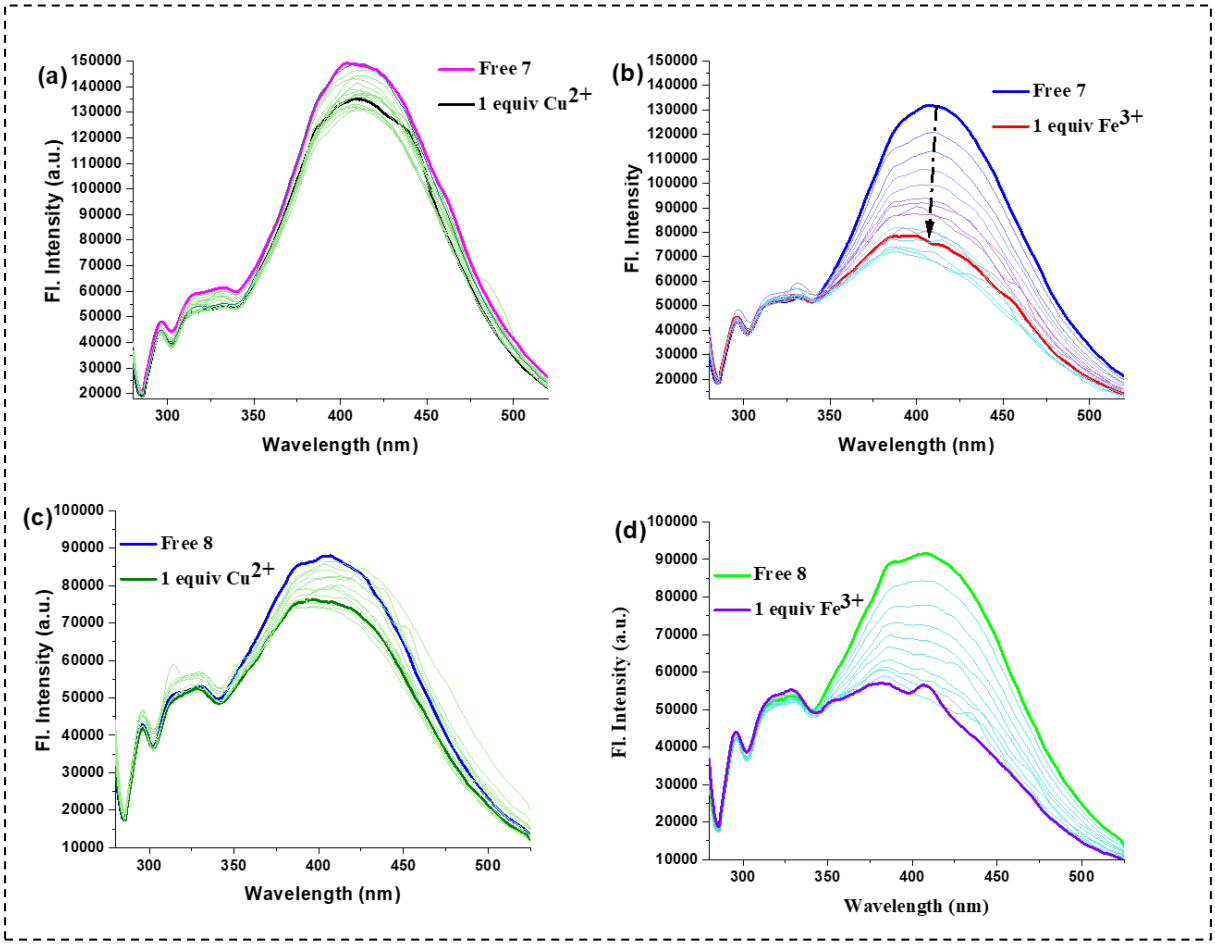

Figure 6.2.7: Fluorescence titrations of compounds (a), (b) **7** and (c), (d) **8** in presence of up to 1 equiv Cu^{2+} and Fe^{3+} ions (CH_3CN, 9.7×10^{-7} M).

6.2.2.4. Electrochemical studies

The acyclic and cyclic derivatives, **7** and **8**, are electroactive due to the presence of the ferrocene unit which can undergo feasible one-electron oxidation and reduction reactions reversibly within the potential window of 0-1 V under electrochemical conditions. Electrochemically compounds **7** and **8** (2.5×10^{-4} M, CH_3CN) displayed a pair of reversible redox peaks with $E_{1/2}$ at 0.590 V and 0.580 V respectively. Upon gradual addition of Hg^{2+} ion up to 2 equiv into **7**, a gradual shift in potential ($\Delta E_{1/2}$ = 172 mV) towards the anodic side was observed by cyclic voltammetry (CV) (Figure 6.2.8(a)). Similar results were reproduced by differential pulse voltammetry (DPV) (Figure 6.2.8(b)) indicating the formation of a new metal complex species [**7**·$2Hg^{2+}$]. On the other hand, upon Hg^{2+} addition to compound **8**, an anodic shift of half-wave potential by 100 mV occurs for up to 1 equiv Hg^{2+}, as obtained from both the aforementioned voltammetric methods (Figure 6.2.8(c) and (d)). Remarkably, no significant changes were observed beyond the addition of 1 equiv Hg^{2+}. Thus, it can be

concluded that there is a resistance in the binding of the second Hg^{2+} ion with probe **8** after the binding of the first ion. There is probability of Hg^{2+} ion interacting with either one alkyne unit at a time. Such difference in response between **7** and **8** arises owing to their structural differences and the feasible flexibility arising out of it.

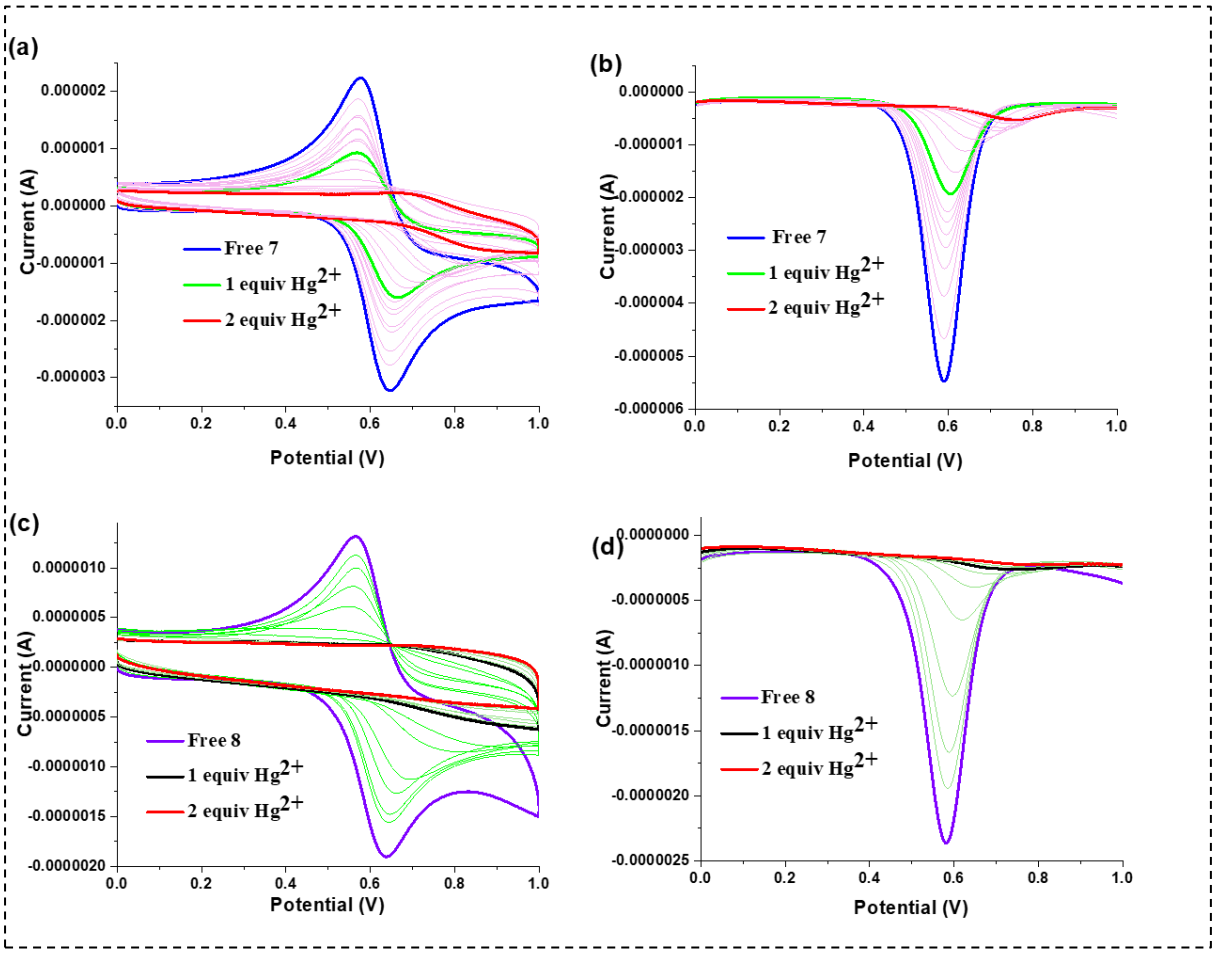

Figure 6.2.8. (a) CV and (b) DPV titrations of **7** with Hg^{2+} and (c) CV and (d) DPV titrations of **8** with Hg^{2+} ion (2.5×10^{-4} M, CH_3CN) with $[(n\text{-}Bu)_4N]ClO_4$ as the supporting electrolyte and with a scan rate 0.06 Vs^{-1}.

To investigate the nature of interactions of cyclic and acyclic probes with Hg^{2+} ion in terms of reversibility, a suitable Hg^{2+}-complexing agent, Na_2EDTA was administered to the solution containing the Hg^{2+}-complexed probes and cyclic voltammograms were recorded (Figure 6.2.9). Upon administering aqueous solution of Na_2EDTA (2.5×10^{-4} M) to CH_3CN solutions of each of the [**7**·$2Hg^{2+}$] and [**8**·Hg^{2+}] complexes, the oxidation and reduction waves shifted back to the positions corresponding to the free probes, signifying a stronger complexation of Hg^{2+} ion by EDTA. Upon further addition of Hg^{2+} ion, the waves did not shift

back to the corresponding positions of the two complexed species, which implied that the nature of interaction of the two probes with Hg^{2+} ion is reversible up to one cycle. Such observation may be associated with the weaker complexing ability of the probes with soft metal like Hg^{2+} ion.

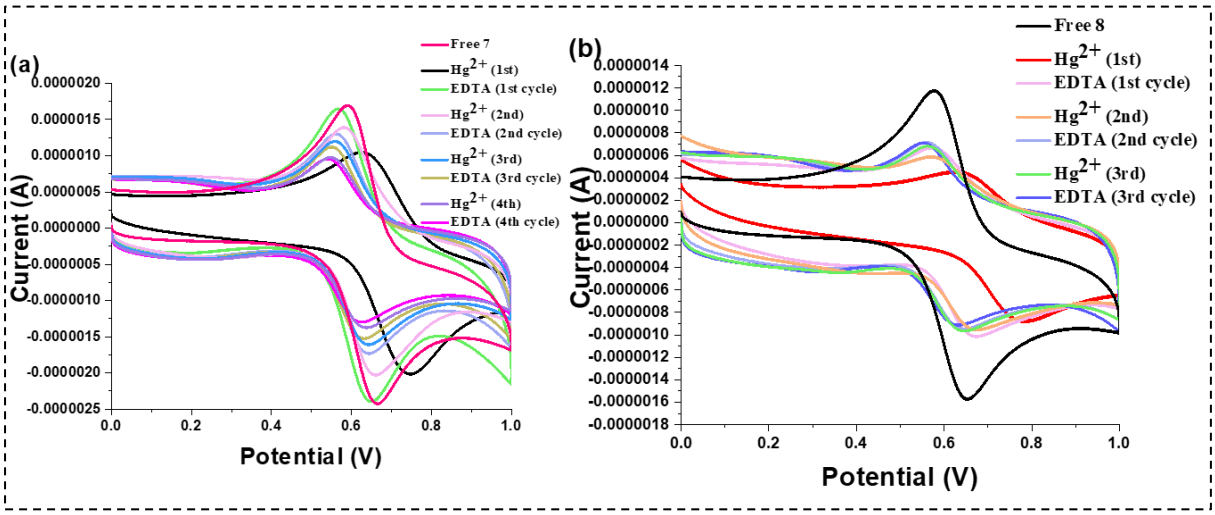

Figure 6.2.9: Reversibility of the interactions of compounds (a) **7** and (b) **8** (CH_3CN, 2.5×10^{-4} M) with Hg^{2+} (CH_3CN, 2.5×10^{-4} M) tested by employing aqueous solution of Na_2EDTA (H_2O, 2.5×10^{-4} M).

Apart from Hg^{2+}, changes of voltammograms (CV and DPV) of probes **7** and **8** after addition of Cu^{2+} and Fe^{3+} ions were also obtained among all other tested metal ions (Figure 6.2.10). Both the analytes did not impart any significant shift to the voltammograms of **7** and **8** in terms of potential, but reduced the cathodic current with addition of each aliquot up to 1 equiv of the analytes. This corroborates to the oxidation phenomenon occurring in the ferrocene unit of each probe by the oxidizing Cu^{2+} and Fe^{3+} ions. Beyond 1 equiv addition of Cu^{2+} and Fe^{3+} ions no significant changes in voltammograms were observed indicating that no ferrocene units are left to be oxidised (Figures 6.2.11 and 6.2.12).

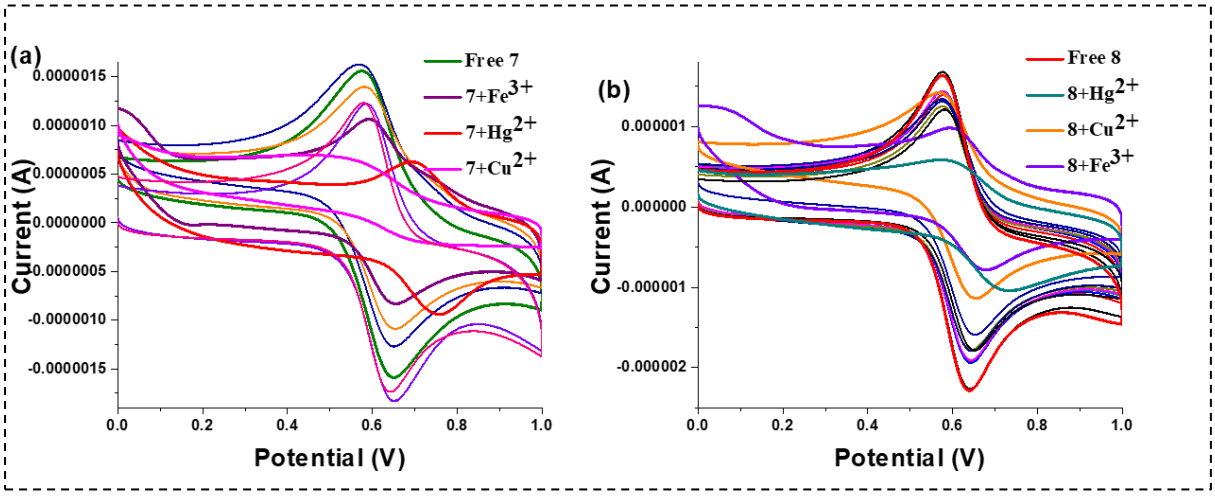

Figure 6.2.10: CV of compounds (a) **7** and (b) **8** in presence of all metal ions (CH_3CN, 2.5 × 10^{-4} M).

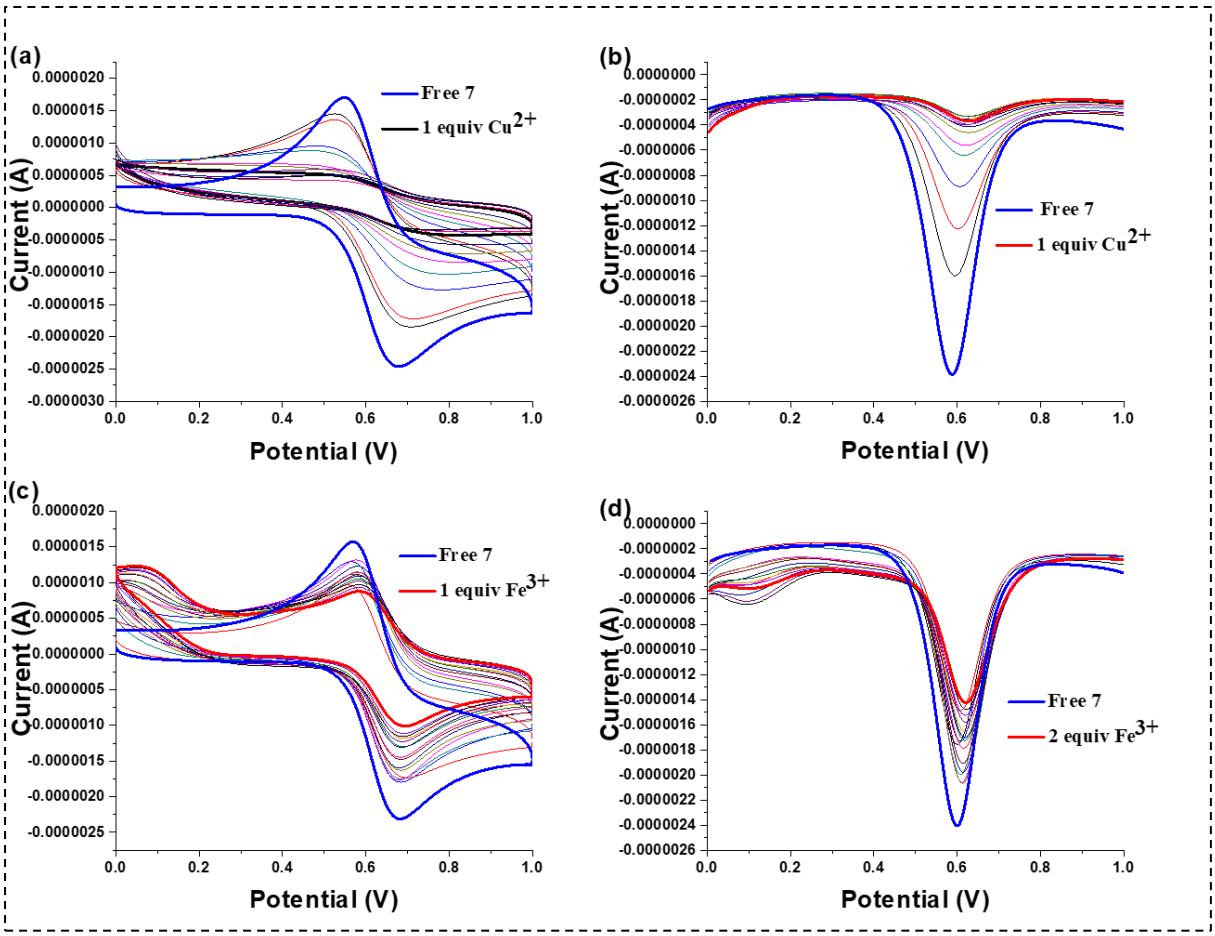

Figure 6.2.11: CV and DPV of compound **7** in presence of up to (a), (b) 1 equiv Cu^{2+} and (c), (d) Fe^{3+} ions (CH_3CN, 2.5 × 10^{-4} M).

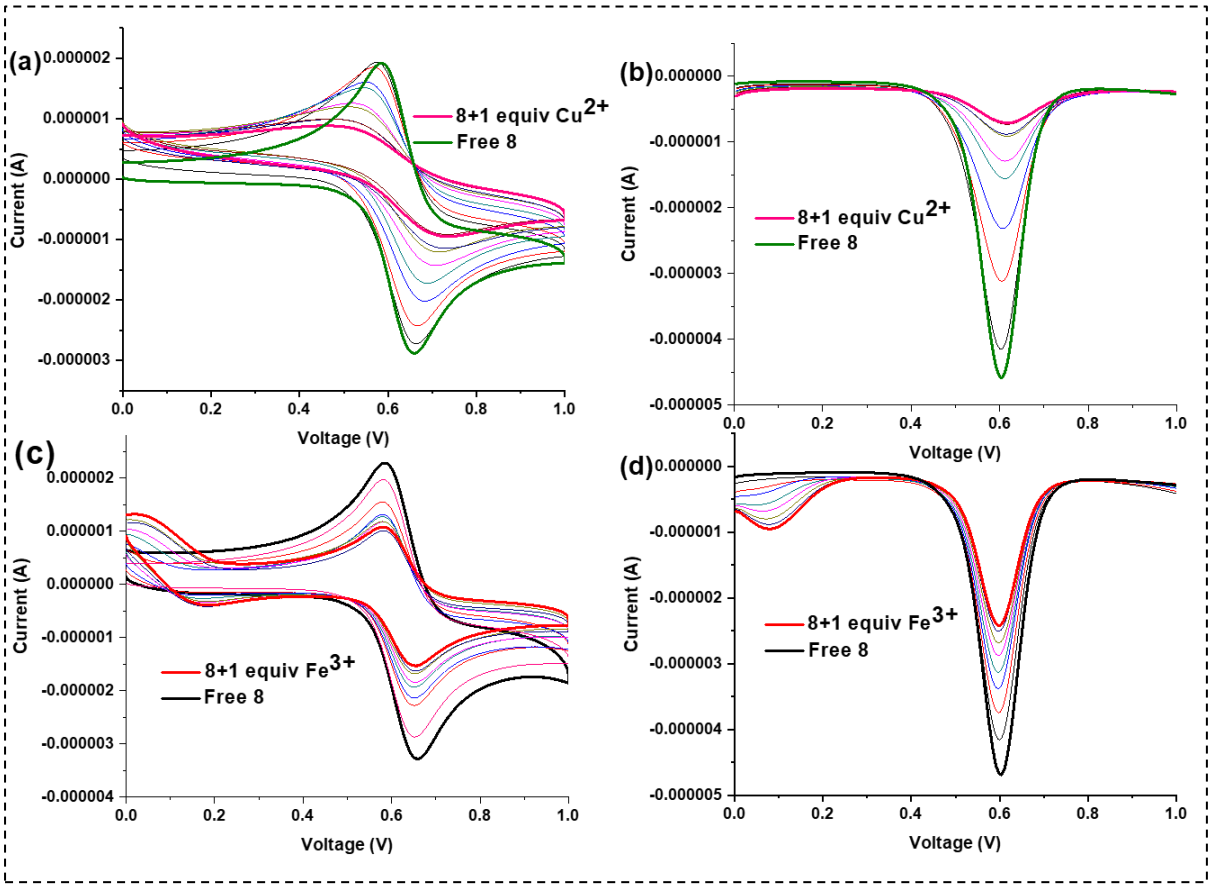

Figure 6.2.12: CV and DPV of compound **8** in presence of up to 1 equiv Cu^{2+} and Fe^{3+} ions (CH_3CN, 2.5 × 10^{-4} M).

6.2.2.5. Competition experiment

A closer look into interference of these three metal ions by the presence of each other was examined using cyclic voltammetry, utilizing their differential electrochemical response towards our synthesized probes **7** and **8**, since voltammetry gives differential response for the oxidizing Cu^{2+} and Fe^{3+} ions (reduction in current) and the binding Hg^{2+} ion (anodic shift). The acyclic derivative, **7** (1.25×10^{-4} M, CH_3CN), was first exposed to oxidation by Cu^{2+} ion (1.25×10^{-4} M, CH_3CN) and then Hg^{2+} ion (1.25×10^{-4} M, CH_3CN) was added, which induced an anodic shift in potential of the redox waves (Figure 6.2.13(a)). When the same experiment was repeated with Fe^{3+} (1.25×10^{-4} M, CH_3CN) instead of Cu^{2+} ion, similar results were obtained (Figure 6.2.13(c)). This indicates that the oxidation of the ferrocene unit to ferrocenium does not affect the Hg^{2+} ion binding mechanism. This also suggests that the ferrocene unit is not actively involved in the binding procedure. On the other hand, reversing the addition sequence of the metal ions to probe **7**, *i.e.*, addition of Hg^{2+} ion first and then the oxidizing agents Cu^{2+}/Fe^{3+} oxidizes the Hg^{2+}-bounded ligand producing changes in the current

intensity (Figures 6.2.13(b) and (d)). When the same set of experiments were performed with probe **8**, similar results were observed (Figure 6.2.14). This indicates that the two processes, binding and oxidation, are mutually exclusively to each other. The competition in terms of anodic shift or no shift have been portrayed in the bar diagrams as shown below.

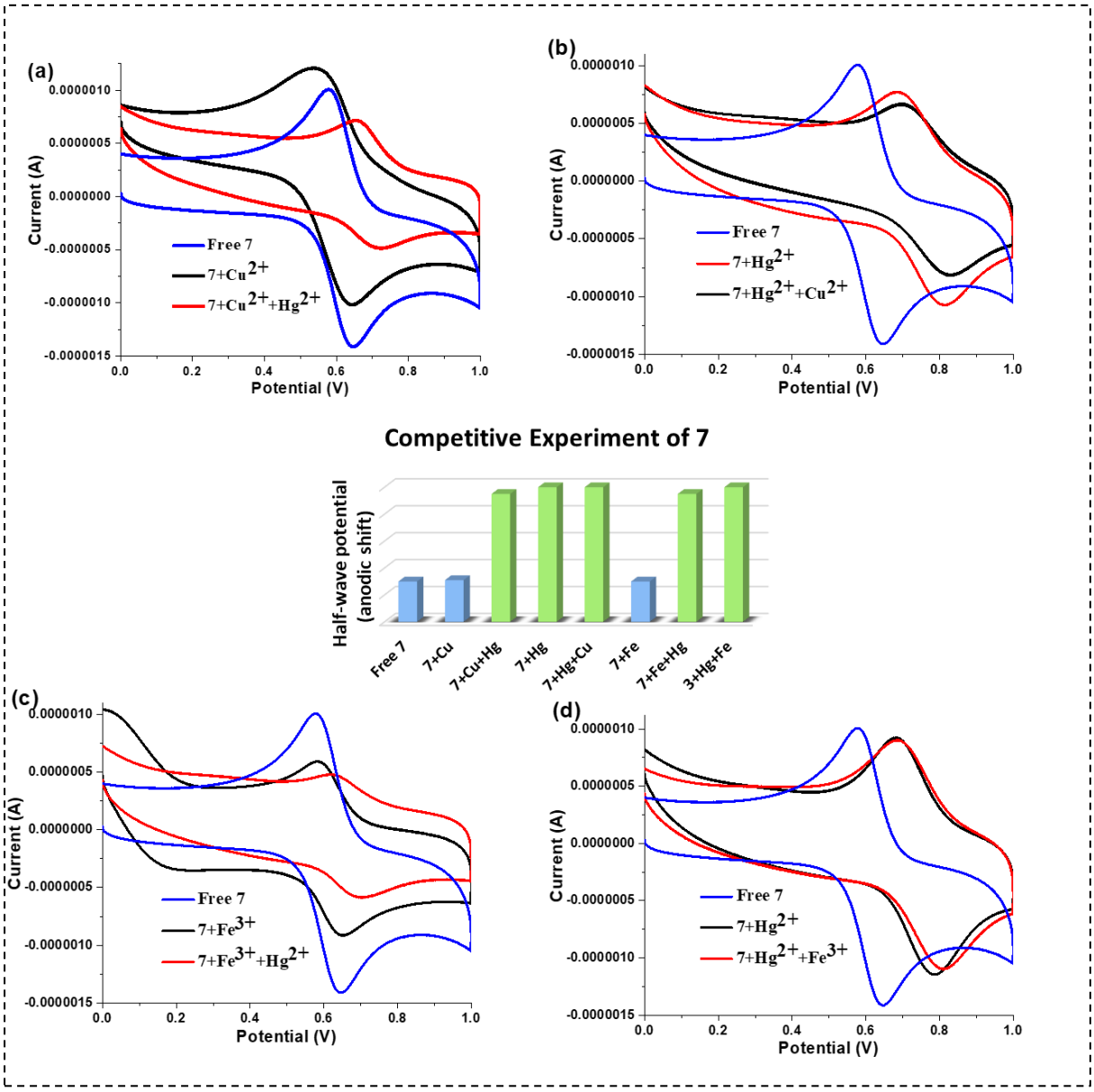

Figure 6.2.13. Competition experiment of compound **7** with (a), (b) Cu^{2+}/Hg^{2+} couple and (c), (d) Fe^{3+}/Hg^{2+} couple (1.25×10^{-4} M CH_3CN) under scan rate 0.06 Vs^{-1}.

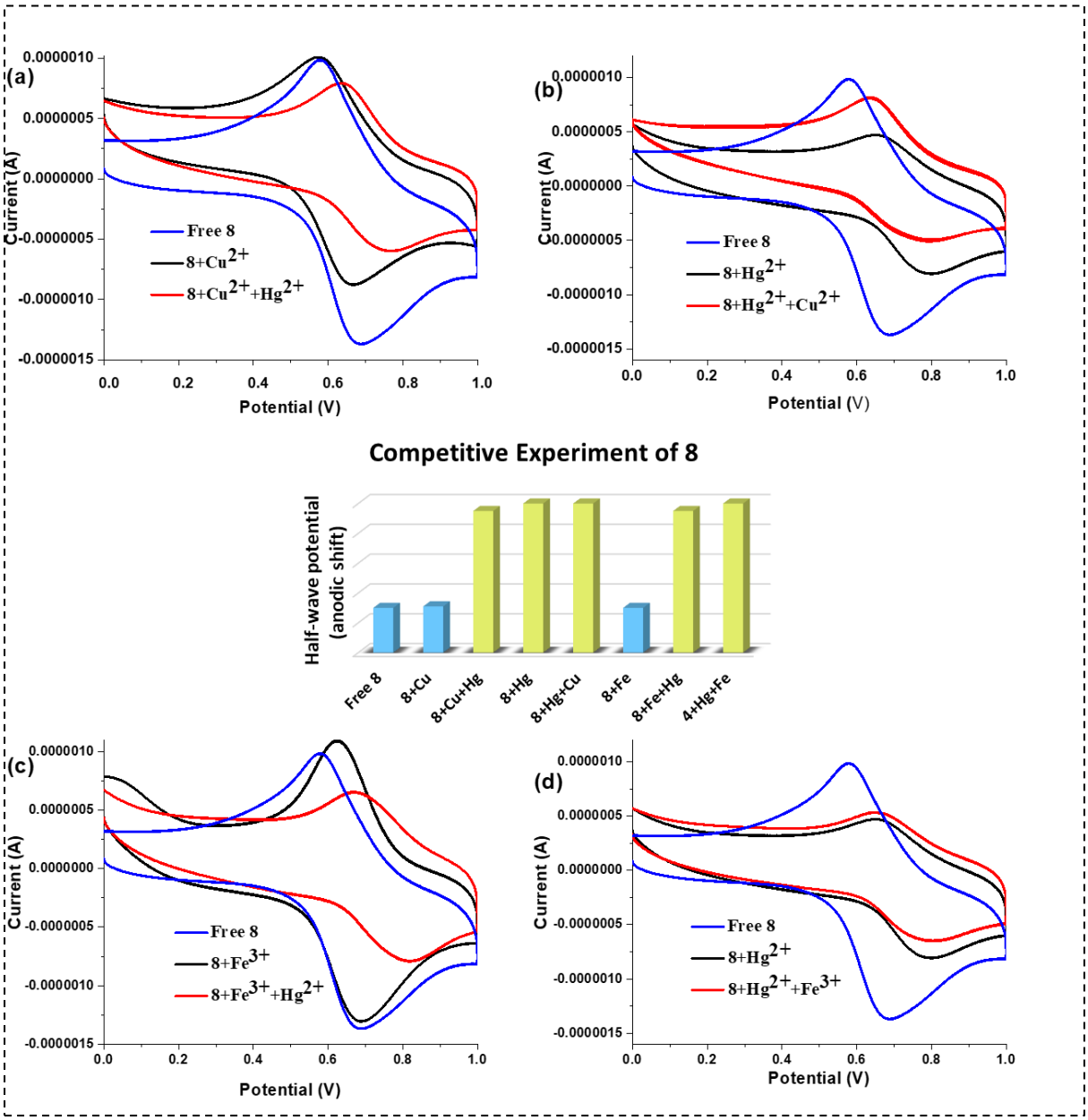

Figure 6.2.14: Competition experiment of compound **8** with (a), (b) Cu^{2+}/Hg^{2+} couple and (c), (d) Fe^{3+}/Hg^{2+} couple (1.25×10^{-4} M CH_3CN) under scan rate 0.06 Vs^{-1}.

6.2.2.6. ^{1}H NMR and IR titrations

In assessing the exact site of interaction of molecules **7** and **8**, the ^{1}H NMR as well as IR spectral titrations have played a crucial role. The NMR spectra of the molecules **7** and **8** before and after interaction with stoichiometric amount of Hg^{2+} ion, were recorded in CD_3CN solvent and compared. From Figure 6.2.15(a), which shows the ^{1}H NMR spectral changes of **7**, it can be observed that after complexation with Hg^{2+} ion (2 equiv.), noticeable changes from the spectral pattern of free **7** occur in two peaks: the terminal alkyne-*H* and its adjacent -OC*H*$_2$

unit. The peak associated with the terminal alkyne-*H* at 2.89 ppm and H atoms of -OCH_2 unit at 5.21 ppm got diminished, with negligible change of other peaks. This indicates the participation of the alkyne unit as well as its neighbouring -OCH_2 group in the Hg^{2+}-binding phenomenon. Furthermore, no peak in the 9-10 ppm region got generated after Hg^{2+} ion addition, which is expected to arise from reaction between terminal alkyne and Hg^{2+} ion giving -CHO group. Hence, from the ^{1}H NMR titration, the plausible binding mode of Hg^{2+} ion with **7** can be concluded to be: the π-cloud of alkyne and lone pair of adjacent O atom. Since the probe **7** contains two symmetrical terminal alkyne units and the symmetry restores even after Hg^{2+} addition, hence the two alkyne units are bound to interact with two Hg^{2+} ions with 1:2 (L:M) ratio of interaction. Remarkably addition of Hg^{2+} ion beyond 2 equiv led to the deformation of entire NMR spectra. On the other hand, upon addition of 1 equiv of Hg^{2+} into the CD_3CN solution of the cyclic compound **8**, the peaks corresponding to the H's attached to the heteroatoms did not suffer sufficient change to conclude their participation in Hg^{2+} attachment (Figure 6.2.15(b)). This can possibly indicate that, not the heteroatoms, but the internally conjugated 1,3-dialkyne unit participates in the Hg^{2+}-binding process, since all peaks are left undisturbed by Hg^{2+} addition. Further addition of Hg^{2+} ion beyond 1 equiv perturbed the whole system. Thus, the binding patterns are evidenced to be different for the acyclic and cyclic alkyne systems. These observations were supported by IR titrations with Hg^{2+} ion (Figures 6.2.15(c) and (d)). The IR fingerprint of the two compounds **7** and **8** clearly denotes the presence of a carbonyl group at 1757 cm^{-1} corresponding to the phenolphthalein carbonyl unit. The peak at 3282 cm^{-1} for **7** arises due to the C-H stretching of the terminal alkyne units, which is absent in **8**, giving a signature difference between the structures of **7** and **8**. In **7**, the C≡C stretching of the terminal alkyne arises in a weak band at 2163 cm^{-1}, however, in **8**, the conjugated alkyne cannot be traced by the C≡C stretching frequency. Upon the addition of Hg^{2+} ion up to 2 equiv for **7** and 1 equiv for **8**, no significant shift in the stretching frequency corresponding to carbonyl functional units can be observed, however, the peaks at 3282 cm^{-1} and 2163 cm^{-1} got diminished in case of **7**. This may imply the participation of the terminal alkyne units in binding with Hg^{2+} ion for probe **7**. The most distinct observation is that there is no generation of any additional carbonyl peak upon Hg^{2+} ion addition to both the acyclic and cyclic analogues, which indicates that there is no chemical reaction occurring between the analyte and the probes, rather there is a fine interaction.

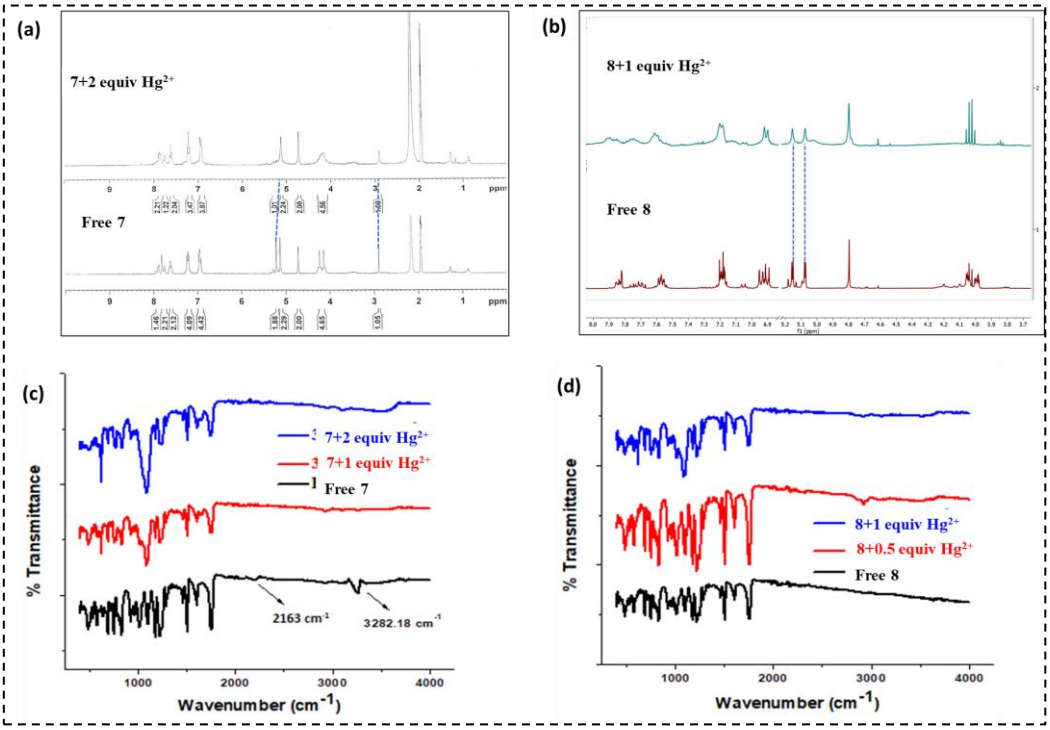

Figure 6.2.15. ^{1}H NMR of compound (a) **7** before and after addition of 2 equiv of Hg^{2+} ion and (b) **8** before and after addition of 1 equiv of Hg^{2+} ion in CD_3CN. IR titration of compound (c) **7** and (d) **8** with gradual addition of Hg^{2+} up to 2 and 1 equiv respectively.

On the basis of all the experimental studies, the plausible binding mode can be evidenced to be happening *via* the participation of the alkyne units, in both isolated and conjugated forms, for both the probes as given below in Figure 6.2.16:

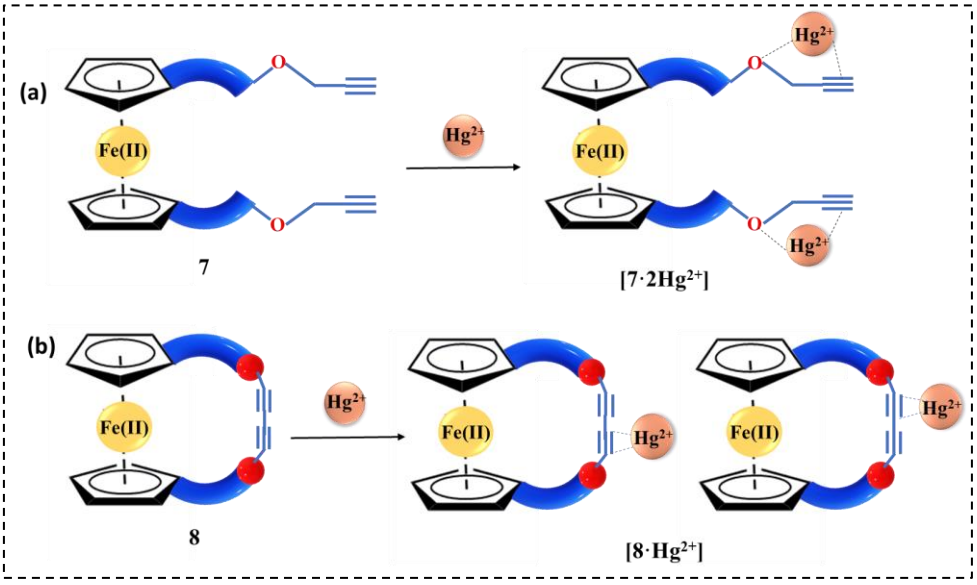

Figure 6.2.16. Plausible interaction modes of (a) **7** and (b) **8** in presence of Hg^{2+} ion, **8** showing a sweeping motion with probability of interaction with either alkyne unit at a time.

6.2.2.7. Colorimetric tests

The fluorescence lifetime experiments convey the information about the ground-state complexation between both the cyclic/acyclic probes and Hg^{2+} ion. To realize such changes by naked eye, colorimetric test with a set of several metal ions have been performed with both the cyclic and acylic molecules. Colorimetric test of compound **7** (10^{-3} M CH_3CN) with Fe^{3+}, Fe^{2+}, Cu^{2+}, Co^{2+}, Cd^{2+}, Hg^{2+}, Zn^{2+}, K^+, Pb^{2+}, Ni^{2+} and Mg^{2+} ions as their perchlorate salts and Cu^+ as $[(CH_3CN)_4Cu]PF_6$, displayed the color changes in presence of Fe^{3+}, Cu^{2+} and Hg^{2+} ions only, by changing its color from yellow to light green, blue and purple respectively (Figure 6.2.17(a)). However, when compound **8** (10^{-3} M CH_3CN) was tested with the same set of metal ions, Hg^{2+} ion deepened the pale yellow color, which eventually got faded away with time and Fe^{3+}/Cu^{2+} ions gave similar bluish green color as in **7** (Figure 6.2.17(b)). The color changes due to Fe^{3+} and Cu^{2+} ions originate from the oxidation of the chromophore unit *i.e.*, ferrocene in the ligand, as was previously discussed, but the color change for Hg^{2+} ion originated by the complexation phenomenon occurring with the probes.

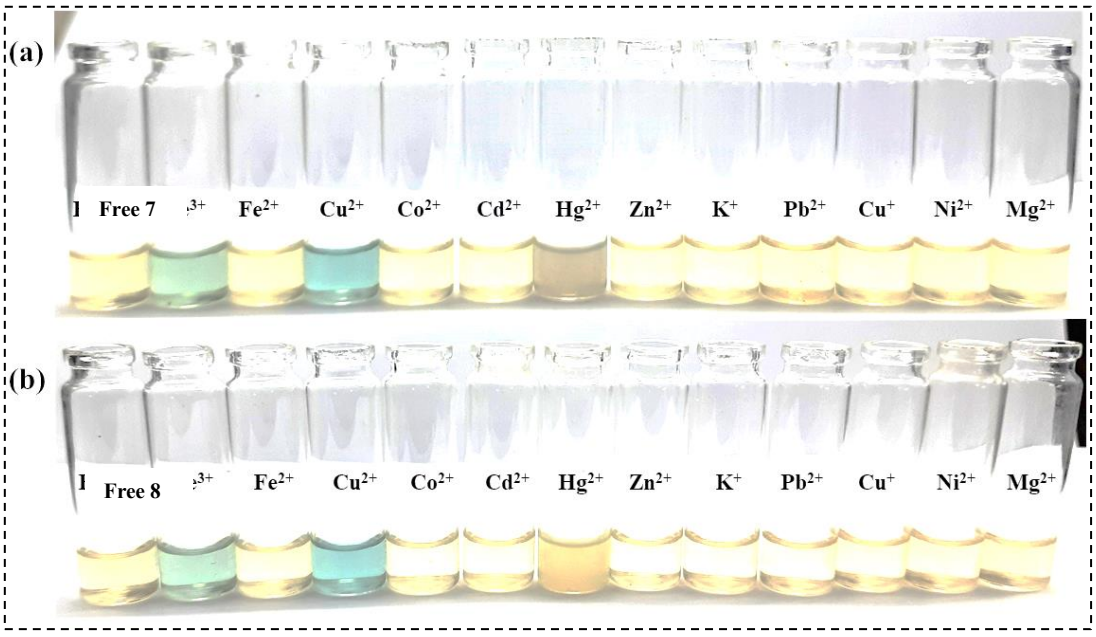

Figure 6.2.17. Colorimetric test of (a) compound **7** (10^{-3} M CH_3CN) and (b) compound **8** in presence of several metal ions.

6.2.2.8. pH, Time and Temperature Effects

Creation of a complete profile about any fluorescent probe needs the consideration of its surrounding environment, so as to render it suitable for application in the physiological

systems. This encouraged the thorough examination of the ambient working conditions of our synthesized molecules with respect to change in pH and temperature. These examinations can be conducted by a series of monitoring a particular output (here fluorescence intensity) with respect to the different kinds of stimuli (pH and temperature). For the acyclic compound **7** (9.7×10^{-7} M, CH_3CN), the optimum working pH was observed to be around 7, which is also valid for its Hg^{2+} ion complex (9.7×10^{-7} M, CH_3CN) (Figure 6.2.18(a)). This was verified by comparing with the fluorescence intensity of **7** and its Hg^{2+}-complex, devoid of any particular pH buffer solution. It was observed that the fluorescence intensities of the solutions without any particular pH and with pH around 7 produced similar results. Any value of pH above and below produced radical changes in the fluorescence intensities. Hence, when using this molecule practically, the pH should be maintained around the physiological range. For the cyclic analogue, **8** and its Hg^{2+} complex also, the optimum working pH was also found to be around 7 (Figure 6.2.18(b)). Since both the structures of **7** and **8** contain the phenolphthalein unit, which constitutes of pH sensitive lactone ring,[55,56] they are supposed to be sensitive towards pH changes in the strong acidic and basic media. Interestingly, the pattern of fluorescence intensity changes in **7** and its complex in the acidic and basic media are widely different than that in **8**. This may be due to the presence of two acidic H atoms in the terminal alkyne units in the acyclic analogue **7**, which is supposed to get deprotonated in basic medium.[1]

The stability to temperature variations is the most important factor in terms of real time utility of the probe. The pattern of the fluorescence intensity for free **7** and **8** (9.7×10^{-7} M, CH_3CN) as well as [**7**·$2Hg^{2+}$] and [**8**·Hg^{2+}] (9.7×10^{-7} M, CH_3CN) were found to be almost undeflected within the temperature range of 25˚C-60˚C, however, the pattern changed a bit for **7** and hugely for **8** when heated to above 60˚C (Figure 6.2.18(c) and (d)). Although the compounds are extremely stable to moisture and do not lose its activity even after a long time, but its optimum temperature domain should be from room temperature to 60˚C.

Apart from the two factors described above, response time is another important factor. Notably, the response time of the probe **7** (9.7×10^{-7} M, CH_3CN) was lesser than that of **8**, as it (**7**) responded within the first 20 seconds of Hg^{2+} ion addition, giving instant results of quenched fluorescence intensity, which remained almost constant afterwards up to about 10 minutes (Figure 6.2.19). The response of the cyclic analogue **8** was rather slower, which was around one minute, however, afterwards it produced similar results with lapse in time.

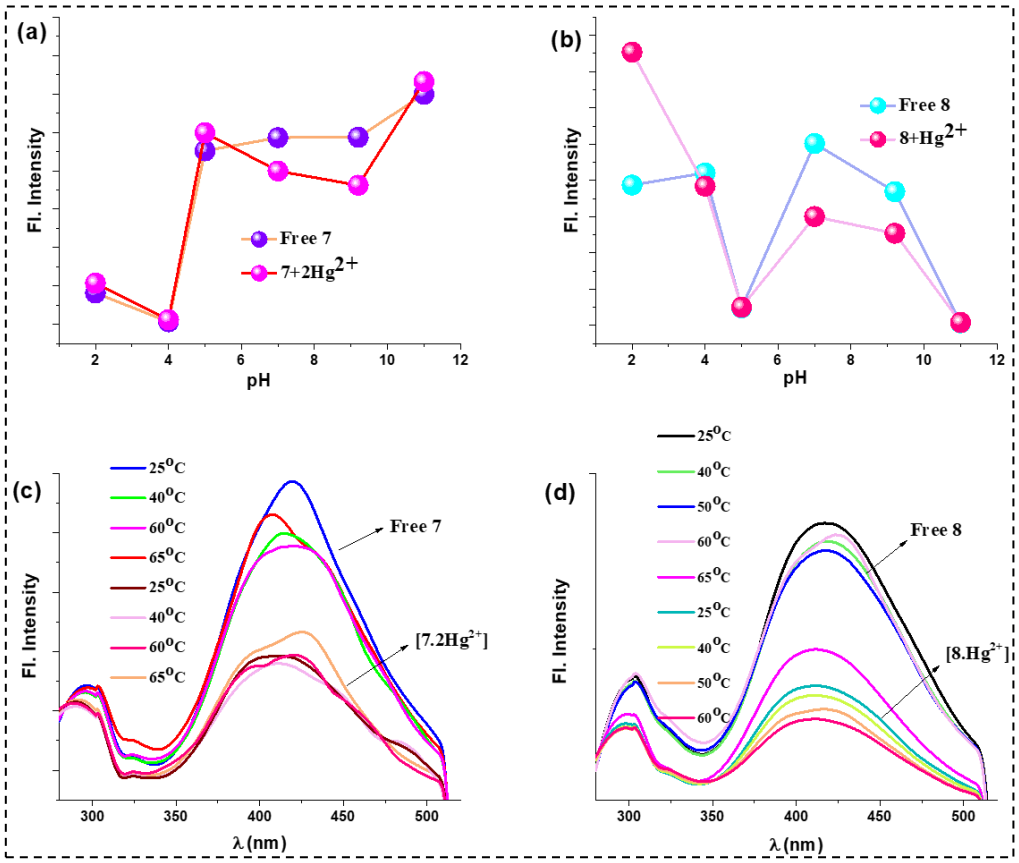

Figure 6.2.18. Study of the stability of free **7** and **8** (9.7×10^{-7} M, CH_3CN) and their respective Hg^{2+} complex (9.7×10^{-7} M, CH_3CN) with the aspects of (a), (b) pH and (c), (d) temperature.

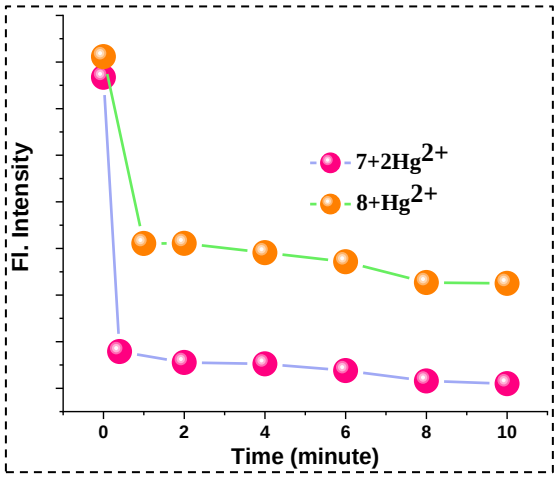

Figure 6.2.19. Study of the response time of **7** and **8** (9.7×10^{-7} M, CH_3CN) and their respective Hg^{2+} complex (9.7×10^{-7} M, CH_3CN).

6.2.2.9. Real sample analysis

Application of the probes in the quantitative detection of Hg^{2+} ion in real water samples promotes its ability in real time use. Here, the detection has been carried out using voltammetric

output with tap water samples collected from Jadavpur University. The water sample was filtered on a Whatman 41 filter paper to filter off any undesired particles and pH value was maintained around 6.5−7. Gradual addition of known quantities of aqueous solution of the Hg^{2+} ion into **7** and **8** (1.25×10^{-4} M, CH_3CN) gave voltametric shifts yielding linear equations y = 1432.3x + 0.0079 and y = 1310.4x + 0.0076 with correlation coefficients, R^2 = 0.9768 and 0.978 respectively (Figure 6.2.20). Any unknown sample concentration of Hg^{2+} ion can be obtained from these equations of the two probes and the average added and recovered metal ion concentrations obtained from these equations are provided in Table 6.2.1.

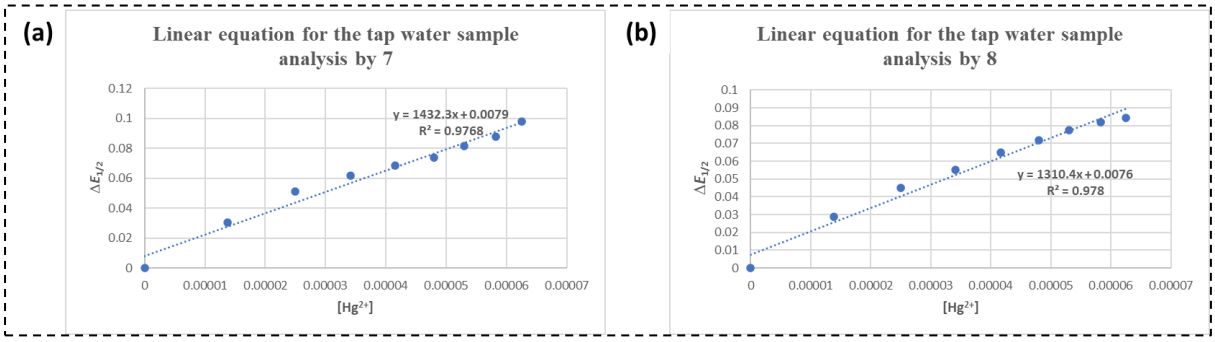

Figure 6.2.20: Real sample analysis of tap water samples for the determination of Hg^{2+} ion by probes (a) **7** and (b) **8**.

Table 6.2.1: Real sample analysis of tap water for the quantitative determination of Hg^{2+} ion by probes **7** and **8**.

Probe	Added Metal conc. (M)	Recovered Metal conc. (M)	% Recovery	% Error
Compound **7**	4.2×10^{-5}	4.18×10^{-5}	99.5	0.5
Compound **4**	4.2×10^{-5}	4.12×10^{-5}	98.09	1.91

6.2.2.10. Theoretical (DFT) Studies

In order to get further insights into the structural and electronic parameters that control the responses (*as mentioned earlier*) of ligands **7** and **8** towards the Hg^{2+} ion, theoretical studies were performed using density functional theory (DFT) (*cf. below*, Experimental Section). Optimization of the geometry of each of the ligands **7** and **8** was carried out at the B3LYP/Lanl2dz level of theory. Starting with few possible geometries of **7** and **8**, they were finally converged at the global minima, giving us the energy-minimized structures (Figure

6.2.21), and their respective frontier molecular orbitals are presented in Figures 6.2.22 and 6.2.23. Energy-minimized conformation of the acyclic ligand **7** reveals that the ferrocene bound two triazole units have occupied a trans/anti arrangement with respect to each other. The C≡C bond length of the terminal alkyne units in **7** are found as 1.222 Å (WBI = 2.886), such lengths being typical with ligands containing free terminal alkyne units.[93]

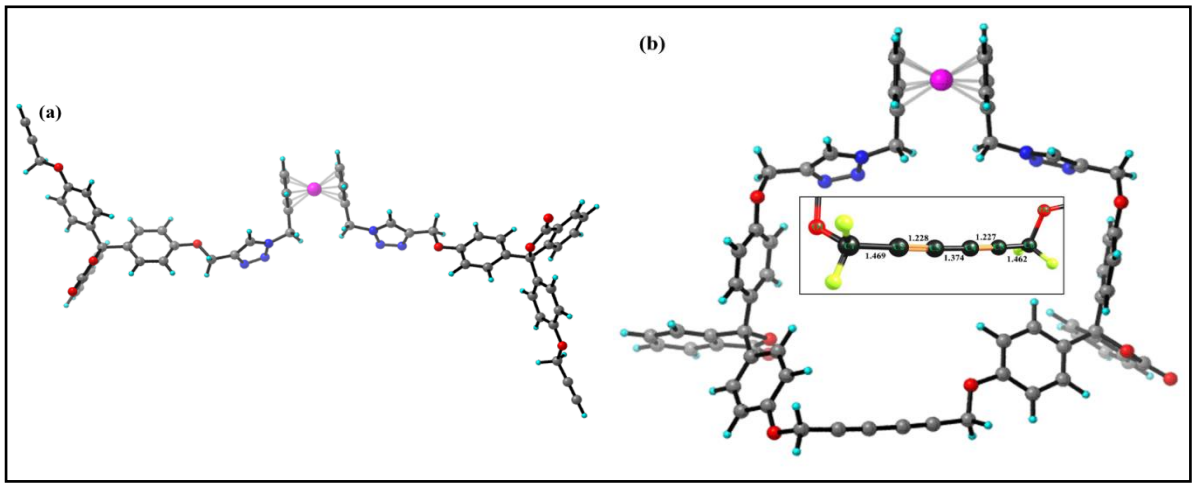

Figure 6.2.21: Optimized structures of the receptors (a) **7** and (b) **8**. Zoomed structure of a middle 1,3-dialkyne unit of the receptor **8** (inset).

The optimized structure of the cyclic receptor **8** displays a little distorted structure, where the 1,3-dialkyne unit is linear. It is noteworthy to mention here that the 1,3-dialkyne bound –CH_2–O units are at 80.4˚ angles, and triazole moieties bound to ferrocene moieties are at trans/anti arrangement to each other. Furthermore, natural bond orbital (NBO) calculation has been performed at the same level of theory to get insights into the bonding scenario. In cyclic ligand, **8**, the C≡C bond lengths of the middle 1,3-dialkyne units are found as 1.228 Å (WBI = 2.614) and 1.227 Å (WBI = 2.608), such lengths being usual for ligands containing 1,3-dialkyne units.[42] Interestingly C-C bond that connects two alkyne units in 1,3-dialkyne has a bond length of 1.374 Å (WBI=1.239) which indicates delocalised nature of the dialkyne units. Such typical behaviour is congruent with our earlier reported literature.[92] The calculated bond lengths and Wiberg bond indices (WBI) are presented in Table 6.2.2.

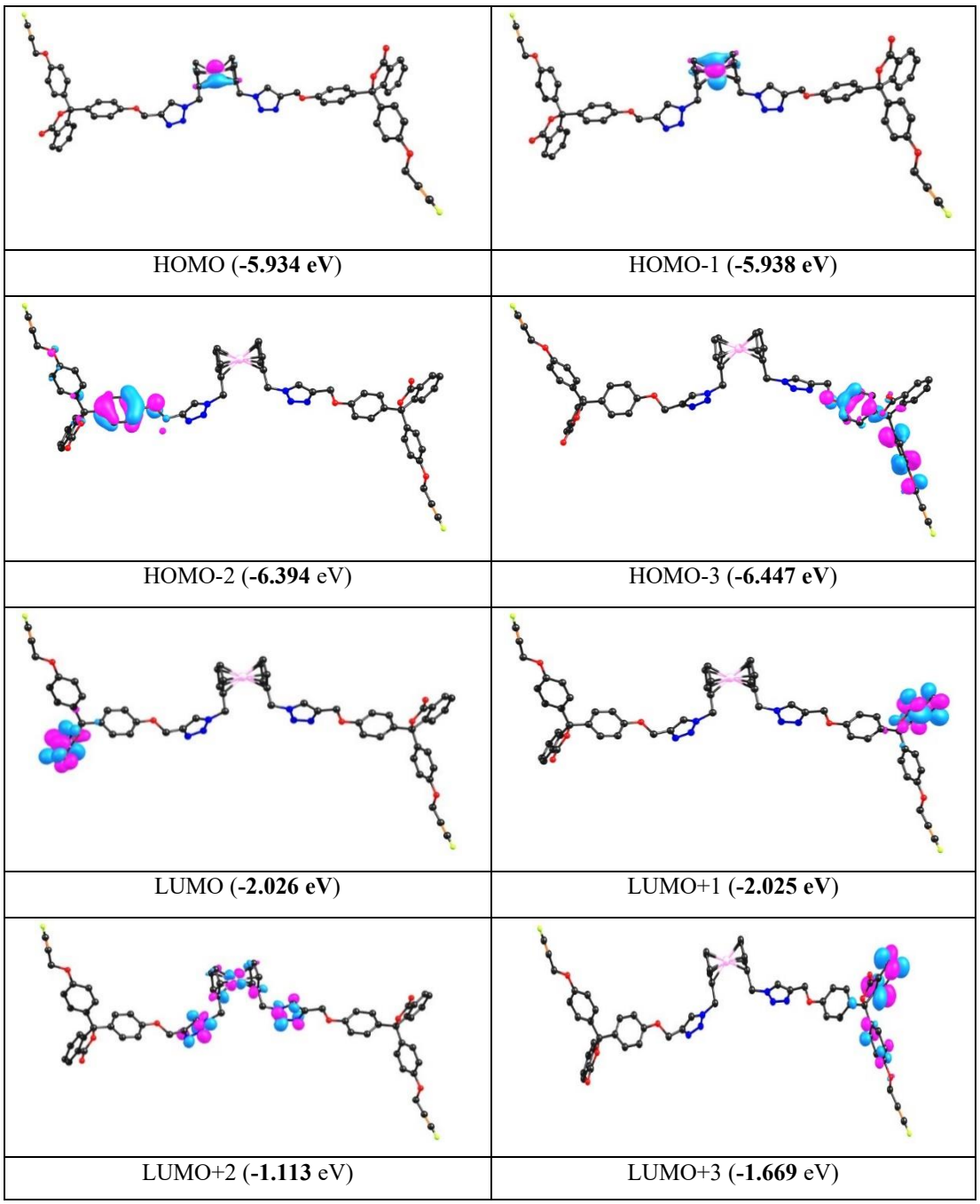

Figure 6.2.22: Frontiers MOs of the acyclic ligand **7** with energy at B3LYP/ lanl2dz / CPCM (acetonitrile) level. (iso value= 0.04)

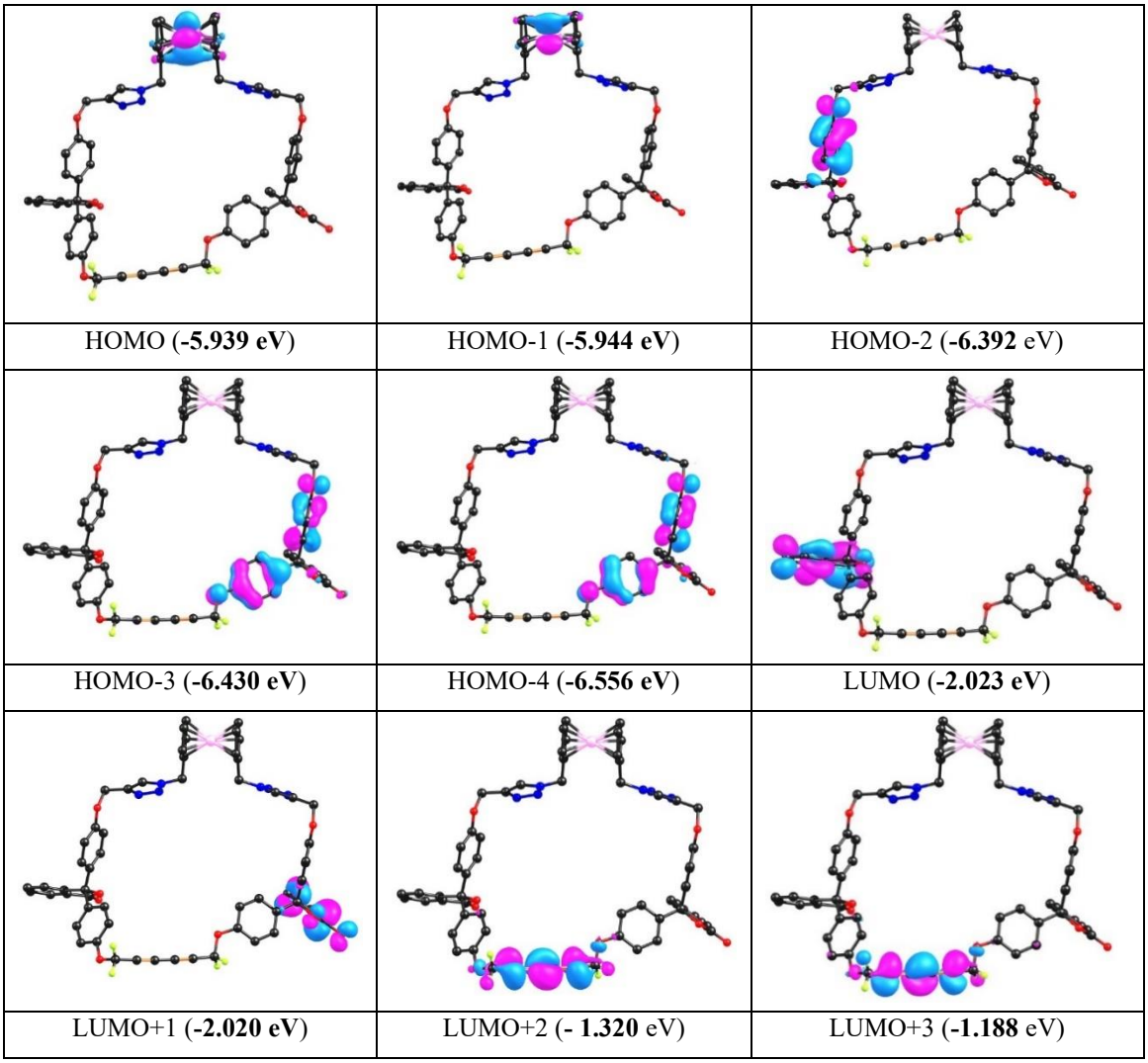

Figure 6.2.23: Frontiers MOs of the cyclic ligand **8** with energy at B3LYP/ lanl2dz / CPCM (acetonitrile) level. (iso value=0.04)

Table 6.2.2. The selected distances (Å) and Wiberg Bond Index (WBI) of ligand/receptor **7** and **8** (involving only terminal alkynes as a binding unit) calculated at B3LYP/lanl2dz/cpcm (acetonitrile) level (The zoomed portions of the primary binding core of **7** (left) and **8** (right) with atom labeling are shown below the table).

	contact	Distance (Å)	WBI
Receptor **[3]**	**C1-C2/ C4-C5**	1.222	2.886
	C2-C3/ C5-C6	1.466	1.466
	C3-O1	1.475	0.855
	C6-O2	1.474	0.856
Receptor **[4]**	**C1-C2**	1.469	1.084
	C2-C3	1.228	2.614

	C3-C4	1.374	1.239
	C4-C5	1.227	2.608
	C5-C6	1.462	1.088
	C1-O1	1.473	0.859
	C6-O2	1.475	0.853

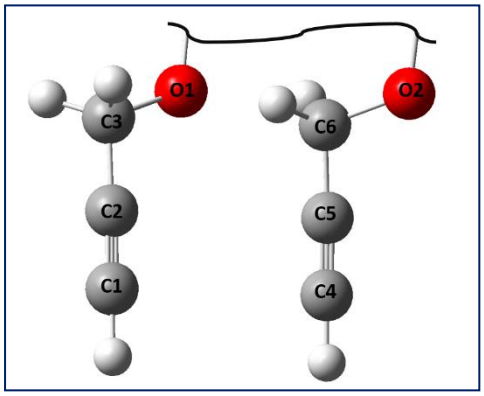

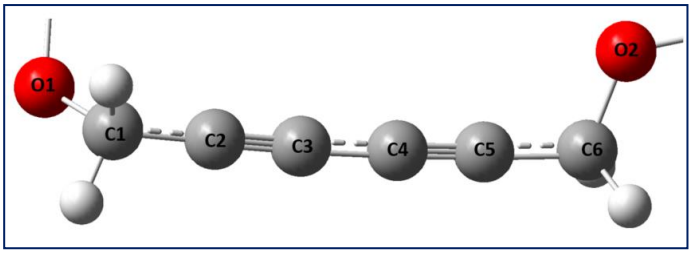

To understand the exact binding site of Hg^{2+} ion with receptor **7**, we have performed theoretical calculation at B3LYP/Lanl2DZ level of theory. To get started, different possible geometries with various binding sites has been optimized. Among all the possible geometries, we have observed that two (2) Hg^{2+} ions bind with each terminal alkyne unit and nearby O-atom of –O-CH_2- unit, adjacent to alkyne, with a slight conformational change from the free acyclic ligand framework in the optimized structure (Figure 6.2.24). This observation corroborates well with our experimental results, where the ligand binds with the metal in 1:2 ratio. Among the coordinates, both Hg-O interactions ($d_{Hg\text{-}O1}$ = 2.844 and $d_{Hg\text{-}O2}$ = 2.944) and Hg-alkyne interactions ($d_{Hg1\text{-}C1}$ = 3.300, $d_{Hg1\text{-}C2}$ = 3.019, $d_{Hg2\text{-}C4}$ = 3.143 and $d_{Hg2\text{-}C5}$ = 3.402) are comparatively weak, as observed from their low Wiberg bond index values (*ca.* 0.02) respectively. Furthermore, from the optimized structures of the **7** and [**7**·2Hg^{2+}], a very small change in alkyne bond lengths (1.221 Å to 1.226 Å) has been observed upon coordination of Hg^{2+} ion to the receptor, which indicated a soft interaction of the receptor, **7** with Hg^{2+} ion. Further, calculation of NBO showed a small change in WBI value from 2.886 to 2.860 (Table 6.2.3) which suggests a soft-soft interaction between the π-orbital of alkyne and the Hg^{2+} ion. In the optimized structure, Hg-C bond distances are in the range of 3.0−3.4 Å, which is a good agreement with the literature reported value.[58]

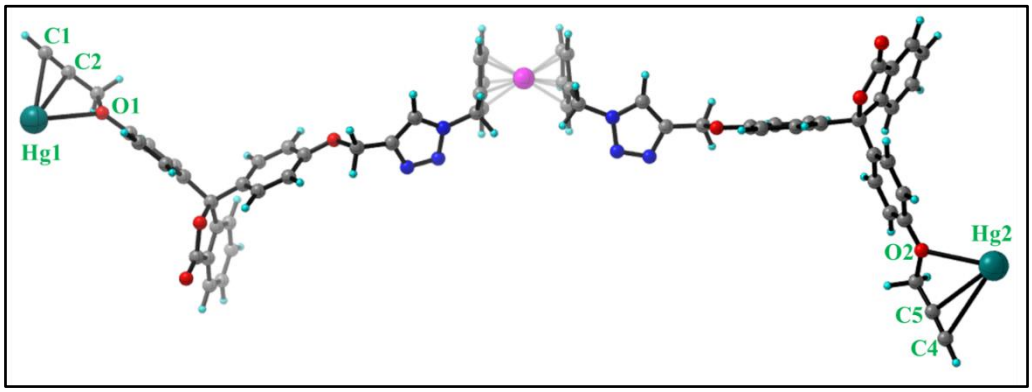

Figure 6.2.24: Optimized structure of the receptor [**7**·2Hg^{2+}].

Table 6.2.3. The selected distances (Å) and Wiberg Bond Index (WBI) of **[7·2Hg^{2+}]** and **[8·Hg^{2+}]** (involving only terminal alkynes and nearby –*O*–CH_2– as a binding unit) calculated at B3LYP/lanl2dz/cpcm (acetonitrile) level (The zoomed portions of the primary binding core of **[7·2Hg^{2+}]** (left) and **[8·Hg^{2+}]** (right) with atom labelling are shown above the table).

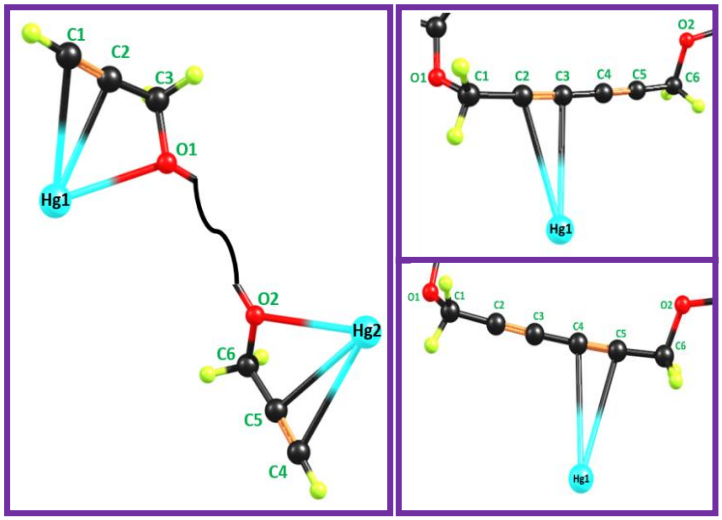

Receptor **[3·2Hg^{2+}]**			*Receptor* **[4·Hg^{2+}]**				
contact	distance(Å)	WBI	contact	Left side alkyne unit		Right side alkyne unit	
C1-C2	1.226	2.859		distance(Å)	WBI	distance(Å)	WBI
C2-C3	1.462	1.088	**C1-O1**	1.471	0.861	1.471	0.861
C3-O1	1.502	0.831	**C1-C2**	1.470	1.081	1.470	1.083
C4-C5	1.224	2.866	**C2-C3**	1.229	2.604	1.228	2.604
C5-C6	1.461	1.086	**C3-C4**	1.375	1.237	1.374	1.237
C6-O2	1.496	0.836	**C4-C5**	1.227	2.612	1.228	2.609
C1-Hg1	3.300	0.0157	**C5-C6**	1.463	1.087	1.463	1.085

C2-Hg1	3.019	0.0170	**C6-O2**	1.474	0.855	1.474	0.855
O1-Hg1	2.844	0.0412	**C2-Hg1**	3.697	0.0063	------	------
C4-Hg2	3.402	0.0120	**C3-Hg1**	3.668	0.0072	------	------
C5-Hg2	3.143	0.0128	**C4-Hg1**	------	------	3.654	0.0070
O2-Hg2	2.944	0.0340	**C5-Hg1**	------	------	3.662	0.0063

Following our earlier findings,[92] we have also tried to optimize another possibility of Hg^{2+} coordination with only terminal alkyne units. Interestingly, in this optimized geometry, we have found that Hg^{2+} ions are far apart from the alkyne units and higher in energy than the aforementioned binding mode. As a noticeable shift of $-OCH_2-$ group is observed in ^1H NMR of receptor **7**, after addition of 2 equiv Hg^{2+} ion, thus, the possibility of this optimized model (only terminal alkyne binding) can be discarded. Therefore, from both experimental (IR analysis, ^1H NMR study), and theoretical analysis, it is concluded that two Hg^{2+} ions bind with the terminal alkyne units of the receptor and oxygen atom of the adjacent $-OCH_2-$ group, which provides the more stable conformation.

To confirm Hg^{2+} ion binding with the receptor **8**, theoretical calculations were performed at the same level of theory. Furthermore, optimization of all the possible geometries of receptor **8** with different ratios of Hg atoms finally converged into the energy-minimized structure with the most stable conformation where only one (1) Hg^{2+} ion binds with the alkyne unit. Surprisingly, this Hg^{2+} ion can bind either one alkyne unit from the two internal alkyne units in 1,3-dialkyne system of **8**. Energy comparison between the interaction of either alkyne unit with Hg^{2+} ion concludes that they are almost equal in energy (~1.3 kcal/mol). The optimized structures are shown in Figure 6.2.25.

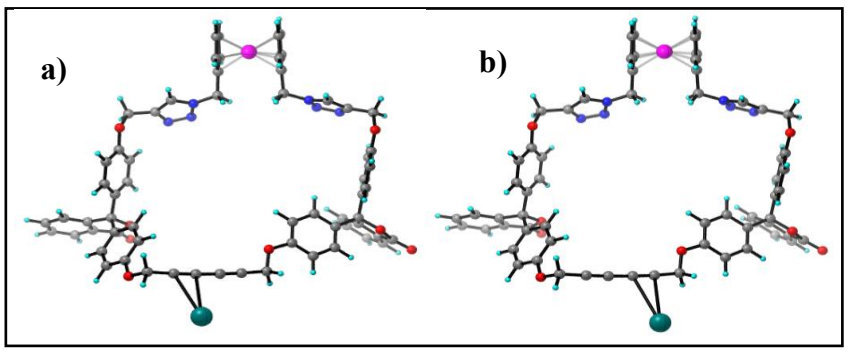

Figure 6.2.25: Optimized structures of the receptor [**8**·Hg^{2+}] when Hg^{2+} ion is bounded to the internally conjugated alkyne in the (a) left alkyne and (b) right alkyne.

Their respective frontier molecular orbitals are presented in Figures 6.2.26-6.2.28. This 1:1 ligand to metal binding nature is also in line with our experimental observation. The Hg-C bond distances are found in the range of 3.4−3.6 Å, which is typical for such interactions as per literature reports.[58]

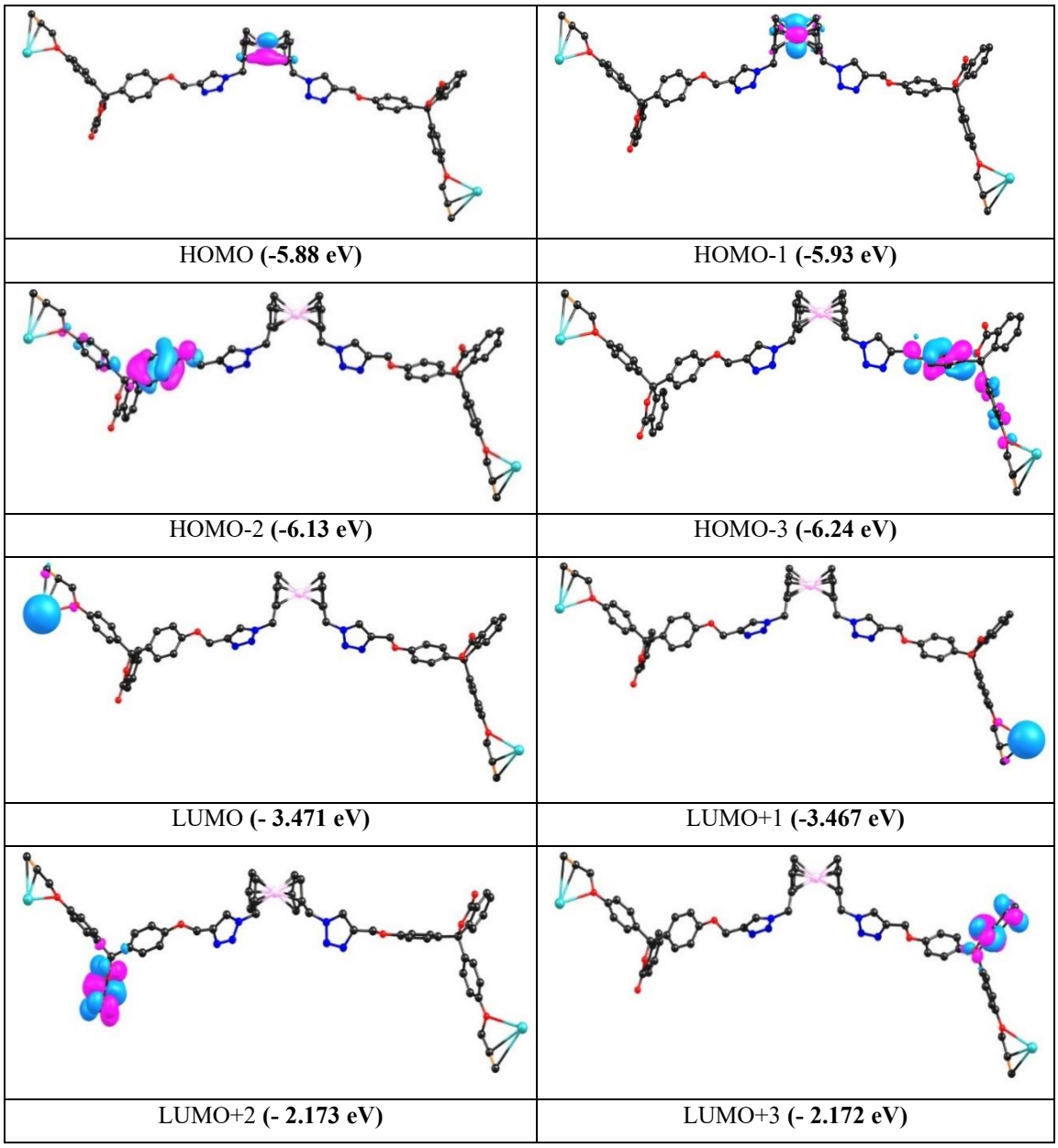

Figure 6.2.26: Frontiers MOs of the free ligand [**7**·2Hg^{2+}] with energy at B3LYP/ lanl2dz / CPCM (acetonitrile) level. (iso value=0.04)

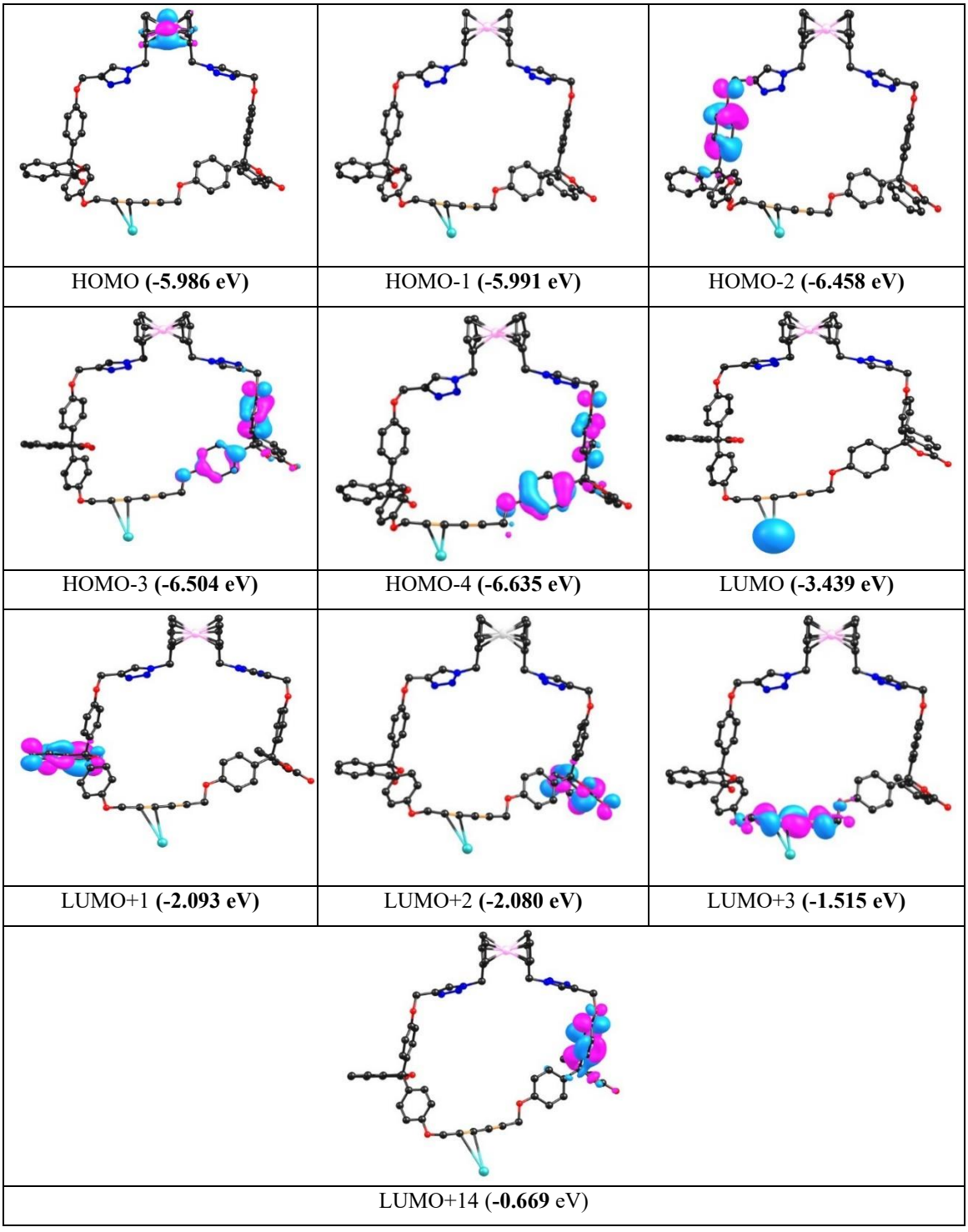

Figure 6.2.27: Frontiers MOs of **[8·Hg^{2+}]** with energy at B3LYP/ lanl2dz / CPCM (acetonitrile) level. (iso value=0.04) (left side)

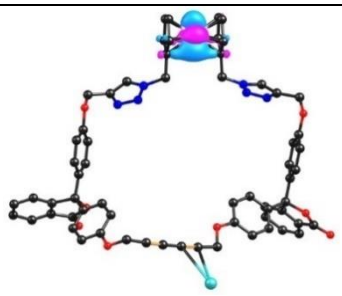	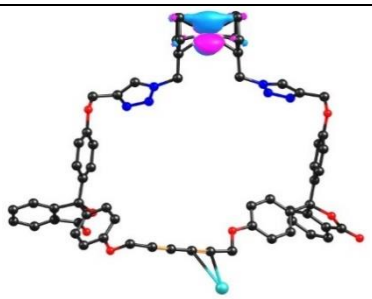	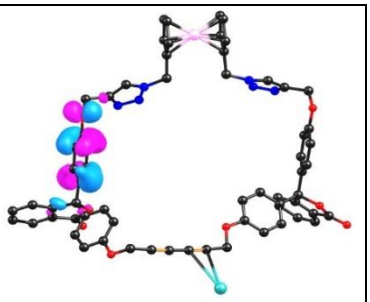
HOMO **(-5.987 eV)**	HOMO-1 **(-5.992 eV)**	HOMO-2 **(-6.454 eV)**
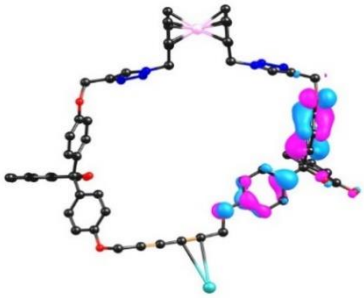	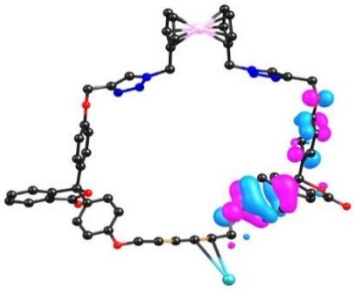	
HOMO-3 **(-6.517 eV)**	HOMO-4 **(-6.654 eV)**	LUMO **(-3.433 eV)**
	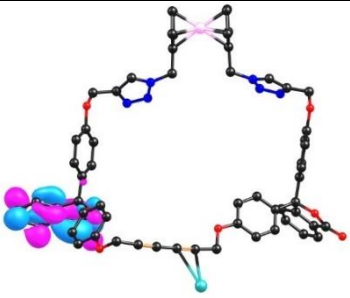	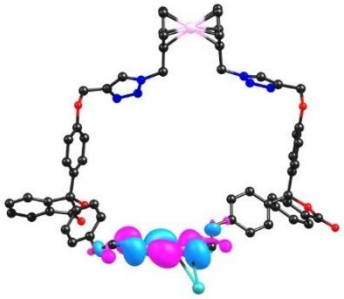
LUMO+1 **(-2.092 eV)**	LUMO+2 **(-2.088 eV)**	LUMO+3 **(-1.525 eV)**
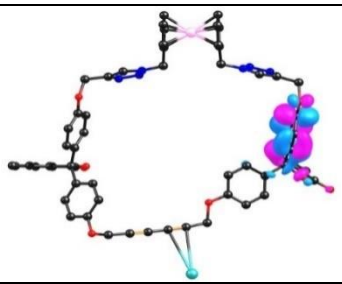		
LUMO+14 **(-0.682 eV)**		

Figure 6.2.28: Frontiers MOs of **[8·Hg^{2+}]** with energy at B3LYP/ lanl2dz / CPCM (acetonitrile) level. (iso value=0.04) (right side)

Further, to rationalize the detailed information about the UV-vis and emission spectra, time-dependent DFT (TD-DFT) calculations were carried out on **7**, **8**, [**7**·2Hg^{2+}] and [**8**·Hg^{2+}] at cam-B3LYP/LANL2DZ/CPCM level of theory using acetonitrile as a solvent. TD-DFT calculations on the acyclic receptor **7** revealed an intense transition at 216 nm (oscillator strength, f = 1.23) involving HOMO−4 to LUMO+10 (phenolphthalein π* type with a conjugation to the benzene ring) orbitals which matches the experimental results (Figure 6.2.29 and Table 6.2.4). Notably, TD-DFT calculations of the cyclic receptor **8** showed a major transition at 223 nm (oscillator strength, f = 0.19) involving HOMO−18 to LUMO+1 (phenolphthalein π* type) orbitals (Figure 6.2.30 and Table 6.2.5). Similarly, TD-DFT calculations on [**7**·2Hg^{2+}] predict a strong HOMO−1 (ferrocene centred) to LUMO+12 (benzene π* type with a delocalisation to benzene ring) transition at 225 nm (oscillator strength f = 0.64), congruent with the experimental UV−vis results (Figure 6.2.31 and Table 6.2.6). Notably, TD-DFT calculations on [**8**·Hg^{2+}] showed a strong HOMO−3 (benzene π type with a delocalization to O-atom) to LUMO+14 (phenolphthalein π* type with a conjugation to the benzene ring) transition at 215 nm (oscillator strength f = 0.5868), and both of the results corroborated with the UV−vis results, obtained experimentally (Figure 6.2.32 and Table 6.2.7). Interestingly, the calculated gaps between the orbitals involved in significant transitions for the acyclic ligand, **7** and complex [**7**·2Hg^{2+}] are found as 3.9 eV and 2.41 eV, respectively, demonstrating a significant shift in UV−vis absorption bands. Similarly, the calculated gaps between the orbitals involved in significant transitions for the cyclic ligand, **8** and complex, [**8**·Hg^{2+}] are found 3.92 eV and 2.55 eV, respectively. DFT calculations revealed a slight decrease (~1.4 eV) in HOMO−LUMO gap upon complex formation for both the receptors **7** and **8** (Figure 6.2.33), which explains the observed small red shifts (~3/4 nm) in the experimental UV-vis study.

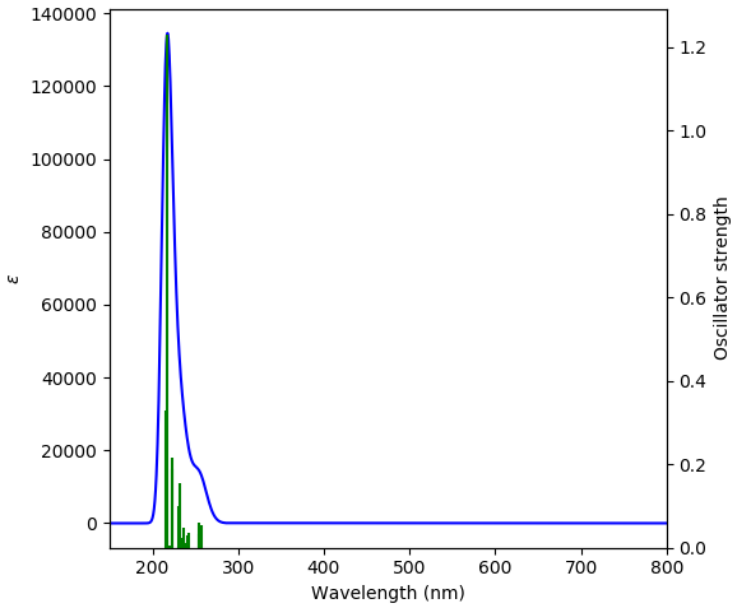

Figure 6.2.29: Calculated absorption spectrum of the ligand/receptor **7**.

Table 6.2.4. Major excited state transitions of the ligand/receptor **7** with Osc. Strength and λ_{ex}.

λ_{ex} (nm) (Exp.)[a]	**λ_{ex} (nm) (Calc.)[b]**	**Oscillator Strength (*f*)**	**Major Transitions[c]**
227	216.5	1.2303	H-4 → L+10 (32%), H-3 → L+10 (19%)
273	253.6	0.0615	H-27 → L+1 (13%), H-13 → L+1 (29%), H-4 → L+1 (32%)
281	257.1	0.0556	H-28 → L (16%), H-12 → L (15%), H-2 → L (52%)

[a]Experimental wavelength in acetonitrile. [b]TD-DFT calculated wavelength of ligand **7** in acetonitrile. [c]Transitions with greater than 10% contribution are represented.

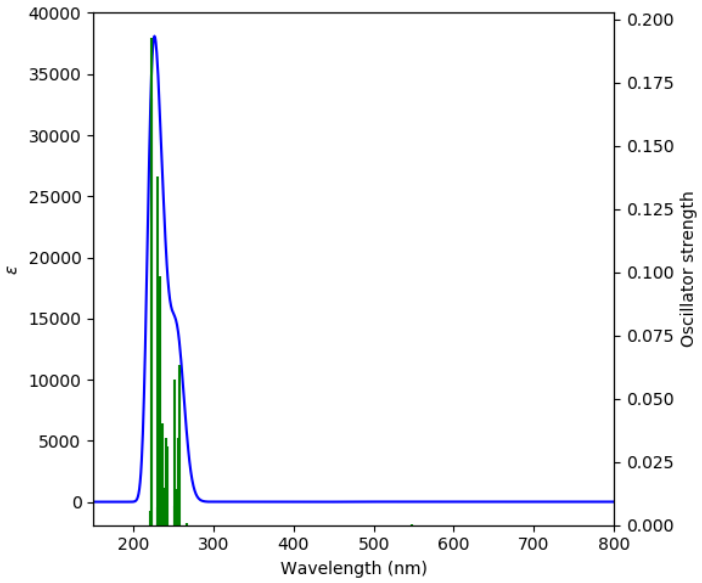

Figure 6.2.30: Calculated absorption spectrum of the ligand/receptor **8**.

Table 6.2.5. Major excited state transitions of the ligand/receptor **8** with Osc. Strength and λ_{ex}.

λ_{ex} (nm) (Exp.)[a]	λ_{ex} (nm) (Calc.)[b]	Oscillator Strength (*f*)	Major Transitions[c]
227	223.0	0.193	H-18 → L+1 (62%)
273	252.1	0.0575	H-26 → L+1 (24%), H-14 → L+1 (26%), H-4 → L+1 (24%)
281	257.3	0.0633	H-15 → L (16%), H-1 → L (52%)

[a]Experimental wavelength in acetonitrile. [b]TD-DFT calculated wavelength of ligand **8** in acetonitrile. [c]Transitions with greater than 10% contribution are represented.

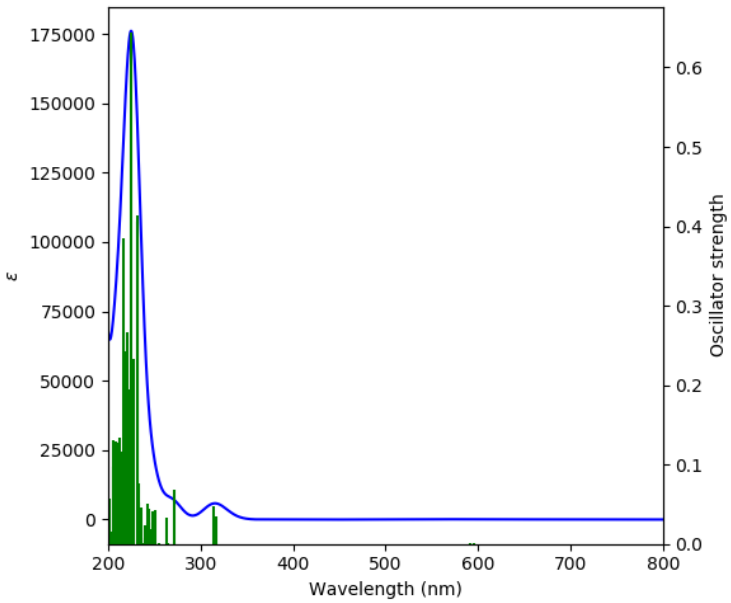

Figure 6.2.31: Calculated absorption spectrum of the complex [**7·2Hg**$^{2+}$]

Table 6.2.6. Major excited state transitions of [**7·2Hg**$^{2+}$] (involving only terminal alkynes and nearby –***O***–CH_2– atom as a binding unit) with Osc. Strength and λ_{ex}.

λ_{ex} (nm) (Exp.)[a]	λ_{ex} (nm) (Calc.)[b]	Oscillator Strength (*f*)	Major Contributions[c]
231	225.2	0.6445	H-1 → L+12 (25%), H-4 → L+3 (14%), H-1 → L+9 (18%), H-1 → L+16 (13%)
	231.26	0.4055	H-5 → L+2 (23%), HOMO → L+8 (15%)
274	251.2	0.0426	HOMO → L+5 (18%), HOMO → L+14 (12%), HOMO → L+17 (44%)
	263.6	0.0339	H-1 → L+3 (84%)
281	271.2	0.0676	HOMO → L+2 (88%)
	314.5	0.0468	H-5 → LUMO (62%), HOMO → LUMO (34%)
	316.9	0.0343	H-4 → L+1 (54%), H-1 → L+1 (41%)

[a]Experimental wavelength in acetonitrile. [b]TD-DFT calculated wavelength of complex [**7·2Hg**$^{2+}$] in acetonitrile. [c]Transitions with greater than 10% contribution are presented.

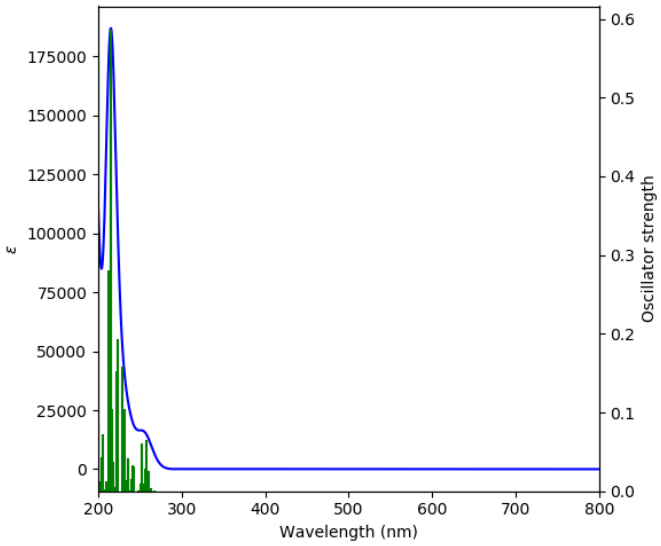

Figure 6.2.32: Calculated absorption spectrum of the complex [**8·Hg^{2+}**].

Table 6.2.7. Major excited state transitions of [**8·Hg^{2+}**] (involving only conjugated alkynes as a binding unit) with Osc. Strength and λ_{ex}.

λ_{ex} (nm) (Exp.)[a]	**λ_{ex} (nm) (Calc.)**[b]	**Oscillator Strength (*f*)**	**Major Contributions**[c]
230	215.5	0.6378	H-4 → L+14 (16%), H-3 → L+14 (41%)
273	251.9	0.0644	H-26 → L+1 (19%), H-14 → L+1 (27%), H-4 → L+1 (27%)
281	257.4	0.0644	H-13 → L+2 (15%), H-2 → L+2 (57%)
[a]Experimental wavelength in acetonitrile. [b]TD-DFT calculated wavelength of complex [**8·Hg^{2+}**] (right side alkyne unit) in acetonitrile. [c]Transitions with greater than 10% contribution are presented.			

λ_{ex} (nm) (Exp.)[a]	**λ_{ex} (nm) (Calc.)**[b]	**Oscillator Strength (*f*)**	**Major Contributions**[c]
230	215.4	0.5868	H-4->L+14 (20%), H-3->L+14 (42%)
273	251.9	0.0601	H-25->L+2 (19%), H-14->L+2 (24%), H-4->L+2 (25%)
281	257.4	0.0649	H-13->L+1 (14%), H-2->L+1 (57%)

[a]Experimental wavelength in acetonitrile. [b]TD-DFT calculated wavelength of complex [**8**·**Hg**$^{2+}$] (left side alkyne unit) in acetonitrile. [c]Transitions with greater than 10% contribution are presented.

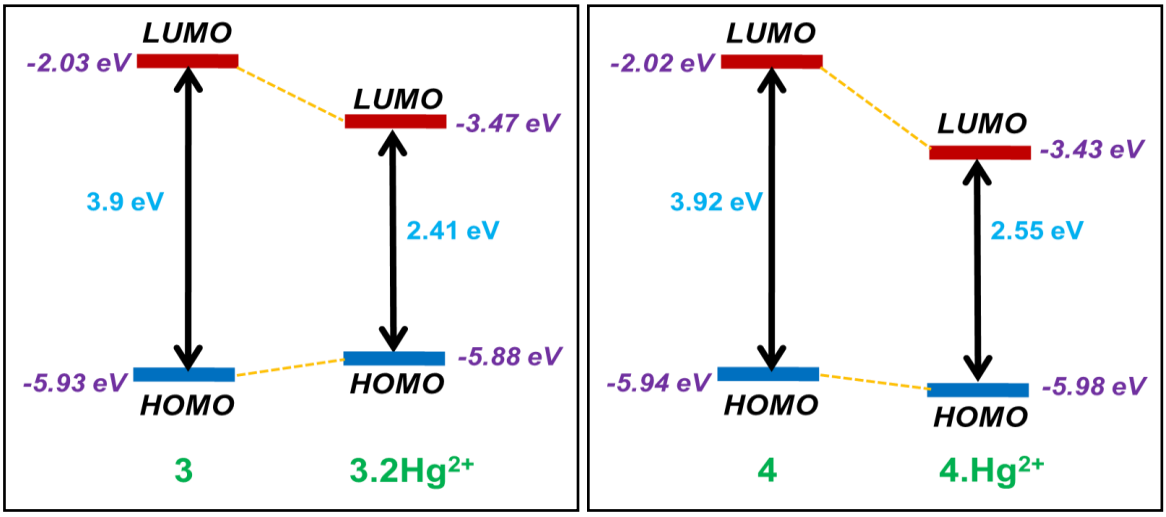

Figure 6.2.33: Energy diagram of the frontier molecular orbitals of receptor **7** and [**7**·2Hg^{2+}] (left) and that of receptor **8** and [**8**·Hg^{2+}] (right) as obtained from DFT calculations.

Furthermore, to understand fluorescence-quenching mechanism, TD-DFT calculations were performed. TD-DFT calculations on [**7**·2Hg^{2+}] revealed that the mercury centered vacant orbital (LUMO) lies between the phenolphthalein *fl*uorophore and phenolphthalein attached benzene ring (Figure 6.2.34). This transcends the electron in the excited state of the phenolphthalein-centered orbital (LUMO+12) to the energetically favourable mercury-centered vacant orbital (LUMO) and not to HOMO-1 state. Such orientation of orbitals might promote an additional pathway for *fl*uorescence quenching of acyclic receptor, **7** in the presence of Hg^{2+} ion.

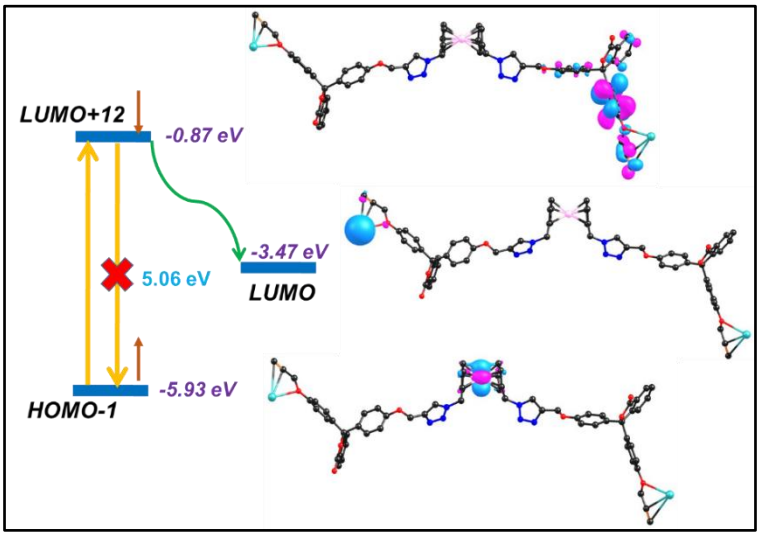

Figure 6.2.34. Schematic representation of fluorescence quenching due to $2Hg^{2+}$ ions binding to the receptor **7**.

Similarly, TD-DFT calculations on [**8**·Hg^{2+}] revealed that the mercury-centered empty orbital (LUMO) dwells in between the phenolphthalein *fl*uorophore and the phenolphthalein attached benzene ring (Figure 6.2.35). This type of orientation of orbitals promotes the transfer of the electron from benzene-centered orbital (LUMO+14) to the energetically favorable mercury-centered empty orbital (LUMO), instead of HOMO-3 state. Thus, an additional pathway for *fl*uorescence quenching of cyclic receptor, **8** in the presence of Hg^{2+} ion may be obtained by such orientation of the respective orbitals.

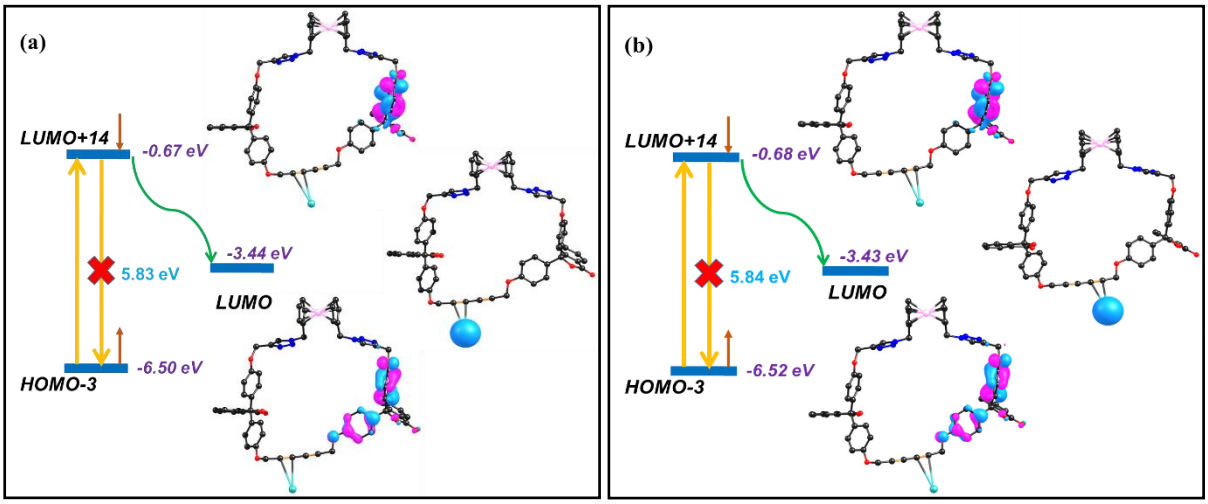

Figure 6.2.35. Schematic representations of fluorescence quenching due to Hg^{2+} ion binding to the receptor **8** when Hg^{2+} ion is bounded to (a) the left alkyne and (b) the right alkyne of the 1,3-dialkyne unit.

6.2.3. Conclusion

Herein, we have designed and successfully synthesized one acyclic and one cyclic alkyne containing probes bearing similar molecular architecture. We have explored their comparative reactivity studies towards metal ion detection for the 1st time. Owing to the different positioning of the alkyne units in the probes, they show differential binding patterns with Hg^{2+} ion. Acyclic probe **7** interacts with Hg^{2+} ion in the ratio of 1:2, whereas probe **8** gives a 1:1 binding stoichiometry. Probe **7** readily accommodates two Hg^{2+} ions by the π-clouds of the two sterically accessible discrete terminal alkyne units, with the assistance of the vicinal -OCH_2 groups, whereas probe **8** finds it difficult to accommodate two Hg^{2+} ions simultaneously by its rigid internally conjugated C_2-symmetric 1,3-dialkyne unit present in the ring architecture. In this study, we are able to focus on the comparative reactivity studies of different alkyne units towards a soft metal, Hg^{2+} ions and extended its application towards the detection of Hg^{2+} ion in real water samples as well. The exploration of difference in the cyclic and acyclic cores are important from the point of view of knowing their overall potential in any interactive environment. We believe that this present study will certainly open up a new aspect in organometallic chemistry involving alkyne moiety as a reactive synthon to get further detailed insight about the differential reactivity of cyclic and acyclic (terminal as well as internal) alkyne towards the metal ions. Such studies on the divergent behaviour of different alkynes, engulfed in different structural cores will permit the overall assessment of the functionality from a separate perspective and allow the scientific community to explore the functionality in differentiating between analogous motifs.

6.2.4. Experimental Section

6.2.4.1. Materials and reagents

Among the metal ions used, K^+, Fe^{2+}, Fe^{3+}, Cu^{2+}, Cd^{2+} and Hg^{2+} were purchased from Sigma Aldrich and Mg^{2+}, Zn^{2+}, Pb^{2+}, Ni^{2+} and Co^{2+} were purchased from Alfa Aesar, as their respective perchlorate salts and used directly without further purification. Cu^+ was purchased from Sigma Aldrich as $[(CH_3CN)_4Cu]PF_6$. Glacial AcOH was purchased from Merck. DMF and acetonitrile (HPLC) were purchased from Thermo Fisher Scientific and freshly distilled prior to use. Rest of the chemicals were purchased from local brand. Bis(azidomethyl)ferrocene was prepared according to literature reported procedure.[59] The compound **2** was prepared from commercially available phenolphthalein by propargylation of phenolic alcohol.[92] Chromatography was carried out using 60-120 mesh silica gel in a column of 2.5 cm diameter.

All the necessary solvents were dried by conventional methods and distilled under N_2 atmosphere. The cyclic voltammetry (CV) was performed with a conventional three electrode configuration consisting of glassy carbon as working electrode, platinum as an auxiliary electrode and Ag/Ag^+ as a reference electrode. The experiment was carried out with 10^{-4} M solution of sample in CH_3CN containing 0.1 M (TBAP) [$(n\text{-}C_4H_9)_4NClO_4$] as supporting electrolyte. The working electrode was cleaned after each run. The cyclic voltammograms were recorded at a scan rate 0.06 Vs^{-1} and readings were taken considering ferrocene/ferrocenium couple as the standard. The UV-vis spectra were carried out in CH_3CN solutions at c = 10^{-5} M and the fluorescence spectra were carried out at c = 10^{-6} M, as it is stated in the corresponding Figure captions.

6.2.4.2. Preparation of pH solutions

10^{-3} M solution of both the probes and their Hg^{2+} complexes were prepared in CH_3CN, where buffer solutions of pH 2, 4, 5, 7, 9.2 and 11 were added separately. The pH of resulting solutions were verified by testing with pH paper strip and were directly used for the pH studies.

6.2.4.3. Preparation of samples for IR and CHN analysis

The acyclic and cyclic compounds **7** and **8** were dissolved in minimum amount of CH_3CN and 2 equiv and 1 equiv of $Hg(ClO_4)_2$ in CH_3CN were mixed with them respectively. The two solutions were subjected to evaporation under reduced pressure. The resulting solid complexes were washed several times with H_2O to remove any extra perchlorate anion, which is followed by filtration by suction and dried under vacuum for several hours. The resulting dry solid powder were used directly for IR and elemental analysis. Elemental analysis: Anal. Calcd for $C_{64}H_{48}FeN_6O_8Hg_2$ [**7**·$2Hg^{2+}$]: C, 51.72; H, 3.26; N, 5.66. Found: C, 62.23; H, 4.05; N, 7.29 and for $C_{64}H_{46}FeN_6O_8Hg_2$ [**8**·Hg^{2+}]: C, 59.89; H, 3.61; N, 6.55. Found: C, 60.56; H, 4.01; N, 6.71.

6.2.4.4. Instrumentation

^1H and ^{13}C NMR spectra were obtained with 300 MHz and 500 MHz FT-NMR spectrometers. The chemical shifts are reported in ppm, using tetramethylsilane as an internal standard and were referenced to the residual solvent as follows: $CDCl_3$ = 7.26 (^1H), 76.16 (^{13}C) ppm, CD_3CN = 1.94 (^1H) at room temperature. For ^1H NMR, coupling constants *J* are given in Hz and the resonance multiplicity is described as s (singlet), d (doublet), t (triplet), m (multiplet). IR spectral studies were done on Perkin Elmer LX-1 FTIR spectrophotometer. The absorption spectra were recorded with a Shimadzu-UV-1900i UV-vis spectrophotometer at

room temperature. Fluorescence was recorded with SHIMADZU RF-5301pc spectrophotometer. Fluorescence lifetime experiments was recorded in Horiba Jobin-Yvon. FT-IR spectra were obtained from PerkinElmer LX-1 FT-IR spectrophotometer. CH Instruments Electrochemical Analyzer was used to perform the cyclic voltammetry (CV) and differential pulse voltammetry (DPV) studies. HRMS were taken using electrospray ionization (ESI) technique. CHN analysis was performed on a CHNS analyser. Microwave reaction has been done in CEM microwave.

6.2.4.5. Synthesis of Compounds 7 and 8

6.2.4.5.1. Synthesis of Compound 7

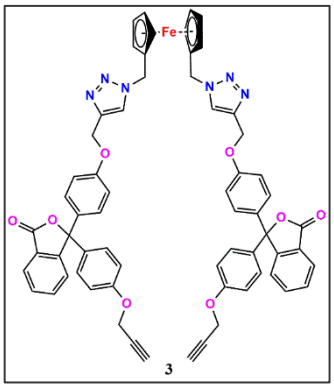

Compound **7** was synthesized from compounds **2** and bis(azidomethyl)ferrocene (**6**). Compound **2** (532 mg, 1.351 mmol) and bis(azidomethyl)ferrocene (**6**) (400 mg, 1.351 mmol) were taken in a 100mL round bottom flask and dissolved in ^{t}BuOH (26 mL) solvent. $CuSO_4 \cdot 5H_2O$ (134.92 mg, 0.5404 mmol) and Sodium-L-ascorbate (214.11 mg, 1.0808 mmol) were dissolved in a total of 13mL of H_2O and added to the reaction mixture one by one at room temperature. After 1 h, a greenish suspension was formed which was allowed to stir for 24 h at room temperature. Reaction mixture was diluted with ethyl acetate and washed with distilled water. The organic phase was separated, dried over sodium sulphate and the solvent was removed under reduced pressure. Then the crude product was purified by silica gel column chromatography. Elution with 60% EtOAc/Hexane gave yellow coloured solid compound **7** (512 mg, 0.473 mmol, yield 35 %) along with some amount of side product. It is to be noted that adding the two reactants in 1:2 ratio (compound **6**:compound **2**) keeping the equivalence of the rest of the reagents intact, also produced same product. ^{1}H NMR ($CDCl_3$, 300 MHz) δ = 7.93 (d, 1H, J = 7.5 Hz, $H_{aromatic}$), 7.69 (t, 1H, J = 7.2 Hz, $H_{aromatic}$), 7.57 (s, 1H, $H_{triazole}$), 7.52 (t, 2H, J = 7.8 Hz, $H_{aromatic}$), 7.26-7.21 (m, 4H, $H_{aromatic}$), 6.92 (d, 4H, J = 8.4 Hz, $H_{aromatic}$), 5.27 (s, 2H, OCH_2), 5.17 (s, 2H, NCH_2), 4.68 (s, 2H, OCH_2), 4.21 (s, 2H, H_{Fc}), 4.18 (s, 2H, H_{Fc}) 2.52 (s, 1H, H_{alkyne}); ^{13}C NMR ($CDCl_3$, 75 MHz) δ = 169.8, 158.2, 157.5, 152.3, 143.6, 134.2, 133.8, 133.4, 129.3, 128.6, 128.4, 125.9, 125.3, 124.0, 122.7, 114.6, 91.4, 82.2, 78.3, 75.9, 69.8, 69.5, 61.8, 55.82, 49.5; HRMS *m/z* calcd for $C_{64}H_{48}FeN_6O_8$

$[M+H]^+$ 1085.2961; found 1085.2932; Anal. Calcd for $C_{64}H_{48}FeN_6O_8$, C, 70.85; H, 4.46; N, 7.75. Found: C, 70.23; H, 4.05; N, 8.01.

6.2.4.5.2. Synthesis of compound 8

The coupling reaction of compound **7** had been performed in microwave reactor under closed reaction system. Compound **7** (100 mg, 0.092 mmol) was soaked with pyridine and grounded with the catalyst $Cu(OAc)_2 \cdot H_2O$ (3 equiv, 55 mg, 0.276 mmol) and the resulting mixture was taken into the closed system vessel. Microwave radiation in the reactor under 50 watt power was applied maintaining a constant 60°C for 30 mins. After cooling the reaction vessel, it was taken out and the reaction mixture was diluted with EtOAc and layered with water to remove the pyridine. The collected organic layer is dried over sodium sulphate and solvent removed under vacuum. Column chromatography by 70% EtOAc/hexane yielded pure compound **8** (30 mg, 0.027 mmol, yield 30 %). ^{1}H NMR ($CDCl_3$, 500 MHz) δ = 7.94-7.91 (q, 1H, J = 3 Hz, $H_{aromatic}$), 7.72-7.67 (m, 1H, $H_{aromatic}$), 7.65 (s, 1H, $H_{triazole}$), 7.58-7.50 (quin, 2H, J = 6 Hz, $H_{aromatic}$),7.28 (s, 2H, $H_{aromatic}$), 7.24 (s, 2H, $H_{aromatic}$), 6.96-6.90 (q, 4H, J = 6 Hz, $H_{aromatic}$), 5.24 (d, 2H, J = 6 Hz, OCH_2), 5.135 (d, 2H, , J = 3 Hz, OCH_2), 4.76 (s, 2H, NCH_2), 4.08 (s, 2H, H_{Fc}) 4.04 (s, 2H, H_{Fc}); ^{13}C NMR ($CDCl_3$, 75 MHz) δ = 169.9, 158.3, 157.4, 152.4, 143.9, 134.3, 134.2, 133.6, 129.4, 128.8, 128.7, 126.1, 125.6, 124.1, 123.1, 114.8, 91.5, 83.2, 74.6, 71.3, 69.5, 69.4, 62.0, 56.2, 49.4; HRMS *m/z* calcd for $C_{64}H_{46}FeN_6O_8$ $[M+H]^+$ 1083.2805; found 1083.2775; Anal. Calcd for $C_{64}H_{46}FeN_6O_8$, C, 70.98; H, 4.28; N, 7.76. Found: C, 70.55; H, 4.58; N, 7.51.

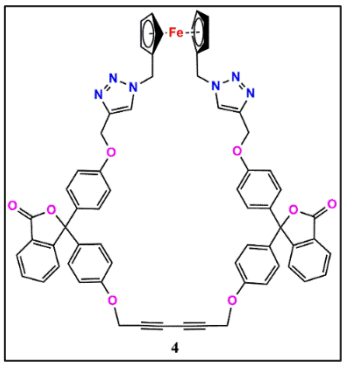

6.2.5. Computational details

All computational calculations (DFT and TDDFT) presented in this paper were carried out using the density functional theory (DFT) method in the Gaussian 16 program package.[60] The ground-state geometry optimizations were performed employing the B3LYP (Becke, three-parameter, Lee−Yang−Parr) functional[94-96] in combination with the LANL2DZ basis set.[97,98] The vibrational frequency calculations were performed to confirm that the optimized geometries represent the local minima and obtain only positive eigen values. The molecular orbital calculation incorporates the solvent effect through the conductor-like polarizable continuum model[62] (CPCM) using acetonitrile as a solvent. Natural bond orbital (NBO)

analysis[63] and Wiberg bond indices (WBI)[64] were performed at the same level[97,98] using the NBO Version 3.1 program implemented in the Gaussian package. TDDFT calculation on the optimized structures was carried out using the Coulomb—attenuated functional CAM-B3LYP at the aforementioned level of theory. Canonical orbitals were rendered in the Chemcraft[65] visualization software with an isosurface value of 0.05. The 3D images of the optimized geometries were visualized using CYLview visualization software.[99]

Table 6.2.8. DFT Optimized coordinates of all the compounds.

Ligand/Receptor 7

Electronic Energy: -3520.714616 a.u.; **EE + Free Energy Correction**: -3519.857175 a.u.

C	11.835709000	5.892083000	6.052102000	N	5.852974000	-9.904769000	-2.517817000
C	-2.657700000	-20.156587000	-8.863806000	C	4.572182000	-10.327852000	-2.731656000
O	11.094324000	6.666755000	5.040231000	C	14.492475000	6.370673000	-1.778812000
O	-2.549032000	-18.787468000	-8.325776000	C	14.007632000	7.268891000	-2.759628000
C	11.116783000	6.201769000	3.717562000	C	12.624459000	7.414655000	-2.967537000
C	-2.010821000	-18.630942000	-7.042568000	C	11.759772000	6.641407000	-2.175436000
C	10.395375000	6.980805000	2.789663000	C	12.235835000	5.745370000	-1.204339000
C	10.355308000	6.604410000	1.440460000	C	13.612158000	5.600873000	-0.990075000
C	11.022012000	5.441709000	0.993947000	C	10.283816000	6.619606000	-2.176174000
C	11.736941000	4.672915000	1.932934000	O	9.866636000	5.731823000	-1.175746000
C	11.792499000	5.041426000	3.289684000	C	11.060853000	5.065090000	-0.494313000
C	-1.929115000	-17.298759000	-6.580491000	O	9.466107000	7.234032000	-2.880778000
C	-1.401777000	-17.034366000	-5.313322000	C	10.918291000	3.566652000	-0.765538000
C	-0.948828000	-18.084187000	-4.476930000	C	9.920987000	2.832516000	-0.077065000
C	-1.045542000	-19.405387000	-4.950160000	C	9.703590000	1.479180000	-0.350716000
C	-1.566841000	-19.689508000	-6.227260000	C	10.487824000	0.822787000	-1.326221000
C	1.608435000	-20.701715000	-1.596914000	C	11.482390000	1.536374000	-2.023822000
C	0.761288000	-21.012737000	-0.506420000	C	11.683738000	2.900759000	-1.740398000
C	-0.419131000	-20.278914000	-0.292577000	O	10.197907000	-0.529894000	-1.521957000
C	-0.717382000	-19.244017000	-1.194254000	C	10.981160000	-1.273371000	-2.536241000
C	0.117113000	-18.934510000	-2.280824000	C	10.526004000	-2.691578000	-2.521947000
C	1.296500000	-19.658978000	-2.494128000	N	11.120085000	-3.647329000	-1.705889000
C	-1.867519000	-18.319184000	-1.185014000	N	10.512022000	-4.827528000	-1.895017000
O	-1.708491000	-17.425218000	-2.252277000	N	9.515761000	-4.615296000	-2.844856000
C	-0.459438000	-17.751469000	-3.065829000	C	9.506187000	-3.310507000	-3.247456000
O	-2.844658000	-18.250487000	-0.421516000	C	8.671484000	-5.751659000	-3.289190000
C	0.477408000	-16.536563000	-3.002000000	H	12.899193000	5.850246000	5.780276000
C	1.536473000	-16.424038000	-3.933668000	H	11.442364000	4.867413000	6.095654000
C	2.460480000	-15.376007000	-3.847776000	H	-3.297714000	-20.761871000	-8.207746000
C	2.339826000	-14.411537000	-2.823911000	H	-1.661265000	-20.616510000	-8.907383000
C	1.285333000	-14.504092000	-1.893575000	H	9.876128000	7.869076000	3.136860000
C	0.368382000	-15.568852000	-1.987564000	H	9.790415000	7.209446000	0.739853000
O	3.313502000	-13.406711000	-2.823566000	H	12.253428000	3.770275000	1.619187000
C	3.244933000	-12.366133000	-1.772010000	H	12.353239000	4.420622000	3.979875000
C	4.422036000	-11.468685000	-1.940687000	H	-2.279404000	-16.495371000	-7.221281000
N	5.620088000	-11.694769000	-1.273066000	H	-1.344028000	-16.005826000	-4.968758000
N	6.502542000	-10.745509000	-1.617435000	H	-0.714293000	-20.235308000	-4.334433000

H	-1.617759000	-20.721590000	-6.556212000
H	2.518148000	-21.277273000	-1.744862000
H	1.029731000	-21.820959000	0.167607000
H	-1.079483000	-20.498290000	0.541217000
H	1.961145000	-19.433244000	-3.322167000
H	1.638764000	-17.149643000	-4.735950000
H	3.274262000	-15.289476000	-4.561524000
H	1.161915000	-13.771552000	-1.103481000
H	-0.441906000	-15.627522000	-1.269056000
H	2.304912000	-11.811792000	-1.877355000
H	3.276856000	-12.846392000	-0.786685000
H	3.884697000	-9.823835000	-3.390158000
H	15.564462000	6.273656000	-1.630171000
H	14.711013000	7.848705000	-3.350108000
H	12.232554000	8.102298000	-3.711122000
H	14.002168000	4.919552000	-0.240178000
H	9.309932000	3.324158000	0.674581000
H	8.938021000	0.917108000	0.175577000
H	12.097396000	1.059114000	-2.778627000
H	12.451658000	3.432211000	-2.293251000
H	10.817864000	-0.816649000	-3.519389000
H	12.045789000	-1.216863000	-2.279469000
H	8.819484000	-2.922909000	-3.981293000
C	6.878066000	-8.950868000	-4.567346000
H	8.720468000	-10.251121000	-4.547943000
C	7.962110000	-9.732908000	-5.118919000
H	5.214822000	-7.817918000	-5.585583000
C	6.096128000	-8.439283000	-5.671222000
H	10.723981000	-7.406747000	-4.682868000
C	8.891015000	-6.094225000	-4.737186000
C	9.961613000	-6.909182000	-5.266779000
Fe	8.088423000	-7.735260000	-5.806762000
C	7.846702000	-9.705900000	-6.554729000
C	6.694404000	-8.905324000	-6.896378000
C	8.103877000	-5.618781000	-5.853655000
C	9.836577000	-6.932964000	-6.701907000
H	8.516801000	-10.185631000	-7.254336000
H	6.349599000	-8.681990000	-7.896266000
C	8.687908000	-6.136440000	-7.064790000
H	10.479453000	-7.468902000	-7.386077000
H	8.320961000	-5.970270000	-8.067914000
H	7.231159000	-4.983361000	-5.784635000
H	8.944382000	-6.581129000	-2.631440000
H	7.625459000	-5.487650000	-3.102978000
C	6.584532000	-8.755557000	-3.104677000
H	5.983998000	-7.855202000	-2.940952000
H	7.502976000	-8.674180000	-2.517193000
C	-3.238680000	-20.076392000	-10.206990000
C	11.669660000	6.554100000	7.349317000
C	-3.720311000	-20.045928000	-11.329813000
C	11.552501000	7.080473000	8.446094000
H	-4.141596000	-20.017166000	-12.311232000
H	11.448580000	7.541854000	9.404106000

*Ligand/Receptor **8***

Electronic Energy: -3519.532780 a.u.; **EE + Free Energy Correction**: -3518.682147 a.u.

C	8.865360000	-6.934177000	8.709249000
C	3.775666000	-11.371205000	8.842008000
O	9.363515000	-7.018496000	7.323387000
O	4.182768000	-12.777621000	8.999989000
C	10.353864000	-6.115059000	6.912241000
C	4.859725000	-13.423032000	7.954436000
C	10.951225000	-5.143748000	7.738947000
C	11.931524000	-4.287452000	7.199869000
C	12.314008000	-4.378903000	5.849166000
C	11.705783000	-5.363950000	5.036739000
C	10.736644000	-6.227361000	5.559941000
C	5.251288000	-12.806141000	6.749492000
C	5.930061000	-13.561970000	5.778145000
C	6.219800000	-14.927128000	5.977765000
C	5.817659000	-15.525522000	7.194569000
C	5.144033000	-14.785816000	8.174686000
C	6.130435000	-19.476695000	5.065854000
C	7.395523000	-19.979322000	5.454637000
C	8.473435000	-19.101773000	5.668212000
C	8.243937000	-17.728426000	5.483082000
C	6.990963000	-17.225086000	5.097619000
C	5.915063000	-18.094926000	4.881843000
C	9.193217000	-16.607921000	5.632185000
O	8.516079000	-15.424547000	5.308002000
C	7.055792000	-15.699970000	4.954410000
O	10.387293000	-16.598961000	5.973476000
C	6.838678000	-15.280869000	3.493237000
C	5.525019000	-15.120558000	2.993043000
C	5.301836000	-14.825921000	1.642183000
C	6.394877000	-14.686423000	0.759908000
C	7.710080000	-14.835954000	1.241967000
C	7.917663000	-15.136994000	2.601774000
O	6.059158000	-14.397928000	-0.569417000
C	7.093393000	-14.462630000	-1.625930000
C	7.931449000	-13.225005000	-1.736747000
N	9.241335000	-13.172392000	-1.272969000
N	9.757252000	-11.963114000	-1.537223000
N	8.758021000	-11.236233000	-2.178076000

C	7.627712000	-11.990135000	-2.315777000
C	16.649678000	-5.669964000	5.395381000
C	17.437571000	-4.800582000	6.186683000
C	16.909790000	-3.577692000	6.638022000
C	15.592782000	-3.258480000	6.269211000
C	14.810254000	-4.111496000	5.472694000
C	15.327957000	-5.336192000	5.032281000
C	14.796604000	-2.072753000	6.640653000
O	13.515426000	-2.228904000	6.095034000
C	13.423715000	-3.497092000	5.256867000
O	15.097793000	-1.073365000	7.313373000
C	13.118304000	-3.043059000	3.826514000
C	11.915956000	-2.331269000	3.592400000
C	11.577592000	-1.892416000	2.309521000
C	12.435626000	-2.170397000	1.221269000
C	13.637104000	-2.870900000	1.434877000
C	13.971511000	-3.292578000	2.737761000
O	12.000303000	-1.687073000	-0.018070000
C	12.700970000	-2.088442000	-1.257700000
C	12.457920000	-3.521094000	-1.624407000
N	13.473330000	-4.470065000	-1.621488000
N	12.968372000	-5.659840000	-1.983758000
N	11.610237000	-5.460916000	-2.214449000
C	11.272512000	-4.154144000	-2.006747000
C	10.763682000	-6.601258000	-2.644483000
H	8.502573000	-5.917517000	8.916227000
H	9.676224000	-7.169131000	9.412625000
H	3.089756000	-11.199613000	9.676318000
H	3.217547000	-11.246810000	7.904499000
H	10.675495000	-5.037360000	8.782789000
H	12.379848000	-3.535807000	7.840882000
H	11.977642000	-5.452000000	3.988932000
H	10.264362000	-6.981407000	4.937763000
H	5.051587000	-11.758001000	6.557379000
H	6.236674000	-13.071149000	4.859513000
H	6.027265000	-16.573063000	7.387362000
H	4.834089000	-15.246015000	9.107857000
H	5.309386000	-20.170119000	4.905381000
H	7.529783000	-21.048950000	5.586678000
H	9.451811000	-19.467539000	5.965541000
H	4.938334000	-17.727433000	4.582692000
H	4.669685000	-15.220464000	3.655619000
H	4.293378000	-14.706767000	1.257416000
H	8.566157000	-14.702411000	0.590162000
H	8.934595000	-15.241660000	2.963577000
H	7.732570000	-15.337863000	-1.464102000
H	6.508407000	-14.611429000	-2.536080000
H	6.732833000	-11.630007000	-2.794976000
H	17.070555000	-6.614939000	5.062850000
H	18.451774000	-5.086212000	6.450125000
H	17.493687000	-2.902372000	7.256386000
H	14.737031000	-6.022362000	4.433645000
H	11.243283000	-2.123765000	4.419921000
H	10.656956000	-1.345685000	2.128527000
H	14.306231000	-3.106815000	0.615465000
H	14.905404000	-3.826142000	2.879755000
H	12.281583000	-1.410536000	-2.004030000
H	13.776048000	-1.897113000	-1.169388000
H	10.271876000	-3.775518000	-2.131434000
C	8.772115000	-9.624214000	-4.066512000
H	10.618661000	-10.467294000	-5.050590000
C	9.646819000	-10.004086000	-5.153971000
H	6.730542000	-8.668147000	-4.085226000
C	7.576717000	-9.048430000	-4.641549000
H	12.092840000	-7.313238000	-5.212479000
C	10.328593000	-6.484305000	-4.079727000
C	11.108837000	-6.865046000	-5.235710000
Fe	9.274321000	-7.921666000	-5.221978000
C	8.990747000	-9.668190000	-6.391960000
C	7.712439000	-9.075465000	-6.075547000
C	9.082924000	-5.921490000	-4.553071000
C	10.349813000	-6.536146000	-6.415178000
H	9.393785000	-9.816328000	-7.384025000
H	6.990102000	-8.703878000	-6.788715000
C	9.097339000	-5.953930000	-5.993476000
H	10.656449000	-6.712264000	-7.436720000
H	8.302882000	-5.616019000	-6.643995000
H	8.284543000	-5.541817000	-3.929729000
H	11.379437000	-7.490269000	-2.482515000
H	9.899949000	-6.647413000	-1.973704000
C	9.030677000	-9.839141000	-2.601102000
H	8.408997000	-9.171451000	-1.994990000
H	10.078743000	-9.668002000	-2.341821000
C	4.897373000	-10.424227000	8.898290000
C	7.772513000	-7.897504000	8.834152000
C	5.817421000	-9.610898000	8.918896000
C	6.851247000	-8.706540000	8.891602000

Complex [7·2Hg^{2+}]

Electronic Energy: -3604.849652 a.u.; **EE + Free Energy Correction**: -3604.012116 a.u.

C	13.101785000	5.476790000	5.866466000
C	-3.114054000	-21.120483000	-8.229379000
O	12.339080000	6.378993000	4.949447000
O	-3.697107000	-20.395441000	-7.050797000

C	12.191563000	6.022716000	3.612105000
C	-2.849066000	-19.809834000	-6.113371000
C	11.163667000	6.704245000	2.912692000
C	10.958396000	6.448363000	1.557746000
C	11.782713000	5.519844000	0.867051000
C	12.784449000	4.817436000	1.592069000
C	13.003234000	5.068365000	2.949668000
C	-3.435098000	-18.804763000	-5.303566000
C	-2.683362000	-18.209224000	-4.295049000
C	-1.329818000	-18.600569000	-4.069835000
C	-0.747717000	-19.578180000	-4.916414000
C	-1.497866000	-20.196960000	-5.922513000
C	2.530081000	-20.081090000	-1.810314000
C	2.073848000	-20.433825000	-0.519679000
C	0.822256000	-19.976256000	-0.055010000
C	0.060094000	-19.176327000	-0.914963000
C	0.494340000	-18.840089000	-2.213002000
C	1.749800000	-19.279421000	-2.668829000
C	-1.249764000	-18.551440000	-0.636816000
O	-1.592216000	-17.793293000	-1.814967000
C	-0.584972000	-17.969848000	-2.881750000
O	-1.985617000	-18.571570000	0.336926000
C	-0.067871000	-16.582368000	-3.272238000
C	0.888679000	-16.419283000	-4.324916000
C	1.411854000	-15.169759000	-4.617597000
C	0.988576000	-14.021121000	-3.866872000
C	-0.001670000	-14.165756000	-2.840737000
C	-0.522642000	-15.424291000	-2.566815000
O	1.574169000	-12.855966000	-4.220036000
C	1.380185000	-11.572184000	-3.441061000
C	2.611474000	-10.753583000	-3.559481000
N	3.727946000	-11.048759000	-2.778227000
N	4.666832000	-10.135562000	-2.991896000
N	4.141794000	-9.227127000	-3.927555000
C	2.877421000	-9.594665000	-4.294009000
C	14.986163000	6.203761000	-2.375371000
C	14.477707000	7.165756000	-3.276749000
C	13.104312000	7.479955000	-3.281185000
C	12.276374000	6.803488000	-2.375314000
C	12.769208000	5.828725000	-1.487021000
C	14.140150000	5.526975000	-1.471599000
C	10.827050000	6.998198000	-2.162432000
O	10.454493000	6.122567000	-1.086077000
C	11.600624000	5.294839000	-0.641731000
O	10.005865000	7.726535000	-2.701430000
C	11.191805000	3.836910000	-0.898239000
C	9.828607000	3.471464000	-0.675287000
C	9.383703000	2.187478000	-0.956265000
C	10.294082000	1.215061000	-1.470977000
C	11.666439000	1.554973000	-1.664257000
C	12.097972000	2.850377000	-1.373818000
O	9.745948000	-0.000455000	-1.756834000
C	10.576068000	-1.099701000	-2.349204000
C	9.712881000	-2.292077000	-2.551816000
N	9.658197000	-3.299207000	-1.591198000
N	8.844709000	-4.263632000	-2.007520000
N	8.360428000	-3.864766000	-3.265623000
C	8.890033000	-2.654014000	-3.620353000
C	7.482024000	-4.795333000	-4.001673000
H	14.156858000	5.459312000	5.567781000
H	12.676515000	4.468418000	5.785475000
H	-2.563331000	-22.002569000	-7.883299000
H	-2.434311000	-20.432101000	-8.746216000
H	10.548431000	7.423341000	3.444851000
H	10.176531000	6.966629000	1.015790000
H	13.398628000	4.071063000	1.098247000
H	13.788451000	4.530287000	3.470145000
H	-4.470255000	-18.523590000	-5.470368000
H	-3.141518000	-17.477029000	-3.639757000
H	0.275392000	-19.902158000	-4.760217000
H	-1.035868000	-20.968865000	-6.529318000
H	3.502623000	-20.431161000	-2.144172000
H	2.697178000	-21.050805000	0.120537000
H	0.457721000	-20.224471000	0.937579000
H	2.143179000	-19.009472000	-3.644384000
H	1.217601000	-17.274633000	-4.905893000
H	2.154806000	-15.026313000	-5.395251000
H	-0.358525000	-13.309006000	-2.279992000
H	-1.274543000	-15.546543000	-1.796131000
H	0.501067000	-11.082541000	-3.870625000
H	1.207917000	-11.834716000	-2.393447000
H	2.276646000	-9.041139000	-4.997564000
H	16.050330000	5.984894000	-2.375834000
H	15.153061000	7.672019000	-3.959928000
H	12.692228000	8.227586000	-3.952660000
H	14.569888000	4.808979000	-0.779059000
H	9.128409000	4.223828000	-0.330171000
H	8.347081000	1.898866000	-0.816854000
H	12.374486000	0.828815000	-2.048452000
H	13.134628000	3.107244000	-1.561903000
H	10.995301000	-0.728897000	-3.291887000
H	11.377198000	-1.340648000	-1.641744000
H	8.663344000	-2.153147000	-4.547574000
C	5.953647000	-8.449239000	-5.428057000
H	7.413240000	-9.772103000	-4.340142000
C	7.097187000	-9.315106000	-5.267856000
H	5.117764000	-7.441160000	-7.266385000
C	5.869957000	-8.078592000	-6.820685000
H	9.587229000	-6.887470000	-3.839750000
C	8.242771000	-5.556709000	-5.061862000
C	9.269510000	-6.541137000	-4.813980000
Fe	7.766119000	-7.431722000	-6.060086000
C	7.702233000	-9.497718000	-6.560856000
C	6.946057000	-8.732011000	-7.522100000
C	8.150683000	-5.365692000	-6.488898000
C	9.829708000	-6.931492000	-6.081633000
H	8.574216000	-10.100085000	-6.773309000
H	7.148922000	-8.661935000	-8.581454000

C	9.135711000	-6.208135000	-7.119361000
H	10.628909000	-7.644060000	-6.229550000
H	9.324088000	-6.280385000	-8.181255000
H	7.477380000	-4.687786000	-6.996885000
H	7.076175000	-5.462615000	-3.235244000
H	6.655952000	-4.227150000	-4.442472000
C	4.982348000	-8.077216000	-4.334773000
H	4.316627000	-7.268299000	-4.651861000
H	5.505614000	-7.760528000	-3.427282000
C	-4.217348000	-21.503713000	-9.108449000
C	12.952232000	5.983237000	7.229082000
C	-5.060147000	-21.840381000	-9.932839000
C	12.857502000	6.317100000	8.403255000
H	-5.782200000	-22.130749000	-10.670449000
H	12.773042000	6.589547000	9.435591000
Hg	-6.182870000	-21.759693000	-6.830921000
Hg	12.749737000	8.972730000	6.279221000

*Complex [**8**·**Hg**$^{2+}$] (left side)*

Electronic Energy: -3562.039179 a.u.; **EE + Free Energy Correction**: -3561.192992 a.u.

C	8.788299000	-6.947029000	8.661317000
C	3.684837000	-11.370941000	8.729519000
O	9.287013000	-7.030078000	7.276768000
O	4.105042000	-12.770057000	8.904534000
C	10.280545000	-6.127228000	6.868913000
C	4.815302000	-13.412200000	7.877448000
C	10.877656000	-5.159001000	7.699088000
C	11.859337000	-4.302198000	7.163463000
C	12.243646000	-4.390654000	5.813078000
C	11.636271000	-5.373667000	4.997631000
C	10.665296000	-6.237382000	5.517248000
C	5.227291000	-12.795179000	6.679596000
C	5.936801000	-13.547086000	5.727396000
C	6.238235000	-14.907712000	5.940157000
C	5.815831000	-15.505723000	7.150016000
C	5.110503000	-14.770012000	8.110956000
C	6.268421000	-19.468930000	5.076333000
C	7.537937000	-19.936924000	5.492870000
C	8.590952000	-19.031723000	5.715043000
C	8.332450000	-17.666329000	5.510291000
C	7.074810000	-17.197312000	5.097633000
C	6.023752000	-18.094744000	4.872923000
C	9.252685000	-16.522221000	5.661362000
O	8.553789000	-15.358960000	5.309973000
C	7.106391000	-15.672974000	4.937794000
O	10.439925000	-16.480412000	6.023085000
C	6.900306000	-15.274704000	3.469348000
C	5.590487000	-15.141747000	2.951543000
C	5.379151000	-14.867046000	1.594558000
C	6.480505000	-14.720842000	0.723750000
C	7.792012000	-14.844170000	1.223310000
C	7.987732000	-15.125202000	2.589071000
O	6.156422000	-14.453054000	-0.612573000
C	7.203906000	-14.514026000	-1.656473000
C	8.026417000	-13.266290000	-1.769864000
N	9.329497000	-13.191338000	-1.290247000
N	9.832358000	-11.977834000	-1.560020000
N	8.831671000	-11.270926000	-2.220596000
C	7.713429000	-12.041362000	-2.364937000
C	16.583061000	-5.675444000	5.373386000
C	17.366483000	-4.806086000	6.169123000
C	16.835076000	-3.584711000	6.620328000
C	15.518989000	-3.266979000	6.246972000
C	14.740921000	-4.120038000	5.446124000
C	15.262211000	-5.343163000	5.005681000
C	14.719713000	-2.082864000	6.616802000
O	13.440975000	-2.239830000	6.065249000
C	13.354506000	-3.507149000	5.225201000
O	15.016269000	-1.084302000	7.292694000
C	13.054512000	-3.052387000	3.794044000
C	11.850422000	-2.345451000	3.554140000
C	11.517577000	-1.905819000	2.270069000
C	12.383272000	-2.177831000	1.186330000
C	13.586919000	-2.872813000	1.405948000
C	13.915468000	-3.295508000	2.709901000
O	11.952751000	-1.695135000	-0.054734000
C	12.664096000	-2.089560000	-1.290814000
C	12.434651000	-3.523687000	-1.660270000
N	13.456315000	-4.465877000	-1.645597000
N	12.963194000	-5.659291000	-2.011743000
N	11.606257000	-5.469731000	-2.257245000
C	11.257663000	-4.165001000	-2.054665000
C	10.772022000	-6.617432000	-2.691701000
H	8.432396000	-5.928777000	8.872691000
H	9.595505000	-7.191431000	9.365712000
H	2.968528000	-11.206970000	9.539057000
H	3.157365000	-11.254002000	7.773426000
H	10.601250000	-5.055104000	8.743013000
H	12.307256000	-3.552499000	7.806983000
H	11.910124000	-5.459869000	3.950236000
H	10.193558000	-6.989637000	4.892507000
H	5.019950000	-11.750292000	6.477589000
H	6.258267000	-13.057110000	4.813391000
H	6.033564000	-16.549744000	7.352322000
H	4.784264000	-15.230230000	9.038529000
H	5.467124000	-20.183528000	4.909094000
H	7.695226000	-21.001537000	5.639149000
H	9.572380000	-19.371017000	6.032944000

H	5.044301000	-17.753835000	4.551996000	H	12.124422000	-7.309274000	-5.253014000
H	4.728940000	-15.248090000	3.605033000	C	10.342770000	-6.505806000	-4.129033000
H	4.373735000	-14.768964000	1.196121000	C	11.133935000	-6.875889000	-5.281088000
H	8.653730000	-14.705654000	0.580046000	Fe	9.315723000	-7.960009000	-5.274123000
H	9.001801000	-15.209731000	2.964055000	C	9.066071000	-9.713529000	-6.441810000
H	7.852787000	-15.378856000	-1.478278000	C	7.776815000	-9.140729000	-6.133338000
H	6.631568000	-14.679850000	-2.571681000	C	9.090999000	-5.962067000	-4.608581000
H	6.820028000	-11.698061000	-2.859012000	C	10.375463000	-6.559423000	-6.464266000
H	17.006865000	-6.619058000	5.040733000	H	9.476485000	-9.857440000	-7.431464000
H	18.380190000	-5.090416000	6.435821000	H	7.052258000	-8.782593000	-6.851119000
H	17.415676000	-2.909337000	7.241722000	C	9.112497000	-5.995725000	-6.048868000
H	14.674902000	-6.029007000	4.403107000	H	10.689379000	-6.731790000	-7.484229000
H	11.172096000	-2.142095000	4.378095000	H	8.316164000	-5.670200000	-6.703396000
H	10.595624000	-1.362809000	2.084627000	H	8.284150000	-5.593766000	-3.989329000
H	14.262016000	-3.103928000	0.590123000	H	11.395201000	-7.500599000	-2.526258000
H	14.851079000	-3.824811000	2.856392000	H	9.905276000	-6.671478000	-2.025353000
H	12.243842000	-1.414116000	-2.038835000	C	9.090119000	-9.873117000	-2.650338000
H	13.737003000	-1.889722000	-1.195438000	H	8.458668000	-9.209489000	-2.049836000
H	10.256002000	-3.793050000	-2.190695000	H	10.135209000	-9.689007000	-2.387847000
C	8.834941000	-9.667699000	-4.117620000	C	4.794541000	-10.410560000	8.819234000
H	10.699768000	-10.483266000	-5.090386000	C	7.687291000	-7.902487000	8.780682000
C	9.721089000	-10.036116000	-5.199745000	C	5.719220000	-9.601508000	8.852305000
H	6.778312000	-8.744517000	-4.149078000	C	6.759623000	-8.704358000	8.832686000
C	7.633359000	-9.112434000	-4.700140000	Hg	3.648622000	-8.146312000	11.507892000

*Complex **[8·Hg^{2+}]** (right side)*

Electronic Energy: -3562.039334 a.u.; **EE + Free Energy Correction**: -3561.194498 a.u.

C	8.709781000	-6.845185000	8.683286000	C	6.922138000	-15.255939000	3.468923000
C	3.680365000	-11.351822000	8.711536000	C	5.610803000	-15.130217000	2.953184000
O	9.211530000	-6.952444000	7.301665000	C	5.395711000	-14.862730000	1.595340000
O	4.112683000	-12.746439000	8.893652000	C	6.494727000	-14.716901000	0.721558000
C	10.221908000	-6.071682000	6.886115000	C	7.807704000	-14.833956000	1.218818000
C	4.827598000	-13.387688000	7.869798000	C	8.007201000	-15.107517000	2.585540000
C	10.832936000	-5.103896000	7.706348000	O	6.166892000	-14.455877000	-0.615224000
C	11.833551000	-4.273114000	7.164432000	C	7.212488000	-14.516364000	-1.660874000
C	12.222321000	-4.386993000	5.817389000	C	8.032995000	-13.267511000	-1.777282000
C	11.598749000	-5.367648000	5.011275000	N	9.339005000	-13.192768000	-1.305704000
C	10.609316000	-6.205934000	5.537373000	N	9.839415000	-11.978375000	-1.575977000
C	5.237329000	-12.772468000	6.670153000	N	8.834183000	-11.270698000	-2.228720000
C	5.951919000	-13.523589000	5.721156000	C	7.715517000	-12.041527000	-2.367797000
C	6.260838000	-14.881813000	5.938769000	C	16.519993000	-5.794775000	5.367180000
C	5.841177000	-15.477917000	7.150545000	C	17.330012000	-4.946493000	6.159083000
C	5.130831000	-14.742952000	8.108302000	C	16.835109000	-3.709360000	6.608868000
C	6.319633000	-19.446381000	5.096016000	C	15.527678000	-3.354786000	6.238148000
C	7.592591000	-19.904227000	5.513361000	C	14.723566000	-4.187045000	5.441261000
C	8.639999000	-18.991255000	5.730165000	C	15.208298000	-5.425530000	5.002062000
C	8.372511000	-17.628515000	5.519312000	C	14.763428000	-2.147441000	6.606982000
C	7.111421000	-17.169587000	5.105857000	O	13.479320000	-2.268892000	6.058477000
C	6.065900000	-18.074770000	4.886477000	C	13.354447000	-3.535680000	5.222795000
C	9.285501000	-16.477753000	5.663805000	O	15.089767000	-1.156268000	7.279965000
O	8.578892000	-15.320793000	5.307507000	C	13.062620000	-3.078346000	3.790914000
C	7.132743000	-15.645901000	4.938951000	C	11.868361000	-2.356002000	3.547885000
O	10.472912000	-16.426668000	6.023996000	C	11.544759000	-1.911593000	2.263128000

C	12.410132000	-2.193891000	1.181772000	H	18.335833000	-5.259195000	6.423866000
C	13.604632000	-2.903630000	1.404586000	H	17.436621000	-3.049653000	7.227177000
C	13.923988000	-3.331197000	2.709194000	H	14.599876000	-6.095319000	4.402307000
O	11.988666000	-1.706061000	-0.060265000	H	11.190010000	-2.144619000	4.369832000
C	12.699879000	-2.106673000	-1.294421000	H	10.630145000	-1.357140000	2.075272000
C	12.459236000	-3.538757000	-1.664750000	H	14.279203000	-3.142571000	0.590578000
N	13.473954000	-4.488386000	-1.650719000	H	14.852402000	-3.872412000	2.858167000
N	12.972112000	-5.677916000	-2.017639000	H	12.287621000	-1.427428000	-2.043453000
N	11.616602000	-5.478258000	-2.262899000	H	13.774241000	-1.916283000	-1.195975000
C	11.277513000	-4.171175000	-2.059435000	H	10.278512000	-3.791989000	-2.195066000
C	10.773858000	-6.619969000	-2.696607000	C	8.824199000	-9.661520000	-4.120986000
H	8.351097000	-5.823855000	8.874108000	H	10.678972000	-10.481238000	-5.109440000
H	9.515854000	-7.074380000	9.394192000	C	9.701255000	-10.030041000	-5.210464000
H	2.963186000	-11.188506000	9.520906000	H	6.770958000	-8.730478000	-4.135060000
H	3.151745000	-11.244138000	7.755095000	C	7.620678000	-9.099933000	-4.693286000
H	10.553269000	-4.980733000	8.747329000	H	12.114875000	-7.313448000	-5.263683000
H	12.293650000	-3.523891000	7.799839000	C	10.340582000	-6.503913000	-4.132366000
H	11.874684000	-5.471618000	3.965968000	C	11.126161000	-6.875790000	-5.287676000
H	10.125822000	-6.956928000	4.920178000	Fe	9.303495000	-7.952291000	-5.275863000
H	5.023861000	-11.729545000	6.464473000	C	9.038650000	-9.701274000	-6.446883000
H	6.271134000	-13.034998000	4.805600000	C	7.753858000	-9.124417000	-6.127541000
H	6.064668000	-16.519978000	7.356652000	C	9.089447000	-5.954299000	-4.606826000
H	4.806329000	-15.201740000	9.037189000	C	10.364897000	-6.554522000	-6.467776000
H	5.522780000	-20.166911000	4.933030000	H	9.441466000	-9.843816000	-7.439851000
H	7.756890000	-20.967111000	5.664462000	H	7.025576000	-8.761411000	-6.839077000
H	9.623908000	-19.322781000	6.048593000	C	9.105752000	-5.986112000	-6.047220000
H	5.083941000	-17.741572000	4.565083000	H	10.674502000	-6.726848000	-7.489063000
H	4.751059000	-15.236506000	3.609026000	H	8.308495000	-5.656389000	-6.698512000
H	4.389137000	-14.769859000	1.198588000	H	8.286342000	-5.583463000	-3.984230000
H	8.667654000	-14.696295000	0.573017000	H	11.392165000	-7.507114000	-2.534272000
H	9.022366000	-15.186917000	2.958702000	H	9.908808000	-6.669681000	-2.027698000
H	7.863342000	-15.379772000	-1.482848000	C	9.089218000	-9.871606000	-2.656110000
H	6.638672000	-14.684412000	-2.574751000	H	8.461660000	-9.209878000	-2.049459000
H	6.818797000	-11.697567000	-2.855372000	H	10.135980000	-9.688115000	-2.399935000
H	16.915770000	-6.750821000	5.035495000	C	4.779884000	-10.380708000	8.799074000

****

6.2.6. References:

1. Shi, W.; Lei, A. *Tetrahedron Lett*. **2014**, *55*, 2763-2772.
2. Liu, J.; Lam, W. Y. J.; Tang, B. Z. *Chem. Rev*. **2009**, *109*, 5799-5867.
3. Michl, J.; Sykes, E. C. H. *ACS Nano.* **2009**, *3*, 1042-1048.
4. Wu, S. T.; Meng, H. H. B.; Dalton, L. R. *Appl. Phys*. *Lett.* **1991**, *70*, 3013-3017.
5. Wu, S. T.; Margerum, J. D.; Meng, H. B.; Dalton, L. R.; Hsu, C. S.; Lung, S. H. *Appl. Phys. Lett*. **1992**, *61*, 630-632.

6. Wu, S. T.; Neubert, M. E.; Keast, S. S.; Abdallah, D. G.; Lee, S. N.; Walsh, M. E.; Dorschner, T. A. *Appl. Phys. Lett*. **2000***, 77*, 957-959.
7. Beristain, M. F.; Ogawa, T.; Gomez-Sosa, G.; Munoz, E.; Maekawa, Y.; Halim, F.; Smith, F.; Walser, A.; Dorsinville, R. *Mol. Cryst. Liq. Cryst*. **2010**, *521*, 237-245.
8. Sari, O.; Roy, V.; Balzarini, J.; Snoeck, R.; Andrei, G.; Agrofoglio, L. A. *Eur. J. Med. Chem*. **2012**, *53*, 220-228.
9. Kivala, M.; Diederich, F. *Pure Appl. Chem.* **2008**, *80*, 411-427.
10. McConnell, A. J.; Beer, P. D. *Chem. Eur. J.* **2011**, *17*, 2724-2733.
11. Sugino, H.; Kawai, H.; Umehara, T.; Fujiwara, K.; Suzuki, T. *Chem. Eur. J.* **2012**, *18*, 13722-13732.
12. Langton, M. J.; Matichak, J. D.; Thompson, A. L.; Anderson, H. L. *Chem. Sci.* **2011**, *2*, 1897-1901.
13. Shi Shun, A. L. K.; Tykwinski, R. R. *Angew. Chem. Int. Ed*. **2006**, *45*, 1034-1057.
14. Hu, R.; Tang, B. Z. In multi-component and sequential reactions in polymer synthesis; *Springer International Publishing: Switzerland*. **2015**, 17-42.
15. Vilhanova, B.; Vaclavik, J.; Artiglia, L.; Ranocchiari, M.; Togni, A.; Bokhoven, J. A.van. *ACS Catal*. **2017**, *7*, 3414-3418.
16. Eglinton, G.; Galbraith, A. R. *J. Chem. Soc*. **1959**, 889-896.
17. Hay, A. S. *J. Org. Chem*. **1962**, *27*, 3320-3321.
18. Pati, A. K.; Mohapatra, M.; Ghosh, P.; Gharpure, S. J.; Mishra, A. K. *J. Phys. Chem. A*. **2013**, *117*, 6548-6560.
19. Wang, D.; Li, J.; Li, N.; Gao, T.; Hou, S.; Chen, B. *Green Chem.* **2010**, *12*, 45–48.
20. Atta, A. K.; Kim, S. B.; Heo, J.; Cho, D. G. *Org. Lett*. **2013**, *15*, 1072-1075.
21. Dong, M.; Wang, Y. W.; Peng, Y. *Org. Lett*. **2010**, *12*, 5310-5313.
22. Tian, M.; Liu, L.; Li, Y.; Hu, R.; Liu, T.; Liu, H.; Wanga, S.; Li, Y. *Chem. Commun*. **2014**, *50*, 2055-2057.
23. Kaur, M.; Choi, D. H. *Sens. Actuators, B. Chemical* **2014**, *190*, 542-548.
24. Lee, D. N.; Kim, G. J.; Kim, H. J. *Tetrahedron Lett*. **2009**, *50*, 4766-4768.
25. Chattaraj, P. K.; Lee, H.; Parr, R. G. *J. Am. Chem. Soc.* **1991**, *113*, 1855–1856.
26. Harris, H. H.; Pickering, I. J.; George, G. N. *Science* **2003**, *301*, 1203.
27. Onyido, I.; Norris, A. R.; Buncel, E. *Chem. Rev*. **2004**, *104*, 5911-5922.
28. Bernhoft, R. A. *J. Environ. Public Health* **2012**, *2012*, 460508-460518.
29. Toyota, S.; Oki, T.; Inoue, M.; Wakamatsu, K.; Iwanaga, T. *Chem. Lett*. **2015**, *44*, 978-980.

30. He, X.; Liu, H.; Li, Y.; Wang, S.; Li, Y.; Wang, N.; Xiao, J.; Xu, X.; Zhu, D. *Adv. Mater*. **2005**, *17*, 2811-2815.
31. Nolan, E. M.; Lippard, S. J. *Chem. Rev*. **2008**, *108*, 3443-3480.
32. Aragay, G.; Pons, J.; Merkoci, A. *Chem. Rev*. **2011**, *111*, 3433-3458.
33. Jia, K.; Zhou, X.; Pan, L.; Yuan, L.; Wang, P.; Wu, C.; Huang, Y.; Liu, X. *RSC Adv*. **2015**, *5*, 71652-71657.
34. Erdemir, S.; Malkondu, S.; Kocyigit, O. *Luminescence* **2019**, *34*, 106-112.
35. Sun, R.; Wang, L.; Yu, H.; Abdin, Z.; Chen, Y.; Huang, J.; Tong, R. *Organometallics* **2014**, *33*, 4560−4573.
36. Behr, O. M.; Eglinton, G.; Galbraith, R. A.; Raphael, R. A. *J. Chem. Soc.* **1960**, 3614-3625.
37. Sharifi, A.; Mirzaei, M.; Naimi-Jamal, MR. *J. Chem. Research* **2002**, *2002*, 628-630.
38. Liu, Z.; Liu, J.; Chen, T. *J. Polym. Sci. Part A: Polym Chem*. **2005**, *43*, 1019-1027.
39. Zhao, L.; Ling, Q.; Liu, X.; Hang, C.; Zhao, Q.; Liu, F.; Gu, H. *Appl. Organomet. Chem.* **2018**, *32*, 4000-4012.
40. Kaiser, K.; Scriven, L. M.; Schulz1, F.; Gawel, P.; Gross, L.; Anderson, H. L. *Science* **2019**, *365*, 1299-1301.
41. Roberts, H. N.; Brown, N. J.; Edge, R.; Fitzgerald, E. C.; Ta, Y. T.; Collison, D.; Low, P. J.; Whiteley, M. W. *Organometallics* **2012**, *31*, 6322–6335.
42. Woodcock, H. L.; Schaefer, III, H. F.; Schreiner, P. R. *J. Phys. Chem. A* **2002**, *106,* 11923-11931.
43. Kim, J.; Swager, T. M. *Nature* **2001**, *411*, 1030-1034.
44. Yu, M.; Shi, M.; Chen, Z.; Li, F.; Li, X.; Gao, Y.; Xu, J.; Yang, H.; Zhou, Z.; Yi, T.; Huang, C. *Chem. Eur. J*. **2008**, *14*, 6892-6900.
45. Quang, D. T.; Kim, J. S. *Chem. Rev.* **2010**, *110*, 6280-6301.
46. Ahmad, A.; Kurkina, T.; Kern, K.; Balasubramanian, K. *Chem. Phys. Chem*. **2009***, 10*, 2251-2255.
47. Yi, X. Q.; He, Y. F.; Cao, Y. S.; Shen, W. X.; Lv, Y. Y. *ACS Sens.* **2019**, *4*, 856-864.
48. Keizer, J. *J. Am. Chem. Soc*. **1983**, *105*, 1494-1498.
49. Kaneyoshi, S.; Zou, T.; Ozaki, S.; Takeuchi, R.; Udou, A.; Nakahara, T.; Fujimoto, K.; Fujii, S.; Sato, S.; Takenaka, S. *Chem. Eur. J.* **2020**, *26*, 139-142.
50. Bhatta, S. R.; Bheemireddy, V.; Thakur, A. *Organometallics* **2017**, *36*, 829-838.
51. Alfonso, M.; Tarraga, A.; Molina, P. *Inorg. Chem.* **2013**, *52*, 7487-7496.

52. Uliniuc, A.; Popa, M.; Drockenmuller, E.; Boisson, F.; Leonard, D.; Hamaide T. *Carbohydrate Polymers* **2013**, *96*, 259– 269.
53. Bhatta, S. R.; Pal, A.; Sarangi, U. K.; Thakur, A. *Inorg.Chim.Acta*. **2019**, *498*, 119097-119108.
54. Wittke, G. *J. Chem. Educ.* **1983**, *60*, 239-240.
55. Yates, E. A.; Philipp, B.; Buckley, C.; Atkinson, S.; Chhabra, S. R.; Sockett, R. E.; Goldner, M.; Dessaux, Y.; Camara, M.; Smith, H.; Williams, P. *Infect. Immun.* **2002**, *70*, 5635.
56. Fugit, K. D.; Anderson, B. D. *J. Control. Release* **2014**, *174*, 88–97.
57. Schäfer, A.; Huber, C.; Ahlrichs, R. *J. Chem. Phys.* **1994**, *100*, 5829-5835.
58. Taylor, T. J.; Gabbai, F. P. *Organometallics* **2006**, *25,* 2143-2147.
59. Casas-Solvas, J. M.; Vargas-Berenguel, A.; Capitan-Vallvey, L. F.; Santoyo-Gonzalez, F. *Org. Lett*. **2004**, *21,* 3687-3690.
60. Gaussian 16, Revision B.01, Frisch, M. J.; Trucks, G. W.; Schlegel, H. B; Scuseria, G. E.; Robb, M. A.; Cheeseman, J. R.; Scalmani, G.; Barone, V.; Petersson, G. A.; Nakatsuji, H.; Li, X.; Caricato, M.; Marenich, A. V.; Bloino, J.; Janesko, B. G.; Gomperts, R.; Mennucci, B.; Hratchian, H. P.; Ortiz, J. V.; Izmaylov, A. F.; Sonnenberg, J. L.; Williams-Young, D.; Lipparini, F. D.; Egidi, F.; Goings, J.; Peng, B.; Petrone, A.; Henderson, T.; Ranasinghe, D.; Zakrzewski, V. G.; Gao, J.; Rega, N.; Zheng, G.; Liang, W.; Hada, M.; Ehara, M.; Toyota, K.; Fukuda, R.; Hasegawa, J.; Ishida, M.; Nakajima, T.; Honda, Y.; Kitao, O.; Nakai, H.; Vreven, T.; Throssell, K.; Montgomery, Jr. J. A.; Peralta, J. E.; Ogliaro, F.; Bearpark, M. J.; Heyd, J. J.; Brothers, E. N.; Kudin, K. N.; Staroverov, V. N.; Keith, T. A.; Kobayashi, R.; Normand, J.; Raghavachari, K.; Rendell, A. P.; Burant, J. C.; Iyengar, S. S.; Tomasi, J.; Cossi, M.; Millam, J. M.; Klene, M.; Adamo, C.; Cammi, R.; Ochterski, J. W.; Martin, R. L.; Morokuma, K.; Farkas, O.; Foresman, J. B.; Fox, D. J. *Gaussian, Inc.*, Wallingford CT, **2016**.
61. Zhao, Y.; Truhlar, D. G. *Theor. Chem. Acc*. **2008**, *120,* 215-241.
62. (a) Klamt, A.; Schuurmann, G. *J. Chem. Soc. Perkin Trans*. **1993**, *2*, 799-805. (b) Barone, V.; Cossi, M. *J. Phys. Chem. A.* **1998**, *102*, 1995-2001.
63. (a) Glendening, E. D.; Reed, A. E.; Carpenter, J. E.; Weinhold, F. NBO, version 3.1; University of Wisconsin: Madison, WI, **2001**. (b) Reed, A. E.; Curtiss, L. A.; Weinhold, F. *Chem. Rev.* **1988**, *88*, 899-926.
64. Wiberg, K. B. *Tetrahedron Lett.* **1968**, *24*, 1083-1096.
65. Andrienko, G. A. http://www.chemcraftprog.com.

66. Ouellette, R. J.; Rawn, J. D. 7 - Alkynes, Organic Chemistry (Second Edition). *Academic Press*, **2018**, 195-211.
67. Hopkinson, A. C. "The chemistry of the carbon-carbon triple bond", S. Patai, ed., *John Wiley and Sons, Chichester,* **1978**, 97.
68. Tidwell, T. T. *J. Chem. Educ.* **1996**, *73*, 1081.
69. Chen, S.; Liu, L.; Gao, X., Hua, Y.; Peng, L.; Zhang, Y.; Yang, L.; Tan, Y.; He, F.; Xia, H. *Nat. Commun.* **2020**, *11***,** 4651.
70. Frenking, G.; Fröhlich, N. *Chem. Rev.* **2000**, *100,* 717-774.
71. Ward, B. C.; Templeton, J. L. *J. Am. Chem. Soc.* **1980**, *102*, 1532–1538.
72. Ginnebaugh, J. P.; Maki, J. W.; Lewandos, G. S. *J. Organometal. Chem.* **1980**, *190*, 403-416.
73. Mandal, R.; Garai, B.; Sundararaju, B. *J. Org. Chem.* **2021**, *86*, 9407−9417.
74. Freeman, F. *Chem. Rev.* **1975**, *75*, 439–490.
75. Kiselev, V. D.; Kornilov, D. A. *Int. J. Chem. Kinet.* **2017**, *49*, 562-575.
76. West, J. K.; Fondong, G. L.; Noll, B. C.; Stahl, L. *Dalton Trans.* **2013**, *42*, 3835–3842.
77. Mereshchenko, A. S.; Ivanov, A. V.; Baranovskii, V. I.; Mloston, G.; Rodina, L. L.; Nikolaev, V. A. *Beilstein J. Org. Chem.* **2015,** *11,* 504–513.
78. Shaw, R. A. *Pure & Appl. Chem.* **1980**, *52*, 1063–1097.
79. Martin, D.; Canac, Y.; Lavallo, V.; Bertrand, G. *J. Am. Chem. Soc.* **2014**, *136*, 5023−5030.
80. Bryce M. R. *J. Mater. Chem. C* **2021**, *9*, 10524-10546.
81. Zirzlmeier, J.; Schrettl, S.; Brauer, J. C.; Contal, E.; Vannay, L.; Brémond, É.; Jahnke, E.; Guldi, D. M.; Corminboeuf, C.; Tykwinski, R. R.; Frauenrath, H. *Nat. Commun.* **2020**, *11*, 4797.
82. Gibtner, T.; Hampel, F.; Gisselbrecht, J. -P.; Hirsch, A. *Chem. Eur. J.* **2002**, *8*, 408−432.
83. (a) Lin, W.; Cao, X.; Ding, Y.; Yuan, L.; Long, L. *Chem. Commun.* **2010**, *46*, 3529-3531. (b) Song, F.; Watanabe, S.; Floreancig, P. E.; Koide, K. *J. Am. Chem. Soc.* **2008**, *130*, 16460–16461. (c) Kaur, M.; Cho, M. J.; Choi, D. H. *Dyes Pigments* **2016**, *125*, 1-7.
84. (a) Bhatta, S. R.; Bheemireddy, V.; Vijaykumar, G.; Debnath, S.; Thakur, A. *Organometallics* **2017**, *36*, 2141–2152. (b) Karmakar, M.; Bhatta, S. R.; Giri, S.; Thakur, A. *Inorg. Chem.* **2020**, *59*, 4493–4507. (c) Bhatta, S. R.; Mondal, B.; Vijaykumar, G.; Thakur, *Inorg. Chem.* **2017**, *56*, 11577–11590.
85. Giel, M. -C.; Barrow, A. S.; Smedley, C. J.; Lewis, W.; Moses, J. E. *Chem. Commun.* **2021**, *57*, 6991–6994.

86. Zhang, Y.; Tanabe, Y.; Kuriyama, S.; Nishibayashi, Y. *J. Org. Chem.* **2021**, *86*, 12577–12590.

87. Salvio, R.; Bassetti, M. *Inorg. Chim. Acta* **2021**, *522*, 120288.

88. Peng, K.; Moreth, D.; Schatzschneider, U. *Organometallics* **2021**, *40*, 2584−2593.

89. Xiao, N.; Zhan, Y. -Z.; Meng, H.; Shu, W. *Org. Lett.* **2021**, *23*, 5186−5191.

90. Wang, Z. -L.; Zhang, F. -L.; Xu, J. -L.; Shan, C. -C.; Zhao, M.; Xu, Y. -H. *Org. Lett.* **2020**, *22*, 7735−7742.

91. Chen, H.; Yang, M.; Wang, G.; Gao, L.; Ni, Z.; Zou, J.; Li, S. *Org. Lett.* **2021**, *23*, 5533−5538.

92. Pal, A.; Das, K. M.; Goswami, B.; Thakur, A. *Inorg. Chem.* **2020**, *59*, 10099−10112.

93. Hencher, J. L. The structural chemistry of the C≡C bond. In The Carbon–Carbon Triple Bond **1978**, S. Patai (Ed.).

94. Becke, D. *J. Chem. Phys.* **1993**, *98*, 5648-5652.

95. Lee, C.; Yang, W.; Parr, R. G. *Phys. Rev. B: Condens. Matter Mater. Phys.* **1988**, *37*, 785-789.

96. Becke, A. D. *Phys. Rev. A: At., Mol., Opt. Phys.* **1988**, *38*, 3098-3100.

97. Wadt, W. R.; Hay, P. J. *J. Chem. Phys.* **1985**, *82*, 284-298.

98. Hay, P. J.; Wadt, W. R. *J. Chem. Phys.* **1985**, *82*, 299-310.

99. Legault, C. Y. CYLView 1.0b, Universitéde Sherbrooke; 2009. See http://www.cylview.org.

Spectroscopic details

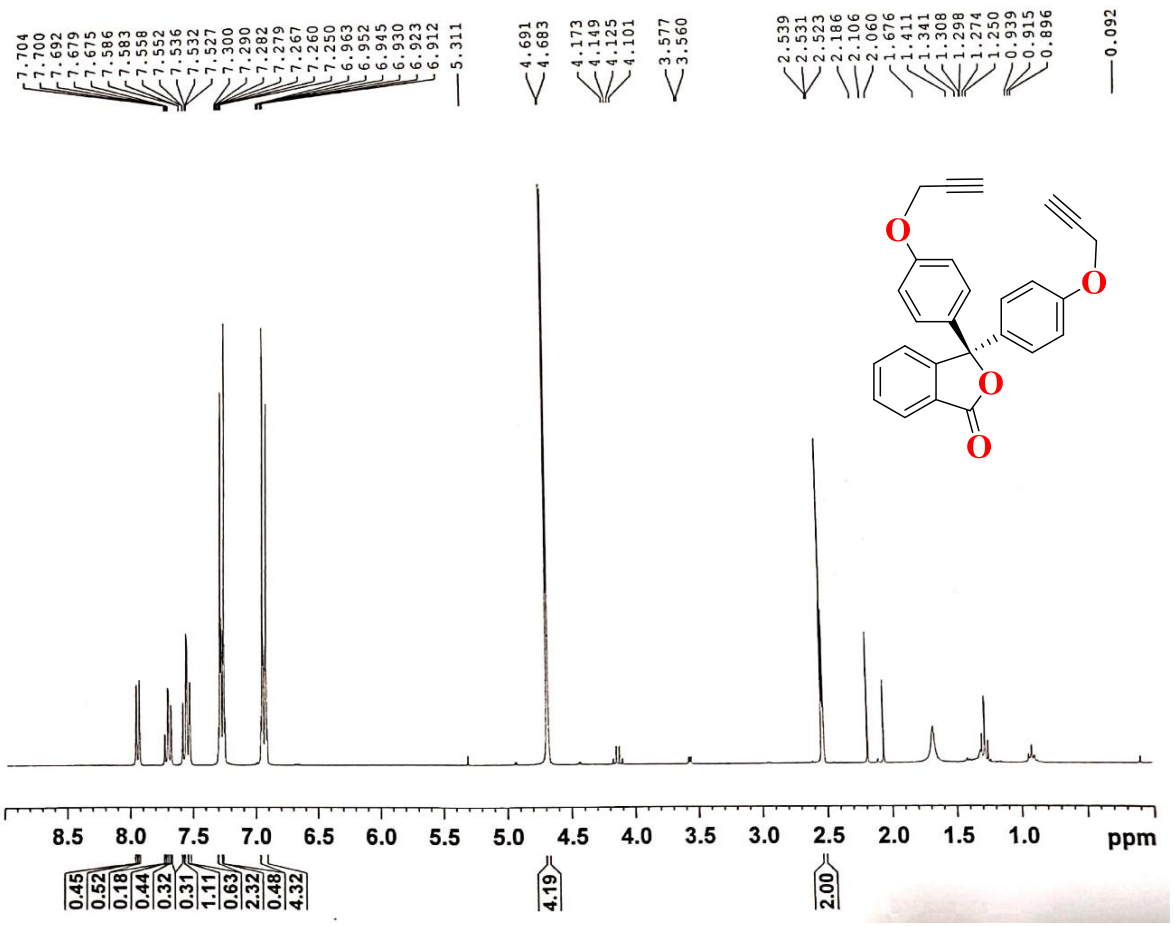

Figure 6.1. ^{1}H NMR spectrum of compound **2** in $CDCl_3$.

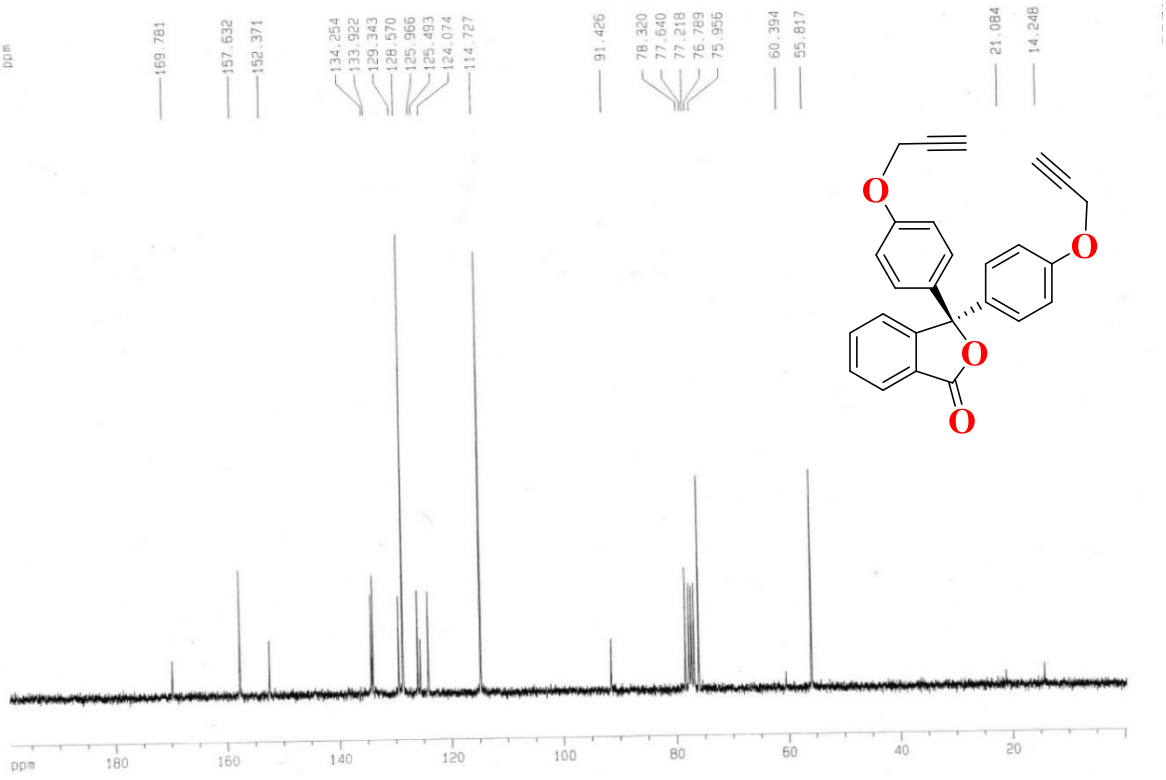

Figure 6.2. ^{13}C NMR spectrum of compound **2** in $CDCl_3$.

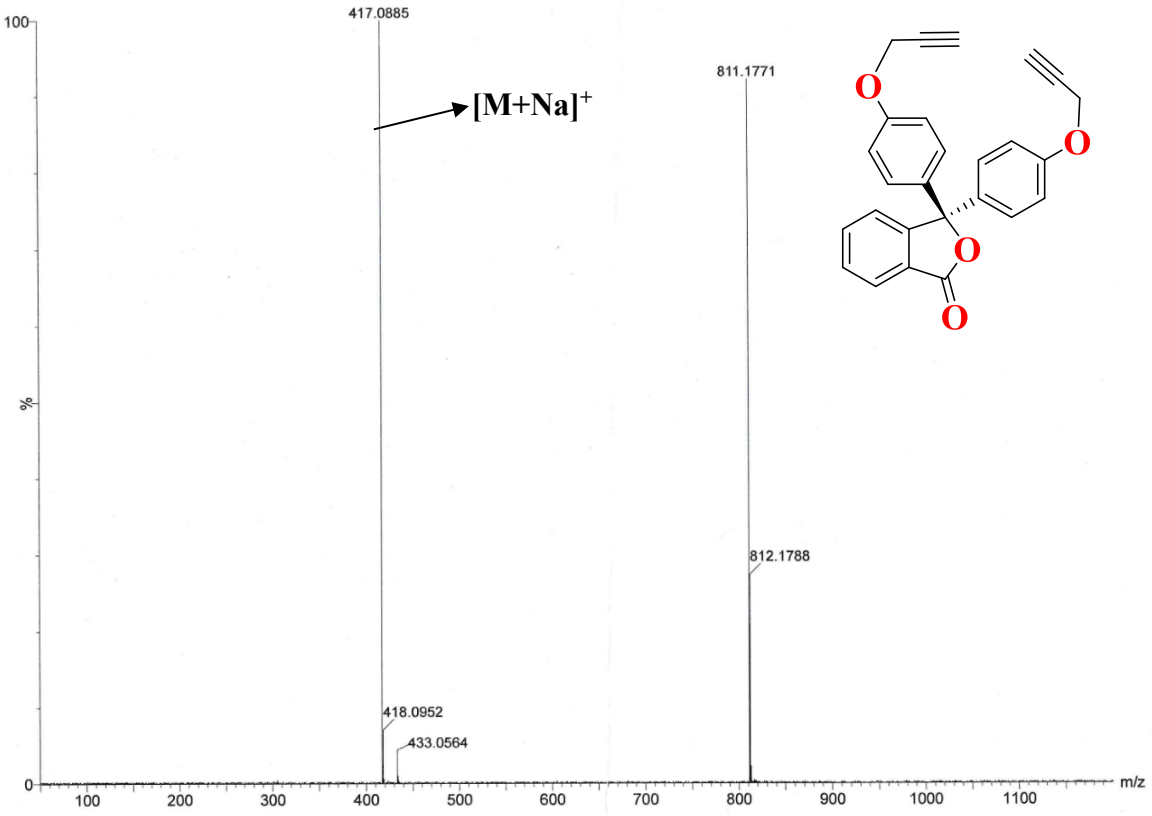

Figure 6.3. HRMS spectra of compound **2**.

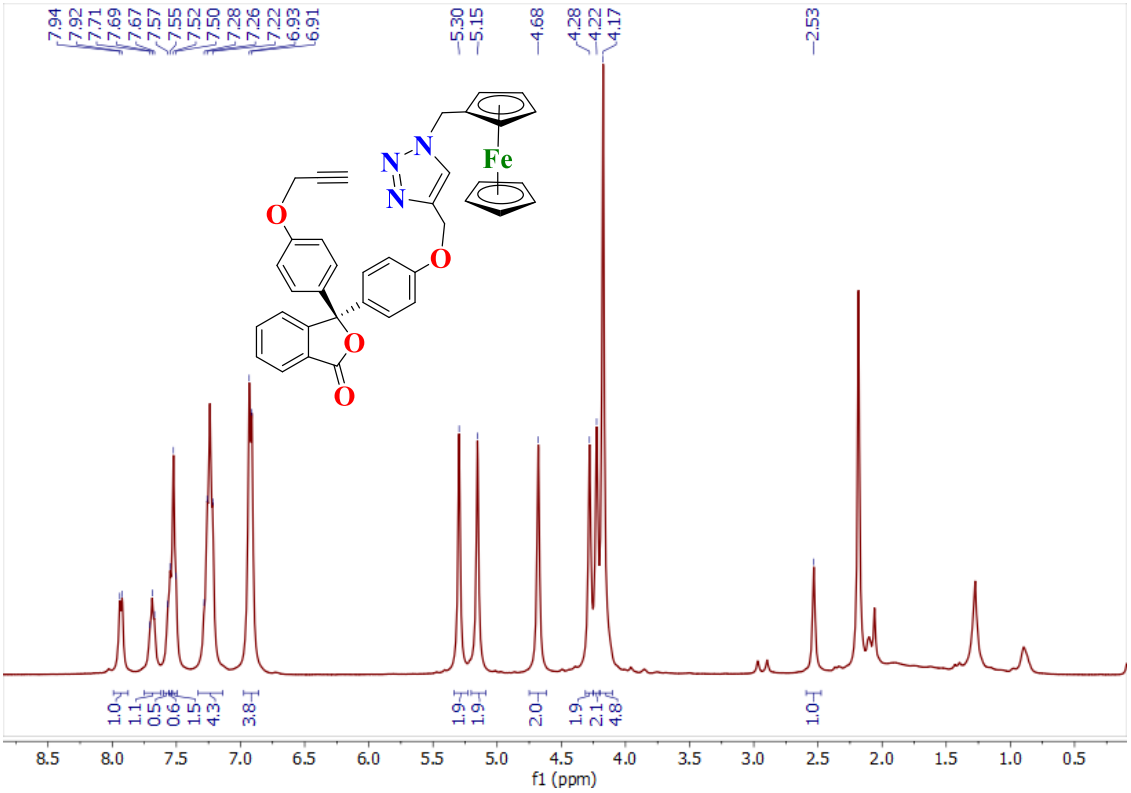

Figure 6.4. ^{1}H NMR spectra of compound **3** in $CDCl_3$.

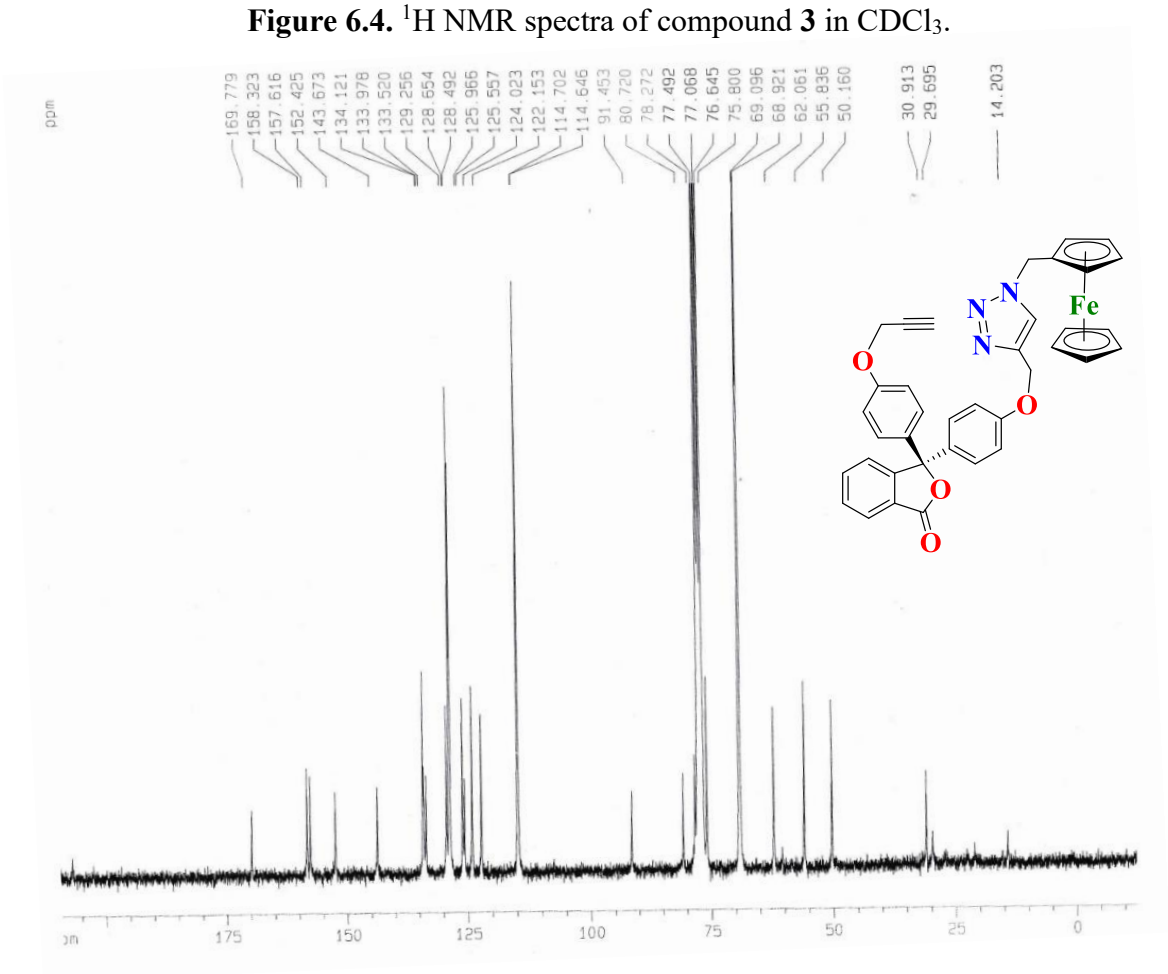

Figure 6.5. ^{13}C NMR spectra of compound **3** in $CDCl_3$ as solvent.

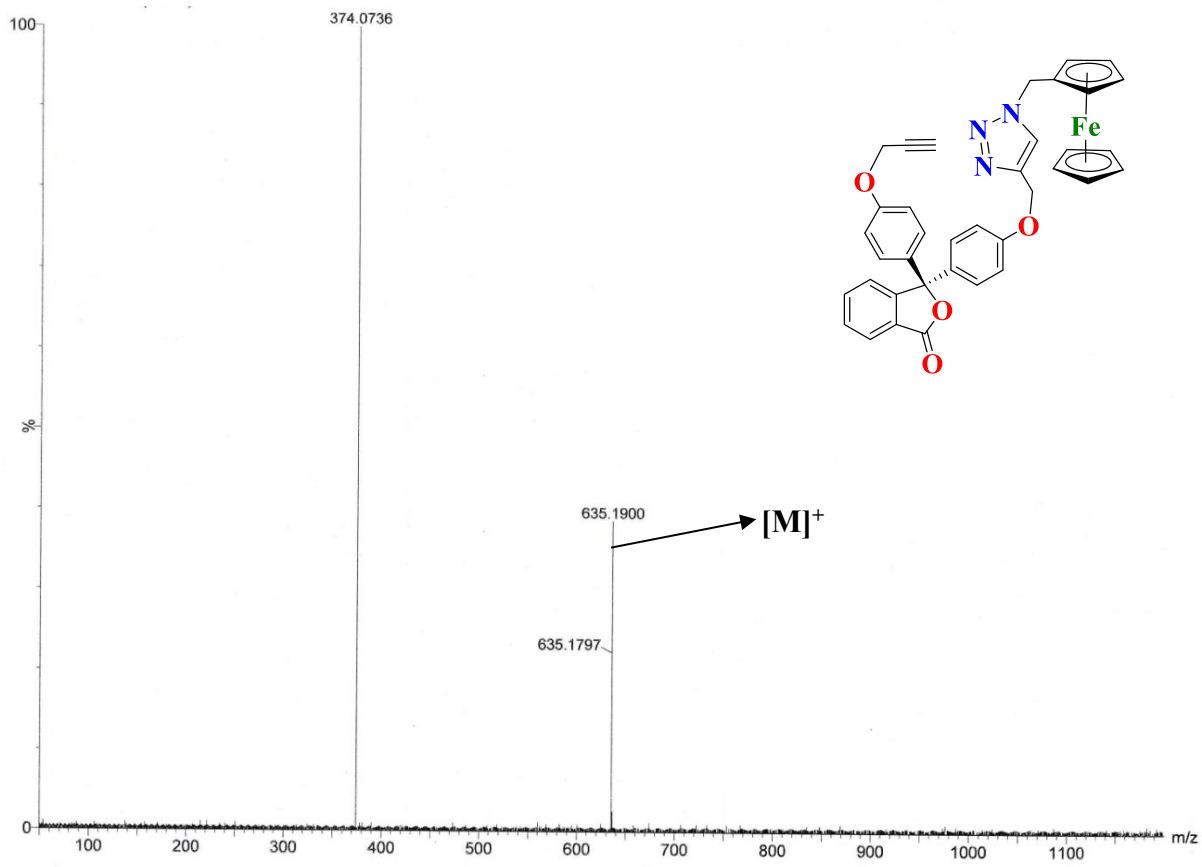

Figure 6.6. HRMS spectra of compound **3**.

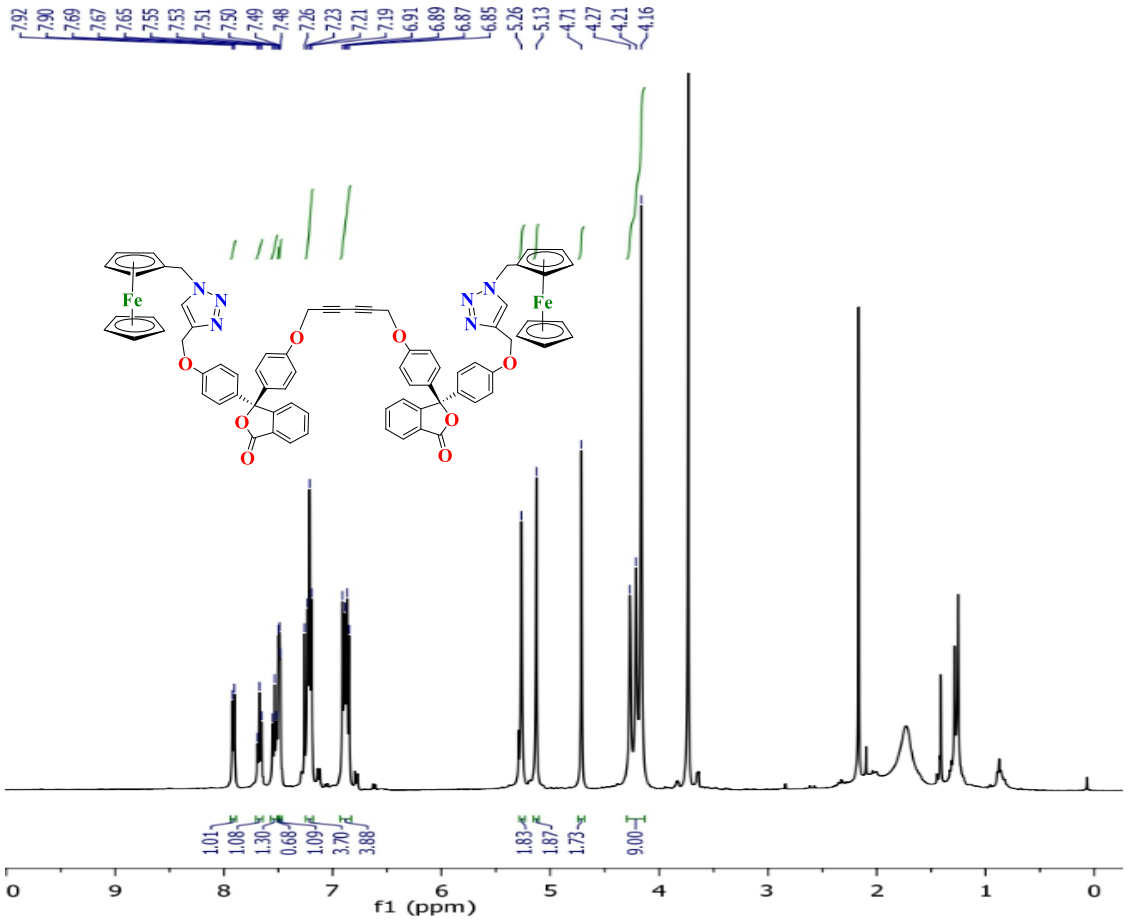

Figure 6.7. ^{1}H NMR spectra of compound **5** in $CDCl_3$.

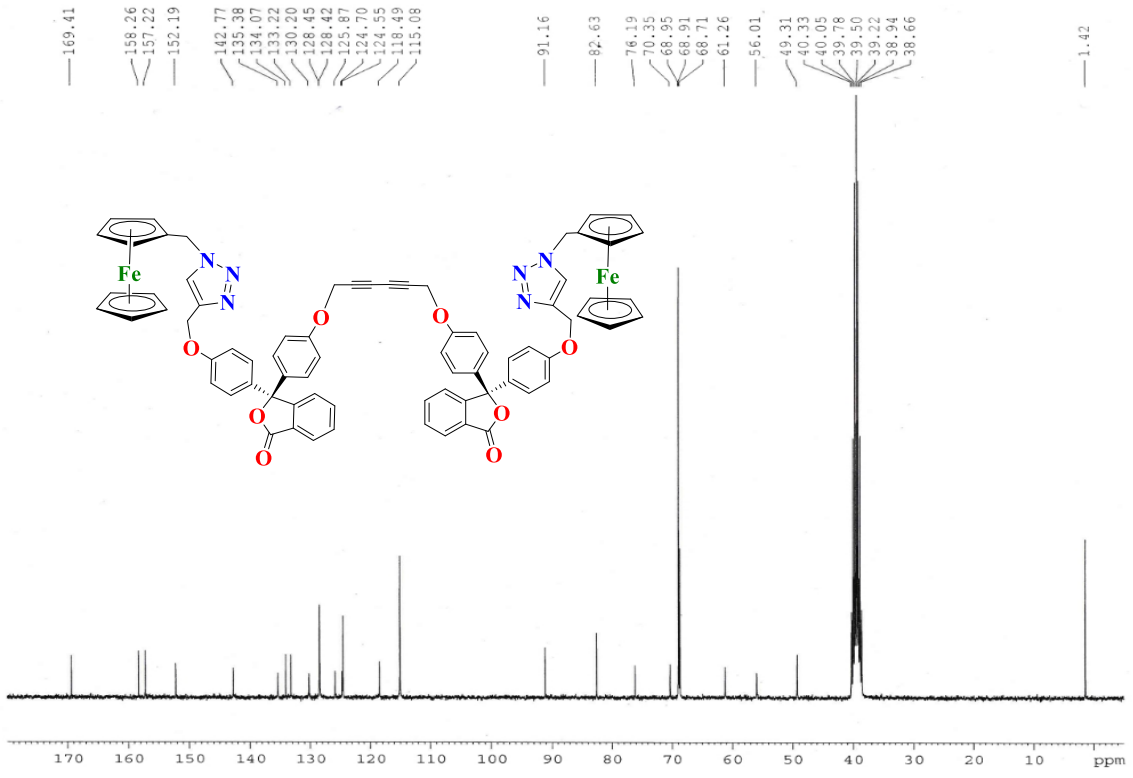

Figure 6.8. ^{13}C NMR spectra of compound **5** in DMSO-d_6.

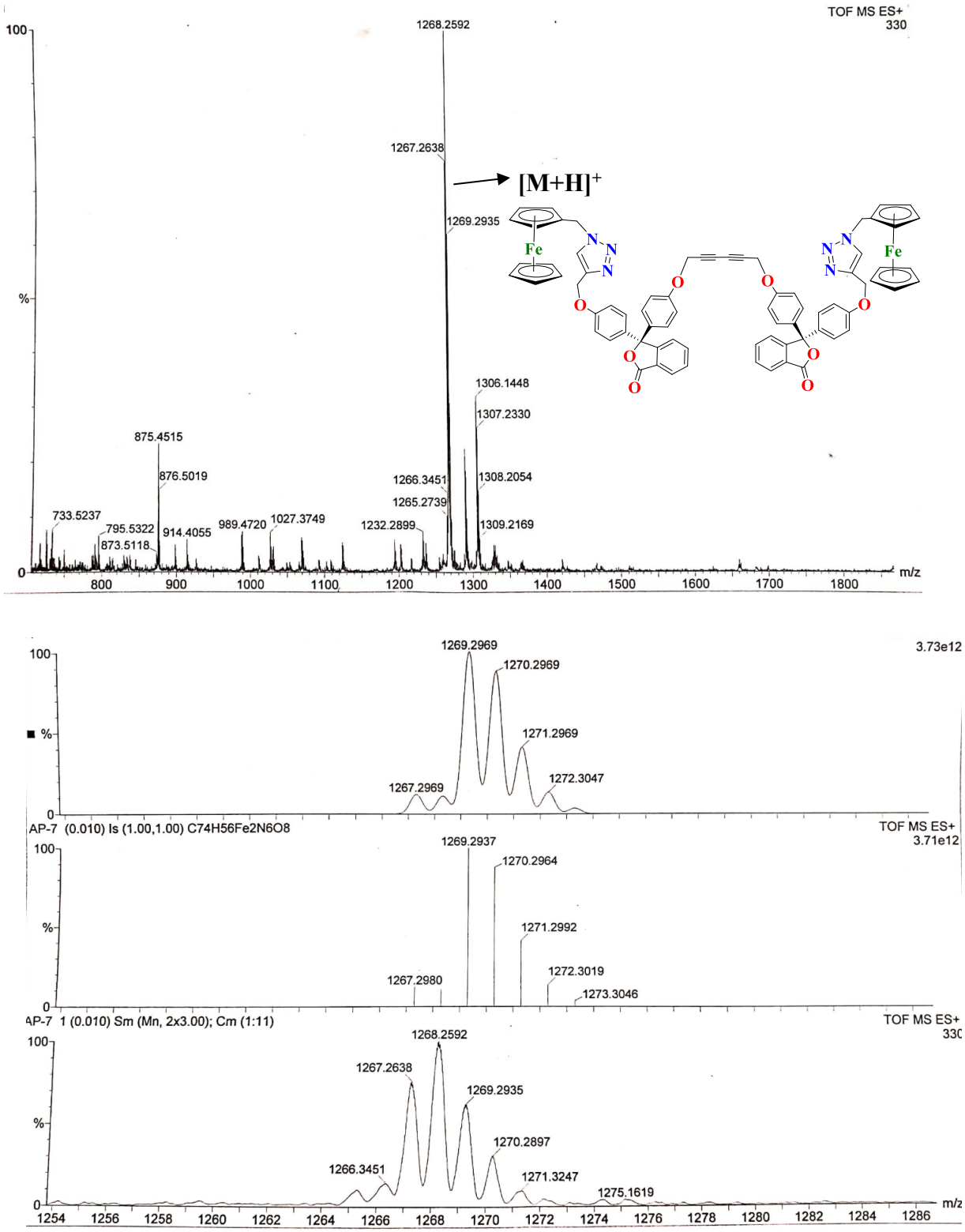

Figure 6.9. HRMS spectra of compound **5**.

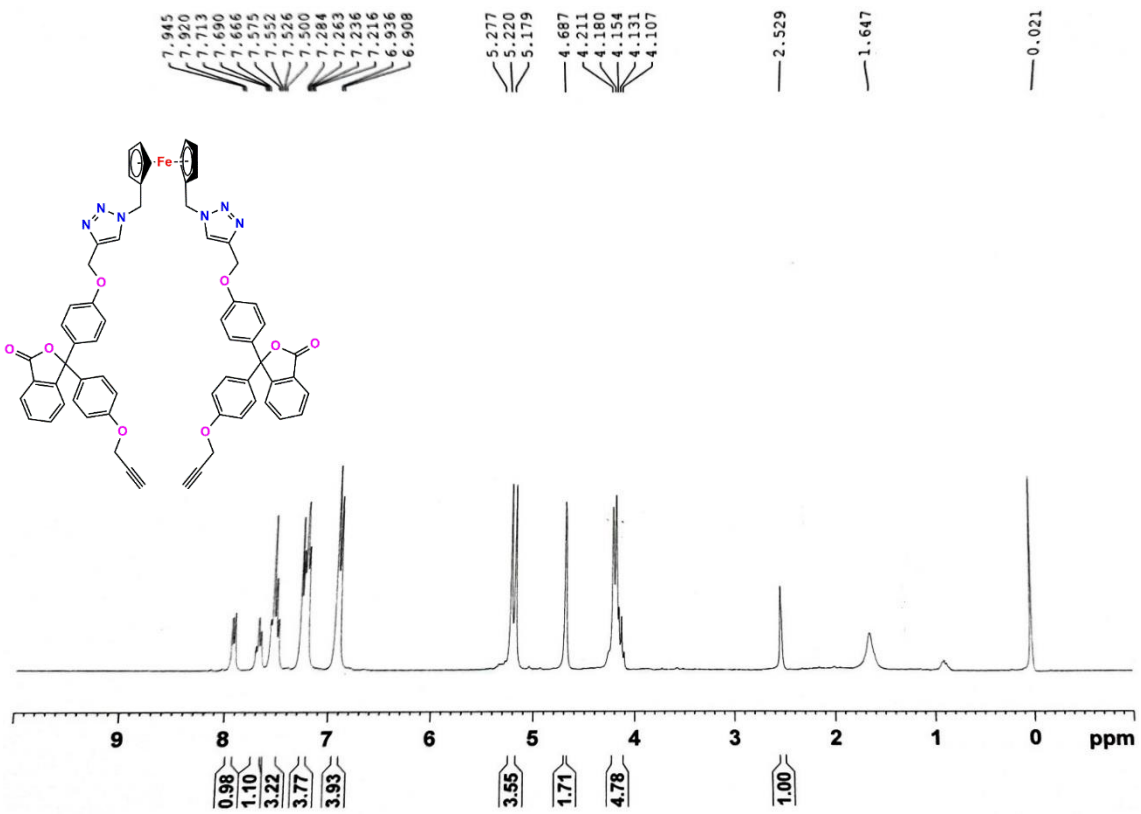

Figure 6.10. ^{1}H NMR spectra of **7** in $CDCl_3$.

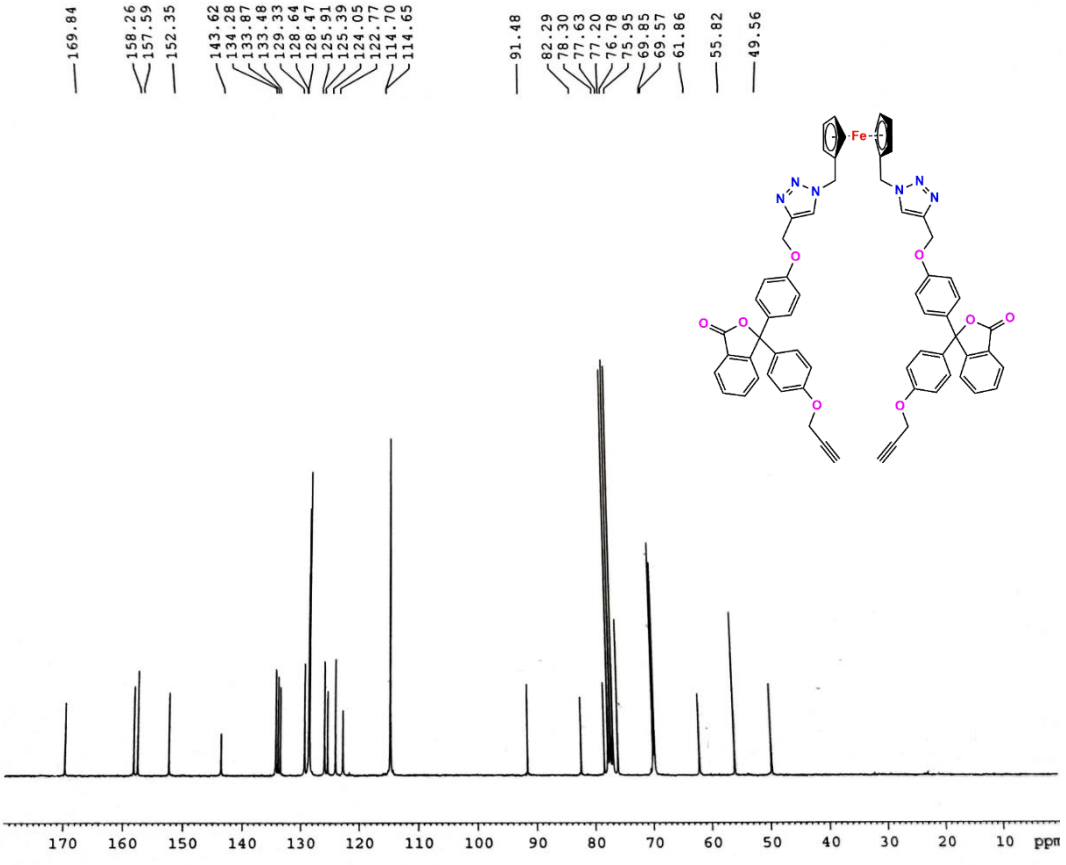

Figure 6.11. ^{13}C NMR spectra of **7** in $CDCl_3$.

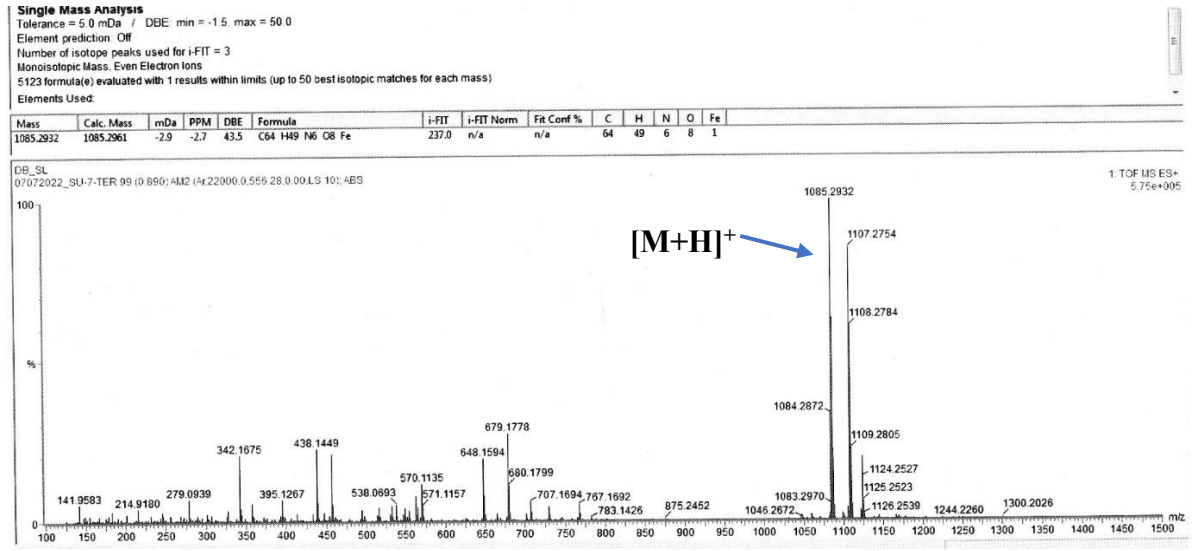

Figure 6.12. HRMS of **7**.

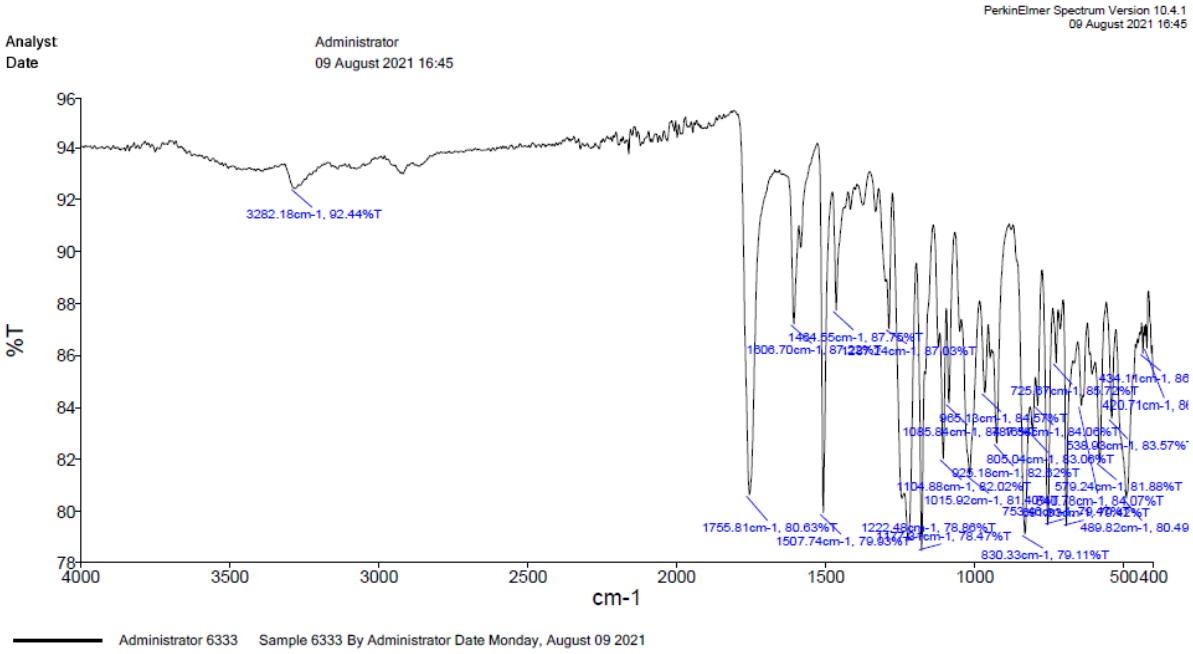

Figure 6.13. IR spectrum of **7**.

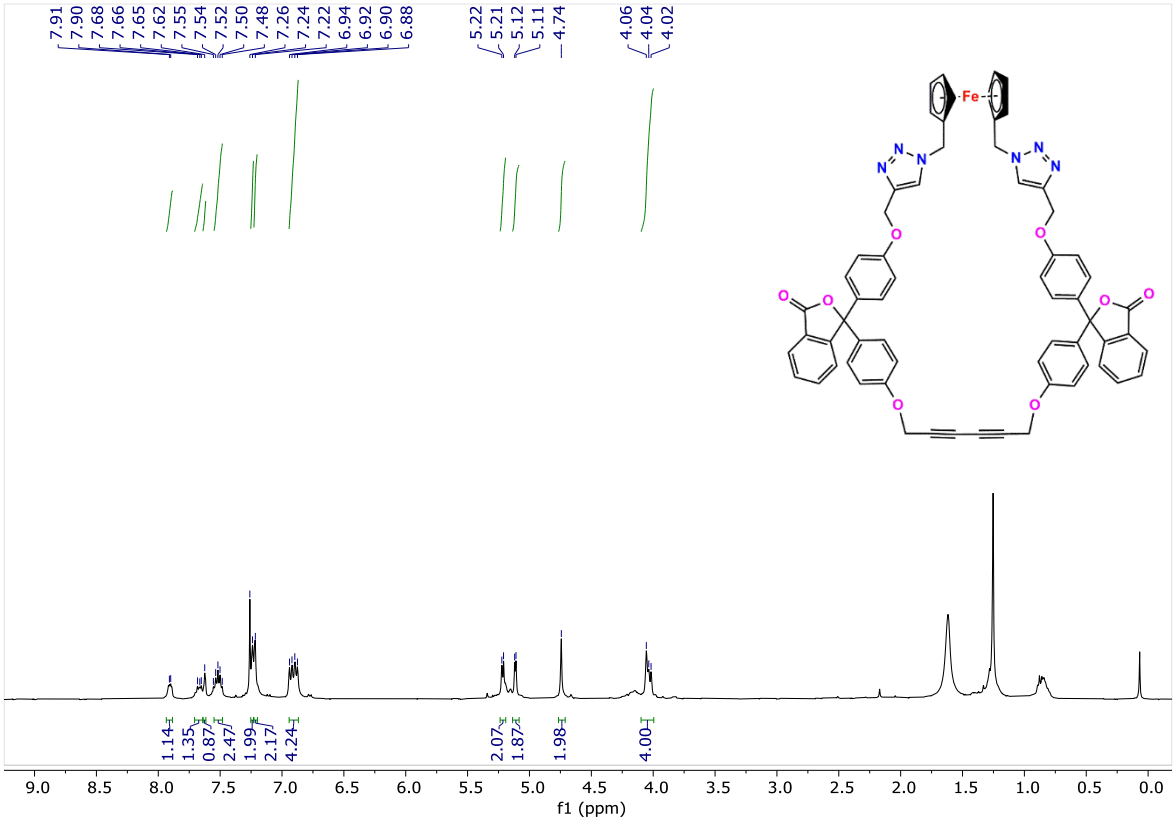

Figure 6.14. ^{1}H NMR spectra of **8** in $CDCl_3$.

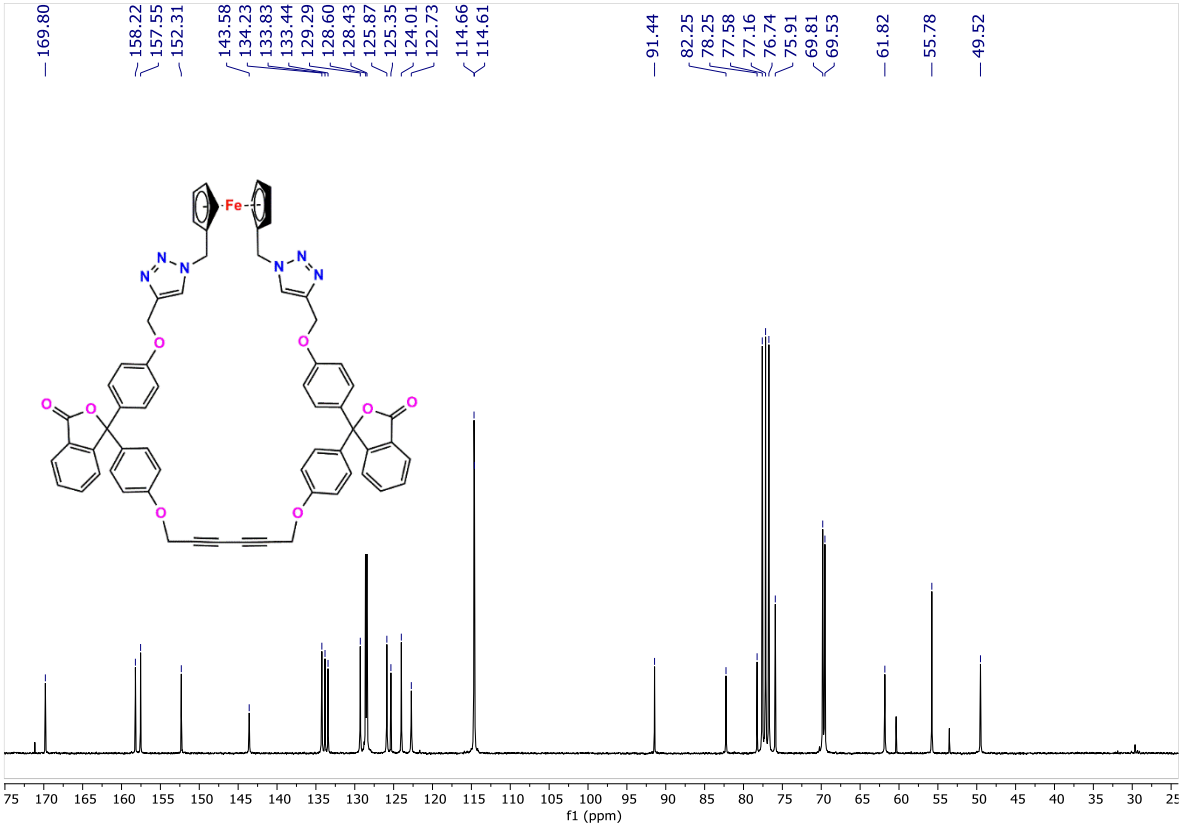

Figure 6.15. ^{13}C NMR spectra of **8** in $CDCl_3$.

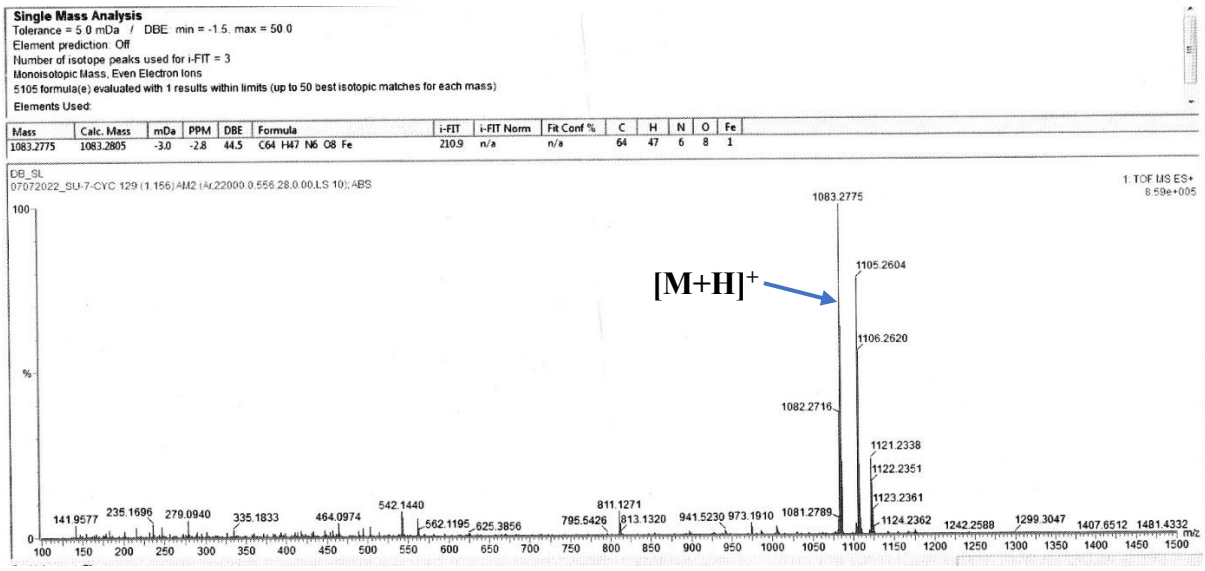

Figure 6.16. HRMS of **8**.

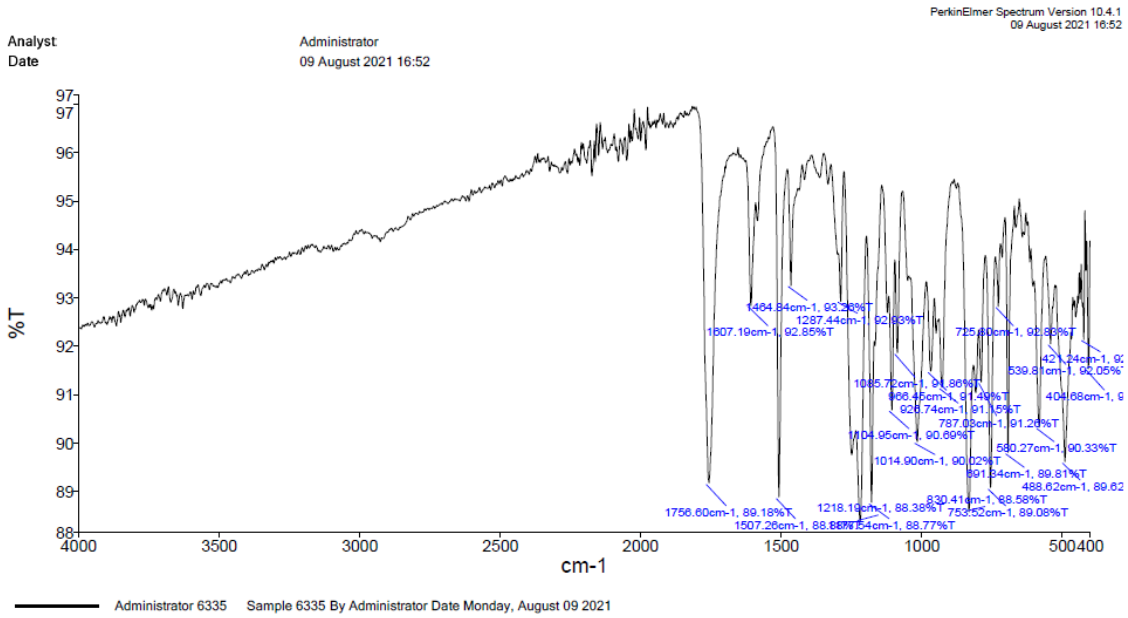

Figure 6.17. IR spectrum of **8**.

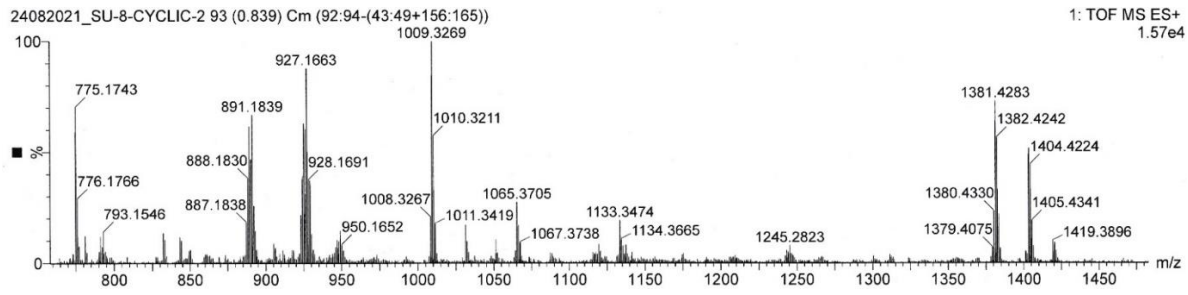

Figure 6.18. HRMS of [**8**+Hg+ClO_4].

Conclusion and Future Scope:

In conclusion, this doctoral work has explored the unexplored potential of a new Co-complex and commercially available Co-salts in various important synthetic organic transformations in greener and atom-economic ways. A variety of substrates were synthesized with our developed methodologies. Additionally, advancement in Cu-based alkyne-alkyne coupling has also been developed, where the developed molecules can be rendered to selective sensing of Hg^{2+} ion *via* an unusual binding pattern. The entire work has been categorized into six (6) chapters.

Chapter 1 gives an introduction to catalysis, in general, the historical development of catalysis, types of catalysis, leading to the development of transition metal catalysts, their importance, and a literature survey of Co-based C-C, C-N coupling, and Cu-based C-C coupling. These literature reports give an overall idea about the catalytic mechanisms that the metals Co and Cu can undergo in reactions which are relevant to this thesis. This chapter also highlights the synthetic utility of these catalytic routes in the preparation of drugs and natural products. At the end of this chapter, another aspect of molecular recognition, which is a potential application of organic probes has been discussed.

Chapter 2 describes the development of a new methodology for the synthesis of structurally beneficial dimerized arenes and heteroarenes, by employing a sustainable catalyst system of a Co(II) catalyst, coupled with freshly activated Zn powder. Compared to literature reported procedures, our developed synthetic strategy is fast, occurs at room temperature, and requires very low catalyst loading. This methodology can be a step forward towards utilizing cheaper earth-abundant metals in replacing the expensive metals in the catalysis industry with high efficiency of output.

Chapter 3 describes an easy, fast, convenient, and atom-economic methodology of *E*-aldimine and *N*-heterocycles synthesis *via* acceptorless dehydrogenative coupling between aromatic primary amines and benzyl alcohols by using low-cost commercially available $CoCl_2$ catalyst under a microwave reactor for the first time. A variety of aniline and benzyl alcohol derivatives furnished the reaction with moderate to good yield without the need of inert atmosphere protection.

Chapter 4 describes an easy-to-use and sustainable one-pot methodology catalyzed by commercially available $Co(OAc)_2 \cdot 4H_2O$ salt where acyl hydrazone derivatives can directly be synthesized in excellent yields from acyl hydrazides without the need for another

component to be coupled. The reaction proceeds under mild conditions and exhibits a wide substrate scope. Further useful synthetic modification for the synthesis of *N*-heterocycles has also been demonstrated with the resulting acyl hydrazone derivatives. This chapter also describes the modulation of its *E/Z* switchability of some of the new products, that may be useful to construct organic molecular photoswitches.

Chapter 5 describes the development of the first Co-based homogeneous photocatalytic route, which provides a straightforward and convenient method for the synthesis of a wide range of *α,β*-epoxy ketones in water. This method is facile, low-cost, and is devoid of any harsh reaction conditions. The present photocatalyzed strategy features a good substrate scope including aliphatic analogues and diverse functional groups, providing innovative approaches to construct synthetically significant *α,β*-epoxy ketones and their various post-modified heterocycles.

Chapter 6 contains two parts. The **1st part** describes the development of a new microwave-assisted Cu-catalyzed Glaser-hay coupling in neat condition giving a C_2-symmetric internally conjugated 1,3- di-alkyne system. The synthesized conjugated 1,3-di-yne system, containing ferrocene as redox unit and phenolphthalein as fluorophore has been explored as a Hg^{2+} ion sensor. Following this work, to find out the comparative reactivity studies towards metal ion detection, two more probes one acyclic with terminal alkyne unit and another cyclic with 1,3-di-yne unit were described in the **2nd part**. Different positioning of the alkyne units in the probes show differential binding patterns with Hg^{2+} ion. The exploration of difference in the cyclic and acyclic cores are important from the point of view of knowing their overall potential of using the π-cloud for metal ion binding, in any interactive environment.

Following the results presented in this thesis, there are several scopes of development of Co-based catalytic systems that can replace expensive metals like Ir, Pd, Ru in important transformations. Such an untouched area of research is the $C(sp^3)$-$C(sp^3)$ cross-coupling reaction. So far, this $C(sp^3)$-$C(sp^3)$ cross-coupling is known with Ni and Ir as catalysts, and not explored by Co as catalyst till date. This coupling is traditionally known to be carried out by organometallic reagents as one of the coupling partners. The main limitation of this strategy is the stringently sensitive reaction conditions and low functional group tolerance. Instead, a direct cross-coupling of two reagents is much more facile to handle, however is much more challenging and hence, demanding. This can be achieved by

breaking of $C(sp^3)$-X bond as in haloalkanes or $C(sp^3)$-H bond as in simple alkanes or by decarboxylative, deaminative or deoxygenative methods, with one coupling partner being the haloalkane. These reactions are so far explored by NHC-Ni or Ir complexes with the aid of photoexcitation. Hence, the exploration of suitable Co-complexes in these important coupling reactions is an unrealized goal, which is highly sustainable, since the alcohols or amines are readily available chemical feedstocks. Not only simple couplings, but there is tremendous scope for stereoselective $C(sp^3)$-$C(sp^3)$ cross-coupling reactions, and a compatible chiral NHC-Co complex can be explored here, which is also virtually unknown to the scientific community to date.

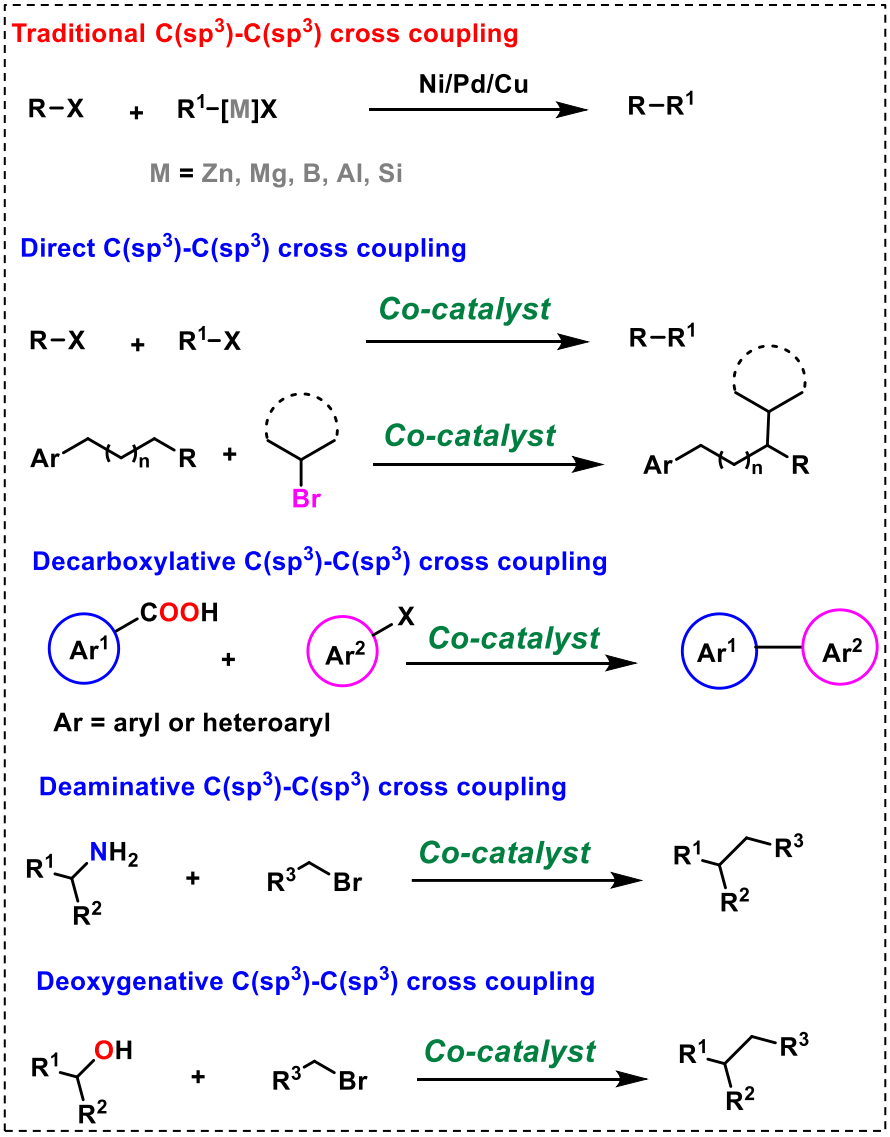

Proposed Scheme: The proposed $C(sp^3)$-$C(sp^3)$ cross-coupling reactions by Co as catalyst.

List of Publications

As 1st author:

1. **Pal, A.**; Das, K. M.; Goswami, B.; Thakur, A. Microwave-assisted neat synthesis of a ferrocene appended phenolphthalein diyne: A designed synthetic scaffold for Hg^{2+} ion. ***Inorg. Chem.*** **2020**, *59*, 10099–10112.
2. **Pal, A.**; Bhatta, S. R.; Thakur, A. Recent advances in the development of ferrocene based electroactive small molecules for cation recognition: A comprehensive review of the years 2010–2020. ***Coord. Chem. Rev.*** **2021**, *431*, 213685.
3. **Pal, A.**; Karmakar, M.; Bhatta, S. R.; Thakur, A. A detailed insight into anion sensing based on intramolecular charge transfer (ICT) mechanism: A comprehensive review of the years 2016 to 2021. ***Coord. Chem. Rev.*** **2021**, *448*, 214167.
4. **Pal, A.**; Goswami, B.; Thakur, A. Cyclic vs. acyclic alkyne towards Hg^{2+} ion detection: combined experimental and theoretical studies. ***New J. Chem.*** **2022**, *46,* 2989–3005.
5. Das, K. M.; **Pal, A.**; Goswami, B.; Thakur, A. Strategic Design of a 2,6-Disubstituted Pyridine-based Probe having Hard-Soft Centers: Responsive Divergence from One Core. ***New J. Chem.*** **2022**, *46,* 12103-12119. (**Equal 1st author**)
6. **Pal, A.**; Thakur, A. One-pot synthesis of dimerized arenes and heteroarenes under mild conditions using Co(I) as an active catalyst. ***Org. Biomol. Chem.*** **2022**, *20*, 8977-8987.
7. **Pal, A.**; Das, K. M.; Thakur, A. Microwave-Assisted Synthesis of *E*-Aldimines, *N*-Heterocycles, and H_2 by Dehydrogenative Coupling of Benzyl Alcohol and Aniline Derivatives Using $CoCl_2$ as a Catalyst. ***J. Org. Chem.*** **2023**, *88,* 8955-8968.
8. **Pal, A.**; Das, K. M.; Sau, S.; Thakur, A. Co(II) acetate assisted direct synthesis of acyl hydrazones from acyl hydrazides under mild condition. ***Chem. Asian. J.*** **2023**, e202300755.
9. Bag, S. K.; **Pal, A.**; Jana, S.; Thakur, A. Recent Advances on diarylethene-based photoswitching materials: Applications in bioimaging, controlled singlet oxygen generation for photodynamic therapy and catalysis. ***Chem. Asian. J.*** **2024**, e202400238. (**Equal 1st author**)
10. **Pal, A.**; Sau, S.; Mondal, B.; De, S.; Thakur, A. Visible-light-mediated Co(II) catalyzed synthesis of α,β-epoxyketones by oxidative coupling of alkenes and aldehydes in water. *Communicated*

As co-author:

11. Bhatta, S. R.; **Pal, A.**; Sarangi, U. K.; Thakur, A. Ferrocene appended fluorescein-based ratiomeric fluorescence and electrochemical chemosensor for Fe^{3+} and Hg^{2+} ions in aqueous media: Application in real samples analysis. ***Inorg. Chim. Acta*** **2019**, *498*, 119097-119108.
12. Karmakar, M.; **Pal, A.**; Mondal, B.; Narayanan, A. N.; Thakur, A. Light triggered metal coordination dynamics in photoswitchable dithienylethene-ferrocene system. ***Inorg. Chem.*** **2021**, *60*, 6086−6098.
13. Das, K. M.; **Pal, A.**; Thakur, A. A Novel quinoline-based NNN-pincer Cu(II) complex as a superior catalyst for oxidative esterification of allylic C(sp^3)-H bonds. ***Org. Biomol. Chem.*** **2022***, 20,* 3540-3549.
14. Pabi, B.; Marek, S.; **Pal, A.**; Kumari, P.; Roy, S. J.; Thakur, A.; Korytar, R.; Pal, A. N. Resonant transport in a highly conducting single molecular junction *via* metal–metal covalent bond. ***Nanoscale*** **2023**, *15*, 12995-13008.
15. Das, K. M.; **Pal, A.**; Thakur, A. Cu(II) promoted C(sp^3)-H activation in unactivated cycloalkanes: Oxo-alkylation of styrenes to synthesize *β*-disubstituted ketones. ***Chem. Eur. J.*** **2023**, e202303776.

List of Scientific Conferences attended and Poster Presentations

1. Chemical Sciences: Today and Tomorrow (CSTT-**2019**), Jadavpur University, Kolkata, India.
2. Celebration of the International Year of the Periodic Table (CIYPT-**2019**), Jadavpur University, Kolkata, India.
3. Modern Trends in Inorganic Chemistry (MTIC XVIII) **2019**, Indian Institute of Technology (IIT) Guwahati, India.
4. Emerging Trends in Chemical Sciences **2020**, Jadavpur University, Kolkata, India.
5. 27th CRSI-National Symposium in Chemistry, Indian Institute of Science Education and Research (IISER) Kolkata, India.
6. One Day Symposium in Chemical Sciences **2022**, Chemical Research Society of India (CRSI), Kolkata Chapter, Indian Association for the Cultivation of Science, Kolkata, India.
7. Indo-French Seminar on Catalysis for Sustainability **2023**, Indian Institute of Science Education and Research (IISER) Thiruvananthapuram, India.